THE
PROCEEDINGS
OF
THE PHYSICAL SOCIETY

Section A

FROM JANUARY 1957 TO DECEMBER 1957

VOLUME 70

Published by
THE PHYSICAL SOCIETY
1 Lowther Gardens, Prince Consort Road,
London S.W. 7

OFFICERS AND COUNCIL 1957–58

PRESIDENT

N. F. Mott, M.A., D.Sc., F.R.S.

VICE-PRESIDENTS who have filled the Office of President

Sir Frank Smith, G.C.B., G.B.E., D.Sc., LL.D., F.R.S. (1924–26)
Sir Owen Richardson, M.A., D.Sc., F.R.S. (1926–28)
W. H. Eccles, D.Sc., M.I.E.E., F.R.S. (1928–30)
T. Smith, M.A., F.R.S. (1936–38)
Sir Charles Darwin, K.B.E., M.C., M.A., Sc.D., F.R.S. (1941–43)
E. N. da C. Andrade, Ph.D., D.Sc., LL.D., F.R.S. (1943–45)
Sir David Brunt, M.A., Sc.D., F.R.S. (1945–47)
G. I. Finch, M.B.E., D.Sc., F.R.S. (1947–49)
S. Chapman, M.A., D.Sc., F.R.S. (1949–50)
L. F. Bates, D.Sc., Ph.D., F.R.S. (1950–52)
R. Whiddington, C.B.E., M.A., D.Sc., F.R.S. (1952–54)
H. S. W. Massey, B.A., Ph.D., F.R.S. (1954–56)

VICE-PRESIDENTS

S. Devons, M.A., Ph.D., F.R.S.
F. Llewellyn Jones, M.A., D.Phil.
H. Jones, Ph.D., F.R.S.
K. Mendelssohn, M.A., D.Phil., F.R.S.

HONORARY SECRETARIES

C. G. Wynne, B.A., Ph.D. (*Business*)
H. H. Hopkins, D.Sc. (*Papers*)

HONORARY FOREIGN SECRETARY

E. N. da C. Andrade, Ph.D., D.Sc., LL.D., F.R.S.

HONORARY TREASURER

A. J. Philpot, C.B.E., M.A., B.Sc.

HONORARY LIBRARIAN

R. W. B. Pearse, D.Sc., Ph.D.

ORDINARY MEMBERS OF COUNCIL

W. E. Burcham, Ph.D., F.R.S.
A. G. Peacock, B.Sc.
D. A. Wright, D.Sc.
N. Feather, B.A., Ph.D., B.Sc., F.R.S.
D. W. Fry, M.Sc.
V. E. Cosslett, M.A., M.Sc., Ph.D.
D. Gabor, Dr. Ing., F.R.S.
E. S. Shire, M.A.
B. H. Flowers, M.A., D.Sc.
F. C. Frank, O.B.E., B.A., B.Sc., D.Phil., F.R.S.
M. H. L. Pryce, M.A., Ph.D., F.R.S.
E. W. H. Selwyn, B.Sc.

OFFICERS OF THE SPECIALIST GROUPS

COLOUR GROUP

Chairman

R. G. Horner, B.A.

Honorary Secretary

R. A. Weale, M.Sc., Ph.D.

LOW TEMPERATURE GROUP

Chairman

K. Mendelssohn, M.A., D.Phil., F.R.S.

Honorary Secretary

R. W. Powell, D.Sc., Ph.D.

OPTICAL GROUP

Chairman

W. D. Wright, D.Sc., Ph.D.

Honorary Secretary

W. Weinstein, B.Sc., Ph.D.

ACOUSTICS GROUP

Chairman

E. G. Richardson, B.A., D.Sc., Ph.D

Honorary Secretaries

J. Lamb, Ph.D.
R. W. B. Stephens, B.Sc., Ph.D.

SECRETARY-EDITOR

Miss A. C. Stickland, M.Sc., Ph.D.
1 Lowther Gardens, Prince Consort Road, London, S.W.7
(*Telephone* : KENsington 0048, 0049)

CONTENTS

Part 1. *January* 1957

PAGE

Dr. A. Sugie, Dr. P. E. Hodgson and Dr. H. H. Robertson. The Contribution of Tensor Forces to n–α Scattering . . . 1

Dr. P. Baxter and Dr. F. R. Stannard. The Use of Multiple Scattering and the Effects of Distortion in a High-Pressure Cloud Chamber . . . 17

Prof. J. D. Jackson. On the Use of the Complete Interaction Hamiltonian in Atomic Rearrangement Collisions . . . 26

Dr. R. F. Barrow, Mr. P. G. Dodsworth and Prof. P. B. Zeeman. Rotational Analysis of Bands of the $A^3\Pi_0{}^+$, $B^3\Pi_1-X^1\Sigma^+$ Systems of Gallium Monofluoride . . . 34

Dr. R. McWeeny and Mr. T. E. Peacock. The Electronic Structure and Spectra of some Nitrogen Heterobenzenes . . . 41

Dr. D. B. Gayther and Mr. K. P. Nicholson. The Average Neutron Total Cross Sections of Heavy Elements at Low Energy . . . 51

Dr. Mohamed El Nadi. Some Aspects of the Stripping Reactions . . . 62

Mr. N. Sarma, Mr. M. Govindjee and Dr. H. R. Allan. A Study of the Reaction $^{12}C(d, p)^{13}C$ . . . 68

Dr. J. M. Calvert, Dr. A. A. Jaffe and Mr. E. E. Maslin. An Investigation of the Reactions ^{12}C (d, n)^{13}N and ^{28}Si (d, n)^{29}P . . . 78

Mr. J. H. Towle, Mr. R. Berenbaum and Mr. J. H. Matthews. γ–Radiation following Proton Capture in ^{35}Cl, ^{37}Cl and ^{39}K . . . 84

Letters to the Editor :

Mr. P. C. Russell and Prof. E. A. Stewardson A Re-measurement of the $L\alpha_{1,2}$ Lines of Lanthanum . . . 91

Reviews of Books . . . 93

Contents of Section B . . . 96

Part 2. *February* 1957

Dr. C. A. ten Seldam. Calculation of the Interatomic Distance at which a Model of Compressed Solid Helium becomes a Metal . . . 97

Mr. T. J. M. Boyd, Dr. B. L. Moiseiwitsch and Dr. A. L. Stewart. Inelastic Collisions between Heavy Particles. Part V : Electron Loss for Fast He^+ Ions passing through Atomic Hydrogen, and Ionization of Hydrogen Atoms by Fast He^+ Ions . . . 110

Mr. J. Adler and Dr. B. L. Moiseiwitsch. Inelastic Collisions between Heavy Particles. Part VI : The $2s^3S$–$2p$ and $3p^3P$ Excitations of Fast He Atoms by H and Ne Atoms . . . 117

Dr. T. B. Grimley. Homopolar Effects in Crystals having the Sodium Chloride Type of Lattice . . . 123

Mr. F. W. Bullock. Nuclear Disintegrations produced by Cosmic Ray Particles in a High Pressure Cloud Chamber . . . 134

Mr. V. Knapp. Nuclear Resonant Scattering of Gamma Rays in ^{199}Hg . . . 142

Mr. A. J. Apostolakis and Mr. I. Macpherson. An Emulsion Spectrograph—A New Technique for the Determination of the Momenta of Fast Charged Particles. Part I : Design Consideration and Theory . . . 146

Mr. A. J. Apostolakis and Mr. I. Macpherson. An Emulsion Spectrograph—A New Technique for the Determination of the Momenta of Fast Charged Particles. Part II : Construction and Applications of a Normal Incidence Stack . . . 154

Letters to the Editor :

Mr. C. J. Batty and Dr. S. J. Goldsack. Polarization of Protons Scattered from Carbon at 970 Mev . . . 165

Reviews of Books . . . 167

Contents of Section B . . . 168

Part 3. *March* 1957

PAGE

Dr. N. H. March. A Variational Method for the Calculation of Particle Densities and Sums of Eigenvalues in Wave Mechanics 169
Dr. A. Dalgarno and Mr. N. Lynn. Curve Crossing and Orthogonality of Molecular Orbitals 176
Dr. F. Mandl. Dispersion Relations for Forward Scattering of Spin Zero Particles by an Extended Potential 183
Dr. C. Henderson and Mr. A. Scott. The Multiple Scattering of Positrons and Electrons 188
Mr. D. L. Allan. Protons from the Interaction of 14 mev Neutrons with Medium Weight Neuclei 195
Mr. N. E. Booth, Mr. B. Ledley, Mr. D. Walker and Mr. D. H. White. Nuclear Cross Sections for 900 mev Protons 209
Dr. R. F. Barrow and Prof. E. Miescher. Fine Structure Analysis of NO Absorption Bands in the Schumann Region 219
Research Notes :
Dr. A. Dalgarno and Mr. N. Lynn. An Exact Calculation of Second Order Long Range Forces 223
Letters to the Editor :
Prof. N. Feather. Note on the Population of Segments of a Random Series which include the Origin 226
Reviews of Books 228
Contents of Section B 232

Part 4. *April* 1957

Dr. F. A. El Bedewi and Mr. I. Hussein. Magnetic Analysis of Tritons and Alpha Particles Emitted from the Deuteron Bombardment of Teflon . . 233
Dr. I. C. Percival. Electron Excitation of 3p Levels of OI 241
Dr. J. C. Barton. The First Passage Problem in the Theory of Multiple Scattering 253
Prof. J. A. V. Fairbrother, Mr. D. G. Parkyn and Mr. B. M. O'Connor. The K Auger Yield for Tin 262
Dr. A. D. Brailsford. The Magnetic Energy Levels of Electrons in Metals . 275
Dr. R. Marriott. The Conversion of Metastable Helium from the Singlet to the Triplet State by Electron Collisions 288
Dr. R. Marriott and Dr. M. J. Seaton. A Simple Analytic Wave Function for He 1s2s ^{1}S 296
Dr. W. F. Miller and Prof. R. L. Platzman. On the Theory of the Inelastic Scattering of Electrons by Helium Atoms 299
Research Notes :
Mr. S. A. Husain and Mr. J. L. Putman. The Absorption of Beta Particles as a Function of Atomic Number 304
Prof. D. R. Bates and Mr. A. Williams. Inelastic Collisions between Heavy Particles. VII : Electron Loss from Fast Hydrogen Atoms passing through Helium 306
Prof. W. E. Burcham. Light Output of Potassium Iodide Crystals under Bombardment by Carbon Ions 309
Letters to the Editor :
Mr. L. S. Kothari and Dr. K. S. Singwi. Thermal Inelastic Scattering of Cold Neutrons in Polycrystalline Graphite 314
Reviews of Books 316
Contents of Section B 320

Part 5. *May* 1957

Dr. J. C. Polkinghorne, Dr. D. L. Pursey and Dr. H. A. Santa Maria. K-meson Decays through a Fermi Interaction 321
Prof. S. N. Ghoshal and Mr. B. B. Baliga. Elastic Scattering of 32 mev Protons from Gold 324

PAGE
Dr. G. W. Greenlees, Mr. B. C. Haywood, Miss L. G. Kuo and Mr. M. Petravić. The Elastic and Inelastic Scattering of Protons by Mg . . 331
Mr. J. Randles. Incoherent Scattering of Gamma Rays from the Bound Electrons of Heavy Elements 337
Dr. K. Takayanagi. Rotational Transition of Hydrogen Molecule by Collision . 348
Mr. K. R. Allen, Mr. E. A. Finlay, Mr. M. Lipsicas, Mr. D. Major and Mr. K. Phillips. The Scattering of Fast Charged Particles : II—On the Single Scattering of 9·8 mev Positrons in Xenon 355
Dr. G. E. Brown. Polarization of gev Protons Scattered by Complex Nuclei . 361
Mr. R. J. Huck. The Effectiveness of Variational Methods for Inelastic Scattering Problems 369
Prof. R. E. Peierls and Dr. J. Yoccoz. The Collective Model of Nuclear Motion. 381
Dr. J. Yoccoz. On the Moments of Inertia of Nuclei 388

Research Notes :

Mr. B. H. Bransden and Mr. J. S. C. McKee. A Variational Calculation of the Cross Section for the 1s–2s Excitation of Hydrogen by Electron Impact 398
Reviews of Books 401
Contents of Section B 404

Part 6. *June* 1957

Prof. J. M. Cassels, Dr. G. Fidecaro, Mr. A. M. Wetherell and Dr. J. R. Wormald. The Capture of Stopped Negative Pions by Hydrogen . . 405
Dr. J. H. Carver, Dr. R. D. Edge and Mr. K. H. Lokan. Direct Excitation in the Photodisintegration of Tantalum above the Giant Resonance . . . 415
Mr. J. L. Lloyd, Dr. E. Rössle and Dr. A. W. Wolfendale. The Scattering of High Energy μ-Mesons in Lead 421
Mr. T. H. R. Skyrme. Nuclear Moments of Inertia 433
Mr. R. Berenbaum and Mr. J. H. Matthews. Gamma Radiation following Proton Capture in ^{35}Cl, ^{37}Cl and ^{39}K : II—Angular Distributions and Correlations . 445
Dr. E. W. Kellermann, Dr. T. Shaw and Dr. N. Dickinson. On the Structure of Extensive Cosmic Ray Air Showers : Core Detection and Core Structure . 452
Mr. R. McCarroll. The Excitation of the Discrete Levels of Atomic Hydrogen by Fast Electrons 460
Dr. H. R. Moore. The L-Series Emission Spectrum of Krypton . . . 466

Research Notes :

Mr. N. Lynn and Dr. B. L. Moiseiwitsch. The Mobility of He$^+$ Ions in Helium 474
Prof. N. Feather, Dr. N. Miller and Mr. S. W. Peat. Search for a Rare α-Emission in ^{228}Ra (MsTh 1) 478
Dr. J. Berkowitz. On a New Phenomenon in Activated Nitrogen . . 480
Contents of Section B 484

Part 7. *July* 1957

Dr. G. K. Woodgate and Mr. J. S. Martin. Hyperfine Structure in Manganese $^{55}_{25}$Mn 485
Mr. A. M. Arthurs and Mr. J. Hyslop. The Oscillator Strengths of the 1sσ–2pπ, 2pπ–2sσ and 2pπ–3dσ Transitions of HeH^{2+} 489
Dr. I. C. Percival. A Box Variational Method for Scattering Phases . . 494
Dr. A. Dalgarno and Mr. R. McCarroll. Properties of the Hydrogen Molecular Ion : VII—Magnetic Dipole Oscillator Strengths of the 1sσ_g–3dπ_g Transition 501
Mr. R. McCarroll and Dr. B. L. Moiseiwitsch. Approximate Molecular Orbitals : VI—The 2pσ state of HeH^{2+} 507
Dr. J. Irving and Mr. F. B. Boucher. A Variation–Iteration Method for Short Range Potential Problems 512
Mr. J. Bowcock. Compound Nuclear Theory and the Optical Model . . . 515

PAGE

Mr. C. A. ten Seldam. Calculations of the Interatomic Distance at which a Model of Compressed Solid Helium becomes a Metal 529

Research Notes :

- Mr. R. D. Amado and Dr. R. J. Blin-Stoyle. Weak Collective Effects in the Nuclear Shell Model 532
- Mr. K. R. Allen, Mr. K. Phillips and Miss F. Whittaker. The Scattering of Fast Charged Particles : III—On the Single Scattering of High Energy Positrons and Electrons at Small Angles 536
- Prof. D. R. Bates and Miss D. Miskelly. Electron Collision Partial Cross Sections for the 1s–2s and 1s–3s Transitions of Atomic Hydrogen . . 539
- Prof. J. M. Cassels, Mr. T. W. O'Keeffe, Miss M. Rigby, Mr. A. M. Wetherell and Dr. J. R. Wormald. Experiments with a Polarized Muon Beam 543

Dr. L. Marquez. On the Interpretation of High Energy Fission 546

Letters to the Editor :

- Dr. P. K. Carroll and Mr. P. J. Daly. Bands Assigned to ZrF . . . 549
- Mr. D. K. Aitken. A Means of avoiding the ' Electron Rest Mass ' Limitation in a Microtron 550
- Mr. J. S. Bell. Time Reversal in Beta-decay 552

Corrigendum :

- Dr. J. Yoccoz. On the Moments of Inertia of Nuclei 553

Reviews of Books 554

Contents of Section B 556

Part 8. *August* 1957

Dr. A. M. Lane and Mr. J. E. Lynn. Fast Neutron Capture below 1 mev : The Cross Sections for ^{238}U and ^{232}Th 557

Mr. J. W. Stephenson and Mr. K. Smith. Tabulation of the Wigner 9*j* Coefficients 571

Dr. W. D. Allen and Dr. A. T. G. Ferguson. The Fission Cross Sections of ^{233}U, ^{235}U, ^{238}U and ^{239}Pu for Neutrons in the Energy Range 0·030 mev to 3·0 mev 573

Mr. A. W. Dalton, Mr. S. Hinds and Dr. G. Parry. An Investigation of the Reaction ^{31}P(d, p)^{32}P by Magnetic Analysis 586

Dr. R. McWeeny. Electronic Absorption Spectra of Heterocyclic Systems. I : A Comparison of Theoretical Methods : Pyridine and Pyrazine . . 593

Dr. J. C. Barton, Mr. D. A. Campbell and Mr. R. C. Read. An Analogue Method for Studying Multiple Scattering. 605

Research Notes :

- Dr. E. W. Elcock. A Note on the Ising Model with Second Nearest Neighbour Interactions 615
- Mr. A. M. Arthurs, Mr. R. A. B. Bond and Mr. J. Hyslop. The Oscillator Strengths of the $1s\sigma$–$2p\sigma$, $2p\sigma$–$2s\sigma$, $2p\sigma$–$3d\sigma$ and $2p\sigma$–$2p\pi$ Transitions of HeH^{2+} 617
- Dr. M. J. Seaton. The Use of Extrapolated Quantum Defects as a Check on Calculated Phases for Scattering of Electrons by Positive Ions . . 620

Letters to the Editor :

- Dr. R. F. Barrow. On the Rotational Analysis of Bands of the $\mathrm{A}^3\Pi_0{}^+$–$\mathrm{X}^1\Sigma^+$ System of TlCl 622

Reviews of Books 624

Book Notices 627

Contents of Section B 628

Part 9. *September* 1957

Dr. E. W. Laing and Dr. R. G. Moorhouse. Photoproduction of Pions at Complex Nuclei 629

Dr. W. D. Allen and Dr. A. T. G. Ferguson. The Measurement of Fast Neutron Flux over the Neutron Energy Range 0·03 mev to 3·0 mev 639

PAGE
Mr. T. E. Peacock. Electronic Absorption Spectra of Heterocyclic Systems II: Applications to some Two-ring Nitrogen Heterocyclics 654
Dr. P. C. Price. The Radiative Capture of Alpha Particles in ^{15}N . . . 661
Dr. G. E. Brown and Dr. C. T. De Dominicis. Elastic Scattering of Low Energy Nucleons by Complex Nuclei 668
Dr. G. E. Brown. Resonances in a Complex Well 681
Dr. G. E. Brown and Dr. C. T. De Dominicis. Direct Interaction and Nuclear Dispersion Theory 686
Dr. T. V. Kanellopoulos and Dr. G. E. Brown. Polarization Experiments in Proton–Proton Scattering 690
Dr. G. E. Brown and Dr. T. V. Kanellopoulos. Analysis in Coincidence in Proton–Proton Scattering 703
Corrigenda:
Dr. J. Bowcock. Compound Nuclear Theory and the Optical Model . 708
Reviews of Books 709
Contents of Section B 712

Part 10. *October* 1957

Prof. R. Eisenschitz and Mr. P. Dean. Electronic Levels of a Model of Liquid Potassium 713
Dr. R. J. N. Phillips. A Phase-Shift Analysis of Nucleon–Nucleon Scattering at 95 Mev 721
Prof. J. M. Cassels, Miss M. Rigby, Mr. A. M. Wetherell and Dr. J. R. Wormald. Radiative Beta Decay of the Pion 729
Mr. A. Ashmore, Mr. R. G. Jarvis, Mr. D. S. Mather and Dr. S. K. Sen. The Energy Spectrum of the 350 Mev Neutron Beam from the Liverpool Synchrocyclotron 735
Mr. A. Ashmore, Mr. R. G. Jarvis, Mr. D. S. Mather and Dr. S. K. Sen. Nuclear Total Cross Sections for 350 Mev Neutrons 745
Research Notes:
Dr. A. L. Stewart. Wave Functions for Helium and Similar Atomic Systems 756
Dr. D. M. S. Bagguley, Dr. J. A. Powell and Mr. D. J. Taylor. Cyclotron Resonance over a wide Temperature Range 759
Dr. E. H. Bellamy, Mr. R. W. P. McWhirter and Mr. P. Palit. The Elastic Photoproduction of Neutral Pions from Helium 763
Mr. P. J. Wood and Prof. G. S. Rushbrooke. On the High Temperature Susceptibility for the Heisenberg Model of a Ferromagnetic. . . . 765
Letters to the Editor:
Dr. R. D. Connor and Mr. I. L. Fairweather. The β-Spectrum of Sulphur 35 769
Corrigendum:
Prof. J. A. V. Fairbrother, Mr. D. G. Parkyn and Mr. B. M. O'Connor. The K Auger Yield for Tin 770
Reviews of Books 771
Contents of Section B 776

Part 11. *November* 1957

Dr. P. G. Burke and Dr. H. H. Robertson. The Low Energy Elastic Scattering of Neutrons by Deuterons 777
Dr. N. Corngold. Slowing Down of Neutrons in Infinite Homogeneous Media 793
Dr. A. Dalgarno and Mr. N. Lynn. Properties of the Helium Atom . . . 802
Mr. T. J. M. Boyd and Dr. B. L. Moiseiwitsch. Inelastic Heavy Particle Collisions involving the Crossing of Potential Energy Curves: V—Charge Transfer from Neutral Atoms to Doubly and Triply Charged Ions 809
Mr. W. R. S. Garton and Mr. A. Rajaratnam. Flash-Absorption Spectra of the Plasmas of Arcs and other Discharges 815
Dr. J. L. Symonds, Dr. J. Warren and Dr. J. D. Young. Excitation Functions up to 980 Mev for Proton-induced Reactions in some Light Elements . . 824

Research Notes : PAGE
Dr. P. G. Klemens. Thermal Resistance due to Isotopic Mass Variation . 833
Mr. K. H. Lokan. The Integrated Cross Section from Threshold to 30 MeV for the Reaction $^9Be(\gamma, 2n)^7Be$ 836
Letters to the Editor :
Dr. N. H. March. The Density Matrix and the Foundations of the Statistical Theory 839
Reviews of Books 842
Contents of Section B 848

Part 12. *December* 1957

Mr. A. M. Arthurs and Mr. J. Hyslop. Radiative Charge Transfer from H Atoms to He^{2+} Ions 849
Dr. D. G. Ravenhall and Dr. D. R. Yennie. Electron Scattering and Model Independence 857
Dr. D. L. Booth, Dr. R. S. Hill, Dr. F. V. Price and Dr. D. Roaf. The Reaction $^3He(d, p)^4He$ between 100 kev and 500 kev 863
Mr. S. J. Biel. The Binding Energy of ^8Be and ^{12}C 866
Dr. J. M. Anderson, Dr. A. D. Kavadas and Dr. R. W. McKay. The Decay of the Nitrogen Afterglow 877
Dr. J. M. Anderson. The Nature of Active Nitrogen 887
Research Notes :
Mr. S. Hinds, Dr. R. Middleton and Dr. G. Parry. Angular Distributions of some Inelastically Scattered Deuteron Groups from ^{24}Mg and ^{28}Si . 900
Mr. S. Abid Husain and Mr. A. K. Hilmi. Absorption of Beta Particles in Liquids 902
Mr. W. Hayes, Mr. P. D. McCarvill and Mr. T. E. Nevin. The Structure of the $x^7\Sigma$ State of MnH and MnD 904
Dr. D. Park. An Improved Born Approximation 905
Letters to the Editor :
Dr. A. P. Stone. Expressions for certain Wigner Coefficients 908
Corrigendum :
Dr. R. D. Connor and Mr. I. L. Fairweather. The β-spectrum of Sulphur. 909
Reviews of Books 910
Contents of Section B 912
Subject Index, Section A, Vol. 70 913
Index of Authors (with Titles), Section A, Vol. 70 919
Index to Reviews of Books, Section A, Vol. 70 927

Contents of the Physical Society Year Book

(*For reference only*)

Frontispiece : Professor N. F. Mott, M.A., D.Sc., F.R.S. . . *Facing page* 1
Presidential Address : The Physics and Chemistry of Metals. By N. F. Mott . 1
41st Guthrie Lecture : Some Chemical Limitations on Theories for the Origin of the Solar System. By H. C. Urey 14
19th Thomas Young Oration : Observations on the Behaviour of Diffraction Gratings. By J. Guild 30
33rd Duddell Medal Address (summary) : The Magnetic Refrigerator for Temperatures below 1°K. By J. G. Daunt 49
34th Duddell Medal Address : The Scale-of-two Counter. By C. E. Wynn-Williams 53
12th Charles Vernon Boys Address : The Discovery of V-particles and the Properties of Hyperons. By G. D. Rochester and C. C. Butler . . . 61
13th Charles Vernon Boys Address : Measurement of the Velocity of Light. By L. Essen 74
Discourses given at the 41st Physical Society Exhibition, 25th–28th March, 1957 :
The International Geophysical Year. By Sir Harold Spencer Jones . 77
The Supply and Distribution of Liquid Helium. By E. Mendoza . . 90
Recent Developments in Acoustics. By E. G. Richardson . . . 93
Obituary Notices 101
Proceedings of the Meetings of the Physical Society 111
Report of Council for Year ended 31st December, 1956 117
Instructions to Authors 129

THE PROCEEDINGS OF
THE PHYSICAL SOCIETY
Section A

VOL. 70, PART 1 1 January 1957 No. 445 A

The Contribution of Tensor Forces to n–α Scattering

BY A. SUGIE[†], P. E. HODGSON[§] AND H. H. ROBERTSON[‡]
Department of Physics, University College London

MS. received 12*th July* 1956

Abstract. The splitting of the p-phase shifts due to tensor forces is calculated for n–α scattering using the resonating group method and Gaussian wave functions and potentials. It is found that the tensor force can account for about 30% of the observed splitting.

§ 1. INTRODUCTION

THE study of systems of several nucleons provides a valuable test of the nuclear forces postulated to account for two-body systems. In particular, the scattering of neutrons by alpha particles gives information on the spin–orbit force, and ^{5}He is the lightest system showing the doublet splitting on the shell model.

The alpha particle has two characteristics that simplify the study of its interactions. Firstly, it is very tightly bound so that it is a good approximation to neglect its polarization during the scattering process. (This will be referred to here as the deformation to avoid confusion with the polarization of the spin.) Secondly, its spin is zero. This makes the channel spin (the vector sum of the spins of the incident and target nuclei) $\frac{1}{2}$ for n–α scattering and consequently, for a given total angular momentum J, there are only two relative orbital angular momenta, namely $J \pm \frac{1}{2}$. Since the parities of the systems corresponding to these two angular momenta are different they do not mix, that is, the orbital angular momentum is also a good quantum number. This is no longer true if the deformation of the alpha particle is taken into account.

The doublet splitting of the lower levels of nuclei is often interpreted in terms of the vector spin–orbit force of the type (Hughes and Le Couteur 1950, Inglis 1953, Elliott 1953)

$$(\mathbf{s}_1+\mathbf{s}_2) \,.\, \{(\mathbf{r}_1-\mathbf{r}_2)\times(\mathbf{p}_1-\mathbf{p}_2)\}\, v(r_{12}). \qquad \ldots\ldots(1)$$

In this way Hochberg, Massey, Robertson and Underhill (1955), extending earlier work of Hochberg, Massey and Underhill (1954), accounted for the splitting of the p state in n–α scattering. However, the tensor spin–orbit force, introduced to account for the quadrupole moment of the deuteron, can also produce some splitting. In this paper the splitting of the p phases in n–α scattering due to the tensor force alone is studied.

The effect of the tensor force on the neutron–alpha-particle system (^{5}He) was first studied by Dancoff (1940). He treated it as a bound state problem, although there is no bound state in ^{5}He, and estimated the energy difference between the $J=\frac{3}{2}$ and $J=\frac{1}{2}$ states by second order perturbation theory with the tensor force as the perturbation. Finding that the very many intermediate states gave contributions of the same order of magnitude, he used the closure approximation to evaluate the sum. The splitting was obtained from the difference in the mean energy in the denominator of the expression for the closure approximation for the two states $J=\frac{3}{2}$ and $J=\frac{1}{2}$. This calculation showed that these two states form a very small normal doublet, a result contrary to experiment.

[†] Now at the Department of Physics, University of Toyko, Japan.

[‡] At the Department of Physics, University of Reading, from April 1957.

[§] Now at C.E.R.N., Geneva, Switzerland.

Later Feingold (1952) considered the problem of ^{5}He, but he also used a formalism appropriate to the bound state problem and included the tensor force in a perturbation-variational way. That is, a variational wave function very similar to the first order perturbation wave function was used, and the parameters in it determined in principle by minimizing the ground state binding energy. Then the difference of the binding energies for the ground and the excited state was evaluated using wave functions of the same form but with different zero order wave functions corresponding to the different total angular momenta. His result depends very strongly on the ratio of the range of the force to the radius of the alpha particle. If ^{5}He is very loosely bound (this means not only the last neutron but also the alpha particle itself) the doublet is normal and the splitting very small (about 0·1 MeV), while if it is tightly bound the doublet is inverted and the splitting fairly large (about 3 MeV). His later work (1956) gives essentially the same result.

Experimentally, it has been established by Seagrave (1953) and others that in the $p_{1/2}$ state there is no virtual level at all in the sense that the phase shift of the $p_{1/2}$ wave does not pass through 90 degrees. Although it is possible to define some formal resonance energy even in this case, the bound state approximation is inadequate.

The tensor force contributes to the splitting of the $p_{1/2}$ and $p_{3/2}$-phase shifts in two ways. The first is through the D state of the alpha particle. The D state probability is of the order 4%, but the amplitude ratio between the S and D states is about 0·2. Since the SD cross term contributes to the splitting, this D state can be important. Secondly, the deformation of the alpha particle also contributes, but this possibility is not considered here. If a vector spin–orbit force of the form (1) is included in the two-body potential the probability of the ^{3}P state may become as large as that of the ^{5}D state, but this state does not contribute to the splitting as the tensor force vanishes for the SP cross terms. In both Dancoff's and Feingold's treatment the D state and the deformation were taken into account on the same footing since the sum of the tensor forces

$$\sum_{i>j=1}^{5} S_{ij} v_{ij}{}^{t}$$

was taken as the perturbation.

Inclusion of the tensor force necessitates a change of the central potential of the n–α system if the accord with experiment is to be maintained. This will be studied in a later paper.

§ 2. FORMULATION OF THE PROBLEM

The Schrödinger wave equation of the n–α system may be written

$$\left(\sum_i T_i + \sum_{i>j} \mathscr{V}_{ij}\right)\Psi = (E_\alpha + E)\Psi \qquad \ldots\ldots(2)$$

where T_i is the kinetic energy of the ith nucleon, $T_i = -(\hbar^2/2M)\nabla_i{}^2$, and $\mathscr{V}_{ij}$ is the potential energy between the ith and the jth nucleon. $E_\alpha + E$ is the total energy of the system, E_α being the binding energy of the target nucleus and E the kinetic energy of the incident neutron.

The potential $\mathscr{V}_{ij}$ has central and tensor components

$$\mathscr{V}_{ij} = \mathscr{V}_{ij}^{\mathrm{c}}(r_{ij}) + S_{ij}\mathscr{V}_{ij}^{\mathrm{t}}(r_{ij}) \qquad \ldots\ldots(3)$$

where S_{ij} is the tensor operator

$$S_{ij} = \{3(\boldsymbol{\sigma}_i\,.\,\mathbf{r}_{ij})(\boldsymbol{\sigma}_j\,.\,\mathbf{r}_{ij}) - r_{ij}^2(\boldsymbol{\sigma}_i\,.\,\boldsymbol{\sigma}_j)\}/r_{ij}^2. \qquad \ldots\ldots(4)$$

The central part of the potential has four exchange components

$$\mathscr{V}_{ij}^{\mathrm{c}}(r_{ij}) = (wW + mM + bB + hH)\,V^{\mathrm{c}}(r_{ij}) \qquad \ldots\ldots(5)$$

while the tensor part has only two because the tensor force contributes only in the triplet state of the two particles:

$$\mathscr{V}_{ij}^{\mathrm{t}}(r_{ij}) = (wW + mM)\,V^{\mathrm{t}}(r_{ij}). \qquad \ldots\ldots(6)$$

When the deformation is neglected the total antisymmetrical wave function Ψ of the system can be written in the form

$$\Psi = \psi(-1)\phi(1) + \psi(-2)\phi(2) + \psi(-3)\phi(3) \qquad \ldots\ldots(7)$$

where $\psi(-i)$ is the antisymmetrized wave function of the target nucleus which does not contain the ith particle and ϕ is the wave function of the incident neutron. Particles 1, 2 and 3 are neutrons, and 4 and 5 are protons.

The ground state of the alpha particle is known to be principally the S state with a small admixture of D state due to the tensor force (Gerjuoy and Schwinger 1942, Irving 1953, Abraham, Cohen and Roberts 1955). The P state is also a possible component but it is quite negligible for a nuclear force of the above type. The alpha particle wave function $\psi(-1)$ is of the form

$$\begin{aligned}\psi(-1) &= \sum_{S}\psi_{L,S,0}(-1) = \sum_{S,p}\psi^{p}{}_{L,S,0}(-1)\\ &= \sum_{S,p} g_S{}^{p}(\mathbf{u},\mathbf{v},\mathbf{w})\,w_S{}^{p}(\mathbf{u},\mathbf{v},\mathbf{w};\,\boldsymbol{\sigma}_2,\boldsymbol{\sigma}_4)\,\chi(\widetilde{23},\widetilde{45}) \qquad \ldots\ldots(8)\end{aligned}$$

in which S = 0 and S = 2 are important. The superscript p distinguishes the many possible spin angular wave functions; **u**, **v**, and **w** are the three independent internal space coordinates; and χ is the spin wave function of the singlet state

$$\chi(\widetilde{23},\widetilde{45}) = \tfrac{1}{2}(\alpha_2\beta_3 - \beta_2\alpha_3)(\alpha_4\beta_5 - \beta_4\alpha_5) \equiv \chi(-1). \qquad \ldots\ldots(9)$$

All the possible spin–angular wave functions were derived by Gerjuoy and Schwinger and the six independent D-state wave functions listed by Abraham, Cohen and Roberts (1955). Here only the most important among them will be considered, namely the symmetric

$$w_2{}^{1}(\mathbf{u},\mathbf{v},\mathbf{w};\;\boldsymbol{\sigma}_2,\boldsymbol{\sigma}_4)\,\chi = \{3(\boldsymbol{\sigma}_2\,.\,\mathbf{r}_{23})(\boldsymbol{\sigma}_4\,.\,\mathbf{r}_{45}) + 3(\boldsymbol{\sigma}_2\,.\,\mathbf{r}_{45})(\boldsymbol{\sigma}_4.\mathbf{r}_{23}) - 2(\mathbf{r}_{23}.\mathbf{r}_{45})(\boldsymbol{\sigma}_2.\boldsymbol{\sigma}_4)\}\chi. \qquad \ldots\ldots(10)$$

The superscript 1 is omitted below. In the S state there are two spin–angular wave functions, one corresponding to the state in which the spins of the two similar particles couple to zero, and the other to the state in which they couple to one. In the ground state the former predominates and the latter will be neglected.

The wave function of the alpha particle can then be written

$$\psi = \{\psi_{\mathrm{S}} + C\psi_{\mathrm{D}}\}/(1 + C^2)^{1/2} \qquad \ldots\ldots(11)$$

where $\psi_{\mathrm{S}} = g_0(\mathbf{u},\mathbf{v},\mathbf{w})\,\chi$ and $\psi_{\mathrm{D}} = g_2(\mathbf{u},\mathbf{v},\mathbf{w})\,w_2(\mathbf{u},\mathbf{v},\mathbf{w};\;\boldsymbol{\sigma}_2\boldsymbol{\sigma}_4)\,\chi$

and the ψ_{S} and ψ_{D} are both normalized.

The wave function of the incident neutron can be decomposed into partial waves by writing it in the form

$$\phi = \sum_{l,\,J=l\pm\frac{1}{2}}\{f_{lJ}(r)/r\}\,\chi_{lJ}{}^{m}(\theta,\phi,s) \qquad \ldots\ldots(12)$$

where (r,θ,ϕ) are the polar coordinates of the neutron relative to the centre of mass of the alpha particle and $\chi_{lJ}{}^{m}$ is the spin–angular wave function of the neutron. Its magnetic quantum number m is also the magnetic quantum number of the whole system since the spin of the alpha particle is zero.

The equation for the wave function ϕ of the incident neutron is obtained by multiplying the Schrödinger wave equation (2) by $\bar{\psi}(1)\,\bar{\chi}_{lj}{}^{m}(\theta_1, \phi_1, s_1)$from the left, summing over the spins, and integrating over all the relative spatial coordinates except r. In this calculation it is assumed that ψ is a good variational wave function. The result can be written in the form

$$\begin{aligned}\left\{\frac{d^2}{dr^2}+k^2-\frac{l(l+1)}{r^2}\right\}&f_{lJ}(r)\\ =\int \bar{\psi}(-1)\,\bar{\chi}_{lJ}{}^{m}(1)&\sum_{j=2}^{5}(U_{1j}{}^{\mathrm{c}}+S_{1j}U_{1j}{}^{\mathrm{t}})\psi(-1)\,\chi_{lJ}{}^{m}(1)f_{lJ}(r)\,d\tau_{-1}d\Omega\\ +2\int \bar{\psi}(-1)\,\bar{\chi}_{lJ}{}^{m}(1)&\sum_{i>j=1}^{5}(U_{ij}{}^{\mathrm{c}}+S_{ij}\,U_{ij}{}^{\mathrm{t}})\,\psi(-2)\,\chi_{lJ}{}^{m}(2)\,\{f_{lJ}(r')/r'\}\,d\tau_{-1}r\,d\Omega\\ -2\int \bar{\psi}(-1)\,\bar{\chi}_{lJ}{}^{m}(1)&\,(\mathrm{K.E.}-\kappa^2)\,\psi(-2)\,\chi_{lJ}{}^{m}(2)\,\{f_{lJ}(r')/r'\}d\tau_{-1}\,r\,d\Omega\end{aligned}\qquad\ldots\ldots(13)$$

$$\left.\begin{aligned}\text{where}\quad k^2=\frac{2M'}{\hbar^2}E\,;\ M'=\frac{4}{5}M\,;\ \kappa^2=\frac{2M'}{\hbar^2}(E_\alpha+E)\,;\ U_{ij}=\frac{2M'}{\hbar^2}\mathscr{V}_{ij}\\ \mathbf{r}=\mathbf{r}_1-\tfrac{1}{4}(\mathbf{r}_2+\mathbf{r}_3+\mathbf{r}_4+\mathbf{r}_5),\\ \mathbf{r}'=\mathbf{r}_2-\tfrac{1}{4}(\mathbf{r}_3+\mathbf{r}_1+\mathbf{r}_4+\mathbf{r}_5)\end{aligned}\right\}\ldots\ldots(14)$$

and K.E. stands for the kinetic energy operators in the centre-of-mass system.

In this equation the integral sign means both the summation over spins and the integration over the spatial coordinates. The m's in $\bar{\chi}_{lJ}{}^{m}$ and $\chi_{lJ}{}^{m}$ are equal because of the conservation of the magnetic quantum number, and the result should not depend on m because of the isotropy of the space.

Hochberg, Massey and Underhill, and Hochberg, Massey, Robertson and Underhill have already evaluated the terms $\bar{\psi}_{\mathrm{S}}\,U^{\mathrm{c}}\,\psi_{\mathrm{S}}$ and $\bar{\psi}_{\mathrm{S}}\,(\mathrm{K.E.}-\kappa^2)\,\psi_{\mathrm{S}}$.

In the present case there are the following additional terms:

$$\bar{\psi}_{\mathrm{D}}U^{\mathrm{c}}\psi_{\mathrm{D}},\ \ \bar{\psi}_{\mathrm{D}}\,U^{\mathrm{t}}\psi_{\mathrm{D}},\ \ \bar{\psi}_{\mathrm{D}}\,(\mathrm{K.E.}-\kappa^2)\,\psi_{\mathrm{D}},\ \ \psi_{\mathrm{S}}\,U^{\mathrm{t}}\psi_{\mathrm{D}}+\psi_{\mathrm{D}}\,U^{\mathrm{t}}\psi_{\mathrm{S}}.\qquad\ldots\ldots(15)$$

All the other terms may be shown by explicit calculation or by general invariance considerations to vanish after integration. Since the D state probability of the alpha particle is small only the SD terms are calculated here, and the effect of the DD terms is neglected. The SD terms are of two types; one has only the coordinates of particle 1 as the outer neutron and the other has the coordinates of both particles 1 and 2 as the other outer neutrons. These types of terms will be referred to as direct and exchange respectively.

All the direct SD Wigner terms vanish after the spin summation because each of the four operators $S_{1j}w_2(\mathbf{u},\mathbf{v},\mathbf{w}\,;\ \boldsymbol{\sigma}_2,\boldsymbol{\sigma}_4)+\bar{w}_2(\mathbf{u},\mathbf{v},\mathbf{w}\,;\ \boldsymbol{\sigma}_2,\boldsymbol{\sigma}_4)\,S_{1j}$ have either $\boldsymbol{\sigma}_2$ or $\boldsymbol{\sigma}_4$ only once and the expectation values of $\boldsymbol{\sigma}_2$ or $\boldsymbol{\sigma}_4$ between two similar χ's is zero. The direct SD Wigner terms also vanish for the other S or D states (see Appendix 1). The direct DD Wigner terms vanish also.

There are ten pairs of exchange SD Wigner terms. S_{12}, S_{13} and S_{23} vanish because each operator contains $\boldsymbol{\sigma}_4$ only once. The terms containing $\boldsymbol{\sigma}_2$ do not vanish because of the exchange nature of the functions. S_{45} vanishes because there is a singlet state in the S-state wave function. This is not the case for the S state neglected here, but the contribution from it is unimportant. Only three of the remaining terms are independent since $S_{14}=S_{15}$, $S_{24}=S_{25}$, and $S_{34}=S_{35}$.

Using the relations $\boldsymbol{\sigma}_3\chi = -\boldsymbol{\sigma}_2\chi,\ \boldsymbol{\sigma}_5\chi = -\boldsymbol{\sigma}_4\chi,$ ......(16)

$$(\boldsymbol{\sigma}\,.\,\mathbf{a})(\boldsymbol{\sigma}\,.\,\mathbf{b}) = (\mathbf{a}\,.\,\mathbf{b}) + i\boldsymbol{\sigma}\,.\,(\mathbf{a}\times\mathbf{b}) \quad \text{if} \quad [\mathbf{a},\mathbf{b}] = 0, \quad \text{and} \quad (\boldsymbol{\sigma}\,.\,\boldsymbol{\sigma}')^2 = 3 - 2(\boldsymbol{\sigma}\,.\,\boldsymbol{\sigma}'), \qquad \text{......(17)}$$

$$\bar{\chi}(-1)\bar{w}_0(-1)\,S_{14}\,w_2(-2)\chi(-2)$$

becomes

$$\chi(-1)[18\,(\mathbf{r}_{13}\,.\,\mathbf{r}_{14})(\mathbf{r}_{14}\,.\,\mathbf{r}_{45}) - 6r_{14}{}^2\,(\mathbf{r}_{13}\,.\,\mathbf{r}_{45}) + 9i\boldsymbol{\sigma}_3\,.\,(\mathbf{r}_{13}\times\mathbf{r}_{14})(\mathbf{r}_{14}\,.\,\mathbf{r}_{45})$$
$$-9i\boldsymbol{\sigma}_3\,.\,(\mathbf{r}_{14}\times\mathbf{r}_{45})(\mathbf{r}_{13}\,.\,\mathbf{r}_{14})]\chi(-2). \qquad \text{......(18)}$$

The value of $\bar{\chi}\,\bar{w}_2(-1)\,S_{14}\,w_0(-2)\chi$ is obtained from the above expression by interchanging $\mathbf{r}_{13}$ and $\mathbf{r}_{23}$. The expression for the term with S_{24} becomes the same as (18) after the interchanges $\mathbf{r}_{14}\rightleftharpoons\mathbf{r}_{24}$ and $\boldsymbol{\sigma}_3\rightleftharpoons-\boldsymbol{\sigma}_3$. In the same way $\bar{\chi}(-1)\bar{w}_0(-1)\,S_{34}\,w_2(-2)\chi(-2)$ is

$$\chi(-1)[-18\,(\mathbf{r}_{34}\,.\,\mathbf{r}_{45})(\mathbf{r}_{34}\,.\,\mathbf{r}_{13}) + 6r_{34}{}^2\,(\mathbf{r}_{13}\,.\,\mathbf{r}_{45}) + 9i\boldsymbol{\sigma}_3\,.\,(\mathbf{r}_{13}\times\mathbf{r}_{34})(\mathbf{r}_{34}\,.\,\mathbf{r}_{45})$$
$$+9i\boldsymbol{\sigma}_3\,.\,(\mathbf{r}_{34}\times\mathbf{r}_{45})(\mathbf{r}_{13}\,.\,\mathbf{r}_{34})]\chi(-2) \qquad \text{......(19)}$$

and $\bar{\chi}\,\bar{w}_2\,(-1)\,S_{34}\,w_0\,(-2)\chi$ is again derived by the interchange $\mathbf{r}_{13}\rightleftharpoons\mathbf{r}_{23}$. In these expressions the terms containing $\boldsymbol{\sigma}_3$ produce splitting of the P phases, while those without it do not. Although, due to the high symmetry of the alpha particle, the direct SD tensor terms give neither central nor spin–orbit force, it follows from general invariance considerations that, if the target nucleus has spin zero and deformation is neglected, the spin–orbit force can only come from the exchange integrals. In fact, for the velocity-independent forces, the independent variables of the incident neutron are $\boldsymbol{\sigma}$ and $\mathbf{r}$ for the direct term and it is not possible to form from them any operator invariant under rotation and reflection. On the other hand there are three variables $\boldsymbol{\sigma}$, $\mathbf{r}$ and $\mathbf{r}'$ in the exchange term and the invariant operator $i\boldsymbol{\sigma}\,.\,(\mathbf{r}\times\mathbf{r}')$ can be formed from them. It will be shown later that this is actually the form of the spin–orbit force derived from (18) and (19) after the integration over the coordinates of the alpha particle.

The SD Heisenberg (or Majorana) terms either vanish after the spin summation or may be shown by suitable exchanges of the numbering of the spatial coordinates to equal the corresponding Wigner terms. This is true for any S-state wave function that does not change under any permutation of the numbering of the spatial coordinates. It does not hold, however, for the S-state wave function

$$(\mathbf{r}_{23}\,.\,\mathbf{r}_{45})(\boldsymbol{\sigma}_2\,.\,\boldsymbol{\sigma}_4)\,\chi g_0\left(\sum_2^5 r_{ij}{}^2\right). \qquad \text{......(19')}$$

§ 3. CHOICE OF POTENTIAL AND WAVE FUNCTION

To avoid prohibitively complex mathematical analysis Gaussian potentials and wave functions were chosen. It is known from nucleon–nucleon scattering experiments that the s-phase shifts decrease fairly rapidly at higher energies (50 MeV), and this is usually attributed to a potential with a hard core. According to the effective range theory the hard core is equivalent, for the energy range important within the nucleus, to a reduction of the shape dependent factor P, which is fairly large for the Yukawa well (cf. Blatt and Jackson 1949). The Gaussian well, for which P is fairly small, is thus similar to the Yukawa well with a hard core.

It has been shown by Gerjuoy and Schwinger (1942) that the tensor force makes an important contribution to the binding energy of the deuteron but not to that of the alpha particle. Therefore, although the low-energy two-body data are fairly well reproduced by tensor forces alone, without central forces, it is necessary to keep the central forces fairly strong to reproduce the binding energy of the alpha particle. The parameters for the singlet state are completely determined by the scattering length and the effective range. In the triplet state, there are two variable parameters for fixed scattering length and effective range, or alternatively, for fixed scattering length a_t and deuteron binding energy, which is more accurately known. One of these is fixed by the quadrupole moment $\underset{\sim}{Q}$ of the deuteron. The other could, in principle, be fixed by the D-state probability, but this is not reliable because of relativistic and mesonic effects. There is thus one variable parameter still remaining after the requirements of the two-body system have been satisfied and this can be chosen to fit the binding energy of the alpha particle. If this is done, however, the calculation becomes more complicated because of the difference in the ranges of the central forces in the singlet and triplet states. As the variational wave function used in this calculation is a simple but not a very good one, this refinement would hardly be justified. A compromise was therefore made by choosing a force with the same central range in the singlet and triplet states, and which also reproduces the low-energy two-body data to within about ten per cent and gives a tolerable value for the binding energy of the alpha particle.

The values of the constants were interpolated from the tables of Kalos, Biedenharn and Blatt (1956), which give a wide range of constants consistent with the two-body scattering data. The central range b_c and the depth parameter s_c for both the singlet and triplet states were chosen to be 0·5 and 0·9, and the tensor range b_t fixed so that the corresponding $\underset{\sim}{Q}$ and a_t are near the experimental values.

The value chosen for b_t was 0·618 and for this the parabolically interpolated values of $\underset{\sim}{Q}$ and a_t are 0·01289 and 1·254, compared with the experimental values $0{\cdot}0147 \pm 0{\cdot}0001$ and $1{\cdot}249 \pm 0{\cdot}006$ respectively. (The unit of length is $4{\cdot}315 \times 10^{-13}$cm.)

The explicit form chosen for the potential is

$$V_{12} = V_c{}^0 \exp(-\mu r^2) + S_{12} V_t{}^0 \exp(-\nu r^2) \qquad \ldots\ldots(20)$$

where

$$V_c{}^0 = -44{\cdot}3 \text{ MeV}, \qquad V_t{}^0 = -30{\cdot}7 \text{ MeV},$$
$$\mu = 0{\cdot}443 \times 10^{26} \text{ cm}^{-2}, \qquad \nu = 0{\cdot}290 \times 10^{26} \text{ cm}^{-2}$$

and the spatial wave functions of the alpha particle

$$g_0 = N_0 \exp\left\{-\tfrac{1}{2}\alpha \sum_{i>j=2}^{5} r_{ij}{}^2\right\}; \quad g_2 = N_2 \exp\left\{-\tfrac{1}{2}\beta \sum_{i>j=2}^{5} r_{ij}{}^2\right\} \qquad \ldots\ldots(21)$$

where N_0 and N_2 are the normalization constants.

The variational expression for the binding energy of the alpha particle is

$$(1+C^2)E_\alpha = \frac{\hbar^2}{2M}\{18\alpha + 26\beta C^2\} + V_c{}^0\{6A^{3/2} + C^2(\tfrac{5}{2}A'^{3/2} + 3A'^{5/2} + \tfrac{1}{2}A'^{7/2})\}$$
$$- V_t{}^0\left\{\frac{12C}{\sqrt{5}}B' + C^2\left(\frac{21}{5}B^{5/2} + B^{7/2}\right)\right\} \qquad \ldots\ldots(22)$$

where
$$A = \frac{2\alpha}{2\alpha+\mu}; \qquad B = \frac{2\beta}{2\beta+\nu};$$
$$A' = \frac{2\beta}{2\beta+\mu}; \qquad B' = \left(\frac{2\alpha}{\alpha+\beta}\right)\left(\frac{2\beta}{\alpha+\beta}\right)^2\left(\frac{2\sqrt{(\alpha\beta)}}{\alpha+\beta+\nu}\right)^{5/2}.$$

This was minimized with respect to the parameters α, β and C, with the result

$$\alpha = 0{\cdot}195 \times 10^{26} \text{ cm}^{-2}; \quad \beta = 0{\cdot}307 \times 10^{26} \text{ cm}^{-2}; \quad C = -0{\cdot}19; \quad E_{\alpha(\min)} = -17{\cdot}8 \text{ MeV}. \qquad \ldots\ldots(23)$$

A rough calculation has shown that if the low-energy data are fitted more precisely by using different ranges for the central force in the singlet and triplet states, the binding energy increases by several MeV.

The numerical calculation is greatly simplified if g_0 and g_2 are chosen the same, so we use in the subsequent work the values $\alpha=\beta=0{\cdot}22\times10^{26}\,\mathrm{cm}^{-2}$ and $C=-0{\cdot}2$.

Hochberg, Massey, Robertson and Underhill used $\alpha=0{\cdot}16\times10^{26}\,\mathrm{cm}^{-2}$ and obtained a satisfactory result for both the s-phase shift and the unsplit p-phase shift. The present calculation of the p-phase shift splitting was repeated with this value of α in order to see the effect of the change in the wave function of the alpha particle.

§ 4. DERIVATION OF THE EXPLICIT KERNELS

For the direct terms it is convenient to use the coordinates

$$\left.\begin{array}{ll}\mathbf{r}=\mathbf{r}_1-\frac{1}{4}(\mathbf{r}_2+\mathbf{r}_3+\mathbf{r}_4+\mathbf{r}_5) & \mathbf{v}=\mathbf{r}_2-\mathbf{r}_3\\ \mathbf{u}=\frac{1}{2}(\mathbf{r}_2+\mathbf{r}_3-\mathbf{r}_4-\mathbf{r}_5) & \mathbf{w}=\mathbf{r}_4-\mathbf{r}_5\end{array}\right\}\qquad\ldots\ldots(24)$$

and for the exchange terms the coordinates

$$\left.\begin{array}{ll}\mathbf{r}=\mathbf{r}_1-\frac{1}{4}(\mathbf{r}_2+\mathbf{r}_3+\mathbf{r}_4+\mathbf{r}_5) & \boldsymbol{\rho}=\mathbf{r}_3-\frac{1}{2}(\mathbf{r}_4+\mathbf{r}_5)\\ \mathbf{r}'=\mathbf{r}_2-\frac{1}{4}(\mathbf{r}_1+\mathbf{r}_3+\mathbf{r}_4+\mathbf{r}_5) & \boldsymbol{\rho}'=\mathbf{r}_4-\mathbf{r}_5.\end{array}\right\}\qquad\ldots\ldots(25)$$

Then, with the approximation $g_0=g_2$, $g_0(-1)g_2(-2)\exp(-\nu r_{14}{}^2)$ becomes

$$N_0N_2\exp\left[-\tfrac{3}{2}\alpha(\mathbf{s}^2+\mathbf{s}'^2)-\tfrac{8}{3}\alpha\rho^2-2\alpha\rho'^2-\nu(\mathbf{s}+\tfrac{1}{3}\boldsymbol{\rho}+\tfrac{1}{2}\boldsymbol{\rho}')^2\right]$$

where $$\mathbf{s}=\tfrac{16}{15}\mathbf{r}+\tfrac{4}{15}\mathbf{r}';\quad \mathbf{s}'=\ \mathbf{r}+\tfrac{16}{15}\mathbf{r}'.$$

The $r_{14}{}^2$ term in the denominator of the tensor operator makes the direct evaluation of this term very complicated, so we make use of the relation†

$$\frac{1}{r_{14}{}^2}\exp(-\nu_0r_{14}{}^2)=\int_{\nu_0}^{\infty}\exp(-\nu r_{14}{}^2)\,d\nu\qquad\ldots\ldots(26)$$

and perform the integration over ν later on.

After the integration over $\boldsymbol{\rho}$ and $\boldsymbol{\rho}'$ the above term becomes

$$\begin{aligned}&\frac{3}{2}\left(\frac{16}{15}\right)^3\left(\frac{3}{2}\right)^3\left(\frac{\pi}{2\alpha}\right)^{3/2}N_0N_2\exp\left[-\tfrac{3}{2}\alpha(s^2+s'^2)\right]\int_{\nu_0}^{\infty}\left(\frac{\pi}{6\alpha+\nu}\right)^{3/2}\\ &\quad\times\left[\frac{45}{(6\alpha+\nu)^2}-\frac{30}{6\alpha+\nu}b(1+2a)s^2-\frac{30}{6\alpha+\nu}b(\mathbf{s}\,.\,\mathbf{s}')+12ab^2(1+a)s^4\right.\\ &\quad\left.+12ab^2s^2(\mathbf{s}\,.\,\mathbf{s}')+\frac{45}{2}b\frac{1}{6\alpha+\nu}i\boldsymbol{\sigma}_3\,.\,(\mathbf{s}\times\mathbf{s}')-9ab^2i\boldsymbol{\sigma}_3\,.\,(\mathbf{s}\times\mathbf{s}')\,s^2\right]\\ &\quad\times\exp\left[-(6\alpha+\nu)\,abs^2\right]d\nu\qquad\ldots\ldots(27)\end{aligned}$$

where $a=\nu/(6\alpha+\nu)$; $b=6\alpha/(6\alpha+\nu)$. The corresponding expression for the (2, 4) term may be obtained by the interchanges $\mathbf{s}\rightleftharpoons\mathbf{s}'$ and $\boldsymbol{\sigma}_3\rightleftharpoons-\boldsymbol{\sigma}_3$.

To perform the angular integrations we expand the factor

$$\exp[-c(\mathbf{r}\,.\,\mathbf{r}')]=4\pi\sum_{L=0}^{\infty}\sum_{M=-L}^{L}q_L(crr')\;\mathrm{Y}_L{}^M(\theta,\phi)\,\overline{\mathrm{Y}}_L{}^M(\theta',\phi')\qquad\ldots\ldots(28)$$

where $$q_l(crr')=i^l\mathrm{j}_l(i\,crr')\quad\text{and}\quad c=\frac{3}{4}\left(\frac{16}{15}\right)^2\frac{6\alpha}{6\alpha+\nu}(2\alpha+\nu)$$

where j_l is the spherical Bessel function of order l. Using the orthonormality of the Clebsch–Gordan coefficients we have

$$\int\bar{\chi}(-1)\,\bar{\chi}_{lJ}{}^m(1)\sum_M\mathrm{Y}_L{}^M(\Omega)\,\overline{\mathrm{Y}}_L{}^M(\Omega')\,\chi_{lJ}{}^m(2)\,\chi(-2)\,d\Omega\,d\Omega'=-\tfrac{1}{2}\delta_{lL}$$

---

† We are indebted to Dr. Tamura for suggesting this device.

The terms with $(\mathbf{r}\,.\,\mathbf{r}')$ outside the exponential can be derived from those without it by differentiation with respect to c. The method of integrating the terms in $i\boldsymbol{\sigma}_3\,.\,(\mathbf{r}\times\mathbf{r}')$ is outlined in Appendix IV. The result is

$$\int \chi(-1)\bar{\chi}_{lJ}{}^{m'}(1)\, i\boldsymbol{\sigma}_3\,.\,(\mathbf{r}\times\mathbf{r}')\sum_{M} \mathrm{Y}_L{}^M(\Omega)\,\bar{\mathrm{Y}}_L{}^M(\Omega')\chi_{lJ}{}^{m'}(2)\chi(-2)\; d\Omega\, d\Omega' = -\tfrac{1}{2}rr'C_{lJL}$$

$$(L=l\pm 1) \qquad \ldots\ldots(29)$$

where

$$C_{l,\,l+1/2,\,l\mp 1} = \pm\frac{l}{2l+1},\quad C_{l,\,l-1/2,\,l\mp 1} = \mp\frac{l+1}{2l+1},\ \text{for } l\neq 0. \qquad \ldots\ldots(30)$$

This calculation can also be done using Racah's technique (cf. Biedenharn, Blatt, and Rose 1952) with the result

$$C_{lJL} = 6(-)^{J+1/2-l}(2l+1)(l100|\,l1L0)^2\, W(11\,ll;1L)\, W(\tfrac{1}{2}\tfrac{1}{2}\,ll;1J)$$

This reduces to (30) on substitution of the explicit formulæ for the Clebsch–Gordan and Racah coefficients.

The integration of the (3, 4) term can be performed analytically, with the result

$$-\frac{3}{2}\left(\frac{16}{15}\right)^3\left(\frac{3}{2}\right)^3\left(\frac{\pi}{6\alpha}\right)^{3/2} N_0N_2\exp\left[-\tfrac{3}{2}\alpha(s^2+s'^2)\right]\left(\frac{\pi}{2\alpha+\nu}\right)^{3/2}\frac{6}{2\alpha+\nu}\,.$$

$$\ldots\ldots(31)$$

The splitting terms vanish because $\mathbf{r}_{13}+\mathbf{r}_{23}$ is the only variable involving $\mathbf{s}$ and $\mathbf{s}'$, and $\mathbf{r}\times\mathbf{r}'$ cannot be formed from this alone. This is not the case for the S state of the form (19′), but the effect of this is negligible.

Using the relations

$$\left.\begin{aligned} &\frac{\partial}{\partial c}q_l(crr') = -\frac{1}{c}\{(l+1)\,q_l(crr') + crr'\,q_{l-1}(crr')\} \\ &\text{and} \\ &\frac{\partial^2}{\partial c^2}q_l(crr') = \frac{1}{c^2}[\{(l+1)(l+2)+(crr')^2\}\,q_l(crr') + 2crr'\,q_{l-1}(crr')] \end{aligned}\right\} \qquad \ldots\ldots(32)$$

and defining the function

$$\mathscr{I}_{l+1/2}(x) = xq_l(x) = i^l\left(\frac{\pi x}{2i}\right)^{1/2}\mathrm{J}_{l+1/2}(ix) \qquad \ldots\ldots(33)$$

the complete expression for the tensor SD exchange integral becomes

$$\left[2\int \bar{\psi}(-1)\bar{\chi}_{lJ}{}^{m'}(1)\sum_{i>j} S_{ij}\,U_{ij}{}^{\mathrm{t}}\,\psi(-2)\,\chi_{lJ}{}^{m'}(2)\{f_{lJ}(r')/r'\}\,d\tau_{-1}\,rd\Omega\right]_{\mathrm{S-D}}$$

$$=\Big[4\int \bar{\psi}(-1)\,\bar{\chi}_{lJ}{}^{m}(1)\,(S_{34}\,U_{34}{}^{\mathrm{t}} + S_{14}\,U_{14}{}^{\mathrm{t}} + S_{24}\,U_{24}{}^{\mathrm{t}})$$

$$\times\,\psi(-2)\,\chi_{lJ}{}^{m'}(2)\,\{f_{lJ}(r')/r'\}d\tau_{-1}\,rd\Omega\Big]_{\mathrm{S-D}}$$

$$=\int\{k_{\mathrm{cm}}{}^{l}(r,r') + k_{\mathrm{cm}}{}'^{l}(r,r') + k_{\mathrm{cm}}{}'^{l}(r'\,r) + k_{\mathrm{sp}}{}^{lJ}(r,r') + k_{\mathrm{sp}}{}^{lJ}(r',r)\}f_{lJ}(r')\,dr' \quad (34)$$

where

$$k_{\mathrm{cm}}{}^{l}(r,r') = \frac{64}{15}\left(\frac{18}{5\pi}\right)^{1/2}\frac{C}{1+C^2}\,U_{\mathrm{t}}{}^{0}\,(6\alpha)^{1/2}\,2\left(\frac{2\alpha}{2\alpha+\nu}\right)^{5/2}$$

$$\times\exp\left[-\frac{136}{75}\,\alpha\,(r^2+r'^2)\right]\mathscr{I}_{l+1/2}(crr'); \qquad c=\frac{128}{75}\,\alpha. \qquad \ldots\ldots(35)$$

$k_{\mathrm{cm}}{}'^{l}(r,r')$

$$
\begin{aligned}
&= -\frac{64}{15}\left(\frac{18}{5\pi}\right)^{1/2}\frac{c}{1+c^2}\,U_{\mathrm{t}}^{0}\,\frac{1}{(6\alpha)^{1/2}}\int_{\nu_0}^{\infty}\left(\frac{6\alpha}{6\alpha+\nu}\right)^{1/2}\left(\frac{2\alpha}{2\alpha+\nu}\right)\exp\left[-\gamma_1 r^2-\gamma_2 r'^2\right]\\
&\quad\times\left[\left\{S_l-\left(\frac{16}{15}\right)^2(6\alpha)\left(T_l r^2+T_l' r'^2\right)+\left(\frac{16}{15}\right)^4(6\alpha)^2\left(Ur^4+2U'r^2r'^2+U''r'^4\right)\right\}\right.\\
&\quad\times\mathscr{I}_{l+1/2}(\gamma_3 rr')+\left(\frac{16}{15}\right)^2(6\alpha)rr'\left\{-V+\left(\frac{16}{15}\right)^2(6\alpha)\left(Wr^2+W'r'^2\right)\right\}\\
&\quad\left.\times\mathscr{I}_{l+3/2}(\gamma_3 rr')\right]d\nu \qquad \dots\dots(36)
\end{aligned}
$$

in which

$$
\gamma_1=\frac{68}{225}(6\alpha)+\left(\frac{16}{15}\right)^2\frac{6\alpha\nu}{6\alpha+\nu}\qquad \gamma_2=\frac{68}{225}(6\alpha)+\frac{1}{16}\left(\frac{16}{15}\right)^2\frac{6\alpha\nu}{6\alpha+\nu}
$$

$$
\gamma_3=\frac{64}{225}(6\alpha)+\frac{1}{2}\left(\frac{16}{15}\right)^2\frac{6\alpha\nu}{6\alpha+\nu} \qquad \dots\dots(37)
$$

$$
\left.
\begin{aligned}
S_l&=5\left(\frac{6\alpha}{6\alpha+\nu}\right)^2+25l\frac{6\alpha}{6\alpha+\nu}\frac{2\alpha}{2\alpha+\nu}\frac{5\alpha+(41/30)\nu}{6\alpha+\nu}\\
&\quad+20l(l-1)\frac{\nu}{6\alpha+\nu}\left(\frac{2\alpha}{2\alpha+\nu}\right)^2\frac{5\alpha+(11/10)\nu}{6\alpha+\nu}\\
T_l&=5\left(\frac{6\alpha}{6\alpha+\nu}\right)^2\frac{5\alpha+(13/6)\nu}{6\alpha+\nu}\\
&\quad+14l\frac{\nu}{6\alpha+\nu}\frac{6\alpha}{6\alpha+\nu}\frac{2\alpha}{2\alpha+\nu}\frac{5\alpha+(17/14)\nu}{6\alpha+\nu}\\
T_l'&=\frac{5}{4}\left(\frac{6\alpha}{6\alpha+\nu}\right)^2\frac{5\alpha+(7/6)\nu}{6\alpha+\nu}\\
&\quad+\frac{13}{8}l\frac{\nu}{6\alpha+\nu}\frac{6\alpha}{6\alpha+\nu}\frac{2\alpha}{2\alpha+\nu}\frac{5\alpha+(27/26)\nu}{6\alpha+\nu}\\
U&=2\left(\frac{\nu}{6\alpha+\nu}\right)\left(\frac{6\alpha}{6\alpha+\nu}\right)^2\frac{5\alpha+(3/2)\nu}{6\alpha+\nu}\\
U'&=\frac{15}{16}\left(\frac{\nu}{6\alpha+\nu}\right)\left(\frac{6\alpha}{6\alpha+\nu}\right)^2\frac{5\alpha+(11/10)\nu}{6\alpha+\nu}\\
U''&=\frac{1}{32}\left(\frac{\nu}{6\alpha+\nu}\right)\left(\frac{6\alpha}{6\alpha+\nu}\right)^2\frac{5\alpha+\nu}{6\alpha+\nu}\\
V&=\frac{25}{4}\left(\frac{6\alpha}{6\alpha+\nu}\right)^2\frac{5\alpha+(41/30)\nu}{6\alpha+\nu}\\
&\quad-10\frac{\nu}{6\alpha+\nu}\frac{6\alpha}{6\alpha+\nu}\frac{2\alpha}{2\alpha+\nu}\frac{5\alpha+(11/10)\nu}{6\alpha+\nu}\\
W&=\frac{7}{2}\left(\frac{\nu}{6\alpha+\nu}\right)\left(\frac{6\alpha}{6\alpha+\nu}\right)^2\frac{5\alpha+(17/14)\nu}{6\alpha+\nu}\\
W'&=\frac{13}{32}\left(\frac{\nu}{6\alpha+\nu}\right)\left(\frac{6\alpha}{6\alpha+\nu}\right)^2\frac{5\alpha+(27/26)\nu}{6\alpha+\nu}
\end{aligned}
\right\}\qquad \dots\dots(38)
$$

and $k_{\mathrm{sp}}{}^{lJ}(r,r')$

$$
\begin{aligned}
&= -\frac{64}{15}\left(\frac{18}{5\pi}\right)^{1/2}\frac{C}{1+C^2}\,U_{\mathrm{t}}^{0}\,\frac{1}{(6\alpha)^{1/2}}\int_{\nu_0}^{\infty}\left(\frac{6\alpha}{6\alpha+\nu}\right)^{3/2}\left(\frac{2\alpha}{2\alpha+\nu}\right)\exp\left[-\gamma_1 r^2-\gamma_2 r'^2\right]\\
&\quad\times\sum_{L=l\pm1}C_{lJL}\left[\left\{X_L-\left(\frac{16}{15}\right)^2(6\alpha)\left(Yr^2+Y'r'^2\right)\right\}\mathscr{I}_{l+1/2}(\gamma_3 rr')\right.\\
&\quad\left.-\left(\frac{16}{15}\right)^2(6\alpha)rr'\,Z\mathscr{I}_{L+3/2}(\gamma_3 rr')\right](6\alpha)\,rr'\,d\nu \qquad \dots\dots(39)
\end{aligned}
$$

in which

$$\left.\begin{aligned} X_L &= \frac{8}{3}\left(\frac{6\alpha}{6\alpha+\nu}\right)+L\frac{32}{15}\left(\frac{\nu}{6\alpha+\nu}\right)\left(\frac{2\alpha}{2\alpha+\nu}\right)\equiv\bar{X}+L\bar{X}',\\ Y &= \frac{16}{15}\left(\frac{\nu}{6\alpha+\nu}\right)\left(\frac{6\alpha}{6\alpha+\nu}\right),\quad Y'=\frac{1}{15}\left(\frac{\nu}{6\alpha+\nu}\right)\left(\frac{6\alpha}{6\alpha+\nu}\right),\\ Z &= \frac{8}{15}\left(\frac{\nu}{6\alpha+\nu}\right)\left(\frac{6\alpha}{6\alpha+\nu}\right).\end{aligned}\right\}\qquad\ldots\ldots(40)$$

In the case $l=1$, $k_{\mathrm{sp}}{}^{lJ}$ may be more simply expressed by using the relations

$$\left.\begin{aligned} C_{lJ0} &= \tfrac{1}{2}(-1)^{J+1/2}-\tfrac{1}{6}=-C_{1J2}\\ \mathscr{I}_{l-1/2}(x)-\mathscr{I}_{l+3/2}(x) &= -\frac{2l+1}{x}\mathscr{I}_{l+1/2}(x)\\ \gamma_3\bar{X}' &= \left(\frac{16}{15}\right)^2(6\alpha)Z\end{aligned}\right\}\qquad\ldots\ldots(41)$$

Hence

$$\begin{aligned} k_{\mathrm{sp}}{}^{1J}(r,r') = {} & \left[\frac{3}{2}(-1)^{J+1/2}-\tfrac{1}{2}\right]15\left(\frac{18}{5\pi}\right)^{1/2}\frac{C}{1+C^2}U_{\mathrm{t}}{}^{0}\frac{1}{(6\alpha)^{1/2}}\int_{r_0}^{\infty}\left(\frac{6\alpha}{6\alpha+\nu}\right)^{1/2}\left(\frac{2\alpha}{2\alpha+\nu}\right)^2\\ & \times\exp[-\gamma_1 r^2-\gamma_2 r'^2]\left[\left\{\bar{X}-\left(\frac{16}{15}\right)^2(6\alpha)(Yr^2+Y'r'^2)\right\}\mathscr{I}_{3/2}(\gamma_3 rr')\right.\\ & \left.-\bar{X}'\gamma_3 rr'\mathscr{I}_{5/2}(\gamma_3 rr')\right]d\nu.\end{aligned}\qquad\ldots\ldots(42)$$

§ 5. NUMERICAL RESULTS FOR THE SPLITTING OF THE P-PHASE

Some of the potential terms of the Schrödinger equation derived from (13)

$$\frac{d^2f_{lJ}(r)}{dr^2}+\left\{k^2-\frac{l(l+1)}{r^2}-W(r)-U_{l,J}(r)\right\}f_{lJ}(r)=\int_0^{\infty}\{k_l(r,r')+n_{l,J}(r,r')\}f_{lJ}(r')\,dr'\qquad\ldots\ldots(43)$$

produce a splitting of the phase shifts and others do not. The non-splitting potential determines, approximately, the weighted mean of the two phase shifts $\delta_{l,\,l+1/2}$ and $\delta_{l,\,l-1/2}$. This weighted mean is very sensitive to the exchange character of the central force. The coefficient of the central force term $W(r)$ can be written

$$(4w+2b-m-2h)\ V_0=\tfrac{3}{4}V_0(^3\mathrm{S})+\tfrac{3}{4}V_0(^1\mathrm{S})+\tfrac{9}{4}V_0(^3\mathrm{P})+\tfrac{1}{4}V_0(^1\mathrm{P})\qquad\ldots\ldots(44)$$

where $V_0(^3\mathrm{S})$ is the strength of the central potential in the S state of the two-body system, and similarly for the other symbols. It is known that the central force in the ^{3}P state cannot be very strong, but it is difficult to obtain definite information about it in the presence of the spin–orbit force. Although some preliminary analyses of two-nucleon scattering processes have been made (Garren 1953, Klein 1956) which indicate a fairly strong spin–orbit force, they are not related to the potential and so the contribution of the central force is unknown. It can be seen from (44) that the strength of the non-splitting central potential in neutron–helium scattering depends most strongly on the strength of the ^{3}P central potential in the two-nucleon interaction.

On the other hand, the magnitude of the splitting potential does not depend on the exchange character of the forces. To see the effect of the tensor force on the doublet splitting for the state of lowest orbital angular momentum, $l=1$, we used the near-Serber potential of Hochberg, Massey, Robertson and Underhill and superposed the splitting term given by (39). The near-Serber potential determines the weighted mean of $\delta_{l,l+\frac{1}{2}}$ and $\delta_{l,l-\frac{1}{2}}$, and was chosen to be in good accord with the experimentally determined phase shifts.

To see the effect of tensor forces alone neglect the vector spin–orbit force. Then $U_{lJ}(r)$ in (43) is zero and $n_{lJ}(r,r)$ is given by (39) and (40) or, for the P state, by (42) and (40). The integrand was evaluated at six values of ν, and the integration performed numerically, a small correction being made for the tail of the integrand outside the computed range. Using this kernel the resulting integro-differential equation was also solved numerically. The results are shown in figure 1, together with the 'experimental' phase shifts of Seagrave. They are qualitatively in agreement with each other, but the magnitude of the splitting is about one-third of the experimental value. It decreases by about 10% at 2·4 MEV for values of α corresponding to radii of the alpha particle larger by about 20% (see Appendix II). If the radius is increased the range of the resultant potential also increases, but its strength is reduced. These two effects partly cancel, so the magnitude of the splitting is not very sensitive to changes of α.

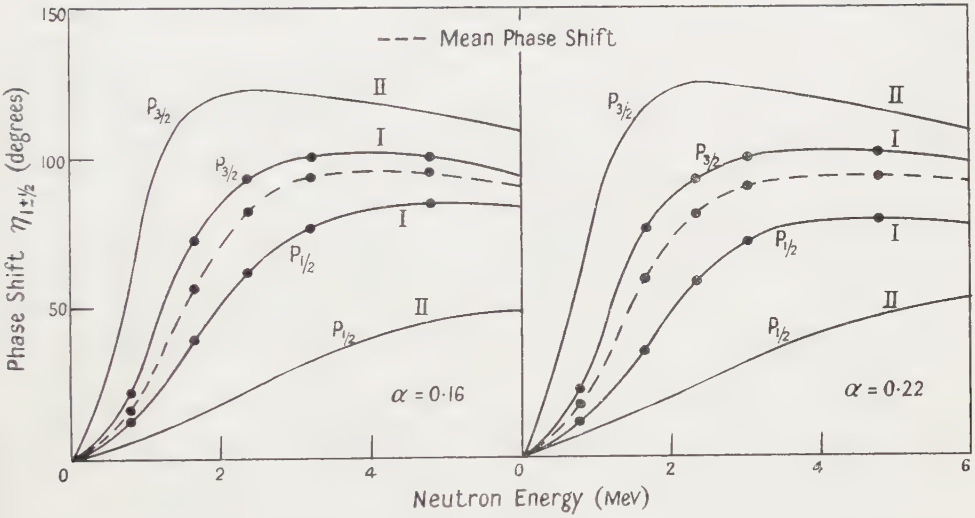

Figure 1. Curves I, Calculated $P_{1/2}$ and $P_{3/2}$ phase shifts for neutron-alpha-particle scattering with tensor forces. Curves II, Experimental results of Seagrave.

A subsidiary calculation was performed to determine the dependence of the splitting on ν_0, and it was found that, at an energy of 2·4 MEV, an increase of ν_0 by about 20% decreases the splitting by about 25%. This result is in marked contrast to the ordinary perturbation calculation in which the splitting depends on a high power of the ratio α/ν.

The results of the calculation of the S phases is shown in figure 2. The agreement with experiment is not too unsatisfactory in view of the relative insensitivity of the angular distribution to the S phase shifts.

All the numerical work was done on the ACE pilot model electronic computer, using programmes made by Robertson (1956).

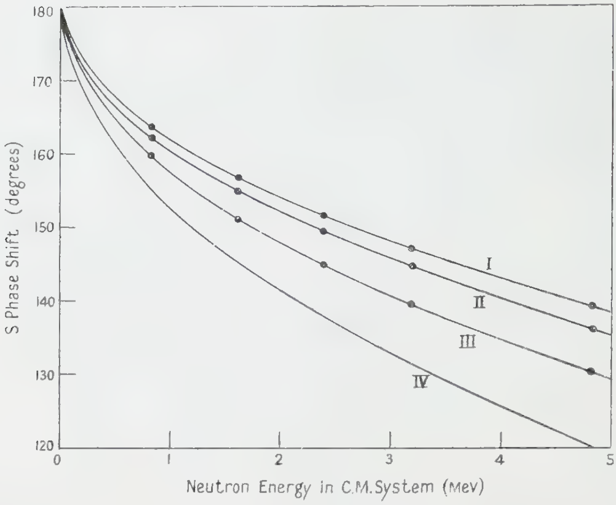

Figure 2. Calculated S-phase shifts for neutron-alpha particle scattering with tensor forces compared with experimental results of Seagrave.
I, SS terms only; II, SS+SD terms; III, Hochberg *et al.* (1955); IV, Seagrave (1953).

§ 6. Discussion

This work shows that the tensor force gives the correct sign for the splitting of the p phases in n–α scattering through the D state of the α-particle. The estimated magnitude of the splitting is only about one-third of the experimental value, but the real value may well be larger. This splitting will seriously compete with that due to the spin–orbit force, and cannot be neglected.

Only the principal S state and principal D state have been taken into account here. Some of the remaining D states may well be as important as the principal D state, as was found by Abraham, Cohen and Roberts for the binding energy of the alpha particle. It would be a laborious task to take these states into account.

There are several possible ways of increasing the magnitude of the splitting. If the strength of the tensor force is increased, the D state probability of the alpha particle will also increase, and the splitting will be roughly proportional to the square of the strength of the tensor force. But this cannot be done without destroying the consistency with the two-body data, in particular it would make the binding energy of the alpha particle too small. However, the variational wave function used is poor particularly for the SD term because the 'radial' wave function depends only on

$$\rho^2 = \sum_{i>j=2}^{5} r_{ij}^2 = 4 \sum_{i=2}^{5} r_i^2$$

where r_i is the coordinate of the ith nucleon relative to the centre of mass of the alpha particle. If the dependence on the individual r_{ij}'s were taken into account, the contribution to the binding energy from the tensor force through the SD term would increase considerably. Such an improved 'radial' wave function would allow a stronger tensor force and larger D-state probability and hence larger splitting. A tensor force with a sharp dip near $r=0$ would also make the splitting larger, since such a change would have little effect on a loose system like the deuteron but would make the SD cross term large for a tight system like the alpha particle.

Among the DD exchange terms that were neglected those related to the kinetic energy are more important than those related to the potential energy. The former terms would tend to reduce the splitting, but only by an amount of the order of one-third of the contribution of the SD terms. The remainder of the splitting is due to a velocity-dependent vector spin–orbit force of the type (1). The combination of the tensor and the vector spin–orbit forces is of interest in connection with the energy levels of light nuclei, especially the very small splitting of the lowest two levels of ^{7}Li.

APPENDIX I

It will be shown that the direct SD and DD Wigner tensor terms vanish. There are four independent D-state spin operators. Writing

$$|\mathbf{a},\mathbf{b}\rangle=\{3(\boldsymbol{\sigma}_2.\mathbf{a})(\boldsymbol{\sigma}_4.\mathbf{b})+3(\boldsymbol{\sigma}_2.\mathbf{b})(\boldsymbol{\sigma}_4.\mathbf{a})-2(\mathbf{a}.\mathbf{b})(\boldsymbol{\sigma}_2.\boldsymbol{\sigma}_4)\}$$

these are

$$|\mathbf{v},\mathbf{w}\rangle,\qquad (\mathbf{v}.\mathbf{w})|\mathbf{u},\mathbf{u}\rangle,$$
$$(\mathbf{v}.\mathbf{u})|\mathbf{w},\mathbf{u}\rangle+(\mathbf{w}.\mathbf{u})|\mathbf{v},\mathbf{u}\rangle,\qquad (\mathbf{v}.\mathbf{w})|\mathbf{v},\mathbf{v}\rangle+(\mathbf{w}.\mathbf{v})|\mathbf{w},\mathbf{w}\rangle;$$

all these operate on $\chi(-1)$. These are the only spin operators invariant under rotation and reflection and antisymmetric with respect to the pairs (2, 3) and (4, 5) that can be constructed from $\mathbf{u}$, $\mathbf{v}$, $\mathbf{w}$, $\boldsymbol{\sigma}_2$ and $\boldsymbol{\sigma}_4$. All the direct SD tensor terms between the principal S state and the above D states vanish because they essentially contain $\boldsymbol{\sigma}_2$ and $\boldsymbol{\sigma}_4$ only once each.

For the other S state

$$(\mathbf{v}.\mathbf{w})(\boldsymbol{\sigma}_2.\boldsymbol{\sigma}_4)g_0'\left(\sum_2^5 r_{1j}^2\right)\chi(-1)$$

it is necessary to calculate

$$\bar{\chi}(\boldsymbol{\sigma}_2.\boldsymbol{\sigma}_4)S_{1j}|\mathbf{a},\mathbf{b}\rangle\chi\qquad(j=2,3,4,5).$$

For $j=2$, $\bar{\chi}(\boldsymbol{\sigma}_2.\boldsymbol{\sigma}_4)\{3(\boldsymbol{\sigma}_1.\mathbf{r})(\boldsymbol{\sigma}_2.\mathbf{r})-r^2(\boldsymbol{\sigma}_1.\boldsymbol{\sigma}_2)\}(1/r^2)|\mathbf{a},\mathbf{b}\rangle\chi$

$$=\bar{\chi}\{3(\boldsymbol{\sigma}_1.\mathbf{r})i\boldsymbol{\sigma}_2.(\boldsymbol{\sigma}_4\times\mathbf{r})-r^2i\boldsymbol{\sigma}_2.(\boldsymbol{\sigma}_4\times\boldsymbol{\sigma}_1)\}(1/r^2)$$
$$\times\{3(\boldsymbol{\sigma}_2.\mathbf{a})(\boldsymbol{\sigma}_4.\mathbf{b})+3(\boldsymbol{\sigma}_2.\mathbf{b})(\boldsymbol{\sigma}_4.\mathbf{a})-2(\mathbf{a}.\mathbf{b})(\boldsymbol{\sigma}_2.\boldsymbol{\sigma}_4)\}\chi.$$

Now

$$\bar{\chi}\boldsymbol{\sigma}_2.(\boldsymbol{\sigma}_4\times\mathbf{r})\{3(\boldsymbol{\sigma}_2.\mathbf{a})(\boldsymbol{\sigma}_4.\mathbf{b})+3(\boldsymbol{\sigma}_2.\mathbf{b})(\boldsymbol{\sigma}_4.\mathbf{a})+2(\mathbf{a}.\mathbf{b})(\boldsymbol{\sigma}_2.\boldsymbol{\sigma}_4)\}\chi$$
$$=\bar{\chi}\{3\mathbf{a}.(\boldsymbol{\sigma}_4\times\mathbf{r})(\boldsymbol{\sigma}_4.\mathbf{b})+3\mathbf{b}.(\boldsymbol{\sigma}_4\times\mathbf{r})(\boldsymbol{\sigma}_4.\mathbf{a})+2(\mathbf{a}.\mathbf{b})\boldsymbol{\sigma}_4.(\boldsymbol{\sigma}_4\times\mathbf{r})\}\chi$$
$$=\bar{\chi}\{3\mathbf{r}.(\mathbf{a}\times\mathbf{b})+3\mathbf{r}.(\mathbf{b}\times\mathbf{a})-2(\mathbf{a}.\mathbf{b})\mathbf{r}.(\boldsymbol{\sigma}_4\times\boldsymbol{\sigma}_5)\}\chi=0$$

since $\bar{\chi}(\boldsymbol{\sigma}_4\times\boldsymbol{\sigma}_5)\chi=-\bar{\chi}(\boldsymbol{\sigma}_4\times\boldsymbol{\sigma}_4)\chi=0.$

All the other terms vanish in the same way.

As an example of the calculation for the direct DD tensor terms, consider the pair (1, 2):

$$\bar{\chi}\{3(\boldsymbol{\sigma}_2.\mathbf{a})(\boldsymbol{\sigma}_4.\mathbf{b})+3(\boldsymbol{\sigma}_2.\mathbf{b})(\boldsymbol{\sigma}_4.\mathbf{a})-2(\mathbf{a}.\mathbf{b})(\boldsymbol{\sigma}_2.\boldsymbol{\sigma}_4)\}r^2S_{12}$$
$$\times\{3(\boldsymbol{\sigma}_2.\mathbf{a})(\boldsymbol{\sigma}_4.\mathbf{b})+3(\boldsymbol{\sigma}_2.\mathbf{b})(\boldsymbol{\sigma}_4.\mathbf{a})-2(\mathbf{a}.\mathbf{b})(\boldsymbol{\sigma}_2.\boldsymbol{\sigma}_4)\}\chi$$
$$=\bar{\chi}\{9(\boldsymbol{\sigma}_2.\mathbf{a})r_{45}^2S_{12}(\boldsymbol{\sigma}_2.\mathbf{a})+9(\boldsymbol{\sigma}_2.\mathbf{b})r_{23}^2S_{12}(\boldsymbol{\sigma}_2.\mathbf{b})-3(\mathbf{a}.\mathbf{b})(\boldsymbol{\sigma}_2.\mathbf{a})S_{12}(\boldsymbol{\sigma}_2.\mathbf{b})$$
$$-3(\mathbf{a}.\mathbf{b})(\boldsymbol{\sigma}_2.\mathbf{b})S_{12}(\boldsymbol{\sigma}_2.\mathbf{a})+4(\mathbf{a}.\mathbf{b})^2(\boldsymbol{\sigma}_2.\boldsymbol{\sigma}_4)S_{12}(\boldsymbol{\sigma}_2.\boldsymbol{\sigma}_4)\}\chi.$$

Now

$$\bar{\chi}(\boldsymbol{\sigma}_2.\mathbf{a})(\boldsymbol{\sigma}_1.\mathbf{r})(\boldsymbol{\sigma}_2.\mathbf{r})(\boldsymbol{\sigma}_2.\mathbf{a})\chi=\bar{\chi}(\boldsymbol{\sigma}_1.\mathbf{r})(\boldsymbol{\sigma}_2.\mathbf{a})(\boldsymbol{\sigma}_2.\mathbf{r})(\boldsymbol{\sigma}_2.\mathbf{a})\chi$$
$$=(\boldsymbol{\sigma}_1.\mathbf{r})\bar{\chi}i\boldsymbol{\sigma}_2.(\mathbf{a}\times\mathbf{r})(\boldsymbol{\sigma}_2.\mathbf{a})\chi$$
$$\bar{\chi}(\boldsymbol{\sigma}_2.\mathbf{a})(\boldsymbol{\sigma}_1.\mathbf{r})(\boldsymbol{\sigma}_2.\mathbf{r})(\boldsymbol{\sigma}_2.\mathbf{b})\chi=(\boldsymbol{\sigma}_1.\mathbf{r})\bar{\chi}i\mathbf{b}.(\mathbf{a}\times\mathbf{r})$$
$$\bar{\chi}(\boldsymbol{\sigma}_2.\mathbf{b})(\boldsymbol{\sigma}_1.\mathbf{r})(\boldsymbol{\sigma}_2.\mathbf{r})(\boldsymbol{\sigma}_2.\mathbf{b})\bar{\chi}=(\boldsymbol{\sigma}_1.\mathbf{r})\bar{\chi}i\mathbf{a}.(\mathbf{b}\times\mathbf{r}).$$

These two terms add to zero and

$$\bar{\chi}(\boldsymbol{\sigma}_2 . \boldsymbol{\sigma}_4)(\boldsymbol{\sigma}_1 . \mathbf{r})(\boldsymbol{\sigma}_2 . \mathbf{r})(\boldsymbol{\sigma}_2 . \boldsymbol{\sigma}_4)\chi = -(\boldsymbol{\sigma}_1 . \mathbf{r})\bar{\chi}(\boldsymbol{\sigma}_2 . \boldsymbol{\sigma}_4)(\boldsymbol{\sigma}_2 . \mathbf{r})(\boldsymbol{\sigma}_2 . \boldsymbol{\sigma}_5)\chi$$
$$= -(\boldsymbol{\sigma}_1 . \mathbf{r})\bar{\chi} i\boldsymbol{\sigma}_5 . (\boldsymbol{\sigma}_4 \times \mathbf{r})\chi = 0.$$

All the other terms vanish in the same way.

APPENDIX II

The Binding Energy of the Alpha Particle

If the expression (22) for the binding energy of the alpha particle is written in the form

$$(1+C^2)W = P + CQ + C^2R$$

and use made of $\partial W/\partial C = 0$, then the D-state probability C and the binding energy W can be calculated for any assumed pair of values of α and β using the equations $C^2 + 2C(P-R)/Q - Q = 0$, $W = P + \frac{1}{2}CQ$. Some of the values found are shown in the table. Neither C nor W is very sensitive to α and β. The values corresponding to the minimum of the binding energy were found by parabolic interpolation with respect to α and β separately.

α (10^{26} cm^{-2})	0·20	0·20	0·20	0·18	0·22	0·20	0·195
β (10^{26} cm^{-2})	0·28	0·30	0·32	0·30	0·30	0·307	0·30
$-C$	0·197	0·191	0·186	0·189	0·199	0·189	0·189
$-W$ (MEV)	17·76	17·81	17·80	17·65	17·37	17·81	17·81

The contributions to the binding energy from the SS, SD and DD terms are, for $\alpha = 0{\cdot}20$, $\beta = 0{\cdot}30$, SS: $-12{\cdot}29$ MEV, SD: $-11{\cdot}03$ MEV, DD: $+5{\cdot}51$ MEV.

APPENDIX III

The Radius of the Alpha Particle

It is of interest to calculate the radii of the alpha particle corresponding to the wave functions used here and compare them with the radii obtained by other methods. The radius is defined by

$$R^2 = \sum_i \langle \psi(\mathbf{r}_i - \mathbf{R}_{\mathrm{cm}})^2 \psi \rangle = 4 \langle \psi(\mathbf{r}_2 - \mathbf{R}_{\mathrm{cm}})^2 \psi \rangle$$
$$= \frac{4}{1+C^2} \{ \langle \psi_{\mathrm{S}}(\mathbf{r}_2 - \mathbf{R}_{\mathrm{cm}})^2 \psi_{\mathrm{S}} \rangle + C^2 \langle \psi_{\mathrm{D}}(\mathbf{r}_2 - \mathbf{R}_{\mathrm{cm}})^2 \psi_{\mathrm{D}} \rangle \}.$$

Since $C^2 \simeq 0{\cdot}04$, the second term is negligible. Expressing $\mathbf{r}_2 - \mathbf{R}_{\mathrm{cm}}$ in terms of $\mathbf{u}$, $\mathbf{v}$, the integration gives $R = 3/2(2\alpha)^{1/2}$.

The radii corresponding to $\alpha = 0{\cdot}22$ and $\alpha = 0{\cdot}16$ (the values used here and by Hochberg, Massey, Robertson and Underhill) are $R = 2{\cdot}26 \times 10^{-13}$ cm and $R = 2{\cdot}65 \times 10^{-13}$ cm respectively. The values derived from the empirical formulae are $R = 1{\cdot}2A^{1/3} = 1{\cdot}90 \times 10^{-13}$ cm and $R = 1{\cdot}4A^{1/3} = 2{\cdot}22 \times 10^{-13}$ cm, the first being the formula derived from electron scattering and the second from high-energy neutron scattering. Although it may be that the alpha particle is outside the region of applicability of these formulae, it does seem that the value chosen by Hochberg, Massey, Robertson and Underhill is a little too large.

APPENDIX IV

Evaluation of C_{lJL}

By definition,

$$C_{lJL} = -\frac{2}{rr'} \sum \iint \chi(-1)\bar{\chi}_{lJ}^{\,m}(1) i\boldsymbol{\sigma}_3 . (\mathbf{r} \times \mathbf{r}') \{ \sum_M \mathrm{Y}_L^M(\theta, \phi) \bar{\mathrm{Y}}_L^M(\theta', \phi') \}$$
$$\times\ \chi(-2)\chi_{lJ}^{\,m'}(2)\, d\Omega\, d\Omega'.$$

Using

$$\chi_{lJ}{}^{m}(1)=c_1\alpha_1 \mathrm{Y}_l{}^{m-1/2}(\theta,\phi)+c_2\beta_1 \mathrm{Y}_l{}^{m+1/2}(\theta,\phi)$$

where

$$c_1=(l\tfrac{1}{2}m-\tfrac{1}{2}\tfrac{1}{2}|l\tfrac{1}{2}Jm), \qquad c_2=(l\tfrac{1}{2}m+\tfrac{1}{2}\tfrac{1}{2}|l\tfrac{1}{2}Jm)$$

and summing over the spins 2, 4 and 5, this becomes

$$\begin{aligned}C_{lJL}=\frac{1}{rr'}\sum\iint &[\alpha_3\{i\boldsymbol{\sigma}_3\,.\,(\mathbf{r}\times\mathbf{r}')\}\alpha_3\overline{\mathrm{Y}}_l{}^{m+1/2}(\theta,\phi)\mathrm{Y}_l{}^{m'+1/2}(\theta',\phi')c_2{}^2\\ &+\beta_3\{i\boldsymbol{\sigma}_3\,.\,(\mathbf{r}\times\mathbf{r}')\}\beta_3\overline{\mathrm{Y}}_l{}^{m-1/2}(\theta,\phi)\mathrm{Y}_l{}^{m'-1/2}(\theta',\phi')c_1{}^2\\ &-\beta_3\{i\boldsymbol{\sigma}_3\,.\,(\mathbf{r}\times\mathbf{r}')\alpha_3\overline{\mathrm{Y}}_l{}^{m+1/2}(\theta,\phi)\mathrm{Y}_l{}^{m'-1/2}(\theta',\phi')c_1c_2\\ &-\alpha_3\{i\boldsymbol{\sigma}_3\,.\,(\mathbf{r}\times\mathbf{r}')\}\beta_3\overline{\mathrm{Y}}_l{}^{m-1/2}(\theta,\phi)\mathrm{Y}_l{}^{m'+1/2}(\theta',\phi')c_1c_2]\\ &\times[\sum_M \mathrm{Y}_L{}^M(\theta,\phi)\overline{\mathrm{Y}}_L{}^M(\theta'\phi')]\,d\Omega\,d\Omega'.\end{aligned}$$

Then since

$$\begin{aligned}i\frac{(\mathbf{r}\times\mathbf{r}')_x}{rr'}-\frac{(\mathbf{r}\times\mathbf{r}')_y}{rr'}&=-\frac{4\pi}{3}\sqrt{2}\{\mathrm{Y}_1{}^1(\theta,\phi)\overline{\mathrm{Y}}_1{}^0(\theta',\phi')+\mathrm{Y}_1{}^0(\theta,\phi)\overline{\mathrm{Y}}_1{}^{-1}(\theta'\phi')\}\\ i\frac{(\mathbf{r}\times\mathbf{r}')_x}{rr'}+\frac{(\mathbf{r}\times\mathbf{r}')_y}{rr'}&=-\frac{4\pi}{3}\sqrt{2}\{\mathrm{Y}_1{}^{-1}(\theta,\phi)\overline{\mathrm{Y}}_1{}^0(\theta',\phi')+\mathrm{Y}_1{}^0(\theta,\phi)\overline{\mathrm{Y}}_1{}^{1}(\theta',\phi')\}\\ i\frac{(\mathbf{r}\times\mathbf{r}')_z}{rr'}&=-\frac{4\pi}{3}\{\mathrm{Y}_1{}^1(\theta,\phi)\overline{\mathrm{Y}}_1{}^1(\theta',\phi')-\mathrm{Y}_1{}^{-1}(\theta,\phi)\overline{\mathrm{Y}}_1{}^{-1}(\theta',\phi')\}\end{aligned}$$

this becomes

$$\begin{aligned}C_{lJL}=\frac{4\pi}{3}\iint &[-\{\mathrm{Y}_1{}^1(\theta,\phi)\overline{\mathrm{Y}}_1{}^1(\theta',\phi')-\mathrm{Y}_1{}^{-1}(\theta,\phi)\overline{\mathrm{Y}}_1{}^{-1}(\theta',\phi')\}\{c_2{}^2\overline{\mathrm{Y}}_l{}^{m+1/2}(\theta,\phi)\\ &\times\mathrm{Y}_l{}^{m'+1/2}(\theta',\phi')-c_1{}^2\overline{\mathrm{Y}}_l{}^{m-1/2}(\theta,\phi)\mathrm{Y}_l{}^{m'-1/2}(\theta',\phi')\}+\sqrt{2}\{\mathrm{Y}_1{}^1(\theta,\phi)\overline{\mathrm{Y}}_1{}^0(\theta',\phi')\\ &+\mathrm{Y}_1{}^0(\theta,\phi)\overline{\mathrm{Y}}_1{}^{-1}(\theta',\phi')\}c_1c_2\overline{\mathrm{Y}}_l{}^{m+1/2}(\theta,\phi)\mathrm{Y}_l{}^{m'-1/2}(\theta',\phi')+\sqrt{2}\{\mathrm{Y}_1{}^{-1}(\theta,\phi)\\ &\times\overline{\mathrm{Y}}_1{}^0(\theta',\phi')+\mathrm{Y}_1{}^0(\theta,\phi)\overline{\mathrm{Y}}_1{}^1(\theta',\phi')\}c_1c_2\overline{\mathrm{Y}}_l{}^{m-1/2}(\theta,\phi)\mathrm{Y}_l{}^{m'+1/2}(\theta',\phi')]\\ &\times[\sum_M \mathrm{Y}_L{}^M(\theta,\phi)\overline{\mathrm{Y}}_L{}^M(\theta',\phi')]\,d\Omega\,d\Omega'.\end{aligned}$$

The magnetic quantum number is conserved, so $m=m'=\frac{1}{2}$. Using the explicit formulae for the Clebsch–Gordan coefficients (Condon and Shortley 1951), the integral may be evaluated, with the result already given by (30).

ACKNOWLEDGMENTS

We should like to express our gratitude to Professor H. S. W. Massey for suggesting the problem and for many valuable discussions, to the Director of the National Physical Laboratory and to the Superintendent of its Mathematics Division for the use of the pilot ACE electronic computer, to the staff of the Mathematics Division for their patience and help in its use and to the British Council for a Scholarship which enabled one of us (A. S.) to spend a year in England.

REFERENCES

ABRAHAM, G., COHEN, L., and ROBERTS, A. S., 1955, *Proc. Phys. Soc.* A, **68,** 265.
BIEDENHARN, L. C., BLATT, J. M., and ROSE, M. E., 1952, *Rev. Mod. Phys.*, **24,** 249.
BLATT, J. M., and JACKSON, J. D., 1949, *Phys. Rev.*, **76,** 18.
CHRISTIAN, R. S., and HART, E. W., 1950, *Phys. Rev.*, **77,** 441.
CHRISTIAN, R. S., and NOYES, H. P., 1950, *Phys. Rev.*, **79,** 85.
CLARK, A. C., 1955, *Proc. Phys. Soc.* A, **67,** 323.

Condon, E. U., and Shortley, G. H., 1951, *Theory of Atomic Spectra* (Cambridge: University Press).
Dancoff, S. M., 1940, *Phys. Rev.*, **58,** 326.
Elliott, J. P., 1953, *Proc. Roy. Soc.* A, **218,** 345.
Feingold, A. M., 1952, *Ph.D. Thesis*, Princeton University; 1956, *Phys. Rev.*, **101,** 258.
Garren, A., 1953, *Phys. Rev.*, **92,** 213.
Gerjuoy, E., and Schwinger, J., 1942, *Phys. Rev.*, **61,** 138.
Hochberg, S., Massey, H. S. W., Robertson, H. H., and Underhill, L. H., 1955, *Proc. Phys. Soc.* A, **68,** 746.
Hochberg, S., Massey, H. S. W., and Underhill, L. H., 1954, *Proc. Phys. Soc.*, **67,** 957.
Hughes, J., and Le Couteur, K. J., 1950, *Proc. Phys. Soc.* A, **63,** 1219.
Inglis, D. R., 1953, *Rev. Mod. Phys.*, **25,** 390.
Irving, J., 1953, *Proc. Phys. Soc.* A, **66,** 17.
Jackson, J. D., and Blatt, J. M., 1950, *Rev. Mod. Phys.*, **22,** 77.
Kalos, M. H., Biedenharn, L. C., and Blatt, J. M., 1956, *Nucl. Phys.*, **1,** 233.
Klein, C. A., 1956, *Nuovo Cim.*, **1,** 581.
Robertson, H. H., 1956, *Proc. Camb. Phil. Soc.*, **52,** 538.
Seagrave, J. D., 1953, *Phys. Rev.*, **92,** 1222.

The Use of Multiple Scattering and the Effects of Distortion in a High-Pressure Cloud Chamber

By P. BAXTER and F. R. STANNARD
Department of Physics, University College, London

Communicated by E. H. S. Burhop; MS. received 17*th May* 1956, *and in revised form* 5*th October* 1956

Abstract. Multiple scattering measurements on tracks of high energy ionizing particles in a high-pressure cloud chamber are described, and the use of such measurements for estimating the product, $p\beta$, of momentum and velocity of the particles is discussed. Q-values of Λ^0-decays and the masses of particles stopping in the chamber are deduced from such measurements. The various distortions found in this type of chamber and their effect on multiple scattering measurements are discussed.

§ 1. Introduction

Since the summer of 1953 a high-pressure cloud chamber has been operated at an altitude of 2040 m on La Marmolada in the Dolomites, in an investigation of high energy interactions produced by particles of the cosmic radiation in the gas of the chamber and in nearby materials. The experiment is being conducted jointly by a team of physicists from University College London, and the University of Edinburgh.

The chamber operates at a pressure of 75 atmospheres, and with an argon filling the density of the gas is 0·135 g cm^{-3}. In such a medium multiple scattering is appreciable not only on the tracks of electrons but also on those of heavy particles. There is no magnetic field associated with the chamber, and it seemed important to investigate the possible use of multiple scattering measurements as a means of estimating the momenta of the particles. Chamber distortions may produce deflections of the tracks which could be mistaken for multiple scattering, so that it is necessary to investigate these distortions before reliance can be placed on momentum estimates based on scattering measurements.

After a discussion of the multiple scattering method in its application to high-pressure chamber tracks in the first part of the paper, the second part describes the various distortions that have been found and their effect upon these measurements.

§ 2. Multiple Scattering

2.1. *The Evaluation of the Scattering Constant*

The scattering constant is obtained from the formula of Goldschmidt-Clermont (1950), who incorporates into the original theory of Williams (1939, 1940) the expression for the mean free path given by Molière (1948).

The mean deflection of a particle traversing thickness t is given as

$$\bar{\theta} = \theta_0 t^{1/2} \qquad \ldots\ldots(1)$$

where for argon at 75 atmospheres and 0°C

$$\theta_0 = \frac{0{\cdot}330}{p\beta}\left\{1{\cdot}45 + 0{\cdot}80\left(\ln\frac{285t}{\beta^2+0{\cdot}056}\right)^{1/2}\right\}. \qquad \ldots\ldots(2)$$

t is in centimetres, p is the momentum in MeV/c, and βc the velocity of the particle.

The criterion for the application of the statistical theory upon which the scattering formula is based is satisfied to within a few per cent if t is greater than 0·035 cm.

2.2. *Experimental Procedure using Constant Cell Lengths*

The photographs are taken on 35 mm film and the scattering measurements are carried out on the negative itself. It is enclosed between glass plates and mounted on the stage of a Cooke M-4000 microscope. The track, which has a width of about 100 μ on the film, is viewed through a × 4 objective and a × 10 eyepiece.

The track is aligned nearly parallel to one of the directions of motion of the microscope and the coordinate method developed by Fowler (1950) is used with cells normally between 1 and 2 mm in length. These correspond to 0·5 and 1 cm on the actual track in space. To improve the statistics overlapping cells are employed.

Owing to the diffuse and ill-defined edges of the track it is always difficult to decide which point should be taken as the centre, and this gives rise to a noise which has a root mean square value usually lying between 5 and 10 μ. This noise is corrected for in the usual manner by finding the mean square second differences $\overline{D_1^2}$ and $\overline{D_2^2}$ for two different cell lengths t_1 and t_2. The mean square scattering angle for unit cell length is then given by

$$\overline{\theta^2} = \frac{\overline{D_2^2} - \overline{D_1^2}}{t_2^3 - t_1^3} \qquad \ldots\ldots(3)$$

and

$$2\epsilon^2 = \overline{D_1^2} + \overline{D_2^2} - \frac{(\overline{D_2^2} - \overline{D_1^2})(t_1^3 + t_2^3)}{(t_2^3 - t_1^3)} \qquad \ldots\ldots(4).$$

where ϵ^2 is the noise.

It can be shown that the optimum choice of cell length is such that the signal–noise ratio ν defined as $\nu = (\overline{D^2} - \epsilon^2)/\epsilon^2$ should be equal to 5·8. Under such circumstances the standard error on the root mean square second difference is $0{\cdot}9/N^{1/2}$, where N is the number of differences (Biswas, George and Peters 1953).

In addition to the noise correction, a 'cut-off' procedure has been adopted similar to that used by workers with emulsions, whereby all differences greater than four times the mean are excluded.

Many of the tracks which have to be measured dip sharply in the chamber and the magnification of their images on the film changes rapidly along the length of the track. In the present work multiple scattering measurements are made directly on the film and the conversion of the conically projected scattering angle so obtained to a scattering angle on the track in space is derived in the Appendix. The conversion relation given as expression (A) may also be of interest in the similar problem encountered in the analysis of tracks in a bubble chamber.

The conversion procedure is very lengthy and the time required prohibits measurements on all but events of particular interest. Such events are the decays of V-particles. The values of $p\beta$ have been estimated for the decay products of six Λ^0-particles so situated in the chamber as to offer suitable lengths of track for measurement, and a histogram of the resulting Q-values is given in figure 1. These are to be compared with the known Q-value of 37 MeV. The errors quoted are derived from the standard errors involved in the estimation of the values of $p\beta$ for the two decay products.

Owing to the high noise level the number of cells available for a high-pressure chamber track is usually considerably smaller than the number obtainable for a track in emulsion. The size of the chamber is such that the maximum observable length of a track is about 15 cm but, even with this length, the standard error on the scattering angle is about 30% for a $p\beta$ value of 150 Mev/**c**. Thus 150 Mev/**c** may be regarded as the maximum value that can be usefully estimated.

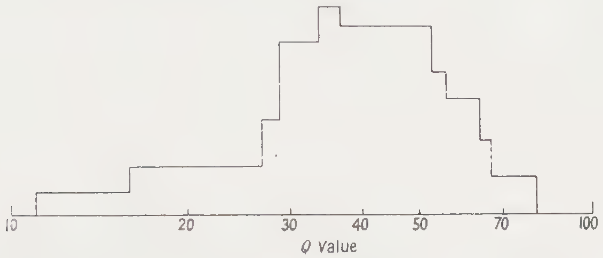

Figure 1. The Q-values obtained from multiple scattering measurements on the decay products of six Λ^0-particles.

2.3. *Constant Sagitta Method for Stopped Particles*

In a high-pressure cloud chamber many particles are brought to rest in the gas. From range and multiple scattering it is possible to make an estimate of their masses, the most convenient procedure being the constant sagitta method developed independently by Biswas, George and Peters (1953) and by Dilworth, Goldsack and Hirschberg (1954). In this method scattering measurements are carried out using variable cell lengths so arranged that the signal–noise ratio remains constant. Such a system of successive cells is called a scattering scheme and the one used most frequently in connection with the present work is given in the table.

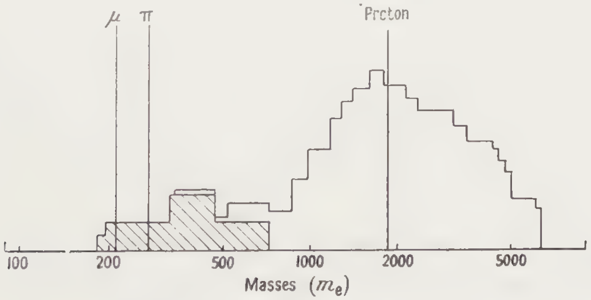

Figure 2. The mass values for 21 protons and 4 light mesons, the latter being indicated by the shaded area.

In figure 2 the masses of 25 stopped particles are plotted on a histogram according to the usual procedure described by Leighton (1953). The particles divide into 21 protons and 4 light mesions. The latter can be identified by decays or stars at the end of their ranges, and their contribution to the histogram is indicated by the shaded area. The displacement of these mesons from their known mass value is not significant as so few have been measured.

When all second differences for the protons are combined together, 371 independent values are obtained which give a resultant mass of $2000^{+300}_{-200}\, m_e$.

Range (cm)	Cell length (cm)	Range (cm)	Cell length (cm)	Range (cm)	Cell length (cm)
0·33	0·16	2·70	0·31	6·38	0·43
0·49	0·18	3·01	0·33	6·81	0·44
0·67	0·20	3·34	0·34	7·25	0·45
0·87	0·22	3·68	0·35	7·70	0·46
1·09	0·23	4·03	0·36	8·16	0·47
1·32	0·25	4·39	0·37	8·63	0·48
1·57	0·26	4·76	0·39	9·11	0·49
1·83	0·28	5·15	0·40	9·60	0·51
2·11	0·29	5·55	0·41	10·11	0·52
2·40	0·30	5·96	0·42	10·63	0·53

§ 3. DISTORTION AND ITS EFFECT ON MULTIPLE SCATTERING MEASUREMENTS

3.1. *Distortion in the Optical System*

The distortion produced by the lenses (Dallmeyer Anastigmatic f/3·5 of focal length 35 mm) and the front window of the chamber was investigated by photographing a grid of straight wires and subsequently measuring the curvature of their images. It was shown that this source of distortion was not serious. For a particle with $p\beta = 150$ Mev/**c** the maximum error in the estimation is only 5% and for most regions of the chamber is substantially less than this.

3.2. *Distortion due to Non-uniform Expansion of the Gas*

This form of distortion usually makes itself apparent near to the walls of the chamber and in regions where irregularities are introduced into the flow of gas during expansion as, for example, near to the supports of the clearing field electrodes. Not a great deal can be done about such distortions except to avoid making measurements in those regions known to be affected.

The main concern, however, has been over a form of distortion transmitted throughout the whole volume. At the rear of the chamber is a back plate perforated with about 500 small holes, and the expansion of the gas is brought about by the movement of a rubber diaphragm behind it. On expansion the gas passes through the holes and, though it is readily understood that the flow must be irregular close to the plate, it has been found that this non-axial flow extends throughout all the chamber.

In the measurement of multiple scattering, the mean square second difference $\overline{D^2}$ is proportional to t^3 so that a graph of $\overline{D^2}$ against t^3 should give a straight line with a slope dependent upon the value of $p\beta$ for the track, and with an intercept on the $\overline{D^2}$ axis equal to the noise ϵ^2. Owing to the variation with cell length of the logarithmic term in the expression for the scattering constant, the line is not, in fact, expected to be perfectly straight. However, when measurements are made on a track, the relation between $\overline{D^2}$ and t^3 is found to be far from linear until $t \geqslant 0{\cdot}5$ mm.

Figure 3 shows a typical graph of $\overline{D^2}$ against t^3 for cells from 0·1 mm to 3·0 mm, while figure 4 shows the same results from 0·1 mm to 0·5 mm on a larger scale.

These values of cell length refer to measurements on the film. The lines drawn show the extent of the variation in slope to be attributed to the logarithmic term.

The value of $\overline{D^2}$ for the smallest cell gives a measure of the noise due to track measurement. At first $\overline{D^2}$ rises rapidly with increase of t^3 and this is attributed to the non-axial component of the gas flow. At $t \simeq 0{\cdot}5$ mm the cell length becomes of the same order as the distance between the holes. The fact that a linear relation between $\overline{D^2}$ and t^3 exists for larger values of t indicates that under these circumstances the irregular flow contributes only a constant amount to $\overline{D^2}$ and can be regarded as a further source of noise, which has become known as 'back-plate noise'. It has been found that all counter-controlled tracks have about the same value for it at the same distance from the plate and, as expected, this value increases the nearer the track is to the plate.

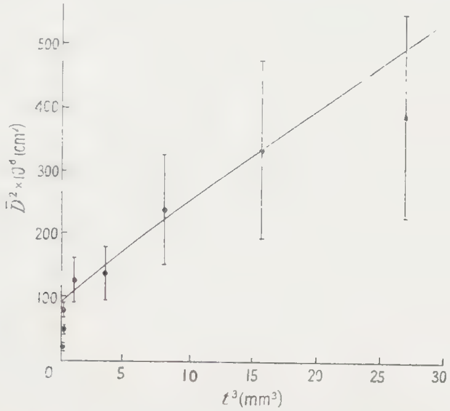

Figure 3. A typical graph of $\overline{D^2}$ plotted against t^3.

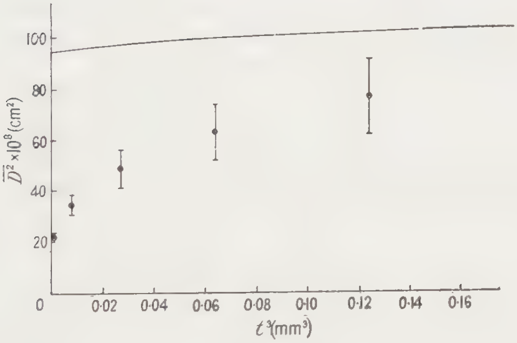

Figure 4. A graph of $\overline{D^2}$ plotted against t^3 for the same track as in figure 3, showing the points for the smaller cells in greater detail.

Tracks that entered the chamber while the expansion was still taking place (a process requiring about 200 msec) can be identified as such from their incomplete condensation. These show a much reduced value of noise due to part of the expansion having already taken place before their entry. Tracks that appear on the second and not on the first photograph of 'the double-flash system' to be described in the next section, are known to have arrived after the expansion was completed, and show no 'back-plate noise'.

The manner of allowing for this distortion is different for the two methods of scattering employed. With the constant cell length method the cell length for noise elimination is shown to be at least 0·5 mm, in order that the back-plate noise should have reached its constant maximum value.

In the constant sagitta method for stopped particles it is not possible to measure noise at cells of 0·5 mm or more because of the high degree of scattering included. Therefore a programme was carried out consisting of the measurement of many tracks at different distances from the back plate to determine the value of noise for all positions in the chamber. The appropriate value is then added to the setting error experimentally found for each track.

This kind of distortion would presuambly not occur in a piston-type chamber.

3.3. *Distortion due to Further Movements of the Gas after the Expansion has been Completed*

For conventional atmospheric pressure chambers, the usual way of detecting such distortion is to measure the curvature on tracks of fast particles in the absence of the magnetic field. Then the temperature control and times of photography can be adjusted to the optimum conditions. In a high-pressure cloud chamber this is not possible as all but very high energy particles are scattered. However, these distortions are time dependent, and the method used in the present investigation for detecting them in the presence of multiple scattering has consisted of photographing the same event twice at different times and comparing the two pictures.

Immediately after the first photograph has been taken, the film in the camera is wound on rapidly and is ready for the second flashing of the lights in 0·1 sec. This is done by means of a solenoid having a 1 inch stroke, which causes a rotation of a wind-on sprocket by means of a gear chain. The armature is then allowed to return on a ratchet. The stroke is adjusted so that one pull interleaves the first and second stereo-pairs of one expansion and three pulls advance the film sufficiently for the next expansion. Figure 5 (Plate I) shows a set of two stereo-pairs.

The usual time delays are 400 msec from the opening of the expansion valve to the first flash and a further 400 msec to the second. So far 5000 photographs have been taken with the apparatus and the distortions found with it can be sub-divided into three classes.

(*a*) *Convection currents due to heating from the walls.* The adiabatically cooled gas near to the walls is heated by the uncooled surface, and convection currents are set up while the central mass of gas falls.

For the chamber under consideration, this effect is imperceptible until 1·5 sec after the expansion, and because this type of distortion is known to increase as $t^{5/2}$ or t^3, it in no way affects the multiple scattering measurements.

(*b*) *Local heating.* When vapour condenses on the track heat is given out and a sleeve of hot gas can be considered to surround the track. Where there is a δ-ray much more heat than normal is released giving rise to the kind of distortion seen on the horizontal track in figure 6 (Plate II). The first signs become noticeable after 800 msec and as it presumably varies according to a high power of time, this form of distortion can also be considered to have no effect on scattering measurements.

(*c*) *Long term convection currents.* By carrying out multiple scattering measurements on the same track for both flashes, any distortion becomes apparent as a change in the scattering on the second photograph.

To analyse this change, it is possible to plot the profile of the track on an enlarged scale using readings at every 0·1 mm. Then, by drawing a smooth curve through the points, movements of the gas show as accentuations on the second photograph of the profile on the first.

As these are long term convection currents, one can assume an approximately linear variation of the distortion with time, and knowing the two time delays, extrapolate to the profile of the track as it was at the moment of expansion. This is done, for example, in the case of equal time delays, by subtracting the difference between the coordinates of a point as measured on the two photographs from the coordinates on the first. Unfortunately, the mean square noise on the extrapolated curve is equal to that on the second photograph plus four times that on the first, and this increase in noise by a factor of about five makes it impossible to carry out scattering measurements for penetrating particles on the distortion-corrected curve.

The double flash system, while being unable to correct multiple scattering measurements for distortion, has proved invaluable for indicating whether particular events are distorted or not, and has been very helpful in guiding efforts to reach the optimum conditions of temperature control and times of photography.

ACKNOWLEDGMENTS

The authors are indebted to Dr. E. H. S. Burhop for his personal supervision and guidance, and to Professor H. S. W. Massey and Dr. G. R. Evans for their interest in this work. We should also like to thank the other members of the team for their helpful discussions and advice and, in particular, Mr. F. W. Bullock and Mr. N. N. Raina, who also carried out many of the measurements.

One of us (F. R. S.) wishes to acknowledge the receipt of a Department of Scientific and Industrial Research maintenance grant and the other (P. B.) a Further Education and Training Scheme award. The programme of work at La Marmolada was made possible as a result of the award of a Department of Scientific and Industrial Research Special Development Grant to Professor Massey, and the friendly co-operation of the Istituto di Fisica, Università di Padova, who granted us facilities in their mountain cosmic-ray laboratory.

REFERENCES

BISWAS, S., GEORGE, E. C., and PETERS, B., 1953, *Proc. Ind. Acad. Sci.* A, **38,** 418.
DILWORTH, C., GOLDSACK, S. J., and HIRSCHBERG, L., 1954, *Nuovo Cim.*, **11,** 113.
FOWLER, P. H., 1950, *Phil. Mag.*, **41,** 169.
GOLDSCHMIDT-CLERMONT, Y., 1950, *Nuovo. Cim.*, **7,** 331.
LEIGHTON, R. B., 1953, *Phys. Rev.*, **89,** 148.
MOLIÈRE, G., 1948, *Z. Naturf.*, **3A,** 78.
WILLIAMS, E. J., 1939, *Proc. Roy. Soc.* A, **169,** 531; 1940, *Phys. Rev.*, **58,** 292.

APPENDIX

BY E. H. S. BURHOP

Relation between Multiple Scattering of Particle Track in Space and that observed after Conical Projection on Film

It is necessary to relate the multiple scattering measured directly on the film with that of the particle track in space. Let O (figure 7) be the pole of the lens and o the foot of the perpendicular from O to the plane of the film, s being the length Oo.

The track PAA′ projects through O to paa′. ox, oy, parallel to OX, OY are taken as coordinate axes on the film. AB, A′B, tangents at two consecutive points A, A′ of the track in space, project into ab, a′b, tangents at the consecutive points a, a′ of the projection of the track on the film. The problem is to calculate the angle a′ba″ ($=\vartheta$) between the two tangents on the film in terms of the angle A′BA″ ($=\theta$) between the two tangents in space and the angle ϕ between the planes OBA″ and A′BA″.

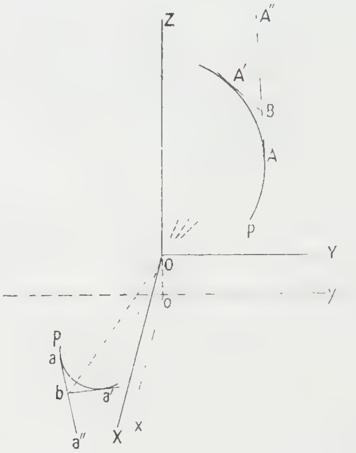

Figure 7.

Take B (XYZ) as new origin and axes ($B\xi\eta\zeta$) such that the ζ axis is taken along BA″ which has direction cosines (l, m, n) relative to the axes (OXYZ) and the ξ axis (direction cosines l_1, m_1, n_1 relative to OXYZ) is taken perpendicular to BA″ in the plane OBA″. The direction cosines of the η axis relative to OXYZ are l_2, m_2, n_2. Let ψ', ψ'' be the angles ba′, ba″ respectively make with ox. Then to the first order in θ,

$$\tan\chi'' = \frac{mZ-nY}{lZ-nX}$$

$$\tan\chi' = \tan\chi'' + \frac{\theta}{(l-nX/Z)^2}$$

$$\left[\cos\phi\left\{\left(l-\frac{nX}{Z}\right)\left(m_1-\frac{n_1Y}{Z}\right)-\left(m-\frac{nY}{Z}\right)\left(l_1-\frac{n_1X}{Z}\right)\right\}\right.$$
$$\left.+\sin\phi\left\{\left(l-\frac{nX}{Z}\right)\left(m_2-\frac{n_2Y}{Z}\right)-\left(m-\frac{nY}{Z}\right)\left(l_2-\frac{n_2X}{Z}\right)\right\}\right]$$

and $$\vartheta = \chi'-\chi'' \simeq \frac{\tan\chi'-\tan\chi''}{1+\tan\chi'\tan\chi''} \simeq -\frac{\theta\sin\phi\,(l_1X+m_1Y+n_1Z)}{Z\left\{\left(l-\frac{nX}{Z}\right)^2+\left(M-\frac{nY}{Z}\right)^2\right\}}.$$

Denoting by R the length OB, ψ the angle OBA″ between the direction of the track and the line joining it to the pole of the lens, α the angle between the track direction BA″ and the axis OZ and β the angle between OB and OZ

$$l_1X+m_1Y+n_1Z = -R\sin\psi$$

and $$\left(l-\frac{nX}{Z}\right)^2+\left(m-\frac{nY}{Z}\right)^2 = 1-\frac{2\cos\alpha\cos\psi}{\cos\beta}+\frac{\cos^2\alpha}{\cos^2\beta},$$

so that $$\vartheta \simeq \frac{\theta\sin\phi\sin\psi\cos\beta}{\cos^2\beta-2\cos\alpha\cos\beta\cos\psi+\cos^2\alpha},$$

and the magnitude of the mean projected angle of deflection is

$$\bar{\vartheta} = \frac{2\bar{\theta}}{\pi} \frac{\cos\beta \sin\psi}{\cos^2\beta - 2\cos\alpha\cos\beta\cos\psi + \cos^2\alpha},$$

where θ is the mean space angle of multiple scattering. Define $\bar{\theta} = \theta_0 T^{1/2}$ where $\bar{\theta}$ is the mean scattering angle in a length T of track, θ_0 the scattering constant and $\bar{\vartheta} = \vartheta_0 t^{1/2}$ where $\bar{\vartheta}$ is the measured mean projected angle of scattering in a projected length t of track and ϑ_0 the scattering constant for the projection of the track on the film. The 'magnification'

$$\frac{t}{T} = \frac{\mathrm{ba}}{\mathrm{BA}} = \frac{s}{Z} \frac{(\cos^2\beta + \cos^2\alpha - 2\cos\alpha\cos\beta\cos\psi)^{1/2}}{\cos\beta},$$

so that the relation between the projected scattering constant measured on the film and the scattering constant on the track may be written

$$\theta_0 = \frac{\pi}{2}\vartheta_0 \left(\frac{s}{z}\right)^{1/2} \frac{(\cos^2\beta - 2\cos\alpha\cos\beta\cos\psi + \cos^2\alpha)^{5/4}}{\sin\psi(\cos\beta)^{3/2}}. \qquad \ldots\ldots(\mathrm{A})$$

In general the quantities Z, α, β, ψ vary along the track so that the second differences measured on the projected image of the track on the film must be weighted according to (A) in order to yield the correct scattering constant θ_0. Fortunately for many tracks measured the variation along the track of the factor in the last bracket of (A) is small and linear so that it is sufficiently accurate to calculate it at each end of the track.

On the Use of the Complete Interaction Hamiltonian in Atomic Rearrangement Collisions

By J. D. JACKSON†

Physical Sciences Centre, McGill University, Montreal, Canada

MS. received 18*th October* 1956

Abstract. The use of the complete interaction Hamiltonian in the problem of the transfer of an electron from a hydrogen-like target atom with nuclear charge Ze to an incident ion of charge $Z'e$ is discussed both qualitatively and quantitatively. The second Born approximation is examined in detail, and it is shown that for $Z'=Z=1$ the second Born approximation correction to the matrix element very nearly vanishes when the complete interaction Hamiltonian is employed. This gives a theoretical explanation for the good agreement between theory and experiment for electron capture by protons in hydrogen even at incident velocities such that $\hbar v/e^2 \sim 1$, and the poor agreement for alpha particles in hydrogen in the same velocity range.

§ 1. INTRODUCTION

In recent years there has been a renewed interest in charge exchange reactions between atoms and molecules, both from the experimental and theoretical sides. The present paper is concerned with the theory of the simplest charge transfer problem, the transfer of an electron from one structureless atomic ion to another. Recent experimental data bearing on this problem are those of Keene (1949), Ribe (1951), Whittier (1954), Stedeford and Hasted (1955) and Stier and Barnett (1956) for electron capture by protons passing through hydrogen gas, and of Allison, Cuevas and Murphy (1956) for alpha particles in hydrogen gas. Earlier experiments are described by Massey and Burhop (1952). Early theoretical work was done by Brinkman and Kramers (1930), among others, while recent calculations have been performed by D. R. Bates and co-workers at Belfast and by the author and collaborators (appropriate references cited below).

If the relative velocity of impact is high, it is customary to use the Born approximation to give the lowest order approximation for the charge-transfer cross section. The cross section is proportional to the absolute square of the matrix element of the interaction Hamiltonian between initial and final unperturbed states. For the simple problem considered here—a hydrogen-like atom of atomic number Z is struck by an incident ion of charge $Z'e$, the electron being transferred to a bound state around the incident ion—the interaction Hamiltonian consists of the (incident ion)–(electron) Coulomb interaction and the (incident ion)–(struck ion) Coulomb interaction. Brinkman and Kramers (1930) calculated the Born approximation cross section using the (incident ion)–(electron) interaction, and neglecting the ion–ion interaction. Such neglect can be readily justified in inelastic collisions processes (Mott and Massey 1949, p. 224, Schiff 1949, p. 200), but not so readily for rearrangement collisions.

---

† At present on sabbatical leave as a John Simon Guggenheim Fellow at Princeton University, Princeton, New Jersey, U.S.A.

Bates and Dalgarno (1952, 1953) and Jackson and Schiff (1953) independently and by different techniques treated the capture of electrons by protons passing hydrogen atoms, using the complete interaction Hamiltonian in the first Born approximation. In contrast to the Brinkman–Kramers result, which is from five to ten times too large, these new calculations are in excellent agreement with experiment (Keene 1949, Ribe 1951, Whittier 1954, Stedeford and Hasted 1955, Stier and Barnett 1956) for proton energies above 25 kev ($\hbar v/e^2 > 1$). Even below this energy a considerable part of the discrepancy between theory and experiment can be traced to the replacement of the actual hydrogen molecules by a collection of independent hydrogen atoms for ease in calculation (unpublished work by the author). It appears, then, that for protons in hydrogen the first Born approximation with the complete interaction as the perturbation gives a good description of the charge exchange process, not only for high velocities ($\hbar v/e^2 \gg 1$), where it might be expected, but also for incident ion velocities of the same order as the electronic orbital velocities ($\hbar v/e^2 \sim 1$). On the other hand, for capture of electrons by alpha particles (He^{2+} ions) in hydrogen, the theoretical cross section calculated in the same way (Schiff 1954) is considerably larger than experiment (Allison, Cuevas and Murphy 1956) for velocities such that $\hbar v/e^2 \sim 1$, although at high velocities the agreement is better.

The purpose of the present paper is two-fold: firstly, to give qualitative arguments why the complete interaction must be employed for the perturbation, and why it might be expected to give good results in lowest approximation for protons in hydrogen but not for other ions; secondly, to show explicitly that the second Born approximation with the complete interaction very nearly vanishes for protons in hydrogen, but not for other ions. The latter point clarifies the reason for the good agreement between theory and experiment for protons in hydrogen, even at low velocities, and the poor agreement for alpha particles in hydrogen at the same velocities.

In § 2 the qualitative arguments are set forth; § 3 contains a summary of general formalism on rearrangement collisions, while § 4 is devoted to a detailed examination of the first-order correction terms (second Born approximation) for the problem at hand. A summary and conclusions appear in § 5.

§ 2. QUALITATIVE ARGUMENTS

Although use of the complete interaction as a perturbation has led to striking agreement with experiment for protons in hydrogen, the logic of its employment has been questioned. For example, G. C. Wick (quoted in footnote by Jackson and Schiff 1953) has argued that the (incident ion)–(struck ion) interaction would give a vanishing contribution to the exact cross section in the limit of infinitely heavy ions. In view of the actual large ratio of ion mass to electron mass, Wick would expect the inclusion of the ion–ion interaction to have a very small effect on the cross section, rather than the large effect found in the first Born approximation. This state of affairs can presumably be blamed on the approximation scheme employed. Wick's argument can be roughly summarized as follows: the angular distribution of the charge–exchange cross section is very sharply peaked in the forward direction. In fact the angles are measured in terms of a characteristic angle θ_0 defined (Jackson and Schiff 1953) by:

$$\theta_0 = \frac{A + A'}{2AA'} \frac{m}{M} \qquad \ldots\ldots(1)$$

where AM and $A'M$ are the masses of the struck and incident ions and m is the electron mass. In the limit $M \gg m$, the angle θ_0 approaches zero. This means that the motion of the heavy ions can be treated as classical straight-line trajectories, i.e. an impact parameter treatment can be employed in which the heavy ion coordinates and momenta are classical variables. If the heavy ion variables are classical quantities, the (incident ion)–(struck ion) interaction is a known function of time and can be removed from the wave equation by a canonical transformation. Consequently, it cannot influence the exact cross section for the charge-transfer process.

The above argument can be challenged by a semi-classical examination of the transverse momentum impulse occurring in the charge-transfer reaction on the one hand, and that due to the ion–ion interaction on the other. If these impulses are, in the velocity range of interest, comparable, then it seems clear that the complete interaction must be taken into account to give a proper description of the process. From a wave viewpoint, one can think of the various Fourier component wavelets arising from the different interactions interfering in a decisive way.

Deflection through an angle of the order of θ_0 implies a transverse momentum impulse of the order

$$\Delta p \sim mv, \qquad \ldots\ldots(2)$$

where v is the relative velocity between the incident ion and the struck atom. This small momentum is characteristic of the charge-transfer process, whether evaluated in the Brinkman–Kramers approximation or with the complete interaction, and is intuitively what one would expect. On the other hand, the Coulomb interaction between an ion of charge Ze and one of charge $Z'e$, colliding at an impact parameter b, gives rise to a small transverse impulse:

$$\Delta p_{\mathrm{c}} \simeq \frac{2ZZ'e^2}{bv},$$

provided b is large compared with the classical closest distance of approach $2ZZ'e^2/Mv^2$. In the charge-transfer reaction it can be shown (Brinkman and Kramers 1930, Schiff 1954) that the important region of impact parameters is

$$b \sim \frac{2e^2}{\hbar v} a_0 = \frac{2\hbar}{mv},$$

for $v > e^2/\hbar$. For impact parameters near this value the momentum impulse from the ion–ion interaction is roughly

$$\Delta p_{\mathrm{c}} \sim ZZ'\, me^2/\hbar. \qquad \ldots\ldots(3)$$

The ratio of the two values of transverse momentum impulse, (2) and (3), is therefore

$$\frac{\Delta p_{\mathrm{c}}}{\Delta p} \sim \frac{ZZ'e^2}{\hbar v}. \qquad \ldots\ldots(4)$$

It is true that for high velocities the ion–ion interaction gives a negligible impulse relative to the charge-transfer impulse, but for the velocity range $\hbar v/e^2 \sim 1$ where charge-exchange is appreciable the two impulses are comparable.

The question of why the first Born approximation with the complete interaction is quite successful for protons in hydrogen and not for other ions in hydrogen has been discussed earlier (Jackson and Schiff 1953). The force exerted on an ion by a neutral atom is of relatively short range. For hydrogen it is a sort of dipole interaction. This means that the distortion of the wave function of relative motion occurs only at relatively close distances, and the approximation of plane waves is fairly good, especially as the capture of the electron occurs at distances of the order of the Bohr radius from the struck ion. For an ion of charge $Z'e$ incident on hydrogen (or any neutral atom), the incoming wave feels only a short-range interaction, but in the rearranged system the outgoing wave feels a long-range Coulomb interaction which becomes $(Z'-1)e^2/R'$ at large separations. Only if $Z'=1$ is there a short-range dipole force for both incoming and outgoing waves. Consequently, it can be expected that the first Born approximation will give better results for $Z'=1$ than for $Z'>1$. This is borne out by the results of § 4 which show that the second-order Born approximation very nearly vanishes for $Z'=1$, but not for $Z'>1$.

§ 3. FORMAL THEORY

The theory of rearrangement collisions in atomic physics is presented by Mott and Massey (1949, Chapter VIII). In nuclear physics the general problem has been discussed by Austern (1953) and Gerjuoy (1953) in terminology appropriate to (d, p) and (d, n) reactions. Both these authors obtain an integral equation for the problem. It is easy to show that the lowest order approximation to the solution of their integral equation is just the first Born approximation of Bates and Dalgarno (1952) and Jackson and Schiff (1953). Recently Lippmann (1956) has treated general rearrangement collisions in an elegant and concise operator formalism. The essential results of Lippmann will now be summarized and applied to the problem at hand. The notation, with minor obvious changes, is that of Lippmann (1956).

In a rearrangement collision there is an 'original' and a 'rearranged' system. Unprimed quantities describe the original system, while primed quantities apply to the rearranged system. The Hamiltonian of the whole system can be broken into an 'unperturbed' part and an 'interaction' part in two different ways:

$$H=H_0+V=H_0'+V', \qquad \ldots\ldots(5)$$

where the first form is appropriate for the original system, and the second form for the rearranged system. The unperturbed Hamiltonians have eigenvectors Φ_{a} and Φ_{b}' such that:

$$H_0\Phi_{\mathrm{a}}=E_{\mathrm{a}}\Phi_{\mathrm{a}}, \quad H_0'\Phi_{\mathrm{b}}'=E_{\mathrm{b}}'\Phi_{\mathrm{b}}'. \qquad \ldots\ldots(6)$$

The operator Green's functions G_0 and G_0' are defined by:

$$G_0(\lambda)=\frac{1}{\lambda-H_0}, \quad G_0'(\lambda)=\frac{1}{\lambda-H_0'}, \qquad \ldots\ldots(7)$$

where $\lambda=E\pm i\epsilon$ for outgoing (incoming) waves. The solutions describing incident 'plane waves' plus scattered waves satisfy the integral equation

$$\Psi_{\mathrm{a}}^{(\pm)}=\Phi_{\mathrm{a}}+G_0(E_{\mathrm{a}}\pm i\epsilon)V\Psi_{\mathrm{a}}^{(\pm)} \qquad \ldots\ldots(8)$$

and the corresponding primed equation. This can be written

$$\Psi_{\mathrm{a}}^{(\pm)}=U(E_{\mathrm{a}}\pm i\epsilon)\Phi_{\mathrm{a}}, \qquad \ldots\ldots(9)$$

where the operator $U(\lambda)$ is defined by

$$[1-G_0(\lambda)V]\,U(\lambda)=1. \qquad \ldots\ldots(10)$$

Equations corresponding to (9) and (10) also hold for primed quantities.

Lippmann shows that the transition probability for a rearrangement collision is rigorously

$$w_{\rm ba}=\frac{2\pi}{\hbar}\,|(\Phi_{\rm b}',\, V'\,\Psi_{\rm a}^{(+)})|^2\,\delta(E_{\rm a}-E_{\rm b}'), \qquad \ldots\ldots(11)$$

and, furthermore, that if both H_0 and H_0' are Hermitian

$$(\Phi_{\rm b}',\, V'\,\Psi_{\rm a}^{(+)})=(\Psi_{\rm b}^{(-)\prime},\; V\,\Phi_{\rm a});\; E_{\rm b}'=E_{\rm a} \qquad \ldots\ldots(12)$$

and also

$$(\Phi_{\rm b}',\, V'\,\Phi_{\rm a})=(\Phi_{\rm b}',\, V\,\Phi_{\rm a});\; E_{\rm b}'=E_{\rm a}. \qquad \ldots\ldots(13)$$

The first Born approximation consists of replacing $\Psi_{\rm a}^{(+)}$ by $\Phi_{\rm a}$ in (11). This leads directly to the cross section formula (9) in the paper of Jackson and Schiff (1953) for the electron capture problem discussed here. The second-order approximation to the matrix element (12) can be obtained by taking the next approximation to the operator U:

$$U(\lambda)\simeq 1+G_0(\lambda)\,V. \qquad \ldots\ldots(14)$$

Substitution into (9) yields the result

$$\Psi_{\rm a}^{(\pm)}\simeq\Phi_{\rm a}+G_0(E_{\rm a}\pm i\epsilon)\,V\,\Phi_{\rm a}. \qquad \ldots\ldots(15)$$

When (15) is inserted into the left-hand side of (12), the first-order correction to the matrix element is

$$\Delta M=(\Phi_{\rm b}',\, V'\,\Psi_{\rm a}^{(+)})-(\Phi_{\rm b}',\, V'\,\Phi_{\rm a})=(\Phi_{\rm b}',\, V'G_0\,V\,\Phi_{\rm a}). \qquad \ldots\ldots(16)$$

Another equivalent approach is to substitute in the right-hand side of (12) the second-order approximation for the state vector $\Psi_{\rm b}'^{(-)}$. This leads to an alternative to (16):

$$\Delta M'=(\Phi_{\rm b}',\; V'\,G_0'\;V\Phi_{\rm a}). \qquad \ldots\ldots(17)$$

The two forms, (16) and (17), for the correction to the Born approximation differ by the appearance of the 'original' Green's function G_0 in (16) and the 'rearranged' Green's function G_0' in (17). The first form arises from a systematic improvement (15) of the wave function explicitly in terms of the original system (the description of the rearranged system being contained implicitly and in a complicated way), while the second form occurs in an improvement of the rearranged wave function. There seems to be no obvious choice between (16) and (17) as the better representation of the correction to the matrix element. It can perhaps be argued that, in order to treat the original and rearranged systems in a symmetrical way, one should take an average of the two. For definiteness in what follows, the second form (17) will be used. Some remarks on the use of (16) and the reason for emphasis on (17) will be made at the end of § 4.

§ 4. DETAILED DISCUSSION

The formal expression (17) for the first-order correction to the Born approximation will now be analysed in detail for the problem of electron capture by an ion of charge $Z'e$, and mass $A'M$, colliding with a hydrogen-like atom of nuclear charge Ze, and mass AM. The notation will be that of Jackson and Schiff (1953, to be referred to as JS[†]). The Green's function G_0' in coordinate representation is

$$G_0'=\sum_j \psi_j^*(\mathbf{r}_1')\,\psi_j(\mathbf{r}')\,G_j(\mathbf{R}',\mathbf{R}_1'), \qquad \ldots\ldots(18)$$

where $\psi_j(\mathbf{r}')$ is the 'internal' wave function for the jth eigenvalue of the rearranged system (electron around ion Z'), and $G_j(\mathbf{R}', \mathbf{R}_1')$ is the Green's function describing the relative motion between atom Z' and ion Z:

[†] and equations in the form (JS9).

$$G_j = \frac{2\mu_f}{4\pi\hbar^2}\frac{\exp(ik_j'\,|\mathbf{R}'-\mathbf{R}_1'|)}{|\mathbf{R}'-\mathbf{R}_1'|} = \frac{2\mu_f}{\hbar^2(2\pi)^3}\int\frac{d\mathbf{q}\exp\{i\mathbf{q}\,.\,(\mathbf{R}'-\mathbf{R}_1')\}}{q^2-k_j'^2-i\epsilon}, \qquad \ldots\ldots(19)$$

where the limit $\epsilon \to 0^+$ is to be taken at the end of the calculation. The state vectors Φ_a and Φ_b are given by

$$\Phi_a = \psi_0(\mathbf{r})\,e^{i\mathbf{k}.\mathbf{R}}, \quad \Phi_b' = \psi_f(\mathbf{r}')\,e^{i\mathbf{k}'.\mathbf{R}'}. \qquad \ldots\ldots(20)$$

The interaction energies V and V' are equal to V_i (J S 5) and V_f (J S 8), respectively. Using (18), (19) and (20), the correction term (17) can be written out explicitly:

$$\Delta M' = \frac{2\mu_f}{\hbar^2}\frac{1}{(2\pi)^3}\sum_j\int d\mathbf{q}\,\frac{1}{q^2-k_j'^2-i\epsilon}\iiiint d\mathbf{r}\,d\mathbf{r}'\,d\mathbf{r}_1\,d\mathbf{r}_1'$$

$$\cdot\ \exp\{i(\mathbf{q}-\mathbf{k}')\,.\,\mathbf{r}\}\exp\left\{i\frac{A'M}{A'M+m}(\mathbf{k}'-\mathbf{q})\,.\,\mathbf{r}'\right\}\psi_f^*(\mathbf{r}')\,\psi_j(\mathbf{r}')\,V_f(\mathbf{r},\mathbf{r}')$$

$$\cdot\ \exp\left\{i\left(\frac{AM}{AM+m}\mathbf{k}-\mathbf{q}\right).\,\mathbf{r}_1\right\}\exp\left\{-i\left(\mathbf{k}-\frac{A'M}{A'M+m}\mathbf{q}\right).\,\mathbf{r}_1'\right\}V_i(\mathbf{r}_1,\mathbf{r}_1')$$

$$\cdot\ \psi_j^*(\mathbf{r}_1')\,\psi_0(\mathbf{r}_1).$$

The interactions V_i and V_f each involve two terms, so that $\Delta M'$ is made up of four different parts. These will be designated as follows:

$$\left.\begin{array}{l}\Delta M_1' \longleftrightarrow (ZZ'e^4/r\,r_1')\\ \Delta M_2' \longleftrightarrow (-ZZ'^2e^4/r_1'\,|\mathbf{r}-\mathbf{r}'|)\\ \Delta M_3' \longleftrightarrow (-Z^2Z'e^4/r\,|\mathbf{r}_1-\mathbf{r}_1'|)\\ \Delta M_4' \longleftrightarrow (Z^2Z'^2e^4/|\mathbf{r}-\mathbf{r}'|\,|\mathbf{r}_1-\mathbf{r}_1'|)\end{array}\right\} \qquad \ldots\ldots(21)$$

where the various parts of the product $V_f(\mathbf{r},\mathbf{r}')\,V_i(\mathbf{r}_1,\mathbf{r}_1')$ identify the components of $\Delta M'$.

At this stage it is convenient to introduce the quantity:

$$\mathscr{M}_j(\mathbf{K}) = -\left[\frac{\hbar^2}{2m_f}(\mathbf{C}+\mathbf{K})^2+\epsilon_j'\right]\phi_j^*(\mathbf{C}+\mathbf{K})\,\phi_0(\mathbf{B}+\mathbf{K}), \qquad \ldots\ldots(22)$$

where the ϕ's are the Fourier transforms of the internal wave functions (J S 14), and $\mathbf{B}$ and $\mathbf{C}$ are defined by (J S 13). If $\mathbf{K}=0$, $\mathscr{M}(0)$ is just the transition matrix element in the Brinkman–Kramers approximation (see J S I.3). Similarly,

$$\mathscr{N}_j(\mathbf{K}) = \phi_j^*(\mathbf{C}+\mathbf{K})\;\phi_0(\mathbf{B}+\mathbf{K}). \qquad \ldots\ldots(23)$$

With these definitions it is straightforward to transform $\Delta M_1'$ and $\Delta M_2'$ into the form $(i=1,\,2)$:

$$\Delta M_i' = \frac{Ze^2}{\pi^2}\frac{\mu_f}{\hbar^2}\sum_j\int d\mathbf{q}\,\frac{1}{q^2-k_j'^2-i\epsilon}\,\frac{\mathscr{M}_j(\mathbf{k}'-\mathbf{q})}{|\mathbf{k}'-\mathbf{q}|^2}\,\mathscr{I}_i \qquad \ldots\ldots(24)$$

where $$\mathscr{I}_1 = -\int\psi_f^*(\mathbf{r}')\,\exp i\,\frac{A'M}{A'M+m}(\mathbf{k}'-\mathbf{q})\,.\,\mathbf{r}'\,\psi_j(\mathbf{r}')\,d\mathbf{r}' \qquad \ldots\ldots(25)$$

and $$\mathscr{I}_2 = Z'\int\psi_f^*(\mathbf{r}')\exp -i\,\frac{m}{A'M+m}(\mathbf{k}'-\mathbf{q})\,.\,\mathbf{r}'\,\psi_j(\mathbf{r}')\,d\mathbf{r}'. \qquad \ldots\ldots(26)$$

To obtain the form (24) an insignificant error was introduced by replacing $A'M/(A'M+m)$ by unity in the $d\mathbf{r}_1'$ integration.

In the integration in (24) over $d\mathbf{q}$ the integrand has a sharp peak around $\mathbf{q}=\mathbf{k}'$

because of the factor $|\mathbf{k}'-\mathbf{q}|^{-2}$. Consequently, to a good approximation the exponential in $\mathscr{I}_1$ can be replaced by unity. Then $\mathscr{I}_1=-\delta_{\mathrm{f}j}$, and $\Delta M_1'$ becomes:

$$\Delta M_1' \simeq -\frac{Ze^2\mu_{\mathrm{f}}}{\pi^2\hbar^2}\int d\mathbf{p}\,\frac{\mathscr{M}_{\mathrm{f}}(\mathbf{k}'-\mathbf{q})}{(q^2-k'^2-i\epsilon)\,|\mathbf{k}'-\mathbf{q}|^2}\,. \qquad \ldots\ldots(27)$$

Regardless of the peaking of the integrand around $\mathbf{q}=\mathbf{k}'$, the exponential in $\mathscr{I}_2$ can be put equal to unity with negligible error. Then $\mathscr{I}_2=Z'\delta_{\mathrm{f}j}$, and

$$\Delta M_2' \simeq -Z'\,\Delta M_1'\,. \qquad \ldots\ldots(28)$$

In a very similar manner $\Delta M_3'$ and $\Delta M_4'$ can be written $(i=3, 4)$:

$$\Delta M_i' = \frac{Z^2Z'e^4\mu_{\mathrm{f}}}{2\pi^4\hbar^2}\sum_j\int d\mathbf{p}\int d\mathbf{q}\,\frac{\mathscr{N}_{\mathrm{f}}(\mathbf{k}'-\mathbf{q}+\mathbf{p})}{p^2(q^2-k_j'^2-i\epsilon)\,|\mathbf{k}'-\mathbf{q}|^2}\,\mathscr{I}_{i-2}. \qquad \ldots\ldots(29)$$

The same arguments as led to (27) can be applied here. Consequently one finds:

$$\Delta M_3' \simeq \frac{Z^2Z'e^4\mu_{\mathrm{f}}}{2\pi^4\hbar^2}\int d\mathbf{p}\int d\mathbf{q}\,\frac{\mathscr{N}_{\mathrm{f}}(\mathbf{k}'-\mathbf{q}+\mathbf{p})}{p^2(q^2-k'^2-i\epsilon)\,|\mathbf{k}'-\mathbf{q}|^2} \qquad \ldots\ldots(30)$$

and

$$\Delta M_4' \simeq -Z'\Delta M_3'. \qquad \ldots\ldots(31)$$

The preceding analysis shows that, to a good approximation, the matrix element correction (17) can be written:

$$\Delta M' \simeq (1-Z')(\Delta M_1'+\Delta M_3'), \qquad \ldots\ldots(32)$$

where $\Delta M_1'$ and $\Delta M_3'$ are given by (27) and (30), respectively. For $Z'=1$, (32) obviously vanishes, showing that for protons in hydrogen the second-order terms vanish. Admittedly there has been an approximation in going from (24) to (27) and (28), but it is clear that there is a large amount of cancellation between the various terms and that the correction $\Delta M'$ is actually very small.

If one insisted on using only the (incident ion)–(electron) interaction, as did Brinkman and Kramers, then the correction term reduces to $\Delta M_1'$. For ground-state capture by protons in hydrogen, a rough evaluation of (27), obtained by factoring out $\mathscr{M}_{\mathrm{f}}(\mathbf{k}'-\mathbf{q})$ evaluated at $\mathbf{k}'=\mathbf{q}$, gives a correction to the Brinkman–Kramers cross section, to first order in $(e^2/\hbar v)$, of the form $1-\pi e^2/\hbar v$. This does not give even qualitative agreement with experiment, or with the first Born approximation with the complete interaction.

A word should be said about the use of (16) to represent the first-order correction instead of (17), as was done above. A calculation starting with (16) leads to the same form of result as (32) with Z' replaced by Z, and a re-ordering of the terms in (21). This must be so because of the obvious symmetry between the original system and the rearranged system under the substitution $(Z', A')\to(Z, A)$. It is clear then that the second-order approximation very nearly vanishes only for $Z=Z'=1$, i.e. only when the short-range, dipole type of force exists in the initial *and* final states. It is significant that (16), which comes from an explicit improvement of the 'original' wave function, vanishes when long-range forces are absent in the *initial* state, while (17) vanishes if the long-range forces are absent in the final state.

Of course, to the extent that the struck atom can be approximated by a one-electron system, Z is effectively unity for all targets since the target material consists of neutral atoms. Therefore, the emphasis can be correctly placed on the condition $Z'=1$ for the vanishing of the second Born approximation.

§ 5. CONCLUSIONS

The essential result of the present paper is embodied in equation (32), which shows that the second-order Born approximation to the charge-exchange cross section very nearly vanishes for $Z'=1$. Arguments were presented in § 2 about why the complete interaction Hamiltonian should be used, and why it might be anticipated that the lowest order approximation to the charge-transfer cross section should be good for protons in hydrogen and not good for more highly charged ions. The result (32) gives detailed confirmation to these qualitative arguments, and explains the observed fact that the calculated cross sections for protons in hydrogen (Bates and Dalgarno 1952, 1953, Jackson and Schiff 1953) agree well with experiment for $(\hbar v/e^2) \gtrsim 1$, while those calculated for He^{2+} ions in hydrogen (Schiff 1954) do not agree with experiment, except perhaps for $(\hbar v/e^2) \gg 1$.

ACKNOWLEDGMENTS

The author wishes to take this opportunity to thank the National Research Council of Canada for its financial support, over a number of years, of graduate assistants employed in a theoretical study of electron capture and loss phenomena.

REFERENCES

ALLISON, S. K., CUEVAS, J., and MURPHY, P. G., 1956, *Phys. Rev.*, **102,** 1041.
AUSTERN, N., 1953, *Phys. Rev.*, **89,** 318.
BATES, D. R., and DALGARNO, A., 1952, *Proc. Phys. Soc.* A, **65,** 919; 1953, *Ibid.*, **66,** 972.
BRINKMAN, H. C., and KRAMERS, H. A., 1930, *Proc. Acad. Sci. Amsterdam,* **33,** 973.
GERJUOY, E., 1953, *Phys. Rev.*, **91,** 645.
JACKSON, J. D., and SCHIFF, H., 1953, *Phys. Rev.*, **89,** 359.
KEENE, J. P., 1949, *Phil. Mag.*, **40,** 369.
LIPPMANN, B. A., 1956, *Phys. Rev.*, **102,** 264.
MASSEY, H. S. W., and BURHOP, E. H. S., 1952, *Electronic and Ionic Impact Phenomena* (Oxford : University Press).
MOTT, N. F., and MASSEY, H. S. W., 1949, *Theory of Atomic Collisions*, 2nd Edn (Oxford : University Press).
RIBE, F., 1951, *Phys. Rev.*, **83,** 1217.
SCHIFF, H., 1954, *Canad. J. Phys.*, **32,** 393.
SCHIFF, L. I., 1949, *Quantum Mechanics* (New York : McGraw-Hill),
STEDEFORD, J. B. H., and HASTED, J. B., 1955, *Proc. Roy. Soc.* A, **227,** 466.
STIER, P. M., and BARNETT, C. F., 1956, *Phys. Rev.*, **103,** 896.
WHITTIER, A. C., 1954, *Canad. J. Phys.*, **32,** 275.

Rotational Analysis of Bands of the A $^3\Pi_{0^+}$, B $^3\Pi_1$ – X $^1\Sigma^+$ Systems of Gallium Monofluoride

By R. F. BARROW†, P. G. DODSWORTH† and P. B. ZEEMAN‡

† Physical Chemistry Laboratory, University of Oxford

‡ Merensky Institute for Physics, University of Stellenbosch

MS. received 11*th July* 1956

Abstract. Rotational analyses of the 0, 0 band of the A–X system and of the 0, 0 and 0, 1 bands of the B–X system, for both molecules Ga^{69}F and Ga^{71}F, have been made. The internuclear distance r_e'' in the ground state is 1·775 Å; the energy of dissociation D_0'' (for Ga^{69}F) is found to be 143·$_3$ kcal mole^{-1}.

---

§ 1. Introduction

The present work forms part of a general study of the thermodynamic and spectroscopic properties of the gaseous monohalides of the Group IIIb elements. The spectrum of gallium monofluoride may be observed both in absorption (Welti and Barrow 1952) and in emission (Barrow, Jacquest and Thompson 1954). For the rotational analysis, plates of the emission spectrum were taken in the 21 ft concave grating at the University of Stellenbosch: experimental details are given in the paper describing the rotational analysis of the indium monofluoride bands (Barrow, Glaser and Zeeman 1955). The rotational structure of the C $^1\Pi$–X$^1\Sigma^+$ system of GaF, like that in InF, proved too close to be resolved.

§ 2. Analysis

The GaF bands are immediately more complicated in appearance than those of InF for, whereas the latter bands are isotopically simple, the former arise from the two species Ga^{69}F (abundance 61·2%) and Ga^{71}F (38·8%). As with InF, the range of values of J for which there are well observed values of $\Delta_2F_0(J)$ from the 0, 0 bands of either system A–X or B–X is limited and the analysis had to be carried out by conventional trial-and-error methods which are as unnecessary to describe as they were tedious to perform. In the end, a fairly complete analysis of the 0, 0 bands of both systems for both Ga^{69}F and Ga^{71}F was obtained. The lines of the Ga^{69}F bands are given in table 1, and observed and calculated isotope separations are illustrated in figure 1.

A somewhat less complete analysis of the 0, 1 band of the B–X system for both isotopic species was also obtained. Values of $\Delta_1F_0'(J)$ for the 0, 0 and 0, 1 bands are in satisfactory agreement.

For the determination of the rotational constants, it was decided to take as primary standards the values of B_0'' derived from the 0, 0 bands of the A, B–X systems. In cases where only unresolved isotopic blends (especially in the P branches) were measured, the positions of the individual Ga^{69}F and Ga^{71}F lines were calculated from the measured blends, weighting according to the isotopic abundance and using the calculated isotope separations (figure 1). The results

Table 1. The 0, 0 Bands of the A $^3\Pi_0{}^+$, B $^3\Pi_1 -$ X$^1\Sigma^+$ Systems of Ga^{69}F.

	A $^3\pi_0{}^+$–X $^1\Sigma^-$		B $^3\pi_1$–X $^1\Sigma^+$		
J	R	P	R	O	P
6		33122·19*§			
7		21·68*§			
8		21·10*§			
9		20·56*§			
10		20·01*§			
11	33136·57*	19·52*§		33449·70*§	33441·57*§
12	37·58*	19·09*§	33459·57*§	50·01*	41·14*§
13	38·63*		60·74*	50·36*§	40·72*§
14	39·64*		61·93*§	50·67*	40·33*§
15	40·72*		62·81*§	51·07*§	39·97*§
16	41·82*		64·10*	51·41*	39·62*§
17	42·97*		65·25*	51·82*	39·27*§
18	44·06*		66·37*§	52·32*	39·03*§
19	45·25*		67·40*§	[illegible]	
20	46·43*		68·87*	53·26*	
21	47·66*		70·25§	53·80*	
22	48·86*		71·44*§	54·31*	
23	50·08*		72·57*§	54·91*	
24	51·35*		74·00*	55·50*	
25	52·69*		75·44	56·15*	
26	54·03*		76·94	56·76*	
27	55·39		78·25§	57·43*	
28				58·13*	37·45*§
29	58·07	14·71*		58·80*	37·45*§
[illegible]	[illegible]	14·71*	82·60	59·57*§	37·45*§
[illegible]	[illegible]	14·71*	84·15	[illegible]	
[illegible]	62·48	14·71*	85·65	61·13*	
[illegible]	[illegible]	14·71*	87·23§	61·91*§	
[illegible]	[illegible]	14·71*	88·75§	62·81*§	
[illegible]	[illegible]			[illegible]	
[illegible]	68·59		92·00§	64·55*	
[illegible]	70·11		93·56	65·41*	
[illegible]	[illegible]		95·30	66·37*§	
39	73·40		97·03	67·40*§	
40	75·02			68·32*	39·03*§
41	76·62		500·54	69·39*	39·27*§
42	78·30		02·21	70·46	39·62*§
43	80·05		04·16	71·44*§	39·97*§
44	81·78		05·90	72·57*§	40·33*§
45	83·50		07·78	73·69	40·72*§
46	85·27		09·69	74·87	41·14*§
47	87·06		11·50	76·06	41·57*§
48	88·95		13·45	77·28	42·05*
49	90·73		15·32	78·47	42·56*
50	92·64		17·46		43·04*
51	94·49	19·09*§		80·97	43·58*
52	96·44	19·52*§	21·27	82·25§	44·13*
53	98·31	20·01*§	23·29	83·57	44·71*
54	200·28	20·56*§	25·53	84·95	45·35*
55	02·31	21·10*§	27·63	86·31	45·98*
56	04·30	21·68*§	29·71	87·67	46·64*
57	06·28	22·19*§	31·79	89·08	47·39*
58	08·37	22·78*	33·93	90·51	48·15*
59	10·42	23·42*	36·24	92·00§	48·86*
60	12·44	24·06*	38·41	93·63§	49·70*§
61	14·57	24·72*	40·63	94·98§	50·36*§
62	16·77	25·41*	42·98	96·59§	
63	18·93	26·15*	45·25	98·05	
64	21·05	26·84*	47·52	99·75	
65	23·34	[illegible]			
66	25·56	[illegible]			
67	27·79	[illegible]			
68	29·94	[illegible]			
69	32·36	31·05*			
70	34·75	31·91*			
71	37·12	[illegible]			
72	39·23	[illegible]			
73	41·78	[illegible]			
74		[illegible]			

* unresolved isotope doublet.

§ blended line.

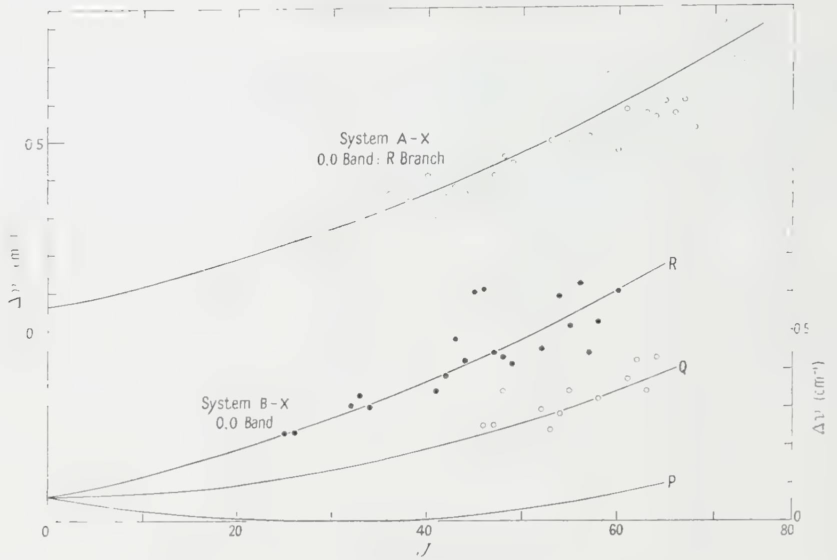

Figure 1. Isotope separations $\Delta\nu$ cm^{-1} in the 0, 0 bands of the A, B–X systems.

are given in figure 2, in which are plotted values of $\Delta_2 F_0''(J)/(J+\frac{1}{2})$ against $(J+\frac{1}{2})^2$ for Ga^{69}F and Ga^{71}F. The lines are drawn with slopes $8D''$ calculated according to Kratzer's relation $D = 4B^3/\omega^2$.

In the B–X system it was, in addition, possible to assign a number of lines to the strong Q branches of the 1, 2 and 2, 3 bands, and use was made of these in determining the rotational constants. Neglecting terms in ΔD, we have

$$\nu(Q) = \nu_0 + (B'^{\mathrm{d}} - B'')J(J+1).$$

Values of $\nu(Q) - 0{\cdot}015\,J(J+1)$ are plotted against $J(J+1)$ in figure 3.

The results are as follows:

(i) From figure 2:
Ga^{69}F: $B_0'' = 0{\cdot}3576_4$, assuming $D_0'' = 4{\cdot}7_8 \times 10^{-7}$ cm^{-1};
Ga^{71}F: $B_0'' = 0{\cdot}3555_1$, assuming $D_0'' = 4{\cdot}7_2 \times 10^{-7}$ cm^{-1}.

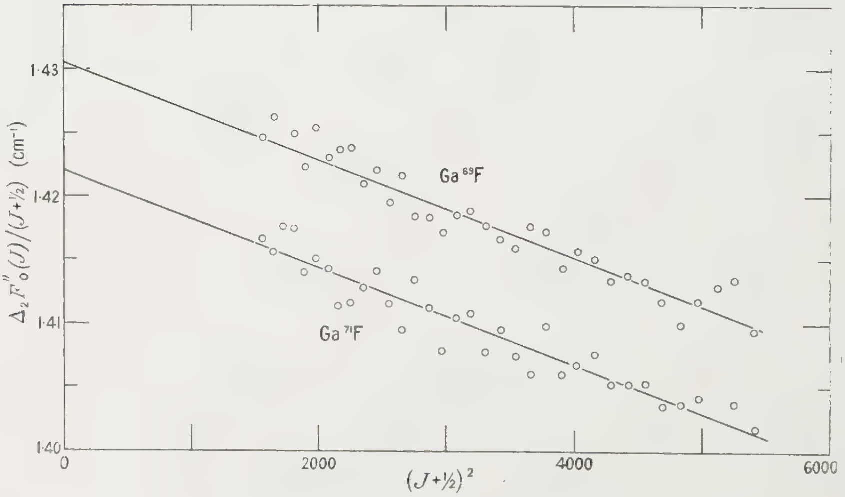

Figure 2. $\Delta_2 F_0''(J)/(J+\frac{1}{2})$ plotted against $J+\frac{1}{2}$ for Ga^{69}F and Ga^{71}F.

(ii) From the Q branches:

	$Ga^{69}F$		$Ga^{71}F$	
v', v''	ν_0	ΔB	ν_0	ΔB
0, 0	33448·12	0·01236	33448·05	0·01230
0, 1	32832·36	0·01518	32834·18	0·01506
1, 2	32880·69	0·01502	32882·38	0·01489
2, 3	32928·69	0·01477		

(iii) From the values of $R(J-1)+P(J)$ for the A–X 0, 0 band:
for $Ga^{69}F$: $\nu_0 = 33126{\cdot}2$, $\Delta B = 0{\cdot}0114_0$ cm^{-1}.

(iv) From the differences
$\{R_{B-X}(J-1) - R_{A-X}(J-1)\}_{0,0} = \{P_{B-X}(J+1) - P_{A-X}(J+1)\}_{0,0}$:
for $Ga^{69}F$: $(\Delta\nu_{B-A})_{0,0} = 321{\cdot}95$ cm^{-1}, $(B_0{}^c)_B - (B_0)_A = 0{\cdot}00105$ cm^{-1}.

(v) The Λ-type doubling in B $^3\Pi_1$ is small, and the measurements are hardly good enough to determine the trend with J. If it is assumed that the doubling varies as $J(J+1)$, then roughly

$$\epsilon/2 = 6 \times 10^{-5} J(J+1), \text{ or } q = B^c - B^d = 6 \times 10^{-5}\ \text{cm}^{-1}.$$

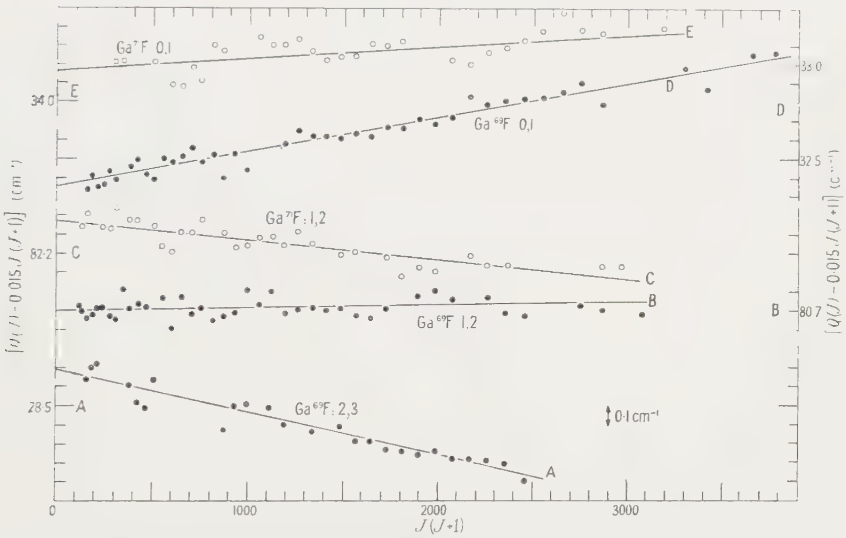

Figure 3. $\{Q(J) - 0{\cdot}015\, J(J+1)\}$ plotted against $J(J+1)$ for the 0, 1 and 1, 2 and 2, 3 bands of $Ga^{69}F$ and for the 0, 1 and 1, 2 bands of $Ga^{71}F$.

This may be compared with the still less reliable value $q = 5 \times 10^{-5}$ cm^{-1} which may be derived from the measurements on the InF bands.

The rotational constants may be derived as follows:

State $X^1\Sigma^+$

From (i) and (ii),

for $Ga^{69}F$: $B_v = 0{\cdot}3590_5 - 0{\cdot}0028_2(v+\frac{1}{2})$;
for $Ga^{71}F$: $B_v = 0{\cdot}3568_9 - 0{\cdot}0027_6\,(v+\frac{1}{2})$.

If we use the isotopic relations to calculate the constants for $Ga^{71}F$ from those of $Ga^{69}F$, we obtain, with $\rho = 1{\cdot}00305_5$, $B_v = 0{\cdot}3568_7 - 0{\cdot}0027_9\ (v+\frac{1}{2})$, in satisfactory agreement with the values determined directly.

State $\text{B}\,{}^3\Pi_1$

From (i) and (ii),

for Ga^{69}F: $B_0{}^{\text{d}} = 0{\cdot}3700_0$, $B_1{}^{\text{d}} = 0{\cdot}3670_2$, $B_2{}^{\text{d}} = 0{\cdot}3639_5\ \text{cm}^{-1}$.

Thus, $B_v{}^{\text{d}} = 0{\cdot}3715_1 - 0{\cdot}0030_2\,(v + \tfrac{1}{2})$.

If $q = 6 \times 10^{-5}\ \text{cm}^{-1}$, $B_e = 0{\cdot}3715_7$ and $B_e = 0{\cdot}3715_1\ \text{cm}^{-1}$.

For Ga^{71}F: $B_0{}^{\text{d}} = 0{\cdot}3677_7$ and $0{\cdot}3677_4$, $B_1{}^{\text{d}} = 0{\cdot}3647_8\ \text{cm}^{-1}$.

These may be compared with the values calculated from the constants of Ga^{69}F using the isotopic relations, i.e., $B_0{}^{\text{d}} + 0{\cdot}3677_8$, $B_1{}^{\text{d}} = 0{\cdot}3647_9\ \text{cm}^{-1}$.

State $\text{A}\,{}^3\Pi_{0+}$.

From (iii), for Ga^{69}F: $B_0 = 0{\cdot}3690_4\ \text{cm}^{-1}$;

From (iv) and (v), $B_0 = 0{\cdot}3690_1\ \text{cm}^{-1}$.

We conclude that $B_0 = 0{\cdot}3690_2\ \text{cm}^{-1}$.

If it is assumed that $\alpha({}^3\Pi_{0+}) \simeq \alpha({}^3\Pi_1)$, then $B_v = 0{\cdot}3705_3 - 0{\cdot}0030_2\,(v + \tfrac{1}{2})$.

The rotational constants for the state $\text{C}\,{}^1\Pi$ have been estimated from the observed R Q or P Q head separations, using the new values of the rotational constants for the ground state. The vibrational constants for all the states have also been evaluated using the accurate values for the band origins obtained here. The constants are summarized in table 2.

Table 2. Constants for the Electronic States of Ga^{69}F †

State	T_0	ω_e	$x_e\omega_e$	$y_e\omega_e$	B_e	α_e	r_e (Å)
$\text{C}\,{}^1\Pi$	47324·1	$542{\cdot}3_5$	$9{\cdot}5_5$	$-0{\cdot}6_0$	$(0{\cdot}358_{05})$	$(0{\cdot}0053_5)$*	1·778
$\text{B}\,{}^3\Pi_1$	$33448{\cdot}1_2$	662·1	1·45	$-0{\cdot}43_3$	$0{\cdot}3715_4$	$0{\cdot}0030_2$	$1{\cdot}745_3$
$\text{A}\,{}^3\Pi_{0+}$	$33126{\cdot}1_7$	$663{\cdot}0_2$	2·18	$-0{\cdot}3_1$	$0{\cdot}3705_3$	$(0{\cdot}0030_2)$	$1{\cdot}747_6$
$\text{X}\,{}^1\Sigma^+$	0	622·2	3·2	—	$0{\cdot}3590_5$	$0{\cdot}0028_2$	$1{\cdot}775_4$

* $-0{\cdot}0003\,(v + \tfrac{1}{2})^2$.

With the new vibrational constants for $\text{C}\,{}^1\Pi$, the vibrational levels are found to converge to a dissociation limit at 51170 cm^{-1} above $v'' = 0$. If this state correlates with $\text{In}\,({}^2\text{P}_{3/2}) + \text{F}\,({}^2\text{P})$, then $D_0'' = 143{\cdot}_3 \pm 0{\cdot}6$ kcal, where the limits correspond to the uncertainty in the state, ${}^2\text{P}_{3/2}$ or ${}^2\text{P}_{1/2}$, of the fluorine atom.

§ 3. DISCUSSION

Two points arising out of this work may be briefly discussed. The first relates to the values of the internuclear distances in the ground states of GaF and related molecules. Present information is summarized in table 3. It will be seen that the new value for GaF fits well into the sequence AlF, GaF, InF. The figures in this table also indicate that, as found by Honig *et al.* (1954) for the ionic, alkali-metal halides, there are deviations of the order of 0·03 Å from the additivity rule. As a matter of practical interest, we can also conclude that at least one of the values r_e(InI) or r_e(TlI) is seriously in error: one would guess that r_e for InI should be about 2·75 Å. Likewise, an earlier estimate for r_e(TlF) at $2{\cdot}07_5$ Å seems to be somewhat too small: we should predict $r_e \sim 2{\cdot}15$ Å for this molecule.

Secondly, the properties of the excited triplet states of the fluorides are of some interest. For both GaF and InF, the case-*a* relations

$$B_{\text{eff}}({}^3\Pi_1) = B_v;\quad B_{\text{eff}}({}^3\Pi_0) = B_v(1 - 2B_v/A)$$

---

† In the corresponding table for InF (Barrow, Glaser and Zeeman 1955) the entry $29935{\cdot}5_8$ should read $30465{\cdot}5_2$.

are approximately fulfilled, though much more closely for GaF than for InF. Thus

	$\{B_e(^3\Pi_1) - B_e(^3\Pi_{0^+})\}$ obs	calc
GaF	$0{\cdot}0010_1$	$0{\cdot}00086$
InF	$0{\cdot}0004_5$	$0{\cdot}00019$

For TlF, this relation no longer holds, even qualitatively, for

$$B_0(\text{A}, 0^+) > B_0(\text{B}, 1).$$

The ground states of these molecules arise from the configuration

$$\ldots.(z\sigma)^2(y\sigma)^2(w\pi)^4(x\sigma)^2,\ {}^1\Sigma^+$$

and the $^3\Pi$ states presumably from

....[illegible] $^3\Pi_r$, $^1\Pi$.

Table 3. Internuclear Distances r_e'' (Å)

	F	Δr	Cl	Δr	Br	Δr	I
B	$1{\cdot}262$	$(0{\cdot}454)$	$1{\cdot}716$	$(0{\cdot}171)$	$1{\cdot}88_7{}^a$		—
Al	$1{\cdot}65_4{}^b$	$(0{\cdot}49)$	$2{\cdot}14^c$	$(0{\cdot}16)$	$2{\cdot}295$		—
Ga	$1{\cdot}775$	$(0{\cdot}433)$	$2{\cdot}208^d$		—		—
In	$1{\cdot}985^e$	$(0{\cdot}416)$	$2{\cdot}401_2{}^f$	$(0{\cdot}1_{40})$	$2{\cdot}540_8{}^f$	$(0{\cdot}3_2)$	$2{\cdot}86^h$
Tl	—		$2{\cdot}541^g$	$(0{\cdot}1_4)$	$2{\cdot}68^h$	$(0{\cdot}1_9)$	$2{\cdot}87^h$

Notes: The values have been taken from Herzberg (1950) except where otherwise stated:

a, value of α'' uncertain.

b, Barrow, Johns and Smith (1956).

c, the values of B'' observed are from B_{11}'' to B_{16}'': the extrapolation to B_e'' is about 10% of B_e''. α'' is given as $0{\cdot}002\ \text{cm}^{-1}$, but the measurements suggest $\alpha'' = 0{\cdot}0016\ \text{cm}^{-1}$.

d, there are some doubtful points about the rotational analysis: see reference under **e.**

e, Barrow, Glaser and Zeeman (1955).

f, from the microwave spectra: Barrett and Mandel (1955).

g, from molecular-beam electric resonance: Carlson *et al.*, (1952). Kadesch *et al.* (1956) find $r_e'' = 2{\cdot}466$Å.

h, from electron diffraction: see Herzberg (1950).

Table 4 gives values of $\omega(^3\Pi_1)/\omega(^1\Sigma^+)$ and also of the multiplet splitting constants, which are compared with those for the metal atoms ... $s^2p\,(^2P)$.

Table 4.

Molecule	$\omega(^3\Pi_1)/\omega(^1\Sigma^+)$	a_{atom}	a_{mol}	$a_{\text{mol}}/a_{\text{atom}}$
BF	$0{\cdot}945$	$10{\cdot}_7$	(14)	$(1{\cdot}3)$
AlF	$1{\cdot}033$	75	93	$1{\cdot}24$
GaF	$1{\cdot}064$	551	644	$1{\cdot}17$
InF	$1{\cdot}069$	1475	1617	$1{\cdot}10$
TlF	$0{\cdot}759$	5195	3378	$0{\cdot}65$

We conclude that the $^3\Pi$ states of AlF, GaF and InF are very closely related, rather near to Hund's case *a*, with some tendency towards case *c* coupling for InF. However, it is not until we come to TlF that the similarity in properties is lost and states are obtained which are more properly described as 1 and 0^+. For BF the analogous triplet state, a $^3\Pi$, approaches case-*b*: we estimate $A = +7\ \text{cm}^{-1}$. Paul and Knauss (1938) give $A = -17{\cdot}9\ \text{cm}^{-1}$ (see, however, Dodsworth and Barrow 1955). It is hoped that rotational analyses of the triplet bands of BF now in progress will settle this question.

References

Barrett, A. H., and Mandel, M., *Phys. Rev.*, 1955, **99**, 666.

Barrow, R. F., Glaser, D. V., and Zeeman, P. B., 1955, *Proc. Phys. Soc.* A, **68**, 962.

Barrow, R. F., Jacquest, J. A. T., and Thompson, E. W., 1954, *Proc. Phys. Soc.* A, **67**, 528.

Barrow, R. F., Johns, J. W. C., and Smith, F. J., 1956, *Trans. Faraday Soc.*, **52**, 913.

Carlson, R. O., Lee, C. A., and Fabricand, B. P., 1952, *Phys. Rev.*, **85**, 784.

Dodsworth, P. G., and Barrow, R. F., 1945, *Proc. Phys. Soc.* A, **68**, 824.

Herzberg, G., 1950, *Molecular Structure* : I : *Spectra of Diatomic Molecules* (New York : van Nostrand).

Honig, A., Mandel, M., Stitch, M. L., and Townes, C. H., 1954, *Phys. Rev.*, **96**, 629.

Kadesch, R. R., Moldenhauer, J. C., and Winans, J. G., 1956, *Spectroscopia Molecular*, **5**, 18.

Paul, F. W., and Knauss, H. P., 1938, *Phys. Rev.*, **54**, 1072.

Welti, D., and Barrow, R. F., 1952, *Proc. Phys. Soc.* A, **65**, 629.

The Electronic Structure and Spectra of some Nitrogen Heterobenzenes

By R. McWEENY and T. E. PEACOCK
Department of Physical Chemistry, King's College, Newcastle

MS. received 16th July 1956

Abstract. The π-electron charge distributions and spectra are calculated for some nitrogen heterobenzenes, using self-consistent molecular orbital theory with configuration interaction. A single parameter is introduced to account for the difference in electron affinity between nitrogen and carbon atoms in the molecular framework. The assumption that this parameter is insensitive to changes in environment of the nitrogen atom is found to be satisfactory. There is a close (though superficial) resemblance between the present approach and that originally suggested by Hückel, elaboration being necessary mainly in discussion of spectra.

§ 1. Introductory Survey

In this paper we shall discuss the mono- and di-substituted benzenes; pyridine, pyridazine, pyrimidine and pyrazine, using self-consistent field molecular orbital theory. In order to place this approach in its context it is useful to distinguish three phases in the development of the molecular orbital theory of the π-electronic structure of aromatic molecules.

The Hückel theory (Hückel 1931), although based conceptually on the atomic self-consistent field method, is an essentially empirical theory, whose underlying assumptions are well known. Here it need only be noted that the one-electron self-consistent field Hamiltonian, referred to a basis of atomic 2p orbitals, is characterized by empirically determined elements, α (the 'Coulomb' integral) being associated with a carbon atom and β (the 'resonance' integral) with a C–C bond, that α, β are assumed independent of molecular environment, and that the introduction of a hetero-atom is represented merely by a change of α at the given atomic site, the change, δ, being assumed characteristic of the hetero-atom. This crude theory has been of great value in discussing not only ground state properties but also electronic spectra, even though a transition energy is naively identified with the energy change of a single electron as it jumps from one orbital to another (electron interaction effects being ignored). Since, however, the charge shifts induced by foreign atoms invalidate the Hückel assumptions, calculations on hetero-cyclic systems have always been open to suspicion. Efforts to improve the theory have been made, for instance by Wheland and Pauling (1935) who assumed some apparently more reasonable pattern of self-consistent field α's in the locality of a hetero-atom, 'sharing out' δ over a number of centres. As might be expected, it has not proved possible to obtain unique and completely satisfactory values for the parameters; thus, for nitrogen, δ-values range from $\delta = 2{\cdot}0\beta$ in the older work to $\delta = 0{\cdot}6\beta$ (Chalvet and Sandorfy 1949, Löwdin 1951, Davies 1955). And it has recently been shown (McWeeny 1956 b) that the practice initiated by Wheland and Pauling is theoretically unsound.

The second phase of development is marked by the appearance of entirely *non*-empirical methods in which a complete Hamiltonian is considered, wave functions are set up for ground and excited state molecular orbital configurations, and *total* π-electron energies are calculated (after a tedious evaluation of all integrals over the basic set of 2p atomic orbitals). This makes possible, in particular, a more realistic quantitative discussion of spectra. It is, moreover, possible to make a more genuine self-consistent field calculation of the 'best' molecular orbitals (Roothaan 1951) and further to improve matters by allowing functions of like symmetry, but in general from different configurations, to mix. Unfortunately, the results of such calculations have on the whole been extremely disappointing.

More recently, however, this theoretically more satisfactory approach has been modified (Moffitt 1954, Pariser and Parr 1953), *ab initio* evaluation of the dominant basic integrals giving way to estimations based upon experimental ionization potential and electron affinity data. Besides overcoming the purely mathematical difficulty of handling sufficiently accurate orbitals, this makes it possible to allow in some measure for effects which can be distinguished physically (e.g. electron correlation, 'polarization' of the framework) but which cannot be introduced precisely within the existing mathematical framework. At the same time, so much simplification is achieved by the consistent neglect of many small integrals that self-consistent field and many-configuration calculations present little difficulty (see, for example, Pople 1953, 1955, Pariser and Parr 1953), and this simplification is also supported by theoretical considerations (McWeeny 1956 b). The results of these rather complete, but still *semi*-empirical, calculations have so far been remarkably satisfactory. In particular, self-consistent field calculations on pure hydrocarbons lead to almost uniform charge distributions (Pople 1953), providing some explanation of the success of Hückel theory in this field: and the interaction of degenerate excited configurations has provided a much more complete and satisfying interpretation of the main features of π-electron spectra (e.g. Dewar and Longuet-Higgins 1954, Pople 1955).

It now remains to be shown that the semi-empirical approach can lead to an equally satisfactory explanation of the structure and spectra of *hetero*-aromatic molecules. The present work, which is directed towards this end, employs an improved self-consistent field method (McWeeny 1956 a, b) in determining the charges and bond orders in nitrogen substituted benzenes; the three main bands in the spectrum of each molecule are then predicted by a configuration interaction analysis. An important secondary aim is to preserve a close parallel with the original Hückel theory, showing that the nitrogen atom is still characterized essentially by one parameter which, like δ, measures its electron affinity relative to carbon, and that this parameter (unlike δ) is indeed independent of charge shifts and molecular environment. Calculations on the mono- and di-substituted benzenes, for which abundant experimental data exist, provide a stringent test of this possibility.

§ 2. FORMULATION: METHOD OF CALCULATION

Using a one-determinant approximation to the ground state, the n doubly occupied molecular orbitals $A, B, C, \ldots$ may be expressed in terms of the m basic atomic orbitals $a, b, c, \ldots$ by $\mathbf{A} = \mathbf{a}\,\mathbf{T}$, where $\mathbf{A}$ and $\mathbf{a}$ are abbreviations for the row matrices $(ABC\ldots)$ and $(abc\ldots)$ and $\mathbf{T}$ is an $m \times n$ matrix of coefficients. The matrix of charges and bond orders is then $\mathbf{P} = 2\mathbf{R}$, where $\mathbf{R} = \mathbf{T}\mathbf{T}^{\dagger}$. With an appropriate decomposition into basic quantities (cf. Pople 1953) the matrix elements of the self-consistent field Hamiltonian h^{F} may be written (for a full discussion see McWeeny 1956 b)‡

$$\left.\begin{aligned} \alpha^{F}_{r}\ (=h^{F}_{rr}) &= \delta\omega_r + (R_{rr}\gamma_{rr} - \tfrac{1}{2}\gamma_{C}^{(0)}) + \sum_{s \neq r}(2R_{ss} - Z_s)\gamma_{rs} \\ \beta^{F}_{rs}\ (=h^{F}_{rs}) &= \beta_{rs} - R_{rs}\gamma_{rs}. \end{aligned}\right\} \qquad \ldots\ldots(1)$$

Here γ_{rs} is the Coulomb repulsion (rr, ss) between electrons in orbitals r and s, β_{rs} is the usual (bare framework) resonance integral $(r\,|\,h\,|\,s)$, and $\delta\omega_r = \omega_r - \omega_C$ where ω_r measures the electron affinity of the single framework ion at r (a more useful quantity than α_r—which depends on the whole molecule) and takes the value ω_C for a carbon atom: $\gamma_C^{(0)}$ is the value of γ_{rr} for a carbon atom (more generally we shall use $\gamma_{CC}^{(j)}$ for the γ_{rs} of jth carbon neighbours, etc.) and Z_s is the number of π electrons contributed by atom s. The energy zero is then such that $\alpha^{F}_{r} = 0$ for a carbon atom in an alternant hydrocarbon. It is, moreover, convenient to work in units of $\beta = \beta^{F}_{CC}$ (benzene), the self-consistent field resonance integral for a C–C bond in benzene: and with this choice of unit the quantities α^{F}_{r} and β^{F}_{rs} will in general differ only slightly from their Hückel counterparts (0 for a carbon atom and 1 for a C–C bond). When the carbon atom r is replaced by a hetero-atom, Hückel theory replaces the zero by δ_r: and it has been pointed out (McWeeny 1956 b) that a reasonable correspondence between the Hückel and self-consistent field theories is obtained by making the identification

[illegible] $(Z$ [illegible]$)$. ......(2)

At this point it should perhaps be stressed that the approximate validity of (1) is associated with the fact that orbitals $a, b, c, \ldots$ *can be found* such that (rs, tu) is very small unless $r = s$ and $t = u$. It must be borne in mind, both in estimating integrals and in making physical predictions, that $a, b, c, \ldots$ *cannot* be regarded as ordinary atomic 2p orbitals. Orbitals of the required type have in fact been constructed (Hall 1954, McWeeny 1955 a) and corresponding non-empirical values of the integrals $\gamma_{CC}^{(2)}, \gamma_{CC}^{(3)}$ will here be adopted. For $\gamma_C^{(0)}$ and $\gamma_{CC}^{(1)}$ however, which represent repulsions between electrons close together, we accept the reduced values suggested by Pariser (1956), reducing the nitrogen integral $\gamma_N^{(0)}$ in a similar way. The resonance integrals β_{CC}, β_{CN} will be taken from Pariser and Parr (1953), those for more distant neighbours being neglected: and it will be assumed that $\gamma_{CN}^{(r)} = \gamma_{CC}^{(r)}\ (r \neq 0)$. With these values, β^{F}_{CC} for benzene is $-4{\cdot}79$ ev and with this energy unit we find

$$\gamma_C^{(0)} = 2{\cdot}380 \qquad \gamma_N^{(0)} = 2{\cdot}672 \qquad \gamma_{CC}^{(1)} = 1{\cdot}593 \qquad \gamma_{CC}^{(2)} = 1{\cdot}148$$
$$\gamma_{CC}^{(3)} = -1{\cdot}044 \qquad \beta_{CC} = 0{\cdot}500 \qquad \beta_{CN} = 0{\cdot}538.$$

This leaves one parameter, $\delta\omega_N$, whose choice completely determines all our predictions and whose non-empirical calculation will not be attempted: the value provisionally accepted will be $\delta\omega_N = 0{\cdot}35$ (i.e. $-1{\cdot}68$ ev).

We shall now calculate, for each molecule, a self-consistent ground state (i.e. the self-consistent field Hamiltonian and the bonding matrix **P**) and, secondly, the first few singlet and triplet excited levels. The self-consistent field method is fully explained elsewhere (McWeeny 1956 a, b) and requires no comment. The calculation of the excited states requires configuration interaction and is similar to that made by Pople in the case of alternants: a slightly more general formalism is, however, required.‡ For this purpose we use $(A)(B)$.. to denote the columns of atomic orbital coefficients representing the molecular orbitals A B, . . and (AB) to denote the column whose rth element is the product of corresponding elements§ of (A) and (B); then the energies (relative to the ground state) of the singlet and triplet functions of the configuration in which an electron has been excited from orbital I into orbital K are given by

---

‡ The interaction term $(r\,|\,v_s\,|\,r)$ (McWeeny 1956 b) will here be approximated by $-Z_s\gamma_{rs}$: this seems to be preferable to the inverse distance approximation (Pople 1953).

$$^{1,3}E_{I\to K}=(I\to K\,|\,H\,|\,I\to K)=\epsilon_K-\epsilon_I-[(II)^\dagger(\gamma)(KK)-(IK)^\dagger(\gamma)(IK)] \pm(IK)^\dagger(\gamma)(IK) \quad \ldots\ldots(3)$$

where ϵ_K, ϵ_I are orbital energies and (γ) is the matrix of Coulomb integrals γ_{rs}. The inter-configurational matrix elements for all other cases may be written in a similar way

$$^{1,3}(I\to K\,|\,H\,|\,J\to L)=-[(IJ)^\dagger(\gamma)(KL)-(LJ)^\dagger(\gamma)(KI)]\pm(LJ)^\dagger(\gamma)(KI). \quad \ldots\ldots(4)$$

Owing to the existence of symmetry in all the molecules considered the configuration functions interact only in pairs. For the same reason the dimensionality of the matrix self-consistent field equations is also reducible, and in practice it is most convenient to work throughout in terms of symmetry orbitals, using transformed analogues of the equations (1) (cf. McWeeny 1956 a, p. 501).

§ 3. Results : Discussion

3.1. *The Ground State*

Calculations were made for values of $\delta\omega_{\mathrm{N}}$ in the range 0·2 to 0·75, the iterative method employed making it a particularly simple matter to correct the $\mathbf{R}$-matrix and self-consistent field Hamiltonian directly, without recalculation of the self-consistent field orbitals, after any change of parameters. Some individual orbitals are of course required in the excited state calculations: these were obtained by the steepest descent method (McWeeny 1956 a, Appendix I) from Hückel first approximations.|| The most satisfactory agreement with experiment resulted when $\delta\omega_{\mathrm{N}}\simeq 0{\cdot}35$ and this value was therefore provisionally adopted.

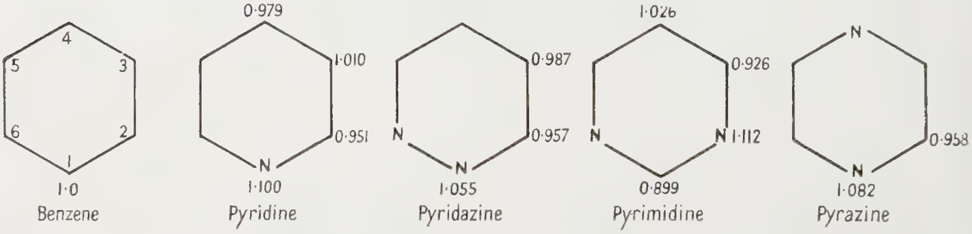

Figure 1. Self-consistent charges.

---

‡ This is a development from McWeeny (1956 b). An almost identical matrix formalism has recently been adopted independently by Pariser (1956).

§ Generally, the *second* factor (i.e. the element from (B)) should be starred, and a dagger indicates starring and transposition.

|| The simple method sometimes leads to an undesired eigenvector. The undesired solution $\mathbf{c}_r$ (with eigenvalue ϵ_r) may effectively be removed by using a revised Hamiltonian $\mathbf{h}-\epsilon_r\mathbf{c}_r\mathbf{c}_r^\dagger$.

The diagonal elements of **P**, which are the Coulson charges, are indicated for each molecule in figure 1. Again it must be stressed that the 'formal' charges represent the populations of *modified* atomic orbitals, which are neither well-localized nor centro-symmetrical, and that it would be unwise to employ them, without further analysis, in estimating dipole moments etc. (for a full discussion see McWeeny 1951, 1955 b). For this reason, such applications (along with the calculation of transition moments) will not be taken up at this stage. Nevertheless the elements of **P** undoubtedly have a fundamental bearing on the behaviour of the molecule (McWeeny 1956 b), besides indicating in a general way the disposition of charge. Two useful conclusions emerge:

(i) Using a 'corresponding' Hückel model with

$$\delta = \delta\omega_N + \tfrac{1}{2}(\gamma_N^{(0)} - \gamma_C^{(0)}) = 0{\cdot}20,$$

the charges given in figure 1 are reproduced to within one or two units in the second decimal place.

(ii) The shifts in the di-substituted molecules are almost exactly given by superimposing the effects of the separate nitrogens: so the shifts are large if the nitrogens are meta to one another but are diminished if they are ortho or (to a lesser extent) para.

A third conclusion follows on examination of the self-consistent field Hamiltonian matrices. The diagonal elements of $\mathbf{h}^F$, the (α^F)'s, are given in figure 2 and should be compared with the Hückel elements, $\alpha^F = 0{\cdot}20$ (nitrogen) $= 0$ otherwise. On the other hand, deviations from the Hückel resonance integrals ($\beta^F = 1$ for r, s neighbours, $= 0$ otherwise) are negligible, except that for para positions $\beta_{rs}{}^F \simeq -0{\cdot}17$. Moreover the deviations introduced by different nitrogens are again roughly additive: it might in fact be said that:

(iii) The corresponding Hückel model may be refined by slightly modifying the δ-values at and about a nitrogen substituent, exactly as in pyridine (figure 2), and assuming that *each* nitrogen makes its own pattern of changes. In addition a resonance integral of approximately $-0{\cdot}17$ should be adopted between para positions.

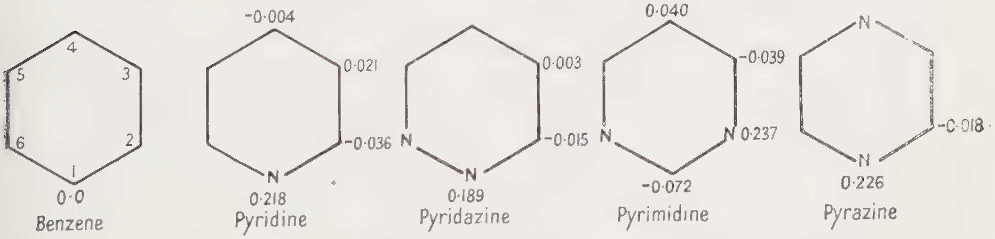

Figure 2. Self-consistent Coulomb integrals ($\delta\omega_N = 0{\cdot}35$).

On balance, the results provide a surprising justification for Hückel's original assumptions rather than for those of Wheland and Pauling. It seems possible that quite good approximations to true self-consistent field results might be obtained, even for more elaborate nitrogen hetero-cyclics, along these lines.

The ground state results admit one direct numerical comparison between experiment and theory, the ionization potential usually being estimated as the negative of the highest occupied orbital energy. In dealing with absolute energies it is necessary to fix ω_C by appeal to the result for benzene: the ionization potentials for the hetero-cyclics are then found to be (compared with $I_{\text{benzene}}=9{\cdot}42$ ev) $I_{\text{pyridine}}=9{\cdot}50$, $I_{\text{pyridazine}}=9{\cdot}64$, $I_{\text{pyrimidine}}=9{\cdot}60$, $I_{\text{pyrazine}}=9{\cdot}40$ ev. Unfortunately, experimental results are available only for pyridine ($I=9{\cdot}70$ ev; Omura, Baba and Hagasi 1955), and in any case the first order theory invoked (Koopman's theorem) is probably inadequate for the prediction of such small differences. These matters are being investigated elsewhere.

3.2. *Excited States*

The most satisfactory comparison between experiment and theory is undoubtedly provided by an analysis of the spectra. All previous work on hetero-cyclics has been concentrated on fitting the first singlet transition and explaining the observed energy sequence pyrazine < benzene < pyridine < pyridazine < pyrimidine. In the first place however it seems more important to explain why all these benzene derivatives have spectra which so closely resemble that of the parent molecule, consisting of the three main peaks often designated by α, p and β, β' (Clar 1941, Klevens and Platt 1949). The simple Hückel theory is unable to interpret the spectrum even of the pure hydrocarbon, where the highest occupied and lowest unoccupied orbitals are each degenerate: but (see Goeppert-Mayer and Sklar 1938, Dewar and Longuet-Higgins, 1954, Pople 1955) the admission of configuration interaction gives a satisfactory interpretation of the splitting into three main bands. On the other hand, the presence of one or two nitrogen atoms removes the benzene degeneracy and it might have been hoped that even a Hückel picture would be of some value. In fact, however, even when self-consistent field orbitals are used and electron interaction is properly included, one-configuration functions fail to give an adequate description of the excited states. Turning to figure 3, it is seen how the situation is completely restored when configuration interaction is admitted. These results should be compared with those for benzene which are given in figure 4, computed with similar parameter values.

In order fully to understand the correspondence between the results for the hetero-benzene and benzene itself, it is instructive to re-label the molecular orbitals A, B, C, . . . in order to emphasize the *alternant*‡ character of the parent molecule. For a general alternant the occupied orbitals might be labelled $A, B, \ldots$, going downwards from our present energy zero; the unoccupied orbitals, A', B', . . . would then be symmetrically located on the upper side of the energy zero and any pair K and K' would differ merely by a sign change in the coefficients of one set of atomic orbitals. We shall use the same notation for the *substituted* alternant in the sense that K will mean that orbital which goes over into K of the parent hydrocarbon as the substituents, regarded as a perturbation, are removed: but this will not generally imply that $\ldots B, A, A', B', \ldots$ lie in ascending energy order.

Now for an alternant hydrocarbon the one-configuration functions $\Phi(B\rightarrow A')$ and $\Phi(A\rightarrow B')$ are degenerate and therefore mix equally, explaining the α and β bands, while $\Phi(A\rightarrow A')$ and $\Phi(B\rightarrow B')$ are usually non-degenerate and separately can account for the p and β' bands (Dewar and Longuet-Higgins 1954, Pople 1955). In the case of the substituted molecule it is important to know whether a parallel assignment will depend upon the *energies* of the orbitals (A, A', B, B') or upon their unperturbed *forms* in the parent molecule. For instance: Is the

---

‡ For treatments of alternant molecules see, for example, Coulson and Rushbrooke (1940) and Pople (1953).

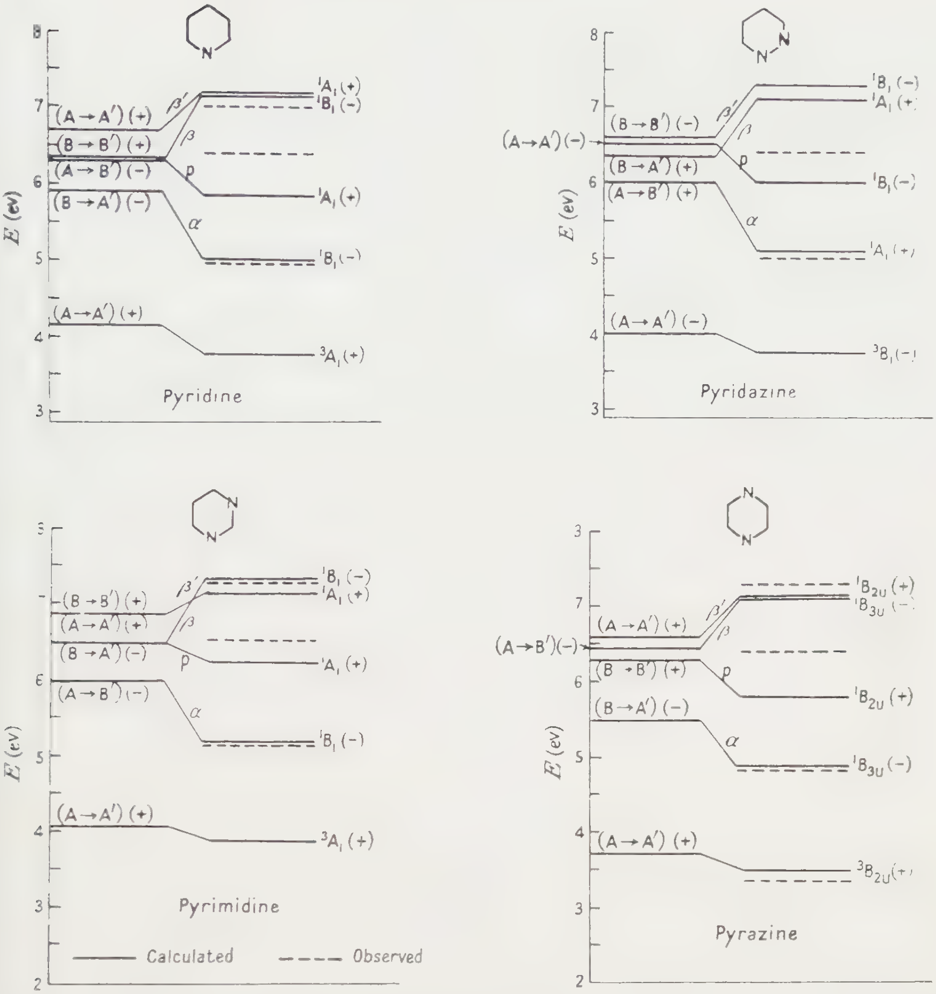

Figure 3. Excited states of nitrogen hetero-benzenes (in each case relative to the ground state as energy zero).

observed p band in a hetero-molecule to be associated with an electron jump from the highest occupied to the lowest unoccupied orbital ?—or to a jump between orbitals which go over into A and A' in the parent ? Our results shed some light on this question since they refer to systems in which the 'normal' energy order $(\ldots B, A, A', B', \ldots)$ is disturbed by substitution. In benzene itself, of course, there is an additional degeneracy between $\Phi(A \rightarrow A')$ and $\Phi(B \rightarrow B')$, arising from the fact that $\epsilon_A = \epsilon_B$ and $\epsilon_{A'} = \epsilon_{B'}$ (figure 4), but in the hetero-molecules all degeneracy is resolved (figure 3). The energy order of the molecular orbitals is then of importance; using orbitals whose unperturbed forms are as shown in figure 5,‡ the order in the hetero-molecules (energy increasing) is

pyridine	A	B	A'	B'
pyridazine	B	A	B'	A'
pyrimidine	B	A	B'	A'
pyrazine	A	B	A'	B'

‡ The unperturbed forms for pyridazine differ trivially by an anticlockwise rotation through 60°.

and the symmetry about the energy zero, typical of alternants, is absent. This is easily understood, for the energies of A and A' (or of B and B') move the *same* way under the perturbations, instead of symmetrically with respect to the energy zero: and it is clear that even with initially *non*-degenerate levels a substantial perturbation could have a similar effect on the sequence of energies. Reference to figure 3, however, shows that this energy order is not in any way responsible for the general pattern of the splitting, which in every case resembles that in the parent hydrocarbon. This appears to confirm a conclusion which might have been reached on general grounds: The α, p, β and β' bands for *hetero*-substituted alternants are to be correlated pictorially with electron jumps between orbitals whose *forms* resemble those of their counterparts in the parent hydrocarbon, without regard to their energies, and the alternant character of the parent is the factor responsible for the spectral similarities of the hydrocarbon and its hetero-derivatives.

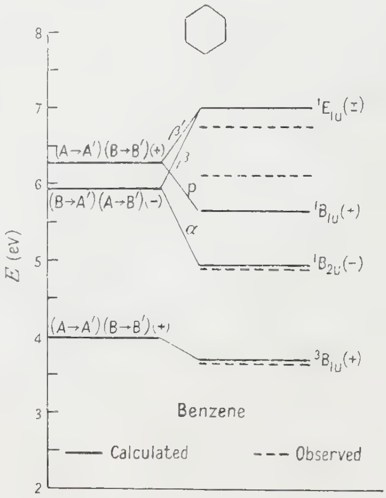

Figure 4. Excited states of benzene (relative to the ground state as energy zero).

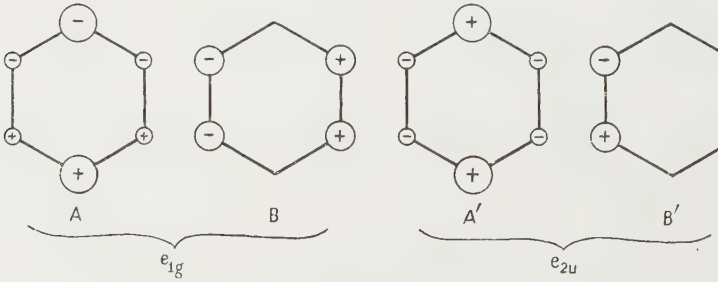

Figure 5. Forms of the orbitals (diagrammatic).

Another conclusion from figure 3 concerns the importance of configuration interaction, for in spite of the absence of degeneracies, and therefore of 'first order' interaction, there is heavy mixing wherever it is allowed by symmetry. In fact, as other writers have pointed out, it is impossible to make any clear cut distinction between first and second order configuration interaction. In particular, the functions $\Phi(A \rightarrow A')$ and $\Phi(B \rightarrow B')$, which account for the p and β' bands in a hydrocarbon, interact strongly and there is no convincing reason why this mixing should occur only in hetero-molecules. It should also be noted that the Hückel theory, which associates the first transition with the jump of an electron from the highest filled to the lowest empty orbital, does give a rough description of the α band in the hetero-benzenes. But in the general alternant (and probably, in many cases, in its hetero-derivatives) the Hückel first transition is to be correlated with the p band. This makes it clear that a too naive application of Hückel theory can easily lead to confusion in identifying even the first absorption peak and its behaviour under substitution.

Finally, quantitative agreement with experiment is seen to be as good as could reasonably be hoped. The symmetries of the states are indicated in the usual notation (see, for example, Eyring, Walter and Kimball 1944) and appear to agree with accepted assignments: to facilitate comparison a + or − has been added to indicate symmetry or antisymmetry under rotation about the in-plane axis which remains in each hetero-molecule‡ (according to which the benzene degeneracies are resolved). The observed (singlet) peaks, indicated by broken lines, are taken from Klevens and Platt (1953): the first transitions are all predicted to within 0·1 ev and their energy order, in the five molecules, is correct. The agreement is less good for the higher transitions but still satisfactory, and could no doubt be improved by a more exhaustive analysis of parameter values. The lowest triplet level is also shown in each case and agrees well with what few experimental data are at present available.

§ 4. CONCLUSION

It has been shown that the self-consistent field molecular orbital theory in its semi-empirical form can give a good account of the structure and spectra of the nitrogen hetero-benzenes, provided configuration interaction is admitted in dealing with the excited states. The introduction of a nitrogen is described essentially by means of one empirically determined parameter $\delta\omega_N$, and the assumption that $\delta\omega_N$ is characteristic of trigonally bonded nitrogen and insensitive to change of neighbours and shifts of π-electron density is justified by the success of these calculations. There is, in fact, a strong superficial resemblance between the present approach and that first proposed by Hückel (1931), and a Hückel model, with slight modifications, is capable of quite accurately reproducing the charge distribution predicted by self-consistent field theory. It is in discussion of spectra that the simple Hückel picture is most inadequate: in particular, heavy mixing of close-lying excited configurations appears to be essential to any understanding of the character and general arrangement of the excited states, and the interaction due to configurational degeneracy in a parent hydrocarbon quite evidently persists, with undiminished importance, when the degeneracy is removed by the substitution of hetero-atoms.

ACKNOWLEDGMENT

One of the authors (T. E. P.) would like to acknowledge the award of a Levin Research Studentship, during the tenure of which this investigation was carried out.

---

‡ In the case of pyrazine, the axis through the nitrogen atoms.

REFERENCES

CHALVET, P., and SANDORFY, C., 1949, *C.R. Acad. Sci., Paris*, **228,** 566.

CLAR, E., 1941, *Aromatische Kohlenwasserstoffe* 1st Edn (Berlin : Springer).

COULSON, C. A., and RUSHBROOKE, G. S., 1940, *Proc. Camb. Phil. Soc.*, **36,** 193.

DAVIES, B. W., 1955, *Trans. Faraday Soc.*, **51,** 449.

DEWAR, M. J. S., and LONGUET-HIGGINS, H. C., 1954, *Proc. Phys. Soc.* A, **67,** 795.

EYRING, H., WALTER, J., and KIMBALL, G. E., 1944, *Quantum Chemistry* (New York : Wiley).

GOEPPERT-MAYER, M., and SKLAR, A. L., 1938, *J. Chem. Phys.*, **6,** 645.

HALL, G. G., 1954, *Trans. Faraday Soc.*, **50,** 773.

HÜCKEL, E. P., 1931, *Z. Phys.*, **72,** 310.

KLEVENS, H. B., and PLATT, J. R., 1949, *J. Chem. Phys.*, **17,** 470; 1953–54 Technical Report (Pt. I), Laboratory of Molecular Structure and Spectra, Chicago, U.S.A.

LÖWDIN, P.-O., 1951, *J. Chem. Phys.*, **19,** 123.

McWEENY, R., 1951, *J. Chem. Phys.*, **19,** 1614 (Errata : *Ibid.*, **20,** 920); 1955 a, *Proc. Roy. Soc.* A, **227,** 288; 1955 b, Technical Report No. 7, Solid State and Molecular Theory Group M.I.T. (Ch. V. §8); 1956 a, *Proc. Roy. Soc.* A, **233,** 496; 1956 b, *Ibid.*, **237,** 355.

MOFFITT, W., 1954, *J. Chem. Phys.*, **22,** 1820.

OMURA, I., BABA, M., and HIGASI, K., 1955, *J. Phys. Soc. Japan*, **10,** 317.

PARISER, R., 1956, *J. Chem. Phys.*, **24,** 250.

PARISER, R., and PARR, R. G., 1953, *J. Chem. Phys.*, **21,** 466, 767.

POPLE, J. A., 1953, *Trans. Faraday Soc.*, **49,** 1375; 1955, *Proc. Phys. Soc.* A, **68,** 81.

ROOTHAAN, C. C. J., 1955, *Rev. Mod. Phys.*, **23,** 69.

WHELAND, G. W., and PAULING, L., 1935, *J. Amer. Chem. Soc.*, **57,** 2086.

The Average Neutron Total Cross Sections of Heavy Elements at Low Energy

By D. B. GAYTHER and K. P. NICHOLSON
Atomic Energy Research Establishment, Harwell, Berks.

MS. received 11*th September* 1956 *and in final form* 5*th November* 1956

Abstract. A method is developed for determining the total cross section averaged over many resonances of an element from a direct measurement of the average transmission of a thick sample. This is used to obtain the average total cross sections of fourteen elements at energies from 1 to 30 kev from transmission measurements made with the Harwell Fast Chopper. Values of the potential scattering cross section and the ratio of average neutron width to level spacing are also obtained. The variations of these quantities with atomic weight are compared with the predictions of the strong and weak coupling models of the nucleus developed by Weisskopf *et al.* The fluctuations which are observed near atomic weight 150 are in qualitative agreement with the weak-coupling theory provided the nuclear radius is $1{\cdot}45\,A^{1/3}\times10^{-13}$ cm.

§ 1. Introduction

The average behaviour of neutron total cross sections at energies below several Mev has been discussed by Feshbach, Peaslee and Weisskopf (1947) and by Feshbach and Weisskopf (1949) using a model in which the incident particle is assumed to be strongly absorbed by the target nucleus. It was found that the average total cross sections predicted with this 'strong-coupling' model did not agree with experimental results taken at energies of several Mev. In order to explain these discrepancies Feshbach, Porter and Weisskopf (1953, 1954) proposed a 'weak-coupling' model in which the incident neutron has a mean free path in nuclear matter comparable with the nuclear radius. This model shows the essential features of the measured cross sections at these energies. At energies below about 100 ev the available data also show qualitative agreement with the weak-coupling model. At intermediate energies, however, very few measurements are available which can be compared with the predictions of the two theories.

In the present experiment the average neutron total cross sections of a number of elements in the region $A\sim150$ have been measured at energies from 1 kev to 30 kev with the Harwell Fast Chopper. The results are compared with the theoretical values for each of the models. It is also shown that values of the potential scattering cross section and the ratio of average neutron width to level spacing can be obtained from these data.

§ 2. Theoretical Predictions

Using the Breit–Wigner relation, it can be shown that for s-wave neutrons ($l=0$) the neutron total cross section averaged over many resonances $\bar{\sigma}_t$ can be expressed approximately in the form

$$\bar{\sigma}_t=4\pi R'^2-\pi^3\lambda\!\!\!^{-2}\langle\Gamma_n/D\rangle^2+2\pi^2\lambda\!\!\!^{-2}\langle\Gamma_n/D\rangle, \qquad \ldots\ldots(1)$$

where λ is the wavelength of the incident neutron, Γ_n is the neutron width of a resonance, D is the spacing of the resonances, $\langle\Gamma_n/D\rangle$ is the ratio of average neutron width to average level spacing, and R' is a length of the same order of magnitude as the nuclear radius R.

In the above equation a second order term in Γ_n/D is included (Lane and Lynn, private communication) which was omitted by Weisskopf *et al.* This term is energy independent and can therefore be combined with the potential scattering cross section $4\pi R'^2$. It will be shown later that this term is numerically significant.

The form of equation (1) is fundamental, however the behaviour of the individual terms depends on the choice of nuclear model.

2.1. *Strong-Coupling Model*

It is assumed that an incident neutron on entering the target nucleus immediately forms a compound nucleus and is absorbed into the collective motion of the system. It is predicted that R′ is equal to the geometrical radius of the nucleus R, and that $\langle[\Gamma_n/\sqrt{E}]/D\rangle$ is constant, where E is the energy of the resonance. Consequently, $\bar{\sigma}_t$ should be a monotonically decreasing function of neutron energy, and a monotonically increasing function of atomic weight. The quantity $\Gamma_n/\sqrt{E}$ is known as the reduced neutron width and is denoted by the symbol Γ_n^0.

2.2. *Weak-Coupling Model*

In both models, the nucleus is replaced by a potential well which acts upon the incoming neutron. In the weak-coupling model this potential is complex and is expressed as

$$\begin{aligned} V(r)&=V_0(1+i\zeta) \quad &&\text{for } r<R \\ V(r)&=0 &&\text{for } r>R. \end{aligned}$$

V_0 is a real number which is the depth of the potential well, and ζ is an absorption coefficient which indicates the probability of compound nucleus formation. For this theory R' is of the same order as R, but the ratio R'/R shows regular maxima and minima as a function of atomic weight. In addition $\langle\Gamma_n^0/D\rangle$ exhibits strong fluctuations for changes in atomic weight. The average total cross section $\bar{\sigma}_t$ also shows such fluctuations for changes in both atomic weight and energy.

§ 3. Comparison with Experiment

3.1. *Previous Measurements*

At the present time the characteristics of the theories have been compared with two different types of data.

At high energies (0·1–3·0 Mev) average total cross sections have been measured for a wide range of elements (Barschall 1952, Miller *et al.* 1952, Walt *et al.* 1953, Okazaki *et al.* 1954). Feshbach *et al.* (1954) find that the essential features of these data are reproduced by the weak-coupling model with the parameters $V_0=-42$ Mev, $R=1{\cdot}45\times A^{1/3}\times10^{-13}$ cm, and $\zeta=0{\cdot}03$ to $0{\cdot}05$. Later, the expression for R was modified to $R=(1{\cdot}26\,A^{1/3}+0{\cdot}7)\times10^{-13}$ cm to give a better fit in the first few Mev (Weisskopf 1956).

The above comparison deals with the combined behaviour of $4\pi R'^2$ and $\langle\Gamma_n^0/D\rangle$. The properties of $\langle\Gamma_n^0/D\rangle$, alone, can be determined at low energies, where individual resonances can be analysed. Measurements of this type have been made by Harvey *et al.* (1955) for elements in the region $A\sim150$ where the weak-coupling model predicts a large peak in $\langle \Gamma_n^0/D \rangle$. Bollinger (private communication) has made a similar comparison in the region $A \sim 50$ where another peak is predicted. When the parameters obtained from the comparison at high energies are used in the weak-coupling model, qualitative agreement is found with these experiments, in that peaks are observed near the predicted mass numbers. A limitation of this method is that for some elements $\langle \Gamma_n^0/D \rangle$ cannot be measured accurately since only a few resonances can be resolved with existing spectrometers. In addition one cannot be certain that the levels studied are truly representative of the system, because of fluctuations which occur in the average properties of relatively large groups of resonances (Egelstaff, private communication).

3.2. *The Present Experiment*

In the intermediate energy region (1–100 kev) where it is difficult to measure individual resonance parameters, it is possible to use measurements of the average total cross section $\bar{\sigma}_t$ as a basis for comparison with the theories.

To investigate the behaviour of $\bar{\sigma}_t$ in the region of the predicted peak near $A = 150$, fourteen elements in the range of atomic weight 96 to 210 were selected. In the choice of samples those elements which have small level spacings and a number of isotopes were preferred to obtain good averaging over the resonances. Hence magic number and even–even nuclei were avoided where possible, though this is difficult with the rare earths because of their relative abundances.

The elements measured were Mo, In, Te, Ce, Pr, Sm, Eu, Gd, Dy, Yb, Ta, W, Pt and Bi. The rare earths were obtained from Messrs. Johnson, Matthey and Co. Ltd., in the form of ‘ Specpure ’ oxides, which were heated to 900°c for approximately 10 hours before use to remove water which may be present in chemical combination with the oxide. For measurement on the Chopper the oxide powders were loaded into aluminium containers and then compressed to ensure a uniform sample. The remainder of the elements were used in the form of pure metal. The thickness of each sample was chosen to give an average transmission of about 0·5, which is near the optimum for accurate cross-section determinations.

The transmissions of the samples were then measured on the Fast Chopper in the interval 1 kev to 30 kev. The full width at half height of the resolution function of the machine was set at 0·18 μsec m^{-1}, so that in general resonances could not be resolved and the average transmission of the samples over a large number of resonances was measured. This quantity is not always simply related to $\bar{\sigma}_t$. The method of obtaining $\bar{\sigma}_t$ from the measurements is treated in the following section.

§ 4. THE MEASUREMENT OF AVERAGE CROSS SECTIONS

In the present experiment the resolution width of the spectrometer is much greater than the mean spacing of the resonances, so that the transmission averaged over many resonances is measured. Also the resolution width is small compared with the neutron energy. The latter condition is not strictly true at the high energy end of our measurements, but is accounted for to a first approximation by a small adjustment to the mean energy of the spectrometer timing channels. The observed transmission $\bar{T}$ can then be written as

$$\bar{T} = \frac{1}{E_2 - E_1} \int_{E_1}^{E_2} \exp\left[-n\sigma_t(E)\right] dE \qquad \ldots\ldots(2)$$

where n is the number of atoms cm^{-2} of the sample, $\sigma_t(E)$ is the total cross section at neutron energy E and $E_2 \gg E_2 - E_1 \gg D$. The true average cross section $\bar{\sigma}_t$ is given by

$$\bar{\sigma}_t = \frac{1}{E_2 - E_1} \int_{E_1}^{E_2} \sigma_t(E)\, dE. \qquad \ldots\ldots(3)$$

It can be seen that $\bar{\sigma}_t$ is obtained directly from equation (2) when $\sigma_t(E)$ is constant or, for a sample with resonances, when $n\sigma_t(E)$ is always small. This latter condition entails the use of a sample which is too thin for accurate transmission measurements.

To obtain $\bar{\sigma}_t$ from the measurement of transmission for a relatively thick sample we shall define the quantity T_0 such that

$$T_0 = \exp(-n\bar{\sigma}_t) \qquad \ldots\ldots(4)$$

and then determine the behaviour of the ratio $\bar{T}/T_0$. This ratio depends in a complicated way on the resonance parameters and in principle could be obtained directly by using a sufficient number of sample thicknesses to eliminate the unknown quantities. However, this procedure would be laborious and in the present experiment only one sample was measured, approximate values of the resonance parameters being used to estimate the ratio $\bar{T}/T_0$ as a function of energy for each particular sample. In this treatment the following assumptions are made: (i) the resonance scheme of a single spin state consists of a set of similar resonances which are uniformly spaced; (ii) the resonances always satisfy the single level Breit–Wigner relations.

The problem is now considered in two stages: firstly, when the resonance spacing is much greater than the total width (including Doppler broadening) so that no overlap occurs when the spin states of all the isotopes are considered together. This argument is then extended to overlapping resonances.

4.1. *Separate Resonances*

Consider a sample of an element for which the ith isotope has a thickness n_i atoms cm^{-2}, spin states of statistical weights g and $1-g$ and completely separate resonances. For the spin state of weight g the contribution of the idealized resonances to the average total cross section is $2\pi^2 \lambda\!\!\!^{-2} g \langle \Gamma_n/D \rangle_g$ where $\langle \Gamma_n/D \rangle_g$ is the average value of Γ_n/D for the resonances of this particular spin state. Hence if both spin states are considered together and $4\pi R'^2$ is the cross section between resonances, $\bar{\sigma}_t$ can be written

$$\bar{\sigma}_t = 4\pi R'^2 + 2\pi^2 \lambda\!\!\!^{-2} [g\langle \Gamma_n/D \rangle_g + (1-g)\langle \Gamma_n/D \rangle_{1-g}]. \qquad \ldots\ldots(5)$$

Assuming $\langle \Gamma_n/D \rangle$ to be the same for both spin states, i.e.

$$\langle \Gamma_n/D \rangle_g = \langle \Gamma_n/D \rangle_{1-g} = \langle \Gamma_n/D \rangle_i \qquad \ldots\ldots(6)$$

equation (5) becomes

$$\bar{\sigma}_t = 4\pi R'^2 + 2\pi^2 \lambda\!\!\!^{-2} \langle \Gamma_n/D \rangle_i \qquad \ldots\ldots(7)$$

which is the first approximation to equation (1).

Using equation (4) the contribution of the ith isotope to the transmission of the sample can then be written as

$$T_0 = T_b \exp(-n_i 2\pi^2 \lambda\!\!\!^{-2} \langle \Gamma_n/D \rangle_i), \qquad \ldots\ldots(8)$$

where $T_b = \exp(-n_i 4\pi R'^2)$ and represents the component of the transmission which is due to potential scattering.

The observed average transmission as defined in equation (2) can be expressed in the form

$$\bar{T}=T_{\mathrm{b}}\left(1-\frac{A_g}{D_g}-\frac{A_{1-g}}{D_{1-g}}\right) \qquad \ldots\ldots(9)$$

where the term A_g/D_g is the area above the Doppler broadened transmission dip of one of the idealized resonances divided by the spacing for that particular spin state. Since most heavy elements have either a high spin or zero spin, it is reasonable to consider only the statistical weighing factors $(\frac{1}{2}, \frac{1}{2})$ and $(1, 0)$. For the case $(1, 0)$ one of the terms of equation (9) disappears and the observed resonance spacing D_i is that of the single spin state. However for statistical weights of $(\frac{1}{2}, \frac{1}{2})$ there are two separate but similar resonance schemes and hence the observed spacing for the isotopes will be half that of the individual spin states and A_g will equal A_{1-g}. Equation (9) can then be rewritten to cover all cases as

$$\bar{T}=T_{\mathrm{b}}\left(1-\frac{A_g}{D_i}\right). \qquad \ldots\ldots(10)$$

The ratio we wish to investigate, $\bar{T}/T_0$, is then

$$\frac{\bar{T}}{T_0}=\frac{1-A_g/D_i}{\exp\left(-2\pi^2\lambda^2 n_i\langle\Gamma_{\mathrm{n}}/D\rangle_i\right)}. \qquad \ldots\ldots(11)$$

In the general case of several isotopes each of n_i atoms cm^{-2}, equation (11) becomes

$$\frac{\bar{T}}{T_0}=\frac{1-\Sigma_i(A_g/D_i)}{\exp\left(-2\pi^2\bar{\lambda}^2\Sigma_i n_i\langle\Gamma_{\mathrm{n}}/D\rangle_i\right)}. \qquad \ldots\ldots(12)$$

Hence from equation (4), putting $n=\Sigma_i n_i$,

$$\bar{\sigma}_{\mathrm{t}}=\frac{2\pi^2\bar{\lambda}^2}{n}\sum_i n_i\langle\Gamma_{\mathrm{n}}/D\rangle_i \ln\left[\frac{1}{\bar{T}}\left(1-\sum_i\frac{A_g}{D_i}\right)\right]. \qquad \ldots\ldots(13)$$

Thus the true average cross section can be obtained provided $n_i\langle\Gamma_{\mathrm{n}}/D\rangle_i$ and A_g/D_i are known. The first term can be evaluated when the resonance parameters Γ_{n} and D_i are known. If g is known the corresponding value of A_g for the particular sample thickness can be read off the standard curves used for the area method of analysis of single resonances (Hughes 1955). Suitable values of the radiation width Γ_γ and the Doppler width Δ are also required. These parameters were estimated in the following way: Δ is calculated for each element (Lamb 1939), g is chosen to be either $(\frac{1}{2}, \frac{1}{2})$ or $(1, 0)$ from tables of nuclear spins, Γ_γ is derived from the systematics (Levin and Hughes 1956). $\langle\Gamma_{\mathrm{n}}/D\rangle_i$ and D_i were based on the low-energy measurements of Harvey *et al.* (1955).

4.2. *Overlapping Resonances*

At high energies overlap of resonances occurs and equation (10) does not apply. This overlap reduces the variations in cross section moving from level to level, thereby reducing the difference between $\bar{T}$ and T_0. Allowance can be made for this effect by replacing the Doppler broadened area A_g used in equation (10) by a smaller area A_g'.

As before, consider a single isotope for which the resonances are similar and equally spaced, but which now overlap. To obtain A_g' we must add the cross sections in the region of overlap and find the area above the resultant transmission curve. Neglecting the interference between resonance and potential scattering, Bethe (1937) has shown that the total cross section of a Doppler broadened resonance σ_Δ can be written as

$$\sigma_\Delta = \sigma_0 \left(\frac{E_0}{E}\right)^{1/2} \psi(\beta, x) \qquad \ldots\ldots(14)$$

where σ_0 is the total cross section at the resonance energy E_0, $\beta = 2\Delta/\Gamma$, $x = (E - E_0)/\frac{1}{2}\Gamma$, $\Gamma = \Gamma_n + \Gamma_\gamma$, the total width of the resonance, and

$$\psi(\beta, x) = \frac{1}{\beta\sqrt{\pi}} \int_{-\infty}^{\infty} \frac{\exp[-\{(x-y)/\beta\}^2]}{1+y^2}\, dy.$$

For the energy range considered in this experiment we can assume that $E = E_0$. In addition it is generally found that $\beta > 8$ for most heavy elements, and with these conditions $\psi(\beta, x)$ is adequately represented by a Gaussian error function:

$$\psi(\beta, x) = \frac{\sqrt{\pi}}{\beta} \exp\left(-\frac{x^2}{\beta^2}\right).$$

Hence equation (14) reduces to

$$\sigma_\Delta = \sigma_0 \frac{\sqrt{\pi}}{\beta} \exp\left(-\frac{x^2}{\beta^2}\right). \qquad \ldots\ldots(15)$$

It can be seen that $\beta\psi$ is a function of x/β only, that is of $(E - E_0)/\Delta$, and therefore we can obtain a universal curve for the Doppler broadened shape in terms of $\beta\psi$ and $(E - E_0)/\Delta$. By taking two such curves and adding them for different separations (in units of D_i/Δ), we can obtain the resultant value of $n\sigma_\Delta$ for the overlapping resonances. Then, by plotting the resultant transmission curve and measuring the area above it, we arrive at the value of A_g'/Δ for the particular separation. It is possible to compute curves of A_g'/Δ as a function of the parameter $2n_i\sigma_0/\beta = n_i\sigma_0\Gamma/\Delta$ for a range of sample thickness n_i and separations D_i/Δ. These curves are shown in figure 1 and are somewhat similar to those used in the area analysis of separate resonances.

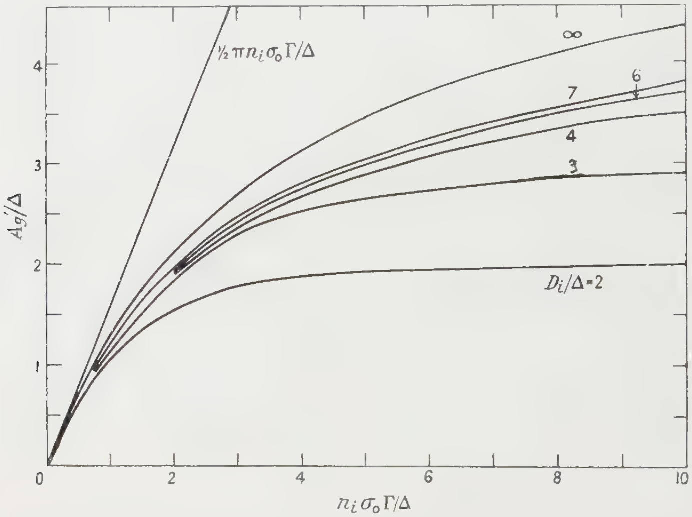

Figure 1. Area curves giving values of A_g'/Δ for the case of overlapping resonances.

The required behaviour of $\overline{T}/T_0$ is found by substituting values of A_g'/Δ for various D_i/Δ in equation (11) and computing a family of curves with respect to D_i/Δ for various values of $n_i\sigma_0\Gamma/\Delta$. These curves are shown in figure 2. It is seen that the ratio $\overline{T}/T_0$ goes through a maximum when D_i/Δ is approximately equal to 5, a behaviour which can be explained as follows: At small values of D_i/Δ the levels overlap considerably, resulting in quite small variations in the combined cross section, so that $\bar{T}/T_0$ approaches one. As D_i/Δ increases the levels separate, the effect of exponential averaging of the resonances increases and $\bar{T}/T_0$ increases. Finally, when the spacing parameter D_i/Δ is large, the contribution of the resonances to the measured transmission is small compared with that of the potential scattering and $\bar{T}/T_0$ again approaches unity. In the region $D_i/\Delta > 20$, A_g'/Δ closely approaches A_g/Δ, the value for separate resonances, provided $\beta > 8$.

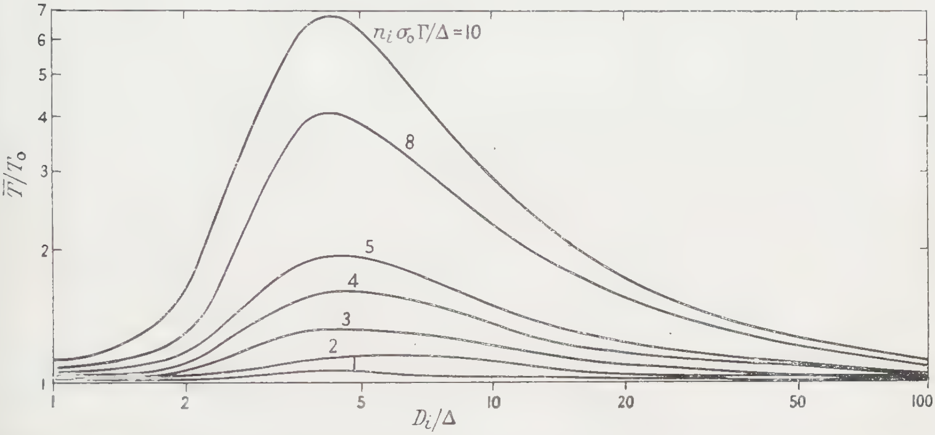

Figure 2. The effect of sample thickness (in terms of $n\sigma_0\,\Gamma/\Delta$) on the ratio of the observed to effective thin sample transmission ($\bar{T}/T_0$) for overlapping resonances.

A few of the heavy elements measured had wide spaced level schemes for which $\beta \sim 1$ and equation (15) does not apply. In these cases figure 2 cannot be used to deduce the values of $\bar{T}/T_0$ and so a separate evaluation of equation (11) is made by using values of A_g/Δ obtained from the usual area analysis curves (Hughes 1955). Elements for which both $D_i/\Delta < 10$ and $\beta \sim 1$ are few, and were avoided where possible because of the extra complication.

With the curves of figure 2, or a separate calculation if necessary, the correction for exponential averaging $T_0 - \bar{T}$ can be established as a function of neutron energy for each of the samples used.

§ 5. Results and Analysis

Some examples of the measured cross sections plotted as functions of time of flight are shown in figure 3. The continuous lines represent the observed cross sections when it is assumed that $\bar{T} = T_0$ for all points. The broken lines show our estimates of the corrected cross sections using the method described in the previous section. These results were analysed in two ways.

5.1. *Average Total Cross Sections*

The results were divided into two energy ranges and the average cross sections for the whole of each range were plotted against atomic weight. To obtain an average of the form defined in equation (3) the cross section for each counting channel was weighted by the factor $E^{3/2}$, where E is the mean energy of the channel. This procedure corrects for the fact that the channels have constant width in time and not in energy.

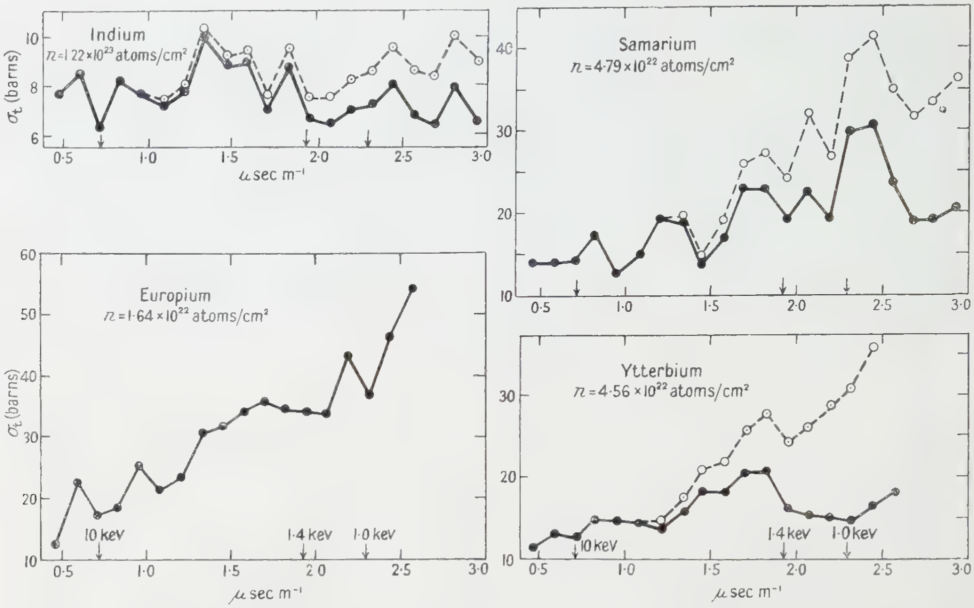

Figure 3. Some examples of the total cross sections measured on the Harwell Fast Chopper. The experimental points are joined by a full line and those corrected for exponential averaging by a broken line. For these cases the cut-off energy is near 1·4 kev which is shown on the figures. A special case is europium, for which the level spacing is so small that there is negligible correction for exponential averaging over the whole of the energy range shown.

The energy ranges chosen were: I, (31·6–6·5) kev, and II, (6·5–∼1·4) kev. In range I the correction for exponential averaging is negligible except for the magic number nuclei bismuth and cerium, which were treated in the same way as the results in range II.

In range II, corrected cross-section curves were calculated for each sample for a range of estimated possible values of the adopted resonance parameters. An

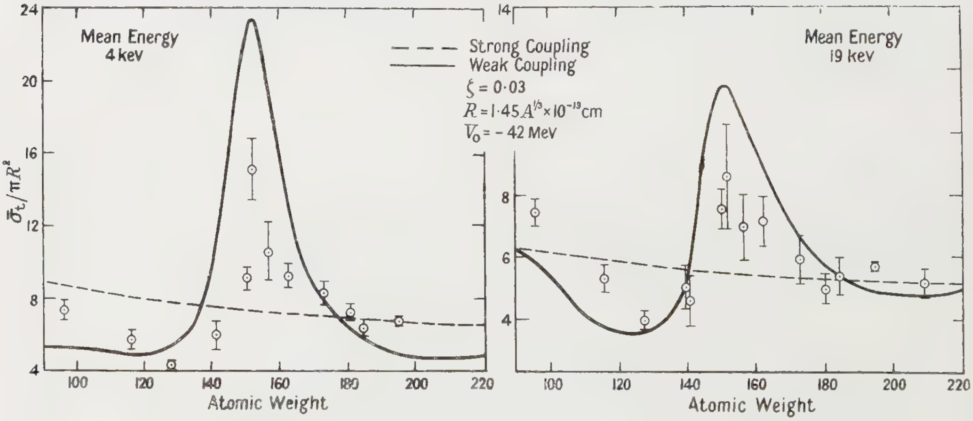

Figure 4. The measured cross sections averaged over the energy intervals 6·5 to *c.* 1·4 kev, mean energy 4 kev, and 31·6 to 6·5 kev, mean energy 19 kev. For both ranges the correction for exponential averaging can be neglected. The curves show the predictions of the strong and weak coupling models for the parameters given on the figures.

energy was then chosen such that the values of $\bar{\sigma}_t$ obtained from these curves did not differ by more than the statistical error. Above this energy $\bar{\sigma}_t$ was determined from the curve based on the best values of the resonance parameters. Below the limit the measurements were rejected. Although this energy limit is different for each sample, the mean energy of the range does not change appreciably and is approximately 4 kev.

The results are shown in figure 4, the errors indicated are the statistical errors and do not include possible systematic errors. It can be seen that for both ranges, the experimental points are in qualitative agreement with the curve predicted by the weak-coupling model with parameters $V_0 = -42$ Mev and $R = 1{\cdot}45\, A^{1/3} \times 10^{-13}$ cm in that there is definite evidence for a peak near atomic weight 150. Both experimental peaks are about one third of the amplitude predicted by this model with $\zeta = 0{\cdot}03$. It appears that a better fit would be obtained by increasing ζ to 0·05 or a little higher. Recently Weisskopf (1956) has used the radius $R = (1{\cdot}26\, A^{1/3} + 0{\cdot}7) \times 10^{-13}$ cm, which changes the position of the peak to $A \sim 170$, in marked disagreement with our observations.

5.2. *Slope and Intercept Analysis*

If we assume that only s-wave effects are of importance at energies below about 30 kev, the observed average cross sections will satisfy equation (1). This can be rewritten in the form,

$$\bar{\sigma}_t = \sigma_\infty + 5{\cdot}65 \times 10^4 \langle \Gamma_n{}^0/D \rangle t \text{ barns}, \qquad \ldots\ldots(16)$$

where t is the time of flight in μsec m^{-1}, $\sigma_\infty = 4\pi R'^2 - 6{\cdot}44 \times 10^6 \langle \Gamma_n{}^0/D \rangle^2$, and $\langle \Gamma_n{}^0/D \rangle$ is in units of (ev)$^{-1/2}$. Hence, by fitting the best straight line to a plot of

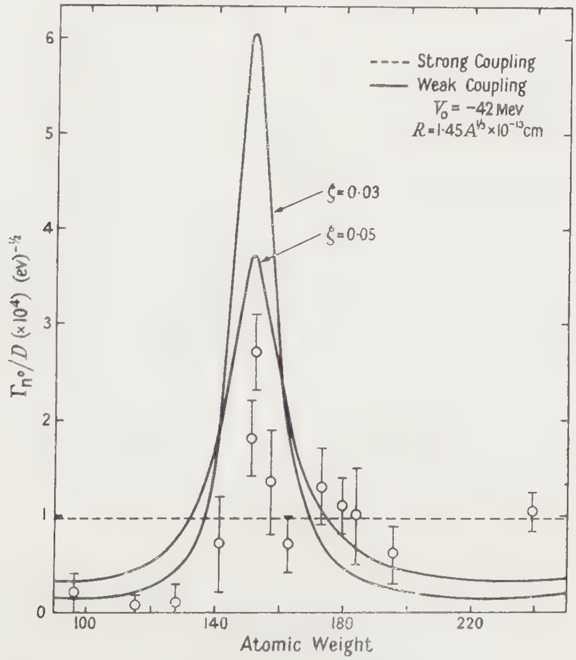

Figure 5. Values of $\langle \Gamma_n{}^0/D \rangle$ obtained by the slope and intercept method of analysis as a function of atomic weight. An additional point is included derived from direct measurement of the low-energy resonance parameters of ^{239}Pu.

$\bar{\sigma}_t$, against t, as shown in figure 3, the values of $\langle \Gamma_n^0/D \rangle$ and σ_∞ can be determined. For each sample an energy limit was chosen at which the correction for exponential averaging was equal to the statistical error on a single measurement, and only results above this limit were used in the analysis. It is found that, with this approach, the results are insensitive to reasonable changes in the assumed resonance parameters and it is considered that any systematic errors due to incorrect choice of parameters will be less than the statistical errors.

The results of this analysis for $\langle \Gamma_n^0/D \rangle$ are shown in figure 5, and although the errors are comparatively large, there is again definite evidence of a peak near $A \sim 150$ with amplitude about one third of that predicted by the weak-coupling model with $\zeta = 0{\cdot}03$. As before, increasing ζ to 0·05 or higher results in better agreement.

It can be seen from equation (16) that the intercept at $t=0$ of the best straight line σ_∞ is approximately equal to the potential scattering cross section $4\pi R'^2$ except when $\langle \Gamma_n^0/D \rangle$ is large. In figures 6(*a*) and 6(*b*) the measured values of $\sigma_\infty/\pi R^2$ for two different nuclear radii are compared with the values of $4\pi R'^2/\pi R^2$ predicted with the weak-coupling model. For the radius $R = 1{\cdot}45\, A^{1/3} \times 10^{-13}$ cm, a more exact evaluation of $\sigma_\infty/\pi R^2$ due to Lane and Lynn (private communication) is also presented. This calculation is based on equation (1) and includes the effect of p-waves. The intercept obtained is that for the part of the curve between 1 kev and 10 kev, and it is found that the p-wave contribution is only important near $A = 90$ and can be neglected in the range $A = 150$ to 170.

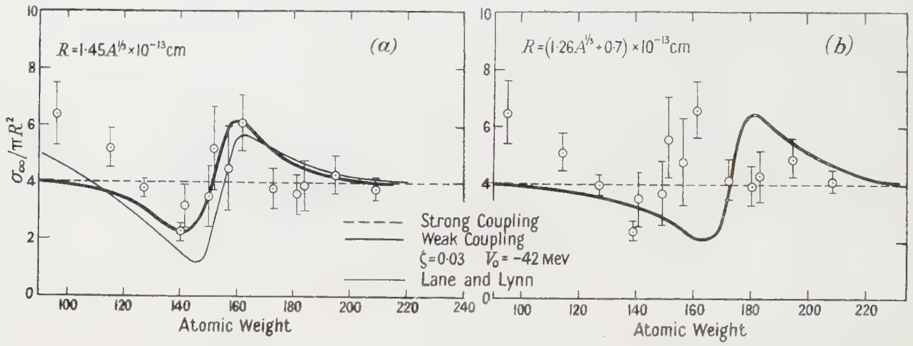

Figure 6. The experimental intercept $\sigma_0/\pi R^2$ as a function of atomic weight for (*a*) $R = 1{\cdot}45A^{1/3} \times 10^{-13}$cm, and (*b*) $R = (1{\cdot}26A^{1\cdot3} + 0{\cdot}7) \times 10^{-13}$ cm. In both cases these results are compared with the value of $4\pi R'^2/\pi R^2$ given by the strong and weak coupling models. (*a*) also shows the corresponding value of $\sigma_\infty/\pi R^2$ computed by Lane and Lynn for the weak-coupling model.

The results appear to have a systematic fluctuation similar to that predicted by the weak-coupling model, the agreement being best for $R = 1{\cdot}45\, A^{1/3} \times 10^{-13}$ cm. The rise of the experimental points towards $A = 90$ could be due to a p-wave contribution which is larger than that used by Lane and Lynn.

ACKNOWLEDGMENTS

The authors wish to express their gratitude to Dr. P. A. Egelstaff for valuable advice in all stages of the work, and to Dr. A. M. Lane and Mr. J. E. Lynn for helpful discussions and computations on some aspects of the theory. We are also grateful to Mr. C. R. T. Heard, Mr. L. A. Wraight, Mr. G. S. G. Tuckey and Miss B. R. Harrison for assistance in operating the Fast Chopper and computing the results.

REFERENCES

BARSCHALL, H. H., 1952, *Phys. Rev.*, **86**, 431.
BETHE, H. A., 1937, *Rev. Mod. Phys.*, **9**, 140.
FESHBACH, H., PEASLEE, D. C., and WEISSKOPF, V. F., 1947, *Phys. Rev.*, **71,** 145.
FESHBACH, H., PORTER, C. E., and WEISSKOPF, V. F., 1953, *Phys. Rev.*, **90,** 116; 1954, *Ibid.*, **96**, 448.
FESHBACH, H., and WEISSKOPF, V. F., 1949, *Phys. Rev.*, **76,** 1550.
HARVEY, J. A., HUGHES, D. J., CARTER, R. S., and PILCHER, V. E., 1955, *Phys. Rev.*, **99,** 10.
HUGHES, D. J., 1955, *J. Nuclear Energy*, **1,** 237.
LAMB, W. E., 1939, *Phys. Rev.*, **55,** 160.
LEVIN, J. S., and HUGHES, D. J., 1956, *Phys. Rev.*, **101,** 1328.
MILLER, D. W., ADAIR, R. K., BOCKELMAN, C. K., and DARDEN, S. E., 1952, *Phys. Rev.*, **88,** 83.
OKAZAKI, A., DARDEN, S. E., and WALTON, R. B., 1954, *Phys. Rev.*, **93,** 461.
WALT, M., BECKER, R. L., OKAZAKI, A., and FIELDS, R. E., 1953, *Phys. Rev.*, **89,** 1271.
WEISSKOPF, V. F., 1956, *Proceedings of the International Conference on the Peaceful Uses of Atomic Energy*, Vol. 2 p. 23 (New York : United Nations).

Some Aspects of the Stripping Reactions

By MOHAMED EL NADI

Cairo University, Cairo, Egypt

MS. received 15*th May* 1956 *and in revised form* 29*th August* 1956

Abstract. The Born approximation method for calculating the stripping cross section is applied to the (d, α) reactions, in which it is assumed that the incident deuteron picks up a proton and a neutron from the target nucleus. The angular distribution shows a peak in the forward direction. Agreement between theory and experimental curves is satisfactory.

In the bombardment of nuclei with deuterons, there is now a great deal of evidence that the reactions occurring do not go primarily through the formations of a compound nucleus, but rather that one of its two constituents is stripped off and captured by the target nucleus. Butler (1951) has shown that the angular distribution of the stripped deuterons (i.e. the outgoing protons or neutrons) will have a maximum in the forward direction. The appearance of this forward maximum has been one of the characteristic features of the stripping reactions.

Newns (1952) has found agreement of the triton stripping theory with the observed angular distributions of the inverse reactions ^{9}Be(d, t)^{8}Be and ^{7}Li(d, t)^{6}Li.

On the other hand, early measurements of the angular distribution in (d, α) reactions (Gibson *et al.* 1952) at moderate energies have given evidence in favour of the compound nucleus formalism. Recently, however, some interesting aspects of the (d, α) reactions have appeared. Green and Middleton (1956) observed that the angular distributions at small angles of emission are similar to those obtained from (d, p) stripping reactions and those predicted by the theory of (d, t) pick-up reactions. This may suggest that the mechanism of (d, α) reactions at intermediate deuteron energies might be similar to that of (d, t) pick-up reactions; the incident deuteron picks up a neutron and a proton from the target nucleus.

A similar process could occur in a (p, ^{3}He) reaction or its inverse (Holmgren *et al.* 1955). Such reactions refer to the possibility of this double picking-up or stripping possibility. The double stripping of the H_3 and He_3 nuclei seems more likely than He_4 because of their relatively small binding energy and larger size. We shall now consider this process and proceed to calculate its cross section by the Born approximation method for both the (He_3, p) and the (α, d) reactions. We shall neglect the Coulomb effect, although the error will be larger than the corresponding one in the treatment of the (d, p) reactions (Bhatia *et al.* 1952).

Let us denote by p, n the proton, neutron in the projectile that are captured by the target nucleus, and by d the residual part of the projectile which comes out of the reaction. V_n and V_p will denote the interactions between p and n and the target nucleus. We shall neglect (as an approximation) the interaction V_d between the product particle d and the target nucleus. Following Gerjuoy's formalism (1952), with the above approximation, we get for the Born approximation differential cross section for the double stripping process

$$\sigma = \frac{1}{4\pi^2 \hbar^4} M_d{}^* M_\alpha{}^* \frac{k_d}{k_\alpha} |I|^2 \qquad \ldots\ldots(1)$$

where

$$I = \int d\mathbf{r}_p \, d\mathbf{r}_n \, d\mathbf{r}_d \, d\xi \exp(-i\mathbf{k}_d \mathbf{r}_d') \phi^* (\mathbf{r}_p \mathbf{r}_n \xi)(V_n + V_p) \psi_\alpha \phi(\xi). \qquad \ldots\ldots(2)$$

M^* and K will refer to the reduced mass and propagation vector, ψ_α is the wave function of the projectile, $\phi(\xi)$ and $\phi(\mathbf{r}_p \mathbf{r}_n \xi)$ are the wave functions of the initial and final nuclei.

$$M_d{}^* = \frac{M_d M_f}{M_d + M_f}, \quad M_\alpha{}^* = \frac{M_\alpha M_i}{M_\alpha + M_i}, \quad \mathbf{r}_d' = \mathbf{r}_d - \frac{M_n + M_p}{M_f} \mathbf{R}, \quad \mathbf{R} = \tfrac{1}{2}(\mathbf{r}_n + \mathbf{r}_p).$$

The rest of the notation will be similar to that used by Bhatia *et al.* (1952). ξ represents all the internal coordinates of the initial nucleus.

Assuming the capture to occur at the surface of the nucleus of radius R, we may replace $\mathbf{r}_p$ and $\mathbf{r}_n$ of the nucleons by (R, θ_p, ϕ_p) and (R, θ_n, ϕ_n) in the factors of the integrand which represent the incident wave in (2), and expand the integral

$$f(\theta_p \phi_p \theta_n \phi_n) = \int \phi^* (\mathbf{r}_p \mathbf{r}_n \xi)(V_n + V_p) \phi(\xi) r_n{}^2 r_p{}^2 \, dr_n \, dr_p \, d\xi,$$

which is only a function of the angular coordinates of the captured nucleons, in spherical harmonics,

$$\sum_{\substack{l_n m_n \\ l_p m_p}} \langle f | V_n + V_p | i, l_n m_n, l_p m_p \rangle Y^*{}_{l_n}{}^{m_n}(\theta_n \phi_n) \, Y^*{}_{l_p}{}^{m_p}(\theta_p \phi_p), \qquad \ldots\ldots(3)$$

where the matrix element

$$\langle f | V_n + V_p | i, l_n m_n, l_p m_p \rangle = \int f(\theta_p \phi_p \theta_n \phi_n) \, Y_{l_n}{}^{m_n}(\theta_n \phi_n) \, Y_{l_p}{}^{m_p}(\theta_p \phi_p) \, d\Omega_p \, d\Omega_n \qquad \ldots\ldots(4)$$

and $d\Omega_p$ and $d\Omega_n$ are the corresponding elements of the solid angle. Inserting (3) into (2), the latter becomes:

$$I = \sum_{\substack{l_n m_n \\ l_p m_p}} \langle f | V_n + V_p | i, l_n m_n, l_p m_p \rangle \int d\mathbf{r}_d \, d\Omega_n \, d\Omega_p \exp(-i\mathbf{k}_d \mathbf{r}_d')$$
$$\times Y^*{}_{l_n}{}^{m_n}(\theta_n \phi_n) \, Y^*{}_{l_p}{}^{m_p}(\theta_p \phi_p) \, \chi(h) \exp\{\tfrac{1}{3}\mathbf{k}_h (2\mathbf{R} + \mathbf{r}_d)\}, \qquad \ldots\ldots(5)$$

where we have assumed, first, that the incident particle is He_3, and that $\chi(h)$ is its internal wave function. Now:

$$-i\mathbf{k}_d \mathbf{r}_d' + \tfrac{1}{3} i \mathbf{k}_h (2\mathbf{R} + \mathbf{r}_d) = i\left(\mathbf{k}_h - \frac{M_i}{M_f} \mathbf{k}_d\right) \mathbf{R} - i(\mathbf{k}_d - \tfrac{1}{3}\mathbf{k}_h)\mathbf{r}$$
$$= i\mathbf{g} . \mathbf{R} - i\mathbf{G} . \mathbf{r}, \qquad \ldots\ldots(6)$$

where:

$$\left.\begin{aligned} \mathbf{r} &= \mathbf{r}_d - \mathbf{R} \\ G^2 &= (k_d - \tfrac{1}{3}k_h)^2 + \tfrac{4}{3} k_d k_h \sin^2 \tfrac{1}{2}\theta \\ g^2 &= \left(k_h - \frac{M_i}{M_f} k_d\right)^2 + \frac{M_i}{M_f} k_h k_d \sin^2 \tfrac{1}{2}\theta \end{aligned}\right\} \qquad \ldots\ldots(7)$$

and θ is the angle between $\mathbf{k}_d$ and $\mathbf{k}_h$.

To evaluate the integral (5), we must choose a form for the internal wave function $\chi(h)$. For this we shall take the gaussian wave function:

$$\begin{aligned}\exp(-\gamma^2 \Sigma r_{ij}^2) &= \exp[-\gamma^2(2r^2+\tfrac{3}{2}r_{\mathrm{np}}^2)] \\ &= \exp[-3\gamma^2 R^2 - 2\gamma^2 r^2 + 3\gamma^2 R^2 \cos\omega], \qquad \ldots\ldots(8)\end{aligned}$$

where the angle ω is shown in figure 1. Now

$$\exp(3\gamma^2 R^2 \cos\omega) = \left(\frac{2\pi}{3\gamma^2 R^2}\right)^{1/2} \sum_{n=0}^{\infty} (n+\tfrac{1}{2})\,\mathrm{I}_{n+1/2}(3\gamma^2 R^2)\,\mathrm{P}_n(\cos\omega), \qquad \ldots\ldots(9)$$

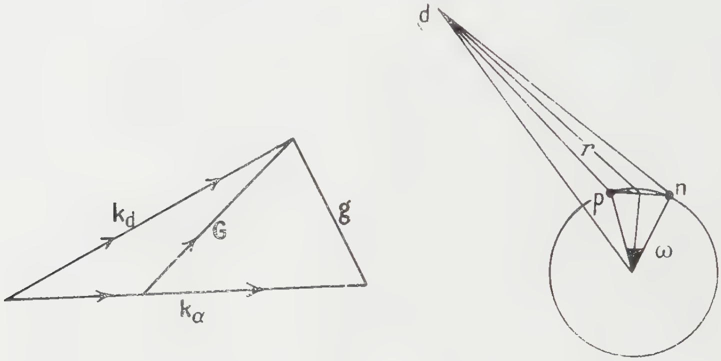

Figure 1.

where $\mathrm{I}_{n+1/2}$ is the modified Bessel function (Petiau 1955). The function $\mathrm{P}_n(\cos\omega)$ in (9) can be expanded in terms of the angles of $\mathbf{R}_{\mathrm{p}}$ and $\mathbf{R}_{\mathrm{n}}$ by the addition theorem:

$$P_n(\cos\omega) = \sum_{m=-n}^{n} \frac{4\pi}{2n+1} Y^{*m}_{n}(\theta_{\mathrm{p}}\phi_{\mathrm{p}})\, Y_n^m(\theta_{\mathrm{n}}\phi_{\mathrm{n}}).$$

Combining the two spherical harmonics in each of the variables $(\theta_{\mathrm{n}}, \phi_{\mathrm{n}})$ and $(\theta_{\mathrm{p}}, \phi_{\mathrm{p}})$ in terms of the Clebsch–Gordan coefficients C, and performing the integration over $\mathbf{r}$, we get for the integral in (5):

$$\begin{aligned} I = A \sum_{\substack{l_{\mathrm{n}} m_{\mathrm{n}} \\ l_{\mathrm{p}} m_{\mathrm{p}}}} \langle f|V_{\mathrm{n}}+V_{\mathrm{p}}|i, l_{\mathrm{n}} m_{\mathrm{n}}, l_{\mathrm{p}} m_{\mathrm{p}}\rangle \{(2l_{\mathrm{n}}+1)(2l_{\mathrm{p}}+1)\}^{1/2} \exp(-G^2/8\gamma^2) \\ \times \sum_{n=0}^{\infty} (n+\tfrac{1}{2})\,\mathrm{I}_{n+1/2}(3\gamma^2 R^2) \sum_{m=-n}^{n} (-1)^{m_{\mathrm{n}}+m_{\mathrm{p}}+m} \sum_{LML'M'} C_{l_{\mathrm{n}}n}(L0, 00) \\ \times C_{l_{\mathrm{n}}n}(L0, -m_{\mathrm{n}} m)\, C_{l_{\mathrm{p}}n}(L'0;\, 00)\, C_{l_{\mathrm{p}}n}(L'0, -m_{\mathrm{p}} m)\, i^{L+L'} \mathscr{I}_L\left(\frac{gR}{2}\right) \mathscr{I}_L\left(\frac{gR}{2}\right) \\ \ldots\ldots(10)\dagger \end{aligned}$$

where $\mathscr{I}_L(gR/2)$ is the spherical Bessel function of order L, and A is a constant factor. This is the general expression for I when the nucleons are captured in the states l_{n} and l_{p}. We have taken the direction of $\mathbf{g}$ as the principal axis for determining l_{n} and l_{p}. This expression is more complicated than the corresponding expression for the (d, p) reaction. If we now consider the simple case when the nucleons are captured in the states $l_{\mathrm{n}} = l_{\mathrm{p}} = 0$, the matrix element (10) takes the simple form

$$I = A' \exp(-G^2/8\gamma^2) \sum_{n=0}^{\infty} (-1)^n (n+\tfrac{1}{2})\,\mathrm{I}_{n+1/2}(3\gamma^2 R^2)\,\mathscr{I}_n^2(gR/2) \qquad \ldots\ldots(11)$$

---

† In this summation we have $M = m - m_{\mathrm{n}} = 0$ and $M' = m - m_{\mathrm{p}} = 0$, i.e., $m = m_{\mathrm{n}} = m_{\mathrm{p}}$.

where A' is a constant containing all terms independent of n; G and g are defined in equation (7).

If the projectile is an α-particle instead of a He_3 nucleus, then if the two nucleons are captured in the states l_n and l_p, the value of the matrix element in this case is:

$$I = A \sum_{\substack{l_n m_n \\ l_p m_p}} \langle \mathrm{f} | V_n + V_p | \mathrm{i}, l_n m_n, l_p m_p \rangle \{(2l_n+1)(2l_p+1)\}^{1/2} \exp(-G^2/16\gamma^2)$$
$$\times \sum_{n=0}^{\infty} (n+\tfrac{1}{2}) \mathrm{I}_{n+1/2}(4\gamma^2 R^2) \sum_{m=-n}^{n} (-1)^{m_n+m_p+m} \sum_{LML'M'} C_{l_n n}(L0, 00)$$
$$\times C_{l_n n}(L0, -m_n m) C_{l_p n}(L'0, 00) C_{l_p n}(L'0, -m_p m) i^{L+L'} \mathscr{I}_L\left(\frac{gR}{2}\right) \mathscr{I}_{L'}\left(\frac{gR}{2}\right) \qquad \ldots\ldots(12)$$

and for the simple case $l_n = l_p = 0$:

$$I = A' \exp(-G^2/16\gamma^2) \sum_{n=0}^{\infty} (-1)^n (n+\tfrac{1}{2}) \mathrm{I}_{n+1/2}(4\gamma^2 R^2) \mathscr{I}_n^{\,2}(gR/2) \qquad \ldots\ldots(13)$$

where

$$G^2 = (k_d - k_{\alpha\,2})^2 + 2k_d k_\alpha \sin^2 \tfrac{1}{2}\theta.$$

The series (12) is convergent and terms become negligible after the first few terms.

In the above discussion we have neglected the spin of the particles considered. If this is taken into account, then we expect to have the following selection rule, associated with the matrix element for the general case:

$$|J_f - J_i| - 1 \quad l_n + l_p \quad J_f + J_i + \tfrac{1}{2} + \tfrac{1}{2}$$

or

$$\mathbf{J}_f = \mathbf{J}_i + \mathbf{l} + \tfrac{1}{2} + \tfrac{1}{2}, \quad \mathbf{l} = \mathbf{l}_p + \mathbf{l}_n. \qquad \ldots\ldots(14)$$

J_i and J_f are the spins of the initial and final nuclei respectively. Also from the conservation of parity the total orbital angular momentum l must be even or odd according as the parities of the initial and final nuclei are the same or different.

The differential cross section will now be given by equations (1) and (12). Performing now the summation over the final magnetic quantum numbers of the target nucleus (Huby 1953), and averaging over the initial magnetic quantum numbers (denoted by the symbols f and i respectively in (12) above) we get for the factor giving the angular distribution:

$$\exp(-G^2/8\gamma^2) \left| \sum_{\substack{m_n=-l_n \\ m_p=-l_p}}^{l_n l_p} \sum_{n=0}^{\infty} (n+\tfrac{1}{2}) \mathrm{I}_{n+1/2}(4\gamma^2 R^2) \sum_{m=-n}^{n} (-1)^{m_n+m_p+m} \right.$$
$$\times \sum_{LML'M'} C_{l_n n}(L0, 00) C_{l_n n}(\mathrm{L}0, -m_n m) C_{l_p n}(L'0, 00)$$
$$\left. \times C_{l_p n}(L'0, -m_p m) i^{L+L'} \mathscr{I}_L(gR/2) \mathscr{I}_{L'}(gR/2) \right|^2. \qquad \ldots\ldots(15)$$

For the purpose of comparison with experiment we have chosen some recent results for the (d, α) reaction. For the constant γ in the internal wave function, we have chosen the value $1/\gamma = 6{\cdot}1 \times 10^{-13}$ cm (Gunn and Irving 1952).

The experimental data chosen were given by Green and Middleton (1956) for the reaction $^{16}O(d, \alpha)^{14}N$, for the ground level. This has the spin values

$J = 1^+$ (Ajzenberg and Lauritsen 1955). Now the ground state of ^{16}O has the spin $J = 0^+$. Assuming that the picked up particles were in the $p_{1/2}$ state, i.e. $l_n = l_p = 1$, we see in figure 2 the theoretical curve together with the experimental points.

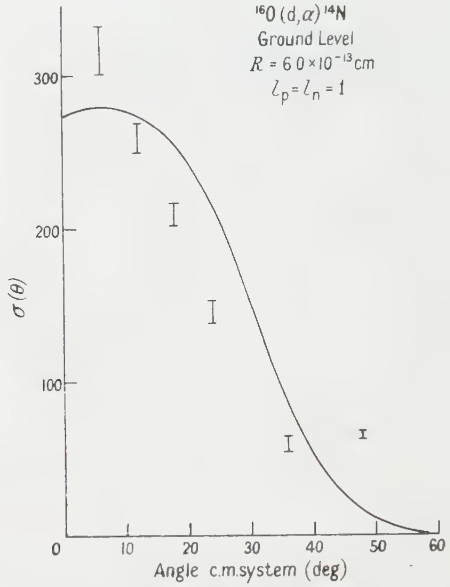

Figure 2. Reaction ^{16}O (d, α)^{14}N, corresponding to the ground state. The points are the results of Green and Middleton (1956). $E_d = 9$ MeV. The full curve is calculated from the theoretical formulae (15) for $l_p = l_n = 1$, and $R = 6{\cdot}0 \times 10^{-13}$ cm.

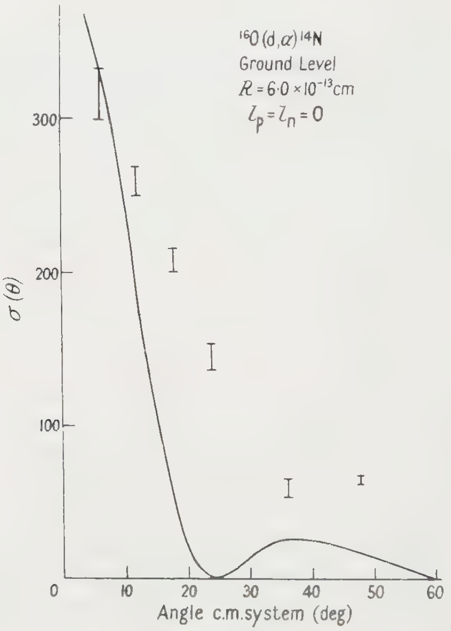

Figure 3. The same reaction ^{16}O(d, α)^{14}N as in figure 2. Full curve is calculated from the theoretical formulae (13), for $l_p = l_n = 0$, and $R = 6{\cdot}0 \times 10^{-13}$ cm.

Better agreement could perhaps be obtained by assuming different radii for the captured particles. For the purpose of comparison we calculated the curve for the case $l_n = l_p = 0$ in figure 3.

This may show that the multiple stripping processes give also angular distributions which are peaked in the forward direction.

This also may show further that some (d, α) reactions could be explained on the stripping or picking-up basis, although undoubtedly, in many cases, the compound nucleus formation is predominant. But due to the complexity of the formulae in the present case, its value in nuclear spectroscopy is not as powerful as it is in the case of the single stripping and picking-up processes. Also the angular distribution, as expected, is not as sensitive for slight changes in the nuclear radius R as the corresponding distribution for the (d, p) reactions.

ACKNOWLEDGMENTS

It is a pleasure to thank Dr. G. Källén of CERN for helpful discussions in evaluating the integral (5).

REFERENCES

AJZENBERG, F., and LAURITSEN, T., 1955, *Rev. Mod. Phys.*, **27,** 125.
BHATIA, A. B., *et al.*, 1952, *Phil. Mag.*, **43,** 485.
BUTLER, S. T., 1951, *Proc. Roy. Soc.* A, **208,** 559.
GERJUOY, E., 1953, *Phys. Rev.*, **91,** 453.
GIBSON, W. M., *et al.*, 1952, *Proc. Roy. Soc.* A, **210,** 549.
GREEN, T. S., and MIDDLETON, R., 1956, *Proc. Phys. Soc.* A, **69,** 28.
GUNN, J. B., and IRVING, J., 1952, *Phil. Mag.*, **43,** 1362.
HOLMGREN, H. D., *et al.*, 1955, *Phys. Rev.*, **100,** 436.
HUBY, R., 1953, *Progress in Nuclear Physics*, Vol. 3, p. 195.
NEWNS, H. C., 1952, *Proc. Phys. Soc.* A, **65,** 916.
PETIAU, G., 1955, *La theorie des fonctions de Bessel* (Paris : Centre National de la Recherche Scientifique), p. 170.

A Study of the Reaction $^{12}C(d, p)^{13}C$

By N. SARMA, M. GOVINDJEE, and H. R. ALLAN
Imperial College, London

MS. received 14*th August* 1956

Abstract. Yields and angular distributions for the reaction $^{12}C(d,p)^{13}C$ have been studied for deuteron bombarding energies between 800 kev and 1·7 Mev. It is shown that the reaction proceeds, at these energies, almost entirely through the formation of a compound nucleus, and not by a stripping process. Assignments of quantum numbers to the resonance levels observed in the compound nucleus are suggested.

§ 1. Introduction

Nuclear transformations of the type (d, p) and (d, n) caused by the deuteron bombardment of various targets have been much studied recently, and the stripping theories of Butler (1951) and Bhatia *et al.* (1952) have been formulated to account for the angular distribution of reaction products. At deuteron energies $E_d = 8$ Mev the stripping process is predominant (Rotblat 1951), and the predictions of simple stripping theories agree with experiment, except for a small background in the angular distribution which is attributed to compound nucleus formation. However, the simple stripping theory neglects the effects of Coulomb and other, nuclear, interactions; Tobocman and Kalos (1955) have computed the angular distributions due to the stripping process taking these effects into account, and show that the angular distributions at deuteron energies comparable with the barrier height, are very sensitive to the assumptions made with respect to the nuclear interactions. The problem at these lower energies is to distinguish between a distorted stripping angular distribution and one due to compound nucleus formation. Marion and Weber (1956) have shown that compound nucleus formation predominates in the reaction $^{13}C(d,p)^{14}C$ at deuteron energies of up to 1·7 Mev. Study of the reaction $^{12}C(d,p)^{13}C$ at energies $E_d \sim 2$ to 3 Mev has shown that compound nucleus formation is comparable with the stripping contribution (Holmgren *et al.* 1954, Bonner *et al.* 1956). At still lower energies, E_d less than 2 Mev, it would therefore be unwise to attempt to analyse the angular distributions in terms of stripping theory alone (cf. Juric 1956).

We have studied the reaction $^{12}C(d,p)^{13}C$ in the range of deuteron energies up to 1·7 Mev. Our analysis of the yield and angular distributions of the protons leading to the ground state of ^{13}C shows that, at these energies, the process proceeds almost entirely through the formation of a compound nucleus, the stripping contribution being negligible. We have also attempted to make assignments of spins, parities and isotopic spins to the levels concerned in the compound nucleus.

§ 2. Experimental Techniques

The target chamber is shown schematically in figure 1. It was connected to the beam port of the Imperial College Van de Graaff generator via a liquid air trap which helped to filter out the residual oil vapour in the system. The deuterons passed through the thin target and were collected in a Faraday cup. Secondary electron suppression was effected by a negatively charged ring in front of the collecting cup. The beam current was measured by a current integrator.

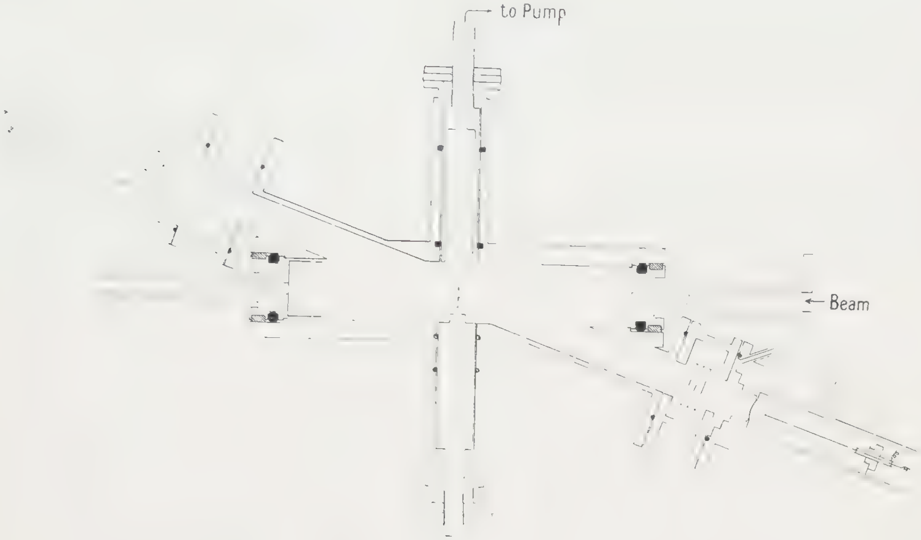

Figure 1. Target chamber.

The beam was collimated by aluminium apertures of 1 mm diameter, set one metre away from the beam deflection magnet. The magnetic field was kept constant, within 0·04%, so that the energy of the deuterons striking the target remained constant to within 2 kev. Stabilizing circuits kept the voltage of the machine close to these limits, and so the beam current was reasonably constant.

The targets were self-supporting films of natural carbon from 30 to 90 $\mu g\,cm^{-2}$ thick, mounted over holes 6 mm in diameter punched in brass foils. These were prepared by an evaporation technique. The carbon was deposited on a glass microscope slide covered with evaporated NaCl, then floated off on a water surface. The films when mounted, washed and dried were fairly uniform and very robust. The thickness of each film was estimated by measuring the Coulomb scattering from it at forward angles. The effect due to ^{13}C in natural carbon was considered negligible because of its low isotopic abundance, 1·1% (Hollander *et al.* 1953).

The emergent particles were detected by end-window proportional counters (see figure 1). The angle between the counters and the incident beam could be varied continuously from 20° to 160° by a worm drive mechanism without breaking the vacuum. The counters were filled with a mixture of argon and carbon dioxide. They were separated from the vacuum by thin windows; mica windows (thickness 2 $mg\,cm^{-2}$) were used for counting long-range protons, but thinner windows of celluloid were necessary for detecting the scattered deuterons and short-range protons. It was necessary to distinguish the different groups of particles by the pulse heights they produced. Maximum discrimination was obtained by sliding suitable absorbers in front of the counter windows and adjusting the pressure of the gas filling. The active volume of the counter was defined by using a special counter seal similar to that developed by Cockroft and Curran (1951). The insulation between the counter wire, field tube and counter wall was of Araldite casting resin.

The counter pulses were amplified by a fast amplifier and recorded with a discriminator and scaler. Single channel kicksorters were used to separate the pulses produced by the deuterons and short-range protons.

§ 3. Results

The yield of long-range protons from the reaction $^{12}C(d,p)^{13}C$ for deuteron energies between 0·8 Mev and 1·7 Mev at angles $\theta_{c.m.} = 21{\cdot}3^\circ$ and $161{\cdot}2^\circ$ (in centre-of-mass coordinates) is given in figure 2. The angular distributions were measured at seventeen different energies, and were analysed into a series of Legendre polynomials:

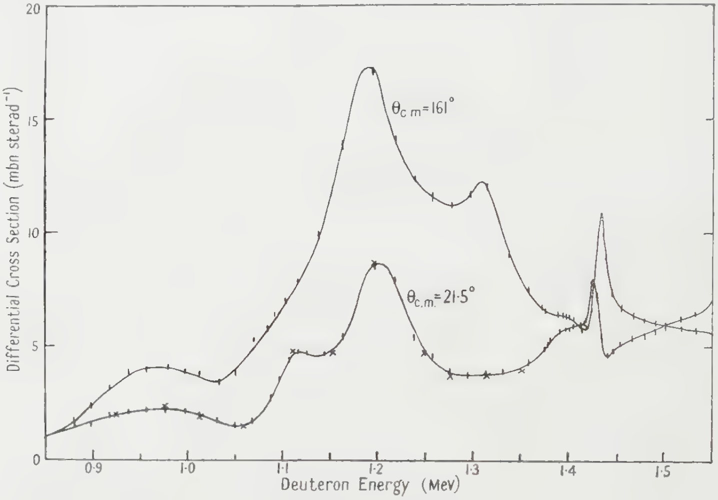

Figure 2. Excitation curves for the long-range protons from the $^{12}C(d,p)^{13}C$ reaction.

$$Y(E,\theta) = f(E)\left\{1 + \sum_{n=1}^{4} a_n P_n(\cos\theta)\right\}.$$

Figures 3–6 give typical experimental points with the results of the analysis. The coefficients, a_n, of the Legendre polynomials at different energies have been tabulated in table 1. The analysis was carried out up to the eighth order polynomial, $P_8(\cos\theta)$, and it was found that coefficients of polynomials of order greater than four were negligible. The finite angle subtended by the counter at the target was less than 3°; hence the effect of this on the analysis of our results was not considered in these calculations.

The excitation curves for the short-range protons leading to the first excited state, $^{13}C^*$, are given in figure 7 for the angles $\theta_{c.m.} = 93{\cdot}6^\circ$, $134{\cdot}1^\circ$ and $161{\cdot}3^\circ$.

§ 4. Discussion

4.1. *Absence of Stripping*

From the excitation functions and the angular distributions, the total cross-section excitation function for the reaction $^{12}C(d,p)^{13}C$ was evaluated, and is

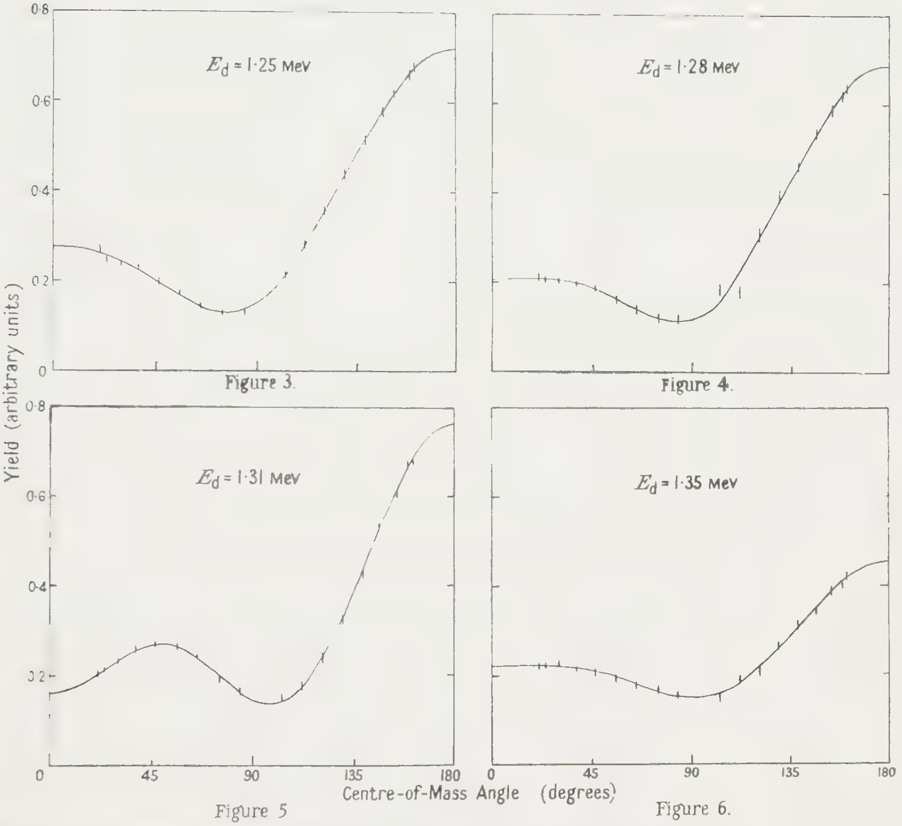

Figure 3.

Figure 4.

Figure 5

Figure 6.

Figures 3–6. Typical angular distribution curves of the long-range protons from the $^{12}C(d, p)^{13}C$ reaction.

Table 1. Coefficients of Legendre Polynomials in the Angular Distributions of Long Range Protons

Energy (kev)	a_1	P.E.	a_2	P.E.	a_3	P.E.	a_4	P.E.
872	+0·019	0·005	−0·009	0·008	−0·107	0·008	0·032	0·010
925	−0·331	0·003	0·170	0·005	−0·020	0·004	0·008	0·006
976	−0·384	0·005	0·178	0·008	0·059	0·007	0·006	0·009
1013	−0·557	0·005	0·385	0·007	0·118	0·007	−0·017	0·009
1060	−0·695	0·011	0·526	0·016	−0·054	0·016	−0·092	0·021
1111	−0·541	0·016	0·801	0·023	0·078	0·023	0·018	0·030
1154	−0·732	0·012	0·960	0·018	−0·115	0·018	−0·027	0·023
1195	−0·638	0·010	0·965	0·015	0·046	0·015	−0·041	0·019
1249	−0·748	0·006	0·963	0·013	−0·063	0·008	−0·065	0·011
1277	−0·763	0·014	0·936	0·022	−0·228	0·021	−0·099	0·027
1314	−0·481	0·005	0·834	0·008	−0·658	0·008	−0·076	0·010
1352	−0·307	0·007	0·603	0·010	−0·241	0·010	−0·024	0·013
1391	−0·207	0·009	0·495	0·013	−0·072	0·012	−0·152	0·016
1413	−0·046	0·007	0·497	0·009	0·013	0·009	−0·104	0·011
1432	−0·686	0·007	0·734	0·014	−0·292	0·011	0·024	0·013
1458	−0·628	0·005	0·593	0·007	−0·271	0·008	0·030	0·010
1477	−0·276	0·006	0·314	0·008	−0·120	0·008	−0·102	0·011

P.E. = probable error.

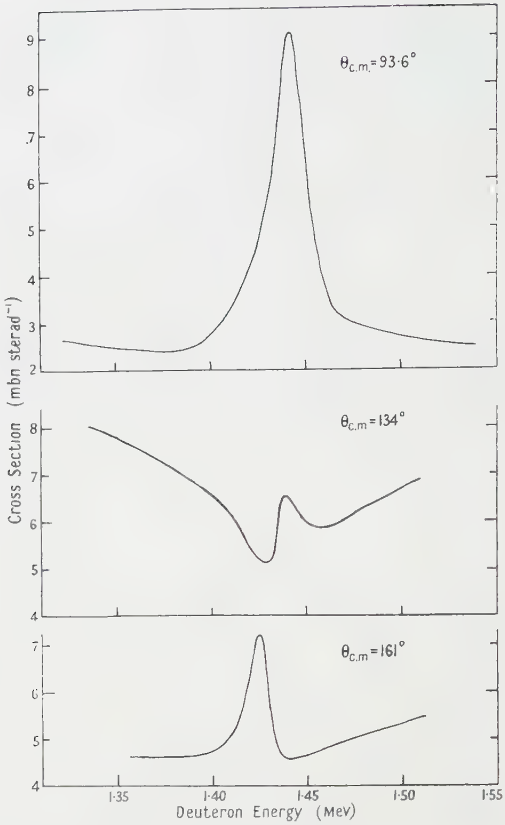

Figure 7. Excitation curves for the short-range protons in the $^{12}C(d, p)^{13}C$ reaction.

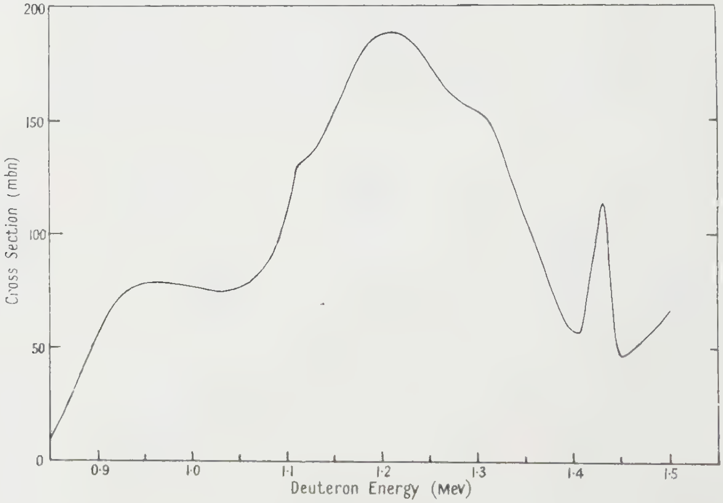

Figure 8. The total cross section excitation function for the long-range protons in the $^{12}C(d, p)^{13}C$ reaction.

given in figure 8. We have been able to analyse this total cross-section curve into a sum of five Breit–Wigner functions appropriate to standard compound nucleus theory. The energies, the total widths of these resonances (corrected for experimental resolution) and their relative intensities are given in table 2. There is no indication of any non-resonant background that could be attributed to a stripping process. Because of this, and also because there is no evidence for the presence of any Legendre polynomials of order greater than four in the angular distributions, we infer that any contribution due to a direct interaction process must be less than 3 mbn, i.e. 2% of the observed yield. This compares with a stripping cross section of the order of 30 mbn at 3·3 Mev (Holmgren *et al.* 1954).

Table 2

(1)	(2)	(3)	(4)	(5)	(6)
0·94	140	8·5	1^+	11·04	3·78
1·13	45	3	—	11·23	4·01
1·16	245	33	2^-	11·26	4·10
1·30	65	6·8	3^+	11·38	4·18
1·44	15	10·0	3^+	11·49	—

(1) E_d (Mev); (2) Γ_{tot} (kev); (3) relative intensity; (4) $J.\ \pi$; (5) $E\ (^{14}N^*)$; (6) $E_p^{Res}\ [^{13}C(p,n)^{13}N]$: (Bair 1953).

The resonances we obtain may be correlated in energy with those obtained by Phillips (1950) and with those $^{13}C(p,n)^{13}N$ resonances obtained by Bair *et al.* (1953). We identify the resonances that appear at $E_d = 0·94$, 1·13, 1·16 and 1·30 Mev with those that were observed by Bair *et al.* at $E_p = 3·78$, 4·01, 4·10 and 4·18 Mev respectively; however, they did not detect any (p, n) resonance corresponding to the (d, p) one found here at $E_d = 1·44$ Mev. It is interesting to note that the same state of the compound nucleus fails to show a resonance in the (d, n) reaction (Bonner *et al.* 1949).

4.2. *Assignments of Spins and Parities*

The reaction having been shown to proceed almost entirely through states of the compound nucleus ^{14}N, the results may be discussed in terms of compound nucleus theory. Before considering each resonance individually certain features may be noted.

1. Since, in the range of energies studied, the coefficients of the Legendre polynomials of order greater than four were negligible, the smaller of the two l-values for the incoming or the outgoing particles participating in the reaction must be 2 or less (Blatt and Weisskopf 1952). Reference to table 3, which gives the possible channel spins and orbital angular momentum values associated with each value of J, π in the compound nucleus, shows that J must be equal to or greater than the smaller of the two l values. Thus the complexity of the angular distribution is determined by the l values and not by J. It also follows that the J values concerned cannot exceed 3.

2. The total cross section at energies between two resonances will contain contributions from both levels of the compound nucleus. Cross product terms in this cross section will normally produce interference effects, but unless the two levels have identical spin and parity, these terms, although present in the differential cross section, will be absent in the total cross section.

Since the measured total cross section does not show interference effects between resonances, levels close enough to interfere cannot have identical spins and parities.

Table 3. Reaction Schemes for $^{12}C(d, p)^{13}C$
Incident spin = 1^+, exit spin = 0, 1^-

		$S_{\text{out}} = 0^-$		$S_{\text{out}} = 1^-$	
$L_{\text{incid.}}$	J, π (^{14}N)	(*a*)	(*b*)	(*a*)	(*b*)
1	0^-	0	0	—	—
0	1^+	1	0	1	0
2	1^+	1	2	1	2
1	1^-	—	—	2, 0	2, 0
2	2^+	—	—	3, 1	4, 2
1	2^-	2	2	2	2
3	2^-	2	4	2	4
2	3^+	3	4	3	4
4	3^+	3	6	3	6
3	3^-	—	—	4, 2	6, 4
4	4^+	—	—	5, 3	8, 6
3	4^-	4	6	4	6
5	4^-	4	8	4	8
5	5^-	—	—	6, 4	10, 8
4	5^+	5	8	5	8

(*a*) l_{out}; (*b*) max. $P_n(\cos\theta)$

3. The existence of odd order Legendre polynomials $P_1(\cos\theta)$ and $P_3(\cos\theta)$ in the distributions indicates interference between states of different parity. For this reaction, $^{12}C(d, p)^{13}C$, the four levels at resonance energies $E_d = 0{\cdot}94$, 1·13, 1·30 and 1·44 MeV appear to interfere with the broad 1·16 MeV resonance. However, as the four resonances are fairly narrow and widely separated, the interference between them is small.

4. The compound nucleus ^{14}N is very highly excited (about 11 MeV) in this reaction and contains equal numbers of protons and neutrons. Emission of the long-range protons and of neutrons leads to the ground states of the mirror nuclei, ^{13}C and ^{13}N respectively. In these circumstances one could expect the intrinsic decay probabilities, that is the reduced widths for emission of protons and neutrons, to be of the same order of magnitude. This should be true also for the emission of the short-range protons which leave the nucleus ^{13}C in an excited state.

The observed widths are influenced also by the barriers (Coulomb and angular momentum) to particle emission. We have computed values of penetrability using the tables of Coulomb functions given by Sharp *et al.* (1953), assuming a radius of $R = 3{\cdot}53 \times 10^{-13}$ cm for all channels. Neutron penetrabilities were evaluated from the paper by Lax and Feshbach (1948); (d, n) cross sections were taken from Bonner *et al.* (1949). Comparisons of the reduced width for the emission of protons and neutrons were then obtained for each resonance. Spin assignments were made to bring the neutron and proton reduced widths to the same order of magnitude. However, for reasonable values of channel radius, the neutron reduced widths were always appreciably smaller than the proton reduced widths. On the other hand, at the higher excitations produced by the reaction of ^{10}B with alpha particles (Shire *et al.* 1953), the neutron width becomes consistently greater than the proton width. The reduced widths are always much less than the limit of $3\hbar^2/2MR$ set by Teichmann and Wigner (1952). This is consistent with the assumption of many particle excitation in the compound nucleus.

5. Confirmation of the spin assignments was obtained in some cases from the agreement of the interference pattern in the angular distribution with that computed theoretically. This is true particularly of the narrow level, 15 kev wide, at $E_d = 1{\cdot}44$ Mev (resonance 5).

Resonance 1. $E_d = 0{\cdot}94$ Mev, $E(^{14}N) = 11{\cdot}04$ Mev.

The (d, p) angular distribution is almost isotropic at 872 kev and the anisotropy at 925 kev may be ascribed to interference effects with the broad resonance at 1·16 Mev. The cross sections of the (d, p), (d, n) and (d, p_1) reactions are all fairly large at this bombarding energy. The level may, therefore, be formed by s-wave capture, which implies a compound nucleus state with $J = 1^+$ (table 3). Further, $\sigma(d, p_1) > \sigma(d, n)$ (Bonner *et al.* 1949), and in order to make the reduced widths inferred for neutron and proton emission of comparable magnitude, we put $l_{p_1} < l_n$. The residual states concerned are $\frac{1}{2}^+$ in ^{13}C for the (d, p_1) reaction, and $\frac{1}{2}^-$ in ^{13}N for the (d, n) reaction which allows us to put $l_{p_1} = 0$, $l_n = 1$. Even so, the reduced width for neutrons is about 0·1 the reduced width for protons. Conservation of isotopic spin suggests that this state of $^{14}N^*$ may have $T = 0$.

Resonance 2. $E_d = 1{\cdot}13$ Mev, $E(^{14}N^*) = 11{\cdot}23$ Mev.

This resonance is visible in the total yield curve only as a small bulge on the side of the broad resonance. Its presence is more apparent in the change in the (d, p) angular distribution through the resonance energy. This resonance was not observed by Bonner for the (d, n) reaction, but in the $^{13}C(p, n)^{13}N$ there is a pronounced resonance corresponding to this same energy in the compound nucleus ^{14}N. The cross sections for the deuteron reactions are less than 2% of those of the (p, n) reactions. This may indicate a $T = 1$ assigment for this level with a small admixture of $T = 0$ that allows some (d, p) reaction to take place.

Resonance 3. $E_d = 1{\cdot}16$ Mev, $E(^{14}N^*) = 11{\cdot}26$ Mev.

This level is extremely broad and is characterized by the large cross sections for the (d, p) process. However, the cross sections for (d, n) and (p, n) are fairly small. The (d, p) angular distribution is not isotropic, but does not contain terms of higher order than $P_2(\cos\theta)$. To account for this limited complexity, the smaller of the two l-values for the incoming and outgoing particles must be $l = 1$. According to table 3 this leads to a spin for the compound nucleus state of $J = 2$. An assignment which would make the reduced widths for proton and neutron emission comparable is $J = 2^-$. The reduced width for neutron emission is then about 0·1 the reduced width for proton emission. Again, we suggest a $T = 0$ state.

Resonance 4. $E_d = 1{\cdot}30$ Mev, $E(^{14}N^*) = 11{\cdot}38$ Mev.

The cross sections for the three reactions (d, p), (d, n) and (p, n) are all large. The (d, p) angular distributions contain significant values for the coefficients of the Legendre polynomials $P_3(\cos\theta)$ and $P_4(\cos\theta)$. Therefore, as d-waves must be the less complex of the incident or emergent particle waves, the spin of the 11·41 Mev state may be estimated as $J = 3$ (table 3). The assignment of $J = 3^-$ is dismissed because this gives an unduly large width for the emission of a neutron as compared to that for a proton. The spin of 3^+ gives this ratio $\gamma_n^2/\gamma_{p_1}^2 = 0{\cdot}2$. The large deuteron reaction cross sections indicate a $T = 0$ state.

Resonance 5. $E_d = 1{\cdot}44$ MeV, $E(^{14}N^*) = 11{\cdot}49$ MeV.

This resonance is very narrow, with $\Gamma_{tot} \sim 15$ kev. The partial width for neutron emission is extremely small compared with the widths for proton and deuteron emission, which are of comparable magnitude. The coefficients of $P_3(\cos\theta)$ and $P_4(\cos\theta)$ in the (d, p) angular distribution are again significant, implying that one l value, incident or emergent must be $l=2$; the other one must be greater. Of the two alternative assignments thus presented, $J = 3^+$ or 3^- (table 3), we choose 3^+ in an attempt to bring the neutron and proton widths to the same order of magnitude. Even so, the ratio $\gamma_n^2/\gamma_{p_1}^2 = 0{\cdot}025$.

Confirmation of the assignment 3^+ was obtained from the angular distribution measurements. The angular distribution due to the interference between this state, assumed to be of spin 3^+, and the broad 2^- state, was computed using the formulae of Blatt and Biedenharn (1952). The Racah coefficients required were taken from the tables of Sharp *et al.* (1954). The simplifying assumption was made that in the formation and break-up of any one compound nuclear state, only the smallest l value allowed by the selection rules plays any part. By conservation of parity, the next l value concerned must be greater by two units and the penetrability through angular momentum barriers is, therefore, greatly reduced.

With this simplification, the effect of interference between two levels of a compound nucleus was calculated; it was found that the ratio of the coefficients of the odd order polynomials, $P_1(\cos\theta)$ and $P_3(\cos\theta)$, i.e. a_1/a_3, is constant through a resonance and depends only on the quantum numbers involved. For the resonance under consideration, assumed to be 3^+, we calculate the ratio for a_1/a_3 the value 2·13. This agrees with the experimental values obtained from three angular distributions at and close to the resonance energy, viz., 2·29, 2·32 and 2·33 (±0·2). Calculations based on other assignments give very different values.

ACKNOWLEDGMENTS

We wish to offer our most sincere thanks to Dr. G. Manning of the English Electric Company, Ltd., and Mr. P. Wynn of the Scientific Computing Service Ltd. for their help in the analysis of the angular distribution curves. The target box used in this experiment was modified from one designed by Dr. A. V. Cohen. We are grateful to Professor S. Devons for his help and encouragement throughout this work.

One of us (N. Sarma) wishes to thank the Government of India, Department of Atomic Energy, for a scholarship.

REFERENCES

BAIR, J. K., KINGTON, J. D., and WILLARD, H. B., 1953, *Phys. Rev.*, **90**, 575.
BHATIA, A. B., KUN HUANG, HUBY, R., and NEWNS, H. C., 1952, *Phil. Mag.*, **43**, 485.
BLATT, J. M., and BIEDENHARN, L. C., 1952, *Rev. Mod. Phys.*, **24**, 258.
BLATT, J. M., and WEISSKOPF, V., 1952, *Theoretical Nuclear Physics* (New York : John Wiley).
BONNER, T. W., EISINGER, J. T., KRAUS, A. A., and MARION, J. B., 1956, *Phys. Rev.*, **101**, 209.
BONNER, T. W., EVANS, J. E., HARRIS, J. C., and PHILLIPS, G. C., 1949, *Phys. Rev.*, **75**, 1501.
BUTLER, S. T., 1951, *Proc. Roy. Soc.* A, **208**, 559.
COCKROFT, A. L., and CURRAN, S. C., 1951, *Rev. Sci. Instrum.*, **22**, 37.
HOLLANDER, J. M., PERLMAN, I., and SEABORG, G. T., 1953, *Rev. Mod. Phys.*, **25**, 478.

Holmgren, H. D., Blair, J. M., Simmons, B. E., Stratton, T. F., and Stuart, R. V., 1954, *Phys. Rev.*, **95,** 1544.
Juric, M. K., 1956, *Bull. Inst. Nucl. Sci.*, ' Boris Kidrich ', **6,** 36.
Lax, M., and Feshbach, H., 1948, *J. Acoust. Soc. Amer.*, **20,** 108.
Marion, J. B., and Weber, G., 1956, *Phys. Rev.*, **103,** 167.
Phillips, G. C., 1950, *Phys. Rev.*, **80,** 164.
Rotblat, J., 1951, *Phys. Rev.*, **83,** 1271.
Sharp, W. T., Gove, H. E., and Paul, E. B., 1953, TPI 70, Atomic Energy of Canada, Ltd., Ontario.
Sharp, W. T., Kennedy, J. M., Sears, B. J., and Hoyle, M. G., 1954, CRT 556, Atomic Energy of Canada, Ltd., Ontario.
Shire, E. S., Wormald, J. R., Lindsey-Jones, G., Lundén, A., and Stanley, A. G., 1953, *Phil. Mag.*, **44,** 1197.
Teichmann, T., and Wigner, E. P., 1952, *Phys. Rev.*, **87,** 123.
Tobocman, W., and Kalos, M. H., 1955, *Phys. Rev.*, **97,** 132.

An Investigation of the Reactions $^{12}C\,(d, n)^{13}N$ and $^{28}Si\,(d, n)\,^{29}P$

By J. M. CALVERT†, A. A. JAFFE† and E. E. MASLIN
Nuclear Physics Research Laboratory, University of Liverpool

Communicated by H. W. B. Skinner; MS. received 20*th August* 1956, *and in final form* 8*th November* 1956

Abstract. The angular distributions of several neutron groups from stripping of deuterons on targets of ^{12}C and ^{28}Si have been measured, and compared with theoretical curves. The parity and possible spin of the final state have been determined for those cases showing a 'stripping distribution'. Absolute cross sections for formation of the final states were measured, and from these the reduced widths were determined for several levels in the final nuclei ^{13}N and ^{29}P.

§ 1. Introduction

Several investigators have measured the angular distributions of proton and neutron groups from deuteron stripping reactions and, by application of stripping theory, have been able to determine spins and parities of the resultant nuclear levels. Holt and Marsham (1953), among these, have shown the importance of also measuring the absolute or relative cross section of a group at the same time as its angular distribution, for this gives information on another quantity involved in the reaction, namely the nucleon–nucleus matrix element. In particular, Holt and Marsham have studied (d, p) reactions on several target nuclei having either closed shells or closed sub-shells so that the final nuclei might be expected to show 'single-particle' characteristics. In fact, their cross-section measurements indicated that the majority of low-lying levels in these particular nuclei are due to single-particle excitation. Basing their interpretation on the Mayer shell model (1950), terms have been proposed for these levels in the final nuclei.

It is of interest to compare the properties of mirror nuclei, and stripping provides a useful tool in this respect since mirror (d, p) and (d, n) reactions can be compared. The present work was carried out for the purpose of studying the $^{28}Si(d, n)^{29}P$ reaction, being the parallel (d, n) reaction to $^{28}Si(d, p)^{29}Si$ previously studied by Holt and Marsham.

The $^{28}Si(d, n)^{29}P$ reaction has been investigated previously by Peck (1948) and by Mandeville *et al.* (1952), the Q-value only being measured. The values quoted by these workers differed by about 1 Mev. More recent measurements at this laboratory by Green (1955), using nuclear emulsions, give a Q-value differing from the earlier work mentioned above but approximately in accord with the value estimated from masses (Endt and Kluyver 1954). They found the value to be $0{\cdot}74 \pm 0{\cdot}10$ Mev.

A target of silicon was bombarded by a beam of 9·0 Mev deuterons from the 37 in. cyclotron at the University of Liverpool. The angular distributions were investigated for several neutron groups from this target and the cross sections for the formation of these groups were measured. In addition, the cross sections for three groups from a carbon target, the angular distributions for which have been reported earlier (Middleton *et al.* 1953), were also measured. The fast-neutron spectrometer and procedure were the same as those described in detail in an earlier paper (Calvert *et al.* 1955 b). The analysis of the results and their comparison with the work of Holt and Marsham are given below.

---

† Now at the University of Manchester.

§ 2. EXPERIMENTAL DETAILS

The silicon target was prepared by deposition from a suspension in alcohol of silicon powder, having natural isotopic abundance, on to a layer of bismuth covering a thick gold backing. Targets of about 1 mg cm^{-2} and 3 mg cm^{-2} were prepared in this way and used in the measurements. The requirements of the backing have been discussed previously (Calvert *et al.* 1955 a) and are determined by the monitoring technique used.

The carbon target was prepared by burning camphor and collecting soot on a gold backing.

The fast-neutron spectrometer was calibrated by using neutrons from the ground state and first two excited states of the reaction $^{12}C(d, n)^{13}N$, for which the $\underset{\sim}{Q}$-values are quite well known, thus making it possible to identify the levels in the silicon reaction accurately.

§ 3. RESULTS

The reactions were studied for neutron energies of 5 MeV and above. This low-energy limit corresponds in each case to an excitation in the final nucleus of about 4–5 MeV, as the ground-state $\underset{\sim}{Q}$-values are in the region of zero. Figure 1 shows the neutron spectrum obtained from the silicon reaction. It should be noted that the relative intensities of the neutron groups in this spectrum are modified by the efficiency of the spectrometer, which increases at the higher neutron energies.

Theoretical curves have been calculated according to the stripping theory of Butler (1951), using a value for the radius parameter of $(1{\cdot}7 + 1{\cdot}22\,A^{1/3}) \times 10^{-13}$ cm.

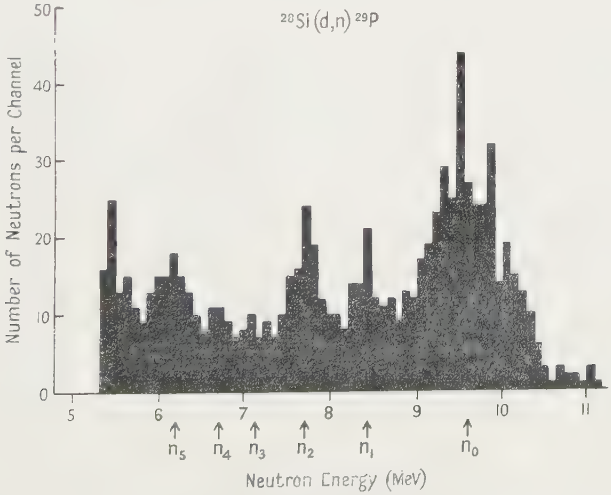

Figure 1. Neutron energy spectrum obtained at 15° from the reaction $^{28}Si(d, n)^{29}P$.

In addition, calculations of values for the reduced widths of the levels concerned have been made at the maxima of the experimental angular distributions.

3.1. $^{28}Si(d, n)^{29}P$

The ground-state Q-value for the silicon reaction was measured to be $0{\cdot}6 \pm 0{\cdot}1$ MeV, in reasonable agreement with that calculated from beta-decay and reaction data. Other levels were identified at excitation energies of 1·4 and 1·9 MeV. The positions of these levels are in fair agreement with those in the mirror nucleus ^{29}Si at 1·28 and 2·03 MeV, although more levels have been identified in the latter. Angular distributions for the first three levels are given in figure 2. The l-values fitted by application of stripping theory are in agreement with the results of Holt and Marsham on the mirror reaction, and also in agreement with work in this laboratory on the reaction ^{28}Si(d, n)^{29}P by Green (1955) using photographic plates.

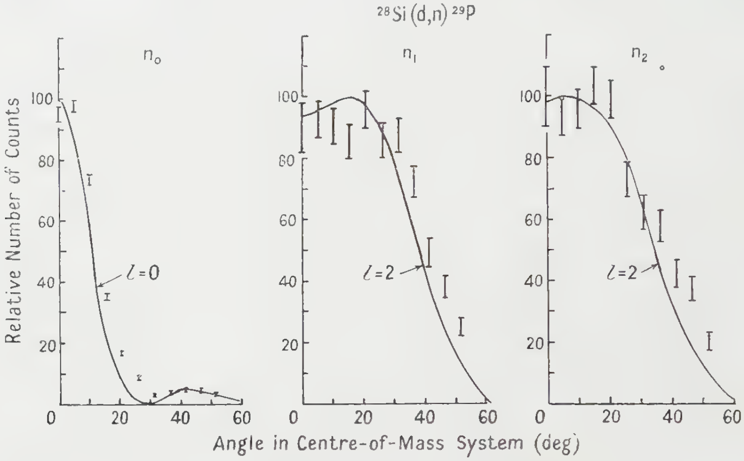

Figure 2. Angular distributions of neutron groups corresponding to the ground state of ^{29}P, and states at 1·30 and 1·92 MeV.

One further group (n_5) was identified at 15° only. Intensity considerations prevented it from being resolved at other angles. The excitation energy of the group agrees with that of the corresponding proton group p_5 in the work of Holt and Marsham. Their proton groups p_3 and p_4 are both weak and it appears that the corresponding neutron groups in our work, n_3 and n_4, are also too weak to be properly resolved. The positions of these groups indicated on the spectrum are taken from the measurements by Green. An upper limit to their cross sections appears in table 1.

Measurements of the absolute cross sections were made by the method described in the previous paper. Range-energy curves of Rich and Madey (1954) and n–p scattering data of Adair (1950) were used in the calculations. Results are summarized in table 1. The accuracy of the absolute cross sections is of the order of 50%, although the relative values are correct to about 15%.

3.2. $^{12}C(d, n)^{13}N$

The angular distributions of three neutron groups from this reaction were measured and found to be in agreement with the previous work of Middleton *et al.*

Table 1.

(1)	(2)	(3)	(4)	(5)	(6)	(7)
			Reaction ^{28}Si(d, n)^{29}P			
n_0	0	0	1/2	even	$28{\cdot}0\times10^{-27}$ (0°)	$9{\cdot}0\times10^{-20}$
n_1	1·30	2	3/2, 5/2	even	$7{\cdot}5\times10^{-27}$ (0°)	$11{\cdot}0\times10^{-20}$
n_2	1·92	2	3/2, 5/2	even	$7{\cdot}0\times10^{-27}$ (0°)	$8{\cdot}0\times10^{-20}$
n_3	2·5				$< 3{\cdot}0\times10^{-27}$ (15°)	
n_4	2·9				$< 4{\cdot}0\times10^{-27}$ (15°)	
n_5	3·5				$\sim 9{\cdot}5\times10^{-27}$ (15°)	
			Reaction ^{12}C(d, n)^{13}N			
n_0	0	1	1/2	odd	$3{\cdot}9\times10^{-26}$ (0°)	$2{\cdot}4\times10^{-19}$
n_1	2·37	0	1/2	even	$7{\cdot}5\times10^{-26}$ (0°)	
n_2	3·51	2	3/2	odd	$2{\cdot}7\times10^{-25}$ (0°)	
n_3	3·56		5/2	even		$2{\cdot}5\times10^{-18}$

(1) Neutron group. (2) Excitation energy of level in Mev. For ^{13}N the values of Ajzenberg and Lauritsen are given. The ^{29}P level positions are those estimated from the present work, except for n_3 and n_4 where the values are taken from the work of Green. (3) *l*-value. (4) Spin of state where known or alternative values derived from stripping theory. (5) Parity. (6) Differential cross section at centre-of-mass angle shown. (7) Reduced width of level in c.g.s. units multiplied by $2J_f+1$, where J_f is equal to the spin of the final state.

(1953). In addition we have measured the absolute cross sections for these three groups and the results are given in table 1. The three groups are known to correspond to neutrons from four levels in ^{13}N, the excitation energies being given by Ajzenberg and Lauritsen (1955). The levels at excitations of 3·51 and 3·56 Mev form a close doublet which we are unable to resolve, and the cross section quoted is for the two groups combined.

§ 4. Discussion

The spins and parities of the levels of ^{29}Si and ^{29}P have, where known, been presented in a review article by Endt and Kluyver (1954). Holt and Marsham have discussed the implications of their results for the (d, p) stripping reaction on ^{28}Si in terms of the nuclear shell model. Levels showing a large capture probability were identified as single-particle levels and given spectroscopic terms according to their *l*-values. The same arguments can be applied to the mirror reaction. For those levels in ^{29}P which can be identified and compared with ^{29}Si agreement is obtained for both *l*-values and excitation energies.

The ground state of ^{29}P is known to have spin $\frac{1}{2}$ and even parity, from a consideration of the *ft* values observed in beta decay. As the angular distribution of the neutrons corresponding to the formation of this state is characteristic of $l=0$, this indicates that the captured proton enters the $2s_{1/2}$ shell-model orbit, since ^{28}Si must be regarded as represented by a closed $1d_{5/2}$ shell.

The calculated reduced width for the first excited state is of the same order of magnitude as the value for the ground state. One may therefore suppose that this state, also, is formed by the excitation of a single particle into the appropriate shell-model orbit. The neutron group n_1 has an angular distribution characteristic of $l=2$, and so stripping theory gives spin values of 3/2 or 5/2 and even parity for this level. However, the first excited state of the mirror nucleus ^{29}Si is known to be $3/2^+$ and so there seems little doubt that the first excited state of ^{29}P is also $3/2^+$.

The value of $l=2$ then agrees with the interpretation that this level is formed by the captured particle entering the $1d_{3/2}$ orbit.

The distribution of neutrons from the second excited state of ^{29}P is also characteristic of $l=2$, and so has spin either 3/2 or 5/2 and even parity. It is not possible, however, for this state also to be a simple single-particle state since the next d-level does not occur until after the 1f, 2p and 1g shells. Hence the configuration must be supposed to be more complex and this is supported by the fact that the reduced width, calculated for a spin value of 5/2, is some 25% of the value for the ground state.

Table 2 gives values of the reduced widths of the first three excited states of ^{29}P, calculated for the spin values shown, and also gives these values expressed as a fraction of the Wigner limit. The reduced widths for the corresponding states of ^{29}Si have also been calculated from the published cross sections of Holt and Marsham and the agreement between these values and those for ^{29}P can be seen to be quite good. This agreement has been confirmed by work (Calvert *et al.* 1956) in which the ratio of cross sections for (d, p) and (d, n) reactions has been measured more accurately.

Table 2.

Reaction ^{28}Si(d, n)^{29}P

(1)	(2)	(3)	(4)
0	$4{\cdot}5\times10^{-20}$ (1/2)	0·025	$5{\cdot}6\times10^{-20}$ (1/2)
1·3	$2{\cdot}7\times10^{-20}$ (3/2)	0·015	$4{\cdot}6\times10^{-20}$ (3/2)
1·92	$1{\cdot}3\times10^{-20}$ (5/2)	0·007	$1{\cdot}1\times10^{-20}$ (5/2)

(1) Excitation energy of level in Mev for ^{29}P. (2) Reduced width of level in c.g.s. units calculated for spin values shown. (3) Reduced width expressed as a fraction of the Wigner limit $3\hbar^2/2ma$. (4) Reduced width for corresponding levels in ^{29}Si calculated from the cross sections of Holt and Marsham.

The spins and parities of the levels of ^{13}N obtained from stripping have been discussed by Middleton *et al.* (1953) and the levels have also been compared with those of ^{13}C in that paper. Table 3 contains the values of the reduced widths for the first three excited states of ^{13}N calculated by Jackson and Galonsky (1951) and also that for the ground state calculated by Thomas (1952). From these values it is apparent that the neutron group from the second excited state would be expected to be much weaker than that for the third excited state, and this is borne out by the

Table 3.

Reaction ^{12}C(d, n)^{13}N

(1)	(2)	(3)	(4)	(5)	(6)
0	$1{\cdot}2\times10^{-19}$ (1/2)	0·056	$0{\cdot}48\times10^{-19}$	$1{\cdot}2\times10^{-19}$	$1{\cdot}28\times10^{-19}$
2·37	—	—	$12{\cdot}1\times10^{-19}$	$6{\cdot}5\times10^{-19}$	$3{\cdot}8\times10^{-19}$
3·51	—	—	$0{\cdot}6\times10^{-19}$	$0{\cdot}38\times10^{-19}$	$0{\cdot}48\times10^{-19}$
3·56	$4{\cdot}1\times10^{-19}$ (5/2)	0·19	$3{\cdot}76\times10^{-19}$	$1{\cdot}4\times10^{-19}$	$2{\cdot}56\times10^{-19}$

(1) Excitation energy of level in Mev for ^{13}N. (2) Reduced width of level in c.g.s. units, calculated for spin values shown. (3) Reduced width expressed as a fraction of the Wigner limit $3\hbar^2/2ma$. (4) Reduced width for ground state of ^{13}N as calculated by Thomas and reduced widths for first, second and third excited states as determined by Jackson and Galonsky. (5) Reduced widths for states of ^{13}C determined by Green and Middleton, (6) Reduced widths for states of ^{13}C determined by El Bedewi.

fact that the angular distribution of the combined group has a typical $l=2$ shape with no sign of any $l=0$ contribution which could come from the second excited state. Assuming, then, that the third neutron group contains mainly neutrons from the third excited state, a value for the reduced width of this state has been calculated and this is seen to agree with the value of Jackson and Galonsky. Also given in this table is the reduced width for the ground-state group, but that for the first excited state could not be calculated because of the known singularity in the Butler theory at these Q-values. The reduced width for the ground-state group does not agree with that obtained by Thomas but, on the other hand, agrees with the ground-state value for ^{13}C measured by Green and Middleton (1956) and by El Bedewi (1956). The latter authors, however, give different values for the reduced width of the third excited state and neither of these values agrees with that for ^{13}N, although they are all of the same order of magnitude.

Acknowledgments

The authors would like to thank Professor H. W. B. Skinner and Dr. J. R. Holt for their encouragement and advice, and Dr. H. C. Newns for many helpful comments on the theory of stripping reactions. Thanks are also due to Mr. W. H. Ward for his assistance in operating and maintaining the cyclotron. One of us (E. E. M.) wishes to thank the Department of Scientific and Industrial Research for the award of a research grant.

References

Adair, R. K., 1950, *Rev. Mod. Phys.*, **22**, 249.
Ajzenberg, F., and Lauritsen, T., 1955, *Rev. Mod. Phys.*, **27**, 77.
Butler, S. T., 1951, *Proc. Roy. Soc.* A, **208**, 559.
Calvert, J. M., Jaffe, A. A., Litherland, A. E., and Maslin, E. E., 1955 a, *Proc. Phys. Soc.* A, **68**, 1008.
Calvert, J. M., Jaffe, A. A., and Maslin, E. E., 1955 b, *Proc. Phys. Soc.* A, **68**, 1017; 1956, *Phys. Rev.*, **101**, 501.
El Bedewi, F. A., 1956, *Proc. Phys. Soc.* A, **69**, 221.
Endt, P. M., and Kluyver, J. C., 1954, *Rev. Mod. Phys.*, **26**, 95.
Green, T. S., 1955, *Ph.D. Thesis*, University of Liverpool.
Green, T. S., and Middleton, R., 1956, *Proc. Phys. Soc.* A, **69**, 28.
Holt, J. R., and Marsham, T. N., 1953, *Proc. Phys. Soc.* A, **66**, 467.
Jackson, H. L., and Galonsky, A. I., 1951, *Phys. Rev.*, **84**, 401.
Mandeville, C. E., Swann, C. P., Chatterjee, S. D., and Van Patter, D. M., 1952, *Phys. Rev.*, **85**, 193.
Mayer, M. G., 1950, *Phys. Rev.*, **78**, 16.
Middleton, R., El Bedewi, F. A., and Tai, C. T., 1953, *Proc. Phys. Soc.* A, **66**, 95.
Peck, R. A., 1948, *Phys. Rev.*, **73**, 947.
Rich, M., and Madey, R., 1954, *University of California*, U.C.R.L. 2301.
Thomas, R. G., 1952, *Phys. Rev.*, **88**, 1109.

γ-Radiation Following Proton Capture in ^{35}Cl, ^{37}Cl and ^{39}K

By J. H. TOWLE†, R. BERENBAUM‡ AND J. H. MATTHEWS‡
Department of Physics, Imperial College, London

MS. received 10*th September* 1956, *and in final form* 13*th November* 1956

Abstract. The excitation functions of the reactions Cl (p, γ) A and ^{39}K (p, γ) ^{40}Ca in the region 0·8–1·8 MEV have been obtained using targets of natural isotopic composition. At the prominent resonances measurements with a NaI scintillation spectrometer have yielded information on the decay schemes of ^{36}A, ^{38}A and ^{40}Ca. The yield of the more intense γ-rays has been measured.

Bound levels have been located in ^{36}A at $1{\cdot}95 \pm 0{\cdot}05$ and $4{\cdot}1 \pm 0{\cdot}1$ MEV.

§ 1. INTRODUCTION

BROSTRÖM, MADSEN AND MADSEN (1951) have reported 86 sharp resonances in the yield of the reaction Cl (p, γ) A for proton energies between 500 and 2150 kev using targets containing natural chlorine. Using enriched targets some of the more prominent resonances were assigned to their isotopes, viz. ^{36}A, 858, 888, 1102, 1258, 1484 and 1510 kev and ^{38}A, 1090 kev.

The present paper describes measurements of the γ-ray spectra at four resonances in ^{36}A and four in ^{38}A. The results lead to the location of bound levels in these nuclei.

The reaction ^{39}K(p, γ)^{40}Ca has not previously been reported. Transitions have been observed to known levels in ^{40}Ca.

I. EXPERIMENTAL PROCEDURE

§ 2. EXCITATION FUNCTIONS

Targets were made from ‘ Specpure ’ $BaCl_2$ and Kl evaporated on to molybdenum or tantalum backings. The target thickness used was, in general, about 5 kev for protons of 1 mev energy. Tantalum apertures were used to define the proton beam of the electrostatic generator. Beam currents of up to 5 μA were used.

The γ radiation was detected by a NaI (Tl) crystal of dimensions 2 in. long × 1·7 in. diameter, in conjunction with a Du Mont photomultiplier. The detector was placed at 0° to the proton direction for measurements of the excitation function and thick target yields. In general, the angular distribution of the γ-rays concerned in the yield measurements was measured and taken into account in estimating the absolute yields. The intensity calibration was obtained from the ^{19}F(pα, γ)^{16}O reaction at the 340 kev resonance using the results of Chao *et al.* (1950). The angular distribution of the γ-rays at this resonance is isotropic (Devons and Hine 1949).

The probable error of the yield measurements is $\pm 15\%$.

---

† Now at the Atomic Weapons Research Establishment, Aldermaston, Berks.
‡ Now at the Physical Laboratories, The University of Manchester.

§ 3. γ-RAY SPECTRA

Pulses from the photomultiplier were taken via an amplifier to a 50-channel kicksorter. The amplifier also provided facilities for gating the spectra (Folkierski 1956). Line shapes and calibration were obtained from convenient radiaoctive sources and the following reactions: ^{9}Be(α, n)^{12}C (4·44 MeV), ^{19}F(p, α)^{16}O (6·14 MeV), ^{13}C(p, γ)^{14}N (8·06 MeV). Curves of A/PH were plotted against γ-ray energy for the total capture and the two escape peaks; A = area under the curve, P = pulse height of a peak and H = counts per channel at the peak. These curves enable the area under a curve to be determined from a knowledge of P and H only, and thus simplify the measurement of intensities in a complex spectrum (after Flack *et al.* 1954).

The intensity measurements are accurate to within about 20% unless otherwise stated.

§ 4. COINCIDENCE MEASUREMENTS

γ–γ coincidence measurements were made using a second NaI spectrometer in conjunction with that already described. The pulses from this spectrometer were fed into a single-channel kicksorter which could be set to cover any part of the spectrum. The pulses from this energy band were used to trigger the 10 μsec gate which preceded the 50-channel analyser. A delay of 3 μsec preceding the gate in the measuring channel ensures that the gate is opened before the coincident pulse arrives.

II. RESULTS. Cl(p, γ)A

§ 5. EXCITATION FUNCTION

Using a target of 5 kev thickness to 1 MeV protons and with the detector biased at 2·5 MeV, prominent well resolved resonances were found at 855, 1070, 1135, 1484, 1510, 1533, 1580 and 1725, all ± 5 kev. None of these resonances has a width greater than 5 kev. The resonances at 888, 1090, 1102 and 1258 kev mentioned by Broström *et al.* were not clearly resolved. The resonances not assigned by Broström we assign (by means of their γ-ray spectra) as follows: 1070, 1135, 1533, 1725 to ^{38}A and 1580 kev to ^{36}A. Broström has given the excitation curves for the (p, γ) and (p, n) reactions on natural chlorine for the region 1·6–1·8 MeV proton energy. The large γ resonance at 1725 kev is evidently a neutron resonance also. This confirms the assignment of this resonance to ^{38}A since the threshold of the ^{35}Cl(p, n)^{35}A reaction is at 6 MeV.

We have measured the yields of the more intense γ-rays at the above resonances. The results are given in table 1. Angular distributions have not been taken into account in estimating the yield at three of these resonances but this omission is not expected to put these results in error by more than 30%.

In estimating $\omega\Gamma_\gamma$ we have made the reasonable assumption that $\Gamma_p \gg \Gamma_\gamma$. ω is the statistical factor $(2J+1)/(2S+1)(2I+1)$ where J, S and I are the spins of the resonance level, proton and target nucleus respectively.

§ 6. γ-RAY SPECTRA

(i) 855, 1484, 1510 *and* 1580 *kev resonances in* ^{36}*A*.

From measurements made at 0° and 90° to the proton direction we find γ-rays of energies and relative intensities as shown in table 2. These measurements

Table 1.

	E_{res} (kev)	E_γ (Mev)	Yield $\gamma/10^{10}$p	$\omega\Gamma_\gamma$ (ev)
^{36}A	855	5·1	1·8	1·2
	1484	9·9	1·1	1·0
	1510	9·9	4·6	4·0
	1580	10·0	3·1	2·7
^{38}A	1070	7·5	†0·5	1·1
	1135	6·4	†0·8	1·8
	1533	9·5	1·4	3·5

† Not corrected for any anisotropy of the γ-ray distributions : see text.

Table 2.

E_{res}	E_{exc} (^{36}A)	E_γ	Rel. Int.	Interpretation
0·855	9·2	5·1	10	9·2 → 4·1
		1·95	11	1·95 → 0
		2·15	9	4·1 → 1·95
		4·1	5	4·1 → 0
		4·3		9·2 → 4·9 ?
		~3	~2	4·9 → 1·95 ?
		0·77	~1	4·9 → 4·1 ?
		7·2	$\lesssim$0·5	9·2 → 1·95
1·484	9·83	9·9	$\gtrsim$90%†	9·83 → 0
1·510	9·86	9·9		9·86 → 0
1·580	9·93	9·9		9·93 → 0

Energies are in Mev.
† $\gtrsim$90% of transitions from top level.

suggest a decay scheme as given in figure 1, which shows the data fitted to a minimum number of energy levels. No bound levels have previously been reported for this nucleus. Coincidence measurements have confirmed the 5·1–4·1 and 5·1–2·15–1·95 Mev cascades. It appears probable also that the 770 kev radiation is in coincidence with both the 2·15 and 1·95 Mev radiations. It is possible that the 770 kev transition connects a level in the 4·3–3·0 Mev cascade to the level at 4·1 Mev as shown with broken lines in figure 1.

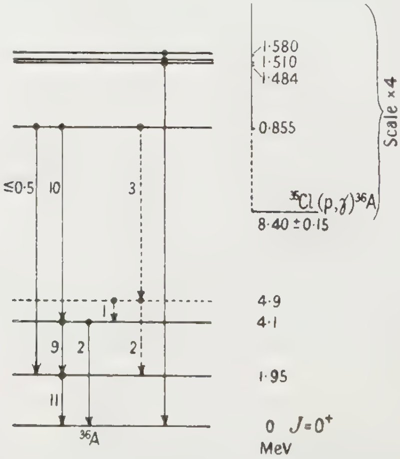

Figure 1. Decay scheme for ^{36}A. The numbers on the arrows denote relative intensities at the 855 kev resonance.

The resonances at 1484, 1510 and 1580 kev decay mainly to the ground state and provide no check on the decay scheme. The low-energy spectrum of the 1580 kev resonance shows a small amount of radiation in the region of 1·6 and 2·1 Mev. Coincidence measurements have shown however that this is due to transitions in ^{38}A owing to the resonance being insufficiently resolved from a smaller one in ^{38}A.

(ii) 1070, 1135, 1533, 1725 *kev resonances in* ^{38}A.

γ-ray spectra were measured at 0° to the proton direction.

Levels at 2·16 Mev ($J=2^+$) and 3·75 Mev ($J=3^-$) are known in ^{38}A: for references see Endt and Kluyver (1954). The 3·75 Mev level is known to decay mainly through the 2·16 Mev level. This cascade is prominent in the spectra of three of the above resonances.

Owing to the complexity of the spectra, particularly at the 1725 kev resonance, we cannot present a complete picture of the decay scheme at each resonance. Relative intensities have not been corrected for anisotropy of the γ-rays. The main features of the decay scheme may however be deduced.

The 1070 and 1135 kev resonances decay mainly to the levels at 2·16 and 3·75 Mev and to a level at approximately 5 Mev.

The resonance at 1533 kev decays mainly to the 2·16 Mev level; this has been confirmed by coincidence measurements. A lesser amount of radiation of 6·7 Mev presumably goes to the 5 Mev level. There is little evidence for a transition to the 3·75 Mev level at this resonance. The 5 Mev level decays mainly to the first excited and ground states.

The resonance at 1725 kev appears to decay mainly by a radiation of about 5·2 Mev which would lead to a level at 6·7 Mev excitation. There is also evidence for a γ-ray of 3 Mev which probably connects the above level to that at 3·75 Mev. The 1·6–2·16 Mev cascade is the main feature of the low-energy spectrum.

§ 7. DISCUSSION

The Q values obtained for proton capture in ^{35}Cl and ^{37}Cl are $8{\cdot}4 \pm 0{\cdot}15$ and $10{\cdot}15 \pm 0{\cdot}15$ Mev respectively, as compared with $8{\cdot}50 \pm 0{\cdot}1$ and $10{\cdot}15 \pm 0{\cdot}1$ Mev obtained from the results of mass spectrometry etc. (Wapstra 1955).

The three resonances in ^{36}A which decay predominantly to the ground state probably have spin unity. There is little evidence for a transition to a first excited state (expected to have $J=2^+$) although the radiation would have the same character as the ground state transition.

The decay scheme for ^{36}A given in figure 1 is consistent with the levels at 1·95 and 4·1 Mev having spin 2, though we note that the transition direct to the 1·95 Mev level is weak compared with that to the level at 4·1 Mev.

In a survey of the excited states of even–even nuclei (Scharff-Goldhaber 1953) it has been recognized that the "addition of two protons to a nucleus" in general alters very little the position of the first excited state, except when the initial or final nucleus has a 'magic' number of protons. ^{34}S has a first excited state at 2·1 Mev, and one would thus expect that of ^{36}A to be located within a few hundred kev of 2·1 Mev. Thus, there is reason to believe that the level we report at 1·95 Mev in ^{36}A is the first excited level.

In ^{38}A we have seen no appreciable decay to the ground state. This may be due, at the 1070, 1135 and 1725 kev resonances, to these resonance levels probably having spin greater than unity. However, the 1533 kev resonance probably does have spin unity since it does not decay appreciably to the 3·75 Mev (3^-) level either. A spin of zero for this resonance is ruled out as we have found the γ-rays to be anisotropically distributed.

The 1725 kev resonance level probably has spin 4 or 5 since it does not decay appreciably to the 2·16 or 3·75 Mev levels. It seems likely that the proposed level at 6·7 Mev has spin 4 (or greater) since it decays mainly through the level with $J = 3^-$.

III. RESULTS. ^{39}K(p, γ)^{40}Ca

§ 8. Excitation Function

With the detector biased at 2·5 Mev prominent resonances were observed at proton energies of 1120, 1300, 1338, 1566 all ±5 kev. 5 kev is an upper limit to the width of the resonance levels. The yield of the more intense γ-rays is given in table 3.

Table 3.

E_{res} (kev)	E_γ (Mev)	Yield $\gamma/10^{10}$p	$\omega\Gamma_\gamma$ (ev)
1120	9·5	0·65	0·5
1300	9·7	1·1	1·0
1338	5·8 6·0	1·5	—
1566	9·9	1·8	1·7

§ 9. γ-ray Spectra

The bound levels shown in figure 2 have been located by Braams (1956). The first excited state at 3·35 Mev is known to have $J = 0^+$ (Bent *et al.* 1955).

We have observed the γ-ray spectra with the detector at 0° to the proton direction at the four resonances mentioned. Results are given in table 4. The predominant mode of decay is seen to be direct to the ground state except at the 1338 kev resonance which cascades through the levels at 3·73 and 3·9 Mev. Coincidence measurements show that less than 10% of the transitions from the 3·9 Mev level are to the 3·73 Mev level.

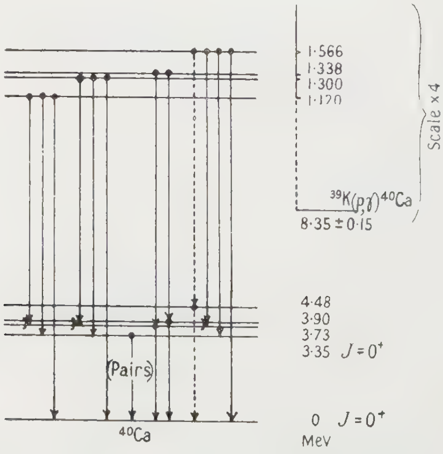

Figure 2. Transitions in ^{40}Ca.

§ 10. DISCUSSION

The Q value of $8{\cdot}35 \pm 0{\cdot}15$ MeV we obtain for proton capture in ^{39}K is in agreement with the value 8·34 ($\pm 0{\cdot}12$) MeV deduced from other data (Wapstra 1955).

At the 1300 kev resonance the 3·7–3·9 MeV radiation is much more intense than the radiation direct to these levels. This effect seems rather large to explain on the grounds of angular distributions and may indicate a triple cascade via a level at much higher excitation.

From the results in table 4 we obtain the probability of a transition to the 0^+ pair-emitting level, relative to that of a transition to the 0^+ ground state, $\Gamma_\pi/\Gamma_{\rm g.s.}$. The angular distributions of these radiations are the same, since 'mixed' transitions cannot occur, and thus we may compare the intensities measured at one angle. For the 1120, 1300 and 1566 kev resonances we obtain respectively $\Gamma_\pi/\Gamma_{\rm g.s.}<0{\cdot}13$, $\Gamma_\pi/\Gamma_{\rm g.s.}<0{\cdot}08$ and $\Gamma_\pi/\Gamma_{\rm g.s.}<0{\cdot}23$. If the reduced transition probabilities for decays to the two 0^+ levels were equal, the γ-ray energy factor would give us $\Gamma_\pi/\Gamma_{\rm g.s.}\simeq 0{\cdot}27$ for dipole and $\Gamma_\pi/\Gamma_{\rm g.s.}\simeq 0{\cdot}12$ for quadrupole transitions. It is probable that the resonance levels at 1120, 1300 and 1566 kev have spin unity since they decay mainly to the ground state. If this is so, the above-mentioned transitions are dipole, and we see that the reduced probability of a transition to the pair-emitting level is rather less, though perhaps not remarkably so, than that of a transition to the ground state.

Table 4.

$E_{\rm res}$	$E_{\rm exc}(^{40}{\rm Ca})$	E_γ	† Rel. Int.	Interpretation
1·120	9·45	9·5	100	9·45 → 0
		6·1	9 ± 4	9·45 → 3·35
		5·6	4 ± 2	$9{\cdot}45 \rightarrow \begin{cases}3{\cdot}9\\3{\cdot}73\end{cases}$
		3·8	14	$\left.\begin{matrix}3{\cdot}9\\3{\cdot}73\end{matrix}\right\}\rightarrow 0$
1·300	9·65	9·65	100	9·65 → 0
		6·3	5 ± 3	9·65 → 3·35
		5·8	6 ± 3	$9{\cdot}65 \rightarrow \begin{cases}3{\cdot}73\\3{\cdot}9\end{cases}$
		3·8	65	$\left.\begin{matrix}3{\cdot}73\\3{\cdot}9\end{matrix}\right\}\rightarrow 0$
		5·2	$\lesssim 5$	9·65 → 4·5 ?
1·338	9·69	9·7	<5	9·7 → 0
		5·96	35	9·7 → 3·73
		5·79	65	9·7 → 3·9
		$\left.\begin{matrix}3{\cdot}7\\3{\cdot}9\end{matrix}\right\}$	100	$\left.\begin{matrix}3{\cdot}73\\3{\cdot}9\end{matrix}\right\}\rightarrow 0$
1·566	9·9	9·9	100	9·9 → 0
		6·6	17 ± 6	9·9 → 3·35
		6·1	17 ± 6	$9{\cdot}9 \rightarrow \begin{cases}3{\cdot}73\\3{\cdot}9\end{cases}$
		~5·4	8 ± 4	9·9 → 4·5 ?
		~4·5	8 ± 4	4·5 → 0 ?
		3·8	25	$\left.\begin{matrix}3{\cdot}73\\3{\cdot}9\end{matrix}\right\}\rightarrow 0$

Energies in MeV.
† Relative intensity at 0° to the proton direction.

Support for the assignment of unit spin to two of the above resonance levels is obtained from meaurements of the angular distribution of the γ-rays emitted in the transitions from the resonance levels directly to the ground state (1120 and 1300 kev resonances).

It is hoped to present at a later date the results of angular distribution measurements on these and some other of the γ-rays observed from both argon and calcium.

ACKNOWLEDGMENTS

We would like to thank Professor S. Devons for suggesting this work and for his continued interest. We are indebted for maintenance awards during the course of this work to the Department of Scientific and Industrial Research (J. H. T. and R. B.) and to the Beaverbrook Overseas Scholarship Fund (J. H. M).

REFERENCES

BENT, R. D., BONNER, T. W., and MCCRARY, J. H., 1955, *Phys. Rev.*, **98,** 1325.
BRAAMS, C. M., 1956, *Phys. Rev.*, **101,** 1764.
BROSTRÖM, K. J., MADSEN, B. S., and MADSEN, C. B., 1951, *Phys. Rev.*, **83,** 1265 (L).
CHAO, C. Y., TOLLESTRUP, A. V., FOWLER, W. A., and LAURITSEN, C. C., 1950, *Phys. Rev.*, **79,** 108.
DEVONS, S., and HINE, M. G. N., 1949, *Proc. Roy. Soc.* A, **199,** 56, 73.
ENDT, P. M., and KLUYVER, J. C., 1954, *Rev. Mod. Phys.*, **26,** 95.
FLACK, F. C., RUTHERGLEN, J. G., and GRANT, P. J., 1954, *Proc. Phys. Soc.* A **67,** 973.
FOLKIERSKI, A., 1956, *J. Sci. Instrum.*, **33,** 187.
SCHARFF-GOLDHABER, G., 1953, *Phys. Rev.*, **90,** 587.
WAPSTRA, A. H., 1955, *Physica*, **21,** 385.

LETTER TO THE EDITOR

A Re-measurement of the L$\alpha_{1,2}$ Lines of Lanthanum

Precision measurements of the principal lines of the L spectra of the rare earth elements were first made thirty five years ago by Hjalmar (1921). Re-measurements have been made more recently in a number of cases (Yb and Lu by Allais (1942), Dy by Barriere (1947), Eu, Gd, Tb, Ho, Er and Tm by Sakellaridis (1953)). With one exception (Eu Lα_2, Sakellaridis (1953)) the results of the re-measurements have been to raise the wavelengths of the L$\alpha_{1,2}$ lines by a small amount—a few tenths of one X.U. in most cases. In the case of lanthanum, however, no recent measurements seem to have been made. The wavelengths of the Lα lines given by Hjalmar are: Lα_1—2659·7 X.U., Lα_2—2668·9 X.U. These yield a ν/R difference of 1·18 for the difference in energy between the M_{IV} and the M_V levels. (Throughout this note energy differences will be expressed in terms of the difference in ν/R). The $M_{IV,V}$ energy difference may also be derived from the wavelengths of the Mα, β lines. These lines have so far been observed only by Kiessig (1938) who gives their wavelengths as 14·88 Å and 14·51 Å respectively. This corresponds to an $M_{IV,V}$ energy difference of 1·56, which is considerably greater than Hjalmar's value. Kiessig's value is to some extent supported by the values yielded by the two pairs of quadrupole lines K$\beta_5^{\mathrm{I,II}}$ and L$\beta_{9,10}$. The former were measured by Ingelstam (1937) and give an energy difference of 1·47, the latter by Coster (1922) (who, however, used Hjalmar's L$\alpha_{1,2}$ wavelengths as reference standards) giving an energy difference of 1·40. Rouault (1939) also gives the difference as 1·50 but this is presumably based on Ingelstam's measurements.

As we required a knowledge of this energy difference in connection with some investigations into the M spectrum of lanthanum at present being carried out in this laboratory, it seemed worth while, in view of these discrepancies, to re-measure the L$\alpha_{1,2}$ lines. For this purpose we used a focusing X-ray spectrometer with a crystal of muscovite mica bent to a nominal radius of 200 cm. As reference lines the K$\alpha_{1,2}$ lines of Ni and Cu were used. These were photographed in the 5th order simultaneously with the lanthanum lines in the 3rd order by using a copper target coated with a mixture of lanthanum and nickel oxides. The photographic plates were placed normal to the X-ray beam and measurements were made in the manner described by Haglund (1941). Eight photographs were used in the wavelength determinations. Two micro-photometer recordings of each plate were taken, and two calculations of the wavelengths made from measurements on each recording, one using Ni Kα_1 and Cu Kα_1 as reference lines, the other using the corresponding Kα_2 radiations. This gave 32 values for each of the lanthanum Lα_1 and Lα_2 lines. The values obtained were well distributed about the means, conforming fairly well to a normal distribution, of probable error ±0·07 X.U. The mean values obtained were:

	λ(X.U.)	ν/R
Lα_1	2660·06	342·58
Lα_2	2669·71	341·34

The probable error mentioned is, of course, a statistical one. Instrumental error is probably greater than this, but it is unlikely, in our opinion, to exceed ± 0·15 X.U. The greatest uncertainty is in the values of the effective lattice constants for different orders in mica. In our determinations we have used the values given by Siegbahn (1931) which were derived from measurements made by Larsson (1929). No allowance has been made for anomalous dispersion in the mica as this effect is presumably small for wavelengths appreciably shorter than the K absorption edge of potassium—the heaviest element normally present in muscovite mica. The wavelengths of the Ni and Cu K lines were taken from the list of wavelengths given by Bragg (1947) as suitable first class standards. These were converted to X.U. by division by 1·00202.

In common with the recent re-determinations of the L lines of other rare earth elements our wavelengths are a few tenths of one X.U. greater than Hjalmar's; the $M_{IV, V}$ energy difference of 1·24 yielded by our measurements reduces slightly the discrepancy between the $L\alpha_{1, 2}$ value and the $M\alpha, \beta$ value, but not significantly. The major part of the discrepancy still remains. In this connection it is worth recalling that the occurrence of the $M\alpha, \beta$ lines in lanthanum remains a matter for surprise as it is still generally accepted that this element possesses no 4f electrons. Further investigation of the M spectrum is obviously needed and as mentioned above such work is now in progress.

The discrepancy in the case of the quadrupole lines is probably not very surprising. In case of the K quadrupole lines the $M_{IV, V}$ energy difference is given by the small difference between two very high frequencies, and changes in the appropriate directions in Ingelstam's wavelengths of the order of 1 part in 30 000 would suffice to bring the $K\beta_5^{I, II}$ energy difference into agreement with that of our $L\alpha_{1, 2}$. Similarly, in the case of $L\beta_{9, 10}$ the discrepancy is probably no greater than is attributable to the experimental error inherent in the measurement of very weak lines. In passing, it is worth noting that similar discrepancies exist in the data at present available for the nearby elements Cs and Ba.

Department of Physics,
University College of Leicester.
7th November 1956.

P. C. Russell.
E. A. Stewardson.

References

Allais, M., 1942, *Cah. Phys.*, **7**, 13.
Barriere, G., 1947, *J. Phys. Radium*, (8), **8**, 72.
Bragg, W. L., 1947, *Phys. Rev.*, **72**, 437.
Coster, D., 1922, *Phil. Mag.*, **43**, 1070.
Haglund, P., 1941, *Ark. Mat. Astr. Fys.*, **28A**, No. 8.
Hjalmar, E., 1921, *Z. Phys.*, **7**, 341.
Ingelstam, E., 1937, *Nova Acta Soc. Sci. Upsal.*, Ser. IV, **10**, No. 5.
Kiessig, H., 1938, *Z. Phys.*, **109**, 671.
Larsson, A., 1929, *Uppsala Univ. Årsskr.*
Rouault, M., 1939, *C. R. Acad. Sci., Paris*, **209**, 434.
Sakellaridis, P., 1953, *C. R. Acad. Sci., Paris*, **236**, 1014; *Ibid.*, **236**, 1244; *Ibid.*, **236**, 1547.
Siegbahn, M., 1931, *Spektroskopie der Röntgenstrahlen* (Berlin: Springer).

REVIEWS OF BOOKS

Expanding Universes, by E. Schrödinger. Pp. viii + 93. (Cambridge: University Press, 1956.) 17*s*. 6*d*.

The study of expanding universes using the theory of general relativity has three stages : the derivation of the general form of the space-time to be used for representing the career of a (smoothed-out) universe, the derivation of the properties of this space-time as regards the behaviour of test-particles and test-signals, the application of Einstein's field relations resulting in the study of particular classes of models. Professor Schrödinger's book deals exclusively with the second stage. It is concise but it is also almost certainly the most thorough single account of this part of the subject.

The first chapter is devoted to the de Sitter universe which is the simplest case for the purpose and which admits comparatively simple geometrical treatments not demanding the general theory of the following chapter. This is the theory of geodesics and its applications to free particles and light rays in the general case. The remaining two chapters treat the same physical phenomena by the wave theories of matter and of light. The connection between the two treatments is based upon the Hamilton–Jacobi theory of particle-motion. The treatments give concordant results and so provide valuable insight into each other.

This summary fails to indicate both the originality of the discussion, particularly that of the wave-theory of which Schrödinger is an unrivalled master, and the liveliness of its presentation. Naturally, these can be appreciated only by the reading of the book itself. This is heartily recommended to all students of relativity theory, whether or not they have special interests in the subject of expanding universes on its own account.

When the subject is developed in the stages I have mentioned, the first two stages are independent of the last. They give the behaviour of test-particles and test-signals in the presence of whatever may be the material and radiational contents of the universe as determined in the last stage. This determination need not be made to depend on Einstein's field-relations. For instance, Schrödinger's study of the de Sitter universe, so far as he takes it, applies equally to the model given by the ' steady state ' theory.

On the other hand, the liberty to go so far without appealing to field-relations is paid for by the fact that, when we do appeal to them to determine the general contents of the universe, there is no necessity for an element of these contents to behave in the same way as one of the test-particles already considered. Therefore the sort of discussion on pp. 60–61 of the book, in which Schrödinger makes inferences about the behaviour of the general contents from his results for test-particles, seems to require further justification. In the cases of physical interest, I think such justification would be forthcoming, but only from a part of the subject that is just outside the scope which Schrödinger has set for himself.

W. H. McCREA.

Structure Report for 1942–1944, Edited by A. J. C. Wilson, N. C. Baenziger, J. M. Bijvoet and J. M. Robertson. Pp. viii + 448 with many figs. (Utrecht: Oosthoek, 1955, published for the International Union of Crystallography.) 65 Dutch florins; $17.50; £6 6*s*. 0*d*.

This is the fifth volume of *Structure Reports* to appear under the auspices of the International Union of Crystallography and follows closely the style of the previous volumes, now well known among crystallographers; the only change introduced is the inclusion of an additional index of carbon compounds. As in the preceding volumes, it has been the policy of the editors and their assistants to attempt to report the structural information in every published paper so fully that no further information would be gained by consulting the paper itself. When it is added that the coverage of the world literature is virtually complete, and that extensive editorial comment is appended to many of the reports, something of the magnitude of the task undertaken by the editors will be appreciated. Crystallographers are exceptionally fortunate in having at their disposal this and the other excellent publications of the International Union of Crystallography, and in view of the unselfish services of the many editors it must seem almost churlish to venture any critical comment. Nevertheless, it might be suggested that there is scope for improvement in the figures in the volume under consideration. Possibly more of the structures could with advantage be represented diagrammatically, and certainly the appearance of the work would be more pleasing if the illustrations were more nearly uniform in style, size and lettering.

It is satisfactory to learn that after the publication of one further volume (that for 1940–41), the editors propose to produce a cumulative index for the years 1940–50. R. C. EVANS.

Valency and Molecular Structure, by E. Cartmell and G. W. A. Fowles. Pp. xi + 256. (London: Butterworths Scientific Publications; New York: Academic Press, 1956.) 32*s*. 6*d*.

Previous accounts of the quantum theory of valency have almost all either been too mathematical for the experimental physicist and chemist or have concentrated on one particular type of approximate wave function. The authors of the present book have done a notable service by providing an accurate, simple, and reasonably comprehensive account of this field in a manner that does not lie too far beyond the mathematical attainments of even the first-year undergraduate. It is true that concepts like electron spin are stumbling blocks in such a policy, since no physical picture can be safely appealed to; and there are several occasions where the authors are obliged to fall back on " Mathematical theory shows . . .". It is also true that some parts, such as the solution of the wave equation for the hydrogen atom, are much heavier and less ' chemical ' than the rest. But this is a useful book, and one that may safely be put in the hands of students (which is saying a lot more than may be said about several other attempts at simplifying wave mechanics !). It leans quite heavily on one or two larger well-known books, but, particularly towards the end, it shows itself to be up to date, with accounts of the electron-deficient borohydrides and the interesting cyclopentadienyls. It makes free use of both the valence-bond and molecular-orbital techniques.

In a book of this kind, which starts right at the beginning, there are bound to be some obscurities. But they appear to be relatively rare in this case.

A particular example occurs on p. 170 where no one could be sure how to describe the bonding in H_2O_2, since two alternative descriptions are given, without critical comment, and the most important factor—the strong repulsion of the lone-pair electrons on the two oxygen atoms—is hardly stressed at all. These, however, are not fundamentally serious objections. Cartmell and Fowles are to be congratulated on making a success of a difficult task. C. A. COULSON.

Electron Physics Tables, by L. MARTON, C. MARTON and W. G. HALL. Pp. 83. (Washington : National Bureau of Standards (Circular 571) 1956.) 50 cents

These tables replace *Miscellaneous Physics Tables—Part II. Electronic Functions* (Mathematical Tables 17 of the National Bureau of Standards, 1941). Eight quantities, calculated on the Standards Electronic Automatic Computor (SEAC), are tabulated with eight-figure accuracy. In the first column are values of V, the potential difference in absolute volts, required to impart to an electron initially at rest a kinetic energy E expressed in electron volts. The next column contains corresponding values of the ' effective relativistic potential difference ' $V^* = V + \boldsymbol{e}V^2/2\boldsymbol{m}_0\boldsymbol{c}^2$ which makes the classical expression $p = (2\boldsymbol{em}_0V^*)^{1/2}$ for the momentum give the relativistically correct result, $\boldsymbol{e}$ being the electronic charge, $\boldsymbol{m}_0$ the rest mass of the electron and $\boldsymbol{c}$ the velocity of light. In the third column, the product $H\rho$ of the magnetic field (in oersteds) and the radius of curvature (in cm) of the path of an electron in a plane perpendicular to the field is tabulated. The remaining columns contain, respectively, values of the wavelength $\lambda = h/p$ of the electron, the momentum in units of $\boldsymbol{m}_0\boldsymbol{c}$, i.e. $p/\boldsymbol{m}_0\boldsymbol{c}$, the kinetic energy in terms of $\boldsymbol{m}_0\boldsymbol{c}^2$, i.e. $E/\boldsymbol{m}_0\boldsymbol{c}^2$, the total energy in the same units and the ratio $\beta = v/\boldsymbol{c}$ of the electron velocity to the velocity of light.

There are over 3000 entries in each column. The range of V, for example, is from just over 2×10^{-1} to just over 3×10^{12}. Each parameter is treated as an independent variable at selected intervals, so that in this sense we have eight separate tables combined into one. A glance at any given column shows the entries which are tabulated at equal intervals. In between any two of these entries there are others which are not tabulated at equal intervals. These correspond to entries in other columns which have taken over the role of independent variable. This plan makes interpolation an easy matter. There are four pages of explanation at the beginning of the book. Care has been taken to make a proper choice of values of the physical constants on which the tables are based. The tables are nicely produced and should be useful to many physicists. M. R. HOPKINS.

CONTENTS OF SECTION B

PAGE

Dr. W. B. Thompson. Thermonuclear Reaction Rates 1

Mr. J. D. Lawson. Some Criteria for a Power Producing Thermonuclear Reactor 6

Mr. R. S. Pease. Equilibrium Characteristics of a Pinched Gas Discharge Cooled by Bremsstrahlung Radiation 11

Dr. J. E. Allen. An Elementary Theory of the Transient Pinched Discharge . 24

Dr. R. J. Tayler. Hydromagnetic Instabilities of an Ideally Conducting Fluid . 31

Mr. R. Carruthers and Dr. P. A. Davenport. Observations of the Instability of Constricted Gaseous Discharges 49

Dr. R. S. Tebble and Dr. R. W. Teale. Magneto-Thermal Effects in Nickel and Cobalt 51

Dr. E. R. Wooding. Concentration Changes in an Aerosol 65

Dr. J. H. Andreae. Ultrasonic Relaxation in Methylene Chloride . . . 71

Dr. D. H. Martin. Surface Structures and Ferromagnetic Domain Sizes . . 77

Dr. J. D. Macpherson. The Effect of Gas Bubbles on Sound Propagation in Water 85

Mr. R. C. Srivastava. Clusius and Dickel Column Constants for a Gas consisting of Hard Spherical Molecules 93

Dr. R. T. Spurr and Mr. T. P. Newcomb. The Adhesion Theory of Friction . 98

Dr. J. McK. Ellison. Extinction of Light by Suspensions of Silica Dust . . 102

Dr. J. K. Lancaster. The Influence of Temperature on Metallic Wear . . 112

Dr. R. J. Elliott. Theory of Nuclear Magnetic Resonance in Eu^{3+} . . 119

Dr. D. J. Howarth, Dr. R. H. Jones and Dr. E. H. Putley. The Dependence of the Hall Coefficient of a Mixed Semiconductor upon Magnetic Induction as Exemplified by Indium Antimonide 124

Mr. M. Redwood and Dr. J. Lamb. On the Propagation of High Frequency Compressional Waves in Isotropic Cylinders 136

Research Notes :

Mr. T. D. S. Hamilton. Photofluorescence Decay Times of Organic Phosphors 144

Mr. D. Haneman and Mr. A. J. Mortlock. Point Contact Transistor Studies using Radioactive Collectors 145

Mr. A. C. McLaren. The Absorption Spectra of Single Crystals of Pure and Partially Decomposed Silver Azide 147

Prof. C. Domb. Melting Curves of Helium and Hydrogen Isotopes . . 150

Letter to the Editor :

Dr. J. C. Woolley and Mr. B. A. Smith. Solid Solution in the GaAs–InAs System 153

Reviews of Books 155

Corrigendum :

P. T. Landsberg 154

Contents of Section A 160

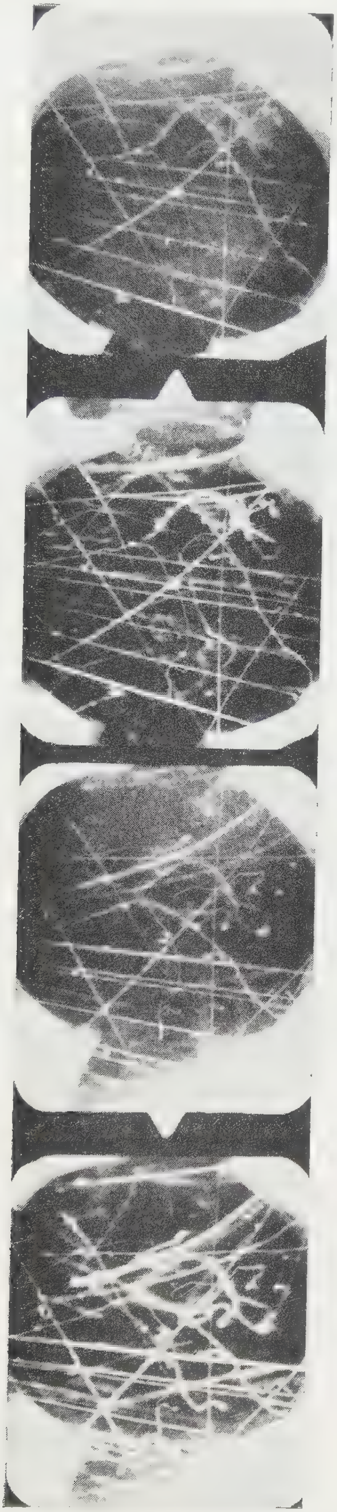

Figure 5. A set of two stereo-pairs. The first and third pictures from the right were taken with the first flash.

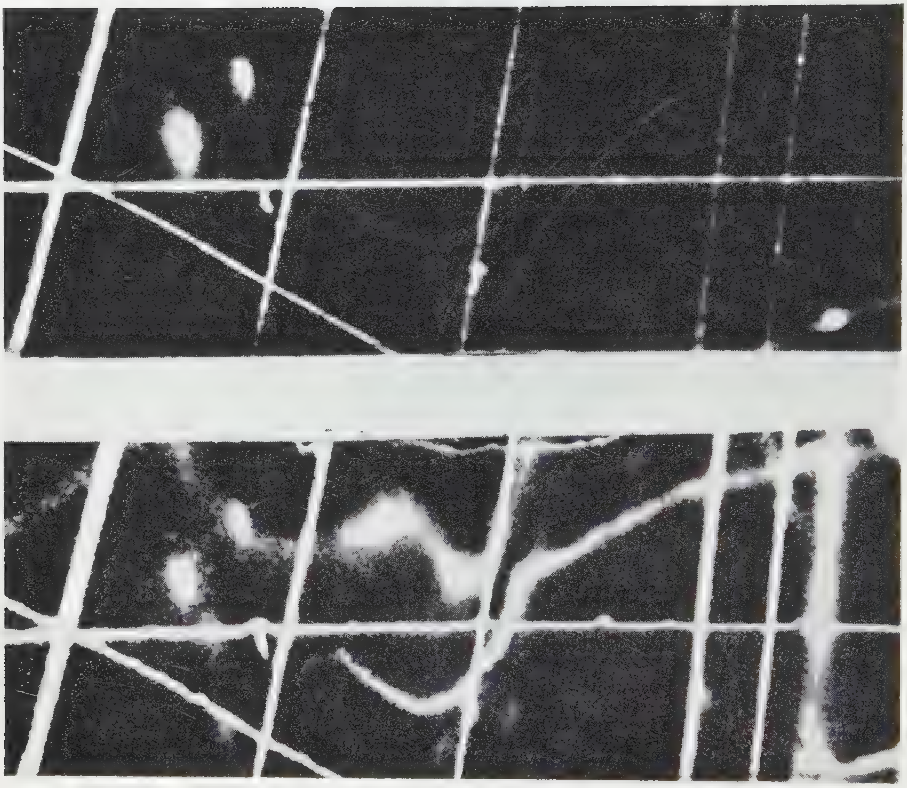

Figure 6. The first and second flash photographs of a horizontal track, the lower picture showing the distortion arising from local heating.

Calculation of the Interatomic Distance at which a Model of Compressed Solid Helium becomes a Metal

By C. A. ten SELDAM†
Cavendish Laboratory, Cambridge

Communicated by N. F. Mott; MS. received 20th September 1956

Abstract. In this paper, a calculation is attempted of the interatomic distance at which a face-centred cubic lattice of helium atoms becomes a metal, i.e., at which valence and conduction bands begin to overlap. Furthermore, the pressure which corresponds to this interatomic distance is estimated by means of the Thomas–Fermi equation of state. In one model used (the 'ionic' one) an electron in the crystal sees a helium ion at the lattice position to which it is nearest, and neutral helium atoms at the other lattice positions; thus the 'Fermi hole' is crudely accounted for. A slightly more refined model deals with exchange and correlation in a way similar to that of Bohm and Pines. In both cases, points of high symmetry in the Brillouin zone are used, and the Bloch wave functions are expanded in terms of the corresponding suitable linear combinations of simple plane waves; the convergence problem involved is discussed.

§ 1. Introduction

THERE has been much interest recently in the metallic properties (conduction at low temperatures, Hall effect, etc.) shown by impurity centres in semiconductors above a certain concentration. These impurities in silicon and germanium are normally in groups III and V in the periodic table and, consequently, contribute one electron or hole each to the conduction and behave like monovalent atoms. The conditions under which an ordered or disordered array of monovalent atoms will give electric conductivity are not yet clear. For divalent atoms, on the other hand, all theories suggest that conductivity will occur when, at a certain interatomic distance, overlap from one electron zone into another first takes place. It seemed worth while, for one atom (helium), to attempt a calculation of the interatomic distance at which this overlap would begin. This is the purpose of this paper.

Though near 0°K the solid helium crystal lattice is hexagonal close packed, at higher temperatures it is face-centred cubic (Dugdale and Simon 1953). Therefore, and because it is simpler to deal with, the face-centred cubic case has been used in the calculation. With two electrons per atom, the first Brillouin zone of a face-centred cubic lattice of helium atoms (the truncated octahedron of the figure) is just full, unless the first and second bands overlap. This overlapping will presumably occur at sufficiently small interatomic distances, and the purpose of the present calculations is to determine the distance at which this first occurs. At smaller distances the material then is a divalent metal. We wish, therefore, to determine the relative energies of the highest level in the first band and the lowest level in the second, as a function of interatomic distance.

Some preliminary calculations showed that the sequence L, X, W (cf. caption of the figure) is one of increasing energy in both first and second zones, as in the free-electron model. Thus subsequent calculations were confined to the energies at W in the first zone, and L in the second. Spill-over of electrons into the second zone will start at the centres L of the eight hexagonal faces, and will leave empty regions around the 24 corners W in the first zone.

---

† On leave from the Netherlands Foundation for Fundamental Research of Matter (F.O.M.), Van der Waals Laboratory, University of Amsterdam, Netherlands.

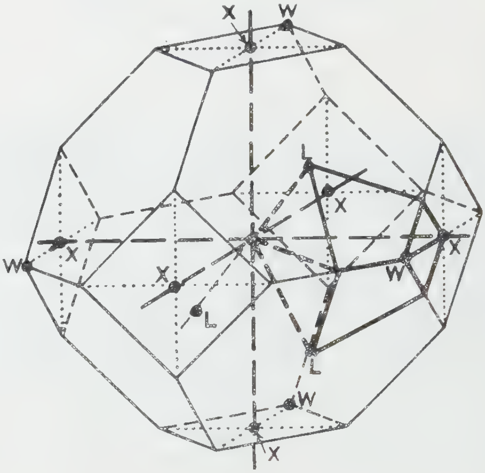

The first Brillouin zone boundary and the coordinate axes.

Some points of high symmetry :

L : $(a/\pi)\,\mathbf{k}=\pm\frac{1}{2},\ \pm\frac{1}{2},\ \pm\frac{1}{2}$ (8 points : centres of hexagonal faces);

X : $(a/\pi)\,\mathbf{k}=\pm 1,\ \ 0,\ \ 0$ (cycl.) (6 points : centres of squares);

W : $(a/\pi)\,\mathbf{k}=\pm 1,\ \pm\frac{1}{2},\ \ 0$ (cycl.) and $\pm 1,\ 0,\ \pm\frac{1}{2}$ (cycl.) (24 points : corners of squares).

Also shown are two 48th parts of the zone (cf. § 6).

The energies E of the two states mentioned above were calculated for several values of the interatomic distance. The effective potential $V(\mathbf{r})$ to be used in these calculations, as seen by an electron in the crystal, can be thought of as consisting of two terms,

$$V(\mathbf{r})=V_{\mathrm{e}}(\mathbf{r})+V_{\mathrm{X}}(\mathbf{k},\mathbf{r})=\sum_{j} v(\mathbf{r}-\mathbf{R}_j)+V_{\mathrm{X}}(\mathbf{k},\mathbf{r}), \qquad \ldots\ldots(1)$$

where the first term $V_{\mathrm{e}}(\mathbf{r})$ represents the sum of the *electrostatic* potentials due to the individual (neutral) atoms, and the second term gives the contribution of the *exchange hole*. The following two methods of approximation suggest themselves : (i) we can take for $V_{\mathrm{X}}(\mathbf{k},\mathbf{r})$ the average value $V_{\mathrm{X}}(\mathbf{k})$, since $V_{\mathrm{X}}(\mathbf{k},\mathbf{r})$ is determined principally by the electron *density* which is fairly uniform (Slater 1951); (ii) we can drop the second term, but account for the exchange hole by using altered atomic potentials $v'(\mathbf{r}-\mathbf{R}_j)$, which are such that the electron sees a He$^+$ *ion* at the lattice point to which it is nearest, and neutral He *atoms* at the other lattice points.

The first of these approximations is used in §§ 2–6. Since in that case the exchange potential $V_{\mathrm{X}}(\mathbf{k})$ is independent of the position of the electron, we can *first* calculate the energy $E_{\mathrm{e}}(\mathbf{k})$, using the first term $V_{\mathrm{e}}(\mathbf{r})$ only, and *afterwards* add $V_{\mathrm{X}}(\mathbf{k})$.

The first part of this procedure is discussed in §§ 2–4. We may expand the one-electron wave functions in terms of ordinary plane waves. The energy $E_{\mathrm{e}}(\mathbf{k})$ is then the lowest solution of the infinite secular equation

$$\det|\,V_{\mathrm{e},ij}+\{k_i^2-E_{\mathrm{e}}(\mathbf{k})\}\,\delta_{ij}\,|=0, \qquad \ldots\ldots(2)$$

where $$V_{\mathrm{e},ij}=\Omega^{-1}\int_{\Omega}\exp(-i\mathbf{k}_j\,.\,\mathbf{r})\,V_{\mathrm{e}}(\mathbf{r})\exp(i\mathbf{k}_i\,.\,\mathbf{r})\,d\mathbf{r}, \qquad \ldots\ldots(3)$$

and Ω is the volume of the unit cell. Also, $\mathbf{k}_i=\mathbf{k}+\mathbf{K}_i$ where $\mathbf{K}_i$ is 2π times a reciprocal lattice vector. If we cut off the determinant (2) at some finite order n, the solution of the equation converges rather slowly as we increase n.

Since L and W are points of high symmetry, the secular equation can be separated into several independent ones of lower order whose convergence is correspondingly better, by setting up the secular equation, not in terms of simple plane waves as in (2), but in terms of the appropriate linear combinations of plane waves, determined by group-theoretical considerations. However, the convergence is still not very satisfactory, but the difficulties due to this have been overcome to a sufficient degree of approximation.

As to the exchange potential $V_{\mathrm{x}}(\mathbf{k})$ (§§ 5, 6) we shall use a model of the electron gas similar to that of Bohm and Pines (1953) and of Pines (1953), i.e., of virtual electrons of slightly augmented mass, effectively interacting by screened Coulomb forces. The long-range part of the *un*screened Coulomb interactions of the real electrons is accounted for in terms of a collective description, by ' plasma waves ', which, however, are not usually excited. $V_{\mathrm{x}}(\mathbf{k})$ has been calculated using several different approximations the accuracy of which can be judged by comparing the various results.

The second approximate method using $v'(\mathbf{r})$ (the ' ionic ' one) is discussed in § 7. For the solution of the resulting secular equation (with $V(\mathbf{r})$ equal to $V_{\mathrm{e}}'(\mathbf{r})=\Sigma_j v'(\mathbf{r}-\mathbf{R}_j)$ instead of to $V_{\mathrm{e}}(\mathbf{r})$), the same remarks apply as in the first part of the first method.

We shall give the final results in § 8. From the values of the interatomic distance at which overlap takes place, we shall estimate the pressure at which this occurs. We shall also compare our results with those of Baltensperger (1954).

§ 2. THE SECULAR EQUATION FOR THE CALCULATION OF $E(\mathbf{k})$ IN TERMS OF THE LINEAR COMBINATIONS OF PLANE WAVES

First, we shall consider the factorization of the secular equation for the case of points of high symmetry in **k**-space. (For a discussion of the potential $V(\mathbf{r})$, see §§ 1 and 3.)

Let $u_{\mathbf{k}}(\mathbf{r})$ be a Bloch wave function with reduced wave vector **k**. Thus

$$u_{\mathbf{k}}(\mathbf{r}+\mathbf{R}_i)=u_{\mathbf{k}}(\mathbf{r})\exp(i\mathbf{k}\,.\,\mathbf{R}_i). \qquad \ldots\ldots(4)$$

Let us consider the set of actual wave vectors $\mathbf{k}_{ih}=\mathbf{k}+\mathbf{K}_{ih}$. To a certain $\mathbf{k}_{i1}$ there are g_i-1 equivalent ones, $\mathbf{k}_{ih}$ $(h=2,\ldots,g_i)$, where g_i equals the order g of the ' symmetry group of **k** ' or (sometimes) a divisor of g. These $\mathbf{k}_{ih}$ have the same length k_i and they may be obtained from $\mathbf{k}_{i1}$ by using the g operations of the symmetry group of **k** (each one g/g_i times).

From the plane waves $P_{ih}=\Omega^{-1/2}\exp(i\mathbf{k}_{ih}\,.\,\mathbf{r})$ we can form the g_i independent orthonormal linear combinations

$$f_{ij}(\mathbf{r})=\sum_{h=1}^{g_i}c_{jh}\,P_{ih}(\mathbf{r}), \qquad \ldots\ldots(5)$$

where $$\int_{\Omega}f_{i'j'}{}^{*}f_{ij}\,d\mathbf{r}=\delta_{ii'}\delta_{jj'}.$$

Since $$|\mathbf{k}_{i1}|=\ldots=|\mathbf{k}_{ig_i}|=k_i,$$

$$-\nabla^2 f_{ij}=k_i^2 f_{ij}. \qquad \ldots\ldots(6)$$

If we expand $u_{\mathbf{k}}(\mathbf{r})$ in the form

$$u_{\mathbf{k}}(\mathbf{r}) = \sum_i \sum_{j=1}^{g_i} c_{ij}(\mathbf{k}) f_{ij} \qquad \ldots\ldots(7)$$

the wave equation $(-\nabla^2 + V - E)u = 0$ leads to the secular equation

$$\det |\{k_i^2 - E(\mathbf{k})\}\delta_{ii'}\delta_{jj'} + \langle i'j' \,|\, V \,|\, ij \rangle| = 0, \qquad \ldots\ldots(8)$$

where

$$\langle i'j' \,|\, V \,|\, ij \rangle = \int_\Omega f_{i'j'}{}^* \, V f_{ij} \, d\mathbf{r}. \qquad \ldots\ldots(9)$$

We can choose the coefficients c_{jh} in (5) such that each f_{ij} transforms according to an irreducible representation of the group of $\mathbf{k}$ (Bouckaert, Smoluchowski and Wigner 1936). This can be done in the same way that was used by Von der Lage and Bethe (1947) to set up corresponding linear combinations of spherical harmonics ('cubic harmonics'). Then $\langle i'j' \,|\, V \,|\, ij \rangle$ is zero whenever j and j' correspond to different irreducible representations. Thus the secular equation factorizes into several independent ones. In practice this means that if we wish to include n terms in (5) we do not have to solve a secular equation of order n but several equations of lower order. Furthermore, we may only have to consider one of these if we are interested in one particular energy level, e.g. the lowest. The appropriate f_{ij} for the points L and W are given in the Appendix.

§ 3. The Potential

In accordance with the remarks of § 1, we will calculate $E(\mathbf{k})$ from (8) using the potential

$$\sum_j v(\mathbf{r} - \mathbf{R}_j), \qquad \ldots\ldots(10)$$

and later (§§ 5 and 6) add the term $V_{\mathrm{x}}(\mathbf{k})$. Then

$$\int_\Omega V \exp(i\mathbf{K}_i \,.\, \mathbf{r}) \, d\mathbf{r} = \int_{\text{crystal}} v(\mathbf{r}) \exp(i\mathbf{K}_i \,.\, \mathbf{r}) \, d\mathbf{r}, \qquad \ldots\ldots(11)$$

where $\mathbf{K}_i$ is 2π times a reciprocal lattice vector. For a $v(\mathbf{r})$ which is spherically symmetric and falls off sufficiently rapidly, the last integral can be transformed to

$$w(K_i) = 4\pi K_i^{-1} \int_0^\infty v(r) \, r \sin K_i r \, dr. \qquad \ldots\ldots(12)$$

Since (10) is the potential in a neutral lattice of helium atoms, $v(r)$ has been taken as $4Z_{\mathrm{p}}(r)/r$ rydbergs, where $Z_{\mathrm{p}}(r)$ is the effective nuclear charge per electron as calculated for the free helium atom by Wilson and Lindsay (1935). It can be represented (with an error of 0·0004) by the expression

$$Z_{\mathrm{p}} = 1{\cdot}42243 \, \mathrm{e}^{-2{\cdot}55095r} - 0{\cdot}42243 \, \mathrm{e}^{-4{\cdot}46615r} + 0{\cdot}0511r \, \mathrm{e}^{-8{\cdot}750r}, \qquad \ldots\ldots(13)$$

for which the integrals $w(K_i)$ can readily be calculated analytically.

The matrix elements (9) of V between the f_{ij}'s are (because of (4)), linear combinations of the integrals (11).

§ 4. Further Details of the Calculation of $E(\mathbf{k})$

In this section we shall give the results of the calculation of $E(\mathbf{k})$ excluding $V_{\mathrm{x}}(\mathbf{k})$ and considering the problems arising from cutting off of the secular equation (8) at a finite order n. We are interested in the lowest solutions of (8), or rather of its appropriate factor equations, for the point W and f_{ij}'s of the type $f_1(\mathrm{W})$ (top level of first band: for the function types indicated here see the Appendix) and, for point L, functions of type f_{1s} (L) (lowest level of second band). Table 1 gives the results for these two states for different values of n.

Table 1. Lowest Eigenvalues (in rydbergs)

(a, given in atomic units, is half the length along one of the coordinate axes of the Wigner cell, which is a rhombic dodecahedron. The distance between nearest neighbours is $2^{1/2}a$; the volume of the Wigner cell is $2a^3$).

Point	n	$a=2$	$a=1\cdot5$	$a=1\cdot25$
L(f_{1s})	6	1·48954	2·23918	2·74548
	8	1·48876	2·23818	2·74440
	10	1·48810	2·23737	2·74356
	∞_e	1·4845	2·2339	2·7406
W(f_1)	6	1·24683	2·18981	3·09483
	8	1·19875	2·13972	3·04605
	10	1·16402	2·10498	3·01290
	∞_e	1·074	2·027	2·942
	∞_{pp}	1·111	2·049	2·956
Correction to W(f_1, 10) by ‘perturbation’ method (§ 4)				
	90	−0·04733	−0·04993	−0·05081
	100	−0·04784	−0·05044	−0·05133
	110	−0·04827	−0·05087	−0·05176
	∞_e	−0·050	−0·053	−0·054
	∞_p	−0·053	−0·056	−0·057
Lowest eigenvalues for the ‘ionic’ field (§ 7)				
L(f_{1s})	6	1·25004	2·21463	3·08877
	8	1·24889	2·21348	3·08765
	10	1·24805	2·21268	3·08689
	∞_e	1·2458	2·2109	3·0852
W(f_1)	6	0·32912	1·54589	2·84742
	8	0·26372	1·48716	2·79361
	10	0·21720	1·44670	2·75711
	∞_e	0·103	1·357	2·680
	∞_{pp}	0·164	1·391	2·700

The values marked ∞_e were obtained by exponential extrapolation, i.e. by fitting a curve $E_n = E_\infty + ae^{-bn}$ through the three values calculated for $n=6, 8, 10$. Especially for the W state the extrapolation amounts to a rather large change. Therefore, in this case another more accurate method of extrapolation was used, which corresponds to second-order perturbation theory. The values obtained thus are indicated by ∞_{pp} in table 1.

We can represent approximately the effect on the energy level of including in (7) f_{ij}'s beyond the tenth, by adding to E_{10} the quantity

$$\Delta E = -\sum_{i'=11}^{\infty} \langle i'j' \mid V \mid ij\rangle^2 \, (k_i^2 - k_i'^2)^{-1}. \qquad \ldots\ldots(14)$$

ΔE was calculated by summing the terms in (14) up to $n=110$, and then by extrapolating by fitting a power-of-n curve $y(n) = y(\infty) + an^{-b}$ through the three values $\sum_{11}^{90}$, $\sum_{11}^{100}$, and $\sum_{11}^{110}$ of $y(n)$ (see table 1).

If K_{11} were very large, the value of b would be about unity, (since

$$\sum_{k>k_0} \langle \mathbf{k} \,|\, V \,|\mathbf{k}_1 \rangle^2 (k^2-k_1{}^2)^{-1} \sim \text{const.} \int_{k>k_0} d\mathbf{k}\, (k^2-k_1{}^2)^{-1} (k^{-2})^2 \sim \text{const.}\; k_0{}^{-3}$$

and $n(k_0)$ = number of $\mathbf{k}$'s up to $k_0 \sim \text{const.} \int_{k<k_0} d\mathbf{k} = \text{const.}\; k_0{}^3$) :

the mean value found was about 0·88. For comparison, the values obtained by exponential extrapolation are added: the power extrapolation is thought to be more appropriate and therefore used for the final values.

§ 5. THE EXCHANGE-CORRELATION TERM V_x ('COMPLETELY FREE ELECTRON GAS' TREATMENT)

We shall now consider the second part of the programme, i.e., the calculation of the exchange and correlation term by means of the Bohm and Pines scheme. The calculations differ from theirs for the completely free-electron gas only by the use of a slightly different interelectronic potential: instead of their $V(r_{12})$ with Fourier coefficients

$$\left.\begin{aligned} \int_{\text{unit volume}} V \exp(i\mathbf{k}\,.\,\mathbf{r}_{12})\, d\mathbf{r}_{12} &= -4\pi e^2 k^{-2} \text{ for } k > k_c, \\ &= 0 \text{ for } k < k_c, \end{aligned}\right\} \qquad \ldots\ldots(15)$$

we shall use the potential $V(r_{12}) = r_{12}{}^{-1} \exp(-k_c r_{12})$, with Fourier coefficients

$$-4\pi e^2 (k_c{}^2 + k^2)^{-1} \qquad \ldots\ldots(16)$$

throughout. This potential is very near the former one (Bohm and Pines 1953, figure 1, p. 613), but seems somewhat more realistic missing the sudden cut-off in the Fourier spectrum.

We have to calculate, just as Pines (1953, p. 636), the quantity

$$W(\mathbf{k}) = -4\pi e^2 (2\pi)^{-3} \int_{E(\mathbf{k}')} d\mathbf{k}' \,[k_c{}^2 + (\mathbf{k}-\mathbf{k}')^2]^{-1}, \qquad \ldots\ldots(17)$$

the integral being over occupied levels.

In the case of free electrons, the integral is to be extended over the Fermi sphere of radius k_0. Straightforward integration yields (in rydbergs)

$$W(k) = -0{\cdot}611\, r_s{}^{-1} \left[\frac{\beta^2+1-x^2}{2x} \ln \frac{\beta^2+(1+x)^2}{\beta^2+(1-x)^2} + 2 - 2\beta \tan^{-1}\frac{1-x}{\beta} - 2\beta \tan^{-1}\frac{1+x}{\beta} \right], \qquad \ldots\ldots(18)$$

where $x = k/k_0$; $\beta = k_c/k_0$; r_s is such that $(4\pi/3) r_s{}^3$ is the volume per electron (in our case $r_s = a(3/4\pi)^{1/3} = 0{\cdot}62035a$).

This gives only the effect of the exchange between the virtual electrons: to it must be added the effect of the apparent mass m^* of difference between the virtual electrons and the free electrons, i.e.

$$3{\cdot}68\, k^2 r_s{}^{-2} \{(1-\beta^3/6)-1\} = 0{\cdot}611\, \beta^3 k^2 r_s{}^{-2} \qquad \ldots\ldots(19)$$

(m^* has nothing to do with the apparent mass of electrons *in the band*).

These quantities have been calculated for $\mathbf{k}a/\pi = \frac{1}{2}\frac{1}{2}\frac{1}{2}$ (i.e. L), and $= 1\frac{1}{2}0$ (i.e. W), with $\beta = \beta(r_s)$ taken from Pines (1953, figure 3 and table I, p. 629). The results are given in table 2, row IV. For comparison the results obtained by Bohm and Pines' original formula (based on (15)) are also given (row III).

§ 6. Exchange and Correlation ('Non-spherical' Treatment).

In both cases (III and IV) mentioned above, we integrated over the Fermi *sphere* of the free-electron gas: however, it is preferable in our case to integrate over the first Brillouin zone (whose volume equals that of the sphere). The corresponding results are obtained by numerical integration (row V): as was expected, the values for W and L were slightly larger and smaller, respectively, than the corresponding values of row IV.

Table 2. $V_X(\mathbf{k}_i) = W_i$ (contribution of exchange hole) $+ E_{em}$ (due to the difference in effective mass).

	Energy (Ryd)	Case	Integrated over	Formula	Functions
A	$V_x(k_i)$	III	Fermi sphere	(15)†	plane waves
B	$V_x(k_i)$	IV	Fermi sphere	(16)	plane waves
C	$V_x(k_i)$	V	1st zone	(16)	plane waves
D	$V_x(k_i)$	VI	1st zone	(16)	lin. comb.
E	E_{em}			(19) used in all cases	
F	ratio $W_i(\mathrm{V})/W_i(\mathrm{IV})$				
G	ratio $W_i(\mathrm{VI})/W_i(\mathrm{IV})$				

	Point L			Point W		
	$a=2$	$a=1{\cdot}5$	$a=1{\cdot}25$	$a=2$	$a=1{\cdot}5$	$a=1{\cdot}25$
A	−0·6801	−0·9590	−1·1948	−0·5654	−0·7812	−0·9574
B	−0·6428	−0·9017	−1·1204	−0·4985	−0·6895	−0·8460
C	−0·6263	−0·8772	−1·0874	−0·4990	−0·6919	−0·8505
D	−0·4498	−0·6323	−0·7870	−0·5730	−0·7881	−0·9617
E	−0·0292	−0·0403	−0·0479	−0·0487	−0·0672	−0·0798
F	0·9743	0·9728	0·9705	1·0010	1·0035	1·0053
G	0·6998	0·7012	0·7024	1·1494	1·1430	1·1368

† that of Pines (1953).
a in atomic units.

However, there is the additional consideration that in the free-electron scheme simple plane waves are used, whereas in our case the use of the linear combinations (5), or at least of functions resembling these, seems more appropriate. This is discussed in what follows.

The exchange term in a Hartree–Fock wave equation for the state *i* is, in the case of an arbitrary potential $eV_{12} = eV(\mathbf{r}_{12})$ between electrons at positions $\mathbf{r}_1$ and $\mathbf{r}_2$,

$$W_i\phi_i(\mathbf{r}_1) = -e^2 \sum_j \left[\int_v \phi_j^*(\mathbf{r}_2)\phi_i(\mathbf{r}_2)\, V_{12}\, d\mathbf{r}_{12}\right]\phi_j(\mathbf{r}_1), \qquad \ldots\ldots(20)$$

(where v is the volume of the crystal and j runs over all occupied states); this may be written

$$-e^2 \sum_j \frac{\int_v \phi_j^*(\mathbf{r}_2)\phi_i^*(\mathbf{r}_1)V_{12}\,\phi_j(\mathbf{r}_1)\phi_i(\mathbf{r}_2)d\mathbf{r}_2}{\phi_i^*(\mathbf{r}_1)\phi_i(\mathbf{r}_1)}\,\phi_i(\mathbf{r}_1). \qquad \ldots\ldots(20\mathrm{a})$$

This operator W_i depends on the state i as well as on $\mathbf{r}_1$, and corresponds, therefore, to our $V_X(\mathbf{k}_i, \mathbf{r})$ (apart from the contribution due to the difference in effective mass).

In order to obtain the average value corresponding to $V_{\mathrm{X}}(\mathbf{k}_i)$, we integrate this with respect to $\mathbf{r}_1$ using the weight factor $\phi_i^*(\mathbf{r}_1)\phi_i(\mathbf{r}_1)$ and also the relation

$$\int_v \phi_i^*(\mathbf{r}_1)\phi_i(\mathbf{r}_1)\,d\mathbf{r}_1 = 1.$$

This yields

$$W_i\phi_i(\mathbf{r}_1) = \sum_j W_{ij}\phi_i(\mathbf{r}_1) = \\ -e^2\sum_j\left[\int_v \phi_j^*(\mathbf{r}_2)\phi_i^*(\mathbf{r}_1)\,V_{12}\,\phi_i(\mathbf{r}_2)\,\phi_j(\mathbf{r}_1)\,d\mathbf{r}_1\,d\mathbf{r}_2\right]\phi_i(\mathbf{r}_1)$$

which depends on i only.

In the case of plane waves $\phi_i(\mathbf{r}) = v^{-1/2}\exp(i\mathbf{k}_i\,.\,\mathbf{r})$, and we obtain

$$W_i = \sum_j W_{ij} = -e^2v^{-1}\sum_j\int_v V_{12}\exp[i(\mathbf{k}_i - \mathbf{k}_j)\,.\,\mathbf{r}_{12}]\,d\mathbf{r}_{12}. \qquad \ldots\ldots(21)$$

If we use the short-range interaction $V_{12} = r_{12}^{-1}\exp(-k_{\mathrm{c}}r_{12})$, we obtain (apart from irrelevant constants)

$$W_{ij} = -4\pi e^2\{k_{\mathrm{c}}^2 + (\mathbf{k}_i - \mathbf{k}_j)^2\}^{-1}.$$

This expression, when integrated over the Fermi sphere, leads to equation (18), and when integrated over the first zone to the results labelled V above.

However, we shall now try to find linear combinations which, for the points L and W, have approximately the symmetry characteristics of $f_{1\mathrm{s}}(\mathrm{L})$ and $f_1(\mathrm{W})$. In order to reduce the calculations to a minimum, normalized linear combinations

$$\phi_i(\mathbf{r}) = \sum_{\alpha=1}^{4} c_\alpha(k_i)\,v^{-1/2}\exp[i(\mathbf{k}_i + \mathbf{K}_\alpha)\,.\,\mathbf{r}] \qquad \ldots\ldots(22)$$

were used. Four is the minimal number of different values $\mathbf{K}_\alpha$ required to include the first-order approximations to the wave functions at the points L, X and W. If we vary $\mathbf{k}$ through the two 48th parts of the truncated octahedron shown in the figure, the appropriate values of $\mathbf{K}_\alpha a/\pi$ are $0\,0\,0$, $2\,0\,0$, $\bar{1}\,\bar{1}\,1$ and $\bar{1}\,\bar{1}\,\bar{1}$ for $\alpha = 1, \ldots, 4$, since for $\mathbf{k}a/\pi = 1\,\tfrac{1}{2}\,0$ this gives just the four equivalent points W. However, in case we vary $\mathbf{k}$ through some other of the 48th parts, other values of $\mathbf{K}_\alpha a/\pi$ have to be used, for the same reason, though $\mathbf{K}_1 a/\pi$ can always be taken $0\,0\,0$ and the same values of the c_α's are obtained for corresponding values of $\mathbf{k}$ in different 48th parts. However, in what follows, the above values of $\mathbf{K}_\alpha a/\pi$ have been used throughout, and this gives the results of $V_{\mathrm{X}}(\mathbf{k})$ shown in row VI of tables 2 and 4. This procedure does not use for all $\mathbf{k}_i$ the best wave functions that can be formed from four plane waves, but it simplifies the computations and shows (see table 2) that the use of linear combinations instead of plane waves markedly affects the values of $V_{\mathrm{X}}(\mathbf{k})$ obtained. It is hoped to carry out in the near future calculations using better wave functions. This is expected to increase the absolute magnitude of V_{X} for both L and W, but it is not possible to predict its effect on their difference.

The sets of c's referred to above are the eigenvectors of the secular equation of order four,

$$\det|V_{\alpha\beta} + [(\mathbf{k} + \mathbf{K}_\alpha)^2 - E(\mathbf{k})]\,\delta_{\alpha\beta}| = 0 \qquad \ldots\ldots(23)$$

with $V_{\alpha\beta} = \Omega^{-1}\int_\Omega \exp[-i(\mathbf{k} + \mathbf{K}_\beta)\,.\,\mathbf{r}]\,V(\mathbf{r})\exp[i(\mathbf{k} + \mathbf{K}_\alpha)\,.\,\mathbf{r}]\,d\mathbf{r}$; $\qquad \ldots\ldots(24)$

i.e. we solve the original wave equation crudely in terms of these four-wave linear combinations (22).

The eigenvectors of (23) have been calculated for 20 values of **k** inside one representative 48th part of the Brillouin zone. Some of those corresponding to the lowest eigenvalues are shown in table 3, and also the eigenvector corresponding to the second lowest eigenvalue at L. It shows that for internal points the value of c corresponding to the term in (22) with $\mathbf{K}=0$ is nearly unity, but that on nearing the surface the other c's increase, giving linear combinations of about the right symmetry for points *on* the surface.

Table 3. The c_α's for some values of **k**, for $a=2$
(For $a=1{\cdot}5$ and $=1{\cdot}25$ the c_α's show the same trend, with no strikingly different values.)

α			1	2	3	4
Centre of cell			000	$\bar{2}00$	$\bar{1}\bar{1}1$	$\bar{1}\bar{1}\bar{1}$ $\times\pi/a$
k_ja/π	000^1	(lowest eigenvalne)	0·99817	0·02521	0·03882	0·03882
	$\frac{1}{2}00^1$		0·99499	0·05231	0·06021	0·06021
	$\frac{1}{2}\frac{1}{2}0^1$		0·98314	0·05818	0·12258	0·12258
	$\frac{3}{4}\frac{1}{2}0^1$		0·92884	0·13099	0·24505	0·24505
(X)	100^2		0·69180	0·69180	0·14631	0·14631
	$1\frac{1}{4}0^2$		0·66118	0·66118	0·25068	0·25068
(L)	$\frac{1}{2}\frac{1}{2}\frac{1}{2}^3$		0·70355	0·07083	0·07083	0·70355
	$\frac{3}{4}\frac{1}{2}\frac{1}{4}^3$		0·69396	0·13575	0·13575	0·69395
(W)	$1\frac{1}{2}0^4$		0·5	0·5	0·5	0·5
	$1\frac{1}{4}\frac{1}{4}^5$		0·56392	0·56392	0·14492	0·58566
	$\frac{3}{4}\frac{3}{4}0^5$		0·58566	0·14492	0·56392	0·56392
k_ja/π						
(W)	$1\frac{1}{2}0$ (lowest eigenvalue). The same as above.					
(L)	$\frac{1}{2}\frac{1}{2}\frac{1}{2}^6$ (second eigenvalue).					
			−0·70708	0·00636	−0·00636	0·70708

1. Internal points. The point in cell 000 always preponderant; as the surface is approached the other c's grow.

2, 3. Symmetric with respect to the plane through 000 ⊥ the 100 (111) axis in case 2(3). The c's which correspond to the two boundary points of cell 000 are near $2^{-\frac{1}{2}}=0{\cdot}70711$.

4. Symmetric in $\pm 1, \frac{1}{2}, 0;\ 0, -\frac{1}{2}, \pm 1$, i.e., as $f_1(\mathrm{W})$.

5. The c's corresponding to the 3 boundary points of cell 000 are near $3^{-\frac{1}{2}}=0{\cdot}57735$.

6. As 3, but antisymmetric, i.e., as $f_{1S}(\mathrm{L})$.

Using these approximate wave functions, we have

$$\left.\begin{aligned} W_i=\sum_j W_{ij} &= -e^2 v^{-1}\sum_j\sum_{\alpha=1}^{4}\sum_{\beta=1}^{4}\sum_{\gamma=1}^{4}\sum_{\delta=1}^{4}\iint_v d\mathbf{r}_1\,d\mathbf{r}_2\,c_\alpha(\mathbf{k}_i)\,c_\beta(\mathbf{k}_j)\,c_\gamma(\mathbf{k}_i)\,c_\delta(\mathbf{k}_j)\\ &\times\exp i[-(\mathbf{k}_i+\mathbf{K}_\alpha)\,.\,\mathbf{r}_1-(\mathbf{k}_j+\mathbf{K}_\beta)\,.\,\mathbf{r}_2+(\mathbf{k}_i+\mathbf{K}_\gamma)\,.\,\mathbf{r}_2+(\mathbf{k}_j+\mathbf{K}_\delta)\,.\,\mathbf{r}_1]V(r_{12}).\end{aligned}\right\} \quad .(25)$$

Each W_{ij} is the sum of 256 terms, of which (at least in the case of the use of constant $\mathbf{K}_\alpha$'s throughout) only 28 are non-zero: unless $\mathbf{K}_\gamma+\mathbf{K}_\delta=\mathbf{K}_\alpha+\mathbf{K}_\beta$, the double integral is of the form

$$\int_v d\mathbf{r}_1\exp(i\mathbf{K}\,.\,\mathbf{r}_1)\int_v d\mathbf{r}_{12}\exp(i\mathbf{L}\,.\,\mathbf{r}_{12})\,V(r_{12}), \qquad \ldots\ldots(26)$$

which vanishes for $\mathbf{K}\neq 0$. In analogy to (16) one obtains

$$W_{ij}=-4\pi e^2\sum_\alpha\sum_\beta\sum_\gamma\sum_\delta c_\alpha(\mathbf{k}_i)\,c_\beta(\mathbf{k}_j)\,c_\gamma(\mathbf{k}_i)\,c_\delta(\mathbf{k}_j)[k_c^2+(\mathbf{k}_i-\mathbf{k}_j+\mathbf{K}_\gamma-\mathbf{K}_\beta)^2]^{-1}\ldots.(27)$$

(with the above relation between the four **K**'s).

$W_i\propto\int d\mathbf{k}_j\,W_{ij}$ was integrated numerically over all occupied levels, with $\mathbf{k}_ja/\pi$ having the values $\frac{1}{2}\,\frac{1}{2}\,\frac{1}{2}$ (L) and $1\,\frac{1}{2}\,0$ (W) using that set of four $c(\mathbf{k}_i)$'s which correspond to the states at L and W in the second and first zones respectively. For $\mathbf{k}_j$

values from the whole (not only the 48th part) of the zone were taken, with the $c(\mathbf{k}_j)$'s belonging to the lowest eigenvalues throughout, since these represent the occupied levels.

The values of $c_\alpha(\mathbf{k}_j)$ for $\mathbf{k}_j$ running over the whole zone were obtained by symmetry from those calculated for one 48th part of the zone. The integral $\int d\mathbf{k}_j\, W_{ij}$ was approximated to by the sum $(\pi/2a)^3 \Sigma_j g\, W_{ij}$ for $\mathbf{k}_j/a\pi = \frac{1}{2}(I, I', I'')$ (I etc. arbitrary integers), using 57 values of $\mathbf{k}_j$. For each internal point $\mathbf{k}_j$ a weight factor $g=1$ was used, for a point on a zone face $g=\frac{1}{2}$ and for the point W, $g=\frac{1}{4}$, giving $\Sigma_j g = 32$.

The same was done in the previous case of row V of table 2, with $\Sigma_j g = 32$ and 256 respectively, i.e. the above sum and the sum $(\pi/4a)^3 \Sigma_j g\, W_{ij}$ for $\mathbf{k}_j a/\pi = \frac{1}{4}(I, I', I'')$ were calculated: in case V this was a much faster calculation than in case IV. By the ratio of the case V results for $\Sigma g = 256$ and 32 respectively the result of the present case of row VI, using $\Sigma g = 32$, was corrected: it was assumed to have thus applied a sufficiently accurate correction for the coarseness of the point grid used (this correction does not exceed 1·2% of the value of W_i).

The results are given in row VI of table 2. The remark has to be made that in all cases (19) was simply used for the effective-mass correction E_{em}, which in no case exceeds $8\frac{1}{2}$% of the total correction.

§ 7. THE 'IONIC' METHOD

Another, cruder, attempt at taking into account the exchange hole, is the 'ionic' one, in which the atomic potential v is changed so that an electron sees the potential of a He$^+$ ion if within the Wigner cell or sphere, and the potential of a neutral He *atom* otherwise. Thus the Fermi hole follows 'its' electron from cell to cell.

An appropriate assumption for the potential is then (in rydbergs)

$$\left.\begin{aligned} v'(\mathbf{r}) &= 2Z_{\mathrm{p}}(r)/r + 2/r - 2/r_{\mathrm{W}} \quad \text{for } r<r_{\mathrm{W}}\,, \\ &= 2Z_{\mathrm{p}}(r)/r \quad \text{for } r>r_{\mathrm{W}}\,; \end{aligned}\right\} \qquad \ldots\ldots(28)$$

i.e. within the *Wigner* sphere with radius r_{W} (given by $(4\pi/3)r_{\mathrm{W}}^3 = \Omega = 2a^3$) the potential is that of an ion, whereas outside of the sphere it is the screened Coulomb potential of a neutral atom. (The constant $-2/r_{\mathrm{W}}$ has been added to order in ensure continuity at $r = r_{\mathrm{W}}$.)

Table 4. Results

Case	Remarks	$L(f_{1s})-W(f_1)$(Ryd)$\equiv F$ $a=2$	$a=1{\cdot}5$	$a=1{\cdot}25$	$F=0$ at $a=$	density (g cm^{-3})	pressure (megatm) p_0	 p
I	without any corr.	0·373	0·185	−0·215	1·368	8·70	63·3	52·0
II	do., 'ionic' case	1·082	0·820	0·385	1·090	17·20	222	191
III	with exch. + correl. corr. (cf. table 2)	0·258	0·007	−0·452	1·495	6·66	38·4	30·9
IV		0·229	−0·027	−0·489	1·519	6·35	35·0	28·1
V		0·246	0·000	−0·452	1·500	6·60	37·6	30·2
VI		0·496	0·341	−0·040	1·271	10·85	96·9	80·9
	Baltensperger's density limits and pressures calc. from them					4·8	20·5	16·0
						5·7	28·6	22·7
	His estimate of transition pressure							18

a is in atomic units.

The results are given in table 1, and in table 4 (row II). (However, for ∞_{pp} the 'perturbation' correction is not recalculated, but simply taken from the previous calculations, row I.) No further corrections have been applied.

§ 8. RESULTS AND CONCLUSIONS

For the different cases the difference of the levels for L (f_{1s}, ∞_e) and W (f_1, ∞_{pp}) is given in table 4, together with the value of a (i.e. $2^{-1/2}$ times the interatomic distance) at which overlap starts, found by quadratic interpolation. Finally, the atomic volume, density and pressure corresponding to that value of a are given. These latter are of importance as indications of order of magnitude only: they are calculated by means of the results of Latter (1956) for the Thomas–Fermi gas without any exchange or correlation correction (p_0 column), and (p column) the same, crudely corrected by the factor $p/p_0 = 1 - 0{\cdot}2072r_s - 0{\cdot}1303r_s^3(r_s + 5{\cdot}1)^{-2}$ which is the pressure ratio between a free-electron gas *with* exchange and (Wigner) correlation [$\epsilon = 2{\cdot}21r_s^{-2} - 0{\cdot}916r_s^{-1} - 0{\cdot}576(r_s + 5{\cdot}1)^{-1}$] and *without* ($r_s$ again as in (18) and (19)).

The most realistic estimate seems to be VI. This gives a much higher density and pressure for the transition to occur than does the estimate made by Baltensperger (1954), according to whom at about 18 megatmospheres the density would jump from 4·8 to 5·7 g cm^{-3}. However, the even higher results corresponding to the 'ionic' potential (case II) are felt to be unrealistic.

Baltensperger expected a density *jump*, because, according to his calculations, the metallic and non-metallic states behave like different allotropic modifications. The total energy of our material has not been calculated: therefore, nothing definite can be said at the moment as to the question whether the curve of total energy against atomic volume has a positive curvature throughout, in which case the density would go continuously through the transition point, or a pair of flexion points, so that there would be a bi-tangent and, accordingly, a density jump at the pressure given by its slope.

ACKNOWLEDGMENTS

I am grateful to Professor N. F. Mott for the hospitality I enjoyed at the Cavendish Laboratory, Cambridge, and for his suggesting this problem. I am also indebted to the Director of the Mathematical Laboratory, Cambridge, for allowing me to use the electronic computer EDSAC, and to its staff for helpful advice. I am very much indebted to Mr. V. Heine for many helpful discussions and suggestions. My stay in Cambridge was made possible by a grant received from the Netherlands Organization for Pure Scientific Research, Z.W.O.

REFERENCES

BALTENSPERGER, W., 1954 (Unpublished work cited in RAMSEY, W. H., 1954, *Occ. Notes R. Astr. Soc.*, **3**, 87 : and private communication).
BOHM, D., and PINES, D., 1953, *Phys. Rev.*, **92**, 609.
BOUCKAERT, L. P., SMOLUCHOWSKI, R., and WIGNER, E., 1936, *Phys. Rev.*, **50**, 58.
DUGDALE, J. S., and SIMON, F. E., 1953, *Proc. Roy. Soc.* A, **218**, 291.
LATTER, R., 1956, *J. Chem. Phys.*, **24**, 280.
PINES, D., 1953, *Phys. Rev.*, **92**, 626.
SLATER, J. C., 1951, *Phys. Rev.*, **81**, 385.
VON DER LAGE, F. C., and BETHE, H. A., 1947, *Phys. Rev.*, **71**, 612.
WILSON, W. S., and LINDSAY, R. B., 1935, *Phys. Rev.*, **47**, 681.

APPENDIX

(1) *Abbreviations used.*

A_{xy} = antisymmetric } with respect
S_{xy} = symmetric } to x and y
e_x = even } with respect
o_x = odd } to x
c = cosine
s = sine
Ω = Wigner unit cell
$\mathbf{R}_i$ = translation vector of the lattice in ordinary space.
V = potential function, always supposed to be fully symmetric (i.e., $e_x e_y e_z S_{xy} S_{yz} S_{zx}$) and periodic with respect to the lattice.

I, E, O = general, even, odd integers
K, L, M = components of $\mathbf{k}$
$\mathbf{K}_i$ = translation vector of the lattice in $\mathbf{k}$ space,
= $(E, E', E'')\pi/a$ or $(O, O', O'')\pi/a$
$\mathbf{k}_i = \mathbf{k} + \mathbf{K}_i$ with components K_i, L_i, M_i.

(2) *Point W*

$\mathbf{k} = (0, -\frac{1}{2}, 1)\pi/a$. $\mathbf{k}_i = \mathbf{k} + \mathbf{K}_i = (E, O+\frac{1}{2}, O')\pi/a$ or $(O, E+\frac{1}{2}, E')\pi/a$. For general (K_i, L_i, M_i) there are eight equivalent tripels, $\pm K_i, L_i, \pm M_i$ and $\pm M_i, -L_i, \pm K_i$ (Group of $\mathbf{k}$: isomorph with D_4). It is, therefore, sufficient to consider only $\mathbf{k}_{i1}$'s of the form $(E \geqslant 0, O+\frac{1}{2} \leqslant 0, O' > 0)\pi/a$.

The eight (*un*normalized) linear combinations of plane waves are

$f_1 = cK_i x \exp(iL_i y)\, cM_i z + cM_i x \exp(-iL_i y)\, cK_i z$	$e_x e_z$	W_1
$f_2 = cK_i x \exp(iL_i y)\, cM_i z - cM_i x \exp(-iL_i y)\, cK_i z$	$e_x e_z$	W_2'
$f_3 = sK_i x \exp(iL_i y)\, sM_i z + sM_i x \exp(-iL_i y)\, sK_i z$	$o_x o_z$	W_1'
$f_4 = sK_i x \exp(iL_i y)\, sM_i z - sM_i x \exp(-iL_i y)\, sK_i z$	$o_x o_z$	W_2
$f_5 = sK_i x \exp(iL_i y)\, cM_i z$	$o_x e_z$	
$f_6 = \qquad sM_i x \exp(-iL_i y)\, cK_i z$	$o_x e_z$	
$f_7 = cK_i x \exp(iL_i y)\, sM_i z$	$e_x o_z$	
$f_8 = \qquad cM_i x \exp(-iL_i y)\, sK_i z$	$e_x o_z$	

The numbers 1 . . . 8 correspond to the suffix j of f_{ij} in the text; the suffix i is found affixed to $\mathbf{K}_i$. Last column: the 'small representations' of Bouckaert *et al.* (1936) to which the f_j correspond. $f_5 \ldots f_8$ correspond to W_3, taken twice.

Normalization Constants (Volume of $\Omega = 2a^3$): $1 . a^{-3/2}$ $(f_1 \ldots f_4)$; $2^{1/2} a^{-3/2}$ $(f_5 \ldots f_8)$. For $K_i = 0$: $2^{-1/2} a^{-3/2} (f_1, f_2)$; $1 . a^{-3/2} (f_6, f_7)$; the other f's vanish.

Values of $(2a/\pi)\mathbf{k}_i$ used: $0\bar{1}2$, 032, $4\bar{1}2$, 432, $0\bar{5}2$, $0\bar{1}6$, 036, $4\bar{5}2$, $4\bar{1}6$, and 072.

$f_j(\mathbf{k}) \perp f_{j'}(\mathbf{k}')$ for $j \neq j'$ and/or $\mathbf{k} \neq \mathbf{k}'$. The only $\langle f_j | V | f_{j'} \rangle$ (for $j \neq j'$, $\mathbf{k} =$ or $\neq \mathbf{k}'$) which are not zero are $\langle f_5 | V | f_6 \rangle$ and $\langle f_7 | V | f_8 \rangle$.

(3) *Point L.*

$\mathbf{k} = (\frac{1}{2}, \frac{1}{2}, \frac{1}{2})\pi/a$. $\mathbf{k}_i = \mathbf{k} + \mathbf{K}_i = (E+\frac{1}{2}, E'+\frac{1}{2}, E''+\frac{1}{2})\pi/a$ or $(O+\frac{1}{2}, O'+\frac{1}{2}, O''+\frac{1}{2})\pi/a$. For general K_i, L_i, M_i there are 12 equivalent tripels: the 2×6 permutations of (K_i, L_i, M_i) and $(-K_i, -L_i, -M_i)$.

Group of $\mathbf{k}$: D_3 (around trigonal axis through $\mathbf{k}$) $\times J$. It is therefore sufficient to consider only $\mathbf{k}_i$'s with, for example, $K_i \leqslant L_i \leqslant M_i$ and $K + L_i + M_i \geqslant 0$. The twelve (*un*normalized) linear combinations of plane waves are: six functions f_{jc} of the form

$$f_{jc} = A_j c(K_i x + L_i y + M_i z) + B_j c(L_i x + K_i y + M_i z) + C_j c(L_i x + M_i y + K_i z)$$
$$+ D_j c(K_i x + M_i y + L_i z) + E_j c(M_i x + K_i y + L_i z) + F_j c(M x + L_i y + K_i z)$$

and six functions f_{js} with sines instead of cosines. The suffixes jc and js correspond to the suffix j of f_{ij} in the text: the suffix i is found affixed to $\mathbf{K}_i$.

The $f_{jc}(f_{js})$ are $e_J(o_J)$, therefore correspond to the 'small representations' $L_h(L_h')(h=1, 2, 3)$ of Bouckaert *et al.*

Function	A	B	C	D	E	F	Corresp. to	
f_{1c}, f_{1s}	1	1	1	1	1	1	L_1, L_1'	S_{xy} S_{xz} S_{yz}
f_{2c}, f_{2s}	1	-1	1	-1	1	-1	L_2, L_2'	A_{xy} A_{xz} A_{yz}
f_{3c}, f_{3s}	2	2	-1	-1	-1	-1	L_3, L_3' (taken twice)	S_{xy}
f_{4c}, f_{4s}	0	0	1	-1	-1	1		S_{xy}
f_{5c}, f_{5s}	2	-2	-1	1	-1	1		A_{xy}
f_{6c}, f_{6s}	0	0	1	1	-1	-1		A_{xy}

Since for $K_i=L_i=M_i$ only $f_{1c}, f_{1s}\neq 0$, I am interested in the normalization constants (volume of $\Omega=2a^3$) of these only. For $K_i\neq L_i\neq M_i\neq K_i$, this constant is $6^{-1/2}a^{-3/2}$. For $K_i=L_i\neq M_i$, $f_{1c}=2c(K_ix+K_iy+M_iz)+\text{cycl.}$ (and similarly for f_{1s}), and one gets $2^{-1}3^{-1/2}a^{-3/2}$. For $K_i=L_i=M_i$, $f_{1c}=6cK_i(x+y+z)$, $f_{1s}=6sK_i(x+y+z)$ and one gets $6^{-1}a^{-3/2}$.

Values of $(2a/\pi)\mathbf{k}_i$ used: 111, $\bar{1}\bar{1}3$, $\bar{1}33$, 333, 115, $\bar{3}15$, $\bar{5}33$, 155, $\bar{1}\bar{1}7$ and $\bar{1}37$.

$f_j(\mathbf{k})_\perp f_{j'}(\mathbf{k}')$ for $j\neq j'$ and/or $\mathbf{k}\neq\mathbf{k}'$. The only $\langle f_j|V|f_{j'}\rangle$ (for $j\neq j'$ and $\mathbf{k}=$ or $\neq\mathbf{k}'$) which are not zero are those with $j, j'=3c, 4c$; $3s, 4s$; $5c, 6c$; $5s, 6s$.

Inelastic Collisions between Heavy Particles

V: Electron Loss for Fast He$^+$ Ions passing through Atomic Hydrogen, and Ionization of Hydrogen Atoms by Fast He$^+$ Ions

By T. J. M. BOYD,† B. L. MOISEIWITSCH† and A. L. STEWART‡

† Department of Applied Mathematics, ‡ Department of Physics, The Queen's University of Belfast

Communicated by D. R. Bates; MS. received 20th August 1956

Abstract. Born's approximation is used to calculate the cross sections for the processes

$$\mathrm{He^+(1s)+H(1s)\rightarrow He^{2+}+e+H(1s,\ 2\overline{sp},\ 3\overline{spd}\ or\ C)},$$

where C represents the continuum. The effect of double transitions is found to be important for impact energies greater than about 300 kev. The agreement between the calculated electron loss cross section and the experimental data of Allison, Cuevas and Murphy for energies of the incident He$^+$ ion lying between 100 and 450 kev is quite good except at the limits of the experimental energy range. The ratio of the electron loss cross section to the electron capture cross section is also computed and compared with experiment. Again, the agreement is quite good.

In addition, Born's approximation is employed to calculate the cross section for the process

$$\mathrm{He^+(1s)+H(1s)\rightarrow He^+(1s)+H^++e},$$

which provides the dominant contribution to the total ionization cross section.

---

§ 1. Introduction

Recently, a detailed study using Born's approximation has been made of some of the more important high energy collision processes involving protons and hydrogen atoms (cf. Bates and Dalgarno (1956) for a brief summary of this work). Considerable interest is also attached to the analogous processes involving collisions between He$^+$ ions and H atoms. In this paper the processes

$$\mathrm{He^+(1s)+H(1s)\rightarrow He^{2+}+e+H(1s,\ 2\overline{sp},\ 3\overline{spd}\ or\ C)}, \qquad \ldots\ldots(1)$$

where C represents the continuum, are treated. All of these result in the formation of an α-particle by ionization of the incident He$^+$ ion. Calculation of their cross sections enables the electron loss cross section for He$^+$ ions passing through atomic hydrogen gas to be readily obtained.

An investigation is also carried out of the ionization of hydrogen atoms by fast He$^+$ ions. Calculations using Born's approximation have been made on the process

$$\mathrm{He^+(1s)+H(1s)\rightarrow He^+(1s)+H^++e}, \qquad \ldots\ldots(2)$$

which gives the dominant contribution to the total ionization cross section.

§ 2. Theory

We are concerned with collisions between He$^+$ ions and H atoms, both particles being initially in their ground states. Ignoring the effects of exchange and making use of Born's approximation, the cross section for the process in which the helium ion is ionized to the state in which the free electron has momentum $\hbar\boldsymbol{\kappa}$ and the hydrogen atom is excited to the state with quantum numbers nl, is given by

$$Q(1s-\kappa;1s-nl)=\frac{8\pi^3M^2}{K_i^2h^4}\int_{K_{\min}}^{K_{\max}}|\mathcal{N}|^2 K\,dK, \qquad \ldots\ldots(3)$$

where

$$\mathcal{N}=\iint\phi(1s,\boldsymbol{\rho})\,\phi^*(\kappa,\boldsymbol{\rho})\exp(i\mathbf{K}.\mathbf{R})\,V(\mathbf{R},\boldsymbol{\rho})\,d\boldsymbol{\rho}\,d\mathbf{R}; \qquad \ldots\ldots(4)$$

$$\mathbf{K}=\mathbf{K}_i-\mathbf{K}_f,\ \ \mathbf{K}_i=2\pi M\mathbf{v}_i/h,\ \ \mathbf{K}_f=2\pi M\mathbf{v}_f/h; \qquad \ldots\ldots(5)$$

M is the reduced mass; $\mathbf{v}_i$ and $\mathbf{v}_f$ are the initial and final velocities of relative motion; $\mathbf{R}$ is the relative position vector of the nuclei of the atom and ion and $\boldsymbol{\rho}$ is that of the ionic electron relative to the α-particle; the ϕ's are the wave functions of the He$^+$ ion in the bound and free states indicated; and $V(\mathbf{R},\boldsymbol{\rho})$ is the interaction potential, which may be written in the form

$$V(\mathbf{R},\boldsymbol{\rho})=e^2\int\psi(1s,\mathbf{r})\left[\frac{2}{R}-\frac{2}{|\mathbf{R}+\mathbf{r}|}-\frac{1}{|\mathbf{R}-\boldsymbol{\rho}|}+\frac{1}{|\mathbf{R}+\mathbf{r}-\boldsymbol{\rho}|}\right]\psi(nl;\mathbf{r})\,d\mathbf{r} \qquad \ldots\ldots(6)$$

the ψ's being the wave functions of the hydrogen atom and $\mathbf{r}$ the position vector of the atomic electron relative to the proton. Due to the orthogonality of the He$^+$ wave functions, the first two terms in (6) give no contribution to $\mathcal{N}$.

If the collision does not result in the excitation of the hydrogen atom, we obtain from the integration formula of Bethe (1930) that

$$\mathcal{N}=\frac{4\pi a_0^2e^2}{t^2}\,|I(1s-1s)-1|\,|J(1s-\kappa)|, \qquad \ldots\ldots(7)$$

where

$$\mathbf{t}=\mathbf{K}a_0, \qquad \ldots\ldots(8)$$

$$I(1s-nl)=\int\psi(1s;\mathbf{r})\,\psi^*(nl;\mathbf{r})\,e^{-i\mathbf{t}.\mathbf{r}}\,d\mathbf{r}, \qquad \ldots\ldots(9)$$

and

$$J(1s-\kappa)=\int\phi(1s;\boldsymbol{\rho})\,\phi^*(\kappa,\boldsymbol{\rho})\,e^{-i\mathbf{t}.\boldsymbol{\rho}}\,d\boldsymbol{\rho}, \qquad \ldots\ldots(10)$$

$\mathbf{r}$ and $\boldsymbol{\rho}$ now being in units of a_0, the radius of the first Bohr orbit of hydrogen. It follows that

$$Q(1s-\kappa;\ 1s-1s)=\left[\frac{8}{s^2}\int_{t_{\min}}^{t_{\max}}|I(1s-1s)-1|^2\,|J(1s-\kappa)|^2t^{-3}\,dt\right]\pi a_0^2 \qquad \ldots\ldots(11)$$

where $s^2=\frac{1}{2}mv_i^2/I_H$, I_H being the ionization potential of a hydrogen atom.

In the case of double transitions, simplification due to the orthogonality of the hydrogen wave functions takes place and we obtain

$$Q(1s-\kappa;\ 1s-nl)=\left[\frac{8}{s^2}\int_{t_{\min}}^{t_{\max}}|I(1s-nl)|^2\,|J(1s-\kappa)|^2t^{-3}\,dt\right]\pi a_0^2. \qquad \ldots\ldots(12)$$

The I and J integrals can be readily evaluated and have been given by Bates and Griffing (1953) for discrete transitions and by Massey and Mohr (1933) for transitions into the continuum. Substituting these expressions for I and J into (11) and (12), $Q(1s-\kappa;\ 1s-nl)$ can be obtained by numerical integration. Introducing the ionization cross section defined by

$$Q(1s-C;\ 1s-nl)=\int Q(1s-\kappa;\ 1s-nl)\,d\kappa \qquad \ldots\ldots(13)$$

the electron loss cross section for He$^+$ ions passing through atomic hydrogen gas is given by

$$Q(1\mathrm{s}-\mathrm{C};\ 1\mathrm{s}-\Sigma)=\sum_{nl}Q(1\mathrm{s}-\mathrm{C};\ 1\mathrm{s}-nl) \qquad \ldots\ldots(14)$$

where the summation includes an integration over the continuum. The calculation of the cross sections $Q(1\mathrm{s}-\mathrm{C};\ 1\mathrm{s}-nl)$ is very lengthy, especially in the case of double ionization for which a triple numerical integration has to be performed.

At sufficiently high energies a closed asymptotic formula for the electron loss cross section may be derived. Thus

$$Q(1\mathrm{s}-\mathrm{C};\ 1\mathrm{s}-\Sigma)\sim Q(1\mathrm{s}-\mathrm{C};\ 1\mathrm{s}-1\mathrm{s})$$
$$+\left[\frac{8}{s^2}\int d\kappa\int_0^\infty |J(1\mathrm{s}-\kappa)|^2 \sum_{\substack{nl\\ nl\neq 1\mathrm{s}}} |I(1\mathrm{s}-nl)|^2 t^{-3}\,dt\right]\pi a_0^2 \qquad \ldots\ldots(15)$$

and since (cf. Bethe 1930)

$$\sum_{nl}|I(1\mathrm{s}-nl)|^2=1 \qquad \ldots\ldots(16)$$

it follows that

$$Q(1\mathrm{s}-\mathrm{C};\ 1\mathrm{s}-\Sigma)\sim\left[\frac{16}{s^2}\int d\kappa\int_0^\infty |J(1\mathrm{s}-\kappa)|^2|1-I(1\mathrm{s}-1\mathrm{s})|t^{-3}\,dt\right]\pi a_0^2 \qquad \ldots\ldots(17)$$

$$=(2{\cdot}21/s^2)\pi a_0^2. \qquad \ldots\ldots(18)$$

An analogous treatment to the one given above yields for the cross section corresponding to process (2)

$$Q(1\mathrm{s}-1\mathrm{s};\ 1\mathrm{s}-\mathrm{C})=\left[\frac{8}{s^2}\int d\kappa\int_{t_{\mathrm{min}}}^{t_{\mathrm{max}}} |J(1\mathrm{s}-1\mathrm{s})-2|^2|I(1\mathrm{s}-\kappa)|^2 t^{-3}\,dt\right]\pi a_0^2 \qquad \ldots\ldots(19)$$

where

$$|J(1\mathrm{s}-1\mathrm{s})|=\frac{256}{(16+t^2)^2}. \qquad \ldots\ldots(20)$$

Also, in the limit of high energies, the total cross section for the ionization of hydrogen atoms by He$^+$ ions has the asymptotic form

$$Q(1\mathrm{s}-\Sigma;\ 1\mathrm{s}-\mathrm{C})\sim Q(1\mathrm{s}-1\mathrm{s};\ 1\mathrm{s}-\mathrm{C})$$
$$+\left[\frac{8}{s^2}\int d\kappa\int_0^\infty \{1-|J(1\mathrm{s}-1\mathrm{s})|^2\}|I(1\mathrm{s}-\kappa)|^2 t^{-3}\,dt\right]\pi a_0^2. \qquad \ldots\ldots(21)$$

The integral occurring in (19) tends to infinity in this limit whereas the integral in (21) remains finite, so that the contribution of double transitions to the total ionization cross section eventually becomes small compared with that from single transitions. A similar occurrence was noted by Moiseiwitsch and Stewart (1954) in connection with the $1\mathrm{s}^2-1\mathrm{s}2\mathrm{p}\,{}^1\mathrm{P}$ excitation of He atoms by fast He$^+$ ions.

§ 3. DISCUSSION OF RESULTS

In figure 1 are shown the cross sections

$$Q(1\mathrm{s}-\mathrm{C};\ 1\mathrm{s}-2\overline{\mathrm{sp}}),\ Q(1\mathrm{s}-\mathrm{C};\ 1\mathrm{s}-3\overline{\mathrm{spd}})\ \text{and}\ Q(1\mathrm{s}-\mathrm{C};\ 1\mathrm{s}-\mathrm{C})$$

as functions of the energy $\mathscr{E}$ of the incident He$^+$ ion, while in figure 2 a comparison is made between the cross section $Q(1\mathrm{s}-\mathrm{C};\ 1\mathrm{s}-1\mathrm{s})$ which involves a single transition only and the electron loss cross section $Q(1\mathrm{s}-\mathrm{C};\ 1\mathrm{s}-\Sigma)$. It can be

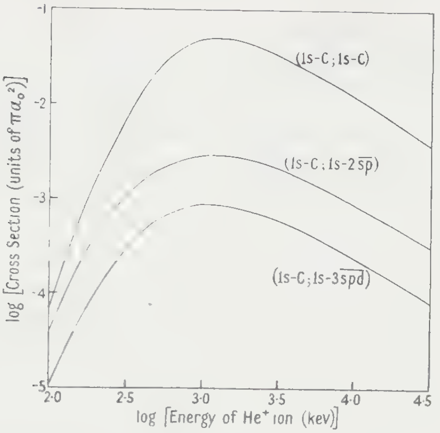

Figure 1. Cross sections $Q(1s-C;\ 1s-2\overline{sp})$, $Q(1s-C;\ 1s-3\overline{spd})$ and $Q(1s-C;\ 1s-C)$.

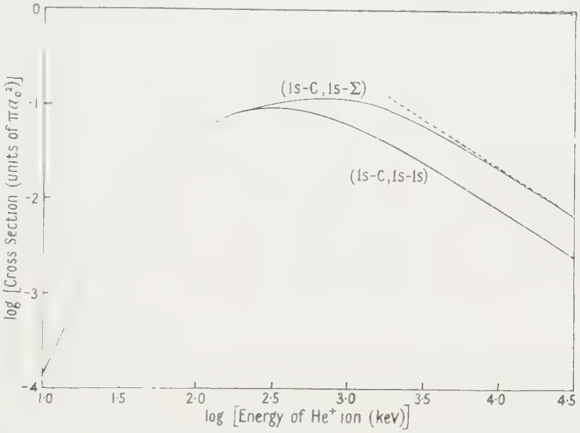

Figure 2. Cross sections $Q(1s-C;\ 1s-1s)$ and $Q(1s-C;\ 1s-\Sigma)$. The broken line represents the asymptotic behaviour of $Q(1s-C;\ 1s-\Sigma)$ as given by formula (18).

seen that the effect of double transitions is important for energies of the incident ion greater than about 300 kev. The electron loss cross section has an exceptionally broad maximum in agreement with the calculations of Bates and Griffing (1955) in the analogous case for collisions between hydrogen atoms.

There is no experimental information for He$^+$ ions passing through *atomic* hydrogen gas. However, experiments have been carried out recently using molecular hydrogen. Comparison between theory and experiment can be made by regarding each molecule as two atoms. Snitzer (1953) and Stier, Barnett and Evans (1954) have observed the equilibrium ratio $r=n(\mathrm{He}^{+})/n(\mathrm{He}^{2+})$ in an He$^+$ ion beam passing through molecular hydrogen, particle concentrations being denoted by n. Provided changes of charge involving two electrons are neglected, this ratio is given by σ_{21}/σ_{12}, where σ_{if} denotes the cross section for a process in which i is the initial ionic charge and f is the final charge. The capture cross section σ_{21} has been calculated by Schiff (1954) using Born's approximation† and so r can be determined at once from the values for the electron loss cross section σ_{12} obtained in this paper. The theoretical values for σ_{21}/σ_{12} and the ratio of the experimental to the theoretical value for r as a function of the energy $\mathscr{E}$

---

† The contribution from capture into states for which $n\geqslant 3$ was only estimated rather crudely.

of the He$^+$ ion beam are given in the table, the experimental results being due to Snitzer except for those marked with an asterisk at 100 and 150 kev which are due to Stier *et al.* Below 200 kev the doubly charged component of the helium ion beam in Snitzer's investigation appears to be only slightly larger than his detectable limit and so the data of Stier *et al.* should be more reliable. The agreement between theory and experiment is surprisingly good, especially at the lower energies where Schiff's calculations are not strictly applicable, capture from atomic hydrogen by He^{2+} into the $n=2$ level being a quasi-resonance process whereas such capture from H_2 is not. It would thus be expected that the calculated values of σ_{21} should substantially overestimate at low energies.

$\mathscr{E}$ (kev)	100	150	200	250	300	350	400	450	500	600	700	800	900	1000
σ_{21} (calc.) / σ_{12} (calc.)	380	120	57	28	15	8·8	5·4	3·5	2·3	1·2	0·62	0·38	0·24	0·16
r (calc.) / r (exp.)	1·3*	(2·5) 1·2*	1·8	1·3	1·2	1·2	1·2	1·0	(1·1)	(1·1)				

The experimental results for r used in this table are due to Snitzer (1953) except for those marked with an asterisk which are due to Stier, Barnett and Evans (1954). The values in brackets have been obtained by using the extrapolated results given by Snitzer.

Allison, Cuevas and Murphy (1956) have measured $\sigma_{21}+\sigma_{20}$ for He$^+$ ions passing through molecular hydrogen gas and get a cross section at low energies much smaller than the capture cross section σ_{21} calculated by Schiff, in agreement with the above conjecture. Using the experimental values of r obtained by Snitzer for energies above 200 kev and by Stier *et al.* below 200 kev, they have determined the electron loss cross section σ_{12}. In figure 3 their results are compared with the theoretical values of σ_{12} calculated in this paper. The agreement is seen to be quite good except at the two ends of their experimental energy range. At 100 kev the theoretical cross section is more than three times the experimental cross section. This might appear to be a surprisingly large error in view of the fact that using the data of Stier *et al.* r(calculated)/r(experimental) is 1·3 at this energy. However, it may be that the Born approximation

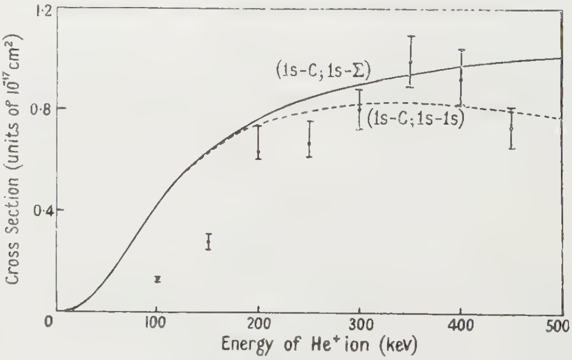

Figure 3. Experimental data of Allison, Cuevas and Murphy compared with theoretical calculations for the cross sections $Q(1s-C;\ 1s-\Sigma)$ and $Q(1s-C;\ 1s-1s)$.

overestimates the loss cross section at low energies by about the same amount as it does the capture cross section. It may be noted that if the values of r observed by Snitzer at low energies are in fact correct, the experimental and theoretical values for σ_{12} would be in harmony.

Little can be said concerning the discrepancy at the higher energies. It is conceivable that Born's approximation overestimates the contribution from double transitions in the energy region where these first begin to become appreciable, but neglect of such transitions does not bring about complete agreement between theory and experiment (cf. figure 3). It is perhaps of relevance to mention that at the higher energies the measured capture cross sections of Allison *et al.* (on which their loss cross sections are based) deviate from the corresponding theoretical capture cross section of Schiff in a peculiar manner.

The total cross section $Q(1s-\Sigma;\ 1s-C)$ for the ionization of hydrogen atoms by He^+ ions is displayed in figure 4 as a function of the energy $\mathscr{E}$ of the incident ion. This cross section has been obtained by the addition of

$$Q(1s-1s;\ 1s-C) \quad \text{and} \quad Q(1s-C;\ 1s-C),$$

the remaining terms contributing to the total cross section being small, as can be seen from the sum rule (equation (21)) which is valid at high energies of impact. For comparison the cross section for the ionization of hydrogen by protons calculated by Bates and Griffing (1953) is also included in figure 4. On the log–log scale of this figure the two curves are nearly parallel to each other over a wide range of energies, the cross section for He^+ ion impact being the larger of the two. At very high energies the two curves eventually coincide.

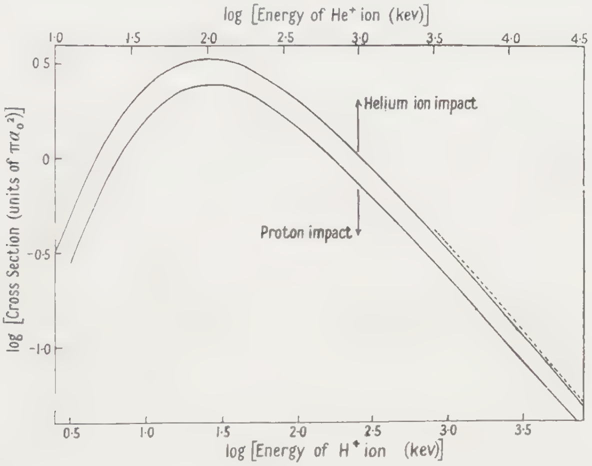

Figure 4. Comparison of the cross sections for the ionization of hydrogen atoms by He^+ ions and by protons. The broken line represents the asymptotic behaviour of $Q(1s-\Sigma;\ 1s-C)$ as given by formula (21). The abscissae have been chosen so that points on the two curves corresponding to equal velocities of relative motion lie on the same ordinate.

The only experimental data available on the cross section for the ionization of hydrogen by He^+ ions are due to Keene (1949) and Gilbody and Hasted (to be published).† Their energy ranges only extend up to about 40 kev and their results are in poor agreement with the theoretical cross section calculated in this paper †. A similar lack of accord was also found for the ionization of hydrogen by protons (Bates and Griffing 1955).

---

† We are indebted to these authors for communicating their results to us prior to publication.

ACKNOWLEDGMENTS

It is a pleasure to thank Professor D. R. Bates for his continued interest in this investigation.

One of us (T.J.M.B.) wishes to thank the Antrim County Education Committee and the Ministry of Education for Northern Ireland for research grants.

REFERENCES

ALLISON, S. K., CUEVAS, J., and MURPHY, P. G., 1956, *Phys. Rev.*, **102,** 1041.

BATES, D. R., and DALGARNO, A., 1956, *Airglow* and *Aurorae*, edited by Armstrong E. B., and Dalgarno, A. (London : Pergamon Press).

BATES, D. R., and GRIFFING, G. W., 1953, *Proc. Phys. Soc.* A, **66,** 961; 1955, *Ibid.*, **68,** 90.

BETHE, H. A., 1930, *Ann. Phys., Lpz.*, **5,** 325.

KEENE, J. P., 1949, *Phil. Mag.*, **40,** 369.

MASSEY, H. S. W., and MOHR, C. B. O., 1933, *Proc. Roy. Soc.* A, **140,** 613.

MOISEIWITSCH, B. L., and STEWART, A. L., 1954, *Proc. Phys. Soc.* A, **67,** 1069.

SCHIFF, H., 1954, *Canad. J. Phys.*, **32,** 393.

SNITZER, W., 1953, *Phys. Rev.*, **89,** 1237.

STIER, P. M., BARNETT, C. F., and EVANS, G., 1954, *Phys. Rev.*, **96,** 973.

---

† In comparing the experimental and theoretical cross sections one hydrogen molecule was as usual assumed equivalent to two hydrogen atoms. It is realized that this assumption is not fully justified.

Inelastic Collisions between Heavy Particles
VI: The $2s^3S$–$2p$ and $3p^3P$ Excitations of Fast He Atoms by H and Ne Atoms

By J. ADLER and B. L. MOISEIWITSCH
Department of Applied Mathematics, The Queen's University of Belfast

Communicated by D. R. Bates; MS. received 1*st October* 1956

Abstract. Born's approximation is used to calculate the cross sections for the processses

$$\mathrm{He}(2s\,^3S)+\mathrm{Ne}(2p^6\,^1S)\rightarrow\mathrm{He}(2p\text{ or }3p\,^3P)+\mathrm{Ne}(2p^6\,^1S)$$

and

$$\mathrm{He}(2s\,^3S)+\mathrm{H}(1s)\rightarrow\mathrm{He}(2p\text{ or }3p\,^3P)+\mathrm{H}(1s\text{ or }2\overline{sp}).$$

In addition, the *total* cross sections at high energies for the $2s\,^3S-2p$ or $3p\,^3P$ excitations of He atoms by Ne and H atoms are obtained.

§ 1. Introduction

The Balmer lines of hydrogen have been observed in the auroral spectrum by Vegard (1939), Gartlein (1950) and Meinel (1951). In particular Meinel found that the λ 6563 H_α line underwent a Doppler shift indicating the presence of fast protons in the primary auroral stream. It is of considerable interest to determine if any heavier particles such as those of helium are also present. A number of lines of helium were originally thought to have been found in the auroral spectrum by Bernard (1948) but these identifications have been rejected by later workers and it seems likely that if any such lines are present they are so weak as to escape detection. It is important to determine what limit this sets on the helium content of the stream.

Bates (1956) has discussed the processes controlling the photon yield in the helium lines. Amongst these is the excitation of fast He atoms from the $2s\,^3S$ state to the $3p\,^3P$ state in encounters with atmospheric atoms and molecules. The cross sections for collisions with atmospheric particles cannot be calculated without great difficulty. However, the cross sections should be given to an adequate approximation by considering Ne atoms in their place. In the present paper the cross sections for the processes

$$\mathrm{He}(2s\,^3S)+\mathrm{Ne}(2p^6\,^1S)\rightarrow\mathrm{He}(2p\text{ or }3p\,^3P)+\mathrm{Ne}(2p^6\,^1S) \qquad \ldots\ldots(1)$$

and

$$\mathrm{He}(2s\,^3S)+\mathrm{H}(1s)\rightarrow\mathrm{He}(2p\text{ or }3p\,^3P)+\mathrm{H}(1s\text{ or }2\overline{sp}) \qquad \ldots\ldots(2)$$

have been obtained, excitation to the $2p\,^3P$ state of He (which gives rise only to emission in the infra-red) and collisions with H atoms being investigated for comparison purposes.

Double transitions are important at quite moderate energies of the incident He atoms, and so asymptotic formulae for the total cross sections at high energies for the $2s\,^3S$–$2p$ or $3p\,^3P$ excitations of He atoms by Ne and H atoms have been obtained.

Finally, it should be noted that before the auroral problem can be answered it will be necessary to obtain cross sections for processes not treated in this paper.

§ 2. Theory

Ignoring the effects of electron exchange and making use of Born's approximation, the cross section for the process

$$\mathrm{He}\,(2\mathrm{s}\,{}^3\mathrm{S}) + \mathrm{Ne}\,(0) \rightarrow \mathrm{He}\,(n\mathrm{p}\,{}^3\mathrm{P}) + \mathrm{Ne}\,(m) \qquad \ldots\ldots(3)$$

in which the He atom is excited from the $2\mathrm{s}\,{}^3\mathrm{S}$ state to the $n\mathrm{p}\,{}^3\mathrm{P}$ state where $n=2$ or 3, and the Ne atom is excited from the initial $2\mathrm{p}^6\,{}^1\mathrm{S}$ ground state denoted by 0 to the final state denoted by m, can be written in the form

$$Q\,(2\mathrm{s}\,{}^3\mathrm{S}\text{–}n\mathrm{p}\,{}^3\mathrm{P};\;0\text{–}m) = \frac{8\pi^3 M^2}{K_\mathrm{i}^2 h^4}\int_{K_{\min}}^{K_{\max}} |\mathcal{N}\,(2\mathrm{s}\,{}^3\mathrm{S}\text{–}n\mathrm{p}\,{}^3\mathrm{P};\;0\text{–}m)|^2\,K\,dK \qquad \ldots.(4)$$

where

$$\mathcal{N}\,(2\mathrm{s}\,{}^3\mathrm{S}\text{–}n\mathrm{p}\,{}^3\mathrm{P};\;0\text{–}m)$$

$$= \iiint \phi\,(2\mathrm{s}\,{}^3\mathrm{S};\;\boldsymbol{\rho}_1,\;\boldsymbol{\rho}_2)\,\phi^*\,(n\mathrm{p}\,{}^3\mathrm{P};\;\boldsymbol{\rho}_1,\;\boldsymbol{\rho}_2)\exp i\mathbf{K}\,.\,\mathbf{R}\,V\,(\mathbf{R},\boldsymbol{\rho}_1,\boldsymbol{\rho}_2)\,d\boldsymbol{\rho}_1\,d\boldsymbol{\rho}_2\,d\mathbf{R}\,; \qquad \ldots\ldots(5)$$

$$\mathbf{K} = \mathbf{K}_\mathrm{i} - \mathbf{K}_\mathrm{f}, \quad \mathbf{K}_\mathrm{i} = 2\pi M\mathbf{v}_\mathrm{i}/h, \quad \mathbf{K}_\mathrm{f} = 2\pi M\mathbf{v}_\mathrm{f}/h\,; \qquad \ldots\ldots(6)$$

M is the reduced mass; $\mathbf{v}_\mathrm{i}$ and $\mathbf{v}_\mathrm{f}$ are the initial and final velocities of relative motion; $\mathbf{R}$ is the relative position vector of the two nuclei of the colliding atoms and $\boldsymbol{\rho}_1$, $\boldsymbol{\rho}_2$ are the position vectors of the helium electrons relative to the α-particle; the ϕ's are the wave functions of the He atom in the states indicated; and $V\,(\mathbf{R},\,\boldsymbol{\rho}_1,\,\boldsymbol{\rho}_2)$ is the interaction potential. If r_i is the position vector of the ith electron of the Ne atom relative to the Ne nucleus, we have that

$$V\,(\mathbf{R},\,\boldsymbol{\rho}_1,\,\boldsymbol{\rho}_2)$$

$$= e^2\int \psi_0\,(\mathbf{r}_1,\ldots,\mathbf{r}_{10})\,\psi_m^*\,(\mathbf{r}_1,\ldots,\mathbf{r}_{10})\left[\frac{20}{R} - \frac{10}{|\boldsymbol{\rho}_1-\mathbf{R}|} - \frac{10}{|\boldsymbol{\rho}_2-\mathbf{R}|}\right.$$

$$\left. + \sum_{i=1}^{10}\left\{\frac{1}{|\boldsymbol{\rho}_1-\mathbf{R}-\mathbf{r}_i|} + \frac{1}{|\boldsymbol{\rho}_2-\mathbf{R}-\mathbf{r}_i|} - \frac{2}{|\mathbf{R}+\mathbf{r}_i|}\right\}\right]d\mathbf{r}_1\ldots d\mathbf{r}_{10} \qquad \ldots\ldots(7)$$

where ψ_0 and ψ_m are the wave functions of the 0 and m states of Ne.

It is necessary to use approximate atomic wave functions to evaluate the cross section. A suitable variational wave function for the $2\mathrm{s}\,{}^3\mathrm{S}$ state of He has been obtained by Morse, Young and Haurwitz (1935). In atomic units it is given by

$$\phi\,(2\mathrm{s}\,{}^3\mathrm{S};\;\boldsymbol{\rho}_1,\;\boldsymbol{\rho}_2) = 2^{-1/2}\{u_1(\boldsymbol{\rho}_1)\,u_2(\boldsymbol{\rho}_2) - u_1(\boldsymbol{\rho}_2)\,u_2(\boldsymbol{\rho}_1)\} \qquad \ldots\ldots(8)$$

where

$$u_1(\boldsymbol{\rho}) = \left(\frac{\mu^3 a^3}{\pi}\right)^{1/2} \mathrm{e}^{-\mu a \rho}, \qquad \ldots\ldots(9)$$

$$u_2(\boldsymbol{\rho}) = \left(\frac{\mu^5}{3\pi N}\right)^{1/2}\left\{\rho\,\mathrm{e}^{-\mu\rho} - \frac{3A}{\mu}\,\mathrm{e}^{-\mu b\rho}\right\}, \qquad \ldots\ldots(10)$$

$$A = \frac{(a+b)^3}{(1+a)^4}, \quad N = 1 - \frac{48A}{(1+b)^4} + \frac{3A^2}{b^3}, \qquad \ldots\ldots(11)$$

and

$$\mu = 0{\cdot}61, \quad \mu a = 2{\cdot}00, \quad \mu b = 1{\cdot}57. \qquad \ldots\ldots(12)$$

The wave function of the 2p and 3p ^{3}P states of He were taken to be

$$\phi(np\,^3\mathrm{P};\ \boldsymbol{\rho}_1, \boldsymbol{\rho}_2) = 2^{-1/2}\{u_1(\boldsymbol{\rho}_1)\,v_n(\boldsymbol{\rho}_2) - u_1(\boldsymbol{\rho}_2)\,v_n(\boldsymbol{\rho}_1)\} \qquad \ldots\ldots(13)$$

with

$$\left.\begin{aligned} v_2(\boldsymbol{\rho}) &= \frac{1}{8}\sqrt{\frac{2}{\pi}}\,\rho\,\mathrm{e}^{-\rho/2}\cos\theta, \\ v_3(\boldsymbol{\rho}) &= \frac{1}{18}\sqrt{\frac{2}{\pi}}\,\rho(6-\rho)\,\mathrm{e}^{-\rho/3}\cos\theta. \end{aligned}\right\} \qquad \ldots\ldots(14)$$

Using the integration formula of Bethe (1930) we obtain

$$\mathcal{N}(2\mathrm{s}\,^3\mathrm{S} - np\,^3\mathrm{P};\ 0-m) = \frac{4\pi a_0{}^2 e^2}{t^2}\,|I(2\mathrm{s}-np)|\left|\sum_{i=1}^{10}(J_{0m}{}^i - \delta_{0m}{}^i)\right| \qquad \ldots\ldots(15)$$

where

$$I(2\mathrm{s}-np) = \int u_2(\boldsymbol{\rho})\,v_n(\boldsymbol{\rho})\exp(i\mathbf{K}.\boldsymbol{\rho})\,d\boldsymbol{\rho}, \qquad \ldots\ldots(16)$$

$$J_{0m}{}^i = \int \psi_0(\mathbf{r}_1, \ldots, \mathbf{r}_{10})\,\psi_m{}^*(\mathbf{r}_1, \ldots, \mathbf{r}_{10})\exp(-i\mathbf{K}.\mathbf{r}_i)\,d\mathbf{r}_1 \ldots d\mathbf{r}_{10}; \qquad \ldots\ldots(17)$$

$\delta_{0m}{}^i$ is a delta function and $\mathbf{t} = \mathbf{K}a_0$, $\boldsymbol{\rho}$ and $\mathbf{r}$ now being in units of a_0, the radius of the first Bohr orbit of hydrogen.

To calculate the cross section for process (1) we require an approximate wave function for the 2p^6 ^{1}S ground state of Ne. Such a function has been obtained by Duncanson and Coulson (1944) in the form of a Slater determinant with 1s, 2s and 2p orbitals given respectively by

$$w_1(\mathbf{r}) = \left(\frac{\nu^3\alpha^3}{\pi}\right)^{1/2}\mathrm{e}^{-\nu\alpha r}, \qquad \ldots\ldots(18)$$

$$w_2(\mathbf{r}) = \left(\frac{\nu^5}{3\pi M}\right)^{1/2}\left\{r\,\mathrm{e}^{-\nu r} - \frac{3B}{\nu}\,\mathrm{e}^{-\nu\beta r}\right\}, \qquad \ldots\ldots(19)$$

$$w_3(\mathbf{r}) = \left(\frac{\nu^5\gamma^5}{\pi}\right)^{1/2} r\,\mathrm{e}^{-\nu\gamma r}\cos\theta, \qquad \ldots\ldots(20)$$

$$w_4(\mathbf{r}) = \left(\frac{\nu^5\gamma^5}{2\pi}\right)^{1/2} r\,\mathrm{e}^{-\nu\gamma r}\sin\theta\,\mathrm{e}^{\pm i\phi}, \qquad \ldots\ldots(21)$$

where

$$B = \frac{(\alpha+\beta)^3}{(1+\alpha)^4}, \quad M = 1 - \frac{48B}{(1+\beta)^4} + \frac{3B^2}{\beta^3}, \qquad \ldots\ldots(22)$$

and

$$\nu = 2{\cdot}934, \quad \alpha = 3{\cdot}29, \quad \beta = 3{\cdot}06, \quad \gamma = 0{\cdot}98. \qquad \ldots\ldots(23)$$

Substitution in (17) yields

$$\sum_{i=1}^{10} J_{00}{}^i = 2L(1-1) + 2L(2-2) + 2L(3-3) + 4L(4-4) \qquad \ldots\ldots(24)$$

where

$$L(m-n) = \int w_m(\mathbf{r})\,w_n{}^*(\mathbf{r})\exp(-i\mathbf{K}.\mathbf{r})\,d\mathbf{r}. \qquad \ldots\ldots(25)$$

It follows that

$$\begin{aligned} &Q(2\mathrm{s}\,^3\mathrm{S} - np\,^3\mathrm{P};\ 0-0) \\ &\quad = \left[\frac{32}{\mathrm{s}^2}\int_{t_{\min}}^{t_{\max}} |I(2\mathrm{s}-np)|^2\,|L(1-1) + L(2-2) + L(3-3) + 2L(4-4) - 5|^2 \right. \\ &\qquad \left. \times\, t^{-3}\,dt\right]\pi a_0{}^2 \end{aligned} \qquad \ldots\ldots(26)$$

where $s^2 = \frac{1}{2}mv_i{}^2/I_{\mathrm{H}}$, I_{H} being the ionization potential of a hydrogen atom.

At sufficiently high energies closed asymptotic formulae for the total cross sections for the excitation of the 2p or 3p ^{3}P levels of He can be derived which make allowance for the excitation of all states of Ne.

In the limit of high impact energies we have

$$\sum_m{}' Q(2\mathrm{s}\,{}^3\mathrm{S}-n\mathrm{p}\,{}^3\mathrm{P};\ 0-m)$$
$$\sim\left[\frac{8}{\mathrm{s}^2}\int_{t_{\min}}^{\infty}|I(2\mathrm{s}-n\mathrm{p})|^2\sum_m{}'\left|\sum_{i=1}^{10}J_{0m}{}^i\right|^2 t^{-3}\,dt\right]\pi a_0{}^2 \qquad \ldots\ldots(27)$$

where the prime indicates that the summation excludes the ground state of Ne. Using the closure property of a complete set of functions we obtain

$$\sum_m\left|\sum_{i=1}^{10}J_{0m}{}^i\right|^2 = 10+\sum_{i=1}^{10}\sum_{j=1}^{10}\int|\psi_0(\mathbf{r}_1,\ldots,\mathbf{r}_{10})|^2\exp(i\mathbf{K}\,.\,(\mathbf{r}_i-\mathbf{r}_j))\,d\mathbf{r}_1\ldots d\mathbf{r}_{10}. \qquad \ldots\ldots(28)$$

Hence, from the expression for $\sum_{i=1}^{10} J_{00}{}^i$ given by (24) we get

$$\sum_m{}'\left|\sum_{i=1}^{10}J_{0m}{}^i\right|^2$$
$$=10-2\,|L(1-1)|^2-2\,|L(2-2)|^2-2\,|L(3-3)|^2-4\,|L(4-4)|^2$$
$$-4\,|L(1-2)|^2-4\,|L(1-3)|^2-4\,|L(2-3)|^2. \qquad \ldots\ldots(29)$$

The value of $t_{\min}$ used in (27) is that corresponding to the excitation of the first excited state of Ne, in which case the estimates of the total cross sections

$$Q(2\mathrm{s}\,{}^3\mathrm{S}-n\mathrm{p}^3\,\mathrm{P};\ 2\mathrm{p}^6\,{}^1\mathrm{S}-\textstyle\sum)=\sum_m Q(2\mathrm{s}\,{}^3\mathrm{S}-n\mathrm{p}\,{}^3\mathrm{P};\ 0-m)$$

obtained by using (26) and (27) give upper limits for the total cross sections.

For processes (2), involving collisions between He atoms and H atoms, the treatment used in this paper is very similar to the one given by Moiseiwitsch and Stewart (1954) who calculated the cross sections for the 1s^2 ^{1}S – 1s 2p ^{1}P excitation of He atoms in fast encounters with H atoms. It thus need not be given here.

§ 3. DISCUSSION OF RESULTS

It can be seen from figures 1 and 2 that the maximum value of the cross section $Q(2\mathrm{s}\,{}^3\mathrm{S}-2\mathrm{p}\,{}^3\mathrm{P};\ 2\mathrm{p}^6\,{}^1\mathrm{S}-2\mathrm{p}^6\,{}^1\mathrm{S})$ for impact between He and Ne atoms is nearly 30 times that of $Q(2\mathrm{s}\,{}^3\mathrm{S}-3\mathrm{p}\,{}^3\mathrm{P};\ 2\mathrm{p}^6\,{}^1\mathrm{S}-2\mathrm{p}^6\,{}^1\mathrm{S})$ and arises at an energy $\mathscr{E}$ of the incident He atom of about 560 ev whereas the latter cross section attains its maximum value at an energy $\mathscr{E}$ of about 3200 ev. This occurs because the energy difference between the 2s ^{3}S and 2p ^{3}P states of He is only 1·14 ev while the energy difference between the 2s ^{3}S and 3p ^{3}P states of He is 3·19 ev. The limitations of the Born approximation (which is, of course, poor at low impact energy) must be borne in mind. Double transitions begin to play an important part in both cases at about 50 kev as can be seen from the values obtained with the asymptotic formulae for the total cross sections $Q(2\mathrm{s}\,{}^3\mathrm{S}-2\mathrm{p}$ or $3\mathrm{p}\,{}^3\mathrm{P};\ 2\mathrm{p}^6\,{}^1\mathrm{S}-\Sigma)$ which are also displayed in figures 1 and 2. The major contribution to the total cross section at high energies arises from the excitation and ionization of the 2p shell electrons of Ne, the contribution from the inner shells being negligible.

The cross sections for the processes (2) involving impact between He and H atoms and the total cross sections $Q(2\mathrm{s}\,{}^3\mathrm{S}-2\mathrm{p}$ or $3\mathrm{p}\,{}^3\mathrm{P};\ 1\mathrm{s}-\Sigma)$ given by the asymptotic formulae are shown in figures 3 and 4. It was found in previous papers

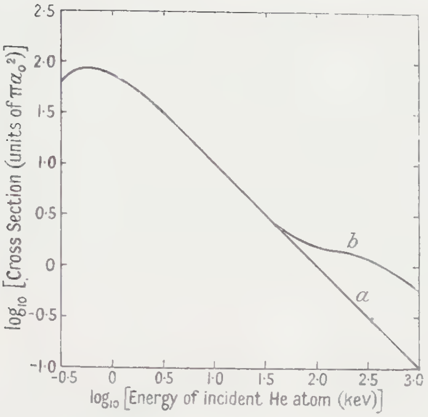

Figure 1. (*a*) Cross section Q ($2s^3S$–$2p^3P$; $2p^6\,{}^1S$); (*b*) cross section Q ($2s^3S$–$2p^3P$; $2p^6\,{}^1S$–Σ).

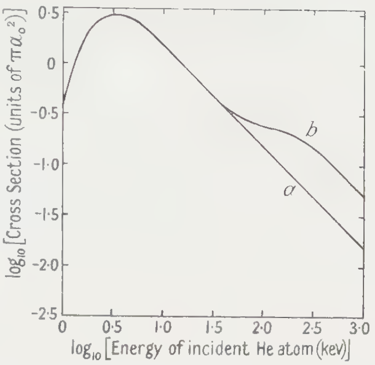

Figure 2. (*a*) Cross section Q ($2s^3S$–$3p^3P$; $2p^6\,{}^1S$–$2p^6\,{}^1S$); (*b*) cross section Q ($2s^3S$–$3p^3P$; $2p^6\,{}^1S$–Σ).

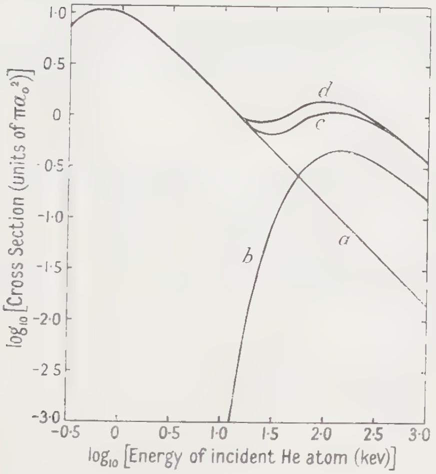

Figure 3. (*a*) Cross section Q ($2s^3S$–$2p^3P$; 1s–1s); (*b*) cross section Q ($2s^3S$–$2p^3P$; 1s–$2\overline{sp}$); (*c*) cross section Q ($2s^3S$–$2p^3P$; 1s–Σ) estimated in the manner explained in the text; (*d*) cross section Q ($2s^3S$–$2p^3P$; 1s–Σ) obtained by use of asymptotic formula.

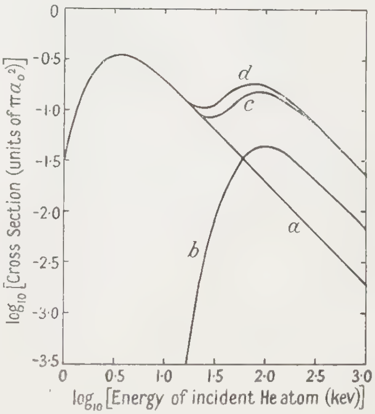

Figure 4. (*a*) Cross section Q ($2s^3S$–$3p^3P$; 1s–1s); (*b*) cross section Q ($2s^3S$–$3p^3P$; 1s–$2\overline{sp}$); (*c*) cross section Q ($2s^3S$–$3p^3P$; 1s–Σ) estimated in the manner explained in the text; (*d*) cross section Q ($2s^3S$–$3p^3P$; 1s–Σ) obtained by use of asymptotic formula.

on heavy particle collisions (Bates and Griffing 1954, Moiseiwitsch and Stewart 1954, Boyd, Moiseiwitsch and Stewart 1957) that the ratio between the cross sections for the 1s – $2\overline{sp}$ excitation and for the 1s–C excitation to the continuum C of H atoms by other atoms is approximately constant down to quite low impact energies. This behaviour enables the total cross sections Q ($2s\,{}^3S - 2p$ or $3p\,{}^3P$; $1s - \Sigma$) to be estimated since they are known at high energies. These estimates of the total cross sections are given in figures 3 and 4. They are not very different from the total cross sections obtained by using the asymptotic formulae only. It seems likely that the cross sections Q ($2s\,{}^3S - 2p$ or $3p\,{}^3P$; $1s - \Sigma$) calculated in this way are quite accurate estimates of the total cross section as in the analogous case of the $1s^2-1s\,2p\,^1P$ excitation of He atoms by H atoms investigated by Moiseiwitsch and Stewart (1954) the error was found to be no greater than about 7%.

The maximum values of the cross sections $Q(2s\,^3S-2p$ or $3p\,^3P;\ 2p^6\,^1S-2p^6\,^1S)$ for impact between He and Ne atoms are about 8 times greater than the maximum values of the corresponding cross sections $Q(2s\,^3S-2p$ or $3p\,^3P;\ 1s-1s)$ for impact between He and H atoms. However, at very high energies where double transitions are important, the former cross sections are only about 2 times greater than the latter.

ACKNOWLEDGMENT

It is a pleasure to thank Professor D. R. Bates for his continued interest in this work.

REFERENCES

BATES, D. R., 1956, *Airglow and Aurorae*, edited by Armstrong, E. B., and Dalgarno, A., (London : Pergamon Press).

BATES, D. R., and GRIFFING, G. W., 1954, *Proc. Phys. Soc.* A, **67**, 663.

BERNARD, R., 1948, *The Emission Spectra of the Night Sky and Aurorae*—Report of conference held under the auspices of the Gassiot Committee of the Royal Society (London : Physical Society).

BETHE, A., 1930, *Ann. Phys., Lpz.*, **5**, 325.

BOYD, T. J. M., MOISEIWITSCH, B. L., and STEWART, A. L., 1957, *Proc. Phys. Soc.* A, **70**, 110.

DUNCANSON, W. E., and COULSON, C. A., 1944, *Proc. Roy. Soc. Edinb.* A, **62**, 37.

GARTLEIN, C. W., 1950, *Trans. Amer. Geophys. Un.*, **31**, 18.

MEINEL, A. B., 1951, *Astrophys. J.*, **113**, 50.

MOISEIWITSCH, B. L., and STEWART, A. L., 1954, *Proc. Phys. Soc.* A, **67**, 1069.

MORSE, P. M., YOUNG, L. A., and HAURWITZ, E. S., 1935, *Phys. Rev.*, **48**, 948.

VEGARD, L., 1939, *Nature, Lond.*, **114**, 1089.

Homopolar Effects in Crystals having the Sodium Chloride Type of Lattice

By T. B. GRIMLEY

Department of Inorganic and Physical Chemistry,
University of Liverpool

MS. received 4th September 1956

Abstract. In an ionic crystal, the outer electrons from the negative ions will be shared to some extent with the surrounding metal ions. Allowing for this possibility in constructing approximate solutions of Fock's equations for the valence electrons, it is shown that the expression for the lattice energy contains an extra negative term representing the homopolar contribution. Numerical calculations are made for LiF and it is found that the homopolar contribution is only about 0·1% of the lattice energy. It is also shown that, whilst homopolar effects provide an additional source of attraction between nearest (unlike) neighbours, they enhance the repulsion between like neighbours.

§ 1. Introduction

Let $\mathscr{H}_{\mathrm{op}}$ be the Hamiltonian operator for an ionic crystal containing N molecules. Assume, for simplicity, that the atomic nuclei are fixed so that the total energy of the system in the ground state is given by the lowest eigenvalue E of the equation

$$(\mathscr{H}_{\mathrm{op}} - E)\Phi = 0, \qquad \ldots\ldots(1)$$

for antisymmetric functions $\Phi(1, 2, \ldots n)$ of the coordinates (including spin) of the n electrons. Even when relativistic effects (including all spin couplings) are neglected the many-body problem posed in (1) is of great complexity. We introduce, therefore, the Hartree–Fock approximation in which Φ is represented by a single Slater determinant. Thus

$$\Phi = \det|u_1(1)\,u_2(2)\ldots.u_n(n)|, \qquad \ldots\ldots(2)$$

where each u_μ is a function of the coordinates of only one electron.

The functions u_μ which give the best approximation to E in (1) are determined from the variation principle $\delta E = 0$. On requiring that the u_μ form an orthonormal set, we arrive at Fock's (1930) equations for the solid. The approximate eigenvalues of (1) may then be expressed in terms of the energy parameters of Fock's equations and certain exchange and Coulomb integrals. However, the difficulties encountered in following this method for any ionic crystal are so great that further approximations have to be made. Landshoff (1936), in his work on NaCl, took for the u_μ the solutions of the Hartree–Fock equations for the free ions. These functions, which we shall call ϕ_μ, have the character of atomic spin-orbitals so that the calculations are carried out in the Heitler–London approximation. Calculations on these lines have been taken further by Löwdin (1948) who also gave a full treatment of the overlapping problem which arises with this choice of the u_μ. In view of the assumption that the normally occupied free ion orbitals are adequate approximations to the one-electron functions, even when the ions are brought together in the crystal, it is convenient to refer to this work as the *ionic approximation.*

Although Löwdin's results for the lattice energy, lattice parameter and compressibility of the alkali halides leave little room for improvement, it does not follow that a true picture of the electronic structure of the crystal (in the Hartree–Fock approximation) is derived from this ionic approximation. To discuss the electronic structure it is essential that some attempt be made to determine the best one-electron functions u_μ by solving Fock's equations for the crystal. This procedure inevitably leads to one-electron functions, which we shall call ψ_μ, having the character of crystal spin–orbitals, i.e. they extend throughout the lattice. Calculations of this sort have been made by Shockley (1936) for NaCl and by Ewing and Seitz (1936) for LiF and LiH. Only the electronic band structure was investigated; the lattice energy was not computed.

The present work was undertaken with a view to improving upon the ionic approximation used by Löwdin. An important effect ignored in the ionic approximation is the possibility that, when the ions are brought together to form a crystal, the outermost electrons on the negative ions may be shared with the surrounding metal ions. Such a sharing of electrons will give rise to an additional cohesive force. Following Mott and Gurney (1940, p. 9) we shall call this force homopolar. Our purpose is to estimate the extent of this sharing and the contribution which homopolar forces make to the lattice energy.

Numerical calculations will be carried out for LiF. For simplicity we shall not, at this stage, attempt to treat all the twelve electrons per molecule but introduce instead an approximation already used by Benson and Wyllie (1951). Thus, we treat only the 2p electrons on F^- and regard the remaining electrons together with the nuclei as constituting structureless ion cores. Even so we do not try to solve Fock's equations directly for this simplified system but suppose that the solutions may be expressed as linear combinations of atomic orbitals (LCAO). The atomic orbitals selected are the $6N$ 2p-orbitals on the F^- ions and the (normally unoccupied) $2N$ 2s-orbitals on the Li^+ ions. The ionic approximation corresponds to the choice of the $6N$ 2p-orbitals as the basic set.

The numerical results for LiF show that, for this crystal, the homopolar effects are of minor importance. However, the general formulae of this paper are applicable with only trivial modifications to all monovalent metal halides, divalent metal oxides, sulphides, selenides and tellurides having the NaCl structure. This work, therefore, provides a basis for the investigation of homopolar effects in a large number of crystals.

§ 2. THE LCAO APPROXIMATION TO FOCK'S EQUATIONS

In this section we treat Fock's equations for the solid in the LCAO approximation. The approximation takes into account the sharing of the outer electrons on the negative ions with the surrounding metal ions in the crystal. For definiteness we consider LiF.

2.1. *Basic Formulae*

It is well known (Fock 1930) that for our system of $6N$ electrons with no complications due to spin degeneracy, the best one-electron functions in the single determinant (2) are the crystal spin-orbitals ψ_μ defined by the eigenvalue equation†

---

† Atomic units are used throughout.

$$[H+2\sum_{\nu}\int\psi_{\nu}^{*}(2)\psi_{\nu}(2)G\,d\tau_{2}]\,\psi_{\mu}(1)-2\sum_{\nu}\int\psi_{\nu}^{*}(2)\psi_{\mu}(2)G\,d\tau_{2}\psi_{\nu}(1)=\epsilon_{\mu}\psi_{\mu}(1), \qquad \ldots\ldots(3)$$

where $$G=1/2r_{12}, \qquad H=-\nabla_{1}^{2}-\sum_{g}Z_{\mathrm{g}}/r_{1\mathrm{g}}.$$

Here Z_{g} is the charge on the ion core at lattice point g and $r_{1\mathrm{g}}$ is the distance of the electron from g. The eigenvalues ϵ_{μ} are the orbital energies.

In our LCAO approximation we assume that the ψ_{μ} in equation (3) may be expressed as linear combinations of $8N$ free ion spin–orbitals ϕ_{α}, namely the $6N$ 2p spin–orbitals on the F^{-} ions and the $2N$ 2s spin–orbitals on the Li^{+} ions. In matrix form

$$\boldsymbol{\psi}=\boldsymbol{\varphi}\mathbf{C}', \qquad \ldots\ldots(4)$$

where $\boldsymbol{\psi}$ and $\boldsymbol{\varphi}$ are row matrices. $\mathbf{C}'$ is taken as a square $(8N\times 8N)$ matrix so that equation (4) defines a set of $8N$ crystal spin–orbitals. Only $6N$ of these are occupied in the ground state; the remaining $2N$ may be used to describe certain excited states of the crystal. It is convenient to order the row matrix $\boldsymbol{\varphi}$ such that the first $6N$ elements are the atomic spin–orbitals on the F^{-} ions and the last $2N$ elements are the atomic spin–orbitals on the Li^{+} ions. Similarly, $\boldsymbol{\psi}$ is ordered such that the first $6N$ elements are the ground state crystal spin–orbitals. We use the indices μ, ν, λ, η to denote any of the first $6N$ elements of $\boldsymbol{\varphi}$ or $\boldsymbol{\psi}$, and m and n to denote any of the last $2N$ elements. The indices α, β, γ or δ will be used to denote *any* of the $8N$ elements of $\boldsymbol{\varphi}$.

The set of atomic spin–orbitals $\boldsymbol{\varphi}$ are not all orthogonal at any finite lattice parameter. We introduce, therefore, an orthonormal set $\boldsymbol{\Phi}$ of atomic spin–orbitals by Löwdin's (1948) transformation. Thus

$$\boldsymbol{\Phi}=\boldsymbol{\varphi}\mathbf{L}, \qquad \ldots\ldots(5)$$

$$\left.\begin{aligned}\mathbf{L}&=(\mathbf{1}+\mathbf{S})^{-1/2}=\mathbf{1}-\tfrac{1}{2}\mathbf{S}+\tfrac{3}{8}\mathbf{S}^{2}-\ldots,\\ S_{\alpha\beta}&=\int\phi_{\alpha}^{*}(1)\,\phi_{\beta}(1)\,d\tau_{1}-\delta_{\alpha\beta}.\end{aligned}\right\} \qquad \ldots\ldots(6)$$

We note that $\mathbf{S}$ is Hermitian.

In terms of the orthonormal atomic spin–orbitals $\boldsymbol{\Phi}$, equation (4) becomes

$$\boldsymbol{\psi}=\boldsymbol{\Phi}\mathbf{C}, \qquad \mathbf{C}^{\dagger}\mathbf{C}=\mathbf{C}\mathbf{C}^{\dagger}=\mathbf{1}. \qquad \ldots\ldots(7)$$

Using (7) in (3) our fundamental approximation is expressed as

$$\mathbf{C}^{\dagger}\mathbf{F}\mathbf{C}=\boldsymbol{\epsilon}, \qquad \ldots\ldots(8)$$

where $\boldsymbol{\epsilon}$ is a diagonal $(8N\times 8N)$ matrix and $\mathbf{F}$ a square $(8N\times 8N)$ matrix with elements $F_{\alpha\beta}$ defined by

$$F_{\alpha\beta}=H_{\alpha\beta}+2\sum_{\nu\gamma\delta}C_{\nu\gamma}{}^{\dagger}G_{\alpha\beta}{}^{\gamma\delta}\,C_{\delta\nu}, \qquad \ldots\ldots(9)$$

$$\left.\begin{aligned}H_{\alpha\beta}&=\int\Phi_{\alpha}^{*}(1)\,H\,\Phi_{\beta}(1)\,d\tau_{1},\\ G_{\alpha\beta}{}^{\gamma\delta}&=\int[\Phi_{\alpha}^{*}(1)\,\Phi_{\gamma}^{*}(2)\,G\,\Phi_{\beta}(1)\,\Phi_{\delta}(2)-\Phi_{\alpha}^{*}(1)\,\Phi_{\gamma}^{*}(2)G\,\Phi_{\delta}(1)\,\Phi_{\beta}(2)]\,d\tau_{1}\,d\tau_{2}.\end{aligned}\right\} \qquad \ldots\ldots(10)$$

The matrix equation (8) is our LCAO approximation to equation (3) (Roothaan 1951 a). The self-consistent field problem still arises since $\mathbf{F}$ is defined in terms of $\mathbf{C}$, The matrix $\mathbf{F}$ has the block form

$$\mathbf{F}=\begin{bmatrix} \mathbf{F}_1 & \mathbf{f} \\ \mathbf{f}^\dagger & \mathbf{F}_2 \end{bmatrix} \qquad \ldots\ldots(11)$$

where $\mathbf{F}_1$ has elements $F_{\mu\nu}$ (μ and ν are halide ion functions) $\mathbf{F}_2$ has elements F_{mn} (m and n are metal atom functions) and $\mathbf{f}$ has elements $F_{\mu m}$. Let $\mathbf{B}$ be the unitary matrix which reduces $\mathbf{F}$ to the form $\boldsymbol{\epsilon}'$ where

$$\boldsymbol{\epsilon}'=\mathbf{B}^\dagger\,\mathbf{F}\mathbf{B}=\begin{bmatrix} \boldsymbol{\epsilon}_1{}' & \mathbf{0} \\ \mathbf{0} & \boldsymbol{\epsilon}_2{}' \end{bmatrix}. \qquad \ldots\ldots(12)$$

Then $\mathbf{B}$ and $\mathbf{C}$ are connected by a unitary transformation $\mathbf{V}$ of the form

$$\mathbf{V}=\begin{bmatrix} \mathbf{V}_1 & \mathbf{0} \\ \mathbf{0} & \mathbf{V}_2 \end{bmatrix}. \qquad \ldots\ldots(13)$$

Explicitly $\mathbf{C}=\mathbf{B}\mathbf{V}$ so that instead of equation (9) we may write

$$F_{\alpha\beta}=H_{\alpha\beta}+2\sum_{\nu\gamma\delta} B_{\nu\gamma}{}^\dagger\, G_{\alpha\beta}{}^{\gamma\delta} B_{\delta\nu} \qquad \ldots\ldots(14)$$

as the definition of $\mathbf{F}$. The matrix $\mathbf{B}$ defines a set $\boldsymbol{\chi}$ of orthonormal atomic spin-orbitals according to

$$\boldsymbol{\chi}=\boldsymbol{\Phi}\mathbf{B} \qquad \ldots\ldots(15)$$

which differ from the 'best' one-electron functions $\boldsymbol{\psi}$ by the unitary transformation $\mathbf{V}$ of equation (13). Since the total energy of the system in the ground state is invariant under such unitary transformations of the set $\boldsymbol{\psi}$, it follows that the set $\boldsymbol{\chi}$ may be used as one-electron functions in equation (2) to calculate this energy.‡ Hence we only need the matrix $\mathbf{B}$ which reduces $\mathbf{F}$ to the form $\boldsymbol{\epsilon}'$ in equation (12); the complete reduction of $\mathbf{F}$ to diagonal form is only required to discuss the electronic structure.

2.2. *The Matrix* **B** *in First Order*

The matrix $\mathbf{B}$ is obtained in first order by treating all non-diagonal elements of $\mathbf{F}$ as first-order small quantities and applying perturbation theory. Writing

$$\mathbf{B}=\mathbf{1}+\mathbf{X}, \qquad \ldots\ldots(16)$$

we have in first order

$$\left.\begin{aligned} X_{m\mu}&=-F_{m\mu}/(F_{mm}-F_{\mu\mu}),\\ X_{\mu m}&=-X_{m\mu}{}^*,\\ X_{\mu\nu}&=X_{mn}=0, \end{aligned}\right\} \qquad \ldots\ldots(17)$$

and $\mathbf{X}$ has the block form

$$\mathbf{X}=\begin{bmatrix} \mathbf{0} & -\mathbf{x}^\dagger \\ \mathbf{x} & \mathbf{0} \end{bmatrix}+\text{2nd order terms}. \qquad \ldots\ldots(18)$$

From equation (14)

$$F_{\alpha\beta}=H_{\alpha\beta}+2\sum_{\gamma\delta} G_{\alpha\beta}{}^{\gamma\delta} R_{\delta\gamma}, \qquad \ldots\ldots(19)$$

where

$$R_{\delta\gamma}=\sum_{\nu} B_{\delta\nu} B_{\nu\gamma}{}^\dagger. \qquad \ldots\ldots(20)$$

---

‡ This invariance expresses the equivalence of the Heitler–London and Bloch schemes for systems whose constituents have closed shell configurations.

$\mathbf{R}$ has been called the charge- and bond-order matrix with respect to the orthonormal atomic spin-orbitals $\boldsymbol{\Phi}$ (Löwdin 1955). Its non-diagonal elements represent the *formal* valencies of the separated ions. Writing

$$\mathbf{R}=\begin{bmatrix}\mathbf{1} & \mathbf{0}\\ \mathbf{0} & \mathbf{0}\end{bmatrix}-\mathbf{P} \qquad \ldots\ldots(21)$$

we find from (16) and (18) that

$$\mathbf{P}=\begin{bmatrix}\mathbf{x}^{\dagger}\mathbf{x} & -\mathbf{x}^{\dagger}\\ -\mathbf{x} & -\mathbf{x}\mathbf{x}^{\dagger}\end{bmatrix}+\text{3rd order terms.} \qquad \ldots\ldots(22)$$

The first matrix on the right in (21) is the charge- and bond-order matrix for separated ions in the *ionic approximation.* Its non-diagonal elements are zero corresponding to the absence of bonds between closed shell systems, but, in addition, the diagonal elements are zero in that portion of the matrix which refers to orbitals on the metal atoms. This latter corresponds to the non-existence of electrons in these orbitals in the ionic approximation. All homopolar effects are, therefore, contained in the matrix $\mathbf{P}$, and we note that from (18) and (22) we can write in first order

$$P_{m\mu}=-X_{m\mu},\quad P_{\mu m}=X_{\mu m},\quad P_{\mu\nu}=P_{mn}=0. \qquad \ldots\ldots(23)$$

Now we are treating non-diagonal elements of $\mathbf{F}$ as first-order small quantities. Thus, in (19), $H_{\alpha\alpha}$ is zero order, $H_{\alpha\beta}$ $(\alpha\neq\beta)$ is first order, $G_{\alpha\alpha}{}^{\gamma\gamma}$ is zero order, $G_{\alpha\beta}{}^{\gamma\gamma}$ $(\alpha\neq\beta)$ is first order, and $G_{\alpha\beta}{}^{\gamma\delta}$ $(\alpha\neq\beta,\ \gamma\neq\delta)$ is second order. The symmetry relations

$$G_{\alpha\beta}{}^{\gamma\delta}=-G_{\alpha\delta}{}^{\gamma\beta}=-G_{\gamma\beta}{}^{\alpha\delta}=G_{\gamma\delta}{}^{\alpha\beta}$$

should be noted.‡ With these concepts concerning the orders of magnitude of the various terms involved we find from (17), (19) and (23)

$$P_{m\mu}=K_{m\mu}/(K_{mm}'-K_{\mu\mu})\ +\text{2nd order terms,} \qquad \ldots\ldots(24)$$

where

$$\left.\begin{aligned}K_{\alpha\beta}&=H_{\alpha\beta}+2\sum_{\nu}G_{\alpha\beta}{}^{\nu\nu},\\ K_{mm}'&=K_{mm}-2G_{mm}{}^{\mu\mu}.\end{aligned}\right\} \qquad \ldots\ldots(25)$$

Corresponding to the expansion (15) of the 'best' orthonormal atomic spin orbitals $\boldsymbol{\chi}$ in terms of the basic set of orthonormal atomic spin-orbitals $\boldsymbol{\Phi}$, the formulae of this section are expressed in terms of the quantities $H_{\alpha\beta}$ and $G_{\alpha\beta}{}^{\gamma\delta}$ (and hence $F_{\alpha\beta}$, $K_{\alpha\beta}$ and K_{mm}'). These are defined by equation (10) in terms of the set $\boldsymbol{\Phi}$. Let $\mathcal{H}_{\alpha\beta}$ and $\mathcal{G}_{\alpha\beta}{}^{\gamma\delta}$ (and hence $\mathcal{F}_{\alpha\beta}$, $\mathcal{K}_{\alpha\beta}$ and $\mathcal{K}_{mm}'$) be defined in the same way but with matrix elements formed from the non-orthogonal atomic spin-orbitals $\boldsymbol{\varphi}$. In terms of this set

$$\boldsymbol{\chi}=\boldsymbol{\varphi}\,\mathfrak{B},\quad \mathfrak{B}=\mathbf{L}\mathbf{B}, \qquad \ldots\ldots(26)$$

and

$$\left.\begin{aligned}\mathbf{F}&=\mathbf{L}^{\dagger}\mathfrak{F}\mathbf{L},\\ \mathcal{F}_{\alpha\beta}&=\mathcal{H}_{\alpha\beta}+2\sum_{\gamma\delta}\mathcal{G}_{\alpha\beta}{}^{\gamma\delta}\mathcal{R}_{\delta\gamma},\\ \mathcal{R}_{\delta\gamma}&=\sum_{\nu}\mathcal{B}_{\delta\nu}\mathcal{B}_{\nu\gamma}{}^{\dagger}.\end{aligned}\right\} \qquad \ldots\ldots(27)$$

---

‡ This four-index symbol can be written as a tensor of the fourth rank in the space spanned by the set $\boldsymbol{\Phi}$.

$\mathfrak{R}$ is the charge- and bond-order matrix with respect to the atomic spin–orbitals $\boldsymbol{\varphi}$ (Löwdin 1955). Its non-diagonal elements represent the *actual* bond strengths in the crystal. Now $\mathbf{L}$ is defined in (6) and the matrix $\mathbf{S}$ has the block form

$$\mathbf{S}=\begin{bmatrix}\mathbf{S}_1 & \mathbf{s}\\ \mathbf{s}^{\dagger} & \mathbf{S}_2\end{bmatrix},$$

where $\mathbf{S}_1$ involves only halide ion functions and $\mathbf{S}_2$ only metal atom functions. Put

$$(\mathbf{1}+\mathbf{S}_1)^{-1}=\mathbf{T} \qquad \ldots\ldots(28)$$

and write $\mathfrak{R}$ in the form

$$\mathfrak{R}=\begin{bmatrix}\mathbf{T} & \mathbf{0}\\ \mathbf{0} & \mathbf{0}\end{bmatrix}-\mathfrak{P}. \qquad \ldots\ldots(29)$$

The first term on the right in equation (29) is the charge- and bond-order matrix for the crystal in the ionic approximation. The non-diagonal elements of $\mathbf{T}$ are negative corresponding to the repulsion between closed shell ions (Lundqvist 1954). Even the diagonal elements are zero in that portion of the matrix which refers to orbitals on the metal atoms. This corresponds to the absence of electrons in these orbitals in the ionic approximation. All homopolar effects are contained in the matrix $\mathfrak{P}$. In second order its elements are

$$\left.\begin{aligned}\mathscr{P}_{\mu\nu}&=(\mathbf{x}^{\dagger}\mathbf{x}+\tfrac{1}{2}\mathbf{x}^{\dagger}\mathbf{s}^{\dagger}+\tfrac{1}{2}\mathbf{s}\mathbf{x}-\tfrac{3}{4}\mathbf{s}\mathbf{s}^{\dagger})_{\mu\nu}\\ \mathscr{P}_{mn}&=(-\mathbf{x}\mathbf{x}^{\dagger}+\tfrac{1}{2}\mathbf{x}\mathbf{s}+\tfrac{1}{2}\mathbf{s}^{\dagger}\mathbf{x}-\tfrac{1}{4}\mathbf{s}^{\dagger}\mathbf{s})_{mn}\\ \mathscr{P}_{m\mu}&=(\tfrac{1}{2}\mathbf{s}^{\dagger}-\mathbf{x}+\tfrac{1}{2}\mathbf{x}\mathbf{S}_1+\tfrac{1}{2}\mathbf{S}_2\mathbf{x}-\tfrac{5}{8}\mathbf{s}^{\dagger}\mathbf{S}_1-\tfrac{3}{8}\mathbf{S}_2\mathbf{s}^{\dagger})_{m\mu}\\ \mathscr{P}_{\mu m}&=\mathscr{P}_{m\mu}{}^{*},\end{aligned}\right\} \qquad \ldots\ldots(30)$$

and as far as first-order terms

$$\mathfrak{B}=\mathbf{1}-\mathfrak{P}, \quad \mathfrak{P}=\mathbf{P}+\tfrac{1}{2}\mathbf{S}^{\dagger}.$$

Finally, from equation (24) we obtain as the only finite elements of $\mathfrak{P}$ in first order,

$$\left.\begin{aligned}\mathscr{P}_{m\mu}&=(\mathscr{K}_{m\mu}-S_{m\mu}{}^{\dagger}\,\mathscr{K}_{\mu\mu})/(\mathscr{K}_{mm}{}'-\mathscr{K}_{\mu\mu}),\\ \mathscr{P}_{\mu m}&=\mathscr{P}_{m\mu}{}^{*},\end{aligned}\right\} \qquad \ldots\ldots(31)$$

where

$$\left.\begin{aligned}\mathscr{K}_{\alpha\beta}&=\mathscr{H}_{\alpha\beta}+2\sum_{\nu}\mathscr{G}_{\alpha\beta}{}^{\nu\nu},\\ \mathscr{K}_{mm}{}'&=\mathscr{K}_{mm}-2\,\mathscr{G}_{mm}{}^{\mu\mu}.\end{aligned}\right\} \qquad \ldots\ldots(32)$$

The homopolar contribution $\mathfrak{P}$ to the charge- and bond-order matrix $\mathfrak{R}$ may be calculated, in first order, from (31). The corresponding 'best' orthonormal atomic spin–orbitals $\boldsymbol{\chi}$ are given, in first order, by the equation

$$\boldsymbol{\chi}=\boldsymbol{\varphi}(\mathbf{1}-\mathfrak{P}). \qquad \ldots\ldots(33)$$

§ 3. THE LATTICE ENERGY

In this section we obtain an expression for the total energy of the crystal in Fock's approximation. The expression is written as the sum of two terms, the first is the total energy in the ionic approximation whilst the second contains the extra terms which arise through the sharing of the outer electrons on the halide ions with the surrounding metal ions.

3.1. *The Energy Expression*

Since the ground state orthonormal crystal spin–orbitals ψ_μ and the ground state orthonormal atomic spin–orbitals χ_μ are equivalent to within a unitary transformation ($\mathbf{V}_1$ of (13)), either set may be used as the one-electron functions in the Slater determinant (2) to calculate the mean value of the Hamiltonian operator for the crystal. We choose the set χ_μ. The ground state energy E is then given by

$$E = W + \sum_{\alpha\beta} R_{\beta\alpha} H_{\alpha\beta} + \sum_{\alpha\beta\gamma\delta} R_{\beta\alpha} G_{\alpha\beta}{}^{\gamma\delta} R_{\delta\gamma}, \qquad \ldots\ldots(34)$$

where W is the interaction energy of the ion cores. We shall assume that W is represented with sufficient accuracy by the ordinary electrostatic interaction. Equation (34) shows that the total energy may be expressed in terms of the matrix elements (10) and the charge- and bond-order matrix $\mathbf{R}$. In terms of the matrix elements $\mathscr{H}_{\alpha\beta}$ and $\mathscr{G}_{\alpha\beta}{}^{\gamma\delta}$ formed with the ordinary atomic spin–orbitals $\boldsymbol{\varphi}$ and the charge- and bond-order matrix $\mathfrak{R}$ we have

$$E = W + \sum_{\alpha\beta} \mathscr{R}_{\beta\alpha} \mathscr{H}_{\alpha\beta} + \sum_{\alpha\beta\gamma\delta} \mathscr{R}_{\beta\alpha} \mathscr{G}_{\alpha\beta}{}^{\gamma\delta} \mathscr{R}_{\delta\gamma}.$$

Using (29) this expression may be put in the form

$$E = E_{\mathrm{I}} + E_{\mathrm{H}}, \qquad \ldots\ldots(35)$$

where

$$E_{\mathrm{I}} = W + \sum_{\mu\nu} T_{\nu\mu} \mathscr{H}_{\mu\nu} + \sum_{\mu\nu\lambda\eta} T_{\nu\mu} \mathscr{G}_{\mu\nu}{}^{\eta\lambda} T_{\lambda\eta}, \qquad \ldots\ldots(36)$$

$$E_{\mathrm{H}} = -\sum_{\alpha\beta} \mathscr{P}_{\beta\alpha} \mathscr{H}_{\alpha\beta} - 2\sum_{\mu\nu\alpha\beta} \mathscr{P}_{\beta\alpha} \mathscr{G}_{\alpha\beta}{}^{\mu\nu} T_{\nu\mu} + \sum_{\alpha\beta\gamma\delta} \mathscr{P}_{\beta\alpha} \mathscr{G}_{\alpha\beta}{}^{\gamma\delta} \mathscr{P}_{\delta\gamma}. \qquad \ldots\ldots(37)$$

E_{I} is the total energy calculated using the atomic spin–orbitals ϕ_μ (or the orthonormal atomic spin–orbitals $\Phi_\mu' = \sum_\nu \phi_\nu (\mathbf{1} + \mathbf{S}_1)_{\nu\mu}{}^{-1/2}$) as one-electron functions in the Slater determinant (2). This is the ionic approximation. E_{H} contains the extra terms which arise because the valence electrons of the halide ions are shared with the surrounding metal ions in the crystal. E_{I} is conveniently referred to as the *energy in the ionic approximation* and E_{H} as the *homopolar contribution to the lattice energy*.‡

3.2. E_{H} *in Second Order*

Making use of the orders of magnitude of the elements of $\mathfrak{P}$ indicated in (30) and the definition (28) of $\mathbf{T}$ we find from (37)

$$E_{\mathrm{H}} = -\sum_{\mu} \mathscr{P}_{\mu\mu} \mathscr{K}_{\mu\mu} - \sum_{m} \mathscr{P}_{mm} \mathscr{K}_{mm} - \sum_{\mu m} (\mathscr{P}_{\mu m} \mathscr{K}_{m\mu} + \mathscr{K}_{\mu m} \mathscr{P}_{m\mu})$$
$$+ 2\sum_{\mu m} \mathscr{P}_{\mu m} \mathscr{G}_{m\mu}{}^{\mu m} \mathscr{P}_{m\mu} + \text{3rd order terms.} \qquad \ldots\ldots(38)$$

Using (30) the following results are easily proved in second order:

$$\left.\begin{aligned} \mathscr{P}_{mn} &= -\sum_{\mu} \mathscr{P}_{m\mu} \mathscr{P}_{\mu n}, \\ \mathscr{P}_{\mu\nu} &= \sum_{m} (\mathscr{P}_{\mu m} \mathscr{P}_{m\nu} - \mathscr{P}_{\mu m} S_{m\nu}{}^{\dagger} - S_{\mu m} \mathscr{P}_{m\nu}). \end{aligned}\right\} \qquad \ldots\ldots(39)$$

Hence (38) may be written in the compact form

$$E_{\mathrm{H}} = \sum_{\mu m} \mathscr{P}_{\mu m} \mathscr{P}_{m\mu} (\mathscr{K}_{\mu\mu} - \mathscr{K}_{mm}{}') + \text{3rd order terms.} \qquad \ldots\ldots(40)$$

Thus we only need the matrix $\mathfrak{P}$ in first order to calculate E_{H} in second order. The only finite elements of $\mathfrak{P}$ in first order are $\mathscr{P}_{m\mu}$ and $\mathscr{P}_{\mu m}$; these may be calculated from (31).

---

‡ No absolute significance is attached to these terms. They have meaning only with reference to the approximations made in solving the fundamental equation (1).

It is of some importance to notice that although we have used a simplified model in which the crystal is regarded as a system of $6N$ electrons and $2N$ ion cores, no major modifications are required to include the effects of the neglected electrons. All that is necessary is to use the indices μ, ν, λ, η to denote any occupied orbital in the free ions, halide or metal, and to take Z_g in (4) as the nuclear charge.

Finally, we note that by using the addition properties of spherical harmonics, it can be shown that E_{H} is independent of the orientation of the axes of quantization chosen to describe the space parts of the atomic orbitals $\boldsymbol{\varphi}$ associated with each ion in the lattice. This is a general property of the interaction energy in a system whose constituents may be regarded as having closed shell configurations.

§ 4. NUMERICAL RESULTS

We take for the basic set $\boldsymbol{\varphi}$ of atomic spin-orbitals the solutions of the Hartree–Fock equations for the free halide ions and metal atoms. Regarding all quantities associated with the overlapping of the orbitals as first order small quantities at the most, it is easy to prove that, in terms of this set,

$$\left.\begin{aligned} \mathscr{K}_{\mu\mu} &= \lambda_\mu - (\alpha_{\mathrm{M}}/r_0) + \text{1st order terms}, \\ \mathscr{K}_{mm}' &= \lambda_m + (\alpha_{\mathrm{M}}/r_0) - (1/r_{\mu m}) + \text{1st order terms}, \\ \mathscr{K}_{m\mu} &= S_{m\mu}\lambda_\mu + (m|\,V^{(\mu)}|\,\mu) + \text{2nd order terms}. \end{aligned}\right\} \qquad \ldots\ldots(41)$$

Here, α_{M} is Madelung's constant ($\alpha_{\mathrm{M}} = 1{\cdot}7476$ for LiF), r_0 is the inter-ionic distance, $r_{\mu m}$ is the distance between the nuclei on which ϕ_μ and ϕ_m are centred, λ_μ and λ_m are the Hartree–Fock energy parameters associated with ϕ_μ and ϕ_m in the free ion and atom respectively. $V^{(\mu)}$ is defined as follows. Let all ions in the lattice be replaced by corresponding point charges ± 1. Remove the charge at the lattice point on which ϕ_μ is centred. $V^{(\mu)}$ is the potential energy of an electron in the remaining array of charges.

E_{H} will be calculated from (40) assuming that only overlap between nearest neighbours (i.e. halide ion–metal atom overlap) is important. Then, with the axes of quantization for the orbitals on the halide ions orientated to point towards the nearest metal ions,

$$\left.\begin{aligned} E_{\mathrm{H}} &= -12|\mathscr{P}_{m\mu}|^2\theta, \\ \theta &= \lambda_m - \lambda_\mu + (2\alpha_{\mathrm{M}} - 1)/r_0. \end{aligned}\right\} \qquad \ldots\ldots(42)$$

It is to be understood henceforth that ϕ_m and ϕ_μ are centred on ions which are nearest neighbours in the lattice and that the metal ion lies in a direction perpendicular to the nodal plane of ϕ_μ. From (31) and (41)

$$\left.\begin{aligned} \mathscr{P}_{m\mu} &= (J_{m\mu} + S_{m\mu}\alpha_{\mathrm{M}}/r_0)\theta, \\ J_{m\mu} &= (m|\,V^{(\mu)}|\,\mu). \end{aligned}\right\} \qquad \ldots\ldots(43)$$

Because of the definition of $V^{(\mu)}$, $J_{m\mu}$ contains certain integrals which depend upon the relative positions of three nuclei. In a first calculation these three-body potentials will be ignored. Hence we use the approximation

$$J_{m\mu} = (m|\,1/r_m|\,\mu),$$

where r_m is the distance from the nucleus on which ϕ_m is centred.

Calculations have been made for LiF. The space parts of ϕ_μ and ϕ_m are of the form $r^{-1}f(r)Y(\theta,\phi)$, where $Y(\theta,\phi)$ is a normalized real spherical harmonic and $f(r)$ is the usual radial function calculated by the self-consistent field method. To calculate the integrals in (43), $r^{-1}f(r)$ was approximated by a finite series of Slater-type radial functions (Slater 1932) of the form

$$R(r\,;\,nl,\zeta)=(2\zeta)^{n+1/2}[(2n)\,!]^{-1/2}r^{n-1}e^{-\zeta r}.$$

For the 2p-orbitals on F⁻, the two-term expression

$$r^{-1}f_{2p}(r)=0{\cdot}724R(r\,;\,2p,2{\cdot}37)-0{\cdot}403R(r\,;\,2p,0{\cdot}85),$$

already given by Benson and Wyllie (1951), was used. We note that only Hartree's equations have been solved for F⁻ (Hartree 1935). For the 2s-orbital on Li, the two-term expansion

$$r^{-1}f_{2s}(r)=0{\cdot}522R(r\,;\,1s,0{\cdot}767)-1{\cdot}435R(r\,;\,2s,0{\cdot}767),$$

was used. This expansion was obtained by Fock and Petrashen (1935) using the variation method as a preliminary to solving the self-consistent field problem with exchange. It is a fair approximation to their final result.

The integrals $S_{m\mu}$ and $J_{m\mu}$ were evaluated at several values of the inter-ionic distance r_0. $S_{m\mu}$ was calculated from the formulae given by Mulliken, Rieke, Orloff and Orloff (1949) and $J_{m\mu}$ from Roothaan's (1951 b) formulae. The final results are shown in figures 1 and 2 where E_H and $|\mathscr{P}_{m\mu}|$ are plotted against r_0.

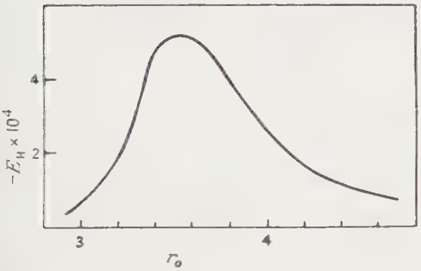

Figure 1. The homopolar contribution to the lattice energy of LiF.

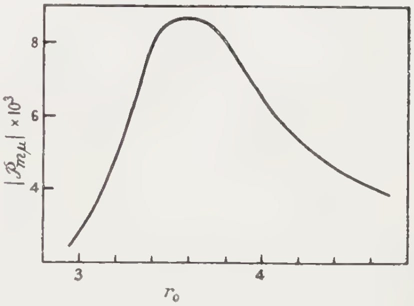

Figure 2. $|\mathscr{P}_{m\mu}|$ as a function of the inter-ionic distance for LiF.

$6|\mathscr{P}_{m\mu}|^2$ is the homopolar charge-order of each ordinary atomic spin-orbital on the metal atoms. The other elements of the charge- and bond-order matrix may be calculated from (39). For $r_0=3{\cdot}80$ (the observed inter-ionic distance in LiF)

$$-2\mathscr{P}_{mm}=0{\cdot}00076 \text{ (homopolar charge-order on Li}^+) \quad\ldots\ldots(44)$$

$$-6\mathscr{P}_{\mu\mu}=0{\cdot}043 \text{ (homopolar charge-order on F}^-) \quad\ldots\ldots(45)$$

$$-2\mathscr{P}_{mn}=-0{\cdot}000126 \quad\ldots\ldots(46)$$

(homopolar bond-order between next-nearest neighbours in the Li⁺ lattice)

$$-2\mathscr{P}_{\mu\nu}=-0{\cdot}0071 \quad\ldots\ldots(47)$$

(homopolar bond-order between next-nearest neighbours in the F⁻ lattice)

$$-4\mathscr{P}_{\mu\nu}=-0{\cdot}0142 \quad\ldots\ldots(48)$$

(homopolar bond-order between nearest neighbours in the F⁻ lattice).

These results show that homopolar effects, whilst giving an extra attraction between nearest (unlike) neighbours also enhance the repulsive character of the interaction between like neighbours in the lattice. Of course, the nearest neighbour attraction is dominant and the total energy of the system is lowered.

§ 5. DISCUSSION

The lattice energy W_L is obtained from (35) by subtracting the total energy of the free ions. The result may be put in the form

$$W_L = W_I + E_H,$$

where W_I is the lattice energy in the ionic approximation. In the simplified theory in which the crystal is treated as a system of $6N$ electrons and $2N$ ion cores and halide–halide overlap is neglected, W_I reduces to the formula for the lattice energy already given by Benson and Wyllie (1951) under the heading 'Simple Perturbation Calculation'. W_I has its minimum value of $-0{\cdot}3945$ at $r_0 = 3{\cdot}57$. From figure 1 we see that E_H has its minimum value at about the same value of r_0 but E_H is only about $0{\cdot}1\%$ of W_L. We conclude, therefore, that homopolar forces play an insignificant part in determining the lattice energy of LiF. This general conclusion has, of course, already been reached both from a study of the physical and chemical properties of the alkali halides and from the fact that, when the classical theory of ionic crystals is combined with the Born–Haber cycle and applied to each of the alkali fluorides to give the electron affinity of F, the values obtained are almost the same. The important, and perhaps surprising, point which emerges from the present work is the complete insignificance of the homopolar contribution to the lattice energy. The effect is small for LiF because $J_{m\mu}$ and $S_{m\mu}\alpha_M/r_0$ are almost equal in magnitude but opposite in sign. Otherwise, a homopolar contribution amounting to some 5% of the lattice energy would arise.

It is natural to enquire whether the importance of the homopolar term may be assessed from any measured physical properties of the crystal. According to (42) and (43) this would be possible if any two of the quantities $|\mathscr{P}_{m\mu}|$, θ and $(J_{m\mu} + S_{m\mu}\alpha_M/r_0)$ could be inferred from the experimental data. θ presents little difficulty. It is a zero-order (large) quantity corresponding to the energy difference between the ground state and the excited state formed by transferring an electron from an orbital χ_μ centred on F^- to a normally unoccupied orbital χ_m centred on one of the nearest Li^+ ions. A proper treatment of the excited state gives the familiar exciton bond. However, the exciton band width is a first-order effect whereas θ is required only in zero order to obtain E_H in second order from (42). Hence θ may be calculated from the position of the first ultraviolet absorption band in the crystal (cf. Mott and Gurney 1940, p. 98). Neither the individual terms $J_{m\mu}$ and $S_{m\mu}\alpha_M/r_0$ nor their sum are related in a simple way to any physical property of the solid and it remains, therefore, to consider $\mathscr{P}_{m\mu}$. The whole matrix $\mathfrak{P}$ is responsible for the deviation of the charge distribution in the solid from that represented by the ionic approximation. However, the ionic approximation is a theoretical concept and has no practical counterpart, so that a knowledge of the actual charge distribution is no help in determining $\mathfrak{P}$. It does not, therefore, appear possible to devise a scheme whereby the homopolar term may be obtained from the physical properties of the solid.

REFERENCES

BENSON, G. C., and WYLLIE, G., 1951, *Proc. Phys. Soc.* A, **64,** 276.
EWING, D. H., and SEITZ, F., 1936, *Phys. Rev.*, **50,** 760.
FOCK, V., 1930, *Z. Phys.*, **61,** 126.
FOCK, V., and PETRASHEN, M. J., 1935, *Phys. Z. Sowjet*, **8,** 547.
HARTREE, D. R., 1935, *Proc. Roy. Soc.* A, **151,** 96.
LANDSHOFF, R., 1936, *Z. Phys.*, **102,** 201.
LÖWDIN, P. O., 1948, *A Theoretical Investigation into Some Properties of Ionic Crystals* (Thesis) (Uppsala : Almquist and Wicksell); 1950, *J. Chem. Phys.*, **18,** 365 ; 1955, *Phys. Rev.*, **97,** 1490.
LUNDQVIST, S. O., 1954, *Ark. Fys.*, **8,** 177.
MOTT, N. F., and GURNEY, R. W., 1940, *Electronic Processes in Ionic Crystals* (Oxford : Clarendon Press).
MULLIKEN, R. S., RIEKE, C. A., ORLOFF, D., and ORLOFF, H., 1949, *J. Chem. Phys.*, **17,** 1248.
ROOTHAAN, C. C. J., 1951 a, *Rev. Mod. Phys.*, **23,** 69 ; 1951 b, *J. Chem. Phys.*, **19,** 1445.
SHOCKLEY, W., 1936, *Phys. Rev.*, **50,** 754.
SLATER, J. C., 1932, *Phys. Rev.*, **42,** 33.

Nuclear Disintegrations produced by Cosmic Ray Particles in a High Pressure Cloud Chamber

By F. W. BULLOCK

Department of Physics, University College London

Communicated by E. H. S. Burhop; MS. received 10*th September* 1956, *and in final form* 26*th November* 1956

Abstract. Cosmic ray stars produced in argon at 75 atmospheres pressure have been analysed to give size distributions and angular distributions of the prongs. In a discussion of the star-producing flux entering the chamber, the natural rate of occurrence of interactions in the chamber is compared with rates obtained by other workers.

§ 1. Introduction

Photographs of the cosmic radiation at 2040 m, obtained with a high-pressure cloud chamber containing argon at 75 atmospheres pressure,† have been scanned for nuclear disintegrations occurring in the chamber gas. This report gives results obtained from an analysis of the 212 disintegrations observed.

Data are presented on star size distribution and on the angular distributions of star primaries and secondaries. The properties of the star-producing flux entering the chamber have been studied by means of the randomly occurring interactions, and it has also been possible to estimate the cross section for production of stars by the ionizing secondaries of interactions occurring in the

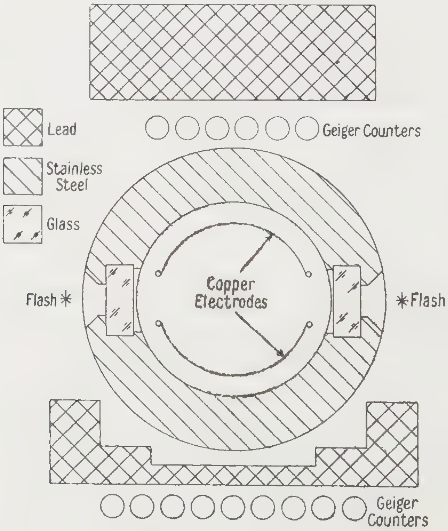

Figure 1. Diagrammatic representation of apparatus.

---

† Operated by a joint group from University College London and the University of Edinburgh (Burhop 1954, Evans 1954).

absorber above the chamber. This is found to be 0·33 ± 0·08 barn, appreciably smaller than the geometric cross section for argon.

§ 2. EXPERIMENTAL ARRANGEMENT

The high pressure cloud chamber and its characteristics have been described elsewhere (Astbury *et al.* 1955). The points mentioned in the following are only those which have not been adequately dealt with previously. A diagrammatic representation of the apparatus is shown in figure 1.

The clearing field electrodes for this experiment have been two copper plates running the length of the chamber and bent to form two sections of a cylinder, so that they fit round the inside of the chamber wall, being about 2 cm away from the wall at all points. With this electrode system the illuminated volume photographed is about 2·5 litres.

Throughout most of the experiment there have been 10 cm of lead absorber covering the whole of the effective area of the chamber gas, making, together with the chamber wall, a total absorber thickness of about 170 g cm^{-2}. For a short run, however, (about 800 pictures) no lead absorber was used, the total thickness due to the stainless steel wall alone then being 53 g cm^{-2}.

Expansion of the chamber is controlled by two trays of Geiger counters, one above and one below the chamber. The counter control system has been arranged to detect penetrating showers initiated in the absorber. The electronic apparatus for the counter system, hodoscope recording unit and chamber control was designed and built by Mr. P. Baxter and Mr. A. J. Metheringham.

§ 3. SELECTION AND MEASUREMENT OF EVENTS

Emulsion studies of stars in general consider only events having three or more charged particles and the criterion used for selection of small stars usually means that the minimum visible energy of the ionizing particles emitted is about 3 MEV. Cloud chamber results, on the other hand, particularly those obtained with a high pressure chamber, do not give such precise information on the number of charged particles emitted since low energy particles produce only blobs of ionization around the star apex and cannot definitely be distinguished as tracks. In the present work no track has been included unless at least 2 mm in length, and the estimated minimum ionization energy observed is then about 5 MEV.

One-prong stars have been included in the analysis only if the prong commences and completes its range within the chamber gas.

Interactions have been separated into those with charged and those with neutral primaries, according to the following criterion. If a star has a lightly ionizing track in the upper hemisphere about the point of disintegration, then this is taken to be the track of the star-producing particle. In the event of there being more than one such track, the one making the smallest angle to the vertical is taken as the star primary.

Since the chamber control system is designed to select penetrating showers originating in the absorber, not all the stars formed in the chamber gas are observed, for there will be a number of cases where a star occurs in the gas of insufficient energy itself, or unaccompanied by enough shower particles, to trigger the required combination of counters. The stars photographed may be divided into two groups. The first contains those which have occurred as the result of an event triggering the chamber and can be distinguished as 'counter-controlled' by the appearance of the tracks (counter-controlled minimum ionization tracks are about 0·7 mm thick in space) (figures 2 and 4, Plate). The second contains stars which have occurred during the sensitive time immediately preceding or following an expansion. Such stars may be distinguished as 'random' either by the fact that all tracks are doubled due to field separation, in which case those concerned were classified as pre-expansion (figure 3, Plate), or else the tracks are very fine, due to incomplete condensation, indicating them to have been formed post-expansion.

During the experiment, 7200 photographs have been obtained showing a total of 212 disintegrations in the chamber gas. Table 1 shows how stars with charged and neutral primaries are distributed in the counter-controlled and random groups.

Table 1

	Counter-controlled			Random	
	a	b	c	a	b
No. of stars under absorber A	4	1	0	2	8
No. of stars under absorber B	57	51	2	13	74

Absorber A. 53 g cm^{-2} stainless steel (chamber wall alone).
Absorber B. 53 g cm^{-2} stainless steel + 114 g cm^{-2} lead.

a : charged primary; b : neutral primary; c : unknown primary. The two stars noted in column c occur in very dense showers, so that the nature of the primary cannot be decided.

Two methods have been employed in the measurement of track orientation in the chamber.

The first involves no re-projection, but consists of direct measurement of the event from the stereo pair on the film, using a Pye two-dimensional travelling microscope. This method, whilst capable of giving angles to an accuracy of better than 1°, involves a great deal of tedious calculation and has been superseded by a re-projection method developed by Dr. G. R. Evans of Edinburgh University.

Here, the film is placed in a re-projection camera of the same dimensions as the chamber camera and either the image is picked up and measured directly on a freely moving screen as in conventional re-projection techniques, or, for more accurate work, the coordinates of any point in space can be obtained. For this purpose a vertical scale with a vernier carrying a fine pointer can be added to the above-mentioned Pye instrument. The pointer is moved until its tip coincides with the required point in the re-projected volume, when its coordinates can be read directly from the three mutually perpendicular scales of the instrument. By this method an accuracy to 1 to 2 degrees can be obtained.

§ 4. Size Distribution of the Stars

The size distribution of all stars, plotted as number of stars $N(>n)$ with more than n ionizing secondaries against n, is shown in figure 5. Distributions are not plotted separately for random and counter-controlled stars, since no significant differences are observed between these. With the exception of $n=0$, all the points lie, on a logarithmic plot, very close to a straight line given by $N(>n)=ke^{-0\cdot5n}$, where k is a constant. The discrepancy at $n=0$ is due to a deficiency of $n=1$ events, which can be explained as a combination of two effects. Firstly, the criterion for selecting one-prong stars leads one to expect a deficiency of $n=1$ events. This effect, however, is emphasized by the fact that a star caused by a neutral primary which passes through the nucleus, imparting enough excitation energy for the nucleus to emit an evaporation particle, will be classified as an $n=1$ event, whereas a similar star caused by a charged primary will be classified as an $n=2$ event. Secondly, it is probable that many true $n=1$ charged primary stars are initiated by slow ionizing particles. These would be classed as $n=2$ neutral primary stars.

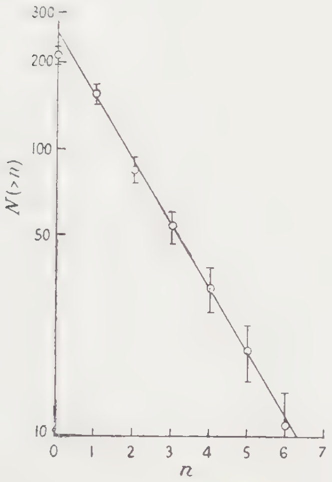

Figure 5. Size distribution for all stars. The line is given by the relation $N(>n)=k\exp(-0{\cdot}5n)$.

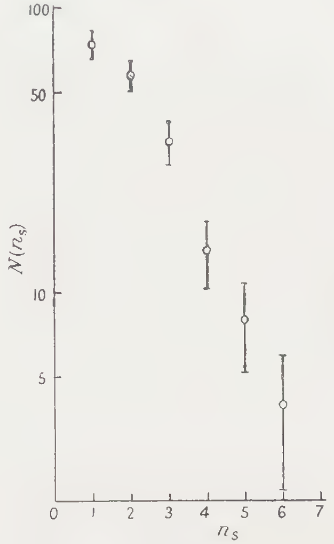

Figure 6. Differential size distribution of number of stars $N(n_S)$ having n_S heavily ionizing secondaries.

The distribution of all stars, plotted as number of stars $N(n_S)$ with n_S slow secondaries against n_S (figure 6) shows the usual exponential decrease in star abundance with increase in number of heavily ionizing secondaries. In a high pressure cloud chamber, difference in intensity of ionization is not so marked as in atmospheric chambers or emulsions since all tracks, even minimum ionization, appear solid. Therefore, in some cases, a distinction between heavily and lightly ionizing particles is necessarily rather difficult to make, particularly so if the star is in a badly illuminated region of the chamber. However, of the present work it is true to say that very few, if any, evaporation particles have been included in the lightly ionizing category, although possibly some lightly ionizing particles have been included in the heavily ionizing category. The separation between heavily and lightly ionizing particles is about four times minimum ionization.

§ 5. ANGULAR DISTRIBUTIONS OF STAR PRIMARIES AND SECONDARIES

Since the clearing field is not uniform over the chamber volume, one expects that pre-expansion events will not be suitable for providing angular data. However, as can be seen from figure 3, distortion is not always present in such stars and, in the majority of cases, it was found possible to make angular measurements on them. All the distributions given, therefore, include data obtained from random stars which were judged to be distortion-free.

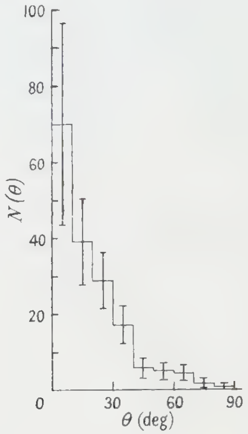

Figure 7. Angular distribution of star primaries with respect to the vertical.

In figure 7 is shown the distribution of angles θ to the vertical of the ionizing star-producing primaries under absorbers B, in which $N(\theta)$ is a measure of the number of particles per steradian in the interval $\Delta\theta$ expressed in arbitrary units. No attempt has been made to allow for the effect of some star-producing primaries coming from below and producing lightly ionizing particles in the upper hemisphere. It can be shown that such a correction would be small (Lohrmann 1955). The distribution can best be fitted by the relation $N(\theta) = A \cos^7 \theta$, where A is a constant.

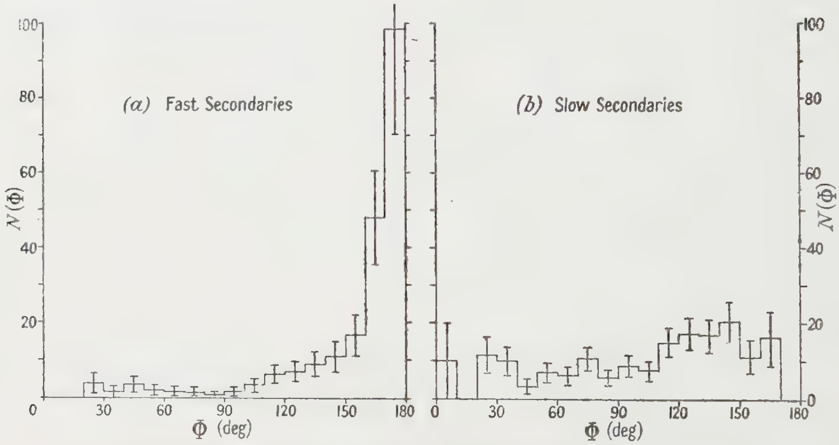

Figure 8. Angular distribution of (*a*) fast secondaries and (*b*) slow secondaries with respect to the primary.

The distribution of angles Φ to the primary of (*a*) lightly ionizing and (*b*) heavily ionizing secondaries is shown in figure 8, both distributions being plotted in the laboratory system. In spite of the comparatively large statistical errors, a downward excess of heavily ionizing secondaries can be distinguished in figure 8(*b*). Isotropic emission from the moving nucleus and 'knock-on' particles in the evaporation-energy region would be expected to produce such a downward excess in the laboratory system (Harding *et al.* 1949, Bernardini *et al.* 1950). Difficulty in differentiating between heavily and lightly ionizing prongs, leading to the inclusion of some lightly ionizing particles in the distribution, may be expected to accentuate the effect in the present work.

§ 6. PROPERTIES OF THE STAR-PRODUCING FLUX ENTERING THE CHAMBER

Information can be obtained about the natural star-producing flux entering the chamber by studying the randomly occurring interactions. Only about half the stars discussed above were random events and in analysing these alone the statistical errors are correspondingly increased.

The selection system used during the experiment causes a biasing of the random stars against two types of event. Firstly, there will be a bias against events whose primaries are in fact secondaries of large interactions in the absorber (figure 4, Plate), since the accompanying particles will normally trigger the expansion. The effect of the bias is found to decrease the number of random stars observed below that which would have been observed without a selection system by about 0·5%. Secondly, stars produced by ionizing primaries and having three or more fast secondaries will, in general, produce an expansion of the chamber and therefore be observed as counter-controlled. Since very few stars are observed of this energy under our conditions, this effect is found to be quite negligible (0·01% less than the abundance expected without a selection system).

6.1. *Ratio of Charged to Neutral Particles in the Flux*

Assuming that the average cross section for production of the interactions is the same for neutral and charged particles, then the ratio of charged to neutral particles in the star-producing flux entering the chamber is $0{\cdot}18 \pm 0{\cdot}05$. It is expected that this ratio will differ from the natural ratio because of the large amount of absorber present in this experiment. However, W. W. Brown (1954) finds that the ratio under $\frac{1}{2}$-inch brass is 0·27 at 3240 m and 0·18 at sea level.

6.2. *Rate of Occurrence of Interactions*

To determine this from the random stars, the total sensitive time, τ sec per expansion, must be known. τ is given by $\tau = \tau_1 + \tau_2$, where τ_1 and τ_2 are respectively the pre-expansion and post-expansion sensitive times, and τ_2 is given directly by the imposed flash delay. τ_1 has been calculated from the chamber dimensions and the applied clearing field,† assuming that the mobility K of A^+ ions in argon is given by $K = K_0 760/p$, where p = gas pressure in mm mercury and $K_0 = 2{\cdot}5$ cm^2 sec^{-1} volt^{-1} (Tyndall 1938).

Several assumptions have been made in this calculation, the most drastic of which is that the lines of force between the semi-cylindrical electrodes are taken as being parallel and vertical in all regions of the chamber. One then arrives at a value of 2·3 sec for τ, the estimated error in which is about ±15%.

---

† A further method for obtaining τ_1 would be to determine the ratio of pre-expansion to post-expansion tracks, and multiply this by τ_2. This was found to be unsatisfactory, however, due to difficulty in differentiating between counter-controlled and post-expansion random tracks in all cases.

Using this value for the sensitive time, the rate of occurrence of all interactions as calculated from the random stars is $2{\cdot}7 \pm 0{\cdot}6$ (g atom)$^{-1}$ h^{-1}. This figure can conveniently be compared with that obtained by W. W. Brown in a cloud–ion chamber at 3240 m, if allowance is made for absorption of the star-producing radiation through (*a*) 110 g cm^{-2} of atmosphere to the altitude of the present experiment, (*b*) 114 g cm^{-2} lead absorber, (*c*) 53 g cm^{-2} stainless steel chamber wall. The best values for the attenuation lengths in air and lead, based on nuclear emulsion data (e.g. Bernardini *et al.* 1949, Rosser and Swift 1951, Barford and Davis 1952), are taken to be 135 g cm^{-2} and 310 g cm^{-2}, respectively. The attenuation length for stainless steel has been taken as 200 g cm^{-2}, the value for iron assuming an attenuation length proportional to $A^{1/3}$. Reduced to the altitude and conditions of the present experiment, Brown's rate then becomes $2{\cdot}0$ (g atom)$^{-1}$ h^{-1}. A higher rate is expected in the present work, since the minimum star energy considered is about 5 MeV whereas Brown's minimum was 8 MeV.

The rates of occurrence of stars having three or more ionizing prongs in emulsions vary considerably according to scanning efficiency. Table 2 gives the rates obtained in six emulsion experiments.

Table 2

1	2	3	4
3660	10·0	0·67	Perkins (1947)
3570	10·8	0·84	Brown *et al.* (1949)
2860	9·0	1·10	Rosser and Swift (1951)
3500	14·2	1·11	Bernardini *et al.* (1950)
3570	17·0	1·32	Barford and Davis (1952)
3570	22·0	1·71	Lord (1951)

1, Altitude of observation in metres; 2, observed star rate per cm^3 per day in emulsion; 3, equivalent rate (g atom)$^{-1}$ h^{-1} in argon under conditions of present experiment; 4, reference.

The rate obtained from the present work for stars having three or more ionizing prongs is $1{\cdot}0 \pm 0{\cdot}2$ (g atom)$^{-1}$ h^{-1}. The effect of losing small prongs in the cloud chamber would be expected to decrease the chamber rate below that observed in emulsions.

§ 7. Cross Section for Star Production by Ionizing Secondaries of Interactions in the Absorber

This has been obtained using only those stars whose primaries are produced in local penetrating showers (figure 4). The whole collection of photographs was scanned for local penetrating showers and the number of particles present in each shower counted. Since large showers could not be counted accurately, and, in any case, could easily be confused in many cases with fast electron showers, only those containing from three to ten penetrating particles were used. From the number of stars occurring in such showers, it was then possible to obtain a value for the cross section. This was found to be $0{\cdot}33 \pm 0{\cdot}08$ barn, compared with a geometric cross section for argon of 0·52 barn.

Acknowledgments

I should like to thank Dr. E. H. S. Burhop for his personal supervision, also Professor H. S. W. Massey and Dr. G. R. Evans for their interest in this work, and to acknowledge several useful discussions with Dr. J. P. Astbury and Dr. P. E. Hodgson. Thanks are also due to the other members of the group for their helpful discussions and advice—in particular to Mr. N. N. Raina who carried out many of the measurements. The group as a whole is indebted to the University of Padua for providing space for this experiment in their laboratory at Marmolada.

The programme was made possible by the award of a Department of Scientific and Industrial Research Special Development Grant to Professor H. S. W. Massey.

References

Astbury, J. P., Baxter, P., Burhop, E. H. S., Evans, G. R., Massey, H. S. W., Metheringham, A. J., Morris, N., Stannard, F. R., Tomlinson, H. S., and Williams, E. J., 1955, *Nature, Lond.*, **175**, 445.

Barford, N. C., and Davis, G., 1952, *Proc. Roy. Soc.* A, **214**, 225.

Bernardini, G. ,Cortini, G., and Manfredini, A., 1949, *Phys. Rev.*, **76**, 1792; 1950, *Ibid.*, **79**, 952.

Brown, R. H., Camerini, U., Fowler, P. H., Heitler, H., King, D. T., and Powell, C. F., 1949, *Phil. Mag.*, **40**, 862.

Brown, W. W., 1954, *Phys. Rev.*, **93**, 528.

Burhop, E. H. S., 1954, *Nuovo Cim.*, **11** (Suppl.), 343.

Evans, G. R., 1954, *Nuovo Cim.*, **12** (Suppl.), 335.

Harding, J. B., Lattimore, S., and Perkins, D. H., 1949, *Proc. Roy. Soc.* A, **196**, 325.

Lohrmann, E., 1955, *Nuovo Cim.*, **6**, 1126.

Lord, J. J., 1951, *Phys. Rev.*, **81**, 901.

Perkins, D. H., 1947, *Nature, Lond.*, **160**, 707.

Rosser, W. G. V., and Swift, M. W., 1951, *Phil. Mag.*, **42**, 856.

Tyndall, A. N., 1938, *Mobility of Positive Ions in Gases* (Cambridge : University Press), p. 71.

Nuclear Resonant Scattering of Gamma Rays in ^{199}Hg

By V. KNAPP

Physics Department, University of Birmingham

Communicated by P. B. Moon; MS. received 13*th August* 1956, *and in final form* 9*th November* 1956

Abstract. The resonant nuclear scattering of the 209 kev gamma ray in ^{199}Hg has been studied by the high speed rotor technique, and the decrease of scattering at speeds above the optimum has been observed.

From the measured ratio of resonant scattering to Rayleigh scattering, and with allowance for internal-conversion transitions, the mean life of the 209 kev level is found to be $(7{\cdot}8 \pm 1{\cdot}2) \times 10^{-11}$ second.

---

§ 1. INTRODUCTION

RESONANT scattering of gamma rays in ^{199}Hg has been studied and the width of the 209 kev excited level measured, using the high speed rotor technique for compensation of energy loss due to nuclear recoil at emission and absorption of gamma rays (Moon 1951).

This particular experimental technique has the advantage of a well-defined compensation speed, and as the highest speed attainable (800 m sec^{-1}) was considerably greater than the theoretical resonant speed (336 m sec^{-1}) for the level concerned, measurements with ^{199}Hg were possible well beyond the maximum of the resonance curve. The results were compared with theory, on the assumptions of complete degradation of beta recoil and free recoils in gamma-ray processes.

§ 2. EXPERIMENTAL TECHNIQUE

The apparatus employs the rotor used in the earlier experiments with ^{198}Hg by Davey and Moon (1953). Rotor tips were loaded with a ^{199}Au source having a 209 kev gamma ray activity of about 4 mc. The source was produced by separation from neutron-irradiated platinum and contained no observable admixtures. Lead shielding was carefully arranged in order to minimize the non-elastic background; this is important since the resonant effect is considerably smaller than in the case of ^{198}Hg. Gamma rays emitted from the source when on the non-shielded arc of the rotor path (figure 1) were scattered by interchangeable scatterers into the scintillation counter. A mean scattering angle of 90° was chosen. Since the angular distribution for resonant scattering is symmetrical about this angle, the experimentally determined scattering cross section is insensitive to small changes of mean scattering angle. As resonant scatterer, liquid mercury was used; it contains 17% of ^{199}Hg. Lead was used as non-resonant scatterer. A single-channel pulse height analyser was set to admit the photoelectric peak from gamma rays with energies in the region of 209 kev; the lower and upper channel limits being about 195 kev and 230 kev.

The ratios of scattering from resonant and non-resonant scatterers were observed at different speeds, the scatterers being exchanged every minute.

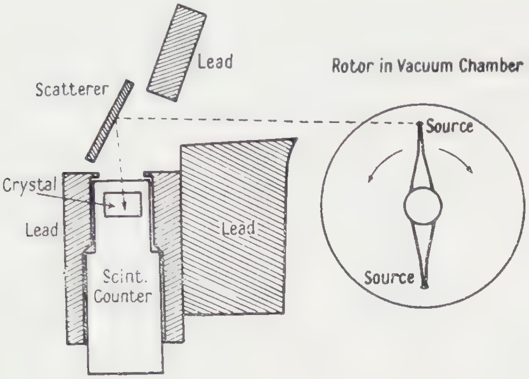

Figure 1. A horizontal section of the apparatus. Part of the shielding and the rotor driving coils are omitted.

Every 25 minutes the calibration of the counter was checked and the pulse discriminator reset. Due to the large number of exchanges, errors other than statistical were effectively reduced, the spread of experimental ratios at any one speed being within the limits of statistical expectation.

§ 3. Results and Discussion

The ratio of counting rates in the selected channel with resonant and non-resonant scatterer was measured for speeds from 800 rev $\sec^{-1}$ (360 m $\sec^{-1}$), the source receding from the scatterer, to 1600 rev $\sec^{-1}$ (720 m $\sec^{-1}$), the source moving towards the scatterer.

With two sources, over 200 000 counts were recorded in 47 experimental runs characterized by well defined rotor speeds.

The cross section for resonant scattering as calculated by Moon and Storruste (1953) is:

$$\sigma = 3{\cdot}6 \times 10^{-3} \frac{f(\theta)}{4\pi} \frac{I\Gamma}{E_0{}^3} \frac{g_a}{g_b} \left(\frac{A}{T}\right)^{1/2} \exp\left[3 \times 10^{-9} \frac{A}{T}(U - U_m)^2\right] \quad \ldots\ldots(1)$$

where I is the isotopic abundance of the resonantly scattering isotope, A its atomic weight, g_a and g_b the multiplicities of the excited and ground states respectively, and T the mean of the temperatures of the source and the scatterer; $f(\theta)$ is the angular distribution factor normalized so as to be equal to unity for isotropic scattering; U and U_m are the actual and optimum speeds of approach of source to scatterer. Γ is the width of excited state and, like the resonant energy E_0, is measured in electron volts. For comparison with the experimental results the exponential factor in formula (1) was averaged so as to take into account the spread of relative source–scatterer velocities for any given rotor speed. This is necessary because gamma rays can reach the scatterers from a 90° arc of the source path.

The maximum of the curve obtained in this way lies at about 880 rev $\sec^{-1}$, 100 rev $\sec^{-1}$ above the speed calculated from the condition $U = U_m$ which gives maximum value to the resonant scattering cross section as given by (1). This is the expected effect of the geometry of the arrangement.

If this calculated curve is expressed as $\sigma = F(u)$, the experimental ratios should fit a curve of the form $A + BF(u)$ where A represents a correction for inequality of the non-resonant scattering from the two specimens and B is a scale factor.

Figure 2 shows such a curve fitted by the least-squares method to the 47 individual experimental ratios; it also shows the points obtained by grouping the experimental ratios into speed regions 200 rev sec^{-1} wide, and calculating arithmetic means for each section. Probable errors are indicated. Apart from a discrepancy in the region of 300 m sec^{-1}, which might have appeared less noticeable if the speed regions had been differently chosen, there is satisfactory agreement with the theoretical curve. In particular, the decrease of scattering above the resonant speed is more clearly apparent than in any previous experiment. At the maximum of the curve the resonant scattering amounts to about 7% of the total counting rate and to $(13 \pm 2)\%$ of elastic (i.e. Rayleigh) scattering. Thomson scattering by the nuclear charge is completely negligible at this energy, being smaller by a factor of about 10^4.

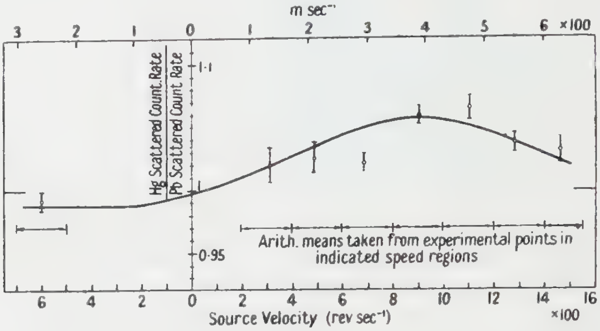

Figure 2. The least squares fit of the theoretical nuclear resonance curve to all experimental points.

Apart from the background, the main counting corrections are due to the presence of elastically scattered 159 kev and Compton scattered 209 kev gamma rays in the selected channel. Analysis of direct and scattered radiation spectra shows that of all recorded counts, about 53% are due to the elastic scattering. The absolute value of the resonant scattering cross section has been determined from the percentage effect by using the theoretical Rayleigh scattering cross section. This was considered a reliable procedure in view of good agreement between the theory of Rayleigh scattering (Franz 1935) and experiments performed with medium energy gamma rays (Storruste 1950). The absolute cross section, in conjunction with formula (1) and the angular distribution function $f(\theta) = 1 + 0{\cdot}25\,P_2(\cos\theta)$ for the sequence of spins $\frac{1}{2}-\frac{3}{2}-\frac{1}{2}$ gives a level width

$$\Gamma = (1{\cdot}76 \pm 0{\cdot}26) \times 10^{-6} \text{ ev}.$$

As pointed out by Jackson (1955), such a calculation does not give a correct level width in presence of internal conversion or branching to lower excited states. The scattering cross section for a gamma ray of energy E by a level with total width Γ and partial width $\Gamma_{\gamma 0}$ for gamma decay to the ground state is determined by the Breit–Wigner formula:

$$\sigma = \frac{g_a}{g_b}\frac{\lambda^2}{8\pi}\frac{\Gamma_{\gamma 0}{}^2}{(E - E_0)^2 + \Gamma^2/4}. \qquad \ldots\ldots(2)$$

If the gamma decay is the only de-excitation process from the level in consideration i.e., if $\Gamma_{\gamma 0}=\Gamma$, then

$$\sigma=\frac{g_a}{g_b}\frac{\lambda^2}{8\pi}\frac{\Gamma^2}{(E-E_0)^2+\Gamma^2/4}$$

from which expression formula (1) is obtained integrating over the Maxwellian energy distribution of the incident gamma rays.

If, however, there are competing de-excitation processes, the right-hand side of formula (1) must be multiplied by $(\Gamma_{\gamma 0}/\Gamma)^2$ in order to comply with (2); consequently, the correct total level width is obtained if the value for Γ as given above is multiplied by $(\Gamma/\Gamma_{\gamma 0})^2$.

If the partial level-width for gamma-transition to the ground state is wanted, the correction factor is $\Gamma/\Gamma_{\gamma 0}$. For resonance in the second excited state, $\Gamma/\Gamma_{\gamma 0}=1+\alpha_0+(1+\alpha_1)\Gamma_{\gamma 1}/\Gamma_{\gamma 0}$ where α_1, α_0 and $\Gamma_{\gamma 1}$, $\Gamma_{\gamma 0}$ are respectively the conversion coefficients and the probabilities for transitions to the first excited and ground state. The available conversion data are not very accurate. A factor $\Gamma/\Gamma_{\gamma 0}$ of about 2·2 seems to be in agreement with both the experimental data (Sherk and Hill 1951) and the theoretical values. The correct partial level width for the resonance transition is then

$$\Gamma_{\gamma 0}=(3{\cdot}87\pm 0{\cdot}58)\times 10^{-6}\text{ ev.}$$

The partial gamma mean life corresponding to this level width would be

$$T_\gamma=(1{\cdot}71\pm 0{\cdot}26)\times 10^{-10}\text{ sec.}$$

From a thermal broadening experiment, Metzger (1956) quotes a value $T_\gamma=(1{\cdot}2\pm 0{\cdot}4)\times 10^{-10}$ sec using $\Gamma/\Gamma_{\gamma 0}=2{\cdot}66$. The corresponding result with $\Gamma/\Gamma_{\gamma 0}=2{\cdot}2$ is $(1{\cdot}45\pm 0{\cdot}5)\times 10^{-10}$ sec. From the present experiment, with $\Gamma/\Gamma_{\gamma 0}=2{\cdot}2$, the mean life of the level including conversion is

$$T=(7{\cdot}8\pm 1{\cdot}2)\times 10^{-11}\text{ sec.}$$

This can be compared with the delayed coincidence mean life measurement by Graham *et al.* (1955), $T=(10\pm 6)\times 10^{-11}$ sec.

ACKNOWLEDGMENTS

The author wishes to express gratitude to Professor P. B. Moon for his interest and advice, and to the Institut Rudjer Bošković for a maintenance grant.

REFERENCES

DAVEY, W. G., and MOON, P. B., 1953, *Proc. Phys. Soc.* A, **66,** 956.
FRANZ, W., 1935, *Z. Phys.*, **98,** 314.
GRAHAM, R. L., *et al.*, 1955, *Bull. Amer. Phys. Soc.*, **30,** 20.
JACKSON, J. D., 1955, *Canad. J. Phys.*, **33,** 575.
METZGER, F. R., 1956, *J. Franklin Inst.*, **261,** 219.
MOON, P. B., 1951, *Proc. Phys. Soc.* A, **64,** 76.
MOON, P. B., and STORRUSTE A., 1953, *Proc. Phys. Soc.* A, **66,** 585.
SHERK, P. M., and HILL, R. D., 1951, *Phys. Rev.*, **83,** 1097.
STORRUSTE, A., 1950, *Proc. Phys. Soc.* A, **63,** 1197.

An Emulsion Spectrograph—A New Technique for the Determination of the Momenta of Fast Charged Particles

Part I: Design Considerations and Theory

By A. J. APOSTOLAKIS † and I. MACPHERSON ‡§

† Department of Physics, The Durham Colleges in the University of Durham
‡ The Physical Laboratories, University of Manchester

Communicated by G. D. Rochester; MS. received 22nd October 1956

Abstract. An account is given of a relatively simple device by which the signs and momenta of fast, charged particles can be measured accurately. The particles traverse normally a stack of thin layers of emulsion, separated by large gaps, in a magnetic field. Particle trajectories are reconstructed after the emulsions are developed. Consideration is given in Part I of the paper to the requirements that a stack must satisfy in order to give a maximum detectable momentum of 300 GEV/***c***. In Part II the construction of an actual stack will be described and an account will be given of some applications.

§ 1. Introduction

Several investigators have examined the possibility of determining the signs and momenta of particles traversing photographic emulsions by their deflection in a magnetic field. Two types of experiment have been performed. In the first, exemplified by the work of Dilworth *et al.* (1950) with glass backed emulsions, the particles were deflected within the emulsion itself by a magnetic field directed normal to the surface of the emulsion. The track left by the particle shows the result of the combined effect of magnetic deflection, scattering and distortion. The effect of scattering is usually so pronounced that exceptionally large fields over long tracks are needed in order to determine momenta accurately. However, with fields of the order of 30 000 gauss, the correct sign of a particle may be obtained with relatively short tracks (Dilworth *et al.* 1950). Steady fields of this order represent an upper limit for work in cosmic rays. Very high pulsed fields up to 600 000 gauss over a volume of 100 mm^3 have recently been produced by Furth and Waniek (1955); with such fields it may be possible to determine not only the signs but also the momenta of charged particles produced artificially by the great accelerators.

In the second, typified by the work of Franzinetti (1950) on the slow particles of the cosmic radiation, two emulsion films are mounted parallel to each other and separated by a narrow air gap. The emulsion–air sandwich is placed in a magnetic field directed normal to the emulsion surfaces. Particles pass through the sandwich at glancing angles to the surfaces of the emulsions, and their signs and momenta are determined from measurements of the directions of their tracks at the points of exit and entry to the free surfaces. This technique is suitable only for particles of relatively low momenta, e.g. for protons less than 1 GEV/***c***.

---

§ Now at Rolls-Royce Ltd., Derby.

It is clear that with the magnetic fields usually available ($\lesssim$15 000 gauss) neither method is suitable for the measurement of momenta above 5 GeV/**c**. Both methods are seriously affected by distortion and scattering. In the method described in this paper, distortion is eliminated and scattering is considerably reduced, and with magnetic fields of the order of 10 000 gauss momenta as high as 100 GeV/**c** can be measured. In the new technique the magnetic field is directed along and not normal to the surfaces of the emulsions and the particles to be examined traverse the emulsions almost normally. Scattering is reduced by using only thin layers of emulsion and glass. Such a set of emulsions will be termed a 'normal incidence stack'.

§ 2. THE THEORY OF THE NORMAL INCIDENCE STACK

We assume that the following requirements can be met. (i) The trajectories of steeply moving particles can be followed from plate to plate. (ii) There exists a common coordinate system which can be calibrated with an accuracy of the order of a micron. (iii) The points at which a particle penetrates a plate can be located in the coordinate system with an accuracy of the order of a micron.

A typical 'normal incidence stack' is shown in figure 1. Let the plate to plate separation be t cm and let there be $2m$ cells formed by $2m+1$ plates. The magnetic field H is directed along the Y-axis. The magnetic field produces a curvature, in the XZ plane, in the trajectory of a charged particle which penetrates the stack, and the momentum of the particle can be determined from the sagitta of this curvature. The projected sagitta U_H (assumed small) of a particle of momentum p incident normally to the plates located in the 1st, $(m+1)$th and $(2m+1)$th plates is given by the equation:

$$U_H = 1{\cdot}5(mt)^2 H/p. \qquad \text{......(1)}$$

U_H is in microns when t is in cm, H in units of 1000 gauss and p in GeV/**c**.

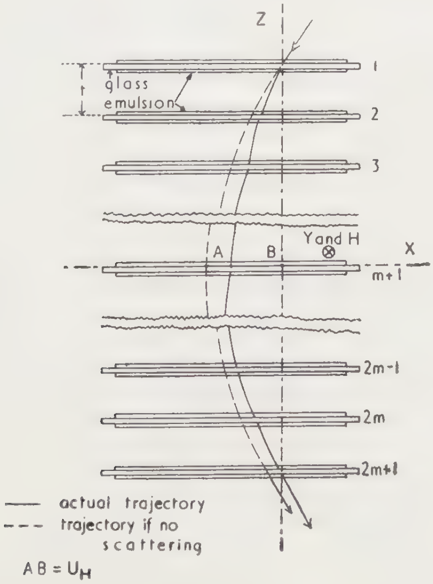

Figure 1. A diagrammatic representation of part of a 'normal incidence stack' to illustrate the symbols used in the text.

The sagitta U_H is a precise quantity only in the absence of scattering and errors of measurement, and in practice it can be regarded as a signal to be measured in the presence of noise, due to multiple scattering and reading errors. It is shown in the Appendix that the mean square sagitta, $\overline{U_S^2}$, due to multiple scattering of a particle located in the 1st, $(m+1)$th, and $(2m+1)$th plates is given by the equation:

$$4\overline{U_S^2} = t^2\overline{\theta^2}(\tfrac{2}{3}m^3 + \tfrac{1}{3}m) - t\overline{\theta x}2m + \overline{x^2}2m \qquad \ldots\ldots(2)$$

where $\overline{\theta^2}$ is the mean square of the projected deflections per cell; $\overline{\theta x}$ is the mean value of the product (deflection times lateral displacement) per cell; and $\overline{x^2}$ is the mean square lateral displacement per cell. The second and third terms are generally small compared with the first term.

In addition to the noise due to scattering, an observed 'magnetic' sagitta contains noise arising from uncertainties in the calibration of the coordinate system and errors of measurement. If the standard deviation of the combined random errors at each point of observation is σ, averaged over all plates, then the standard deviation of an estimate for the sagitta derived from three points is $(1{\cdot}5)^{1/2}\sigma$.

Combining multiple scattering and errors of measurement the root mean square noise becomes $(\overline{U_S^2} + 1{\cdot}5\sigma^2)^{1/2}$. Setting $\overline{U_S^2} = \overline{U_0^2}/\beta^2$ the signal to noise ratio is:

$$R = \frac{U_H\beta}{(\overline{U_0^2} + 1{\cdot}5\beta^2\sigma^2)^{1/2}}. \qquad \ldots\ldots(3)$$

For those particles for which $\beta \simeq 1$ and for $\overline{U_0^2}$ large compared with $1{\cdot}5\sigma^2$, equation (3) may be written as:

$$R_0 = U_H/(\overline{U_0^2})^{1/2}$$

where R_0 is a constant independent of momentum. It is desirable to make R_0 as great as possible. We note from equation (1) that U_H varies as $(mt)^2H$ for a given momentum and from equation (2) $(\overline{U_S^2})^{1/2} \propto (t^2\overline{\theta^2}m^3)^{1/2}$ for a given momentum (and a fixed value of β). Now for a given type of plate, e.g. thickness of emulsion and glass, $\overline{\theta^2}$ is a constant for a given momentum and velocity. Therefore $(\overline{U_0^2})^{1/2} \propto (m^3t^2)^{1/2}$ and R_0 varies as $m^{1/2}tH$. Thus for the greatest value of the ratio of the signal to noise the magnetic field should be as large as possible and for the same total length of the stack a few long cells are better than many short cells. R_0 may also be increased by reducing the amount of solid material in each cell, thereby reducing $\overline{\theta^2}$. In figure 2, R_0 is shown as a function of field strength in a stack composed of two cells ($m=1$). Two plate thicknesses are considered; one produces scattering equivalent to layers of G5 emulsion 400 μ in thickness, the other to 800 μ G5 emulsion. Four cell lengths, 0·5 cm, 1·0 cm, 1·5 cm and 2·0 cm are shown. The variation of R_0 with the number of cells in a stack is shown in figure 3. The signal to noise ratio for two cells (R_{02}) has been taken as unity.

The variation of R with momentum will now be considered. Consider first fast particles ($\beta \simeq 1$). As the momentum increases the magnetic sagitta and the sagitta due to scattering decrease at the same rate and eventually $1{\cdot}5\sigma^2$ becomes comparable with $\overline{U_0^2}$: R thus falls below R_0. A maximum detectable momentum may be defined by setting R_{MDM} equal to unity. Similarly, when $\beta \ll 1$, R again falls below R_0. A lowest detectable momentum may then be defined in a similar manner, i.e. R_{LDM} equal to unity ($\beta < 1$). The lowest momentum measured in a practical stack need not necessarily correspond to the lowest detectable momentum as defined above. The lower limit in certain circumstances is fixed by the ease with which low momentum particles can be traced from one plate to the next. The time and computation required to trace particles with momentum below some low momentum cut-off are so great that this cut-off is the effective lowest detectable momentum.

Figure 4 shows the variation of R with momentum for a stack of twelve cells, each 1·5 cm long, containing material equivalent to a 400 μ thick G5 emulsion.

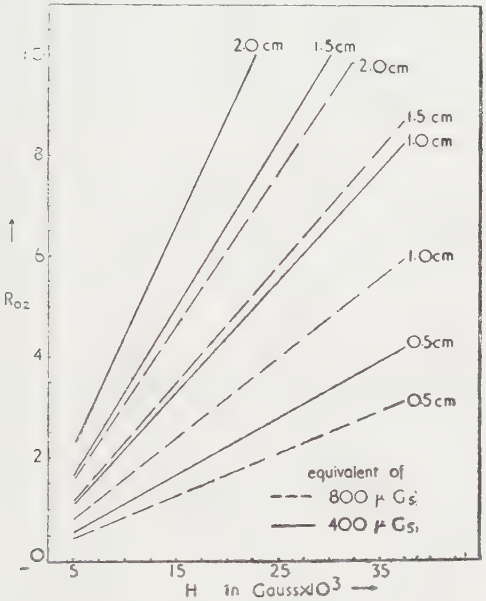

Figure 2. The signal to noise ratio R_{02} as a function of field strength H for two cells only. Two plate thicknesses are considered with equivalent scattering of 400 μ and 800 μ G5 emulsion. Four cell lengths, 0·5 cm, 1·0 cm, 1·5 cm, and 2·0 cm, are shown.

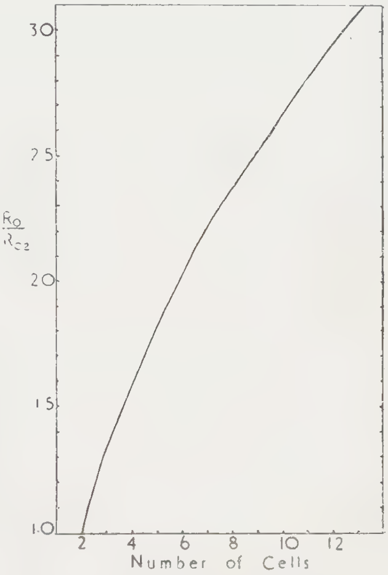

Figure 3. The variation of the ratio R_0/R_{02} with the number of cells.

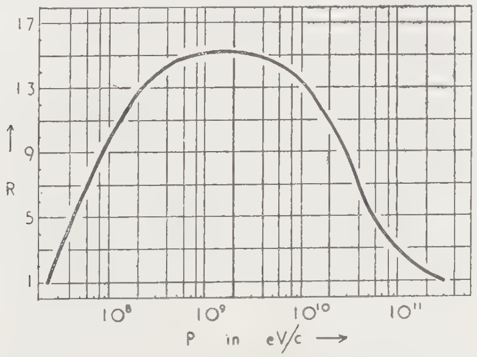

Figure 4. The variation of the signal to noise ratio R with momentum p for a typical stack.

The value of H is 15 000 gauss and σ is 5 μ. The particles passing through the stack are assumed to be μ-mesons. It is emphasized that figures 2, 3 and 4 refer to particles measured in only the first, centre and final plates. Such particles would be located in the intermediate plates in order to trace their trajectories through the stack.

§ 3. GENERAL REQUIREMENTS OF A NORMAL INCIDENCE STACK

In order to trace a particle through the stack it is necessary to locate its position with the greatest possible precision in the frame of reference of each plate and to know the relation of each frame of reference to its neighbours. It will be shown in Part II how this has been achieved with an actual stack but it is necessary to mention here two important general points. In the first place a stack must be designed so that it can readily be taken to pieces and built up again while still maintaining the exact relationship between the frames of reference. The reasons for this are as follows: (i) to reduce the number of no-field tracks, that is, tracks left by fast particles traversing the stack when it is not in the magnetic field: it should, therefore, be possible to build up the stack or to take it down while still in the magnetic field; (ii) to enable the individual plates to be coated, processed and examined separately. The desired rigidity and reproducibility have been achieved by kinematically located plates with gravity constraint secured by spring loading.

Again it is most important that there should be at least one point where the particle passes through the plate which is not displaced by processing. This requirement prevents the use of unsupported emulsion. It has been met by constructing each plate from a thin sheet of glass coated with a thin layer of emulsion on each side (as in figure 1). With this arrangement the glass remains quite flat and the points at which the particle enters and leaves the glass remain fixed relative to the glass during processing. Since two fixed points are known for the particle at each plate its direction through the plate may be determined accurately and it may therefore be followed easily from plate to plate. A further practical advantage of the arrangement is that if any single plate is spoiled by bad development the rest of the stack can be used to determine the trajectory with little loss of accuracy.

§ 4. THE DETERMINATION OF MOMENTUM

The problem of estimating the momentum of a particle which is subject to magnetic deflection and multiple scattering has been given much detailed consideration (see e.g. Scott 1949, Moyal 1950). The treatment can be based on the coordinate method or the tangent method. It appears that the best estimate of momentum is obtained when perfect measurements of the tangent of the ends of the trajectory are available. The uncertainty due to multiple scattering has then its minimum value. However, this method cannot be used with any precision here. In the normal incidence stack the position of a particle is measured at $N+1 \leqslant 2m+1$ points along its trajectory. Therefore, the coordinate method is directly applicable to the calculation of momentum. Two cases may be distinguished, namely, when the uncertainties produced by multiple scattering are greater or less than the errors of measurement. When the former condition holds the error produced by scattering may be minimized (Scott 1949) if the *Kth* curvature obtained from the coordinates $K-1$, K, $K+1$ is weighted by a quantity b_K which is given by

$$b_K = \frac{3[(-1)^{N-1}\Delta_{N-1} - (-1)^{N-K-1}\Delta_{N-K-1} - (-1)^{K-1}\Delta_{K-1}]}{(3N+2)(-1)^{N-1}\Delta_{N-1} + (-1)^N\Delta_N - 1}$$

$$\textstyle\sum_K b_K - 1 \qquad \text{and} \qquad \Delta_i = 4\Delta_{i-1} - \Delta_{i-2}$$

$$\Delta_1 = 4 \qquad \Delta_2 = 15.$$

In deriving this formula it is assumed that the $(N+1)$ points are equally spaced along the trajectory and that the $N-1$ curvatures are obtained from overlapping pairs of cells.

While this is the best method, the simplest is to use the coordinates of the ends and the mid-point of the trajectory. This method, which may be termed the 'three point method', wastes some information; but the amount rejected is not necessarily large compared with that utilized. This is clearly shown from equations developed by Scott (1949) who shows that the curvature error produced by scattering and determined by the three-point method, is simply related to its equivalent determined by the $(N+1)$-point method. Adapting Scott's results to the normal incidence stack, the ratio of the mean square sagittas measured by the three-point and the $(N+1)$-point methods is

$$\frac{\overline{U_{s\,(3)}^{2}}}{\overline{U_{s\,(N+1)}^{2}}} \simeq \frac{4}{3}\left(1 - \frac{0{\cdot}577}{N}\right).$$

When $N \to \infty$ the error is identical with the one for perfect measurements on the tangents at the ends of the trajectory. In a practical stack, in order to have a big signal to noise ratio the number of plates is small, consequently the number of points where one can measure the coordinates of a trajectory is limited. Thus the effort involved in applying the $(N+1)$-point formula does not result in any worthwhile increase in accuracy. For example, using the sagitta method in a 10-cell stack with $t = 1{\cdot}5$ cm and $H = 15\ 000$ gauss, the noise due to scattering only is approximately 7% of the signal. If the $N+1$ formula is used, the noise level becomes approximately $0{\cdot}796^{1/2} \times 7\% = 6{\cdot}3\%$ of the signal. The second condition, that is, errors due to scattering less than errors of measurement, applies particularly to particles of great energies near the maximum detectable momentum. The observations under these conditions are independent and the least squares method may therefore be used to fit a parabola† to the observations.

Thompson (1955) has applied such a method to cloud chamber tracks and the same analysis can be taken over to the normal incidence stack.

Summarizing, it can be said that the three-point (sagitta) method is adequate for momenta in the design range. It can be applied very quickly and by unskilled persons. The least squares method is suitable for high momenta near the maximum detectable momentum when errors of measurement predominate.

REFERENCES

Dilworth, C. C., Goldsack, S. J., Goldschmidt-Clermont, Y., and Levy, F., 1950, *Phil. Mag.*, **41**, 1032.

Franzinetti, C., 1950, *Phil. Mag.*, **41**, 86.

Furth, H. P., and Waniek, R. N., 1955, *Nuovo Cim.*, **2**, 1350.

Moyal, J. E., 1950, *Phil. Mag.*, **41**, 1058.

Scott, W. T., 1949, *Phys. Rev.*, **76**, 212.

Thompson, R. W., 1955, *Nuovo Cim.*, **1**, 735.

† A segment of a circle reduces to a parabola in the small-angle approximation.

APPENDIX

DERIVATION OF FORMULA

$$4\overline{U_S^2} = t^2\overline{\theta^2}\left(\tfrac{2}{3}m^3 + \tfrac{1}{3}m\right) - t\overline{\theta x}\,2m + \overline{x^2}\,2m$$

Consider a system of $2m$ cells each of length t. Scattering takes place in each cell giving rise to an angular deflection and a lateral displacement. The problem is to find the mean square sagitta for a particle observed at the beginning of the 1st cell, the interface of the mth and the $(m+1)$th cell and at the end of the $2m$th cell. The system is shown in figure 5. Consider a particle incident at an angle ϕ_0 to the Z-axis. After penetrating the 1st cell it will move at an angle $\phi_0 + \theta_1$ and will be displaced by a distance x_1 from the incident trajectory. It will suffer a further deflection θ_2 in the second cell and will be displaced by a distance x_2 from the extension of its incident trajectory on the second cell. Further deflections $\theta_3, \theta_4, \ldots \theta_i, \ldots \theta_{2m}$ will occur together with displacements $x_3, x_4, \ldots x_i, \ldots x_{2m}$.

Expressing the X coordinate of the particle in terms of the initial angle ϕ_0 and the small subsequent displacements we have:

$$X_1 = \phi_0 t + x_1$$

$$X_2 = \phi_0 2t + t\theta_1 + x_1 + x_2$$

$$X_3 = \phi_0 3t + 2t\theta_1 + t\theta_2 + x_1 + x_2 + x_3$$

. . . .

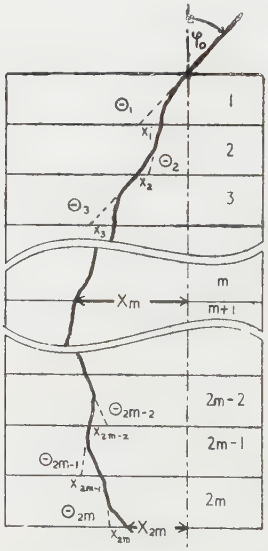

Figure 5. Diagrammatic representation of the track of a particle which undergoes scattering in different layers of material.

These equations have been derived assuming that the multiple scattering in each cell is equivalent to a single scatter of θ_i at a distance x_i/θ_i before the particle leaves the ith cell.

In general, for m cells

$$X_m = \phi_0 nt + t\sum_{i=1}^{m}\theta_i(n-i) + \sum_{i=1}^{m}x_i \quad \text{where} \quad i = 1, 2, 3, \ldots m. \qquad \ldots(1)$$

The sagitta U of a particle penetrating the stack is defined by the equation $2U = |X_{2m} - 2X_m|$. Using equation (1)

$$2U_S = t\sum_{i=1}^{2m} \theta_i(2m-i) - 2t\sum_{i=1}^{m} \theta_i(m-i) + \sum_{i=1}^{2m} x_i - 2\sum_{i=1}^{m} x_i.$$

Splitting the summation range 1 to $2m$ into 1 to m together with $m+1$ to $2m$ we obtain

$$2U_S = t\sum_{i=1}^{m} (i\theta_i) + t\sum_{i=m+1}^{2m} (2m-i)\theta_i + \sum_{i=m+1}^{2m} x_i - \sum_{i=1}^{m} x_i. \quad \ldots\ldots(2)$$

With this equation we may now obtain the mean square sagitta. The angles θ_i are all independent of each other. Consequently, the averages $\overline{\theta_i}^2$ can all be calculated as single sums because $\overline{\theta_i\theta_j} = 0$ if $i \neq j$, thus terms like

$$\sum_{i=1}^{m} \theta_i \cdot \sum_{i=m+1}^{2m} \theta_i$$

will disappear. Assuming that all cells are identical the complexity of the equation for $4\overline{U_S}^2$ is somewhat reduced by taking averages, giving

$$4\overline{U_S^2} = t^2\overline{\theta^2}\sum_{i=1}^{m} i^2 - t^2\overline{\theta^2}\sum_{i=m+1}^{2m} (4m^2 - 4mi + i^2) + \overline{x^2}\sum_{i=1}^{2m} 1 - 2t\overline{\theta x}\sum_{i=1}^{m} i + 2t\overline{\theta x}\sum_{i=m+1}^{2m} (2m-i).$$

Carrying out the summations we obtain the desired result

$$4\overline{U_S^2} = t^2\overline{\theta^2}(\tfrac{2}{3}m^3 + \tfrac{1}{3}m) - t\overline{\theta x}2m + \overline{x^2}2m.$$

For cells which are not homogeneous but are stratified it can be shown from first principles that

$$\overline{\theta^2} = (p\beta)^{-2}\sum_{i=1}^{n} K_i^2 t_i$$

$$\overline{\theta x} = \tfrac{1}{2}(p\beta)^{-2}\sum_{i=1}^{n} K_i^2\left[\left(t - \sum_{j=1}^{i-1} t_j\right)^2 - \left(t - \sum_{j=1}^{i} t_j\right)^2\right]$$

and

$$\overline{x^2} = \tfrac{1}{3}(p\beta)^{-2}\sum_{i=1}^{n} K_i^2\left[\left(t - \sum_{j=1}^{i-1} t_j\right)^3 - \left(t - \sum_{j=1}^{i} t_j\right)^3\right]$$

where $t_1 + t_2 + t_3 + \ldots + t_n = t$ are the thicknesses of the respective materials and $K_1, K_2, \ldots K_n$ are the scattering constants for layers $1, 2, 3 \ldots n$.

An Emulsion Spectrograph—A New Technique for the Determination of the Momenta of Fast Charged Particles

II: Construction and Applications of a Normal Incidence Stack

By A. J. APOSTOLAKIS† AND I. MACPHERSON‡§

† Department of Physics, The Durham Colleges in the University of Durham
‡ The Physical Laboratories, University of Manchester

Communicated by G. D. Rochester; MS. received 22nd October 1956

Abstract. An account is given of a relatively simple device by which the signs and momenta of fast, charged particles can be measured accurately. The particles traverse normally a stack of thin layers of emulsion, separated by large gaps, in a magnetic field. Particle trajectories are reconstructed after the emulsions are developed. Consideration was given in Part I of the paper to the requirements that a stack must satisfy in order to give a maximum detectable momentum of 300 GeV/***c***. In Part II the construction of an actual stack is described and an account is given of some applications.

---

§ 1. Introduction

It was shown in Part I (Apostolakis and Macpherson 1957, to be referred to as I) that a stack consisting of layers of emulsion separated by gaps can, in principle, be used to measure the signs and momenta of charged particles over a wide range of energies. In this paper the construction and performance of one form of a stack is described. Special emphasis is placed on the form of the mechanical system used for mounting the plates, since the maximum detectable momentum which can be realized depends entirely on the degree of perfection of this system, especially on its reliability and reproducibility.

The performance of such a stack could best be assessed by means of a mono-energetic beam of fast particles. In practice such particles are not readily available and, instead, the fast particles present in the cosmic radiation at sea level have been used. These particles have the disadvantage that they are not mono-energetic. However, the majority are non-interacting μ-mesons and some have very great energies, well outside the range of machine energies. Both these features make the radiation suitable for testing the stack. In this paper an account is given of an exposure made at Manchester using one of the magnets of the double-magnet spectrograph (Hyams *et al.* 1950).

§ 2. Construction and Calibration

A photograph of the apparatus is shown in figure 1 (Plate). It consists of a stack of fourteen brass frames supported on a rectangular brass container C. Each frame (one of which is shown in detail in figure 2) is 5 cm wide by 10 cm long and has a central window 4 cm by 8 cm. A shallow step is recessed round the top edge of the window and a plate, which consists of a thin sheet of glass with an

§ Now at Rolls–Royce Ltd., Derby.

emulsion layer on each side, is cemented into this step. The emulsions are $100\,\mu$ thick, and the glass is about $850\,\mu$ thick. The plate to plate separation (cell length of I) is 1·5 cm, except between frames 13 and 14 where it is 2 cm. The frame to frame location, perhaps the most important feature of the apparatus, is kinematic. A hole, slot and plane arrangement has been used. The hole and slot are cut in pieces of glass cemented to the top of the frame; the plane is formed by the polished surface of a similar piece. The complementary members of the location are steel balls, 2 mm in diameter, soldered to the bottom of the frame. Steel and glass have been used in order to minimize the effects of plastic deformation. The configuration can be seen in figure 2. The weight of the frames provides the constraint for the location, the frames resting one on top of another. This is not the best method, because errors in location are cumulative. However, the results obtained have proved the arrangement to be adequate and have facilitated the construction of plates parallel to within an angle of $\tan^{-1} 0{\cdot}001$.

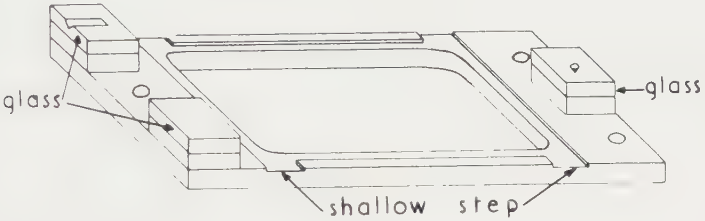

Figure 2. Isometric drawing of a frame showing the recess in which the plates are mounted and the hole, slot and plane of the plate to plate location.

The whole stack is secured by a top plate (T in figure 1), connected to C by the rods a, b, and c. The lowest frame, No. 14, is rigidly connected to the base container C, which has been designed to hold a block of stripped emulsions with their planes at right angles to the plates of the stack. The block in the present exposure consisted of twenty-nine G5 emulsion films each $12\,\text{cm} \times 8\,\text{cm} \times 600\,\mu$. The top edge of the block was machined flat, a uniform gap of about $200\,\mu$ being left between the machined surface and the fourteenth plate. This relation was maintained by two brass pegs (P_1, P_2 in figure 1), fitting closely into Perspex sleeves passing through the block.

To reconstruct the trajectories of particles recorded in the plates, a common coordinate 'lattice' is essential. Moreover, as shown in I, to attain a maximum detectable momentum of 300 GeV/c this coordinate system must be established to an accuracy of the order of one micron. The system which has been adopted for the plates is a rectilinear grid of 1 cm spacing, engraved on the glass before the emulsions were attached. The grid lines were produced in the following manner. Frame No. 14 of the stack was fixed on to the carriage of a milling machine. An engraving diamond was mounted in a holder which could rotate only in a vertical plane parallel to one direction of movement, X, of the carriage. A line was made by moving the frame relative to the diamond. The Y-movement of the carriage was locked, and a corresponding line was marked on each plate by building up the stack. The cutting angle of the diamond was kept constant by lowering the carriage each time a frame was added. With care, it was possible to make straight, parallel lines with lateral displacements, plate to plate, as small as $10\,\mu$.

By having parallel lines, the work involved in tracing trajectories is eased, whereas the small lateral displacements make the calibration by a special vertical microscope possible (Apostolakis and Macpherson, in the press).

In terms of Cartesian coordinates, the rectilinear grids formed (X, Y) systems at regularly spaced intervals along the Z axis. The grid lines were 4–5 μ wide and were visible under 10 × objectives and 45 × oil-immersion objectives, even when covered by the processed emulsion. A setting accuracy of about one micron has been achieved, as the lines had a fine structure formed by the engraving diamond. The (X, Y) system of each plate was satisfactorily calibrated using a Cooke, Troughton and Simms M 40 000 microscope. The common Z axis has been established using a microscope with a vertical movement of 11·5 cm. The total height of the assembled frames is 20 cm. The calibration has therefore been carried out in two parts, the measurements overlapping at plates 7 and 8. The calibration procedure involved measuring the lateral displacement, plate to plate, of the same (X, Y) point (say $x_i = 0$, $y_i = 0$, $i = 1, 2, 3, \ldots . 14$) in the grid systems. Two sets of measurements were required for one calibration. In the first set the microscope was focused on the chosen point in each plate as the stack was assembled in the correct order. The coordinates of this point were recorded for each plate in terms of an eyepiece scale. The second set of measurements was made in the same manner, using the same (X, Y) point, but with the stack rotated through 180° in a horizontal plane. By forming the differences of the observed relative displacements, the motion of the microscope has been eliminated. In this way, the positions of the chosen (X, Y) points have been determined relative to a linear axis—the common axis of rotation. The errors in establishing the axis depend on the reproducibility of the microscope movement, the errors of observation and the errors in the frame to frame location. In all, the calibration procedure was repeated twelve times for three coordinate points. In this way the relative rotation and translation of each grid system have been measured.

In table 1 some quantitative details of the calibration are given. Specifically, the coordinates of the point $x_i = 0$, $y_i = 0$ with respect to the common axis passing through $x_{14} = 0$, $y_{14} = 0$ of the fourteenth plate are listed, as are the plate to plate separations Z. The latter parameter has been measured using 'Matrix' slip gauges and a conventional dial gauge graduated in thousandths of an inch. The errors quoted for X and Y are the standard deviation of one set of observations: because the stack was rebuilt between each set of observations these errors are those encountered when the stack is assembled for the exposure. The estimated random error in Z is about 10 μ. The coordinate system was extended into the block of stripped emulsions by means of x-rays. When the fourteenth frame had been

Table 1.

Plate No.	$X (\mu)$	$Y (\mu)$	$Z (\mu)$
1	58·9 ± 7·6	55·0 ± 9·6	200 563
2	48·3 ± 6·9	57·5 ± 8·7	185 524
3	49·0 ± 5·6	52·1 ± 7·1	170 588
4	49·8 ± 4·6	58·4 ± 4·8	155 541
5	46·3 ± 3·7	51·3 ± 4·2	140 512
6	45·5 ± 3·3	53·1 ± 2·8	125 422
7	45·1 ± 3·3	47·4 ± 2·4	110 388
8	42·9 ± 2·8	42·9 ± 2·2	95 537
9	41·5 ± 2·2	32·1 ± 2·1	80 421
10	34·7 ± 1·6	24·0 ± 1·8	65 298
11	31·8 ± 1·3	17·5 ± 1·9	50 269
12	26·0 ± 0·9	6·4 ± 2·2	35 313
13	20·2 ± 0·9	2·0 ± 1·2	20 175
14	0	0	0

finally screwed to the top of the container C, in which was the emulsion block B, x-rays were used to mark lines across the plate. The x-rays penetrated about 500 μ into the top edge of the block. Six lines were used: they formed X-shaped patterns across the top edge of the block and provided the required link between the grid system of the plates and the emulsions in the block. Experience has shown that trajectories can be extrapolated from the plates to the block to intersect within 100 μ of the true trajectory.

§ 3. Field Exposure and Processing

An important factor controlling the duration of an exposure is the available flux of particles. For the present experiment with cosmic-ray particles at sea-level, sufficient particles to test the technique were recorded in a week's exposure, but not so many as to produce ambiguity in the reconstruction of trajectories. Unprotected thin emulsions are liable to fading, especially when the exposure takes place at temperatures above 20°c. To avoid fading it was found necessary to control the condition of the atmosphere round the stack. The whole apparatus was placed in a container filled with commerical argon at atmospheric pressure and relative humidity 60% at 16°c. Between the pole faces of the magnet and the container of the stack a cooling system was introduced which maintained the temperature of the stack at about 16°c. Cooling was required because of the high ambient temperature at the time of the exposure.

Only particles which pass through the whole stack when it is in the magnetic field are useful. To reduce the background of unwanted tracks fresh emulsions were used: less than 24 hours elapsed between the manufacture of the emulsions and the start of the exposure. For the same reason the stack was covered throughout the exposure by 10 cm of lead. During the final assembly of the stack the top four plates were placed in position with the rest of the stack already in the magnetic field. Similarly, at the end of the exposure the same four plates were separated from the stack with the magnetic field at full strength. In the analysis of the particles recorded in the stack a particle has been accepted as useful only if its trajectory penetrated the top four plates. The duration of the exposure was 160·5 hours and the magnet current was observed both regularly and randomly over this period. The observed variation in the current produced an uncertainty of less than 1% in the magnetic field. The mean field strength was 15 460 ± 200 gauss and it was uniform to within 2% over the volume occupied by the plates.

After the exposure the plates were developed by the usual 'temperature-cycle' method. The plates were left in the frames for ease of handling. The metallic surfaces were covered with celluloid varnish to prevent chemical reactions between the metal and the processing solutions. In the hot stage, where the temperature of the plates should rise as quickly as possible from 5°c to 23°c, special care was taken to allow for the large thermal capacity of the frames.

4. Examination of the Stack

There are three stages in the examination of a normal incidence stack. The first is the selection of pairs of tracks in the two emulsions of one plate, the second is the following of the trajectories across the first gap, and the third is the tracing of the trajectories through the whole stack. It is evident that for each of these operations it is important that at least one point of the track in each plate is not displaced by processing. The only part of the track which satisfies this condition is at the emulsion–glass interface (F-point, see § 5.2).

In the first stage the best processed pair of plates is selected and the top emulsion of one of them scanned for steep tracks. The partners of these tracks are then identified in the emulsion on the other side of the plate. A long working-distance 45 × oil-immersion objective is capable of focusing the lower emulsion through the supporting glass and the upper emulsion. Tracks are accepted as partners if (*a*) the parts of the tracks near the emulsion surfaces are parallel (Apostolakis and Major 1957) and (*b*) the projected separation of their F-points is about eight times the projected length of each track. In this way the selection of true partners is independent of the effect of distortion. From the coordinates of the F-points in the top and bottom emulsion the direction of the trajectory in the scanned plate is estimated. The intersection of the trajectory with the following plate is predicted from this direction. However, several effects produce an uncertainty in the predicted position. These are (i) error in the estimate of the direction, (ii) the magnetic deflection in the gap between the plates, and (iii) scattering in the first plate. The first effect is mainly due to the uncertainty of each F-point because the fractional error in the thickness of the glass is relatively small. The magnitudes of the second and third effects are not known *a priori* since measurements in one plate give no indication of either the sign or momentum of the particle.† Because of these uncertainties it is necessary to search for the expected tracks in a rectangular area of the following plate. The dimensions of this rectangle are inversely proportional to the momentum of the particle, the longer side being in the direction of the magnetic deflection. An effective lowest detectable momentum of approximately 350 MeV/**c** has been imposed on the experiment by limiting the length of this side to 600 μ. The width of the rectangle was fixed at 200 μ: this length adequately allowed for multiple scattering and errors of measurement. Tracks in the second plate are accepted as a correlated pair if they can satisfy the conditions (*a*) and (*b*) used in the first plate. In addition, any difference in the projected separation of the F-points of the two pairs must be proportional to the displacement of the second pair from its expected position. The final stage, i.e. the exploration of the complete trajectory, is the simplest but the most laborious. The estimated direction and magnetic deflection from the previous cell are used to predict the location of the tracks in the next plate. When these tracks have been found the process is repeated until the trajectory has been traced through all the plates.

§ 5. ANALYSIS OF THE RECORDED PARTICLES

5.1. *Confirmation of the Calibration*

A total of 106 particles have been traced through the fourteen plates of the stack, their derived momenta varying from 0·3 to 100 GeV/**c**. In what follows these particles are assumed to be μ-mesons. The foundation for the calculation of the momenta is the calibration made with the vertical microscope. Considering the processes which occur between the calibration and the examination of the plates, confirmation of the calibration figures is desirable. Two post-calibration defects that can occur in the coordinate system may be distinguished. One is a *dislocation* of some frames during the final assembly of the stack. The other is a *displacement*, caused by a plate slipping in its frame. Both of these defects can be detected using high-energy trajectories as described in the Appendix. Application of the method has not revealed any dislocations, but there is evidence for small displacements. The trajectories of six particles with momenta greater than 20 GeV/**c** have been used. It has been found that plates 6 and 10 were displaced, the former by $8 \pm 2\,\mu$ in the magnetic direction, and the latter by $5 \pm 2\,\mu$ at right angles to this direction. The simplest way of allowing for these defects is to modify the calibration figures of table 1. Doing this is equivalent to classing the displacement errors as systematic errors of the calibration. One other explanation of the observed defects can be suggested. It is possible that the cement holding the plates in the frames was distorted when the emulsions were mounted on the plates.

---

† The grain density of the tracks does not indicate the momentum of the particles because the tracks are steep. Even particles at minimum ionization give rise to black tracks.

5.2. *Determination of the Error of the Momentum Measurements*

The error in the momentum measurement arises from the errors of measurement, errors of the calibration and scattering. The first two are independent of momentum and an estimate for their combined effect, including any slip of the emulsion at the emulsion–glass interface of a plate, has been obtained as follows. The r.m.s. value ϵ of the second differences in the Y-direction of twelve high-momentum particles has been calculated. Because the momenta were high, greater than 10 GeV/**c**, ϵ is an estimate for the combined errors of measurement and calibration for three adjacent plates. The corresponding combination for one plate, $\epsilon/\sqrt{6}$, has been found to be $\pm 1{\cdot}8\,\mu$. This figure is the overall accuracy with which a track can be located in one plate. To combine observations from three plates which are not adjacent, the calibration errors listed in table 1 have to be taken into account. For example, the combined error for observations in plates Nos. 1, 7 and 13 is $\pm 5{\cdot}5\,\mu$. This quantity is the $(1{\cdot}5)^{1/2}\sigma$ of I and corresponds to a maximum detectable momentum of 340 GeV/**c**. In I it is also shown that, for the purposes of measurement, two extreme types of particles can be distinguished. For one type scattering errors predominate, whereas for the other only the errors of measurement and calibration are significant. It is pointed out that the momentum of the second type should be calculated by the least-squares method; then the error of the momentum can be evaluated, in principle, from the known values of the errors of measurement and calibration. However, if the simpler three-point method is used, an estimate $\epsilon(p)$ for the error of the momentum p is given by the relation

$$\epsilon(p)/p = p/\text{M.D.M.}\ [p > (\text{M.D.M.})/10]$$

in which the maximum detectable momentum (M.D.M.) of the present experiment is 340 GeV/**c**.

When the scattering predominates and $\beta \simeq 1$, the fractional error of the momentum is constant. In this case the fractional error for the three-point method can be expressed as

$$\epsilon(p)/(p) = 1/R_0,$$

where R_0 is defined as in I. Sixty-seven of the 106 particles traced through the stack had momenta in the region to which this relation applied and, using them, a verification of the scattering formulae presented in I has been attempted. The momenta of the 67 particles covered a wide range and straightforward comparison of a theoretical scattering parameter with its observed value was not possible. An indirect comparison has been made using the ratio

$$\frac{\text{Observed sagitta due to scattering}}{\text{Observed magnetic sagitta}} = \frac{S_y}{S_x},$$

which is independent of momentum for the selected particles. It is easily shown that

$$\text{Variance } (S_y/S_x) = 1/R_0^2.$$

The ratio (S_y/S_x) for 2, 4, 6, 8, 10 and 12 cells has been determined for each of the 67 tracks and the r.m.s. value of the six distributions (assumed normal) calculated. A χ^2-test has shown a good fit between the experimental values and those calculated using the formulae of I. Figure 3 shows the experimental values and the theoretical curve based on the following scattering constants (r.m.s. values)

$$\text{Emulsion}: \quad K_e = 39{\cdot}4 \text{ deg MeV}/\mathbf{c}\,(100\,\mu)^{-1/2}$$

$$= 6{\cdot}9 \times 10^{-4} \text{ rad GeV}/\mathbf{c}\,(100\,\mu)^{-1/2}$$

$$\text{Glass}: \quad K_g = 3{\cdot}6 \times 10^{-4} \text{ rad GeV}/\mathbf{c}\,(100\,\mu)^{-1/2}.$$

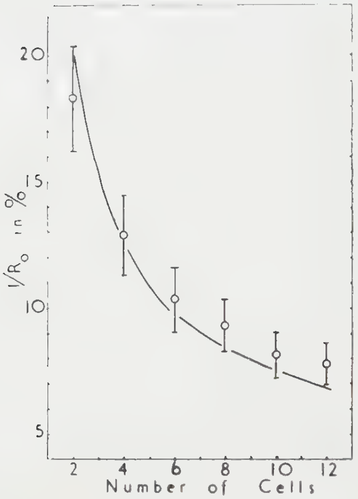

Figure 3. Comparison of the experimental points with the theoretical curve for the quantity $1/R_0$, where R_0 is the signal-to-noise ratio.

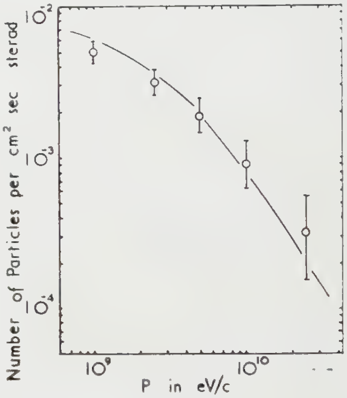

Figure 4. Comparison of the experimental points for the integral momentum spectrum with the established spectrum of unassociated singly charged particles at sea level (Owen and Wilson 1955). The errors quoted are the Poisson fiducial limits (Regener 1951).

5.3. *The Observed Momentum Spectrum*

The integral momentum spectrum of the measured particles is compared in figure 4 with the established spectrum of unassociated singly charged particles at sea level (Owen and Wilson 1955). The experimental points are absolute quantities derived from the duration of the exposure, the solid angle of acceptance (±7° in two directions at right angles), the area scanned and the number of tracks found. A correction has been made for the momentum loss in the 10 cm of lead which covered the aperture of the stack during the exposure. No other correction has been made. The agreement between the accepted and observed spectrum is satisfactory considering the low statistics of the present experiment. It furnishes strong evidence that the normal incidence technique can, in fact, be used to measure momentum.

It will be noticed that the lowest momenta of the experimental points is 1 GeV/**c**, not 350 MeV/**c** which is the effective lowest detectable momentum discussed in § 4. There are two reasons for this. One is that the stack was well immersed in the magnetic field and under 10 cm of lead. Consequently the solid angle of acceptance for the lowest momentum particles was distorted. The second reason is that the cut-off at 350 MeV/**c** is not sharp. This lowest detectable momentum was based on observations from two plates only; for these observations, the signal-to-noise ratio is only about 2:1 and therefore some particles with momenta greater than 350 MeV/**c** are incorrectly rejected, with the converse applying to lower momenta. This uncertainty is illustrated by the fact that a particle with a momentum as low as 250 MeV/**c** has been traced through the stack. For a linear region of the spectrum, and good statistics, the difference between the number (wrongly) gained to the number (wrongly) rejected can be calculated. Neither of these conditions apply to the present results for this part of the spectrum.

5.4. *The Observed Positive–Negative Ratio*

Of the 106 particles traced through the stack, 95 had momenta above 1 GeV/**c** and of these 45 were positive and 40 negative. The corresponding positive–negative ratio is $1{\cdot}12 \pm 0{\cdot}22$ and agrees within the experimental errors with the average value $1{\cdot}25 \pm 0{\cdot}02$ given by Owen and Wilson (1951), for particles with momenta greater than 1 GeV/**c**.

5.5. *Comparison of the Momentum Measured by Magnetic Deflection in the Stack and by Multiple Scattering in the Block*

With the help of the block of stripped emulsions it is possible to compare the momenta measured by two different techniques. In the stack the momentum p is measured by the sagitta method. In the block the value of the $p\beta$ of the same tracks can be determined by measuring the multiple scattering inside the emulsions. Ten tracks with momentum from 0·6–2·5 GeV/**c** have been selected as suitable for measurement. Each of these tracks is sufficiently long in the 600 μ thick emulsions of the block to enable an accurate determination of $p\beta$ to be made. For the measurements of $p\beta$, a Cooke M 40 000 microscope has been used with stage noise 0·1 μ for 500 μ cell length. Each track was measured on a cell length such as to give a signal-to-noise ratio of 6:1. The noise taken was the stage noise for the correct cell plus the grain and reading errors. To avoid surface defects, the multiple scattering was measured only in the middle part of the emulsions. The top and bottom 30 μ of the emulsions and a 1 cm margin round the edge of the plates were excluded from the measurements. The standard errors of the value of $p\beta$ were calculated from the number of non-overlapping cells. The error in the momentum measured by the sagitta method was 7%.

In figure 5, corresponding values of p and $p\beta$ are plotted; the continuous line is the theoretical relation, assuming that all particles are μ-mesons. The results show that p and $p\beta$ measured by these two techniques agree within the experimental error. It is shown elsewhere, however, that in this block for momenta greater than 2·5 GeV/**c** spurious scattering becomes important (Biswas *et al.* 1955, Apostolakis, Clarke and Major 1957).

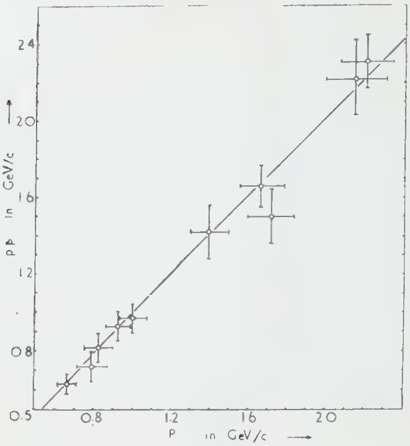

Figure 5. Comparison of corresponding values of p and $p\beta$. The continuous line is the theoretical relation for μ-mesons.

§ 6. Application of the Normal Incidence Technique

In I it has been shown that it is possible to design a 'normal incidence stack' which can be used to determine the signs and momenta of high-energy particles. In the present paper it has been shown that the design may be carried out in practice. Two types of application may be envisaged: (1) experiments on the cosmic radiation and (2) experiments on artificially accelerated particles. In both cases the weight of the frames can be used to provide the constraint for the location of the frames—an important feature since gravity constraint is reproducible and least likely to distort the coordinate system. The magnetic field can be produced by electromagnets or permanent magnets. For artificially accelerated particles the field can be produced by Helmholtz coils, the field being synchronized with the output of the accelerator. The shape and dimensions of a stack are dictated by the aim of the experiment, the available field and the field volume.

The value of the momentum measurements is enhanced if it is possible to trace the measured particle into blocks of stripped emulsions. This has been achieved for one block only placed at the end of the stack, but the use of more blocks could very easily be introduced. By placing vertical stripped emulsions at the centre of a stack it should be possible to measure the momenta of primary and secondary particles of high-energy interactions. Problems such as the variation of grain density with momentum and scattering constant measurements can be studied provided that the stack has been designed to give a large signal-to-noise ratio. The spectrum of particles at different levels above and below sea level could be measured with zenith angles varying from 0° to 90°. Such spectrum determinations are attractive for two reasons (*a*) because the system of selection is unbiased and can in general give the absolute flux of particles and (*b*) the magnetic field may be provided by a permanent magnet which is easily transported.

For experiments which require a large number of measured particles the time consumption of the technique is important. The time taken for the preliminary scanning for steep tracks is inversely proportional to their density D. The rate at which trajectories can be traced is independent of D for small D, but decreases rapidly for large D. A density of 10^3 tracks/cm^2 is reasonable. A second factor which strongly affects the rate of working is, obviously, the quality of the development. In the present work the grain density was not high, less than 18 grains/100 μ, and the track density was roughly 400/cm^2. The time taken in finding the constituent tracks of a trajectory was small, about 10% of the time in computing, changing plates and setting up coordinates. It was, therefore, found convenient to explore twenty trajectories at a time. Towards the end of the examination of the stack an overall rate of about three particles per man–day was attained. It is felt that this figure would have been at least twice as great if a grain density of 25–30 grains/100 μ had been used.

The scanning efficiency for steep tracks is surprisingly high. No efficiency correction has been applied to the points used to compare the observed spectrum and the established spectrum. Using a 45 × oil-immersion objective, experienced observers had no difficulty in detecting the type of track used in this experiment, even when the track was near the edge of the field of view. In view of the total time taken to measure the momentum of a particle, some form of selection is advisable.

In conclusion, it should be emphasized that the major advantage of the normal incidence technique is the precision with which the trajectory of a particle can be reconstructed, using a compact and simple apparatus. This precision, allied to a long trajectory and a strong magnetic field, results in an accurate estimate of momentum. The determination of signs is correspondingly certain.

ACKNOWLEDGMENTS

Our thanks are due to Professor G. D. Rochester for his constant advice and encouragement, to Dr. S. J. Goldsack for discussions in the earlier part of the work and to our colleagues, Mr. J. O. Clarke, Mr. J. V. Major and Dr. A. W. Wolfendale. Mr. C. Waller and his staff at Messrs. Ilford Ltd. are particularly thanked.

REFERENCES

Apostolakis, A. J., Clarke, J. O., and Major, J. V., 1957, *Nuovo Cim.*, in the press.

Apostolakis, A. J., and Macpherson, I., 1957, *Proc. Phys. Soc.* A, **70,** 146.

Apostolakis, A. J., and Major, J. V., 1957, *Brit. J. Appl. Phys.*, **8,** 9.

Biswas, S., Peters, B., and Rama, 1955, *Proc. Indian Acad. Sci.* A, **41,** 156.

Hyams, B. D., Mylroi, M. G., Owen, B. G., and Wilson, J. G., 1950, *Proc. Phys. Soc.* A, **63,** 1053.

Owen, B. G., and Wilson, J. G., 1951, *Proc. Phys. Soc.* A, **64,** 417; 1955, *Ibid.*, **68,** 409.

Regener, H. V., 1951, *Phys. Rev.*, **84,** 161.

APPENDIX

THE USE OF HIGH ENERGY PARTICLES FOR DETECTING STACK DEFECTS

Consider the trajectory of a particle which passes through a stack of equispaced plates. Let the x-coordinate in successive plates be $x_1\ x_2\ x_3 \ldots x_i \ldots x_n$, referred to a perfect coordinate lattice. If the particle is not deflected by a magnetic field and if scattering can be neglected then the first differences $D_i = x_i - x_{i+1}$ are constant. If the particle is deflected by a magnetic field the second differences $S_i = x_i - 2x_{i+1} + x_{i+2}$ are constant within the small-angle approximation. Consequently, the third differences

$$T_i = x_i - 3x_{i+1} + 3x_{i+2} - x_{i+3}$$

are identically equal to zero for a particle which suffers a small magnetic deflection. Hence, the third differences of high-energy tracks should be normally distributed about zero. If, however, a fault is introduced into the coordinate lattice of the type described in the text, that is a dislocation or displacement, the differences are no longer centred about zero. The systematic shifts can be detected by calculating the mean values of the third differences of several high-energy trajectories. Moreover, the nature of the fault can be ascertained. Consider first an unknown displacement error of δ in the ith plate, that is, the correct coordinate is $x_i + \delta$. It is easily shown that if the assumed coordinate x_i is used to calculate the third differences, then the following relations pertain:

Third differences	T_{i-4}	T_{i-3}	T_{i-2}	T_{i-1}	T_i	T_{i+1}
Mean value	0	$-\delta$	$+3\delta$	-3δ	$+\delta$	0

Similarly, for a dislocation of δ at the ith plate, i.e. correct coordinates $x_i + \delta$, $x_{i+1} + \delta$, $x_{i+2} + \delta$, . . , the following relations pertain:

Third differences	T_{i-3}	T_{i-2}	T_{i1}	T_i	T_{i+1}
Mean value	0	$+\delta$	-2δ	$+\delta$	0

Hence, by examining the sequence of the mean third differences for several tracks, it is possible to discriminate between the types of fault, and to locate the fault. The magnitude of the fault is determined with an accuracy to $[20/(n-1)]^{1/2}\sigma$, where n is the number of tracks used and σ is the standard deviation of the errors of measurement.

The above method is only applicable when the number of faults is small compared with the number of plates.

If by some mischance a large number of faults occur then the highest energy track may be used as a reference axis.

LETTERS TO THE EDITOR

Polarization of Protons Scattered from Carbon at 970 Mev

We report here some preliminary experiments on the polarization of 970 Mev protons scattered from the Birmingham proton synchrotron. Experiments at lower energies (see for example Chamberlain *et al.* 1956) have shown that particles scattered by nuclei may be polarized and it is of interest to look for similar effects at higher energies.

The internal circulating beam of the synchrotron is scattered to the right through 4° from a carbon target inside the vacuum chamber and emerges through a thin window into the atmosphere. Here it is collimated by two successive channels in heavy material to form a well defined beam of divergence $\pm 0{\cdot}3^\circ$ and angular spread $\pm 0{\cdot}25^\circ$ in the horizontal plane. The second scatterer is placed in the beam about one metre from the collimator. Owing to the gradient of the synchrotron fringing field the beam passes through a horizontal focal line 25 cm from the second scatterer. At this position the scattered tracks are recorded in Ilford G5 plates 200 μ thick, 5 inches by 1 inch. These plates lie horizontally and the beam of unscattered protons passes through the central region of the plates, normal to their long edge.

Scanning of the plates has been performed on Cooke Troughton and Simms type M3000 microscopes using 45 × oil immersion objectives and 15 × eyepieces. Each microscope has been fitted with a special swivelling stage which can be rotated about a point 25 cm from the plate corresponding to the original position of the second scatterer. This, combined with a special eyepiece with a protractor graticule which can be displaced to the position of the track, enables tracks to be counted at a rate of 50–100 per hour with reasonable efficiency. Angles are measured to the nearest $\frac{1}{4}^\circ$ but the results have so far been grouped in degree intervals.

The unscattered beam direction is determined by examining the tracks of particles in the centre of the plates. This can be done with an accuracy of $\pm 0{\cdot}125^\circ$ on each plate. As the results contain the measurements from 20 plates the error in the mean beam angle should be less than $\pm 0{\cdot}03^\circ$.

The presence of a magnetic field of about 3500 oersteds in the region of the plates does not in itself disturb the measurements since all angles are measured at the same distance from the scatterer. There is, however, a gradient of 100 oersted cm^{-1}. It can be shown that this introduces an error in the polarization approximately equivalent to an error in the beam angle determination of $0{\cdot}03^\circ$, or an error in the asymmetry of $-0{\cdot}01$ (i.e. the true asymmetry is greater than that observed by 0·01).

A few of the tracks will not have come from the second target. Exposures were therefore made without a second target in position. Corrections for this background have been found necessary only at the smaller angles of 2 and 3°.

If the polarization $P(\theta_0)$ is produced by scattering at a given angle, then a second scattering at the same angle produces an asymmetry $\epsilon = P^2(\theta_0)$ where ϵ is defined by the relation between R and L, the tracks counted at the right and the left respectively

$$P^2(\theta_0) = \epsilon = \frac{R-L}{R+L}\,. \qquad \ldots\ldots(1)$$

At other angles of second scattering the asymmetry $\epsilon(\theta) = P(\theta_0)P(\theta)$. Thus, once the polarization of the beam is known from equation (1), the polarization at any other angle of scattering may be determined by studying the asymmetry at other angles of second scatter.

Figure 1 shows the observed polarization as a function of angle for 5000 tracks so far counted in this work. Figure 2 shows the angular distribution, summed over right and left. The errors shown in figure 2 are statistical only and the absolute values of the cross section may be in error by ±50% owing to poor beam monitoring.

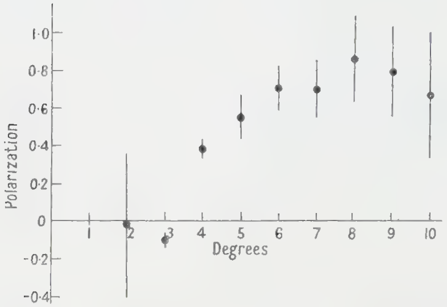

Figure 1. Polarization as a function of angle for 970 MeV protons scattered from carbon.

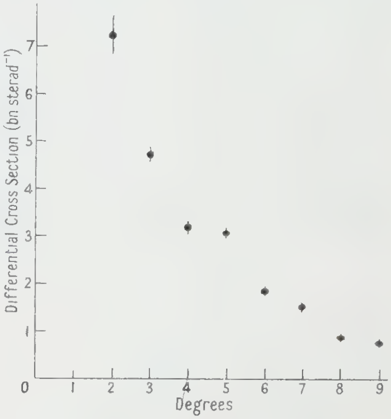

Figure 2. Differential cross section as a function of angle for 970 MeV protons scattered from carbon.

These results show that considerable polarization effects exist at this energy. Theoretical calculations by Dr. G. E. Brown (1957, private communication) are in good agreement with these experimental results.

Recently some exposures have been made using a $5\frac{1}{2}°$ first angle of scatter. Unfortunately, probably because the first target is much closer to the plates in this arrangement, the shielding was less efficient for this exposure, and the background correction was much bigger. Hence the results have larger errors than those at 4° presented here, but they are in qualitative agreement.

To improve our results it is hoped to make more satisfactory exposures and to modify the scanning procedure to increase the scanning efficiency. Elements other than carbon will also be studied.

Our thanks are due to Professor P. B. Moon and Dr. P. V. March who initiated the work on this problem, to Miss P. Cole for help with the scanning, and to the synchrotron staff for their efficient operation of the machine. One of us (C. J. B.) wishes to acknowledge the receipt of a Department of Scientific and Industrial Research maintenance grant.

Department of Physics,
University of Birmingham.
10th December 1956.

C. J. Batty.
S. J. Goldsack.

Chamberlain, O., Segrè, E., Tripp, R. E., Wiegand, C., and Ypsilantis, T., 1956, *Phys. Rev.*, **102,** 1659.

REVIEWS OF BOOKS

Physics in my Generation. A selection of papers by MAX BORN, F.R.S., N.L. Pp. viii + 232. (London and New York: Pergamon Press, 1956.) 40*s.*

In 1921, classical physics, enlarged and enriched by the relativity theory of Einstein, seemed to promise an objective picture of the physical universe in which the succession of events was governed by rigid equations of motion and in which apparently irrational features such as Planck's constant would ultimately appear as logical consequences of the fundamental equations. Less than ten years later the foundations of this orderly structure had been undermined, deterministic laws in natural phenomena had been replaced by statistical averages, and the new theory of quantum mechanics had been developed to acknowledge and describe the indeterminacy of atomic processes. Professor Max Born is one of the founders of quantum mechanics; in his early years as a student he was closely in touch with Einstein and Minkowski, and later he numbered among his pupils in Göttingen both Heisenberg and Jordan. His work and experience embrace the period of transition between the classical and quantum manner of thought and in common with many great theoretical physicists he has been much concerned with the philosophical implications of his methods. In the present collection of essays and lectures, nearly all of which have been published elsewhere but which are brought together in this volume for the first time, Professor Born surveys the development of physical thinking over a period of some thirty years or more. The articles are, as might be expected from their various purposes, of widely different length and standard of difficulty, and there is a good deal of repetition, but they are beautifully written and easily readable. Some, notably those on *Cause, Purpose and Economy in Natural Laws* and *Astronomical Recollections*, deviate somewhat from the theme of the majority, and in some of the later lectures there are remarks on the responsibility of scientists for nuclear warfare to which not all physicists will subscribe. The excellence of this book is however, in the accounts which it gives of the work of the great German physicists, of the difficulty which Einstein and Planck found in accepting the fundamental indeterminacy of nature described by Heisenberg's uncertainty principle, of the reluctance of Schrödinger to accept the reality of anything but wave functions, of the place of Lorentz and Poincaré in the history of relativity, of the unification of alternative descriptions of matter made by Bohr in his principle of complementarity. The physicist learns at first hand how Born brought matrix algebra to Heisenberg's theory of observables, how he was led to identify the square of a wave function with a particle density and how the method of approximation which bears his name became a powerful tool of the new quantum mechanics. All this is of course familiar to many and is to be found tidily presented in numerous textbooks, but most of these fail to convey the excitement of discovery and the spirit of adventure which animated the great men whose names move through Professor Born's pages. Those for whom quantum mechanics is a human achievement as well as a successful technique will find both pleasure and profit in reading and re-reading this book.

W. E. BURCHAM.

CONTENTS OF SECTION B

PAGE

Dr. E. W. Elcock and Dr. P. T. Landsberg. Temperature Dependent Energy Levels in Statistical Mechanics 161

Dr. R. Cooper, Mr. D. T. Grossart and Dr. A. A. Wallace. Directional Effects in the Electric Breakdown of Single Crystals of KC1 and NaC1 169

Mr. P. T. Wedepohl. Electrical and Optical Properties of Type IIb Diamonds . 177

Mr. J. C. Anderson and Dr. B. Donovan. On the Complex Permeability of Iron–Nickel Alloys at High Frequencies 186

Mr. H. N. V. Temperley. The Influence of Boundary Conditions on the Onsager–Ising Partition Function for the Plane Square Lattice 192

Dr. R. T. Spurr and Mr. T. P. Newcomb. The Variation of Friction with Velocity 198

Mr. J. J. Benbow and Dr. F. C. Roesler. Experiments on Controlled Fractures . 201

Prof. K. S. W. Champion. High Power Discharges in an Intense Longitudinal Field. 212

Dr. A. K. Jonscher. Drift of Minority Carriers in the Presence of Trapping . 223

Dr. A. K. Jonscher. Diffusion of Minority Carriers in the Presence of Trapping 230

Mr. L. Jacob. The Electron Bombardment of Thin Barium Films . . . 235

Research Notes :

Dr. R. Mansfield. The Galvanomagnetic and Thermomagnetic Effects in Semiconductors 240

Dr. D. J. Oliver. Fluctuations in the Number of Electrons and Holes in a Semiconductor 244

Dr. T. S. Moss. Theory of the Spectral Distribution of Recombination Radiation from InSb 247

Mr. R. B. Jackson and Mr. A. K. Walton. Abnormal Noise in Junction Transistors during Secondary Ionization 251

Dr. F. H. Herbstein. A Note on the Structure of Evaporated Silver Deposits Prepared at High Temperatures 251

Dr. E. O. Hall. Domain Patterns on Cobalt Crystals 254

Dr. N. Barakat. The Formation of White Light Fringes of Equal Chromatic Order 256

Letters to the Editor :

Mr. J. Starkiewicz, Mr. G. Bate, Mr. H. Bennett and Mr. C. Hilsum. A Single Crystal Photodiode of Lead Sulphide 258

Reviews of Books 260

Contents of Section A 264

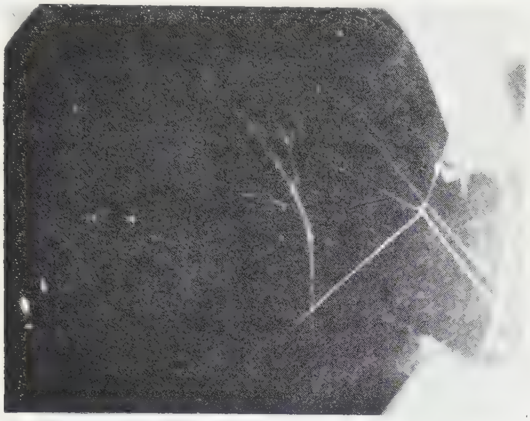

Figure 2. An example of a ‘counter-controlled’ star.

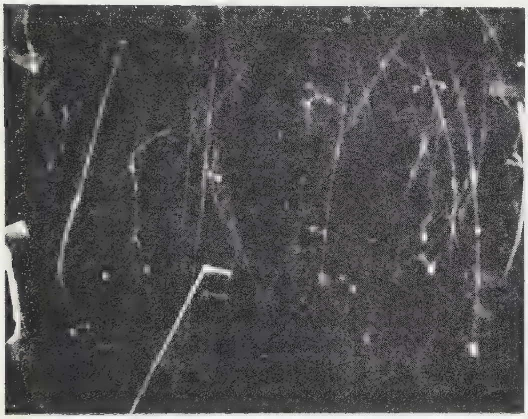

Figure 3. An example of a ‘pre-expansion’ random star, showing separation of the ion pairs by the clearing field.

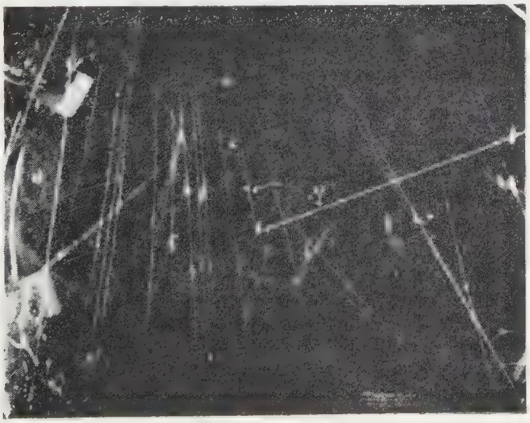

Figure 4. An example of an interaction occurring in a local penetrating shower initiated in the chamber wall.

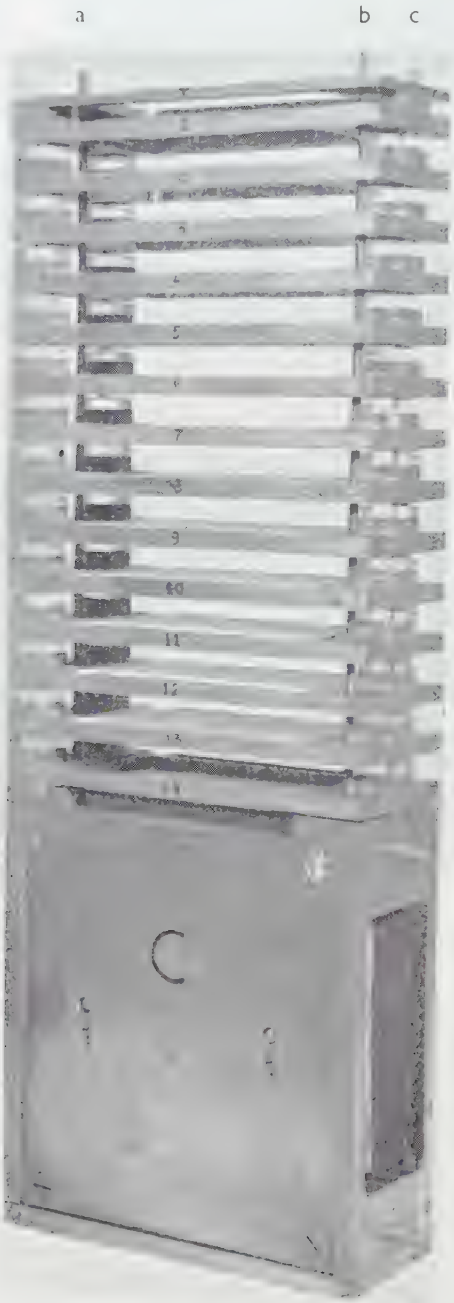

Figure 1.

A Variational Method for the Calculation of Particle Densities and Sums of Eigenvalues in Wave Mechanics

By N. H. MARCH

Department of Physics, The University, Sheffield

MS. received 17th October 1956

Abstract. Adopting a recent proposal made by Macke, the problem of calculating approximate particle densities and sums of eigenvalues by a variational method is examined thoroughly for the case of particles moving along the x axis in a given potential. An Euler equation is derived, which can, in principle, be solved to obtain the best possible density in the sense of the restricted variational method employed. Connection is made with previous work of von Weizsäcker, and it is pointed out that the solution of von Weizsäcker's equation may often be used to obtain a good initial approximation to the optimum results of the present treatment.

Illustrative calculations have been carried through for the linear harmonic oscillator with the first ten levels singly occupied, and the results for the particle density are extremely encouraging.

§ 1. INTRODUCTION

MACKE (1955 a, b) has recently proposed a very interesting method of dealing with many-particle problems in quantum mechanics, based on the Ritz variational principle. This treatment starts from approximate wave functions which are automatically orthogonal and normalized, being formed from a known set of eigenfunctions which are, however, essentially expressed in a different space. In three-dimensional cases, Macke proposed the use of the eigenfunctions representing the motion of a particle confined in a unit cube but otherwise free. It was then shown, in the limit of a very large number of particles, that the method yields the usual equations of the statistical theory, and, in particular, Macke emphasized a connection with von Weizsäcker's extension of the Thomas–Fermi method (von Weizsäcker 1935). Elsewhere, in a survey article (March 1957), the writer has pointed out that, whilst the connection with von Weizsäcker's method is not in dispute, Macke's arguments as they stand cannot be taken as providing a firm foundation for von Weizsäcker's method. The reason for this is that, in the evaluation of the kinetic energy, approximations were made which are only valid in the limiting case of a very large number of particles and there is no assurance that terms of the same order of magnitude as von Weizsäcker's kinetic energy correction are not omitted in this way. Furthermore, by making such approximations, the method is no longer certain to lead to an upper bound for the total energy of the many-particle system.

In the present investigation, the emphasis has been placed on working out fully the consequences of Macke's proposals for the simpler case of particles moving in a common one-dimensional potential $V(x)$, where it has proved possible to carry through the formal development without further approximation once the basic choice of variational function has been made. Attention will be focused on the calculation of the particle density and the sum of the eigenvalues.

§ 2. A VARIATIONAL METHOD FOR ONE-DIMENSIONAL PROBLEMS

Starting from the one-dimensional Schrödinger equation

$$-\frac{\hbar^2}{2m}\frac{d^2\psi}{dx^2}=[E-V(x)]\psi, \qquad \ldots\ldots(1)$$

we wish to approximate to the particle density ρ, given by

$$\rho=\sum_1^N \psi_n{}^2 \qquad \ldots\ldots(2)$$

if we assume that we are dealing with N singly occupied levels, and to the sum of the eigenvalues

$$\sum_1^N E_n. \qquad \ldots\ldots(3)$$

To do this we attempt to approximate the wave function ψ_n by another function u_n defined by

$$u_n=\left(\frac{dy}{dx}\right)^{1/2}\phi_n(y) \qquad \ldots\ldots(4)$$

where the functions $\phi_n(y)$ form a known orthonormal set, and are taken, following Macke, to be the wave functions of a particle confined to move in a one-dimensional 'box' of unit length. Thus

$$\phi_n(y)=2^{1/2}\sin n\pi y, \qquad n=1, 2, \ldots \qquad \ldots\ldots(5)$$

where $0\leqslant y\leqslant 1$, but otherwise the functional relation between y and x is to be determined by the variational method. The approximation to the particle density thus obtained is

$$\rho=\sum_1^N u_n{}^2=\frac{dy}{dx}\sum_1^N \phi_n{}^2(y). \qquad \ldots\ldots(6)$$

This immediately focuses attention on the function

$$\begin{aligned}\chi_N(y)&=\sum_1^N \phi_n{}^2(y)\\ &=\sum_1^N 2\sin^2 n\pi y,\end{aligned} \qquad \ldots\ldots(7)$$

and this turns out to be of central importance in the present treatment. Fortunately the sum in (7) can be evaluated; the relatively simple result for χ_N may be written

$$\chi_N(y)=N+\tfrac{1}{2}-\frac{\sin\{\pi(2N+1)y\}}{2\sin\pi y} \qquad \ldots\ldots(8)$$

and ρ is then given by

$$\rho=\frac{dy}{dx}\chi_N. \qquad \ldots\ldots(9)$$

It should be noted from (8) that as $N\to\infty$, χ_N approximates more and more closely to the constant value N throughout the unit 'box'.

We wish now to determine the form of $y(x)$ by the variational method and in order to do this we note first of all, assuming $y(x)$ to lie between 0 and 1 and to be the same function for all levels under consideration, that equations (4) and (5) define a special orthonormal set u_n such that an upper bound for the nth eigenvalue E_n is given by

$$-\frac{\hbar^2}{2m}\int u_n\frac{\partial^2 u_n}{\partial x^2}dx+\int u_n V u_n dx. \qquad \ldots\ldots(10)$$

Indeed, if u_n is at all a reasonable approximation to ψ_n, then (10) should give a useful estimate of E_n. Thus the sum of the eigenvalues for the first N levels may be approximated by

$$\begin{aligned} \mathscr{E} &= -\frac{\hbar^2}{2m}\int\sum_1^N u_n\frac{\partial^2 u_n}{\partial x^2}\,dx + \int\sum_1^N u_n{}^2 V\,dx \\ &= \qquad T \qquad + \qquad U, \end{aligned} \qquad \ldots\ldots(11)$$

where T is the kinetic energy and U is the potential energy.

With the particular choice of functions given in equations (4) and (5) the potential energy U may immediately be expressed in the form

$$U = \int y_1 V \chi_N\,dx, \qquad \ldots\ldots(12)$$

where we have written y_1 for dy/dx; in general, we shall for convenience put y_n for $d^n y/dx^n$. Following Macke, the kinetic energy T can easily be placed in the form

$$\begin{aligned} T &= \frac{\hbar^2}{2m}\int\left\{y_1\sum_1^N\left(\frac{\partial\phi_n}{\partial x}\right)^2 + \tfrac{1}{2}y_2\sum_1^N\frac{\partial}{\partial x}(\phi_n{}^2) + \left(\frac{\partial}{\partial x}y_1{}^{1/2}\right)^2\sum_1^N\phi_n{}^2\right\}dx \\ &= \frac{\hbar^2}{2m}\int\left\{y_1\sum_1^N\left(\frac{\partial\phi_n}{\partial x}\right)^2 + \tfrac{1}{2}y_2\frac{\partial\chi_N}{\partial x} + \left(\frac{\partial}{\partial x}y_1{}^{1/2}\right)^2\chi_N\right\}dx. \end{aligned} \qquad \ldots\ldots(13)$$

The summation in (13) may now be evaluated by writing

$$\sum_1^N\left(\frac{\partial\phi_n}{\partial x}\right)^2 = \sum_1^N\left(y_1\frac{\partial\phi_n}{\partial y}\right)^2 = y_1{}^2\sum_1^N 2n^2\pi^2\cos^2 n\pi y,$$

from (5). Thus we find immediately that

$$\sum_1^N\left(\frac{\partial\phi_n}{\partial x}\right)^2 = 2\pi^2 y_1{}^2\left[\frac{N(N+1)(2N+1)}{6} - \sum_1^N n^2\sin^2 n\pi y\right]$$

and by differentiating $\chi_N(y)$ it is easy to show that

$$2\sum_1^N n^2\sin^2 n\pi y = \frac{N(N+1)(2N+1)}{6} - \frac{\chi_N''}{4\pi^2}$$

where we have written χ_N'' for $\partial^2\chi_N/\partial y^2$; we shall use a similar notation for other derivatives of χ_N with respect to y. The kinetic energy may then be written

$$\begin{aligned} T = \frac{\hbar^2\pi^2}{m}\int y_1{}^3\left[\frac{N(N+1)(2N+1)}{12} + \frac{\chi_N''}{8\pi^2}\right]dx + \frac{\hbar^2}{4m}\int y_1 y_2\chi_N'\,dx \\ + \frac{\hbar^2}{8m}\int\frac{y_2{}^2}{y_1}\chi_N\,dx. \end{aligned} \qquad \ldots\ldots(14)$$

The terms involving χ_N' and χ_N'' are then easily shown to cancel, using an integration by parts, and we have finally

$$T = \frac{\hbar^2\pi^2}{12m}N(N+1)(2N+1)\int y_1{}^3\,dx + \frac{\hbar^2}{8m}\int\frac{y_2{}^2}{y_1}\chi_N\,dx. \qquad \ldots\ldots(15)$$

Thus $\mathscr{E}$ is known from (11), (12) and (15), and for a suitable variational function $y(x)$ we can in this way obtain an upper bound to the sum of the eigenvalues.

§ 3. EULER EQUATION FOR THE DETERMINATION OF $y(x)$

We can now, of course, ask for the best possible function $y(x)$, in the sense that the approximation to the sum of the eigenvalues given by (11), (12) and (15) shall be as close as possible to the correct sum. Formally, we may write the approximate sum of the eigenvalues as

$$\mathscr{E}=\int F(x,y,y_1,y_2)dx \qquad \ldots\ldots(16)$$

and then by minimizing $\mathscr{E}$ with respect to the function y we find the Euler equation

$$\frac{\partial F}{\partial y}-\frac{d}{dx}\left(\frac{\partial F}{\partial y_1}\right)+\frac{d^2}{dx^2}\left(\frac{\partial F}{\partial y_2}\right)=0. \qquad \ldots\ldots(17)$$

We note that χ_N depends only on y and not on y_1 and y_2 and after some manipulation we obtain the explicit Euler equation

$$-\frac{\hbar^2\pi^2}{4m}N(N+1)(2N+1)\frac{d}{dx}(y_1{}^2)-\chi_N\frac{dV}{dx}-\frac{\hbar^2}{8m}\chi_N\frac{d}{dx}(y_2{}^2y_1{}^{-2})$$
$$+\frac{\hbar^2}{4m}\chi_N\frac{d}{dx}(y_3y_1{}^{-1})+\frac{\hbar^2}{2m}\chi_N{}'y_3+\frac{\hbar^2}{4m}y_1y_2\chi_N{}''=0. \qquad \ldots\ldots(18)$$

Thus a fourth-order equation must be solved for $y(x)$ and among its solutions will be one which satisfies the physical conditions of the problem and is such that $0<y<1$; this will then give the best possible function $y(x)$ in the sense of the variational method used here.

§ 4. THE VIRIAL THEOREM

If $y(x)$ is indeed obtained by solution of the Euler equation (18) and is then used to calculate T and ρ as given by (15) and (9) respectively, it is not difficult to show that the virial theorem is exactly satisfied. The most straightforward procedure seems to be to form the customary virial as

$$\int \rho x\frac{dV}{dx}\,dx$$

and from equation (9) this is equal to

$$\int xy_1\chi_N\frac{dV}{dx}\,dx.$$

But $\chi_N dV/dx$ can now be obtained from equation (18) and, substituting in the above integral, the value can be shown, after considerable manipulation, to be equal to twice the kinetic energy, that is we have

$$2T=\int \rho x\frac{dV}{dx}\,dx. \qquad \ldots\ldots(19)$$

§ 5. CONNECTION WITH VON WEIZSÄCKER'S METHOD

Often, however, it may suffice to use a function $y(x)$ which is not the optimum one but is a good approximation to it, and the method will now be discussed from this point of view. We have already noted that the function χ_N becomes progressively nearer to the constant value N over the whole 'box' as N becomes very large. In this case, the derivatives of χ_N will become negligibly small and we shall also be able to replace $N(N+1)(2N+1)$ by $2N^3$. Equation (18) then reduces to

$$-\frac{\hbar^2\pi^2}{2m}N^3\frac{d}{dx}(y_1{}^2)-N\frac{dV}{dx}-\frac{\hbar^2}{8m}N\frac{d}{dx}(y_2{}^2y_1{}^{-2})+\frac{\hbar^2}{4m}N\frac{d}{dx}(y_3y_1{}^{-1})=0, \qquad \ldots\ldots(20)$$

where we have replaced χ_N by N. It will be seen that (20) no longer depends on y, and also that it can be integrated immediately to yield

$$-\frac{\hbar^2\pi^2}{2m}N^3y_1{}^2-NV-\frac{\hbar^2}{8m}Ny_2{}^2y_1{}^{-2}+\frac{\hbar^2}{4m}Ny_3y_1{}^{-1}=\text{const.}$$

If we now put $\gamma=Ny_1$ then the differential equation to be solved for γ is

$$-\frac{\hbar^2\pi^2}{2m}\gamma^2-V-\frac{\hbar^2}{8m}\frac{\gamma_1{}^2}{\gamma^2}+\frac{\hbar^2}{4m}\frac{\gamma_2}{\gamma}=\text{const.,} \qquad \ldots\ldots(21)$$

and this is simply von Weizsäcker's equation (see, for example, Plaskett 1953). The argument given is not intended to do more than suggest that a reasonable approximation to y_1 might often be obtained from (21), and then y can be calculated by integration. Further, in the case when the solution of the von Weizsäcker equation is not very different from the simple Thomas–Fermi density, it might be a useful approximation to calculate y_1 and y from this latter density. The details of the procedure by which we can therefore make use of the Thomas–Fermi or preferably the von Weizsäcker results within the framework of the present method will become clearer when we work out a specific example in the following paragraph.

§ 6. ILLUSTRATIVE EXAMPLE—THE LINEAR HARMONIC OSCILLATOR

We shall now illustrate the formal method by considering the simple case of the linear harmonic oscillator with the first ten levels singly occupied. This example has been used previously (Ballinger and March 1954) in an investigation of the extended Thomas–Fermi methods of Plaskett (1953) and von Weizsäcker and, in particular, the particle density obtained from von Weizsäcker's method is known. Figure 1 shows the results obtained in this previous work using the exact wave functions (curve 1), the Thomas–Fermi approximation (curve 2) and the von Weizsäcker method (curve 3). Actually, in figure 1 we have plotted $\rho/\alpha^{1/2}$ against $\alpha^{1/2}x$ where $\alpha=4\pi^2m\nu_0/\boldsymbol{h}$, ν_0 being the classical frequency of the oscillator.

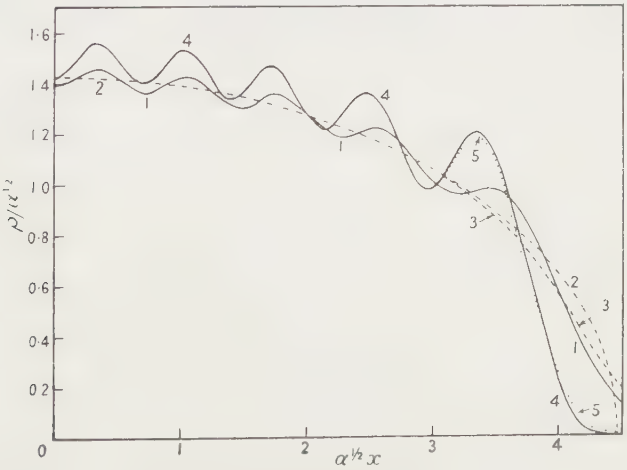

Figure 1. Densities for harmonic oscillator. Curve 1, wave-mechanical ; 2, Thomas-Fermi ; 3, von Weizsäcker ; 4, variational density with $y(z)=\bar{v}(z)$; 5, variational density in von Weizsäcker approximation.

Figure 1 shows that the results of von Weizsäcker's method are indistinguishable from the Thomas–Fermi results out to $\alpha^{1/2}x \sim 3$, although after that the curves deviate markedly. However, the agreement between the Thomas–Fermi and the von Weizsäcker densities is sufficient to suggest that a reasonable variational function $y(x)$ can be obtained from the simple Thomas–Fermi approximation to the density which may be written

$$\begin{aligned}\rho_{\mathrm{TF}} &= \frac{2}{\boldsymbol{h}}(2m)^{1/2}(E'-V)^{1/2}\\ &= \frac{2}{\boldsymbol{h}}(2m)^{1/2}(E'-2\pi^2 m\nu_0{}^2x^2)^{1/2}. \qquad \ldots\ldots(22)\end{aligned}$$

Expressing this in terms of $\alpha^{1/2}x=z$, and using the fact that $E'=N\boldsymbol{h}\nu_0$ (see March and Plaskett (1956) for the basic reasons for this value) we find the following approximation, denoted by $\bar{y}(z)$, for $y(z)$:

$$\left.\begin{aligned}&\bar{y}=0, && z<-(2N)^{1/2}\\ &\bar{y}=\tfrac{1}{2}+\frac{z}{2N\pi}(2N-z^2)^{1/2}+\frac{1}{\pi}\sin^{-1}\left\{\frac{z}{(2N)^{1/2}}\right\}, && -(2N)^{1/2}\leqslant z\leqslant(2N)^{1/2}\\ &\bar{y}=1, && z>(2N)^{1/2}.\end{aligned}\right\}\quad(23)$$

This function is shown in curve 1 of figure 2 for the case $N=10$, and the variational density which results from it is

$$\rho=\frac{d\bar{y}}{dx}\chi_{10}(\bar{y}).$$

We have plotted this in curve 4 of figure 1 for comparison with the exact results. The oscillations of the correct wave-mechanical density are now seen to be reproduced and the agreement with the exact results is extremely encouraging. The fact that the density is identically zero in the classically forbidden region is a consequence of the use of the Thomas–Fermi approximation (22) to calculate $\bar{y}(z)$. In fact, the use of the von Weizsäcker density formally avoids this defect, and using the numerical results obtained earlier by Ballinger and March (1954), we have indicated in curve 2 of figure 2 the (very small) modifications thereby introduced. Curve 5 of figure 1 shows how such a change in $y(z)$ affects the

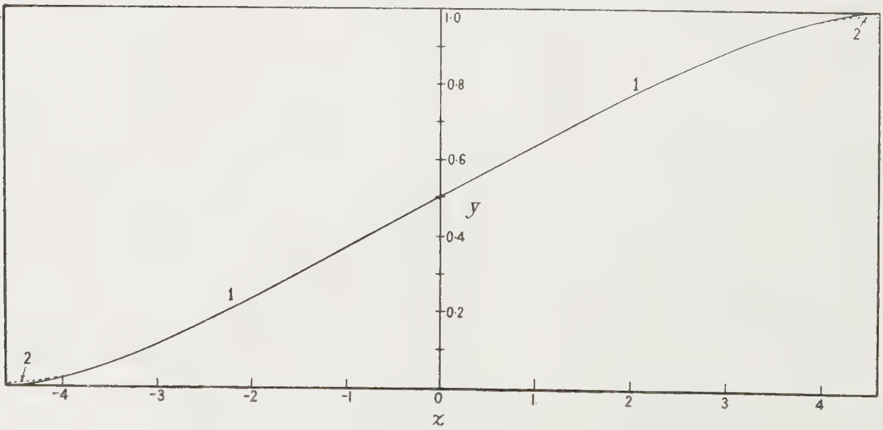

Figure 2. Transformation of space $y(z)$ for harmonic oscillator. Curve 1, Thomas–Fermi approximation ; 2, von Weizsäcker approximation.

density in the outer regions; it will be seen that the density in the classically forbidden region, while not identically zero, is very small.

With either of these forms of $y(z)$, the sum of the eigenvalues could be calculated from equations (11), (12) and (15), and, although we have not done this, values which are higher than the correct sum would be obtained. Actually, it is known that, in the case of the linear harmonic oscillator, the simple Thomas–Fermi formula for the sum of the eigenvalues gives the exact result; but, as March and Plaskett (1956) have shown, this is firstly because the exact values E_n for the energy levels of the linear harmonic oscillator are given by the WKB formula, and secondly because E_n depends linearly on n: a combination of exceptional circumstances. It cannot, of course, be expected that the present method can give the exact sum except in the limit $N \rightarrow \infty$.

§ 7. CONCLUSION

The treatment worked out fully in this paper, along lines suggested by Macke's work, is rigorously founded on the variational method, and thus the sum of the eigenvalues given by (11), (12) and (15), when a suitable variational function is specified, is always greater than the correct sum. This property is not, of course, shared by the simple Thomas–Fermi formula for the sum of the eigenvalues (see March and Plaskett (1956) for a thorough discussion of this formula), nor have we been able to show that it always holds for the extended method of von Weizsäcker, although it could conceivably do so. The present method reduces to the Thomas–Fermi method as the number of particles becomes very large, as Macke emphasized, and furthermore the form of the Euler equation (18) suggests that solutions of von Weizsäcker's equation might lead to results quite near to the optimum ones in some cases. It should not be expected that the method will give good results for a small number of particles in general, although it will, of course, still yield upper bounds to the sum of the eigenvalues.

In the example considered, namely the linear harmonic oscillator with ten levels singly occupied, variational functions obtained from the Thomas–Fermi and the von Weizsäcker methods have been used to calculate the particle density, and the agreement with the correct wave-mechanical results is very encouraging. Even better results could be obtained by solving (18) for $y(x)$: this will be a somewhat laborious task, but should be tractable numerically, especially when a good initial approximation is known.

Further work along these lines is in progress, particularly attempts to deal with the three-dimensional case.

REFERENCES

BALLINGER, R. A., and MARCH, N. H., 1954, *Proc. Phys. Soc.* A, **67,** 378.
MACKE, W., 1955 a, *Phys. Rev.*, **100,** 992 ; 1955 b, *Ann. Phys., Lpz.*, **17,** 1.
MARCH, N. H., 1957, *Advanc. Phys.*, **6,** 1.
MARCH, N. H., and PLASKETT, J. S., 1956, *Proc. Roy. Soc.* A, **235,** 419.
PLASKETT, J. S., 1953, *Proc. Phys. Soc.* A, **66,** 178.
VON WEIZSÄCKER, C. F., 1935, *Z. Phys.*, **96,** 431.

Curve Crossing and Orthogonality of Molecular Orbitals

By A. DALGARNO and N. LYNN
Department of Applied Mathematics, The Queen's University of Belfast

Communicated by D. R. Bates; MS. received 1*st October* 1956, *and in final form* 1*st November* 1956

Abstract. The approximate representation of states whose potential energy curves cross (or nearly cross) is discussed quantitatively, by comparing the energies and transition integrals of the $2s\sigma$ and $3d\sigma$ states of HeH^{2+} calculated using various approximate molecular orbitals with the exact values. It is concluded that, whilst the usual methods of taking mixing with neighbouring states into account may lead to accurate values of the energies provided orthogonality is imposed, the oscillator strengths may be seriously in error, especially if they are associated with weak transitions.

§ 1. Introduction

Because of the separability of the wave equation of a diatomic molecule with a single electron, it is possible for the potential energy curves of states, whose crossing would ordinarily be prohibited by the Wigner–Witmer non-crossing rule, to intersect at some value of the nuclear separation. This crossing actually occurs for the $2s\sigma$ and $3d\sigma$ states of both $H_2{}^+$ and HeH^{2+} (Bates, Ledsham and Stewart 1953, Bates and Carson 1956). The non-crossing rule does, however, apply to potential-energy curves derived from approximate wave functions. The problem thereby posed is of more than academic interest, for near-crossing must be common in more complex molecules.

§ 2. Approximate Wave Functions and Energies

Because of the symmetry requirements which must be imposed upon wave functions of states of $H_2{}^+$ it is simpler to consider the heteronuclear molecule HeH^{2+}. We shall be concerned with the $1s\sigma$ state which at infinite separation consists of a proton and a positive helium ion in the 1s state, with the $2s\sigma$ and $3d\sigma$ states, which consist of a proton and a positive helium ion in a mixture of the 2s and 2p states, and with the $2p\sigma$ state, which consists of an alpha particle and a hydrogen atom in the ground 1s state.

2.1. *The LCAO Approximation*

The LCAO approximations to the wave functions of the $2s\sigma$ and $3d\sigma$ states of HeH^{2+} are given by

$$\Psi(2s\sigma) = l\psi(2s_b) + m\psi(2p_b) \qquad \ldots\ldots(1)$$

$$\Psi(3d\sigma) = m\psi(2s_b) - l\psi(2p_b) \qquad \ldots\ldots(2)$$

and the normalization requirement that $l^2 + m^2$ be unity.

Here

$$\psi(2s_b) = (\pi)^{-1/2}(1 - r_b)\exp(-r_b) \qquad \ldots\ldots(3)$$

$$\psi(2\mathrm{p_b}) = (\pi)^{-1/2} r_\mathrm{b} \exp(-r_\mathrm{b}) \cos\theta_\mathrm{b}; \qquad \ldots\ldots(4)$$

$\mathbf{r}_\mathrm{b}$ is the position vector of the electron referred to the helium nucleus B as origin, and l and m are determined by minimization of the electronic energy E, given in rydbergs by

$$E = -\int \Psi^* \left(\nabla^2 + \frac{2}{r_\mathrm{a}} + \frac{4}{r_\mathrm{b}}\right) \Psi d\mathbf{r} \qquad \ldots\ldots(5)$$

where $\mathbf{r}_\mathrm{a}$ is the position vector of the electron referred to the hydrogen nucleus A. The two wave functions are orthogonal at all values of the nuclear separation R both to each other and, since there has been no rearrangement, also to the LCAO approximation to the $1s\sigma$ state which is given by

$$\Psi(1s\sigma) = (8/\pi)^{1/2} \exp(-2r_\mathrm{b}). \qquad \ldots\ldots(6)$$

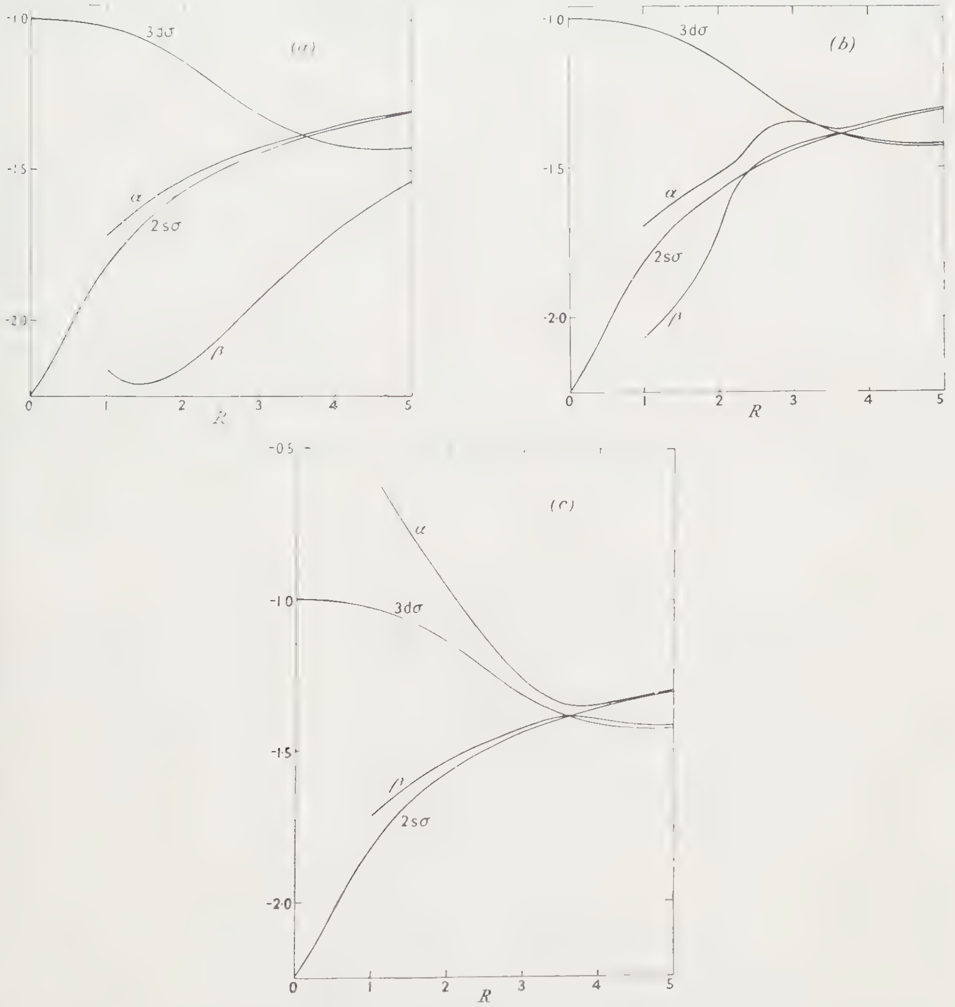

Figure 1 (*a*), (*b*) and (*c*). The energies of the $2s\sigma$ (curves α) and $3d\sigma$ (curves β) states, calculated using the wave functions of §§ 2.1, 2.2, and 2.3 respectively. The curves labelled $2s\sigma$ and $3d\sigma$, common to all three figures, are the corresponding exact energies.

The energies derived from equations (1) and (2) are illustrated in figure 1(*a*) together with the exact energies computed by Bates and Carson (1956), the approximate curves being labelled by supposing that at large values of R they have the same ordering as the exact curves. Although it is unlikely, the harmony of the approximate and exact 2sσ energies may be fortuitous, for the approximate 3dσ binding energies are grossly in error and there is no tendency for the two curves to approach each other. Since the approximate 3dσ binding energies are *larger* than the exact, part of their error must be attributed to lack of orthogonality to wave functions of lower states, in particular to lack of orthogonality to the wave function of the 2pσ state.

2.2. *The LCAO Approximation with Mixing*

The orthogonality of wave functions of the 2sσ and 3dσ states to each other and to the wave function of the 2pσ state can be achieved approximately, by defining new wave functions

$$\Psi(2\mathrm{p}\sigma, 3\mathrm{d}\sigma, 2\mathrm{s}\sigma) = l\psi(2\mathrm{s_b}) + m\psi(2\mathrm{p_b}) + n\psi(1\mathrm{s_a}), \qquad \ldots\ldots(7)$$

the LCAO approximation to the 2pσ state being given by

$$\psi(1\mathrm{s_a}) = (\pi)^{-1/2} \exp(-r_\mathrm{a}). \qquad \ldots\ldots(8)$$

Regardless of considerations of orthogonality, equation (7) is a natural refinement of equations (1) and (2), for the energies of the 2pσ, 3dσ and 2sσ states are equal at infinite separation R, so that considerable mixing is to be anticipated at finite values of R.

Minimizing equation (5), using equation (7), gives three potential energy curves and three corresponding sets of values of l, m and n. The wave functions so obtained are, of course, mutually orthogonal. The energies of the 2sσ and 3dσ states only are shown in figure 1(*b*), those for the 2pσ state having been reported previously (McCarroll and Moiseiwitsch 1957). A strong tendency for the curves to approach each other is now evident and this tendency is apparently reflected in the values of the ratios $l:m:n$ which change sign in the region of the near-crossing, whereas, for the ordinary LCAO approximation discussed in § 2.1, no change of sign occurred. A similar behaviour is suggested by some work of Coulson and Lester (1955) on the analogous states of H_2^+. For values of R greater than the crossing point R_X the approximate energies of both the 2sσ and 3dσ states are in harmony with the exact energies, whilst for values of R slightly less than R_X the original approximate 2sσ energy curve follows closely the exact 3dσ curve and the original approximate 3dσ energy curve follows closely the exact

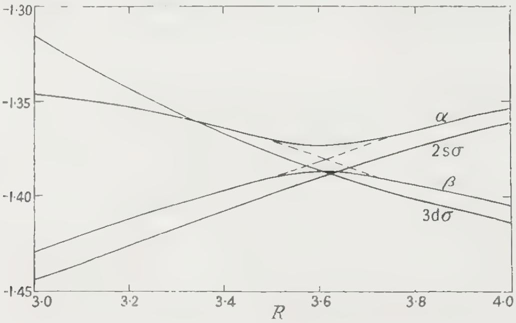

Figure 2. A more detailed reproduction of figure 1 (*b*) in the crossing region.

$2s\sigma$ curve. Thus more accurate energies would be obtained by supposing that the approximate curves do cross and figure 2, which shows the crossing region in more detail, demonstrates how the two pairs of curves may be connected through the crossing point.

For smaller values of R the situation is rather similar to that for the ordinary LCAO approximation and is again presumably due to lack of orthogonality, for the introduction of the $2p\sigma$ component causes the automatic orthogonality to the LCAO $1s\sigma$ wave function to be lost.

2.3. *The LCAO Approximation with Mixing and Orthogonality*

In order to obtain a set of four mutually orthogonal wave functions, it is usually necessary to introduce a wave function with four components, the weighting of the components being determined from the roots of a quartic in the energy. However, for the states of interest here, we may, following McCarroll and Moiseiwitsch (1957), define a wave function

$$\Psi(2\mathrm{p}\sigma, 2\mathrm{s}\sigma, 3\mathrm{d}\sigma) = l\psi(2\mathrm{s_b}) + m\psi(2\mathrm{p_b}) + n\{\psi(1\mathrm{s_a}) - \lambda\psi(1\mathrm{s_b})\}, \quad \ldots\ldots(9)$$

where $\lambda = \int \psi(1\mathrm{s_a})\psi(1\mathrm{s_b})d\mathbf{r}$. The three wave functions corresponding to (9) are then mutually orthogonal to each other and also to the LCAO $1s\sigma$ wave function. For the method to be accurate, it is necessary for the LCAO $1s\sigma$ wave function to be a good representation of the exact $1s\sigma$ wave function and this appears to be the case except at very small values of R (Moiseiwitsch and Stewart 1956).

The energies derived from equation (9) are shown in figure 1(*c*).† The good agreement obtained in § 2.2 for values of R greater than R_X is retained and a marked improvement is found for values of R less than R_X provided it is again assumed that the curves do cross. A change of sign of the ratios $l:n:m$ corresponding to the $2s\sigma$ and $3d\sigma$ states also occurs for equation (9) in the region of the near-crossing.

§ 3. TRANSITION INTEGRALS

It is important to ascertain whether the accuracy with which the energies are reproduced (if it is assumed that the curves cross) is reflected in the prediction of other molecular properties. The calculation of the transition integrals connecting the $1s\sigma$, $2s\sigma$ and $3d\sigma$ states by Dalgarno, Lynn and Williams (1956), using exact wave functions, provides suitable comparison data. The $1s\sigma$–$2s\sigma$, $1s\sigma$–$3d\sigma$ and $2s\sigma$–$3d\sigma$ transition integrals $\underset{\sim}{Q}$ have been computed using the wave functions of §§ 2.1, 2.2 and 2.3 in both the dipole length and dipole velocity forms:

$$Q_{\mathrm{L}}\mathbf{t} = \int \chi_{\mathrm{i}}\mathbf{r}\chi_{\mathrm{f}}d\mathbf{r} \text{ (dipole length)} \qquad \ldots\ldots(10)$$

$$Q_{\mathrm{V}}\mathbf{t} = -\frac{2}{\Delta E}\int \chi_{\mathrm{i}}\nabla\chi_{\mathrm{f}}d\mathbf{r} \text{ (dipole velocity)} \qquad \ldots\ldots(11)$$

where χ_{i} and χ_{f} are the wave functions of the initial and final states, ΔE is the photon energy of the radiation in rydbergs, $\mathbf{t}$ is some unit vector and $\mathbf{r}$ is the position vector of the electron relative to an arbitrary origin.

The results for the $1s\sigma$–$2s\sigma$ and $1s\sigma$–$3d\sigma$ transitions computed using the wave functions derived in § 2.2 will not be reproduced since, due to the lack of orthogonality of the initial and final wave functions, Q_L is a function of the position of the (arbitrary) origin of coordinates‡, but the results using the wave functions in §§ 2.1 and 2.3 are illustrated in figures 3 and 4, the ordinary LCAO approximation and the exact results being reproduced from the paper by Dalgarno, Lynn and Williams (1956).

---

† We are indebted to Mr. R. McCarroll and Dr. B. L. Moiseiwitsch for allowing us the use of some auxiliary computation that they carried out in connection with the $2p\sigma$ state.

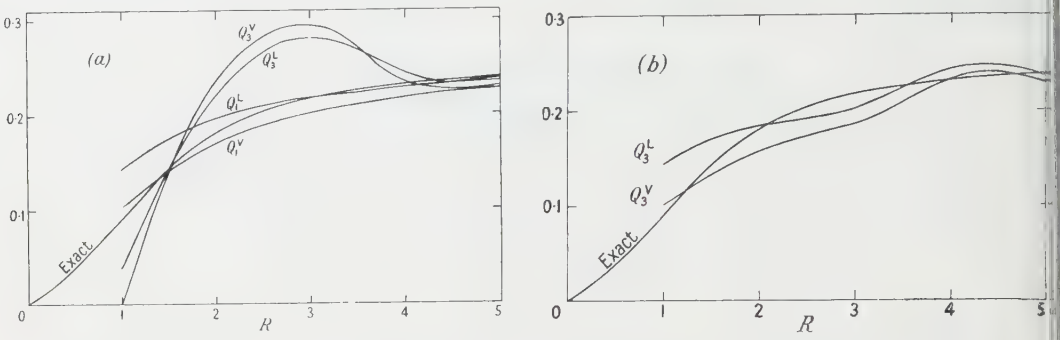

Figure 3 (*a*) and (*b*). The 1sσ — 2sσ transition integrals, computed using the wave functions of § 2.1 (curves $Q_1{}^L$ and $Q_1{}^V$) and § 2.3 (curves $Q_3{}^L$ and $Q_3{}^V$). Figure 3 (*a*) without, and (*b*)† with interchange of the labelling of the states. (In calculating Q_V, the exact energies have been used.)

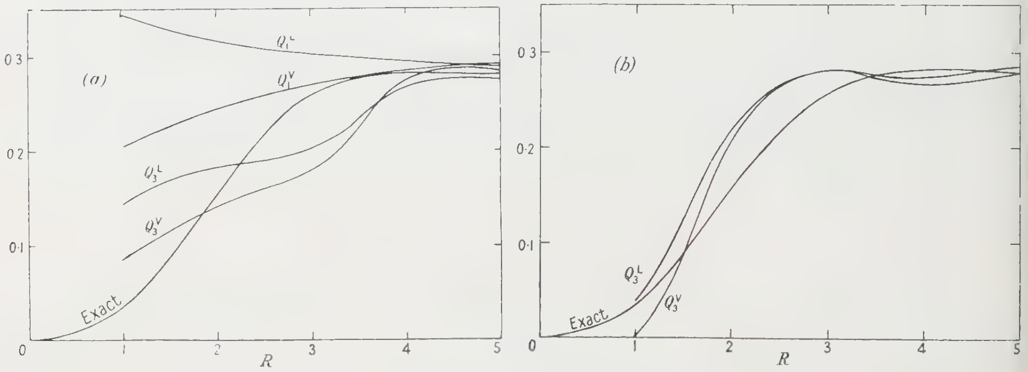

Figure 4 (*a*) and (*b*). The 1sσ — 3dσ transition integrals, computed using the wave functions of § 2.1 (curves $Q_1{}^L$ and $Q_1{}^V$) and § 2.3 (curves $Q_3{}^L$ and $Q_3{}^V$). Figure 4 (*a*) without, and (*b*)† with interchange of the labelling of the states. (In calculating Q_V, the exact energies have been used.)

† The transition integrals through the crossing point have been smoothed, using a method like that for the crossing of the energy curves (cf. figure 2).

The LCAO values for the 1sσ–2sσ transition are reasonably accurate, those for the 1sσ–3dσ transition less so. When mixing and orthogonality are included, there is strong evidence (compare figures 3(*a*) and 4(*a*) with 3(*b*) and 4(*b*) to support the expectation that, for values of R less than R_X, the labelling of the approximate wave functions should be interchanged. When this is done the predicted transition integrals are in good agreement with the exact values over the entire range of R, suggesting that the approximate molecular orbitals possess high accuracy.

---

‡ This point has been frequently overlooked, since it is customary to take the origin at the centre of charge or at the mid-point of the nuclear axis. It must be stressed that the computation of a transition integral, connecting states represented by non-orthogonal wave functions, is a meaningless procedure.

However, the 1sσ–2sσ and 1sσ–3dσ transition integrals are not very sensitive to the wave functions employed (provided they are correct at infinite separation) and the 2sσ–3dσ transition, which is of the *sub-Rydberg* type, provides a much severer test of the accuracy of the wave functions.

The results computed using the wave functions of § § 2.1, 2.2 and 2.3 in Q_L are shown in figure 5, but the values of Q_V are ridiculous, changing sign in a haphazard fashion, and are omitted. On comparing with the exact values, it can be seen that neither mixing nor mixing with orthogonality lessens the serious disagreement of the LCAO and exact values, in contrast to the marked improvement obtained previously. Indeed, the results do not even have qualitative accuracy. The situation is one made familiar by the recent detailed calculations on H_2^+ (Dalgarno and Poots 1954, Moiseiwitsch and Stewart 1954, Carson and Dalgarno 1955, Dalgarno and Lewis 1956) and on HeH^{2+} (Moiseiwitsch and Stewart 1956, McCarroll and Moiseiwitsch, to be published).

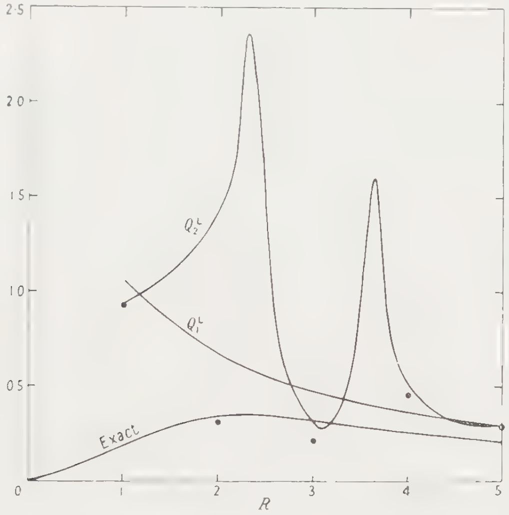

Figure 5. The 2sσ – 3dσ transition integrals, computed using the wave functions of § 2.1 (curve Q_1^L), § 2.2 (curve Q_2^L) and § 2.3 (denoted by points only, since insufficient points have been computed to determine the shape of the curve; it is probably rather similar to Q_2^L).

In general, the conventional variational method for dealing with closely neighbouring states is unsatisfactory unless accurate and simple initial trial wave functions can be found (such as those used by Carson and Dalgarno (1955)) and it may be preferable to attempt direct perturbation-type calculations of matrix elements, in which the convergence of the successive orders can be examined (cf. Dalgarno and Stewart 1956).

ACKNOWLEDGMENT

The authors are indebted to Professor D. R. Bates for several interesting comments on the subject matter of this paper.

REFERENCES

BATES, D. R., and CARSON, T. R., 1956, *Proc. Roy. Soc.* A, **234**, 207.

BATES, D. R., LEDSHAM, K., and STEWART, A. L., 1953, *Phil. Trans. Roy. Soc.* A, **246**, 215.

CARSON, T. R., and DALGARNO, A., 1955, *Proc. Phys. Soc.* A, **68**, 569.

COULSON, C. A., and LESTER, G. R., 1955, *Trans. Faraday Soc.*, **51**, 1605.

DALGARNO, A., and LEWIS, J. T., 1956, *Proc. Phys. Soc.* A, **69**, 285.

DALGARNO, A., LYNN, N., and WILLIAMS, E. J. A., 1956, *Proc. Phys. Soc.* A, **69**, 610.

DALGARNO, A., and POOTS, G., 1954, *Proc. Phys. Soc.* A, **67**, 343.

DALGARNO, A., and STEWART, A. L., 1956, *Proc. Roy. Soc.* A, **238**, 276.

MOISEIWITSCH, B. L., and STEWART, A. L., 1954, *Proc. Phys. Soc.* A, **67**, 457; 1956, *Ibid.*, **69**, 480.

Dispersion Relations for Forward Scattering of Spin Zero Particles by an Extended Potential

By F. MANDL
Atomic Energy Research Establishment, Harwell, Berks.

Communicated by B. H. Flowers; MS. received 4th December 1956

Abstract. Dispersion relations are derived for the scattering in the forward direction of spin zero (scalar or pseudo-scalar) particles by a real, extended potential. The contribution from the bound states is expressed in terms of the residues of the bound-state wave functions in momentum space at the resonance energies.

§ 1. INTRODUCTION

In this paper, we shall study the scattering of spin zero (scalar or pseudo-scalar) particles by an extended potential, with a view to deriving dispersion relations for forward scattering. This problem has previously been studied by van Kampen (1953) who considered the non-relativistic problem, i.e. assuming no maximum velocity for the propagation of signals, for s waves. The problem has also been treated by Gell-Mann, Goldberger and Thirring (1954), who show that the behaviour of the forward scattering amplitude is much simpler than that of the individual partial waves. However, their analysis is not satisfactory (Goldberger 1955).

More recently, Goldberger (1955) has derived dispersion relations for forward scattering of mesons by nucleons, using the symmetric pseudo-scalar point interaction. His derivation is now believed not to be rigorous due to convergence difficulties arising from the bound-state contributions.†

In this paper we use the Goldberger approach to consider the scattering of spin zero particles, described relativistically, by a non-relativistic three-dimensional potential. This leads to certain simplifications, particularly conceptually, as we deal with only one quantized field. On the other hand, we do not have conservation of momentum now and this rather complicates the analysis. To treat the bound-state contribution rigorously, we have used a device suggested by Bogoliubov at the Seattle Conference. The dispersion relations which we derive correspond, very roughly, to describing the scattering of mesons by a nucleus in terms of an optical model. A comparison with experiment does not seem reasonable at this stage, as we have only considered a real potential.

§ 2. DERIVATION

We consider spin zero particles of mass μ described by the Klein–Gordon equation

$$[\Box^2 - \mu^2 - V(\mathbf{x})]\phi(x) = 0 \qquad \ldots\ldots(1)$$

where x denotes the four-vector $(\mathbf{x}, x_0)$. For simplicity we shall assume that the potential $V(\mathbf{x})$ does not contain any charge exchange operators. We can then treat $\phi(x)$ as a real field. We shall not assume $V(\mathbf{x})$ spherically symmetric, but only the weaker condition

---

† These points were discussed at the Conference on Theoretical Physics held at Seattle, U.S.A., in September 1956.

$$V(-\mathbf{x})=V(\mathbf{x}). \qquad \ldots\ldots(2)$$

The Feynman amplitude for an incident meson of momentum $\mathbf{k}=(0,0,k)$ to be scattered into a state of momentum $\mathbf{k}'$ is given in the Heisenberg representation (Low 1955, Lehmann *et al.* 1955) by

$$\mathscr{F}(\mathbf{k}',\mathbf{k},k_0',k_0)=i\int d^4x d^4y \exp(-ik'x+iky)$$
$$\times(\Box_x{}^2-\mu^2)(\Box_y{}^2-\mu^2)(\Phi_0,(\phi(x)\phi(y))_+\Phi_0). \qquad \ldots\ldots(3)$$

Here Φ_0 represents the 'vacuum', i.e. the no-meson state, which is assumed to be the eigenstate of the *total* Hamiltonian H corresponding to the lowest eigenvalue E_0. Eigenstates with eigenvalues $E_n \geqslant E_0+\mu$ correspond to scattering states, states with energies in the interval $E_0<E_n<E_0+\mu$ to bound states.

Introducing equation (1) into (3), defining the operator

$$T(\mathbf{k},x_0)=\int d\mathbf{x} \exp(i\mathbf{k}\mathbf{x})V(\mathbf{x})\phi(x), \qquad \ldots\ldots(4)$$

and using the time dependence of Heisenberg operators to separate out the conservation of energy, we obtain

$$\mathscr{F}(\mathbf{k}',\mathbf{k},k_0',k_0)=2\pi\delta(k_0'-k_0)F(\mathbf{k}',\mathbf{k},k_0) \qquad \ldots\ldots(5)$$

where

$$F(\mathbf{k}',\mathbf{k},k_0)=i\int dx_0 \exp(ik_0x_0)(\Phi_0,(T(-\mathbf{k}',x_0)T(\mathbf{k},0))_+\Phi_0). \qquad \ldots\ldots(6)$$

Following Goldberger, we introduce instead of $F(\mathbf{k}',\mathbf{k})$, a causal function $M(\mathbf{k}',\mathbf{k})$, which vanishes outside the light cone, by

$$M(\mathbf{k}',\mathbf{k},k_0)=i\int dx_0 \exp(ik_0x_0)(\Phi_0,\eta(x_0)[T(-\mathbf{k}',x_0),T(\mathbf{k},0)]\Phi_0), \qquad \ldots\ldots(7)$$

where

$$\eta(x_0)=\tfrac{1}{2}(1+\epsilon(x_0))=\begin{cases}1 \text{ if } x_0>0,\\ 0 \text{ if } x_0<0.\end{cases} \qquad \ldots\ldots(8)$$

Introducing the abbreviation

$$f(\mathbf{k}',\mathbf{k},x_0)=(\Phi_0,[T(-\mathbf{k}',x_0),T(\mathbf{k},0)]\Phi_0), \qquad \ldots\ldots(9)$$

one can write F and M in terms of dispersive and absorptive parts

$$D(\mathbf{k}',\mathbf{k},k_0)=\frac{i}{2}\int_{-\infty}^{\infty} dx_0 \exp(ik_0x_0)\epsilon(x_0)f(\mathbf{k}',\mathbf{k},x_0), \qquad \ldots\ldots(10)$$

$$A(\mathbf{k}',\mathbf{k},k_0)=\tfrac{1}{2}\int_{-\infty}^{\infty} dx_0 \exp(ik_0x_0)f(\mathbf{k}',\mathbf{k},x_0), \qquad \ldots\ldots(11)$$

as

$$F(\mathbf{k}',\mathbf{k},k_0)=D(\mathbf{k}',\mathbf{k},k_0)+i\epsilon(k_0)A(\mathbf{k}',\mathbf{k},k_0), \qquad \ldots\ldots(12)$$

$$M(\mathbf{k}',\mathbf{k},k_0)=D(\mathbf{k}',\mathbf{k},k_0)+iA(\mathbf{k}',\mathbf{k},k_0). \qquad \ldots\ldots(13)$$

We now specialize to consider forward scattering only, $\mathbf{k}'=\mathbf{k}=(0,0,k)$. One can then prove the following properties for $f(\mathbf{k},x_0)\equiv f(\mathbf{k},\mathbf{k},x_0)$:

If

$$\phi(-\mathbf{x},x_0)=\lambda\phi(\mathbf{x},x_0), \qquad \ldots\ldots(14)$$

where $\lambda=+1(-1)$ for a scalar (pseudo-scalar) boson field, then

$$T(\mathbf{k},x_0)=\lambda T(-\mathbf{k},x_0) \qquad \ldots\ldots(15)$$

$$f(\mathbf{k},x_0)=-f(\mathbf{k},-x_0) \qquad \ldots\ldots(16)$$

$$f(\mathbf{k},x_0)=f(-\mathbf{k},x_0); \qquad \ldots\ldots(17)$$

thus $f(\mathbf{k}, x_0)$ is a function of k^2 only, and we shall write $f(\omega, x_0)$ where

$$\omega = \omega_k = \{\mu^2 + k^2\}^{1/2}.$$

One can then prove that for real ω

$$f(\omega, x_0) = -f^*(\omega, x_0) \qquad \ldots\ldots(18)$$

i.e. $f(\omega, x_0)$ is purely imaginary. We can now rewrite equations (10) and (11) as

$$A(\omega) = i\int_0^\infty dx_0 \sin \omega x_0 f(\omega, x_0), \qquad \ldots\ldots(19)$$

$$D(\omega) = i\int_0^\infty dx_0 \cos \omega x_0 f(\omega, x_0), \qquad \ldots\ldots(20)$$

and from equations (19) and (20):

$$\begin{aligned} A(-\omega) &= -A(+\omega) \\ D(-\omega) &= D(+\omega). \end{aligned} \qquad \ldots\ldots(21)$$

We can express $A(\omega)$, equation (11), differently by inserting the unit operator $\Sigma_n \Phi_n)(\Phi_n$, between the two T-operators and extracting the time dependence of the matrix elements. One obtains

$$\begin{aligned} A(\omega) &= \tfrac{1}{2}\int_{-\infty}^{\infty} dx_0 \exp(i\omega x_0) \sum_n g_n(\omega)[\exp(-i\omega_n x_0) - \exp(i\omega_n x_0)] \\ &= \pi \sum_n g_n(\omega)[\delta(\omega - \omega_n) - \delta(\omega + \omega_n)] \end{aligned} \qquad \ldots\ldots(22)$$

where

$$g_n(\omega) = (\Phi_0, T(-\mathbf{k}, 0)\Phi_n)(\Phi_n, T(\mathbf{k}, 0)\Phi_0) \qquad \ldots\ldots(23)$$

and

$$\omega_n \equiv E_n - E_0. \qquad \ldots\ldots(24)$$

For $|\omega| < \mu$, we are dealing with the discrete set of bound states, and $A(\omega) = 0$ in this interval except at the bound-state energies $\omega = \omega_n$, and at $\omega = -\omega_n$. In particular, $A(\omega)$ vanishes throughout this interval if there are no bound states. In the above analysis, as throughout, we always assume that the time integration is carried out before the space integrations (our notation, $T(\mathbf{k}, 0)$, is perhaps misleading, but convenient). In fact, some convention such as this must be used, so that our definitions make sense in the range $|\omega| < \mu$, where k is imaginary, so that we would deal with exponentially divergent integrals. No such difficulty arises if the potential $V(\mathbf{x})$ vanishes outside some finite range or decreases sufficiently rapidly.

In the same way, we can overcome the difficulties when there are bound states. We have merely to consider, instead of $A(\omega)$, the quantity

$$A(\omega) \prod_n (\omega^2 - \omega_n^2), \qquad \ldots\ldots(25)$$

the product being over all bound states. In this way one obtains factors $(\omega \pm \omega_n)\delta(\omega \pm \omega_n)$ in equation (22), which again vanishes identically throughout $(-\mu, \mu)$. This way of treating bound states was suggested by N. Bogoliubov at the Seattle Conference.

To obtain dispersion relations, we now consider the integral

$$I = \frac{(\omega_{\mathfrak{b}}^2 - \omega_{\mathfrak{a}}^2)}{\pi} P\int_{-\infty}^{\infty} \frac{\omega\, d\omega}{(\omega^2 - \omega_{\mathfrak{b}}^2)(\omega^2 - \omega_{\mathfrak{a}}^2)} A(\omega) \prod_n \frac{\omega^2 - \omega_n^2}{\omega^2 - \alpha_n^2}. \qquad \ldots\ldots(26)$$

Here $\omega_{\mathfrak{b}}$ and $\omega_{\mathfrak{a}}$ are real, and we shall take $\omega_{\mathfrak{b}} > \omega_{\mathfrak{a}} \geqslant \mu$. Ignoring the last factor for the moment, the denominator $(\omega^2 - \omega_{\mathfrak{b}}^2)(\omega^2 - \omega_{\mathfrak{a}}^2)$ has been introduced to give convergence. (From the optical theorem, the total cross section is given by

$$\sigma_{\mathrm{T}}(\omega)=\frac{4\pi}{k}A(\omega). \qquad \ldots\ldots(27)$$

Hence, if $\sigma_{\mathrm{T}}(\omega)$ tends to a constant as $|\omega|\to\infty$, equation (26) will converge.) In the last factor we have introduced the denominators so as not to reduce the degree of convergence. The α_n are real numbers in $0<\alpha_n<\mu$, and we shall ultimately go to the limit $\alpha_n\to\omega_n$. Finally, all integrations over poles are to be taken as principal values.

Substituting equation (19) for $A(\omega)$ and changing the order of integration equation (26) becomes

$$I=\int_0^\infty dx_0\left[\frac{(\omega_{\mathrm{b}}^2-\omega_{\mathrm{a}}^2)}{\pi}P\int_{-\infty}^{\infty}d\omega\frac{\omega\sin\omega x_0}{(\omega^2-\omega_{\mathrm{b}}^2)(\omega^2-\omega_{\mathrm{a}}^2)}if(\omega,\,x_0)\left\{\prod_n\frac{\omega^2-\omega_n^{\,2}}{\omega^2-\alpha_n^{\,2}}\right\}\right]. \qquad \ldots\ldots(28)$$

The rigorous justification of this change of order of integration is very difficult; it has been discussed by Goldberger (1955).

We shall only briefly indicate how this expression is evaluated. We carry out the ω-integration by contour integration, replacing $\sin\omega x_0$ by $\exp(i\omega x_0)$. The contribution of the infinite semicircle in the half plane $Im\omega>0$ vanishes, since the integrand contains the factor $\exp\{i\omega x_0+i\mathbf{k}(\mathbf{x}-\mathbf{y})\}$. As $\omega\to i\infty$, this exponential will give convergence provided $x_0>|\mathbf{x}-\mathbf{y}|$, i.e. provided $(x-y)$ is time-like. This condition is satisfied: for on account of the causality condition, $[\phi(x),\,\phi(y)]=0$, if $(x-y)$ is space-like, only time-like vectors $(x-y)$ contributing to equation (28). In the resulting expression, the integrals over x_0 can be expressed in terms of $D(\omega)$ by means of equation (20). Finally, we proceed to the limit $\alpha_n\to\omega_n$ and obtain the dispersion relation

$$\begin{aligned}D(\omega_{\mathrm{b}})-D(\omega_{\mathrm{a}})&=\frac{2(\omega_{\mathrm{b}}^2-\omega_{\mathrm{a}}^2)}{\pi}P\int_\mu^\infty d\omega\frac{\omega A(\omega)}{(\omega_{\mathrm{b}}^2-\omega^2)(\omega_{\mathrm{a}}^2-\omega^2)}\\&\quad+2(\omega_{\mathrm{b}}^2-\omega_{\mathrm{a}}^2)\sum_n\frac{\omega_n}{(\omega_{\mathrm{b}}^2-\omega_n^{\,2})(\omega_{\mathrm{a}}^2-\omega_n^{\,2})}g_n(\omega_n). \qquad \ldots\ldots(29)\end{aligned}$$

In this equation, the terms on the left-hand side originate from the residues in equation (28) at $\omega=\pm\omega_{\mathrm{a}}$ and $\omega=\pm\omega_{\mathrm{b}}$. The first term on the right-hand side is the original expression I, equation (26), rewritten using the fact that the integrand vanishes in $(-\mu,\mu)$ and that $A(-\omega)=-A(\omega)$. The second term is the contribution from the residues at $\omega=\pm\alpha_n$, the summation being over all bound states. Equation (29) is completely analogous to Goldberger's dispersion relation and can similarly be rewritten in various ways, by using momentum instead of energy variables, taking the special case $\omega_{\mathrm{a}}=\mu$, etc.

§ 3. THE BOUND STATE CONTRIBUTION

We can express the bound-state contribution in equation (29), i.e. the last term:

$$B\equiv 2(\omega_{\mathrm{b}}^2-\omega_{\mathrm{a}}^2)\sum_n\frac{\omega_n}{(\omega_{\mathrm{b}}^2-\omega_n^{\,2})(\omega_{\mathrm{a}}^2-\omega_n^{\,2})}g_n(\omega_n), \qquad \ldots\ldots(30)$$

differently, bringing out its significance more clearly.

On account of the field equations (1) we can write

$$\begin{aligned}(\Phi_0,\,V(\mathbf{x})\phi(\mathbf{x},0)\Phi_n)&=(\Box^2-\mu^2)(\Phi_0,\,\phi(\mathbf{x},0)\Phi_n)\\&=(\omega_n^{\,2}-\mu^2+\nabla^2)(\Phi_0,\,\phi(\mathbf{x},0)\Phi_n)\\&=(2\omega_n)^{-1/2}(\omega_n^{\,2}-\mu^2+\nabla^2)\phi_n(\mathbf{x}), \qquad \ldots\ldots(31)\end{aligned}$$

where $\phi_n(\mathbf{x})$ represents the one-particle eigenfunction satisfying

$$H\phi_n(\mathbf{x}) = E_n\phi_n(\mathbf{x}).$$

Going over to momentum space,

$$\phi_n(\mathbf{x}) = \int d\mathbf{p} \exp(i\mathbf{px})\psi_n(\mathbf{p}), \qquad \ldots\ldots(32)$$

we know that $\psi_n(\mathbf{p})$ has the form (Salpeter 1951)

$$\psi_n(\mathbf{p}) = \frac{\chi_n(\mathbf{p})}{\omega_n{}^2 - (\mu^2 + \mathbf{p}^2)}, \qquad \ldots\ldots(33)$$

with χ_n in general non-vanishing at the bound-state energy. We thus have

$$(\Phi_0, V(\mathbf{x})\phi(\mathbf{x}, 0)\Phi_n) = (2\omega_n)^{-1/2} \int \chi_n(\mathbf{p}) \exp(i\mathbf{px})\, d\mathbf{p}, \qquad \ldots\ldots(34)$$

and from (4),

$$(\Phi_0, T(-\mathbf{k}, 0)\Phi_n) = \frac{(2\pi)^3}{(2\omega_n)^{1/2}}\chi_n(\mathbf{k}). \qquad \ldots\ldots(35)$$

In this way one finds

$$g_n(\omega) = \frac{(2\pi)^6}{2\omega_n} |\chi_n(\omega)|^2 \qquad \ldots\ldots(36)$$

where I have written $\chi_n(\omega)$, indicating that we are throughout only considering forward scattering and $\mathbf{k} = (0, 0, k)$. From equations (36) and (30) we finally obtain

$$B = (2\pi)^6(\omega_b{}^2 - \omega_a{}^2) \sum_n [(\omega_b{}^2 - \omega_n{}^2)(\omega_a{}^2 - \omega_n{}^2)]^{-1} |\chi_n(\omega_n)|^2. \qquad \ldots\ldots(37)$$

Thus the bound-state contribution can be expressed in terms of the residues of the wave functions in momentum space at the bound-state energies.

We have derived dispersion relations for the scattering of a spinless particle by an extended potential. Our final result is given in equation (29). The problem which we have here considered is too idealized to allow comparison with experiment and corresponds to the scattering of mesons by a nucleus described by an optical model with a real potential. In order to allow for inelastic events one requires, of course, a complex potential. It is hoped to treat this more realistic problem in due course.

ACKNOWLEDGMENTS

It is a pleasure to express to Professor A. Salam my indebtedness for several lengthy discussions about dispersion relations and for a full report on the Seattle Conference, in particular on the treatment of bound states as proposed by N. Bogoliubov.

REFERENCES

GELL-MANN, M., GOLDBERGER, M. L., and THIRRING, W. E., 1954, *Phys. Rev.*, **95**, 1612.
GOLDBERGER, M. L., 1955, *Phys. Rev.*, **99**, 979.
VAN KAMPEN, N. G., 1953, *Phys. Rev.*, **91**, 1267.
LEHMANN, H., SYMANZIK, K., and ZIMMERMANN, W., 1955, *Nuovo Cim.*, **1**, 205.
LOW, F. E., 1955, *Phys. Rev.*, **97**, 1392.
SALPETER, E. E., 1951, *Phys. Rev.*, **84**, 1226.

The Multiple Scattering of Positrons and Electrons

By C. HENDERSON and A. SCOTT
Department of Physics, University College London

Communicated by H. S. W. Massey ; MS. received 14th November 1956

Abstract. The multiple scattering of electrons and positrons at an energy of 0·4 MeV has been measured with a scintillation counter. The difference between the distribution width for electrons and that for positrons after scattering by aluminium, silver and gold is smaller than previous measurements have indicated, and is given approximately by the calculations of Mohr.

Further work with electrons only, using silver and Ilford G5 emulsion as the scattering foil material shows good agreement with the theory of Molière.

§ 1. Introduction

Experiments show that at electron energies greater than 1 MeV there is substantial agreement with the Molière (1948) theory of multiple scattering. The results of Hisdal (1952), who measured the scattering of electrons in G5 emulsions at 0·59 MeV show a distribution some forty per cent narrower than the theory predicts. Cusack and Stott (1955), working with a cloud chamber, present results which could be interpreted as a deficiency in scattering at 0·4 MeV. Heymann and Williams (1956) survey work using nuclear emulsions which again shows the possibility of a systematic divergence of theory and experiment with decreasing energy.

Experimental evidence for the difference in multiple scattering between electrons and positrons is sparse and contradictory. Groetzinger, Humphrey and Ribe (1952), using a cloud chamber, found the r.m.s. value for the angle of multiple scattering for positrons in argon to be less, by approximately 10%, than for electrons at energies between 0·3 and 2 MeV. This is much greater than the 1% predicted by the calculations of Mohr (1954). Cusack and Stott, working with greater accuracy, found no statistically significant difference. Bosley and Hughes (1955), using nuclear emulsions at 10 MeV show a difference of 15% between the scattering constants of electrons and positrons, compared with less than 1% calculated by Mohr for these conditions.

The experiments to be described were designed to provide further information on both topics—the possible deviations from Molière's theory at energies below 1 MeV, and the ratio of positron to electron multiple scattering. The apparatus was such that the detailed shape of the distribution could not be found with great accuracy. In interpreting the results, the Molière shaped distribution which gave the best fit to the experimental data has been compared with the Molière distribution calculated for the measured thickness of the foil. The Molière distributions used were derived from the paper of Bethe (1953), which takes into account the scattering by the atomic electrons.

§ 2. Apparatus

The large β-ray spectrometer described by Rundle, Ellis, Griffith and Tomlinson (1954) provided a strong flux of the particles required, in the form of a converging hollow conical beam. The same equipment was used by Ellis and Henderson (1955) in single scattering measurements on positrons and electrons, but a much more strongly collimated beam was possible in the experiments described in this paper, because of the larger numbers of the counts in the multiple scattering region. A further improvement was the introduction of a brass plate which could be moved in front of the radioactive source, entirely cutting out the primary beam when necessary. The essentials of the experiment are shown in figure 1.

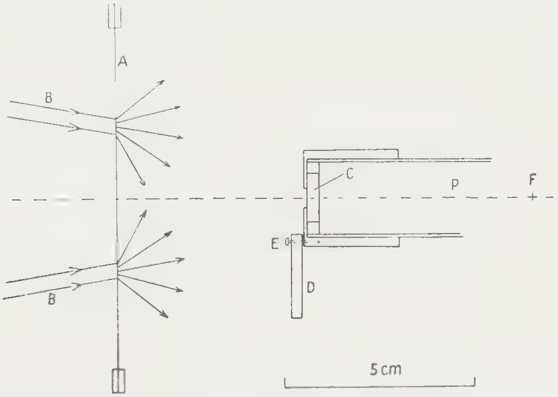

Figure 1. The scattered beam and crystal counter.

The beam of particles B converges as a hollow cone towards the focus F. The scattering foil A intercepts and spreads this beam along the axis, where it is measured by the scintillations from an anthracene crystal C supported upon the long Perspex light pipe P. The acceptance of the crystal is defined by a hole of diameter 5 mm in a thin brass plate. The Perspex rod is connected rigidly to a photomultiplier and the whole unit is mounted axially with respect to the outer vacuum tube of the spectrometer, in which it can slide, its axial position being controlled by spacing rods. The purpose of the light pipe P is to keep the photomultiplier out of the magnetic field of the spectrometer coils. D is a disc of Perspex, pivoted at E, which closes the aperture to charged particles when the counting unit is rotated through 180° about its own axis.

§ 3. Experimental Details

3.1. *The Scattering Geometry*

The energy of the experiments concerned with the electron–positron ratios was decided by the theoretical predictions of Mohr existing at the time, and by the positron sources available. Copper 64 offered the best compromise, having a somewhat lower energy than desired, but with the excellent property of providing roughly equal numbers of positrons and electrons at 0·4 Mev, the energy finally chosen. An axial helical baffle in the spectrometer transmitted either a pure electron beam or a pure positron beam depending upon the direction of the current in the spectrometer coils.

Much attention was given to the production of a well defined primary beam by the careful choice and modification of the spectrometer baffle system. Measurements were made of beam shape and size by means of photographic films placed perpendicularly to the axis and at various distances along the axis of the system. The axial distribution of the unscattered beam was also measured, using the scintillation counter. By combining the above information the beam was found to consist of rays converging to the axis at nearly 10°, having an angular spread of less than 1°, but with a radial width of about 4 mm. The beam cross section at the scattering foil was annular, bounded by radii of 1·7 and 2·1 cm.

The radial distribution of particles at the foil position was determined by a separate experiment in which a series of concentric apertures of progressively decreasing radii were placed in turn at the foil position. A large crystal capable of accepting the complete flux was situated at the focus and the way in which this flux decreased with decreasing aperture gave the desired distribution of the primary beam at the foil.

3.2. *The Radioactive Sources and the Scattering Foils*

In the experiments for determining the difference between electron and positron multiple scattering the sources were in the form of a disc of pure copper having a diameter of 5 mm and a thickness of 0·005 inch. Appreciably thicker sources gave increased numbers of particles but a relatively larger background of annihilation gamma rays due to the self absorption of positrons by the source. The copper disc was mounted in a small aluminium holder and the material was activated by an exposure of one week to neutrons in the pile at Harwell. In exploratory experiments the aluminium holder was unnecessarily large and the 1·39 MeV β activity of 14·9-hour ^{24}Na produced in the reaction Al–n–α was observed as a time variation of the electron positron ratio of the primary beam. The initial activity of the copper was about 10 mc permitting the experiments to start with primary beams of some 60 000 pulses per minute, with a half-life of 12·9 hours. An indium source of half-life 48 days, having the same diameter as the copper, was used in the experiments involving electrons only.

The scattering foils of gold and silver were prepared by vacuum evaporation of the pure metals from an eight-filament jig designed to give high uniformity over the regions used in the experiment. A backing of thin Melinex film enabled a flat, mirror-like surface to be obtained. The foil of Ilford G5 emulsion was obtained by stripping a film of about 25μ from its glass plate. This film was then cut to a circular shape and fixed to a rigid ring shaped aluminium foil holder of greater diameter by means of an interposed annulus of thin rubber sheet. The presence of this rubber annulus was necessary to prevent the foil cracking as it dried under vacuum conditions. This foil was weighed at zero moisture content immediately after the experiment in which it was used. No use was made of the electron-sensitive properties of the G5 emulsion, the material acting purely as a scattering foil.

3.3. *Procedure*

With the scattering foil removed the counter was placed at the focus to give a measure of the incident flux of electrons and positrons in turn. This measurement was repeated at intervals to check that the ratio of the numbers of particles remained constant, and that they decayed with a 12·9-hour half life. The scattering foil was then placed in position and a series of five-minute background counts taken with the Perspex plate over the counter aperture, alternating with overall checks of the stability of the counting system, as described by Ellis and Henderson

(1955, p. 270). An improvement in the present work was that, during these stability checks, the primary beam was cut off entirely by a brass plate placed in front of the radioactive source.

Five-minute electron counts were then taken using the same procedure. The whole experiment was carried out for positrons, but with the background counts taken last to avoid rotating the counter between the electron and positron counts. The amplifier was set to give a pulse height of twelve volts for the energy of the particles selected, and all pulses over six volts were counted.

The counter was then moved to a different axial position and another set of results taken, continuing in this manner to obtain the axial distribution of the scattered electrons and positrons. By so working the electron–positron ratio was determined in a way that minimized uncertainties in the decay exponent of the source. The lowest signal to background ratio was about ten.

§ 4. ANALYSIS OF RESULTS

4.1. *Absolute Distribution Widths*

It was necessary to be sure that the difference of counts with and without the Perspex absorber gave a correct measure of the scattered charged particles, subtracting away any true gamma background without introducing any extra due to bremsstrahlung, or due to annihilation radiation in the case of positrons. The measurement of the primary beam with the counter at the focus gave the necessary assurance. For example, the counting rate with positrons at 70 000 pulses per minute became 360 with the Perspex in position. Corresponding counts for electrons were 45 000 and 10. The maximum uncertainty was thus only 0·5% which was less than the statistical error associated with the 10 000 counts taken at each axial position.

Due to the radial spread of the primary beam it was not possible to derive the multiple scattering distribution directly from the observed axial distribution. The calculated data of table 1 were obtained from the Molière distributions corresponding to the actual foil thickness, including the effect of the Melinex backing, at the energy of the experiment. The half-width ω of the Molière distribution is the angle at which the intensity falls to a factor $1/e$ of its maximum value. It is, therefore not equal to $\chi_c B^{1/2}$ which is the half-width of the gaussian part of the Molière distribution. The data designated 'observed' were obtained using the Molière distribution which gave a predicted axial distribution in best agreement with the experimental one. To do this Molière distributions corresponding to slightly

Table 1. Comparison of the Observed and Calculated Half-widths ω of the Molière Distributions

1	2	3	4	5	6	7	8	9	10
0·40	Au	1·98	0·45	17	4·06	2·62	18·7°	19·8°	+5
	Ag	2·64	0·45	31	4·96	2·29	19·3°	18·3°	−6
	Al	6·04	none	83	6·03	1·64	18·0°	18·8°	+4
0·59	G5	9·34	none	90	6·17	3·18	25·4°	25·2°	−1
	Ag	2·64	0·45	29	4·85	1·20	13·8°	13·2°	−4
1·2	Ag	2·64	0·45	26	4·71	0·367	7·54°	7·25°	−4

1, Energy (MeV), 2, Material, 3, Thickness (mg cm^{-2}), 4, Backing, Melinex, 5, Ω_0, 6, B, 7, $\chi_c{}^2 \times 10^2$, 8, ω_{calc}, 9, ω_{obs}, 10, $(\omega_{\mathrm{obs}}-\omega_{\mathrm{calc}})/\omega_{\mathrm{calc}}$ (%). Ω_0 is the number of scatters in traversing the foil (see Molière 1948, p. 82). 5, 6, 7 and 8 are for measured thickness.

different foil thicknesses, in the vicinity of the measured thickness, were used to evaluate predicted axial distributions. The best Molière distribution was selected by a criterion of least percentage squares between the experimental and predicted axial distributions. Figure 2 shows such a comparison for the gold foil at 0·4 Mev. Here the experimental points are shown circled, but, to avoid confusion, the theoretical points are not shown in the figure. The full line passes through the computed points corresponding to the best fit and the broken line passes through the points calculated entirely from the measured foil thickness, including Melinex backing. The difference between theory and experiment is then taken as the difference in parameters of the Molière distributions from which the two theoretical axial distributions were derived.

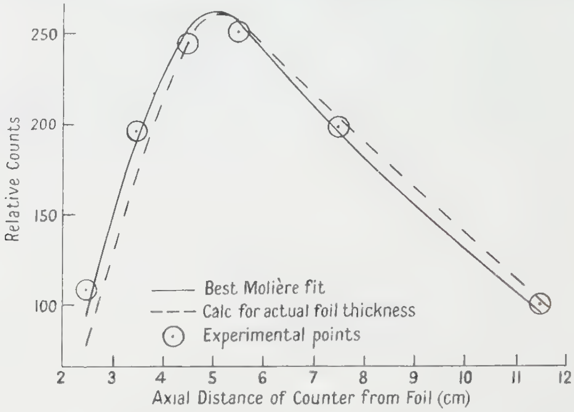

Figure 2. Theoretical and experimental axial distributions, for gold at 0·4 Mev.

In determining the best fit the results for the counter position nearest to the foil were not used since they correspond to scattering angles near 30° where the $\sin\theta = \theta$ approximation of the Molière theory is not good and where also the narrowing of the solid angle of acceptance of the counter aperture due to its finite thickness is over 10%. This effect of counter aperture thickness as well as the variation in radial intensity at the scattering foil is included in the numerical computations to find the theoretical axial distributions.

4.2. *Differences in Electron and Positron Distributions*

To evaluate the difference in multiple scattering between electrons and positrons the following procedure was used to minimize any arbitrariness in interpretation. Consider the ratios of counts for gold shown in figure 3.

Making the assumption that the Molière distributions for electrons and positrons differed only in the size of the parameter $\chi_c^2 B$ the calculated values of the ratios were derived from the series of trial Molière distributions already to hand from the curve fitting described in the previous section. It is true that these trial values correspond to Molière distributions for foils of slightly varying thickness whereby χ_c^2 and B varied separately. Nevertheless, the major change over the range of about 15% in thickness used in the calculations is due to the change in $\chi_c^2 B$, the effect of B alone in the Molière expansion $B^{-1}f^{(1)} + B^{-2}f^{(2)}$ (see Bethe 1953, eqn 25) being much smaller. This remark applies equally well to the figures of table 1.

It was found that for a given scattering foil, if the electron–positron ratios calculated from Molière distributions with a given difference of $\chi_c^2 B$ were plotted against the cube of the counter to focus distance, a straight line resulted. The slope of this line depended on the difference of $\chi_c^2 B$ assumed. Further this slope itself varied linearly with the difference of $\chi_c^2 B$ over the small range involved.

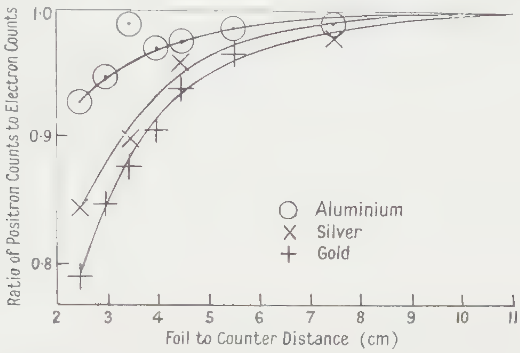

Figure 3. Positron–electron ratios as a function of the axial position of the counter. Normalized to unity at approximately 11 cm, corresponding to zero angle of scatter.

Hence the observed ratios were plotted against the cube of the distance from foil to counter; a best straight line obtained by a least squares fit and the slope of this line could then be directly interpreted as a definite difference in $\chi_c^2 B$. The standard deviation of this difference was evaluated, and is included in table 2.

Table 2. The Percentage Difference in Widths of the Gaussian Part of the Multiple Scattering Distributions for Electrons ω_{g-} and Positrons ω_{g+} at 0·4 MeV.

Material	Au	Ag	Al	
$\frac{\omega_{g-}-\omega_{g+}}{\omega_{g-}}$ (%)	5·79 ± 0·46	4·60 ± 1·04	1·19 ± 0·70	1·56 ± 0·55†.

† Obtained when the point exceptionally far from the smooth curve for aluminium (see figure 3) is excluded from the analysis.

§ 5. Discussion

Since the analysis of the experiment is based on the theory of Molière it is necessary to consider how well this theory can be expected to apply here. Four corrections will be discussed. They are the effect of the $\sin\theta=\theta$ approximation, deviations from the Rutherford single scattering law, U. Fano's (1954) modification of the inelastic scattering correction, and uncertainties connected with the rather thin foils used.

Bethe (1953 eqn 58) shows that the Molière distribution can be made applicable to higher angles by the corrective multiplying factor $(\theta/\sin\theta)^{1/2}$. The largest effect in the present experiment is for the G5 emulsion and produces an increase in width of about $\frac{1}{2}\%$, and is hardly significant.

The effect of deviations from the Rutherford single scattering formula due to relativistic effects are difficult to estimate. They will be at their largest for the G5 emulsion, because its relatively high effective Z is combined with a broad multiple scattering distribution. If the correction factor of Spencer and Blanchard (1954) is assumed, in which the ordinates of the Molière distribution are increased by a factor of exact cross section/Molière's cross section, then the calculated width for the G5 emulsion could be increased by as much as 5% and the gold and silver by 2%. These figures are likely to give an upper limit to the correction rather than a reliable estimate under the conditions of this experiment.

The correction of Fano takes into account the difference in cut-off angles for electron–nuclear and electron–electron collisions. There is an error, pointed out by Williams (1956), in Fano's equation (17), repeated in the summary, where the term in $zZe^2/\hbar v$ should appear squared. This correction is a maximum for the aluminium foil, where the Molière width is increased by 1%.

The thickness of the foils used was governed by the requirement that the bulk of the distribution should be in the range 0° to 30°, which was best suited to the apparatus. To satisfy this condition the number of collisions (see table 2) made by the particles in traversing the foils of silver and gold were somewhat small. Molière (p. 93) estimates the errors of his theory to be about 1% when Ω_0 is twenty, whilst Bethe (p. 1259) finds errors of approximately $1/\Omega_0$. The thickness of the G5 emulsion corresponds closely to the cell length of $17{\cdot}5\mu$ used by Hisdal.

The corrections discussed above are small, and can have little effect on the calculations of the ratio of positron to electron multiple scattering.

§ 6. CONCLUSION

The results show that pronounced deviations from the Molière theory do not occur. This is in direct contradiction of the G5 experiments of Hisdal.

Further the electron–positron ratios shown in table 2 are at most some 6% for gold and in general are compatible with extrapolations of the calculations of Mohr and of Tassie (1956). They are much smaller than the differences reported by Groetzinger *et al.* and by Bosley and Hughes.

ACKNOWLEDGMENTS

The authors wish to express their thanks to Professor H. S. W. Massey for his interest in the work described here, to Mr. R. A. Hudson of the Plastics Division, I.C.I., for his efforts in making the especially thin Melinex film which he gave us, to Dr. C. Waller, of Ilford Limited, for providing the thin G5 emulsion, and to the staff of the Departmental and Rocket Research workshops for their technical advice and for making apparatus.

REFERENCES

BETHE, H. A., 1953, *Phys. Rev.*, **89**, 1256.
BOSLEY, W., and HUGHES, J. S., 1955, *Phil. Mag.*, **46**, 1281.
CUSACK, N., and STOTT, P., 1955, *Phil. Mag.*, **46**, 632.
ELLIS, J., and HENDERSON, C., 1955, *Proc. Roy. Soc.* A, **229**, 260.
FANO, U., 1954, *Phys. Rev.*, **93**, 117.
GROETZINGER, G., HUMPHREY, W., and RIBE, F. L., 1952, *Phys. Rev.*, **85**, 78.
HEYMANN, F. F., and WILLIAMS, W. F., 1956, *Phil. Mag.*, **1**, 212.
HISDAL, E., 1952, *Phil. Mag.*, **43**, 790.
MOHR, C. B. O., 1954, *Proc. Phys. Soc.* A, **67**, 730.
MOLIÈRE, G., 1948, *Z. Naturforsch.*, **3a**, 78.
RUNDLE, G. P., ELLIS, J., GRIFFITH, T. C., and TOMLINSON, H. S., 1954, *Proc. Phys. Soc.* B, **67**, 52.
SPENCER, L. V., and BLANCHARD, C. H., 1954, *Phys. Rev.*, **93**, 114.
TASSIE, L. J., 1956, *Austr. J. Phys.*, **9**, 54.
WILLIAMS, W. F., 1956, *Thesis*, University of London.

Protons from the Interaction of 14 MeV Neutrons with Medium Weight Nuclei

By D. L. ALLAN
Atomic Energy Research Establishment, Harwell, Didcot, Berks.

MS. received 14th August 1956, and in final form 11th December 1956

Abstract. The energies of the protons emitted by ^{27}Al, ^{54}Fe, ^{56}Fe, ^{58}Ni, ^{60}Ni, and ^{63}Cu when bombarded by 14 MeV neutrons have been determined using a photographic plate method. In addition, the angular distribution of the protons emitted by ^{63}Cu has been measured. The energy distribution of the protons is consistent with some of them being produced by the (n, np) reaction and others by a direct interaction. Rough cross sections for these processes are given; in the course of the work a cross section of 10 ± 4 mbn has been measured for the reaction ^{54}Fe (n, 2n). The results, generally, are in good agreement with the statistical and direct interaction theories.

---

§ 1. Introduction

The determination of the energy distribution of neutrons and protons inelastically scattered by medium weight nuclei in the energy region 14–18 MeV has received considerable attention in recent years (e.g. Graves and Rosen 1953, Gugelot 1954). The work now reported was begun in order to compare the energy distribution of protons from (n, p) reactions with the results of the inelastic scattering experiments. A brief report of a determination of the energy distribution of protons from the reaction Cu (n, p) Ni at 14 MeV appeared in a recent research note (Allan 1955). A photographic plate technique was used in this study, and the most significant feature of the results was that a large proportion of the tracks observed (85%) had ranges corresponding to proton energies well below the coulomb barrier energy (7 MeV). According to the statistical theory of nuclear reactions (Weisskopf and Ewing 1940) the emission of protons with energies below the barrier energy should be strongly inhibited by the competition from neutron emission.

Three hypotheses might account for these results: (i) The short range tracks, which look as if they were produced by low energy protons might, in fact, have been produced by deuterons of higher energy. (ii) The coulomb barrier might be lower for highly excited nuclei than for nuclei in their ground states. (iii) The low energy protons might come from the (n, np) reaction.

This paper is concerned with an investigation of these hypotheses.

§ 2. Method

The first of these possibilities (i) was investigated by careful grain counting of the tracks; however, it was not possible to resolve such short tracks into proton and deuteron groups. A further test of (i) was made by determining the range distributions of the tracks from a Cu target at angles 0°, 45°, 90° and 120° to the incident neutrons. If deuterons are produced, they should result from a pick-up process, and consequently marked anisotropy should be apparent in their angular distribution.

The second and third possibilities were investigated by determining the yields and energy distributions of protons from a number of targets prepared from separated isotopes. This work will be discussed in § 6.

§ 3. Apparatus

The target chamber is shown in figure 1 (*a*). An evacuated brass cylinder of 1⅝ in. diameter and 1/16 in. wall thickness contained the target and the photographic plate. To ensure that as few protons as possible were ejected from parts of the apparatus near the source, the targets were attached to a 4 cm diameter circular disc of 0·02 in. gold sheet ('end disc') placed inside the cylinder at the end nearer the neutron source. The cylindrical walls were also lined internally with 0·02 in. gold sheet to prevent protons from the brass walls reaching the plate. Ilford C_2 photographic plates, 3 in. by 1 in. and 300 μ thick, were clamped in a plate holder making an angle of 10° with the axis of the cylinder, the mid-point of the plate being 8 cm from the surface of the gold end disc.

The targets were in the form of strips 1 cm wide and varied in thickness from 5 to 12 mg cm^{-2}. Where available as metal foils, they were laid on the end disc, bent over, and fixed to the back of the disc with soft wax. The cylindrical gold lining clamped over the bent portion of these foils and the extra thickness at the bends was not visible at the plate. Separated isotopes were electroplated directly on to the end discs.

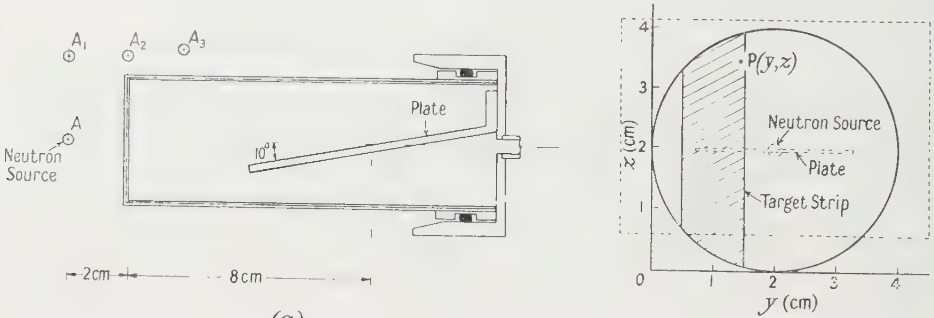

(*a*) (*b*)

Figure 1. (*a*) Target chamber, (*b*) end disc and coordinate system.

The source of neutrons was the ^{3}H (d, n) ^{4}He reaction in which 250–300 kev deuterons bombarded a zirconium tritide target. The target chamber was placed with the end disc 2 cm from the source and with its axis making an angle of 90° with the deuteron beam. It was essential to place the targets close to the neutron source in order to minimize the flux of direct neutrons at the centre of the plate relative to that at the target.

§ 4. Experimental

4.1. *General Procedure*

The irradiation of the targets continued until they had received an integrated flux of $1{\cdot}4 \times 10^{10}$ neutrons cm^{-2}, corresponding to a flux of $5{\cdot}6 \times 10^{8}$ neutrons cm^{-2}

at the centre of the plate. This flux was determined by counting the α-particles emitted by the source into a known small solid angle.

The plates were scanned across their width, starting at the centre and proceeding strip by strip towards the targets. Only tracks entering the surface of the emulsion from the direction of the end disc were measured. However, owing to the finite depth of focus of the microscope objective, tracks originating within the top $1\,\mu$ layer of the emulsion could not be distinguished from those caused by charged particles from outside. 85% of the measured background was due to this cause, the remainder came from the gold end disc. About half of the background was caused by high energy proton recoils with ranges well outside the main region of interest in this work. Most of the short range background was found to be caused by protons from the bromine content of the emulsion.

The background was kept low by ensuring that only tracks of particles which could have come from the targets were accepted for analysis. For this purpose, the points of origin P (figure 1 (*b*)), real or apparent, in the plane of the end disc were calculated. The coordinates y of points P were obtained from the position and horizontal angle of each track, and z from the position and dip of the track. Tracks originating at points outside the dotted square were rejected at the time of measurement by referring to tables, but the coordinates of all other tracks were computed later. Figure 2 shows a plot of such points of origin observed when the target was a 1 cm wide deposit of ^{58}Ni.

4.2. *Energy Distributions*

In the earlier work, in order to measure the background, separate runs were made with and without the target strip. The background subtraction was not always satisfactory, particularly for higher energies, because of slight day to day changes in the track selection criteria applied by the scanner, and to small differences in the quality of the plates. This difficulty was overcome in the later work now reported by placing the target strip in the position shown in figure 1 (*b*), for this enabled the tracks from the target to be measured at the same time and in the same plate as the corresponding background tracks. In this arrangement, apart from the presence of the target strip on one side, there is complete symmetry between the two sides of the plane through the neutron source and the line $y = 2$ cm. Tracks with y coordinates between 0·25 cm and 1·75 cm were regarded as coming from the target, those with y coordinates between 2·25 cm and 3·75 cm were regarded as background. The two sets of tracks were both present in the plate and the observer could not know to which set a track belonged until the analysis was completed. Thus, observer bias was completely eliminated.

Range histograms, corrected for background, were plotted at $4\,\mu$ range intervals for each target. Small corrections were applied to the range measurements to allow for the average dip angle of the tracks in the emulsion, and to the energy spectra derived from them to allow for target thickness. The background at the peak of the energy spectrum varied from 11% to 25%, according to the yield of the target.

4.3. *Angular Distribution*

The method of determining the energy spectra of protons at angles 45°, 90° and 120° to the incident neutrons was essentially the same as described in the previous paragraph. The positions of the Cu target and plate remained the same, but the chamber was placed so that the neutron source appeared at A_1, A_2, and A_3 in successive exposures (figure 1 (*a*)). The source was always in the plane of symmetry through $y = 2$ cm and therefore the principle of background measurement and subtraction remained unchanged, although the magnitude and range distribution of the background changed considerably. The spectrum at 0° was determined by placing the Cu target in the central position as described below.

The relative yields of tracks at different angles could be obtained from these observations, but the calculation of differential cross sections required some rather uncertain corrections to allow for the very different neutron flux distributions along the length of the target strip as the source position changed. In order to avoid these corrections a comparison was made of the yields at 0° and 90° using a different arrangement. The target strip was placed on the end disc along the line $y = 2$ cm, and the chamber was placed as in figure 1 for the 0° measurements, but with the target 2·5 cm from the neutron source. The chamber was then rotated through 90° about $y = 2$ cm for the 90° measurements. With the target strip in the central position separate background exposures were necessary at each angle, but the background was made smaller than usual by using a thicker target. The neutron flux in this arrangement required a correction for variation across the foil; it was very small.

4.4. *Grain Density Measurements*

Grain density comparisons were made by placing two target strips on the end disc, a copper target at $y = 1$ cm, and a layer of deuterated paraffin wax at $y = 3$ cm. The wax target was covered with two different thicknesses of gold foil in order to reproduce a continuous spectrum of recoil deuteron tracks with approximately the same range distribution as the proton tracks from the copper. Thus, a mixture of proton tracks from the copper target and deuteron tracks, which could be identified by the usual method of determining the track origin, occurred in the same plate, and each set could be compared directly with neighbouring long range proton recoil tracks. Grain counts were made over the last $60\,\mu$ and $120\,\mu$ of tracks which had been selected to have ranges corresponding to 3–5 Mev protons, and ends which were free from dip. In order to avoid errors due to the differential development of the plate, the selection of the tracks was arranged so that comparisons were made on neighbouring track ends at approximately the same depth in the emulsion.

4.5. *Cross Section Measurements*

Cross sections were determined, in the first instance, by a double target method similar to that described in the preceding section. The yield from a standard Cu target placed at position $y = 1$ cm was compared with that from other targets placed at $y = 3$ cm. Histograms, representing the number of tracks with origin coordinates $z = 0{\cdot}5$–4 cm, $y = 0$–4 cm, were plotted against y at 0·5 mm intervals. These were in the form of double peaks representing the relative yields from the targets. After subtracting a background distribution obtained from a separate exposure, the numbers of tracks in each peak gave the yields and cross sections relative to copper.

Absolute cross sections required a knowledge of the neutron flux at the targets and of the solid angle for proton detection inside the chamber. The neutron flux in the double target experiments was assumed to have the calculated value of $1{\cdot}4 \times 10^{10}$ neutrons cm^{-2}. The internal solid angle was measured by replacing the target with a ^{239}Pu deposit of the same shape and of known activity. A plate was exposed in the usual position to give a convenient α-track density, and the solid angle for any number of plate search strips was simply related to the number of α-tracks found in the same number of strips. The agreement between the measured and calculated solid angle was very good.

In order to retain the advantages of simultaneous background measurement a second series of exposures with single targets was made. All the cross section measurements suffered from uncertainties arising from the close proximity of the targets to the neutron source. The size of the deuteron beam spot on the zirconium tritide target was not negligible compared with the neutron source–target distance, and its tendency to wander during an exposure could have caused large errors. In a number of exposures with single targets the neutron flux was determined by using a copper foil detector in which the activity produced by the ^{65}Cu(n, 2n) reaction was measured. The foil was placed in the position of the target strip; its activity was then compared with that induced in similar foils placed at 5, 8 and 10 cm from the source, at which distances the neutron flux could be reliably calculated from the α-particle monitor. The yield of protons from different portions of the target strip varies considerably, as is demonstrated by the variation of the density of points in figure 2. Although the correct area over which the neutron flux should be measured was calculated for a fixed point source, no correction could be applied to allow for the fact that the neutron source wandered during an exposure. The measured neutron flux varied from exposure to exposure from $1{\cdot}2$ to $1{\cdot}6 \times 10^{10}$ neutrons cm^{-2} for the same total neutron emission, indicating that the source–target disposition was not constant. The average of eight such measurements agreed with the calculated flux of $1{\cdot}4 \times 10^{10}$ neutrons cm^{-2}.

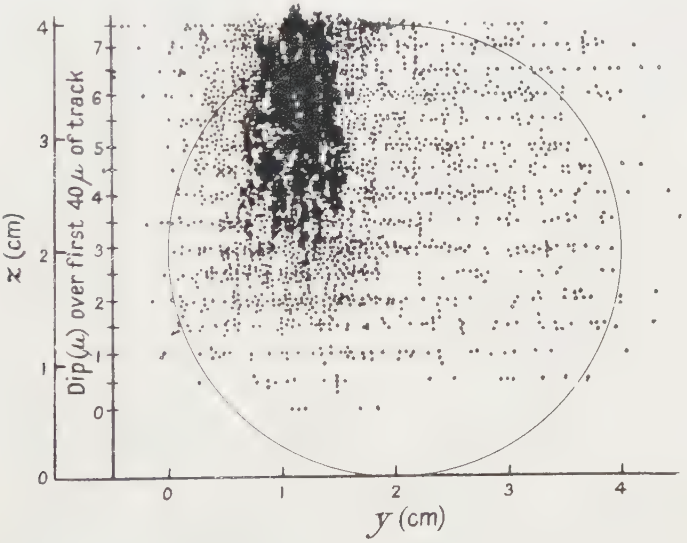

Figure 2. Points of origin (P) of protons in plane of end disc.

The cross section figures given in § 5.4 are the best averages derived from all the measurements available. From the scatter of values from two targets for which 4 or 5 independent measurements had been made, the error on all the cross section figures is estimated to be ± 20%.

§ 5. RESULTS

5.1. *Energy Distributions*

The proton energy distributions are shown in figure 3. The angle of observation was 34 ± 20° with respect to the incident neutrons. The errors shown are the statistical errors derived from the track counts of the target and background data. The statistical accuracy deteriorates above 12·5 MeV and the points are rather scattered because of the large number of 14 MeV recoils measured in this region.

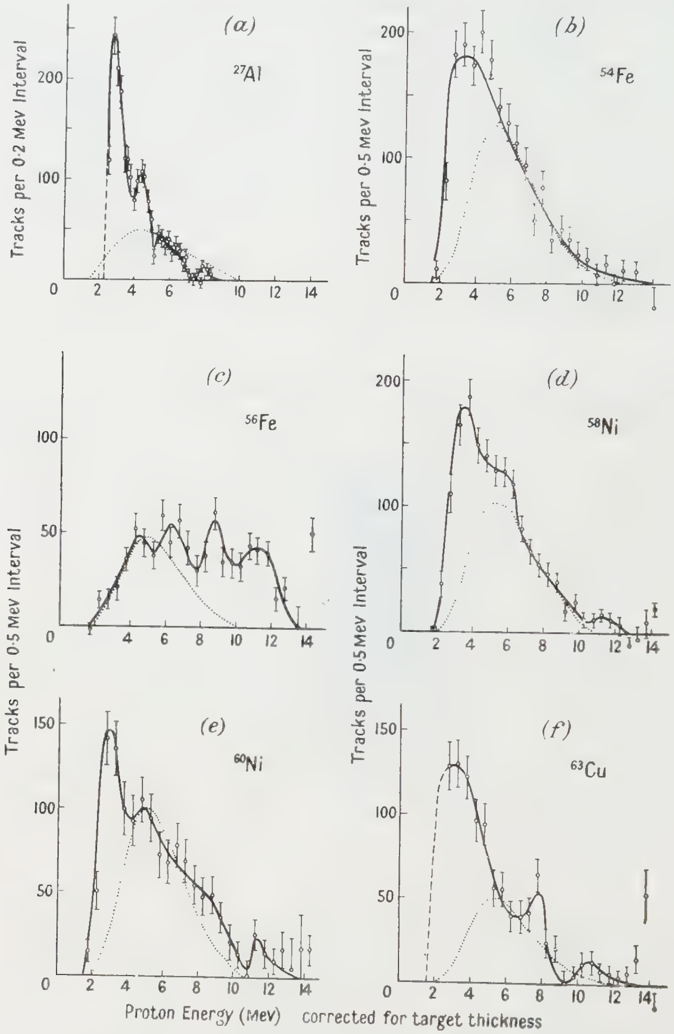

Figure 3. Proton energy distributions.
(In the ordinate scale, background is subtracted.)

The scatter of the points is due to the fact that a slight error in the alignment of the chamber causes a small shift in the balance of both the number and the energy of recoil protons apparently coming from the two sides of the gold end disc. Because of the large numbers involved (100 to 200 tracks per point) the scatter of points caused by this shift is quite large compared with the rest of the distribution, and any features above 12·5 MeV are likely to be spurious. Below 12·5 MeV the background is particularly low and the small peaks observed between 10 and 12·5 MeV are believed to be genuine.

It was found that α-particle emission from ^{27}Al, although small, was not negligible, and for most of the exposures the less sensitive E_1 type photographic plates were used in order to improve the discrimination against them. The use of E_1 plates resulted in some of the very long range tracks being missed, and the observations above 9 MeV are therefore unreliable. For this reason no points are given in the ^{27}Al spectrum above 9 MeV.

With the exception of ^{54}Fe which contained 33% ^{56}Fe, and ^{63}Cu for which a foil of natural Cu was used, all the targets used were close to 100% of isotopic purity. The curve drawn for the ^{54}Fe distribution has been corrected for the ^{56}Fe content. No such correction was necessary in the case of ^{63}Cu because an experiment with a ^{65}Cu target failed to resolve target protons from the background.

The dotted curves represent the proton energy distributions for 14 MeV (n, p) reactions calculated on the basis of the statistical theory. The calculated curves have been adjusted to fit the experimental curves at a proton energy between 5 and 7 MeV (see § 6). In these calculations the formula for level density as a function of the excitation energy U derived from equation (27) in a paper by Lang and Le Couteur (1954) was used, together with the nuclear temperature given by $U=\frac{1}{8}At^2-t$. The coulomb barrier penetrabilities were obtained from the tables of Blatt and Weisskopf (1952).

It is apparent that in no case does the calculated distribution fit the whole of the measured distribution. For ^{56}Fe the fit is good at low energies but there is a considerable excess of high energy protons. In all the other spectra there is a reasonable fit at the higher energies but a large excess of low energy protons.

5.2. *Angular Distributions*

The energy distributions from a 28 mg cm^{-2} Cu target at angles 0°, 45°, 90° and 120° (each ± 20°) are given in figure 4 (*a*–*d*). The curves have been adjusted so that the area beneath each for proton energies less than 8 MeV is the same.

The spurious effects due to 14 MeV proton recoils become progressively worse as the angle is increased because the neutron source is placed nearer to the plate as it moves from A to A_3 (figure 1 (*a*)). The lower limit of the recoil track group also occurs at a lower energy because of the steeper angle of approach of the neutrons to the plate, until at 120° the observations above about 8·5 MeV are probably all spurious.

The yields of protons at 90° and 0° were compared by the method referred to in § 4.3. The ratios of the yield at 90° to the yield at 0° for protons of energy less than 8 MeV and less than 5 MeV were each unity to an accuracy of 15%. This result, and the fact that the shape of the spectrum does not change between 0° and 120°, strongly suggests that the angular distribution is isotropic.

5.3. *Grain Density Measurements*

The results obtained from histograms of grain counts on the last 60 μ and 120 μ of proton (P) and deuteron (D) recoils are given in table 1.

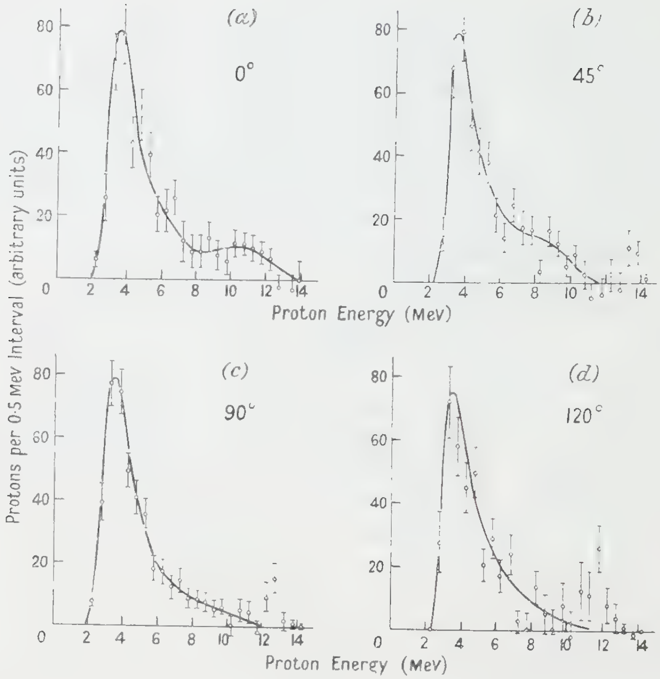

Figure 4. Proton energy distribution from ^{63}Cu.

Table 1

1	2	3	4	5
Last 120 μ	P	199·4	10	22·2
Last 120 μ	D	221·6	11	
Last 60 μ	P	107·5	8·5	9·3
Last 60 μ	D	116·8	9·0	

(1) Track segment used ; (2) type ; (3) mean grain count ; (4) half-width at half height (grains) ; (5) difference between mean grain counts.

These results show that some degree of resolution can be obtained provided 120 μ of track is available for measurement. However, 120 μ corresponds (after allowance has been made for the 28 mg cm^{-2} target thickness) to protons of energy 4·75 Mev from the Cu target, and this energy is too high to include the low energy peak in figure 3 (*f*). 3·5 Mev protons have tracks of length 60 μ in the plate and for this length the half-widths of the grain count distributions are about equal to the difference in mean grain counts for protons and deuterons. It would be necessary, therefore, to make grain counts on a large number of tracks from the Cu target in order to determine the mean grain count to the accuracy required for a comparison with the proton and deuteron recoil tracks. Even with the thick target used, the density of 3·5 Mev proton tracks from the Cu target, which were suitable for grain counting, was very low and the search for them laborious. It was, therefore, decided to abandon the attempt to check the identity of the short range tracks by grain counting.

5.4. *Cross Sections*

The isotopic cross sections, integrated over 4π assuming an isotropic angular distribution, are given in table 2.

Table 2

Target nucleus	^{27}Al	^{54}Fe	^{56}Fe	^{58}Ni	^{60}Ni	^{63}Cu	^{65}Cu
mbn	140	680	190	530	300	250	<40

§ 6. DISCUSSION

The fact that the calculated (n, p) proton energy distributions can be adjusted to fit the experimental curves reasonably well for proton energies above 5 MEV for ^{54}Fe, ^{58}Ni, ^{60}Ni and ^{63}Cu, suggests that these higher energy protons arise primarily from the (n, p) reaction in accordance with the statistical theory for the decay of a compound nucleus. On the other hand a considerable modification of the theory of coulomb barrier penetrabilities, or of the level density functions of the residual nuclei, would be required to explain the fact that the experimental curves peak at 3 MEV. The good agreement between the observed and calculated shapes of the low energy part of the proton energy distribution for ^{56}Fe (figure 3 (*c*)) shows that the conventional coulomb barrier penetrability is applicable for this nucleus. The penetrability for ^{54}Fe should be identical; however, the proton spectrum for this nucleus shows a large low energy excess.

If ^{63}Cu may be regarded as typical, the isotropic angular distribution suggests that the low energy particles are emitted as the result of compound nucleus decay and therefore the identification of these particles with protons is probably correct.

An explanation of the occurrence of the excess of low energy protons appears when the binding energies of neutrons and protons in the target nucleus are considered. At 14 MEV, two particle emission of the types (n, 2n), (n, np), and (n, 2p) are energetically possible, as illustrated in figure 5. These reactions may be regarded as proceeding in two separate stages along two different branches. The (n, n′) branch can proceed further to give (n, 2n) and (n, np) reactions, and the (n, p) branch can give rise to (n, pn) and (n, 2p) reactions. Owing to the coulomb barrier, the emission of two successive protons is unlikely, for at each stage proton emission is in competition with neutron emission. Protons from the reaction

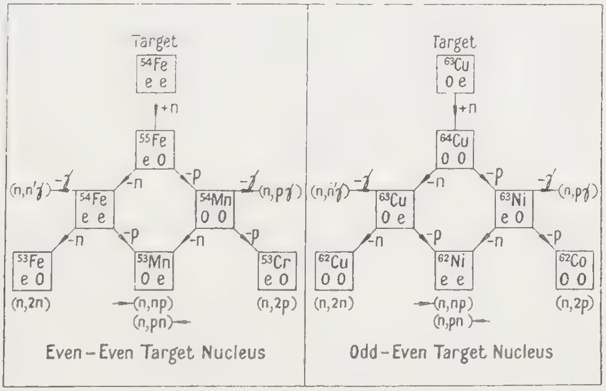

Figure 5. Schematic representation of 14 MEV neutron reactions.

(n, pn) will have the same energy distribution as those from (n, pγ), for here only protons from the first stage are detected, and their manner of emission should be quite independent of the way the second stage proceeds. In the (nn′) branch, it is only the second stage leading to (n, np) reactions which is detected in these experiments. After the inelastic scattering of the neutron the excited target nucleus can decay either by neutron emission (n, 2n), proton emission (n, np) or γ-emission (n, n′γ). The relative probabilities for these processes depend on the binding energies of the neutron and proton in the target nucleus, and on the maximum excitation energy available (14·1 MeV).

These binding energies, derived from the tables of Feather (1953), are given in table 3.

Table 3. Energies in MeV

Target nucleus	^{27}Al	^{54}Fe	^{56}Fe	^{58}Ni	^{60}Ni	^{63}Cu	^{65}Cu
B.E. of neutron	12·99	13·8	11·16	11·7	11·45	10·85	10·05
B.E. of proton	8·29	9·2	10·17	7·7	9·6	6·13	7·59
Difference in B.E.	4·7	4·6	0·99	4·0	1·85	4·72	2·46
Exitation energy for 2 MeV proton emission	10·29	11·2	12·17	9·7	11·6	8·13	9·59
Neutron energy for same excitation	−2·7	−2·6	+0·99	−2·0	+0·15	−2·72	−0·46
Maximum proton energy (n, np)	5·81	4·9	3·93	6·4	4·5	7·97	6·51

It is clear that for ^{54}Fe the emission of a second neutron is energetically impossible over most of the range of target nucleus excitation, and that proton emission (n, np) is in competition only with γ-emission from zero proton energy up to 4·6 MeV, which is the difference between the neutron and proton binding energies. Let us suppose that the excess of low energy protons is caused by the (n, np) reaction. Then from the experimental data it appears that proton emission competes favourably with γ-emission (for $Z = 26$ to 29) provided that the kinetic energy available to the proton is greater than about 2 MeV, for this is the minimum proton energy observed. Row 4 of table 3 gives the excitation energy of the target nucleus required for 2 MeV proton emission, and row 5 the energy for neutron emission corresponding to this excitation energy. It is apparent that for ^{27}Al, ^{54}Fe, ^{58}Ni, ^{63}Cu, and ^{65}Cu neutron emission is energetically impossible, that it is improbable for ^{60}Ni, but for ^{56}Fe neutron emission is very probable. Thus, for ^{56}Fe neutron competition is already severe at the minimum proton energy of 2 MeV, and no low energy peak is observed.

The excess of high energy protons observed for ^{56}Fe and ^{60}Ni may be ascribed to the effect of direct interactions of the type discussed by Hayakawa, Kawai, and Kikuchi (1955). There are therefore three possible contributions to the total observed proton energy distributions:

(i) (n, p) reactions involving the decay of a compound nucleus

(ii) (n, np) reactions involving the decay of a compound nucleus

(iii) (n, p) reactions involving the direct interaction of the incident neutron.

These three contributions are represented diagramatically in figure 6. The individual contributions overlap and they can be separated only by calculating the contribution from reaction (i) according to the statistical model of the nucleus

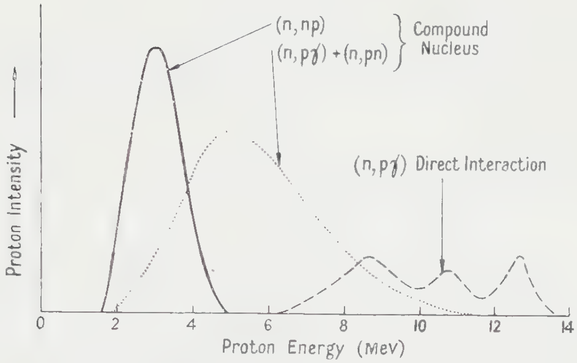

Figure 6. Schematic representation of proton spectra.

and subtracting it from the total. Figure 5 shows that the branching to (n, p) and (n, n′) reactions is between odd–odd and even–even nuclei where the target nucleus is even–even, and between even–odd and odd–even nuclei when the target nucleus is odd–even. The calculated (n, p) cross sections will depend, therefore, on the assumptions made concerning the ratios of level densities for these types of nuclei. As these ratios are not known with any certainty a somewhat arbitrary adjustment was made in normalizing the calculated curves shown in figure 3 (*a–f*). The calculated curves representing reaction (i) have been adjusted to fit the experimental data between 5 and 7 MeV because in this energy region the contributions from both reactions (ii) and (iii) appeared to be very small. Table 4 gives the proportions of the total measured proton emission cross section which have been assigned to the three reactions using this method of normalizing.

Table 4. Cross Sections (mbn)

Target nucleus	^{27}Al	^{54}Fe	^{56}Fe	^{58}Ni	^{60}Ni	^{63}Cu	^{65}Cu
σ (n, p) compound nucleus	70	460	100	310	200	100	<40
σ (n, np) compound nucleus	70	220	0	220	60	130	<40
σ (n, p) direct interaction	—	—	90	—	40	20	—
R	—	6·7	12·5	4·4	18·1	0·7	—

These results are discussed below under separate headings for the three reactions.

(i) (n, p) reaction : compound nucleus

The variations in the cross sections of the compound nucleus part of the (n, p) reaction are caused mainly by the variations in the Q value. There is a regular increase in the cross sections of the even–even target nuclei from ^{56}Fe ($Q = -2{\cdot}93$ MeV), through ^{60}Ni ($Q = -2{\cdot}03$ MeV), to ^{54}Fe and ^{58}Ni for both of which the (n, p) reaction has positive Q values ($+0{\cdot}34$, $+0{\cdot}62$ MeV). The (n, p) cross sections of the two odd–even nuclei ^{63}Cu and ^{65}Cu are several times lower than is expected from their Q values ($+0{\cdot}78$, $-1{\cdot}02$ MeV), and this demonstrates the effect of the enhanced proton competition in the even–even target nuclei, where the (n, p) reaction leads to an odd–odd nucleus (see figure 5).

We have calculated the ratio R of the level density of the residual nucleus produced by proton emission to that produced by neutron emission at the same excitation energy. Assuming that competition from the (n, α) reaction is negligible, the cross section of the (n, p) reaction involving the decay of a compound nucleus is given by

$$\sigma(\mathrm{n,p}) = \sigma_{\mathrm{c}}(\mathrm{n}) \frac{RF_{\mathrm{p}}}{F_{\mathrm{n}} + RF_{\mathrm{p}}} \qquad \ldots\ldots(1)$$

where $\sigma_{\mathrm{c}}(\mathrm{n})$ is the total reaction cross section for 14 MeV neutrons and F_{p}, F_{n} are the proton and neutron emission probabilities assuming no distinction between odd–odd, even–even, and even–odd nuclei (Blatt and Weisskopf 1952). $\sigma_{\mathrm{c}}(\mathrm{n})$ was taken to be 1400 mbn (Taylor, Lönsjö and Bonner 1955) and F_{p}, F_{n}, were calculated using the formula given by Blatt and Weisskopf (1952, p. 369), and the level density formula of Lang and Le Couteur (1954).

The values of R obtained from equation (1) by inserting the measured (n, p) cross sections are given in table 4. Roughly, they are of the expected order of magnitude. The spread in values for the even–even target nuclei may be caused by inadequacies in the method of deriving σ(n, p) from the experimental results. Also, the fact that the nickel isotopes are closed proton shell nuclei and ^{54}Fe is a closed neutron shell nucleus may cause anomalies in the values of R in this region. There is, however, a marked contrast between the values of R for the even–even target nuclei and that for ^{63}Cu which is an odd–even nucleus. Thus, the statistical model of the nucleus accounts well for the observed (n, p) cross section of ^{63}Cu with R of the order of unity, but values of R between 4·5 and 18 are required to explain the (n, p) cross sections of the even–even target nuclei.

These considerations also explain the fact that no protons were observed from a ^{65}Cu target. Using equation (1) and the value $R=1$ for an odd–even target nucleus, the calculated cross section of the reaction ^{65}Cu (n, p) was 28 mbn. This is in agreement with the experimental value (19 mbn) found by Forbes (1952) for the reaction ^{65}Cu (n, pγ) ^{65}Ni, and is too low to have been detected in these experiments.

It should be remembered that the (n, p) cross sections in table 4 include those reactions which ultimately lead to the evaporation of a neutron in the second stage ((n, pn) reactions). Measurement of the true (n, pγ) cross sections by activation methods (e.g. Paul and Clarke 1953) do not include such reactions since they lead to different final nuclei.

(ii) (n, np) reaction: compound nucleus.

It will be noticed in table 4 that for the three pairs of isotopes, ^{54}Fe, ^{56}Fe; ^{58}Ni, ^{60}Ni; and ^{63}Cu, ^{65}Cu; the larger (n, np) cross section occurs in the neutron deficient isotope. It is for the neutron deficient isotopes that the neutron and proton binding energies are most favourable to (n, np) reactions. The reverse situation is apparent when the (n, 2n) cross sections of Paul and Clarke (1953) are examined. For example, ^{65}Cu (1085 mbn), ^{63}Cu (482 mbn) and ^{71}Ga (700 mbn), ^{69}Ga (552 mbn). Moreover, the large (n, np) cross section of ^{58}Ni is in contrast to the small (n, 2n) cross section of ^{58}Ni (40 mbn).

Upper limits for the (n, np) cross sections of ^{80}Se, ^{108}Pd, ^{142}Ce and ^{186}W have been measured recently by Cohen, Hyder and White (1956). Their values (0·8, 65, 18 and 1·6 mbn, respectively) are low compared with the present measurements. This is partly a result of the greater coulomb barriers, but also a result of the fact that the nuclei which they studied all have high neutron numbers for the group of isotopes to which they belong. The neutron and proton binding energies are therefore probably unfavourable to the (n, np) reaction.

The (n, np) cross sections of ^{63}Cu and ^{65}Cu are both smaller than would be expected from a comparison of the binding energies with those of the even–even nuclei (table 3). This is another example of the successful competition of the reaction which leads to an odd–odd nucleus which, in this example, is the (n, 2n) reaction.

The effect of the competition between the (n, 2n) and the (n, np) reactions is also apparent in the proton energy spectra of the even-even nuclei (figure 3). The widths of the low energy peaks of the four nuclei, ^{54}Fe, ^{56}Fe, ^{58}Ni, ^{60}Ni increase in a regular manner as the difference between the neutron and proton binding energies increases.

The very high neutron binding energy in ^{54}Fe, which is responsible for the large (n, np) cross section, should also result in a very small (n, 2n) cross section for this nucleus. This has been confirmed by an activation measurement. The radioactive products of the reactions ^{63}Cu(n, 2n)^{62}Cu and ^{54}Fe(n, 2n)^{53}Fe have similar properties. Both are allowed positron emitters of maximum energy 2·9 and 2·6 MeV, and half-life 10·1 and 9 minutes, respectively. This allows a direct comparison of the β-activities induced in thin deposits of the separated isotopes by 14 MeV neutrons to be made, without the necessity of applying corrections for self-absorption and back scattering. Using the figure of Paul and Clarke for ^{63}Cu, a measurement of the activity induced in the ^{54}Fe sample gave an (n, 2n) cross section of 10 ± 4 mbn.

(iii) (n, p) reaction: direct interaction.

The direct interaction process is expected to result in nucleons emitted in a predominantly forward direction and there is some evidence of this in the behaviour of the high energy part of the ^{63}Cu spectrum as the angle of observation is changed (figure 4). The direct interaction cross sections in table 4 are therefore exaggerated because the observations were made in the forward direction and the cross sections have been presented on the basis of an isotropic angular distribution.

The ordinate scales of the proton energy spectra in figure 3 have been chosen so that the experimental results for each target nucleus are clearly presented. It should be noted that the chosen scales are not all the same.

§ 7. CONCLUSIONS

The conclusions of this work are summarized with reference to the three hypotheses suggested in § 1 to account for the emission of the low energy protons.

(i) The isotropic angular distribution of the low energy charged particles strongly suggests that they have been correctly identified as protons. (ii) The agreement with experiment of the calculated ^{56}Fe(n, p) energy spectrum below 5 MeV proton energy suggests that no change in the conventional coulomb barrier penetrabilities is required. (iii) A study of the binding energies of neutrons and protons in the target nuclei provides an explanation of the occurrence of low energy protons as the result of the (n, np) reaction.

ACKNOWLEDGEMENTS

The author wishes to thank Dr. M. L. Smith for the preparation of the separated isotope targets, Dr. M. J. Poole and his group for providing the neutron irradiation facilities, and Dr. B. B. Kinsey for his helpful criticism of the original manuscript.

Thanks are also due to Miss D. Field, Miss M. J. Hewer and Miss M. A. Rose, for their patient work in scanning the plates.

REFERENCES

ALLAN, D. L., 1955, *Proc. Phys. Soc.* A, **68**, 925.
BLATT, J. M., and WEISSKOPF, V. F., 1952, *Theoretical Nuclear Physics* (New York : Wiley).
COHEN, A. V., HYDER, S. B., and WHITE, P. H., 1956, *Nucl. Phys.*, **1**, 278.
FEATHER, N., 1953, *Advanc. Phys.* (*Phil. Mag.* Suppl.), **2**, 141.
FORBES, S. G., 1952, *Phys. Rev.*, **88**, 1309.
GRAVES, E. R., and ROSEN, L., 1953, *Phys. Rev.*, **89**, 343.
GUGELOT, P. C., 1954, *Phys, Rev.*, **93**, 425.
HAYAKAWA, S., KAWAI, M., and KIKUCHI, K., 1955, *Prog. Theor. Phys., Japan*, **13**, 415.
LANG, J. M. B., and LE COUTEUR, K. J., 1954, *Proc. Phys. Soc.* A, **67**, 586.
PAUL, E. B., and CLARKE, R. L., 1953, *Canad. J. Phys.*, **31**, 267.
TAYLOR, H. L., LÖNSJÖ, O., and BONNER, T. W., 1955, *Phys. Rev.*, **100**, 174.
WEISSKOPF, V. F., and EWING, D. H., 1940, *Phys. Rev.*, **95**, 1209.

Nuclear Cross Sections for 900 MeV Protons

By N. E. BOOTH, B. LEDLEY, D. WALKER† and D. H. WHITE
Department of Physics, University of Birmingham

Communicated by P. B. Moon; MS. received 1st *November* 1956, *and in final form* 31*st December* 1956

Abstract. The cross sections of carbon, aluminium, copper, antimony and lead for 900 MeV protons have been measured. Observations were made with a counter telescope in which the final counter subtended a number of different angles at the absorber. Extrapolation of 'poor geometry' results gave the inelastic cross sections. Extrapolations for nuclear cross sections, which require 'good geometry' measurements, were possible only for the lighter elements carbon, aluminium, and copper because of Coulomb scattering.

If the nuclear radius R is assumed to follow the form $R=r_0A^{1/3}$, the value $r_0=(1{\cdot}26\pm0{\cdot}03)\times10^{-13}$ cm is obtained. If the tapered nuclear density distribution of Williams is assumed, a radial parameter of $0{\cdot}73\times10^{-13}$ cm is obtained.

§ 1. Introduction

The optical model of Fernbach, Serber and Taylor (1949) has been successful in describing the scattering of high-energy nucleons by complex nuclei. The model is particularly applicable at energies where the wavelength of the incident nucleon is much less than the distance in which large changes of nuclear potential occur.

The description of the scattering depends on three parameters: R, the nuclear radius, K, the absorption coefficient of nuclear matter and V, the potential of the incident nucleon in the nucleus. It is usually possible to distinguish experimentally between elastic (or diffraction) and inelastic (or absorption) events and to measure their respective cross sections σ_d and σ_a. At low energies the relatively large energy difference of elastically and inelastically scattered nucleons enables one to separate them. At higher energies, use is made of the different angular distributions. In the optical model, σ_d is dependent on the three parameters, and σ_a on R and K. K may be expressed as a function of R and of the free nucleon–nucleon scattering cross sections, corrected for the presence of other component nucleons. V cannot easily be calculated; it depends both on the forward nucleon–nucleon scattering amplitudes and on an assumed shape for the nucleon–nucleon potential. Therefore it is usual to calculate R from the experimental value of σ_a and the relation involving K. The measurement of σ_d then enables V to be found. However, at high energies σ_d is rather insensitive to the nuclear potential and hence only an approximate value of V can be found.

The present paper describes the measurement of absorption and total cross sections of carbon, aluminium, copper, antimony and lead for protons with a mean energy of 895 MeV.

---

† Now at Victoria University College, Wellington, New Zealand.

Other experiments at similar energies include the measurement of the average absorption cross sections of the light and heavy nuclei in nuclear emulsions for 600 and 950 MeV protons (Lock, March, Muirhead and Rosser 1955). Chen, Leavitt and Shapiro (1955) have determined total and absorption cross sections of a number of nuclei with 860 MeV protons, and similar measurements have been made by Coor, Hill, Hornyak, Smith and Snow (1955) with 1·4 GeV neutrons and by Dzhelepov, Satarov and Golovin (1956) with 590 MeV neutrons.

§ 2. APPARATUS

2.1. *Experimental Layout*

Protons are accelerated to an energy of 990 MeV in the Birmingham synchrotron (Moon, Riddiford and Symonds 1955). The circulating beam is then scattered by a target near the outside wall of the vacuum chamber. In this experiment a vertical polythene rod of 2 mm square cross section was used. It is shown as T_1 in figure 1. Protons scattered out of the vacuum chamber described orbits in the fringing field of the magnet. The counter telescope was located to select particles within definite momentum limits. The telescope consisted of three counters C_1, C_2 and C_3 in fast coincidence. Protons which passed through the telescope then traversed a large, fourth scintillation counter C_4. An absorber A was placed between C_3 and C_4. Triple coincidences T, which occurred when a proton passed through the telescope, and quadruple coincidences Q were recorded. Their ratio Q/T, which we shall call the efficiency e, gave the fraction of protons which did not produce a count in the fourth counter. θ is the conical half-angle subtended by the fourth counter at the centre of the absorber.

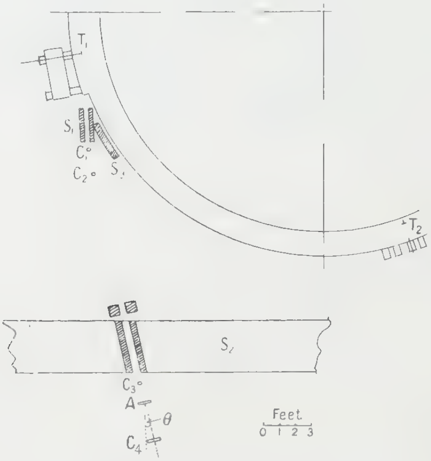

Figure 1. Experimental arrangement. C_1, C_2 and C_3 form the triple coincidence counter telescope. The scintillators C_1 and C_2 are $\frac{1}{2}$ in. by $\frac{1}{2}$ in. perpendicular to the beam and 1 in. long. C_3 is a disc of 1 in. diameter perpendicular to the beam and $\frac{1}{2}$ in. thick. The fourth scintillator C_4 is 4 in. in diameter. A is the absorber. S_1 is a collimating channel 12 in. long constructed of lead–tungsten alloy (density 18 g cm^{-3}). The aperture in S_1 is 1 in. by 1 in. S_2 is a concrete radiation shield with a lead-lined channel of 3 in. by 2 in. aperture. S_3 is an additional lead radiation shield. T_1 and T_2 are described in the text.

The target T_2 intercepted protons which were scattered inwards by T_1 and reduced the background in the region of the counters.

The thickness of each absorber was about 20 g cm^{-2} and was known to an accuracy of better than 1%. The impurity in each absorber was less than 0·5% by weight.† The thickness was chosen by estimating the contribution to the cross section by multiple and single Coulomb scattering and by considering the statistical accuracy obtainable in the available running time. For the lighter elements the thickness was limited by the uncertainty in the solid angle subtended by the fourth counter.

2.2. *Coincidence Apparatus*

A block diagram of the coincidence apparatus is shown in figure 2. The pulses were amplified by 100 Mc/s bandwidth distributed amplifiers which have gains of 100. Limiters on the output of each amplifier delivered pulses of ½ volt into a terminated 91 Ω cable. To detect triple coincidences in the telescope the limited pulses from the corresponding amplifiers were combined at the coincidence mixer, which had a resolving time of 10^{-8} second. A similar method was used to detect double coincidences between C_3 and C_4. Pulses from the coincidence mixer were amplified by amplifiers A_2 which have gains of approximately 3000 and bandwidths of 2 Mc/s. These amplifiers were followed by discriminators and scales of five, having dead times of about 0·3 microsecond. Quadruple coincidences were obtained by mixing the pulses from the discriminators in a further coincidence circuit with a resolving time of 10^{-7} second.

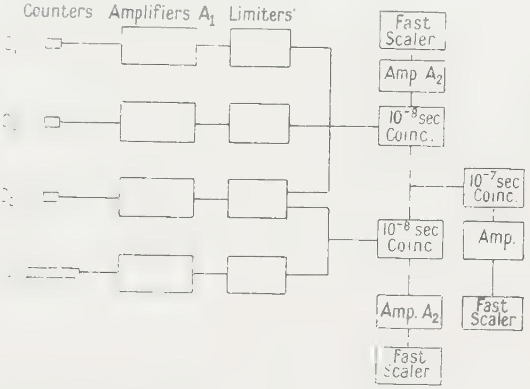

Figure 2. Block diagram of the electronic arrangement.

Frequent checks were made of the operation of the electronics. One check was to measure the efficiency with no absorber, e_0, over a range of delays in the fourth signal cable. Another test was made by attenuating the coincident pulses at the input to one of the amplifiers A_2, using the coincident pulses from the other amplifier A_2 as a monitor. During experiments no change of counting rate was obtained over a range of 16 dB attenuation.

2.3. *Beam Surveys*

The first three counters were located horizontally in the magnetic median plane by maximizing the triple counting rate. A fourth counter with a small scintillator was used in coincidence with the triple coincidence telescope to investigate the beam in front of C_1. By measuring the quadruple counting rate as a function of the horizontal position of this counter, it was found that the protons originated directly from the target. This was confirmed by another experiment in which a length of heavy alloy was placed along the beam axis. This reduced T to zero. The channel S_1 was located along the axis of the beam. The beam cross section at the position chosen for C_4 was also determined with the small scintillator. The results are shown in figure 3.

---

† The antimony absorber was analysed by Mr. J. C. Sargeant. The carbon absorber was loaned by the Atomic Energy Research Establishment, Harwell.

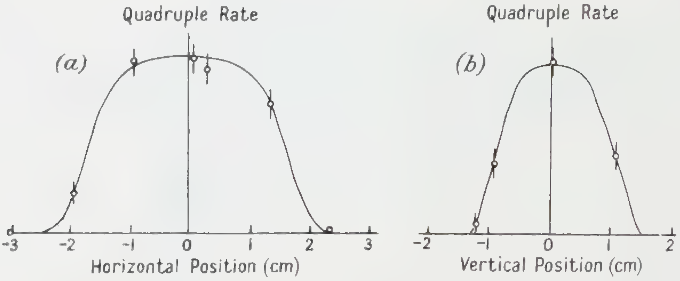

Figure 3. (*a*) Horizontal plot of proton beam at C_4, (*b*) vertical plot of proton beam at C_4. The search crystal was 1·25 cm diameter.

§ 3. Calculation of Cross Sections

The measured cross section $\sigma(\theta)$ at a given subtended angle θ is defined in the following way:

$$\frac{e(\theta)}{e_0} = \exp\left[-\sigma(\theta)\rho x N/A\right]$$

where ρ is the density of the absorber in g cm^{-3}, x is its thickness in cm, A its average atomic weight and N is Avogadro's number. $e(\theta)$ is the efficiency for the geometry θ.

For various reasons discussed below, e_0 does not equal unity. However, the calculation of cross sections from e and e_0 is valid if e_0 remains constant throughout the experiment. In practice, e_0 was observed to vary from run to run between 0·91 and 0·99. Consideration of the material in the third counter and between the third and fourth counters leads one to expect an efficiency of 0·98. It was shown that e_0 was independent of beam intensity. This is to be expected from measurements of counting rates in the individual counters and of random coincidence rates. Measurements of e_0 were made at frequent intervals during the runs, and each half-day's results were used only with the values of e_0 obtained at that time. It seems certain from the reproducibility of cross sections that there was no significant change in e_0 during these periods.

§ 4. Results

Table 1 contains the cross sections at each subtended angle θ. In each synchrotron pulse, about thirty triple coincidences were obtained. For each measurement about three thousand triple coincidences were recorded.

The errors quoted are the standard deviations in the cross sections due to statistical errors in the triple and quadruple counts. The errors are calculated from the formula (Ledley 1956)

$$\frac{(\Delta\sigma)}{\sigma} = \left[\frac{(T_0-Q_0)^{1/2}}{T_0} + \frac{(T_1-Q_1)^{1/2}}{T_1}\right] \Big/ \log_e\left(\frac{e_0}{e(\theta)}\right)$$

where T_0 and Q_0 are respectively the triple and quadruple coincidences recorded during the measurement of e_0, and T_1 and Q_1 those recorded during the measurement of $e(\theta)$.

Certain corrections must be applied to the measured cross sections to enable σ_d and σ_a to be found.

Table 1. Measured Cross Sections (millibarns)

θ (deg)	Carbon	Aluminium	Copper	Antimony	Lead
2·3	375 ± 9	739 ± 21			
3·2			1635 ± 65		
4·1			1090 ± 65		
4·4		554 ± 22			
4·7			1090 ± 65		
5·1	314 ± 9				
5·4			942 ± 65		
5·75			863 ± 60		
5·9		560 ± 22	841 ± 45	1380 ± 55	1980 ± 95
6·5	271 ± 8				
6·9		426 ± 20			
8·1		407 ± 15			
9·9			810 ± 45	1187 ± 55	1670 ± 80
10·4	226 ± 7				
11·0		367 ± 20			
12·7			618 ± 40	1187 ± 65	1598 ± 95
13·3		368 ± 18			
14·2	183 ± 10			1133 ± 60	
15·0			561 ± 60		1700 ± 95
15·5		363 ± 20			
15·8	115 ± 15				
17·1	158 ± 10	347 ± 10	613 ± 40	1178 ± 60	1548 ± 110

(*a*) *Large angles.*

At angles of about 10° and greater, the scattering is largely inelastic. There is still a small contribution from elastically scattered protons. Bratenahl, Fernbach, Hildebrand, Leith and Moyer (1950) have shown that this can be estimated from the diffraction of an equivalent black disc. For this we have chosen a radius given by $R = 1{\cdot}28 \times 10^{-13} A^{1/3}$ cm. The elastic scattering is then given by

$$\sigma(\Omega) = \int_{\Omega}^{2\pi} \left(\frac{d\sigma}{d\Omega}\right) d\Omega,$$

where we take

$$\left(\frac{d\sigma}{d\Omega}\right) = \left(\frac{\sigma_d}{\pi}\right)\left[\frac{J_1(kR\sin\theta)}{\sin\theta}\right]^2.$$

For this correction we have used values for σ_d of 1600 millibarns for lead, and 1400 millibarns for antimony. For the lighter elements we have taken σ_d equal to half of the total cross section. A better approximation is not warranted since the corrections are always less than 15%. The corrected cross sections are plotted against solid angle $\Omega = 2\pi(1 - \cos\theta)$ in figure 4. The points would lie on a straight line if the secondary charged particles were emitted isotropically. The angular distribution of the secondary charged particles from inelastic processes is in fact nearly isotropic (Lock, March, Muirhead and Rosser 1955) and hence a large region may be used for extrapolation; increasing the precision of the method. The error is slightly greater for nuclei of small mass due to the effect of the motion of the centre of momentum of the system on the angular distribution.

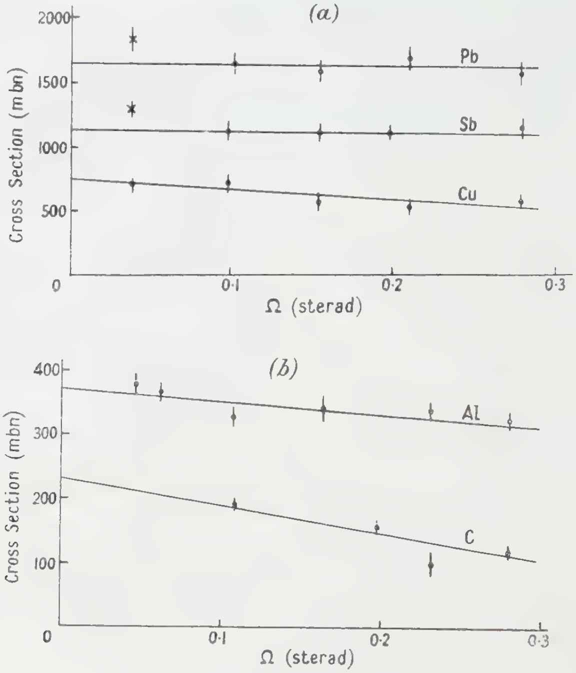

Figure 4. Cross sections at large angles Ω, corrected for diffraction scattering. Extrapolation gives the following values for σ_a : (*a*) Pb, 1660 ± 50 mbn; Sb, 1153 ± 22 mbn; Cu, 740 ± 52 mbn; (*b*) Al, 370 ± 29 mbn; C, 230 ± 20 mbn.

A proportion of the inelastic events produce secondary ionizing particles in the forward direction. These may be detected in the fourth counter and reduce the measured cross section. From nuclear emulsion studies these are known to consist mainly of protons of energy less than 50 MeV. To reduce their effect, a brass disc sufficiently thick to stop 60 MeV protons was placed in front of the fourth counter.

Because of the uncertainty in the magnitude of the interference between Coulomb and elastic scattering, the smallest-angle point was ignored in the extrapolations for antimony and lead.

(*b*) *Small angles.*

At small angles, multiple and single Coulomb scattering made important contributions. Multiple nuclear elastic scattering was not important. Sternheimer's calculations (1954) were used to correct for multiple Coulomb scattering. For these corrections it was assumed that the unattenuated protons were distributed uniformly over a circular area of 3·6 cm diameter at the fourth counter. (This corresponds to the diameter determined in figure 3 (*a*).) If the density of protons falls off towards the periphery of the beam, this correction will be too large. The correction was always less than 5% of the measured cross sections. The single Coulomb scattering cross section was calculated by assuming the protons were concentrated in a line along the axis of the beam and that the scattering occurred at the centre of the absorber. While this underestimates the contribution, this cross section was always less than 3% of the total.

The corrected cross sections may be extrapolated linearly to zero subtended angle to give the total cross section $\sigma_t = \sigma_d + \sigma_a$. A linear extrapolation is justified because the major contribution to the corrected cross section is derived from larger angle scattering and absorption processes. Thus the cross section for a given θ is not strongly dependent upon the differential elastic scattering cross section at the angle θ, and a linear relation may be assumed over a limited range of θ. The range of measurement is restricted at the small angles by the preponderance of Coulomb scattering over diffraction scattering and is smaller for the heavier elements. The extrapolations for carbon, aluminium and copper are shown in figure 5. The extrapolations for carbon and aluminium provide a reasonable estimate of the total cross sections, although the extrapolation would be expected to make the values slightly high. For copper and heavier elements the extrapolation method loses its precision. However, it is interesting to make a rough estimate of σ_t for copper.

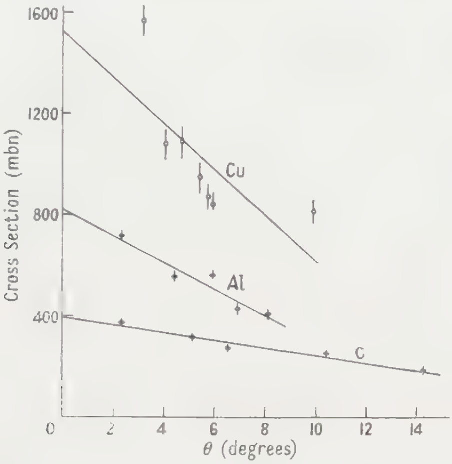

Figure 5. Extrapolation of small-angle cross sections, corrected for Coulomb scattering, to give σ_t for carbon = 392 ± 24 mbn, for aluminium = 823 ± 30 mbn and for copper = 1530 ± 160 mbn.

§ 5. Energy Spread

The radial variation of the fringing magnetic field of the synchrotron has been used to compute the trajectories of protons scattered at the target. The counter telescope accepted protons of energies greater than 902 ± 10 MeV. The maximum proton energy, allowing for the Fermi energy of the component nucleons in the target nuclei, was 970 MeV. Allowing for energy loss in the scintillators and the absorber we have a mean energy of 895 MeV with a *total* spread of 70 MeV.

§ 6. The Uniform Optical Model Constants

The cross sections have been analysed using the uniform optical model of Fernbach, Serber and Taylor (1949). To find R from σ_a, a value of K was calculated as a function of R from the formula

$$K = (3/4\pi R^3)[Z\sigma_{pp} + (A-Z)\sigma_{np}]$$

where $\sigma_{pp}(\sigma_{np})$ is the free p–p (n–p) cross section. We have taken $\sigma_{pp} = 48$ millibarns and $\sigma_{np} = 34$ millibarns. σ_{pp} was chosen from the results of Chen, Leavitt and Shapiro (1956) and from measurements made in this laboratory (to be published). σ_{np} was obtained by interpolation of the results at 590 MeV (Dzhelepov, Kazarinov, Golovin, Fljagin and Satarov 1956) and 1400 MeV (Coor, Hill, Hornyak, Smith and Snow 1955).

The calculated values of R and K and the opacity, $\sigma_a/\pi R^2$, are shown in table 2 together with the extrapolated values of σ_a and σ_t. Figure 6 is a graph of R versus $A^{1/3}$. The straight line which passes through the points for the three heavier elements and the origin has a slope $r_0 = (1{\cdot}26 \pm 0{\cdot}02) \times 10^{-13}$ cm. This value of r_0 agrees within statistical errors with the results of Chen, Leavitt and Shapiro ($1{\cdot}25 \pm 0{\cdot}02$) using 860 MeV protons and Coor, Hill, Hornyak, Smith and Snow ($1{\cdot}28 \pm 0{\cdot}015$) using 1400 MeV neutrons. The values of K obtained in the present experiment are significantly lower than those obtained by Chen, Leavitt and Shapiro; this is largely due to their choice of a higher value (43 mbn) for σ_{np}. The value of r_0 does not depend strongly on the choice of σ_{pp} and σ_{np}.

Table 2

Element	Extrap. Values (mbn)		$R \times 10^{13}$ (cm)	$K \times 10^{-12}$ (cm^{-1})	$\sigma_a/\pi R^2$	$k_1 K$
	σ_a	σ_t				
Carbon	230 ± 20	392 ± 24	$3{\cdot}09 \pm 0{\cdot}15$	3·65	0·77	0·4
Aluminium	370 ± 29	823 ± 30	$3{\cdot}65 \pm 0{\cdot}13$	5·40	0·89	0·6
Copper	740 ± 52	1530 ± 160	$5{\cdot}07 \pm 0{\cdot}15$	4·69	0·92	0·4
Antimony	1153 ± 22		$6{\cdot}23 \pm 0{\cdot}07$	4·79	0·95	
Lead	1160 ± 50		$7{\cdot}41 \pm 0{\cdot}19$	4·78	0·96	

$r_0 = (1{\cdot}26 \pm 0{\cdot}02) \times 10^{-13}$ cm. Mean value of $K = (4{\cdot}7 \pm 0{\cdot}5) \times 10^{12}$ cm^{-1}.
Radius parameter of Williams' tapered model, $a = 0{\cdot}730 \pm 0{\cdot}005 \times 10^{-13}$ cm.

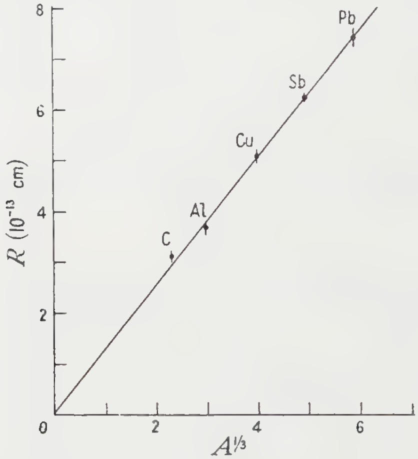

Figure 6. Plot of R against $A^{1/3}$.

k_1, the increase in the wave number of the incident proton as it enters the potential of the complex nucleus, was obtained from the curves of Bethe and Wilson (1951) which give k_1/K as a function of σ_d, σ_a and R. Our results, tabulated in table 2, give a mean value of $k_1/K = 0{\cdot}5$ for carbon, aluminium and copper.

§ 7. The Tapered Density Model

The measurements of σ_a are not adequate to determine the form of the nuclear density distribution. With the uniform optical model there is an apparent discrepancy between radii obtained by nucleon scattering and by electromagnetic methods. Several authors have shown that the assumption of a square potential well is unrealistic, and in this paper a distribution suggested by Williams (1955) has been used to fit the data. By using this distribution, radii have been obtained which conform with the results of electron scattering by complex nuclei and of μ-mesonic x-ray studies. It has been pointed out that the equivalent square well radius (the radius obtained when a uniform distribution is assumed) would not be the same for all experiments if the density distribution were non-uniform. If the nuclear density distribution is assumed to have a gently tapered edge, Williams finds that the neutron measurements of Coor, Hill, Hornyak, Smith and Snow (1955) give a nuclear size in agreement with the electromagnetic results.

Thus the apparent difference in the nuclear size as determined by the electromagnetic and nuclear methods may be largely resolved by the assumption of a smoothed out density distribution in the nucleus. In addition it appears that the smoothed out distributions are least affected by the finite range of nuclear forces. In fact by assuming a finite range for nuclear forces, an effective potential has been calculated using the uniform density model. The uniform potential is modified to a shape closely approximating that of the tapered nucleus.

Williams has expressed his results graphically as a plot of the opacity $\sigma_a/\pi R^2$ against $(K_0R)^{-1}$. K_0^{-1} is the mean free path at the centre of the nucleus. All nuclei are assumed to be similar in shape with the radius $R = aA^{1/3}$, where a is the parameter which is determined from the experimental data. The analysis of the results obtained with 1400 MeV neutrons gave $a = 0{\cdot}736 \times 10^{-13}$ cm. In the present experiment the value of a was found by a least squares fit of the three elements Pb, Sb, and Cu to the theoretical curve. This curve is plotted in figure 7 together with the values for all the elements measured.

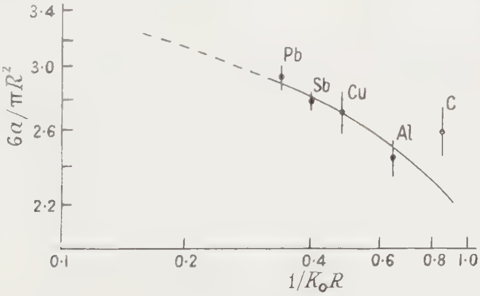

Figure 7. $\sigma_a/\pi R^2$ as a function of $(K_0R)^{-1}$ where K_0^{-1} is the mean free path at the centre of the nucleus.

Voss and Wilson (1956) have analysed data obtained from neutron total cross sections in the region 80–300 MeV. By comparing the measured variation in total cross section with energy with that to be expected assuming various potential well shapes, they deduce an upper limit to the taper that may be allowed. The 'Williams' taper is excluded by this reasoning as too large.

The situation may be summarized as follows. The nuclear radii obtained from electromagnetic and nuclear scattering data may be made to agree by a suitable choice of potential distribution. Some doubt is cast on this distribution by qualitative information on the variation of the total cross section with energy. This doubt could be resolved by assuming different radii for the neutron and proton distributions in the nucleus.

Acknowledgments

We are grateful to Dr. G. W. Hutchinson for many fruitful discussions during the later stages of the work and to the synchrotron team for their tireless efforts. We also wish to thank Dr. J. Woodward and Mr. J. Studdard who performed the trajectory calculations.

N. E. Booth is indebted to Imperial Oil Limited for the award of a Graduate Research Fellowship, D. H. White to the Department of Scientific and Industrial Research for a maintenance grant, and B. Ledley to the Trustees of the Gowrie Scholarship Fund for a Travelling Scholarship and to the University of Birmingham for a University Scholarship.

References

Bethe, H. A., and Wilson, R. R., 1951, *Phys. Rev.*, **83,** 690.

Bratenahl, A., Fernbach, S., Hildebrand, R. H., Leith, C. E., and Moyer, B. J., 1950, *Phys. Rev.*, **77,** 597.

Chen, F. F., Leavitt, C. P., and Shapiro, A. M., 1955, *Phys. Rev.*, **99,** 857; 1956, *Ibid.*, **103,** 211.

Coor, T., Hill, D. A., Hornyak, W. F., Smith, L. W., and Snow, G., 1955, *Phys. Rev.*, **98,** 1369.

Dzhelepov, V. P., Kazarinov, Ju. M., Golovin, B. M., Fljagin, V. B., and Satarov, V. I., 1956, *Nuovo Cim. Suppl.*, **3,** 61.

Dzhelepov, P. V., Satarov, V. I., and Golovin, B. M., 1956, *Doklady Akad. Nauk, S.S.S.R.*, **104,** 717.

Fernbach, S., Serber, R., and Taylor, T. B., 1949, *Phys. Rev.*, **75,** 1352.

Ledley, B., 1956, *Thesis*, University of Birmingham.

Lock, W. O., March, P. V., Muirhead, H., and Rosser, W. G. V., 1955, *Proc. Roy. Soc.* A, **230,** 215.

Moon, P. B., Riddiford, L., and Symonds, J. L., 1955, *Proc. Roy. Soc.* A, **230,** 204.

Sternheimer, R. M., 1954, *Rev. Sci. Instrum.*, **25,** 1070.

Voss, R. G. P., and Wilson, R., 1956, *Proc. Roy. Soc.* A, **236,** 52.

Williams, R. W. 1955, *Phys. Rev.*, **98,** 1387.

Fine Structure Analysis of NO Absorption Bands in the Schumann Region

By R. F. BARROW[†] and E. MIESCHER[‡]
[*] Physical Chemistry Laboratory, University of Oxford
[†] Department of Physics, University of Basel

MS. received 3rd December 1956

Abstract. Rotational analyses of bands in the far ultra-violet absorption spectrum of nitric oxide have been carried out. The bands studied include the 0,0, 1,0, 2,0, 3,0 and 4,0 bands of the ϵ system ($D^2\Sigma^+-X^2\Pi$), the 4,0 and 5,0 bands of the γ system ($A^2\Sigma^+-X^2\Pi$), and the 8,0, 13,0 and 17,0 bands of the β system ($B^2\Pi-X^2\Pi$), as well as other bands ascribed to new systems. Summaries are given of the constants for the states $A^2\Sigma^+$, $B^2\Pi$ and $D^2\Sigma^+$. All bands in the absorption spectrum above 1600 Å have now been assigned. Possible Rydberg series are briefly discussed.

---

§ 1.

Herzberg, Lagerqvist and Miescher (1956) have recently carried out, on high-dispersion plates of the absorption spectrum of nitric oxide (NO), rotational analyses of bands of the interacting systems $\beta(B^2\Pi-X^2\Pi)$ and $\delta(C^2\Pi-X^2\Pi)$ which lie in the region 2000–1600 Å. In the same region are the bands of the strong $\epsilon(v', 0)$ progression ($D^2\Sigma^+-X^2\Pi$). Some β bands, γ bands ($A^2\Sigma^+-X^2\Pi$), as well as bands of other systems, are overlapped by the ϵ bands. Therefore, and in order to improve the knowledge of the $D^2\Sigma^+$ level, fine-structure analyses of the ϵ bands in the Schumann region have now been made, using the same plates. Former analyses of ϵ bands in emission (Gaydon 1944, Gerö, Schmid and von Szily 1944, Ogawa 1955) include upper levels $v' = 0$ and 1 only.

The ϵ bands are found to contain, as expected, structure, in some cases quite well resolved, of bands belonging to other systems. The $\epsilon(0, 0)$ band contains the $\gamma(4, 0)$ and $\beta(8, 0)$ bands; $\epsilon(1, 0)$ contains $\gamma(5, 0)$; $\epsilon(2, 0)$ contains $\beta(13, 0)$ and, although it has not yet proved possible to identify $\gamma(6, 0)$ with certainty, there remain weak unassigned lines in the region predicted for this band; $\epsilon(3, 0)$ contains the $(0, 0)$ band of the β' system ($B'^2\Delta-X^2\Pi$) (Miescher 1956 a) and the tail of $\beta(16, 0)$. $\epsilon(4, 0)$ is found to contain a strong band at 1612 Å of a new system $F^2\Sigma-X^2\Pi$. The $\epsilon(5, 0)$ band cannot be seen: the extrapolated position ($Q_{11}(\frac{1}{2}) = 64147\ \mathrm{cm}^{-1}$) falls in a region of strong absorption which is probably that of the $\beta(21, 0)$ and $\delta(5, 0)$ bands.

§ 2.

The ϵ bands present few features worthy of remark. The interaction between $B^2\Pi$ and $D^2\Sigma^+$ is weak. The following levels coincide approximately in energy:

$D^2\Sigma^+$	$B^2\Pi$	J
$v = 0\ F_2$	$v = 8\ F_2$	$3\frac{1}{2}$
$v = 1\ F_2$	$v = 11\ F_1$	$18\frac{1}{2}$
$v = 3\ F_2$	$v = 16\ F_1$	$16\frac{1}{2}$

The first interaction occurs at too low, the second at too high, a value of J to be followed in detail, but the interactions seem to be weak. Only in the last case is there some evidence of interaction, so that the value of $B_3(\mathrm{D}^2\Sigma^+)$ is a little smaller than would be expected (see table 1). From the vibrational intervals,

$$G(v) = 2323{\cdot}90(v+\tfrac{1}{2}) - 22{\cdot}885(v+\tfrac{1}{2})^2 + 0{\cdot}75(v+\tfrac{1}{2})^3 - 0{\cdot}22(v+\tfrac{1}{2})^4.$$

Table 1. Constants for $\mathrm{D}^2\Sigma^+$

v	$Q_{11}(\frac{1}{2})$ D–X	B_{obs}	$B_{\mathrm{obs-calc}}$†
0	53 291·2	1·9917	0·0000
1	55 570·6	1·9701	+0·0001
2	57 804·7	1·9484	+0·0002
3	59 987·4	1·9209	−0·0056
4	62 107·2	1·9047	0·0000

† With $B_v = 2{\cdot}0026 - 0{\cdot}02175(v+\frac{1}{2})$.

Further small perturbations have been observed in $\mathrm{D}^2\Sigma^+$ at $N=10$ in $v=1$ and $N=7$ in $v=3$: the former arises by interaction with $v=5$ of $\mathrm{A}^2\Sigma^+$; the origin of the latter is not known.

§ 3.

The question as to the independent existence, or not, of the γ and ϵ systems has received much attention in the past. The problem was settled by the observation of lines of the $\gamma(4, 0)$ band (Herzberg, Lagerqvist and Miescher 1956) which lie within $\epsilon(0, 0)$. The analysis of the $\gamma(4, 0)$ band has now been extended by the identification of the ${}^{S}\mathrm{R}_{21}$ branch and of some lines of the $\mathrm{A}^2\Sigma^+ - \mathrm{X}^2\Pi_{1\frac{1}{2}}$ sub-band. The $\gamma(5, 0)$ band has also been identified: $v=5$ in $\mathrm{A}^2\Sigma^+$ lies only about 9 cm^{-1} above $v=1$ of $\mathrm{D}^2\Sigma^+$, and only the lines of the R_{11} and ${}^{S}\mathrm{R}_{21}$ branches are free from overlapping by the stronger ϵ-band lines. As has been noted, these levels coincide approximately in energy at $N=10$, where small displacements, up to 0·3 cm^{-1}, are found. The origin of the $\gamma(6, 0)$ band is expected to lie at about 50 cm^{-1} below the origin of $\epsilon(2, 0)$. The strongest lines should fall in a region already containing lines of $\epsilon(2, 0)$ and the isotopic lines of $\epsilon(2, 0)$ and lines of $\beta(13, 0)$. It has not, on this account, been possible to draw any definite conclusions about the existence or otherwise of this band.

Constants for the $\mathrm{A}^2\Sigma^+$ state are given in table 2. From vibrational intervals,

$$G(v) = 2374{\cdot}8(v+\tfrac{1}{2}) - 16{\cdot}46(v+\tfrac{1}{2})^2.$$

Table 2. Constants for $\mathrm{A}^2\Sigma^+$

v	$Q_{11}(\frac{1}{2})$ A–X	B_{obs}	$B_{\mathrm{obs-calc}}$†
0	44 199·2‡	1·9870‡	−0·0006
1	46 540·6‡	1·9688‡	+0·0005
2	48 850·5‡	1·9498‡	+0·0008
3	51 127·2‡	1·9290‡	−0·0007
4	53 369·9	1·9108	+0·0004
5	55 579·6	1·8906	−0·0006

† With $B_v = 1{\cdot}9972 - 0{\cdot}01928(v+\frac{1}{2})$.
‡ From Gerö and Schmid (1948).

§ 4.

Table 3 summarizes present knowledge of the $\mathrm{B}^2\Pi$ levels including the results of the analyses of the $\beta(8,0)$, $\beta(13,0)$ and $\beta(17,0)$ bands. The lines of the $\beta(13,0)$ band, whose origin lies inside the $\epsilon(2,0)$ band, cannot be traced at all on the low-temperature plates, this band being anomalously weak. But lines for high J are readily measurable on a plate taken with nitric oxide at room temperature in the region between $\delta(2,0)$ and $\epsilon(2,0)$, where the perturbation between $\delta(2,0)$ and $\beta(13,0)$ sets in. The B-value given for $v=13$ has been calculated by extrapolation from these lines. No lines of the $\beta(17,0)$, $(\mathrm{B}^2\Pi_{1\frac{1}{2}}-\mathrm{X}^2\Pi_{1\frac{1}{2}})$ sub-band could be measured in the presence of the numerous strong lines of $\beta'(1,0)$. The spin coupling constant, $Y=A/B$, increases regularly with vibrational quantum number (table 3), that is with strengthened field along the internuclear axis.

Table 3. Constants for $\mathrm{B}^2\Pi$

v	$\mathrm{Q}_{11}(\frac{1}{2})$	Y_v†	B_v	v	$\mathrm{Q}_{11}(\frac{1}{2})$	Y_v†	B_v
0	45 485·7	28	1·118	10	55 090·5	—	1·022
1	46 507·7	29	1·105(1)	11	55 960·3	47	1·010
2	47 515·5	31	1·093	12	56 739·4	—	— (3)
3	48 509·6	32	1·081	13	57 746		1·02
4	49 484·0	29	1·068(2)	14	58 539·0	49	1·034
5	50 452·6	36	1·056	15	59 208·0	—	— (4)
6	51 406·4	38	1·041	16	60 313·2	56	0·997
7	52 347·1	41	1·028	17	61 074·6	—	0·955
8	53 273·5	42	1·021	18	61 862·5	57	0·98
9	54 183·4	44	1·019	19	62 588·8	69	0·914

† $Y_v=A_v/B_v$.

(1) Jenkins, Barton and Mulliken (1927).

(2) Gerö and Schmid (1948), Schmid (1930).

(3) Perturbed by $\delta(2, 0)$.

(4) Perturbed by $\delta(3, 0)$.

§ 5.

Several other bands have structures sufficiently well resolved on the present plates for rotational analysis, and results are given in table 4. These include, besides the $(\mathrm{E}^2\Sigma^+-\mathrm{X}^2\Pi)$ system with the well-known $\mathrm{E}^2\Sigma^+$ upper state (Feast 1950), the 1612 Å band found to overlap $\epsilon(4,0)$. It has a structure apparently identical with and a B'-value of comparable magnitude with that shown by the γ and

Table 4.

Band Å	$\mathrm{Q}_{11}(\frac{1}{2})$ cm⁻¹	B cm⁻¹	Assignment	Ueda's† notation
1612	62 039·6	1·964	$\mathrm{F}^2\Sigma-\mathrm{X}^2\Pi$	U_0
1567	63 826·4	1·43	$\mathrm{I}^2\Pi-\mathrm{X}^2\Pi$	S_2
1546	64 660·0	2·010	$\mathrm{M}^2\Sigma-\mathrm{X}^2\Pi$	
1543	64 800·4	0·916	$\beta(22, 0)$	S_3
1513	66 100·8	0·90	$\beta(24, 0)$	
1493	66 973·1	1·994	$\mathrm{P}^2\Sigma-\mathrm{X}^2\Pi$	W_0

† Ueda (1955).

ϵ bands; we ascribe it to a transition to a new state, $\mathrm{F}^2\Sigma$. With this, all bands observed above 1600 Å in the NO absorption spectrum have been assigned. Below this limit, two bands, one at 1546 Å and one at 1493 Å, have the structure of $^2\Sigma$–$^2\Pi$ transitions and show upper-state B-values close to that for the ion NO^+ (Miescher 1956 b). The upper state $\mathrm{P}^2\Sigma$ of the 1493 Å band fits rather well as the third member of the $\mathrm{A}^2\Sigma^+$, $\mathrm{E}^2\Sigma^+$, ... Rydberg series proposed by Sutcliffe and Walsh (1953). The upper state $\mathrm{M}^2\Sigma$ of the 1546 Å band can, together with the $\mathrm{D}^2\Sigma^+$ state of the ϵ bands, form a new Rydberg series going to the same ionization limit.

The $\mathrm{A}^2\Sigma^+$ and $\mathrm{D}^2\Sigma^+$ states dissociate certainly to an excited atomic state with $n=3$. It may be significant that the difference in energy ($\mathrm{D}^2\Sigma^+ - \mathrm{A}^2\Sigma^+ = 9100\ \mathrm{cm}^{-1}$) is of the same size as the difference of the 3s excitation energies in the N and O atoms:

$$\left[\mathrm{N}^{*}\,\substack{(^4\mathrm{P})\\(^2\mathrm{P})}+\mathrm{O}(^3\mathrm{P})\right]-\left[\mathrm{N}(^4\mathrm{S})+\mathrm{O}^{*}\,\substack{(^5\mathrm{S})\\(^3\mathrm{S})}\right]=\substack{9500\\9400}\ \mathrm{cm}^{-1}.$$

Sutcliffe and Walsh have already suggested that the $\sigma 3s$ orbital in the state A is strongly localized on the O atom. The D state may well be in the analogous state in which this orbital is localized on the N atom.

The three remaining bands of table 4 are red degraded and have small B-values. One of these, the 1567 Å band, is strong and lies in a region free from other bands. The fact that it shows no isotope heads leads us to assign it to a new state $\mathrm{I}^2\Pi$. The other two may well be higher members of the β progression, as is indicated in table 4.

ACKNOWLEDGMENTS

We would like to acknowledge our debt to Dr. G. Herzberg, in whose laboratories the plates were taken, to the Swiss National Fund, and to the Leverhulme Trustees for a Research Grant to one of us (R. F. B.).

REFERENCES

FEAST, M. W., 1950, *Canad. J. Res.* A, **28,** 488.
GAYDON, A. G., 1944, *Proc. Phys. Soc.*, **56,** 160.
GERÖ, L., and SCHMID, R., 1948, *Proc. Phys. Soc.*, **60,** 533.
GERÖ, L., SCHMID, R., and VON SZILY, F. K., 1944, *Physica*, **11,** 144.
HERZBERG, G., LAGERQVIST, A., and MIESCHER, E., 1956, *Canad. J. Phys.*, **34,** 622.
JENKINS, F. A., BARTON, H. A., and MULLIKEN, R. S., 1927, *Phys. Rev.*, **30,** 150.
MIESCHER, E., 1956 a, *Helv. Phys. Acta*, **29,** 401; 1956 b, *Ibid.*, **29,** 135.
OGAWA, M., 1955, *Science of Light* (Japan), **3,** 90.
SCHMID, R., 1930, *Z. Phys.*, **64,** 84.
SUTCLIFFE, L. H., and WALSH, A. D., 1953, *Proc. Phys. Soc.* A, **66,** 209.
UEDA, M., 1955, *Science of Light* (Japan), **3,** 143.

RESEARCH NOTES

An Exact Calculation of Second Order Long Range Forces

By A. DALGARNO and N. LYNN
Department of Applied Mathematics, The Queen's University of Belfast

Communicated by D. R. Bates; MS. received 26th November 1956

§ 1. Introduction

In calculations of long-range forces between atomic systems it is customary to expand the interaction potential V in inverse powers of the nuclear separation R (cf. Margenau 1939). The accuracy of this procedure for particular cases has been discussed semi-quantitatively by Dalgarno and Lewis (1956) and by Dalgarno and Stewart (1956), who evaluated the second-order expression for the energy $\mathscr{E}_2$:

$$\mathscr{E}_2 = \sum{}' (0 \,|\, V \,|\, p)^2/(E_0 - E_p) \qquad \ldots\ldots(1)$$

in the usual notation, by using Unsöld's approximation (1927) in which $E_0 - E_p$ is replaced by a constant Δ with the result that

$$\mathscr{E}_2 = \Delta^{-1}\{(0 \,|\, V^2 \,|\, 0) - (0 \,|\, V \,|\, 0)^2\}, \qquad \ldots\ldots(2)$$

Δ being to some extent arbitrary. There is no difficulty in evaluating (2) with the expanded and complete forms of V (Eisenschitz and London 1930) but the evaluation of (1) is less easy. It has been carried out for various single-electron cases by Dalgarno and Lewis (1956) and by Dalgarno and Stewart (1956) with the expanded form of V, but not hitherto with the complete form.

§ 2. Theory

We restrict attention to the case of an atom consisting of a nucleus A of charge ζ and a single 1s electron perturbed by a nucleus B, of charge ζ', a distance R from A. Then if $\mathbf{r}_\mathrm{a}$ and $\mathbf{r}_\mathrm{b}$ are the position vectors of the electron from the nuclei A and B respectively, the interaction potential V is given in rydbergs by

$$V = 2\zeta' \left(\frac{\zeta}{R} - \frac{1}{r_\mathrm{b}} \right) \qquad \ldots\ldots(3)$$

which, for $r_\mathrm{a} < R$, may be expanded according to

$$V \sim 2\zeta' \left\{ \frac{\zeta - 1}{R} - \frac{1}{R} \sum_{n=1}^{\infty} \left(\frac{r_\mathrm{a}}{R} \right)^n P_n(\cos\theta_\mathrm{a}) \right\}. \qquad \ldots\ldots(4)$$

Dalgarno and Lewis (1955) have shown that equation (1) is equivalent to

$$\mathscr{E}_2 = (0 \,|\, Vf \,|\, 0) - (0 \,|\, V \,|\, 0)(0 \,|\, f \,|\, 0) \qquad \ldots\ldots(5)$$

where f satisfies the equation

$$2\nabla f \,.\, \nabla\psi_0 + \psi_0 \nabla^2 f = V\psi_0 - (0 \,|\, V \,|\, 0)\psi_0, \qquad \ldots\ldots(6)$$

ψ_0 being the unperturbed wave function. Introducing confocal elliptical coordinates $\lambda=(r_a+r_b)/R$, $\mu=(r_a-r_b)/R$, ψ_0 may be written

$$(\zeta^3/\pi)^{1/2}\exp\left[-\zeta R(\lambda+\mu)/2\right]$$

and (6) becomes

$$\frac{\partial}{\partial\lambda}\left[(\lambda^2-1)\frac{\partial f}{\partial\lambda}\right]+\frac{\partial}{\partial\mu}\left[(1-\mu^2)\frac{\partial f}{\partial\mu}\right]-t(\lambda^2-1)\frac{\partial f}{\partial\lambda}-t(1-\mu^2)\frac{\partial f}{\partial\mu}$$
$$=a(\lambda^2-\mu^2)-b(\lambda+\mu) \quad \ldots\ldots(7)$$

where $2a=\zeta' R\{1-(t+1)\exp[-2t]\}$, $b=\zeta' R$ and $t=\zeta R$. Applying the condition that $f(\lambda,\mu)$ be non-singular, it may be shown that

$$\begin{aligned}f(\lambda,\mu)=&-\frac{a}{t}(\lambda+\mu)+\frac{b}{t^2}\{(t-1)+(t+1)\exp[-2t]\}\log(\lambda+1)\\&-\frac{b}{t^2}(t+1)\log(1-\mu)+\frac{b}{t^2}(t+1)\exp[-2t]\log(1+\mu)\\&+\frac{b}{t^2}(t+1)\exp[-t]\{\exp[t]\mathrm{Ei}[-t(1-\mu)]-\exp[-t]\mathrm{Ei}[t(1+\mu)]\}\end{aligned}$$
$$\ldots\ldots(8)$$

where

$$\mathrm{Ei}(x)=-\int_{-x}^{\infty}s^{-1}\exp(-s)\,ds.$$

Expression (5) may then be evaluated and is given by

$$\begin{aligned}\mathscr{E}_2=&\frac{\zeta'^2}{t^2}\{5-(4t^2+8t+10)\exp[-2t]+(4t^3+7t^2+8t+5)\exp[-4t]\}\\&-\frac{2\zeta'^2}{t^2}\{(t+1)^2\exp[-2t](1+\exp[-2t])\mathrm{Ei}[2t]\\&+\left[(t-1)^2\exp[2t]+(t^2+2t-3)+(4t+4)\exp[-2t]\right]\mathrm{Ei}[-2t]\\&-2(t+1)^2\exp[-2t](1+\exp[-2t])(\gamma+\log 2t)\}\end{aligned} \quad \ldots\ldots(9)$$

where γ is Euler's constant, 0·577 215 7.

If exponentially decreasing terms are ignored, equation (9) simplifies to

$$\mathscr{E}_2=\frac{2\zeta'^2}{t^2}\left[\tfrac{5}{2}-(t+1)^2\exp[-2t]\mathrm{Ei}[2t]-(t-1)^2\exp[2t]\mathrm{Ei}[-2t]\right] \quad \ldots\ldots(10)$$

which on expanding the exponential integrals becomes

$$\mathscr{E}_2=-2\zeta'^2\sum_{s=1}^{\infty}\frac{(2s+2)!\,(s+2)}{(2t)^{2s+2}s(s+1)}, \quad \ldots\ldots(11)$$

in agreement with the result of Dalgarno and Stewart (1956).

§ 3. Results and Discussion

The expressions (9), (10) and (11) are given in table 1 at a number of values of t, the series (11) being summed as described by Dalgarno and Lewis (1956). It is clear that the error arising from the (asymptotically) divergent nature of the series is small compared with that arising from ignoring the exponentially decreasing terms and that the series is very accurate for large values of t and still useful for t as small as 4.

Table 1. Values of $-\mathscr{E}_2/\zeta'^2$

t	Eqn (9)	Eqn (10)	Eqn (11)	
1	3·9862	3·6386	22·500	$\times 10^{-1}$
2	1·4051	2·6481	3·9844	10^{-1}
3	5·1372	7·1175	8·6134	10^{-2}
4	1·9548	2·2845	2·2242	10^{-2}
5	8·1857	8·6624	8·6049	10^{-3}
6	3·8579	3·9255	3·9196	10^{-3}
7	2·0286	2·0381	2·0374	10^{-3}
8	1·1658	1·1672	1·1671	10^{-3}
9	7·1794	7·1812	7·1811	10^{-4}
10	4·6659$_5$	4·6662	4·6662	10^{-4}

In tables 2 and 3 the exact energies of the 1sσ and 2pσ states of HeH^{2+} (Bates and Carson 1956) are compared with those obtained from perturbation theory taken to the second order using both the expanded and complete forms of V. The accuracy of the perturbation method (which is valid in the limit of infinite R) at *all* values of R for the 1sσ state occurs because the 1sσ state consists in the limit of vanishing R of a nucleus of charge $\zeta+\zeta'$ and a 1s electron, and the perturbation calculation of the energy of such a system on the basis of unperturbed hydrogenic wave functions corresponding to a charge ζ is *exactly* correct when taken to the second order (Trees 1956, Dalgarno 1956).

Table 2. Total Energies, $-\mathscr{E}$, of the 1sσ State of HeH^{2+}

R	Exact	Using Complete V	Using Expanded V
0	$9-4/R$	$9-4/R$	∞
1	2·06671	2·03061	2·39844
2	3·02439	3·01787	3·02224
3	3·33765	3·33716	3·33725
4	3·50121	3·50117	3·50117
5	3·60047	3·60047	3·60047

Table 3. Total Energies, $-\mathscr{E}$, of the 2pσ State of HeH^{2+}

R	Exact	Using Complete V	Using Expanded V
0	$2{\cdot}25-4/R$	$9-4/R$	∞
1	−1·32333	1·51178	10·00000
2	0·69037	1·45214	2·59375
3	1·02432	1·19227	1·34453
4	1·06216	1·07652	1·08897
5	1·04509	1·03253	1·03442

References

Bates, D. R., and Carson, T. R., 1956, *Proc. Roy. Soc.* A, **234,** 207.

Dalgarno, A., 1956, *Proc. Phys. Soc.* A, **69,** 784.

Dalgarno, A., and Lewis, J. T., 1955, *Proc. Roy. Soc.* A, **233,** 70; 1956, *Proc. Phys. Soc.* A, **69,** 57.

Dalgarno, A., and Stewart, A. L., 1956, *Proc. Roy. Soc.* A, **238,** 276.

Eisenschitz, R., and London, F., 1930, *Z. Phys.*, **60,** 491.

Margenau, H., 1939, *Rev. Mod. Phys.*, **11,** 1.

Trefs, R. E., 1956, *Phys. Rev.*, **102,** 1553.

Unsöld, A., 1927, *Z. Phys.*, **43,** 563.

LETTERS TO THE EDITOR

Note on the Population of Segments of a Random Series which include the Origin

If a segment of length l is arbitrarily chosen within a linear array of points randomly distributed, and of mean spacing $1/N$, the probability that precisely n points are included in the segment is given by the Poisson formula

$$P(n)=\frac{(Nl)^n}{n!}\,\mathrm{e}^{-Nl}. \qquad \ldots\ldots(1)$$

The distribution of developed grains along the track of a high-energy β-particle in a photographic emulsion is approximately random, and the problem has recently arisen (Stanners and Ross 1956) of calculating the probability of finding precisely n grains in an initial segment of such a track, the length of the segment, λ, being statistically determined by a frequency function which is constant-valued over the range $0\leqslant\lambda\leqslant l$ and is otherwise zero. The result of this calculation was so unexpected that it was thought worth while to treat a slightly more general case in a separate note.

Let there be a point O in a one-dimensional continuum such that to one side of O there is a constant probability Nds of finding a singularity (point-event) in a constant length ds arbitrarily placed, whereas to the other side of O this probability is everywhere zero. O is then defined as the origin of the random series of point-events, of average concentration N per unit length, stretching in (say) the positive direction from O (which is also taken as origin of coordinates). We consider now a segment of this one-dimensional continuum, of length l, stretching from $\mathrm{P}_1(\xi)$ to $\mathrm{P}_2(\xi+l)$. We assume that $-(l-x)\leqslant\xi\leqslant x$ $(0\leqslant x\leqslant l)$ and that over this range the frequency function describing the distribution of ξ values is constant-valued. Then the probability of finding precisely n point-events in $\mathrm{P}_1\mathrm{P}_2$ is given by

$$P(n,x)=\int_{-(l-x)}^{0}\frac{\{N(l+\xi)\}^n}{n!}\,\mathrm{e}^{-N(l+\xi)}\frac{d\xi}{l}+\frac{(Nl)^n}{n!}\,\mathrm{e}^{-Nl}\int_0^x\frac{d\xi}{l}$$

or

$$P(n,x)=\frac{1}{Nl}\left(\mathrm{e}^{-Nx}\sum_0^n\frac{(Nx)^r}{r!}-\mathrm{e}^{-Nl}\sum_0^n\frac{(Nl)^r}{r!}\right)+\frac{x}{l}\frac{(Nl)^n}{n!}\,\mathrm{e}^{-Nl}. \qquad \ldots\ldots(2)$$

Writing $Nl=\nu$, $x=fl$ in (2), we have

$$\frac{n!\mathrm{e}^{\nu}}{\nu^{n-1}}\{P(n,f)-P(n-1,f)\}=f^n\mathrm{e}^{\nu(1-f)}+f(\nu-n)-1. \qquad \ldots\ldots(3)$$

When $f=0$, (3) reduces to

$$P(n,0)-P(n-1,0)=-\frac{\nu^{n-1}}{n!}\,\mathrm{e}^{-\nu}.$$

This is the unexpected result already referred to: it implies

$$P(0,0)>P(1,0)>P(2,0)>\ldots \qquad \ldots\ldots(4)$$

or that, whatever the value of ν, the integral part of which is the most probable number of point-events to be found in a segment of length l wholly contained in the random series according to the Poisson formula, the most probable number of such events to be found in a segment of equal length is uniquely zero when the segment is so placed that the origin of the series always falls within the segment and has a uniform probability of falling anywhere in the segment.

Note that, when $f=1$, equation (3) reduces to

$$P(n,1)-P(n-1,1)=(\nu-n)\frac{\nu^{n-1}}{n!}e^{-\nu}$$

which, as it should be, is consistent with (1) and gives the result quoted above, that, for a segment wholly within the series, the most probable value of n is the integer immediately less than ν.

In the general case, when $0<f<1$, with ν and f given, the solution, $n=n_0$, of

$$f^n e^{\nu(1-f)}+f(\nu-n)-1=0 \qquad \ldots\ldots(5)$$

determines the most probable number of point-events in a segment of specified placing (as the integer immediately less than n_0); alternatively, with ν and n (integral, $\geqslant 1$) given, the solution of (5) for f determines the placing of the segment such that the probabilities of finding precisely n or $n-1$ point-events in the segment are equal and greater than the probability of finding any other specified number of point-events in the segment. Explicit solutions of equation (5) are not possible, nor, in general, are good approximations easily obtained. In all circumstances $f(\nu-n)<1$, but this inequality provides only a poor approximation to f, when ν and n are given. Similarly, when ν and f are given, it imposes no significant definition on n_0, at least when f is smaller than $1/\nu$. Writing equation (5) in the form

$$n\log f+\nu(1-f)-\log\{1-f(\nu-n)\}=0$$

we obtain a crude approximation for f when $\nu\gg n\geqslant 1$. This approximation is

$$f_0=e^{-\frac{\nu-1}{n}}.$$

Returning to the case $f=0$, the result of our calculation, expressed as in the multiple inequality (4), may appear somewhat surprising, as it certainly did when the calculation was first made, but it should be noted that when $\nu\gg 1$ in this case the probabilities of finding 0, 1, 2, ... point-events in the segment are very nearly equal, and the probability of finding ν events in the segment is still of the order $\frac{1}{2}P(0,0)$.

The particular result may then have been unexpected, but it is not unaccountably so.

The University,
Edinburgh.
19th December 1956.

N. FEATHER.

STANNERS, W. F., and ROSS, M. A. S., 1956, *Proc. Phys. Soc.* A, **69**, 836.

REVIEWS OF BOOKS

Quantum Field Theory, by H. UMEZAWA. Pp. xiv + 364. (Amsterdam: North Holland, 1956.) 70*s*.

In this book Dr. Umezawa describes the mathematical framework of relativistic quantum field theory. It is written from a somewhat advanced standpoint which would be suitable for a graduate student in theoretical physics who has already acquired some knowledge both of non-relativistic quantum field theory and of the physics which the theory is seeking to explain. The emphasis of the book is on the mathematical theory rather than on its physical interpretation or application. This emphasis has enabled Dr. Umezawa to write an elegant exposition of the subject unencumbered by many of the tedious details and the mountainous formulae which always occur when quantum field theory is applied to physical problems.

Following a historical introduction, four chapters are devoted to a discussion of relativistic wave equations for free fields. These describe the algebraic properties of the Dirac equation for the electron, the use of spinors, and general equations for particles of higher spin. The next four chapters describe the Lagrangian formalism and the quantization of free fields, and illustrate the general theory by giving its form for a variety of particular fields. The Heisenberg, the Schrödinger and the interaction representations are described in the next three chapters and are illustrated by different interacting fields.

A chapter is devoted to the perturbation solution for the scattering matrix; this follows closely the methods of Dyson and Feynman. Two chapters describe renormalization theory, and include an indication of the calculation of the Lamb-shift in lowest approximation. The last two chapters contain an outline of work on the relation between scattering phase shifts and potentials, and on the general theory of propagators; the latter includes a brief mention of the Bethe–Salpeter equation.

Extensive (but strongly selective) references are given to original papers; those in *Progress of Theoretical Physics* being somewhat over-emphasized. The book is essentially an introduction to the subject with a few random incursions to advanced topics, but it is unfortunate that it does not contain some elementary chapters which would make it more suitable for a student having no previous knowledge of quantum field theory. It is a welcome addition to the available literature. R. J. EDEN.

Resonance in Organic Chemistry, by G. W. WHELAND. Pp. xiii + 846. (New York: John Wiley; London: Chapman and Hall, 1955.) 120*s*.

When published in 1944, Wheland's *Theory of Resonance and its Applications to Organic Chemistry* was an extremely timely and welcome volume, as it set down in simple terms the information then available regarding the interpretation of the properties of organic compounds in terms of their electronic structures. This new book, with a shortened title, is the natural successor to the previous one, but it is rightly not regarded as a second edition since it is a much more comprehensive work.

The first eight chapters deal with the general theory of resonance, the nature of valence, resonance energy, the steric effects of resonance, and resonance in relation to dipole moments, molecular spectra, chemical equilibrium, and chemical reaction. Though these chapters bear the same titles as in the previous book, whilst the sub-headings have been added to rather than revised, the material included has swollen from 285 pages to 543. This extension has been produced not only by the introduction of summaries of more recently discovered facts, but also by the inclusion of much more profound theoretical discussions. In particular the value of the book has been immensely enhanced by the introduction of the molecular orbital treatments of valence and of the structures of conjugated molecules, in addition to the complementary valence-bond treatment. A further major addition to the book arises from the removal of the short section on the mathematical basis of resonance, previously appearing in Chapter 1, to form an extra chapter of 150 pages. This provides a good general introduction to wave mechanical theory as used by chemists. In addition the original 11-page Appendix, giving a table of bond lengths, has been expanded to 101 pages and now also includes bond angles.

Throughout the book is very well written and the arguments used are easy to follow. The production, too, is excellent, a feature which the reviewer found particularly pleasing being that benzene rings appear as regular hexagons instead of the badly distorted hexagons so frequently used. The book is written primarily for chemists, and it is to organic chemists that it should make its strongest appeal. On the other hand, it should be of very great value to all physicists who are interested in the mechanics of molecules. Perhaps an even more important function which it will serve, however, is to illustrate to the physicist the applications which the chemist is making of the principles of quantum mechanics, even in relation to molecules of very complex structures. J. W. SMITH.

Ordinary Non-Linear Differential Equations in Engineering and Physical Sciences, 2nd Edn., by N. W. McLachlan. Pp. viii + 271. (Oxford: Clarendon Press, 1956.) 35*s*.

The mathematical theory of non-linear differential equations has received a good deal of attention in the last decade but as yet there are not many expositions of its results in engineering terms. The book under review aims at filling this gap. Its first edition was published in 1950 (for a review, see *Proc. Phys. Soc.* B, 1951, **64,** 620); the fact that a second edition was called for is at the same time an indication of the interest taken in the subject and a tribute to the value of Professor McLachlan's book. The text of the first edition has been left substantially unaltered but two new chapters have been added. One of these gives an account of the theory of singular points of differential equations of the first order, with applications to stability questions, and some further useful stability criteria. This is a welcome addition since the subject is a basic part of the theory; it should prove very useful to the readers of the book. The other new chapter deals with a particular problem of laminar fluid flow that leads to an ordinary differential equation and with the numerical solution of that equation. The already extensive bibliography has been further enlarged and is to be commended for its exhaustiveness. A number of problems (with answers) have also been appended.

F. G. FRIEDLANDER.

Progress in Nuclear Energy. Series I: Physics and Mathematics. Vol. 1, edited by R. A. Charpie, J. Horowitz, D. J. Hughes and D. J. Littler. Pp. x + 398. (London: Pergamon Press, 1956). 84*s.*

Progress in Nuclear Energy will comprise eight series of annual publications. The first series, entitled *Physics and Mathematics*, begins with this volume of eleven articles which deal with the material on neutron physics presented at the Geneva Conference on the Peaceful Uses of Atomic Energy. There is an assurance that these reviews are not only summaries of the sessions of the Geneva Conference, but represent a subsequent " evaluation and distillation " of the material.

The first two articles (*Summary of Data on the Cross Sections and Neutron Yields of* ^{233}U, ^{235}U, and ^{239}Pu by P. A. Egelstaff and D. J. Hughes) survey the work of several countries, and emphasize the great measure of agreement between the data of independent workers, much of which was published for the first time at Geneva. *Techniques for Measuring Elastic and Non-Elastic Neutron Cross Sections* are reviewed comprehensively by Cranberg, Day, Rosen, Taschek and Walt. Both the theoretical and experimental aspects of fast reactors and discussed in some detail by Codd, Shepherd and Tait; delayed neutrons and their effect on reactor behaviour are described by G. R. Keepin.

The remaining six articles,† though contributing much to the usefulness of the book, are in themselves neither summaries nor the results of distillation but are reprinted, virtually word for word, from Volumes 4 and 5 of the Proceedings of the Geneva Conference. The assertion, on the dust cover, that " Almost every article has been specially written for this volume " is difficult to understand.

It is surprising that none of the authors includes a survey of available information on the energy spectrum of neutrons resulting from fission, which must be involved in, or indeed be a starting point of, many reactor calculations. The index lists only one reference to this subject, a mention of the Watt spectrum, though both a method of measuring the spectrum and results for ^{235}U, albeit incidentally, occur elsewhere in the book (pp. 139–140).

† *Theoretical Analysis of Neutron Resonances in Fissile Materials,* by H. A. Bethe.
The Cross Section of the Fission Product Poison ^{135}Xe *as a Function of Energy,* by S. Bernstein and E. C. Smith.
Resonance Captive Integrals, by R. L. Macklin and H. S. Pomerance.
Homogeneous Critical Assemblies, by Dixon Callihan.
Heterogeneous Methods for Calculating Reactors, by S. M. Feinberg.
Highly Enriched Intermediate and Thermal Assemblies, by M. Hurwitz and R. Ehrlich.

A. A. JAFFE.

Proceedings of the Second International Congress of the International Union for the Philosophy of Science: Zurich, 1954. (Neuchâtel/Suisse: Editions du Griffon; Paris: Dunod, 1955). 5 vols. (pp. 159, 152, 170, 136, 107). 3,000 *fr.*

Five volumes have been published of the proceedings of this Congress which was convened by Swiss philosophers of science. These volumes are devoted to (1) *Plenary Sessions*, (2) *Physics and Mathematics*, (3) *Theory of Knowledge and Linguistics*, (4) *Philosophy and Science, History of Philosophy*, (5) *Sociology and Psychology*. The printing was done in Switzerland and is very neat and clear.

Unfortunately, the papers themselves form a very curious hotch-potch, reflecting the equally curious way in which this Congress was organized. Some are of considerable interest, but many are of little value and others quite out of place. There seems, too, to be very little sense of arrangement. For example Adolf Grünbaum's mathematical paper on the clock paradox in the special theory of relativity appears in the third volume under Theory of Knowledge, whereas the abstract of Pierre Vernotte's paper *Les principes de la méthode scientifique* is included in the second volume under Physics.

Among the comparatively few papers which I can strongly recommend to readers of these *Proceedings* are the review of *The Philosophy of Science of Logical Empiricism* by Herbert Feigl and Piaget's paper on *Les lignes générales de l'epistemologie génétique*, both in the first volume, the paper by E. H. Hutten *On the Pauli Principle* in the second volume, and the paper on the clock paradox, already referred to, in the third volume.

Feigl's paper is the most valuable. It is a lucid discussion of some of the more important recent changes and developments in the outlook of Logical Empiricism. Feigl distinguishes three main trends. The first, exemplified in the work of Philipp Frank, combines informal logical analyses of the sciences with awareness of the psychological and cultural factors which lead to the selection of problems and may be regarded as the sequel to the work of Ernst Mach. Second is the development of analytic philosophy by G. E. Moore and Wittgenstein (to the reviewer this development seems to have very little to do with science and justifies Gustav Bergmann's appelation of ' futilitarian '). The third method is exemplified in the work of Carnap, Reichenbach, Woodger, Braithwaite, Tarski and others. Feigl argues incisively against Quine's contention that there is no sharp distinction between analytic and synthetic statements. Although the reviewer tends to sympathize with Quine in principle, he found Feigl's discussion clear and cogent, e.g. " The applicability of a certain formal structure such as transitivity to a set of empirically given facts is clearly a matter for synthetic statements. And although it might be said that Newtonian time is analytically transitive, or that Euclidean triangles are analytically equiangular, it cannot be claimed that the transitivity of experienced (or physically measured) time is a matter of analytic truth. Nor can it be said that it is logically true that a physical triangle *empirically* determined as equilateral must therefore also be equiangular." Furthermore, his discussion of Duhem's view of the impossibility of crucial experiments in science contains much sound sense, and his serious doubts concerning the role of alternative multi-valued logics as a solvent of scientific problems seem to be well-founded. All in all, a very stimulating paper.

G. J. WHITROW.

CONTENTS OF SECTION B

PAGE

Dr. L. E. Collins and Dr. O. S. Heavens. The Epitaxial Growth and Oxidation of Nickel, Cobalt and Iron on Rocksalt 265

Dr. P. T. Landsberg. A Contribution to the Recombination Statistics of Excess Carriers in Semiconductors 282

Dr. J. E. Allen, Dr. R. L. F. Boyd and Dr. P. Reynolds. The Collection of Positive Ions by a Probe Immersed in a Plasma 297

Dr. R. J. Bickerton. The Lateral Diffusion of an Electron Swarm in a Magnetic Field 305

Dr. B. K. P. Scaife. Dipole Moment Fluctuations of a Dielectric Body . . 314

Dr. F. C. Champion and Mr. D. L. O. Humphreys. Variations in the Ultra-Violet Absorption of Counting Diamonds. 320

Research Notes :

Mr. A. Danielian and Dr. K. W. H. Stevens. High Temperature Susceptibilities 326

Mr. B. Rowson. Measurements of the Angular Diameters of Two Galactic Radio Sources at a Wavelength of 10·7 cm 328

Letters to the Editor :

Dr. D. J. Oliver. Current Noise in Indium Antimonide 331

Reviews of Books 333

Contents of Section A 344

Magnetic Analysis of Tritons and Alpha Particles Emitted from the Deuteron Bombardment of Teflon

By F. A. EL BEDEWI and I. HUSSEIN

Faculty of Science, University of Alexandria, Egypt

MS. received 14th August 1956, and in final form 18th December 1956

Abstract. The energy spectra for particles emitted from the $^{19}F(d,t)^{18}F$ and $^{12}C(d,\alpha)^{10}B$ reactions have been measured by magnetic analysis. The mean energy of the incident deuterons is 8·9 Mev. The energy levels of ^{18}F are determined at $0{\cdot}94 \pm 0{\cdot}02$ Mev and $1{\cdot}07 \pm 0{\cdot}02$ Mev. The latter level is found to have $T=1$. The energy levels of ^{10}B are only observed at 0·72 Mev and 2·14 Mev. The absence of an alpha particle group corresponding to a level at 1·74 Mev, characterized by $T=1$, is good evidence for the operation of the isobaric spin selection rule.

Angular distributions of these triton and alpha particle groups are presented. The triton distributions are fitted to theoretical pick-up curves. The angular momenta carried away by the picked-up neutron leaving the nucleus ^{18}F at the ground, 0·94 Mev and 1·07 Mev states are found to be 0, 1 and 0 respectively.

---

§ 1. Introduction

At moderate deuteron energy the angular distributions of (d, pn) reactions at small angles are found to contain large contributions from deuteron stripping. Also, the pronounced forward structure first observed by El Bedewi (1951) in the distribution for the $^{9}Be(d,t)^{8}Be$ reaction suggests an inverse process, i.e. a deuteron pick-up. In this process, a neutron attached to the initial nucleus is captured by the deuteron in its flight near the target nucleus. Beside these well established processes, the recent distributions for the $^{16}O(d,\alpha)^{14}N$ reaction reported by Green and Middleton (1956 b) show similar features to those of stripping reactions. El Nadi (private communication) proposes a theory for this reaction on the assumption that the incident deuteron picks up a neutron and a proton from the target nucleus.

The object of this work is to report some angular distributions from $^{19}F(d,t)^{18}F$ and $^{12}C(d,\alpha)^{10}B$ reactions which can illustrate these single and double pick-up processes. Moreover, the nuclear properties of the residual nuclei in both these reactions are of particular interest since they are odd–odd self-mirrored nuclei each containing an equal number of neutrons and protons. Also, some light could be given on the validity of the conservation of isobaric spin since both ^{10}B and ^{18}F should contain a low-lying level having $T=1$.

§ 2. Procedure

A thin teflon (CF_2) target of 1 mg cm^{-2} surface density was bombarded by a beam of deuterons of $8{\cdot}90 \pm 0{\cdot}02$ Mev mean energy provided by the Liverpool 37 inch cyclotron. A heavy particle magnetic spectrograph (Green and Middleton

1956 a) was used to sort out the outgoing charged particles. They were detected in Ilford C2 emulsion 100 μ thick and examined with a binocular microscope with magnification of about 1000.

A detailed description of the present experiment was reported by El Bedewi (1956). Although the difference in range and initial ionization permit the discrimination between protons and deuterons yet in case of tritons and alpha particles mere observation is not adequate. Reliable identification is achieved by dividing each plate into small portions and the tritons are sorted from the alpha particles by range measurements. When these particles are mixed together in one of these portions, tritons should be slightly shorter and because of their greater energy dispersion, the triton groups are broader than those of alpha particles. A typical range distribution at an angle of observation of 10° for these triton groups mixed with alpha particles emitted from the $^{19}F(d,\alpha)^{17}O$ reaction is shown in figure 1. The abscissa represents the range in scale divisions (1 s.d. = 2·410 μ) and the ordinate represents the number of accepted tracks observed in an area of 8 mm wide and about 1 cm long. Since at any point in the emulsion the energy of the recorded particle is proportional to Z^2/m, where Z and m are the charge and mass of the particle respectively, a further check was given by the requirement of consistency in the mean energy of the particles belonging to each group as derived from the following procedures: (i) the mean ranges of the tritons and alpha particles corrected for the emulsion shrinkage and using the range–energy relations of El Bedewi (1951) and Rotblat (1951); (ii) the mean ranges of the deuteron background measured at the position of the weighted mean of each group; (iii) the position of each group with respect to

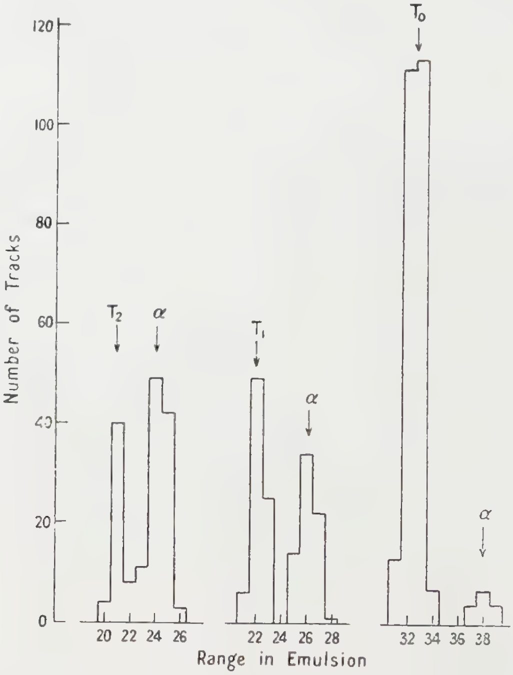

Figure 1. Histograms of tritons and background alpha particles emitted from the deuteron bombardment of fluorine at 10°. In the abscissa, 1 scale division = 2·410μ.

those defined by the protons emitted from the $^{12}C(d,p)^{13}C$ reaction and using the energy–distance relation as described by El Bedewi (1956).

The Q values of the triton and alpha particle groups were calculated at each angle of observation, from their corresponding mean energy. The loss of particle energy in escaping from the target was taken into consideration.

§ 3. Results and Discussion

3.1. *The $^{19}F(d,t)^{18}F$ Reaction*

(*a*) *Energy spectrum.*

The triton spectrum of an angle of observation of 10° is shown in figure 2.

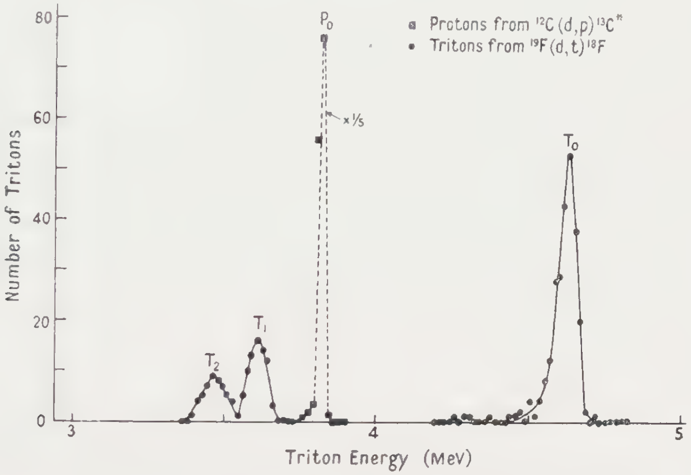

Figure 2. Spectrum of the triton groups from the deuteron bombardment of teflon at an angle of observation of 10°.

The group denoted by P_0 is due to protons from the $^{12}C(d,p)^{13}C$ reaction leaving the residual nucleus at its ground state. Groups denoted by T_0, T_1 and T_2 are identified as being due to tritons emitted from the $^{19}F(d,t)^{18}F$ reaction. These correspond to the ground state and two levels of the residual nucleus ^{18}F at $0{\cdot}94 \pm 0{\cdot}02$ Mev and $1{\cdot}07 \pm 0{\cdot}02$ Mev. The reaction energy Q_0 was found to be $-4{\cdot}17 \pm 0{\cdot}02$ Mev and from this the mass of ^{18}F was calculated to be $18{\cdot}006665 \pm 0{\cdot}000034$ m.u., using the masses of ^{2}H and ^{19}F as given by Scolman, Quisenberry and Nier (1956) and the triton mass as quoted by Li, Whaling, Fowler and Lauritsen (1951). This result is in good agreement with the value of $18{\cdot}006651 \pm 0{\cdot}000022$ m.u. reported by Li (1952) from the $^{18}F(\beta^+)^{18}O$ and $^{18}O(p,n)^{18}F$ reactions.

(*b*) *Angular distribution.*

The angular distributions of these triton groups are plotted in the centre-of-mass system as shown in figure 3. The experimental errors are the statistical standard deviation. Although these results are presented in arbitrary units yet, when using the known cross sections for $^{12}C(d,p)^{13}C$ reaction, they can be converted to millibarns per steradian by multiplying by $0{\cdot}0085 \pm 0{\cdot}0017$ (El Bedewi 1956). The theoretical curves are calculated from the Born approximation

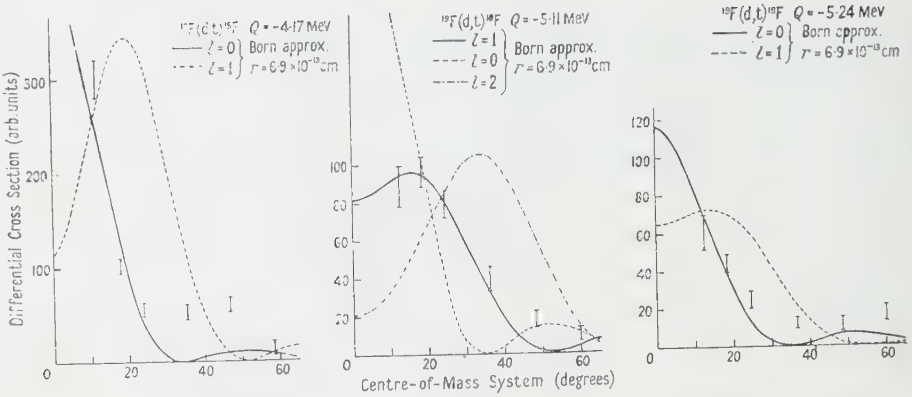

Figure 3. Angular distribution of triton groups emitted from ^{19}F(d, t)^{18}F reaction corresponding to the ground, 0·94 Mev and 1·07 Mev states of ^{18}F.

pick-up theory (Newns 1952). The radius of interaction used in the theoretical formula to give the best fit was found to be $6 \cdot 9 \times 10^{-13}$ cm, i.e. the Gamow radius plus 2×10^{-13} cm. Good agreement was obtained by assuming that the transitions to the ground, 0·94 Mev and 1·07 Mev levels in ^{18}F are characterized by angular momenta $l = 0$, 1 and 0 respectively. Assuming the initial nucleus ^{19}F to have $J = \frac{1}{2}^{+}$, the results concerning the nuclear properties of the energy levels in ^{18}F are given in the table.

(1)	(2)	(3)	(4)	(5)	(6)	(7)	(8)
T_0	0	0	even	0,1	1	2·55	40
T_1	0·94	1	odd	0,1 or 2		0·75	53
T_2	1·07	0	even	0,1	0	0·52	25

(1) Group ; (2) energy level (Mev) ; (3) l-value ; (4) parity ; (5) possible spins of the final nucleus J_f; (6) suggested spin J_f; (7) absolute cross section at 10°(mbn sterad^{-1}) ; (8) pick-up probability (arbitrary units) Λ.

(c) *Discussion.*

Up to now no results from the ^{19}F(d, t)^{18}F reaction have been reported The low energy levels of ^{18}F have been investigated by using the ^{20}Ne(d, α)^{18}F reaction (Middleton and Tai 1951) and the ^{14}N(α, γ)^{18}F reaction (Price 1955). No experimental assignments for the spin and parity of these levels are yet known.

With regard to the ground state of ^{18}F our results are consistent with the positron decay to the ground state of ^{18}O (Ruby and Richardson 1951). Since the present transition to both the ground and the 1·07 Mev states of ^{18}F has $l = 0$, it is easily seen from the calculation of Elliot and Flowers (1955) that if one of these states has $T = 0$ the other should have $T = 1$. As shown later, the ground state of ^{18}F must have $T = 0$. Now, since the ground state of ^{18}O is known to have $J = 0^{+}$ and $T = 1$ and since the 0–0 transition requires $\Delta T = 0$ then the observed β^{+} transition will thus indicate that the ground state of ^{18}F must have $J = 1^{+}$. This is a reasonable assignment as it agrees with the systematics of odd–odd nuclei. Recently, Reynolds and Standing (1956) used 19·8 Mev protons to investigate the ^{19}F(p, d)^{18}F reaction. The angular distribution of the deuteron group corresponding to the ^{18}F ground state gave a fit with the theory when $l = 0$

in agreement with the present work. It is of interest to point out that these authors have reported the differential cross section in the centre-of-mass system at 11° as 8·5 millibarns per steradian which is three times as large as the value found for the present (d, t) reaction at the same angle.

The energy levels in ^{18}F are of considerable theoretical importance since it contains a proton and a neutron outside a symmetrical ^{16}O core. Elliot and Flowers (1955) pointed out that the even parity levels of this nucleus could be formed by linear combinations of single particle orbitals represented by $\Sigma_x(1d)^{2-x}(2S)^x$ where x is 0, 1 or 2. In terms of these configurational mixing and intermediate coupling these authors calculated the relative positions of the lowest levels of $T=0$ and $T=1$ as functions of the strength V_c of the central interaction. Since the positions of the $T=1$ levels relative to the $T=0$ levels are found to be very sensitive to the spin exchange character of the central interaction and since no experimental results on the nature of these levels are yet known, it was difficult to choose with certainty the type of force or even the value of V_c to fix the exact positions of these levels.

The first level with $T=1$ corresponding to the ground state of ^{18}O calculated from the coulomb energy should appear at about 1·1 Mev. The level at $1{\cdot}05 \pm 0{\cdot}03$ Mev observed by Middleton and Tai (1951) from the ^{20}Ne(d, α)^{18}F reaction is unlikely to have $T=1$ on account of the isobaric spin selection rule. Although Price (1955) has reported from the radioactive capture of alpha particles in ^{14}N an identical level at $1{\cdot}075 \pm 0{\cdot}010$ Mev yet no intepretation of a transition of energy $0{\cdot}945 \pm 0{\cdot}010$ Mev was given. It seems from the present work that the observed two neighbouring levels at 0·94 Mev and 1·07 Mev can thus give some light to clear the situation of the conservation of isobaric spin. The former level in agreement with the 0·945 Mev transition of Price is in fact identical to the 1·05 Mev level previously reported by Middleton and Tai. This level can have $T=0$, odd parity and spin 0, 1 or 2. The other level at 1·07 Mev, which agrees well with the transition of 1·075 Mev observed by Price, is found to have even parity and spin 0 or 1. It is likely that this level has $J=0^+$ and $T=1$ as it may represent the $T_z=0$ member of the $T=1$ triplet, of which the ^{18}O and ^{18}Ne ground states are the $T_z=+1$ and -1 components respectively. On this assumption, the calculations of Elliott and Flowers (1955) will not require a Serber force but rather a modified form of the Rosenfeld mixture has to be used to lower the $T=1$ group to the position required for an energy difference of 1·07 Mev between the $T=0$ and $T=1$ lowest levels. Hence, the value of V_c could be adjusted to fulfil this requirement.

3.2. *The $^{12}C(d,\alpha)^{10}B$ Reaction*

(*a*) *Energy spectrum.*

The spectrum of alpha particles of energy less than 9 Mev at an angle of observation of 10° is represented in figure 4. Also shown in this figure is a proton group P_1 from the ^{12}C(d, p)^{13}C* reaction leaving the residual nucleus at the known level 3·09 Mev. While the observed background is mainly due to the ^{19}F(d, α)^{17}O reaction, the groups denoted by α_0, α_1 and α_3 are identified as being due to the ^{12}C(d, α)^{10}B reaction. These groups correspond to the ground state and two levels of ^{10}B at $0{\cdot}72 \pm 0{\cdot}02$ Mev and $2{\cdot}14 \pm 0{\cdot}02$ Mev. The energy of this reaction Q_0 is calculated from different angles of observation and the mean value is found to be $-1{\cdot}39 \pm 0{\cdot}02$ Mev. Using the masses of ^{2}H, ^{10}B and ^{12}C as

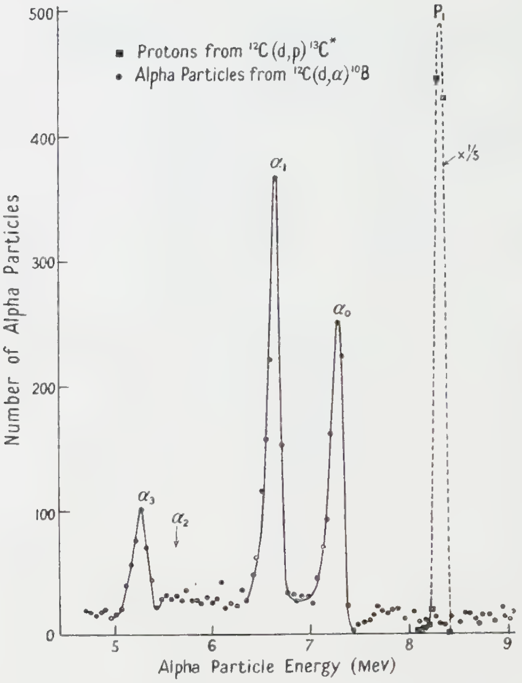

Figure 4. Spectrum of alpha particle groups from the deuteron bombardment of carbon at an angle of observation of 10°.

reported by Scolman *et al.* (1956) the mass of an alpha particle is found to be 4·003923 ± 0·000025 m.u. in agreement with the value 4·003944 ± 0·000019 m.u. given by Nier (1951).

(*b*) *Angular distribution.*

The angular distributions of the groups α_0, α_1 and α_3 are shown in the centre-of-mass system in figure 5. These distributions are represented in the same units and can be converted to millibarns per steradian by multiplying by 0·017 ± 0·003 (El Bedewi 1956). It is of interest to point out that the cross sections of deuteron induced reactions with carbon are considerably larger than those with fluorine.

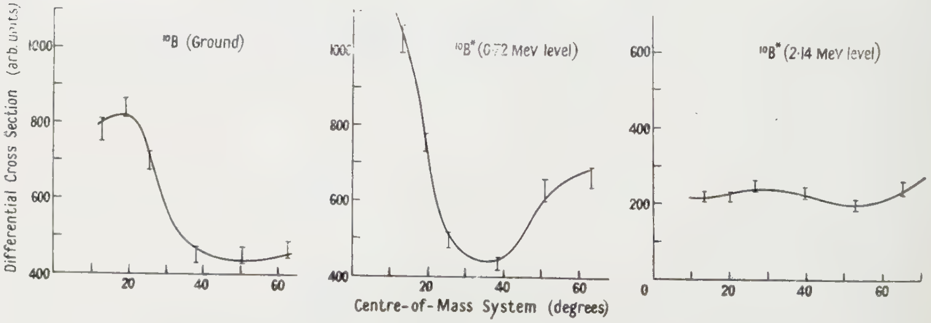

Figure 5. Angular distribution of alpha particle groups emitted from $^{12}C(d, \alpha)^{10}B$ reaction corresponding to the ground, 0·72 Mev and 2·14 Mev states of ^{10}B.

(*c*) *Discussion.*

This reaction was first investigated by Berlman (1950) using nuclear emulsions to detect the charged particles emitted from the bombardment of 10 MeV deuterons with thin carbon target. The author has reported the energy of this reaction Q_0 as $-1{\cdot}44$ MeV in agreement with the present work. Two levels at 0·41 MeV and 0·71 MeV were also reported. Ashmore and Raffle (1951) used a magnetic spectrometer with proportional counter as a detector to study this reaction and were able to confirm the existence of the latter level. The level at 0·41 MeV has neither been observed in the present work nor in all investigations of other reactions leading to this residual nucleus ^{10}B (Ajzenberg and Lauritsen 1955). The most accurate determination of these energy levels was obtained from the inelastic scattering of protons from ^{10}B reported by Bockelman, Browne, Buechner and Sperduto (1953). These authors have reported, in our region of investigation, levels at 0·717, 1·739 and 2·152 MeV with errors of $\pm 0{\cdot}005$ MeV. In the present work the levels observed at 0·72 MeV and 2·14 MeV are in good agreement with those of Bockelman *et al.* With regard to the level at 1·739 MeV an arrow at α_2 is shown in figure 4 to represent its position. As is seen, only a uniform background of alpha particles is observed. A similar conclusion has been obtained from the inelastic scattering of deuterons from ^{10}B reported by Bockelman *et al.* (1953). The absence of this level is consistent with the isobaric spin selection rule since it is known to have $T=1$, the analogue to the ground states of ^{10}Be and ^{10}C.

With regard to the nature of the angular distribution, although in some cases it resembles those of deuteron stripping or pick-up yet the compound nucleus influence is hardly to be ruled out. It is advisable that some experiment be performed to extend these measurements to backward angles. However, El Nadi (private communication) has successfully fitted the distribution belonging to the level 0·72 MeV ($J=1^+$) by a theoretical curve calculated on the assumption that the angular momentum transferred by the captured neutron and proton are $l_n=l_p=0$. The radius of interaction used in this calculation is $5{\cdot}3\times10^{-13}$ cm.

ACKNOWLEDGMENTS

One of the authors (F. B.) is grateful to Professor H. W. B. Skinner for his encouragement and advice during the performance of this experiment at the Nuclear Physics Research Laboratory, Liverpool.

The authors would also like to express their gratitude to Professor M. A. El Sherbini for his interest and discussion.

REFERENCES

AJZENBERG, F., and LAURITSEN, T., 1955, *Rev. Mod. Phys.*, **27**, 77.
ASHMORE, A., and RAFFLE, J. F., 1951, *Proc. Phys. Soc.* A, **64**, 754.
BERLMAN, J. B., 1950, *Phys. Rev.*, **80**, 775.
BOCKELMAN, C. K., BROWNE, C. P., BUECHNER, W. W., and SPERDUTO, A., 1953, *Phys. Rev.*, **92**, 665.
EL BEDEWI, F. A., 1951, *Proc. Phys. Soc.* A, **64**, 947, 1079 ; 1956, *Ibid.*, **69**, 221.
ELLIOT, J. P., and FLOWERS, B. H., 1955, *Proc. Roy. Soc.* A, **229**, 536.
GREEN, T., and MIDDLETON, R., 1956 a, *Proc. Phys. Soc.* A, **69**, 16 ; 1956 b, *Ibid.*, **69**, 28.
LI, C. W., 1952, *Phys. Rev.*, **88**, 1038.
LI, C. W., WHALING, W., FOWLER, W. A., and LAURITSEN, C. C., 1951, *Phys. Rev.*, **83**, 512.

Middleton, R., and Tai, C. T., 1951, *Proc. Phys. Soc.* A, **64,** 801.
Newns, H. C., 1952, *Proc. Phys. Soc.* A, **65,** 916.
Nier, A. O., 1951, *Phys. Rev.*, **81,** 624.
Price, P. C., 1955, *Proc. Phys. Soc.* A, **68,** 553.
Reynolds, J. B., and Standing, K. G., 1956, *Phys. Rev.*, **101,** 158.
Rotblat, J., 1951, *Nature, Lond.*, **167,** 550.
Ruby, L., and Richardson, J. R., 1951, *Phys. Rev.*, **83,** 698.
Scolman, T. T., Quisenberry, K. S., and Nier, A. O., 1956, *Phys. Rev.*, **102,** 1076.

Electron Excitation of 3p Levels of OI

By I. C. PERCIVAL
Department of Physics, University College London

Communicated by H. S. W. Massey; MS. received 12*th December* 1956

Abstract. The collision strengths for low-energy electron excitation of OI from the ground level to the $2p^3(^4S)3p\,^3P$ and ^5P excited levels have been calculated using the distorted wave Born–Oppenheimer approximation, and the ^5P collision strength using the exchange-distorted wave Born–Oppenheimer approximation.

Difficulty with the orthogonality properties of the radial functions of the 3p orbitals leads to an investigation of the approximate atomic wave functions used in the calculations. A comparison of fine-structure separations suggests that for the ^3P excited level a single-configuration Hartree–Fock wave function with one parent term is insufficiently accurate for the calculation of these collision strengths. A similar comparison leads to an improved estimate of the ^5P collision strength, though various corrections to the estimate might modify it within wide bounds.

A method of calculating certain exchange integrals is described.

It is concluded that before calculating collision cross sections for similar processes, great care should be taken to ensure that the atomic wave functions are sufficiently accurate.

---

§ 1. INTRODUCTION

In order to determine the importance of the processes

$$\mathrm{OI}\,2p^4\,^3P + e \rightarrow \mathrm{OI}\,2p^3(^4S)3p\,^3P + e \quad (10{\cdot}74\,\mathrm{ev}) \qquad \ldots\ldots(1)$$

$$\rightarrow \mathrm{OI}\,2p^3(^4S)3p\,^5P + e \quad (10{\cdot}99\,\mathrm{ev}) \qquad \ldots\ldots(2)$$

in aurorae, the collision cross sections, or the closely related collision strengths (equation (5)), are required for incident electrons with energies slightly above the indicated excitation thresholds. For this purpose approximate wave functions for the initial and final levels of the oxygen atom must be obtained. The derivation and accuracy of such functions are considered in § 2.

Since magnetic effects are negligible, the second process, with change of spin, must involve rearrangement of electrons, and this may also be of importance for the first process, so exchange must be considered. As the energies of the incident electrons are small, distortion will also be important, so that either the distorted wave Born–Oppenheimer (DBO), or the more complex but more exact exchange-distorted wave Born Oppenheimer (EDBO) approximations (Seaton 1953 a, Massey and Moiseiwitsch 1954) may be used, as described in §§ 3–5.

Inevitably, in calculations relating to complex collision processes, one must have recourse to further approximations, and estimates of the consequent errors introduced into the calculated ^5P collision strength, together with a revised evaluation, appear in § 6.

Unless other units are specified, all quantities are expressed in Hartree units, for which the unit of energy is the Rydberg unit and of any other quantity is the atomic unit.

§ 2. THE OXYGEN ATOM: INITIAL AND FINAL LEVELS

We shall use the following abbreviations:

Level	Usual notation	
0	$\mathrm{O\,I\,2p^4\,{}^3P}$	
1	$\mathrm{O\,I\,2p^3({}^4S)3p\,{}^3P}$	......(3)
2	$\mathrm{O\,I\,2p^3({}^4S)3p\,{}^5P}$.	

The radial function of an orbital of level *i* will be distinguished by a suffix *i* to the principal quantum number.

The most thorough calculations of the wave functions of the oxygen atom at present available are those of Hartree, Hartree and Swirles (1939–40), who have tabulated the normalized radial functions of the Hartree–Fock electron orbitals for the ground configurations of O I and O II.

The central field obtained from their $\mathrm{O\,II\,2p^3\,{}^4S}$ functions was used to calculate the radial function $P(3\mathrm{p})$ of levels 1 and 2, neglecting exchange and perturbation of the ${}^4\mathrm{S}$ core by the 3p electron. This approximate $P(3\mathrm{p})$ will be denoted P_{E}. It will be shown later that P_{E} is a bad approximation to $P(3\mathrm{p})$ near the origin, where the other orbitals are large. $P(3\mathrm{s})$ for the corresponding ${}^3\mathrm{S}$ and ${}^5\mathrm{S}$ levels of O I was calculated to the same approximation, and both functions appear in table 1.

The 2p radial function $P(2_{\mathrm{II}}\mathrm{p})$ of $\mathrm{O\,II\,2p^3\,{}^4S}$ was used for the ${}^4\mathrm{S}$ core of levels 1 and 2 throughout.

Orthogonality Properties of P(3p)

For our purposes two distinct orthogonality properties of atomic wave functions are of importance:

(A) Exact atomic wave functions for different energy levels are orthogonal. In the calculation of inelastic collision strengths, the approximate atomic wave functions of the initial and final states should also be orthogonal, or there will be contributions from elastic scattering terms.

(B) In the Hartree–Fock approximation the electron orbitals belonging to the same determinant are usually made orthogonal, thus simplifying the calculations without modifying the approximate wave function of the whole atom. Such orthogonality is necessary for the derivation of equations (15) and (16) which are used for the calculation of collision strengths.

The orthogonality properties of P_{E} make it unsatisfactory for the calculation of collision strengths. The 3p radial functions for levels 1 and 2, denoted $P(3_1\mathrm{p})$ and $P(3_2\mathrm{p})$ respectively, will be considered separately.

(i) By (A), the atomic wave functions of levels 0 and 1 must be orthogonal. Since for our approximate wave functions this is not ensured by angular or spin factors, the radial functions must be appropriately modified. For this purpose a second approximate $P(3\mathrm{p})$, denoted P_{G}, was formed by subtracting sufficient $P(2_0\mathrm{p})$ of level 0 from P_{E} to make the difference orthogonal to $P(2_0\mathrm{p})$, and normalizing. As shown in the figure, the overlap between $P(2_0\mathrm{p})$ and $\mathrm{P_E}$ is small, and about $\frac{1}{5}P(2_0\mathrm{p})$ had to be subtracted, so that P_{G} is several times smaller than P_{E} near the origin.

Condition (B) is automatically satisfied by level 1 through the spin quantum numbers of the orbitals.

(ii) The orthogonality conditions for $P(3_2\mathrm{p})$ are the converse of those for $P(3_1\mathrm{p})$.

Table 1. $P(3p, r)$ of O I $2p^3(^4S)3p\,^3P$ and ^5P, and $P(3s, r)$ of O I $2p^3(^4S)3s\,^3S$ and ^5S Calculated Neglecting Exchange in the Field of an Unperturbed ^4S Core.

r	$P(3p, r)$ $P_E(r)$	$P(3s, r)$
0	0	0
0·01	0·000	0·020
0·02	0·001	0·037
0·03	0·003	0·052
0·04	0·005	0·063
0·06	0·009	0·080
0·08	0·016	0·090
0·10	0·023	0·094
0·12	0·031	0·093
0·14	0·039	0·088
0·16	0·048	0·081
0·18	0·056	0·072
0·20	0·065	0·060
0·15	0·043	0·085
0·25	0·088	0·028
0·30	0·109	−0·007
0·35	0·128	−0·042
0·40	0·146	−0·075
0·45	0·161	−0·104
0·50	0·174	−0·129
0·6	0·194	−0·167
0·7	0·207	−0·190
0·8	0·214	−0·200
0·9	0·217	−0·201
1·0	0·217	−0·193
1·1	0·214	−0·179
1·2	0·209	−0·160
1·4	0·193	−0·114
1·6	0·174	−0·061
1·8	0·151	−0·006
2·0	0·125	0·051
2·2	0·098	0·105
2·4	0·069	0·157
2·6	0·039	0·205
2·8	0·009	0·249
3·0	−0·021	0·289
3·2	−0·052	0·324
3·4	−0·081	0·354
3·6	−0·110	0·380
3·8	−0·138	0·401
4·0	−0·164	0·418
3·5	−0·096	0·368
4·5	−0·224	0·444
5·0	−0·274	0·450
5·5	−0·313	0·440
6·0	−0·341	0·420
6·5	−0·360	0·392
7·0	−0·370	0·360
7·5	−0·373	0·326
8·0	−0·369	0·292
8·5	−0·359	0·258
9·0	−0·346	0·227
9·5	−0·330	0·197
10·0	−0·311	0·171
10·5	−0·291	0·147
11·0	−0·271	0·125
11·5	−0·250	0·107
12·0	−0·230	0·090
13	−0·191	0·064
14	−0·156	0·045
15	−0·125	0·031
16	−0·099	0·021
17	−0·078	0·014
18	−0·060	0·010
19	−0·046	0·006
20	−0·035	0·004

$P(3p, r)$, $P_E(r)$

Calculated energy parameter 2·20 ev.
Experimental energy parameter 2·25 ev.
For small r : $P = 3{\cdot}30 r^2 (1 - 4r)$.
For large r : $P = -0{\cdot}0750 \exp(-0{\cdot}4032 r) r^{2{\cdot}48} (1 - 2{\cdot}07/r)$.

$P(3s, r)$

Calculated energy parameter 3·57 ev.
Experimental energy parameter 3·75 ev.
For small r : $P = 2{\cdot}20 r (1 - 8r)$.
For large r : $P = 0{\cdot}399 \exp(-0{\cdot}5135 r) r^{1{\cdot}95} (1 - 1{\cdot}8/r)$.

Condition (A) is satisfied for states 0 and 2 through the atomic spin.

But neither angular nor spin factors ensure orthogonality of the 2p and 3p orbitals of state 2 so, by condition (B), $P(3_2\text{p})$ must be orthogonal to $P(2_{\text{II}}\text{p})$ of the ^{4}S core. The radial function P_{F} is the normalized linear combination of P_{E} and $P(2_{\text{II}}\text{p})$ which is orthogonal to the latter. The overlap in this case is even smaller: about $\frac{1}{4}P(2_{\text{II}}\text{p})$ had to be subtracted from P_{E}, and this so dominated the shape of the function P_{F} near the origin as to introduce an additional zero there. Thus by the usual definition of principal quantum number in terms of the number of zeros, P_{F} could not be the radial function of a 3p orbital.

At the end of the detailed calculations to be described, it was found that the estimated collision strengths were very sensitive to the approximate $P(3\text{p})$ in the region $0{\cdot}3 < r < 1{\cdot}3$, where $P(3\text{p})$ is dependent on the orthogonality conditions imposed.

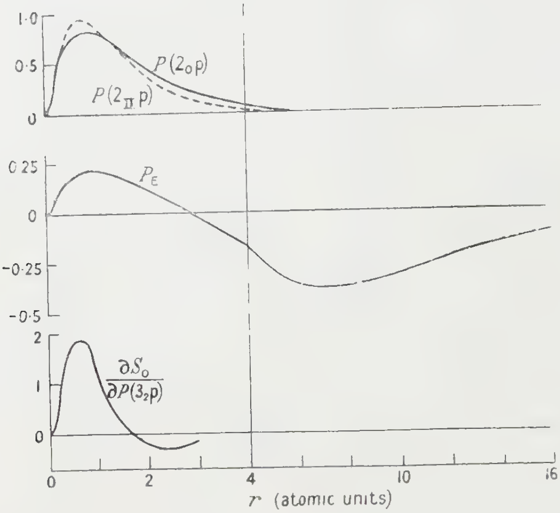

The radial wave functions $P(2_0\text{p})$ of OI and $P(2_{\text{II}}\text{p})$ of OII were calculated by Hartree, Hartree and Swirles (1939–40). P_{E} is the approximate radial wave function $P(3\text{p})$ of OI calculated without exchange in the static field of OII. $\partial S_0/\partial P(3_2\text{p})$ is a measure of the sensitivity of S_0 to errors in the function $P(3_2\text{p})$.

Massey (private communication, 1954) suggested that a good check on the magnitude near the origin of such a radial function might be afforded by comparing calculated and observed fine-structure separations. The observed separations (Moore 1949) and those calculated using P_{G} are shown in table 2.

The observed separations for level 1 do not obey the Landé interval rule, so that assuming only first-order spin–orbit interaction to be important in determining the fine structure, this level is not representable as a single configuration with one parent term. Other considerations suggest mixing of level 1 with OI$2\text{p}^3(^2\text{D})3\text{p}\,^3\text{P}$. Separations for level 2 calculated with P_{G} are too small, and P_{F} would give even worse results, as it is smaller than P_{G} near the origin. However, as the interval rule is nearly obeyed in this case, a better approximation P_{H} to $P(3_2\text{p})$ was sought.

Table 2. Observed (Moore 1949) and Calculated Fine-Structure Separations

Level	J	(1)	(2)	(3)
$2p^3(^4S)3p\,^3P$	2			
1		0·54	−0·047	
	1			
		−0·70	−0·023	
	0			
$2p^3(^4S)3p\,^5P$	1			
2		2·02	0·047	0·92
	2			
		3·67	0·070	1·38
	3			

(1) Observed intervals (cm^{-1}); (2) intervals calculated using P_G (cm^{-1}); (3) intervals calculated using P_H (cm^{-1}).

P_H was obtained by a scaling process, using the free radial wave functions $\mathscr{F}_{II}(r)$ of the system O II $2p^3(^4S)+kp\,^5P$ for the zero-energy limit ($k=0$) calculated with the inclusion of exchange distortion by Seaton (1953 b, 1955). The system is the same as that of level 2, so that, except for the differences in the energy parameters, the wave equations are identical. Within a distance of 2 atomic units of the origin the potential and kinetic energies are separately very large compared with the energy parameter of level 2. Thus within this region the corresponding radial functions calculated using the same approximation differ only slightly if appropriately normalized, e.g. P_G and the corresponding free radial wave function $F_{II}(r)$ have their first maxima at $r=1{\cdot}3$ and $r=1{\cdot}1$ respectively. For $r<2$, $\mathscr{F}_{II}(r)$ may be closely approximated by appropriate scaling of $F_{II}(r)$. $P_H(r)$ was obtained by scaling $P_G(r)$ in substantially the same way, giving

$$P_H(r)=2{\cdot}41P_G(1{\cdot}8r). \qquad \ldots\ldots(4)$$

P_H is not normalized to unity, and is unlikely to be useful beyond $r=2$.

The fine-structure comparison is more satisfactory for P_H but suggests that $1{\cdot}5P_H$ might be a better approximation to $P(3_2p)$ near $r=0{\cdot}7$.

§ 3. WEAK COUPLING DISTORTED WAVE APPROXIMATIONS

A convenient measure of the probability of a collisionally induced atomic transition (say $i\to j$), is the collision strength (Hebb and Menzel 1940, Seaton 1953 a):

$$\Omega(ij)=k_i^2\omega_i Q(i\to j) \qquad \ldots\ldots(5)$$

where Q is the collision cross section for the process in units of πa_0^2, and ω_i the degeneracy of the state i of the atom.

We shall use $\Omega^a(ij)$ to denote a contribution from a state a of the whole system to the total collision strength $\Omega(ij)$, where

$$\Omega(ij)=\sum_a \Omega^a(ij). \qquad \ldots\ldots(6)$$

It may be shown (Seaton 1953 a, Percival 1956) that for weak coupling, if L^T and S^T are the total orbital and spin angular momentum quantum numbers for the whole system, atom + electron, and l is the orbital quantum number† of the free electron:

$$\Omega^{lL^{\mathrm{T}}S^{\mathrm{T}}}(ij)=\frac{8(2L^{\mathrm{T}}+1)(2S^{\mathrm{T}}+1)}{k_ik_j}\left|\frac{C_{ij}^{lL^{\mathrm{T}}S^{\mathrm{T}}}}{A_i(k_ilL^{\mathrm{T}}S^{\mathrm{T}})A_j(k_jlL^{\mathrm{T}}S^{\mathrm{T}})}\right|^2, \qquad \ldots\ldots(7)$$

where

$$C_{ij}^{lL^{\mathrm{T}}S^{\mathrm{T}}}=\int_0^\infty F_i(k_ilL^{\mathrm{T}}S^{\mathrm{T}},r)[V_{ij}{}^{L^{\mathrm{T}}S^{\mathrm{T}}}(r)-X_{ij}{}^{lL^{\mathrm{T}}S^{\mathrm{T}}}]F_j(k_jlL^{\mathrm{T}}S^{\mathrm{T}},r)\,dr, \qquad \ldots\ldots(8)$$

which will be referred to as the scattering integrals, V and X are potential and integral exchange operators, and F_i, F_j are radial functions of the free electron orbital with asymptotic amplitudes of A_i, A_j respectively.

If exchange distortion is considered, then for weak coupling the radial functions F_i are solutions of the equations

$$\left[\frac{d^2}{dr^2}-\frac{l(l+1)}{r^2}-2V_{ii}{}^{L^{\mathrm{T}}S^{\mathrm{T}}}(r)+k_i{}^2\right]F_i(k_ilL^{\mathrm{T}}S^{\mathrm{T}},r)=-2X_{ii}{}^{lL^{\mathrm{T}}S^{\mathrm{T}}}F_i(k_ilL^{\mathrm{T}}S^{\mathrm{T}},r) \qquad \ldots\ldots(9)$$

where the potential functions V and integral exchange operators X are dependent on L^{T} and S^{T}, as for the analogous Hartree–Fock equations for bound orbitals. F_j are solutions of similar equations. This is the EDBO approximation.

When the exchange operators X are omitted, together with the non-central potential terms, the DBO approximation is obtained. The radial functions are then independent of L^{T} and S^{T}, as for the Hartree self-consistent field equations. $V_{ii}{}^{L^{\mathrm{T}}S^{\mathrm{T}}}(r)$ with the non-central terms omitted will be denoted $\bar{V}_{ii}(r)$.

For the general explicit form of V and X, see the above references.

For charge to be conserved (Seaton 1953 a):

$$\sum_{j\neq i}\Omega^{lL^{\mathrm{T}}S^{\mathrm{T}}}(ij)\leqslant\tfrac{1}{2}(2L^{\mathrm{T}}+1)(2S^{\mathrm{T}}+1). \qquad \ldots\ldots(10)$$

§ 4. OXYGEN EXCITATION: DBO APPROXIMATION

The DBO approximation was used to find the collision strengths $\Omega(01)$ and $\Omega(02)$ of the processes (1) and (2). As the outer electrons are all in p-orbitals, it was to be expected that the most important contribution to the collision strength might come from the p-wave of the free electron. For *partial* collision strengths of larger l, distortion is insignificant, even for the lowest energies, and exchange is negligible, so the Born approximation was used.

Let $\bar{V}_i(r)$ be the central field in Hartree units of the oxygen atom for level i. Then the equations for the initial and final p-waves are

$$\left[\frac{d^2}{dr^2}-\frac{2}{r^2}+\bar{V}_i(r)+k_i{}^2\right]F_i(k_i\mathrm{p},r)=0 \quad (i=0,1,2) \qquad \ldots\ldots(11)$$

where

$$\bar{V}_i(r)=-2\bar{V}_{ii}(r). \qquad \ldots\ldots(12)$$

The central field of levels 1 and 2 was calculated using the equation

$$\bar{V}_1(r)=\bar{V}_2(r)=\bar{V}_{11}(r)-2y_0(3\mathrm{p}3\mathrm{p},r), \qquad \ldots\ldots(13)$$

where

$$y_\lambda(\mathrm{ab},r)=r^{-(\lambda+1)}\int_0^r P(\mathrm{a},r')P(\mathrm{b},r')r'^{\lambda}\,dr'+r^\lambda\int_r^\infty P(\mathrm{a},r')P(\mathrm{b},r')r'^{-(\lambda+1)}\,dr', \qquad \ldots\ldots(14)$$

---

† Collisions for which a change in l is important are not considered.

$V_{\rm II}(r)$ is the central field of O II $2p^3\,{}^4S$, and $y_0(3p3p, r)$ was calculated using P_F or $P(3p)$.

The equations were solved for final electron energies of 1·35 ev and 4·06 ev.

Making the assumption that *bound* orbitals of the initial and final levels are dentical or orthogonal, the method described by Seaton (1953 a) was used to btain

$$\Omega^{pL^TS^T}(01) = 8(2L^T+1)(2S^T+1)\left\{\sum_{\lambda=0,\,2}[\epsilon_\lambda(pL^TS^T, 01)R_\lambda(p, V) + \delta_\lambda(pL^TS^T, 01)S_\lambda(p, X)]\right\}^2 \quad \ldots\ldots(15)$$

$$\Omega^{pL^TS^T}(02) = 8(2L^T+1)(2S^T+1)\left\{\sum_{\lambda=0,\,2}[\delta_\lambda(pL^TS^T, 02)S_\lambda(p, X)]\right\}^2 \quad \ldots\ldots(16)$$

where the algebraic coefficients ϵ_λ and δ_λ are shown in table 3. R_λ and S_λ are defined by the equations

$$\left.\begin{aligned} R_\lambda(p, V) &= R_\lambda(3_jp\,k_jp, 2_0p\,k_0p) \\ S_0(p, X) &= R_0(3_jp\,k_jp, k_0p\,2_0p) - [4R_0(2_0p\,3_jp, 2_0p\,k_0p) \\ &\qquad - 3R_0(2_jp\,3_jp, 2_0p\,k_0p)]\Delta_r(k_jp|2_0p) \\ S_2(p, X) &= R_2(3_jp\,k_jp, k_0p\,2_0p) \end{aligned}\right\} \quad \ldots\ldots(17)$$

where

$$\left.\begin{aligned} R_\lambda(ab, cd) &= \int_0^\infty P(a, r)P(c, r)y_\lambda(bd, r)\,dr \\ \Delta_r(a|b) &= \int_0^\infty P(a, r)P(b, r)\,dr \end{aligned}\right\} \quad \ldots\ldots(18)$$

Table 3. Algebraic Coefficients. α simplifies tabulation.

Final State	Term of whole system	α	$\alpha\epsilon_0$	$\alpha\epsilon_2$	$\alpha\delta_0$	$\alpha\delta_2$	η_2	η_3
1	^2D	$\sqrt{3}$	-2	$-\frac{2}{25}$	2	$\frac{2}{25}$	$-\frac{1}{3}$	1
1	^2P	$\sqrt{3}$	-2	$\frac{2}{5}$	-2	$\frac{2}{5}$	$-\frac{1}{3}$	-1
1	^2S	$\sqrt{3}$	2	$\frac{4}{5}$	2	$\frac{4}{5}$	$-\frac{1}{3}$	1
1	^4D	$2\sqrt{3}$	-4	$-\frac{4}{25}$	1	$\frac{1}{25}$	$\frac{11}{12}$	$\frac{1}{4}$
1	^4P	$2\sqrt{3}$	-4	$\frac{4}{5}$	-1	$\frac{1}{5}$	$\frac{11}{12}$	$-\frac{1}{4}$
1	^4S	$2\sqrt{3}$	-4	$-\frac{8}{5}$	1	$\frac{2}{5}$	$\frac{11}{12}$	$\frac{1}{4}$
2	^4D	$2\sqrt{5}$	0	0	5	$\frac{1}{5}$	$-\frac{1}{4}$	$-\frac{1}{4}$
2	^4P	$2\sqrt{5}$	0	0	-5	1	$-\frac{1}{4}$	$\frac{1}{4}$
2	^4S	$2\sqrt{5}$	0	0	5	2	$\frac{1}{4}$	$-\frac{1}{4}$

The results for various $P(3p)$ and energies are shown in table 4. Evidently they are very sensitive to the choice of $P(3p)$. This table also gives a DBO approximation to Ω^s and a Born approximation to Ω^d for both transitions. No other partial collision strength is significant, and it was confirmed that to this approximation the p-wave makes the largest contribution to the collision strengths.

All partial collision strengths are small in comparison with the conservation limit (10), so the use of weak-coupling approximations is justified.

Table 4. Partial Collision Strengths. The symbols are defined in the text.

Approxn.	Energy above threshold (ev)	l	$P(3p)$	$y_0(d)$	$\Omega^l(01)$ (^3P)	$\Omega^l(02)$ (^5P)
DBO	1·35	p	P_F	$y_0(2_0 2_1)$	0·013	0·006
DBO	1·35	p	P_G	$y_0(d)$	0·777	0·046
DBO	4·06	p	P_G	$y_0(d)$	0·514	0·047
EDBO	2·32	p	P_G	$y_0(d)$		0·003
EDBO	2·32	p	P_H	$y_0(d)$		0·025
EDBO	2·32	p	P_H	$y_0(2_0 2_0)$		0·005
DBO	1·35	s	P_G		0·039	0·000
Born	1·35	d	P_G		0·000	0

§ 5. EDBO APPROXIMATION TO $\Omega^p(02)$

Seaton (1953 a) has made a thorough study of the transitions between the ground configuration terms ^3P ($i=0$), ^1D and ^1S of OI, and has obtained exact resonance solutions with exchange distortion for the p-waves. To this approximation there is no coupling except for the ^2P terms of the whole system, and, with this exception, the p-wave radial functions for state 0 are constant multiples of a single function $\mathscr{F}(r)$ for each free electron energy. His comparison of $\mathscr{F}(r)$ with the non-exchange solution (for an energy below the thresholds for processes (1) and (2)) shows the importance of exchange distortion for the ground-state radial wave functions.

Neglecting strong coupling and all non-central terms it may be shown that the EDBO radial equations for the p-waves of states 1 and 2 reduce to the form

$$\left[\frac{d^2}{dr^2} - \frac{2}{r^2} + \bar{V}_1(r) + k_j^2\right] F_j(k_j \mathrm{p} L^{\mathrm{T}} S^{\mathrm{T}}, r) = -2[\eta_2 \Theta_2(r) + \eta_3 \Theta_3(r)] \quad (j=1,\ 2). \qquad \ldots\ldots(19)$$

η_2 and η_3 are shown in table 3.

If e_n ($n=2,\ 3$) is defined by the equation

$$2e_n = k_j^2 + \epsilon_n \qquad \ldots\ldots(20)$$

where ϵ_n is the energy parameter of $P(n\mathrm{p})$, then

$$\Theta_n(r) = [e_n \Delta_r(n\mathrm{p}|k_j\mathrm{p}) + y_0(n\mathrm{p}\ k_j\mathrm{p}, r)] P(n\mathrm{p}, r) \qquad \ldots\ldots(21)$$

subject to the conditions

$$e_n \Delta_r(n\mathrm{p}|k_j\mathrm{p}) = R_0(n\mathrm{p}\ n\mathrm{p}, n\mathrm{p}\ k_j\mathrm{p}). \qquad \ldots\ldots(22)$$

For the derivation of these relations see Percival (1956).

The set of six differential equations (19) are soluble by a method which is an extension of that due to Seaton (1953 b) to the case of two independent exchange terms. In practice the scattering integrals and asymptotic amplitudes were obtained without calculating the exchange-distorted wave functions explicitly, but the method was still very tedious as the terms including exchange with $P(3\mathrm{p})$ range a great distance from the origin, and a two-dimensional array of functions $f_{\mathrm{st}}(r)$ had to be computed. Unfortunately no useful estimate of the collision strength $\Omega^{\mathrm{P}}(01)$ could be obtained, as shown, for instance, by the fine-structure comparison of § 2, which was performed after the above calculations.

Consistently neglecting non-central terms:

$$\Omega^{\mathrm{p}L^{\mathrm{T}}S^{\mathrm{T}}}(02)=\frac{8(2L^{\mathrm{T}}+1)(2S^{\mathrm{T}}+1)}{k_0k_2}\left[\frac{\delta_0(\mathrm{p}L^{\mathrm{T}}S^{\mathrm{T}},02)S_0(\mathrm{p},X)}{A_0(k_0\mathrm{p}L^{\mathrm{T}}S^{\mathrm{T}})A_2(k_2\mathrm{p}L^{\mathrm{T}}S^{\mathrm{T}})}\right]^2. \quad \ldots\ldots(23)$$

On keeping the second derivative of the free waves at the origin fixed, the inclusion of exchange distortion acted more through increasing the asymptotic amplitudes $A_2(k_2\mathrm{p}L^{\mathrm{T}}S^{\mathrm{T}})$ than modifying the scattering integrals $S_0(\mathrm{p},X)$. As would be expected from equation (23), there was a resultant decrease in the estimated collision strength when exchange distortion was included. The result using P_{G} for $P(3\mathrm{p})$ is given in table 4.

§ 6. INTEGRATION OF $S_0(\mathrm{p}, X)$

$S_0(\mathrm{p},X)$ is defined by equation (17). It was found that the two terms on the right-hand side were large and of opposite sign, so that evaluation of $S_0(\mathrm{p},X)$ as it stands would entail considerable loss of accuracy. The following method of evaluation was therefore used.

If, by definition:

$$4y_0(2_0\mathrm{p}\ 2_0\mathrm{p},r)-3y_0(2_2\mathrm{p}\ 2_0\mathrm{p},r)=y_0(\mathrm{d},r), \quad \ldots\ldots(24)$$

$$y_0(k_2\mathrm{p}\ 2_0\mathrm{p},r)-y_0(\mathrm{d},r)\Delta_r(k_2\mathrm{p}|2_0\mathrm{p})=Q(r), \quad \ldots\ldots(25)$$

we may replace equation (17) by

$$S_0(\mathrm{p},X)=\int_0^\infty P(3_2\mathrm{p},r)F(k_0\mathrm{p},r)Q(r)\,dr. \quad \ldots\ldots(26)$$

Both terms on the left-hand side of equation (25) are of order $1/r$ for large r, and outside the effective range of the bound orbitals they cancel approximately.†

We arrange that the cancellation takes place before numerical integration, n the first term on the right-hand side of the following equation:

$$Q(r)=[r^{-1}-y_0(\mathrm{d},r)]\int_0^r F(k_2\mathrm{p},r')P(2_0\mathrm{p},r')\,dr'+\int_r^\infty F(k_2\mathrm{p},r')P(2_0\mathrm{p},r')r'^{-1}\,dr'$$

$$-y_0(\mathrm{d},r)\int_r^\infty F(k_2\mathrm{p},r')P(2_0\mathrm{p},r')\,dr'. \quad \ldots\ldots(27)$$

In general, if P represents the radial function of a bound orbital, and F that f a free orbital, many non-diagonal exchange integrals do not differ essentially rom the form

$$S_0(l,X)=R_0(PF,FP)-R_0(PP,PF)\Delta_r(F|P)$$

$$=\int_0^\infty F(r)P(r)Q(r)\,dr \quad \ldots\ldots(28)$$

where

$$Q(r)=y_0(FP,r)-y_0(PP,r)\Delta_r(F|P) \quad \ldots\ldots(29)$$

---

† Since these are exchange integrals the integrand should be identically zero where here is no overlap between the exchanged orbitals. That it is not exactly zero there is consequence of the approximations made.

and to reduce cancellation of large quantities of opposite sign, this may be converted to the form in which

$$Q(r)=[r^{-1}-y_0(PP,r)]\int_0^r FP\,dr+\int_r^\infty FPr^{-1}\,dr-y_0(PP,r)\int_r^\infty FP\,dr \quad \ldots\ldots(30)$$

before computation begins.

§ 7. $\Omega^{\mathrm{p}}(02)$: RELIABILITY, AND NEW ESTIMATE

The most uncertain feature in the calculations was the accuracy of P_G as an approximation to $P(3\mathrm{p})$. It was therefore necessary to find the range of r over which the magnitude of this function was important in the estimation of $\Omega^{\mathrm{p}}(02)$. This range is that for which (cf. Hartree and Hartree 1936) the formal derivative $\partial S_0/\partial P(3\mathrm{p})$ of $S_0(\mathrm{p}, X)$ with respect to $P(3\mathrm{p})$ is large. As the inclusion of exchange distortion acted more through increasing the asymptotic amplitudes than modifying the scattering integral, it suffices to calculate $\partial S_0/\partial P(3\mathrm{p})$ using for the colliding electron a final p-wave radial function without exchange distortion. This formal derivative is shown in the figure, calculated for $k_2{}^2=0{\cdot}171$. Unfortunately P_G is inaccurate near the origin, as shown by the fine-structure comparison in table 2. The estimated $\Omega^{\mathrm{p}}(02)$ given in § 6 is thus unreliable.

For this reason P_H, as described in § 2, was calculated, and a new estimate of $\Omega^{\mathrm{p}}(02)$ based on this function made, as in table 4. The fine-structure comparison shows that any corrections to P_H will leave the estimated $\Omega^{\mathrm{p}}(02)$ inside the range

$$0{\cdot}025 \leqslant \Omega^{\mathrm{p}}(02) < 0{\cdot}06. \quad \ldots\ldots(31)$$

$S_0(\mathrm{p}, X)$ is linear, but not homogeneous, in $y_0(\mathrm{d}, r)$, as may be seen from equation (25), so (for small r) there is scope for cancellation between terms of large magnitude but opposite sign. This is demonstrated in table 4, where $\Omega^{\mathrm{p}}(02)$ calculated using $y_0(2_0\mathrm{p}\,2_0\mathrm{p}, r)$ in place of $y_0(\mathrm{d}, r)$ may be compared with the original estimate. $y_0(2_0\mathrm{p}\,2_0\mathrm{p}, r)$ and $y_0(\mathrm{d}, r)$ do not differ anywhere by more than $\frac{1}{6}$ of the latter, clearly exhibiting the sensitivity.

$y_0(\mathrm{d}, r)$ was originally calculated using $P(2_{\mathrm{II}}\mathrm{p})$ for $P(2_2\mathrm{p})$, which amounts to neglecting the perturbation by the 3p electron. Although this perturbation is small, since a 3p electron has only a small probability of being in the region where the 2p orbital is large, the comparison of the previous paragraph shows that a very small perturbation could have an appreciable effect on the scattering integral. Inclusion of this perturbation would make $P(2_2\mathrm{p})$ resemble $P(2_0\mathrm{p})$ more closely, and consequently make $y_0(\mathrm{d}, r)$ more like $y_0(2_0\mathrm{p}\,2_0\mathrm{p}, r)$.

We conclude that if the perturbation of $P(2_2\mathrm{p})$ were included, then $S_0(\mathrm{p}, X)$ would be multiplied by a factor μ_1, where probably $0{\cdot}7 < \mu_1 \leqslant 1$.

Configuration superposition may be significant for levels 0 and 2. The effect that this would have on the scattering amplitude is difficult to estimate, but a reasonable range for the corresponding error factor μ_2 is $0{\cdot}5 < \mu_2 < 2$.

Corrections to the free waves must also be considered. Those arising from strong coupling generally tend to decrease an estimated inelastic collision strength (Mott and Massey 1949). There are two possibly serious cases of strong coupling with level 2. For potential coupling with $\mathrm{O\,I}\,2\mathrm{p}^3(^4\mathrm{S})3\mathrm{s}(^5\mathrm{S})+k\mathrm{d}\,^4\mathrm{D}$, the term $2(2/15)^{1/2}y_1(3\mathrm{s}3\mathrm{p}, r)F(k\mathrm{d}, r)$ will appear in the equation for $F_2(k_2\mathrm{p})$. As $r\to\infty$

$$y_1(3\mathrm{s}3\mathrm{p}, r)\to r^{-2}\int_0^\infty P(3\mathrm{s}, r')P(3\mathrm{p}, r')r'\,dr' \simeq -6/r^2. \quad \ldots\ldots(32)$$

The expression $$\int_0^\infty P(3s)P(3p)r'\,dr'$$

was calculated using P_E for $P(3p)$, and approximates to its asymptotic form around $r=6$. The integral in (32) depends on large values of r, and is not sensitive to the particular $P(3p)$ used. Probably the error factor μ_3 associated with this strong coupling is in the range $0{\cdot}7<\mu_3\leqslant 1$. Potential coupling with O I $2p^3(^4S)3d(^5D)+ks\,^4D$ could also be serious, and its effect may be similar to that of the previous case: $0{\cdot}7<\mu_4\leqslant 1$.

It is not evident how these error factors should be combined, for it is most improbable that all should have their estimated maximum or minimum values together, besides which one error may alter the sensitivity to another. But it appears probable that if μ is the error factor for all the effects together, then $0{\cdot}03<\mu^2<4$ where μ^2 is the combined error factor for $\Omega^P(02)$.

Using (31), $$0{\cdot}001<\Omega^P(02)<0{\cdot}24. \qquad \ldots\ldots(33)$$

§ 8. CONCLUSIONS

The principal conclusion to be drawn is that in calculating inelastic collision cross sections for processes similar to (1) and (2), the greatest care should be taken to ensure that the atomic wave functions are sufficiently accurate.

For example the angular and spin symmetries of the initial and final levels of process (1) are the same, and the calculated scattering amplitudes contain contributions from elastic scattering amplitudes, which swamp the inelastic scattering amplitude, unless the approximate atomic wave functions of the initial and final states are made orthogonal.

Also the observed fine-structure separations for the $3p\,^3P$ excited level do not even approximately obey the Landé interval rule, so that level probably cannot be represented in terms of a single configuration with one parent term, in which case approximations which assume such a simple structure are of little value in the calculation of collision cross sections. For the $3p\,^5P$ excited level 2, the Landé interval rule is approximately obeyed. In this case both fine-structure separations and the inelastic collision cross section for excitation from the ground level 0 are dependent on the magnitude of the 3p orbital near its first maximum. An approximate atomic wave function which does not give reasonable values for the fine-structure separations is unlikely to give an accurate cross section.

Comparison of observed and calculated fine-structure separations would be a useful preliminary to the evaluation of cross sections for similar inelastic collisions.

The difference between DBO and EDBO cross sections shows that exchange distortion was important, confirming the conclusions of Massey and Mohr (1952).

When exchange integrals for inelastic collisions are being computed the cancellation of large numbers of opposite sign may be reduced by the method of § 6.

Finally, the inequality (33), although very weak, suggests that electron excitation of oxygen atoms is not the principal agent responsible for the observed auroral lines mentioned in the introduction. For details, see Percival and Seaton (1956).

ACKNOWLEDGMENTS

I am indebted to Professor H. S. W. Massey for suggesting this research, and to Dr. M. J. Seaton for his interest and advice throughout its progress.

I should also like to thank Miss J. Nicholson for helping with the computations, and the Department of Scientific and Industrial Research for a grant.

REFERENCES

HARTREE, D. R., and HARTREE, W., 1936, *Proc. Roy. Soc.* A, **154,** 588.

HARTREE, D. R., HARTREE, W., and SWIRLES, B., 1939-40, *Phil. Trans. Roy. Soc.* A, **238,** 229.

HEBB, M. H., and MENZEL, D. H., 1940, *Astrophys. J.*, **92,** 408.

MASSEY, H. S. W., and MOHR, C. B. O., 1952, *Proc. Phys. Soc.* A, **65,** 485.

MASSEY, H. S. W., and MOISEIWITSCH, B. L., 1954, *Proc. Roy. Soc.* A, **227,** 38.

MOTT, N. F., and MASSEY, H. S. W., 1949, *The Theory of Atomic Collisions* (Oxford : University Press), p. 265.

MOORE, C. E., 1949, *Atomic Energy Levels*, Vol. 1, Circular 467, (Washington : National Bureau of Standards).

PERCIVAL, I. C., 1956, *Ph.D. Thesis*, University of London.

PERCIVAL, I. C., and SEATON, M. J., 1956, *The Airglow and the Aurorae* (London : Pergamon Press), p. 244.

SEATON, M. J., 1953 a, *Phil. Trans. Roy. Soc.* A, **245,** 469; 1953 b, *Proc. Roy. Soc.* A, **218,** 400; 1955, *Ibid.*, **231,** 37.

The First Passage Problem in the Theory of Multiple Scattering

By J. C. BARTON†
University College of the West Indies

Communicated by R. Fürth; MS. received 9th November 1956, *and in revised form 9th January* 1957

Abstract. A new formal method of solving first passage problems is developed and applied to the multiple scattering equation for the simplest cases of single- and double-sided boundaries. The latter problem is also treated by an alternative method which enables the moments of the distribution to be calculated more readily.

§ 1. INTRODUCTION

THE first passage problem consists of finding the distribution of the times, or values of an equivalent variable, at which a stochastic variable first reaches some particular value. For the case of one-dimensional Brownian motion the problem was first solved by Fürth (1917). In this treatment, and also in those of subsequent workers, it is assumed that the 'relaxation time' is very short compared with the time of observation so that the simple Einstein equation of Brownian motion is applicable. When this is not true and the damping forces restricting the motion of the particle are small it becomes necessary to use the more complicated equation of Kramers (1940). Wang and Uhlenbeck (1945) pointed out that the first passage problem then becomes much more difficult and that they were unable to find a solution.

The equation governing the distribution of high-energy particles which are undergoing multiple scattering was first derived by Fermi (see Rossi and Greisen 1941). In the two-dimensional case this equation is

$$\frac{\partial P}{\partial x}+\theta\frac{\partial P}{\partial y}=\mu\frac{\partial^2 P}{\partial\theta^2} \qquad \ldots\ldots(1)$$

where x and y are position coordinates, θ the angle, which is assumed to be small, between the track of the particle and the x axis, $P=P(x,y,\theta)$ the distribution function and μ half the mean square angle of scattering per unit length. It can be seen that this is a particular case of the Kramers equation, in which the damping forces have become vanishingly small.

The first passage problem for multiple scattering has arisen in several branches of high-energy-particle physics. Thus it is of relevance in determining the effective width of a collimating slit, the necessary width of material for absorption measurements and the proportion of particles scattered out of nuclear emulsions. The first of these problems was considered by Courant (1951) who attempted to solve it by using an image method. His solution is clearly incorrect since the resulting distribution function was negative for some values of the coordinates. This is not very surprising as the image method does not in fact satisfy the correct boundary condition for the scattering equation.

The first passage problem arises with nuclear plates, because the distribution in length of randomly oriented particle tracks is altered by scattering in the emulsion. The method used by Chartres and Tidman (1955) is to consider that the space outside the emulsion is also filled with scattering material. By integrating Fermi's fundamental solution for equation (1) they are able to calculate upper and lower limits to the number of tracks of any given length in the finite slice of emulsion. In some cases the calculated limits are very close together; in other cases a method of interpolating between the limits is suggested, but it is admitted that the reliability of this estimate is uncertain.

---

† Now at Birkbeck College, London.

The present paper develops the method used by Chartres and Tidman into a general one for treating a certain type of first passage problem. A formal solution is obtained which in principle could be evaluated to any required accuracy. The method is applied to the multiple-scattering problem and results are calculated for two particular sets of boundary conditions. The theory applies only to true multiple scattering but the effect of occasional large angles of scatter can be considered independently, as has been shown by Chartres and Tidman. The latter part of the paper shows how the moments of the first passage distribution can be obtained by a relaxation method. The values for the first two moments are evaluated and compared with those calculated by the first method.

§ 2. FORMAL SOLUTION OF FIRST PASSAGE PROBLEM

We consider only problems in which: (1) A particle is moving in a two-dimensional region. (2) One coordinate of the position of the particle increases monotonically. (3) The locus of the boundary can be expressed as a single-valued function of the same coordinate. (This means that the region must be unbounded on one side.)

Suppose a particle starts from the origin and moves as shown in figure 1. We want to calculate the probability of the particle first crossing the boundary between $x = x_0$ and $x = x_0 + dx_0$. Let the probability of the particle going from $(0, 0, 0)$ to (x, y, θ) be given by $P(x, y, \theta)$.

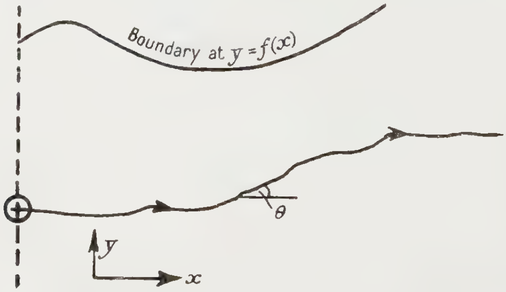

Figure 1. Coordinate system for single-sided first passage problem.

Using the method of Chartres and Tidman (1955, § 5) we can obtain the upper limit to the fraction of particles which have not yet crossed the boundary before reaching x_0 as

$$N_1 = \int_{y=-\infty}^{f(x_0)} \int_{\theta=-\pi/2}^{+\pi/2} P(x_0, y, \theta)\, dy\, d\theta. \qquad \ldots\ldots(2)$$

Next we consider the integral

$$S_1 = \int_{x_1=0}^{x_0} \int_{\theta=\tan^{-1} f'(x_1)}^{\pi/2} P(x_1, f(x_1), \theta_1) \sin\{\theta - \tan^{-1} f'(x_1)\}\, dx_1\, d\theta, \qquad \ldots\ldots(3)$$

which represents the total probability of finding a particle moving outward across the boundary. But some particles will cross and re-cross the boundary more than once so that $1-S_1$ is only a lower limit to the proportion of particles which have not crossed the boundary before reaching x_0.

We now develop the method by introducing quantities S_r which represent the probability that a particle will have made at least r outward crossings before reaching x_0. We find:

$$S_r=\int_{x_1=0}^{x_0}\int_{x_2=x_1}^{x_0}\dots\int_{\theta_1=\tan^{-1}f'(x_1)}^{\pi/2}\int_{\theta_2=\tan^{-1}f'(x_2)}^{\pi/2}\dots P\{x_1,f(x_1),\theta_1\}$$
$$\times P\{x_2-x_1,f(x_2)-f(x_1)-\tan\theta_1(x_2-x_1),\theta_2-\theta_1\}\dots dx_1\,dx_2\dots d\theta_1\,d\theta_2\dots \qquad \dots\dots(4)$$

where the particle crosses the boundary in an outward direction at $x=x_1$, x_2, $x_3,\dots x_r$, at angles $\theta=\theta_1$, θ_2, $\theta_3.\dots\theta_r$. Suppose that the probability that a particle crosses the boundary in either direction exactly i times is given by p_i. Then

$$p_0+p_1+p_2+p_3+p_4+\dots=1. \qquad \dots\dots(5)$$

A particle contributes to S_1 each time it crosses the boundary in an *outward* direction, so

$$(p_1+p_2)+2(p_3+p_4)+3(p_5+p_6)+\dots=S_1. \qquad \dots\dots(6)$$

Again, by considering the number of ways in which a particle making more than two outward crossings contributes to S_2, we find

$$(p_3+p_4)+3(p_5+p_6)+6(p_7+p_8)+\dots=S_2. \qquad \dots\dots(7)$$

Similarly, in general,

$$(p_{2r-1}+p_{2r})+{}_{r+1}C_r(p_{2r+1}+p_{2r+2})+{}_{r+2}C_r(p_{2r+3}+p_{2r+4})+\dots=S_r. \qquad \dots\dots(8)$$

By alternately adding and subtracting the equations (5) to (8) it is found that the coefficients of the terms (p_1+p_2) etc. all vanish, leaving

$$p_0=1-S_1+S_2-S_3+\dots+(-1)^rS_r+\dots. \qquad \dots\dots(9)$$

Thus we have a complete solution for the probability of the particle not crossing the boundary before reaching x_0; the first passage distribution follows immediately on differentiating p_0 with respect to x_0.

It is seen that the approximate solution of Chartres and Tidman consists of cutting off the series at the term S_1. The complete solution may be only of formal interest as the computation of the higher terms in the series will generally be very difficult, but it will be shown below that even one additional term may lead to much greater accuracy.

We have not investigated the requirements on the probability function $P(x,y,\theta)$ which ensure that the S's do form a converging series but the method appears to be satisfactory for dealing with the generalized Brownian motion. For the otherwise simpler case when the relaxation time becomes negligible, the integrals themselves diverge (similarly the concept of 'recurrence time' becomes meaningless). Fortunately this is the one case in which the image method can be used.

§ 3. SINGLE-SIDED FIRST PASSAGE PROBLEM IN MULTIPLE SCATTERING

Only the simplest case will be considered, in which the boundary is specified by $y=b$. It is assumed that the angle θ is always small so that $\sin\theta$ can be replaced by θ.

For the scattering equation (1) Fermi's solution is

$$P(x,y,\theta)=\frac{\sqrt{3}}{2\pi\mu x^2}\exp\left\{-\frac{1}{\mu x^3}(3y^2-3xy\theta+x^2\theta^2)\right\}. \qquad \ldots\ldots(10)$$

The expressions for the integrals of § 2 are then:

$$N_1=\int_{y=-\infty}^{b}\int_{\theta=-\pi/2}^{\pi/2}\frac{\sqrt{3}}{2\pi\mu x_0^2}\exp\left\{-\frac{1}{\mu x_0^3}(3y^2-3x_0y\theta+x_0^2\theta^2)\right\}dy\,d\theta, \qquad \ldots\ldots(11)$$

$$S_1=\int_{x_1=0}^{x_0}\int_{\theta_1=0}^{\pi/2}\frac{\sqrt{3}}{2\pi\mu x_1^2}\exp\left\{-\frac{1}{\mu x_1^3}(3b^2-3x_1b\theta_1+x_1^2\theta_1^2)\right\}\theta_1\,dx_1\,d\theta_1, \qquad \ldots\ldots(12)$$

$$S_2=\int_{x_1=0}^{x_0}\int_{x_2=x_1}^{x_0}\int_{\theta_1=0}^{\pi/2}\int_{\theta_2=0}^{\pi/2}\frac{3}{4\pi^2\mu^2x_1^2(x_2-x_1)^2}\exp\left\{-\frac{1}{\mu x_1^3}(3b^2-3x_1b\theta_1+x_1^2\theta_1^2)\right\}$$
$$\times\exp\left\{-\frac{1}{\mu(x_2-x_1)^3}[3\theta_1^2(x_2-x_1)^2+3\theta_1(x_2-x_1)^2(\theta_2-\theta_1)+(x_2-x_1)^2(\theta_2-\theta_1)^2]\right\}$$
$$\times\,\theta_1\theta_2\,dx_1\,dx_2\,d\theta_1\,d\theta_2. \qquad \ldots\ldots(13)$$

These integrals can be computed without undue labour and the values of N_1, $1-S_1$ and $1-S_1+S_2$ are plotted as functions of $\xi=(4\mu/3b^2)^{1/3}x_0$ in figure 2. Whereas the theory of Chartres and Tidman gave N_1 as the upper limit for the correct value, this can now be replaced by $1-S_1+S_2$. The uncertainty in the proportion of particles which have not yet crossed the boundary at a depth corresponding to $\xi=3$ is reduced from 2·8% to 0·5%. For larger values of ξ the approximation is less satisfactory and the next term of the series becomes significant. Unfortunately, it is very difficult to obtain the value of S_3 without an excessive amount of numerical integration.

The distribution of the distances at which particles cross the boundary is given by differentiating these curves. This is done for the best estimate, $1-S_1+S_2$, in figure 3.

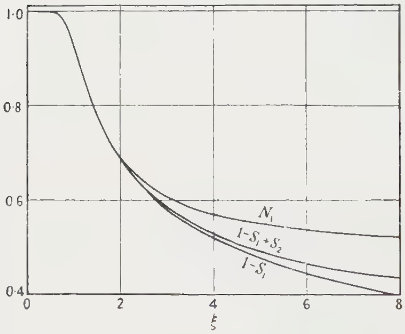

Figure 2. Values of N_1, $1-S_1$ and $1-S_1+S_2$ for single-sided problem.

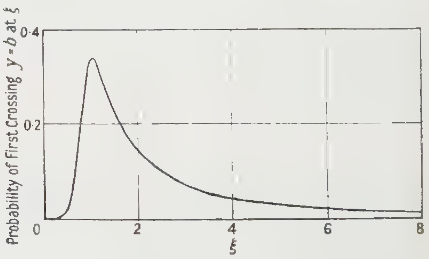

Figure 3. Distribution of first passage distances for single-sided problem.

§4. SYMMETRICAL DOUBLE-SIDED FIRST PASSAGE PROBLEM IN MULTIPLE SCATTERING

We assume in this case that the particle starts with coordinates (0, 0, 0) and that the boundaries are at $y=\pm b$.

The expression for N_1 must then be modified by restricting the range of integration over y to the interval from $-b$ to $+b$ and each of the expressions S_1 and S_2 must be doubled. There is a further modification which results from the double boundary, as the general theory of §2 assumed that the function describing the boundary was single-valued. There are now two ways in which a particle can make two outward crossings of the boundary before reaching x_0.

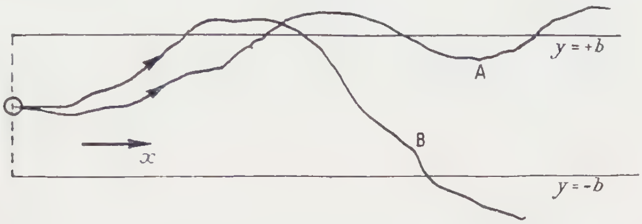

Figure 4. Two types of tracks making double outward crossing.

These are marked A and B in figure 4; only trajectories of type A are included in the expression (13) for S_2. The corresponding expression for the type B tracks is:

$$S_2' = 2\int_{x_1=0}^{x_0}\int_{x_2=x_1}^{x_0}\int_{\theta_1=0}^{\pi/2}\int_{\theta_2=0}^{\pi/2} \frac{3}{4\pi^2\mu^2 x_1^2 (x_2-x_1)^2} \\ \times \exp\left\{-\frac{1}{\mu x_1^3}(3b^2 - 3x_1 b\theta_1 + x_1^2\theta_1^2)\right\} \exp\left\{-\frac{1}{\mu(x_2-x_1)^3}[3(x_2-x_1)^2(\theta_1+2b)^2 \right. \\ \left. -3(x_2-x_1)(\theta_1+2b)(\theta_1+\theta_2)(x_2-x_1) + (\theta_1+\theta_2)^2(x_2-x_1)^2]\right\} \theta_1\theta_2\, dx_1\, dx_2\, d\theta_1\, d\theta_2. \qquad \ldots\ldots(14)$$

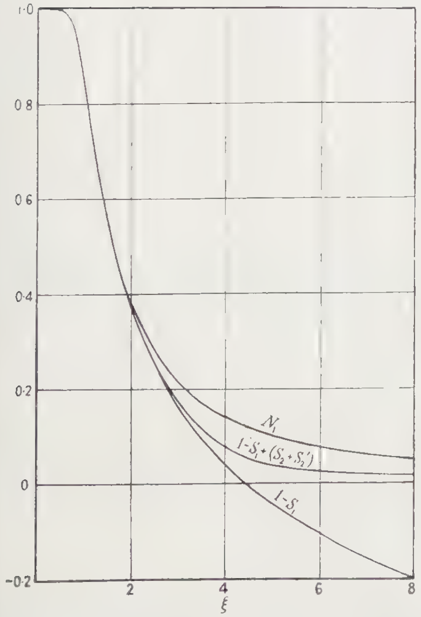

Figure 5. Values of N_1, $1-S_1$, and $1-S_1+(S_2+S_2')$ for double-sided problem.

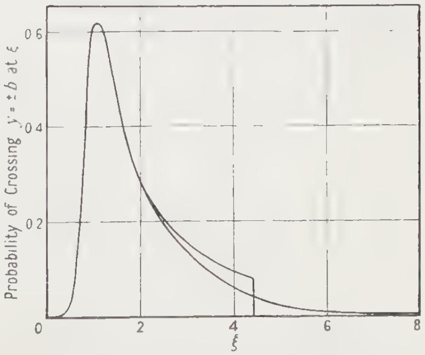

Figure 6. Distribution of first passage distances for double-sided problem.

This term, for which the numerical evaluation is very tedious, must be added to S_2. The dependence of N_1, $1-S_1$, and $1-S_1+S_2+S_2'$ on ξ is shown in figure 5. It is again seen that the new upper limit is a much closer bound than the one given by N_1. The lower limit is of course zero for values of ξ greater than 4·46.

The distribution of the distances at which particles cross either boundary is shown in figure 6 for both the upper and lower limits to the true value. In this problem the moments of the distribution are finite and may be determined numerically. The upper and lower limits for the mean depth are 2·00 and 1·92 respectively, in units of ξ. The exact value should be quite close to the upper limit. The corresponding limits for the second moment are 6·0 and 4·5.

§ 5. MOMENTS FOR DOUBLE-SIDED FIRST PASSAGE PROBLEM

The method described in the last section provides a reasonably good approximation to the distribution function at the expense of rather lengthy numerical computations. It appears very tedious to repeat the calculation for all possible initial values of y_1 and θ_1 or for more complicated boundaries. In this section we outline an alternative method which only enables the first few moments of the distribution to be calculated but provides these for all values of the initial coordinates.

Suppose the boundaries are again at $y = \pm b$ and let $p(y, \theta, x)$ be the probability that a particle starting from $(y, \theta, 0)$ reaches the boundary at a depth x.

By a method similar to that used in deriving Fermi's equation we find that p satisfies an equation very similar to (1), viz.:

$$\frac{\partial p}{\partial x} = \theta \frac{\partial p}{\partial y} + \mu \frac{\partial^2 p}{\partial \theta^2}. \qquad \ldots\ldots(15)$$

Next introduce the moment generating function

$$G(y, \theta, \alpha) = \int_0^\infty p(y, \theta, x) e^{-\alpha x}\, dx \qquad \ldots\ldots(16)$$

so that (15) leads to

$$\alpha G = \theta \frac{\partial G}{\partial y} + \mu \frac{\partial^2 G}{\partial \theta^2} \qquad \ldots\ldots(17)$$

which must be true for any value of α. But $G = 1 - \bar{x}\alpha + \frac{1}{2}\bar{x}^2\alpha^2 - \ldots$ whence equating coefficients of α in (17) provides the set of equations

$$\left.\begin{aligned} 1 + \theta \frac{\partial \bar{x}}{\partial y} + \mu \frac{\partial^2 \bar{x}}{\partial \theta^2} &= 0 \\ 2\bar{x} + \theta \frac{\partial \overline{x^2}}{\partial y} + \mu \frac{\partial^2 \overline{x^2}}{\partial \theta^2} &= 0 \\ 3\overline{x^2} + \theta \frac{\partial \overline{x^3}}{\partial y} + \mu \frac{\partial^2 \overline{x^3}}{\partial \theta^2} &= 0 \\ \cdots\cdots\cdots\cdots & \end{aligned}\right\} \qquad \ldots\ldots(18)$$

It can be shown that (18) is a special case of a general result. This is derived from a much longer but more rigorous analysis in a paper by Wasow (1951) which treats a whole class of random motion problems.

It is obvious that the equations in (18) must be solved successively, starting with the equation for the mean. The boundary conditions are:

$$\left.\begin{array}{lll}\overline{x^n}=0 & \text{for} & y=+b,\ \theta>0 \\ & \text{and} & y=-b,\ \theta<0; \\ \overline{x^n}\to 0 & \text{for} & \theta \text{ not small compared to unity.}\end{array}\right\} \qquad \ldots\ldots(19)$$

There does not seem to be any analytical method for solving partial differential equations of this type. Approximate solutions can be found by replacing them by finite difference equations and solving these by a type of relaxation method.

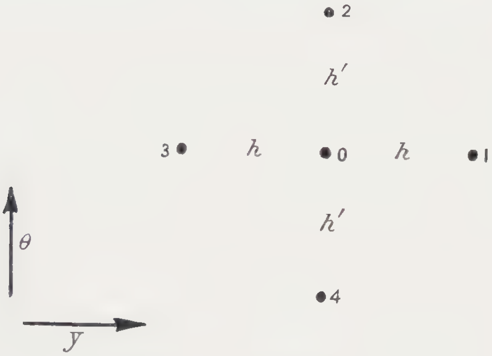

Figure 7. Relaxation net.

Using the net pattern of figure 7 the difference equation for $\bar{x}$ is:

$$\frac{\mu}{h'^2}(\overline{x_4}+\overline{x_2}-2\overline{x_0})+\frac{\theta}{2h}(\overline{x_1}-\overline{x_3})+1=0.$$

Putting $\theta=rh'$ where r is the row number

$$(\overline{x_4}+\overline{x_2}-2\overline{x_0})+r\frac{h'^3}{2\mu h}(\overline{x_1}-\overline{x_3})+\frac{h'^2}{\mu}=0. \qquad \ldots\ldots(20)$$

It has been pointed out by Allen and Severn (1951) that the usual relaxation technique is not strictly applicable to non-elliptic partial differential equations. This is true for the present equation and is reflected in the fact that $\bar{x}$ is unknown on the boundaries $y=b$ for $\theta<0$ and $y=-b$ for $\theta>0$. In practice it means that the relaxation technique does not necessarily converge to the true solution. When the relaxation method was first applied to this problem, the lack of convergence showed up as an oscillatory behaviour of the values of $\bar{x}$ along any row of the array of net points. Adjacent points would be alternately maxima and minima with the amplitude of the oscillation increasing at points towards the boundary where $\bar{x}$ was unknown.

Allen and Severn suggest that this difficulty, which is a consequence of replacing a differential equation by a finite difference one, can be avoided by converting the differential equation into one of higher order but with more suitable boundary conditions. This has the disadvantage that the individual relaxation operation becomes more complicated. It has been avoided in the solutions found for the present equations by imposing an additional but physically reasonable condition. Any oscillation in the values is clearly spurious as its ‘wavelength’ changes with the net size, so the requirement is imposed that second differences along any row should be small. After some experience had been gained in the use of the particular relaxation pattern it was found quite easy to arrange that this should be so.

The usual procedure of solving the problem for successively finer nets was adopted; the finest had an interval of $b/10$ in the y direction and of $(\mu b/5)^{1/3}$ in the θ direction. The unit of θ was chosen to give simple integral values for the relaxation pattern.

The resulting values of $\bar{x}$ and $\bar{x}^2$ are shown in figures 8 and 9 as functions of initial position y_1 and with the initial angle θ_1 as parameter. The ordinates have been expressed in terms of the dimensionless quantity ξ which was introduced in § 3.

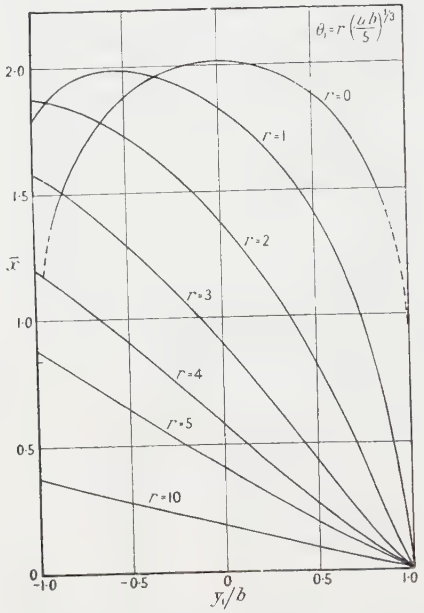

Figure 8. Mean first passage distance for double-sided problem.

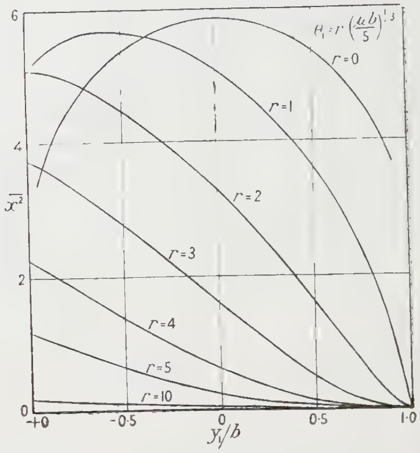

Figure 9. Mean square of first passage distance for double-sided problem.

The accuracy of a numerical solution obtained by relaxation methods can only be estimated by observing how the values converge when the net size is reduced. In this case the rate of convergence suggests that the accuracy of the values for $\bar{x}$ should not be worse than 1%. The values for $\overline{x^2}$ may be slightly less accurate as these depend on those for $\bar{x}$.

§ 6. COMPARISON AND DISCUSSION

The methods of §§ 4 and 5 each yield values of the mean and mean square first passage distances for particles which start from (0, 0, 0).

The comparison is made in the following table.

	1st Method		2nd Method
	Upper limit	Lower limit	
$\overline{x}$	2·00	1·92	2·02 ± 0·02
$\overline{x^2}$	6·0	4·5	5·8 ± 0·1

Since it was pointed out in § 4 that we should expect the upper limit to be very close to the true value, the agreement is satisfactory.

It may be useful to summarize the relative advantages of the two methods. Only the first one gives the complete distribution function and, at least in principle, can have any accuracy that is required. Its disadvantages are that lengthy computations are needed for even one set of initial conditions and only very simple boundary shapes can be treated. On the other hand the relaxation method only provides the moments of the distribution function but these are obtained for all values of the initial coordinates at the same time. There should be little difficulty in adapting this method for any shape of the boundaries. It could not, of course, be applied to cases like that treated in § 3 in which the moments are infinite.

ACKNOWLEDGMENTS

I am indebted to Drs. Chartres and Tidman for sending me an extended version of their published paper. Mr. D. Hum provided valuable advice on the application of relaxation methods. I am very grateful to Dr. Fürth for his continued interest and criticism.

REFERENCES

ALLEN, D. N. DE G., and SEVERN, R. T., 1951, *Quart. J. Mech.*, **4**, 209.
CHARTRES, B. A., and TIDMAN, D. A., 1955, *Proc. Phys. Soc.* A, **68**, 841.
COURANT, E. D., 1951, *Rev. Sci. Instrum.*, **22**, 1003.
FÜRTH, R., 1917, *Ann. Phys., Lpz.*, **53**, 177.
KRAMERS, H. A., 1940, *Physica, 's Grav.*, **7**, 284.
ROSSI, B., and GREISEN, K., 1941, *Rev. Mod. Phys.*, **13**, 267.
WANG, M. C., and UHLENBECK, G. E., 1945, *Rev. Mod. Phys.*, **17**, 323.
WASOW, W., 1951, *Ann. Math. Statist.*, **22**, 199.

The K Auger Yield for Tin

By J. A. V. FAIRBROTHER, D. G. PARKYN and B. M. O'CONNOR
Department of Physics, University of Natal

MS. received 12*th April* 1956, *and in revised form* 15*th December* 1956

Abstract. The principle employed by Martin and Stockmeyer in their determination of the fluorescent yield for gases is extended in the present paper to a determination of the fluorescent yield for metals. Preliminary measurements, using Burhop's probability values for the possible Auger transitions, give 0·164 ± 8% as the K Auger yield for tin or 0·836 ± 1·5% for the fluorescent yield. Though not forming part of the present paper the method allows the relative probability of the possible Auger transitions to be determined.

§ 1. THEORY

If a thin sheet of metal is traversed by a monochromatic beam of X-rays of slightly longer wavelength than that required to excite its K fluorescent radiation, groups of photoelectrons will be ejected from the metal atoms with energies

$$(E_S - E_L), (E_S - E_M), (E_S - E_N), \ldots$$

where E_S is the quantum energy of the radiation, the suffix S denoting that it is on the soft side of the K critical absorption limit, and E_L, E_M, $E_N, \ldots$ denote the quantum energies of the critical absorption edges of the L, M, N, ... levels of the metal atoms. If R_m is the mean component of the range in the metal of any one of these groups in a direction normal to the surface it is possible for photoelectrons in this group which are generated to a depth R_m below the surface to carry energy across the surface. If N_S is the number of photoelectrons generated per unit volume of the metal by a beam of unit cross section, N_S being constant over R_m, the total number generated per unit area in a surface layer of thickness R_m is $N_S \times R_m$ and the total energy possessed by this number is $N_S \times R_m \times (E_S - E)$ where E is the critical quantum absorption energy of the particular level being considered.

Assuming a range–energy relationship in the metal of the form $R \propto E^\beta$ elementary considerations show that the energy carried across the surface is proportional to

$$N_S \times (E_S - E)^{1+\beta} \times \beta/(1+\beta) \quad \text{or} \quad N_S \times (E_S - E)^\gamma \times \alpha \qquad \ldots\ldots(1)$$

putting $1+\beta=\gamma$ and $\beta/1+\beta=\alpha$.

The fraction of the total photoelectron energy in a surface layer R_m carried across the surface is therefore proportional to $\beta/(1+\beta)$ and is only dependent on the range through β. The energies of the photoelectron groups appearing in these experiments lie between 0·02 and 0·03 MeV and the energy range relationship used is the one proposed by Katz and Penfold (1952) for aluminium, namely $R = 412\,E^\beta$ mg cm^{-2} for the energy range $0{\cdot}01 \leqslant E \leqslant 2{\cdot}5$ MeV, where $\beta = 1{\cdot}265 - 0{\cdot}0954 \ln E$. The range in aluminium given by the formula for

0·03 MEV electrons is $5{\cdot}6\times10^{-4}$ cm and the range in tin will be some 2·7 times less than this. Since the intensities of the X-ray beams used in the present experiments can be considered to remain constant over this thickness of metal, N_S can be considered constant over R_m.

If the directional distribution of the ejected photoelectrons does not change with energy the total energy carried across the surface by all groups is proportional to the sum of all such expressions as (1) and can be written for convenience as

$$\sum_{i=L,M,N,\dots} N(Si)\times[\alpha E^{\gamma}]_{Si}$$

where (Si) refers to the photoelectrons possessing energy E_S-E_i. Since $N(SN)\ll N(SM)\ll N(SL)$ and $E(SM)$ and $E(SN)$ are nearly equal to and only a little larger than $E(SL)$, E_S being only slightly different from E_K, it is permissible to write $N_S\times[\alpha E^{\gamma}]_{SL}$ in place of the above expression, where N_S is now the total number of atoms per cubic centimetre of the metal ionized in all levels below the K level by the radiation of quantum energy E_S. The energy possessed by all the photoelectrons escaping into the air will be dissipated in the formation of ion pairs which will constitute an ion current Z_S where

$$Z_S\propto N_S\times[\alpha E^{\gamma}]_{SL}. \qquad \dots\dots(2)$$

If the metal is now irradiated with monochromatic radiation of wavelength slightly shorter than the critical K absorption limit of the metal the ionization due to the above group of electrons will be augmented by that due to the group ejected from the K shell and those arising from internal conversion. This new ionization current then becomes

$$Z_H\propto N_H\Big[[\alpha E^{\gamma}]_{HL}+(J_H-1)[\alpha E^{\gamma}]_{HK}+A(J_H-1)\sum P_{ij}[\alpha E^{\gamma}]_{Ki,j}\Big]$$

where N_H is the total number of atoms per cubic centimetre of the metal ionized in all levels below the K level by the radiation of quantum energy E_H (the suffix H denoting that it is on the hard side of the K critical absorption limit), J_H is the K absorption jump at λ_H, A is the Auger yield and P_{ij} is the fraction of the Auger transitions in the energy group $E_{Ki}-E_j$, where $i, j=L, M, N, \dots$ and $\sum P_{ij}=1$.

Since there is a limit in practice to the thinness of the foil a fraction of the fluorescent radiation will be absorbed in the foil and give rise to a group of electrons which will contribute to Z_H. The number of fluorescent photons emitted per unit volume of the metal is $N_H(J_H-1)(1-A)$ and if a fraction f of these is reabsorbed a number $N_Hf(J_H-1)(1-A)$ photoelectrons will be emitted per unit volume each with energy $E_{KL}-E_L$ (the number emitted from the $M, N, \dots$ rings is negligibly small) and the contribution to Z_H by this energy group is represented by the term

$$N_Hf(J_H-1)(1-A)[\alpha E^{\gamma}]_{KL,L}.$$

Collecting terms containing A, the complete expression for Z_H then becomes

$$\begin{aligned}Z_H\propto N_H\Big[&[\alpha E^{\gamma}]_{HL}+(J_H-1)[\alpha E^{\gamma}]_{HK}+f(J_H-1)[\alpha E^{\gamma}]_{KL,L}\\&+A(J_H-1)\Big\{\sum P_{ij}[\alpha E^{\gamma}]_{Ki,j}-f[\alpha E^{\gamma}]_{KL,L}\Big\}\Big]. \qquad \dots\dots(3)\end{aligned}$$

If I_{H} and I_{S} are the intensities of the hard and soft beams, and if these produce ionization currents S_{H} and S_{S} when measured in the same ionization chamber then

$$\left.\begin{aligned} &I_{\mathrm{S}}({}_{\mathrm{a}}\tau_{\mathrm{S}}+{}_{\mathrm{a}}\omega_{\mathrm{S}}) \propto S_{\mathrm{S}} \\ \text{and}\quad &I_{\mathrm{H}}({}_{\mathrm{a}}\tau_{\mathrm{H}}+{}_{\mathrm{a}}\omega_{\mathrm{H}}) \propto S_{\mathrm{H}} \end{aligned}\right\} \qquad \ldots\ldots(4)$$

where the ${}_{\mathrm{a}}\tau$'s denote the portion of the total absorption coefficient due to photoelectric absorption and the ${}_{\mathrm{a}}\omega$'s the portion associated with the Compton recoil electrons ($\mu=\tau+\omega+\sigma$). Also

$$\left.\begin{aligned} &I_{\mathrm{S}}\,{}_{\mathrm{m}}\tau_{\mathrm{S}} \propto N_{\mathrm{S}}E_{\mathrm{S}} \\ \text{and}\quad &I_{\mathrm{H}}\,{}_{\mathrm{m}}\tau_{\mathrm{H}} \propto N_{\mathrm{H}}E_{\mathrm{H}}J_{\mathrm{H}} \end{aligned}\right\} \qquad \ldots\ldots(5)$$

where the ${}_{\mathrm{m}}\tau$'s are the photoelectric absorption coefficients in the metal for the two radiations and J_{H} is the photoelectric absorption jump at λ_{H}. Combining equations (2), (3), (4) and (5)

$$\frac{Z_{\mathrm{H}}}{Z_{\mathrm{S}}}=\frac{S_{\mathrm{H}}}{S_{\mathrm{S}}}\frac{1}{J_{\mathrm{H}}}\frac{{}_{\mathrm{a}}\tau_{\mathrm{S}}+{}_{\mathrm{a}}\omega_{\mathrm{S}}}{{}_{\mathrm{a}}\tau_{\mathrm{H}}+{}_{\mathrm{a}}\omega_{\mathrm{H}}}\frac{{}_{\mathrm{m}}\tau_{\mathrm{H}}}{{}_{\mathrm{m}}\tau_{\mathrm{S}}}\frac{E_{\mathrm{S}}}{E_{\mathrm{H}}}\frac{1}{[\alpha E^{\gamma}]_{\mathrm{SL}}}\Big[[\alpha E^{\gamma}]_{\mathrm{HL}}+(J_{\mathrm{H}}-1)[\alpha E^{\gamma}]_{\mathrm{HK}}$$
$$+f(J_{\mathrm{H}}-1)[\alpha E^{\gamma}]_{\mathrm{KL,\,L}}+A(J_{\mathrm{H}}-1)\Big\{\sum P_{ij}[\alpha E^{\gamma}]_{\mathrm{K}i,\,j}-f[\alpha E^{\gamma}]_{\mathrm{KL,\,L}}\Big\}\Big]. \qquad \ldots\ldots(6)$$

Equation (6) is of the form

$$a=b+A(J_{\mathrm{H}}-1)[\textstyle\sum c_{ij}P_{ij}+d] \qquad \ldots\ldots(7)$$

in which a, b, c_{ij} and d are dependent on E_{H} and E_{S}. By working with different combinations of E_{H} and E_{S} and setting up as many equations as there are P_{ij}'s from experimental determinations of the ratios $Z_{\mathrm{H}}/Z_{\mathrm{S}}$ and $S_{\mathrm{H}}/S_{\mathrm{S}}$ the P_{ij}'s can in principle be determined from the equations. Considering the K, L, M and N levels only, possible transitions are K→LL, K→LM, K→MM, K→LN, K→MN and K→NN. Since there is an approximate seven-fold fall off in the critical absorption energies in passing outwards through successive electron shells these possible transitions fall into three main groups, namely, K→LL (group 1), K→LM, K→LN (group 2), and K→MM, K→MN, K→NN (group 3), so that in practice partial resolution is possible by solving three equations.

Experimentally the problem resolves itself into: (*a*) Generating monochromatic beams of x-rays on the hard and soft side of the K absorption edge of the metal of sufficient intensity to produce measurable saturation currents in an ionization chamber. (*b*) Measuring $S_{\mathrm{H}}/S_{\mathrm{S}}$, the ratio of the beam intensities. (*c*) Measuring $Z_{\mathrm{H}}/Z_{\mathrm{S}}$ the ratio of the energies of the photoelectrons ejected from the metal by the two beams.

Knowing the S and Z ratios the Auger yield can be calculated from known absorption data. The metal forming the subject of investigation in the present paper is tin.

§ 2. THE RADIATION AND MONOCHROMATIZATION

The radiation used was obtained from a Machlett tube fitted with a tungsten anticathode and operated at a peak voltage of 45 kv. A sheet of aluminium 2 mm thick was fitted over the exit port of the tube to take out the soft radiation. The tube was controlled by a Victor X-ray Corporation autotransformer unit adapted to give independent and continuously variable control of the filament current and high tension. The tube current was read on a Victor 0–20 mA X-ray milliameter which gave a deflection of about 6 mm per milliampere.

The ionization currents were fed to the grid of an FP54 electrometer valve used in a circuit described by DuBridge and Brown (1933). Using a galvanometer with a sensitivity of $2{\cdot}2 \times 10^{-8}$ amperes per cm on a scale distant 1 metre the electrometer circuit had an initial sensitivity of 725 centimetres per volt change on the grid. With this sensitivity and a tube current of 5 mA the ionization currents were large enough to operate the electrometer circuit with a grid resistance of 10^{10} ohms. The electrometer and its circuit was contained in an earthed metal box kept dry with silica gel. Under these conditions the circuit was very stable and gave trouble free operation throughout the course of the experiments. In the absence of mains voltage fluctuations, it was possible to hold the beam intensity steady, as judged by the deflection of the galvanometer, to within $\pm 1\%$ and to repeat readings to within $\pm 2\%$.

Monochromatic beams of radiation were obtained using the balanced filter method introduced by Ross (1928). Silver, tin and iodine filters were employed. The silver–tin pair provided the equivalent of a narrow beam of radiation on the soft side of the K absorption edge of tin of width 0·061 Å and the tin–iodine pair a band of radiation on the hard side of width 0·05 Å. The silver and tin foils used for the filters were each 0·05 mm thick and could be rotated about an axis perpendicular to the beam so as to vary their effective thickness.

The iodine filter was prepared by dropping a solution of iodoform (CHI_3) in chloroform on to a filter paper, thereby leaving it impregated with a uniform layer of small iodoform crystals after the chloroform had evaporated off. A thin protective coating of paraffin wax served to prevent the evaporation of iodoform which has an appreciable vapour pressure at room temperature. The three filters fitted into a box attached to the ionization chamber (figure 1). The filters were balanced by running the tube at 25 kv, i.e. just on the soft side of the K absorption edge of silver, and adjusting their effective thickness so that each produced the same reduction in beam intensity when placed in the path of the beam. For this purpose the iodine filter was held at right angles to the beam and the tin and silver filters were tilted. To compensate for the reduction in X-ray

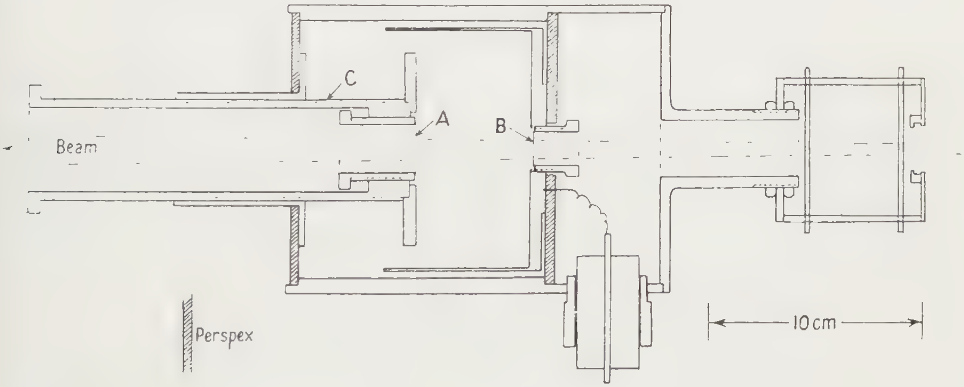

Figure 1. The variable gap chamber.

output at the lower operating voltage employed in balancing, the 2 mm aluminium filter was replaced by a 0·3 mm aluminium filter.

The ratio of the difference of the ionization currents due to the tin and silver filtered beams to the ionization current due to the tin filtered beam, for peak operating voltages greater than the K absorption edge for tin, was taken as a measure of the fraction of the total beam energy in the soft wave band. The maximum value of this ratio occurred at 45 kv peak and the tube was therefore operated at this voltage throughout the experiments. The measured ratio was about 1/3·2.

§ 3. THE MEASUREMENTS OF Z_H/Z_S

The ratio Z_H/Z_S was measured by means of the chamber shown in figure 1 in which A and B are thin sheets of tin foil $8{\cdot}75 \times 10^{-4}$ cm thick mounted on the ends of aluminium cylinders which screw into position in the chamber. A served as high tension electrode and B as collector. The distance between the foils could be varied from 0–10 cm by turning the threaded brass tube C. Curves of saturation current versus foil separation were plotted with the iodine, tin and silver filters placed in turn in the beam. A typical plot (in this case for the unfiltered beam) is shown in figure 2. The contribution to the ionization in the chamber by the photoelectrons ejected from the metal foil (denoted by Z_I, Z_{Sn}, Z_{Ag} for the iodine, tin and silver filtered beams) is given by the intercept on the current axis of the extrapolated straight part of the curve after correction for the ionization in the chamber due to the fluorescent radiation from the foil and the absorption in the foil of the photoelectrons ejected from the air by the main beam. The ratio of Z_H/Z_S is then given by

$$Z_H/Z_S = (Z_I - Z_{Sn})/(Z_{Sn} - Z_{Ag}).$$

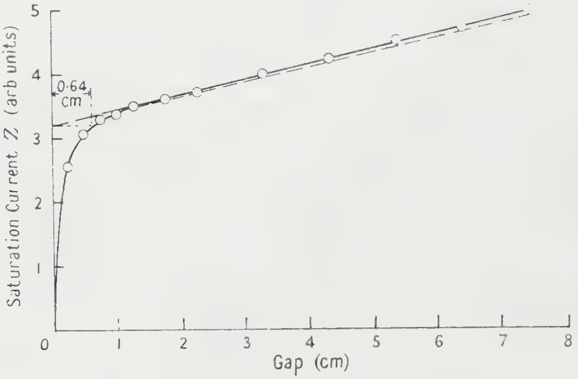

Figure 2. A typical plot of saturation current versus foil separation using the variable gap chamber. The broken line is corrected for fluorescent radiation.

The nature and magnitude of the corrections to be applied for the ionization due to the fluorescent radiation and the loss of photoelectrons in the foil is illustrated by reference to figure 3 in which curve I represents the ionization due to the photoelectrons ejected from the air by the main beam, curve II is the ionization in the chamber due to the fluorescent radiation from the foil and curve III is the ionization due to the photoelectrons ejected from the foil. Each curve is a plot of the total ionization contained in a parallel slab, of which the foil forms one face, against slab thickness.

Curve I. Since the ionization of the air in the immediate vicinity of the foil is due to the photoelectrons received from one side only the slope of Curve I increases with slab thickness until the latter reaches a value equal to the mean component of the range of the ejected photoelectron normal to the foil. From this point onwards, assuming the intensity of the beam to remain constant, the slope is constant. Compton and Allison (1935) give $R = V^2/440$ as a rough working formula for the mean total range of an electron in air at atmospheric pressure, where V is the energy in kev and R is the range in centimetres. The energy peak in the spectrum of the radiation used in these experiments is in the neighbourhood of the absorption edge for tin, namely 29·12 kv. From the formula this corresponds to a total mean range of 1·93 cm. The mean component of the range perpendicular to the plates (represented by OC) will be about one third of this, namely 0·64 cm. The intensity of ionization at the foil, and hence the slope of the curve at O, depends upon the width of the beam relative to the mean component of the range. When the beam width is small compared with the mean range, so that the intensity of ionization at any point in the beam is due principally to photoelectrons proceeding in the direction of the beam, the slope of the curve O will be one half of the slope at B since photoelectrons are received from one side only. In this case elementary considerations show that $OO' = \frac{1}{3}BC'$. When the beam width is large compared with the range the slope at O will be one sixth of the slope at B in which case $OO' = (1/9)BC'$. The beam width in these experiments was about 6 mm, i.e. about equal to the mean component of the range in the direction of the beam so that OO' lies between 1/3 and 1/9 of BC' and the intercept on the current axis of the straight portion of the curve (obtained after correction for the ionization due to the fluorescent radiation) must be increased by this amount. Reference to figure 2 shows that it is of the order of 1%. Reference to figure 5 also shows that the slopes of the linear parts of the curves are approximately proportional to the current intercepts so that OO' is proportional to Z. Since $Z_H/Z_S = (Z_I - Z_{Sn})/(Z_{Sn} - Z_{Ag})$ the correction therefore largely disappears in the ratio.

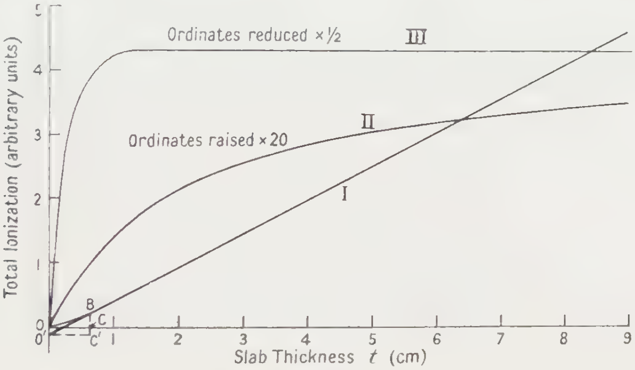

Figure 3. Plot of total ionization in a slab of thickness t against t due to (I) the photoelectrons ejected from the air by the main beam, (II) the fluorescent radiation, (III) the photoelectrons ejected from the foil. The foil forms one face of the slab.

Curve II. Curve II is a plot of the mean path of the fluorescent radiation in the chamber given by the expression

$$P = Y\left(\frac{\pi}{2} - \tan^{-1}\frac{Y}{X}\right) - X \ln\cos\left(\tan^{-1}\frac{Y}{X}\right)$$

for different values of the foil separation X. Y is the radius of the chamber. The expression is derived on the assumption that the fluorescent radiation is emitted equally in all directions from the centre of each foil. This assumption is permissible since the radius of the chamber was some fifteen times that of the cross section of the beam. The product of P and the absorption coefficient of the fluorescent radiation in air is a measure of the ionization produced.

Curve III. The ionization due to the photoelectrons ejected from the metal form a sheath in the vicinity of the foils of thickness equal to the mean component of the range in the direction of the beam. Outside the sheath the ionization is zero. Though the energy peak in the x-ray spectrum is in the neighbourhood of the absorption edge for tin, the high energy photoelectrons in the metal make a relatively greater contribution to the ionization in the chamber on account of their greater numbers, the high energy photoelectrons being drawn from a greater thickness of metal in accordance with the energy range relationship in the metal. The mean component of the range in air of the photoelectrons ejected from the metal might therefore be expected to lie somewhere between values corresponding to 29·12 and 45 kv electrons. Using Compton and Allison's formula these voltages correspond to total ranges of 1·93 and 4·6 cm and to mean ranges in the direction of the beam equal to a third of these, namely, 0·64 and 1·53 cm. The mean component of the range in the direction of the beam in figure 2 is about 12 mm and lends support to the assumption that the mean range in a particular direction can be taken as about equal to one third of the total range. The relative magnitude of curves I and II, figure 3 are obtained from the curves given in figure 4. Curve I, figure 4, is the output spectrum of the tube plotted from standard data and corrected for absorption in the 2 mm aluminium filter. Curve II is the spectrum of the radiation after passing through

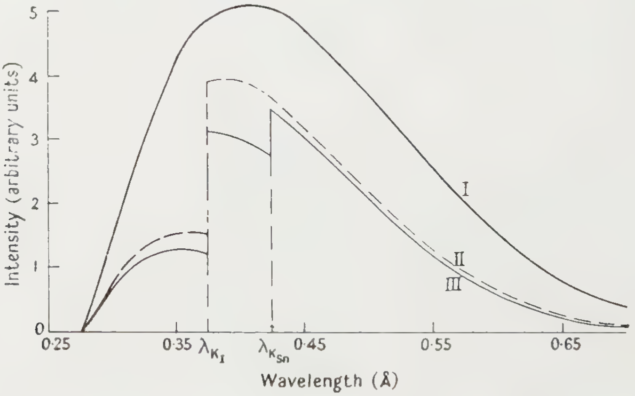

Figure 4. Output spectrum of the tube filtered through (I) 2 mm of aluminium, (II) 2 mm aluminium and the iodine filter, (III) 2 mm aluminium, the iodine filter and the first foil of the variable gap chamber.

the iodine filter (effective thickness 0·066 mm) and Curve III is the spectrum of the radiation after passing through the first foil of the variable gap chamber. A fraction

$$\int_{\lambda=29\cdot12\,\mathrm{kv}}^{\lambda=45\,\mathrm{kv}} I_\lambda \frac{J_\lambda-1}{J_\lambda}\,\frac{E_\mathrm{K}-E_\mathrm{L}}{E_\lambda}(1-A)(1-f)\,d\lambda$$

of the area contained between Curves II and III on the hard side of the K absorption edge for tin represents the energy entering the chamber as fluorescent radiation. The integral is taken over all wavelengths from the absorption edge for tin to the shortest in the spectrum. The energy of the fluorescent radiation lies between 24·66 and 25·20 kv and its contribution to the ionization in the chamber is given by the product of the above integral, the mean path length in the chamber and the absorption coefficient in air for radiation of this wavelength. The ionization due to the radiation in the main beam is computed by replotting Curve III with all its ordinates multiplied by the appropriate absorption coefficient in air and measuring the area under the curve. The ratio of the ionization due to the fluorescent radiation to the sum of the ionization due to the main beam and the fluorescent radiation expressed as a percentage for foil separations increasing by steps of 1 cm, is given in table 1 for the iodine, tin and silver filtered radiation. The table also includes the figures for the unfiltered radiation, i.e. for the radiation after it has passed through 2 mm of aluminium only.

Table 1

Separation (cm)	1	2	3	4	5	6	7	8	9
Iodine (%)	12·21	9·25	7·53	6·37	5·49	4·85	4·32	3·90	3·56
Tin (%)	5·61	4·18	3·36	2·81	2·42	2·13	1·89	1·70	1·55
Silver (%)	7·09	5·29	4·27	3·58	3·09	2·71	2·41	2·17	1·98
Unfiltered (%)	10·65	8·05	6·51	5·50	4·75	4·16	3·72	3·34	3·05

The contribution to the ionization by the fluorescent radiation is small compared with the contribution from the beam which in turn is small compared with the ionization due to the photoelectrons from the metal. This is evidenced by the fact that the graph in figure 2 appears linear for foil separations greater than the range of the photoelectrons ejected from the foil. To obtain Z, the contribution to the ionization of the photoelectrons from the foil, the contribution due to the fluorescent radiation (obtained from the data in table 1) is subtracted from the ionization current readings and the straight portion of the curve obtained is extrapolated to cut the current axis to give Z. The replotted curve of figure 2 is shown in broken line.

The intercept on the current axis of the replotted curve differs from that of the original by less than the error in drawing either curve and such difference as there is tends to disappear by difference as in the case of the correction for the loss of photoelectrons by absorption in the foils. The accuracy of the final result is also aided by the two effects acting in opposite directions and operating so as to cancel each other out.

A typical set of curves showing the variation of total ionization with foil separation for the iodine, tin and silver filtered beams is shown in figure 5.

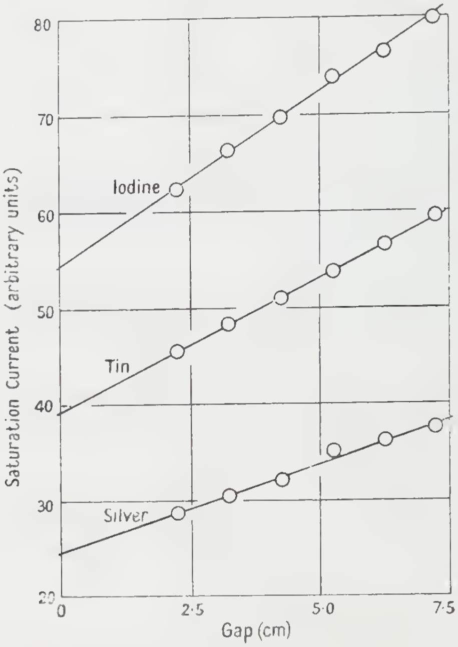

Figure 5. Plot of saturation current against gap for the iodine, tin and silver filtered beams.

§ 4. MEASUREMENT OF S_H/S_S

Since the ionization due to absorption in the air in the variable gap chamber was only a small portion of the measured saturation current, the bulk of it being due to ionization by photoelectrons from the metal, S_H/S_S was measured by substituting a parallel plate chamber of standard pattern for the variable gap chamber. A sheet of tin foil of the same thickness as that used for the variable gap chamber was placed in the path of the beam sufficiently far from the chamber to ensure that the radiation scattered from it made no contribution to the ionization in the chamber. The beam thus had the same spectral composition as it had on entering the air space of the variable gap chamber. Ionization currents S_I, S_{Sn}, S_{Ag} were taken for iodine, tin and silver filtered beams and S_H/S_S calculated from the relationship

$$S_H/S_S=(S_I-S_{Sn})/(S_{Sn}-S_{Ag}).$$

§ 5. SATURATION CHARACTERISTICS OF THE VARIABLE GAP CHAMBER

Figure 6 shows the ionization current–voltage characteristic of the variable gap chamber for 2·5, 5·0 and 7·5 cm gaps respectively. The operating voltages chosen for these three gaps were 120, 400 and 800 as being well into the region of the flat plateau. Intermediate voltages were used for intermediate distances.

§ 6. RESULTS

A set of values of Z_H/Z_S and S_H/S_S are given in table 2 and the energy terms in kev used in the equations in table 3. E_H and E_S are the energies

Table 2

							Mean
Z_H/Z_S	1·06	1·08	1·01	1·05	1·02		1·04
S_H/S_S	0·421	0·414	0·415	0·429	0·409	0·403	0·415

Table 3

		Sn					Sb				Sn & Sb
E_H	E_S	E_K	$E_{L(I)}$	$E_{L(II)}$	$E_{L(III)}$	E_M	$E_{L(I)}$	$E_{L(II)}$	$E_{L(III)}$	E_M	E_N
31·09	27·30	29·12	4·46	4·15	3·92	0·51	4·99	4·37	4·13	0·54	$<0{\cdot}1$

corresponding to the middle wavelengths of the hard and soft bands, namely $\lambda_H = 0{\cdot}399$ Å and $\lambda_S = 0{\cdot}454$ Å.

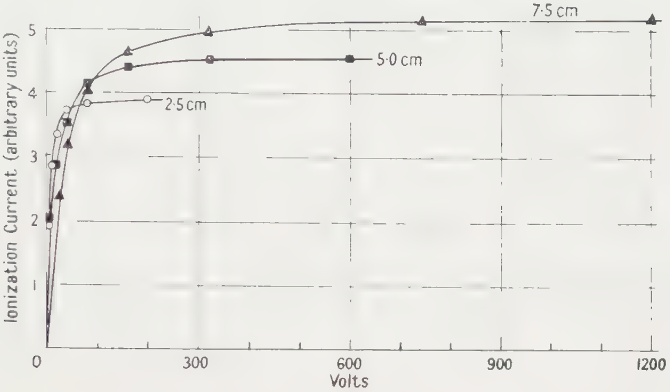

Figure 6. Plot of ionization current versus voltage for 2·5, 5·0 and 7·5 cm gaps.

A term like $[\alpha E^\gamma]_{HL}$ (equation (6)) is a composite term which can be written

$$[\alpha E^\gamma]_{HL} = a[\alpha E^\gamma]_{HL(I)} + b[\alpha E^\gamma]_{HL(II)} + c[\alpha E^\gamma]_{HL(III)}$$

where a, b, c are the fractions of photoelectrons ejected by the E_H radiation from the L(I), L(II), L(III) subshells. Using Wentzel's (1927) formula relating the rate of ejection of photoelectrons from the sublevels with the exciting wavelength

$$a = \lambda_L/(10\lambda + \lambda_L) \quad \text{and} \quad b + c = 10\lambda/(10\lambda + \lambda_L)$$

where λ is the exciting wavelength and λ_L the mean of the critical absorption wavelengths for the L level. Counting the L(II) and L(III) levels as one level and employing the formula,

$[\alpha E^\gamma]_{LH}$ is replaced by $0{\cdot}427[\alpha E^\gamma]_{H,\,L(I)} + 0{\cdot}573[\alpha E^\gamma]_{H,\,(L(II)+L(III))/2}$

$[\alpha E^\gamma]_{SL}$ by $0{\cdot}395[\alpha E^\gamma]_{S,\,L(I)} + 0{\cdot}605[\alpha E^\gamma]_{S,\,(L(II)+L(III))/2}$

and

$[\alpha E^\gamma]_{KL,\,L}$ by $0{\cdot}376[\alpha E^\gamma]_{KL(III),\,L(I)} + 0{\cdot}624[\alpha E^\gamma]_{KL(III),(L(II)+L(III))/2}$.

The $E_{L(III)}$ term is used for $E_{KL(III)} (= E_K - E_{L(III)})$ since the KL(I) transition does not occur.

E_{Ki} in the term $E_{Ki,\,j}$ denotes the energy difference for the appropriate energy levels of tin (50) and E_j represents the energy levels of antimony (51) the next higher element in the atomic series. When i represents an L level it is taken as L(III). Using Burhop's (1952) probability values for the transitions K→LL, K→LM, K→MM, K→LN, K→MN, K→NN, the term $\sum P_{ij}[\alpha E^{\gamma}]_{Ki,j}$ becomes

$$0\cdot55\{0\cdot337[\alpha E^{\gamma}]_{\mathrm{KL(III),L(I)}}+0\cdot663[\alpha E^{\gamma}]_{\mathrm{KL(III),(L(II)+L(III))/2}}$$
$$+0\cdot317[\alpha E^{\gamma}]_{\mathrm{KL(III),M(Sb)}}+0\cdot041[\alpha E^{\gamma}]_{\mathrm{KM,M(Sb)}}$$
$$+0\cdot076[\alpha E^{\gamma}]_{\mathrm{KL(III),N(Sb)}}+0\cdot0136[\alpha E^{\gamma}]_{\mathrm{KM,N(Sb)}}+0\cdot0019[\alpha E^{\gamma}]_{\mathrm{KN,N(Sb)}}.$$

The photoelectric absorption coefficients for tin are taken from data compiled by Allen (1954) and from Coade's (1930) experimental data on the scattering coefficient.

For tin Allen gives $\mu_H(\lambda_H=0\cdot40\text{ Å})=39$ and $\mu_S(\lambda_S=0\cdot45\text{ Å})=9\cdot6$ and Coade gives for the scattering coefficient $\sigma_H=0\cdot6$ and $\sigma_S=0\cdot7$ so that, taking differences, the photoelectric absorption coefficients for tin are $\tau_H=38\cdot4$ and $\tau_S=8\cdot9$. The absorption due to Compton recoil electrons in the metal is negligible compared with the photoelectric absorption for the wavelengths used in these experiments.

For air, compounding Allen's data for nitrogen and oxygen in the ratio of 79/21, $\mu_H=0\cdot304$ and $\mu_S=0\cdot370$ and from Compton and Allison $\sigma_H=0\cdot191$ and $\sigma_S=0\cdot199$ so that, by difference, $\tau_H+\omega_H=0\cdot113$ and $\tau_S+\omega_S=0\cdot171$. Using data from the same sources the ratio of the photoelectric absorption jump at λ_H is $J_H=38\cdot4/6\cdot1=6\cdot29$.

An expression for the fraction f of the fluorescent radiation which is reabsorbed is derived in an addendum. The value of f is not constant through the foil even on the assumption of uniform excitation, but falls off fairly steeply towards the surface. When in addition the exponential decay of the exciting radiation, about 24% across the foil, is taken into account the f-profile becomes appreciably unsymmetrical.

The mean range of the ejected photoelectrons in the metal (R_m) is of the order of 2×10^{-4} cm and it is necessary (cf. § 1) to evaluate the mean of f over a surface layer of this depth. Further, since the contribution to Z_H arises from the exit face of the first foil and the incident face of the second, f was calculated as the average of these two means the resulting value being 12·12%.

Inserting the above data equation (7) becomes

$$8\cdot67=6\cdot42+A(6\cdot29-1)[2\cdot87-0\cdot29]$$

giving

$$A=0\cdot164\pm8\% \qquad \text{(the Auger yield)}$$

and

$$\omega=0\cdot836\pm1\cdot5\% \qquad \text{(the fluorescent yield).}$$

Previous experimental determinations of the fluorescent yield for tin are as follows:

Arends (1935)	0·825
Backhurst (1936)	0·855
Berkey (1934)	0·66
Roos (1954)	0·81
Stephenson (1937)	0·84

ACKNOWLEDGMENTS

We wish to record our thanks to the South African Council of Scientific and Industrial Research for a bursary and equipment grant to one of us (B. M. O'C.), to Dr. A. J. Barnard and Mr. M. Leask for helpful discussions, to Messrs. The Aluminium Company of South Africa (Pty) Limited, for gifts of aluminium and tin foil, to Messrs. the South African General Electric Company (Pty) Ltd. and Messrs. The General Electric Company of England for gifts of x-ray apparatus, and to Mr. Abel Phelps for his expert assistance in constructing the apparatus.

APPENDIX

THE FRACTIONAL ABSORPTION OF FLUORESCENT RADIATION IN A METAL FOIL

The problem is idealized to that of an infinite metal foil of thickness t irradiated by a parallel beam of x-rays. If the rate of fluorescent energy emission generated at the incident face is e_0, τ' the linear absorption coefficient for the exciting radiation and τ that for the fluorescent radiation within the foil, then the total fluorescent energy outflow rates from the incident and exit faces may be seen to be respectively

$$E^-(t) = \frac{e_0 \pi R^2}{2} \int_0^t \int_0^{\pi/2} \exp(-\tau z \sec\theta) \sin\theta \, d\theta \exp(-\tau' z) \, dz$$

and $$E^+(t) = \frac{e_0 \pi R^2}{2} \int_0^t \int_0^{\pi/2} \exp(-\tau z \sec\theta) \sin\theta \, d\theta \exp[-\tau'(t-z)] \, dz$$

where R is the radius of the irradiated disc. Of these, the integral for $E^+(t)$ is singular but may be evaluated using a Cauchy principal value. On the assumption $\tau' > \tau$, the integrals may be reduced to

$$E^-(t) = \frac{e_0 \pi R^2}{2\tau'} \left\{ 1 - \frac{\tau}{\tau'} \ln\left(\frac{\tau'}{\tau} + 1\right) - \exp(-\tau' t) H_2(\tau t) + \frac{\tau}{\tau'} \exp(-\tau' t) H_1(\tau t) \right.$$
$$\left. - \frac{\tau}{\tau'} H_1[(\tau' + \tau)t] \right\}$$

$$E^+(t) = \frac{e_0 \pi R^2}{2\tau'} \exp(-\tau' t) \left\{ -1 - \frac{\tau}{\tau'} \ln\left(\frac{\tau'}{\tau} - 1\right) + \exp(+\tau' t) H_2(\tau t) \right.$$
$$\left. + \frac{\tau}{\tau'} \exp(+\tau' t) H_1(\tau t) + \frac{\tau}{\tau'} \mathrm{Ei}[(\tau' - \tau)t] \right\}$$

where the integrals $H_n(t) = \int_1^\infty x^{-n} e^{-tx} \, dx$ $(n = 1, 2)$ are Gold's (1909) integrals

$$\mathrm{Ei}(t) = \int_{-\infty}^t \frac{e^x}{x} \, dx.$$

The Gold integrals may be reduced to those of the form $\mathrm{Ei}(t)$, these being very fully tabulated in the National Bureau of Standards Mathematical Tables (1940). In particular $H_1(t) = -\mathrm{Ei}(-t)$.

Since the total rate of fluorescent energy production within the foil (E_0) is given by $E_0 = (e_0 \pi R^2/\tau')[1 - \exp(-\tau' t)]$, the mean absorption rate

$$[1 - (E^+ + E^-)/E_0],$$

may be evaluated. In view of the relatively short range of the photoelectrons, however, it is necessary to investigate the absorption rate in the neighbourhood of the exit face. The total energy outflow rate from an edge sheet, inner face distance z from the incident face, is

$$E^-(t) + E^+(z) - \exp(-\tau' z) E^-(t - z).$$

After differentiating with respect to z, the local fractional absorption rate may be seen to be

$$f(z)=\frac{\tau\exp\left[+\tau'(t-z)\right]}{2\tau'}\left\{\ln\left(\frac{\tau'+\tau}{\tau'-\tau}\right)+\exp\left(+\tau'z\right)H_1(\tau z)-\exp\left[-\tau'(t-z)\right]\right.$$
$$\left.\times H_1[\tau(t-z)]+H_1[(\tau'+\tau)(t-z)]+\mathrm{Ei}[(\tau'-\tau)z]\right\}$$

where the absorption rate is given as a fraction of the rate of energy production at the exit face.

The edge values may be obtained as the limits when $z\to 0$ and t respectively in the forms

$$f(0)=\frac{\tau\exp(\tau't)}{2\tau'}\left\{\ln\frac{\tau'+\tau}{\tau}-\exp\left(-\tau't\right)H_1(\tau t)+H_1[(\tau'+\tau)t]\right\}$$

and

$$f(t)=\frac{\tau}{2\tau'}\left\{\ln\frac{\tau}{\tau'-\tau}+\exp\left(+\tau't\right)H_1(\tau t)+\mathrm{Ei}[(\tau'-\tau)t]\right\}.$$

In the following table $f(z)$ is calculated as a percentage for an exit face with $t=8{\cdot}75\times10^{-4}$, $\tau'=284\,\mathrm{cm}^{-1}$ and $\tau=80\,\mathrm{cm}^{-1}$, z being the distance from the incident face.

$z\times10^4$ (cm)	5	6	7	8	8·75
$f(z)$ (%)	14·96	14·62	14·07	13·24	12·14

The mean value over a surface layer of depth 2×10^{-4} cm is 13·37%.

For the second foil of the ionization chamber the values near the incident face are required and are expressed as a percentage of the rate of energy production at the incident face, this being effectively equal to that at the exit face of the first foil.

$z\times10^4$ (cm)	0	1	2	3	4
$f(z)$ (%)	9·85	10·97	11·47	11·72	11·77

The mean value over a surface layer of depth 2×10^{-4} cm is 10·88%, giving an average value of f for the two foils as 12·12%.

REFERENCES

ALLEN, S. J. M., 1954, *The Chemical Rubber Publishing Company's* 1954 *Handbook.*

ARENDS, E., 1935, *Ann. Phys., Lpz.*, **22,** 281.

BACKHURST, I., 1936, *Phil. Mag.*, **22,** 737.

BERKEY, D. K., 1934, *Phys. Rev.*, **45,** 437.

BURHOP, E. H. S., 1952, *The Auger Effect* (Cambridge : University Press), p. 50.

COADE, E. N., 1930, *Phys. Rev.*, **36,** 1109.

COMPTON, A. H., and ALLISON, S. K., 1935, *X-rays in Theory and Experiment* (London : Macmillan), pp. 494, 122.

DU BRIDGE, L. A., and BROWN, H., 1933, *Rev. Sci. Instrum.*, **4,** 532.

GOLD, E., 1909, *Proc. Roy. Soc.* A, **82,** 62.

KINSEY, B. B., 1948, *Canad. J. Res.* A, **26,** 404, 421.

KATZ, L., and PENFOLD, A. S., 1952, *Rev. Mod. Phys.*, **24,** 28.

MARTIN, L. H., 1927, *Proc. Roy. Soc.* A, **115,** 420.

ROOS, C. E., 1954, *Phys. Rev.*, **93,** 401.

ROSS, P. A., 1928, *J. Opt. Soc. Amer.*, **16,** 433.

STEPHENSON, H. J., 1933, *Phys. Rev.*, **43,** 527; 1937, *Ibid.*, **51,** 637.

STOCKMEYER, W., 1932, *Ann. Phys., Lpz.*, **12,** 71.

U.S. NATIONAL BUREAU OF STANDARDS, 1940, *Tables of Sine, Cosine and Exponential Integrals*, M.T. 5, 6 (New York : National Bureau of Standards).

WENTZEL, G., 1927, *Z. Phys.*, **40,** 574.

The Magnetic Energy Levels of Electrons in Metals

By A. D. BRAILSFORD†

Department of Mathematical Physics, University of Birmingham

Communicated by R. E. Peierls; MS. received 20th December 1956

Abstract. The magnetic energy levels of an electron in a periodic lattice are found using a generalization of the energy band of the simple cubic lattice. It is shown that when the constant-energy curves in a plane normal to the field direction are closed the levels are given by the semi-classical quantization rules, the broadening due to the lattice forces being negligible compared with the level spacing in nearly all cases. When the curves are open, the levels in the presence of a magnetic field are continuous. The relation of the results to a general type of energy band is briefly discussed.

§ 1. Introduction

THE determination of the magnetic energy levels of an electron in a periodic lattice is of importance in the quantitative theory of the diamagnetism of metals. Peierls (1933) has shown that approximate eigenvalues may be obtained by using an equivalent Hamiltonian formed from the energy function $E(\mathbf{k})$ of a particular band by the substitution $\mathbf{k} \to \mathbf{K}$ where $[K_x, K_y] = (ie/\hbar c)H_z$ etc. This theorem is valid provided the mixing of states in different energy bands may be neglected. Consequently, it is known as the single band approximation.

A general approach to this alternative statement of the eigenvalue problem has been suggested by Onsager (1952). As presented by Lifshitz and Kosevitch (1954) this is the following: let the field H be directed along the z-axis, then the commutation relations between the components of $\mathbf{K}$ become

$$[K_x, K_y] = (ie/\hbar c)H : [K_x, K_z] = [K_y, K_z] = 0. \qquad \ldots\ldots(1.1)$$

Thus $(c\hbar^2/eH)K_x$ and K_y play the role of generalized coordinate and canonically conjugate momentum respectively. The Bohr–Sommerfeld quantization rule may then be stated in the form

$$(c\hbar^2/eH)\oint K_y \, dK_x = (n+\gamma)h \qquad \ldots\ldots(1.2)$$

where $0<\gamma<1$. The integral in equation (1.2) is the area enclosed by the curve $E(\mathbf{k}) = E$ in the plane $K_z = k_z =$ constant. Equation (1.2) is an implicit relation between the energy E and the quantum number n.

Recently Lifshitz *et al.* (1956) have pointed out that Onsager's method is not applicable when the constant-energy curves in a plane normal to the field direction cannot be closed within a single zone or by periodic continuation in $\mathbf{k}$-space.‡ A particular example we select to illustrate this feature is

$$E(\mathbf{k}) = E_0(\cos k_x a_x + \lambda \cos k_y a_y + \nu \cos k_z a_z) \qquad \ldots\ldots(1.3)$$

† Now at Bell Telephone Laboratories Inc., Murray Hill, N.J., U.S.A.

‡ These results of work in course of publication were outlined to us in a letter from Mr. A. M. Abrikosov.

this being the simplest non-trivial generalization of the energy band of the simple lattice for which $\lambda=\nu=1$ ($a_x=a_y=a_z$) as found using the tight binding approximation. In figure 1 various curves of constant energy are plotted in the k_x–k_y plane, choosing $\lambda<1$. It will be seen that whilst the area in (1.2) is definite for the energies denoted by 1 and 4, where the orbit† is either closed as drawn or may be closed by using the equivalence of opposite points on the zone boundaries, the quantization rule cannot be applied for an open orbit such as 5. Indeed, this is true for all orbits intermediate between 2 and 3. For such cases Onsager's method does not determine the eigenvalues.

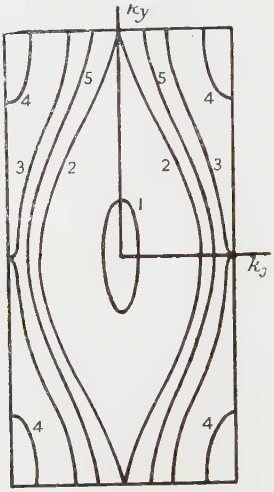

Figure 1. Constant energy curves in k_x–k_y plane for the energy band (1.3).

In this paper the magnetic energy levels for the energy band (1.3) are found. A rigorous derivation of Onsager's result is given for the energies corresponding to the closed orbits. It is shown that where the orbits are open, the energy levels in the presence of a magnetic field form a uniform continuous spectrum.

In § 2 Peierls' theorem is applied to the energy band (1.3) and the eigenequation is derived in the form of a difference equation. This equation has periodic coefficients and is shown to possess eigenvalues which fall into bands, or broadened levels. The broadening is described by two parameters k_x and k_y. Since the method used for solving the eigenequation is insensitive to the presence of both these parameters simultaneously, we first consider the case $k_y=0$. Two general solutions of the eigenequation are given in § 3 and these are used in § 4 to obtain relations giving the eigenvalues for the two separate cases of open and closed orbits. In § 5 the k_y broadening is investigated for $k_x=0$. The results of this study are given in § 6, where the variation of the level spacing and level broadening throughout the band is described. § 7 contains a summary of the results of this paper and a discussion of their relation to other types of energy bands.

---

† In the presence of a magnetic field, the projection of the motion in **k**-space of a representative point in the transverse plane is along a curve of constant energy. The latter are henceforth referred to as orbits.

§ 2. EIGENEQUATION

In applying Peierls' theorem, a convenient representation of $\mathbf{K}$ is

$$\hbar\mathbf{K} = -i\hbar\nabla - (\mathbf{e}/\mathbf{c})\mathbf{A}(\mathbf{r}) \qquad \ldots\ldots(2.1)$$

and we select the gauge $\mathbf{A} = (0, Hx, 0)$ giving a field H along the z-axis. Substituting (2.1) into the eigenequation

$$E_0(\cos K_x a_x + \lambda \cos K_y a_y + \nu \cos K_z a_z)u(\mathbf{r}) = Wu(\mathbf{r})$$

and using the relation

$$\exp\left(a\frac{d}{dx}\right)u(x) = u(x+a) \text{ etc.}$$

gives

$$\tfrac{1}{2}E_0\{u(x+a_x) + u(x-a_x) + \lambda[\exp(-i\epsilon Hxa_y)u(y+a_y) + \exp(i\epsilon Hxa_y)u(y-a_y)] + \nu[u(z+a_z) + u(z-a_z)]\} = Wu(\mathbf{r})$$

where $\epsilon = e/\hbar c$. The variables may be separated by the substitution

$$u(\mathbf{r}) = \exp(ik_y y)\exp(ik_z z)u(x)$$

giving

$$\tfrac{1}{2}[u(x+a_x) + u(x-a_x)] + \lambda\cos(\epsilon Ha_y x - k_y a_y)u(x) = E_0^{-1}(W - E_0\nu\cos k_z a_z)u(x).$$

This is equivalent to the difference equation

$$u_{n+1} + u_{n-1} + 2[\lambda\cos(\alpha n - k_y a_y) - E]u_n = 0 \qquad \ldots\ldots(2.2)$$

where $\alpha = \epsilon H a_x a_y$ and $E = E_0^{-1}(W - E_0\nu\cos k_z a_z)$ is the energy due to motion in the transverse plane measured in units of E_0.

One property of the eigenvalues of (2.2) may be established immediately. Substituting $u_n = (-1)^n w_n$ and changing the origin of n by π/α is equivalent to reversing the sign of E. Thus, the eigenvalues are symmetrical about $E = 0$. In the subsequent analysis E will be considered positive.

In order to obtain the eigenvalues of (2.2) it is convenient to seek solutions satisfying the boundary condition.

$$u_{n+N} = \rho u_n \qquad \ldots\ldots(2.3)$$

where $N = 2\pi/\alpha$ and ρ is a constant. Suppose two linearly independent solutions of (2.2), $y_n^{(1)}$ and $y_n^{(2)}$, are known. Then $y_{n+N}^{(1)}$ and $y_{n+N}^{(2)}$ are also solutions, since the coefficient of u_n is periodic. Hence the latter solutions may be written

$$\left.\begin{aligned} y_{n+N}^{(1)} &= \alpha_{11}y_n^{(1)} + \alpha_{12}y_n^{(2)} \\ y_{n+N}^{(2)} &= \alpha_{21}y_n^{(1)} + \alpha_{22}y_n^{(2)} \end{aligned}\right\} \qquad \ldots\ldots(2.4)$$

where the α's are constants. If u_n is expressed as a linear combination of $y_n^{(1)}$ and $y_n^{(2)}$ and the boundary condition (2.3) is imposed, it may be shown (Fort 1948, p. 189) that ρ must satisfy

$$\rho^2 - (\alpha_{11} + \alpha_{22})\rho + 1 = 0. \qquad \ldots\ldots(2.5)$$

Since for real solutions the α's are real and the product of the roots of (2.5) is unity, it follows that ρ is of the form

$$\rho = \exp(\pm ik_x a_x N) \qquad \ldots\ldots(2.6)$$

where k_x is either real or pure imaginary. If the solutions $y_n^{(1)}$ and $y_n^{(2)}$ are chosen such that

$$\left.\begin{aligned} y_0^{(1)} &= 0, \qquad y_0^{(2)} = 1 \\ y_1^{(1)} &= 1, \qquad y_1^{(2)} = 0 \end{aligned}\right\} \qquad \ldots\ldots(2.7)$$

we have, from (2.4),

$$\alpha_{11}=y_{N+1}^{(1)}-y_N^{(1)} : \alpha_{22}=y_N^{(2)}.$$

Hence, using (2.5) and (2.6)

$$\cos k_x a_x N=\tfrac{1}{2}[y_{N+1}^{(1)}-y_N^{(1)}+y_N^{(2)}]. \qquad \ldots\ldots(2.8)$$

The bounded solutions of (2.2) are those for which k_x is real. Thus the eigenvalues correspond to the bands of energy for which the right-hand member of (2.8) is less than or equal to unity in modulus. Hence the problem is resolved into finding the solutions $y_n^{(1)}$ and $y_n^{(2)}$.

§ 3. GENERAL SOLUTIONS OF THE EIGENEQUATION

The general solutions of (2.2) for the particular case $\lambda=1$ have previously been obtained by Harper (1955, § 2) by means of a WKB method. This method is applicable since for magnetic fields normally used $H\sim10^4$, $\alpha\sim10^{-4}$ and hence $\cos\alpha n$ is a slowly varying function of n. It is worth remarking that whilst the spirit of the WKB method is semi-classical and must lead to the Onsager result for closed orbits, it has the advantage that one may also use the WKB solutions to estimate the level broadening (see § 4).

The adaptation of Harper's solution for a general value of λ is straightforward and only their final form is given. In this section and § 4 we consider the case $k_{//}=0$. When $|E-\lambda\cos\alpha n|<1$ the WKB solutions are

$$u_n=(\sin k_n)^{-1/2}\exp \pm i\left(\sum_l^n k_l-\tfrac{1}{2}k_n\right) \qquad \ldots\ldots(3.1)$$

where

$$\cos k_n=E-\lambda\cos\alpha n. \qquad \ldots\ldots(3.2)$$

When $E-\lambda\cos\alpha n>1$

$$u_n=(\sinh K_n)^{-1/2}\exp \pm \left(\sum_l^n K_l-\tfrac{1}{2}K_n\right) \qquad \ldots\ldots(3.3)$$

where

$$\cosh K_n=E-\lambda\cos\alpha n. \qquad \ldots\ldots(3.4)$$

These solutions are valid for values of n such that

$$\left|\frac{k_n-k_{n-1}}{k_n}\right|\ll1. \qquad \ldots\ldots(3.5)$$

This criterion is not satisfied near the classical turning points, which are the roots of

$$|E-\lambda\cos\alpha n|=1.$$

The required continuation of the WKB solutions across a turning point may be found by expanding $E-\lambda\cos\alpha n$ about such a point. If $E-\lambda\cos\alpha n_0=1$ then the approximate equation for u_n near n_0 is

$$u_{n+1}+u_{n-1}=2(m+n-n_0)u_n/m \qquad \ldots\ldots(3.6)$$

where $m=(\alpha\lambda\sin\alpha n_0)^{-1}\gg1$. Equation (3.6) is a recurrence relation of the Bessel functions

$$\mathrm{J}_{m+n-n_0}(m) \qquad \text{and} \qquad \mathrm{Y}_{m+n-n_0}(m).$$

The asymptotic expansions of these functions for large order and large argument (Watson 1944, p. 244) may be used to find the correct combination of the WKB solutions on either side of the turning point. Labelling successive turning points n_0 and n_1, where $\alpha n_0 < \pi$ and $n_1 = -n_0 + 2\pi/\alpha$ the connections are found to be

(*a*) across n_0

$$\left.\begin{aligned}(\sin k_n)^{-1/2}\cos(k_{n_0,n}-\pi/4) &\to \tfrac{1}{2}(\sinh K_n)^{-1/2}\exp K_{n,n_0}\\ (\sin k_n)^{-1/2}\sin(k_{n_0,n}-\pi/4) &\to -\tfrac{1}{2}(\sinh K_n)^{-1/2}\exp -K_{n,n_0}\end{aligned}\right\} \quad \ldots\ldots(3.7)$$

where

$$\left.\begin{aligned}k_{n_0,n} &= \left(\sum_l^{n_0} k_l - \tfrac{1}{2}k_{n_0}\right) - \left(\sum_l^{n} k_l - \tfrac{1}{2}k_n\right)\\ &= \sum_{l=n}^{n_0} k_l - (\tfrac{1}{2}k_{n_0} + \tfrac{1}{2}k_n)\end{aligned}\right.$$

and similarly

$$\left.K_{n,n_0} = \sum_{l=n_0}^{n} K_l - \tfrac{1}{2}(K_n + K_{n_0}).\right\} \quad \ldots\ldots(3.8)$$

(*b*) Across n_1

$$\left.\begin{aligned}\tfrac{1}{2}(\sinh K_n)^{-1/2}\exp K_{n_1,n} &\to (\sin k_n)^{-1/2}\cos(k_{n,n_1}-\pi/4)\\ \tfrac{1}{2}(\sinh K_n)^{-1/2}\exp -K_{n_1,n} &\to -(\sin k_n)^{-1/2}\sin(k_{n,n_1}-\pi/4).\end{aligned}\right\} \quad \ldots\ldots(3.9)$$

These connection formulae in conjunction with the method given in § 2 will be used to deduce the eigenvalues.

§ 4. EIGENVALUES

In this section we obtain eigenvalue equations for the energy ranges corresponding to open and to closed orbits.

The energy band (1.3), as drawn in figure 1, is for a value $\lambda < 1$. This restriction on λ will be retained in the following analysis, although, as we shall point out later (§ 6), the results are independent of this choice. Thus, for $\lambda < 1$, it is seen that $|E - \lambda\cos\alpha n| < 1$ for all n if $E < 1 - \lambda$. For these energies, which are denoted by the open orbits in the absence of a magnetic field, there are no classical turning points. The WKB approximation may then be used over the whole cycle of the cosine since the validity criterion (3.5) is always satisfied. To find the magnetic eigenvalues for this case we require the combination of solutions (3.1) which obey the boundary conditions (2.7). These are

$$\left.\begin{aligned}y_n^{(1)} &= \left(\frac{\sin k_1}{\sin k_n}\right)^{1/2}\frac{\sin k_{n,0}}{\sin k_{1,0}}\\ y_n^{(2)} &= y_n^{(1)} - \left(\frac{\sin k_0}{\sin k_n}\right)^{1/2}\frac{\sin k_{n,1}}{\sin k_{1,0}}.\dagger\end{aligned}\right\} \quad \ldots\ldots(4.1)$$

Hence, using (2.8), the eigenvalues are given by

$$\cos k_x a_x N = \frac{1}{2}\left[\left(\frac{\sin k_1}{\sin k_{N+1}}\right)^{1/2}\frac{\sin k_{N+1,0}}{\sin k_{1,0}} - \left(\frac{\sin k_0}{\sin k_N}\right)\frac{\sin k_{N,1}}{\sin k_{1,0}}\right].$$

Since k_n is periodic with period N

$$\cos k_x a_x N = \cos\tfrac{1}{2}(k_{N+1,0} + k_{N,1})\sin\tfrac{1}{2}(k_{N+1,0} - k_{N,1})(\sin k_{1,0})^{-1}$$

which, by virtue of the periodicity of k_n reduces to

$$\cos k_x a_x N = \cos k_{N,0}. \quad \ldots\ldots(4.2)$$

Thus, for $E < 1 - \lambda$, k_x is always real. Hence the level spectrum is continuous. Equation (4.2) will be further discussed in § 6.

---

† Note that by (3.8)

$$k_{0,1} = \left(\sum_l^{0} k_l - \tfrac{1}{2}k_0\right) - \left(\sum_l^{1} k_l - \tfrac{1}{2}k_1\right) = -k_{1,0}.$$

We now consider $1-\lambda<E<1+\lambda$. Then there are always two turning points in one cycle of the cosine. The eigenvalues will again be found from (2.8). We require the form of the solutions $y_n^{(1)}$ and $y_n^{(2)}$ after one period. These may be obtained as follows:

(i) For $0<n<n_0$

$$y_n^{(1)}=\left(\frac{\sin k_1}{\sin k_n}\right)^{1/2}\frac{\sin k_{n,0}}{\sin k_{1,0}}$$
$$=\left(\frac{\sin k_1}{\sin k_n}\right)^{1/2}\frac{1}{\sin k_{1,0}}[\sin(k_{n_0,0}-\tfrac{1}{4}\pi)\cos(k_{n_0,n}-\tfrac{1}{4}\pi)$$
$$-\cos(k_{n_0,0}-\tfrac{1}{4}\pi)\sin(k_{n_0,n}-\tfrac{1}{4}\pi)].$$

(ii) Using the connection formulae (3.7) it follows that for $n_0<n<n_1$

$$y_n^{(1)}=\frac{1}{2}\left(\frac{\sin k_1}{\sinh K_n}\right)^{1/2}\frac{1}{\sin k_{1,0}}[\sin(k_{n_0,0}-\tfrac{1}{4}\pi)\exp(K_{n,n_0})$$
$$+\cos(k_{n_0,0}-\tfrac{1}{4}\pi)\exp(-K_{n,n_0})]$$
$$=\frac{1}{2}\left(\frac{\sin k_1}{\sinh K_n}\right)^{1/2}\frac{1}{\sin k_{1,0}}[\exp(K_{n_1,n_0})\sin(k_{n_0,0}-\tfrac{1}{4}\pi)\exp(-K_{n_1,n})$$
$$+\exp(-K_{n_1,n_0})\cos(k_{n_0,0}-\tfrac{1}{4}\pi)\exp(K_{n_1,n})].$$

(iii) Thus applying (3.8), one finds for $n_1<n$

$$y_n^{(1)}=\left(\frac{\sin k_1}{\sin k_n}\right)^{1/2}\frac{1}{\sin k_{1,0}}[\exp(-K_{n_1,n_0})\cos(k_{n_0,0}-\tfrac{1}{4}\pi)\cos(k_{n,n_1}-\tfrac{1}{4}\pi)$$
$$-\exp(K_{n_1,n_0})\sin(k_{n_0,0}-\tfrac{1}{4}\pi)\sin(k_{n,n_1}-\tfrac{1}{4}\pi)]. \qquad \ldots\ldots(4.3)$$

(iv) A similar procedure gives, for $n_1<n$

$$y_n^{(2)}=y_n^{(1)}-\left(\frac{\sin k_1}{\sin k_n}\right)^{1/2}\frac{1}{\sin k_{1,0}}[\exp(-K_{n_1,n_0})\cos(k_{n_0,1}-\tfrac{1}{4}\pi)\cos(k_{n,n_1}-\tfrac{1}{4}\pi)$$
$$-\exp(K_{n_1,n_0})\sin(k_{n_0,1}-\tfrac{1}{4}\pi)\sin(k_{n,n_1}-\tfrac{1}{4}\pi)]. \qquad \ldots\ldots(4.4)$$

Hence, by (2.8), the eigenvalues are given by

$$\cos k_x a_x N=\tfrac{1}{2}(\sin k_{1,0})^{-1}[\exp(-K_{n_1,n_0})\{\cos(k_{n_0,0}-\tfrac{1}{4}\pi)\cos(k_{N+1,n_1}-\tfrac{1}{4}\pi)$$
$$-\cos(k_{n_0,1}-\tfrac{1}{4}\pi)\cos(k_{N,n_1}-\tfrac{1}{4}\pi)\}+\exp(K_{n_1,n_0})\{\sin(k_{n_0,1}-\tfrac{1}{4}\pi)$$
$$\times\sin(k_{N,n_1}-\tfrac{1}{4}\pi)-\sin(k_{n_0,0}-\tfrac{1}{4}\pi)\sin(k_{N+1,n_1}-\tfrac{1}{4}\pi)\}].$$

By repeated use of the periodicity of k_n, this may be reduced to

$$\cos k_x a_x N=\cosh K_{n_1,n_0}\cos(k_{N,n_1}+k_{n_0,0})$$
$$=\cosh K_{n_1,n_0}\cos k_{n_0,-n_0}. \qquad \ldots\ldots(4.5)$$

This equation giving the magnetic energy levels for the energies $1-\lambda<E<1+\lambda$ will be discussed in § 6.

Finally, for $E>1+\lambda$, there are again no turning points. In this case only the unbounded WKB solutions occur and consequently there are no eigenvalues.

The energy is thus confined within the same limits as in the absence of the magnetic field.

§ 5. k_y BROADENING

The dependence of the eigenvalues upon k_y cannot be found directly from the WKB solutions, the reason being that the WKB method is insensitive to the addition of a small phase to the cosine in equation (2.2). The only effect of such a phase is to produce a small change in the position of the turning points, and it is just near these points that the errors in the WKB method are greatest.

In this section it is shown that non-zero k_y produces a broadening of the levels.

Solutions of the eigenequation exist which satisfy the condition

$$u_{n+N} = \exp(ik_x a_x N)u_n.$$

Hence a particular form for u_n is

$$u_n = \exp(ik_x a_x n)v_n \qquad \ldots\ldots(5.1)$$

where v_n is periodic in n with period N. The equation for v_n is

$$\exp(ik_x a_x)v_{n+1} + \exp(-ik_x a_x)v_{n-1} + 2[\lambda \cos(\alpha n - k_y a_y) - E]v_n = 0. \qquad \ldots\ldots(5.2)$$

Since v_n is periodic, it may be expressed as the Fourier series

$$v_n = \sum_m w_m \exp(imn\alpha) \qquad \ldots\ldots(5.3)$$

where m is an integer. Substituting (5.3) into (5.2), multiplying by a particular phase $\exp(imn\alpha)$ and summing over n, one finds the equation satisfied by w_m

$$\exp(ik_y a_y)w_{m+1} + \exp(-ik_y a_y)w_{m-1} + 2\lambda^{-1}[\cos(\alpha n + k_x a_x) - E]w_m = 0. \qquad \ldots.(5.4)$$

Now, from (5.3),

$$w_m = \left(\sum_n\right)^{-1} \sum_n v_n \exp(-imn\alpha).$$

Thus w_m is periodic in m with period N. We may again seek solutions of the type

$$w_m = \exp(-ik_y a_y m)G_m$$

where

$$G_{m+N} = \exp(ik_y a_y N)G_m.$$

The equation for G_m, namely

$$G_{m+1} + G_{m-1} + 2\lambda^{-1}[\cos(\alpha m + k_x a_x) - E]G_m = 0 \qquad \ldots\ldots(5.5)$$

is of the same type as that for u_n. To find the dependence of the eigenvalues upon k_y we may again use the method of § 2.

The general solutions of (5.5) may be found as before using the WKB method given by Harper.

Considering the case $k_x = 0$, one finds

(1) $$G_m = (\sin q_m)^{-1/2} \exp \pm i\left(\sum_l^m q_l - \tfrac{1}{2}q_m\right) \qquad \ldots\ldots(5.6)$$

where

$$\cos q_m = \lambda^{-1}(E - \cos\alpha m) \qquad \ldots\ldots(5.7)$$

when

$$|E - \cos\alpha m| < \lambda;$$

(2) $$G_m = (\sinh Q_m)^{-1/2} \exp \pm \left(\sum_l^m Q_l - \tfrac{1}{2}Q_m\right) \qquad \ldots\ldots(5.8)$$

where

$$\cosh Q_m = \lambda^{-1}(E - \cos\alpha m) \qquad \ldots\ldots(5.9)$$

when

$$E - \cos\alpha m > \lambda.$$

These solutions are sufficient for the calculation of the k_y broadening when $1 - \lambda < E < 1 + \lambda$. The connection formulae across the turning points, the latter being the roots of

$$E - \cos\alpha m = \lambda, \qquad \ldots\ldots(5.10)$$

may be found by the method given in § 3. If we define

$$q_{m,m'} = \sum_{l=m'}^{m} q_l - \tfrac{1}{2}(q_m + q_{m'}) \qquad \ldots\ldots(5.11)$$

$$Q_{m,m'} = \sum_{l=m'}^{m} Q_l - \tfrac{1}{2}(Q_m + Q_{m'}) \qquad \ldots\ldots(5.12)$$

and denote successive turning points by m_0, m_1 $(\alpha m_0 < \pi)$ the connection formulae are then given by (3.7) and (3.9) after the substitutions $k_m \to q_m$, $k_{n,n'} \to q_{m,m'}$, $K_{n,n'} \to Q_{m,m'}$, $n_0 \to m_0$, $n_1 \to m_1$.

The determination of the eigenvalues is now formally equivalent to the calculation of the k_x-broadening (§ 4) for $E > 1-\lambda$. Replacing k_x by k_y in equation (4.5), the implicit relation between k_y and the energy is evidently

$$\cos k_y a_y N = \cosh Q_{m_1, m_0} \cos q_{-m_0, m_0}. \qquad \ldots\ldots(5.13)$$

In the energy interval $E < 1-\lambda$ the problem is slightly more complicated since (5.10) is then satisfied by four values of m in one period. We now consider this case. Successive turning points will be labelled m_0, m_1, m_2, m_3 where m_0 is the smallest positive root of (5.10) and $m_3 = m_0 + N$. Then for $|m| < m_0$, $(E - \cos \alpha m) < -\lambda$. The WKB solutions are found to be

$$G_m = (-1)^m (\sinh Q_m')^{-1/2} \exp \pm \left(\sum_l^m Q_l' - \tfrac{1}{2} Q_m' \right) \qquad \ldots\ldots(5.14)$$

where

$$Q_m' = \lambda^{-1}(\cos \alpha m - E). \qquad \ldots\ldots(5.15)$$

The continuation of (5.14) across m_0, m_3 may again be obtained from the asymptotic expansions of the Bessel function solutions. One finds

(a) across m_0

$$\tfrac{1}{2}(-1)^m (\sinh Q_m')^{-1/2} \exp Q_{m_0, m_0}' \to (-1)^{m_0+1} (\sin q_m)^{-1/2} \sin (q_{m,m_0} - \tfrac{1}{4}\pi)$$

$$\tfrac{1}{2}(-1)^m (\sinh Q_m')^{-1/2} \exp - Q_{m_0, m}' \to (-1)^{m_0} (\sin q_m)^{-1/2} \cos (q_{m,m_0} - \tfrac{1}{4}\pi),$$

(b) across m_3

$$(-1)^{m_3} (\sin q_m)^{-1/2} \sin (q_{m_3, m} - \tfrac{1}{4}\pi) \to \tfrac{1}{2}(-1)^{m+1} (\sinh Q_m') \exp Q_{m, m_3}'$$

$$(-1)^{m_3} (\sin q_m)^{-1/2} \cos (q_{m_3, m} - \tfrac{1}{4}\pi) \to \tfrac{1}{2}(-1)^{m} (\sinh Q_m') \exp - Q_{m, m_3}'.$$

With the aid of these connection formulae, and those obtained from (3.7) and (3.9), the k_y broadening for $E < 1-\lambda$ may be found by the same procedure as in § 4. The result is

$$\cos k_y a_y N = \cos 2q_{m_1, m_0} \cosh Q_{-m_0, m_0}' \cosh Q_{m_2, m_1} - \sinh Q_{-m_0, m_0}' \sinh Q_{m_2, m_1}. \qquad \ldots\ldots(5.16)$$

The equations (5.13) and (5.16) will be discussed in the following section.

§ 6. LEVEL SPACING AND LEVEL BROADENING

The first part of this section is devoted to an examination of the level distribution and broadening for $E > 1-\lambda$, i.e. the region of closed orbits.

When $k_y = 0$, the eigenvalues are given by

$$\cos k_x a_x N = \cosh K_{n_1, n_0} \cos k_{-n_0, n_0}. \qquad \ldots\ldots(4.5)$$

We first consider the magnitude of K_{n_1, n_0}. From (3.4) and (3.8)

$$K_{n_1, n_0} = \sum_{l=n_0}^{n_1} K_l - \tfrac{1}{2}(K_{n_1} + K_{n_0}) \simeq \int_{n_0}^{n_1} \cosh^{-1}(E - \lambda \cos \alpha n) dn.$$

For $E=1-\lambda+\epsilon$ $(\epsilon\ll 1)$, $K_{n_1,n_0}\simeq\pi\epsilon/\alpha\sqrt{\lambda}$. Thus K_{n_1,n_0} is large if $\epsilon\gg\alpha$ and since $\alpha\sim 10^{-4}$ this is a very mild condition on ϵ. Also as K_{n_1,n_0} is an increasing function of E we conclude that $K_{n_1,n_0}\gg 1$ provided $E\neq 1-\lambda$. Hence the solution of (4.5) is

$$k_{-n_0,n_0}=(j+\tfrac{1}{2})\pi+2(-1)^{j+1}\exp(-K_{n_1,n_0})\cos k_x a_x N \quad j=(0,1,2\ldots) \quad \ldots(6.1)$$

or, for $E-(1-\lambda)\gg\alpha$

$$k_{n_0,n_0}\simeq\int_{-n_0}^{n_0}\cos^{-1}(E-\lambda\cos\alpha n)\alpha n=(j+\tfrac{1}{2})\pi \qquad \ldots\ldots(6.2)$$

that is, the eigenvalues are independent of k_x, the broadening being negligible. Similarly, from (5.12) and (5.9) it is found that $Q_{m_1,m_0}\sim\alpha^{-1}$ and hence the solution of (5.13) to a very good approximation is

$$\int_{-m_0}^{m_0}\cos^{-1}[(E-\cos\alpha m)\lambda^{-1}]\,dm=(j+\tfrac{1}{2})\pi. \qquad \ldots\ldots(6.3)$$

Equations (6.2) and (6.3) are two alternative forms of Onsager's result (1.2) for the particular energy band being investigated, being of the form

$$(c\hbar^2/eH)\int K_x\,dK_y=(j+\tfrac{1}{2})h$$

$$(c\hbar^2/eH)\int K_y\,dK_x=(j+\tfrac{1}{2})h$$

respectively. This completes the derivation of Onsager's result for the case considered. From the method we have used it is clear that our investigation is sufficient to ensure the generality of Onsager's result for any closed orbit which is not a re-entrant curve. In the classical approximation, and with our choice of $\mathbf{K}$ (2.1) and $\mathbf{A}$ the problem immediately reduces to finding K_x for a given K_y. If the curve is not re-entrant there will be at most two real values of K_x, the phase integral (6.2) being over the interval in which, for a given energy, these exist.

It is of interest to examine further the energy spectrum of this model. Near the top of the band $E=1+\lambda-\epsilon$, we obtain from (6.2) $\pi\epsilon\lambda^{-1/2}=(j+\tfrac{1}{2})\pi$ or if effective masses are defined by

$$\frac{\hbar^2}{m_x{}^*}=E_0 a_x{}^2\ :\ \frac{\hbar^2}{m_y{}^*}=E_0\lambda a_y{}^2$$

the total energy W is

$$W=E_0(1+\lambda)-\frac{e\hbar H}{(m_x{}^*m_y{}^*)^{1/2}c}(j+\tfrac{1}{2})+E_0\nu\cos k_x a_x. \qquad \ldots\ldots(6.4)$$

The relation (6.4) is analogous to a previous result of Blackman (1938) for anisotropic effective electron masses.

The variation of the level spacing with energy may be obtained from (6.2). Thus

$$k_{-n_0,n_0}(E_j+\Delta E_j)-k_{-n_0,n_0}(E_j)=\pi$$

where

$$\Delta E_j=E_{j+1}-E_j.$$

Hence

$$\Delta E_j=\pi\left[\left(\frac{dk_{-n_0,n_0}}{dE}\right)_{E=E_j}\right]^{-1}. \qquad \ldots\ldots(6.5)$$

Now

$$\frac{dk_{-n_0,n_0}}{dE}=-2\int_0^{n_0}\frac{dn}{\{1-(E-\lambda\cos\alpha n)^2\}^{1/2}}. \qquad \ldots\ldots(6.6)$$

The integral in (6.6) is elliptic and may be put in the standard form

$$\frac{dk_{-n_0,\,n_0}}{dE} = -\frac{2}{\alpha\sqrt{\lambda}}\int_0^{\pi/2}\frac{d\theta}{\left\{1-\left[\dfrac{(1+\lambda)^2-E^2}{4\lambda}\right]\sin^2\theta\right\}^{1/2}} \quad \ldots\ldots(6.7)$$

by means of the substitution

$$\tan\left(\frac{\alpha n}{2}\right) = \left[\frac{1+\lambda-E}{E-1+\lambda}\right]^{1/2}\cos\theta.$$

Using the tabulated values of the integral in (6.7) (Jahnke and Emde 1945, p. 65) its variation with E may be found using equation (6.4). The results are presented in graphical form in figure 2 for different values of λ. In each case it is seen that, going from the top of the band towards its centre ($E=0$) the decrease in the spacing is small over nearly all the interval $1-\lambda<E<1+\lambda$ but becomes very large near the lower limit where the spacing falls to zero. This limit corresponds to the boundary of the region of continuous eigenvalues. We have already shown that near $E=1-\lambda$ the k_x broadening is largest (cf. equation (6.1)) and when combined with the sharp decrease in the spacing this may result in overlapping levels. However, since the magnitude of the broadening decreases like $\exp\{[E-(1-\lambda)]/\alpha\}$ with increasing E, the region in which this overlap may occur constitutes only a small proportion of the total width of the band in energy.

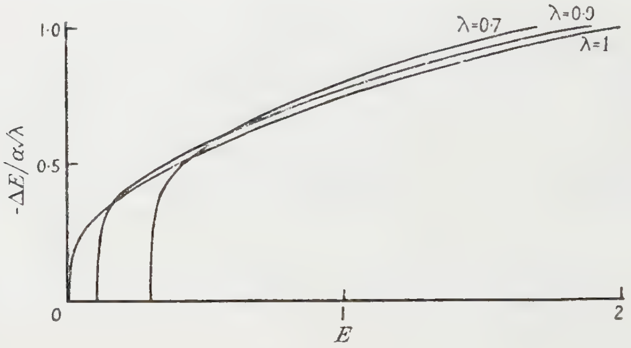

Figure 2. Variation of the level spacing with energy for closed orbits.

The plot in figure 2 for $\lambda=1$ is of interest as this gives the level spectrum for the energy band of the simple cubic lattice. In this instance the sharp decrease in the spacing occurs in an interval approximately equal to 1% of the total bandwidth. It is only in this small region at the band-centre where the levels may overlap; in the remainder of the band the energy levels are discrete and the broadening is negligible compared with the level spacing.†

We now find the eigenvalues of λ other than unity in the energy range $E<1-\lambda$. When $k_x=0$, these are given by equation (5.16). Since $Q_{m_0,\,-m_0}'$ and $Q_{m_2,\,m_1}$ are of the order α^{-1} the approximate solution of (5.16) is

$$q_{m_1,\,m_0}=j\pi \quad (j=0,\,1,\,2\ldots)$$

---

† This description of the eigenspectrum of the simple cubic lattice differs from that given by Harper (1955, § 3). According to figure 1 of this reference the spacing increases towards the centre of the band near $E=0$. This is not correct, the slope of this figure near $E=0$ should tend to infinity. The broadening of the levels as given by Harper is also incorrect since the wave functions, $\exp(ik_xa_xn)v_x$ which are used do not possess the property that v_n be periodic.

that is, the energy is independent of k_y. Hence the equation

$$\cos k_x a_x N = \cos k_{N,0} \qquad \ldots\ldots(4.2)$$

which was obtained for $k_y = 0$, is true for all k_y. Thus the eigenvalues are given by

$$k_{N,0}(E) = 2\pi j + k_x a_x N \qquad \ldots\ldots(6.8)$$

where

$$k_{N,0}(E) \simeq \int_0^N \cos^{-1}(E - \lambda \cos \alpha n)\alpha n.$$

In order to solve (6.8) for E we find the variation in $k_{N,0}(E)$ with E

$$\frac{dk_{N,0}(E)}{dE} = -\frac{2}{\alpha}\int_0^\pi \frac{dx}{\{1-(E+\lambda\cos x)^2\}^{1/2}}$$

which is again an elliptic integral. This may be reduced to the standard form

$$\frac{dk_{N,0}(E)}{dE} = \frac{-4}{\alpha\{(1+\lambda)^2 - E^2\}^{1/2}}\int_0^{\pi/2} \frac{d\theta}{\{1-[4\lambda/\{(1+\lambda)^2-E^2\}]\sin^2\theta\}^{1/2}} \qquad \ldots\ldots(6.9)$$

by the substitution

$$\tan\frac{x}{2} = \left[\frac{1+E+\lambda}{1+E-\lambda}\right]^{1/2}\cot\theta.$$

Using the tabulated values of the integral in (6.9) the variation in $dk_{N,0}(E)/dE$ was found taking $\lambda = 0{\cdot}5$ (figure 3). Thus it is reasonably constant over about 20% of the central region. Approximate eigenvalues are therefore

$$a - bE = 2\pi j + k_x a_x N$$

where a and b are constants depending upon H. Since the energy is linear in k_x, the density of states is a smoothly varying function of the energy.

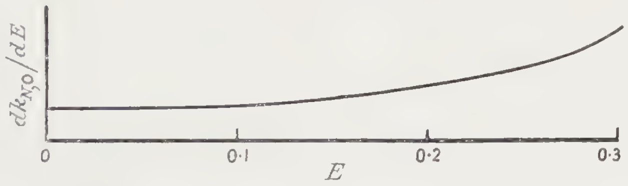

Figure 3. Variation of $dk_{N,0}/dE$ with energy for open orbits.

The eigenvalue equation (6.8) may also be derived directly from the WKB solutions (3.1). Since there are no turning points the progressive wave solutions are valid for all n. The boundary condition (2.3) applied to either of these solutions gives equation (6.8). It will be noted that $k_{N,0}$ is the area enclosed by the constant-energy curve and the zone boundaries. However, for open orbits this area is not quantized since we may regard k_x as continuous.

The results given in this section were obtained for the specific case of $\lambda < 1$. However, the eigenspectrum must be independent of this assumption since a rotation of the energy curves through 90° about the z-axis is merely equivalent to changing the gauge for **A**. Mathematically, this is more easily established by retaining the same gauge but replacing (1.3) by

$$E(\mathbf{k}) = E_0(\lambda\cos k_x a_x + \cos k_y a_y + \nu \cos k_z a_z)$$

and still assuming $\lambda<1$. This has the advantage of being equivalent to taking $\lambda>1$ in the previous analysis whilst still retaining the same maximum energy. The effect of choosing this new energy band is simply to interchange the equations for u_{n} (2.2) and G_{m} (5.5). Thus there is again a continuous distribution of levels near the centre of the band, this now being a result of the k_{y} broadening.

§ 7. SUMMARY AND DISCUSSION

The magnetic energy levels have been found by applying Peierls' theorem to a simple model of an energy band containing both open and closed energy curves in a plane normal to the magnetic field direction. Onsager's result has been derived for the energies corresponding to closed orbits and corrections due to level broadening have been shown to be generally negligible in this region. The occurrence of open orbits has been related to the existence of a continuous spectrum of levels in the presence of a magnetic field.

An investigation of Onsager's result for the particular model we have used has shown that going from the top band the rate of decrease is small initially but becomes large in the immediate vicinity of $E=1-\lambda$. This may be understood by noting that whilst the magnetic field causes groups of states in phase space to coalesce forming degenerate discrete levels, the average density of states in energy is the same as in the absence of the field. Since the degeneracy of each magnetic level is the same, the spacing is therefore inversely proportional to the density of states at a particular value of the energy due to the motion in the transverse plane for the unperturbed system. Now the density of states increases rapidly in the energy region where the relevant contour just touches the zone boundary. For our model (1.3) this is the energy $E=1-\lambda$.† In addition, the density of states for the energy due to transverse motion is proportional to the derivative of the area enclosed by the orbit. Thus this physical argument is equivalent to finding the level spacing by Onsager's method. On the basis of these remarks, the results of this paper do not give any reason for the absence of the oscillatory behaviour of the magnetic susceptibility (de Haas–van Alphen effect) in the monovalent metals. Let us consider the alkali metals, which are body-centred cubic in structure. The density of states curve for the energy band of this structure, in the tight-binding approximation, shows a rapid increase near the centre of the band (Mott and Jones 1936, p. 85) and consequently for a half-filled band the Fermi energy would coincide with this region. However, for the alkalis the free electron approximation is more appropriate and this has the tendency of shifting the discontinuity in the density of states curve towards higher energies. In this case the Fermi energy for a monovalent metal would lie below this discontinuity and the magnetic energy levels would thus be discrete and the lattice broadening negligible compared with the spacing. Hence, although the collision broadening may be important in damping the de Haas–van Alphen effect (Dingle 1952), the broadening due to the equilibrium lattice forces cannot be expected to inhibit the effect in the alkali metals. Because of this negative conclusion it should be remembered that these remarks are based ultimately upon the neglect of inter-band coupling. Adams (1953) has pointed out that this is of importance when the energy gap is small since then transitions, between bands are associated with small energy change. Whether this is more generally the case is not known at present.

† The author is indebted to Professor H. Jones for suggesting this argument.

ACKNOWLEDGMENTS

The author is deeply indebted to Professor R. E. Peierls for his helpful advice and encouragement during the course of this work. He also wishes to thank the Department of Scientific and Industrial Research for the award of a maintenance grant.

REFERENCES

ADAMS, E. N., 1953, *Phys, Rev.*, **89,** 63.
BLACKMAN, M., 1938, *Proc. Roy. Soc.* A, **166,** 1.
DINGLE, R. B., 1952, *Proc. Roy. Soc.* A, **211,** 517.
FORT, T., 1948, *Finite Differences* (Oxford : University Press.).
HARPER, P. G., 1955, *Proc. Phys. Soc.* A, **68,** 874.
JAHNKE, E., and EMDE, F., 1945, *Tables of Functions* (New York : Dover).
LIFSHITZ, I. M., AZBEL, M., and KAGANOV, M. I., 1956, *J. Exp. Theor. Phys. U.S.S.R.*, **30,** 220 (more detailed paper in course of publication).
LIFSHITZ, I. M., and KOSEVITCH, A. M., 1954, *Doklady Akad. Nauk. S.S.S.R.*, **96,** 963.
MOTT, N. F., and JONES, H., 1936, *Properties of Metals and Alloys* (Oxford : University Press).
ONSAGER, L., 1952, *Phil. Mag.*, **43,** 1006.
PEIERLS, R. E., 1933, *Z. Phys.*, **80,** 763.
WATSON, G. N., 1944, *A Treatise on the Theory of Bessel Functions*, 2nd Edn (Cambridge: University Press).

The Conversion of Metastable Helium from the Singlet to the Triplet State by Electron Collision

By R. MARRIOTT
Physics Department, University College London

Communicated by H. S. W. Massey; MS. received 13*th December* 1956

Abstract. The zero-order partial cross section has been calculated for the conversion of He* (2^1S) metastable atoms to He* (2^3S) by superelastic collision with thermal electrons. A numerical method has been used, which retains all the direct-coupling terms between the initial and final atomic states. Full allowance has been made for electron exchange. A cross section of 5×10^{-15} cm^2 was obtained at a temperature of 300°K, which is rather too small to account for the experimental value of 3×10^{-14} cm^2 observed by Phelps.

§ 1. Introduction

In this paper the superelastic collision

$$\mathrm{He}^*(2^1S) + e^- \rightarrow \mathrm{He}^*(2^3S) + e^- + 0{\cdot}78\ \mathrm{ev}$$

is considered from a theoretical point of view.

Recent experimental observations by Phelps (1955) on the rate at which He* (2^1S) is converted to He* (2^3S) in the afterglow of a helium discharge have given a cross section for the process of 3×10^{-14} cm^2 for thermal electrons (300°K).

It has been shown (Mott and Massey 1949) that at such a low collision energy, where the range of the scattering atomic field is small compared with the wavelength of the incident electron, only scattering of the S partial waves of zero angular momentum would be expected to be significant and that conservation theorems then set an upper limit to the cross section of 4×10^{-14} cm^2. It, therefore, appears that the experimental value is very large and it is of interest to attempt to calculate the cross section for the process.

Following the method used by Massey and Moiseiwitsch (1954) for the determination of the cross section for the excitation of metastable helium by electron impact, the cross section was first calculated by the distorted-wave approximation. Although lengthy, this work was greatly simplified by the fact that the required distorted wave functions had already been published by Massey and Moiseiwitsch. However, the cross section obtained violated the conservation limit for incident electron energies below 2·7 ev and it followed that the approximation would not be satisfactory at thermal energies. The approximation depends upon the assumption that the coupling between the final and the initial states of the system is small and may be neglected. Its failure shows that this is not the case.

In order to obtain the cross section for collision with thermal electrons, a numerical method has been constructed which retains all the direct coupling terms between the initial and final atomic states.

§ 2. Scattering Theory

Using atomic units throughout, the wave equation for the system of helium atom plus colliding electron takes the form

$$L\Psi(123) = 0 \qquad \ldots\ldots(1)$$

where $$L=\nabla_1^2+\nabla_2^2+\nabla_3^2+2E-\frac{2}{r_{12}}-\frac{2}{r_{13}}-\frac{2}{r_{23}}+\frac{4}{r_1}+\frac{4}{r_2}+\frac{4}{r_3}.$$
The three electrons are distinguished by the numbers 1, 2 and 3, their mutual separations by r_{12}, r_{13}, r_{23} and E is the total energy of the system.

We expand $\Psi(123)$ in terms of products of free electron functions $\mathscr{F}_n(3)$, the complete set of orthonormal unperturbed helium wave functions $\psi_n(12)$, which are solutions of the equation

$$\left[\nabla_1^2+\nabla_2^2+2E_n-\frac{2}{r_{12}}+\frac{4}{r_1}+\frac{4}{r_2}\right]\psi_n(12)=0$$

and appropriate spin functions $\chi_n(12:3)$. $\Psi(123)$ is required to be antisymmetric in electron exchange and the expansion may be written

$$\Psi(123)=\sum_n[\psi_n(12)\mathscr{F}_n(3)\chi_n(12:3)+\psi_n(23)\mathscr{F}_n(1)\chi_n(23:1)$$
$$+\psi_n(31)\mathscr{F}_n(2)\chi_n(31:2)]. \qquad \ldots\ldots(2)$$

In this case, since the atom is initially in a singlet state and it is assumed that spin–orbit interactions may be neglected, the spin functions $\chi_n(12:3)$ are initially and, therefore, also finally appropriate to doublet spin states.

If then (2) is restricted to include only the initial ($n=1$) and final ($n=3$) atomic states, a procedure exactly similar to that used by Massey and Moiseiwitsch (1954) yields two coupled integro-differential equations

$$[\nabla_3^2+k_1^2+V_{11}]\mathscr{F}_1(3)-\int\psi_1(12)^*L\psi_1(23)\mathscr{F}_1(1)\,d\tau(12)=$$
$$-(3)^{1/2}\int\psi_1(12)^*L\psi_3(23)\mathscr{F}_3(1)\,d\tau(12)\ldots. \qquad \ldots\ldots(3)$$
$$[\nabla_3^2+k_3^2+V_{33}]\mathscr{F}_3(3)-\int\psi_3(12)^*L\psi_3(23)\mathscr{F}_3(1)\,d\tau(12)=$$
$$(3)^{1/2}\int\psi_3(12)^*L\psi_1(23)\mathscr{F}_1(1)\,d\tau(12)\ldots \qquad \ldots\ldots(4)$$

where $$V_{nn}=2\int\psi_n(12)^*\left(\frac{2}{r_3}-\frac{1}{r_{13}}-\frac{1}{r_{23}}\right)\psi_n(12)\,d\tau(12),$$

and $$E_1+\tfrac{1}{2}k_1^2=E_3+\tfrac{1}{2}k_3^2=E.$$

In the case of slow collisions, where only S-wave scattering is expected to be significant, the free-electron functions are to a good approximation purely radial functions and are required to have the asymptotic forms

$$\left.\begin{aligned}&\mathscr{F}_1(3)\sim(k_1r_3)^{-1}\sin k_1r_3+\alpha_{11}r_3^{-1}\exp(ik_1r_3),\\&\mathscr{F}_3(3)\sim\beta_{13}r_3^{-1}\exp(ik_3r_3),\end{aligned}\right\} \qquad \ldots\ldots(5)$$

and to be bounded at the origin.

The cross section for the superelastic collision is then given by

$$\sigma_{1\to3}=4\pi(k_3/k_1)\,|\beta_{13}|^2. \qquad \ldots\ldots(6)$$

§ 3. SOLUTION OF THE COUPLED EQUATIONS

The distorted-wave approximation solves equations (3) and (4) for β_{13} by neglecting the right-hand side of (3). The failure of the approximation shows that this coupling term is, in fact, important.

It appears that no previous attempt has been made to solve fully a set of coupled integro-differential equations such as (3) and (4). This may be effected numerically by an iterative procedure (see Appendix). The equations in general yield two independent solutions that are bounded at the origin. These are distinguished by use of different starting solutions in the numerical-integration routine. The independent solutions have then to be linearly combined to give the particular solution, which satisfies the required asymptotic conditions. This leads to an expression for the zero-order partial cross section in terms of the amplitudes and phases of the independent solutions.

3.1. *Rearrangement of the Coupled Equations*

To obtain (3) and (4) in a form suitable for numerical treatment, we substitute $\mathscr{F}_{n}(r)=F_{n}(r)r^{-1}$ and expand the atomic functions $\psi_1(12)$, $\psi_3(12)$ in terms of their component electron orbital functions $u_1(r)$, $u_2(r)$, as given by Morse, Young and Haurwitz (1935), viz.

$$\left.\begin{aligned}\psi_1(12)&=(2)^{-1/2}\{u_1(1)u_2(2)+u_1(2)u_2(1)\}\\ \psi_3(12)&=(2)^{-1/2}\{u_1(1)u_2(2)-u_1(2)u_2(1)\}\end{aligned}\right\}\qquad\ldots\ldots(7)$$

$$u_1(1)=\alpha\exp(-\mu a r_1),\ \alpha=(\mu^3a^3/\pi)^{1/2},\ a\mu=2\cdot00,$$

$$u_2(1)=\beta r_1\exp(-\mu r_1)-\gamma\exp(-\mu b r_1),\ \beta=(\mu^5/3\pi\nu)^{1/2},\ \nu=1-\frac{48A}{(1+b)^4}+\frac{3A^2}{b^3}$$

$$A=(a+b)^3/(1+a)^4,\ b\mu=1\cdot57,\ \mu=0\cdot61,\ \gamma=3A\beta/\mu.$$

The equations may then be written

$$\frac{d^2F_1(r)}{dr^2}=[\phi(r)-k_1^2]F_1(r)+A_1(r)u_1(r)+A_2(r)u_2(r),\qquad\ldots\ldots(8)$$

$$\frac{d^2F_3(r)}{dr^2}=[\phi(r)-k_3^2]F_3(r)+B_1(r)u_1(r)+B_2(r)u_2(r),\qquad\ldots\ldots(9)$$

subject to the boundary conditions that $F_1(r)$, $F_3(r)$ should be zero at the origin.

The functions $A_1(r)$, $A_2(r)$, $B_1(r)$, $B_2(r)$ are defined by the relations

$$\left.\begin{aligned}
A_1(r_3)=4\pi r_3\Big\{&\int F_1(1)\Big[\chi(1)+\tfrac{1}{2}k_1^2u_1(1)-\frac{u_1(1)}{r_{13}}\Big]r_1\,dr_1\\
&-4\pi\int[F_1(1)+(3)^{1/2}F_3(1)][\tau(1)+\sigma(1)]\,dr_1\\
&+(3)^{1/2}\int F_3(1)\Big[\chi(1)+\tfrac{1}{2}k_3^2u_1(1)-\frac{u_1(1)}{r_{13}}\Big]r_1\,dr_1\Big\}\\
A_2(r_3)=4\pi r_3\Big\{&\int F_1(1)\Big[\xi(1)+\tfrac{1}{2}k_1^2u_2(1)r_1-\frac{u_2(1)r_1}{r_{13}}\Big]dr_1\\
&-4\pi\int[F_1(1)-(3)^{1/2}F_3(1)][\rho(1)+\theta(1)]\,dr_1\\
&-(3)^{1/2}\int F_3(1)\Big[\xi(1)+\tfrac{1}{2}k_3^2u_2(1)r_1-\frac{u_2(1)r_1}{r_{13}}\Big]dr_1\Big\}\\
B_1(r_3)=4\pi r_3\Big\{&(3)^{1/2}\int F_1(1)\Big[\chi(1)+\tfrac{1}{2}k_1^2u_1(1)-\frac{u_1(1)}{r_{13}}\Big]r_1\,dr_1\\
&-4\pi\int[(3)^{1/2}F_1(1)-F_3(1)][\tau(1)-\sigma(1)]\,dr_1\\
&-\int F_3(1)\Big[\chi(1)+\tfrac{1}{2}k_3^2u_1(1)-\frac{u_1(1)}{r_{13}}\Big]r_1\,dr_1.\Big\}\\
B_2(r_3)=-4\pi r_3\Big\{&(3)^{1/2}\int F_1(1)\Big[\xi(1)+\tfrac{1}{2}k_1^2u_2(1)r_1-\frac{u_2(1)r_1}{r_{13}}\Big]dr_1\\
&+4\pi\int[(3)^{1/2}F_1(1)+F_3(1)][\rho(1)-\theta(1)]\,dr_1\\
&+\int F_3(1)\Big[\xi(1)+\tfrac{1}{2}k_2^2u_2(1)r_1-\frac{u_2(1)}{r_{13}}r_1\Big]dr_1\Big\},
\end{aligned}\right\}\ldots(10)$$

and $\phi(r)$, $\theta(r)$, $\tau(r)$, $\rho(r)$, $\sigma(r)$, $\chi(r)$, $\xi(r)$ are given by

$$\left.\begin{aligned}
\phi(r_3) &= 8\pi \int \frac{1}{r_{13}} [u_1(1)^2 + u_2(1)^2]\, r_1^2\, dr_1 - \frac{4}{r_3}, \\
\theta(r_3) &= u_2(3)\, r_3 \int \frac{1}{r_{13}} u_1(1)^2 r_1^2\, dr_1, \\
\tau(r_3) &= u_1(3)\, r_3 \int \frac{1}{r_{13}} u_2(1)^2 r_1^2\, dr_1, \\
\rho(r_3) &= u_1(3)\, r_3 \int \frac{1}{r_{13}} u_1(1)\, u_2(1)\, r_1^2\, dr_1, \\
\sigma(r_3) &= (u_2(3)/u_1(3))\, \rho(r_3), \\
\chi(r_3) &= \left[\frac{1}{2}\frac{1}{r_3^2}\frac{d}{dr}\left(r_3^2 \frac{d}{dr}\right) + \frac{2}{r_3}\right] u_1(3), \\
\xi(r_3) &= r_3 \left[\frac{1}{2}\frac{1}{r_3^2}\frac{d}{dr}\left(r_3^2 \frac{d}{dr}\right) + \frac{2}{r_3}\right] u_2(3).
\end{aligned}\right\} \qquad \ldots\ldots(11)$$

This was the form of the equations treated numerically.

3.2. *Derivation of the Cross Section*

The two independent solutions of (8) and (9) are denoted by

$$\begin{pmatrix} F_1(r) \\ F_3(r) \end{pmatrix} \quad \text{and} \quad \begin{pmatrix} G_1(r) \\ G_3(r) \end{pmatrix},$$

where

$$\begin{pmatrix} F_1(r) \\ F_3(r) \end{pmatrix} \sim \begin{pmatrix} a_1 \sin(k_1 r + \lambda_1) \\ a_3 \sin(k_3 r + \lambda_3) \end{pmatrix}, \quad \begin{pmatrix} G_1(r) \\ G_3(r) \end{pmatrix} \sim \begin{pmatrix} b_1 \sin(k_1 r + \mu_1) \\ b_3 \sin(k_3 r + \mu_3) \end{pmatrix} \ldots\ldots(12)$$

The required particular solution is that linear combination of the independent solutions having, from (5), the asymptotic form

$$u \begin{pmatrix} F_1(r) \\ F_3(r) \end{pmatrix} + v \begin{pmatrix} G_1(r) \\ G_3(r) \end{pmatrix} \sim \begin{pmatrix} k_1^{-1} \sin k_1 r + \alpha_{11} \exp(ik_1 r) \\ \beta_{13} \exp(ik_3 r) \end{pmatrix} \ldots\ldots(13)$$

where u and v are constants to be determined. Substitution of (12) in (13) and equation of coefficients of $\exp(ik_1 r)$, $\exp(-ik_1 r)$, $\exp(ik_3 r)$, $\exp(-ik_3 r)$ gives a set of simultaneous equations, which may be solved for β_{13} and yield for the cross section

$$\sigma_{1\to3} = \frac{4\pi k_3}{k_1^3} \frac{\sin^2(\lambda_3 - \mu_3)}{[(a_1/a_3)^2 + (b_1/b_3)^2 - 2(a_1 b_1/a_3 b_3) \cos(\lambda_1 - \lambda_3 - \mu_1 + \mu_3)]}. \quad \ldots\ldots(14)$$

3.3. *Starting Solutions*

Equations (8) and (9) are both of the inhomogeneous type

$$y''(r) = f(r)\, y(r) + g(r). \qquad \ldots\ldots(15)$$

In order to obtain a starting series $\Sigma_n a_n r^{n+3}$ for $y(r)$, representations for $f(r)$ and $g(r)$ near the origin are required. Examination of the known functions concerned shows that they take the form

$$f(r) = \sum_n b_n r^{n-1}, \quad g(r) = \sum_n d_n r^{n+1}$$

and the permitted values for S in the expansion for $y(r)$ are $S = 1$ or 3.

In this calculation the series based on $S = 1$ was used leading to the recurrence relation

$$a_p = \frac{1}{p(p+1)} \left[\sum_{n=0}^{p-1} a_n \, b_{p-n-1} + d_{p-2} \right] \qquad \ldots\ldots(16)$$

where a_0, i.e. the slope of $y(r)$ at the origin, is undetermined.

The series representing the coupled solutions may be written

$$F_1(r) = \sum_n a_n{}^1 r^{n+1}, \quad F_3(r) = \sum_n a_n{}^3 r^{n+1},$$

where $a_0{}^1$, $a_0{}^3$ are arbitrary.

Linearly independent solutions were distinguished by taking two different values for the ratio $a_0{}^1/a_0{}^3$. At this point it is necessary to consider the effect of the bound-state solutions.

3.4. *Uniqueness of the Solutions*

It may be seen by substitution in the original expansion for $\Psi(123)$ that

$$\begin{pmatrix} F_1(r) \\ F_3(r) \end{pmatrix} = \begin{pmatrix} r\,u_1(r) \\ (3)^{-1/2} r\,u_1(r) \end{pmatrix}, \quad \text{and} \quad \begin{pmatrix} F_1(r) \\ F_3(r) \end{pmatrix} = \begin{pmatrix} r\,u_2(r) \\ -(3)^{-1/2} u_2(r) \end{pmatrix}$$

satisfy $\Psi(123) = 0$ and, therefore, are solutions of equation (1).

Since no restrictions eliminating these bound-state functions have been imposed, the starting solutions derived from § 3.3 would lead to particular solutions of the form

$$\begin{pmatrix} F_1(r) \\ F_3(r) \end{pmatrix} = \begin{pmatrix} f_1(r) \\ f_3(r) \end{pmatrix} + a \begin{pmatrix} r\,u_1(r) \\ (3)^{-1/2} r\,u_1(r) \end{pmatrix} + b \begin{pmatrix} r\,u_2(r) \\ -(3)^{-1/2} r\,u_2(r) \end{pmatrix}$$

where

$$\begin{pmatrix} f_1(r) \\ f_3(r) \end{pmatrix}$$

is that part of the solutions having the required oscillating asymptotic behaviour and a and b are constants determined by $a_0{}^1$ and $a_0{}^3$.

It is necessary to show that the procedure for obtaining linearly independent solutions will lead to an independent oscillating function, not merely to a variation in a and b. That this is so follows from an examination of the recurrence relation (16), which shows that the first and second coefficients in any starting series of the type considered have the same ratio for all solutions. This ratio can only be maintained, when a and b alter, by an appropriate change in

$$\left. \frac{d}{dr} f_1(r) \right|_{r=0} \Big/ \left. \frac{d}{dr} f_3(r) \right|_{r=0}$$

and this gives the required independent solution.

The functions $u_1(r)$, $u_2(r)$ are both asymptotically zero and do not affect the asymptotic forms of $F_1(r)$ and $F_3(r)$. It is, therefore, only necessary to remove the bound-state contributions by making the numerical solution orthogonal to the bound-state solutions, if these contributions are so large as seriously to affect the numerical iterative process. This was not found to be the case in the following calculation.

3.5. *Calculation of the Cross Section*

Following the numerical procedure described in the Appendix, equations (8) and (9) were solved for several energies of the incident electron and the values of the asymptotic phases and amplitudes determined. The cross section was then directly calculated from (14). The results are given in the table. The cross section nowhere violates the conservation limit, but this only shows that there is no gross numerical error. It may be shown that, whereas the distorted-wave approximation can give results greater than the conservation limit, if all the coupling terms are retained this is no longer the case. A more rigorous test of the solutions is afforded by the Wronskian condition

$$F_3''G_3 - F_3 G_3'' + F_1'' G_1 - F_1 G_1'' = 0,$$

which was satisfied to the required accuracy.

Asymptotic Parameters

k_1 (A.U.)	(a)							(b)	(c)
		a_1	a_3	b_1	b_3	$\lambda_1-\mu_1$	$\mu_3-\lambda_3$		
0·044	0·026	3·02	0·90	12·05	0·99	0·125	0·760	180	1630
0·050	0·034	2·64	0·90	10·43	0·98	0·143	0·760	141	1260
0·060	0·048	2·22	0·89	8·57	0·95	0·168	0·760	113	873
0·100	0·134	1·04	0·88	4·14	0·84	0·270	0·652	64·7	314
0·300	1·210	0·39	0·67	1·35	0·67	0·710	0·588	14·6	35

(a) Incident electron energy (ev); (b) cross section $\sigma_{1\to 3}$ (a_0^2); (c) conservation limit πk_1^2 (a_0^2).

§ 4. DISCUSSION

The calculated zero-order partial cross section for the conversion of He* (2^1S) to He* (2^3S) by collision with thermal electrons at 300°K is $\sigma_{1\to 3} = 5 \times 10^{-15}$ cm². The experimental value for this cross section has been given by Phelps (1955) as $\sigma_{1\to 3} = 3 \times 10^{-14}$ cm².

The results are in somewhat worse agreement than appears at first sight, since the experimental cross section represents the value obtained by averaging over a distribution of electron energies, while the calculated value is for one particular electron energy. Correction for this would reduce the calculated cross section further by at least 15%.

This throws some doubts on the validity of the approximations made in the calculations. The magnitude of the cross section depends upon the difference between the independent solutions and these differences depend in turn on the form taken by the inhomogeneous parts of the coupled equations (8) and (9). It was noted that a change in these functions of 10% could have a considerable effect on the cross section. The calculation of these functions involved the use of approximate atomic wave functions and the neglect of terms that would arise from coupling through atomic states other than the initial and final.

In the case of the neglected coupling through intermediate atomic states, the terms involved could be important if their contribution was 10% of those arising from the direct coupling. However, the energy of collision is so small that it is difficult to see how the terms could be as large as this.

In the case of the atomic wave functions these are known to be in error for He* (2^1S) although they give the energy of the atomic states accurately. For example, the function is not orthogonal to the ground-state function for helium. The first indications of a recalculation of the corrected wave function (to be published) are that at large distances from the nucleus the wave function used was far too small. The effect of this on the cross section could be considerable. In view of the disagreement between the experimental and calculated cross sections, it would be of interest to investigate the consequences of this error in the He* (2^1S) function and it is hoped to present this at a later date.

ACKNOWLEDGMENTS

The author wishes to thank Professor H. S. W. Massey for suggesting the problem and Dr. E. H. S. Burhop for his continued interest and many helpful discussions.

REFERENCES

JACKSON, J., 1923, *Mon. Not. R. Astr. Soc.*, **84,** 602.

MASSEY, H. S. W., and MOISEIWITSCH, B. L., 1954, *Proc. Roy. Soc.* A, **227,** 38.

MORSE, P. M., YOUNG, L. A., and HAURWITZ, E. S., 1935, *Phys. Rev.*, **48,** 948.

MOTT, N. F., and MASSEY, H. S. W., 1949, *The Theory of Atomic Collisions*, 2nd Edn, (Oxford : University Press), Chap. viii.

PHELPS, A. V., 1955, *Phys. Rev.*, **99,** 1307.

APPENDIX

Numerical Procedure

Starting series $\Sigma_n a_n r^{n+1}$ were chosen for all functions and the same procedure could then be consistently applied. This had the advantage of often allowing the detection of errors by inspection, an important consideration in view of the very lengthy numerical work involved.

All integrals in $A_1(r)$, $A_2(r)$, $B_1(r)$, $B_2(r)$ were evaluated by Simpson's rule, those of the type

$$\int_0^\infty \frac{r_1 F_1(1) u_1(1)}{r_{13}} dr_1$$

first being expanded :

$$\int_0^\infty \frac{r_1 F_1(1) u_1(1)}{r_{13}} dr_1 = \frac{1}{r_3}\int_0^{r_3} r_1 F_1(1) u_1(1) dr_1 + \int_{r_3}^\infty F_1(1) u_1(1) dr_1.$$

Thus $A_1(r)$, $A_2(r)$, $B_1(r)$, $B_2(r)$ and the inhomogeneous parts of equations (8) and (9) respectively could be tabulated as required.

The series representations $\Sigma d_n r^{n+1}$ of the inhomogeneous parts of (8) and (9) were required for the determination of the starting solutions. Functions of the form ar^2+br were fitted to $A_1(r)$, $A_2(r)$, $B_1(r)$, $B_2(r)$ near the origin. Then using the known coefficients in the expansions of $u_1(r)$ and $u_2(r)$ the appropriate d_n coefficients could be calculated.

Initially taking $d_n=0$ and setting $F_1'(r)|_{r=0}=a_0^1=1$, $F_3'(r)|_{r=0}=a_0^3=1$, equation (8) was solved for $F_1(r)$ by a variation due to Erskine (unpublished) of the backward-difference method for solving linear second-order differential equations containing no first derivative (i.e. equation (15)) originally suggested by Cowell (see Jackson 1923).

This is based on the relation, in central-difference notation

$$y_n=\omega^2\left[\delta^{-2}y_n''+\frac{1}{12}y_n''-\frac{1}{240}\delta^2 y_n''+\ldots\right] \qquad \ldots\ldots(17)$$

where ω is the interval by which r is increased for each value.

Taking ω sufficiently small so that $\frac{1}{240}\delta^{-2}y_n''$ may be neglected and substituting for y_n'' from (15), equation (17) may be written

$$y_n=\frac{\omega^2}{1-\omega^2 f_n/12}\left[\delta^{-2}y_n''+\frac{1}{12}g_n\right]. \qquad \ldots\ldots(18)$$

This was the integrating formula used.

Two starting values are required and were calculated from (16). The solution was used to determine a first approximation to the inhomogeneous part of (9), which was then similarly solved for $F_3(r)$. The iterative cycle was repeated until $F_1(r)$, $F_3(r)$ had converged to the required accuracy.

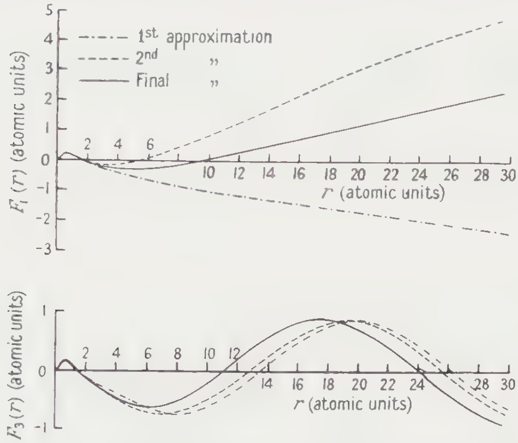

Figure 1. Stages in the numerical solution for $\begin{pmatrix} F_1(r) \\ F_3(r) \end{pmatrix}$ at an incident electron energy of 0·026 ev.

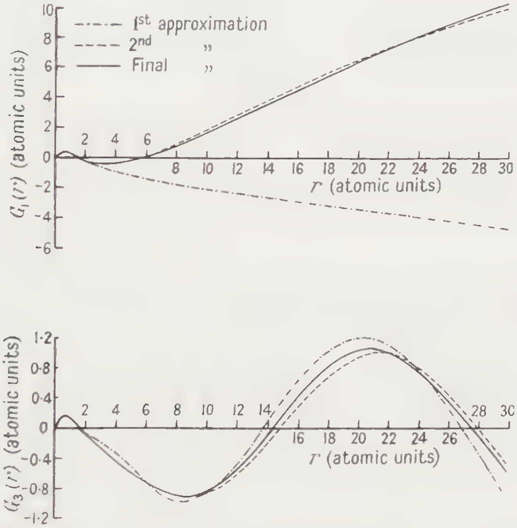

Figure 2. Stages in the numerical solution for $\begin{pmatrix} G_1(r) \\ G_3(r) \end{pmatrix}$ at an incident electron energy of 0·026 ev.

The second particular solution was obtained by setting

$$G_1'(r)|_{r=0} = 2, \quad G_3'(r)|_{r=0} = 1.$$

Successive stages in the iteration for

$$\begin{pmatrix} F_1(r) \\ F_3(r) \end{pmatrix}, \quad \begin{pmatrix} G_1(r) \\ G_3(r) \end{pmatrix}$$

are shown in figures 1 and 2 for an incident electron energy equivalent to 300 K, ($k_1 = 0{\cdot}044$ A.U.), about six iterative cycles being required for convergence to approximately 1%.

The bound-state contribution was less than 10% throughout and, therefore, the procedure was not complicated by its elimination. The numerical error in the calculated cross section at this energy was less than 10%.

The number of iterative cycles required for solutions corresponding to $k_1 + \Delta k_1$ were greatly reduced, where Δk_1 was small, by taking as a first approximation to the inhomogeneous part of (8) the function previously obtained for k_1.

A Simple Analytic Wave Function for He 1s2s ^{1}S

By R. MARRIOTT and M. J. SEATON

Physics Department, University College London

MS. received 14th January 1957

Abstract. An additional restriction is imposed on anti-symmetrized product wave functions for He 1s2s ^{1}S if the 2s orbital is made orthogonal to the 1s orbital of the excited state. Variational calculations have been carried out using simple analytic wave functions. The condition of orthogonality of orbitals is not imposed but the total wave function for 1s2s ^{1}S is made orthogonal to a simple approximate 1s^2 ^{1}S function. Evidence is presented relating to the accuracy of the function obtained.

The simplest wave functions for He 1s2s ^{1}S and ^{3}S having correct symmetry are of the form

$$\Psi_{\pm} = \frac{1}{\sqrt{2}}\{u_{1s}(r_1)\,u_{2s}(r_2) \pm u_{1s}(r_2)\,u_{2s}(r_1)\}. \qquad \ldots\ldots(1)$$

Assuming the orbitals u_{1s} and u_{2s} normalized to unity and putting

$$\Delta = \int u_{1s}(r)\,u_{2s}(r)\,d\tau, \qquad \ldots\ldots(2)$$

the normalized wave function is obtained on multiplying (1) by $[1 \pm \Delta^2]^{-1/2}$. For the ^{3}S state Ψ_- a constant multiple of one orbital may be added to the other without altering the total wave function (1) and in consequence no essential restriction is made by imposing the condition $\Delta = 0$. For the ^{1}S state Ψ_+ this is no longer the case; to put $\Delta = 0$ would here imply an additional restriction on the total wave function.

Morse, Young and Haurwitz (1935) considered orbitals of the form

$$u_{1s}(r) = \frac{M}{(4\pi)^{1/2}}\,e^{-\alpha r}, \quad u_{2s}(r) = \frac{N}{(4\pi)^{1/2}}\,(e^{-\beta r} - Sr e^{-\gamma r}) \qquad \ldots\ldots(3)$$

(M and N being normalizing factors) and imposed the condition $\Delta = 0$ for both ^{1}S and ^{3}S. No difficulty was experienced in varying the parameters to obtain a minimum for E(1s2s ^{3}S) but it was found that no such minimum could be obtained for any reasonable value of E(1s2s ^{1}S). Morse, Young and Haurwitz suggested the use of a function for 1s2s ^{1}S obtained from (1) and (3) using the parameters calculated for 1s2s ^{3}S. This will be referred to as the MYH function.

The lowest ^{3}S state is 1s2s ^{3}S but the lowest ^{1}S state is the 1s^2 ground state. To obtain an energy minimum corresponding to 1s2s ^{1}S it is therefore necessary that the wave function be orthogonalized to the ground-state wave function. We have carried out variational calculations for E(1s2s ^{1}S) using wave functions of the form (1) and (3), without imposing the condition $\Delta = 0$, but imposing the condition of orthogonality to the approximate ground-state function

$$\Psi_+(1s^2) = (z^3/\pi)\exp\{-z(r_1 + r_2)\}, \quad (z = 27/16) \qquad \ldots\ldots(4)$$

(Hylleraas 1929). The function obtained will be referred to as the MS function. For both the MYH and the MS functions, $\alpha = 2{\cdot}00$ and $M = (32)^{1/2}$. The other parameters are given in table 1.

Table 1

	β	γ	N	S	Δ
MYH	1·57	0·61	1·049	0·340	zero
MS	1·136	0·464	0·568	0·317	0·0424

The most elaborate wave functions available for He 1s2s ¹S are those of Coolidge and James (1936). The best Coolidge and James function containing r_1 and r_2 only ($R\Phi$ in their notation) will be referred to as the CJ function. Comparison with the CJ function shows that the MS function is more accurate than the MYH function but suggests that the MS function is too large for r greater than about 8 atomic units. This conclusion is confirmed by comparing with the ‘ Coulomb ’ function of Bates and Damgaard (1949), obtained using the empirically determined effective quantum number $n^*(2s)$.

In order to demonstrate the relative merits of the MYH, MS and CJ functions the following quantities have been calculated :

(i) The term energy T referred to the He⁺ ground state.

(ii) The mean square radius,

$$\overline{r^2} = \int \Psi_+ [r_1{}^2 + r_2{}^2] \Psi_+ \, d\tau_1 \, d\tau_2. \qquad \ldots\ldots(5)$$

(iii) The square of the integral

$$\sigma = \int_0^\infty \mathrm{P}(2s\,|\,r)\, r\, (\pi r)^{1/2} \mathrm{J}_3 (8^{1/2} r^{1/2})\, dr \qquad \ldots\ldots(6)$$

(where $u_{2s} = \mathrm{P}(2s\,|\,r)/(4\pi)^{1/2} r$ and J_3 is a Bessel function) required for the calculation of the threshold photo-ionization cross section (Bates 1946). The corresponding quantity has been calculated by Goldberg (1939) using the CJ function.

The results of these calculations are given in table 2.

Table 2

	(i) T (cm⁻¹)	(ii) $\overline{r^2}$	(iii) $\lvert\sigma\rvert^2$
MYH	32400	21·7	9·6
MS	31690	38·8	37·2
CJ	31620	33·1	40·2
Observed	32033 ± 15	—	—

With 1s2s ¹S trial functions orthogonal to the *exact* ground-state wave function it may be shown that T(calc) cannot exceed T(obs). The fact that T(MYH) exceeds T(obs) must therefore be due to an appreciable admixture of the ground-state wave function in the MYH function. It is apparent from the figures given in table 2, particularly those for $|\sigma|^2$, that use of the MYH function may lead to quite large errors. This function has previously been employed (Marriott 1957) in the course of calculations of the cross section for He 1s2s ¹S → 1s2s ³S produced by impact of slow electrons; the calculated result was found to be smaller, by a factor of 6, than that obtained experimentally by Phelps (1955). These calculations are being repeated, using improved wave functions, in the hope that better agreement with experiment will be obtained.

While the Coolidge and James functions are undoubtedly the most accurate, the merit of the MS function lies in the combination of simplicity with an accuracy which may be adequate for many applications. Orthogonalization to so simple a ground-state function as (4) will entail some loss of accuracy but this particular orthogonality relation may be convenient for calculations in which the function (4) is also employed (Massey and Moiseiwitsch 1954).

REFERENCES

Bates, D. R., 1946, *Mon. Not. R. Astr. Soc.*, **106,** 423.
Bates, D. R., and Damgaard, A., 1949, *Phil. Trans. Roy. Soc.* A, **242,** 101.
Coolidge, A. S., and James, H. M., 1936, *Phys. Rev.*, **49,** 676.
Goldberg, L., 1939, *Astrophys. J.*, **90,** 414.
Hylleraas, E. A., 1929, *Z. Phys.*, **54,** 347.
Marriott, R., 1957, *Proc. Phys. Soc.* A, **70,** 00.
Massey, H. S. W., and Moiseiwitsch, B. L., 1954, *Proc. Roy. Soc.* A, **227,** 38.
Morse, P. M., Young, L. A., and Haurwitz, E. S., 1935, *Phys. Rev.*, **48,** 948.
Phelps, A. V., 1955, *Phys. Rev.*, **99,** 1307.

On the Theory of the Inelastic Scattering of Electrons by Helium Atoms

By W. F. MILLER† and R. L. PLATZMAN
Department of Physics, Purdue University, Lafayette, Indiana, U.S.A.

MS. received 7th December 1956

Abstract. The familiar relationship between the optical properties of an atom and its cross sections for inelastic electron collisions can provide a valuable criterion for the validity of such cross sections. A method of exploiting this relationship is explained and then illustrated by application to two transitions of helium (transitions to the 2 ^{1}P state, and to the ionization limit), thereby correcting erroneous cross sections of long standing in the literature. Other applications are suggested, and a general proposal for obtaining more accurate cross sections is advanced.

The quantum theory of inelastic impacts of swiftly moving, charged atomic particles with atoms or molecules was established and developed in virtually full detail in the monumental 1930 paper of Bethe. However, application of Bethe's theory to a specific medium demands a knowledge of the wave functions of its atoms or molecules, and the only case which has thus far been treated quantitatively (other than atomic hydrogen, which is primarily of didactic importance) is atomic helium, for which extensive calculations of the inelastic scattering cross sections were made by Massey and Mohr (1931, 1933). The cross sections of Massey and Mohr are the ones available in the greatest detail for any chemically stable substance, and they have been used in numerous applications to a variety of topics. It is an objective of the present paper to point out that they are seriously in error and to show why this is so. To this end, suggestions will be made whereby more trustworthy cross sections can be attained.

The differential cross section for a collision in which an incident electron (merely for simplicity, the following discussion is restricted to electron scattering) of kinetic energy T is scattered with momentum change $\mathbf{K}\hbar$, after exciting an atom from the ground state to the excited or ionized state n, is given, to the accuracy of the first Born approximation, by

$$\sigma_n(K)\,dK = \frac{8\pi a_0^2 R^2}{T E_n} f_n(K)\frac{dK}{K}, \qquad \ldots\ldots(1)$$

where a_0 is the first Bohr radius of hydrogen, R is the Rydberg *energy*, E_n is the excitation energy of state n (i.e. energy above the ground state), and $f_n(K)$ is the generalized oscillator strength of Bethe:

$$f_n(K) = \frac{E_n}{R}\left|\frac{1}{Ka_0}\sum_i\int \psi_n{}^*\psi_0 \exp(i\mathbf{K}\,.\,\mathbf{r}_i)\,d\tau_1\,d\tau_2\ldots d\tau_Z\right|^2. \qquad \ldots\ldots(2)$$

The total cross section is thus

$$\sigma_n = \frac{4\pi a_0^2 R^2}{T E_n}\int_{K=K_{\min}}^{K_{\max}} f_n(K)\,d\ln(K^2a_0^2), \qquad \ldots\ldots(3)$$

---

† Now at Argonne National Laboratory, Lemont, Illinois.

where

$$K_{\max}^2 a_0^2 = 4\frac{T}{R}\left[1-\frac{E_n}{2T}+O\left(\frac{E_n^2}{T^2}\right)\right], \quad K_{\min}^2 a_0^2 = \frac{E_n^2}{4TR}\left[1+\frac{E_n}{2T}+O\left(\frac{E_n^2}{T^2}\right)\right]. \qquad \ldots\ldots(4)$$

(These well-known formulae are explained by Bethe (1930) and by Mott and Massey (1949).)

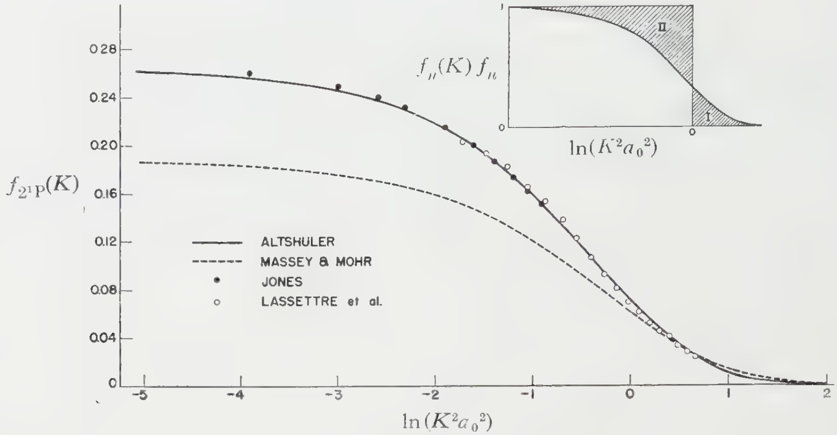

Figure 1. Generalized oscillator strength for the 2 ^{1}P state of helium. Examples of the limits of integration in eqn (3) are: for $T=300$ ev, $\ln(K_{\min}^2 a_0^2)=-3{\cdot}56$ and $\ln(K_{\max}^2 a_0^2)=4{\cdot}44$; for $T=1000$ ev, $\ln(K_{\min}^2 a_0^2)=-4{\cdot}79$ and $\ln(K_{\max}^2 a_0^2)=5{\cdot}67$. The insert provides a graphical illustration of the meaning of the constant c_n that appears in equation 5: $\ln c_n = \ln(R/E_n)^2 +$ area I − area II.

Many features of formulae (1) to (3), for the case of optically allowed transitions, are greatly clarified by a graph of $f_n(K)$ against $\ln(K^2a_0^2)$, as in figures 1 and 2. We recommend the use of such graphs in considerations of differential scattering cross sections. For each excitation process, a single curve of the illustrated shape must embody all information on the differential and total cross sections, for all values of T great enough to ensure validity of the Born approximation. For values of K such that $Ka_0 \ll 1$, the ordinate is constant and equal to the optical (dipole) oscillator strength f_n, to which expression (2) clearly reduces in this limit. The ordinate declines strongly near $Ka_0 = 1$ and is negligible for $Ka_0 \gg 1$, the decline being monotonic for excitation to low levels. The total cross section σ_n is, apart from the simple factor preceding the integral in (3), just the area under the curve between the limits given by (4). Thus the meaning of the Bethe *asymptotic* formula for the total cross section

$$\sigma_n \to \frac{4\pi a_0^2 R^2}{T E_n} f_n \ln(4Tc_n/R) \qquad \ldots\ldots(5)$$

is immediately apparent from the plot: at sufficiently great T, the area is equal to that of the rectangle bounded by ordinates f_n and 0, and abscissae $-\ln(4TR/E_n^2)$ and 0, with a small correction represented by the constant c_n. This constant is of the order of magnitude unity and depends only upon the *shape* of the curve:

$$\ln c_n (E_n/R)^2 = \int_0^\infty \frac{f_n(K)}{f_n}\, d\ln(K^2a_0^2) - \int_{-\infty}^0 \left[1-\frac{f_n(K)}{f_n}\right] d\ln(K^2a_0^2).$$

Now it is obvious that calculated values of the cross sections depend decisively upon the optical constants f_n. However, because most theoretical treatments work directly from equations (1) and (2), this fundamental and familiar relationship is only implicit and has usually been overlooked. An example is provided by the Massey–Mohr calculations for helium, which used approximations for ψ_0 and ψ_n that lead to erroneous oscillator strengths and therefore to cross sections correspondingly in error. Indeed, one might even claim that more accurate results for the total cross sections could be obtained, without calculation, by using realistic optical constants and simply guessing the values of c_n; this is, of course, the philosophy motivating use of the method of impact parameters (Williams 1935).

Two specific examples are now considered, the first being the $2\,^1$P excitation of helium. (Similar arguments are valid for excitation to higher P states.) Here, the wave functions used by Massey and Mohr (1931) give $f_2 = 0{\cdot}187$, whereas the correct value (Miller and Platzman, to be published) is about 0·277. The Massey–Mohr values of $f_2(K)$ are plotted in figure 1. Also plotted there are the results of calculations by Altshuler (1952, 1953) using the same wave functions but an alternative expression for $f_n(K)$ that differs from (2): it is formally equivalent, but emphasizes different regions of coordinate space and therefore leads to a different result when approximate wave functions are employed. (Use of this expression reduces, in the optical region, to use of the momentum matrix element, which was introduced and so successfully exploited by Chandrasekhar (1945); the present case provides another and remarkable example of the improvement effected by this simple transformation, for the latter gives $f_2 = 0{\cdot}262$ with the same wave functions.) The far greater accuracy of Altshuler's results for small values of K suggests, but does not prove, their superiority outside the optical region, i.e. for Ka_0 comparable with unity. This conjecture is substantiated by a few points, also shown in figure 1, which were calculated by Jones (1948) using expression (2) but a greatly superior ψ_0. Jones' results are in excellent accord with those of Altshuler, not only for values of $\ln(K^2 a_0^2)$ between $-3{\cdot}9$ and $-0{\cdot}9$, but also in the limit $K \to 0$, where the wave functions that he employed give $f_2 = 0{\cdot}266$ (Wheeler 1933). Finally, there are plotted a number of values of $f_2(K)$ calculated by means of equation (1) from experimental data obtained by Lassettre *et al.* (1953). (These are relative measurements of the differential cross section, and have been multiplied here by a constant factor chosen so that they agree as closely as possible with the calculations of Altshuler. Lassettre *et al.* also normalized their data, but in a different way.) It is evident that they corroborate the theory up to about $\ln(K^2 a_0^2) = +0{\cdot}6$.

The alternative expression for $f_n(K)$ used by Altshuler was originally proposed by Bates *et al.* (1950) as a means of improving inelastic scattering cross sections calculated with use of approximate wave functions. However, apart from the region of great K (which is of interest in itself but of little consequence in so far as the total inelastic cross section is concerned), the angular distribution, represented by $f_2(K)/f_2$, is almost the same for the calculations of Massey and Mohr and of Altshuler (and also of Jones). The greater accuracy, in this case at least, devolves almost entirely from the superior value of the optical oscillator strength given by the momentum matrix element. This suggests the possibility that improvement in theoretical cross sections may be effected to a greater extent, and more simply than possible from the Bates proposal, by using angular distributions $f_n(K)/f_n$

calculated from approximate wave functions together with the best possible optical oscillator strengths, obtained either from optical experiments or from much more detailed theoretical calculations.

Figure 2 pertains to the differential cross section for ionization of helium, at the ionization threshold. The ordinate is now, by an obvious extension of (2), $R\, df_{\varepsilon}(K)/d\epsilon$, where ϵ is the kinetic energy of the ejected electron, for the particular case $\epsilon = 0$. In treating ionization of helium, Massey and Mohr (1933) adopted a different model : they assumed, in effect, that each atomic electron is hydrogen-like, with $Z = 27/16$ (in both initial and final states). Such an assumption leads at once to the simple relationship of scale:

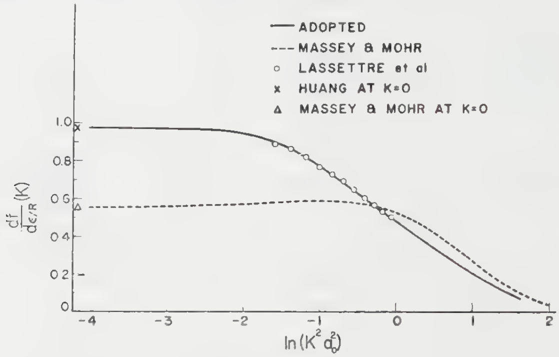

Figure 2. Generalized oscillator strength to the continuum of helium, at the ionization limit (i.e. for $\epsilon = 0$).

$$\left[\frac{df_{\varepsilon}(K)}{d\epsilon/R}\right]^{\mathrm{He}} = 2\,Z^{-2}\left[\frac{df_{\varepsilon/Z^2}(K/Z)}{d\epsilon/R}\right]^{\mathrm{H}}.$$

However, this generalized oscillator strength is again greatly in error in the optical region, for the (differential) optical oscillator strength of atomic hydrogen at the threshold is 0·7815, which gives $2(27/16)^{-2}(0{\cdot}7815) = 0{\cdot}5488$ for helium, compared to the value 0·970 found by Huang (1948). Very little trustworthy information on the (angular) differential ionization cross section of helium is available, but figure 2 shows how a first approximation may be contrived. Based upon a few experimental points obtained by Lassettre *et al.*, normalized by use of the multiplication factor found from consideration of $2\,^1\mathrm{P}$ excitation, a curve is drawn having the same general shape as those in figure 1 and approaching the correct optical limit. This curve is determined accurately enough to establish the constant $c_{\varepsilon=0}$ of equation (5), and is seriously uncertain only in the region of great K.

The same scheme cannot be used for ϵ greater than 0, because, although the optical information is available, the experimental data are inadequate to determine the curves, which are more complex because of the pronounced maximum at a value of K greater than zero. However, a few words may be said about the total ionization cross section, i.e., the integral of $d\sigma_{\varepsilon}(K)$ over K and ϵ. At energies great enough so that the asymptotic formula (5) holds at all values of ϵ for which the optical oscillator strength is not negligibly small, the total ionization cross section is given asymptotically by the simple expression

$$\sigma_i \to (4\pi a_0^2\, R/T)\, M_i^2 \ln(4TC_i/R), \qquad \ldots\ldots(6)$$

where C_i is a constant and M_i^2 is the integrated value of $R^2(df_{\varepsilon}/d\epsilon)/E_{\varepsilon}$, i.e. the 'total' square of the dipole matrix element (divided by a_0^2). The Massey–Mohr calculation would lead to a value of M_i^2 which is $2Z^{-2}$ times that quantity for atomic hydrogen, or $2(27/16)^{-2}(0{\cdot}2833)=0{\cdot}1990$, whereas an integration using the oscillator strengths of Huang yields $M_i^2=0{\cdot}477$. Thus the total ionization cross section of Massey and Mohr is far too small at high energies, a fact which is not incompatible with figure 44 on page 246 of the book of Mott and Massey (1949). The available experimental data do, indeed, agree with equation (6) and the value $M_i^2=0{\cdot}477$ (Miller and Platzman, to be published).

A remark may be appended about the cross sections at low energy. Here the above analysis, confined as it is to the domain of validity of the Born approximation, has no direct consequences. But it does convey the implication that, if the use of crude wave functions leads to serious error at high energy, they may not be without effect at low energies—and since such an effect may be energy dependent, that refinements to the simple Born approximation designed to correct for its various failures at low energy but using crude wave functions may be partially spurious. Moreover, semi-empirical excitation functions at low energy, which are often obtained from *relative* experimental data by adjusting them to agree with theory at some high energy, should, of course, approach the correct theoretical cross sections.

No mention has been made of optically forbidden transitions, but their analysis can also profit from similar considerations based upon quantities analogous to $f_n(K=0)$.

A detailed study of the inelastic scattering cross sections of helium is being prepared for publication.

REFERENCES

ALTSHULER, S., 1952, *Phys. Rev.*, **87**, 992; 1953, *Ibid.*, **89**, 1093.

BATES, D. R., FUNDAMINSKY, A., LEECH, J. W., and MASSEY, H. S. W., 1950, *Phil. Trans. Roy. Soc.* A, **243**, 93.

BETHE, H., 1930, *Ann. Phys., Lpz.*, **5**, 325.

CHANDRASEKHAR, S., 1945, *Astrophys. J.*, **102**, 223.

HUANG, S.-S., 1948, *Astrophys. J.*, **108**, 354.

JONES, E. A., 1948, *Ph. D. Dissertation*, Ohio State University.

LASSETTRE, E. N., KRASNOW, M. E., and SILVERMAN, S., 1953, *Scientific Report* 3, Contract No. AF 19(122)642, Department of Chemistry, Ohio State University.

MASSEY, H. S. W., and MOHR, C. B. O., 1931, *Proc. Roy. Soc.* A, **132**, 605; 1933, *Ibid.*, **140**, 613.

MOTT, N. F. and MASSEY, H. S. W., 1949, *Theory of Atomic Collisions* (Oxford : Clarendon Press), Second Edition.

WHEELER, J. A., 1933, *Phys. Rev.*, **43**, 258.

WILLIAMS, E. J., 1935, *K. Danske Vidensk. Selsk. Mat.-Fys. Medd.*, **13**, No. 4.

RESEARCH NOTES

The Absorption of Beta Particles as a function of Atomic Number

By S. ABID HUSAIN†‡ and J. L. PUTMAN§

† Department of Physics, The University, Karachi.
§ Atomic Energy Research Establishment, Harwell, Didcot, Berks.

MS. received 13th December 1956

The energy loss of beta particles in passing through matter is almost entirely due to their inelastic collisions with the atomic electrons, by which the atoms of the absorber are excited or ionized. The energy transferred in nuclear collisions is negligible because of the large mass difference.

Thus the absorption of beta particles of a given energy distribution is, to a first approximation, a function only of the electron density. It has become common practice to express the thickness of absorbing foils in terms of mass per unit area (e.g. mg cm^{-2}). The thickness in these units is proportional to (electrons per unit area) $\times A/Z$. Absorption curves plotted in this way for absorbers of neighbouring atomic numbers are therefore nearly identical.

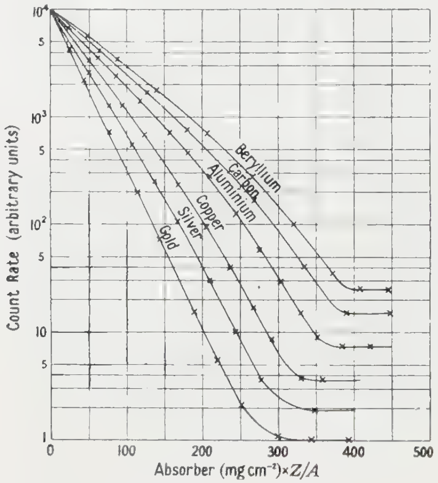

Figure 1. Absorption curves for ^{30}P beta particles.

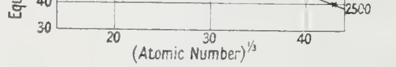

Figure 2. Equivalent thickness as a function of atomic number.

However, when the thicknesses of absorbing foils are plotted in terms of electrons/cm^2 or rather in terms of (mg cm^{-2})Z/A, the resulting absorption curves are not found to be independent of atomic number. Figure 1 shows a series of such curves, obtained with a thin ^{32}P source mounted on an aluminium tray at 20 cm from the window of an end-window Geiger counter (type EHM2). Absorbers were laid directly in contact with the 2 mg cm^{-2} mica window and were all greater than 5 cm in extent (i.e. twice the window diameter). It is seen that the efficiency of absorption increases systematically with Z.

---

‡ Attached to Isotope Division, Atomic Energy Research Establishment, Harwell, under Baghdad Pact Training Scheme.

The effect is almost certainly due to nuclear scattering, the probability of which for a given angle of scatter is proportional to Z^2, whereas the number of nuclei encountered is proportional to $1/Z$ in absorbers with the same number of electrons per cm^2. The energy loss per unit path length of a beta particle (neglecting bremsstrahlung losses) is a function only of the electron density and not of direction. Thus the effect of nuclear scattering will be only to increase the mean path length in the medium. We have found that the extent of this increase bears a simple empirical relationship to atomic number.

Equivalent thicknesses of absorber (i.e. those resulting in the same counting rates) are plotted in figure 2, in terms of $Z^{1/3}$. The linearity of the plots shows that equivalent thicknesses X (in electrons/cm^2) are related to atomic number by the expression:

$$\log X = B - AZ^{1/3}.$$

The lines of figure 2 are not quite parallel so that A is nearly, but not quite, constant.

From the mean value of A it is found that if thicknesses in (mg cm^{-2})Z/A are multiplied by a factor $\exp(\frac{1}{3}Z^{1/3})$, closely similar absorption curves are obtained for all elements from $Z = 4$ to $Z = 79$, down to the level where the curves are modified by bremsstrahlung.

A less accurate but still quite good approximation for atomic numbers above that of aluminium is obtained by multiplying the absorber thickness X by $Z^{1/3}$, that is by plotting the absorber thickness in units of (mass per unit area) × $(Z^{4/3}/A)$ as shown in figure 3.

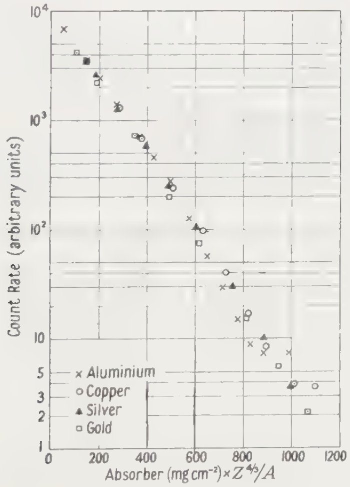

Figure 3. Modified absorption curves for ^{32}P beta particles. (Common scale.)

Further experiments using a ^{90}Sr + ^{90}Y source, providing a mixed spectrum of beta particles, gave results which showed a similar dependence on $Z^{1/3}$.

Inelastic Collisions between Heavy Particles
VII : Electron Loss from Fast Hydrogen Atoms passing through Helium

By D. R. BATES and A. WILLIAMS
Department of Applied Mathematics, The Queen's University of Belfast

MS. received 17*th December* 1956

§ 1. Introduction

It is of some importance to determine the range of validity of Born's approximation for the treatment of inelastic collisions between heavy particles. Even with modern techniques the cross sections associated with such collisions are far from easy to measure (cf. Massey and Burhop 1952, Allison and Warshaw 1953), and the reliability of much of the published data cannot readily be assessed with assurance. This must be borne in mind when making a comparison between theoretical and experimental results. The uncertainty renders the number of processes which have to be studied before a conclusion can be reached greater than it would otherwise be.

To add to the few cases for which there are both theoretical and experimental results (cf. Bates and Dalgarno 1956), we here evaluate the cross section for

$$\mathrm{H}(1\mathrm{s})+\mathrm{He}(1\mathrm{s}^2)\rightarrow \mathrm{H}^+ + \mathrm{e} + \sum_{n'l',n''l''} \mathrm{He}(n'l', n''l''),\dagger \qquad \ldots\ldots(1)$$

which process has been investigated in the laboratory by Stier and Barnett (1956).

§ 2. Theory

The detailed mathematical analysis need not be presented since accounts of the application of Born's approximation to electron loss processes have been given elsewhere (Bates and Griffing 1955, Boyd, Moiseiwitsch and Stewart 1957, Adler and Moiseiwitsch 1957).

Representing the bound and free states of the hydrogen atom by the appropriate exact wave functions and the ground state of the helium atom by the approximate wave function

$$\Psi(1\mathrm{s}^2|\mathbf{r}_1, \mathbf{r}_2) = \frac{\alpha^3}{\pi}\exp[-\alpha(r_1+r_2)], \qquad \alpha = 27/16, \qquad \ldots\ldots(2)$$

it is found that the contribution to the cross section of (1) from the single-transition process

$$\mathrm{H}(1\mathrm{s})+\mathrm{He}(1\mathrm{s}^2)\rightarrow \mathrm{H}^+ + \mathrm{e} + \mathrm{He}(1\mathrm{s}^2) \qquad \ldots\ldots(3)$$

is

$$Q(1\mathrm{s}\text{–C}\,;\,1\mathrm{s}^2\text{–}1\mathrm{s}^2) = \int_\kappa Q(1\mathrm{s}\text{–}\kappa\,;\,1\mathrm{s}^2\text{–}1\mathrm{s}^2)\,d\kappa, \qquad (\pi a_0^2) \qquad \ldots\ldots(4)$$

where

$$Q(1\mathrm{s}\text{–}\kappa\,;\,1\mathrm{s}^2\text{–}1\mathrm{s}^2) = \frac{32}{s^2}\int_{t_{\min}}^{\infty} t^{-3}\left\{1-\frac{16\alpha^4}{(4\alpha^2+t^2)^2}\right\}^2 \mathscr{I}(1\mathrm{s}\rightarrow\kappa)^2\,dt, \quad (\pi a_0^2) \quad \ldots\ldots(5)$$

in which

$$\kappa = \frac{2\pi m v_\mathrm{e} a_0}{h}, \qquad s = \frac{2\pi m v_\mathrm{p} a_0}{h}, \qquad \ldots\ldots(6)$$

v_e being the velocity of the ejected electron relative to its parent nucleus and v_p being the initial velocity of relative motion of the heavy particles, and in which

---

† The summation includes an integration over the continuum.

$t_{\min}$ and $\mathscr{I}(1s\to\kappa)$ are as defined by Bates and Griffing (1953). It is further found that the contribution from the double-transition process

$$\mathrm{H}(1s)+\mathrm{He}(1s^2)\to\mathrm{H}^{+}+e+\sum_{n'l',\,n''l''\neq 1s^2}{}' \mathrm{He}(n'l',n''l'') \qquad \ldots\ldots(7)$$

is

$$Q(1s\text{–}C;\,1s^2\text{–}\Sigma')=\int_{\kappa} Q(1s\text{–}\kappa;\,1s^2\text{–}\Sigma')\,d\kappa, \qquad (\pi a_0^2) \qquad \ldots\ldots(8)$$

where in the high impact energy limit

$$Q(1s\text{–}\kappa;\,1s^2\text{–}\Sigma')=\frac{16}{s^2}\int_0^\infty t^{-3}\left\{1-\frac{256\alpha^8}{(4\alpha^2+t^2)^4}\right\}\mathscr{I}(1s\to\kappa)^2\,dt, \qquad (\pi a_0^2). \qquad \ldots\ldots(9)$$

The computation of $Q(1s\text{–}C;\,1s^2\text{–}1s^2)$ is not unduly lengthy. But the computation of $Q(1s\text{–}C;\,1s^2\text{–}\Sigma')$ is extremely tedious (except in the region where the asymptotic formula cited may be used), since triple numerical integrations must be performed. Fortunately, examination of the results of the earlier calculations indicates that the energy variation of $Q(1s\text{–}C;\,1s^2\text{–}\Sigma')$ may be assumed to be closely the same as that of $Q(1s\text{–}C;\,1s^2\text{–}1s2p,\,{}^1P)$, the cross section of

$$\mathrm{H}(1s)+\mathrm{He}(1s^2)\to\mathrm{H}^{+}+e+\mathrm{He}(1s2p,\,{}^1P), \qquad \ldots\ldots(10)$$

and this may be evaluated comparatively easily since only double numerical integrations are involved. Taking the 2p orbital to be hydrogenic it is found that the associated partial cross section is given by

$$Q(1s\text{–}\kappa;\,1s^2\text{–}1s2p\,{}^1P)=\frac{2^{28}\alpha^6(1+2\alpha)^6}{(2+\alpha)^6 s^2}\int_{t_{\min}}^\infty t^{-1}\{(1+2\alpha)^2+4t^2\}^{-6}\mathscr{I}(1s\to\kappa)^2\,dt,$$
$$(\pi a_0^2). \qquad \ldots\ldots(11)$$

§ 3. Discussion

3.1.

The calculated total loss cross section, $Q(1s\text{–}C;\,1s^2\text{–}\Sigma)$ and the contribution $Q(1s\text{–}C;\,1s^2\text{–}1s^2)$ from the single-transition process (3), are plotted in figure 1 against the energy $\mathscr{E}$ of the incident hydrogen atom, a double logarithmic scale being used. For comparison, the results of the measurements of Stier and Barnett (1956) are similarly plotted. Above about 100 kev the agreement is satisfactory, but, below, the agreement is poor, the theoretical cross sections being much smaller than the experimental.

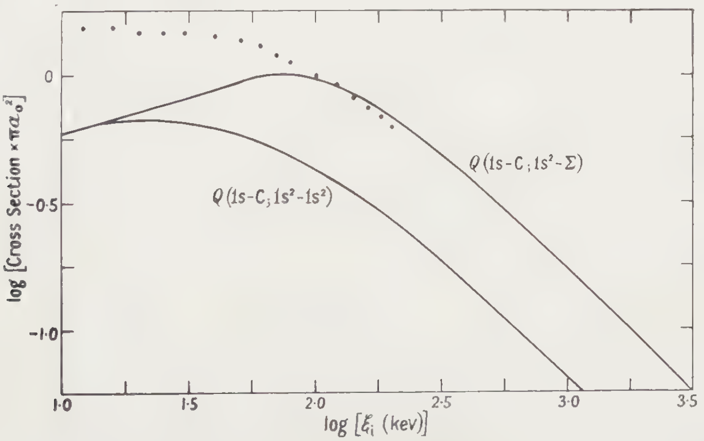

Figure 1. Electron loss from hydrogen atoms in helium. Curves: Born approximation to Q (1s–C; 1s²–1s²) and Q (1s–C; 1s²–Σ), as computed in this paper. Points: loss cross section as measured by Stier and Barnett (1956).

Born's approximation is, of course, expected to fail in the low-energy region. The assumption is often made that in the case of heavy-particle collisions it in general yields cross sections which are too large, just as it does in the case of electron collisions. However, the pattern of its failure is actually complex. One of the factors of importance is the variation with the internuclear distance R of the separation $\Delta E(R)$ of the initial and final potential-energy surfaces (cf. Bates, Massey and Stewart 1953). There is a tendency for Born's approximation to overestimate the cross section if $\Delta E(R)$ is greater than $\Delta E(\infty)$ in the range of R where the perturbing interaction is strong, and to underestimate the cross section if $\Delta E(R)$ is less than $\Delta E(\infty)$ in this range. Now the quasi-molecule formed by the colliding hydrogen and helium atoms has lithium as its united-atom limit; and the ionization potential of lithium is much lower than that of hydrogen or than that of helium.† In view of what has been said, it is therefore not unreasonable that Born's approximation to the cross section of the process under discussion is smaller than the observed cross section at low energies.

Though the united-atom limit of the quasi-molecule may serve as a guide to the sense of the error in Born's approximation it cannot be expected to be an infallible guide, since the error is influenced by several factors. When using it as a guide, account must naturally be taken of which atomic orbitals may be occupied by the active electron after an adiabatic approach. Usually, an excited orbital may be occupied which suggests that cases in which Born's approximation underestimates the cross section may not be uncommon.

3.2.

Stier and Barnett (1956) also carried out measurements with hydrogen as the target gas. These provide comparison data for the calculations of Bates and Griffing (1955) on the cross section of

$$\mathrm{H}(1\mathrm{s})+\mathrm{H}(1\mathrm{s})\rightarrow\mathrm{H}^{+}+\mathrm{e}+\sum_{nl}\mathrm{H}(nl) \qquad \ldots\ldots(12)$$

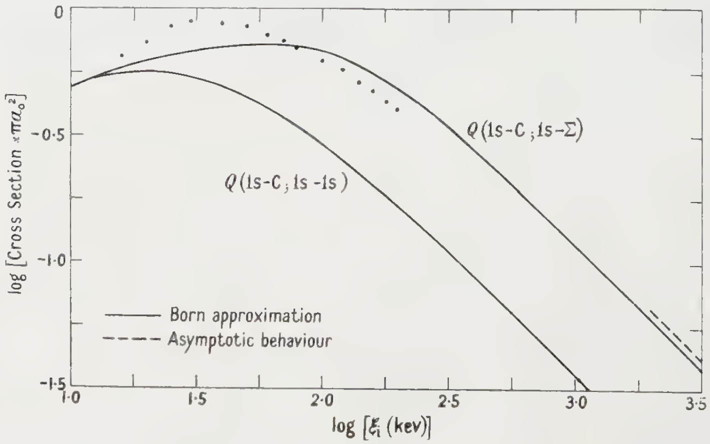

Figure 2. Electron loss from hydrogen atoms in atomic hydrogen. Curves: Born approximation to $Q\,(1\mathrm{s}-\mathrm{C};\ 1\mathrm{s}-1\mathrm{s})$ and $Q\,(1\mathrm{s}-\mathrm{C};\ 1\mathrm{s}-\Sigma)$, and asymptotic behaviour of the latter, all from Bates and Griffing (1955). Points: loss cross section as measured by Stier and Barnett (1956).

---

† The ionization potential of helium is not of direct relevance as far as single-transition collisions are concerned.

if the customary (but not strictly valid) assumption is made that one hydrogen molecule is equivalent to two hydrogen atoms. As may be seen from figure 2, the accord is quite good. It is rather better than that between the theoretical curve and the earlier experimental curve of Montague (1951) (cf. Bates and Griffing 1955, Dalgarno and Griffing 1955).

ACKNOWLEDGMENT

One of us (A. W.) wishes to thank the Colonial Welfare and Development Fund for a grant.

REFERENCES

ADLER, J., and MOISEIWITSCH, B. L., 1957, *Proc. Phys. Soc.* A, **70,** 117.
ALLISON, S. K., and WARSHAW, S. D., 1953, *Rev. Mod. Phys.*, **25,** 779.
BATES, D. R., and DALGARNO, A., 1956, *The Airglow and Aurora* (Eds E. B. Armstrong and A. Dalgarno), (London : Pergamon Press), p. 328.
BATES, D. R., and GRIFFING, G. W., 1953, *Proc. Phys. Soc.* A, **66,** 961 ; 1955, *Ibid.*, **68,** 90.
BATES, D. R., MASSEY, H. S. W., and STEWART, A. L., 1953, *Proc. Roy. Soc.* A, **216,** 437.
BOYD, J. M., MOISEIWITSCH, B. L., and STEWART, A. L., 1957, *Proc. Phys. Soc.* A, **70,** 110.
DALGARNO, A., and GRIFFING, G. W., 1955, *Proc. Roy. Soc.* A, **232,** 423.
MASSEY, H. S. W., and BURHOP, E. H. S., 1952, *Ionic and Electronic Impact Phenomena* (Oxford : Clarendon Press).
MONTAGUE, J. H., 1951, *Phys. Rev.*, **81,** 1026.
STIER, P. M., and BARNETT, C. F., 1956, *Phys. Rev.*, **103,** 896.

Light Output of Potassium Iodide Crystals under Bombardment by Carbon Ions

By W. E. BURCHAM
Department of Physics, University of Birmingham

MS. received 28th January 1957

§ 1. INTRODUCTION

CRYSTALS of the alkali halides, activated by thallium, are much used for determining the energy of charged particles emitted in nuclear reactions. The majority of such applications up to the present have been concerned with hydrogen or helium ions, for which the linearity of the light output of the crystal as a function of incident particle energy has been extensively studied (see Link and Walker 1953, who give references to earlier work, Eby and Jentschke 1954, Brolley and Ribe 1955).

Scintillation spectrometry is also a convenient way of studying the energy distribution of accelerated heavy ions (Walker, Fremlin, Link and Stephens 1954) and for this purpose it is necessary to know how the light pulse produced by a heavy ion in an alkali halide depends on the ion energy. Deviations from linearity in the response of both NaI(Tl) and KI(Tl) crystals to α-particles of energies less than 10 MEV have been reported by several authors. In particular Link and Walker (1953) showed that the light output per unit energy dissipated by α-particles in KI(Tl) fell off as the specific energy loss increased from 0·2 to 0·5 MEV per mg cm^{-2}. Fully charged carbon ions have a specific energy loss nine times as great as that of α-particles of the same velocity and can therefore be used as an alternative to very low energy α-particles to extend observations on the saturation of light output from scintillators. The present note reports on a study of the response curve for ^{12}C ions in KI(Tl).

§ 2. EXPERIMENTAL METHOD

Carbon ions in the 6^+ ionic state were accelerated in the Nuffield cyclotron of the University of Birmingham to an energy of about 110 MeV. It was found possible to extract a small beam of these ions by the normal electrostatic method and to deflect this beam magnetically into an observation chamber 20 feet from the cyclotron. The deflected ions passed through a chamber into which aluminium foils could be rotated *in vacuo* and then struck a crystal of KI (Tl, about 0·1%) of dimensions 4 mm × 4 mm × 1 mm. Aluminium foils could also be inserted into the beam of ions before the magnetic deflection. The crystal was mounted on a 1 inch length of Perspex light guide leading to an EMI Type 5311 photomultiplier, operated at about 140 volts per stage. Tests were made to check that the multiplier was not affected by stray magnetic fields from the cyclotron and deflecting magnet. Impulses from the multiplier were fed from a cathode follower to an amplifier with an integrating time constant of 0·8 μsec and the amplifier output was studied using either a 60-channel pulse analyser or photographic recording.

The energy of the ions incident on the crystal was determined from the current in the deflecting magnet, which was calibrated by using α-particles, protons and deuterons of known energy and also by observing the equilibrium of a current-carrying wire in the field. The maximum energy available from the cyclotron for α-particles was found by observing their tracks in Ilford C2 emulsions and using the range-energy tables given by Rotblat (1951); reduced energies were obtained by allowing the particles to pass through various thicknesses of aluminium foil before entering the deflecting magnet. The energy of the ^{12}C ions indicated by this calibration was also checked by recording tracks of these ions in nuclear emulsions and using the range–energy relation given by Papineau (1956 a). The accuracy of energy measurement was to 3% for particles of maximum energy. At energies below about 50 MeV care was needed to distinguish the beam of 6^+ ions from 5^+ ions formed by electron capture in the absorbing foils. Ambiguity was avoided by observing both beams.

The linearity of the photomultiplier, amplifier and recording system was tested by applying standard light flashes from a neon tube (Garlick and Wright 1952) to the photocathode of the multiplier. Neutral density filters were used to reduce the calibrating signal to a value below that obtained with the lowest ion energy used. Corrections for non-linearity were applied to the observed signals when necessary; the accuracy of output measurement was to about 2% for particles of maximum energy.

§ 3. RESULTS

Figure 1 is a typical pulse-height distribution obtained with the 60-channel analyser showing peaks due to ^{12}C and ^{4}He ions. These particles are accelerated in and extracted from the cyclotron with the same value of e/m and velocity and their energies should be in the ratio 3/1. The low-energy tail on the peak of ^{12}C ions shown in figure 1 is probably due to surface irregularities of the crystal, or to scattering in the collimator system, and was disregarded. The ^{12}C energy obtained for the peak shown was 113 Mev and the amplitude of the signal obtained from these ions was used as a reference value.

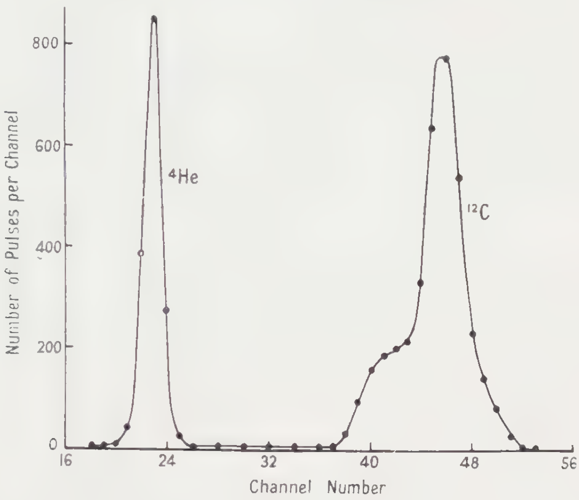

Figure 1. Pulse-size distribution for 38 Mev ^{4}He ions and 113 Mev ^{12}C ions in KI (Tl) crystal.

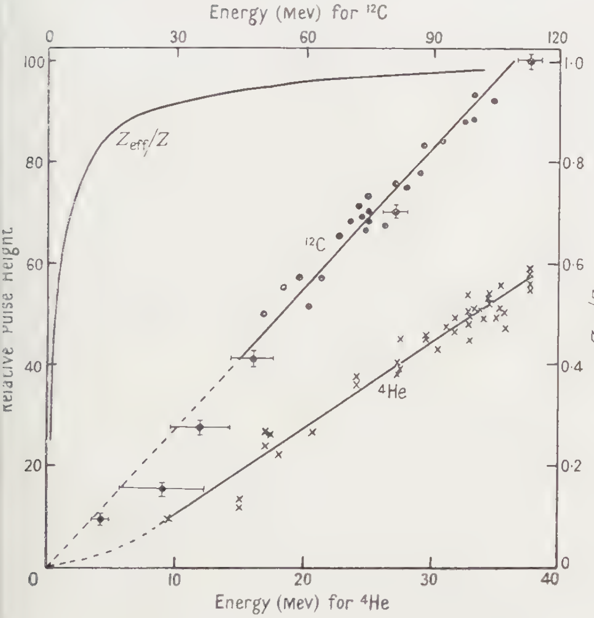

Figure 2. Response of a KI (Tl) crystal to ^{4}He and ^{12}C ions. Zeff is the average charge of the ^{12}C ion.

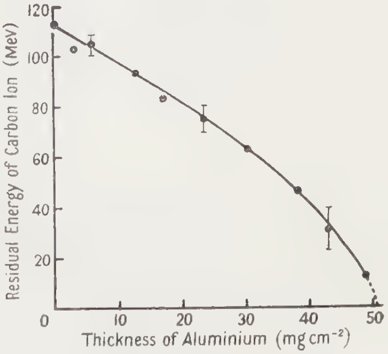

Figure 3. Slowing-down of 113 Mev ^{12}C ions by aluminium.

Figure 2 shows the response of the crystal, in terms of the reference value as 100 units, as a function of incident carbon ion energy. The observations at energies below 50 Mev are inaccurate because of the large scattering and straggling in the absorber foils, resulting in loss of intensity, a broad energy distribution and bad definition of energy. A correction of about 3% may also be necessary (Wright 1954) for the decreased efficiency of light collection from the crystal for short range particles. The point at the energy of 13 MeV was obtained by using the 2^{+} ion beam available from the cyclotron (Walker *et al.* 1954). The figure also shows on the same scale the response obtained from α-particles of different energies.

Some observations were also made of the pulse heights obtained when aluminium foils were placed in the path of the beam of 113 MeV carbon ions between the deflecting magnet and the crystal. The energy remaining to the carbon ion after passage through a given thickness of aluminium is shown in figure 3, from which a range of $51 \pm 2\,\mathrm{mg\,cm^{-2}}$ is deduced.

§ 4. DISCUSSION

From figure 2, the light output per unit energy dissipated by 113 MeV ^{12}C ions in KI(Tl) is 0·55 of that for α-particles of the same velocity. According to information collected by Papineau (1956 a) and shown in figure 2, the effective charge of a 113 MeV carbon ion moving through matter is about 5·9. Using this figure the specific energy loss of the 113 MeV carbon ions may be obtained directly from the energy loss for α-particles (as used for instance by Link and Walker 1953) and is† 1 MeV per $\mathrm{mg\,cm^{-2}}$. The lower light output for a higher energy loss is predicted by the trend of the curve given by Link and Walker (1953, fig. 3) and discussed by them in terms of a limited number of luminescent centres in the crystal. The results of Eby and Jentschke (1954) for slow α-particles in NaI(Tl) suggest that the light output from heavy ions ought to be suppressed even further than observed in this experiment. For carbon ion energies between 70 and 113 MeV the light output from KI(Tl) is linear with energy within the accuracy, to about 5%, of the present work.

The observations below 70 MeV are not sufficiently accurate to establish linearity of light output with energy. At energies less than 10 MeV the average ionic charge decreases rapidly with velocity and a closer study of the response curve may exhibit the importance of nuclear stopping collisions.

The range ($51 \pm 2\,\mathrm{mg\,cm^{-2}}$) obtained for 113 MeV carbon ions in aluminium is close to that predicted ($50{\cdot}0\,\mathrm{mg\,cm^{-2}}$) from the range of protons of the same velocity V, assuming the relationship

$$R_{\mathrm{c}}(V) = \frac{m}{Z^2} R_{\mathrm{p}}(V)$$

where m, Z are the mass and charge of the ion. This agreement is probably fortuitous, since it is known for nuclear emulsion at least (Papineau 1956 a, b) that the effects of charge exchange must be included in the calculation of range–energy curves. The range–velocity relationship derived from figure 3 is of the form $R = kV^3$, but the error of the energy measurements near the end of the range is large and a quadratic velocity dependence cannot be excluded.

ACKNOWLEDGMENT

I am grateful to Miss D. Latham for scanning the nuclear emulsions used in this experiment.

---

† This figure was checked by direct observation of the reduction in carbon ion energy due to insertion of aluminium and silver foils in the beam before the deflecting magnet.

REFERENCES

BOHR, N., 1948, *The Penetration of Atomic Particles through Matter. Det. Kgl. Danske Vidensk. Selskab.*, XVIII, 8.

BROLLEY, J. E., and RIBE, F. L., 1955, *Phys. Rev.*, **98,** 1112.

EBY, F. S., and JENTSCHKE, W. K., 1954, *Phys. Rev.*, **96,** 911.

GARLICK, G. F. J., and WRIGHT, G. T., 1952, *Proc. Phys. Soc.* B, **65,** 415.

LINK, W. T., and WALKER, D., 1953, *Proc. Phys. Soc.* A, **66,** 767.

PAPINEAU, A., 1956 a, *C.R. Acad. Sci., Paris.*, **242,** 2933 ; 1956 b, *J. Phys. Radium.*, **17,** 566.

ROTBLAT, J., 1951, *Nature, Lond.*, **167,** 550.

WALKER, D., FREMLIN, J. H., LINK, W. T., and STEPHENS, K. G., 1954, *Brit. J. Appl. Phys.*, **5,** 157.

WRIGHT, G. T., 1954, *J. Sci. Instrum.*, **31,** 377.

LETTERS TO THE EDITOR

Thermal Inelastic Scattering of Cold Neutrons in Polycrystalline Graphite

Kleinman (1951) has calculated the inelastic scattering cross section for 7 Å neutrons in graphite as a function of temperature, assuming a Debye frequency spectrum. One finds that the calculated variation of the cross section is in complete disagreement with experiment (Hughes 1953). The aim of this communication is to calculate the same for 10 Å neutrons taking into account the anisotropic nature of the graphite lattice.

The anomalous behaviour of the specific heat of graphite at low temperatures, which is also a consequence of its anisotropy, is well known. The model of the graphite lattice proposed by Krumhansl and Brooks (1953) has been found by Keesom and Pearlman (1955) to account satisfactorily for the low temperature variation of the specific heat. We have also used this model for our calculations. In this model the lattice vibrations are divided into two types, (i) z modes with atomic displacements normal to the layer planes, and a Debye temperature Θ_z and (ii) xy modes with atomic displacements in the layer planes and Debye temperature Θ_{xy}. For frequencies less than a certain ν_{0z} the density of z modes is taken to be proportional to ν^2 and for frequencies greater than ν_{0z} but less than a certain maximum ν_{mz}, the density is taken to be proportional to ν. The corresponding Debye temperatures are defined as follows:

$$k\Theta_{0z} = h\nu_{0z}, \quad \text{and} \quad k\Theta_z = h\nu_{mz}.$$

The xy modes are similarly treated. The values of the various constants used are:

$$\left.\begin{array}{lll} n_z = 19 \times 10^{-6}, & \Theta_{0z} = 7^\circ\text{K}, & \Theta_z = 1000^\circ\text{K} \\ n_{xy} = 10 \times 10^{-6}, & \Theta_{0xy} = 7^\circ\text{K}, & \Theta_{xy} = 2500^\circ\text{K} \end{array}\right\}$$

(see Keesom and Pearlman 1955), where n_z and n_{xy} are, respectively, the fractions of the normal modes which have frequencies below ν_{0z} and ν_{0xy}.

Formulae for the multiphonon inelastic scattering cross section, which have been derived by us in an earlier paper (Kothari and Singwi 1955), can easily be modified to the case of an anisotropic lattice of the graphite type. In the present case it is not possible to expand the Debye–Waller factor and use the Placzek expansion (Placzek 1954) for the cross section. We have, therefore, calculated separately the one and two phonon cross sections for 10 Å neutrons using the incoherent approximation. The numerical work involved is long and tedious but straightforward. The results are plotted in the figure. Curves $\sigma_{01}^{(z)}$ and $\sigma_{01}^{(xy)}$ respectively represent the contributions of z and xy modes to the one phonon cross section (the first subscript denotes the number of phonons emitted while the second denotes the number of phonons absorbed). $\sigma_{02}^{(z)}$ represents the contribution of the z modes to the two phonon cross section. In the temperature range considered, the corresponding contribution from the xy modes is expected to be small because of the large value of Θ_{xy}. Further the calculations are tedious and, therefore, we have evaluated $\sigma_{02}^{(xy)}$ only for graphite temperature of 1000°K. The value obtained is indicated in the figure by a circle (this has not been included

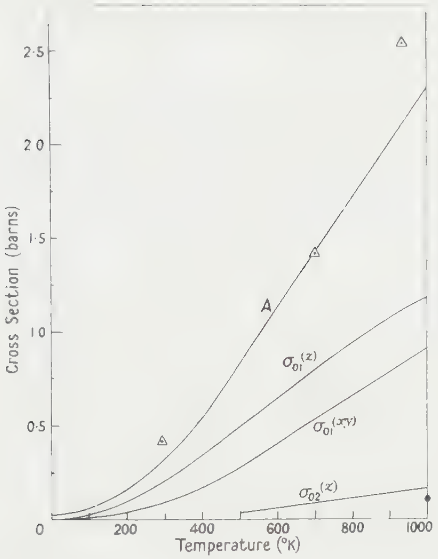

Cross section against graphite temperature for 10 Å neutrons.

in curve A). The contributions σ_{20} and σ_{11} are each much less than σ_{02} and have been neglected. The total calculated scattering cross section plus the absorption cross section ($\sigma_a = 0{\cdot}025\,b$) is shown as curve A in the figure. The experimental points of the Brookhaven group † are also marked there.

It will be seen from the figure that the agreement between the calculated and the experimental values of the cross section is reasonably good. It may, however, be mentioned that for 10 Å neutrons Dr. Palevsky attributes a maximum contribution of 0·1 barn to the observed cross section on account of small angle scattering in the graphite sample. If we subtract 0·1 barn from his experimental values and note that the theoretical values will be slightly increased in the high temperature range on account of the contribution coming from $\sigma_{02}^{(xy)}$, the agreement is further improved. The discrepancy then is not more than about 10%.

In view of the above results and its success in explaining the specific heat at low temperatures, the model of graphite adopted for these calculations appears to be a reasonably good working model.

Atomic Energy Establishment,
Apollo Pier Road,
Bombay 1, India.
27th November 1956.

L. S. Kothari.
K. S. Singwi.

Hughes, D. J., 1953, *Pile Neutron Physics* (Cambridge, Mass : Addison-Wesley), p. 251.
Keesom, P. H., and Pearlman, N., 1955, *Phys. Rev.*, **99**, 1119.
Kleinman, D. A., 1951, *Phys. Rev.*, **81**, 326.
Kothari, L. S., and Singwi, K. S., 1955, *Proc. Roy. Soc.* A, **231**, 293.
Krumhansl, J., and Brooks, H., 1953, *J. Chem. Phys.*, **21**, 1663.
Placzek, G., 1954, *Phys. Rev.*, **93**, 895.

---

† We are thankful to Dr. Palevsky for communicating these results to us prior to publication. According to him the best available experimental results are for 10 Å neutrons.

REVIEWS OF BOOKS

Acht- und Neunstellige Tabellen zu den Elliptischen Funktionen, by M. Schuler and H. Gebelein. Pp. xxiv + 296 (Berlin: Springer, 1955). DM 58.

This volume represents another attempt to tabulate the elliptic functions in a way which will enable them to be used more easily in numerical calculations. Theory introduces them, in the most elementary way, as generalizations of the circular functions, sn u being the inverse of the familiar elliptic integral. In any case, the functions sn u, cn u, dn u, are inconvenient to tabulate. They are functions of two variables, and have awkwardly placed infinities.

In the present volume, the tables of most direct use to the computer give the logarithms of sn u/sin x, cn u/cos x and of dn u as functions of z. There are also tables from which the elliptic integrals K and E may be obtained directly. Here $x = \pi u/2K$ and $z = \cos 2x$. The modulus is taken as Jacobi's q, and the relation between this and Legendre's θ is also tabulated.

The selection of this form in which to tabulate the functions appears likely to be a useful one, but only longer experience can really show whether this is so.

The book is well printed and bound, and the explanation of the tables is given in English as well as German. J. H. AWBERY.

Fünfstellige Tabellen zu den Elliptischen Funktionen, by M. Schuler and H. Gebelein. Pp. x + 114 (Berlin: Springer, 1955). DM 29·60.

The main tables are those of log sn u/sin x, log cn u/cos x, and log dn u, with the modulus taken as Jacobi's q and not Legendre's $k = \sin\theta$, but a table of the relation between q and θ is given. The arguments u and x are related by $u = 2kx/\pi$ where, of course, K is the complete integral of the first kind for the modulus q, which again is tabulated separately.

The quantities mentioned in the first line are actually given as functions of $z = \cos 2x$ and q, so that quite a lot of auxiliary calculation is necessary before the value of sn (u, k) can be obtained from the tables. However, all aid needed for interpolation is supplied, and only experience can show whether these tables will rob computation with elliptic functions of the tedium hitherto associated with it.

J. H. AWBERY.

Elementary Wave Mechanics with Applications to Quantum Chemistry, by W. Heitler, 2nd. Edn, Pp. viii + 193. (Oxford: Clarendon Press, 1956.) 18*s*.

The writer of an elementary and introductory book for the general reader on the principles of wave mechanics must of necessity devote his work to some particular aspect of the subject, or must lay emphasis on a special application of it, in order to bring out its characteristic features. In writing this book Professor Heitler has made it his aim to give a readable account of the fundamental principles of his subject and to show how they can be applied in chemistry.

In this second edition, he has remained faithful to his original purpose and has gone further with it in adding work on diatomic molecules and on the subject of the chemical bond.

This purpose gives direction to his introduction to the principles of the subject. Having explained how the wave equation is derived, he applies it to the case of the hydrogen atom, keeping in mind the practical aspect both of the equations and their solutions. He then discusses the subject of angular momentum and of the ordering of quantum states.

A valuable feature of the book and one which gives it a special character amongst short introductory accounts of the quantum theory is the chapter on the problem of two electrons where the question of exchange degeneracy and the use of symmetrical and anti-symmetrical functions is explained. This part of the book, almost exactly one half of it, ends with a short chapter on perturbation theory.

This account of general principles will be found of value to any student of the quantum theory whether he is interested in special applications or not. The work may certainly be recommended to the general reader and to students of physical chemistry, but on account of its lucidity and directness it will be found of great help to undergraduates whose main interest is in physics.

The second half of the book is concerned with the advances made in our understanding of the interactions existing between molecules as a result of the application of the quantum theory. Especially noteworthy is a chapter on the theory of the homopolar chemical bond, a theory to which the author himself has largely contributed.

In the space of this book it has not been possible to go very deeply into the problems which arise, but the principles are here and the account is stimulating. It would have been a good plan to include references to more extensive works on the topics treated. References given throughout the book are scarce, in fact almost absent. This could well be remedied in future editions, for many readers will wish to continue with the subject after reading this introductory account of it.

H. T. FLINT.

Abacs or Nomograms, by A. GIET. Pp. ix + 225. Translated and revised by J. W. Head and H. D. Phippen. (London: Iliffe; New York: Philosophical Library.) 35*s*.

Even in the age of electronic computers, the nomogram will still be welcomed by physical scientists and engineers to help with routine approximate calculations. This book can be recommended for its lucid exposition of the methods by which the common types of nomogram are constructed. Both author and translators are to be congratulated on the way in which the topic is presented. As is necessary, the diagrams are excellent.

On a first reading it seems free from error and lacking in ambiguities. The many examples are carefully laid out in stepwise progression. There is no index, but the table of contents is very comprehensive. There is also an appendix which summarizes the types of abac appropriate to various forms of relationship between the variables to be plotted.

It is very doubtful whether most people would be prepared to pay much of a price to possess a personal copy, since the construction of nomograms is essentially an occasional exercise for which most of us would rely on library books for guidance. The publishers seem to have us weighed up, and have fixed a sufficiently high price to break even. The book should appear in most libraries and, once it is known, I have little doubt it will become the most popular of the reference books on this topic at present available.

M. J. MORONEY.

Automatic Digital Calculators, by A. D. Booth and K. H. V. Booth. Pp. ix+261. (London: Buttersworths Scientific Publications, 1956). 32*s*.

This book is intended to serve as a guide to the theory of automatic digital computers, and covers both the design of the machines and the methods of application.

The book covers a very wide field and the stress, in the design section of the book, tends to be directed more to a description of the computing units in the form of block diagrams as opposed to a description of the actual circuits themselves.

The last five chapters deal with machines from the users' point of view, and hence will be of most interest to the general reader. Here the authors start by discussing the basic operations necessary for a complete instruction code for a machine, particular reference being made to the authors' own machine, the APE(X)C at Birkbeck College. The next three chapters describe the technique of programming and coding, i.e. the breaking down of the calculation into convenient parts and the translation of these parts into the detailed arithmetical operations which the machine performs. Some numerical methods that might be employed in this connection, for example, interpolation and Chebyshev approximation, are described.

The last chapter describes some applications of computers. These include X-ray crystal structure analysis and the mechanical translation of languages, both of which the authors have helped to develop.

This edition differs little from the first edition (1953), and gives only a very brief account of some of the recent developments in the field, e.g., ferrite core storage and the use of transistors. However, the bibliography, which was a good feature of the first edition, has been considerably expanded to bring it up to date.

R. A. BROOKER.
R. L. GRIMSDALE.

The Theory of Photons and Electrons, by J. M. Jauch and F. Rohrlich. Pp. xiv+488. (Cambridge, Mass.: Addison-Wesley; London: Academic Books, 1955.) $10.

At a time when in so many directions in high-energy physics the accumulation of experimental data has outstripped their theoretical interpretation and the question of the usefulness of the whole elaborate edifice of field theory is sometimes raised, it is refreshing and stimulating to turn to a part of quantum field theory that has been placed on a firm and sure foundation since the end of the war. The basic advance in this field arose, of course, from the discovery of the Lamb–Retherford shift in 1947; this development provided just the stimulus needed for the imaginative and elegant work by Schwinger, Tomonaga, Feynman, Dyson and others, which has led to our present confidence in the power and usefulness of quantum radiation theory. Of course many difficulties remain, in the infinities that continue to plague the theory, and in the bases of the mass and charge renormalization methods that have been developed. But the almost uncanny accuracy with which it is possible to account for the experimental observations in this field tends to minimize the importance of these difficulties in the eyes of the physicist.

The appearance of the present work is timely. It satisfies a need for a clear and consistent presentation of quantum radiation theory in terms of the new methods. Elegance in presentation is the keynote of the whole book. In their preface the authors state, " Elegance, in our opinion, is not just an irrelevant luxury in a scientific theory. We consider it a principle of economy of the greatest pedagogical value ". This approach leads them to break away from the historical development of the quantum field theory from the classical model and the canonical formalism. The quantum theory is taken, right from the start, as the basic theory : the classical theory as a special case, valid under certain conditions.

Nevertheless, the emphasis on elegance of formulation does not mean the submergence of the physical ideas. The last six of the sixteen chapters are indeed devoted to the application of the theory to calculations of great physical interest such as Compton scattering, Delbrück and Rayleigh scattering, pair production and annihilation, bremsstrahlung, electron scattering by electrons and nuclei, and so on.

The book can be conveniently divided into three main parts. In the first six chapters, general principles of relativity and quantum mechanics are set out and the theory of the free radiation field, the free electron field and the coupling of the two fields developed. The next four chapters provide the technique for the application of the theory to specific problems. The S matrix is introduced and its approximate evaluation discussed, the method of use of Feynman–Dyson diagrams being described with great clarity in this connection. This section of the book contains also a discussion and classification of the various divergences that occur and of the methods of mass and charge renormalization. The reader is then in a position to appreciate the applications mentioned above, which are described in the remaining chapters. A series of eight most useful appendices, including one on the powerful methods of Feynman integration, concludes the book.

This work is a most notable contribution to the literature of modern theoretical physics. It does not constitute elementary reading, but it is undoubtedly destined to have a very wide influence on the training of research workers in this field. E. H. S. BURHOP.

CONTENTS OF SECTION B

PAGE

Mr. A. C. Chapman, Dr. P. Rhodes and Dr. E. F. W. Seymour. The Effect of Eddy Currents on Nuclear Magnetic Resonance in Metals 345

Mr. A. M. Goodbody. The Influence of Condenser Aperture on the Resolution of a Pair of Parallel Lines 361

Prof. B. N. Srivastava and Mr. S. C. Saxena. Thermal Conductivity of Binary and Ternary Rare Gas Mixtures 369

Dr. A. R. Stokes. The Theory of Light Scattering by Suspensions of Randomly Oriented Long Prisms 379

Dr. P. G. Harper. The Interaction of Electrons with Lattice Vibrations . . 390

Mr. E. A. Neppiras. Metal Fatigue at High Frequency 393

Dr. R. A. Sack. Relaxation Processes and Inertial Effects. I: Free Rotation about a Fixed Axis 402

Dr. R. A. Sack. Relaxation Processes and Inertial Effects. II: Free Rotation in Space 414

Research Notes:

Mr. J. S. Dryden and Mr. R. J. Meakins. Examples of the Maxwell–Wagner Type of Dielectric Absorption using Wool Wax–Water Mixtures. 427

Mr. E. H. B. Williams. A General Theory of the Surface Friction of Solids 431

Prof. A. Piekara, Mr. J. Małecki, Mr. M. Surma and Mr. J. Gibalewicz. Note on Production of Strong Magnetic Fields of Short Duration and Measurement of their Intensity 432

Mrs. L. M. Roberts. The Atomic Heat of Samarium from 2° to 20°K . 434

Prof. E. R. Andrew and Mr. K. M. Swanson. A Method for Determining the Nuclear Relaxation Mechanism in Crystals 436

Letters to the Editor:

Dr. R. F. Pearson. Domain Patterns on Ferrite Single Crystals 441

Reviews of Books 442

Book Notices 447

Corrigendum:

C. H. Champness 447

Contents of Section A 448

K-meson Decays through a Fermi Interaction

By J. C. POLKINGHORNE, D. L. PURSEY and H. A. SANTA MARIA
Tait Institute of Mathematical Physics, University of Edinburgh

Communicated by N. Kemmer; MS. received 30th January 1957

Abstract. The decay of K-mesons by means of a weak Fermi interaction is investigated. For the decay of the θ^+ into π^+ and π^0 only $\Delta I=3/2$ contributes. It is shown that if the only hyperon taking part is Λ then the interaction must be S-A-P for pure $\Delta I=3/2$. The case in which other hyperons participate is considered. For a Σ-nucleon interaction it is necessary to have S-A-P for pure $\Delta I=5/2$. Some other less specific results are also obtained.

---

§ 1. Introduction

The approximate equality of the strength of the interaction producing the decays of the 'curious' particles with the strength of the β-decay interaction led Gell-Mann (1955 unpublished) to suggest that the decays might take place through an extended Fermi interaction involving hyperons as well as nucleons and leptons. The single weak Fermi interaction would form the only weak link in a chain of otherwise strong virtual interactions producing the decay.

A decay of particular interest is that of the θ^+ into two pions. If the θ^+ has spin zero the pions produced must be in an $I=2$ state. The decay would therefore be characterized by $\Delta I=3/2$.

The ordinary Fermi interactions are those between the pairs of fields (P, N) (μ, ν) and (e, ν). The simplest extension would be to add the pair (P, Λ). In fact it will be convenient to consider also Fermi interactions between four neutral baryons. This is because we are interested in the pure $\Delta I=3/2$ operator and using the Λ this requires the interactions

$$\left.\begin{array}{l}\overline{\Lambda}+\mathrm{P}\rightarrow\overline{\mathrm{N}}+\mathrm{P},\\ \overline{\Lambda}+\mathrm{N}\rightarrow\overline{\mathrm{P}}+\mathrm{P},\\ \overline{\Lambda}+\mathrm{N}\rightarrow\overline{\mathrm{N}}+\mathrm{N}.\end{array}\right\}\qquad\ldots\ldots(1)$$

In § 2 we investigate the case in which Λ is the only hyperon used and all pion radiative corrections are considered. We find that only that part of the interaction given by S-A-P gives $\Delta I=3/2$. In § 3 possible interactions involving the Σ and Ξ are considered. For the Σ-nucleon interaction we require S-A-P to give $\Delta I=5/2$. Other less specific results are also obtained.

§ 2. Interactions Involving Λ

If the Fermi interaction only involves Λ and nucleons there are three isotopic spin $\frac{1}{2}$ fields from which to form an $I=3/2$ isotopic operator. Such an operator must be completely symmetric in the isotopic indices of the fields. For the interaction exemplified by figure 1(a), the operator is given by

$$\begin{aligned}\mathrm{O}_{-1/2}(\tfrac{3}{2})=&\overline{\Lambda}^{(1)}(0)\mathrm{N}_{-1/2}^{(2)}(\tfrac{1}{2})\overline{\mathrm{N}}_{1/2}^{(3)}(\tfrac{1}{2})\mathrm{N}_{1/2}^{(4)}(\tfrac{1}{2})\\ &+\overline{\Lambda}^{(1)}(0)\mathrm{N}_{1/2}^{(2)}(\tfrac{1}{2})\overline{\mathrm{N}}_{1/2}^{(3)}(\tfrac{1}{2})\mathrm{N}_{-1/2}^{(4)}(\tfrac{1}{2})\\ &+\overline{\Lambda}^{(1)}(0)\mathrm{N}_{1/2}^{(2)}(\tfrac{1}{2})\overline{\mathrm{N}}_{-1/2}^{(3)}(\tfrac{1}{2})\mathrm{N}_{-1/2}^{(4)}(\tfrac{1}{2}).\end{aligned}\qquad\ldots\ldots(2)$$

Lorentz indices are omitted. The superscripts refer to the ordering of the fields in the Fermi interactions and $N_i(\frac{1}{2})$, $\overline{N}_i(\frac{1}{2})$, $(i = -\frac{1}{2}, \frac{1}{2})$, are the components of the nucleon and antinucleon isotopic doublets respectively. $O_{-1\,2}(\frac{3}{2})$ is symmetric under the permutation of the subscripts and this implies that there is a symmetry between the three interactions (1). Since particles 2 and 4 belong to the same (nucleon) doublet the isotopic symmetry of their subscripts can be translated into a symmetry of their superscripts. Explicitly the interaction must be symmetric under the permutation P_{24}, interchanging the positions in the interaction of the fields 2 and 4.

Since fields 3 and 4 belong to different doublets we cannot use this argument to obtain symmetry under P_{34}. To investigate the symmetry appropriate to this case it is necessary to consider the effect of Furry's theorem on the second fermion loop. This is somewhat complicated by the need to take isotopic spin and charge conservation into account.

The first case to be considered is that in which a positive charge is carried from the first loop to the second loop by the interaction

$$\overline{\Lambda} + P \rightarrow \overline{N} + P.$$

There must be an odd number of *charged* meson vertices in the second loop, starting and ending with a π^+ vertex and alternating in the sign of charge. Any number of π^0 vertices may be inserted before, or between, and after the charged pions. Furry's theorem links this with the graph in which all the π-vertices appear in reversed order. This is a possible graph for charge conservation. It differs from the first graph in that π^0's formerly coupled to a proton are now coupled to a neutron and vice versa. This introduces an extra sign of $(-1)^{n_{\pi^0}}$, n_{π^0} being the number of π^0 vertices, into the result of Furry's theorem.

The second case to be considered is that in which no charge is carried across from the first loop to the second loop by the interactions

$$\overline{\Lambda} + N \rightarrow \overline{N} + N$$
$$\overline{\Lambda} + N \rightarrow \overline{P} + P.$$

For $\Delta I = 3/2$ the corresponding interactions have equal coupling constants. For the first of them there must be an even number of charged meson vertices in the second loop, starting with a π^- vertex, ending with a π^+ vertex and alternating in the sign of charge. Furry's theorem links this with the graph in which all the π vertices appear in the reversed order. This does not give charge conservation for the first (neutron) process but it does for the second (proton) process. Thus for $\Delta I = 3/2$ there is again a simple Furry's theorem with an extra sign $(-1)^{n_{\pi^0}}$.

For $\Delta I = 3/2$ the results can be summarized:

(i) An even number of π^0 vertices (virtual or real) in the second loop: Simultaneously symmetric under P_{24} and P_{34}.

(ii) An odd number of π^0 vertices in the second loop: Simultaneously symmetric under P_{24} and antisymmetric under P_{34}.

There is no non-vanishing Fermi interaction satisfying the condition (ii) and only the 'remarkable' interaction, S-A-P, of Critchfield and Wigner (1941, 1943) satisfies (i). Thus for pure $\Delta I = 3/2$ we require S-A-P and graphs with an odd number of π^0 vertices in the second loop will vanish.

This result is true taking into account all pion radiative corrections. There does not seem any reason, in view of the strong pion–nucleon coupling, to neglect these. If, however, only the basic graphs are considered it is easy to show that only graph (*a*) need be considered. All other basic graphs may be paired off into graphs giving contributions of opposite sign. To show this use must be made of the symmetry between the pion momenta in the final even parity state. It is then easy to verify the general conclusion explicitly for this case. It is only necessary to consider graph (*a*) and the mutually cancelling pair of graphs in which the π^+ is emitted from the first loop and the π^0 from the second. The symmetry properties are then manifest.

If K-meson radiative corrections are considered it is possible to prove a similar result for most graphs by applying a generalized Furry's theorem to all closed fermion loops connected by virtual K-mesons. This fails, however, for graphs in which the two basic loops are directly or indirectly coupled in this way.

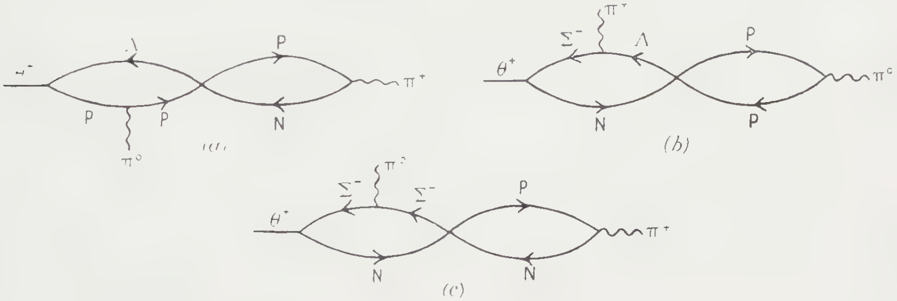

Figure 1.

§ 3. INTERACTIONS INVOLVING OTHER HYPERONS

Interactions such as that given by figure 1(*b*) are essentially the same as those of §2 since they only involve Λ and nucleons at the weak vertex. The interaction

$$\overline{\Lambda}+\mathrm{N}\rightarrow\overline{\Xi}+\Xi$$

will not give the results of §2 since the particles 2 and 4 are now members of different doublets and isotopic symmetry cannot be transformed to P_{24} symmetry.

If the Σ is coupled to the nucleons to give such graphs as figure 1(*c*) it is now possible to form a $\Delta I=5/2$ operator at the weak vertex. This must be symmetric in the isotopic components of all four fields. Again it is possible to use this fact together with the generalized Furry's theorem to show that only S-A-P gives a pure $\Delta I=5/2$ operator. Dalitz (1956) finds that such an operator must represent 6% of the interaction to explain the decay of the τ^+. No very strong results can be deduced for the $\Delta I=3/2$ operator, since the three nucleon fields can combine in an $I=3/2$ or $I=1/2$ operator and still combine with Σ to give $I=3/2$. If basic graphs without radiative corrections are considered some cancellations can be obtained between graphs but they do not substantially reduce the complications.

ACKNOWLEDGMENTS

We wish to thank Professor Kemmer and Professor Salam for a helpful discussion. One of us (H.A.S.) also wishes to thank the British Council for a Scholarship.

REFERENCES

CRITCHFIELD, C. L., 1943, *Phys. Rev.*, **63**, 417.
CRITCHFIELD, C. L., and WIGNER, E. P., 1941, Phys. Rev., **60**, 412.
DALITZ, R. H., 1956, *Proc. Phys. Soc.* A, **69**, 527.

Elastic Scattering of 32 MeV Protons from Gold

By S. N. GHOSHAL† and B. B. BALIGA
Institute of Nuclear Physics, Calcutta

MS. received 13th November 1956 and in revised form 15th January 1957

Abstract. The results of an experiment on the elastic scattering of 32 MeV protons from the Berkeley linear accelerator by gold, which had been performed several years ago, are reported. The photographic plates which had been employed for detection of the scattered protons have been recently scanned systematically. The differential scattering cross section has been plotted as a function of the scattering angle. These include contributions of the inelastic scattering of protons from several low lying levels in ^{197}Au. To estimate this effect, the differential distribution of the ranges of the scattered protons in the photographic emulsion has been determined. From this range distribution curve the upper limit of the differential elastic scattering cross section at various scattering angles has been estimated. The positions of the maxima and minima in the cross section curve agree approximately with those given by the elementary theory of diffraction. The results have been compared with the theoretically calculated cross sections obtained by employing Montroll–Greenberg variational method using the optical type square well potential.

§ 1. INTRODUCTION

The spectacular success of the optical model of the nucleus in explaining the total scattering cross section of neutrons in the energy range of 1 to 3 MeV (Feshbach, Porter and Weisskopf 1954) has prompted investigations of the elastic scattering of intermediate energy protons in order to test the validity of this model in the latter case. In particular, the angular distribution of the elastic scattering of protons of different energies by various nuclei has been measured by a number of investigators (Burkig and Wright 1951, Gugelot 1952, Cohen and Neidigh 1954, Schrank 1955, Gove 1955, Melkanoff *et al.* 1955, Dayton and Schrank 1956). Theoretical interpretation of these results using the optical type complex potential, both with sharp as well as diffused boundaries has been attempted by several workers. The growing interest in this type of work has prompted us to publish an account of an experiment of similar type, performed by one of the authors with the 32 MeV proton beam of the Berkeley linear accelerator during 1949–50. At that time only a few plates (the protons were recorded photographically) had been scanned. These preliminary results had been briefly reported earlier (Ghoshal 1950). Systematic scanning of all the plates was undertaken only recently, and the results of these scannings will be presented here.

§ 2. EXPERIMENTAL METHOD

As already mentioned, the scattered protons were detected photographically. The scattering chamber used was similar to the one developed by Levinthal *et al.* (1950). A schematic diagram of the arrangement used is shown in figure 1.

---

† Now at the Physics Department, Presidency College, Calcutta.

The target and the plate holders were all assembled on a large $\frac{3}{4}$ inch thick plate of dural which constituted the lid of the scattering tank which could be evacuated. The target was gold foil, about 10 mg cm^{-2} thick. The target and the target holder arrangement were such that only protons scattered from the former could reach the plates, while protons scattered from the collimating slits would be prevented from doing so.

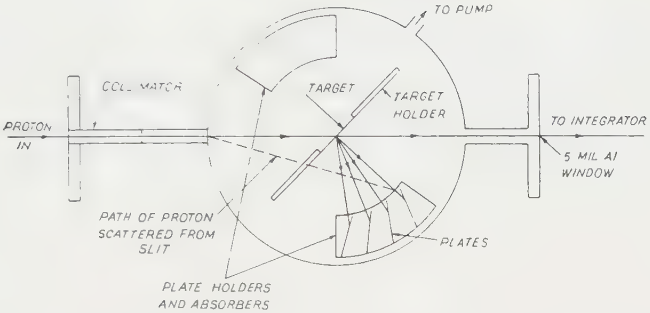

Figure 1. Schematic diagram of scattering chamber and plate holders.

The plates were Ilford C2 of 100 μ thickness. The scattered protons reached them at an angle of 17·5° along the mean direction of scattering for the different scattering angles at which measurements were performed. The range of scattering angles varied from 18° to 150°. There were defining slits whose widths were $\frac{1}{16}$ inch for the forward directions of scattering and $\frac{1}{8}$ inch for the backward directions through which the protons could reach the plates (see figure 2). This defined the angles of scattering to $\pm\frac{3}{4}°$ and $\pm 1·5°$ respectively in these directions.

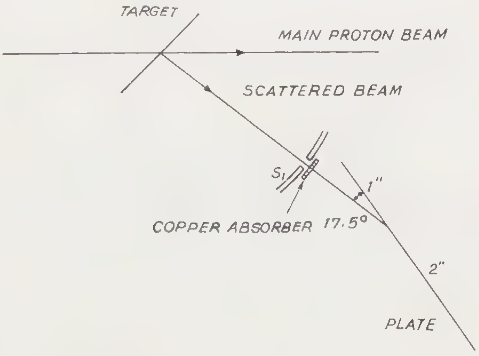

Figure 2. Details of the plate holder.

Behind the slit were copper absorbers of required thicknesses put in such a way that they were perpendicular to the path of the protons reaching the plates. These absorbers were used to reduce the energy of the protons such that the latter would spend their residual ranges within the thickness of the emulsion. Total exposure on each plate was obtained by allowing the main beam to enter into an integrator after it emerged at the back of the scattering chamber.

After the exposed plates had been developed, they were scanned under a microscope with oil immersion objective and the number of proton tracks on a known area was counted. The solid angle subtended by the area scanned at the centre of the target could easily be calculated from the known geometry of the arrangement.

Only those tracks were selected for counting which started at the top of the emulsion and had the right directions. Allowances were, however, made for multiple scattering of the protons within the copper absorbers in front of the defining slits.

For each plate exposed with the target on, a second plate was exposed without the target. Thus the background effect, which was negligible in most cases, could be substracted. The background tracks were usually short, and in order to avoid confusion no tracks were counted as genuine which had a length less than a minimum value. This minimum limit was arbitrarily fixed at 50 μ, since it was found that the genuine tracks with length below 50 μ constituted less than 1% of the total number of tracks in all the plates.

§ 3. Experimental Results

In figure 3, the differential cross sections for the scattering of protons at various angles have been plotted. It should be noted that the cross sections plotted in figure 3 include the effect of inelastic scattering of protons from various low lying levels in gold.

Now the 1415 mg cm^{-2} of copper absorber used in the defining slits in front of the plates cuts out all protons with an energy below about 29·5 Mev. Since the incident energy was 31·5 Mev, this means that protons inelastically scattered from levels in ^{197}Au lying above 2 Mev cannot reach the plates. Between 0 and 2 Mev, ^{197}Au have the known levels shown in the table, reported by various observers.

Levels in ^{197}Au

Levels (Mev)	Reference
0·077	Heydenberg & Temmer (1954).
0·190	Heydenberg & Temmer (1954).
0·277	Heydenberg & Temmer (1954), Huber *et al.* (1953), Goldberg & Williamson (1954).
0·545	Goldberg & Williamson (1954), Ebel & Goodman (1954).
1·200	Martin *et al.* (1954).
1·440	Ebel & Goodman (1954).
2·000	Martin *et al.* (1954).

The above table shows that some of the levels reported are quite close to the ground state in gold and if there is appreciable inelastic scattering from them they cannot be distinguished from the elastically scattered protons. To analyse the spectrum of the scattered protons as recorded on the plates, the differential range versus number of proton tracks were plotted for the plates at different angles. Two of the histograms of these data are given in figure 4, one for a small angle of scattering and another for a large angle of scattering.

If only elastically scattered protons were present, these curves should have been approximately gaussian in nature with one peak. The energy spread of the incident beam would introduce departure from a truly gaussian curve. However, from the histograms it is found that more than one peak is present at all angles of scattering. Of these, the one having the greatest value of the range should correspond to the elastic peak.

In all the histograms there are two close prominent peaks separated by about 40 microns in range. If the peak having the greater range corresponds to the elastically scattered protons, the other would correspond to inelastic scattering from a level about 0·5 MeV higher than the ground state, which is probably the same as the well known 0·55 MeV level in ^{197}Au (see the table). In some of the plates there is evidence for the appearance of another peak whose position indicates that this probably corresponds to the 1·2 MeV level in ^{197}Au. The lengths of the proton tracks scattered from this level are so short that they may escape being recorded in some of the plates if the whole spectrum is slightly shifted to smaller values of ranges in these plates. The reason for such shift could be due to (1) different fractions of energy taken away by the recoiling nucleus at different scattering angles, (2) different thicknesses of the scatterer penetrated by the protons at different scattering angles, (3) non-uniformity of the thicknesses of the copper absorbers used at different scattering angles, the absorbers having been cut from larger sheets of copper whose average thicknesses were known.

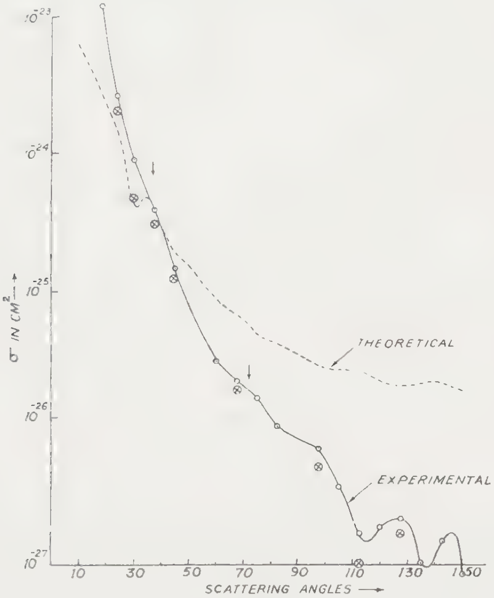

Figure 3. Differential elastic scattering cross section from gold as a function of scattering angle. Crossed circles give upper limits to the differential elastic scattering cross section after subtracting the inelastic contribution from the experimental curve. The arrows indicate the positions of maxima in the differential cross section curve.

It is not possible to say anything definitely regarding the contribution of the inelastically scattered protons from these graphs. However, Dayton and Schrank (1956) have shown that the ratio of inelastic scattering cross section to the differential elastic scattering cross section is quite small at all scattering angles for heavy elements (like Pt, Au) for $E_{\rm p} = 17$ MeV. If we assume that this is also true for $E_{\rm p} = 32$ MeV, then we can take the area under the observed elastic peak in the differential range spectrum curve to give an estimate of the upper limit of the elastically scattered cross section at various angles. In figure 2 these upper limits to the differential elastic scattering cross section have been plotted as a function of the scattering angle. These have been obtained by multiplying the cross sections

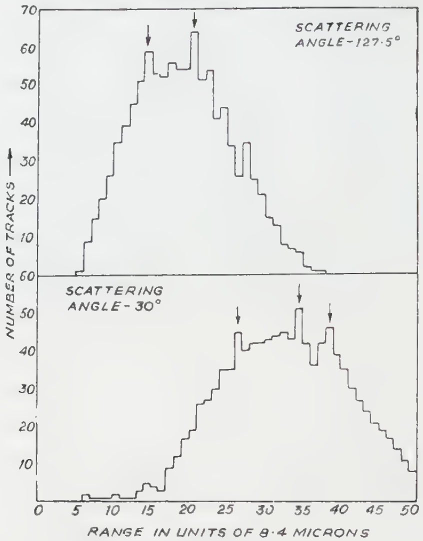

Figure 4. Distribution of the residual ranges of the scattered protons in emulsion at different scattering angles. The positions of the peaks are indicated by arrows. They are shifted to higher values of ranges at smaller scattering angles.

in figure 1 by the ratio of the area under the elastic peak to the total area under the range–frequency curve at various angles. However the corrected points still include the effect of inelastic scattering from levels below 0·55 Mev.

§ 4. Discussion of the Results

A close examination of the experimental cross section curve in figure 3 shows that there is a slight inflection of the curve at the scattering angle of about 37° and another more prominent one at an angle of 72°. When the effect of inelastic scattering is subtracted the first inflection becomes quite pronounced, pointing to the existence of a maximum in the cross-section curve at an angle of 37°. The other inflection point is sufficiently prominent even without correcting for inelastic scattering to reveal the existence of a maximum at the scattering angle of 72°.

Kinsey and Stone (1956) have recently measured elastic scattering cross sections for 31·5 Mev protons from different scatterers with Z up to 47 (silver). Similar measurements have been made for protons at three other energies. They have observed maxima and minima in their cross section curves for the different scatterers, whose positions agree with the predictions of elementary diffraction theory. To demonstrate this, they have plotted the cosecant of the half angle of scattering at the first and second maxima against $2KR$ where K is the wave number outside the nucleus calculated in the centre-of-mass system and R is the radius of the scattering nucleus. The points fall on two straight lines for the two maxima whose slopes agree with those given by the diffraction formula. These straight lines are reproduced in figure 5. In this we have plotted the cosecants of the half angles giving the positions of the two maxima for gold mentioned above. Of these, the

37° point falls close to the Kinsey straight line plot corresponding to the first maximum. The 72° point, however, falls much below the line of the second maximum. We thus associate the 37° inflection with the first diffraction maximum in the case of scattering from gold.

From the Kinsey plot it is found that the second maximum for gold should appear at an angle of about 47°. Unfortunately the plates corresponding to this scattering angle were damaged so that no experimental data are available in this region. The inflection at 72° probably corresponds to the third diffraction maximum for which the theoretically predicted value of x is 11·6, which is in rough agreement with our observation ($x = 12{\cdot}8$). This also agrees with the positions of third maxima in Kinsey's cross-section curves for zirconium and silver ($x = 11{\cdot}6$ and 11·7 respectively). Because of the relatively large angle at which the third maximum appears its observed position is not expected to be in very good agreement with the position predicted by diffraction theory.

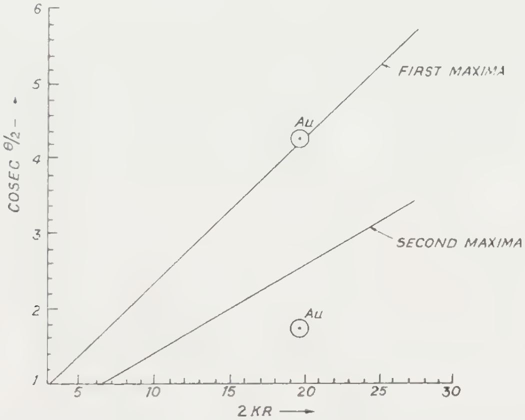

Figure 5. Cosecants of the half angles for the first and second diffraction maxima as functions of $2KR$ from Kinsey and Stone (1956). The straight lines are represented by the equations $2K\,(R+\lambda) = 5{\cdot}2 \operatorname{cosec} \frac{1}{2}\theta$ for the first maximum and $2K\,(R+\lambda) = 8{\cdot}4 \operatorname{cosec} \frac{1}{2}\theta$ for the second maximum. The experimental points corresponding to the first and second maxima for different scatterers (not shown here) determined by Kinsey and Stone fall along these two lines. The points corresponding to diffraction maxima for ^{197}Au at 37° and 72° observed in the present work are shown.

These cross sections have also been calculated using the optical type square-well potential. The calculated cross sections are plotted in the same figure (figure 3). In most of the earlier work on the elastic scattering of protons from nuclei, the calculations have been performed using the partial wave method, since the energies of the protons employed were low (20 MeV). However, because of the relatively higher energy of the protons used in the present experiment, and also due to the high atomic number of the scatterers used ($z = 79$), the partial wave method of calculation was not found very convenient. We therefore employed the Montroll–Greenberg variational method for the calculation of these cross sections (Montroll and Greenberg 1952). The details of the theoretical procedure employed will be published separately. The potential was of the form

$$\begin{aligned} V &= -(V_0 + iW_0) \quad \text{for} \quad r < a \\ &= ze^2/r \qquad\qquad \text{for} \quad r > a \end{aligned}$$

where a is the nuclear radius and Ze is the nuclear charge of the scatterer. The following numerical values were used in the calculations: $V_0 = 45$ MeV, $W_0 = 20$ MeV, $a = 1{\cdot}42 \times A^{1/3} \times 10^{-13}$ cm.

The cross sections calculated from the above considerations have been compared with the experimentally determined cross sections in figure 3. The agreement is not very good.

As is well known, the square-well type complex potential gives results which are in agreement with experimental observations only for scatterers of low nuclear charge, e.g. aluminium. For heavier nuclei, where back scattering is relatively low, this model does not give satisfactory agreement (Peaslee 1955). It appears that a complex potential well with rounded corners gives much better agreement with experimental results both for light as well as for heavy nuclei, up to a proton energy of 22 MeV (Peaslee 1955). Calculations have therefore been started using a complex potential well with rounded corners for proton energy of 32 MeV.

ACKNOWLEDGMENTS

The authors are indebted to Professor Emilio Segrè of the University of California, Berkeley who had suggested the problem to one of the authors (S.N.G.) while he had been working there. Thanks are also due to the crew of the Berkeley linear accelerator for their very close co-operation in making the run of this experiment possible. We are indebted to Professor B. D. Nag Chaudhuri for his kind interest in the work.

REFERENCES

BURKIG, J. W., and WRIGHT, B. T., 1951, *Phys. Rev.*, **82**, 451.
COHEN, B. L., and NEIDIGH, R. V., 1954, *Phys. Rev.*, **93**, 282.
DAYTON, I. E., and SCHRANCK, G., 1956, *Phys. Rev.*, **101**, 1358.
EBEL, A. A., and GOODMAN, C., 1954, *Phys. Rev.*, **93**, 197.
FESHBACH, H., PORTER, C. E., and WEISSKOPF, V. F., 1954, *Phys. Rev.*, **96**, 448.
GHOSHAL, S. N., 1950, *Ph.D. Thesis*, University of California.
GOLDBERG, W. I., and WILLIAMSON, R. M., 1954, *Phys. Rev.*, **94**, 747; *Ibid.*, **95**, 629, 767.
GOVE, H. E., 1955, *Phys. Rev.*, **99**, 1353.
GUGELOT, R. C., 1952, *Phys. Rev.*, **87**, 525.
HEYDENBERG, N. P., and TEMMER, G. M., 1954, *Phys. Rev.*, **93**, 906.
HUBER, O., HALTER, J., JOLY, R., MAEDER, D., and BRUNNER, J., 1953, *Helv. Phys. Acta*, **26**, 591.
KINSEY, B. B., and STONE, T., 1956, *Phys. Rev.*, **103**, 975.
LEVINTHAL, C., MARTINELLI, E. A., and SILVERMAN, A., 1950, *Phys. Rev.*, **78**, 199.
MARTIN, H. C., DIVEN, B. C., and TASCHEK, R. F., 1954, *Phys. Rev.*, **93**, 199.
MELKANOFF, M. A., NODVIK, J., and SAXON, D. S., 1955, *Phys. Rev.*, **100**, 1805.
MONTROLL, E. W., and GREENBERG, S. M., 1952, *Phys. Rev.*, **86**, 889.
PEASLEE, D. C., 1955, *Annu. Rev. Nucl. Sci.*, **5**, 99 (Palo Alto: Annual Reviews Inc.).
SCHRANK, G., 1955, *Phys. Rev.*, **99**, 640.

The Elastic and Inelastic Scattering of Protons by Mg

By G. W. GREENLEES, B. C. HAYWOOD, L. G. KUO AND
M. PETRAVIĆ
Physics Department, University of Birmingham

Communicated by W. E. Burcham; MS. received 23rd November 1956, *and in final form* 19*th February* 1956

Abstract. Absolute differential cross sections are given for the elastic scattering by Mg of protons of energies 9·55 MeV, 9·13 MeV, 8·83 MeV, 8·62 MeV and 7·86 MeV, for an angular range of 25°–165° (centre-of-mass coordinates). The angular distributions show characteristic maxima and minima due to nuclear interference with Coulomb scattering. Absolute differential cross sections for the inelastic scattering of protons at these five energies from the 1·37 MeV level of ^{24}Mg are also given. A marked variation of the angular distribution with energy has been noted.

---

§ 1. Introduction

The elastic scattering of protons of different energies from various elements is of considerable interest in view of the possible theoretical analysis in terms of the complex potential model of the nucleus. This field has been reviewed extensively in a recent paper by Kinsey and Stone (1956).

The angular distributions of proton inelastic scattering in the region of 10 MeV leaving the residual nucleus in discrete excited states have been reported by several authors. In certain cases (Fischer 1954, Freemantle *et al.* 1954, Eisberg and Hintz 1956 and Greenlees and Souch 1956) distributions asymmetric about 90° have been observed. This could be interpreted as evidence for a direct interaction, or, if a compound nucleus mechanism be assumed, a violation of the statistical assumption, provided a sufficient number of overlapping levels are involved in the compound nucleus.

The scattering of protons by Mg has been studied by Greenlees and Souch (1956) at 9·62 and 8·86 MeV and by Fischer (1954) at 9·9 MeV. The elastic scattering at energies of 9·62 and 9·9 MeV show good agreement in their general form as regards angular distribution. The inelastic scattering at these energies, however, show marked differences. While all three distributions are asymmetric about 90°, the one at 8·86 MeV shows a pronounced forward peaking. The present experiments were undertaken with a detecting system different from that of Greenlees and Souch, with a view to investigating more fully the variation of the inelastic and elastic angular distributions with incident proton energy.

§ 2. Apparatus

The 9·8 MeV proton beam from the Nuffield 60 in. cyclotron was extracted and focused in a horizontal plane into the scattering chamber (figure 1). This beam was defined to ± $\frac{3}{4}$° by a collimating telescope and, after passing through the target located at the centre of the chamber, was collected in a Faraday cup and integrated. The integrator used was of the 'charge sharing' type (cf. Lewis and Collinge 1953). The target foil could be set at any angle to the incident beam from outside the chamber.

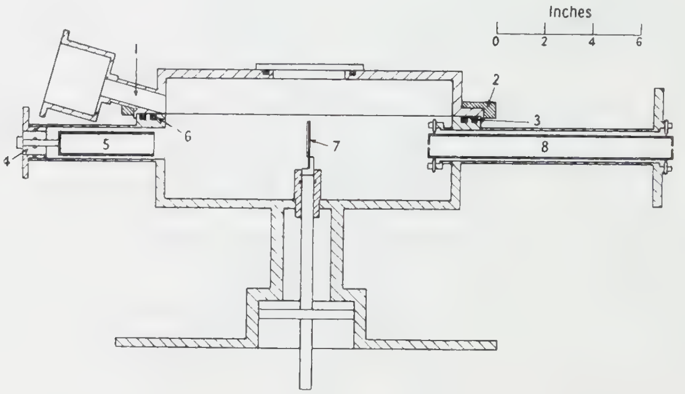

Figure 1. The scattering chamber; 1, counter tube, 2, gear, 3, ball-bearings, 4, insulator, 5, Faraday cup, 6, rubber seal, 7, target holder, 8, collimator.

The detector was attached to the lid of the chamber via a tube set at 15° to the horizontal plane. The end of the tube was vacuum sealed with a mica window which defined the scattered beam accepted to $\pm \frac{1}{2}^\circ$. The whole lid of the chamber could be rotated by means of a motor operated worm drive and gear and was located on ball-bearings with a rubber sealing gasket. Thus the detector could be set at any angle between 15° and 165° to the line of the incident beam. A resistance wire round the lid of the chamber and a bridge circuit enabled the counter angle to be set remotely.

The detector used was a KI (Tl) crystal and photomultiplier arrangement (figure 2). The crystal, 3 mm thick and 13 mm in diameter, was packed in a brass case with a Perspex light guide. The whole was made moisture proof by means of a thin glass plate on one end and a mica window on the other. The light output from the crystal was collected by a Dumont 6292 photomultiplier and the resultant pulses fed via a cathode follower and amplifier into a 60 channel Hutchinson–Scarrott kicksorter.

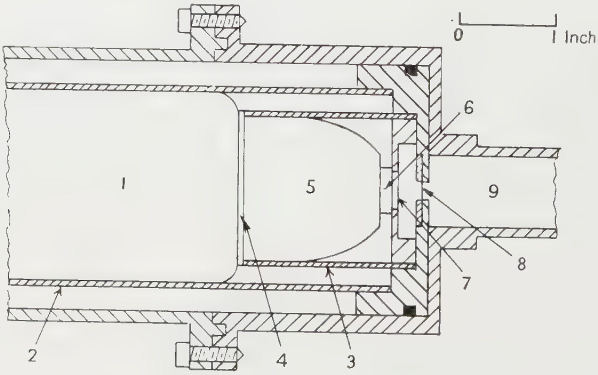

Figure 2. The scintillation crystal mounting; 1, photomultiplier, 2, mumetal shield, 3, brass case, 4, glass plate, 5, Perspex light guide, 6, KI (Tl) crystal, 7, mica window, 8, defining slit and mica window, 9, counter tube.

§ 3. EXPERIMENTAL PROCEDURE

The target used was a piece of natural Mg foil rolled down to a thickness of 2·22 mg cm^{-2}. It was set with its normal at 20° with respect to the incident beam while the counter was in the angular region of 20° to 80°. For counting over the region of 70° to 120°, the target was set at 50°, and for the backward angles, at −10°. This was done in order to minimize loss in resolution due to different loss in energy of protons in the foil. In the regions where the target angle was changed, counter readings were taken at both target angles to provide an overlap which served as a check on the correctness of the target angle setting, and on the uniformity of the foil.

Figure 3 shows a typical spectrum taken at 63° (c.m.) for a known quantity of beam through the target. The two well resolved groups are attributed respectively to elastic scattering from ^{24}Mg, ^{25}Mg, ^{26}Mg and to inelastic scattering from the 1·37 MeV level of ^{24}Mg (cf. Endt and Kluyver 1954). All scattered protons were completely stopped in the crystal. The effective thickness of the target in different positions, which corresponded to proton energy losses of about 150 kev, was mainly responsible for the spread in energy of the incident beam, although the inhomogeneity of the beam from the cyclotron was probably of the same order. As can be seen in figure 3, the final resolution of the peaks in the crystal was about 6%.

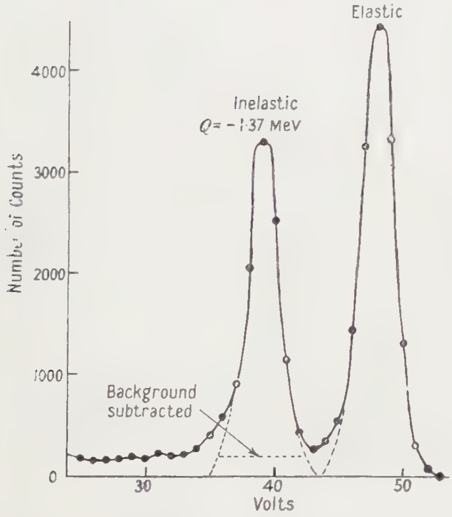

Figure 3. Pulse-height spectrum on the kicksorter for the scattering of 8.83 MeV protons by Mg at 63° (c.m.)

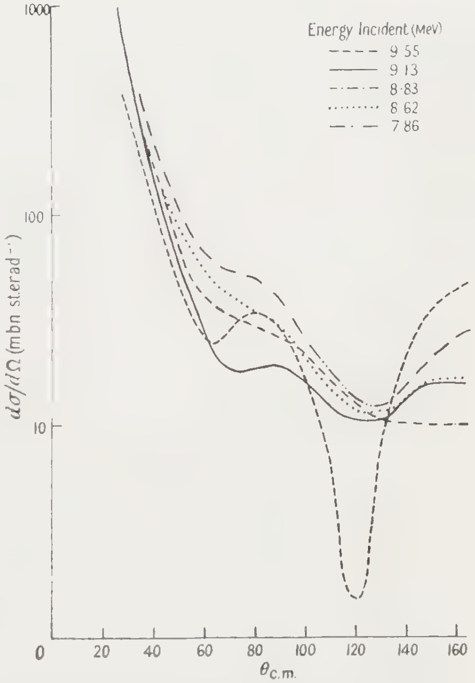

Figure 4. Differential cross sections for elastic scattering of protons of various energies by Mg.

The beam energy was obtained by measurement of the range of protons elastically scattered from a thin gold foil into a photographic emulsion. The energy thus obtained was 9·80 ± 0·07 MeV. Angular distributions were measured at five incident energies: 9·55 Mev, 9·13 Mev, 8·83 Mev, 8·62 Mev and 7·86 Mev; these were obtained by means of a set of Al absorbers in front of the collimator.

§ 4. Results

Since the detection system used recorded all scattered protons, absolute differential cross sections could be obtained from the observed spectra together with a knowledge of the beam intensity used, the thickness of the target, and the solid angle of the detector.

Figure 4 shows the elastic differential cross sections at five energies. In counting the number under the elastic peak (figure 3) no background subtraction was considered necessary. However, the low energy side of the peak always contained some protons inelastically scattered from ^{25}Mg, and the magnitude of this had to be estimated. Uncertainty in dead time corrections (always less than 5%) and in the angular setting of the counter (accurate to $\frac{1}{2}°$) also introduced errors. These were more important at forward angles where counting rates were high and scattering very angle-dependent. The relative values of the cross sections are estimated to be accurate to 3%, while absolute cross sections may have an error of 5%. The angular definition in these measurements was $\pm 1\frac{1}{2}°$.

Figure 5 shows the inelastic differential cross sections at the five incident energies. Here the main uncertainty lay in the estimation of the background which became particularly large at forward angles where elastic scattering was predominant. The error in the relative cross sections is estimated to be 3%. However, the absolute cross sections may only be accurate to 8% owing to systematic errors arising from the background subtraction. There was some indication that all five angular distribution curves showed a rise at 25° (c.m. angle), but because of the uncertainty in the background these points have not been plotted.

The elastic and inelastic angular distributions at 9·55 Mev are shown in figure 6 together with errors on the experimental points.

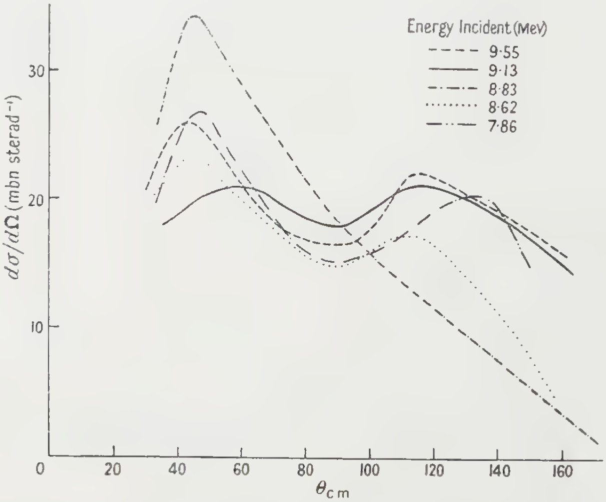

Figure 5. Differential cross sections for inelastic scattering ($Q = -1·37$ Mev) of protons of various energies by ^{24}Mg.

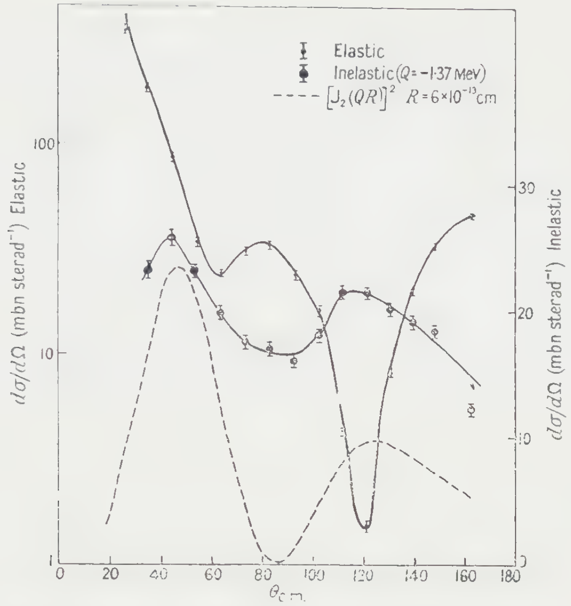

Figure 6. Differential cross sections for elastic and inelastic scattering at 9·55 MeV.

§ 5. Discussion

The elastic scattering of protons in the intermediate energy range by nuclei has been interpreted as scattering from a potential well of the Saxon type

$$V(r) = \frac{V+iW}{1+\exp[(r-R_0)/a]}$$

(Saxon 1955). This has had considerable success for medium heavy nuclei (Glassgold 1956 private communication, Bromley and Wall 1956). Some calculations on the elastic scattering of 10 MeV protons from ^{16}O (Dee 1955, Burge, Fujimoto and Hossain 1956), showed, however, that for such a light nucleus and at such incident energy, the angular distribution could be fitted equally well with a square well of the form $(36+2i)$ MeV and a radius parameter of $R_0 = 1{\cdot}45 \times A^{1/3} \times 10^{-13}$ cm. In the present case it is expected that a square well fit could be obtained at one energy, but it is uncertain whether the same parameters could reproduce the observed variation of cross section with energy. However, since for Mg only a small number of partial waves ($l \leqslant 4$) are important, the change in the relative importance of each of them with energy may be large enough to give the observed effect.

The inelastic angular distributions are all asymmetric about 90° except that of 9·13 MeV. At 8·83 MeV, a pronounced forward peak reported by Greenlees and Souch (1956) is observed, while at a lower energy, 7·86 MeV, the angular distribution is again similar to that at 9·55 MeV. Eisberg and Hintz (1956) in a similar experiment at 9·8 MeV, 9·0 MeV and 8·5 MeV, on ^{40}A (p, p′) ^{40}A* also found a variation of differential cross section with energy which they attributed to the violation of the statistical assumption of compound nucleus theory. In the present case, the excitation of the compound nucleus formed ^{25}Al is about 14 MeV, and its level density at this excitation is unknown. Although it is expected that at least a few levels are involved, it is not certain that the continuum is reached. The theories of McManus and Sharp (1952) and Austern, Butler and McManus (1953) which describe the inelastic scattering in terms of a direct interaction between the incident nucleon and a surface nucleon, and that of Hayakawa and Yoshida (1955 a, b), which considers the excitation of Bohr–Mottelson surface vibrations, both predict an angular dependence of inelastic differential cross section in terms of $(\mathrm{J}_2(\underset{\sim}{Q}R))^2$, for a 0 to 2^+ transition as in the present experiment, where $\underset{\sim}{Q}=|k_{\mathrm{in}}-k_{\mathrm{out}}|$ the momentum difference between the ingoing and outgoing proton, R = nuclear radius, and J_2 = spherical Bessel function of order 2. Gugelot and Phillips (1956), in a similar experiment on ^{24}Mg (p, p′) ^{24}Mg* (1·37 MeV) at 18 MeV found that the maxima obtained agreed with that predicted by $(\mathrm{J}_2(\underset{\sim}{Q}R))^2$ by using $R=(1{\cdot}45\,A^{1/3}+1{\cdot}82)\times10^{-13}\,\mathrm{cm}=6\times10^{-13}\,\mathrm{cm}$. In the present case, agreement has been obtained for $E_{\mathrm{p}}=9{\cdot}55$ MeV, with the same value of R and is shown in figure 6. However $(\mathrm{J}_2(\underset{\sim}{Q}R))^2$ does not vary fast enough with energy to produce a fit with experiment at 8·83 MeV. The present effects observed seem to suggest interference between compound nucleus and direct interaction mechanisms.

Yoshida (1956), in a recent paper, attempted to calculate surface interaction effects for the inelastic scattering of nucleons without using a perturbation approximation, and applied it to the case of ^{24}Mg. He was unable to predict the large asymmetry involved in the present results.

ACKNOWLEDGMENTS

Three of us (B.C.H., L.G.K. and M.P.) wish to thank various bodies for financial support as follows: B.C.H. the Department of Scientific and Industrial Research; L.G.K. the University of Birmingham; and M.P. the Institute “Ruder Bośković” Zagreb.

REFERENCES

AUSTERN, N., BUTLER, S. T., and MCMANUS, H., 1953, *Phys. Rev.*, **92**, 350.
BRINK, D. M., 1955, *Proc. Phys. Soc.* A, **68**, 994.
BROMLEY, D. A., and WALL, N. S., 1956, *Phys. Rev.*, **102**, 1560.
BURGE, E. J., FUJIMOTO, Y., and HOSSAIN, A., 1956, *Phil. Mag.*, **1**, 19.
DEE, A., 1955, *M.Sc. Thesis*, University of Birmingham.
EISBERG, R. M., and HINTZ, N. M., 1956, *Phys. Rev.*, **103**, 645.
ENDT, P. M., and KLUYVER, J. C., 1954, *Rev. Mod. Phys.*, **26**, 95.
FISCHER, G. E., 1954, *Phys. Rev.*, **96**, 704.
FREEMANTLE, R. G., PROWSE, D. J., HOSSAIN, A., ROTBLAT, J., 1954, *Phys. Rev.*, **96**, 1270.
GREENLEES, G. W., and SOUCH, A. E., 1956, *Proc. Phys. Soc.* A, **69**, 686.
GUGELOT, P. C., and PHILLIPS, P. R., 1956, *Phys. Rev.*, **101**, 1614.
HAYAKAWA, S., and YOSHIDA, S., 1955 a, *Progr. Theor. Phys Japan*, , **14**, 1; 1955 b, *Proc. Phys. Soc.* A, **68**, 656.
KINSEY, B. B., and STONE, T., 1956, *Phys. Rev.*, **103**, 975.
LEWIS, I. A. D., and COLLINGE, B., 1953, *Rev. Sci. Instrum.*, **24**, 1113.
MCMANUS, H., and SHARP, W. T., 1952, *Phys. Rev.*, **87**, 188 (A).
SAXON, D. S., 1955, *Statistical Aspects of the Nucleus*, report on conference held at Brookhaven National Laboratory.
YOSHIDA, S., 1956, *Proc. Phys. Soc.*, A, **69**, 668.

Incoherent Scattering of Gamma Rays from the Bound Electrons of Heavy Elements

By J. RANDLES
Department of Mathematical Physics, University of Birmingham

Communicated by R. E. Peierls; MS. received 28th December 1956, *and in final form 28th January* 1957

Abstract. In the experimental study of the coherent (elastic) scattering of gamma rays of energy greater than 1 MeV from the electrons of heavy atoms, the energy resolution of the available detecting instruments makes it impossible to distinguish between photons scattered coherently and those scattered incoherently with an energy loss of up to about 10%. The experimental results therefore include an unknown amount of incoherent scattering, the contribution of which is calculated in this paper. The answer is stated as the ratio of incoherent to coherent cross sections which is observed with a detector with the type of response to radiation assumed in the text, and the derivation is valid for large angles ($\gtrsim 60°$) and the energies of interest ($\simeq 1$ MeV). Since the method of solution is much clearer in non-relativistic quantum mechanics, we have presented the necessary details within this framework and outlined at the end the procedure for the more exact relativistic theory. As will be seen, the ratio of the cross sections for tin is given well by the non-relativistic approximation although the absolute cross section is not. For heavier elements (e.g. mercury), only the relativistic theory is acceptable.

---

§ 1. STATEMENT OF THE PROBLEM

THE measurements made to determine the coherent scattering cross section for photons scattered from heavy elements involve the use of instruments which also record gamma rays scattered with an energy loss of up to about 10% of the incident energy, $\hbar\nu$, the exact figure depending on the particular detector. Radiation scattered with a greater energy loss than this has only a small probability of being recorded. For a typical case, we can simulate this response by using a weighting function

$$\exp\{-(\hbar\nu-\hbar\nu')^2/(0\cdot1\hbar\nu)^2\} \qquad \ldots\ldots(1.1)$$

as a measure of the probability that a photon scattered with an energy $\hbar\nu'$ is recorded by a pulse height analyser set up so that its channel width is small and has at its centre the incident energy $\hbar\nu$. If the analyser channel is adjusted so that it lies about some other energy $\hbar\nu+\omega mc^2$, then we need only replace $\hbar\nu$ by $\hbar\nu+\omega mc^2$ in the numerator of the exponent of (1.1) to obtain the response for this case.

In the light of these considerations, the problem reduces to that of calculating the incoherent differential cross section weighted by the factor (1.1).

§ 2. THE SCATTERING PROCESS

For the process in which a photon of momentum $\hbar c\mathbf{k}$ enters an atom and is scattered with reduced momentum $\hbar c\mathbf{k}'$ by interacting with one of the electrons, we have, from second order perturbation theory, the following expression for the differential scattering cross section

$$\sigma_{\mathrm{f},0}(\theta)=r_0^2\frac{k'}{k}\left|S_{\mathrm{t}}\left\{\frac{(\psi_{\mathrm{f}}|\boldsymbol{\alpha}\,.\,\mathbf{e}'\exp(-i\mathbf{k}'\,.\,\mathbf{r})|\psi_{\mathrm{t}})(\psi_{\mathrm{t}}|\boldsymbol{\alpha}\,.\,\mathbf{e}\exp(i\mathbf{k}\,.\,\mathbf{r})|\psi_0)}{\epsilon_{\mathrm{t}}-\epsilon_0-(\hbar\nu/mc^2)}\right.\right.$$
$$\left.\left.+\frac{(\psi_{\mathrm{f}}|\boldsymbol{\alpha}\,.\,\mathbf{e}\exp(i\mathbf{k}\,.\,\mathbf{r})|\psi_{\mathrm{t}})(\psi_{\mathrm{t}}|\boldsymbol{\alpha}\,.\,\mathbf{e}'\exp(-i\mathbf{k}'\,.\,\mathbf{r})|\psi_0)}{\epsilon_{\mathrm{t}}-\epsilon_0+(\hbar\nu'/mc^2)}\right\}\right|^2, \quad \ldots\ldots(2.1)$$

where $\cos\theta=\mathbf{k}\,.\,\mathbf{k}'/kk'$; r_0 is the classical electron radius; $\boldsymbol{\alpha}$ the usual Dirac matrix; $\mathbf{e}$ and $\mathbf{e}'$ are the polarization vectors of the incident and scattered photons; $(\mathbf{r}|\psi_0)$, $(\mathbf{r}|\psi_{\mathrm{t}})$ and $(\mathbf{r}|\psi_{\mathrm{f}})$ the relativistic ground, intermediate and final Dirac wave functions of the scattering electron; ϵ_0 and ϵ_{t} the ground and intermediate state energies in units of mc^2, $\hbar\nu$ and $\hbar\nu'$ the initial and final photon energies and the coordinate $\mathbf{r}$ is in units of $\hbar/mc$. The Pauli principle is taken account of by demanding that $(\mathbf{r}|\psi_{\mathrm{f}})$ shall not be a bound occupied level of the atom. By ignoring the effect of the nuclear coulomb field in the intermediate states of the electron, it is well known (Franz 1935) that this reduces to

$$\sigma_{\mathrm{f},0}(\theta)=r_0^2\frac{k'}{k}\left|\mathbf{e}\,.\,\mathbf{e}'\int d^3\mathbf{r}\exp(i\Delta\mathbf{k}\,.\,\mathbf{r})(\psi_{\mathrm{f}}|\mathbf{r})(\mathbf{r}|\psi_0)\right|^2, \quad \ldots\ldots(2.2)$$

where $\Delta\mathbf{k}=\mathbf{k}-\mathbf{k}'$. The neglect of binding in intermediate states gives wrong results for $\sigma_{\mathrm{f},0}(\theta)$ when the γ-energies are in the region of 1 Mev, but as we shall show in §7, it is reasonable to assume that this does not affect the ratio of incoherent to coherent scattering.

§ 3. The Scattering Electron

We may use the integral appearing in (2.2) to show that, for large scattering angles, the cross section is nearly all accounted for by transitions of the K electrons to continuum states. Expanding the factor $\exp(i\Delta\mathbf{k}\,.\,\mathbf{r})$ in the usual series of products, $\mathrm{j}_l(\Delta kr)\mathrm{P}_{l,M}(\theta,\phi)$, and performing the angular integrations, this integral becomes

$$\sum_l a_l\int_0^\infty drr^2F_{\mathrm{f},0}(r)\mathrm{j}_l(\Delta kr),$$

where a_l is a constant and $F_{\mathrm{f},0}(r)$ is the product of the radial parts of $(\psi_{\mathrm{f}}|\mathbf{r})$ and $(\mathbf{r}|\psi_0)$. Writing

$$\mathrm{j}_l(y)=\mathscr{R}\mathrm{h}_l(y),$$

where $\mathrm{h}_l(y)$ is the spherical Hankel function of the first kind, we have

$$\int_0^\infty drr^2F_{\mathrm{f},0}(r)\mathrm{j}_l(\Delta kr)=\mathscr{R}\int_0^\infty drr^2F_{\mathrm{f},0}(r)\mathrm{h}_l(\Delta kr).$$

By considering the contour integral

$$\int_\Gamma dzz^2F_{\mathrm{f},0}(z)\mathrm{h}_l(\Delta kz),$$

where Γ is the contour $\Gamma_{\mathscr{I}}+\Gamma_{\mathscr{R}}+\Gamma_\infty$ shown in figure 1, we can see that its value is zero, since there are no poles inside or on Γ and that

$$\int_{\Gamma_\infty} dzz^2F_{\mathrm{f},0}(z)h_l(\Delta kz)=0,$$

since there is always a factor like $\exp(-|z|)$ present in the integrand. Hence

$$\int_{\Gamma_{\mathscr{I}}+\Gamma_{\mathscr{R}}} dzz^2F_{\mathrm{f},0}(z)h_l(\Delta kz)=0.$$

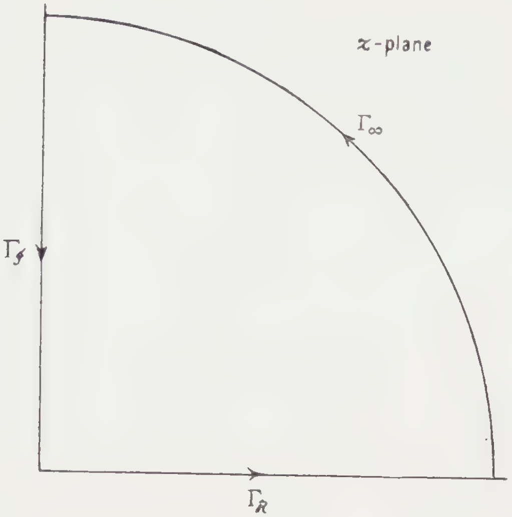

Figure 1.

From this it follows that

$$\int_0^\infty dr r^2 F_{f,0}(r) j_l(\Delta k r) = \mathscr{I}\int_0^\infty dy y^2 F_{f,0}(iy) h_l(i\Delta k y);$$

and since $h_l(i\Delta k y)$ contains a cut-off factor $e^{-\Delta k y}$, then, provided Δk is large, the quantity on the right is only appreciable when $F_{f,0}(iy)$ does not go to zero as $y \to 0$. This means that the scattering of a photon has an appreciable probability only for electrons whose initial and final wave functions have a significant value at the origin. In view of this we can disregard all but the K electrons and the transitions of these to continuum states. According to a rough calculation, the sum of all other processes amounts to less than about 1/6 of the total.

The problem now reduces to a calculation of the cross section for the scattering of a photon and the excitation of a K electron to a continuum level.

§ 4. DERIVATION OF THE CROSS SECTION

To calculate the cross section specified above, we require, explicitly, the wave functions describing the scattering electron in the ground 1s and final continuum states. For a K electron, the nuclear coulomb field is large compared with the field of the other atomic electrons and so the wave function is very nearly that of an electron in the field of the bare nucleus. We denote this by $(\mathbf{r}|m')$, where $m'=0, -1$ for the spin up and spin down electron respectively. For the continuum state we have to use a coulomb wave function because, as we know from § 3, the region of importance in the scattering is the close neighbourhood $(r \lesssim 1/\Delta k)$ of the nucleus where the coulomb field is very strong. We denote this wave function by $(\mathbf{r}|\psi(\mathbf{p}))$, where $mc\mathbf{p}$ is the momentum of the continuum electron at large distances.

It follows from these considerations and (2.2) that the required differential cross section is

$$\sigma(\mathbf{p}, \theta) = r_0^2(\mathbf{e}\cdot\mathbf{e}')^2 \frac{k'}{k} \sum_{m'=-1}^{0} \left| \int d^3\mathbf{r} \exp(i\Delta\mathbf{k}\cdot\mathbf{r})(\psi(\mathbf{p})|\mathbf{r})(\mathbf{r}|m') \right|^2. \qquad \ldots\ldots(4.1)$$

Until now the work has been entirely within the framework of relativistic theory and logically should continue to be, especially since the scattering takes place near the nucleus where the velocity of the electron is large. Nevertheless, we shall now go into the non-relativistic approximation where our calculation will be much clearer and even fairly accurate for the ratio of incoherent to coherent scattering. Equating $(\mathbf{r}|m')$ and $(\mathbf{r}|\psi(\mathbf{p}))$ with the Schrödinger wave functions for the ground and continuum states

$$(\mathbf{r}|m') = \pi^{-1/2}(Z\alpha)^{3/2}\mathrm{e}^{-Z\alpha r}, \qquad \ldots\ldots(4.2)$$

$$(\mathbf{r}|\psi(\mathbf{p})) = \mathrm{e}^{\pi Z\alpha/2p} \sum_{l=0}^{\infty} \frac{\Gamma(l+1-iZ\alpha/p)}{(2l)!}(2ipr)^l \mathrm{e}^{ipr} \times F(l+1-iZ\alpha/p,\ 2l+2,\ -2ipr)P_l(\cos\theta'), \qquad \ldots\ldots(4.3)$$

where $F(l+1-iZ\alpha/p, 2l+2, -2ipr)$ is the confluent hypergeometric function, (4.1) reduces to $\sigma_{\mathrm{NR}}(\mathbf{p},\theta)$, the non-relativistic limit.

Noting that (4.3) has the vector $\mathbf{p}$ as the polar axis of reference and that $(\mathbf{r}|m')$ is independent of m' in the non-relativistic theory, we define

$$R(\mathbf{p}) = \int d^3\mathbf{r} \exp(i\Delta\mathbf{k}\,.\,\mathbf{r})(\psi(\mathbf{p})|\mathbf{r})(\mathbf{r}|m'); \qquad \ldots\ldots(4.4)$$

so that

$$\sigma_{\mathrm{NR}}(\mathbf{p},\theta) = 2r_0^2(\mathbf{e}\,.\,\mathbf{e}')^2\frac{k'}{k}|R(\mathbf{p})|^2. \qquad \ldots\ldots(4.5)$$

In conjunction with equation (4.3) we shall use for $dN(\mathbf{p})$, the number of states lying in the interval $(\mathbf{p}, \mathbf{p}+d\mathbf{p})$, the standard expression

$$dN(\mathbf{p}) = (2\pi)^{-3}p^2\sin\theta_p\,dp\,d\theta_p\,d\phi_p, \qquad \ldots\ldots(4.6)$$

where the angles (θ_p, ϕ_p) are the polar and azimuthal angles of $\mathbf{p}$ with respect to some fixed reference system with $\Delta\mathbf{k}$ as pole. For the factor $\exp(i\Delta\mathbf{k}\,.\,\mathbf{r})$ we use the expansion (which has, as is necessary, the vector $\mathbf{p}$ as polar axis of reference)

$$\exp(i\Delta\mathbf{k}\,.\,\mathbf{r}) = 4\pi\sum_{s=0}^{\infty}\sum_{t=-s}^{s} i^s \mathrm{j}_s(\Delta kr)\mathrm{P}_{s,t}{}^*(\theta',\phi')\mathrm{P}_{s,t}(\theta_p,\phi_1), \qquad \ldots\ldots(4.7)$$

where $\mathbf{r} = (r, \theta', \phi')$ and ϕ_1 is the azimuthal angle of $\Delta\mathbf{k}$ in a reference system with $\mathbf{p}$ as z axis.

Combining (4.2), (4.3), (4.4) and (4.7) and performing the integration over θ' and ϕ', we obtain

$$R(\mathbf{p}) = 4\pi^{1/2}(Z\alpha)^{3/2}\mathrm{e}^{\pi Z\alpha/2p}\sum_{l=0}^{\infty}(2p)^l\frac{\Gamma(l+1+iZ\alpha/p)}{(2l)!}I_l(p)P_l(\cos\theta_p); \qquad \ldots\ldots(4.8)$$

where

$$I_l(p) = \int dr\,r^{l+2}\mathrm{e}^{-Z\alpha r}\mathrm{j}_l(\Delta kr)\mathrm{e}^{-ipr}F(l+1+iZ\alpha/p,\ 2l+2,\ 2ipr). \qquad \ldots\ldots(4.9)$$

The discussion so far refers to the scattering of a photon and the ejection of a K electron with a definite momentum $mc\mathbf{p}$. The differential scattering cross section for an electron emitted into an interval $[mc\mathbf{p}, mc(\mathbf{p}+d\mathbf{p})]$ of the continuum is, by (4.6),

$$\sigma_{\mathrm{NR}}(\mathbf{p},\theta)\,dN(\mathbf{p});$$

and the amount of this which is recorded is, by § 1,

$$\sigma_{\mathrm{NR}}(\mathbf{p},\theta)\exp\{-(\hbar\nu-\hbar\nu')^2/(0{\cdot}1\hbar\nu)^2\}\,dN(\mathbf{p}).$$

Expressing the exponent in terms of $\mathbf{p}$, we thus have for the cross section of experimental significance

$$\sigma_{\mathrm{NR}}(\mathbf{p},\theta)\exp\{-(p^2+(Z\alpha)^2)^2/\Delta^2\}\,dN(\mathbf{p});\ \Delta = \frac{0{\cdot}2\hbar\nu}{mc^2}. \qquad \ldots\ldots(4.10)$$

To obtain the total incoherent scattering affecting the measurements as described in the abstract we simply integrate (4.10) over all momenta. This produces a slight error because the quantity Δk appearing in $\sigma_{\mathrm{NR}}(\mathbf{p}, \theta)$ through $I_l(p)$ is kept constant for this process and consequently different values of k' (or p since $k' = k - (Z\alpha)^2/2 - p^2/2$) give slightly different values of the scattering angle. Clearly, since $\sigma_{\mathrm{NR}}(\mathbf{p}, \theta)$ does not vary rapidly with θ at large angles, this error is negligible and we can take Δk to be

$$\Delta k = 2k \sin\frac{\theta}{2} = 2\frac{h\nu}{mc^2}\sin\frac{\theta}{2}, \qquad \ldots\ldots(4.11)$$

where θ is now the coherent scattering angle.

By (4.5), (4.6), (4.8) and (4.10), we get for the required incoherent differential cross section

$$\sigma_{\mathrm{NR}}{}^{\mathrm{I}}(\theta) = 32 r_0{}^2(\mathbf{e}\,.\,\mathbf{e}')^2(Z\alpha)^4 \int_0^\infty dpp\,\frac{(k'(p)/k)\exp\{-(p^2+(Z\alpha)^2)^2/\Delta^2\}}{1-\mathrm{e}^{-2\pi Z\alpha/p}}$$
$$\times \sum_{l=0}^{\infty} \frac{2^{2l}\prod_{s=1}^{l}(s^2p^2+(Z\alpha)^2)|I_l(p)|^2}{(2l+1)[(2l)!]^2}\,; \qquad \ldots\ldots(4.12)$$

where use has been made of the result

$$|\Gamma(l+1+iy)|^2 = \frac{\pi y}{\sinh \pi y}\prod_{s=1}^{l}(s^2+y^2),$$

and

$$\frac{k'(p)}{k} = 1 - \frac{p^2+(Z\alpha)^2}{10\Delta}.$$

We note that the integrand here cuts off very quickly for

$$\Delta k \gg p > p_{\mathrm{m}} = [\Delta - (Z\alpha)^2]^{1/2}. \qquad \ldots\ldots(4.13)$$

§ 5. Calculation of the Integrals $I_l(p)$

Since the coefficients of $|I_l(p)|^2$ in the series appearing in (4.12) are rapidly convergent, we can expect that all but the first two or three terms ($l=0$, 1, 2) can be neglected. This will be verified later in the section. To evaluate $I_l(p)$ we first apply the transformation worked out for the general case in § 3. This gives

$$I_l(p) = \mathscr{R} i^{l+3}\int_0^\infty dyy^{l+2}\mathrm{e}^{-iZ\alpha y}\mathrm{e}^{py}F(l+1+iZ\alpha/p,\, 2l+2,\, -2py)\mathrm{h}_l(i\Delta ky),$$

where the fact that the integrand of (4.9) is real and the inequality $p < \Delta k$ have been used.

If all of this integrand except the Hankel function is now expanded as a power series in the quantities $Z\alpha y$ and py, then, since $\mathrm{h}_l(i\Delta ky)$ contains a factor $\mathrm{e}^{-\Delta ky}$, these will be, for values of y for which the integrand is significant, less than numbers of order $Z\alpha/\Delta k$ and $p_{\mathrm{m}}/\Delta k$ respectively. For two widely differing cases of interest, viz. 1·33 MeV gamma rays scattered from mercury ($Z\alpha/\Delta k_{60^\circ} \simeq 0{\cdot}2$, $p_{\mathrm{m}}/\Delta k_{60^\circ} \simeq 0{\cdot}1$) and 1·33 MeV gamma rays scattered from tin ($Z\alpha/\Delta k_{60^\circ} \simeq 0{\cdot}1$, $p_{\mathrm{m}}/\Delta k_{60^\circ} \simeq 0{\cdot}2$), these numbers are sufficiently small to justify neglecting all but a few of the terms of the expansion and obtaining an approximation to $I_l(p)$ with these.

Accordingly, we perform the expansion to third degree in y and use the standard formulae for $\mathrm{h}_l(ix)$, obtaining, after some manipulation

$$\left.\begin{aligned} I_0(p) &= \frac{4(Z\alpha)}{\Delta k^4} + \frac{5(Z\alpha)p^2 - 19(Z\alpha)^3}{3\Delta k^6} + \text{higher powers,} \\ I_1(p) &= \frac{12(Z\alpha)}{\Delta k^5} + \frac{20(Z\alpha)p^2 - 76(Z\alpha)^3}{\Delta k^7} + \text{higher powers,} \\ I_2(p) &= \frac{64(Z\alpha)}{\Delta k^6} + \frac{736(Z\alpha)p^2 - 3104(Z\alpha)^3}{7\Delta k^8} + \text{higher powers.} \end{aligned}\right\} \quad \ldots\ldots(5.1)$$

All of these expansions converge in the manner predicted. For mercury, one of the heaviest elements of interest, the least convergent of the group (5.1), $I_2(p)$, which contributes only slightly to the answer in any case, has for the ratio of its second to first term, a quantity less than 0·4 for 60° scattering and 1·33 MEV gamma rays. We may therefore neglect the higher powers of (5.1), the remaining terms giving a result which will be particularly good for large scattering angles.

Squaring the $I_l(p)$ and retaining only terms of degree less than $(1/\Delta k)^{13}$

$$\left.\begin{aligned} [I_0(p)]^2 &= \frac{16(Z\alpha)^2}{\Delta k^8} + \frac{40(Z\alpha)^2p^2 - 152(Z\alpha)^4}{3\Delta k^{10}} + \frac{25(Z\alpha)^2p^4 - 190(Z\alpha)^4p^2 + 361(Z\alpha)^6}{9\Delta k^{12}}, \\ [I_1(p)]^2 &= \frac{144(Z\alpha)^2}{\Delta k^{10}} + \frac{480(Z\alpha)^2p^2 - 1824(Z\alpha)^4}{\Delta k^{12}}, \\ [I_2(p)]^2 &= \frac{2404(Z\alpha)^2}{\Delta k^{12}}, \end{aligned}\right\} \quad \ldots\ldots(5.2)$$

we can compute the first three terms of the series in (4.12). Relative to each other, these terms are given by the table

$$\left.\begin{array}{ll} l; & \dfrac{2^{2l}\prod\limits_{s=1}^{l}(s^2p^2+(Z\alpha)^2)[I_l(p)]^2}{(2l+1)[(2l)!]^2} \\ 0; & 1 \\ 1; & 3\left[\left(\dfrac{p}{\Delta k}\right)^2 + \left(\dfrac{Z\alpha}{\Delta k}\right)^2\right] \\ 2; & \dfrac{64}{45}\left[\left(\dfrac{p}{\Delta k}\right)^2 + \left(\dfrac{Z\alpha}{\Delta k}\right)^2\right]\left[4\left(\dfrac{p}{\Delta k}\right)^2 + \left(\dfrac{Z\alpha}{\Delta k}\right)^2\right] \end{array}\right\} \quad \ldots\ldots(5.3)$$

from which it is clear that only the first two need be considered, the third being negligible.

§ 6. EVALUATION OF THE CROSS SECTION

Neglecting terms in $(1/\Delta k)^{12}$, it follows from (4.12) and (5.2) that

$$\frac{\sigma_{\mathrm{NR}}{}^{\mathrm{I}}(\theta)}{r_0{}^2(\mathbf{e}\,.\,\mathbf{e}')^2} = 512\frac{(Z\alpha)^6}{\Delta k^8}\int_0^\infty dpp\left(\frac{1-[p^2+(Z\alpha)^2]/10\Delta}{1-\mathrm{e}^{-2\pi Z\alpha/p}}\right) \times\left(1+\frac{23p^2-(Z\alpha)^2}{6\Delta k^2}\right)\exp[-(p^2+(Z\alpha)^2)^2/\Delta^2]. \quad \ldots\ldots(6.1)$$

The error due to this approximation is of the order of the neglected terms multiplied by the appropriate members of table (5.3). This is small. Putting $(\mathbf{r}|\psi_{\mathrm{f}}) = (\mathbf{r}|\psi_0) = (\mathbf{r}|m')$ in (2.2), the coherent differential cross section for the K shell in the non-relativistic limit is

$$\sigma_{\mathrm{NR}}{}^{\mathrm{C}}(\theta) = \frac{1024(Z\alpha)^8}{[1+(2Z\alpha/\Delta k)^2]^4\Delta k^8}r_0{}^2(\mathbf{e}\,.\,\mathbf{e}')^2. \quad \ldots\ldots(6.2)$$

Hence, the ratio of incoherent to coherent cross sections, after (6.1) has been evaluated exactly and terms of order greater than $(1/\Delta k)^2$ neglected, is

$$\begin{aligned}\frac{\sigma_{\mathrm{NR}}{}^{\mathrm{I}}(\theta)}{\sigma_{\mathrm{NR}}{}^{\mathrm{C}}(\theta)} = \frac{\Delta}{4(Z\alpha)^2}\biggl\{&\left(1+12\left(\frac{Z\alpha}{\Delta k}\right)^2\right)\int_{(Z\alpha)^2/\Delta}^{\infty}\exp(-x^2)\,dx\\ &+\frac{1}{2}\left(\frac{23}{6}\frac{\Delta}{\Delta k^2}-\frac{6}{5}\left(\frac{Z\alpha}{\Delta k}\right)^2-\frac{1}{10}\right)\exp\left[-\frac{(Z\alpha)^4}{\Delta^2}\right]\\ &-\frac{23}{60}\frac{\Delta}{\Delta k^2}\int_{(Z\alpha)^2/\Delta}^{\infty}\exp(-x^2)x^2\,dx\biggr\}. \qquad \ldots\ldots(6.3)\end{aligned}$$

This result is only valid for large scattering angles ($\gtrsim 60°$) and an incident gamma ray energy large compared with the binding energy of the K shell of the element concerned ($\simeq 1$ MEV).

For tin and 1·33 MEV† incident gamma rays

$$\frac{\sigma_{\mathrm{NR}}{}^{\mathrm{I}}(\theta)}{\sigma_{\mathrm{NR}}{}^{\mathrm{C}}(\theta)} = 0{\cdot}58\left(1+\frac{3{\cdot}035}{\Delta k^2}\right).$$

For mercury and 1·33 MEV gamma rays

$$\frac{\sigma_{\mathrm{NR}}{}^{\mathrm{I}}(\theta)}{\sigma_{\mathrm{NR}}{}^{\mathrm{C}}(\theta)} = 0{\cdot}04\left(1+\frac{8{\cdot}03}{\Delta k^2}\right).$$

These results suggest that the arrangement designed to observe coherent scattering will record an appreciable number of incoherent photons with tin, but only a small number with mercury or lead.

§ 7. EFFECT OF BINDING IN INTERMEDIATE STATES

In § 2 it was seen that the approximate differential scattering cross section is given by the square of the quantity

$$R_{n,0} = \int d^3\mathbf{r}\exp(i\Delta\mathbf{k}\,.\,\mathbf{r})(\psi_n|\mathbf{r})(\mathbf{r}|\psi_0)\,.\,(\mathbf{e}\,.\,\mathbf{e}'), \qquad \ldots\ldots(7.1)$$

a result obtained by ignoring the coulomb field in the intermediate states of the scattering electron. If the vectors **e** and **e**′ are expressed in circular polarizations, the product **e . e**′ has a value depending on whether or not the photon undergoes spin flip

$$\left.\begin{aligned}\mathbf{e}\,.\,\mathbf{e}' &= 1-\cos\theta, \quad \text{for spin flip;}\\ \mathbf{e}\,.\,\mathbf{e}' &= 1+\cos\theta, \quad \text{for no spin flip.}\end{aligned}\right\} \qquad \ldots\ldots(7.2)$$

To find the observable cross section the two cross sections corresponding to these different final states of the photon must be averaged. By (7.1) and (7.2), we have for this average

$$(1+\cos^2\theta)\left|\int d^3\mathbf{r}\exp(i\Delta\mathbf{k}\,.\,\mathbf{r})(\psi_n|\mathbf{r})(\mathbf{r}|\psi_0)\right|^2, \qquad \ldots\ldots(7.3)$$

which is just the quantity, apart from the angular factor, studied in the previous sections.

The effect of including the coulomb field in the intermediate states has been studied by Brown and Mayers (to be published) for the case of coherent scattering. They find that the amplitude for spin flip is not changed by this inclusion while the amplitude for no spin flip can be obtained by replacing $1+\cos\theta$ by

---

† The reason for the choice of this energy is its frequent use in experiments (e.g. Mann, private communication).

$(1+\cos\theta)\underset{\sim}{Q}(r)$ in the integrand of (7.1), $\underset{\sim}{Q}(r)$ being approximately given, in the non-relativistic theory, by

$$\underset{\sim}{Q}(r)=(1+Z\alpha/r)^{-1}. \qquad \text{......(7.4)}$$

The problem of incoherent scattering differs from this only in the employment of a final state $(\mathbf{r}|\psi_n)$ instead of the ground state $(\mathbf{r}|\psi_0)$. However, we would not expect $\underset{\sim}{Q}(r)$ to depend sensitively on the final state and therefore the incoherent scattering cross section is given by the improved approximation

$$\tfrac{1}{2}(1+\cos\theta)^2\left|\int d^3\mathbf{r}\exp(i\Delta\mathbf{k}\,.\,\mathbf{r})(\psi_n|\mathbf{r})(\mathbf{r}|\psi_0)\right|^2$$
$$+\tfrac{1}{2}(1+\cos\theta)^2\left|\int d^3\mathbf{r}\exp(i\Delta\mathbf{k}\,.\,\mathbf{r})(\psi_n|\mathbf{r})(\mathbf{r}|\psi_0)\underset{\sim}{Q}(r)\right|^2, \qquad \text{......(7.5)}$$

where an average over final photon states has been taken. Evidently (7.5) is different from (7.3) at large angles but we can see that the important result in § 6, the ratio of incoherent to coherent scattering, is practically unaffected by the change. To show this we write down this ratio from (7.5):

$$\frac{\left|\int d^3\mathbf{r}\exp(i\Delta\mathbf{k}\,.\,\mathbf{r})(\psi_n|\mathbf{r})(\mathbf{r}|\psi_0)\right|^2}{\left|\int d^3\mathbf{r}\exp(i\Delta\mathbf{k}\,.\,\mathbf{r})|(\mathbf{r}|\psi_0)|^2\right|^2}\left\{\frac{1+\Theta^2|\mathscr{I}_{n,0}|^2}{1+\Theta^2|\mathscr{I}_{0,0}|^2}\right\}, \qquad \text{......(7.6)}$$

where

$$\Theta=\frac{1+\cos\theta}{1-\cos\theta},$$

$$\mathscr{I}_{m.0}=\frac{\int d^3\mathbf{r}\exp(i\Delta\mathbf{k}\,.\,\mathbf{r})(\psi_m|\mathbf{r})(\mathbf{r}|\psi_0)\underset{\sim}{Q}(r)}{\int d^3\mathbf{r}\exp(i\Delta\mathbf{k}\,.\,\mathbf{r})(\psi_m|\mathbf{r})(\mathbf{r}|\psi_0)}.$$

The expression (7.6) is just the result to be obtained by ignoring the potential in intermediate states multiplied by the factor in the brackets. Hence, if the quantities $\mathscr{I}_{m,0}$ can be shown to have only slight dependence on m, the deductions of § 6 will continue to hold. Recalling that only the values of the wave functions near the origin are important, it is clear by inspection of $\mathscr{I}_{m,0}$ that quantities depending sensitively on m cancel in the numerator and denominator provided that $(\mathbf{r}|\psi_m)$ does not vary rapidly within a distance of order $r=1/\Delta k$ from the nucleus. Since, for large scattering angles, the final states of interest all vary slowly in this region, it follows that the $\mathscr{I}_{m,0}$ are practically constant and in particular that $\mathscr{I}_{n,0}\simeq\mathscr{I}_{0,0}$, where n denotes a continuum state. In addition to this, $\mathscr{I}_{m,0}\ll 1$ for large angles, so that if any minor variations remain, they are negligible. The factor in brackets in (7.6) is therefore very near to unity and the inclusion of potential in intermediate states does not affect the conclusions of this paper.

§ 8. The Relativistic Treatment

To carry out the relativistic calculation we have to consider in the place of (4.2) and (4.3) the Dirac wave functions (Bethe 1933) for the ground and continuum states. By inserting these into (4.1) and performing the angular integrations in a manner similar to that in § 4, we obtain

$$\sigma_{\mathrm{I}}(\theta)=r_0^2(\mathbf{e}\,.\,\mathbf{e}')^2\frac{K^2}{\pi}\int_0^\infty dp\,p^2\frac{k'(p)}{k}\exp\left[-\{(p^2+1)^{1/2}-\gamma_0\}^2/(\Delta/2)^2\right]\sum_{\kappa=-\infty}^{\infty}|\kappa|\mathscr{I}_\kappa^2$$
$$\text{......(8.1)}$$

replacing (4.12) for the observed total incoherent differential cross section. In (8.1) we have

$$\sum_{\kappa=-\infty}^{\infty} |\kappa|\,\mathscr{I}_{\kappa}{}^{2} = \frac{2\pi(1+W)}{W}\,\mathrm{e}^{\pi Z\alpha W/p} \sum_{\kappa=-\infty}^{\infty} \frac{|\kappa|\,|\Gamma(\gamma(\kappa)+1+iZ\alpha W/p)|^{2}}{[\Gamma(2\gamma(\kappa)+1)]^{2}}\,, \\ \times 2^{2\gamma(\kappa)-2}\,\mathrm{I}_{\kappa}{}^{2}(p) \quad \ldots\ldots(8.2)$$

where

$$I_{\kappa}(p) = \int_{0}^{\infty} dr r^{\gamma_0+\gamma(\kappa)}\mathrm{e}^{-Z\alpha r}\mathrm{j}_{l}(\Delta k r)\mathscr{Q}_{\kappa}(r), \qquad \kappa=-l-1 \text{ or } l, \qquad \kappa\neq 0, \quad \ldots\ldots(8.3)$$

$$\mathscr{Q}_{\kappa}(r) = \{\exp(i\beta_{\kappa})\mathrm{e}^{-ipr}F(\gamma(\kappa)+1+iZ\alpha W/p,\ 2\gamma(\kappa)+1,\ 2ipr)+\text{c.c.}\} \\ -i\left(\frac{(\gamma_0-1)(W-1)}{(\gamma_0+1)(W+1)}\right)^{1/2}\{\exp(i\beta_{\kappa})\mathrm{e}^{-ipr} \\ \times F(\gamma(\kappa)+1+iZ\alpha W/p,\ \ 2\gamma(\kappa)+1,\ 2ipr)-\text{c.c.}\}, \quad \ldots\ldots(8.4)$$

$$\gamma_0=(1-(Z\alpha)^2)^{1/2}, \quad \gamma(\kappa)=(\kappa^2-(Z\alpha)^2)^{1/2}, \qquad K^2=\frac{(1+\gamma_0)(2Z\alpha)^{2\gamma_0+1}}{2\Gamma(2\gamma_0+1)},$$

$$W=(p^2+1)^{1/2}, \quad \beta\kappa = \begin{cases} \dfrac{1}{2}\left[\tan^{-1}\left(\dfrac{Z\alpha W}{p\gamma(\kappa)}\right)+\tan^{-1}\left(\dfrac{Z\alpha}{p|\kappa|}\right)\right] & \text{when } \kappa<0, \\ \dfrac{1}{2}\left[\tan^{-1}\left(\dfrac{Z\alpha W}{p\gamma(\kappa)}\right)-\tan^{-1}\left(\dfrac{Z\alpha}{p|\kappa|}\right)\right]+\dfrac{\pi}{2} & \text{when } \kappa>0. \end{cases}$$

The series appearing on the right-hand side of (8.2) is rapidly convergent and the structure of $I_{|\kappa|}(p)$ is like that of $I_l(p)$ the corresponding integral in the non-relativistic theory. Therefore, by the same argument as used in § 5, we can expand $I_{|\kappa|}(p)$ to the appropriate order and assume that all but the terms with $|\kappa|=1$, 2 can be neglected. The work involved is very tedious but essentially the same as that in § 5. Denoting the relativistic coherent differential cross section for the K shell by $\sigma_c(\theta)$ we get for 1·33 MeV gamma rays scattered from tin

$$\left(\frac{\sigma_{\mathrm{I}}}{\sigma_{\mathrm{c}}}\right)_{\theta=60^\circ}=0{\cdot}73, \qquad \left(\frac{\sigma_{\mathrm{I}}}{\sigma_{\mathrm{c}}}\right)_{\theta=120^\circ}=0{\cdot}58,$$

and from mercury

$$\left(\frac{\sigma_{\mathrm{I}}}{\sigma_{\mathrm{c}}}\right)_{\theta=60^\circ}=0{\cdot}24, \qquad \left(\frac{\sigma_{\mathrm{I}}}{\sigma_{\mathrm{c}}}\right)_{\theta=120^\circ}=0{\cdot}17.$$

These results show that for tin, the non-relativistic theory gives a good estimate of $\sigma_{\mathrm{I}}/\sigma_{\mathrm{c}}$ while for mercury there is an appreciable discrepancy. In the remaining part of the paper we shall assume that high numerical accuracy is not required and will use the non-relativistic theory to calculate the experimental results for tin. The much smaller value of incoherent scattering for mercury will not be considered, although for higher energies this would be incorrect owing to the rapid increase of σ_{I} with $\hbar\nu$.

§ 9. CONCLUSION: THE OBSERVED SPECTRUM OF PULSES IN THE ANALYSER

The experimental data are usually taken not only by setting the channel of the analyser at the incident γ-ray energy, $\hbar\nu$, but also at other points $\hbar\nu+\omega mc^2$, as shown in figure 2. In the region given by $\omega>0$, this spectrum can be predicted, within the limitation of the assumption of a gaussian response, by displacing the peak of the response function from $\hbar\nu$ to $\hbar\nu+\omega mc^2$ as specified in § 1, and calculating the ratio $\sigma_{\mathrm{I}}(\omega,\theta)/\sigma_{\mathrm{c}}(\theta)$ for a set of values of ω, $\sigma_{\mathrm{I}}(\omega,\theta)$ being the incoherent cross section weighted by the shifted response function.

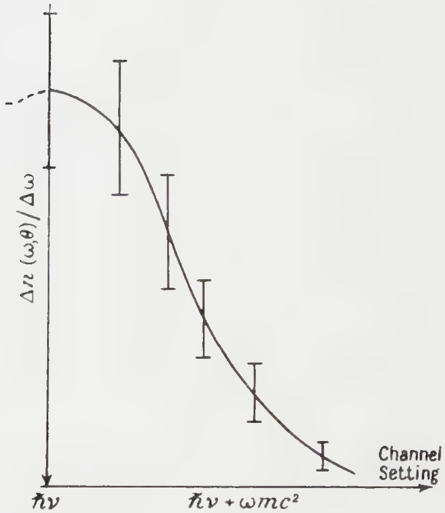

Figure 2. Counting rate per unit channel width as a function of channel setting.

Writing $\Delta n(\omega, \theta)/\Delta\omega =$ the counting rate per unit channel width for the centre of the channel at $\hbar\nu + \omega mc^2$, $N =$ the total counting rate per unit area in the incident beam of γ-rays,

$$N(\omega_0) = N(mc^2/0{\cdot}1\hbar\nu)\pi^{-1/2}\int_0^{\omega_0} \exp[-(\omega mc^2/0{\cdot}1\hbar\nu)^2]\, d\omega$$

$=$ counting rate per unit area of the incident beam recorded when the channel of the analyser lies on an interval $(\hbar\nu,\ \hbar\nu + \omega_0 mc^2)$; it is easy to show that

$$\frac{1}{N(\omega_0)}\frac{\Delta n(\omega, \theta)}{\Delta\omega} = \frac{\exp[-(\omega mc^2/0{\cdot}1\hbar\nu)^2]\sigma_c(\theta) + (\sigma_I(\omega,\theta)/\sigma_c(\theta))\sigma_c(\theta)}{\int_0^{\omega_0} \exp[-(\omega' mc^2/0{\cdot}1\hbar\nu)^2]\, d\omega'}, \quad \ldots\ldots (9.1)$$

from which we can obtain the spectrum of figure 2. If the large channel width ω_0 is employed instead of the narrow one $\Delta\omega$ then the counting rate, $S(\omega_0, \theta)$, in this case will be

$$S(\omega_0, \theta) = \int_0^{\omega_0} \lim_{\Delta\omega\to 0} \frac{\Delta n(\omega, \theta)}{\Delta\omega}\, d\omega,$$

and therefore

$$\frac{S(\omega_0, \theta)}{N(\omega_0)} = \sigma_c(\theta)\left\{1 + \frac{\int_0^{\omega_0} (\sigma_I(\omega,\theta)/\sigma_c(\theta))\, d\omega}{\int_0^{\omega_0} \exp[-(\omega mc^2/0{\cdot}1\hbar\nu)^2]\, d\omega}\right\}. \quad \ldots\ldots (9.2)$$

Using the non-relativistic theory with a displaced response, we get in the place of (6.3)

$$\frac{\sigma_I(\omega,\theta)}{\sigma_c(\theta)} = \frac{\Delta}{4(Z\alpha)^2}\left[1 + 16\left(\frac{Z\alpha}{\Delta k}\right)^2\right]\chi(\omega,\theta), \quad \ldots\ldots (9.3)$$

where

$$\begin{aligned}\chi(\omega,\theta) = {} & \left[1 - \frac{12(Z\alpha)^2 + 23\omega}{3\Delta k^2}\right]\int_{\frac{(Z\alpha)^2+2\omega}{\Delta}}^{\infty} \exp(-x^2)\, dx \\ & + \left(\frac{23}{6}\frac{\Delta}{\Delta k^2}\left(1 + \frac{\omega}{5\Delta}\right) + \frac{12(Z\alpha)^2 + 23\omega}{30\Delta k^2} - \frac{1}{10}\right)\int_{\frac{(Z\alpha)^2+2\omega}{\Delta}}^{\infty} x\exp(-x^2)\, dx \\ & - \frac{23}{60}\frac{\Delta}{\Delta k^2}\int_{\frac{(Z\alpha)^2+2\omega}{\Delta}}^{\infty} x^2\exp(-x^2)\, dx. \quad \ldots\ldots (9.4)\end{aligned}$$

Writing $\sigma_{\mathrm{I}}(\omega,\theta)/\sigma_c(\theta)=A(1+B/\Delta k^2)\times\pi/2$, this gives for tin and 1·33 MEV γ-rays the following results.

ω	0	0·05	0·10	0·15	0·20	0·25
A	0·65	0·47	0·32	0·20	0·13	0·07
B	3·04	2·98	2·97	2·94	2·98	3·03

When $\omega_0=0{\cdot}25$ the channel width is nearly equal to one-half of the resolution of the counter, and for this case we have

$$\frac{S(0{\cdot}25,\theta)}{N(0{\cdot}25)}\simeq 1{\cdot}38\left(1+\frac{0{\cdot}83}{\Delta k^2}\right)\sigma_c(\theta).$$

This then is the expected experimental result.

ACKNOWLEDGMENTS

I wish to thank Professor R. E. Peierls and Dr. G. E. Brown for many helpful discussions and Professor A. K. Mann for his information about the experimental method. I am also very grateful to the Department of Scientific and Industrial Research for financial support.

REFERENCES

BETHE, H. A., 1933, *Handbuch der Physik*, 24/1 (Berlin : Springer).
BRENNER, S., BROWN, G. E., and WOODWARD, J. B., 1954, *Proc. Roy. Soc.* A, **227**, 59.
BROWN, G. E., and MAYERS, D. F., 1955, *Proc. Roy. Soc.* A, **234**, 387.
BROWN, G. E., PEIERLS, R. E., and WOODWARD, J. B., 1954, *Proc. Roy. Soc.* A, **227**, 51.
BROWN, G. E., and WOODWARD, J. B., 1952, *Proc. Phys. Soc.* A, **65**, 997.
FRANZ, W., 1935, *Z. Phys.*, **98**, 314.
HEISENBERG, W., 1931, *Phys. Z.*, **32**, 737.
WHITE, G., *Nat. Bureau of Standards Rep.* 2763.

Rotational Transition of Hydrogen Molecule by Collision

By KAZUO TAKAYANAGI†
Department of Physics, University College London

Communicated by H. S. W. Massey ; MS. received 10th December 1956

Abstract. The previous calculation of rotational transition probability for para-hydrogen gas is improved by adding an attractive term to the intermolecular potential. Using the result of recent calculations by Evett and Margenau of intermolecular force, good agreement is obtained between the calculated and experimental values of transition probability.

The transition probability is also calculated for H_2–H collisions, because of its importance for the cooling of interstellar matter. According to our present knowledge of the intermolecular forces the H_2–H potential shows much more appreciable anisotropy than does the H_2–H_2 potential, so that H_2–H collisions are much more effective than H_2–H_2 collisions for the rotational transition, nearly 10 times for 100–1000°K.

§ 1. INTRODUCTION

IN previous papers (Takayanagi 1952, Takayanagi and Kishimoto 1953) the method of modified wave number has been applied to the calculation of rotational transition rates in para-hydrogen gas. The rates calculated were about four times the empirical value obtained from the ultrasonic dispersion experiment by Rhodes (1946). In that calculation, no account was taken of the van der Waals force. If this is taken into account the effective kinetic energy increases so that the resulting cross section becomes larger and the agreement between the calculated and the empirical values becomes worse.

It should be noted, however, that the intermolecular force used in the previous work was rather different from the recently reported result by Evett and Margenau (1953). This new potential shows less anisotropy. Therefore, it can be expected that, with its use, better agreement between the theory and experiment could be obtained and this is verified in the present work.

The transition probabilities for H_2–H collisions are also calculated. It has been suggested that the collisional excitation of H_2 and the following radiative de-activation is one of the important ways for cooling of the interstellar clouds (Spitzer 1949). For convenience in using the result of our calculation in this sort of problem, the excitation probabilities are calculated, though the de-activation probability has been calculated in the previous papers.

For $H_2 + H$, there is a possibility of the rearrangement (or atom–atom interchange) process

$$H_2 + H \rightarrow H + H_2.$$

It is likely that the molecule thus formed often remains in an excited rotational state. However, the observed reaction rate of this rearrangement process is much less than the rate of the ordinary rotational excitation which has been calculated in this paper. Therefore, we shall omit the further discussions on the rearrangement process.

---

† On leave from Department of Physics, Saitama University, Japan.

§ 2. METHOD OF CALCULATION

The determination of the intermolecular force is one of the difficulties in the collision problems. For H_2–H and for H_2–H_2, however, we have theoretical calculations by Margenau (1943) and Evett and Margenau (1953) respectively. Their results are expressed approximately by the following Morse type functions (in atomic units, which are used throughout this paper unless otherwise specified)

$$V(R, \chi) = D\exp[-2\alpha(R-R_0)] - 2D\exp[-\alpha(R-R_0)] + \beta D\exp[-2\alpha(R-R_0)]P_2(\cos\chi) \qquad \ldots\ldots(1)$$

with $D=1{\cdot}0\times10^{-4}$, $R_0=6{\cdot}3$, $\beta=0{\cdot}26$ for H_2–H, $D=1{\cdot}1\times10^{-4}$, $R_0=6{\cdot}4$, $\beta=0{\cdot}075$ for H_2–H_2, and $2\alpha=1{\cdot}87$ for both cases. For large R, the attractive part in the expression (1) decreases more rapidly than in the real van der Waals force, the main term of which is proportional to R^{-6} for large R. But, in any case, the absolute value of the potential is very small for large R and we may expect that the approximation (1) does not give serious error in the inelastic collision cross section. For H_2–H_2, one of the molecules is assumed to be in the spherically symmetric state throughout collision. As to the notation R, χ, see figure 1.

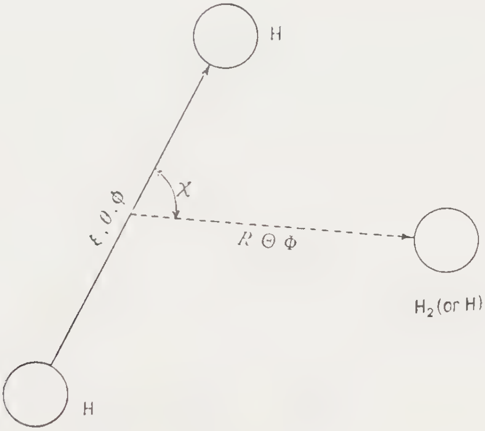

Figure 1.

Neglecting the interference, the method of distorted waves gives the following cross section for the rotational transition

$$H_2(l=0) + H\,(\text{or } H_2) \rightarrow H_2(l=2) + H\,(\text{or } H_2),$$

l being the rotational quantum number.

$$Q_{0\rightarrow2} = 4\pi\frac{k_2}{k_0}\sum_{j,j',\nu}(2j'+1)\,|\,2\mu\beta D(j,\nu,2,-\nu\,|\,P_2(\cos\chi)\,|\,j',0,0,0)J\,|^2, \qquad \ldots\ldots(2)$$

where k_0, k_2 are initial and final wave numbers and μ the reduced mass

$$(j,\nu,2,-\nu\,|\,P_2(\cos\chi)\,|\,j',0,0,0) = \int\!\!\int\!\!\int\!\!\int Y_{j\nu}{}^*(\Theta,\Phi)\,Y_{2-\nu}{}^*(\theta,\phi)\,P_2(\cos\chi) \times Y^{j'0}(\Theta\Phi)\,Y_{00}(\theta,\phi)\sin\Theta\,d\Theta\,d\Phi\sin\theta\,d\theta\,d\phi,$$

$$J = \int_0^\infty G_{2-\nu}{}^{j\nu}(k_2,R)\,e^{-2\alpha(R-R_0)}\,G_{00}{}^{j'0}(k_0,R)\,dR.$$

G's are radial parts of distorted waves and should be normalized as follows :

$$G_2 \sim \sin(k_2R+\delta_2)/k_2, \quad G_0 \sim \sin(k_0R+\delta_0)/k_0.$$

Equation (2) must be multiplied by 2 for H_2–H_2 collision because both molecules can be excited. But the number of collisions for the pair of identical molecules is half the number of collisions for the dissimilar particles, assuming the other conditions to be the same. Therefore, statistically speaking, the reaction rate can be calculated by the same formula for both (H_2–H and H_2–H_2) cases. For this reason, we shall neglect the symmetry effect hereafter.

By making use of the formula

$$P_2(\cos\chi)=\frac{4\pi}{5}\sum_{p=-2}^{2} Y_{2p}{}^*(\Theta,\Phi)\, T_{2p}(\theta,\phi),$$

we get

$$\begin{aligned}(j,\nu,2,-\nu\,|\,P_2(\cos\chi)\,|\,j',0,0,0)&=\frac{\sqrt{2}}{5}\int_0^\pi \Theta_{j\nu}\,\Theta_{2-\nu}\,\Theta_{j'0}\sin\Theta\, d\Theta\\ &=(-1)^\nu\frac{\sqrt{(2j'+1)}}{5}\,c^{j'}(j\nu;\,2\nu).\end{aligned}$$

Here $Y_{lm}(\Theta,\Phi)=\Theta_{lm}(\Theta)\,\Phi_m(\Phi)$, each factor being normalized, and

$$C^j(lm;\ l'm')=\sqrt{\{2/(2j+1)\}}\int_0^\pi \Theta_{lm}(\theta)\,\Theta_{jm-m'}(\theta)\,\Theta_{l'm'}(\theta)\sin\theta\, d\theta$$

is the coefficient defined in the book by Condon and Shortley (1935).

Now as the first step of the simplifications in our calculation, we assume that

$$J(j,\nu,2,-\nu,k_2;\,j',0,0,0,k_0)\simeq J(j',0,0,0,k_2;\,j',0,0,0,k_0). \quad\ldots\ldots(3)$$

Then we have

$$Q_{0\to2}=4\pi\frac{k_2}{k_0}\sum_{j'}(2j'+1)\,[2\mu\beta DJ(j',0,0,0,k_2;\,j',0,0,0,k_0)]^2 \times\sum_{j,\nu}\left[\frac{\sqrt{(2j'+1)}}{5}\,C^{j'}(j\nu;\,2\nu)\right]^2.$$

By using the relation

$$C^k(lm;\ l'm')=(-1)^{g+m'}\frac{[(2l+1)(2l'+1)]^{1/2}}{2k+1}\,s_{k00}{}^{ll'}\cdot s_{k-mm'}{}^{ll'},\qquad 2g=k+l+l',$$

(Racah 1942), the summation in the last factor can be carried out easily:

$$\sum_{j,\nu}\left[\frac{\sqrt{(2j'+1)}}{5}\,C^{j'}(j\nu;\,2\nu)\right]^2=\tfrac{1}{5}.$$

Thus we have

$$Q_{0\to2}=4\pi\frac{k_2}{k_0}\sum_{j'}(2j'+1)\,\tfrac{1}{5}\,[2\mu\beta DJ(j',0,0,0,k_2;\,j',0,0,0,k_0)]^2 \quad\ldots\ldots(4)$$

where, of course, $k_2=(k_0{}^2-2\mu\,\Delta E)^{1/2}$, $\Delta E=$ excitation energy.

As the second step of the simplification, we assume that

$$\begin{aligned}&4k_0k_2\,\tfrac{1}{5}\,[2\mu\beta DJ(j',0,0,0,k_2;\,j',0,0,0,k_0)]^2\\ &\quad\simeq\frac{16}{5}\frac{(\mu\beta D)^2}{\tilde{k}_0\,\tilde{k}_2}\left|\int_0^\infty g(\tilde{k}_2,R)\,e^{-2\alpha(R-R_0)}\,g(\tilde{k}_0,R)\,dR\right|^2=F(\tilde{k}_0),\end{aligned} \quad\ldots\ldots(5)$$

where $\tilde{k}=[k^2-j'^2/R_0{}^2]^{1/2}$ is the modified wave number. This is essentially the method of modified wave number discussed in a previous paper (Takayanagi and Kaneko 1954). The g's are the solutions of the radial wave equation for the S-wave, which are normalized as

$$g(\tilde{k}_l,R)\sim\sin(\tilde{k}_lR+\delta_l)\ \text{ for }\ R\to\infty.$$

F is the probability of transition per collision of a molecule with another.

The cross section is then given by

$$\left.\begin{aligned} Q &\simeq \int_0^{k_0 R_0} \frac{2\pi}{\tilde{k}_0^2} F(\tilde{k}_0)\, j\, dj, \\ \bar{Q} &\simeq \pi R_0^2 \int_0^{\infty} K(k_0)\, dk_0 \int_0^{k_0 R_0} F(k_0^2 - j^2/R_0^2)^{1/2}\, 2j\, dj/k_0^2 R_0^2 \\ &= \pi R_0^2 \int_0^{\infty} \tilde{K}(\tilde{k}_0)\, dk_0\, F(\tilde{k}_0) \equiv \pi R_0^2\, \bar{F}, \end{aligned}\right\} \qquad \ldots\ldots(6)$$

where $K(k)\,dk$ is the ordinary Maxwellian distribution and

$$\tilde{K}(\tilde{k})\, d\tilde{k} = (\mu KT)^{-1} \exp[-\tilde{k}^2/2\mu KT)\, \tilde{k}\, d\tilde{k}$$

is the distribution of the relative velocity component along the line joining the centres of molecules at the instant of collision, the molecules being considered as spheres of diameter R_0.

§ 3. CALCULATION AND RESULTS

For the distorted wave in (5) we may put the solution of the one-dimensional wave equation with the potential

$$\bar{V} = D \exp[-2\alpha(R - R_0)] - 2D \exp[-\alpha(R - R_0)].$$

The solution which has been given by Strachan (1935) is

$$g(\tilde{k}_l, R) = \tfrac{1}{2} \left| \frac{\Gamma[\frac{1}{2} - i(k_l/\alpha) - d]}{\Gamma[-2i(k_l/\alpha)]} \right| (2d e^{-\alpha u})^{-1/2}\, W_{d,\, i\frac{k_l}{\alpha}} (2d\, e^{-\alpha u}),$$

where $d = \sqrt{(2\mu D)}/\alpha$, $u = R - R_0$. Then

$$\int_0^{\infty} g(\tilde{k}_2, R) \exp[-2\alpha(R - R_0)]\, g(\tilde{k}_0, R)\, dR \simeq \int_{-\infty}^{\infty} \ldots\ldots dR$$

$$= \frac{\pi^2}{8d^2\alpha} \left| \frac{\Gamma[\frac{1}{2} - i(\tilde{k}_2/\alpha) - d]}{\Gamma[-2i(\tilde{k}_2/\alpha)]} \right| \left| \frac{\Gamma[\frac{1}{2} - i(\tilde{k}_0/\alpha) - d]}{\Gamma[-2i(\tilde{k}_0/\alpha)]} \right| \left\{ \frac{\tilde{k}_0^2 - \tilde{k}_2^2 + 2d\alpha^2}{\alpha^2 |\Gamma(\frac{1}{2} + i(\tilde{k}_0/\alpha) - d)|^2} \right.$$

$$\left. - \frac{\tilde{k}_0 - \tilde{k}_2^2 - 2d\alpha^2}{\alpha^2 |\Gamma[\frac{1}{2} + i(\tilde{k}_2/\alpha) - d]|^2} \right\} \left(\cosh\frac{2\tilde{k}_0\pi}{\alpha} - \cosh\frac{2\tilde{k}_2\pi}{\alpha} \right)^{-1} \qquad \ldots\ldots(7)$$

(Lennard-Jones and Devonshire 1937).

Numerical calculations are straightforward and the results are shown in table 1 and figure 2.

The mean transition probability $\bar{F}$ can be obtained by numerical integration. The results are shown in table 2.

The rate of excitation is given by $\bar{F}$ multiplied by the collision number per unit time. From the ultrasonic dispersion experiment in para-hydrogen gas by Rhodes (1946) we can derive that

$$\bar{Q}_{0\to 2} = \pi R_0^2\, \bar{F}_{0\to 2} = 5{\cdot}2 \times 10^{-2} \quad \text{for} \quad T = 197{\cdot}7^\circ\text{K}.$$

Assuming $R_0 = 5$, which is a reasonable value, we have

$$\bar{F}_{0\to 2} = 6{\cdot}6 \times 10^{-4}\,(\text{experimental}) \ \text{ for } \ T = 197{\cdot}7^\circ\text{K},$$

which is compared with

$$\bar{F}_{0\to 2} = 3{\cdot}5 \times 10^{-4}\,(\text{theoretical})$$

obtained from the value for $T = 200^\circ$K in table 2. The agreement is quite satisfactory in view of simplifications made in the calculation.

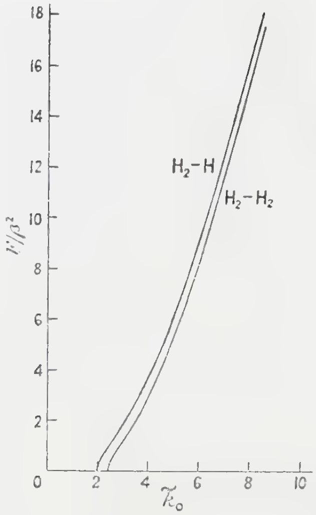

Figure 2.

Table 1. $F(\tilde{k}_0)/\beta^2$

$\tilde{k}_0$	H_2-H_2	H_2-H
2·5	0·230	0·90
4·0	2·83	3·71
5·5	6·74	7·44
7·0	11·6	12·4
8·5	17·4	18·2

Table 2. $\overline{F}/\beta^2$

	H_2-H_2	H_2-H
100°K	0·003	0·003
200°K	0·063	0·047
1000°K	1·99	1·45

§ 4. DISCUSSION ON SOME HIGHER ORDER PROCESSES

(1) $H_2(l=0)+H\,(\text{or } H_2)\rightarrow H_2(l=4)+H\,(\text{or } H_2)$.

No information is available about the higher order terms in $\cos\chi$ in the intermolecular potential so that some assumption must be made about them. Suppose that

$$V(R,\chi)=u(r_{13})+u(r_{23})$$
$$=\sum_{a=1,2}\sum_{ijk}^{\infty}\frac{x_a{}^i y_a{}^j z_a{}^k}{i\,!\,j\,!\,k\,!}\left[\frac{\partial^{i+j+k}u(r)}{\partial X^i\partial Y^j\partial Z^k}\right]_{X=Y=Z=0},\quad (r=[(X-R)^2+Y^2+Z^2]^{1/2}).$$

Then the main parts of $V(R,\chi)$ contributing to the transition considered are the terms for which $i+j+k=4$, i.e.,

$$V^{(4)}=2\left(\frac{\xi}{2}\right)^4\sum_{i+j+k=4}\frac{\cos^i\chi\sin^{j+k}\chi\sin^j\phi\cos^k\phi}{i\,!\,j\,!\,k\,!}\left[\frac{\partial^4 u(r)}{\partial X^i\partial Y^j\partial Z^k}\right]_{X=Y=Z=0}$$
$$=2\left(\frac{\xi}{2}\right)^4\left\{u^{(\text{iv})}(R)\cos^4\chi\cdot\frac{1}{4\,!}+\left(\frac{u'''(R)}{R}-\frac{2u''(R)}{R^2}+\frac{2u'(R)}{R^3}\right)\right.$$
$$\left.\times\cos^2\chi\sin^2\chi\cdot\frac{1}{2\,!\,2\,!}+\left(\frac{u''(R)}{R^2}-\frac{u'(R)}{R^3}\right)\sin^4\chi\,\tfrac{1}{8}\right\}.$$

Neglecting the anisotropy of van der Waals force, assuming that $u(R)=A\,e^{-2\alpha R}$, $2\alpha=1{\cdot}87$, and replacing the slowly varying functions R^{-n} by constant 5^{-n} respectively, we have

$$V^{(4)}(R,\chi)=A\xi^4\{0{\cdot}0075\,P_4(\cos\chi)+\ldots\}\,e^{-2\alpha R}.$$

A similar method gives, for the second order part,

$$V^{(2)}(R,\chi)=A\xi^2\{0{\cdot}52\,P_2(\cos\chi)+\ldots.\}\,e^{-2\alpha R}.$$

Thus, we may put the potential in the following form

$$V(R,\chi)=D\exp[-2\alpha(R-R_0)]-2D\exp[-\alpha(R-R_0)]$$
$$+\beta D\exp[-2\alpha(R-R_0)]\,P_2(\cos\chi)+\beta\gamma D\exp[-2\alpha(R-R_0)]\,P_4(\cos\chi),$$

where

$$\gamma=\frac{\xi^4\times 0{\cdot}0075}{\xi^2\times 0{\cdot}52}\simeq 0{\cdot}03.$$

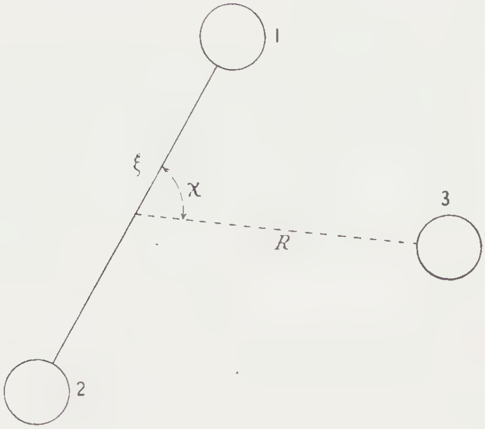

Figure 3.

The cross section for the process considered is given by the formula

$$Q_{0\to 4}=4\pi\frac{k_4}{k_0}\sum_{jj'\nu}(2j'+1)\,|\,2\mu\beta\gamma D(j,\nu,4,-\nu\,|\,P_4(\cos\chi)\,|\,j',0,0,0)J\,|^2.$$

This must be very small compared with $Q_{0\to 2}$ because $Q_{0\to 4}\propto\gamma^2\simeq 10^{-3}$ and furthermore $(\Delta E)_{0\to 4}$ is more than 3 times $(\Delta E)_{0\to 2}$ which makes J very small. It is therefore unnecessary to proceed with the detailed calculations.

(2) For H_2–H_2 collision,

$$H_2(l=0)+H_2(l=0)\to H_2(l=2)+H_2(l=2)$$

may occur more easily than the above process.

Starting from

$$V=u(r_{13})+u(r_{14})+u(r_{23})+u(r_{24}),\quad\text{(see figure 4)},$$

taking out the main part contributing to the process, assuming again that $u(R)=A\,e^{-2\alpha R}$ and neglecting the smaller terms, we have

$$V^{(2,2)}=A\xi^4\{0\cdot 16\,P_2(\cos\chi_1)\,P_2(\cos\chi_2)\\ +0\cdot 26\,P_1(\cos\chi_1)\,P_1(\cos\chi_2)\,P_1(\cos\chi)\}\,e^{-2\alpha R}.$$

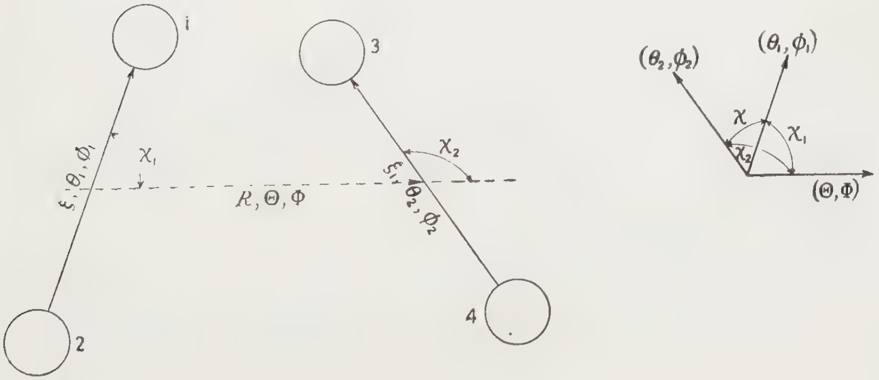

Figure 4.

Thus the angular part of the transition matrix element of this potential may become comparable with that for the process

$$H_2(l=0)+H_2(l=0)\rightarrow H_2(l=2)+H_2(l=0).$$

But, owing to the fact that $(\Delta E)_{0,\,0\rightarrow 2,\,2}=2(\Delta E)_{0,\,0\rightarrow 0,\,2}$, $F(\tilde{k}_0)$ becomes very small for the case we are considering. It is, in fact, less than a tenth of $F(\tilde{k}_0)$ for $(0, 0)\rightarrow(0, 2)$ process for $\tilde{k}_0 < 5$. Therefore, we may conclude that it will cause no serious error to neglect the process $(0, 0)\rightarrow(2, 2)$ at least for lower temperatures (less than 10^3 deg K).

§ 5. CONCLUSION

We have calculated, by the method of modified wave number, the rotational transition cross sections for

$$H_2(l=0)+H\rightarrow H_2(l=2)+H \qquad \text{(A)}$$

and

$$H_2(l=0)+H_2(l=0)\rightarrow H_2(l=2)+H_2(l=0). \qquad \text{(B)}$$

The process (A) shows a larger reaction rate than the process (B), because of the larger anisotropy of the intermolecular potential for H_2–H than for H_2–H_2.

Comparison of the calculated result with the empirical reaction rate has been made for the process (B) at 200°K. Good agreement has been obtained. We may consider this agreement as some evidence for the reliability of our method of approximation as well as the reliability of the potential function of Evett and Margenau. We are now investigating transport phenomena in low temperature hydrogen gas by using the same potential, following the method developed before (Takayanagi and Ohno 1955).

ACKNOWLEDGMENTS

The author would like to express his thanks to Professor H. S. W. Massey for his profound interest in this work and continual encouragement. He also wishes to thank Dr. M. J. Seaton for helpful discussions. Indeed, this work started from a discussion with him. He also wishes to thank Dr. R. A. Buckingham for his interest in the work and for the linguistic help.

The author is also grateful to the British Council for the scholarship, under the help of which he has been studying in the United Kingdom.

REFERENCES

CONDON, E. U., and SHORTLEY, G. H., 1935, *Theory of Atomic Spectra* (Cambridge: University Press).

EVETT, A. A., and MARGENAU, H., 1953, *Phys. Rev.*, **90**, 1021.

LENNARD-JONES, J. E., and DEVONSHIRE, A. F., 1937, *Proc. Roy. Soc.* A, **158**, 253.

MARGENAU, H., 1943, *Phys. Rev.*, **63**, 385.

RACAH, G., 1942, *Phys. Rev.*, **62**, 438.

RHODES, J. E., 1946, *Phys. Rev.*, **70**, 932.

SPITZER, L., 1949, *Astrophys. J.*, **109**, 337.

STRACHAN, C., 1935, *Proc. Roy. Soc.* A, **150**, 456.

TAKAYANAGI, K., 1952, *Progr. Theor. Phys., Japan*, **8**, 497.

TAKAYANAGI, K., and KANEKO, S., 1954, *Sci. Rep. Saitama Univ.* A, **1**, No. 3, 111.

TAKAYANAGI, K., and KISHIMOTO, T., 1953, *Progr. Theor. Phys. Japan*, **9**, 578; **10**, 369.

TAKAYANAGI, K., and OHNO, K., 1955, *Progr. Theor. Phys. Japan*, **13**, 243.

The Scattering of Fast Charged Particles :
II—On the Single Scattering of 9·8 Mev Positrons in Xenon

By K. R. ALLEN, E. A. FINLAY,† M. LIPSICAS, D. MAJOR
and K. PHILLIPS

Research Department, Metropolitan-Vickers Electrical Co. Ltd., Manchester

Communicated by H. S. W. Massey; MS. received 15th June 1956

Abstract. The scattering of 9·8 Mev positrons in xenon in the angular interval 5–40° has been investigated using the cloud chamber method. The results agree reasonably well in this angular interval with the calculations of McKinley and Feshbach, in which Z is replaced by $-Z$. The ratio e^-/e^+ using the previous electron scattering results (Part I), normalized to 9·8 Mev, also agree well with McKinley and Feshbach in the 5–30° interval.

§ 1. INTRODUCTION

MANY measurements have been made on the single scattering of fast electrons by atomic nuclei, but comparatively little work has been done on the scattering of positrons. This is no doubt due to the lack of suitable sources of high energy positrons. The single scattering of positrons and more particularly the ratio of the scattering of positrons and of electrons by similar nuclei is of considerable theoretical importance.

The elementary theory of electron scattering by Rutherford was extended by Mott (1929, 1932) who showed that the scattering cross section was greater than Rutherford's value (with simple relativistic correction) for small angles and decreased to values less than Rutherford's at large angles. Massey (1942) showed that a similar theory could be applied to positrons assuming they act as Dirac particles with a positive charge. The effect of spin–orbital interaction is to reduce the scattering cross section to less than the Rutherford value at all angles. This departure from Rutherford is more pronounced for heavy nuclei and at higher energies.

Until very recently the only experiments which have indicated any distinction between positron and electron scattering are those of Fowler and Oppenheimer (1938) and Lasich (1948). The evidence was based on a small number of scatter events and could only be used as an indication of the difference and not as a quantitative check. More recently Howatson and Atkinson (1951) and Cusack (1952) have used radioactive sources with a cloud chamber to study the scattering of positrons at 0·7 Mev and 0·3 Mev respectively. Lipkin and White (1950) and McDonell (1953) have employed counters to investigate positron scattering in foils. The former found that the ratio of electron to positron scattering was 15% higher than the theoretical value, whilst McDonell's results agreed reasonably well with Massey's calculations and showed for the first time a variation of the ratio with the angle of scatter. Ellis and Henderson (1955) studied the nuclear scattering of electrons and positrons of 0·7 and 1·4 MeV in aluminium, silver and gold. They found good agreement with the theory of Dirac. Bosley and Hughes (1955) investigated the scattering of electrons and positrons at 10 MeV, and found general agreement with the theoretical values of McKinley and Feshbach (1948).

---

† Now at the University of Birmingham.

A summary of the results of previous work on positron scattering is given in table 1. The present measurements were made to determine the absolute scattering cross section for 9·8 MeV positrons in xenon and to compare it with the work on electron scattering by Allen, Lipsicas, Major and Phillips (1956).

Table 1. Summary of Previous Positron Scattering Results

Author	Energy (MeV)	Scattering nucleus	Number of events	Results
	Cloud Chamber			
Fowler and Oppenheimer (1938)	10·5	Pb	9(>14·5°)	$\frac{e^-}{e^+}=1{\cdot}6$
Lasich (1948)	0·45 0·68 0·95	Au	30(>17°)	$\frac{e^-}{e^+}=1{\cdot}6$
Howatson and Atkinson (1951)	0·7	A	65(>20°)	$\frac{N_{\text{exp}}}{N_{\text{theor}}}=0{\cdot}92$
Cusack (1952)	0·3	N	114(>20°)	$\frac{N_{\text{exp}}}{N_{\text{theor}}}=0{\cdot}63$
	Counter			
Lipkin and White (1950)	0·7	Pt	at 58°	$\frac{e^-}{e^+}=3{\cdot}15$
McDonell (1953)	1·07	Au	<40 °	$\frac{e^-}{e^+}=1{\cdot}11$
Ellis and Henderson (1955)	0·7 1·4	Al Ag Au	at 22·8° 34·5° 47·5°	Agreement with theory to within 5%
	Nuclear Plate			
Bosley and Hughes (1955)	10	Average $Z=41$	163(>25°)	General agreement with theory

§ 2. EXPERIMENTAL PROCEDURE

An attempt was made to use the high energy positrons produced in the target of a 20 MeV betatron, since an estimate of the yield indicated that there should be sufficient for the proposed experiment. This source of positrons is not only due to the extremely high x-ray intensity in the target but to the considerable number of pairs formed by the electrons. It was found however that the intensity of low energy particles near the betatron made it impossible to identify the positron beam. The cloud chamber was moved to a position 15 feet from the betatron and electron–positron pairs were produced in a 1 mm thick lead target mounted in the x-ray beam.

The 20 MeV x-rays were collimated into a narrow beam by means of a collimator constructed of lead and steel which was supported in a wall of barytes concrete 8 feet thick, as shown in the experimental arrangement (figure 1). The x-rays were then directed on the lead target and a magnetic channel selected the positrons.

A lead wall was erected round the chamber to reduce the background radiation to a tolerable level. The positrons entered the chamber through a 0·02 in. thick aluminium window 1 inch in diameter, the aluminium window being sealed to the glass with cold setting Araldite.

To ensure that all the particles were positrons a thin lead absorber about 0·02 in. thick was placed in the chamber perpendicular to the path of the entering particle beam and photographs were taken of tracks with the spectrometer magnet field reversed and also with the cloud chamber field reversed. The direction of motion of the particles and direction of curvature indicated the presence of positions. The X-ray beam was pulsed with a single shot circuit which allowed up to 10 pulses to enter the chamber. It was observed that the number of background tracks increased noticeably when xenon was introduced into the chamber. It became impossible to improve the ‘ signal to noise ’ ratio above a certain level and as a result there was difficulty in interpreting some photographs. Nevertheless, it proved to be relatively easy to detect scatters by means of the method of stereoscopic projection. Distortion was detected by noting whether adjacent tracks exhibited the same apparent shift. If they did not, then any departure from a smooth curve was attributed to multiple scattering. Curvature was measured by checking for coincidence with a circular arc at least 5 cm in length. This method was generally preferable to the more tedious chord and sagitta method of radius measurement, which does not allow the observer to detect small changes in track curvature. A total of 3000 pairs of stereoscopic photographs was taken, each containing approximately 1 metre of track. The chamber was filled with a mixture of 80% helium and 20% xenon, and the gas mixture analysed with a mass spectrometer. Gas samples were taken in small

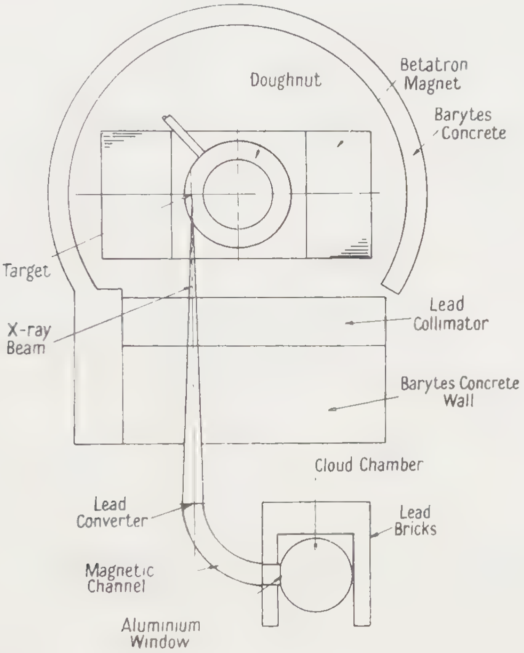

Figure 1. Experimental arrangement of the betatron and cloud chamber.

glass bottles sealed with stainless steel taps with polythene diaphragms. These were tested and found to be leak proof for a period of several months. Gas samples were taken at intervals of a few days and then fed into a mass spectrometer in succession. It was found that over a period of several weeks the concentration of helium was gradually reduced by diffusion through the rubber diaphragm of the chamber, but the concentration of xenon remained unchanged.

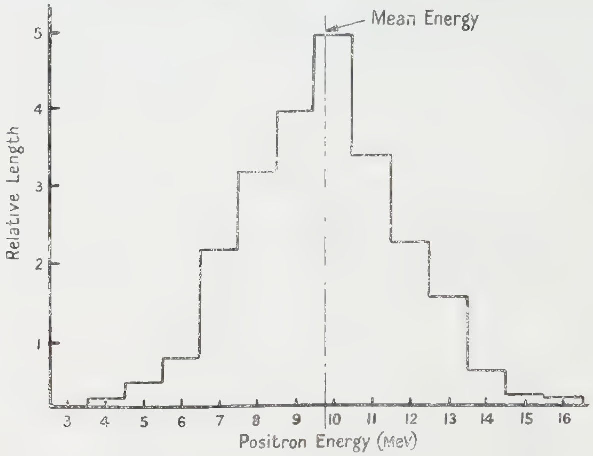

Figure 2. Length–energy histogram of the positrons.

The length–energy histogram of the positrons is shown in figure 2, the mean energy being 9·8 MeV. A total number of 220 single scatters greater than 5° was measured. In order to compare these results with the electron scattering results (Part I) an identical scanning procedure was adopted and the same criteria were used for acceptance of tracks. Corrections were applied to allow for the finite depth of illumination, minimum track length of 5 cm and the presence of water–alcohol vapour.

§ 3. EXPERIMENTAL RESULTS AND COMPARISON WITH THEORY

The theory of scattering of fast electrons was first developed by Mott. Using the Dirac relativistic wave equation he derived an explicit formula for the scattering cross section, which is valid if $Z/137=\alpha$ is small, i.e. for light nuclei only. Mott also obtained an exact expression for the scattering cross section as a series in associated Legendre polynominals. This series has been summed numerically by Bartlett and Watson (1940) for the elastic scattering of electrons in mercury nuclei. The Mott cross section for electron scattering is expressed as

$$\sigma=k^{-2}[q^2(1-\beta^2)\,|F|^2\operatorname{cosec}^2\tfrac{1}{2}\theta+|G|^2\sec^2\tfrac{1}{2}\theta]$$

where $q=\alpha/\beta$, $k^2=m_0{}^2v^2/h^2(1-\beta^2)$ and $\beta=v/c$. Mott, and Bartlett and Watson, showed that it is possible to write

$$F=F_0+F_1 \text{ and } G=G_0+G_1{}^{F_0}+G_1{}^{\phi}+G_1{}^{E}.$$

The theory of elastic scattering of fast positrons by heavy nuclei (mercury) was developed by Massey who pointed out that the change in the sign of the Coulomb force can be expected to affect the scattering distribution through the medium of spin–orbital interaction. Massey based his calculations on the numerical results of Bartlett and Watson and showed that the ratio of the scattering cross section of the positrons to the Rutherford scattering cross section is always less than unity and the ratio decreases as the scattering angle θ increases. This is in contradistinction to the scattering of electrons for which the cross section is greater than the Rutherford value at small angles and becomes less than unity at larger angles. Yadav (1952) calculated the scattering cross section for positrons in the energy range of 1–10 MeV for values of Z from 10–80 using a procedure similar to that used by McKinley and Feshbach for electron scattering. The latter expressed F_1 and G_1 as a power series in α up to α^4 in the form

$$F_1 = A(\theta)\alpha^2 + B(\theta)\alpha^3/\beta + C(\theta)\alpha^4/\beta^2 + D(\theta)\alpha^4$$

$$G_1 = E(\theta)\alpha^2 + H(\theta)\alpha^3/\beta + I(\theta)\alpha^4/\beta^2 + J(\theta)\alpha^4.$$

The numerical coefficients A, B, C etc., of the series were tabulated.

More recently Curr (1955) has extended the calculations of McKinley and Feshbach to the α^6 approximation. None of these results have been calculated for values of θ less than 30 degrees. Bartlett and Watson gave an expression for small angle scattering, but this was an approximation, since G_1 was taken equal to G_1^ϕ and the other terms were ignored. For comparison with theory the numerical coefficients in the power series have been evaluated for scattering angles of 5, 10, 20 and 30 degrees.

The experimental angular scattering distribution is tabulated in table 2, together with the distributions based on Rutherford's theory and on the McKinley and Feshbach α^4 approximation. There is better agreement with the McKinley and Feshbach results than with Rutherford, tending to confirm the theoretical prediction of a difference in the nuclear scattering of positrons and electrons due to the differences in the spin–orbital forces in the two cases. The McKinley and Feshbach theory predicts cross sections of the correct order of magnitude.

Table 2.

(1)	(2)	(3)	(4)	(5)
5–10	199	218	207	0·91
10–20	36	54·5	48·7	0·66
20–30	6	10·2	8·4	0·59
30–40	1	2·4	1·8	0·42

(1) Scattering angle θ (degrees), (2)–(4), number of scatters N, (2) experimental, (3) Rutherford, (4) McKinley and Feshbach, (5) ratio of experimental scattering to Rutherford scattering.

In table 2 it is seen that the ratio of experimental scattering to Rutherford scattering is 0·91 in the angular interval 5°–10° and falls to 0·64 in the angular interval 10°–40°. The experiment therefore supports the theory of McKinley and Feshbach both in absolute magnitude and in angular distribution, although the present results do not permit a detailed examination of the latter in very narrow angular intervals.

Using the normalized results of electron scattering in Part I, the experimental ratio of electron to positron scattering e^-/e^+ at 9·8 MeV was found to be 1·3 for all the scatters between 5 and 30 degrees. This agrees well with the theoretical value of 1·4 obtained from the calculations based on the theory of McKinley and Feshbach. The general agreement with theory tends to confirm the expected difference in the scattering of positively and negatively charged particles due to the change in sign of the spin–orbital interaction term.

ACKNOWLEDGMENTS

The authors wish to thank Mr. B. G. Churcher, Manager of Research Department and Dr. Willis Jackson, Director of Research and Education, Metropolitan-Vickers Electrical Co. Ltd., for permission to publish this paper.

REFERENCES

ALLEN, K. R., LIPSICAS, M. M., MAJOR, D., and PHILLIPS, K., 1956, *Proc. Phys. Soc.* A, **69**, 141.
BARTLETT, J. H., and WATSON, R. E., 1940, *Proc. Amer. Acad. Arts Sci.*, **74**, 53.
BOSLEY, W., and HUGHES, I. S., 1955, *Phil. Mag.*, **46**, 1281.
CURR, R. M., 1955, *Proc. Phys. Soc.* A, **68**, 156.
CUSACK, N., 1952, *Phil. Mag.*, **43**, 671.
ELLIS, J., and HENDERSON, C., 1955, *Proc. Roy. Soc.* A, **229**, 260.
FOWLER, W. A., and OPPENHEIMER, J., 1938, *Phys. Rev.*, **54**, 320.
HOWATSON, A. F., and ATKINSON, J. R., 1951, *Phil. Mag.*, **42**, 1136.
LASICH, W. B., 1948, *Aust. J. Sci. Res.* A, **1**, 249.
LIPKIN, H. J., and WHITE, M. G., 1950, *Phys. Rev.*, **79**, 892.
MASSEY, H. S. W., 1942, *Proc. Roy. Soc.* A, **181**, 14.
McDONELL, J. A., 1953, *Aust. J. Phys.*, **6**, 245.
McKINLEY, W. A., and FESHBACH, H., 1948, *Phys. Rev.*, **74**, 1759.
MOTT, N. F., 1929, *Proc. Roy. Soc.* A, **124**, 425 ; 1932, *Ibid.*, **135**, 429.
YADAV, H. N., 1952, *Proc. Phys. Soc.* A, **65**, 672.

Polarization of GeV Protons Scattered by Complex Nuclei

By G. E. BROWN
Department of Mathematical Physics, University of Birmingham

Abstract. Polarization in the elastic scattering of GeV protons by carbon is calculated, assuming a model in which the nucleus is replaced by a complex spin-dependent phenomenological potential $V(r) = V_1(r) + \boldsymbol{\sigma} . \mathbf{L} V_2(r)$. Results are compared with Birmingham experiments. In order to set the parameters of V_1, a new derivation, valid for high energies, of the relationship between the phenomenological potential and the nucleon-nucleon scattering amplitudes is given.

The results of the comparison with experiment are: (i) V_2 is mainly real, (ii) the same V_2 as was used at 300 MeV can explain experiments at 1 GeV.

---

§ 1. INTRODUCTION

In this paper, general features of the polarization which would be expected in the elastic scattering of protons in the GeV range by complex nuclei are discussed. The points made are illustrated by rough calculations of the polarization of protons scattered by carbon, for which experiments have recently been carried out at approximately 1 GeV (Batty and Goldsack 1957).

Various experiments in the past few years (see for example Chamberlain *et al.* 1956) at energies in the range 100–400 MeV have shown that nucleons scattered elastically by complex nuclei are highly polarized at certain angles. Theoretical investigations (Sternheimer 1954, Fernbach, Heckrotte and Lepore 1955, Levintov 1956) have demonstrated that the experimental polarizations and differential cross sections can be reasonably reproduced by a model which assumes the interaction between the nucleon and nucleus to be described by a phenomenological spin–orbit term of the type $\boldsymbol{\sigma} . \mathbf{L} V_2(r)$ in addition to the complex central potential $V_1(r)$ usually employed in the optical model of the nucleus. Here $\mathbf{L}$ is the angular momentum, $\boldsymbol{\sigma}$ the spin and r the radial coordinate of the nucleon. This model will be used here.

As a background to the discussion of the general features expected at high energies and to the interpretation of the carbon data, relations between the general potential and the nucleon–nucleon scattering amplitudes are derived. This makes it possible to draw some conclusions about the latter from the experimental evidence and it is indicated how these experiments might give information about nuclear forces.

§ 2. RELATION OF NUCLEON–NUCLEON SCATTERING TO SCATTERING BY THE COMPLEX NUCLEUS

Approximate formulae, valid for high energy scattering at small angles, will be applied. These formulae come from a generalization of work by Molière (1947), by R. Glauber (private communication), Shapiro (1955) and the author. A discussion of the approximations involved and an extension to large angle scattering has been given by Schiff (1956). These formulae will be applied here not only to the scattering by the phenomenological potential, but also to that by the nucleon–nucleon potential. This is justifiable, as long as the nucleon–nucleon potential is, in its important region, small compared with the incident energy.[†]

The problem now is to express the effects of the interaction with all the nucleons in the nucleus by a phenomenological potential.

In the high energy approximation, the amplitude for scattering by a spin-dependent potential $V_1(r)+\boldsymbol{\sigma}\,.\,\mathbf{L}V_2(r)$ is given (Shapiro 1955) by

$$f(\theta)=\frac{k}{2\pi i}\int \exp(i\Delta\mathbf{k}\,.\,\mathbf{b})\left\{\exp\left\{-i\frac{E}{k}\int_{-\infty}^{\infty}[V_1(r)+\boldsymbol{\sigma}\,.\,\mathbf{m}kbV_2(r)]dz\right\}-1\right\}d\mathbf{q} \qquad \ldots\ldots(1)$$

where $\mathbf{b}$ is the radius vector in a plane perpendicular to the direction of flight which is taken as the z-axis, and $\mathbf{m}=(-\sin\phi, \cos\phi, 0)$ where ϕ is the azimuthal angle. Also, $\mathbf{k}$ is the incident momentum and $\Delta\mathbf{k}=\mathbf{k}'-\mathbf{k}$, where $\mathbf{k}'$ is the momentum of the particle after the scattering. Carrying out the integration over angles gives, after linearizing in the spin:

$$f(\theta)=A+B\boldsymbol{\sigma}\,.\,\mathbf{n} \qquad \ldots\ldots(2)$$

with

$$\left.\begin{aligned} A&=-\frac{ik}{2}\int_0^{\infty}\{\exp(i\chi_1+i\chi_2)+\exp(i\chi_1-i\chi_2)-2\}\mathrm{J}_0(kb\sin\theta)bdb \\ B&=-\frac{k}{2}\int_0^{\infty}\{\exp(i\chi_1+i\chi_2)-\exp(i\chi_1-i\chi_2)\}\mathrm{J}_1(kb\sin\theta)bdb \end{aligned}\right\} \qquad \ldots\ldots(2.1)$$

and the polarization is given by

$$\mathbf{P}=\frac{AB^*+A^*B}{|A|^2+|B|^2}\mathbf{n}$$

where

$$\chi_1=-\frac{E}{k}\int_{-\infty}^{\infty}V_1dz; \quad \chi_2=-\frac{E}{k}kb\int_{-\infty}^{\infty}V_2dz \qquad \ldots\ldots(2.2)$$

and J_0 and J_1 are Bessel functions.

The potentials V_1 and V_2 result from N neutrons and Z protons, which we describe by this number of nucleon–nucleon potentials distributed over the nucleus. Hence:

$$f(\theta)=\frac{k}{2\pi i}\int \exp(i\Delta\mathbf{k}\,.\,\mathbf{b})\left\{\int\prod_{i=1}^{N+Z}\rho_i(\xi_i)\exp\left[-i\frac{E}{k}\int V_i(\mathbf{r}-\boldsymbol{\xi}_i)dz\right]d^3\xi_i-1\right\}d^3r. \qquad \ldots\ldots(3)$$

Here $\boldsymbol{\xi}_i$ is the radius vector and ρ_i the density of the ith nucleon. At this point the motion of the nucleons in the nucleus both before and after collision has been neglected. This limits the validity of the results to small angles. To illustrate now the relation between the nucleon–nucleon scattering and the scattering for the complex nucleus, a central potential will first be considered,[‡] and the extension to spin-dependent potentials will then be sketched.

The phenomenological potential $V(r)$ can now be defined by requiring it to reproduce the above $f(\theta)$. Hence, $V(r)$ is given by the equation

$$\int\prod_{i=1}^{N+Z}d\xi_i\rho_i(\xi_i)\exp\left[-i\frac{E}{k}\int V_i(\mathbf{r}-\boldsymbol{\xi}_i)dz\right]=\exp\left[-i\frac{E}{k}\int V(r)dz\right]. \qquad \ldots(4)$$

[†] This would not be so in case of a hard core in the nucleon–nucleon interaction, but this high energy method can be generalized to cover this case as well.

[‡] This proof has been given for a central potential by R. Glauber (private communication).

A change of variables will now be made from $\boldsymbol{\xi}_i$ to $\mathbf{b}_i$, the radius vector in the xy plane, and ζ_i the z-coordinate of the ith nucleon. Then

$$-\frac{E}{k}\int_{-\infty}^{\infty} V_i(\mathbf{r}-\boldsymbol{\xi}_i)dz=\chi_i(|\mathbf{b}-\mathbf{b}_i|) \qquad \ldots\ldots(4.1)$$

and equation (4) can be rewritten as

$$\int\prod_{i=1}^{N+Z} d\mathbf{b}_i d\zeta_i \rho_i(\mathbf{b}_i,\zeta_i)\{\Gamma_i+1\}=\exp\left[-i\frac{E}{k}\int V(r)dz\right] \qquad \ldots\ldots(4.2)$$

with

$$\Gamma_i=\Gamma_i(|\mathbf{b}-\mathbf{b}_i|)=\exp[i\chi_i(|\mathbf{b}-\mathbf{b}_i|)]-1. \qquad \ldots\ldots(4.3)$$

Of course Γ_i and χ_i will in general be functions of k, as well as of $|\mathbf{b}-\mathbf{b}_i|$. Now the $\rho_i(\mathbf{b}_i,\zeta_i)$ multiplying Γ_i can be set equal to $\rho_i(\mathbf{b},\zeta_i)$ since Γ_i is non-zero only in the neighbourhood of $\mathbf{b}$. (This amounts to neglecting the range of the nucleon–nucleon potential compared with the radius of the nucleus.) But

$$\int\Gamma_i(|\mathbf{b}-\mathbf{b}_i|)d\mathbf{b}_i=\frac{2\pi i}{k}f_i(0), \qquad \ldots\ldots(5)$$

where $f_i(0)$ is the zero-angle nucleon–nucleon amplitude. Hence (4.2) becomes, for large $N+Z$,

$$\left.\begin{aligned}&\prod_{i=1}^{N+Z}\left\{1+\frac{2\pi i}{k}f_i(0)\int\rho_i(\mathbf{b},\zeta_i)d\zeta_i\right\}\\ &\simeq\exp\left[i\sum_i\frac{2\pi}{k}f_i(0)\int\rho_i(\mathbf{b},z)dz\right],\end{aligned}\right\} \qquad \ldots\ldots(5.1)$$

since the second term in braces is small. Here ζ_i has been replaced by z under the integral sign. Thus, from equation (4),

$$-\frac{E}{k}V(r)=\sum_i\frac{2\pi}{k}f_i(0)\rho_i(\mathbf{r})=\frac{2\pi}{k}\sum_i\bar{f}_i\rho(\mathbf{r}) \qquad \ldots\ldots(5.2)$$

where $\bar{f}_i$ is the amplitude averaged for protons and neutrons, and $\rho(r)$ is the nucleon probability density normalized to unity.

The above method will now be extended to obtain the spin-dependent part of the phenomenological potential. For simplification it will be assumed that the spin of the nucleus is zero, so that the nucleon–nucleon amplitude can easily be averaged over the spins of the nucleons in the nucleus. Equation (4.2) can then be generalized to

$$\int\prod_{i=1}^{N+Z} d\mathbf{b}_i d\zeta_i\rho_i(\mathbf{b}_i,\zeta_i)\{\Gamma_{1i}+\boldsymbol{\sigma}\,.\,\hat{\mathbf{p}}_i\Gamma_{2i}+1\}$$

$$=\exp\left[-i\frac{E}{k}\int V_1(r)dz-i\frac{E}{k}\boldsymbol{\sigma}\,.\,\mathbf{L}\int V_2(r)dz\right] \qquad \ldots\ldots(6)$$

where $\Gamma_{2i}=\Gamma_{2i}(|\mathbf{b}-\mathbf{b}_i|)$ and $\hat{\mathbf{p}}_i$ is a unit vector, for which symmetry allows only the direction

$$\hat{\mathbf{p}}_i=\frac{(\mathbf{b}-\mathbf{b}_i)\times\mathbf{k}}{|\mathbf{b}-\mathbf{b}_i|k} \qquad \ldots\ldots(6.1)$$

and Γ_{1i} is the non-spin-dependent term which we considered above.

First, the spin-dependent part of the nucleon–nucleon amplitude which would result from the term involving Γ_{2i} will be obtained. If the origin is chosen so that $\mathbf{b}_i=0$,

$$\frac{k}{2\pi i}\int\exp[i\Delta\mathbf{k}\,.\,\mathbf{b}]\,\boldsymbol{\sigma}\,.\,\hat{\mathbf{p}}\Gamma_{2i}(b)d\mathbf{b}=-\frac{k}{2\pi}\frac{\boldsymbol{\sigma}\,.\,\mathbf{k}'\times\mathbf{k}}{(\Delta k)k}\frac{d}{d\Delta k}\int\frac{\exp[i\Delta\mathbf{k}\,.\,\mathbf{b}]}{b}\Gamma_{2i}(b)d\mathbf{b}. \qquad \ldots\ldots(7)$$

After an integration over angles, this becomes

$$-k\frac{\boldsymbol{\sigma}\,.\,\mathbf{k}'\times\mathbf{k}}{(\Delta k)k}\int\Gamma_{2i}\mathrm{J}_0{}'(\Delta kb)bdb=k\,\frac{\boldsymbol{\sigma}\,.\,\mathbf{k}'\times\mathbf{k}}{(\Delta k)k}\int\Gamma_{2i}\mathrm{J}_1(\Delta kb)bdb. \qquad \ldots\ldots(7.1)$$

This can be written as $i\boldsymbol{\sigma}\,.\,\mathbf{k}'\times\mathbf{k}g(\Delta k)$ and $g(0)$ will be of particular interest later. It has the simple form

$$g(0)=-\frac{i}{2}\int\Gamma_{2i}(b)b^2db, \qquad \ldots\ldots(7.2)$$

where J_1 has been expanded for small values of the argument and the limit $\Delta k\to 0$ taken.

Now the term $\Gamma_{1i}+1$ in the brackets in equation (6) can be handled in the same way as before, but $\rho_i(\mathbf{b}_i,\zeta_i)$ must be obtained more accurately for the term in Γ_{2i} since in the zero-range approximation, $\rho_i(\mathbf{b}_i,\zeta_i)=\rho_i(\mathbf{b},\zeta_i)$, no contribution is obtained. To a better approximation,

$$\rho_i(\mathbf{b}_i,\zeta_i)\simeq\rho_i(\mathbf{b},\zeta_i)+\nabla\rho_i(\mathbf{b},\zeta_i)(\mathbf{b}_i-\mathbf{b}). \qquad \ldots\ldots(8)$$

Then the left-hand side of equation (6) becomes, after integration over angles,

$$\int\prod_{i=1}^{N+Z}\left\{1+\frac{2\pi i}{k}f_i(0)\int\rho_i(\mathbf{b},\zeta_i)d\zeta_i+\frac{2\pi i}{k}g_i(0)\boldsymbol{\sigma}\,.\,\mathbf{k}\times\int\nabla_i\rho_i(\mathbf{b},\zeta_i)d\zeta_i.\right. \qquad \ldots(8.1)$$

With the introduction of $\bar{g}_i$, the average of g_i for protons and neutrons, and the assumption that the nuclear density is spherically symmetrical (so that $\nabla\rho=(\mathbf{r}/r)(d\rho/dr)$), a phenomenological potential

$$-\frac{EV}{k}=\frac{2\pi}{k}\sum_i\left\{\bar{f}_i(0)\rho(r)+\bar{g}_i(0)\boldsymbol{\sigma}\,.\,\mathbf{L}\frac{1}{r}\frac{d\rho}{dr}\right\} \qquad \ldots\ldots(8.2)$$

is obtained.

The approximations employed in this proof are certainly quite good for energies of the order of 1 GeV and would, in fact, appear to be valid down to lower energies, so long as V_i is considerably less than E in the region of space important for the scattering.

A formula similar to (8.2) has been obtained by Fernbach, Heckrotte and Lepore (1955) by a treatment designed for rather lower energies. Whereas their proof may be applicable in the GeV region, the semi-classical treatment is more transparent in some ways.

§ 3. SCATTERING BY COMPLEX NUCLEI

The choice of the parameters of our complex, spin-dependent phenomenological potential will first be described. Energies of the order of 1 GeV are too high for an extrapolation of the known parameters from the 100–400 MeV region. Therefore the central potential has been chosen from what is known about the 1 GeV nucleon–nucleon scattering. In the analysis (see Fowler *et al.* 1956) of nucleon–nucleon scattering by the optical model a fit to experiment can be obtained by assuming that the nucleon is a 'cloudy crystal ball' of a finite capacity. The striking feature of the nucleon–nucleon scattering is that the inelastic exceeds the elastic scattering and this feature can be easily reproduced by the above model only by assuming that the real part of the nucleon–nucleon potential is zero. This will be done here, although in figure 3 the effect that a small real part would have is shown. Now a purely imaginary potential leads to an imaginary forward scattering amplitude and hence by (5.2) to an imaginary central potential for the complex nucleus. Further, a value for this potential can be deduced from the total cross sections for pp and np scattering. For a nuclear radius of $1{\cdot}3\times10^{-13}A^{1/3}$ cm a value of $4{\cdot}78(12)\,\text{cm}^{-1}$ is obtained for the inverse of the mean free path in a nucleus with uniform density.

The choice of a real spin–orbit phenomenological potential has very striking consequences, if the central potential is imaginary. In this case, both A and B of (2.1) are imaginary. Since A is a decreasing function of angle for small angles, and B an increasing function, there is a point where $A=B$, and here the polarization P of equation (2.1) is 100%. This point is reached just before the diffraction minimum where $A=0$. This conclusion is independent of the functional form of the potential chosen. On the other hand, if the spin–orbit potential is imaginary, the polarization P is zero for all angles, if again the central potential is pure imaginary. These results are in agreement with the general formula derived by Levintov (1956) for lower energies, which gives the maximum polarization equal to $\sin(\beta-\alpha)$ where β and α are the phases of the spin–orbit and central potentials, respectively. The validity of his results depend on the spin–orbit contribution to the phase being small, which does not seem to be the case at 1 GeV and hence his formula cannot be used here.

In the next section, possible origins of an imaginary part of the spin–orbit potential will be discussed. For the moment the spin–orbit potential will be assumed to be real.

With the assumptions of an imaginary central and real spin–orbit potential the polarization must then reach 100% before the diffraction minimum and, as is seen immediately from (2.1), it goes linearly with θ for small angles, beginning at 0 for $\theta=0$. One might expect it to be quite insensitive to changes in the radial dependence of the potential. This is the case as is seen from figure 1 where results from the following three spin–orbit potentials are portrayed:

$$\left.\begin{aligned}
&1.\quad V_2=-u_1R\delta(r-R_1) && \\
&2.\quad V_2=-u_2 && (r<R_2)\\
&\qquad\;\;=0 && (r>R_2)\\
&3.\quad V_2=-u_3\frac{r^2}{R_3^{\,2}}\frac{1}{1+\exp[(r^2-R_3^{\,2})/\beta^2]} &&
\end{aligned}\right\}\qquad\ldots\ldots(9)$$

where the choices $R_1=1{\cdot}3\times10^{-1}A^{1/3}$ cm, $R_2=R_1$, and $R_3=0{\cdot}88R_1$, $\beta=R_3/2$ have been made. Here u_1, u_2 and u_3 are constants. The choices 1 and 2 were made to allow a comparison with the lower energy results of Sternheimer (1954). These models were used in preliminary analyses by Sternheimer and are far from the form (8.2) that would come from a realistic nuclear density distribution. It is believed, however, that they illustrate the main features correctly and the lack of sensitivity with respect to changes (figures 2 and 3) and there is the added advantage that these values of u_1 and u_2 can be compared directly with the values used by Sternheimer. The model 3 reproduces the effects of a diffuse nuclear surface, an important feature not included in 1 and 2. All of these should be proportional to $1/r$ times the derivative of the central potential. In practice, a square central potential was used because the results proved to be quite insensitive to changes in its form. The results come from very rough models, then, and should be considered as only a first orientation. If very accurate

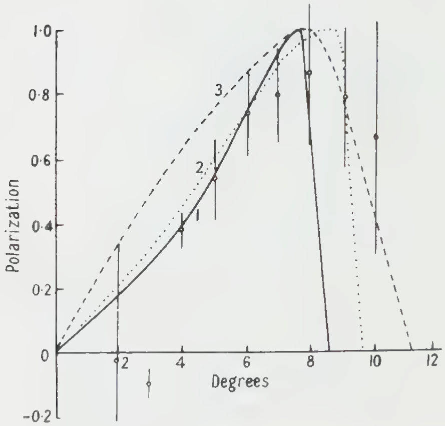

Figure 1. Polarization of GeV protons scattered by carbon assuming various spin–orbit potentials. The curves 1, 2 and 3 result from the potentials 1, 2 and 3, respectively, of (9), with $u_1=0{\cdot}87$ MeV, $u_2=2$ MeV and $u_3=2{\cdot}5$ MeV. A nuclear radius of $1{\cdot}3\times10^{-13}A^{1/3}$ cm and an imaginary central potential giving an inverse mean free path of $4{\cdot}78\times10^{12}$ cm^{-1} were assumed.

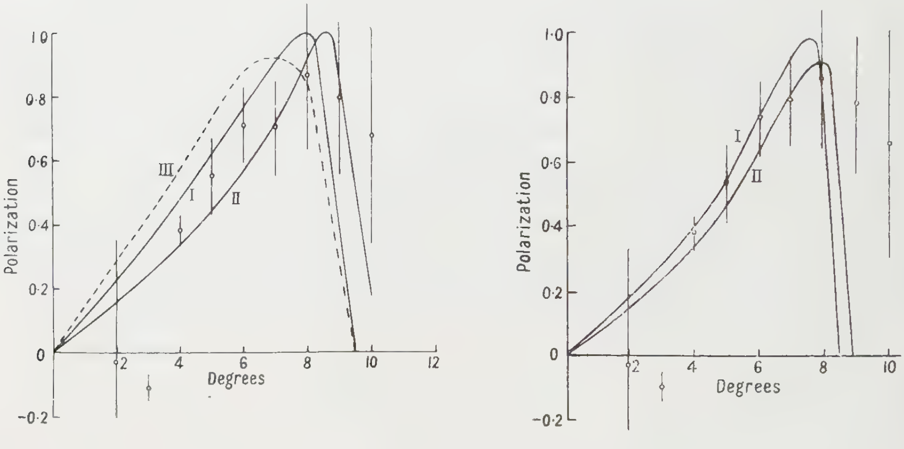

Figure 2. Figure 3.

Figure 2. Polarization of GeV protons scattered by carbon, assuming a spin–orbit potential of type 2, equation (9). Curve I results from assuming $u_2=2$ MeV, curve II from $u_2=1{\cdot}14$ MeV, curve III from $u_2=2+i1{\cdot}37$ MeV. A nuclear radius of $1{\cdot}5\times10^{-13}$ $A^{1/3}$ cm and an imaginary central potential giving an inverse mean free path of $4{\cdot}78\times10^{12}$ cm^{-1} were assumed.

Figure 3. Polarization of GeV protons scattered by carbon, assuming a spin–orbit potential of type 1, equation (9), with $u_1=0{\cdot}87$ MeV. For curve I a purely imaginary central potential, as described in figures 1 and 2, was employed. For curve II, a 30 MeV real part was added to the central potential. A nuclear radius of $1{\cdot}3\times10^{-13}$ $A^{1/3}$ cm was used in both cases.

experimental results are obtained, it may pay to use models with a more realistic radial dependence.

The change in polarization with change in the magnitude and phase of u_2 is shown in figure 2. In figure 3 the effect of the addition of a real part to the central potential is demonstrated. The theoretical results are very insensitive to the various changes in assumptions, and it is not surprising that good agreement with experiment is obtained.

The conclusions from the experiments are then that the larger part of the general spin–orbit potential is real and that the value of the spin–orbit potential depth is in the neighbourhood of those given in figure 1. The implications of both of these results will be discussed in the next section.

§ 4. CONCLUSIONS

The results arrived at are (1) the spin–orbit potential is mainly real and (2) the spin–orbit coupling parameter—which of course depends on the model employed—is roughly in the range of parameters for which curves are shown in figures 1–3. The first and second models, equation (9), were used by Sternheimer at 316 MeV, where fits to experiment indicated u_1 of the order of 0·5 MeV and u_2 of the order of 1·2 MeV, which are slightly lower than the results reported here, although they would probably still fit the experiments. The indication is, then, that the spin–orbit coupling parameter does not change greatly in the region 300–950 MeV, and in fact, the analyses of Levintov (1956) show that it is also more or less constant in the lower energy regions 0–300 MeV.

The question as to whether the experiments can be fitted over the energy region 300–950 MeV with a constant spin–orbit coupling parameter is an important one. If they can, there would seem to be some indication of a nucleon–nucleon spin–orbit force, as can be seen by the following argument:

If the contribution of such a force to $g_i(0)$ in equation (8.3) is taken to first order (Born approximation for the spin–orbit part of the nucleon–nucleon amplitude) it gives rise to a term of the type $\boldsymbol{\sigma} \,.\, \mathbf{L} V_2(r)$, with the energy dependence given by the $|\mathbf{L}|$, i.e. with $V_2(r)$ not a function of energy. Of course, such a phenomenological spin-dependent term can also arise from a nucleon–nucleon tensor force, but this tensor force would have to increase approximately linearly with k to give rise to a phenomenological V_2 which is independent of energy, since $|\mathbf{L}| \simeq k\rho$ increases linearly with k. Unfortunately, the experimental data at 1 GeV and the theoretical models both here and at approximately 300 MeV are not accurate enough to answer this question. A theoretical analysis of experimental data on the scattering of neutrons and protons from carbon over the entire energy range 300–1000 MeV is now being carried out, following the prescriptions of § 2. In particular, the charge distribution, which is known accurately from electron scattering, is used for the density of nuclear matter $\rho(r)$ in (8.2) Preliminary results indicate that the experimental data near 300 MeV can be fitted, and that these fits determine the parameters in (8.2) fairly well. They also indicate, however, that the spin–orbit coupling parameters are substantially different from those obtained by rough fits previously. Also, the energy dependence of the spin–orbit coupling parameter is quite different from that given by rough models. It is hoped to present a detailed analysis in the future, after more accurate experimental results have been obtained at 1 GeV.

The fact that the spin–orbit phenomenological potential is mainly real is not trivial. Such a real potential can arise only if there is a real term in the nucleon–nucleon potential. On the other hand, there is no indication of a real central potential. An imaginary spin–orbit term in the phenomenological potential can arise from a real nucleon–nucleon spin-dependent potential, but at this energy one might expect it to come mainly from meson production. Such a term will result if meson production in nucleon–nucleon collisions is different for states with different j, but the same l. Our results show, however, that this imaginary term does not predominate over the real one.

We have not included the Coulomb force in the above analysis. It is easy to see that for small Z this Coulomb amplitude will be mainly real whereas the above amplitude A from the phenomenological force is purely imaginary. Therefore, the two amplitudes will be almost 90° out of phase and one can add the Coulomb cross section to the above cross section. We have also neglected the relativistic spin-dependent term from the Coulomb potential (Heckrotte 1956). Inclusion of these terms would change our results only at very small angles, of the order of 1°.

ACKNOWLEDGMENTS

The author would like to thank Mr. C. J. Batty and Dr. S. J. Goldsack for many discussions about their results, and Professor R. E. Peierls for criticism. He is also grateful to Professor R. Glauber for several suggestions which improved the treatment.

REFERENCES

BATTY, C. J., and GOLDSACK, S. J., 1957, *Proc. Phys. Soc.* A, **70,** 165.
CHAMBERLAIN, O., SEGRÈ, E., TRIPP, R. D., WIEGAND, C., and YPSILANTIS, T., 1956, *Phys. Rev.*, **102,** 1659.
FERNBACH, S., HECKROTTE, W., and LEPORE, J. V., 1955, *Phys. Rev.*, **97,** 1059.
FOWLER, W. B., SHUTT, R. P., THORNDIKE, A. M., WHITTEMORE, W. L., COCCONI-TONGIORGI, V., HART, E., BLOCK, M. M., HARTH, E. M., FOWLER, E. C., GARRISON, J. D., and MORRIS, T. W., 1956, *Phys. Rev.*, **103,** 1489.
HECKROTTE, W., 1956, *Phys. Rev.*, **101,** 1406.
LEVINTOV, I. I., 1956, *Doklady Akad. Nauk S.S.S.R.*, **107,** 240.
MOLIÈRE, G., 1947, *Z. Naturf.*, **2a,** 133.
SCHIFF, L. I., 1956, *Phys. Rev.*, **103,** 443.
SHAPIRO, I. I., 1955, *Thesis*, Harvard University.
STERNHEIMER, R. M., 1954, *Phys. Rev.*, **94,** 1073 ; **95,** 587.

The Effectiveness of Variational Methods for Inelastic Scattering Problems

By R. J. HUCK
Physics Departments, University College London and Battersea Polytechnic

Communicated by H. S. W. Massey; MS. received 6*th February* 1957

Abstract. The calculation of a partial cross section in atomic collision theory requires the solution of a pair of coupled integro-differential equations when the collision is inelastic and there is a possibility of particle exchange. A discussion is given of some variational procedures available for obtaining approximate solutions of such equations. These procedures are applied to the solution of two sets of model equations which simulate the equations of real problems but permit of exact solution. A comparison of exact and variational solutions enables the effectiveness of the variational methods to be assessed. It is found that a good approximation may be expected when trial functions are used which allow for the mixing of inelastically and elastically scattered waves, but that if only crude trial functions are used the approximation will be poor in cases where coupling is strong.

---

§ 1. INTRODUCTION

Several variational methods have been proposed for the approximate solution of the coupled integro-differential equations arising in inelastic scattering problems in atomic collision theory. A simple example, on which some detailed calculations have been carried out, is the 1s–2s excitation of atomic hydrogen by electron impact. The theory of this problem, treated by the distorted wave method with allowance for electron exchange, is given in a paper by Erskine and Massey (1952). The total wave function for the system of hydrogen-atom and electron is assumed to be

$$\Psi(r_1, r_2) = r_2^{-1}\{f_0^{\pm}(r_2)\psi_0(r_1) + f_1^{\pm}(r_2)\psi_1(r_1)\} \pm r_1^{-1}\{f_0^{\pm}(r_1)\psi_0(r_2) + f_1^{\pm}(r_1)\psi_1(r_2)\}. \qquad \ldots\ldots(1)$$

Here ψ_0 and ψ_1 are the 1s and 2s wave functions of atomic hydrogen, and $f_0^{\pm}(r)$ and $f_1^{\pm}(r)$ are proper functions vanishing at $r=0$ and having suitable asymptotic forms.

The Schrödinger equation (in atomic units) is

$$\left[\nabla_1^2 + \nabla_2^2 + \left(k_0^2 + 2E_0 + \frac{2}{r_1} + \frac{2}{r_2} - \frac{2}{r_{12}}\right)\right]\Psi(r_1, r_2) = 0. \qquad \ldots\ldots(2)$$

The kinetic energies of the incident and inelastically scattered electron are $\frac{1}{2}k_0^2$ and $\frac{1}{2}k_1^2$ respectively, while E_0 is the ground state energy of the hydrogen atom. Substitution of (1) into (2) leads to the coupled integro-differential equations for $f_0^{\pm}$ and $f_1^{\pm}$:

$$L_0(r) = \left[\frac{d^2}{dr^2} - 2V_{00}(r) + k_0^2\right]f_0^{\pm}(r) \pm \int_0^{\infty} K_{00}(r, r')f_0^{\pm}(r')\,dr' - 2V_{01}(r)f_1^{\pm}(r)$$
$$\pm \int_0^{\infty} K_{01}(r, r')f_1^{\pm}(r')\,dr' = 0, \qquad \ldots\ldots(3a)$$

$$L_1(r) \equiv \left[\frac{d^2}{dr^2} - 2V_{11}(r) + k_1^2\right] f_1^{\pm}(r) \pm \int_0^{\infty} K_{11}(r, r') f_1^{\pm}(r') dr' - 2V_{10}(r) f_0^{\pm}(r) \pm \int_0^{\infty} K_{10}(r, r') f_0^{\pm}(r') dr' = 0. \qquad \ldots\ldots(3b)$$

The alternative signs relate to the cases of antiparallel and parallel spins and will be omitted for simplicity in what follows. V and K are defined by

$$V_{pq}(r_1) = \int \psi_p^*(r_2) \left(\frac{1}{r_{12}} - \frac{1}{r_1}\right) \psi_q(r_2) d\tau_2, \qquad K_{pq} = 4\pi r \psi_q(r)(k_{pq}^2 - 2\gamma_0(r, r'))r' \psi_p^*(r').$$

$$k_{pq}^2 = k_0^2 + 2(E_0 - E_p - E_q), \ \gamma_0 = r_>^{-1}.$$

Erskine and Massey obtained approximate solutions of (3) by an iteration method in which coupling was assumed small. This enabled the inelastic cross section to be calculated in terms of the functions $f_0(r)$ and $f_1(r)$ for the corresponding cases of elastic scattering of k_0 electrons by the 1s atom and k_1 electrons by the 2s atom. These functions were found by applying the well-known variational procedures of Hulthén (1944) and Kohn (1948) for elastic scattering problems.

Moiseiwitsch (1951) has shown how to extend the methods of Hulthén and Kohn to inelastic collisions, and Massey and Moiseiwitsch (1953) have carried out an approximate solution of equations (3) by Moiseiwitsch's method, which has the advantage of not assuming weak coupling. For low electron energies, particularly near the threshold, the coupling is in fact strong, and for these cases the cross sections calculated by Massey and Moiseiwitsch differ considerably from those given by the distorted wave Born–Oppenheimer method. The trial functions used by Massey and Moiseiwitsch were quite crude, so that further calculations using more refined trial functions would be highly desirable. However, in view of the very extensive arithmetic involved when trial functions with a large number of parameters are employed, a general investigation of the effectiveness of the variational methods using both simple and elaborate trial functions is called for.

In the present paper two sets of model equations are studied which are obtained by assigning simplified artificial forms to the V's and K's in (3). These are chosen so that exact solutions of the model equations may be obtained, while at the same time the essential features of equations (3) are retained. These model equations are solved by the variational procedures of Hulthén and Kohn, as generalized by Moiseiwitsch, and the results so obtained compared with the exact solutions.

At the same time the opportunity is taken to test a variational procedure suggested by Rubinow (1955) for the solution of coupled differential equations arising in nuclear scattering problems involving tensor forces. Rubinow's formulae are here generalized and adapted to equations of the type (3) where incident and scattered particles have different energies but are both represented by S-waves.

A brief summary of the variational procedures and trial functions used is now given, followed by details of their application to the model equations.

§ 2. THE VARIATIONAL PROCEDURES USED

2.1. *The Hulthén–Moiseiwitsch Method* (*HM Method*)

This method is based on the properties of the integral

$$J = -\int_0^{\infty} [f_0^*(r) L_0(r) + f_1^*(r) L_1(r)] dr = 0. \qquad \ldots\ldots(4)$$

For small functional variations in $f_0(r)$ and $f_1(r)$ such that the functions remain zero at $r=0$ and retain the asymptotic forms

$$f_0(r) \sim \sin k_0 r + \alpha \cos k_0 r, \qquad \ldots\ldots(5a)$$

$$f_1(r) \sim \beta \exp(ik_1 r), \qquad \ldots\ldots(5b)$$

where $\alpha = x+iy$, $\beta = u+iv$, are complex parameters, it may be shown that

$$\delta J = k_0 \delta\alpha - 2ik_1 \beta^* \delta\beta. \qquad \ldots\ldots(6)$$

In this method the condition $\delta J = 0$ is imposed so that $\delta\alpha$ and $\delta\beta$ are not independent variations.

To apply this method trial functions $f_{0t}(r)$ and $f_{1t}(r)$ are chosen which are zero at $r=0$ and have the asymptotic forms (5). In addition to α and β the trial functions may contain n additional complex parameters $c_1 \ldots . c_n$. These trial functions are inserted in (4) to give the integral J_t which is then evaluated as a function of α, β, c_i and their complex conjugates. The values of the parameters α', β', c_i' are then found which satisfy the $n+2$ simultaneous equations

$$J_t = 0; \quad -2i\frac{k_1}{k_0}\beta\frac{\partial J_t}{\partial \alpha^*} + \frac{\partial J_t}{\partial \beta^*} = 0; \quad \frac{\partial J_t}{\partial c_i^*} = 0\ (i = 1, \ldots . n). \qquad \ldots\ldots(7)$$

It is easily shown that

$$\mathscr{I} J_t = k_0 y - k_1 |\beta|^2, \qquad \ldots\ldots(8)$$

from which it follows that the remaining $n+2$ conditions for J_t to be stationary are the complex conjugate equations to (7) and therefore are automatically satisfied. Further, since both J and $J_t(\alpha', \beta', c_i')$ are zero it follows that both the true values of the parameters and the solutions of (7) satisfy the condition

$$y = \frac{k_1}{k_0}|\beta|^2, \qquad \ldots\ldots(9)$$

which ensures the conservation of particles. If a good trial function is used the solution obtained by inserting α', β', c_i' in the trial functions should give a good approximation which is consistent with the conservation of particles.

The inelastic cross section when the forms (5) are used is

$$Q_{\text{in}} = \frac{4\pi k_1 |\beta|^2}{k_0^3 |1 - i\alpha|^2} = \frac{4\pi k_1 (u^2 + v^2)}{k_0^3 [x^2 + (1+y)^2]}. \qquad \ldots\ldots(10a)$$

However, if the conservation condition (9) is satisfied we can write

$$Q_{\text{in}} = 4\pi y / k_0^2 [x^2 + (1+y)^2], \qquad \ldots\ldots(10b)$$

which formula only requires knowledge of the parameter α.

Equation (6) shows that when $\delta J = 0$, $\delta\alpha$ and $\delta\beta$ are not necessarily zero, so that α' and β' found above may not be the best estimates of the true parameters which can be obtained. If

$$I = -\int_0^\infty [f_0(r) L_0(r) + f_1(r) L_1(r)] dr, \qquad \ldots\ldots(11)$$

it is easily shown that

$$\delta I = k_0 \delta\alpha, \qquad \ldots\ldots(12)$$

so that a *corrected* value α'' of the parameter α is obtained from

$$\alpha'' = \alpha' - I_t(\alpha', \beta', c_i')/k_0. \qquad \ldots\ldots(13)$$

From the relation (8) a corresponding value of $|\beta|^2$ exists equal to $k_0 y''/k_1$, and so α'' may be used to calculate an improved value of the cross section from (10*b*).

An alternative is to obtain both real and imaginary parts of a *corrected parameter* β'' by writing (6) in the form

$$J_{\mathrm{t}}(\alpha',\beta',c_i') = I_{\mathrm{t}}(\alpha',\beta',c_i') - 2ik_1\beta''^*(\beta'-\beta''). \qquad \ldots\ldots(14)$$

Since (6) and (12) are only true to the first order, α'' and β'' will not necessarily satisfy the charge conservation condition if the approximation is poor, so that a different estimate of the cross section is given by putting both corrected parameters α'' and β'' in (10*a*).

The extent to which the two estimates of $\underset{\sim}{Q}_{\mathrm{in}}$ agree may be a useful indication of the accuracy of the approximation. This is shown in the following calculations.

In practice the HM method involves extensive arithmetic with complex numbers. A particular disadvantage is that one of the equations (7) is of second degree in the parameters.

2.2. *The Kohn–Moiseiwitsch Method* (*KM Method*)

This method is based on the same integrals J and I as in the HM method, but the condition $J_{\mathrm{t}}=0$ is not imposed. Hence $\delta\alpha$ and $\delta\beta$ are independent variations, and the *uncorrected parameters* α', β', c_i' are the solutions of the $n+2$ simultaneous equations:

$$\frac{\partial J_{\mathrm{t}}}{\partial\alpha^*}=0; \quad \frac{\partial J_{\mathrm{t}}}{\partial\beta^*}=0; \quad \frac{\partial J_{\mathrm{t}}}{\partial c_i^*}=0 \ (i=1,\ldots n). \qquad \ldots\ldots(15)$$

The uncorrected parameters do not obey the conservation relation (9). Corrected parameters α'', β'' are determined as before using (13) and (14). The cross section is calculated by inserting $\alpha''=x''+iy''$ in (10*b*), a check on the approximation being again given by inserting x'', y'', u'' and v'', in (10*a*).

Numerical calculation is much less arduous with the KM procedure since the equations (15) are linear in the parameters.

2.3. *The Rubinow Method*

In this method real parameters are used throughout. The solutions are expressed as linear combinations with a mixing parameter $\tan\epsilon$.

We write

$$f_0(r) = A_i\cos\epsilon\, f_{0i} - A_j\sin\epsilon\, f_{0j},$$

$$f_1(r) = A_i\sin\epsilon\, f_{1i} + A_j\frac{k_0}{k_1}\cos\epsilon\, f_{1j} \qquad \ldots\ldots(16)$$

where

$$f_{0i}\sim\cot\delta_i\sin k_0r+\cos k_0r, \qquad f_{0j}\sim\cot\delta_j\sin k_0r+\cos k_0r,$$

$$f_{1i}\sim\cot\delta_i\sin k_1r+\cos k_1r, \qquad f_{1j}\sim\cot\delta_j\sin k_1r+\cos k_1r. \quad \ldots\ldots(17)$$

The differences between these asymptotic forms and the actual functions are called the *inside wave functions* g and h, and are defined by

$$g_{i,j}=f^{\infty}_{0i,j}-f_{0i,j}, \qquad h_{i,j}=f^{\infty}_{1i,j}-f_{1i,j}. \qquad \ldots\ldots(18)$$

The following expressions are stationary with regard to small functional variations in $g_{i,j}$ and $h_{i,j}$:

$$k_{ii}\cot\delta_i = k_{ii}\cot\Delta_{ii}(1+B_{ii})^2 - C_{ii}, \qquad \ldots\ldots(19a)$$

$$k_{jj}\cot\delta_j = k_{jj}\cot\Delta_{jj}(1+B_{jj})^2 - C_{jj} \qquad \ldots\ldots(19b)$$

$$0 = k_{ij}\cot\Delta_{ij}B_{ij}B_{ji} - C_{ij}. \qquad \ldots\ldots(19c)$$

In these equations $k_{ii}=k_0\cos^2\epsilon+k_1\sin^2\epsilon$; $k_{jj}=(k_0{}^2/k_1)\cos^2\epsilon+k_0\sin^2\epsilon$; $k_{ij}=k_0$. The B's, C's and $\cot\Delta$'s are given below for the case when the K's of (3) are zero:

$$k_{ss}B_{rs}=-2\cos^2\epsilon\int_0^\infty[\alpha_{rs}V_{00}\sin k_0r(g_s-\cos k_0r)+\beta_{rs}V_{01}\sin k_1r(g_s-\cos k_0r)$$

$$+\gamma_{rs}V_{01}\sin k_0r(h_s-\cos k_1r)+\delta_{rs}V_{11}\sin k_1r(h_s-\cos k_1r)]dr,$$

$$C_{rs}=\cos^2\epsilon\int_0^\infty\Bigg[\mu_{rs}\left\{-\frac{dg_s}{dr}\frac{dg_r}{dr}\right\}+k_0^2g_rg_s-2V_{00}(g_r-\cos k_0r)(g_s-\cos k_0r)$$

$$-\nu_{rs}\left\{-\frac{dh_s}{dr}\frac{dh_r}{dr}+k_1^2h_rh_s-2V_{11}(h_r-\cos k_1r)(h_s-\cos k_1r)\right\}$$

$$+2V_{01}\{w_{rs}(g_r-\cos k_0r)(h_s-\cos k_1r)+\pi_{rs}(g_s-\cos k_0r)(h_r-\cos k_1r)\}\Bigg]dr,$$

$$k_{rr}k_{ss}[k_{rs}\cot\Delta_{rs}]^{-1}=-2\cos^2\epsilon\int_0^\infty[l_{rs}V_{00}\sin^2k_0r+m_{rs}V_{01}\sin k_0r\sin k_1r$$

$$+n_{rs}V_{11}\sin^2k_1r]dr,$$

$\alpha_{ii}=\mu_{ii}=l_{ii}=1$, $\beta_{ii}=\gamma_{ii}=-\alpha_{ij}=-\alpha_{ji}=-w_{ii}=-\pi_{ii}=-\mu_{ij}=-l_{ij}=\tan\epsilon$,
$\nu_{jj}=n_{jj}=k_0^2/k_1^2$, $\delta_{ii}=\alpha_{jj}=-\beta_{ij}=-\gamma_{ji}=\nu_{ii}=\mu_{jj}=\pi_{ij}=l_{jj}=n_{ii}=\tan^2\epsilon$,
$\delta_{jj}=\gamma_{ij}=\beta_{ji}=-w_{ij}=k_0/k_1$, $-\beta_{jj}=-\gamma_{jj}=\delta_{ij}=\delta_{ji}=w_{jj}=\pi_{jj}=\nu_{ij}=n_{ij}=(k_0/k_1)\tan\epsilon$,
$m_{ii}=2\tan\epsilon$, $m_{jj}=-2k_0/k_1$, $m_{ij}=(k_0/k_1)-\tan^2\epsilon$.

The procedure is to choose suitable trial functions for $g_{i,j}$ and $h_{i,j}$ and to find values of the parameters in them such that the expressions in the right-hand side of (19*a*) and (19*b*) are stationary. A value of $\tan\epsilon$ must first be assumed for this to be done. The parameters so found are then substituted into (19*c*), which is a quartic equation for $\tan\epsilon$, and an improved value of $\tan\epsilon$ found. This is now put into (19*a*) and (19*b*) and the whole iterative process repeated until a set of parameters is found which simultaneously satisfy (19*c*) while making (19*a*) and (19*b*) stationary. The values of $\cot\delta_i$ and $\cot\delta_j$ are then calculated from (19*a*) and (19*b*) and used together with the final value of $\tan\epsilon$ to calculate the cross section. Although only real quantities are involved, the numerical work may become very tedious, especially if the initial choice of $\tan\epsilon$ is not close to the true value.

The solution may be thrown into the form (5) by writing

$$A_i=\frac{\sec\epsilon(\eta-i)}{\xi(\eta-i)+\lambda\eta(\xi-i)},\quad A_j=\frac{-\operatorname{cosec}\epsilon[\lambda(\xi-i)]}{\xi(\eta-i)+\lambda\eta(\xi-i)},\qquad\ldots\ldots(20)$$

where $\xi=\cot\delta_i$, $\eta=\cot\delta_j$, $\lambda=(k_1/k_0)\tan^2\epsilon$. It is found that

$$\left.\begin{aligned}\alpha&=\frac{(1+\lambda)[\xi\eta(\lambda\xi+\eta)+(\xi+\lambda\eta)]+i\lambda(\xi-\eta)^2}{\xi^2\eta^2(1+\lambda)^2+(\xi+\lambda\eta)^2},\\&=\frac{-\tan\epsilon(\xi-\eta)[\xi\eta(1+\lambda)+i(\xi+\lambda\eta)]}{\xi^2\eta^2(1+\lambda)^2+(\xi+\lambda\eta)^2}.\end{aligned}\right\}\qquad\ldots\ldots(21)$$

It is easily seen that the solution satisfies the condition (9) for conservation of particles, and that the inelastic cross section is given by

$$Q_{\text{in}}=\frac{4\pi k_1\tan^2\epsilon}{k_0(k_0+k_1\tan^2\epsilon)^2}\sin^2(\delta_i-\delta_j).\qquad\ldots\ldots(22)$$

The cross section can thus be calculated directly from the parameters $\cot\delta_i$, $\cot\delta_j$ and $\tan\epsilon$.

In the following investigations α and β were calculated for the purpose of comparison with the results of the other methods.

§ 3. The Trial Functions

The following three sets of trial functions were used in the application of the Moiseiwitsch variational methods HM and KM:

(i) *The Massey–Moiseiwitsch Functions.*

$$f_{0t}(r)=\sin k_0r+(\alpha+\gamma e^{-r})(1-e^{-r})\cos k_0r,$$

$$f_{1t}(r)=(1-e^{-r})\beta\exp(ik_1r).$$

(ii) *The Simplified Massey–Moiseiwitsch Functions.*

$$f_{0t}(r)=\sin k_0r+\alpha(1-e^{-r})\cos k_0r,$$

$$f_{1t}(r)=(1-e^{-r})\beta\exp(ik_1r).$$

(iii) *The Mixed Functions.*

$$f_{0t}(r)=\sin k_0r+\alpha(1-e^{-r})\cos k_0r+\mu e^{-r}\sin k_1r+\nu e^{-r}(1-e^{-r})\cos k_1r,$$

$$f_{1t}(r)=(1-e^{-r})\beta\exp(ik_1r)+\rho e^{-r}\sin k_0r+\sigma e^{-r}(1-e^{-r})\cos k_0r.$$

All these functions have the required asymptotic forms (5) for large r and are zero at the origin. The parameters α, β, ... σ, are all complex. The functions (i) are those used by Massey and Moiseiwitsch in their calculations on the 1s–2s excitation of atomic hydrogen using method HM. It was clearly of interest to test their effectiveness first. Functions (ii) are simplified versions of (i) with $\gamma=0$. Functions (iii) are more elaborate forms based on (ii) but containing additional terms to represent the mixing of elastically and inelastically scattered waves.

The forms of (iii) were arrived at in the following manner. By setting all the V's and K's in the integro-differential equations (3) equal to zero except V_{01}, the simplified equations (23) were formed:

$$\frac{d^2f_0}{dr^2}+k_0^2f_0=2V_{01}f_1, \qquad \text{......(23a)}$$

$$\frac{d^2f_1}{dr^2}+k_1^2f_1=2V_{10}f_0. \qquad \text{......(23b)}$$

An approximate form for $f_1(r)$ was found by setting $f_0(r)=\sin k_0r$ on the right-hand side of (23*b*), and using for V_{10} the appropriate expression for the 1s–2s case of hydrogen viz:

$$V_{01}(r)=V_{10}(r)=\frac{2^{3/2}}{9}e^{-3r/2}(\tfrac{2}{3}+r).$$

The required solution of the resulting differential equation was easily shown to be

$$f_1(r)=-A\exp(ik_1r)+e^{-3r/2}\{(B+Cr)\sin k_0r+(A+Dr)\cos k_0r\}, \qquad \text{....(24)}$$

in which A, B, C, D, are constants. The asymptotic form of this expression for large r represents the inelastically scattered wave at infinity, and in fact gives the Born approximation: $Q_{in}=4\pi|A|^2/k_1k_0^3$. The second term of (24), which is important only in the immediate neighbourhood of the atom, represents a damped elastically scattered wave. A similar term involving k_1r would appear in the approximate form of $f_0(r)$. The trial functions (iii) were suggested by the form of (24).

Physical considerations suggest that the mixed trial functions (iii) should be especially appropriate in cases of close-coupling. When the scattered particles spend a relatively long time in the vicinity of the atomic field there is a possibility of multiple scattering processes: for example, an inelastically scattered particle may 'de-excite' the excited scattering atom and emerge eventually as an elastically scattered particle (Massey and Mohr 1933). Hence the wave function near the atom should include terms representing the elastically scattered particle associated with the excited atomic state and the inelastically scattered particle associated with the unexcited state. In adopting the trial functions (iii) we are in fact introducing terms of the type $\psi_1(r_2)\phi(k_0r_1)$ and $\psi_0(r_2)\phi(k_1r_1)$ into the total wave function (1). The terms remaining in the asymptotic form are of the type $\psi_0(r_2)\phi(k_0r_1)$ and $\psi_1(r_2)\phi(k_1r_1)$, corresponding to the normal association of the elastically scattered wave at infinity with the unexcited atom, and of the inelastically scattered wave at infinity with the excited atom.

In the application of the Rubinow variational method (§ 2.3) only one set of trial functions was used, namely:

(iv) $$g_{i,j}(r)=\mathrm{e}^{-r}\cos k_0r\,; \quad h_{i,j}(r)=\mathrm{e}^{-r}(d_{i,j}\sin k_1r+\cos k_1r).$$

These are the inside wave functions in which the parameters d_i and d_j are real. They are very crude trial functions chosen with the object of keeping the number of parameters small and at the same time having functions roughly equivalent to the functions (ii) used in the Moiseiwitsch methods.

It must be remembered, however, that one cannot directly compare the effectiveness of the Moiseiwitsch and Rubinow methods using the same set of trial functions since the Rubinow method works only with the inside wave functions and the parameters in the asymptotic forms are not varied.

§ 4. Calculations with Model A

For this model the equations (3) were simplified by putting $K_{00}=K_{01}=K_{10}=K_{11}=V_{00}=V_{11}=0$. The direct interaction $2V_{01}$ was assumed to be equal to a constant C for $0<r<a$, and to zero for $a<r<\infty$. The equations are thus reduced to

$$\begin{aligned}\frac{d^2f_0}{dr^2}+k_0^2f_0&=Cf_1 \;(0<r<a)\\ &=0 \quad (a<r<\infty),\end{aligned} \qquad \ldots\ldots(25a)$$

$$\begin{aligned}\frac{d^2f_1}{dr^2}+k_1^2f_1&=Cf_0 \;(0<r<a)\\ &=0 \quad (a<r<\infty).\end{aligned} \qquad \ldots\ldots(25b)$$

The exact solution of these equations for $r<a$ has the form

$$f_0(r)=A\sin mr+B\sin pr,$$

$$f_1(r)=C^{-1}\{A(k_0^2-m^2)\sin mr+B(k_0^2-p^2)\sin pr\},$$

where $2m^2=k_0^2+k_1^2+\{(k_0^2-k_1^2)^2+4C^2\}^{1/2}$; $2p^2=k_0^2+k_1^2-\{(k_0^2-k_1^2)^2+4C^2\}^{1/2}$.

By matching these at $r=a$ to the asymptotic forms (5) the values of α and β, hence the cross section, were obtained. For numerical calculation the values $k_0=1$, $k_1=\frac{1}{2}$, $a=1$, were assumed, and the solution evaluated for integral values of the coupling constant C^2 from zero up to 12. The cross section, in units of

πa_0^2, is shown in figure 1 as a function of C^2. The theoretical *maximum possible value* of the cross section is $1/k_0^2$ (Mott and Massey 1949). Since the solution satisfies the conservation relation (9) it is of course only essential to find the real and imaginary parts of $\alpha = x + iy$, since $\underset{\sim}{Q}_{\mathrm{in}}$ may then be calculated from (10*b*). The values of x and y as functions of C^2 are shown in figures 2 and 3.

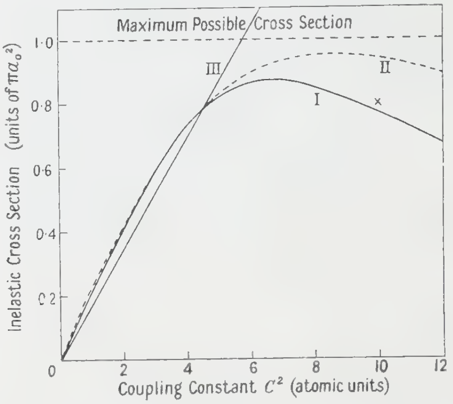

Figure 1. Cross section for inelastic scattering with model A, as a function of the coupling constant C^2. I, Calculated from the exact solution; II, calculated by equation (10*b*) from the corrected parameter α'' given by the Kohn–Moiseiwitsch variational method with trial functions (i); III, calculated by the Born approximation. × marks the value obtained for $C^2 = 10$ using mixed trial functions (iii).

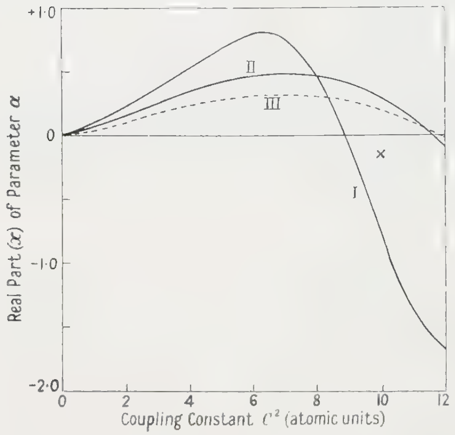

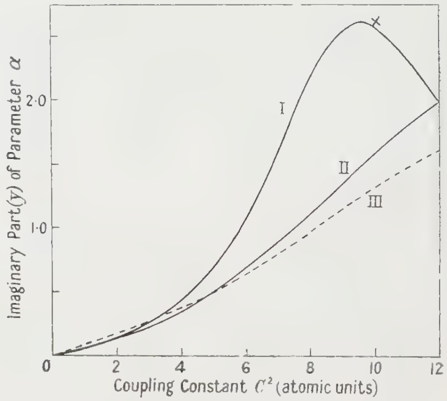

Figure 2. Real part (x) of parameter α, model A, for various values of the coupling constant C^2.

Figure 3. Imaginary part (y) of parameter α, model A, for various values of the coupling constant C^2.

Curve I, The value in the exact solution; II, the value (x'', y'') of the corrected parameter given by the KM method with trial functions (i); III, the value (x', y') of the uncorrected parameter given by the KM method with trial functions (i). × marks the value of (x'', y'') for $C^2 = 10$ using mixed trial functions (iii).

The Born approximation was again found by putting $f_0(r) = \sin k_0 r$ on the right-hand side of equation (25*b*). It gives $\underset{\sim}{Q}_{\mathrm{in}}$ proportional to C^2 and is shown by the straight line in figure 1. It clearly holds only for weak couplings and is in excess of the possible maximum even before the true maximum value of $\underset{\sim}{Q}_{\text{in}}$ is reached.

Equations (25) were first solved, using the crude trial function (i), by the Kohn–Moiseiwitsch variational procedure (§ 2.2). In figures 2 and 3 are shown for comparison the uncorrected and corrected parameters, while in figure 1 are shown the inelastic cross sections, for various values of C^2, calculated by inserting the corrected parameters x'', y'', into (10*b*). It will be seen that over the range for which the Born approximation is good the KM method gives a cross section very close to the true one: for stronger couplings it progressively overestimates the cross section. Thus at the maximum ($C^2=7$) $\underset{\sim}{Q}_{\text{in}}$ is 7% too great; at $C^2=10$ the error is 20%. In this region even the corrected parameters differ considerably from the exact values.

On account of the extensive arithmetical work necessary, further calculations were carried out for one particular value of C^2 only. The value $C^2=10$ was selected as representing a case not too far removed from the region of interest in real problems involving strong coupling. At the same time, it shows a sufficiently large discrepancy between the exact and variational solutions for subsequent improvements with better trial functions to be significant. The results of various calculations for this case are shown in table 1.

Table 1. Variational Solutions of Equations (3) using model A.
$k_0=1,\ k_1=\frac{1}{2},\ C^2=10$

Trial functions	Method used	Corrected Parameters				$\lvert\beta''\rvert^2$	$\underset{\sim}{Q}_{\text{in}}$ (units $\pi a_0{}^2$)	
		α''		β''				
		x''	y''	u''	v''			
—	E	−0·792	−2·582	−0·257	−2·257	5·162	0·767	
(i)	KM	−0·304	−1·579	−0·969	−1·393	2·879	0·937	(0·854)
(ii)	KM	−0·307	−1·577	−0·988	−1·417	2·983	0·937	(0·886)
	HM	−0·285	−1·667	−1·031	−1·460	3·195	0·927	(0·888)
(iii)	KM	−0·170	−2·630	−0·830	−2·133	5·240	0·797	(0·793)
(iv)	R	−1·395	−2·401	−1·357	−1·721	4·802	0·711	

E = exact solution; KM = Kohn–Moiseiwitsch; HM = Hulthén–Moiseiwitsch; R = Rubinow. The values of $\underset{\sim}{Q}_{\text{in}}$ were calculated by insertion of x'', y'', into equation (10*b*). The values in brackets were obtained by insertion of x'', y'', u'', v'', into (10*a*). Equations (21) and (22) were used to calculate the Rubinow parameters and cross section.

When the simplified trial functions (ii) were used with the KM method the difference in the results was negligible. These functions were therefore used instead of (i) to compare the KM with the Hulthén–Moiseiwitsch method (§ 2.1). The improvement brought about by using the HM method was clearly very slight. It was therefore decided to carry out the solution with the mixed functions (iii) using the simpler KM procedure. The evaluation of integral (4) involved very extensive complex arithmetic. The condition (15) gave twelve simultaneous (but linear) equations for the real and imaginary parts of the parameters. It may be seen that the improvement brought about by the use of the more refined trial functions was considerable. The cross section came out to be less than 4% greater than the exact value, while the corrected parameters obeyed the relation for particle conservation almost exactly.

Finally, the equations were solved by the Rubinow procedure (§ 2.3) with the very crude trial functions (iv). These are substantially equivalent to the functions (ii) used above, and it is apparent that the results were better than those obtained with the KM and HM method using these functions.

§ 5. CALCULATIONS WITH MODEL B

In this model the term V_{01} was set equal to zero, while terms were retained to represent the effects of distortion and exchange coupling. The effects of V_{00} and K_{00} were represented by a combined term $v_0(r)$ such that $v_0(r) = -C$ for $r < r_0$, $v_0(r) = 0$ for $r > r_0$. Similarly V_{11} and K_{11} were represented by $v_1(r)$ such that $v_1(r) = -D$ for $r < r_1$, $v_1(r) = 0$ for $r < r_1$.

For $K_{01} = K_{10}$ artificial wave functions $\psi_0(r)$, $\psi_1(r)$, were assumed such that

$$\psi_0(r) = \left(\frac{3}{4\pi r_0^3}\right)^{1/2} \quad r < r_0 \qquad \psi_1(r) = \left(\frac{3}{4\pi r_1^3}\right)^{1/2} \quad r < r_1$$
$$= 0 \qquad r > r_0, \qquad\qquad = 0 \qquad r > r_1.$$

The interaction between the electrons was taken as $Ae^2/2r_{12}$, and $k_{01}^2 = 0$, thus giving $K_{01}(r, r') = -\mathscr{A}^{1/2} rr'/r_>$ for $r < r_0$, $r' < r_1$; and $K_{01}(r, r') = 0$ for $r > r_0$ or $r' > r_1$.

Here $\mathscr{A}^{1/2} = 3A/(r_0 r_1)^{3/2}$ is a parameter measuring the coupling strength.

Exact solutions for this model have already been given by Massey and Mohr (1952). The corresponding forms of equations (3) are given in their paper and will not be written out here.

For carrying out the Moiseiwitsch variational procedures the integral (4) becomes

$$\begin{aligned} J_t = -\Bigg[& \int_0^\infty f_{0t}^*(r) \left\{\frac{d^2}{dr^2} + k_0^2\right\} f_{0t}(r)\,dr + \int_0^{r_0} f_{0t}^*(r) \Bigg\{ 2Cf_{0t}(r) \\ & - \mathscr{A}^{1/2} \left(\int_0^r r' f_{1t}(r')\,dr' + r \int_r^{r_1} f_{1t}(r')\,dr' \right) \Bigg\} dr + \int_0^\infty f_{1t}^*(r) \left\{ \frac{d^2}{dr^2} + k_1^2 \right\} f_{1t}(r)\,dr \\ & + 2D \int_0^{r_1} f_{1t}^*(r) f_{1t}(r)\,dr - \mathscr{A}^{1/2} \Bigg(\int_0^{r_0} f_{1t}^*(r) \left\{ \int_0^r r' f_{0t}(r')\,dr' + r \int_0^{r_0} f_{0t}(r')\,dr' \right\} dr \\ & + \int_{r_0}^{r_1} f_{1t}^*(r) \left\{ \int_0^{r_0} r' f_{0t}(r')\,dr' \right\} dr \Bigg) \Bigg]. \end{aligned}$$

For numerical calculations the following values were used: $k_0 = 1$, $k_1 = \frac{1}{2}$, $r_0 = 1$, $r_1 = 2$, $C = 1{\cdot}1$, $D = 1{\cdot}75$, $\mathscr{A} = 20$. The choice of $\mathscr{A}$ was made to give a coupling strength in a range comparable with $C^2 = 10$ of the previous model.

Calculations were carried out by the Kohn–Moiseiwitsch method only, using both the crude and mixed trial functions (ii) and (iii). The results obtained for the cross sections are given in table 2.

Table 2. Variational Solutions of Equations (3) using model B.
$k_0 = 1$, $k_1 = \frac{1}{2}$, $\mathscr{A} = 20$

Trial functions	—	(ii)	(iii)	—	—
Method used	E	KM	KM	DWBO	BO
Q_{in} (units of πa_0^2)	0·432	0·402 (0·401)	0·409 (0·407)	1·66	11·0

E = exact solution; KM = Kohn–Moiseiwitsch; DWBO = distorted wave Born–Oppenheimer approximation (weak coupling); BO = Born–Oppenheimer approximation. Unbracketed cross sections from (10*b*), bracketed cross sections from (10*a*).

It can be seen that even with functions (ii) a good approximation was obtained, the cross section being then 7·0% below the true value. The mixed functions (iii) gave some improvement, reducing the error to 5·3%. The solutions in both cases obeyed the particle conservation condition almost exactly.

§ 6. Discussion and Conclusions

The foregoing investigation had a twofold purpose: to compare the merits of the different variational principles, and to ascertain if the more refined trial functions of type (iii) will yield more accurate values for the cross section in close coupling cases than the cruder functions so far employed. In assessing the relative merits of the variational methods one has to weigh the accuracy of approximation achieved against the time and labour involved in computation. The HM method (§ 2.1) has the drawback that one of the equations for determining the parameters is of second degree, whereas in both KM and Rubinow methods (§ § 2.2 and 2.3) the simultaneous equations are all linear in the parameters. The calculations with model A suggest that there is no marked gain in accuracy when the HM method is employed so that it is clearly preferable to use one of the other methods. In the foregoing calculations the simultaneous equations were solved by conventional numerical methods. If an electronic computer were available this could be done much more easily and it would become practicable to handle a larger number of parameters in the trial functions.

There is little to choose between the KM and Rubinow procedures with regard to ease of calculation. The KM method has the disadvantage of working with complex parameters and also of involving the calculation of the correction integrals $I(\alpha', \beta', c_i')$ and $J(\alpha,' \beta', c_i')$. Rubinow's method uses real parameters, but the presence of the mixing parameter considerably complicates the algebraic development of the expressions to be varied. Furthermore, the iterative process of alternatively solving the quartic equation for the mixing parameter and the set of simultaneous equations for the parameters in the inside wave functions is very tedious. Given equal numbers of parameters the KM method probably involves less labour than the Rubinow. On the other hand the results of the calculations on model A with crude trial functions (ii), (iv) (see table 1), show the Rubinow method to yield a considerably better result for the cross section than the KM (7% error as against 22%), so that the extra labour could be considered worth while. The Rubinow method was not tried out with the improved trial functions (iii); further calculations here would be of interest.

With regard to the effectiveness of the different trial functions it seems a reasonable conclusion that the use of mixed functions of type (iii) will give a value for the cross section which is a good approximation. In both the models studied the values found were within 5% of the exact solution. With the crude functions, however, there may be a considerable error as shown in the case of model A. Since the crude functions are much more effective in model B, where the term V_{01} is omitted, it seems likely that it is V_{01} rather than the exchange and distortion terms which is responsible for the failure of the crude functions. These conclusions are compatible with the results of recent calculations, on the 1s–2s excitation of hydrogen, by Bransden and McKee (1956), who have obtained exact solutions of equations (3) without exchange terms (i.e. with the K's set equal to zero). Their results indicate that the inelastic cross sections derived for this case by Massey and Moiseiwitsch (1953), using the HM method with the crude trial functions (i), differ from the exact values by about 50%. At the same time, however, they show that the distorted wave (weak coupling) approximation is fairly good for this case. Hence the error in the variational cross section is surprisingly large, for the corresponding calculations with model equations A suggest that the variational result should be good in a case where the weak coupling approximation is not much in error. Even where this approximation gives results which greatly exceed the possible maximum, the variational method, using the crude functions (i), only gives an error of about 20% with the model equations. A re-examination of the variational calculations for the 1s–2s hydrogen case seems desirable. The results obtained in the present paper suggest that a considerable improvement in accuracy might be expected if mixed trial functions of the type (iii) are used, since in the case of model A the error was reduced to about one-fifth of the original amount by this means. The solutions of Bransden and McKee would provide a useful check on the accuracy of the approximation.

Acknowledgments

I should like to thank Professor H. S. W. Massey for his helpful advice and encouragement during the course of this investigation, and for making available the value of the exact cross section in the case of model B.

My thanks are also due to Dr. H. R. Heath for facilities at Battersea Polytechnic.

References

Bransden, B. H., and McKee, J. S. C., 1956, *Proc. Roy. Soc.* A, **69,** 422.
Erskine, G. A., and Massey, H. S. W., 1952, *Proc. Roy. Soc.* A, **212,** 521.
Hulthén, L., 1944, *K. Fysiogr. Sällsk, Lund. Förh.*, **14,** No. 21.
Kohn, W., 1948, *Phys. Rev.*, **74,** 1763.
Massey, H. S. W., and Mohr, C. B. O., 1933, *Proc. Roy. Soc.* A, **140,** 613; 1952, *Proc. Phys. Soc.* A, **65,** 845.
Massey, H. S. W., and Moiseiwitsch, B. L., 1953, *Proc. Phys. Soc.* A, **66,** 406.
Moiseiwitsch, B. L., 1951, *Phys. Rev.*, **82,** 753.
Mott, N. F., and Massey, H. S. W., 1949, *Theory of Atomic Collisions* (Oxford : Clarendon Press), 2nd Edn, Chapter VIII.
Rubinow, S. I., 1955, *Phys. Rev.*, **98,** 183.

The Collective Model of Nuclear Motion

By R. E. PEIERLS and J. YOCCOZ†
Department of Mathematical Physics, University of Birmingham

MS. received 11*th February* 1957

Abstract. Collective motions of a many-body system, such as translation, rotation and oscillation, may be incorporated approximately in a shell-model description by regarding the shell-model wave function as a trial function for a variational approach, and exploiting the fact that the expectation value of the energy is then independent of the location and orientation, and approximately independent of the size and shape of the potential well. If these degeneracies are removed in the usual way, one is led naturally to wave functions containing both shell-model and collective aspects and to approximate values for the translational, rotational and vibrational energies.

§ 1. Introduction

The 'collective' model of the nucleus, due to A. Bohr (1952) and further developed by Bohr and Mottelson (1953), has made important contributions to the understanding of many nuclear problems. In this model the variables which describe the shape and orientation of the nucleus are treated as dynamical variables. This approach has a strong intuitive appeal, and there is ample evidence that it contains many important features of the real behaviour of nuclei, particularly as regards the low-energy rotational states of nuclei with large quadrupole moments.

One would like to connect this model with the quantum equations of the nuclear many-body problem, in which it must evidently be contained. The natural approach to this is to introduce into the description of the many-body problem such a set of variables that the surface parameters are a part of this set. The remainder will represent the single-particle aspects of the motion. If one tries to use simply the surface variables *and* the particle coordinates as dynamical variables, one has a redundant set; a formalism using redundant variables is possible, but liable to lead to mathematical complications. Alternatively, one may reduce the number of variables, but then one must express the particle coordinates in terms of a smaller number of 'internal' coordinates and the surface variables. The implementation of such a programme also leads to considerable mathematical difficulties.

A large number of papers (e.g. Tolhoek 1955, Coester 1955, Tomonaga 1955, Nataf 1955, Lipkin *et al.* 1955, Villars, private communication), have made interesting contributions to this problem, but in each of them some points remain obscure.

In the present paper we discuss an alternative approach to this problem, which seems to have been suggested on a number of occasions (e.g. Hill and Wheeler 1953, Redlich and Wigner 1954), but which we feel deserves further exploration.

---

† Now at Laboratoire de Physique et Chimie Nucléaires du Collège de France, Paris.

It might be argued that a derivation of the model from first principles is a luxury, as long as one knows from intuitive arguments how to work with it. Apart from the intrinsic interest in connecting the model with the basic equation, there are, however, two questions from which such a connection would seem to be essential:

(1) To estimate the magnitude of the moments of inertia (and other parameters appearing in the model). These can be estimated by using the 'cranking model' in which the quantized motion of the surface is replaced by a classical rotation of given angular velocity (Inglis 1954, Bohr and Mottelson 1955, Valatin 1956). It is not clear, however, what approximation is involved in this step.

(2) To determine the limits of validity of the model. It seems that the rotational structure of the spectrum (energy levels proportional to $J(J+1)$) is accurate only for nuclei with large deformations (large quadrupole moments) and one wants to be clear just when the model is expected to be right quantitatively.

§ 2. OUTLINE OF METHOD. MOTION OF CENTRE OF MASS

We shall explain the principle of the method by discussing the motion of the centre of mass of the nucleus, which in a sense is the simplest kind of collective motion. It is easy to separate the motion of the centre of mass in the many-body problem and the kinetic energy due to this motion is then, of course, $k^2/2AM$ if A is the mass number, M the mass of one nucleon and k the total momentum ($\hbar = 1$).

If this separation is performed rigorously, the remaining problem of the internal motion is no longer in a convenient form for applying the shell-model approximation. It is therefore customary to use the shell model directly. This can be understood in the sense of a variation approach. We evaluate the expectation value of the correct Hamiltonian of the system by means of a trial function Φ which is a Slater determinant of one-particle wave functions in a suitable well U around the origin. If we want to allow for exchange terms (Hartree–Fock approximation), we must allow U to be velocity dependent, i.e. to be an integral operation in coordinate space. The Hartree–Fock equations are then

$$\Phi(\mathbf{x}_1, \dots \mathbf{x}_A) = \frac{1}{\sqrt{A_0!}} \sum_P (-1)^P u_{p1}(\mathbf{x}_1) \dots u_{PA}(\mathbf{x}_A) \qquad \dots\dots(2.1)$$

where P is a permutation of $1, 2, \dots, A$ and u_i satisfies the equation

$$\left(E_i + \frac{1}{2M}\nabla^2\right) u_i(\mathbf{x}) = \int U(\mathbf{x}, \mathbf{x}') u_i(\mathbf{x}') d^3\mathbf{x}'. \qquad \dots\dots(2.2)$$

Spin and isotopic spin variables are assumed included in the coordinates of (2.1). We then consider the mean energy

$$E_0 = \frac{\langle \Phi^* H \Phi \rangle}{\langle \Phi^* \Phi \rangle} \qquad \dots\dots(2.3)$$

where the brackets $\langle \dots \rangle$ indicate integration over all particle coordinates (and summation over spin and isotopic spin variables) and H is the complete Hamiltonian:

$$H = \sum \frac{1}{2M} p_i^2 + \tfrac{1}{2} \sum_{i,j} V(x_i - x_j). \qquad \dots\dots(2.4)$$

(2.3) can now be regarded as a variation principle for determining the well potential U, which, in turn, then fixes the trial function Φ by (2.1), (2.2).

Then the required form for U is

$$U(\mathbf{x},\mathbf{x}')=\delta(\mathbf{x}-\mathbf{x}')\sum_i\int V(\mathbf{x}-\mathbf{x}'')u_i^*(\mathbf{x}'')u_i(\mathbf{x}'')d^3\mathbf{x}'' \\ -\sum_i V(\mathbf{x}-\mathbf{x}')u_i(\mathbf{x})u_i^*(\mathbf{x}'). \qquad \ldots\ldots(2.5)$$

(2.2) and (2.5) are the well-known Hartree–Fock equations.

It is now known that the Hartree–Fock approach to real nuclei is probably invalid because of the importance of correlations in the nuclear wave function, and that this does not invalidate the shell model (Bruecker 1954, Bethe 1956). However, we shall use the simple Hartree–Fock method for our present purpose. It is likely that the Brueckner–Bethe type of approach could also be incorporated in our scheme, but it would seem premature to attempt this at the present stage.

The trial function (2.1) does not possess the required translational symmetry, since the potential well represents a centre of attraction. The function (2.1) implies the fiction of an attractive centre around which the centre of mass is capable of oscillating. Skyrme and Elliott (1955) have shown that this in general gives rise to unphysical solutions (representing a nucleus in its ground state oscillating as a whole about the attractive centre) and they show how to eliminate those unphysical states in the particular case of a harmonic well.

This fact can also be expressed by saying that there is a degeneracy in our solution, since the function

$$\Phi(\mathbf{x}-\mathbf{r})=\Phi(\mathbf{x}_1-\mathbf{r},\mathbf{x}_2-\mathbf{r},\ldots\mathbf{x}_A-\mathbf{r}) \qquad \ldots\ldots(2.6)$$

gives the same value to the energy (2.3) as Φ. Now it is well known that such a degeneracy always allows one to improve on the variational energy further by using as a new trial function an arbitrary linear combination of the degenerate ones.

In our case, since the degenerate functions (2.6) form a continuous set, the linear combination is of the form

$$\Psi=\int\chi(\mathbf{r})\Phi(\mathbf{x}-\mathbf{r})d^3\mathbf{r} \qquad \ldots\ldots(2.7)$$

where now $\chi(\mathbf{r})$ has to be determined from the variation principle†

$$\delta E=\delta\frac{\langle\Psi^*H\Psi\rangle}{\langle\Psi^*\Psi\rangle}=0. \qquad \ldots\ldots(2.8)$$

It is easy to prove that this condition is met by the function

$$\chi=\text{const. } e^{i\mathbf{k}.\mathbf{r}} \qquad \ldots\ldots(2.9)$$

so that

$$\Psi(\mathbf{x})=\text{const.}\int e^{i\mathbf{k}.\mathbf{r}}\,\Phi(\mathbf{x}-\mathbf{r})d^3\mathbf{r} \qquad \ldots\ldots(2.10)$$

and that the expectation value of the energy is

$$E=\frac{\int d^3\mathbf{r}\langle\Phi^*(\mathbf{x})H\Phi(\mathbf{x}-\mathbf{r})\rangle e^{i\mathbf{k}.\mathbf{r}}}{\int d^3\mathbf{r}\langle\Phi^*(\mathbf{x})\Phi(\mathbf{x}-\mathbf{r})\rangle e^{i\mathbf{k}.\mathbf{r}}}. \qquad \ldots\ldots(2.11)$$

---

† We here regard Φ as given by (2.1), (2.2), (2.5) so that (2.8) represents a variation principle only for χ. It might be more logical to determine also the u_i from (2.8). This does not change χ, but makes the u_i depend on χ. In spite of its greater complication this procedure may have advantages.

The integrands in numerator and denominator contain the overlap of the wave functions belonging to two wells a distance **r** apart and therefore decrease rapidly as **r** increases. We may therefore expand the exponential and have

$$E=\frac{h_0-\frac{1}{2}k_\mu k_\nu h_{\mu\nu}+\ldots}{n_0-\frac{1}{2}k_\mu k_\nu n_{\mu\nu}+\ldots} \qquad \ldots\ldots(2.12)$$

where

$$\left.\begin{aligned} h_0&=\int h(\mathbf{r})d^3\mathbf{r}, \quad h_{\mu\nu}=\int r_\mu r_\nu h(\mathbf{r})d^3\mathbf{r}, \quad h(r)=\langle \Phi^* H\Phi(\mathbf{x}-\mathbf{r})\rangle \\ n_0&=\int n(\mathbf{r})d^3\mathbf{r}, \quad n_{\mu\nu}=\int r_\mu r_\nu n(\mathbf{r})d^3\mathbf{r}, \quad n(r)=\langle \Phi^*\Phi(\mathbf{x}-\mathbf{r})\rangle. \end{aligned}\right\} \qquad \ldots\ldots(2.13)$$

Here μ, ν denote space directions, summation over repeated suffices being implied. From symmetry for a spherical well $h_{\mu\nu}=\delta_{\mu\nu}h_{11}$, $n_{\mu\nu}=\delta_{\mu\nu}n_{11}$ so that to the leading order in k^2

$$E=\frac{h_0}{n_0}+\tfrac{1}{2}k^2\left(\frac{h_0 n_{11}}{n_0{}^2}-\frac{h_{11}}{n_0}\right). \qquad \ldots\ldots(2.14)$$

(2.12), or its approximate form (2.13), is thus the approximation of our model to the correct centre-of-mass motion. The evaluation of (2.13) for specific cases will be discussed in a later paper. This will show that

(*a*) if U is taken as local oscillator well and we consider a non-degenerate state (2.12) gives exactly the right answer. This is not surprising since according to Skyrme and Elliott (1955) the centre-of-mass coordinates then separate off naturally. It is easy to see that the operation (2.10) then performs this separation correctly.

(*b*) For zero centre-of-mass momentum the operation (2.10) removes the unphysical states, since for these the integral (2.10) with $k=0$ just vanishes. This method therefore appears to give the natural generalization of the procedure of Skyrme and Elliott for an arbitrary shape of well.

(*c*) For a general (non-harmonic) well U the k^2 term is of the correct order of magnitude, but it differs from the correct answer by a numerical factor. This factor appears to be fairly close to unity, but it is now being investigated for a number of interesting cases. (2.12) ceases to be linear in k^2 for very large k. This corresponds to a centre-of-mass velocity of the order of the internal velocity of the nucleons; it is hardly surprising that the approximation based on a stationary well should fail in that region.

It is well known that solutions based on a variation principle must be applied with some caution if one is not dealing with the lowest state of given symmetry. This does not limit the usefulness of the function (2.10) with different k, since k determines the translational symmetry. It does, however, mean that functions with the same k, but different occupation of the shell states u_i in (2.1), will not in general be orthogonal even if one keeps the well potential U fixed. It is probable that, as in other applications, these non-orthogonal states will still lead to useful secular equations, but this needs further investigation.

§ 3. ROTATION OF WELL

The method outlined above can be applied at once to the problem of rotational states. Consider an even–even nucleus but not of a closed-shell configuration. It is then evident from the argument first given by Rainwater (1950) that an ellipsoidal well will in general give a lower value for the energy E_0 (equation (2.3)) than the spherical well. If we choose for U such an ellipsoidal well (whether velocity-dependent or not), we now have, besides the translational degeneracy considered in § 2, a directional degeneracy, since any orientation of the well in space generates a wave function which will give the same value of E_0 in (2.3).

If we assume the well to have axial symmetry, we require two angles θ, ϕ to specify its orientation. The degeneracy is then removed by writing, in analogy with (2.7),

$$\Psi=\int d\theta d\phi \chi(\theta,\phi)\Phi(R_{\theta\phi}\mathbf{x}) \qquad \ldots\ldots(3.1)$$

where $R_{\theta\phi}$ is the operator which brings the axis of symmetry from the z axis into the θ, ϕ direction. Φ is then the solution of (2.1), (2.2) with the symmetry axis of the well in the z direction. Since the ground state of the even–even nucleus in an axially symmetric well has axial symmetry the orientation of the x and y axes in their common plane is immaterial.

It is then evident that the choice of χ which will make (2.8) stationary is

$$\chi(\theta,\phi)=\text{const. } \mathrm{Y}_{lm}(\theta,\phi). \qquad \ldots\ldots(3.2)$$

This energy appears in the form

$$E_{lm}=\frac{\int\langle\Phi^*(R_{\theta\phi}\mathbf{x})H\Phi(R_{\theta'\phi'}\mathbf{x})\rangle \mathrm{Y}_{lm}{}^*(\theta\phi)\mathrm{Y}_{lm}(\theta'\phi')d\omega d\omega'}{\int\langle\Phi^*(R_{\theta\phi}\mathbf{x})\Phi(R_{\theta'\phi'}\mathbf{x})\rangle \mathrm{Y}_{lm}{}^*(\theta,\phi)\mathrm{Y}_{lm}(\theta'\phi')d\omega d\omega'}. \qquad \ldots\ldots(3.3)$$

The matrix elements in the integrands depend only on the angle Θ between the direction θ, ϕ and θ', ϕ'. If we write

$$\left.\begin{aligned}\langle\Phi^*(R_{\theta\phi}\mathbf{x})H\Phi(R_{\theta'\phi'}\mathbf{x})\rangle&=h(\Theta)=\sum h_l\mathrm{P}_l(\cos\Theta)\\ \langle\Phi^*(R_{\theta\phi}\mathbf{x})\Phi(R_{\theta'\phi'}\mathbf{x})\rangle&=n(\Theta)=\sum n_l\mathrm{P}_l(\cos\Theta)\end{aligned}\right\} \qquad \ldots\ldots(3.4)$$

then the addition theorem leads directly to the result

$$E_{lm}=h_l/n_l. \qquad \ldots\ldots(3.5)$$

If the wave function Φ belongs to a well of large anisotropy the overlap between the functions of different orientation is small unless the directions are nearly the same. We may then expand the Legendre polynomial in the definition of the expansion coefficients of (3.4):

$$\begin{aligned}h_l&=\frac{2l+1}{2}\int h(\Theta)\mathrm{P}_l(\cos\Theta)d\cos\Theta=\frac{2l+1}{2}\int h(\Theta)[1-\tfrac{1}{2}l(l+1)\Theta^2+\ldots]\sin\Theta d\Theta\\ n_l&=\frac{2l+1}{2}\int n(\Theta)\mathrm{P}_l(\cos\Theta)d\cos\Theta=\frac{2l+1}{2}\int n(\Theta)[1-\tfrac{1}{2}l(l+1)\Theta^2+\ldots]\sin\Theta d\Theta\end{aligned} \qquad \ldots\ldots(3.6)$$

and

$$E_{lm}=\frac{H_0-\frac{1}{2}l(l+1)H_2}{N_0-\frac{1}{2}l(l+1)N_2} \qquad \ldots\ldots(3.7)$$

$$\left.\begin{aligned}H_n&=\int h(\Theta)\Theta^n\sin\Theta d\Theta\\ N_n&=\int n(\Theta)\Theta^n\sin\Theta d\Theta.\end{aligned}\right\} \qquad \ldots\ldots(3.8)$$

The expression (3.7) is applicable only if $h(\Theta)$ and $n(\Theta)$ decrease sufficiently rapidly for the terms of higher order in (3.6) to be negligible. The work of Yoccoz (1957) shows that for a reasonably large anisotropy this is a good approximation. For the same reason the second terms in numerator and denominator of (3.7) are then small compared with the first, and we may write

$$E_{lm}=\frac{H_0}{N_0}+\tfrac{1}{2}l(l+1)\left[\frac{N_2H_0}{N_0^2}-\frac{H_2}{N_0}\right]. \qquad \ldots\ldots(3.9)$$

This is of the form of a rotational energy, and the last bracket gives, in principle, a value for the reciprocal moment of inertia. This is discussed quantitatively by Yoccoz. It is interesting to note that for smaller anisotropy the dependence of E_{lm} on l is no longer of the simple rotational form (3.9). This agrees with the fact that the exact validity of the $l(l+1)$ law for the excitation is found empirically only in the nuclei with large quadrupole moments.

It is also evident that only even l are possible since for an even–even nucleus Φ is of even parity, so that for an odd spherical harmonic (3.1) vanishes identically.

§ 4. VOLUME AND SURFACE OSCILLATIONS

So far we have regarded the well potential U as given. The trial functions (2.7) and (3.1) combined only shell-model wave functions, for varying location or orientation of the well, which are exactly degenerate in energy. If we compare different well shapes and sizes, their individual energy values will be different, having a minimum for a certain kind of well which is specified by the Hartree-Fock equations. However, near the minimum, the energy varies slowly and one must therefore regard all well forms near the minimum as almost degenerate. If ϵ is a parameter defining the nature of the well we are therefore led to consider the trial function

$$\Psi=\int\chi(\epsilon)\Phi(\mathbf{x},\epsilon)d\epsilon \qquad \ldots\ldots(4.1)$$

in which we expect $\chi(\epsilon)$ to be appreciable only in the neighbourhood of the value ϵ_0 belonging to the optimum well. The condition that the function (4.1) makes the Hamiltonian stationary is then

$$\int d\epsilon'\,[H(\epsilon,\epsilon')-EN(\epsilon,\epsilon')]\,\chi(\epsilon)=0 \qquad \ldots\ldots(4.2)$$

where

$$\left.\begin{aligned}H(\epsilon,\epsilon')&=\langle\Phi^*(\mathbf{x},\epsilon)H\Phi(\mathbf{x},\epsilon')\rangle\\ N(\epsilon,\epsilon')&=\langle\Phi^*(\mathbf{x},\epsilon)\Phi(\mathbf{x},\epsilon')\rangle.\end{aligned}\right\} \qquad \ldots\ldots(4.3)$$

If the matrix elements decrease rapidly with $\epsilon-\epsilon'$, we may expand χ into a Taylor series about ϵ, and have to second order:

$$(H_0-EN_0)\chi(\epsilon)+(H_1-EN_1)\frac{d\chi}{d\epsilon}+\tfrac{1}{2}(H_2-EN_2)\frac{d^2\chi}{d\epsilon^2}=0 \qquad \ldots\ldots(4.4)$$

or

$$\frac{d^2\chi}{d\epsilon^2}+\frac{2(H_1-EN_1)}{H_2-EN_2}\frac{d\chi}{d\epsilon}+\frac{2(H_0-EN_0)}{H_2-EN_2}\chi=0 \qquad \ldots\ldots(4.5)$$

with

$$\left.\begin{aligned}H_n(\epsilon)&=\int(\epsilon'-\epsilon)^nH(\epsilon,\epsilon')d\epsilon'\\ N_n(\epsilon)&=\int(\epsilon'-\epsilon)^nN(\epsilon,\epsilon')d\epsilon'.\end{aligned}\right\} \qquad \ldots\ldots(4.6)$$

(4.5) is an equation of the type of the Schrödinger equation for an oscillator, since the coefficients of χ and $d\chi/d\epsilon$ can again be expanded in Taylor series about the point ϵ_0 for which the last coefficient is a minimum. It differs from the usual oscillator equation by the occurrence of the energy in the denominators, which is connected with the lack of orthogonality of the eigenfunctions, and by the presence of the first-order term which can be eliminated in the usual way.

The lowest eigensolution of (4.5) will give a slightly improved approximation to the ground state of the nucleus, but this is not very interesting. The higher eigenvalues will correspond to the excitation of oscillators in the radius and shape of the nucleus. Since the excitation energies of such oscillations are, however, comparable with the internal excitation of the shell model it is doubtful whether the study of an equation like (4.5), derived from a single Slater determinant for the internal state, is an adequate approximation.

The general method of this paper will be applied to the rotational states in a paper by J. Yoccoz. Results which bear some resemblance to those of this paper have been obtained by Skyrme (1957) using a very different starting point. The authors would like to acknowledge several stimulating discussions with Mr. Skyrme.

REFERENCES

BETHE, H. A., 1956, *Phys. Rev.*, **103,** 1353.
BOHR, A., 1952, *K. Danske Vidensk. Selsk., Mat.-Fys. Medd.*, **26,** No. 14.
BOHR, A., and MOTTLESON, B. R., 1953, *K. Danske Vidensk. Selsk., Mat.-Fys. Medd.*, **27,** No. 16; 1955, *Ibid.*, **30,** No. 1.
BRUECKNER, K. A., 1954, *Phys. Rev.*, **95,** 217.
COESTER, F., 1955, *Phys. Rev.*, **99,** 170.
HILL, D. L., and WHEELER, J. A., 1953, *Phys. Rev.*, **89,** 1102.
INGLIS, D. R., 1954, *Phys. Rev.*, **96,** 1059; 1956, *Ibid.*, 103, 1786.
LIPKIN, H. J., DE SHALIT, A., and TALMI, I., 1955, *Nuovo Cim.*, **2,** 773.
NATAF, R., 1955, *C. R. Acad. Sci., Paris*, **240,** 2510, **241,** 31.
RAINWATER, J., 1950, *Phys. Rev.*, **79,** 432.
REDLICH, M. G., and WIGNER, E. P., 1954, *Phys. Rev.*, **95,** 122.
SKYRME, T. H. R., 1957, *Proc. Roy. Soc.* A, in the press.
SKYRME, T. H. R., and ELLIOTT, J. P., 1955, *Proc. Roy. Soc.* A, **232,** 566.
TOLHOEK, H. A., 1955, *Physica*, **21,** 1.
TOMONAGA, S., 1955, *Progr. Theor. Phys. Japan*, **13,** 467.
VALATIN, J. G., 1956, *Proc. Roy. Soc.* A, **238,** 132.
YOCCOZ, J., 1957, *Proc. Phys. Soc.* A, **70,** 388.

On the Moments of Inertia of Nuclei

By J. YOCCOZ

Laboratoire de Physique et Chimie Nucléaires du Collège de France

Communicated by R. E. Peierls; MS. received 11th February 1957

Abstract. The variational method developed in the previous paper is applied to the calculation of nuclear moments of inertia using an anisotropic harmonic well and neglecting spin–orbit couplings. The inter-nucleon forces are assumed to have a Gaussian form, either with zero range or with a realistic range, and in the latter case either for ordinary (Wigner) forces or for a Serber mixture. The results are shown in the figure. While with such a crude model no detailed agreement can be expected, the orders of magnitude and the trend of the results are encouraging.

Introduction

We wish to present in this paper an application of the general method described in the preceding paper (Peierls and Yoccoz 1957) to the problem of the rotational levels observed in many nuclei, especially in the rare-earth region, and studied extensively in the so-called collective model of Bohr and Mottelson (1953). The potential well, which serves as a basis for the shell model, is chosen to be non-spherical, and the shell-model wave function, defined for a fixed orientation of the well relative to the laboratory frame of reference, is integrated over all the positions of the well with a suitable weight function. The energy is then calculated, and exhibits a term which can be considered as a rotational energy, and gives us a value of the effective moment of inertia, calculated from the shell model. The crudeness of the model, and of the two-body forces used, prevent our results from being comparable with experiment in detail, but the relation between moment of inertia and intrinsic quadrupole moment is satisfactory enough to convince us that our description of collective motion can be useful. In § 1 we shall introduce the shell model and the two-body forces used. In § 2 we shall consider a simple type of rotational motion, and the development of the general method in this case. In § 3 we shall go over the numerical computations and the results. In § 4 we shall treat some aspects of the general rotational case.

§ 1.

The shell model used has been chosen for reasons of convenience, so as to simplify the numerical calculations. The potential well in which each nucleon is supposed to move has the form

$$U(\mathbf{x})=\frac{\hbar^2}{2\mu}\left[\alpha^4(x^2+z^2)+\beta^4y^2\right].$$

The individual levels are characterized by the three quantum numbers l, m, n, the energy

$$\epsilon=(l+n+1)\frac{\hbar^2\alpha^2}{\mu}+(m+\tfrac{1}{2})\frac{\hbar^2\beta^2}{\mu}$$

and the wave function $u_l(\alpha x)u_m(\beta y)u_n(\alpha Z)$ in which

$$u_p(\xi)=\pi^{-1/4}2^{-p/2}(p!)^{-1/2}H_p(\xi)\exp-[\xi^2/2].$$

We shall refer to a state in the ' shell ' P if $l+m+n=P$ by analogy with the spherical case. The parameters α and β will be determined in the following way :

(i) The mean value of $r^2=x^2+y^2+z^2$ will be set equal to the corresponding mean value for a uniform density in a nucleus of radius $R=\rho_0A^{1/3}$ where $\rho_0=1{\cdot}2\times10^{-13}$ cm.

We have
$$A\langle r^2\rangle=\frac{1}{\alpha^2}\sum(l+n+1)+\frac{1}{\beta^2}\sum(m+\tfrac{1}{2})$$

the summation being extended over all the occupied states. This convention will be always implied, if not otherwise stated.

(ii) The intrinsic quadrupole moment Q_0, the mean value of $\Sigma_j(2y_j^2-x_j^2-z_j^2)$ is closely related to the ratio β/α and the configuration of the ground state of our model (which also depends on this ratio) :

$$Q_0=\frac{1}{\alpha^2}\left[\frac{2\alpha^2}{\beta^2}\sum(m+\tfrac{1}{2})-\sum(l+n+1)\right].$$

The ratio β/α has no direct relation to the deformation parameter of Bohr and Mottelson. We have preferred to express our results in terms of Q_0 which is a quantity directly computable in our model and comparable to experiment. We shall suppose $\beta/\alpha<1$, $Q_0>0$ as observed in the nuclei in which we are interested. The computations can easily be extended to $Q_0<0$. We have neglected the spin–orbit coupling, and therefore our shell model will not exhibit the right order of levels, or the correct magic numbers. But as the collective motion involves essentially transport of masses, it is hoped that the introduction of such finer features as the spin–orbit force will have a minor effect. Moreover, it is well known (e.g. Hahn *et al.*, 1956) that the density given by a model based upon the harmonic oscillator potential well does not agree with the evidence, for example, from electron experiments. However, as the moment of inertia and quadrupole moment both involve mean values of quantities like x^2, y^2, z^2 it can be hoped that a modification of the density (giving more weight to the external parts of the nucleus) will modify the moment of inertia and the intrinsic quadrupole moment in the same way and so will not spoil the relation between these two quantities.

For the two-body interactions, we have made the following choice :

(i) The spatial dependence is assumed to be of the form $V(r)=V_0\exp(-r^2/r_0^2)$ (Gaussian potential), in order to obtain algebraic expressions for the various matrix elements. We have in such a case :

$$\langle p,q,r;p',q',r'|V|l,m,n;l,'m,'n'\rangle=V_0\langle p,p'|V_x|ll'\rangle\langle qq'|V_y|mm'\rangle\langle rr'|V_z|nn'\rangle$$
$$\langle pp'|V_x|ll'\rangle=\rho(2+\rho^2)^{-1/2}P_{ll'}{}^{pp'}[(2+\rho^2)^{-1}]$$

where $\rho=r_0\alpha$ and $P_{ll'}{}^{pp'}$ is a polynomial.

So

$$\begin{aligned}\langle p,q,r;p',q',r'|V|l,m,n;l',m',n'\rangle\\ &=V_0r_0^3\alpha^2\beta(2+r_0^2\alpha^2)^{-1}(2+r_0^2\beta^2)^{-1/2}F^{pqr,\,p'q'r'}_{lmn,\,l'm'n'}(r_0\alpha,r_0\beta)\\ &=BF^{pqr,\,p'q'r'}_{lmn,\,l'm'n'}(r_0\alpha,r_0\beta).\end{aligned}$$

$r_0\alpha$, $r_0\beta$ being less than 1, the essential dependence of this matrix element in respect of $r_0\alpha$ is contained in the factor B.

Using the values $s=1{\cdot}43$, $r_0 \simeq 1{\cdot}5 \times 10^{-13}$ cm given by the effective-range theory of Blatt and Jackson in the triplet case, and $\alpha = 4 \times 10^{12}\,\mathrm{cm}^{-1}$, we obtain $r_0\alpha = 0{\cdot}6$; $B_{\mathrm{T}} = 0{\cdot}63\ \hbar^2\alpha^2/\mu$. We shall adopt this value of B_{T} everywhere. $F^{pqr;\,p'q'r'}_{lmn;\,l'm'n'}$ will be calculated for two cases:

(*a*) $r_0\alpha = 0$. This corresponds to a contact interaction of a suitable strength.

(*b*) $r_0\alpha = 0{\cdot}5$. This somewhat unfortunate choice is due to an earlier choice of a larger radius R (and therefore a smaller value of α). We do not believe that this will modify the value of the moment of inertia by more than 10%.

(ii) The spin dependence is given by the factor $0{\cdot}8 + 0{\cdot}2\ P^B$, which gives a single effective strength equal to 0·6 of the triplet strength.

(iii) Majorana exchange forces are introduced by the factor $1 + \lambda P^{\mathrm{M}}/(1+\lambda)$ and computations done for $\lambda = 0$ (Wigner forces—case b_1) and $\lambda = 1$ (Serber force—case b_2). For $r_0\alpha = 0$ evidently, Majorana exchange does not give anything new.

§ 2.

We shall consider here a simple rotation of the nucleus around the Oz axis, perpendicular to the symmetry axis. The position of the potential well is characterized by the angle θ, and $\Phi(\mathbf{r}_1, \mathbf{r}_2 \ldots \mathbf{r}_A; \theta)$ is the wave function of the ground state for this position. The spins can be supposed quantized along the Oz axis, and, as there is no spin-orbit coupling, can be left out in most of the calculations. The nucleus will be treated as an assembly of four kinds of particles (protons with spin up and spin down, neutrons likewise). In order to avoid unnecessary difficulties, we shall restrict ourselves to ground states non-degenerate in our model (this corresponds to even–even nuclei, $K=0$ in the Bohr–Mottelson notation, and even parity). Therefore the weight function $\chi(\theta)$ which must already satisfy $\chi(\theta^2+\pi) = \chi(\theta)$ (cyclic coordinates), must satisfy also $\chi(\theta+\pi) = \chi(\theta)$ the two positions of the well θ and $\theta+\pi$ being indistinguishable. The range of the θ values will be any range of length π.

We will construct the wave function of the nucleus by

$$\Psi(\mathbf{r}_1, \ldots \mathbf{r}_A) = \int \chi(\theta)\Phi(\mathbf{r}_1, \ldots \mathbf{r}_A;\ \theta)\, d\theta.$$

Using the variational equation, we find immediately

$$\chi(\theta) = \exp(\pm iM\theta) \ (M \text{ an even intger})$$

$$E = H(M)/N(M)$$

where

$$H(M) = \int d\theta H(\theta) \exp(-iM\theta)$$

$$= \int e^{-iM\theta}\Phi^*(\mathbf{r}_1 \ldots, \mathbf{r}_A; \theta) H \Phi(\mathbf{r}_1 \ldots \mathbf{r}_A; 0)\, d\mathbf{r}_1 \ldots d\mathbf{r}_A d\theta$$

$$N(M) = \int d\theta N(\theta) \exp(-iM\theta)$$

$$= \int e^{-iM\theta}\Phi^*(\mathbf{r}_1 \ldots \mathbf{r}_A; \theta)\Phi(\mathbf{r}_1 \ldots \mathbf{r}_A; 0)\, d\mathbf{r}_1 \ldots d\mathbf{r}_A d\theta.$$

Due to the symmetries of Φ, $H(\theta)$ and $N(\theta)$ are even functions of θ, and E is an even function of M. The levels $+M$ and $-M$ are degenerate.

Moreover, it is easy to show that

$$L_z\Psi(\mathbf{r}_1 \ldots \mathbf{r}_A) = \pm M\hbar\Psi(\mathbf{r}_1 \ldots \mathbf{r}_A).$$

Before going over detailed computations, we should like to point out some intuitive facts. Physically, what we do is to rotate the potential well (in close analogy with the cranking model), expecting that the nucleons will follow this motion. It is rather obvious that the rotation of the well will operate only if the deformation is large enough, in order to 'catch' at least some nucleons. But then not only the nucleons in the asymmetric part will be involved, but also the inside ones through the nucleon–nucleon interactions and their kinetic energy. The moment of inertia is the complicated outcome of the two effects, and likely not to be the irrotational moment of inertia of Bohr and Mottelson, which involves essentially the nucleons in the symmetric part. Besides, only one configuration ever enters in Φ. This is justified as long as the energy involved in internal excitation is large compared to the energy of collective excitation. This condition, which we must always keep in mind, is not fulfilled when the deformation is small. Therefore, it will not be possible to use the limit $\beta/\alpha \to 1$ in our formulae.

We shall now study the nature of the functions $H(\theta)$ and $N(\theta)$. We have

$$\Phi(\mathbf{r}_1 \ldots \mathbf{r}_A;\theta) = \Phi(\mathbf{r}_1' \ldots \mathbf{r}_A')$$

with

$$\begin{aligned} x' &= x\cos\theta + y\sin\theta \\ y' &= -x\sin\theta + y\cos\theta \\ z' &= z. \end{aligned}$$

With our particular choice of the potential well we have, for a kind of particles

$$\phi_p(\mathbf{r}_1 \ldots \mathbf{r}_p) = GD[x^l y^m z^n] \exp -\tfrac{1}{2}[\alpha^2 \sum_j (x_j^2 + z_j^2) + \beta^2 \sum_j y_j^2] \quad \ldots\ldots (1)$$

where the Slater determinant D is built with the monomials $x^l y^m z^n$ and G a normalization constant.

Transforming

$$\left.\begin{aligned} &\tfrac{1}{2}\alpha^2(x^2 + x'^2 + z^2 + z'^2) + \tfrac{1}{2}\beta^2(y^2 + y'^2) \text{ into } u^2 + v^2 + w^2 \text{ by} \\ &e^2 = \alpha^2 - \beta^2,\ z = w/\alpha, \\ &y = v(\alpha^2 - \tfrac{1}{2}e^2\sin^2\theta)^{1/2}(\alpha^2\beta^2 + \tfrac{1}{4}e^4\sin^2\theta)^{-1/2} \\ &x = u(\alpha^2 - \tfrac{1}{2}e^2\sin^2\theta)^{-1/2} - \tfrac{1}{2}ve^2\sin\theta\cos\theta[(\alpha^2 - \tfrac{1}{2}e^2\sin^2\theta)(\alpha^2\beta^2 + \tfrac{1}{4}e^4\sin^2\theta)]^{-1/2} \end{aligned}\right\} \quad \ldots\ldots (2)$$

and using the fact that $N(\theta=0)=1$, we find that

$$N(\theta) = \left[1 + \frac{e^4}{4\alpha^2\beta^2}\sin^2\theta\right]^{-X} (\cos\theta)^Y.$$

The integers X and Y can be calculated from the quantum numbers of the occupied states.

X involves all the states. The contribution of a complete 'shell' P is $tP = P(P+1)(P+3)/6$. The contribution of an incomplete 'shell' Q (all the levels $l+m+n=Q$ are not occupied) is

$$t_Q = n_Q(n_Q+1)(n_Q+3)/6 + (Q-n_Q)(n_Q+1)(n_Q+2)/2$$

where n_Q is the maximum value of the quantum number n in this shell for the occupied states.

$$X = \tfrac{1}{2}A + \sum_P t(P) + \sum_Q t(Q).$$

Y involves only the incomplete shells

$$Y = \tfrac{1}{2}\sum_{Q}(Q - n_Q)(n_Q + 1)(n_Q + 2).$$

Even for heavy nuclei $A \sim 180$, and for the appropriate values of β/α, the shape of $N(\theta)$ is primarily determined by $(\cos\theta)^Y$. Y is usually of the order of 60–80, and it is, if so, possible to write

$$N(\theta) \simeq \exp - [K\theta^2] \quad \left(K = \frac{Y}{2} + \frac{Xe^4}{4\alpha^2\beta^2}\right). \qquad \ldots\ldots(3)$$

K is of the order of 30–40, and $N(\theta)$ a strongly peaked function of θ near $\theta = 0$.

Our principal aim in the direct study of $H(\theta)$ is to make plausible an expansion of the type

$$H(\theta) = N(\theta)[\mathscr{H}_0 + \mathscr{H}_2\theta^2 + \mathscr{H}_4\theta^4 + \ldots] \qquad \ldots\ldots(4)$$

in which the coefficients $\mathscr{H}_2$, $\mathscr{H}_4$ are at least of the same order. The presence then of the factor $N(\theta)$ will ensure that only small values of θ (and the first few terms of the expansion) will matter. We shall separate H in the kinetic energy part T and the potential energy part V.

For $T(\theta)$, the form (4) is fully justified, if we remember that Φ is a solution of the equivalent Hamiltonian. The contribution to the bracket in (4) comes from the expansion in respect to θ of

$$\text{(i)} \quad \frac{\hbar^2}{2\mu}\Big\{S_1\alpha^2\left[2 - \frac{e^2}{2\alpha^2}\sin^2\theta\left[1 - \frac{e^2}{2\alpha^2}\sin^2\theta\right]^{-1}\right]$$

$$+ S_2\beta^2\left[1 + \frac{e^4}{4\alpha^2\beta^2}\sin^2\theta\right]^{-1}\left[1 - \frac{e^2}{2\alpha^2}\sin^2\theta + \frac{e^4}{4\beta^4}\sin^2\theta\cos^2\theta\left(1 - \frac{e^2}{2\alpha^2}\sin^2\theta\right)^{-1}\right]$$

where

$$S_1 - \sum l + \tfrac{1}{2}; \quad S_2 - \sum m + \tfrac{1}{2}$$

$$\text{(ii)} \quad S_3 e^2 \sin^2\theta\left(1 - \frac{e^2}{2\alpha^2}\sin^2\theta\right)^{-1},$$

in which S_3 is a function, independent of θ, of the quantum numbers of the incomplete shells. We have thus an expansion in respect of quantities of the order of $l^2/2\alpha^2$ ($\sim 0{\cdot}1$) and expansions of trigonometric functions.

The potential energy part $V(\theta)$ is more tricky. If r is the distance between the particles 1 and 2, we have, with the transformation (2) and $u = u_1 - u_2 \ldots$

$$r^2 = \frac{u^2}{\alpha^2}\left(1 - \frac{e^2}{2\alpha^2}\sin^2\theta\right)^{-1}$$

$$+ \frac{v^2}{\beta^2}\left(1 - \frac{e^2}{\alpha^2}\sin^2\theta + \frac{e^4}{2\alpha^4}\sin^2\theta\right)\left(1 - \frac{e^2}{\alpha^2}\sin^2\theta\right)^{-1}\left(1 + \frac{e^4}{4\alpha^2\beta^2}\sin^2\theta\right)^{-1}$$

$$+ \frac{w^2}{\alpha^2} - \frac{uv}{\alpha\beta}\frac{e^2}{\alpha^2}\sin\theta\cos\theta\left(1 - \frac{e^2}{2\alpha^2}\sin^2\theta\right)^{-1}\left(1 + \frac{e^4}{4\alpha^2\beta^2}\sin^2\theta\right)^{-1/2}.$$

The terms in θ are affected by coefficients of the type $e^2/\alpha^2 \simeq 0{\cdot}2$ and therefore we expand the interactions between particles in the form

$$V(r) = \mathscr{U}_0(u, v, w) + e^2\sin\theta\cos\theta\,\mathscr{U}_1(u, v, w) + e^2\sin^2\theta\,\mathscr{U}_2(u, v, w) + \ldots \qquad \ldots\ldots(5)$$

$V(\theta)$ can then be put in the form

$$V(\theta) = N(\theta)[V_0' + V_2'\sin^2\theta + V_4'\sin^4\theta + \ldots]$$

where V_0' is the mean value of the potential energy in the configuration ϕ. V_2' contain three contributions :

(a) The term $\mathcal{U}_2$, in (5), with the coefficient e^2, between all the states.

(b) The term $\mathcal{U}_1$, in (5), with the coefficient e^2, between some states of the incomplete shells and all the others.

(c) The term $\mathcal{U}_0$, in (5), between some states of the incomplete shells and all the others. Due to the absence of the factor e^2, the last term can be (even if the number of the matrix elements is lower) of the same order as the first. The second is less important. This view is supported by the detailed calculation which follows.

V_4' contains five contributions $[\mathcal{U}_0 \dots \mathcal{U}_4]$. The terms $\mathcal{U}_4$, $\mathcal{U}_3$ have the same structure as the terms $\mathcal{U}_2$ in V_2', but with the coefficient e^4. $\mathcal{U}_1$ and $\mathcal{U}_2$ have the same importance as before, and a rough estimate of V_4' can be obtained keeping only the term in $\mathcal{U}_0$. Detailed computations have convinced us that V_4' is a fraction of V_2'.

It is then easy to deduce (4) from (5). An expansion of the type (4) has the following interest. Assuming

$$N(\theta) \simeq \exp[-K\theta^2] \qquad \dots\dots(6)$$

$$H(\theta) \simeq \exp[-K\theta^2][\mathscr{H}_0 + \mathscr{H}_2\theta^2 + \dots] \qquad \dots\dots(7)$$

and using the Taylor series, we get

$$K = \langle L_z^2 \rangle / 2\hbar^2 \qquad \dots\dots(8)$$

$$-\mathscr{H}_2 = [\langle L_z^2 H \rangle - \langle L_z^2 \rangle \langle H \rangle] / 2\hbar^2 \qquad \dots\dots(9)$$

where L_z is the z component of the total orbital angular momentum and the brackets mean that average values with respect to ϕ are taken.

In the following, we shall use equations (8) and (9).

E can then be written

$$E = \mathscr{H}_0 + \frac{\mathscr{H}_2}{2K} + \frac{3\mathscr{H}_4}{4K^2} + \dots - \frac{M^2}{4K^2}\left[\mathscr{H}_2 + 3\frac{\mathscr{H}_4}{K} + \dots\right] + \frac{M^4}{16K^4}[\mathscr{H}_4 + \dots] + \dots \qquad \dots\dots(10)$$

If K is large enough, $\mathscr{H}_2$, $\mathscr{H}_4$ being at least of the same order, we can neglect the terms in M^4, and higher orders, if $M^2/4K^2 \ll 1$. Interpreting the second term as rotational energy, we get, for the moment of inertia

$$I = \frac{2\hbar^2 K^2}{-[\mathscr{H}_2 + 3\mathscr{H}_4/k]} \simeq \frac{2\hbar^2 K^2}{-\mathscr{H}_2} \qquad \dots\dots(11)$$

$$I = \frac{|\langle L_z^2 \rangle|^2}{\langle L_z^2 H \rangle - \langle L_z^2 \rangle \langle H \rangle}. \qquad \dots\dots(11')$$

§ 3.

We shall use the notation :

$$\delta = \beta/\alpha - \alpha/\beta$$

$$\sigma = \beta/\alpha + \alpha/\beta.$$

A summation sign like

$$\sum_{\substack{lmn,\, l+1,\, m-1,\, n \\ (l+2,\, m-2,\, n)}}$$

will mean that the summations are to be extended over all the occupied states l, m, n for which the states $l+1$, $m-1$ are occupied, but $l+2, m-2, n$ are not.

Using (8) we have :

$$K = \frac{\sigma^2}{8} \sum_{\substack{l,\,m,\,n\\(l+1,\,m-1,\,n)}} m(l+1) + \frac{\delta^2}{8} \sum_{\substack{l,\,m,\,n\\(l+1,\,m+1,\,n)}} (l+1)(m+1).$$

The contribution $\mathscr{T}_2$ to $\mathscr{H}_2$ is given by:

$$\mathscr{T}_2 = \frac{\hbar^2}{8\mu}\,\frac{\sigma\delta}{4}(\alpha^2-\beta^2) \sum_{\substack{l,\,m,\,n\\(l,\,m+2,\,n)}} (m+1)(m+2).$$

The $\mathscr{T}_2$ term, when negative, involves to the same extent complete and incomplete shells.

The contribution $\mathscr{V}_2$ is complex. We will limit ourselves to give the type of direct matrix elements we have.

Terms in $\sigma^2/8$

$$\sum_{\substack{lmn;\,l'm'n'\\(l+1,\,m-1,\,n;\,l+1,\,m'-1,\,n')}} [(l+1)m(l'+1)m']^{1/2}\langle l+1, \mathrm{m}-1, n\,;\, l', m', n'|\mathscr{U}|l, m, n\,;\, l', m', n'\rangle$$

$$-\sum_{\substack{lmn;\,l'm'n';\,l+1,\,m-1,\,n\\(l+2,\,m-2,\,n)}} [(l+1)(l+2)(m-1)m]^{1/2}\langle l+2, m-2, n\,;\, l', m', n'|\mathscr{U}|l, m, n\,;\, l', m', n'\rangle$$

$$+\sum_{\substack{lmn,\,l'm'n'\\(l+1,\,m-1,\,n)}} [(l+1)(l+2)(m-1)m]^{1/2}\langle l+2, m-2, n\,;\, l', m', n'|\mathscr{U}|l, m, n\,;\, l', m', n'\rangle$$

Terms in $\sigma\delta/8$

$$-\sum_{\substack{lmn;\,l'm'n'\\(l+1,\,m+1,\,n;\,l'+1,\,m'-1,\,n')}} [(l+1)(l'+1)m'(m'+1)]^{1/2}\langle l+1, m+1, n\,;\, l'+1, m'-1, n'|\mathscr{U}|l, m, n\,;\, l', m', n'\rangle$$

$$+\sum_{\substack{lmn;\,l'm'n'\\(l,\,m+2,\,n)}} [(m+1)(m+2)]^{1/2}\langle l, m+2, n\,;\, l', m', n'|\mathscr{U}|l, m, n\,;\, l', m', n'\rangle$$

$$-\sum_{\substack{lmn;\,l'm'n'\\(l+1,\,m-1,\,n)}} (2m+1)[(l+1)(l+2)]^{1/2}\langle l+2, m, n\,;\, l', m', n'|\mathscr{U}|l, m, n\,;\, l', m', n'\rangle$$

$$-\sum_{\substack{lmn;\,l'm'n';\,l+1,\,m+1,\,n\\(l+1,\,m+1,\,n)}} [(l+1)(l+2)]^{1/2}\langle l+2, m, n\,;\, l', m', n'|\mathscr{U}|l, m, n\,;\, l', m', n'\rangle$$

$$+\sum_{\substack{lmn;\,l'm'n';\,l+1,\,m+1,\,n\\(l+2,\,m,\,n)}} (2m+1)[(l+1)(l+2)]^{1/2}\langle l+2, m, n\,;\, l', m', n'|\mathscr{U}|l, m, n\,;\, l', m', n'\rangle$$

Terms in $\delta^2/8$

$$+\sum_{\substack{lmn;\,l'm'n'\\(l+1,\,m+1,\,n;\,l'+1,\,m'+1,\,n')}} [(l+1)(m+1)(l'+1)(m'+1)]^{1/2}\langle l+1, m+1, n\,;\, l'+1, m'+1, n'|\mathscr{U}|l, m, n\,;\, l', m', n'\rangle$$

$$+\sum_{\substack{lmn;\,l'm'n'\\(l-1,\,m+1,\,n)}} [(l+1)(l+2)(m+1)(m+2)]^{1/2}\langle l+2, m+2, n\,;\, l', m', n'|\mathscr{U}|l, m, n\,;\, l', m', n'\rangle$$

$$-\sum_{\substack{l,\,m,\,n;\,l',\,m',\,n';\,l+1,\,m+1,\,n\\(l+2,\,m+2,\,n)}} [(l+1)(l+2)(m+1)(m+2)]^{1/2}\langle l+2, m+2, n\,;\, l', m', n'|\mathscr{U}|l, m, n\,;\, l', m', n'\rangle$$

With the exchange matrix elements, we shall have to sum up all these contributions, with the modifications introduced by spin exchange and Majorana exchange forces.

We shall give some results for nuclei $N=Z$, and $\beta/\alpha = 0{\cdot}90$. The 'nuclei' will be specified by the total number A of nucleons. I_S is the moment of inertia of the nucleus rotating as a solid. I' is the moment of inertia calculated from (11) by using $\mathscr{T}_2^2$ instead of $\mathscr{H}_2$. I_s, I', I are given in units μ/α^2; $\mathscr{T}_2$, $\mathscr{H}_2$ in units $\hbar^2\alpha^2/\mu$, Q_0 in units $1/\alpha^2$ (to get Q_0 in ordinary units $10^{-24}\,\mathrm{cm}^2$, we have to divide the figure given by a number of the order 16–20). I and $\mathscr{H}_2$ are given for the three cases a, b_1, b_2.

A	120	140	144	152	164	180	200
K	22·2	2·3	12·5	26·9	39·1	43·8	341
I_s	406	469	498	551	620	702	89
Q_0	87	49	74	111	144	162	149
$\mathscr{T}_2$	2	2·1	2·3	2·7	3·1	3·5	3·8
$\mathscr{I}'$	490	5	136	540	990	1080	610
$-\mathscr{H}_2$ (a)	8·6	6·4	9·7	16	17	18·6	15·1
$-\mathscr{H}_2$ (b_1)	8·2	6·6	12·7	18·9	20·9	17·1	14·5
$-\mathscr{H}_2$ (b_2)	6·7	4·8	6·9	9·6	11	12·1	11·2
I (a)	110	2	33	90	180	200	150
I (b_1)	120	1·6	25	80	150	220	160
I (b_2)	150	2	46	150	280	310	210

For the ‘ nuclei ’ 140 and 144, K is small and therefore our results are only for comparison, since our approximations break down in these cases.

From the table, we can draw the following conclusions.

(*a*) With the kinetic energy only, we get large moments of inertia, of the order of I_s. We should like to point out here that it would be highly desirable to have self-consistency between the potential well and the two-body forces used. We use variational methods for the collective motion, based on one hand on the shell model, and on the other hand on the two-body forces. A self-consistency at the level of the shell model would probably improve the results. The fact that I' is sometimes bigger than I_s is due to this lack of self-consistency (a nucleus without interaction would be highly unstable).

(*b*) The introduction of the potential energy improves our results (even if we do not have self-consistency, the situation is somewhat better).

The moments of inertia I are a fraction (0·3–0·4) of I_s, the quadrupole moments Q_0 being of the right order of magnitude. The results are still quite sensitive to the kind of forces we choose, particularly to the amount of exchange. Much more work must be done in this field, but the fact that Serber force gives a qualitatively good relation between Q_0 and I is hopeful.

We have done also some calculations for nuclei $N \neq Z$, with Serber forces, for which the ground state can be considered as non-degenerate in our model.

$^{90}_{60}\mathrm{Nd}^{150}$ Experimental values : $Q_0 = 4{\cdot}8 \times 10^{-24}\,\mathrm{cm}^2$, $E_2 = 3\hbar^2/I = 132$ kev (excitation energy of the first level of rotation).

For $\beta/\alpha = 0{\cdot}88$, we have $\alpha = 4{\cdot}6 \times 10^{12}\ \mathrm{cm}^{-1}$, $Q_{0(\mathrm{calc})} = 4{\cdot}6 \times 10^{-24}\ \mathrm{cm}^2$, $\hbar^2\alpha^2/\mu = 8{\cdot}9$ Mev, $K = 35$, $I_s = 570\,\mu/\alpha^2$, $I' = 510\,\mu/\alpha^2$, $E_{2(\mathrm{calc})} = 110$ kev.

$^{92}_{62}\mathrm{Sm}^{154}$ Experimental values : $Q_0 = 7{\cdot}4 \times 10^{-24}\ \mathrm{cm}^2$; $E_2 = 82$ kev. For $\beta/\alpha = 0{\cdot}84$, $Q_{0(\mathrm{calc})} = 7{\cdot}4 \times 10^{-24}\,\mathrm{cm}^2$, $K = 50$. $E_{2(\mathrm{calc})} = 100$ kev.

$^{96}_{66}\mathrm{Dy}^{162}$ Experimental values : $8 \times 10^{24}\,\mathrm{cm}^2$; $E_2 = 82$ kev. For $\beta/\alpha = 0{\cdot}85$ (we cannot increase this value without introducing some degeneracy)

$$Q_{0(\mathrm{calc})} = 9 \times 10^{24}\ \mathrm{cm}^2, \qquad E_{2(\mathrm{calc})} = 65\ \mathrm{kev}.$$

$^{92}_{66}\mathrm{Dy}^{150}$ The experimental values are not known :

$$Q_{0(\mathrm{calc})} = 9 \times 10^{-24}\ \mathrm{cm}^2, \qquad E_{2(\mathrm{calc})} = 80\ \mathrm{kev}.$$

$^{114}_{76}\mathrm{Os}^{190}$ Experimental values not known, but we have for :

$^{110}_{76}\mathrm{Os}^{186}$ $\quad Q_0 = 5 \times 10^{-24}$ cm², $\quad E_2 = 135$ kev.

$^{112}_{76}\mathrm{Os}^{188}$ $\quad Q_0 = 5{\cdot}6 \times 10^{-24}$ cm², $\quad E_2 = 155$ kev.

For $\beta/\alpha = 0{\cdot}92$ $\quad Q_{0(\mathrm{calc})} = 5 \times 10^{-24}$ cm², $\quad E_{2(\mathrm{calc})} = 185$ kev.

These results are shown in the figure.

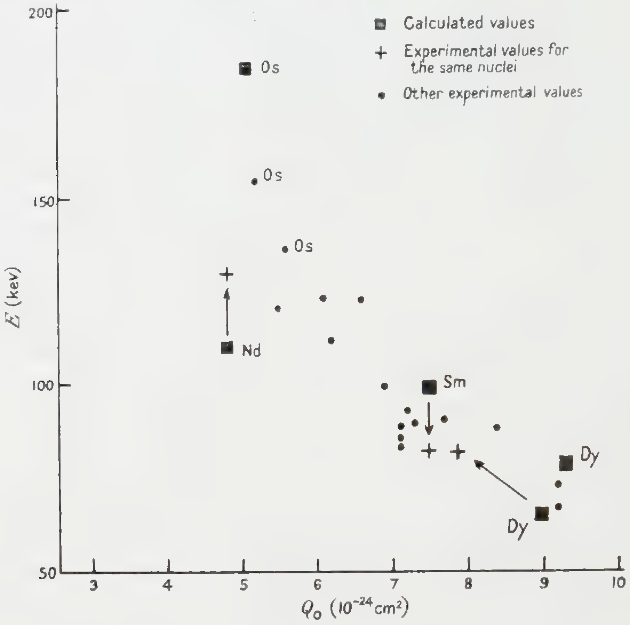

We shall now outline the theory of the general rotation, and give the results, part of which have already been given in the preceding paper (Peierls and Yoccoz 1957). $-\Phi^K(\mathbf{r}_1', \mathbf{r}_2' \ldots \mathbf{r}_A')$ will be the shell model wave function in the intrinsic frame $(Ox'y'z')$, K being the projection of the total intrinsic angular momentum along the axis of symmetry OZ' of the potential well. We can suppose $K > 0$, and use only Φ^K, because the introduction of a mixture of Φ^K and Φ^{-K} does not alter the results.

We use expansion of the type $\Phi^K = \sum a_J f_J^K$ in which the f_J^K functions are a basis of a representation of the rotation group ; we define the wave function of the nucleus as $\Psi(x) = \int Q(R)\Phi^K(x')\, dR$, where R is the rotation connecting the intrinsic frame and the laboratory frame. It can then be shown that a solution of the variational equation, giving a Φ which is an eigenfunction of the total angular momentum and its component along OZ, with the eigenvalues I and M, is the well-known matrix element of the rotation group :

$$Q(R) = \mathscr{D}^{*I}_{MK}(R).$$

The energy E is given by

$$\int d^I_{KK}(\theta)[H(\theta) - EN(\theta)] \sin\theta d\theta, \text{ where } d^I_{KK}(\theta)$$

is the reduced matrix element (Wigner 1931), involving only the rotation θ around Oy, that is an axis perpendicular to the symmetry axis, in complete analogy with the previous treatment. The introduction of the explicit form of $d^I_{KK}(\theta)$ gives a rotational spectrum identical with the spectrum given by Bohr and

Mottelson, with the values of the moment of inertia discussed above. The decoupling factor, for the case $K=\frac{1}{2}$, will be discussed in a subsequent paper.

ACKNOWLEDGMENTS

I wish to thank Professor R. Peierls for his great help, and Professor F. Joliot for his kind interest in this work. I should like to express also my gratitude to the Centre National de la Recherche Scientifique, for its financial support, both in France and in England.

REFERENCES

BOHR, A., and MOTTELSON, B. R., 1953, *K. Danske Vidensk. Selsk. Mat.-fys. Medd.*, **27,** No. 16.

HAHN, B., RAVENHALL, D. G., and HOFSTADTER, R., 1956, *Phys. Rev.*, **101,** 1131.

PEIERLS, R. E., and YOCCOZ, J., 1957, *Proc. Phys. Soc.* A, **70,** preceding paper.

WIGNER, E., 1931, *Phys. Z.*, **32,** 450.

RESEARCH NOTES

A Variational Calculation of the Cross Section for the 1s–2s Excitation of Hydrogen by Electron Impact

By B. H. BRANSDEN† and J. S. C. McKEE‡ §
† University of Glasgow ‡ Queen's University of Belfast

MS. received 31*st January* 1957

§ 1.

The calculation of cross sections for the elastic scattering of slow electrons by atoms or ions has been greatly facilitated by the introduction of variational methods, but corresponding methods for inelastic collisions have not yet been fully explored (Massey 1956). Variational procedures for the solution of coupled equations of the type occurring in inelastic scattering theory have been described, but not yet applied to electron excitation problems, by Blatt and Biedenharn (1954) and by Rubinow (1955); however a method, due to Moiseiwitsch (1951), has been employed in a calculation of zero angular momentum partial cross sections for the 1s–2s electron excitation of hydrogen atoms, by Massey and Moiseiwitsch (1953). These cross sections (in the non-exchange case), are somewhat smaller than those found by direct numerical solution of the appropriate equations (Bransden and McKee 1956), so that it is of interest to examine alternative approaches to the problem.

A version of Schwinger's variational method, with simple polynomial trial wave functions, has been used successfully by Altshuler (1953) to calculate zero angular momentum cross sections for the elastic scattering of electrons by hydrogen atoms, and it is the intention of this note to explore an extension of this procedure to inelastic collisions, by means of a calculation of the zero order 1s–2s electron excitation cross section of hydrogen atoms.

§ 2.

Erskine and Massey (1952) have derived the equations describing the excitation process. Neglecting exchange, they may be written, for zero angular momentum, in the form||:

$$\mathbf{L}(r)\mathbf{\Psi}(r)=\mathbf{V}(r)\mathbf{\Psi}(r)$$

where

$$L_{ij}(r)=\left(\frac{d^2}{dr^2}+k_i^{\,2}\right)\delta_{ij}, \qquad \ldots\ldots(1)$$

$$V_{ij}(r)=2\int\phi_i(r)\phi_j(r')\left\{\frac{1}{|r-r'|}-\frac{1}{r}\right\}d\mathbf{r}'\,; \qquad i,j=0,1$$

and $\mathbf{\Psi}(r)$ is the two-component column vector $\psi_i(r)$. $\phi_0(r)$, $\phi_1(r)$ are the normalized 1s and 2s hydrogen wave functions, $k_0^{\,2}$ is the kinetic energy of the incident electron and $k_1^{\,2}$ that of the inelastically scattered electron.

---

§ Now at the University of Birmingham.

|| Atomic units are used throughout.

Schwinger's variational method may be formulated in terms of two independent solutions of (1), $\boldsymbol{\Psi}^{\mathrm{A}}(r)$, $\boldsymbol{\Psi}^{\mathrm{B}}(r)$ defined so that

$$\boldsymbol{\Psi}^{\mathrm{A}}(r)=\boldsymbol{\Phi}^{\mathrm{A}}(r)+\boldsymbol{\Psi}_{\mathrm{OUT}}{}^{\mathrm{A}}(r), \quad \boldsymbol{\Psi}^{\mathrm{B}}(r)=\boldsymbol{\Phi}^{\mathrm{B}}(r)+\boldsymbol{\Psi}_{\mathrm{IN}}{}^{\mathrm{B}}(r) \quad \ldots\ldots (2)$$

where $\boldsymbol{\Phi}^{\mathrm{A}}(r)$, $\boldsymbol{\Phi}^{\mathrm{B}}(r)$ represent unperturbed waves incident on the 1s and 2s states of hydrogen,

$$\boldsymbol{\Phi}^{\mathrm{A}}(r)=k_0^{-1}\begin{pmatrix}\sin k_0 r\\ 0\end{pmatrix}, \qquad \boldsymbol{\Phi}^{\mathrm{B}}(r)=k_1^{-1}\begin{pmatrix}0\\ \sin k_1 r\end{pmatrix} \qquad \ldots\ldots (3)$$

and $\boldsymbol{\Psi}_{\mathrm{OUT}}{}^{\mathrm{A}}(r)$, $\boldsymbol{\Psi}_{\mathrm{IN}}{}^{\mathrm{B}}(r)$ contain, at great distances, only outgoing and incoming spherical waves respectively.

$\boldsymbol{\Psi}^{\mathrm{A}}(r)$, $\boldsymbol{\Psi}^{\mathrm{B}}(r)$ satisfy

$$\left.\begin{aligned}\boldsymbol{\Psi}^{\mathrm{A}}(r)&=\boldsymbol{\Phi}^{\mathrm{A}}(r)+\int_0^\infty \mathbf{G}(r,r')\mathbf{V}(r')\,\boldsymbol{\Psi}^{\mathrm{A}}(r')dr'\\ \boldsymbol{\Psi}^{\mathrm{B}}(r)&=\boldsymbol{\Phi}^{\mathrm{B}}(r)+\int_0^\infty \mathbf{G}^{\dagger}(r,r')\mathbf{V}(r')\boldsymbol{\Psi}^{\mathrm{B}}(r')dr',\end{aligned}\right\} \qquad \ldots\ldots (4)$$

where $G_{ij}(r,r')=-k_i^{-1}\sin k_i r_< \exp(ik_i r_>)\,\delta_{ij}$, $r_<$ being the smaller and $r_>$ the greater of r and r'.

The partial cross section of zero order for 1s–2s excitation Q_{1s-2s} and that for 2s–1s de-excitation Q_{2s-1s} may be expressed in terms of a scattering amplitude f, so that (in units of $\pi a_0{}^2$)

$$Q_{1s-2s}=\frac{4k_1}{k_0}\,|f|^2, \quad Q_{2s-1s}=\frac{4k_0}{k_1}\,|f|^2. \qquad \ldots\ldots (5)$$

Using (4) it is found that $f=R=S=T$ where

$$\left.\begin{aligned}R&=\int_0^\infty \boldsymbol{\Phi}^{\mathrm{B}\dagger}(r)\,\mathbf{V}(r)\,\boldsymbol{\Psi}^{\mathrm{A}}(r)\,dr\\ S&=\int_0^\infty \boldsymbol{\Psi}^{\mathrm{B}\dagger}(r)\,\mathbf{V}(r)\,\boldsymbol{\Phi}^{\mathrm{A}}(r)\,dr\\ T&=\int_0^\infty\!\!\int_0^\infty \boldsymbol{\Psi}^{\mathrm{B}\dagger}(r)\,\mathbf{V}(r)\,[\delta(r-r')-\mathbf{G}(r,r')\,\mathbf{V}(r')]\,\boldsymbol{\Psi}^{\mathrm{A}}(r')\,dr\,dr'\end{aligned}\right\} \qquad \ldots\ldots (6)$$

and that (RST^{-1}) is an expression for f, stationary with respect to variations of $\boldsymbol{\Psi}^{\mathrm{A}}(r)$, $\boldsymbol{\Psi}^{\mathrm{B}}(r)$.

The trial wave functions $\boldsymbol{\Psi}_{\mathrm{t}}{}^{\mathrm{A}}(r)$, $\boldsymbol{\Psi}_{\mathrm{t}}{}^{\mathrm{B}}(r)$ are taken to be the polynomials

$$\psi_j{}^{\mathrm{A}}(r)=\sum_{n=1}^{N} C_n{}^{\mathrm{A}}(j)r^n, \quad \psi_j{}^{\mathrm{B}}(r)=\sum_{n=1}^{N} C_n{}^{\mathrm{B}}(j)r^n \qquad \ldots\ldots (7)$$

and the constants C_n are determined numerically from the linear equations

$$\frac{\partial R}{\partial C_n}+\frac{\partial S}{\partial C_n}=\frac{\partial T}{\partial C_n}. \qquad \ldots\ldots (8)$$

Using the calculated C_n, $\boldsymbol{\Psi}_{\mathrm{t}}{}^{\mathrm{A}}(r)$, $\boldsymbol{\Psi}_{\mathrm{t}}{}^{\mathrm{B}}(r)$ are substituted into the stationary expression (RST^{-1}) to provide an approximate value of f.

§ 3.

The calculated cross section Q_{1s-2s} is compared with that given by numerical integration of equation (1) in table 1, for a number of incident energies up to 54 ev. Results are given for trial wave functions containing one, two or three terms ($N=1$, 2, 3 in (7)). The complexity of the numerical work increases greatly with increasing N, so that accurate computation beyond $N=3$ has not been undertaken, but it has been verified that the addition of terms in r^4 increases the $N=3$ cross section (column C in the table) by less than 7%. The rapid convergence of the cross section with increasing N, shown by the table, is similar to that found by Altshuler (1953) in his study of elastic scattering.

Zero Order Partial Cross Sections for the 1s–2s Excitation of Hydrogen by Electron Impact (without exchange)

Energy of incident electron	Q_{1s-2s} (units of πa_0^2)			
(ev)	E	A	B	C
10.2	0	0	0	0
13·5	0·204	0·110	0·164	0·189
19·4	0·102	0·055	0·081	0·094
30·4	0·0450	0·027	0·035	0·040
54·0	0·0155	0·003	0·012	0·014

E, from numerical solution of equations (1) (Bransden and McKee 1956). A, B, C, calculated cross sections using trial wave functions with $N=1$, 2, 3 respectively.

The calculated cross section for $N=3$ is in harmony with that found by direct numerical integration of (1) at all energies considered, and the results suggest that this form of the Schwinger variational method may provide a reasonably rapid method for the calculation of inelastic cross sections. The rapidity of convergence depends largely on the potential $\mathbf{V}(r)$ being of such short range that high powers of r do not contribute significantly to a power series expansion of the wave function inside the well, and it remains to be seen whether convergence will be as rapid when allowance is made for exchange.

REFERENCES

Altshuler, S., 1953, *Phys. Rev.*, **89,** 1278.
Blatt, J. M., and Biedenharn, L. C., 1954, *Phys. Rev.*, **93,** 1387.
Bransden, B. H., and McKee, J. S. C., 1956, *Proc. Phys. Soc.* A, **69,** 422.
Erskine, G. A., and Massey, H. S. W., 1952, *Proc. Roy. Soc.* A, **212,** 521.
Massey, H. S. W., 1956, *Rev. Mod. Phys.*, **28,** 199.
Massey, H. S. W., and Moiseiwitsch, B. L., 1953, *Proc. Phys. Soc.* A, **66,** 406.
Moiseiwitsch, B. L., 1951, *Phys. Rev.*, **82,** 753.
Rubinow, S. I., 1955, *Phys. Rev.*, **98,** 183.

REVIEWS OF BOOKS

Elementary Nuclear Theory, by H. A. Bethe and P. Morrison. Pp. xi + 274. (New York: Wiley; London: Chapman and Hall, 1956.) 50*s*.

The second edition of Professor Bethe's well-known book is a much improved and more extensive version of the earlier edition. The eight years that have elapsed between the two editions have brought to light a wealth of new detail and a goodly number of major advances in our understanding of nuclear structure and the characteristics of nuclear reactions. The authors have performed a far-reaching revision to take many of these developments into account, but the style remains clear and elementary. The new topics include the recently elucidated problem of nuclear radii, nucleon–nucleon scattering at high energies and its phenomenological interpretation in terms of phase shifts and nuclear forces, nuclear models, and the resonance theory of nuclear reactions including the interpretation of averaged cross sections by means of a complex potential; many other new topics are introduced more briefly. There is, finally, an appendix giving a table of all known nuclei, their modes of decay, spin, and mass. It is likely that this book will remain for several years to come the best elementary introduction to theoretical nuclear physics. I recommend it warmly to all beginners, and to their lecturers; those who " know all about nuclear physics already " will read it with admiration and delight.

B. H. FLOWERS.

Progress in Nuclear Energy. Series VI. Biological Sciences, Vol. 1, edited by J. C. Bugher, J. Coursaget and J. F. Loutit. Pp. x + 205. (London: Pergamon Press, 1956.) 50*s*.

Progress in Nuclear Energy is the title given to eight separate series of books dealing with nuclear energy and its applications. *Biological Sciences* is the title given to the sixth series and the book under review is the first annual publication of this series. The books were apparently planned before the Geneva Conference on the Peaceful Uses of Atomic Energy, but because such a vast amount of new scientific information was made available at Geneva it was thought that the first book in each series should be devoted to a review of the papers given at the Conference. Therefore, this volume is not typical of the series and the reader will not be able to form an opinion of the scientific value of future publications in this series from the first volume.

The book is divided into eight sections, each written by a worker well known in this branch of science. The first chapter by A. M. Brues and the next two chapters, both written by T. C. Carter, deal with the effects of radiation on living things. The other five chapters deal with the application of radioactive isotopes to the study of various problems in plant and animal research. An abstract of the subject matter is given at the beginning of each chapter (except in the case of the last chapter by Roche) and a long list of references to recent papers is given at the end of each chapter. The way in which the subject matter is treated in each chapter varies considerably. Brues, writing about the modes of radiation injury, summarizes briefly the contents of 24 Geneva Conference Papers in 12 pages whereas Carter, in the next chapter of 30 pages, fully reports four papers on genetics and quotes large parts from each. Only chapter 6, entitled Some Applications of Tracer Technique with C^{14} in Plant Biochemistry, by Bassham, Clavin and Porter is a true review article which is not entirely confined to summarizing Geneva Conference papers.

This book should be useful to those workers applying isotope techniques to biological problems for it gives them a concise account of a large number of papers in this field given at Geneva. It should also prove useful to other scientists not directly engaged in biological work who wish to make themselves familiar with the current research problems in this field. Finally, all who have thought about any possible harmful effects of the widespread use of atomic energy will find the first two chapters, dealing with radiation injury and genetic hazards, of interest.

G. W. DOLPHIN.

Physical Mathematics, by C. H. PAGE. Pp. x+329. (Princeton: van Nostrand; London: Macmillan, 1955.) 42*s*.

It must be emphasized that this is not a book for undergraduates. The opening words of the Preface suggest that the book is addressed to the " average graduate student of physics ", and the author states that his objective is " to help physicists correlate their smatterings of mathematical knowledge in such a way as to improve their feeling for the subject and increase its usefulness ". In spite of the relatively elementary material which makes its appearance here and there, however, the style of the book suggests that the author is really preaching to the converted.

In Chapter One, for instance, entitled " Integration and Differentiation ", the author introduces the Stieltjes integral very reasonably by means of a physical example, but immediately goes on to discuss for a whole page the Riemann and Lebesgue integrals, without defining either of them. In the same place the mathematical conception of *measure* is described, but very inadequately. Indeed, it is difficult to see why this topic was included, for it plays no significant role in the book and will almost certainly confuse the average physicist. Admittedly, in a footnote on page 11 it is pointed out that the *delta function* is not really a function at all, but a measure. None the less, the author's use of the delta function is not appreciably different from that to be found in most physics texts, where this subtlety goes unrecorded.

Later in the book it is somewhat surprising to discover the theory of a complex variable, and, in particular, complex integration, in a section entitled " Application of Fourier Transform Theory ". One cannot escape the conclusion that this was inserted as an afterthought, for on page 211 appears the statement " Hence $F_1(z)$ is analytic in the half-plane by Morera's theorem (the converse of Cauchy's theorem) ", while Cauchy's theorem is not even stated until three pages later and an analytic function defined later still.

It would be a pity, however, if these and other minor irritations should lead to the book being neglected by physicists, for it is in many ways excellent. The average physicist would be well advised to pass lightly over Chapter One and regard the book as essentially a treatise on the differential equations of mathematical physics, with particular emphasis upon Fourier and Laplace transform methods. Eigenvalue problems are very fully considered, and there are useful chapters on function space, integral equations and difference equations. The latter half of the book, dealing mainly with applications of Fourier and Laplace transforms, draws heavily upon electrical circuit theory for its physical examples. This may not appeal to some physicists, but, on the other hand, may prove useful to sophisticated electrical engineers and intending cyberneticists.

Possibly the greatest virtue of the book is its conciseness. A busy physicist might hope to read through it profitably in a finite time, which is more than can be said of some of the compendia of mathematical physics which have appeared recently.

S. RAIMES.

Laboratory Administration, by E. S. HISCOCKS. Pp. xvi + 392. (London: Macmillan, 1956.) 36*s*.

In this book the everyday problems which confront anyone responsible for the administration of a large modern laboratory are discussed in an easily readable manner.

The author describes and compares the methods used in a number of government and industrial laboratories in this country and abroad for dealing with the recruitment, assessment, remuneration and training of staff, with the provision of buildings and services, the flow of information, and with the programming, control, and evaluation of laboratory work.

Prominence is naturally given to the practices followed at the N. P. L. where Mr. Hiscocks is Secretary, but the book also contains much information culled from other sources. Many comparative statistics and examples of rating forms and organization charts are set out in 22 Appendices and together with a bibliography provide a useful source of reference.

Mr. Hiscocks has provided a broad survey of current practice in a field of management which is still developing. He does not claim that any of the administrative practices which he describes are the best or final answer to the problems discussed, and the book contains little that is really new.

T. D. S.

CONTENTS OF SECTION B

PAGE

Dr. H. H. Hopkins. The Aberration Permissible in Optical Sytems 449

Dr. D. H. Parkinson and Mrs. L. M. Roberts. The Atomic Heat of Cerium between 1·5° and 20°K 471

Dr. J. M. Lock. The Magnetic Susceptibility of Ytterbium from 1·3°K to 300°K 476

Mr. J. D. Nixon and Dr. P. C. Banbury. Junctions Induced in Germanium Surfaces by Transverse Electric Fields 481

Dr. J. M. Cowley and Mr. A. F. Moodie. Fourier Images : I—The Point Source 486

Dr. J. M. Cowley and Mr. A. F. Moodie. Fourier Images : II—The Out-of-focus Patterns 497

Dr. J. M. Cowley and Mr. A. F. Moodie. Fourier Images : III—Finite Sources 505

Prof. C. A. Hutchison, Jr., Dr. B. R. Judd and Mr. D. F. D. Pope. Paramagnetic Resonance Absorption in Gadolinium Trichloride 514

Prof. S. Tolansky and Mr. V. R. Howes. Induction of Ring Cracks on Diamond Surfaces 521

Research Notes :

Dr. E. W. J. Mitchell and Mr. P. T. Wedepohl. Magnetoresistance of a p-type Semiconducting Diamond 527

Dr. R. Parker. The Magnetoresistance of the Nickel–Zinc Ferrite System . 531

Mr. D. E. Bradley and Mr. R. Phillips. An Explanation of an Anomalous Form of Sub-boundary in Aluminium 533

Letters to the Editor :

Mr. H. N. V. Temperley. Would a Classical Gas of Non-attracting Rigid Spheres show a Phase Transition ? 536

Dr. K. W. H. Stevens. The Ising Model and Ferrimagnetism 537

Reviews of Books 540

Contents of Section A 544

The Capture of Stopped Negative Pions by Hydrogen

By J. M. CASSELS, G. FIDECARO†, A. M. WETHERELL
AND J. R. WORMALD
Nuclear Physics Research Laboratory, University of Liverpool

MS. received 1st *February* 1957

Abstract. A total absorption Cerenkov γ-ray spectrometer has been used to study the relative probabilities of mesonic and radiative capture. The ratio was found to be $1{\cdot}50 \pm 0{\cdot}15$. This result is collated with other data concerning the interaction of low-energy pions with nucleons and radiation. Reasonable consistency is found.

§ 1. Introduction

The interaction of stopped negative pions with hydrogen was first studied in the classic experiment of Panofsky, Aamodt and Hadley (1951). They showed that two competing reactions occur:

$$\pi^- + \mathrm{p} \rightarrow \pi^0 + \mathrm{n} \rightarrow 2\gamma + \mathrm{n}, \qquad \ldots\ldots(1)$$

$$\pi^- + \mathrm{p} \rightarrow \gamma + \mathrm{n}. \qquad \ldots\ldots(2)$$

The first reaction, referred to as mesonic absorption, leads to the production of a neutron of 0·40 Mev energy. The two γ-rays produced by the decay of the neutral pion share between them an energy of about 138 Mev. Their energy spectrum is therefore centred about 69 Mev, and extends with constant intensity from a lower limit of about 55 Mev to an upper limit of about 83 Mev, because of the neutral pion motion before decay. In order to conserve momentum the two γ-rays are emitted in nearly opposite directions, the minimum angle between them being about 157° (Chinowsky and Steinberger 1954 a).

The second reaction, radiative absorption, produces an 8·8 Mev neutron and a single 129 Mev γ-ray (Crowe and Phillips 1954) moving in opposite directions.

The ratio R of the probabilities of mesonic and radiative absorption was found by Panofsky *et al.* to be

$$R \quad \frac{w(\pi^- + \mathrm{p} \rightarrow \pi^0 + \mathrm{n})}{w(\pi^- + \mathrm{p} \rightarrow \gamma + \mathrm{n})} = 0{\cdot}94 \pm 0{\cdot}30 \qquad \ldots\ldots(3)$$

where, as in the rest of this paper, the uncertainty quoted is a standard deviation. The ratio R is referred to as the Panofsky ratio.

Since the absorption takes place when the pion is in the K shell, the reaction (1) can be related to the s-wave charge exchange scattering of low-energy negative pions. Similarly, reaction (2) can be related to the s-wave radiative capture, and so to the inverse reaction, which is the s-wave part of a photo-production process. The Panofsky ratio can in fact be calculated from the results of scattering and photo-production experiments, but until recently the value so obtained was about twice the experimental value (3).

In view of the obvious need for further data, two experiments on the high-energy γ-rays have been done at Liverpool. Both make use of the external strong-focused 96 Mev negative pion beam.

---

† Now at C.E.R.N., Geneva.

Kuehner, Merrison and Tornabene (to be published) have been using a conventional magnetic pair spectrometer of high resolution but low counting efficiency, while the experiment described here was done with a new type of Cerenkov γ-ray spectrometer, originally suggested by Kantz and Hofstadter (1954). The γ-rays are made to dissipate their energy in a cascade shower inside a block of lead glass. If the shower is fairly complete, the total length of electron track is nearly proportional to the incident electromagnetic energy. Almost all the track is relativistic so that the total amount of Cerenkov light emitted is also nearly proportional to the incident energy. Pulse-height analysis of the output from a large photomultiplier viewing the glass then gives the spectrum directly. The instrument has the advantage of high counting efficiency and, in principle, freedom from systematic errors, since the whole spectrum is observed at once in a very straightforward way. However, as will be seen, these advantages have here been only partially realized, because the resolution of the spectrometer was not quite good enough to resolve completely the two groups of γ-rays. Calibration experiments were therefore necessary in order to arrive at the separate line shapes.

§ 2. THE SPECTROMETER

The spectrometer consisted of two right cylinders of Chance EDF 653335 glass, each 5 in. in diameter and 4 in. long. These were placed in optical contact, to make a cylinder 8 in. in total length. All surfaces were polished, and a 5 in. E.M.I. photomultiplier with a photocathode sensitivity of 37 μA/lumen was placed in optical contact with one end. The γ-rays produced electron pairs in a 2 in. diameter external lead converter, and these pairs were counted by a coincidence counter and put in at the other end. This arrangement ensured that the showers in the glass started near the axis. A coaxial white shield surrounded the glass, and the radiation entered through a thin polished aluminium cap. The multiplier was shielded magnetically by coaxial soft-iron and mumetal shields.

The glass had a density of $3{\cdot}9\,\mathrm{g\,cm^{-3}}$, a refractive index of 1·69, a radiation length of 2·56 cm, and a critical energy of 16 MeV. The transmission of light of various wavelengths through ten radiation lengths of glass is shown in figure 1, together with the relative quantum efficiencies of the photocathode at the same

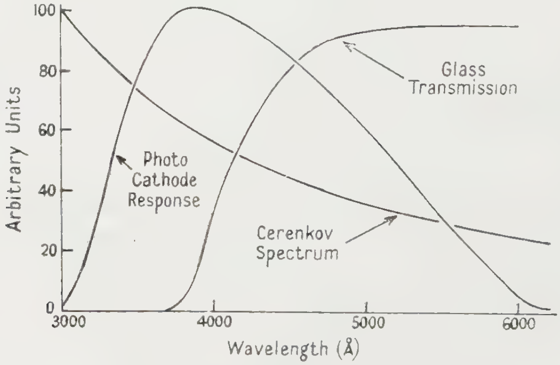

Figure 1. The Cerenkov spectrum, the quantum efficiency of the photomultiplier, and the transmission of the glass through 10 radiation lengths, as functions of photon wavelength.

wavelengths. There are some wavelengths at which both figures are reasonably large but the short wavelength cut-off in the transmission is clearly a limitation, especially since the number of quanta per unit wavelength interval in the Cerenkov radiation is proportional to λ^{-2}. The type of glass used in the spectrometer offered the best transmission per radiation length at short wavelengths.

The arrangement used for calibrating the spectrometer is shown in figure 2. The layout was the normal one for work with 96 MEV negative pions, except

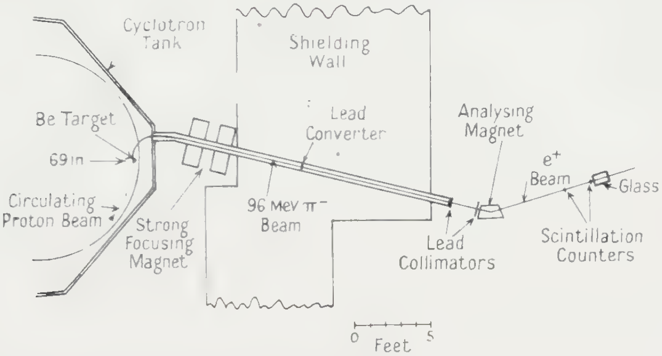

Figure 2. The experimental arrangement used to obtain positrons for calibrating the spectrometer.

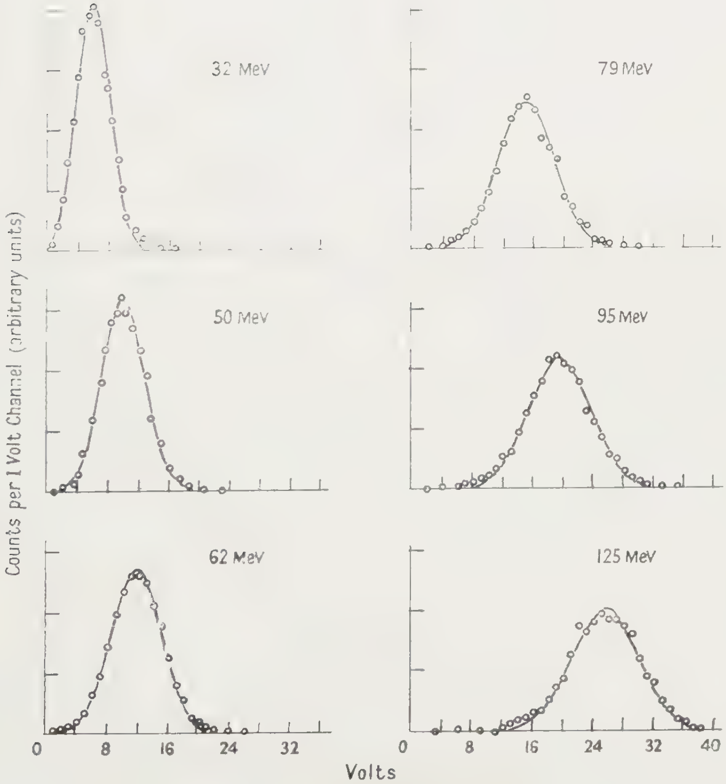

Figure 3. The response of the spectrometer to positrons with various energies in the range 32–125 MEV.

that the beam was passed through a lead converter 6·3 mm thick and the field of the analysing magnet was reversed. The negative pion beam was contaminated in the usual way by 190 MeV negatrons, which started showers in the lead and so produced positrons. Beams of these positrons, with various energies, were selected by the analysing magnet and directed on to the counters. The pions and muons present, being negative, were deflected out of the way by the magnet.

The glass counter, without the lead converter, was put in coincidence with the normal collimating counter and with another scintillation counter defining the line of flight of the positrons. When a triple coincidence occurred an electronic gate opened, and a proportional pulse from the glass counter was sent to a 50-channel pulse analyser. The spectra observed with positrons of various energies are given in figure 3, where the fitted curves are gaussian distributions. The shapes of these spectra, and the ratios of triple coincidences to double coincidences between the two scintillation counters alone, show that the counting efficiency of the glass is 100% in this energy range. Figure 4 shows that the voltage output of the counter is proportional to the positron energy, and that the line widths are nearly proportional to the square root of the energy. In these circumstances the response of the counter to a pair of electrons of a given total energy is essentially the same as the response to a single electron of that energy.

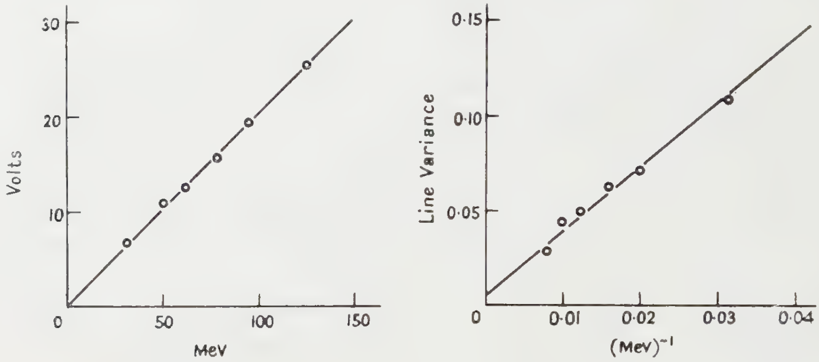

Figure 4. Mean pulse heights, and line widths, of the spectra shown in figure 3.

The positron data were then used to compute the line shapes produced in the complete spectrometer by the γ-rays from mesonic and radiative absorption. The small effects of energy losses by ionization in the converter and collimating counter were taken into account, but bremsstrahlung losses were ignored because the corresponding radiation passed into the glass and made its contribution to the shower.

§ 3. Experimental Procedure and Results

The apparatus used for studying the complete spectrum of the γ-radiation s shown in figure 5 (*a*). The negative pions were slowed down in polyethylene absorbers A and B, passing through the scintillation counter 1 on the way. Some of the pions stopped in the liquid hydrogen target C, which was made from foamed polystyrene. The active volume of the target was a cylinder $1\frac{1}{2}$ in. in diameter and $1\frac{1}{2}$ in. high. As already mentioned, the γ-radiation was observed through the production of electron pairs in a lead converter D. The electrons were counted by the scintillation counter 2 and the glass counter 3 in coincidence, and the anti-coincidence counter 4 eliminated the effects of charged particles scattered from the target area. A coincidence–anti-coincidence event of the type 1234 opened the electronic gate, which allowed a linear pulse from the glass counter to pass through to the pulse analyser. The counts in counter 1 were used for monitoring.

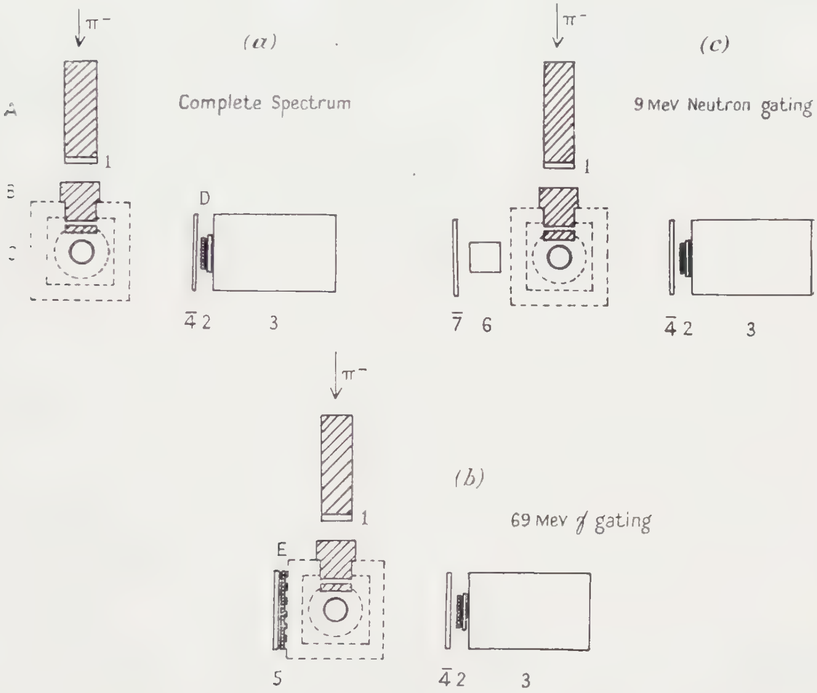

Figure 5. The experimental arrangements used for studying the Panofsky radiation: (*a*) ungated, (*b*) gated by γ–γ coincidences, (*c*) gated by γ–n coincidences.

Figures 6(*a*) and 6(*b*) show the pulse spectra obtained with lead converters $\frac{1}{8}$ in. and $\frac{1}{16}$ in. thick respectively. In each case a background equal to about one third of the total effect has been subtracted. The backgrounds were caused by γ-rays which either originated elsewhere than in the liquid hydrogen or produced pairs elsewhere than in the lead converter. The effects of these were found by running with either the hydrogen or the converter, or both, removed.

The curves shown were fitted to the experimental points by taking the computed pulse spectra for the two groups of γ-rays and adding them together in proportions determined by the method of least squares.

The computed line shapes were checked directly by means of two subsidiary experiments. For the first experiment (figure 5(*b*)) a coincidence counter 5 and a $\frac{1}{4}$ in. thick lead converter E, both 5 in. in diameter, were introduced, and an event of the type 123$\bar{4}$5 was required to open the electronic gate. Such events were produced by mesonic absorption, when one of the two γ-rays was detected by the spectrometer and the other by counter 5. A background equal to about one quarter of the total effect was found after removing either the hydrogen, or the converter E, or both. In figure 6(*c*) the results, with the background subtracted, are compared with the computed pulse spectrum for the lower energy group of γ-rays. The agreement is satisfactory.

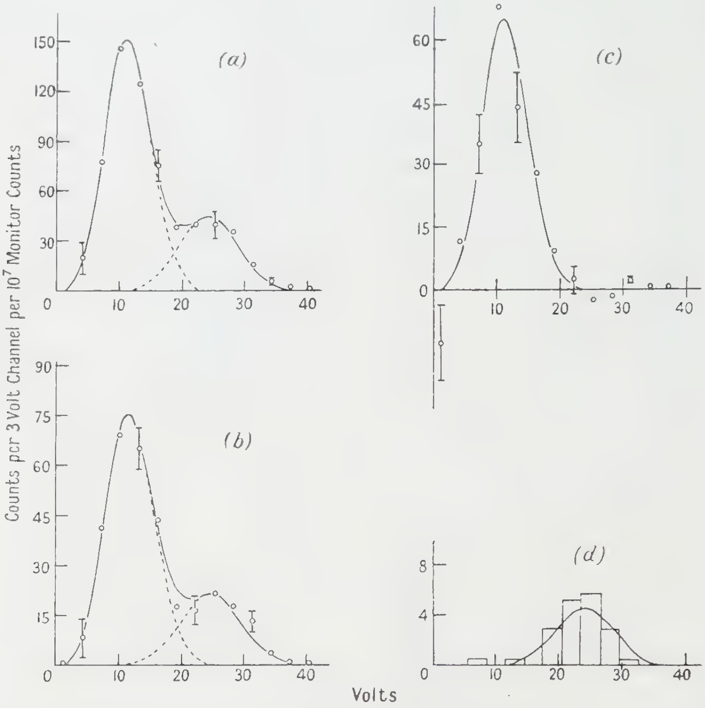

Figure 6. Pulse spectra given by the Panofsky radiation : (*a*) ungated, $\frac{1}{8}$ in. Pb converter ; (*b*) ungated, $\frac{1}{16}$ in. Pb converter ; (*c*) gated by γ–γ coincidences; (*d*) gated by γ–n coincidences.

In the second subsidiary experiment (figure 5(*c*)) the additional counters 6, 7 were used to discriminate in favour of radiative absorption. The electronic gate now opened only when an event of the type $123\bar{4}6\bar{7}$ occurred. Counter 6 had a cylindrical plastic scintillator 2 in. in diameter and 2 in. long; it was able to detect, by means of proton recoils, the 8·8 MeV neutrons from radiative absorption but not the 0·4 MeV neutrons from mesonic absorption. Unfortunately, this counter could also detect high-energy γ-rays, through pair production or Compton scattering in the plastic scintillator. The intrinsic efficiency for counting in this way was about half the efficiency for counting 8·8 MeV neutrons. However, a γ-ray interaction in counter 6 usually produced high-energy electrons which were detected in the 5 in. diameter anti-coincidence counter 7, thus cancelling the event. There was a further geometrical factor, of about three, in favour of radiative absorption. The angle between the two γ-rays produced in mesonic absorption is usually near to the minimum 157°. If one γ-ray was detected in the spectrometer, the other could miss counter 6 altogether.

The counting rate was found to be extremely low, and in fact only 32 events were collected. There was no detectable background effect with the hydrogen removed. Figure 6(*d*) shows the pulse spectrum in histogram form, together with the computed pulse spectrum for the high-energy group of γ-rays. The two small pulses may credibly be attributed to break-through of mesonic absorption events in which a low-energy Compton electron was produced in counter 6. The distribution of the remainder is reasonably consistent with the computed line shape.

The Panofsky ratio is obtained almost directly from the ratios of the areas under the low- and high-energy peaks in figures 6 (*a*) and 6 (*b*). Small corrections have to be applied for the energy dependence of the efficiency of the lead converters. The cross sections for pair production in lead were taken from Davies, Bethe and Maximon (1954), and a minor contribution from Compton scattering was also considered. An additional very small correction (2%) was made for the possibility that both electrons produced by a low-energy γ-ray in the $\frac{1}{8}$ in. converter might stop before reaching counter 2. This was calculated by the method of Wilson (1951).

The results, with their statistical standard deviations, are:

$$R = \begin{cases} 1\cdot48 \pm 0\cdot15 & (\tfrac{1}{8}\text{ in. converter}) \\ 1\cdot52 \pm 0\cdot18 & (\tfrac{1}{16}\text{ in. converter}) \\ 1\cdot50 \pm 0\cdot11 & (\text{combined result}). \end{cases}$$

An attempt was also made to review the possibilities of systematic error. It was not possible, for example, to include all physical effects in the computation of the theoretical line shapes. Some of the electrons produced in the lead converters could be severely scattered before entering the glass, and tests with the calibrating positron beam showed appreciable distortions of the pulse spectra given by electrons entering at angles greater than 45° to the normal. Reassurance about the size of errors of this kind is, however, provided by the good agreement of the results taken with $\frac{1}{8}$ in. and $\frac{1}{16}$ in. converters, and by the gated spectra shown in figures 6 (*c*) and 6 (*d*).

Another kind of error would arise if the background were affected by presence or absence of liquid hydrogen in the target. The distribution of the pions in the foamed polystyrene *behind* the liquid-hydrogen container will indeed be slightly affected by the stopping power and scattering of the hydrogen. In fact, however, the range of the pions in the strong-focused beam was not well defined, so that the thickness of the hydrogen and the foamed polystyrene target walls was small compared with the range straggling. A small upper limit on the background variation can be set by suitable scaling of the background given by he solid polyethylene absorber immediately *in front of* the hydrogen container.

It seemed reasonable, after reviewing these possibilities, to allow an additional standard deviation equal to the statistical one. The final result is then $R = 1\cdot50 \pm 0\cdot15$.

§ 4. DISCUSSION

Table 1 shows that the results of the two Liverpool experiments, which are in good agreement, raise the weighted mean value of R by about 50%. The table also shows the available data on the absorption of negative pions from the K shell of deuterium, the branching ratio S being defined by

$$S = \frac{w(\pi^- + \mathrm{d} \rightarrow 2\mathrm{n})}{w(\pi^- + \mathrm{d} \rightarrow 2\mathrm{n} + \gamma)}. \qquad \ldots\ldots(4)$$

As already mentioned, the ratio R can be used to link the positive energy s-wave cross sections for pion–proton scattering and pion photo-production

Table 1. Branching Ratios in the Capture of Stopped Negative Pions by Hydrogen (R) and Deuterium (S)

Reference	R
Panofsky *et al.* (1951)	$0{\cdot}94 \pm 0{\cdot}30$
Kuehner *et al.* (private communication)	$1{\cdot}60 \pm 0{\cdot}17$
This paper	$1{\cdot}50 \pm 0{\cdot}15$
Weighted Mean	$1{\cdot}52 \pm 0{\cdot}11$
	S
Panofsky *et al.* (1951)	$2{\cdot}36 \pm 0{\cdot}74$
Chinowsky and Steinberger (1954 b)	$1{\cdot}5 \ \pm 0{\cdot}8$
Kuehner *et al.* (private communication)	$2{\cdot}36 \pm 0{\cdot}36$
Weighted Mean	$2{\cdot}31 \pm 0{\cdot}31$

The uncertainties quoted are standard deviations.

(Anderson and Fermi 1952). The link is obtained in an elementary way by taking the transition rate for any one of these low-energy pion absorption processes to be proportional to the square of the modulus of the pion wave function at the position of the proton. It then follows that, apart from Coulomb effects, the absorption cross sections at very low positive energies must obey the '$1/v$ law', $\sigma = A/\eta$, where $\eta = p/\mu\mathbf{c}$ is the pion momentum p divided by the charged pion rest mass μ and the velocity of light $\mathbf{c}$. The constant A is connected with the K-shell absorption rate w by the relation

$$w = \mathbf{c}A/\pi a^3. \qquad \ldots\ldots(5)$$

In this equation the Bohr radius a (a_{H} for hydrogen, a_{D} for deuterium) is calculated from the appropriate reduced pion mass.

With the help of the deuterium data the cross sections for scattering and photo-production may be linked with the s-wave cross section for a third important process, pion production in nucleon-nucleon collisions (Brueckner, Serber and Watson 1951). For this it is necessary to know the ratio

$$T = \frac{w(\pi^- + \mathrm{d} \rightarrow 2\mathrm{n} + \gamma)}{w(\pi^- + \mathrm{p} \rightarrow \mathrm{n} + \gamma)} = \frac{2}{3}\left(\frac{a_{\mathrm{H}}}{a_{\mathrm{D}}}\right)^3 \qquad \ldots\ldots(6)$$

where the value given is that estimated by Brueckner *et al.* using the impulse approximation.

The complete phenomenological scheme is set out in figure 7. The processes which have actually been observed are printed in bold type, and all but one of the connecting links use either equation (5) or (6), or charge independence (c.i.) or detailed balancing (d.b.). In photo-production the ratio of the numbers of negative to positive pions produced in deuterium near threshold is taken to be equal to the ratio of the photo-production cross sections of neutrons and protons separately:

$$r_0 = \frac{\sigma_{\mathrm{S}}(\gamma + \mathrm{n} \rightarrow \mathrm{p} + \pi^-)}{\sigma_{\mathrm{S}}(\gamma + \mathrm{p} \rightarrow \mathrm{n} + \pi^+)} = \frac{\sigma_{\mathrm{S}}(\gamma + \mathrm{d} \rightarrow 2\mathrm{p} + \pi^-)}{\sigma_{\mathrm{S}}(\gamma + \mathrm{d} \rightarrow 2\mathrm{n} + \pi^+)}. \qquad \ldots\ldots(7)$$

Table 2 shows the absolute capture rates from the K shell as predicted from the positive energy data. The corresponding mean lifetimes are all of the order of 10^{15} second. In table 3 the rates are taken in pairs and their ratios compared with the capture data set out in table 1 and equation (6).

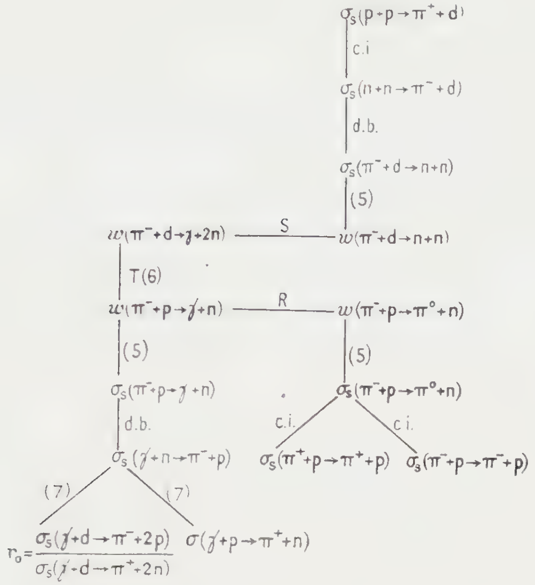
$\sigma_s(p+p\to\pi^++d)$
c.i
$\sigma_s(n+n\to\pi^-+d)$
d.b.
$\sigma_s(\pi^-+d\to n+n)$
(5)
$w(\pi^-+d\to\gamma+2n)$
S
$w(\pi^-+d\to n+n)$
T(6)
$w(\pi^-+p\to\gamma+n)$
R
$w(\pi^-+p\to\pi^0+n)$
(5)
(5)
$\sigma_s(\pi^-+p\to\gamma+n)$
$\sigma_s(\pi^-+p\to\pi^0+n)$
d.b.
c.i.
c.i.
$\sigma_s(\gamma+n\to\pi^-+p)$
$\sigma_s(\pi^++p\to\pi^++p)$
$\sigma_s(\pi^-+p\to\pi^-+p)$
(7)
(7)
$r_0=\frac{\sigma_s(\gamma+d\to\pi^-+2p)}{\sigma_s(\gamma+d\to\pi^++2n)}$
$\sigma(\gamma+p\to\pi^++n)$

Figure 7. Phenomenological scheme of connections between π^- capture processes, pion-proton scattering, photo-production, and production in nucleon–nucleon collisions.

Table 2. Capture Rates from the K Shell, calculated from Positive Energy Data

Capture Process	Transition Rate $10^{-14}w$ (sec^{-1})	Input Data	Ref.
$\pi^-+p\to\pi^0+n$	$7{\cdot}18\pm1{\cdot}08$	(*a*) $\alpha_1-\alpha_3=(0{\cdot}27\pm0{\cdot}02)\eta$	O
		(*b*) $v_0/c=0{\cdot}204\pm0{\cdot}005$	K *et al.*
$\pi^-+p\to\gamma+n$	$4{\cdot}05\pm0{\cdot}33$	(*c*) $\sigma_s(\gamma+p\to\pi^++n)=(1{\cdot}43\pm0{\cdot}06)\eta\times10^{-28}$ cm^2	B *et al.*
		(*d*) $r_0=1{\cdot}87\pm0{\cdot}13$	B *et al.*
$\pi^-+d\to2n$	$6{\cdot}64\pm0{\cdot}72$	(*e*) $\sigma_s(p+p\to\pi^++d)=(1{\cdot}38\pm0{\cdot}15)\eta\times10^{-28}$ cm^2	C & S

In the third column α_1, α_3 are the phase shifts for s-wave pion–nucleon scattering in the $T=\frac{1}{2}$, $\frac{3}{2}$ states respectively; v_0 is the velocity of emission of the neutral pion in the capture process. O, Orear (1956); K *et al.*, Kuehner *et al.* (private communication); B *et al.*, Beneventano *et al.* (1956); C & S, Crawford and Stevenson (1955).

Table 3. Ratios of Transition Rates, calculated from Positive Energy Data and from Capture Data

Ratio	From positive energy data	From capture data	Difference (%)
$\frac{w(\pi^-+p\to\pi^0+n)}{w(\pi^-+p\to\gamma+n)}$	$1{\cdot}77\pm0{\cdot}30$	$R=1{\cdot}52\pm0{\cdot}11$	15 ± 19
$\frac{w(\pi^-+d\to2n)}{w(\pi^-+p\to\gamma+n)}$	$1{\cdot}64\pm0{\cdot}22$	$ST=1{\cdot}88\pm0{\cdot}25$	-14 ± 19
$\frac{w(\pi^-+d\to2n)}{w(\pi^-+p\to\pi^0+n)}$	$0{\cdot}92\pm0{\cdot}17$	$ST/R=1{\cdot}24\pm0{\cdot}19$	-30 ± 24

The difference column is obtained by subtracting the second value from the first and dividing by the mean.

The correspondence is reasonably good in view of the fact that the analysis has ignored several uncertain theoretical points. It is likely that various Coulomb effects have affected the positive energy data by perhaps 5 or 10% and a correction of the same order will probably appear when the calculation of T is considered more closely. Finally, Noyes (1956) has pointed out that deviations from charge independence in the pion–nucleon system have the effect of depressing the value of $w(\pi^- + \mathrm{p} \rightarrow \pi^0 + \mathrm{n})$ as calculated from the scattering data. Noyes proposed a correction of 10% in this sense, but in fact the appropriate correction should probably be much smaller. The effect of the radiative transition is obviously reduced now that the value of R has been raised. It also seems likely that the range of the pion–nucleon s-interaction is much smaller than was thought at the time of the original calculation, and this too has the effect of reducing the correction required.

Acknowledgments

We should like to thank Drs. Kuehner, Merrison and Tornabene for generously making available their results to us before publication. We have had many informative discussions with them and also with Dr. R. H. Dalitz, of Birmingham University.

The glass counter was made possible by the interest and skill of the research department of Pilkington Bros. and the production department of Chance Bros. Much of the electronic equipment was supplied and serviced by Dr. Collinge and his group. The mechanical apparatus was largely built by Mr. Critchley, and supplied with liquid hydrogen by the Atomic Energy Research Establishment at Harwell. We received unfailing co-operation from Mr. Halliday and the cyclotron crew.

References

Anderson, H. L., and Fermi, E., 1952, *Phys. Rev.*, **86**, 794.

Beneventano, M., Bernardini, G., Carlson-Lee, D., Stoppini, G., and Tau, L., 1956, *Nuovo Cim.*, **4**, 323.

Brueckner, K., Serber, R., and Watson, K., 1951, *Phys. Rev.*, **81**, 575.

Chinowsky, W., and Steinberger, J., 1954 a, *Phys. Rev.*, **93**, 586 ; 1954 *b*, *Ibid.*, **95**, 1561.

Crawford, F. S., and Stevenson, M. L., 1955, *Phys. Rev.*, **97**, 1305.

Crowe, K. M., and Phillips, R. H., 1954, *Phys. Rev.*, **96**, 470.

Davies, H., Bethe, H. A., and Maximon, L. C., 1954, *Phys. Rev.*, **93**, 788.

Kantz, A., and Hofstadter, R., 1954, *Nucleonics*, **12**, 36.

Noyes, H. P., 1956, *Phys. Rev.*, **101**, 320.

Orear, J., 1956, *Nuovo Cim.*, **4**, 856.

Panofsky, W. K. H., Aamodt, R. L., and Hadley, J., 1951, *Phys. Rev.*, **81**, 565.

Wilson, R. R., 1951, *Phys. Rev.*, **84**, 100.

Direct Excitation in the Photodisintegration of Tantalum above the Giant Resonance

By J. H. CARVER, R. D. EDGE AND K. H. LOKAN
Research School of Physical Sciences, The Australian National University, Canberra

Communicated by E. W. Titterton; MS. received 27th December 1956, *and in final form 5th March* 1957

Abstract. The bremsstrahlung from the Canberra electron-synchrotron has been used to measure the single and multiple photo-neutron yields of tantalum from the thresholds to 31 MeV. The ratio of the total integrated cross section for the (γ, n) reaction to that for the $(\gamma, 2\mathrm{n})+(\gamma, 3\mathrm{n})$ reactions is found to be

$$\int_0^{31} \sigma_1\, dE \bigg/ \int_0^{31} (\sigma_2+\sigma_3)\, dE = 2{\cdot}6 \pm 0{\cdot}3.$$

For gamma rays of energy exceeding about 17 MeV significant contributions to σ_1 can only come from direct interactions, and the ratio of the integrated cross sections in this region is found to be

$$\int_{17}^{31} \sigma_1\, dE \bigg/ \int_{17}^{31} (\sigma_2+\sigma_3)\, dE = 0{\cdot}86 \pm 0{\cdot}15.$$

The results show that direct interactions account for a large part of the photon absorption in the high-energy tail above the giant resonance.

§ 1. Introduction

The present experiments are concerned with the relative importance of direct emission and compound-nucleus formation in nuclear photodisintegration. The ratio of single to multiple neutron emission has been studied in the higher energy region where, if the statistical conditions were fulfilled, multiple emission would be the predominant process and single-particle emission would occur almost entirely through direct interactions.

Tantalum was chosen for these experiments for the following reasons: (*a*) it is practically mono-isotopic, ^{181}Ta having an abundance of 99·99% (White *et al.* 1955); (*b*) its high Coulomb barrier (13 MeV) suppresses the emission of charged particles so that neutrons are expected to be the chief disintegration products; (*c*) the important ^{181}Ta (γ, n) reaction may be observed simply by measuring the residual 8-hour β-activity of ^{180}Ta.

The gamma-ray thresholds for the emission of one, two and three neutrons from tantalum are 7·6, 14 and 22 MeV respectively. If a compound nucleus is formed proton emission will be negligible owing to the effect of the Coulomb barrier and the nucleus will lose energy by evaporating neutrons. The dependence of the neutron multiplicity upon gamma-ray energy is shown in figure 1 as calculated by Levinger and Bethe (1952) using the statistical theory. For the direct effect both protons and neutrons may be emitted, but only the emission of neutrons has

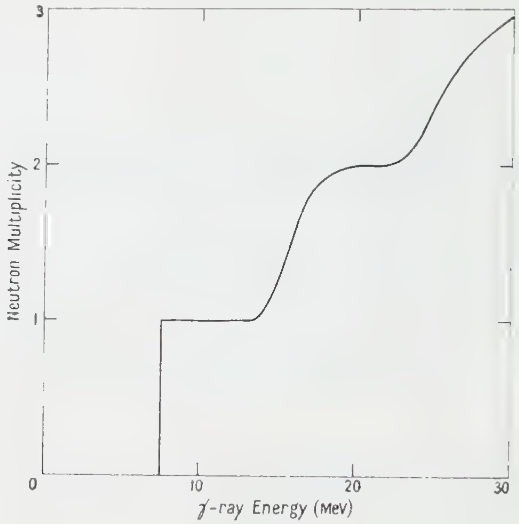

Figure 1. Theoretical neutron multiplicity for the photodisintegration of tantalum according to the statistical theory (Levinger and Bethe 1952)

been measured in the present experiment. Photo-proton emission from tantalum has been studied by Toms and Stephens (1955) and Hoffman and Cameron (1953).

§ 2. EXPERIMENTAL METHOD

In the present experiments, which extend to an energy of 31 Mev, the ^{181}Ta (γ, n) cross section has been measured by residual activity and the cross section for all neutron-producing reactions has been obtained by measuring the total neutron yield. For the latter purpose a Szilard–Chalmers detector was used because of its high efficiency and its insensitivity to gamma radiation. The same irradiations were used for both types of measurements.

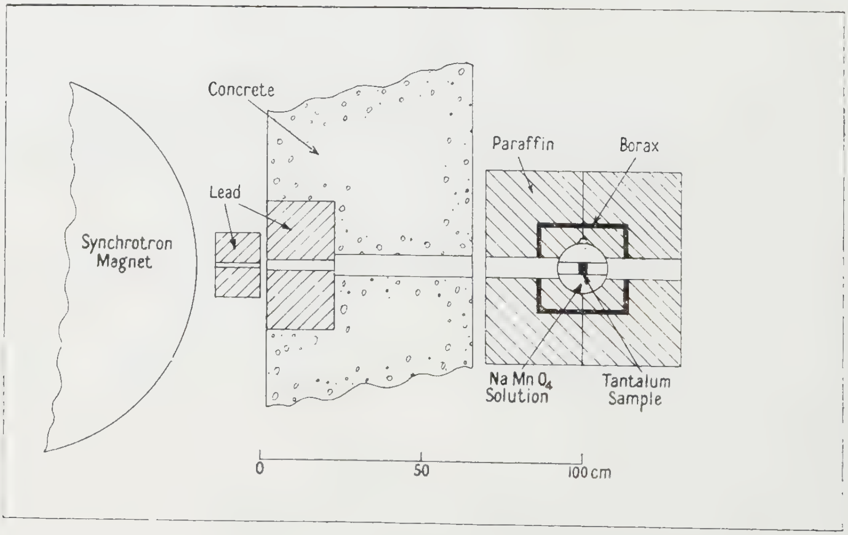

Figure 2. Experimental arrangement.

The experimental arrangement is shown in figure 2. Gamma rays from the Canberra electron-synchrotron traversed a hole in the concrete and lead shielding wall and struck a tantalum sample in the centre of a two-litre volume of aqueous sodium permanganate solution ($650\,\mathrm{g\,l.^{-1}}$) in which the neutrons were detected by the Szilard-Chalmers process. Through the centre of the vessel containing the solution was a hole of such size that the gamma-ray beam did not strike the walls of the vessel or the solution. The detector was surrounded by 15 cm of paraffin to reflect neutrons back into the tank to help in flattening its energy response. A layer of boron and a further 15 cm of paraffin surrounded the detector and shielded it from the background of neutrons in the research room. From the work on the 'long counter' reported by Hanson and McKibben (1947) such a detector is expected to be fairly insensitive to energy changes. The energy spectrum of the evaporation neutrons should not alter sufficiently with changing photon energy to invalidate the assumption of constant efficiency of detection within the accuracy of the experiments. The situation with regard to 'direct' neutrons is more complicated since these may range in energy up to about 20 Mev at the higher photon energies, but this does not affect the determination of the (γ, n) cross section which depends only on the induced activity measurement. To check that large errors were not introduced into the determination of the total neutron yield by the use of the small two-litre tank, a 700-litre tank was employed to measure the neutron yields at bremsstrahlung energies of 18 and 30 Mev. The ratio of the neutron yields at 18 and 30 Mev as measured with the large tank was $0{\cdot}63 \pm 0{\cdot}05$; the same ratio determined with the small tank was $0{\cdot}59 \pm 0{\cdot}03$, indicating that serious errors were not introduced by the use of the small tank.

After the irradiations, which lasted for 20 minutes, the sodium permanganate solution was filtered to extract, as manganese dioxide, the 2·6-hour ^{56}Mn and its activity, which was proportional to the neutron yield, was measured with a thin-walled Geiger counter. Similar irradiations were made without the tantalum sample in order to correct for the neutron background which was found to be less than 5% of the true count for 30-Mev bremsstrahlung.† Tantalum foils were also exposed to the beam and after the irradiation the yield for the ^{181}Ta (γ, n) reaction alone was determined by counting the induced 8-hour ^{180}Ta activity using thin-window Geiger counters.

Copper foils were used to monitor the gamma-ray flux by means of the well-known ^{63}Cu (γ, n) reaction. The induced 10-minute ^{62}Cu activity was measured with the same apparatus as was used to count the tantalum activity. Berman and Brown (1954) have used the Stanford 36-Mev linear accelerator to measure the ^{63}Cu (γ, n) cross section and their result, which is independent of a calculated R-meter response, has been taken as standard for this work. During the runs a continuous indication of the beam was obtained from an ionization chamber which was used to monitor the flux at bremsstrahlung energies below 14 Mev where the copper monitoring was less accurate.

§ 3. Results and Analysis

The measured yield curves are shown in figure 3 where each point is the mean of about four separate determinations. The total neutron yield has been normalized to the Ta (γ, n) yield at 14 MeV, the threshold for the (γ, 2n) reaction, and the difference between these curves gives the multiple-neutron yield which is also shown. The single- and multiple-neutron yield curves have been analysed by an iterative method (Carver and Lokan 1957) to give the (γ, n) cross section σ_1 and the multiple-neutron cross section σ_m shown in figure 4. There are three reactions which may contribute to the multiple-neutron yield, namely (γ, 2n), (γ, 3n) and (γ, np), so that $\sigma_m = 2\sigma(\gamma, 2n) + 3\sigma(\gamma, 3n) + \sigma(\gamma, np)$.

---

† A complication would arise if the gamma-ray beam contained a large contamination of fast neutrons since some of these could be scattered into the solution by the tantalum target. A calculation based on the number of fast neutrons known to be present in the beam (E. W. Titterton, private communication) showed that this effect is small.

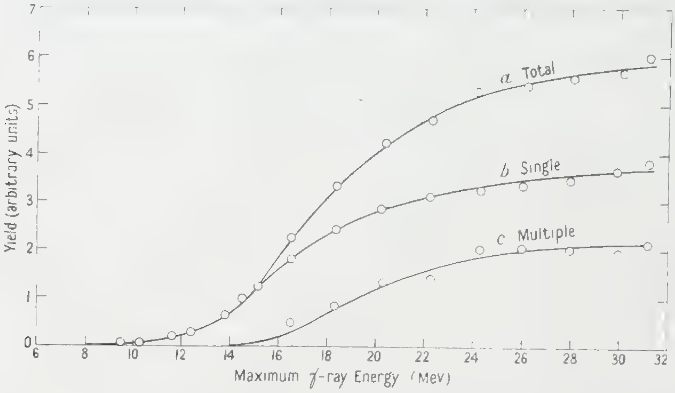

Figure 3. The measured neutron yield curves for tantalum: (*a*) the total yield for all neutron producing reactions obtained from the Szilard–Chalmers measurements; (*b*) the yield for single neutron production obtained from the ^{180}Ta activation measurements; (*c*) the yield for multiple reactions obtained by subtraction.

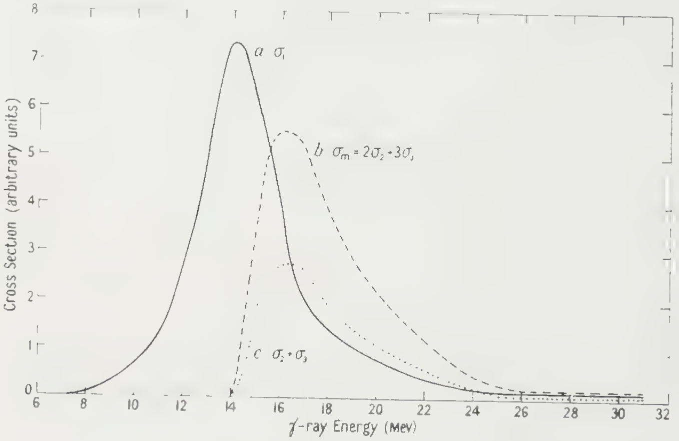

Figure 4.—The measured photoneutron cross sections for tantalum: (*a*) the (γ, n) cross section σ_1; (*b*) the cross section for multiple production $\sigma_m = 2\sigma_2 + 3\sigma_3$; (*c*) the sum of the cross sections for the (γ, 2n) and (γ, 3n) cross sections, $\sigma_2 + \sigma_3$, derived from σ_m assuming the ratio σ_2/σ_3 is as given by the statistical theory.

The (γ, np) reaction will be strongly inhibited by the Coulomb barrier. If a compound nucleus is formed this reaction will be very weak indeed since evaporation protons will be almost entirely suppressed. It will be a somewhat more likely reaction if a direct interaction occurs, but even in this case the proton must receive about 13 MeV if it is to surmount the Coulomb barrier and this will increase the effective threshold for the (γ, np) reaction from 13·4 MeV to about 26 MeV. It seems, therefore, that this reaction can safely be neglected.

Below the $(\gamma, 2\mathrm{n})$ threshold, then, at 22 MeV $\sigma_{\mathrm{m}}=2\sigma(\gamma, 2\mathrm{n})$ and at higher energies $\sigma_{\mathrm{m}}=2\sigma(\gamma, 2\mathrm{n})+3\sigma(\gamma, 3\mathrm{n})$. In a preliminary attempt to separate the $(\gamma, 2\mathrm{n})$ and $(\gamma, 3\mathrm{n})$ reactions above 22 MeV a careful study was made of the tantalum decay curves at the maximum bremsstrahlung energy. The curves showed an apparently pure 8·1-hour decay corresponding to the reaction $^{181}\mathrm{Ta}\,(\gamma, \mathrm{n})$ and no components were found with periods of 10 minutes or 2 hours corresponding to $^{178}\mathrm{Ta}$ (Wilkinson 1950), indicating that the integrated $(\gamma, 3\mathrm{n})$ cross section was less than about 5% of the integrated (γ, n) cross section. This does not however exclude the possibility that $\sigma(\gamma, 3\mathrm{n})$ may contribute a large part of σ_{m} at the higher energies and further work is in progress in this laboratory using a scintillation spectrometer to place a closer limit on the magnitude of the $(\gamma, 3\mathrm{n})$ cross section.

The spectrometer can also be used to investigate the $(\gamma, 2\mathrm{n})$ cross section by observing the resulting 600-day $^{179}\mathrm{Ta}$ activity. In this way an independent measurement of the multiple-neutron yield at 30 MeV has been made in collaboration with Dr. W. Turchinetz. The result agrees with the recent measurement to within 10% and provides a check against any systematic error which might arise from, say, the energy response of the Szilard–Chalmers tank.

§ 4. DISCUSSION

From a comparison of the cross-section data of figure 4 with the predicted neutron multiplicity of figure 1 it is evident that above about 17 MeV the observed (γ, n) cross section is too large a fraction of the total cross section to arise from the statistical decay of a compound nucleus. In this higher energy region the (γ, n) reaction must arise almost entirely from direct interactions.

Only the multiple reactions, $(\gamma, 2\mathrm{n})$ and $(\gamma, 3\mathrm{n})$, which comprise σ_{m} will then involve the formation of a compound nucleus at some stage. If it is assumed that, for these multiple reactions, all the energy of the photon is given to the statistical motion of the nucleons, then statistical theory may be used to divide σ_{m} between σ_2 and σ_3 for gamma-ray energies exceeding the $(\gamma, 3\mathrm{n})$ threshold (22 MeV), and the sum of σ_2 and σ_3 calculated in this way is shown in figure 4. This, of course, is an extreme assumption which overestimates σ_3 since the compound nucleus involved in these multiple processes may follow a direct interaction between a photon and a nucleon in which the nucleon suffers a collision before it can escape from the nucleus, a situation most likely to occur for protons. Alternatively a neutron may be ejected directly from a low-lying nuclear shell leaving sufficient excitation in the nucleus for the evaporation of a second neutron. The uncertainty involved in the division of σ_{m} between σ_2 and σ_3, however, is not very serious for the interpretation of the present results. The other extreme division is to assume that σ_3 is zero, in which case the $\sigma_2+\sigma_3$ curve of figure 4 would be multiplied by a factor which is unity below 22 MeV and increases to 1·5 at 31 MeV.

The ratio of the total integrated cross sections for single- and multiple-neutron emission given by these results is

$$\int_0^{31} \sigma_1\,dE \Big/ \int_0^{31} (\sigma_2+\sigma_3)\,dE = 2{\cdot}6 \pm 0{\cdot}3.$$

For the high energy tail the ratio is

$$\int_{17}^{31} \sigma_1\, dE \Big/ \int_{17}^{31} (\sigma_2+\sigma_3)\, dE = 0{\cdot}86 \pm 0{\cdot}15,$$

and involves a 7% uncertainty, depending on how σ_{m} is divided between σ_2 and σ_3. These results may be compared with the measurements made at 17·6 MeV using the Li(p, γ) radiation (Carver, Edge and Wilkinson 1953, Carver and Hay 1953), in which the ratio of the cross sections at 17·6 MeV was found to be $\sigma_1/\sigma_2 = 0{\cdot}9 \pm 0{\cdot}4$. For gamma rays of energy exceeding 17 MeV the cross sections σ_1 and $\sigma_2+\sigma_3$ shown in figure 4 indicate the relative cross sections for direct emission and compound nucleus formation respectively and the latter probably arises from an initial direct interaction according to one of the mechanisms discussed above. An additional contribution to the direct cross section will come from photo-proton emission. The Coulomb barrier will suppress the emission of protons at low photon energies, but photons of energy exceeding about 20 MeV may produce protons of energy exceeding the barrier height of 13 MeV. At these higher photon energies, then, photo-proton emission will be expected to be comparable with the (γ, n) cross section σ_1 measured in these experiments. The present results show the importance of direct effects in the region above the giant resonance and support the single-particle theory of Wilkinson (1955) although they do not give any information about the enhancement factors which are required on that theory to account for the giant resonance itself.

References

Berman, A. I., and Brown, K. L., 1954, *Phys. Rev.*, **96,** 83.
Carver, J. H., Edge, R. D., and Wilkinson, D. H., 1953, *Phil. Mag.*, **44,** 404.
Carver, J. H., and Hay, H. J., 1953, *Phil. Mag.*, **44,** 1191.
Carver, J. H., and Lokan, K. H., 1957, *Aust. J. Phys.*, in the press.
Hanson, A. O., and McKibben, J. L., 1947, *Phys. Rev.*, **72,** 673.
Hoffman, M. M., and Cameron, A. G. W., 1953, *Phys. Rev.*, **92,** 1184.
Levinger, J. S., and Bethe, H. A., 1952, *Phys. Rev.*, **85,** 577.
Toms, M. E., and Stephens, W. E., 1955, *Phys. Rev.*, **98,** 626.
White, F. A., Collins, T. L., and Rourke, F. M., 1955, *Phys. Rev.*, **97,** 566.
Wilkinson, D. H., 1955, *Proceedings of the* 1954 *Glasgow Conference on Nuclear and Meson Physics* (London : Pergamon Press, 1955), p. 161.
Wilkinson, G., 1950, *Phys. Rev.*, **80,** 495.

The Scattering of High Energy μ-Mesons in Lead

By J. L. LLOYD†, E. RÖSSLE‡ and A. W. WOLFENDALE†
The Physical Laboratories, The University, Manchester

Communicated by G. D. Rochester; MS. received 30th January 1957

Abstract. A study has been made of the scattering of μ-mesons, in the momentum range 5–150 GeV/**c**, by a thick block of lead. The experimental scattering distribution shows an excess of large displacements over the number expected on conventional scattering theory, indicating that the anomalous scattering found at low energies extends to these high energies.

§ 1. Introduction

The experimental study of the scattering of fast μ-mesons by heavy elements, particularly lead, has revealed an anomaly. In every experiment to date the scattering distributions have shown an excess of large momentum transfers over the number expected on the conventional scattering theory. This theory assumes that the nuclear charge is distributed fairly uniformly throughout a sphere of radius $R \sim 1{\cdot}2A^{1/3}\,10^{-13}$ cm, as shown by Hofstadter (1956) and others and the term uniform nuclear model is used to describe the model.

The experimental scattering distributions, on the other hand, simulate the scattering expected from point charges (Molière distribution—Molière 1947). This extreme model has proved useful for comparison purposes although it has no physical significance and it is clear either that some imperfection exists in the multiple scattering theory or that account has not been taken of all the forces acting between fast μ-mesons and nucleons.

It has recently been shown by Fowler (1957) that the large angle scattering may possibly be explained by a mechanism which is essentially the elastic counterpart of μ-meson star production.

In the present experiment the work of Lloyd and Wolfendale (1955) (to be referred to as I) on the scattering of fast μ-mesons in lead has been extended to higher energies. In order to obtain measurable scattering a very thick scattering layer was used—76 cm Pb—and for technical reasons the scattering displacements rather than the scattering angles were studied. The momenta of the particles were determined precisely using the Manchester Cosmic Ray Spectrograph.

§ 2. Experimental Arrangement and Method

2.1. *The Spectrograph*

The Manchester Cosmic Ray Spectrograph (Hyams *et al.* 1950) has been modified by the introduction of three flat cloud chambers, one at each of the measuring levels, so that the maximum detectable momentum has been increased by a factor of about 20 (Holmes *et al.* 1956). In the experiment to be described here the lowest flat chamber was removed and the multi-plate chamber (described in I, but now containing nine 1 cm lead plates) raised so that its top plate became the lowest measuring level of the spectrograph. The bottom flat chamber and associated counter tray were then placed beneath the multi-plate chamber and the thick scattering block. The arrangement is shown in figure 1. All the counters below the flat chambers were connected to a hodoscope circuit so that the discharges of individual counters could be recognized. As in previous experiments with the spectrograph, the magnetic field was reversed for part of the time.

---

† Now at the Department of Physics, Durham Colleges in the University of Durham, Durham.

‡ British Council Fellow, on leave from Hochspannungslaboratorium, Hechingen.

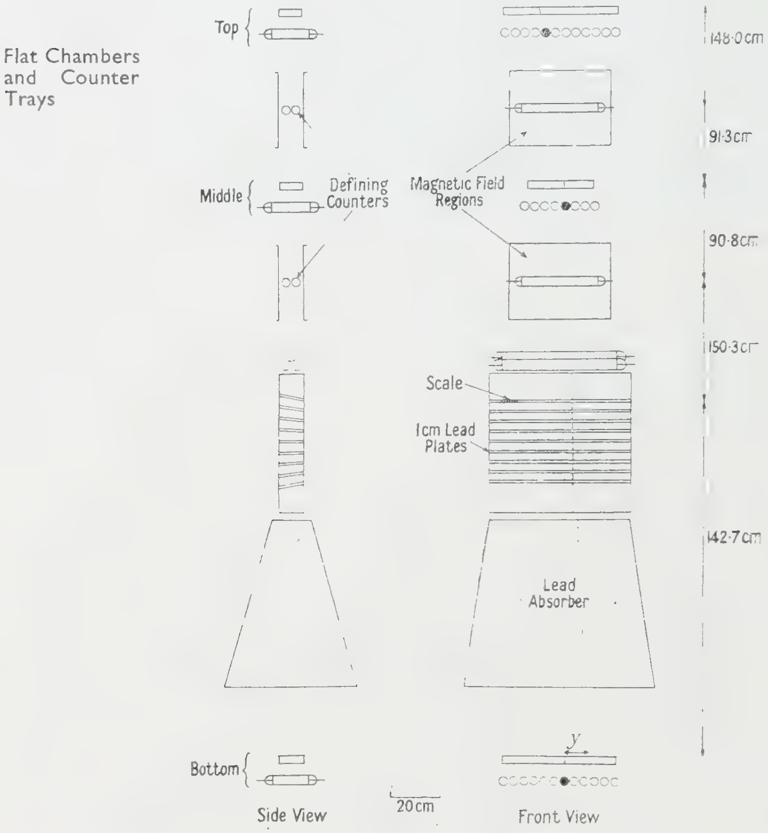

Figure 1. The experimental arrangement.

2.2. *Measurement of the Selected Events*

For the main part of the experiment a 6-fold coincidence was required with one or more counters discharged in each tray. Events in which only single counters were discharged in each of the trays connected to the hodoscope usually corresponded to the passage of a single particle through the apparatus. The selection of trajectories to be measured accurately was made on the basis of the counters discharged in the top and middle layers and the approximate position of the track in the multi-plate chamber. A rough estimate of the momentum was made using these data and events in which the momentum was above about 5 GeV/**c** were selected. The selected trajectories were examined in detail. The coordinates of the intersections of each track in the flat chambers with a ruled grid on the upper glass window were found by visual examination of the stereoscopic photographs. A scale attached to the top plate of the multi-plate chamber was used to give the coordinates of the intersection of the track with the plate. Knowledge of the coordinates T, M and C (in the direction perpendicular to the field) of the track at the upper three measuring levels and the line integrals of the magnetic fields, together with the geometry of the arrangement, permitted evaluation of the momenta of the selected particles. Measurement was made of the longitudinal position B of the track in the bottom flat chamber and the longitudinal position B_0, predicted for no scattering, found from T, M and C (the longitudinal direction is that perpendicular to the field). The difference $y=B-B_0$ was then the projected displacement due to scattering in the lead block.

2.3. *Determination of the Momenta of the Selected Particles*

The magnetic deflection of a particle at the central level of the spectrograph is given approximately by $\Delta=\frac{1}{2}(T+C)-M-\Delta_0$ where Δ_0 is a constant. Δ_0 was found in the following way. An experiment was carried out in which the spectrograph was operated without magnetic field and fast particles were selected from observations on their scattering in the multi-plate chamber. The displacements were then mainly due to random distortion and measuring errors, and $\frac{1}{2}(T+C)-M$ was centred about Δ_0. The derivation of the accuracy with which the measured value of Δ gave the true magnetic deflection of the particle is given in Appendix I. Briefly, for single readings of the coordinates, the standard deviation was $\sigma_\Delta=0{\cdot}12$ cm and for the mean of two readings at each level $\sigma_\Delta=0{\cdot}11$ cm.

The mean current through the magnet coils was 40·15 amp giving $\int H\,dl=6{\cdot}98\times10^5$ gauss cm and $p=31{\cdot}2/\Delta$ with p in GeV/**c** for Δ in cm. The maximum detectable momentum of the instrument was thus 290 GeV/**c**.

In addition to the factors mentioned above two further sources of uncertainty in the momentum arise. These are the variation of $\int H\,dl$ with position of trajectory and time, and the effect of scattering in the counter trays, chambers etc. The total error arising from these sources is 2·8%.

2.4. *Rejection of Spurious Events*

It is possible that the counters discharged at each level and the tracks seen in the cloud chambers did not always correspond to the passage of a single particle through the apparatus. For example, two particles passing through the upper and lower halves of the apparatus within the resolving time of the counter circuits would simulate a single particle. The number of spurious events was reduced by imposing a limit on the value of the transverse deflection δ (i.e. the deflection in the direction of the magnetic field) since for single fast particles this deflection should be almost zero. The measurements of the transverse coordinates were rather inaccurate because of the small angle between the camera lenses used in the stereoscopic photography, and consequently an appreciable spread in transverse deflection existed. A limit of $\pm0{\cdot}8$ cm on δ was imposed and tracks having larger δ-values were rejected; the value of the limit was chosen so that a large fraction of spurious events was rejected with only a small loss of genuine events. A discussion of the rate of spurious particles is given in § 4.1.1. Their effect on the root-mean-square displacement of scattering, to be considered in § 3, is negligible.

2.5. *The Accuracy of the Displacement Measurements*

As mentioned in § 2.2 the displacement is given by $y = B - B_0$: B_0 is computed from the measurements of T, M and C and its accuracy depends on the accuracies of these quantities. From the errors quoted in the Appendix the error in y is calculated to be 0·19 cm for single readings and 0·18 cm for double readings. The errors in p and y are roughly balanced: $\sigma_y / \langle y \rangle = 3{\cdot}5 \sigma_p / p$, where $\langle y \rangle$ is the expected r.m.s. displacement for a particle of momentum p and the σ's are the appropriate standard deviations.

2.6. *The Deflection Spectrum of the Accepted Particles*

From a large number of photographs 272 energetic particles were selected having momenta equal to or greater than 5 GeV/**c** ($\Delta \leqslant 6{\cdot}23$ cm). The deflection spectrum of these particles is given in figure 2. The lower limit to the momentum was chosen to give a reasonable overlap with the region investigated in I. At this limit $\langle y \rangle$ was about 3 cm and large geometrical corrections would have been necessary for slower particles.

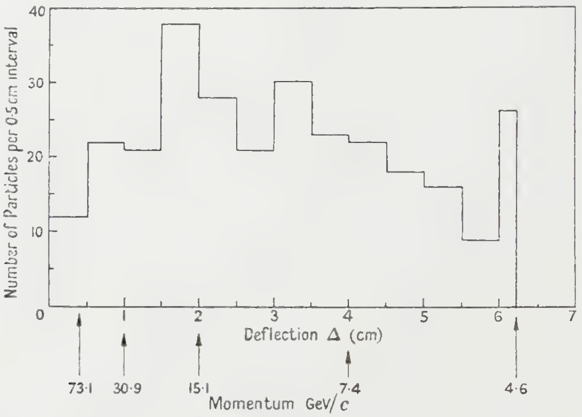

Figure 2. The deflection spectrum of the accepted particles. (Momentum loss by ionization has been allowed for in the momenta indicated.)

§ 3. EXPERIMENTAL RESULTS ON MULTIPLE SCATTERING

The r.m.s. displacement $\langle y \rangle$ has been found from the experimental results. A cut-off procedure has been used whereby displacements greater than 3·5 times the expected r.m.s. displacement (on the uniform nuclear model theory) have been rejected. These large displacements are considered in detail in the section in which the scattering distributions are considered as a whole.

3.1. *Variation of $\langle y \rangle$ with Momentum*

The r.m.s. displacements have been grouped together for different momentum bands and are plotted as a function of mean momentum in figure 3. Small corrections have been applied: to $\langle y \rangle$ for random errors in y, and to p for errors in Δ. Also shown are the expected variations on the uniform nuclear model and Molière theories. It will be noticed that the scattering is rather greater than that expected on the uniform nuclear model theory. The ratios of observed to expected r.m.s. scattering displacements with cut-off at 3·5 × r.m.s. of the uniform nuclear model distribution are

$$1{\cdot}19 \pm 0{\cdot}04 \text{ (uniform nuclear model)}$$

and $$1{\cdot}02 \pm 0{\cdot}04 \text{ (Molière).}$$

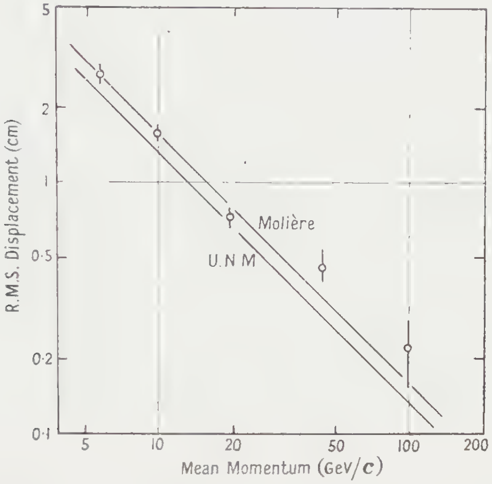

Figure 3. The variation, with momentum, of the r.m.s. scattering displacement for particles of both signs.

Since the scattering at high momenta appears to be appreciably greater than expected it is possible that the effect of errors in y has been underestimated. If it is assumed that the difference between the point at 100 GeV/**c** and the uniform nuclear model theory is due to errors in y, their subtraction, in quadrature, from the other points results in the point at 45 GeV/**c** being reduced by only a third of a standard deviation; the effect on the other points is negligible. The ratios given above are not significantly affected.

3.2. *Variation of $\langle y \rangle$ with the Sign of the Particle*

The ratio of $\langle y \rangle$ for positive and negative particles has been determined, again with a cut-off at 3·5 × r.m.s. displacement. The ratios for different momentum bands are given in table 1. The ratios are independent of systematic instrumental errors and are not inconsistent with unity in any group. The ratio averaged over all momenta is 0·93 ± 0·08.

Table 1. The Variation with Momentum of the Ratio of r.m.s. Scattering Displacement for Positive and Negative Particles

Momentum band (Momenta in GeV/**c**)	Ratio of r.m.s. scattering for positive and negative particles
$30{\cdot}9 < p$	$1{\cdot}02 \pm 0{\cdot}26$
$15{\cdot}1 < p < 30{\cdot}9$	$0{\cdot}76 \pm 0{\cdot}14$
$7{\cdot}4 < p < 15{\cdot}1$	$0{\cdot}99 \pm 0{\cdot}14$
$4{\cdot}6 < p < 7{\cdot}4$	$1{\cdot}03 \pm 0{\cdot}17$

§ 4. The Form of the Scattering Distributions, and the Large Displacements

4.1. *Spurious Contributions to the Scattering*

The tail of the scattering distribution is of considerable interest. Here the number of particles is small and since most spurious processes give rise to events appearing in the tail such contamination must be assessed.

Two main classes of spurious events can be defined: firstly where the event arises from an error in p and secondly where an error in y is responsible.

4.1.1. *Particles of uncertain momentum.*

Defining the genuine particle as that seen in the multi-plate chamber, it is possible that this particle did not pass through the top flat chamber but only through the middle one with a spurious particle passing through the top. The value obtained for the momentum of the genuine particle would then be erroneous. Since the tracks in the flat chambers were short and diffuse two sources of spurious events arise: one in which the genuine particle passed through that region of the Geiger counters outside the chamber and the other where it passed through the chamber and was not seen. In each case it is necessary that an apparently contemporary track be seen in the chamber in the correct region. From the experimentally determined individual probabilities the probability of an event of this type is 0·2%, when allowance is made for the stringent limit set on δ. An independent check on this value is afforded by consideration of the distribution in δ-values. The fraction of events outside the limits $\pm 0{\cdot}8$ cm is 2·9%, giving rise to an estimated spurious fraction within the limit of 0·45%. The two values are in rough agreement.

4.1.2. *Particles of uncertain scattering displacement.*

A similar situation exists in the bottom flat chamber. The probability of the genuine particle passing through a counter outside the chamber and a spurious particle passing through the appropriate counter inside the chamber is 0·4%. There is, of course, no limit on the transverse scattering displacement and another type of check must be made in the region where this degree of contamination is serious.

Another source of spurious events is provided by knock-on electrons produced in the absorber and accompanying the μ-meson. Two types of events can be distinguished.

(i) Where the μ-meson passed outside the counters and the electron passed through a counter and the visible region of the chamber.

(ii) Where the μ-meson passed through a counter but not the visible part of the chamber and the electron passed through the same counter (events where more than one counter was discharged were rejected). From a knowledge of the distribution of μ-meson trajectories and the frequency and spatial distribution of associated electrons, determined experimentally, the expected number of spurious events is approximately 0·02% of the number of accepted events. This fraction is negligible.

4.1.3. *Re-examination of particles with $py > 30$* GEV/**c** cm.

The only serious spurious rate is the 0·4% referred to in § 4.1.2. In order to reduce this rate to negligible proportions further checks were carried out on the particles having large py, that is $py > 30$ GEV/**c** cm. The inclination θ_{ch} to the vertical, in the magnetic deflection plane, of the track in each chamber was measured and compared with the expected inclination θ_c derived from T, M and C. In order to check the accuracy of the angular measurements fast particles, having $\Delta < 1$ cm, were selected which had small values of py and $\theta_{ch} - \theta_c$ determined for each chamber and each particle. The r.m.s. values of $\theta_{ch} - \theta_c$ were 2·8°, 3·2° and 3·2° for the top, middle and bottom flat chambers respectively. These represent distortion and errors of setting on the short tracks. Similar considerations to those giving the range of δ-values to be accepted, give a limit of $\pm 8^\circ$ on $\theta_{ch} - \theta_c$ for acceptance. It is estimated that this results in a reduction of the spurious rate at each level by a factor of about 3. No events were in fact rejected on the basis of anomalous $\theta_{ch} - \theta_c$ values.

The resultant contamination is thus of the order of 1 per 1000 events and it is therefore unlikely that any of the accepted particles is spurious.

Finally, the distribution of pz (where z is the transverse scattering displacement) for the particles with large py was compared with that for particles with small py. No significant difference was found, again indicating that the contamination by spurious particles was negligible.

4.2. *The Scattering Distributions*

The accepted particles having momentum less than 73 GeV/**c** (magnetic deflection greater than 0·4 cm) are grouped according to their values of py and plotted in figure 4. For these particles the uncertainty in momentum measurement

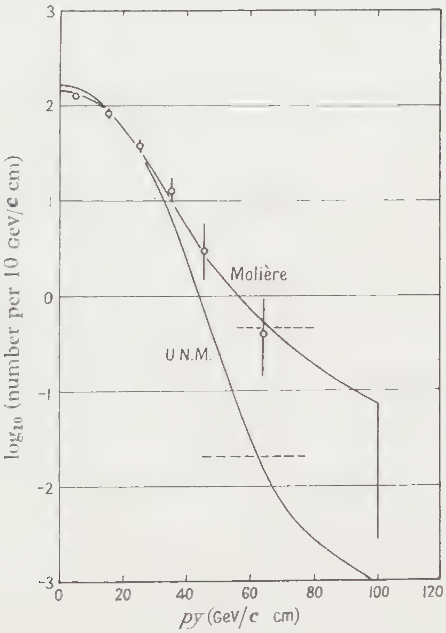

Figure 4. The scattering distribution for particles with momentum between 4·6 and 73 GeV/**c**.

is not large. Also plotted are the scattering distributions expected on the uniform nuclear model and Molière theories. The theoretical distributions were calculated in the following way. The lead absorber was divided into layers each of 4·5 cm thickness and the displacement distributions at the bottom flat chamber found for each layer using the angular scattering distributions given in I. The displacement distributions for the various layers were then folded in together to give the resultant distribution for the whole absorber. The uniform nuclear model distribution tends to $1/Z$ of the Molière distribution for large py, where the Z protons in the nucleus are considered to act as independent scattering centres.

Corrections have been made to the theoretical distributions to allow for the effects of errors in p, y and the geometrical bias introduced by the limited size of the bottom flat chamber (particularly in the transverse direction).

Table 2. The Magnitudes of the Various Errors Contributing to the Error in the Magnetic Deflection

Chamber	Errors (mm)			Total	
	Setting	Cell	Distortion	1 reading	2 readings
Multi-plate	0·37	0·15	0·20	0·45	0·36
Top	0·54	0·29	(0·82)	1·02	0·95
Middle	0·52	0·29	(0·82)	1·02	0·95
Bottom	0·67	0·29	(0·82)	1·10	0·99
Deflection (Δ)				1·16	1·08

The corrections were made using the mean momentum of each group ($0{\cdot}4 < \Delta < 1{\cdot}0$ cm etc.—see § 3.2) and the resultant py distributions were summed according to the number of particles in each group. The determination of the errors in p and y are considered in Appendix I, and the evaluation of their effect on the scattering distribution is straightforward. The geometrical bias was estimated from the distribution of predicted points of intersection of the particle trajectories with the plane of the bottom chamber. This distribution was then mixed with the expected displacement distributions for various momenta, and the fraction of particles expected within the chamber determined. The geometrical correction increases with py reaching a factor of 2 for the lowest momentum group at $py \sim 100$ GeV/**c** cm. Consequently, the expected number of events above 100 GeV/**c** cm ($\simeq 0{\cdot}5$ in Molière distribution) is somewhat uncertain and the scattering distributions have been cut off at 100 GeV/**c** cm. The last experimental point gives the number of events between 50 and 100 GeV/**c** cm. The dotted lines give the numbers expected on the two theories. The experimental point is plotted at the mean abscissa of the two intersections of the dotted lines with their respective curves.

The goodness of fit between the experimental points and the theoretical curves has been inspected using the χ^2-test. The probabilities of the measured χ^2 or greater values being due to chance are 97% for the Molière distribution and 0·24% for the uniform nuclear model distribution.

The agreement with the Molière distribution is unexpectedly good. The inconsistency of the experimental results with the uniform nuclear model distribution is fairly well established. It is found that the major contribution to χ^2 for the uniform nuclear model distribution is from the region 30–50 GeV/**c** cm where both errors and geometrical corrections are small; there are 16 particles in this region.

No pronounced asymmetry in the signs of the particles with large displacements has been observed. Of the particles with $py > 30$ GeV/**c** cm, 10 are positive and 8 are negative compared with a positive–negative ratio for all the particles of 1·14.

§ 5. Discussion and Conclusions

5.1. *The Multiple Scattering*

The results of this investigation, in the region 5–10 GeV/***c***, are in good agreement with those reported in I. For momenta above 10 GeV/***c*** the consistency with the Molière distribution continues. There is no evidence for any appreciable increase in scattering in excess of the Molière distribution at high energies or for any difference in the multiple scattering of positive and negative particles at any energy.

5.2. *The Large-Angle Scattering*

The experiment has shown that the large-angle (or more precisely large-displacement) scattering observed at lower momenta persists to momenta of the order of 100 GeV/***c***.

The present position regarding the experimental aspect of large-angle scattering can be summarized as follows, for the various momentum ranges that have been studied.

(*a*) $p\beta < 200$ MeV/***c***.

Here the experimental evidence on scattering is sparse. Nuclear emulsions are particularly useful in this region since momentum and deflection measurements can be made accurately. However, because of the low flux of slow μ-mesons, experiments of high statistical precision have not been made. Kannangara and Shrikantia (1953) (see also Rochester and Wolfendale 1954) observed the large-angle scattering of a small number of μ-mesons in this region but were unable to distinguish between the uniform nuclear model and Molière distributions.

There are preliminary reports of Russian work in this momentum region. Alichanow and Jelissejew (1955) have studied the scattering of μ-mesons in carbon plates in a cloud chamber in the energy range 40–500 MeV. An excess of scattering was observed throughout this energy range; the cross section for scattering through angles greater than 16° was found to fall with increasing energy of the μ-mesons. This variation suggests some form of Coulomb interaction but the magnitude is considerably greater than expected in the Molière distribution. These results are inconsistent with those of the emulsion experiment where an anomaly of this magnitude would have been detected. It is possible that the reason for the discrepancy is the difference in atomic number of the scattering nuclei in the two experiments.

Alichanjan and Kirillow-Ugrjumow (1955) have studied the scattering of μ-mesons in copper. Over most of the low momentum region (the region studied was below about 300 MeV/***c***) agreement with theory was found, although the statistical precision was too low to distinguish between the Olbert and Molière distributions. In the region 80–135 MeV/***c*** an excess of deflections through angles above 15° was found. Later experiments using the same apparatus have shown that better agreement exists with the Olbert distribution over most of the momentum range but, as before, there is excess scattering in the range 80–135 MeV/***c*** (private communication from A. I. Alichanjan to L. Rosenfeld).

It is of interest to note here that it is in this region that Short (to be published) has found what appears to be a significant difference in the multiple scattering of positive and negative μ-mesons. It is also in this low energy region (<10 MeV kinetic energy) that anomalous effects have been observed in electron scattering by Heymann and Williams (1956) and others.

(*b*) $200 < p\beta < 600$ MeV/**c**.

In this region the statistical weight of the experiment is again poor. Kannangara and Shrikantia found better agreement with the Molière distribution in this region but the result is not conclusive. The experiments of McDiarmid (1954, 1955) are the most precise. For scattering in iron most of the contributions to the large-angle scattering in the two low-momentum bands comes from the regions of 300 and 600 MeV/**c**. In each band rather better agreement is found with the uniform nuclear model than the Molière distribution. For scattering in lead in the lowest momentum band with mean effective momentum of about 300 MeV/**c** McDiarmid found rather better agreement with the Molière distribution. However, comparison is made with the uniform nuclear model for $r_0 = 1{\cdot}4$ and if the more realistic value of $r_0 = 1{\cdot}1$ is used, together with a small correction (Lloyd and Wolfendale 1955, Appendix 1, (1)) for the effect of random errors in the angle measurements, the results are not inconsistent with the uniform nuclear model distribution.

Whittemore and Shutt (1952) observed the scattering of μ-mesons, some of which had momenta below 600 MeV/**c**. The number of mesons in this region was small, however; only 3 particles in this momentum range had $p\phi > 10$ GeV/**c** deg.

(*c*) 600 MeV/**c** $< p\beta < 3$ GeV/**c**.

The results of experiments of moderate statistical precision by Whittemore and Shutt, McDiarmid, and Lloyd and Wolfendale all show scattering in excess of the uniform nuclear model distributions and of magnitude similar to Molière distributions.

(*d*) 3 GeV/**c** $< p\beta < 100$ GeV/**c**.

This region has been studied by the present authors, the part below about 10 GeV/**c** by Lloyd and Wolfendale. Using rather different methods the results are similar and it is concluded that the excessive scattering is still present.

It is useful here to consider information from other sources on the interaction of fast μ-mesons. Masek *et al.* (1956) have recently studied the production of μ-meson pairs by 600 MeV electrons. They find that the ratio of the experimental to the theoretical cross section for the production of a μ-meson pair, in which the negative μ-meson is emitted in a particular angular range, is $1{\cdot}42 \pm 0{\cdot}34$. The theoretical value has been derived by modifying the conventional formula for the pair production of fermions by photons in a Coulomb field for the effect of a finite nuclear size. Although the ratio may differ significantly from unity it is apparent that the anomalous interaction is rather weak. It will be seen by reference to (*a*) and (*b*) above that these results are not inconsistent with the conclusions given there, since apart from the work of Alichanow there is no significant evidence for an anomaly in this energy region.

The theoretical aspect of the large-angle scattering has recently been studied by Fowler (1957) and a possible explanation put forward. The theoretical calculations involve the derivation of elastic scattering phase shifts and these have only been evaluated for μ-meson momenta below 2 GeV/**c**. Fowler's results may be summarized as follows:

(i) Below about $p\beta \sim 270$ MeV/**c** (energy, 200 MeV) little or no anomaly is expected.

(ii) The cross section for the large-angle scattering is proportional to A^2.

(iii) The magnitude of the large-angle scattering is such that the single scattering approaches the Molière distribution for large momentum transfers. For example, for mesons with $p\beta = 2$ GeV/**c**, the ratio of predicted scattering to Molière scattering is $\sim 0{\cdot}1$ at 20 GeV/**c** deg, $\sim 0{\cdot}25$ at 30 GeV/**c** deg and is nearly unity for $p\phi > 40$ GeV/**c** deg (ϕ is the projected angle of scattering).

It is clear that a multiple scattering distribution formed from this single scattering law will be in much better accord with the experimental results. A detailed comparison with the results of the present experiment cannot be made on account of the lack of calculation of the expected scattering at high energies.

ACKNOWLEDGMENTS

We are greatly indebted to Professor G. D. Rochester, formerly Acting Director, and Professor S. Devons, the present Director of the Physical Laboratories, for providing the facilities and for their interest in the work.

We wish to thank Mr. A. L. Rodgers for his assistance in the operation of the spectrograph and for many helpful discussions. Dr. Gey Van Pittius co-operated with us in the early part of the work and we wish to express our thanks to him.

We have benefitted from many discussions with Dr. G. N. Fowler and we should like to thank him for communicating his results prior to publication.

One of us (E. R.) wishes to thank the British Council for provision of a Scholarship.

REFERENCES

ALICHANJAN, A. I., and KIRILLOW-UGRJUMOW, W. G., 1955, *Izv. Akad. Nauk, SSSR, Ser. fiz.*, **19**, 737.

ALICHANOW, A. I., and JELLISSEJEW, G. I., 1955, *Izv. Akad. Nauk, SSSR, Ser. fiz.*, **19**, 732.

FOWLER, G. N., 1957, *Nuclear Phys.*, **3**, 121.

HEYMANN, F. F., and WILLIAMS, W. F., 1956, *Phil. Mag.*, **1**, 212.

HOFSTADTER, R., 1956 *Rev., Mod. Phys.* **28**, 214.

HOLMES, J. R., OWEN, B. G., RODGERS, A. L., and WILSON, J. G., 1956, *Report on the Conference on Recent Developments in Cloud Chamber and Associated Techniques* (London : University College), p. 177.

HYAMS, B. D., MYLROI, M. G., OWEN, B. G., and WILSON, J. G., 1950, *Proc. Phys. Soc.* A, **63**, 1053.

KANNANGARA, M. L. T., and SHRIKANTIA, G. S., 1953, *Phil. Mag.*, **44**, 1091.

LLOYD, J. L., and WOLFENDALE, A. W., 1955, *Proc. Phys. Soc.* A, **68**, 1045.

MASEK, G. E., LAZARUS, A. J., and PANOFSKY, W. K. H., 1956, *Phys. Rev.*, **103**, 374.

McDIARMID, I. B., 1954, *Phil. Mag.*, **45**, 933 ; 1955, *Ibid.*, **46**, 177.

MOLIÈRE, G., 1947, *Z. Naturf.*, **2a**, 133 ; 1948, *Ibid.*, **3a**, 78.

ROCHESTER, G. D., and WOLFENDALE, A. W., 1954, *Phil. Mag.*, **45**, 980.

WHITTEMORE, W. L., and SHUTT, R. P., 1952, *Phys. Rev.*, **88**, 1312.

APPENDIX

THE DETERMINATION OF THE UNCERTAINTIES IN Δ AND y

As mentioned in § 2.3, the magnetic deflection at the central level of the spectrograph is given by $\Delta = \frac{1}{2}(T+C) - M - \Delta_0$. In order to determine Δ_0 the spectrograph was operated without magnetic field and the deflections of fast particles were determined. The fast particles were selected from observations on their scattering in the multi-plate chamber; particles with root-mean-square deflection less than 0·3° were classed as fast. The value found for Δ_0 is $7{\cdot}25 \pm 0{\cdot}02$ cm.

The standard deviation of the distribution in Δ for the fast particles is $1{\cdot}6 \pm 0{\cdot}15$ mm. This value comprises displacements due to: (*a*) The scattering of the fast particles in the various layers of the spectrograph. (*b*) The track distortion in each of the cloud chambers. (*c*) Errors of setting at each of the measuring levels.

The contribution due to scattering has been calculated from the known momentum spectrum of the fast particles with $\phi_{\text{r.m.s.}} < 0{\cdot}3°$; this spectrum had been measured directly in a previous experiment in which the spectrograph was operated normally with magnetic field. The residual r.m.s. displacement, corrected for scattering, is

$$\sigma_\Delta = 1{\cdot}16 \pm 0{\cdot}24 \text{ mm.}$$

This is the error in the deflection when only one measurement is taken at each level; when two measurements are made and the mean taken the error is reduced a little, to 1·08 mm.

In order to find the error in y it is necessary to know the individual errors at the various levels. Only in the case of the multi-plate chamber could the distortion error be determined directly. Photographs of the tracks of fast particles in the multi-plate chamber, spaced at roughly equal intervals of time throughout the experiment, were selected for examination. In each case the best straight line was drawn through the points of intersection of the track with successive lead plates. The displacements between the points of intersection of the track and the best straight line are due to distortion, i.e. the lateral and angular movement of track segments arising from the effects of gas motion in the cloud chamber. It was found that the displacement, at the measuring level in the multi-plate chamber, had a random component with standard deviation 0·16 mm and a systematic component, with respect to the best line, of 0·19 mm. A truly systematic displacement is not important since it is contained in Δ_0. Slowly varying 'systematic' errors may occur, however, and a value of 0·20 mm has been taken as the distortion error.

The errors of setting were determined from a consideration of the differences between repeated settings on the same track.

'Cell' errors arise from the fact that measurements of the position of a track were made to the nearest millimetre in the flat chambers and to the nearest 0·5 mm on each photograph of the multi-plate chamber.

The results are summarized in table 2. The distortion error in each of the flat chambers has been assumed to be the same and has been calculated by subtraction of all the other errors from σ_Δ. The value found, $0{\cdot}82 \pm 0{\cdot}26$ mm, is larger than would be expected. It is probable that systematic distortion, varying slowly over the period of the experiments and arising from the lack of complete temperature control for each of the flat chambers, is responsible for the large distortion error.

The error in y has been calculated using the relation between y and C, T, M, B and the geometrical factors, and the known errors in these quantities. The result is that $\sigma_y = 1{\cdot}92$ mm for one reading at each level and 1·76 mm for two readings.

Nuclear Moments of Inertia

By T. H. R. SKYRME
Atomic Energy Research Establishment, Harwell, Berks.

Communicated by B. H. Flowers; MS. received 14*th March* 1957

Abstract. A formula proposed by the author for the calculation of the moment of inertia of a nuclear system is discussed. A simple calculation using the model of a deformed oscillator well for the mean nuclear potential gives the result $M\Sigma z^2$ for a prolate distribution, approximately half the rigid moment; it is suggested that this result incorporates most of the effects of the residual interactions between nucleons. The problem of other potential shapes and the velocity-dependence of the potential is discussed qualitatively.

§ 1. Introduction

Many nuclei are now known to exhibit bands of energy levels with the spectra

$$E_I = (\hbar^2/2\mathscr{I})I(I+1) \qquad \ldots\ldots(1)$$

where I is the angular momentum of the level and $\mathscr{I}$ is an empirical constant (for each band) called the moment of inertia by analogy with the spectrum of energy levels of a rigid rotating top. These are especially well developed in the nuclei with masses between 150 and 190 and greater than 225, nuclei which are also considered to be markedly deformed into an ellipsoidal shape on the basis of their large electric quadrupole moments (and quadrupole transition matrix elements). The experimental information has been collated by various authors, Bohr and Mottelson (1955), Moszkowski (1956), Blin-Stoyle (1956). The present paper offers some theoretical comments on the magnitude of $\mathscr{I}$.

A qualitative explanation of the deformation of these nuclei was given by Rainwater (1950), who showed that on the basis of the independent particle model of the nucleus the state of lowest energy would generally be deformed due to the polarizing action of those (outermost) nucleons which were in incompletely filled shells. Calculations have been made by various authors, for example Nilsson (1955), showing that indeed large deformations would be expected in the mass-regions mentioned due to the overlapping and mixing of a large number of single-particle levels.

The self-consistency of this deformed potential was discussed by Bohr and Mottelson (1953) in terms of a hydrodynamic model in which the potential was ascribed to a 'core' of nucleons whose motion was assumed to be that of an incompressible, irrotational fluid, having a surface tension tending to oppose the polarizing action of the individual nucleons coupled to the potential. In the 'strong-coupling' limit of this model, the system would execute small vibrations about an equilibrium state characterized by a deformed core and the lowest states of the system would be rotational ones with a moment of inertia given by

$$\mathscr{I}_{\mathrm{irrot}}=\mathscr{I}_{\mathrm{rig}}\epsilon^2 \qquad \ldots\ldots(2)$$

where ϵ is the ratio of the difference of axes to the mean radius of the equilibrium ellipsoidal shape.

The deformation ϵ could be inferred directly from the quadrupole data, and it was found that the observed moments of inertia determined by the level spacing were appreciably greater than given by the formula (2), presumably due to the impropriety of describing the nucleon motion as irrotational fluid flow.

An alternative method of discussing the problem was suggested by Inglis (1954), who introduced the idea of independent particle motion in a deformed potential well rotated with a fixed impressed angular velocity Ω. In a frame of reference fixed with respect to the potential the rotation introduces as a perturbation a Coriolis force. It can then be argued that the reduction in energy caused by this perturbation should be equal to the increase in energy for free rotation of this system, and the moment of inertia is found by equating this energy change to $\frac{1}{2}\mathscr{I}\Omega^2$; this leads to the cranking model formula

$$\mathscr{I}_{\mathrm{cr}}=2\sum_i |\langle 0|J_x|i\rangle|^2/(E_i-E_0). \qquad \ldots\ldots(3)$$

Some of the consequences of this formula have been discussed by Inglis and by Bohr and Mottelson (1955). In particular they have shown that, used in conjunction with a deformed oscillator well, the formula leads to the rigid moment of inertia for the equilibrium configuration; they have also shown that this value may be markedly reduced by the effects of residual interactions between the nucleons.

A number of authors, for example Villars (to be published), have considered the general problem of exhibiting the rotational motion by a suitable transformation of the many-particle Hamiltonian describing the nucleus, but this fundamental approach will not be considered further in this paper. A more phenomenological approach has been used by Yoccoz (1956), applying a variational principle to a wave function of the type suggested by Hill and Wheeler.

The method followed here is that suggested by Skyrme (1957), and is closely related to the method of Yoccoz in this problem. In the following section the basic formula in this approach is derived; in §3 it is applied to a wave function of shell-model type; next a simplified formula is deduced, making use of the fact that the interaction forces are predominantly of short range. In §5 this is used in conjunction with a deformed oscillator well and in the following sections some discussion is given of the problems presented by a more realistic form of potential. The results are discussed in §8.

§2. Formula for the Moment of Inertia

It will be supposed at first that the nuclear system has a set of energy levels E_I, which are given exactly by the formula (1) for a rigid rotator, and corresponding eigenfunctions $\psi_M{}^I(x)$, where the arguments x stand for all the coordinates of the A constituent nucleons. According to the qualitative picture developed by Bohr and Mottelson (1953), these levels can be described phenomenologically in terms of the rotational motion of a top; if θ, ϕ and ψ, or Ω for brevity, are the Eulerian coordinate angles of this top, the wave functions of this model are the well-known transformation matrices $D_{KM}{}^{I}(\Omega)$, the eigenfunctions of the Hamiltonian

$$(1/2\mathscr{I})\mathbf{K}^2 \qquad \ldots\ldots(4)$$

representing the rotational energy, where **K** is the angular momentum operator corresponding to the coordinates Ω.

According to the general procedure suggested by Skyrme (1957) an enlarged state function $\psi(x, \Omega)$ is constructed according to the definition

$$\psi(x, \Omega) = \sum_{IM} A_I \psi_M{}^I(x) D_{KM}{}^{*I}(\Omega). \qquad \ldots\ldots(5)$$

Here K is the intrinsic spin postulated for the set of levels considered and the A_I are coefficients, arbitrary for the moment. Conversely from this equation

$$A_I \psi_M{}^I(x) = \int \psi(x, \Omega) D_{KM}{}^I(\Omega)\, d\Omega \qquad \ldots\ldots(6)$$

which exhibits the wave function in a general form that has been suggested by Hill and Wheeler.

Since it has been assumed that the levels E_I are given by the eigenvalues of (4), it follows from the definition (5) that $\psi(x, \Omega)$ must satisfy the enlarged Schrödinger equation

$$(H - (1/2\mathscr{I})\mathbf{K}^2)\psi(x, \Omega) = E_0 \psi(x, \Omega) \qquad \ldots\ldots(7)$$

where H is the Hamiltonian of the nuclear system, the sum of kinetic energy T and potential energy V. It is also clear from the definition that $\Psi(x, \Omega)$ is invariant under simultaneous rotations of the coordinates x and of the Eulerian angles Ω, so that

$$\mathbf{K}\Psi(x, \Omega) = \mathbf{J}\Psi(x, \Omega) \qquad \ldots\ldots(8)$$

where **J** is the total angular momentum vector of the nucleonic system; in other words $\Psi(x, \Omega)$ can be obtained from $\Psi(x, 0)$ simply by a rotation of coordinates, and since $\mathbf{K}^2$ is equivalent to $\mathbf{J}^2$, all mention of Ω can be eliminated from (7). Hereafter $\Psi(x, 0)$ will simply be written as $\Psi(x)$, which must satisfy

$$(H - (1/2\mathscr{I})\mathbf{J}^2)\Psi(x) = E_0 \Psi(x). \qquad \ldots\ldots(9)$$

In this equation both the function Ψ and the coefficient $(1/2\mathscr{I})$ are unknown. Now it was originally supposed that the energy levels E_I were given exactly by the formula (1); this was unrealistic and the coefficient $(1/2\mathscr{I})$ will be so chosen as to minimize the difference between the actual energy levels and those given by the model formula. One of the simplest ways of doing this is to impose the variational condition

$$\delta \int \Psi^*(x)[H - (1/2\mathscr{I})\mathbf{J}^2 - E_0]^2 \Psi(x)\, dx = 0 \qquad \ldots\ldots(10)$$

on variations both of the state-function and of the parameters $\mathscr{I}$ and E_0. Variation of the state-function Ψ leads back to equation (9), and variation of the parameters leads, after the elimination of E_0, to a formula for the moment of inertia

$$1/2\mathscr{I} = [\langle H\mathbf{J}^2\rangle - \langle H\rangle\langle \mathbf{J}^2\rangle]/[\langle \mathbf{J}^4\rangle - \langle \mathbf{J}^2\rangle^2] \qquad \ldots\ldots(11)$$

where the bracket symbols $\langle\ \rangle$ denote the expectation value with respect to the function Ψ determined by (9), or some approximation to it.

§3. SELF-CONSISTENT POTENTIAL

Further progress in this problem depends upon making some approximation to the function $\Psi(x)$. The qualitative success of the single-particle model of deformed nuclei suggests that $\Psi(x)$, for a suitable choice of A_{I} in equation (5), might be taken as a determinant of single-particle wave functions $\phi_n(x_i)$. It would then be most consistent to determine the best possible set of ϕ_n from the variational condition (10); however, this leads to excessive algebraic complexity and the (more usual) variational condition will be used in which the integrand is not squared, that is

$$\delta\langle H-(1/2\mathscr{J})\mathbf{J}^2-E_0\rangle=0 \qquad \ldots\ldots(12)$$

(this also leads to equation (9) for arbitrary variations of $\Psi(x)$).

The set of ϕ_n determined by this condition (12) are eigenstates of a single-particle Hamiltonian

$$h=t+u-(1/2\mathscr{J})g \qquad \ldots\ldots(13)$$

where t is the kinetic energy of a single nucleon, u is a single-particle non-local potential, the Hartree–Fock potential derived from V and ϕ_n, and g is a similar single-particle operator derived from $\mathbf{J}^2$.† The total determinantal state Ψ is then an eigenstate of the Hamiltonian H' formed by summing the single-particle Hamiltonians h_i,

$$H'=T+U-(1/2\mathscr{J})G \qquad \ldots\ldots(14)$$

and

$$H=H'+(V-U)+(1/2\mathscr{J})G. \qquad \ldots\ldots(15)$$

This last expression is now substituted for H in the formula (11). H' may be dropped since Ψ is supposed now to be an eigenstate of it, and when the terms in $(1/2\mathscr{J})$ are collected together the result is to give

$$(1/2\mathscr{J})=[\langle(V-U)\mathbf{J}^2\rangle-\langle(V-U)\rangle\langle\mathbf{J}^2\rangle]/[\langle(\mathbf{J}^2-G)\mathbf{J}^2\rangle-\langle(\mathbf{J}^2-G)\rangle\langle\mathbf{J}^2\rangle]. \ldots(16)$$

Now the operators V and $\mathbf{J}^2$ may, with respect to the set of functions ϕ_n, be divided into an expectation value, a 'one-particle part' giving rise to excitations of one nucleon from the ground state, a 'two-particle part' and so on. Obviously the expectation value does not contribute to the formula (12) and the one-particle parts are cancelled exactly by U and G respectively; so if the operator $\underset{\sim}{Q}$ is defined to be zero acting upon the ground state and all states derived from it by excitation of only one nucleon, and unity otherwise, the formula may be written more concisely as

$$(1/2\mathscr{J})=\langle V\underset{\sim}{Q}\mathbf{J}^2\rangle/\langle\mathbf{J}^2\underset{\sim}{Q}\mathbf{J}^2\rangle. \qquad \ldots\ldots(17)$$

These expectation values may now easily be written in terms of matrix elements. The matrix element between the states ϕ_m and ϕ_n of the single-particle angular momentum operator $\mathbf{j}$ will be written as $(n|\mathbf{j}|m)$; then

$$\langle\mathbf{J}^2\underset{\sim}{Q}\mathbf{J}^2\rangle=2\sum_m\sum_n\sum_{m'}\sum_{n'}\sum_r\sum_s(m|j_r|m')(n|j_r|n')[(m'|j_s|m)(n'|j_s|n)-(m'|j_s|n)(n'|j_s|m)] \qquad \ldots\ldots(18)$$

where the summation of m and n extends over all occupied states and that of m'

---

† With the notation used below in equation (18) and (19), the matrix elements of u and g are given by

$$(a\,|\,u\,|\,b)=\sum_n(an-na\,|\,v\,|\,bn)$$

$$(a\,|\,g\,|\,b)=(a\,|\,j^2\,|\,b)-2\sum_n\sum_r(a\,|\,j_r\,|\,n)(n\,|\,j_r\,|\,b)$$

and n' over all unoccupied ones. It will be assumed hereafter that V is a sum of two-nucleon interactions

$$\sum_{i<j} v_{ij};$$

then in a similar way

$$\langle VQ\mathbf{J}^2\rangle = 2\sum_m \sum_n \sum_{m'} \sum_{n'} \sum_r (m, n-n, m|v|m'n')(m'|j_r|m)(n'|j_r|n) \qquad \ldots\ldots(19)$$

where the matrix element of v is the difference of the direct and exchange matrix elements.

In the above discussion the question of centre-of-mass motion has been ignored. The wave functions introduced in §2 should be those of the internal motion of the system, whereas the approximate determinantal ones involve some motion of the mass-centre. Then it would be more consistent with the general philosophy used here to replace the total angular momentum $\mathbf{J}$ in formulae (11) and (17) by the internal angular momentum. This has not however been considered in any detail because of the complexity of the modified matrix elements.

§ 4. A Simplified Formula

The formulae found in the preceding sections could be evaluated numerically for particular assumed trial wave functions, but it is difficult to draw general qualitative conclusions from them. For this it would be desirable to have a form which depends principally upon the mean self-consistent potential rather than upon the internucleon potential V. This can be done in the following way.

By the substitution of (15) into the fundamental relation (11), two formally different identities may be obtained

$$(1/2\mathscr{I})\langle \mathbf{J}^2(\mathbf{J}^2 - G - \langle \mathbf{J}^2 - G\rangle)\rangle = \langle \mathbf{J}^2(V - U - \langle V - U\rangle)\rangle \qquad \ldots\ldots(20)$$

$$(1/2\mathscr{I})\langle J_r(\mathbf{J}^2 - G - \langle \mathbf{J}^2 - G\rangle)J_r\rangle = \langle J_r(V - U - \langle V - U\rangle)J_r\rangle + \langle J_r[H', J_1]\rangle \qquad \ldots\ldots(21)$$

of which the former is the same as equation (16). In the latter equation the coefficient of $(1/2\mathscr{I})$ is not very different from (18) being explicitly

$$\sum_r \sum_s \sum_m \sum_n \sum_{m'} \sum_{n'} (m|j_r|m')(n'|j_r|n)[(m'|j_s|m)(n|j_s|n') - (m'|j_s|n')(n|j_s|m)] \qquad \ldots\ldots(22)$$

with the same direct term. The first term on the right is equal to

$$\sum_r \sum_m \sum_n \sum_{m'} \sum_{n'} (m|j_r|m')(n'|j_r|n)(m'n|V|mn' - n'm) \qquad \ldots\ldots(23)$$

and is approximately equal to the negative of (19), for the following reasons:

(*a*) in the heavy deformed nuclei the orbital angular momenta are much larger than the spins, so that $\mathbf{j}$ may be replaced by $\mathbf{l}$; then, if the states are taken to have real orbital wave functions (which is not a significant restriction),

$$(n'|l_r|n) = -(n|l_r|n'), \qquad \ldots\ldots(24)$$

(*b*) the 'direct' matrix elements of V are the same in the two cases; the exchange terms are different, but will be small for short range forces.

A useful formula can be obtained then by assuming this last equality and by retaining only the similar direct terms in (18) and (22). Some further examination of these simplifications is made in Appendix A. Within the framework of the present analysis J_z is a good quantum number, equal to K, so that only J_x and J_y contribute to the matrix elements and in a symmetrical way; for example

$$\sum_m \sum_{m'} (m|j_r|m')(m'|j_s|m) = \delta_{rs}(1 - \delta_{r3})\langle J_x^2\rangle \qquad \ldots\ldots(25)$$

and the simplified formula is

$$\mathscr{I} = 2\langle J_x{}^2\rangle^2/\langle J_x(H' - \langle H'\rangle)J_x\rangle. \qquad \ldots\ldots(26)$$

In a similar notation the formula given by the cranking model is

$$\mathscr{I}_{\mathrm{cr}} = 2\langle J_x(H' - \langle H'\rangle)^{-1}J_x\rangle \qquad \ldots\ldots(27)$$

which will always be greater than (26) unless all the excitation energies involved are equal. The evaluation of (26) is discussed in the following sections.

§ 5. The Oscillator Model

The simplest model and the only one for which explicit calculations can easily be made is that of articles moving in a deformed oscillator well, such as has been used by Inglis (1954, 1955, 1956), Bohr and Mottelson (1955) and other authors. With this assumption

$$H' = -(1/2M)\nabla^2 + \tfrac{1}{2}M\omega^2[(x^2+y^2)e^{2\epsilon/3} + z^2e^{-4\epsilon/3}] \qquad \ldots\ldots(28)$$

where the parameter ϵ is a convenient measure of the deformation, related to the parameter B introduced by Bohr and Mottelson (1953) by

$$B = (16\pi/45)^{1/2}(e^{2\epsilon/3} - e^{-\epsilon/3}) \sim 1{\cdot}06\epsilon. \qquad \ldots\ldots(29)$$

The individual particle wave functions are oscillator wave functions with deformation $\frac{1}{2}\epsilon$, and can be labelled by the oscillator quantum numbers l, m, n corresponding to the x, y, z directions.

The deformation will be assumed to be prolate with cylindrical symmetry, so that

$$\sum(l+\tfrac{1}{2}) = \sum(m+\tfrac{1}{2}) < \sum(n+\tfrac{1}{2}) = C, \quad \text{say}. \qquad \ldots\ldots(30)$$

The assumed potential (28) can only be self-consistent if the density distribution has approximately the same deformation; since the wave functions are distorted only by $\frac{1}{2}\epsilon$, the asymmetry of the configuration must make up the difference; the expectation values of y^2 and z^2 will have the correct ratio if

$$\sum(m+\tfrac{1}{2}) = Ce^{-\epsilon}. \qquad \ldots\ldots(31)$$

This result may also be obtained by minimizing $\langle H'\rangle$ with respect to variations of ϵ, but that argument is dubious (see also § 7).

Acting upon the state $|l, m, n\rangle$ the operator j_x can transform it into any of the four states $|l, m\pm 1, n\pm 1\rangle$ that are unoccupied, and the value of $\langle J_x{}^2\rangle$ is found by summing the squares of all the allowed transition matrix elements (cf. the formula (25)). This summation can easily be performed by summing over all, allowed and forbidden, matrix elements and then subtracting the forbidden ones. The result, as has been found by Bohr and Mottelson and by Inglis, is

$$\begin{aligned}\langle J_x{}^2\rangle &= \cosh^2(\tfrac{1}{2}\epsilon)\sum(n-m) + \sinh^2(\tfrac{1}{2}\epsilon)\sum(m+n+1)\\ &= C\sinh\epsilon \qquad \ldots\ldots(32)\end{aligned}$$

with the help of the condition (31).

The denominator of (26) can be evaluated in just the same way, leading to the result

$$\mathscr{I} = (C/\omega)e^{2\epsilon/3} = M\sum z^2 \qquad \ldots\ldots(33)$$

so that the ratio to the rigid moment $M\sum(y^2+z^2)$ is $1/(1+e^{-2\epsilon})$, a little greater than $\frac{1}{2}$ for the moderate deformations observed.

§ 6. GENERAL ESTIMATE

The oscillator model is only a rough approximation for heavy nuclei, so it is important to investigate the generality of the preceding result and in particular how sensitive it is to the well shape and to the velocity dependence of the mean potential (Blin-Stoyle 1956).

The denominator of formula (26) can reasonably be estimated, since it can be written in terms of commutators as†

$$\langle \tfrac{1}{2}[J_x, [U, J_x]] \rangle. \qquad \ldots\ldots(34)$$

As a model of a distorted velocity-dependent potential it will be assumed that U can be taken in the form

$$U = U_0(r') + \mathbf{p}U_1(r')\mathbf{p} \qquad \ldots\ldots(35)$$

where

$$r'^2 = (x^2+y^2)e^{2\epsilon/3} + z^2 e^{-4\epsilon/3} \qquad \ldots\ldots(36)$$

so that the effective mass is given by

$$1/2M^* = 1/2M + U_1(r'). \qquad \ldots\ldots(37)$$

It will also be assumed, consistently, that the density ρ and 'square-of-momentum' density τ are also functions only of r'. Then the expectation value (34) can be expressed in terms of an integral over r',

$$\frac{4}{3}\sinh^2\epsilon(\tfrac{1}{2}\langle[J_x[U,J_x]]\rangle) = -\frac{2}{15}\sinh^2\epsilon\int\left[\frac{dU_0}{dr'}\frac{d\rho}{dr'} + \frac{dU_1}{dr'}\frac{d\tau}{dr'}\right]r'^2\,dV. \quad \ldots.(38)$$

It can be verified that for the oscillator potential, $U_0 = \frac{1}{2}M\omega^2 r'^2$, this gives the same result as that calculated directly in § 5, which is

$$2\omega C e^{-2\epsilon/3}\sinh^2\epsilon \sim \omega^2 \mathscr{I}_{\text{rig}}\sinh^2\epsilon \qquad \ldots\ldots(39)$$

proportional to A, the total number of nucleons, when the oscillator frequency is adjusted to give constant nuclear density. For a more realistic square potential shape, the integral should be proportional to $A^{4/3}$, at least for large A; an estimate can be made by using the Thomas–Fermi approximation relating ρ and τ to the potential, when (38) can be transformed into

$$\frac{4}{27}\sinh^2\epsilon\int\frac{\tau}{2M^*}\left(\frac{r'}{\rho}\frac{d\rho}{dr'}\right)^2 dV \qquad \ldots\ldots(40)$$

as shown in Appendix B, and of which a numerical estimate is

$$A^{4/3}(7{\cdot}2\,\text{MeV})\sinh^2\epsilon \qquad \ldots\ldots(41)$$

whereas the coefficient of $\sinh^2\epsilon$ in (39), for the oscillator potential, has the numerical value A (22 MeV). Thus for the heavy nuclei with A around 200 the estimate (41) has about twice the value given by the oscillator model.

The estimation of $\langle J_x^2 \rangle$ is more difficult, as this depends upon the configuration of minimum energy for a given deformation. One possible line of approach is to follow the suggestion made by Nilsson (1955) that in the case of large deformations perturbation theory may be applied to the deformed oscillator model. Then the configuration of the oscillator model is retained, but $\langle J_x^2 \rangle$ is altered by the first-order change in the wave functions.

---

† Here the reaction term $(1/2\mathscr{I})G$ in H' has been neglected, or it may be supposed that U is modified to include it.

If U_{pert} is the correction applied to the oscillator potential, then in first order the change in $\langle J_x^2\rangle$ is

$$2\langle J_x^2(E_0-H')^{-1}U_{\text{pert}}\rangle. \qquad \ldots\ldots(42)$$

The perturbation used by Nilsson, proportional to $\mathbf{l}^2$ depresses states of high angular momentum and makes this correction positive. Its numerical value fluctuates with the configuration considered, and suggests increases of 25–50% in $\langle J_x^2\rangle$.

Apart from the crudity of the method of estimation by perturbation theory it is not clear that Nilsson's model is sufficiently realistic to give a reliable value for $\langle J_x^2\rangle$. In the next section a different approach is attempted, to bring in explicitly the condition of optimum configuration.

§ 7. CONDITION OF LEAST ENERGY

The first requirement is a knowledge of the single-particle wave functions in a well with a given distortion, such as (35). The approximation suggested by Moszkowski (1955) will be used, according to which the single-particle wave functions are approximated by those of a spherical system, distorted by some amount η to be fixed by a variational calculation.

The states ϕ_n are functions of the distorted coordinates $x'=xe^{\eta/3}$, $z'=ze^{-2\eta/3}$, so that $d\phi_n/dx=e^{\eta/3}(d\phi_n/dx')$, and so on. The expectation values are worked out by expressing all quantities in terms of the distorted coordinates. For the determination of η only terms of the first and second order in η and ϵ will be retained; thus, dropping the primes from the distorted coordinates, the expectation value of the kinetic energy is

$$\frac{1}{2M}\left\langle \sum(p_x^2+p_y^2+p_z^2)+\frac{2\eta}{3}\sum(p_x^2+p_y^2-2p_z^2)+\frac{2\eta^2}{9}\sum(p_x^2+p_y^2+4p_z^2)\right\rangle. \qquad \ldots\ldots(43)$$

The linear term in η is cancelled exactly, according to the virial theorem, by a similar term arising in first order from the potential energy. The remaining quadratic terms are

$$\tfrac{4}{9}\eta^2Y+\tfrac{4}{9}(\epsilon-\eta)^2X \qquad \ldots\ldots(44)$$

where

$$Y=\tfrac{1}{2}\langle(1/2M^*)\sum(p_x^2+p_y^2+4p_z^2)\rangle\sim\langle(1/2M^*)\sum(p_x^2+p_y^2+p_z^2)\rangle \qquad \ldots\ldots(45)$$

to this order of approximation in the deformation, and where X is the integral defined in equation (38).

Therefore the optimum distortion is given by

$$\eta/\epsilon=(1+Y/X)^{-1}. \qquad \ldots\ldots(46)$$

For the oscillator case $X=Y$ and $\eta=\tfrac{1}{2}\epsilon$, as we already know. For the realistic case X is about doubled in value, and so will be Y for a reduced mass around $\tfrac{1}{2}M$, so their ratio will not differ much from unity.

The second requirement is the fixing of the distortion ϵ. As was mentioned earlier it is not *a priori* satisfactory to do this simply by minimizing with respect to ϵ, because it is possible that the potential varies in other ways with ϵ. It is, however, correct to assert that the energy, calculated as the expectation value of the many-body Hamiltonian, must be stationary for small uniform distortions of the determinantal wave function, since the latter was defined to be the best. In particular then the condition

$$[H,D]=[H,\sum(2zp_z-xp_x-yp_y)]=0 \qquad \ldots\ldots(47)$$

must be satisfied in the equilibrium state.

The potential energy will be taken in the phenomenological form used by Skyrme (1956),

$$V = \sum_{i<j} \delta(x_i - x_j)(t_0 + t_1(p_i - p_j)^2). \qquad \ldots\ldots(48)$$

The commutator with D is easy to evaluate in this form, because the delta-function commutes with the distortion, leading to the result

$$i[H, D] = \langle (1/M^*) \sum (2p_z^2 - p_x^2 - p_y^2) \rangle + B \int [2(d\rho/dz)^2 - (d\rho/dx)^2 - (d\rho/dy)^2]\, dV \qquad \ldots\ldots(49)$$

where B is proportional to t_1 (see reference quoted for the precise definition).

The second term in this result is just the hydrodynamical estimate of the potential energy of distortion, and is a relatively small surface effect. The contribution of the first term may be divided into two parts, one arising from the asymmetry of the configuration and the other, a volume effect, arising from the uniform distribution of the system. Since the latter is much larger, for heavy nuclei, than the surface effect, the vanishing of the whole must be due to a balance between the asymmetry of the configuration and the volume distortion effect, modified slightly by the effects of the last term. If that is neglected, the use of distorted wave functions gives the condition

$$\langle (1/M^*) \sum (2p_z^2 - p_x^2 - p_y^2) \rangle = (8\eta/3) Y \qquad \ldots\ldots(50)$$

on the configuration of the equilibrium state.

Now for oscillator wave functions, in a configuration of minimum energy

$$(1/M) \langle \sum (2p_z^2 - p_x^2 - p_y^2) \rangle = \omega \langle \mathbf{J}^2 \rangle. \qquad \ldots\ldots(51)$$

(Both are proportional to $\sum (2n - m - l)$, see § 5.) Also both these quantities depend only upon the particles in the last partly filled shell, and mainly upon those of higher angular momentum. It is plausible to suppose that the corresponding states in a more realistic well might yield a similar relation

$$\langle (1/M^*) \sum (2p_z^2 - p_x^2 - p_y^2) \rangle = \omega^* \langle \mathbf{J}^2 \rangle \qquad \ldots\ldots(52)$$

for some suitable effective oscillator frequency ω^*. Then from equations (46), (50) and (52), to order ϵ,

$$\langle \mathbf{J}^2 \rangle = (8\epsilon/3)(XY/\omega^*)/(X + Y). \qquad \ldots\ldots(53)$$

The moment of inertia is obtained by substituting this result and (38) into the formula (26), giving

$$\mathscr{I} = \frac{2}{3} \frac{Y}{\omega^{*2}} \frac{4XY}{(X + Y)^2}. \qquad \ldots\ldots(54)$$

Since X and Y are nearly equal the last factor is very close to unity, and will be dropped. Y is the total kinetic energy evaluated with the reduced mass,

$$Y = A \frac{3}{5} \frac{k_F^2}{2M_1} \qquad \ldots\ldots(55)$$

where k_F is the maximum momentum of nucleons and M_1 is a mass close to the value of M^* inside the nucleus. ω^* can be estimated by comparison of the kinetic energies for the topmost nucleons

$$\omega^* k_F R \sim \langle (1/M^*) \mathbf{p}^2 \rangle = k_F^2 / M_2 \qquad \ldots\ldots(56)$$

where M_2 is another 'effective mass' appropriate to a particle at the top of the momentum distribution. Finally then the ratio of the moment of inertia to the rigid one is

$$\mathscr{I} / \mathscr{I}_{\mathrm{rig}} = \tfrac{1}{2}(M_2^2 / M M_1) \qquad \ldots\ldots(57)$$

for small deformations. M_2 will certainly lie between M and M_1 so that the factor (M_2^2/MM_1) will be between $\frac{1}{2}$ and 2, if M_1 is about $\frac{1}{2}M$; a closer estimate does not appear possible without a detailed model of the velocity dependence and of surface shape.

§ 8. Discussion

The first formula (11) derived in § 2 should really be regarded as an identity satisfied by the true state, but since it is in fact stationary for small variations from that state it can be used as an estimator of $\mathscr{I}$ on the basis of an approximate wave function. This latter was then assumed to be the determinantal wave function satisfying (12), and the original formula could then be simplified to (17). Up to this point no assumption is made about the nature of the nuclear interactions, except that they are such as to make the determinantal wave function a reasonable approximation.

In § 4 a much simpler formula (26) was obtained, involving only the mean self-consistent potential, by making some approximations which involved in an essential way the short-range nature of the interactions. This agrees with the prediction of the cranking model only when the excitation energies involved are all equal; applied to the particular case of the deformed oscillator well this is precisely the case in which the irrotational formula is reproduced, a point of only academic interest since there is then no equilibrium deformation. In general, application to this model, with the self-consistent equilibrium deformation, gives a moment of inertia equal to one-half of the rigid value, for small deformations, whereas the cranking model gives the rigid value in these circumstances.

This result does not necessarily imply any contradiction between the two methods of calculating the moment of inertia, for, as has been emphasized by Bohr and Mottelson (1955), residual interactions between nucleons modify considerably the result obtained with the cranking model. On the other hand the original formula (11), being associated with a variational principle, should be insensitive to errors in the wave function so that, in so far as the reduction to (26) is justified, the latter should incorporate most of these residual effects.

The question then arises whether this factor of one-half is a realistic explanation of the tendency of the observed moments to cluster around this value (Blin-Stoyle 1956, Moszkowski 1956). The present analysis shows that there are various effects operating both to raise and to lower this value. In the first place the oscillator model gives, for deformations with $\epsilon = 0{\cdot}3$–$0{\cdot}4$, a rather larger ratio of about 0·65 (§ 5). The effects of the shape of the potential well and of its velocity dependence cannot easily be estimated, but the calculations made in the last two sections indicate that there may be some reduction arising from the velocity dependence, as suggested by Blin-Stoyle; since, however, the rotational phenomena are determined mainly by surface interactions, the effective mass relevant here should be greater than the mean value for all the nucleons. There is a third effect tending to reduce the influence of the velocity dependence: this arises from the fact that the finite range of the nucleon interaction, of which one manifestation is the effective mass, also introduces a correction to the simplified formula (26) tending to increase the moment of inertia (see Appendix A).

Acknowledgment

The author is indebted to Professor R. E. Peierls for several discussions about the work of Yoccoz and Peierls, which has close contact with the analysis in this paper through equation (6), and which provided the stimulus for the present investigation.

APPENDIX A

The main contribution to $\langle J_x^2 \rangle$ comes from transitions within the same shell, i.e. for the oscillator model the first term of (32), which arises by summing $(m+1)n$ over those occupied states from which a transition can be made. The most important effect of the exchange term in (18) is to remove those terms in the sum with $m=n$, introducing therefore a correction of the relative order

$$(\textstyle\sum' (m+1)^2 n^2)/[\sum' (m+1)n]^2. \qquad \ldots\ldots(\mathrm{A}\,1)$$

This must, however, be reduced by a factor $\frac{1}{4}$ because exchange can take place only between particles with the same spin and charge, and by a further factor $\frac{1}{2}$ because the exchange term in (22) is of smaller order, and it is the average of (18) and (22) which occurs in the formula (26). The resultant correction is unlikely to exceed 5% in the heavy nuclei where several states contribute to the sums in (A 1).

The errors arising from the finite range of the potential may be investigated with the help of the potential (48). It will be assumed that the condition (*a*) of § 4 is satisfied so that (24) holds. Then a direct evaluation of the expectation value $2\langle VQJ_x^2 \rangle$ can be made for comparison with the formula (38). The t_0 term gives immediately

$$2t_0 \int (\textstyle\sum' \phi_n l_x \phi_n)^2 \, dV \qquad \ldots\ldots(\mathrm{A}\,2)$$

where $\sum'$ denotes summation over those states from which a transition can be made, or

$$\begin{aligned}\textstyle\sum' \phi_n l_x \phi_n &= \textstyle\sum \phi_n l_x \phi_n - \sum \sum \phi_n \phi_m \int \phi_m l_x \phi_n \, dV \\ &= \tfrac{1}{2} l_x \textstyle\sum \phi_n{}^2 = \tfrac{1}{2} l_x \rho\end{aligned}$$

since the last term vanishes by the condition (24). This leads to a verification of the formula (38) with $U_0 = t_0 \rho$, as was to be expected.

The t_1 term can be analysed in a similar way, but this time the condition (24) is not sufficient to express the result only in terms of the mean potential. When the expressions derived have been simplified as far as possible the result takes the form

$$2\langle VQJ_x^2 \rangle = \tfrac{1}{2}[l_x, U][l_x, \rho] + t_1[\textstyle\sum' (\phi_n l_x \phi_n - \phi_n l_x \phi_n)]^2 \quad \ldots\ldots(\mathrm{A}\,3)$$

of which the first term is positive, leading to (38), and the second residual term is negative (for j_x is an imaginary operator). This second term represents the change in strength of the interaction due to the change of momentum produced by the operator j_x. This momentum change will, for a large system, be of the order of spacing between states in momentum and so small compared with the momenta at the top of the Fermi distribution.

APPENDIX B

Suppose that the potential energy of the system can be written in the form

$$\langle V \rangle = \int W(\rho, \tau) \, dV \qquad \ldots\ldots(\mathrm{B}\,1)$$

then the resultant single-particle potential is of the form (35) with

$$U_0 = \partial W/\partial \rho, \qquad U_1 = \partial W/\partial \tau. \qquad \ldots\ldots(\mathrm{B}\,2)$$

The integrand of (38) can be transformed as follows:

$$-\frac{d\rho}{dr}\frac{dU_0}{dr}-\frac{d\tau}{dr}\frac{dU_1}{dr}=-\frac{d\rho}{dr}\left\{\frac{d}{dr}\left[\frac{\partial W}{\partial\rho}+\frac{d\tau}{d\rho}\frac{\partial W}{\partial\tau}\right]\right\}+\frac{d\rho}{dr}\frac{\partial W}{\partial\tau}\frac{d}{dr}\frac{d\tau}{d\rho}$$

$$=\frac{d\rho}{dr}\left(\frac{1}{2M}+\frac{\partial W}{\partial\tau}\right)\frac{d}{dr}\frac{d\tau}{d\rho} \qquad \ldots\ldots(\mathrm{B}\,3)$$

with the help of the Thomas–Fermi relation

$$(1/2M)(d\tau/d\rho)+\partial W/\partial\rho+(\partial W/\partial\tau)(d\tau/d\rho)=\text{const.}$$

The result (B 3) with $\tau\alpha\rho^{5/3}$ leads immediately to (40). The numerical result (41) was obtained using the density distribution

$$\rho/\rho_0=[1+\exp\{(r-R)/0{\cdot}5\}]^{-1} \qquad \ldots\ldots(\mathrm{B}\,4)$$

and an effective mass $1/2M^*=(1/2M)(1+\rho/\rho_0)$. Closely similar results were obtained by the use of the figures adopted by Skyrme (1956) and by a direct estimate of (38) in terms of density and potential gradients.

REFERENCES

BLIN-STOYLE, R. J., 1956, *Nuclear Phys.*, **2,** 169.

BOHR, A., and MOTTELSON, B. R., 1953, *K. Danske Vidensk. Selsk., Mat.-fys. Medd.*, **27,** no. 16; 1955, *Ibid.* **30,** no. 1.

INGLIS, D., 1954, *Phys. Rev.* **96,** 1059 ; 1955, *Ibid.*, **97,** 701; 1956, *Ibid*, **103,** 1786.

MOSZKOWSKI, S. A., 1955, *Phys. Rev.*, **99,** 803; 1956, *Ibid.*, **103,** 1328.

NILSSON, S. G., 1955, *K. Danske Vidensk. Selsk., Mat.-fys. Medd.*, **29,** no. 16.

RAINWATER, J., 1950, *Phys. Rev.*, **79,** 432.

SKYRME, T. H. R., 1956, *Phil. Mag.*, **1,** 1043; 1957, *Proc. Roy. Soc.* A, **239,** 399.

YOCCOZ, J., 1956, *J. Phys. Radium*, **7,** 517.

Gamma Radiation following Proton Capture in ^{35}Cl, ^{37}Cl and ^{39}K
II: Angular Distributions and Correlations

By R. BERENBAUM‡ and J. H. MATTHEWS†
Physics Department, Imperial College of Science and Technology, London S.W.7

MS received 30th January 1957

Abstract. Angular distribution measurements and one angular correlation measurement have been made on a number of the γ-rays observed in the reactions ^{35}Cl(p, γ)^{36}A, ^{37}Cl(p, γ)^{38}A and ^{39}K(p, γ)^{40}Ca described in an earlier paper. From the results of these measurements the following probable assignments can be made to the levels in ^{36}A, ^{38}A and ^{40}Ca: in ^{39}K + p 1120, 1300 and 1566 kev resonances, $1^{\pm}(2^{-})$; in ^{37}Cl + p 1533 kev resonance, $2^{(-)}$; in ^{35}Cl + p 1510 kev resonance, $1^{\pm}(2^{-})$; and 850 kev resonance, $3^{(+)}$. For the bound states observed in ^{36}A: 1·95 Mev, $2^{(+)}$; 4·1 Mev, $3^{(-)}$.

§ 1. Introduction

In a previous paper (Towle, Berenbaum and Matthews (1957), subsequently referred to as I) the results were reported of measurements of γ-radiation, following proton capture in ^{35}Cl, ^{37}Cl and ^{39}K. The present paper describes measurements of the angular distributions of some of the γ-rays observed, together with one angular correlation measurement (between two γ-rays in the cascade from the 855 kev resonance in ^{35}Cl).

§ 2. Experimental

The target holder used in I was replaced by a brass cylinder of wall thickness 1/32 inch. The target materials, of similar nature and thickness to those used in I, were evaporated on to molybdenum foil approximately 0·004 in. thick and this foil was held in the target chamber in such a way that the foil was oriented along one of two possible diameters of the chamber. The use of two orientations enabled corrections to be made where necessary for any γ-ray absorption in the brass support around the edge of the foil.

The two NaI scintillation spectrometers used were those described in I; one of these was movable, in a plane containing the incident beam, about an axis through the centre of the target. The distance from the target position to the centre of this crystal was 7 cm. In the angular distribution measurements the number of counts in this spectrometer was compared with the number of counts in a second spectrometer which was fixed with the centre of the crystal at a distance from the target of 6 cm. During these measurements the two crystals did not approach each other more closely than 11 cm (centre to centre).

The incident beam of monoenergetic protons from the Imperial College Van de Graaff generator was collimated so as to impinge on the target at the axis of rotation of the NaI spectrometer by means of two tantalum slits. One slit, of width 1 mm, was about 20 cm from the target; the other, of width about 2 mm, was about 50 cm from the target.

---

† Now at The Physical Laboratories, The University, Manchester.

‡ Now at the National Coal Board, Mining Research Establishment, Isleworth, Middlesex.

The apparatus was tested for anisotropy by examining the angular distribution of the 6·13 Mev γ-radiation resulting from the bombardment of ^{19}F by protons at the 340 kev resonance. This radiation is known to be isotropic (Devons and Hine 1949). A small ($\sim$2%) regular deviation was found and corrected for in the subsequent measurements.

The output from the spectrometers could be fed through amplifiers either to a fifty-channel pulse analyser or through single-channel pulse analysers to scalers. In the cases of the angular distributions of the γ-rays from the resonances examined in ^{39}K and ^{37}Cl, and the 1·510 Mev resonance in ^{35}Cl the single-channel analysers were set to pass only pulses of the appropriate energy from both spectrometers. These were calibrated with the multi-channel analyser and gate (Folkierski 1956).

In the measurements of the angular distribution of the γ-radiation from the 0·855 Mev resonance in ^{35}Cl the output of the rotating spectrometer was fed into the multi-channel analyser and the spectrum recorded at each angle examined. In the angular correlation measurement at this resonance, the monitoring spectrometer was placed at 90° to the beam direction at a distance of 7 cm, and its output passed through a single-channel analyser set to pass only pulses corresponding to the higher in energy of the two γ-rays concerned. The output of this analyser was then used to gate the pulses from the rotating counter. The gated output of this counter was then fed into the multi-channel analyser.

In all cases, numbers of measurements were taken in random order at each of the various angles. The final distribution was the sum of these runs. This reduced any errors due to drifts in the amplifying and counting systems. Also spectra of the γ-ray being observed were taken at regular intervals in both channels to confirm the absence of long-term drifts.

The angular distribution of one of the γ-rays found at the 0·855 Mev resonance in ^{35}Cl (7·2 Mev) and the angular correlation at this resonance were obtained from measurements at four angles between 0° and 90° to the proton beam. In all other distributions, measurements were made at ten angles between 335° and 120° to the proton beam.

§ 3. Results

In all measurements, except those on the 855 kev resonance in ^{35}Cl + p, the angular distributions were directly calculated from the numbers of pulses recorded in the two spectrometer channels. A least squares method was employed to fit the observed data to a distribution of the form

$$1 + \sum_{n=1}^{4} a_n P_n(\theta).$$

In the measurments on the 0·855 Mev resonance in ^{35}Cl + p the spectrum obtained at each angle was analysed as described in I; the errors quoted in the results in these cases derive mainly from the uncertainties inherent in this method, which lead to a greater scatter of the experimental points than that due to the statistical uncertainties alone. These results were then similarly fitted by a least squares method.

The angular correlation experimental points (figure 1) were obtained by analysis of the number of counts falling in the various regions of the spectrum, since the total number of counts obtained in this case was too low to apply the usual method of analysis.

In all measurements, the corrections specified above were made, but no correction for the finite acceptance angle of the counter was necessary within the accuracy of the experiments.

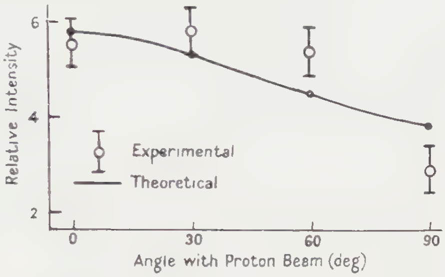

Figure 1. Angular correlation of γ_3 with γ_1 from 855 kev resonance in $^{35}Cl+p$. γ_1 is observed at 90° with the proton beam.

The resulting distributions are shown in the table. The large error in the measurement of the 7·2 Mev γ-ray in ^{36}A results from uncertainty in subtracting the effect of the 'tail' of the 5·1 Mev radiation.

In all cases, the 'best fit' value of the coefficient of P_4 was less than or equal to the error quoted in the coefficient of P_2.

§ 4. Interpretation of Results

In this, and subsequent discussions, incoming protons of orbital angular momentum up to and including three units are considered. The subsequent analyses were carried out using the tables of Sharp *et al.* (1954).

(i) $^{39}K(p,\gamma)^{40}Ca$

(*a*) 1·120 Mev *and* 1·300 Mev *resonances.*

As these two resonances yield the same angular distribution, within the experimental error, they will be considered together. The observed modes of γ-decay of these resonances, principally to the ground state (0^+) of ^{40}Ca (see I), make it likely that they have spin 1 or 2. As the ground state of ^{39}K has spin 3/2, a spin 2 level can result from proton l-values equal to 1, 2 or 3, and channel spin equal to 1, or l-values equal to 0, 1, 2 or 3, and channel spin equal to 2. Mixed multipole radiation cannot occur.

Formation of a level of spin 2 by s-wave protons would of course yield an isotropic distribution of γ-rays, while d-wave protons would introduce a P_4 component into the angular distribution. It is not possible for cancellation of the P_4 components between different channel spin contributions to take place to an extent sufficient to explain the observed absence of a P_4 component ; such a cancellation would require a channel spin mixture which would also lead to cancellation of the P_2 component. This applies also, if interference between s- and d-wave protons is taken into account. If the resonances have the assignment 2^-, then a contribution from f-waves again introduces a higher component than P_2. However, for pure p-wave formation, it is possible to obtain the observed distribution if the levels are formed with a ratio of channel spin contributions given by

$$\frac{\text{formation in channel spin}=1}{\text{formation in channel spin}=2}=\frac{S(1)}{S(2)}\geqslant 15$$

whereas *jj* coupling predicts approximately equal amounts of each channel spin whether the total angular momentum of the incoming proton is taken to be $\frac{1}{2}$ or $\frac{3}{2}$.

If the resonances have the assignment 1^+ or 1^- then formation by s- and d-waves (in the case of even parity) or by p- and f-waves (in the case of odd parity) in almost any ratios (except, of course, pure s-wave formation) can give a distribution as observed if suitable channel spin mixtures are assumed. It is concluded that these resonances have spin 1 although the assignment 2^- is not completely ruled out.

(*b*) 1·566 Mev *resonance.*

The assignment 2^+ can again probably be ruled out (as in (*a*)) but again, for pure p-wave formation, 2^- remains a possibility. There is again no reason to discard either of the possibilities $1^\pm$.

It may be noted that the resonances at 1·120 Mev and 1·300 Mev are those in which the γ-transition to the first excited state of ^{40}Ca appears inhibited, while this is not the case in the 1·566 Mev resonance.

(ii) $^{37}\mathrm{Cl}(\mathrm{p},\gamma)^{38}\mathrm{A}$

1·533 Mev *resonance.*

This exhibits γ-decay almost entirely to the first excited state of ^{38}A (of spin 2^+) (cf. I), rather than to the ground state (0^+), or to the second excited state (3^-). Only the possibilities 2, 3 are considered for the spin of the resonance level. Spin 3 can be ruled out as it is found on calculation that this cannot lead to a distribution of the form $1+aP_2$, where a is positive, for pure multipole radiation. If spin 3^+ is assumed in order to obtain multipole mixing, then it is difficult to explain the almost complete inhibition of the transition to the second excited state.

For the assignment 2^+, reasonable agreement with the observed distribution can be obtained only for pure d-wave formation entirely in channel spin 1. Spin 2^- can yield the measured distribution as a result of p-wave formation with the channel spin ratio $S(1)/S(2)=9$.

If the effect of a small f-wave admixture is considered, then this channel spin ratio can be reduced.

Again the assignment 2^- is expected to be more likely than 2^+, if the relative transition probabilities to the first and second excited states are considered.

(iii) $^{35}\mathrm{Cl}(\mathrm{p},\ \gamma)^{36}\mathrm{A}$

(*a*) 1·510 Mev *resonance.*

Arguments similar to those used in considering the resonances in ^{39}K apply here. Again we obtain the assignments $1^\pm$ (2^-).

(*b*) 0·855 Mev *resonance and the levels of* ^{36}A.

The notation $\gamma_1 \ldots \gamma_4$, shown in figure 2, is here adopted for convenience. This figure shows the decay-scheme proposed in I for this resonance.

In this case, where a number of angular distributions was obtained, it is possible to be much more definite when 'ruling-out' possible sets of values for the spins of the levels.

The following possibilities were considered: the spin of the 1·95 Mev level may be 1, 2 or 3; the spin of the 4·1 Mev level may be 1, 2, 3, 4 or 5; and the resonance level may have spin 2, 3, 4 or 5. In calculating theoretical distributions, those of γ_3 and γ_4 were determined neglecting the contributions to their intensities which come from cascades other than the cascade $\gamma_1\,\gamma_3\,\gamma_4$. In the case of γ_3 this contribution is only of the order of 10%, and can safely be neglected, but in the case of

γ_4 it is thought that as much as 25% may come from other cascades. However, it remains unlikely that there is sufficient contribution to affect the sign of the coefficient of P_2 in this distribution.

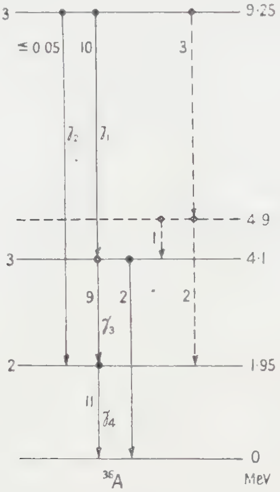

Figure 2. Decay of 855 kev resonance in $^{35}Cl+p$ (cf. figure 1), together with proposed level spins in ^{36}A.

The great majority of the possible level spin schemes, resulting from the above possibilities, can be ruled out on the basis of the signs alone of one or more of the coefficients of P_2 in the various distributions. In particular, if the 1·95 Mev level is assumed to have spin 2, then most of the possible level spin schemes resulting would lead to angular distributions, at least two of which disagree with those observed in the sign of the coefficient of P_2. In some cases, including those in which mixed multipole radiation could occur (only mixtures of E2 and M1 radiation were considered) it was necessary to consider the specific mixtures of channel spins, *l*-values and/or multipolarities which could give rise to the observed distributions. Thus, for any particular level scheme under examination, the limiting values of these mixing parameters necessary to obtain each of the four observed distributions were calculated. Then, if the various angular distributions could not all be fitted, using consistent mixing parameters, the level scheme could be ruled out.

It may be noted that in almost all cases, and in particular in those which might be expected (by comparison with other even–even nuclei) to be the most likely, at least two criteria could be used to rule out a given level scheme. That is, in addition to one or more calculated angular distributions which disagree with those observed, weaker intensity rules were sometimes considered (as, for example, the unlikelihood of an M1 transition being much more favoured than an E1 transition of similar, or larger, energy). It should be emphasized that in no case were such intensity rules considered alone, nor was any scheme ruled out solely because it would not give the observed distribution of γ_4.

The result of these calculations was that only two possible sets of level spin assignments remain; these are (i) the level spin assignments shown in figure 2, and (ii) the assignments 3, 2, 2 (in order of increasing excitation). The assignments (ii) disagree with observation if parities consistent with the observed transition probabilities are assigned (see below) and would not be in accordance with experimental data on other even–even nuclei (see § 4).

With regard to the assignments (i), if the parity of the 1·95 Mev level is taken to be even, then, from the relative intensities of γ_1 and γ_2, it appears that γ_1 may be E1 and γ_2 M1 in nature. With these multipolarity assignments it is seen that the resonance level is also required to have even parity. The resonance can then only be formed by d-wave protons, and we find that the observed distribution for γ_1 can be obtained from a channel spin mixing ratio $S(1)/S(2)=\frac{2}{3}$. (It may be noted that on a *jj* coupling scheme the values predicted for this ratio are $S(1)/S(2)=\frac{3}{5}$ or $\frac{2}{5}$). If this value is taken, then the theoretical values obtained for the other angular distributions are those shown in the table (γ_2 considered pure M1). The theoretical angular correlation of γ_3 with γ_1 is plotted in figure 1. It is seen that these theoretical estimates are in good agreement with the experimental values.

Reaction	Resonance energy (Mev)	γ-ray energy (Mev)	Angular distribution observed	Angular distribution calculated
$^{39}K(p, \gamma)^{40}Ca$	1·120	9·5	$1+(0{\cdot}44\pm0{\cdot}03)P_2$	
	1·300	9·65	$1+(0{\cdot}43\pm0{\cdot}03)P_2$	
	1·566	9·9	$1-(0{\cdot}07\pm0{\cdot}03)P_2$	
$^{37}Cl(p, \gamma)^{38}A$	1·533	9·5	$1+(0{\cdot}27\pm0{\cdot}03)P_2$	
$^{35}Cl(p, \gamma)^{36}A$	1·510	9·9	$1+(0{\cdot}15\pm0{\cdot}02)P_2$	
	0·855	5·1	$1+(0{\cdot}21\pm0{\cdot}03)P_2$	$1+0{\cdot}21P_2$
	0·855	7·2	$1-(0{\cdot}12\pm0{\cdot}06)P_2$	$1-0{\cdot}16P_2$
	0·855	2·15	$1-(0{\cdot}17\pm0{\cdot}04)P_2$	$1-0{\cdot}17P_2$
	0·855	1·95	$1+(0{\cdot}13\pm0{\cdot}04)P_2$	$1+0{\cdot}12P_2$

The parities deduced here cannot be regarded as certain, as agreement with the observed angular distributions and angular correlation can be obtained with any choices of parity for the three levels. It is concluded, nevertheless, that the most probable assignments for the levels at 1·95 Mev, 4·1 Mev and 9·25 Mev in ^{36}A are respectively $2^{(+)}$, $3^{(-)}$ and $3^{(+)}$.

The excited state of ^{36}A suggested at 4·9 Mev (cf. I), could well have, consistent with this scheme, spin 2 or 4 and even parity, with the latter assignment rather more probable in the absence of any observed radiation consistent with the decay of this level directly to the ground state.

§ 5. DISCUSSION

(i) ^{36}A. It is of some interest to compare the level scheme of ^{38}A which has a level of spin 2^+ at 2·16 Mev and a level of spin (probably) 3^- at 3·75 Mev (Endt and Kluyver 1954), with that suggested here for ^{36}A. In ^{38}A the ground state configuration is expected to be $(d_{3/2})^{-2}$. Such a configuration can result in only two levels, of spins 0 and 2 (Mayer and Jensen 1955). Thus, it is natural to expect that the second excited state will be one resulting from excitation of a $d_{3/2}$ nucleon to the $f_{7/2}$ shell and hence leading to a state of odd parity.

As was pointed out in I, consideration of the regularities observed in the excited states of even–even nuclei (Scharff-Goldhaber 1953) suggests that the 1·95 Mev level in ^{36}A is the first excited state and has also spin 2^+. Again the next excited state above this, having even parity and spin 2 or 4, would be expected to have an excitation energy between about 4 and 6 Mev (Scharff-Goldhaber and Weneser 1955). However, a survey by Morinaga (1956) indicates that excited states having odd spin and parity occur in even–even nuclei (especially near, but not at, closed shells) at excitation energies obeying the empirical rule $E_{\text{excitation}} = 67\,A^{-3/4}$ Mev, where A is the number of nucleons in the nucleus. This expression is just the expression for the energy difference of the odd–odd and even–even nuclear mass curves (e.g. Ramsey 1953). It is suggested by Morinaga that this indicates that the states of odd parity arise from excitation of one nucleon into the next nuclear shell and that the resulting weak interaction between the two nucleons of the separated pair is analogous to the weak interaction between the unpaired nucleons in an odd–odd nucleus.

This empirical rule would suggest a level of odd spin and parity at about 4·3 Mev in ^{36}A. Thus, even though in ^{36}A the configuration $(d_{3/2})^{-4}$ would be expected to give rise to more than one excited state of even spin and parity, the level scheme proposed is quite consistent with experimental data from other even–even nuclei.

Acknowledgments

We would like to thank Professor S. Devons for suggesting this work and for his continued interest. We are indebted to the Department of Scientific and Industrial Research (R.B.) and to the Beaverbrook Overseas Scholarship Fund (J.H.M.) for maintenance awards held during the course of this work. We are also indebted to Mr. J. H. Towle for a number of helpful discussions.

References

Devons, S., and Hine, M. G. N., 1949, *Proc. Roy. Soc.* A, **199**, 56, 73.
Endt, P. M., and Kluyver, J. C., 1954, *Rev. Mod. Phys.*, **28**, 95.
Folkierski, A., 1956, *J. Sci. Instrum.*, **33**, 187.
Mayer, M. G., and Jensen, J. H. D., 1955, *Elementary Theory of Nuclear Shell Structure*, (London : Chapman Hall).
Morinaga, H., 1956, *Phys. Rev.*, **103**, 503.
Ramsey, N. F., 1953, *Experimental Nuclear Physics I*, (Ed. Segrè) (New York : Wiley).
Scharff-Goldhaber, G., 1953, *Phys. Rev.*, **90**, 587.
Scharff-Goldhaber, G., and Weneser, J., 1955, *Phys. Rev.*, **98**, 212.
Sharp, W. T., Kennedy, J. M., Sears, B. J., Hoyle, M. G., 1954, Tables of Coefficients for Angular Distribution Analysis.—A.E.C.L. Canada. CRT-556.
Towle, J. H., Berenbaum, R., and Matthews, J. H., 1957, *Proc. Phys. Soc.* A, **70**, 84.

On the Structure of Extensive Cosmic Ray Air Showers: Core Detection and Core Structure

By E. W. KELLERMANN, T. SHAW† and N. DICKINSON‡
Department of Physics, University of Leeds

MS. received 18*th January* 1957

Abstract. A 'core-detecting' apparatus is described for which the efficiency of core detection is uniform for central electron densities from about 20 to 200 m^{-2}. Accuracy of location of shower axes has been studied by means of decoherence curves between two identical units; more than 50% of responses are shown to arise from showers for which the axis falls within 3 m of the centre of the detector.

The performance of the core detector is shown to be consistent with the conclusion that the proportion of energetic electrons in the centre of showers changes little over the range of shower size examined, and in particular that the smaller showers do not show the characteristics of 'old' cascades.

The observations provide no evidence of any core structure of size comparable with the measured accuracy of location.

§ 1. Introduction

Two different methods have been adopted to give the detailed information required for the determination of specific features of shower structure. The first employs numerous recording instruments covering a large area and thus is capable of mapping showers in the plane of observation. The other uses, in general, a smaller array of detectors, but relies on some device which is sensitive to the position of the shower core, taking this as an axis of reference relative to which the shower structure is determined, either for individual showers or for the average of many showers. The value of the second method depends essentially on the precision with which the positions of shower cores are located.

The purpose of this paper is to describe a core detector which has been used since 1952, and to draw conclusions about its efficiency of operation, and about the core structure of showers. The determination of the efficiency of the detectors is a necessary preliminary to the examination of other shower properties; these, in particular the lateral distribution of electrons as well as the nature and distribution of the penetrating particles, will be discussed in another paper.

§ 2. Basis of Core Selection

We understand by a core detector a device sensitive to specific conditions obtaining in the region close to the axis of extensive showers. Provided that cascade development is not too far advanced, the electron cascade can be assumed to possess an axial region, in the direction of motion of the 'primary' electron (or photon), containing electrons (and photons) of relatively higher energies than those in the outer parts of the shower. In the plane of observation, the core region will also show a relatively large electron (and photon) density with electron energies at least as high as the critical energy. This definition of the core region applies even if the core is not unique, but possesses a structure.

---

† Now at British Nylon Spinners, Doncaster.

‡ Now at Atomic Energy Development Group, Ferranti Ltd., Manchester.

It must be emphasized that although relatively high densities characterize the core of the single shower, apparatus sensitive only to high shower densities is not a useful core detector. Large showers possess an extended high density region, and 'cores' selected in this way would accordingly be recorded at considerable distances from the true shower axis even if a particularly high density is required (Singer 1951). Only if the number of large showers was small enough to make their contribution to the recorded average negligible could a core detector based on density selection be successful. This is not the case, and the failure of this approach to core detection has, in fact, served as an indication of the contribution of large showers to the size spectrum of extensive showers. Moreover, there are great numbers of low density showers which contain definite cores of energetic electrons, and these would certainly be missed by high density selection.

That core detection based on the determination of density gradients within showers can be successful has been shown by Kasnitz and Sitte (1954), but the accuracy of this method is not good.

Our apparatus is designed on the assumption that the presence of energetic electrons is the characteristic quality of the core region, which, if detected, is most likely to be reliable in determining the core position, This principle of energy selection has been applied to special cases of single showers by Hazen *et al.* (1954), and to shower averages by Cocconi, Tongiorgi, and Greisen (1949), and by Haddara and Jakeman (1953). The selector of Cocconi *et al.* responded, however, not only to electrons but also to penetrating particles giving rise to nuclear reactions, and its efficiency was for this reason greatly reduced for showers of higher density. The method used by Haddara and Jakeman was not open to this objection but as described had too small a sensitive surface to yield statistically useful results.

Our detector identifies the more energetic electrons by the products of their multiplication under lead, an associated array of unshielded counters serving as a rough indicator of shower density.

§ 3. The Core Detector

3.1. *Construction*

The apparatus was operated 100 metres above sea level. Three unshielded counter trays, 'selecting trays', formed the vertices of an equilateral triangle of side about 5 m, each tray containing two counters of 140 cm^2 effective area and one of 35 cm^2 (figure 1). An extensive shower was recorded if at least one of the larger counters in each tray was discharged. Such an event was classified as (3, 3), i.e. three of the larger counters discharged, three undischarged. Similarly, other events were classified (4, 2), (5, 1), (6, 0). Figure 2 gives the calculated density response corresponding to these events. A further sub-division of the (6, 0) density class is possible if the small counters are taken into consideration. Then (6, 0; 1, 2) denotes a discharge of six large and one small counter, complete saturation being denoted by (6, 0; 3, 0).

A lead block, containing in cavities (figure 3) three counter trays under 5, 12·5, and 20 cm of lead respectively, was placed at the centre of the triangle formed by the selecting trays, the middle tray not being used for the present experiment. The thickness of lead at the bottom was 7·5 cm and the sides were shielded by 15 cm. The top tray contained nine counters each of area 140 cm^2 spaced 1 cm apart, the bottom tray containing ten counters each of area 240 cm^2. All counters used in the experiment were hodoscoped, transmitting their pulses through pre-amplifiers to central equipment containing the remaining electronic

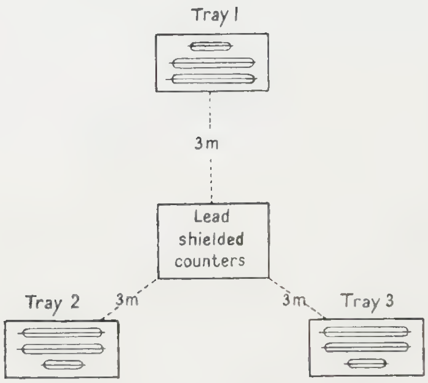

Figure 1. General arrangement of core-selecting apparatus.

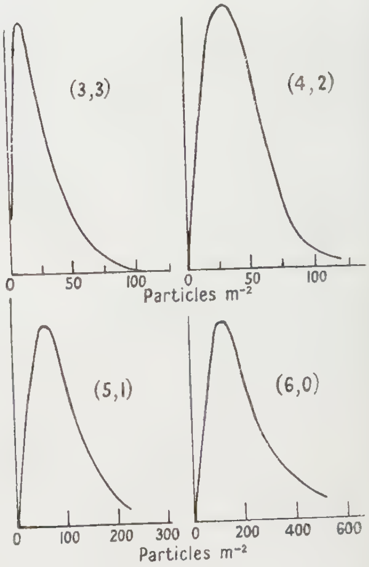

Figure 2. Relative contribution of showers of different density to the response of the unshielded counter array for the four selecting groups employed.

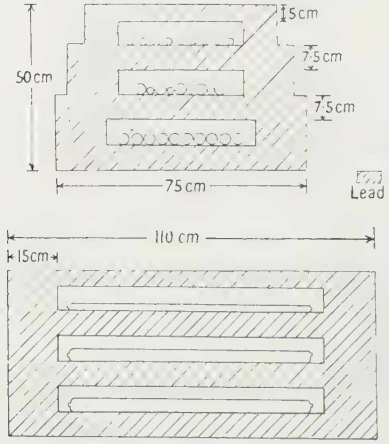

Figure 3. The central (shielded) unit of the core detector.

units and provision for automatic recording. The test routine included a check of the apparatus as a whole in addition to that of the individual counters.

As will be seen below, the selecting trays as well as the shielded counter trays in the lead block were integral parts of the device (the 'core detector').

3.2. *Performance*

For the purpose of core detection the most important part of the lead block at the centre of the triangle of selecting counters was the top tray, containing counters under 5 cm of lead. A 5×10^9 ev electron is expected to give rise to a shower of about nine electrons under this thickness at which shower development will be near maximum. The basis of core selection adopted here is the evidence that a certain degree of cascade multiplication has taken place in the 5 cm lead layer: i.e. a higher particle density is sought under this lead than is to be found immediately outside. This consideration of change of density at the detecting device differs from the approach of Cocconi and his co-workers, and leads to improved core detection efficiency at high density.

Accordingly, a certain minimum number n_i of the counters in the top shielded tray must be discharged if the recorded event is to be classified as a 'core', the number, n_i, being adjusted to values appropriate to the various classes of density response of the selecting counters.

In order to exclude effects of the nucleonic component which might simulate the required electron shower in the top shielded tray, all events were excluded in which more than one counter in the bottom tray, under a total thickness of 20 cm of lead, was discharged. While this selection does not exclude the effect of single μ-mesons, it discriminates effectively against nuclear effects large enough to contribute significantly to the operation of the top shielded tray upon which core selection largely depends. A shortcoming of this procedure which must be borne in mind is that if the part of the core region falling on the lead contains a concentration of energetic nucleons as well as energetic electrons, some genuine core events will be excluded, and it is not clear at this stage whether any bias in this exclusion will be of importance.

§ 4. THE CRITERION FOR CORE SELECTION

The number n_i which indicates adequate multiplication in 5 cm of lead of electrons belonging to the broad density classes selected by the unshielded selecting counters must be determined empirically, although a useful estimate may be made by an analysis of the normal type of the relative counter discharges below lead and in the selecting trays, allowing for the absorption of the lower energy electrons. The determination of n_i is simplified if two detection units are available and de-coherence effects between them studied, for in general, the effectiveness of a core selecting device, or of a criterion of selection in the use of any particular device as a core selector, is measured by the steepness of the de-coherence curve. The operation of two identical units with two different choices for n_i is illustrated in figure 4. With such information, the choice of n_i is a compromise between a slow rate of operation (large n_i) and a less steep de-coherence curve (small n_i). The value $n_i = 6$ has been adopted for the density class (3, 3). Not only does this value afford a suitable compromise of the kind just described, but it also requires significant cascade multiplication in the 5 cm lead layer for a substantial proportion of the incident cascade particles. Increased

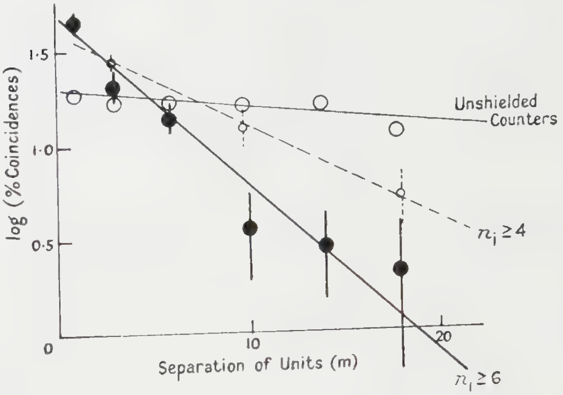

Figure 4. De-coherence curves for detectors with different choice of n_i in the (3, 3) group.

values of n_i have been required for the higher density classes of showers: $n_i = 6, 7, 8, 9$ for the (3, 3), (4, 2), (5, 1) and (6, 0) classes respectively.

Using these criteria, the de-coherence curves for the first three density classes are similar (figures 5, 6), the coincidence rates (black circles) falling by a factor of the order 10 for a change of separation of about 17 metres. The curve for the (6, 0) density class is markedly less steep, but the very large range of densities contributing to this group must be noted, and the probability that for some of these showers the accepted value of n_i does not require cascade multiplication in 5 cm of lead. That this is so is shown when the (6, 0) density class is subdivided into the two sub-groups (6, 0; 0, 3) + (6, 0; 1, 2) and (6, 0; 2, 1) + (6, 0; 3, 0) (figure 6). The first of these, covering a range of shower densities around 200 m^{-2} is found to show a de-coherence curve which agrees with those of the lower density groups; the second, in which almost complete saturation occurs, shows an unsatisfactorily flat de-coherence curve, and must be considered to concern shower densities outside the effective range of the apparatus.

Table 1. De-coherence Effects between Two Identical Core Selectors

The table shows the percentage of responses of a single unit which are in coincidence with a response of the other.

Separation (m) Density class	1	3	6	10	14	18
(3, 3)	44·8 ± 4·0	20·5 ± 3·8	13·7 ± 2·8	3·5 ± 1·7	2·8 ± 1·4	2·1 ± 1·5
(4, 2)	57·2 ± 3·8	22·9 ± 3·6	17·4 ± 2·7	12·1 ± 3·2	5·0 ± 1·5	7·2 ± 2·4
(5, 1)	66·2 ± 3·8	43·3 ± 4·4	31·3 ± 3·6	14·2 ± 3·2	9·7 ± 2·2	3·4 ± 1·9
{(6, 0; 0, 3) (6, 0; 1, 2)}	80·5 ± 6·6	48·9 ± 7·3	35·4 ± 6·9	4·8 ± 4·8	8·2 ± 3·9	4·0 ± 3·9
{(6, 0; 2, 1) (6, 0; 3, 0)}	85·7 ± 5·0	60·4 ± 9·4	52·1 ± 6·0	13·7 ± 6·4	18·4 ± 5·5	15·3 ± 7·1

De-coherence data are summarized in table 1 for separations from 1 to 18 m (for 1 m separation the two lead units were built together to share a common side wall of 20 cm thickness). The open circles in figures 5 and 6 represent the de-coherence data obtained if the events showing multiple discharges in the bottom tray under 20 cm of lead are not excluded. These discharges contribute significantly only in the highest density group, and this can be understood since the density of the nuclear component is a small fraction of the electron density.

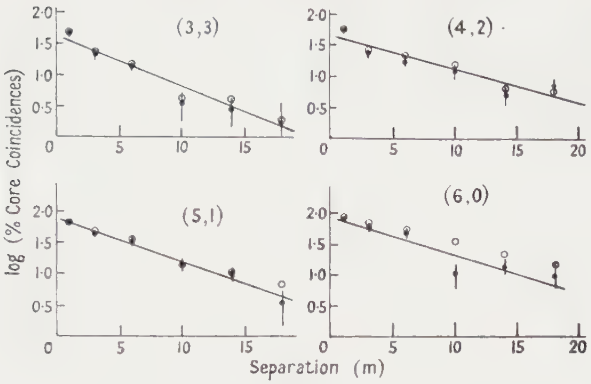

Figure 5. De-coherence curves between two core detectors for the four density groups. For key see text.

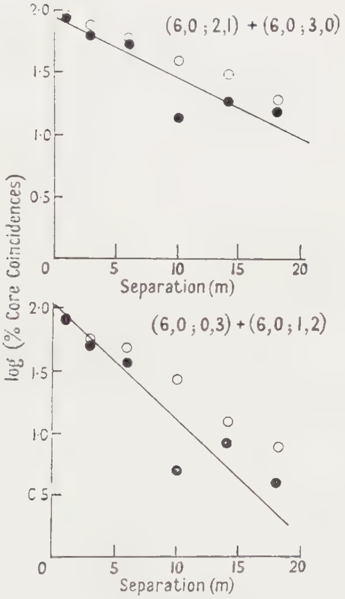

Figure 6. De-coherence curve of group (6, 0) split up into sub-groups by reference to additional small counters in the unshielded shower selecting trays. For key see text.

In the $\{(6, 0;\ 0, 3)+(6, 0;\ 1, 2)\}$ sub-group, containing the largest densities for which our detector is still effective, the accuracy of core detection as indicated by the slope of the de-coherence curve is certainly improved by the omission of the multiple events under 20 cm of lead, although the curve gives no information concerning the number of genuine core events rejected by this selection.

§ 5. ACCURACY OF CORE LOCATION AND SHOWER STRUCTURE

The accuracy with which shower axes are located, upon which the practical value of the selector depends, may be estimated from de-coherence curves of two identical units together with the general measurable characteristics of the showers as a whole.

Since a detailed study of the core region is not attempted here, an average slope of the de-coherence curve is used; this is taken to be a reduction of the probability of a coincident count in the two units by a factor 0·1 per metre increase of separation. The proportion of showers in the four density classes (3, 3), (4, 2), (5, 1), {(6, 0; 0, 3)+(6, 0; 1, 2)}, selected so that the de-coherence curves with an identical unit were similar and of the slope quoted, for which cores were detected is shown in table 2 for a sample of about 3000 showers. In this table values of the median shower size $N_{1/2}$, corresponding to the shower density classes is also given. Although the absolute significance of this quantity is open to question, it here gives an indication of the relative sizes of showers forming the four density classes. It is notable that the efficiency of detecting of cores does not fall away rapidly for the smaller showers, a feature which supports evidence from other shower observations (e.g. Zatsepin and Khristiansen 1956, Kellermann 1956) that these showers are not old in the sense of having a much reduced central concentration of energetic electrons.

Table 2.

Density group	No. of showers	No. of core responses	% core responses	$N_{1/2}$
(3, 3)	1217	86	7	4×10^4
(4, 2)	1053	117	11	8×10^4
(5, 1)	750	118	16	2×10^5
{(6, 0; 0, 3)+(6, 0; 1, 2)}	190	24	13	3×10^5

The probability of operation of a core detecting unit can be treated in a manner similar (cf. Ise and Fretter 1949) to that used for the probability of discharge of unshielded counter arrays, by making the assumption that the number of combinations of incident particles capable of operating the detector is proportional to N, the number of particles in the shower. This assumption essentially ignores any difference of shower structure over the rather small range of shower size concerned.

Assuming a shower size spectrum of the form $\mathcal{N}(N)dN \sim N^{-(\gamma+1)}dN$ where $\gamma=1{\cdot}5$, the observed average de-coherence curve leads directly to a lateral distribution of the particle combinations capable of operating the core detector, measured from the true shower axis, proportional to $r^{-(1.5\pm0.1)}$. The absolute magnitude of this distribution is determined to yield the correct fraction of core events to all shower events, and the actual distribution of detected cores follows immediately. For each density category, rather more than 50% of detected cores lie within 3 metres of the centre of the array.

This result may be compared with the fraction of all showers, selected by the triangular array of unshielded counters, for which the shower axis falls within a distance r_0 of the centre of the array, which may be determined by performing the usual series of integrations of the expression describing the discharge of the counter trays, making last of all the integration over r. The fraction, $n(r_0)$, which differs little from one density group to another, and is not very sensitive to the exact form of the lateral distribution function assumed, has been determined for the size spectrum of showers already quoted: it is tabulated below.

r_0(m)	1	2	3	5	10	20	30
$n(r_0)$ (%)	2	6	12	30	50	80	90

§ 6. CONCLUSION

It follows from this distribution that the core detector responds with an efficiency of about 50% when within 3 metres of a shower axis except in the lowest (3, 3) density group for which the efficiency is about 30%. While it may be that this reduced efficiency in the lowest density group represents a real deficiency of core particles, this effect is clearly not large. The figures agree well with those implied by the direct coincidence rates of two core detectors as given for 1 metre and 3 metre separations in table 1; the average efficiency within 3 metres would be expected to be between the values listed in these two columns of the table.

The agreement noted here, together with the continued rise of the de-coherence curve when the separation of the coincident detectors is reduced from 3 metres to 1 metre has an interesting bearing on the structure of the immediate core region of the showers under investigation. They are entirely in accord with the view that any structure of the sustaining core of the shower is very narrow, and, while they cannot be regarded as necessarily inconsistent with any larger structure, they are certainly inconsistent with a distributed group of cores of comparable importance and of separation of the order 2 or 3 metres.

ACKNOWLEDGMENTS

The authors wish to express their thanks to Professor R. Whiddington and to Professor E. C. Stoner for the facilities provided. They are indebted to Professor J. G. Wilson for valuable discussions of the manuscript and its subsequent improvement. T. S. and N. D. wish to thank the Department of Scientific and Industrial Research for maintenance grants.

REFERENCES

COCCONI, G., TONGIORGI, V., and GREISEN, K., 1949, *Phys. Rev.*, **76**, 1020.
HADDARA, S. R., and JAKEMAN, D., 1953, *Proc. Phys. Soc.* A, **66**, 549.
HAZEN, W. E., WILLIAMS, R. W., and RANDALL, Jr., C.A., 1954, *Phys. Rev.*, **93**, 578.
ISE, J., Jr., and FRETTER, W. B., 1949, *Phys. Rev.*, **76**, 933.
KASNITZ, H. L., and SITTE, K., 1954, *Phys. Rev.*, **94**, 977.
KELLERMANN, E. W., 1956, The Oxford Conference on Extensive Showers (Harwell: Atomic Energy Research Establishment), p. 20.
SINGER, S. F., 1951, *Phys. Rev.*, **81**, 579.
ZATSEPIN, G. T., and KHRISTIANSEN, G. B., 1956, The Oxford Conference on Extensive Showers (Harwell: Atomic Energy Research Establishment), p. 11.

The Excitation of the Discrete Levels of Atomic Hydrogen by Fast Electrons

BY R. McCARROLL
Department of Applied Mathematics, The Queen's University of Belfast

Communicated by D. R. Bates; MS. received 18th January 1957

Abstract. The cross sections for the excitation of normal hydrogen atoms to the fifth and higher levels have been obtained by interpolation from the Born cross sections for the excitation to the second, third and fourth levels, and for ejection into the continuum. The cross section describing the excitation of all levels and the energy loss sustained by the incident electron are hence derived.

---

§ 1. INTRODUCTION

THE calculation of the total cross section for the excitation of any discrete level of atomic hydrogen becomes progressively more tedious as the principal quantum number increases, so that for the excitation of the higher levels some alternative to the direct method of calculation must be adopted. Existing information on the excitation of the three lowest discrete levels (Bethe 1930, Goldstein 1932 and Massey and Burhop 1952), and of the continuum (Dalgarno 1953, unpublished), suggested that an interpolation method might be used to find the intervening discrete levels. Unfortunately, the earlier computations on the lower discrete levels proved to be slightly in error, and had therefore to be repeated.

§ 2. THEORY

Let the total cross section for the excitation of the nth discrete level of hydrogen from the ground state be Q_{1n} and let that for ejection into the continuum, with energy between ϵ and $\epsilon+d\epsilon$ be $Q_\epsilon^i d\epsilon$. The energy E_n of the nth level is $-1/n^2$ rydbergs, so that for large n a small change δn in n is approximately related to a change δE in E by

$$\delta n \simeq n^3 \delta E/2 \qquad \ldots\ldots(1)$$

and the cross section for the excitation of an electron with energy between E_n and E_n+dE_n is correspondingly

$$\tfrac{1}{2}n^3 Q_{1n} dE_n. \qquad \ldots\ldots(2)$$

Therefore $\frac{1}{2}n^3 Q_{1n}$ regarded as a function of E_n is continuous with Q_ϵ^i regarded as a function of ϵ and the limit as n tends to infinity of $\frac{1}{2}n^3 Q_{1n}$ is Q_0^i. Provided Q_{1n} is known for some of the lower values of n and provided Q_ϵ^i is known for a range of ϵ close to the threshold, interpolation should yield the cross sections for the excitation of the higher discrete levels.

The formula for Q_ϵ^i is derived on the basis of Born's approximation by Massey and Mohr (1933), and the evaluation of Q_ϵ^i which involves a numerical integration over the momentum change of the incident particle, has been carried out by Dalgarno (1953, unpublished), for various ϵ over a wide range of energies of the incident electron. When ϵ is zero the integration may be performed analytically, and since $Q_0{}^i = \lim_{n\to\infty} \frac{1}{2} n^3 Q_{1n}$ the value of $Q_0{}^i$ is of particular importance. Defining $\mathbf{k}$ to be $2\pi m\mathbf{v}/h$ where $\mathbf{v}$ is the velocity of the colliding electron, m its mass and h Planck's constant, we find

$$Q_0{}^i = \frac{2^9}{3(ka_0)^2}\left[\exp(-4t)\left\{-\frac{t^4}{2}-\frac{t^3}{4}+\frac{t^2}{16}+\frac{9t}{32}+\frac{41}{128}\right\}+\exp(-4)\mathrm{Ei}(4t)\right]_{t_1}^{t_2}\pi a_0{}^2 \qquad \ldots\ldots(3)$$

in which

$$t_1 = 1/(1+Y_{\max}) \qquad \ldots\ldots(4)$$

$$t_2 = 1/(1+Y_{\min}) \qquad \ldots\ldots(5)$$

$$Y_{\substack{\max\\\min}} = \{ka_0 \pm [(ka_0)^2-1]^{1/2}\}^2 \qquad \ldots\ldots(6)$$

$$\mathrm{Ei}(x) = \int_{-\infty}^{x} (\exp p)/p\, dp \qquad \ldots\ldots(7)$$

and a_0 is the atomic unit of length.

If the magnitude of the momentum change suffered by the incident electron during a collision is K then according to Born's approximation, the total cross section for the excitation of all discrete levels with principal quantum number n is

$$Q_{1n} = \frac{2n^2}{(ka_0)^2}\int_{\zeta\,\min}^{\zeta\,\max}\frac{1}{\zeta^3}\sum_{l=0}^{n-1}|\epsilon_{1,n,l}(\zeta)|^2\,d\zeta\,\pi a_0{}^2 \qquad \ldots\ldots(8)$$

with $\zeta = \frac{1}{2}Kna_0$, $\epsilon_{1,n,l}(\zeta)$ being as given by Mott and Massey (1949). Denoting $\sum\limits_{l=0}^{n-1}|\epsilon_{1,n,l}(\zeta)|^2$ by $\mathscr{I}(1, n, \zeta)$ we have

$$\left.\begin{aligned}\mathscr{I}(1,2,\zeta) &= \frac{2^{15}\zeta^2}{(9+4\zeta^2)^5}\\ \mathscr{I}(1,3,\zeta) &= \frac{81\zeta^2(3\zeta^2+2)}{(\zeta^2+4)^6}\\ \mathscr{I}(1,4,\zeta) &= \frac{2^{20}\zeta^2(16\zeta^4+56\zeta^2+45)}{(4\zeta^2+25)^7}.\end{aligned}\right\} \qquad \ldots\ldots(9)$$

The integrations over ζ may be carried out analytically without difficulty; if we write

$$\frac{2n^2}{(ka_0)^2}\int\frac{1}{\zeta^3}\mathscr{I}(1,n,\zeta)d\zeta \quad \text{as} \quad F_{1n}(\zeta)$$

then

$$Q_{1n} = [F_{1n}(\zeta\,\max) - F_{1n}(\zeta\,\min)]\pi a_0{}^2 \qquad \ldots\ldots(10)$$

where

$$\left.\begin{aligned}F_{12}(\zeta) &= \frac{2^{17}}{9^5(ka_0)^2}\left[\log\frac{4\zeta^2}{4\zeta^2+9}+\sum_{s=1}^{4}\frac{1}{s}\left(\frac{9}{4\zeta^2+9}\right)^s\right]\\ F_{13}(\zeta) &= \frac{3^6}{2.4^5(ka_0)^2}\left[-\frac{6}{5}\left(\frac{4}{\zeta^2+4}\right)^5+\log\frac{\zeta^2}{\zeta^2+4}+\sum_{s=1}^{5}\frac{1}{s}\left(\frac{4}{\zeta^2+4}\right)^s\right]\\ F_{14}(\zeta) &= \frac{2^{23}}{15.25^6(ka_0)^2}\left[-150\left(\frac{25}{4\zeta^2+25}\right)^5+55\left(\frac{25}{4\zeta^2+25}\right)^6\right.\\ &\qquad\left.+54\log\frac{4\zeta^2}{4\zeta^2+25}+54\sum_{s=1}^{6}\frac{1}{s}\left(\frac{25}{4\zeta^2+25}\right)^s\right].\end{aligned}\right\} \ldots(11)$$

§ 3. ENERGY LOSS

The loss of energy suffered by an electron in traversing a path of one centimetre through a gas of atomic hydrogen, which contains N atoms per cm^3 is

$$\Delta W^{e} + \Delta W^{i}$$

where

$$\Delta W^{e} = N \sum_{n} (E_n + I_{H}) Q_{1n} \qquad \ldots\ldots(12)$$

is the contribution due to the excitation of the discrete levels,

$$\Delta W^{i} = N \int_{0}^{\epsilon_{max}} (\epsilon + I_{H}) Q_{\epsilon}^{i} d\epsilon \qquad \ldots\ldots(13)$$

is the contribution due to ejection into the continuum and I_H is the ionization potential of hydrogen. Using the Born approximation, with certain additional assumptions, which are valid in the high energy limit, Bethe finds

$$\Delta W^{e} + \Delta W^{i} = N \frac{8}{(ka_0)^2} \{\log [2(ka_0)^2/c]\} I_{H} \pi a_0^2 \qquad \ldots\ldots(14)$$

c being a constant of numerical value 1·105.

§ 4. CALCULATIONS AND RESULTS

The cross sections for the excitation of the 2nd, 3rd and 4th levels of hydrogen have been computed from formula (10) for a range of energies of the incident electron from 1 rydberg to 72·25 rydbergs, the choice of energies being determined by the already available information on the ionization cross sections. Plotting together for each value of the impact energy, $\frac{1}{2}n^3 Q_{1n}$ versus the energy

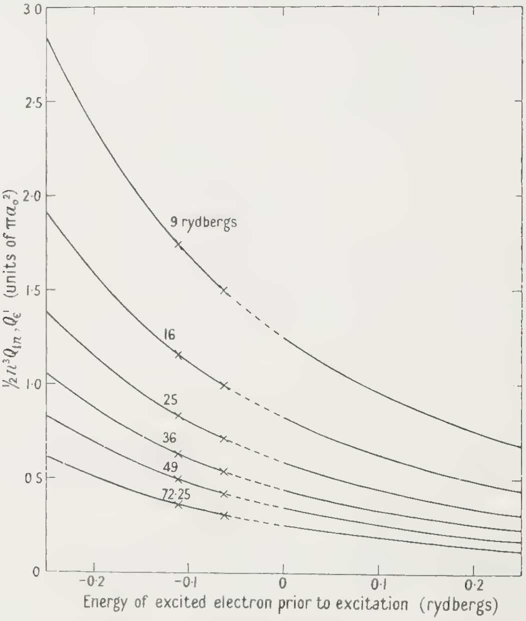

Illustration of the continuity of $\frac{1}{2}n^3 Q_{1n}$ (as a function of E_n) with Q_{ϵ}^{i} (as a function of ϵ). The numbers on the graphs refer to the energy of impact of the incident electron. Positive energies of the excited electron correspond to the ejection of the electron into the continuum and negative energies to the excitation of a discrete level. The interpolated (broken) sections of the curves for which $-1/16 < E_n < 0$, yield information on the cross sections for the excitation of the 5th and higher levels.

of the excited state and $Q_\varepsilon^{\mathrm{i}}$ versus the energy of ejection, smooth, slowly varying curves were obtained, a representative sample of which are shown in the figure. From the interpolated (broken) sections of these graphs, values of the excitation cross section for the 5th and 6th levels were found and these results, together with those for the 2nd, 3rd and 4th levels, are listed in table 1. For the 7th and higher levels, it is sufficiently accurate to fit a straight line to the pertinent section of the curve, giving an empirical form for the cross section

Table 1. Total Cross Sections for the Excitation of the Discrete Levels of Hydrogen

Impact energy (ryd)	Q_{12}	Q_{13}	Q_{14} (units of πa_0^2)	Q_{15}	Q_{16}
1·00	1·2868	0·1787	0·0509	0·0202	0·0092
1·44	1·5354	0·2782	0·0999	0·0476	0·0265
1·96	1·4993	0·2798	0·1021	0·0490	0·0274
2·56	1·3886	0·2600	0·0951	0·0457	0·0256
3·24	1·2630	0·2358	0·0862	0·0413	0·0231
4·00	1·1424	0·2123	0·0775	0·0372	0·0208
6·25	0·8919	0·1637	0·0595	0·0285	0·0159
9·00	0·7101	0·1290	0·0468	0·0224	0·0125
12·25	0·5780	0·1041	0·0377	0·0180	0·0101
16·00	0·4797	0·0858	0·0310	0·0148	0·0083
20·25	0·4050	0·0721	0·0260	0·0124	0·0069
25·00	0·3468	0·0614	0·0221	0·0105	0·0059
36·00	0·2634	0·0463	0·0166	0·0079	0·0044
49·00	0·2075	0·0363	0·0130	0·0062	0·0035
72·25	0·1527	0·0265	0·0095	0·0045	0·0025

$$\tfrac{1}{2}n^3 Q_{1n} = Q_0^{\mathrm{i}} + b/n^2$$

where Q_0^{i} and b are parameters which depend only on the impact energy. Their values are given in table 2.

Table 2. Parameters to Determine Q_{1n} for $n \geqslant 7$

Impact energy (ryd)	1·44	1·96	2·56	3·24	4·00	6·25	9·00
Q_0^{i}	2·615	2·738	2·561	2·313	2·084	1·594	1·247
b	8·7	7·8	7·1	6·4	5·9	4·5	3·6
Impact energy (ryd)	12·25	16·00	20·25	25·00	36·00	49·00	72·25
Q_0^{i}	1·001	0·822	0·687	0·584	0·438	0·342	0·249
b	3·0	2·6	2·2	1·8	1·36	1·08	0·81

This method proved entirely satisfactory for all energies of impact considered, and apart from the special case where the energy of the incident electron corresponded to the ionization potential of hydrogen, the maximum error arising from interpolation is about 0·2 per cent.

The curves of Q_{1n} plotted as a function of the ratio of the energy of impact to the energy of excitation of the *n*th state exhibit close similitude: for example, if the curves for the 4th and 5th levels are fitted for a large impact energy, say at 600 ev, the deviation of one curve from the other at 20 ev is only 5%. Because of this, it was possible to estimate the cross section for the excitation of the 5th and 6th levels by electrons with energy I_{H} from the curve for the excitation of the 4th level. This provided a useful check on the previous interpolated value, which, as already stated, is of doubtful accuracy in this instance.

From tables 1 and 2, the total cross section for the excitation of all discrete states

$$Q^e = \sum_{n=2}^{\infty} Q_{1n} = \sum_{n=2}^{6} Q_{1n} + Q_0^i \sum_{n=7}^{\infty} \frac{2}{n^3} + b \sum_{n=7}^{\infty} \frac{2}{n^5}$$

and the energy loss due to the excitation of discrete states

$$\Delta W^e = N\left\{ \sum_{n=2}^{6} \left(1 - \frac{1}{n^2}\right) Q_{1n} + Q_0^i \sum_{n=7}^{\infty} \frac{2}{n^3} + (b - Q_0^i) \sum_{n=7}^{\infty} \frac{2}{n^5} - b \sum_{n=7}^{\infty} \frac{2}{n^7} \right\}$$

were calculated. The derived values along with the values of Q^i and ΔW^i computed from the results of Dalgarno (1953, unpublished) are displayed in table 3.

Table 3. Total Excitation and Ionization Cross Sections and Energy Loss due to Excitation and Energy Loss due to Ionization in a Gas of Unit Density

Impact energy (ryd)	Q^e (units of πa_0^2)	Q^i† (units of πa_0^2)	$\Delta W^e/N$ (units of $I_H \pi a_0^2$)	$\Delta W^i/N$† (units of $I_H \pi a_0^2$)
1·44	2·0515	0·5632	1·6271	0·661
1·96	2·0241	0·9927	1·6083	1·299
2·56	1·8772	1·1660	1·4919	1·677
3·24	1·7056	1·1899	1·3553	1·856
4·00	1·5409	1·1405	1·2242	1·900
6·25	1·1984	0·9304	0·9514	1·758
9·00	0·9511	0·7428	0·7547	1·529
12·25	0·7721	0·5918	0·6124	1·297
16·00	0·6397	0·4886	0·5072	1·106
20·25	0·5391	0·3994	0·4273	0·950
25·00	0·4609	0·3359	0·3653	0·826
36·00	0·3493	0·2471	0·2767	0·631
49·00	0·2748	0·1900	0·2176	0·502
72·25	0·2018	0·1367	0·1597	0·372

Table 4 compares the Bethe values of $(\Delta W^e + \Delta W^i)$ with the corresponding Born values. It is seen that the Bethe values are in close accord with the Born values at high energies but are considerably larger at low energies: thus the Bethe value exceeds the Born value by only 2% at 50 rydbergs (676 ev), but by 80% at 2 rydbergs (27 ev). This trend is to be anticipated from the fact that the major contribution to the difference arises from Bethe's replacement of $K_{\min}$ in the Born formula by $(E_n + I_H)/2k$ which is smaller than the true value. Dalgarno and Griffing (1955), report a similar trend in the case of collisions between protons and hydrogen atoms.

Table 4. Comparison of the Total Energy Loss in a Gas of Unit Density, according to the Born Approximation and the Bethe Formula

Impact energy (ryd)		1·44	1·96	2·56	3·24	4·00	6·25	9·00
Total energy loss (units of $I_H \pi a_0^2$)	Born	2·288	2·907	3·169	3·211	3·124	2·709	2·284
	Bethe	5·321	5·169	4·791	4·367	3·959	3·105	2·481
Impact energy (ryd)		**12·25**	**16·00**	**20·25**	**25·00**	**36·00**	**49·00**	**72·25**
Total energy loss (units of $I_H \pi a_0^2$)	Born	1·909	1·613	1·377	1·191	0·908	0·720	0·532
	Bethe	2·024	1·681	1·423	1·220	0·928	0·732	0·540

† *Note added in proof.* Since the manuscript was prepared it has appeared that the values of Q^i and $\Delta W^i/N$ may be less accurate than was originally thought. The values given in table 3 for these quantities should therefore be considered as only accurate to two places of decimals.

Table 5.

Impact energy (ryd)		1·44	1·96	2·56	3·24	4·00	6·25	9·00
Average energy	(*a*)	0·7931	0·7946	0·7947	0·7946	0·7945	0·7939	0·7935
loss (ryd)	(*b*)	$1{\cdot}17_3$	$1{\cdot}30_8$	$1{\cdot}43_8$	$1{\cdot}55_9$	$1{\cdot}66_6$	$1{\cdot}89_0$	$2{\cdot}08_9$
	(*c*)	$0{\cdot}87_5$	$0{\cdot}96_4$	$1{\cdot}04_1$	$1{\cdot}10_9$	$1{\cdot}16_5$	$1{\cdot}27_3$	$1{\cdot}35_7$
Impact energy (ryd)		12·25	16·00	20·25	25·00	36·00	49·00	72·25
Average energy	(*a*)	0·7932	0·7929	0·7926	0·7925	0·7922	0·7920	0·7917
loss (ryd)	(*b*)	$2{\cdot}19_2$	$2{\cdot}26_4$	2·38	2·46	2·55	2·64	2·72
	(*c*)	$1{\cdot}40_0$	$1{\cdot}43_0$	$1{\cdot}46_7$	$1{\cdot}49_6$	$1{\cdot}52_1$	$1{\cdot}54_8$	$1{\cdot}57_0$

(*a*) $\Delta\omega^{\mathrm{e}}$ (excitation), (*b*) $\Delta\omega^{\mathrm{i}}$ (ionization), (*c*) $\Delta\omega$ (all inelastic).

Finally, table 5 gives the following average energy losses:

$$\Delta\omega^{\mathrm{e}}=\Delta W^{\mathrm{e}}/N\underset{\sim}{Q}^{\mathrm{e}}$$

$$\Delta\omega^{\mathrm{i}}=\Delta W^{\mathrm{i}}/N\underset{\sim}{Q}^{\mathrm{i}}$$

$$\Delta\omega=(\Delta W^{\mathrm{e}}+\Delta W^{\mathrm{i}})/N(\underset{\sim}{Q}^{\mathrm{e}}+\underset{\sim}{Q}^{\mathrm{i}})$$

$\Delta\omega^{\mathrm{e}}$ being the average for excitation collisions, $\Delta\omega^{\mathrm{i}}$ that for ionization collisions and $\Delta\omega$ that for all inelastic collisions.

ACKNOWLEDGMENTS

This work was carried out under contract for the United Kingdom Atomic Energy Authority, to whom thanks are due for permission to publish. The author is also indebted to Professor D. R. Bates for many helpful suggestions, and for his encouragement during the course of the work; and to Dr. A. Dalgarno for permitting the use to be made of unpublished results.

REFERENCES

BETHE, H., 1930, *Ann. Phys., Lpz.*, **5**, 325.

DALGARNO, A., and GRIFFING, G. W., 1955, *Proc. Roy. Soc.* A, **232,** 423.

GOLDSTEIN, L., 1933, *Ann. Phys., Paris.*, **19**, 305.

MASSEY, H. S. W., and BURHOP, E. H. S., 1952, *Electronic and Ionic Impact Phenomena* (Oxford : Clarendon Press).

MASSEY, H. S. W., and MOHR, C. B. O., 1933, *Proc. Roy. Soc.* A, **140,** 613.

MOTT, N. F., and MASSEY, H. S. W., 1949, *Theory of Atomic Collisions*, 2nd Edn (Oxford : Clarendon Press).

The L-Series Emission Spectrum of Krypton

By H. R. MOORE†

Dominion Physical Laboratory, Department of Scientific and Industrial Research, New Zealand

MS. received 4*th February* 1957

Abstract. The L-spectrum of krypton has been observed in emission from an electrodeless discharge source and recorded photographically with a bent crystal spectrometer. Wavelength values are given for seven diagram lines (Lβ_1: 7547 X.U.; L$\alpha_{1,2}$: 7788 X.U.), one quadrupole line and ten satellite lines. The half widths and intensities of the latter are compared with those of their parent lines Lβ_1 and L$\alpha_{1,2}$. The X-ray energy levels LI(1920 ev), MIV, V (87 ev) and NI (20 ev) are evaluated. A quasi-optical origin for some extra lines observed in this spectrum is proposed.

§ 1. INTRODUCTION

RECENT compilations of X-ray energy levels (Cauchois 1955, Fine and Hendee 1955) reflect the various gaps remaining in our knowledge of X-ray diagram spectra. Thus, certain levels of krypton are absent due to its L-emission spectrum not having been known. The results of a preliminary examination of this spectrum are now given.

The radiation source was an electrodeless discharge tube, the main features of which have been described (Moore and Chalklin 1955). The troublesome 'edge-effect' previously encountered was eliminated by the use of a wider (3 cm × 0·5 cm) discharge tube, otherwise the experimental procedures remain essentially the same. The spectra were recorded in the first order of a bent crystal spectrometer (Moore 1955) on Ilford Q2 plates. With a muscovite mica crystal the inverse plate dispersion was about 95 X.U. mm^{-1} over the wavelength range examined.

The recorded spectrum is extensive and the sharpness of its finer features as seen on a microdensitometer record exhibits some dependence on the wavelength in exact focus. For this reason a composite density contour of the spectrum determined from two plates is shown in figure 1. One of the plates is reproduced as figure 2 (Plate).

The electronic configuration of neutral krypton (atomic number 36) is $1s^2\ 2s^2\ 2p^6\ 3s^2\ 3p^6\ 3d^{10}\ 4s^2\ 4p^6$, the atom being in a $^1S_0$ state. The energy level diagram for krypton given in figure 3 shows that there are eleven L-series lines allowed by the dipole selection rules. As indicated in figures 1 and 2 seven of these lines have been detected, the others (γ_2, γ_3, l, η) lying beyond the region at present examined.

Several other lines were also recorded. On the immediate short wavelength side of $\alpha_{1,2}$ and β_1 occur the satellite groups which have been studied in elements of higher and lower atomic numbers (Hirsh 1935, 1936, Richtmyer and Richtmyer 1929). A further four lines appearing in the krypton spectrum have no apparent analogies in the spectra of adjacent elements.

---

† Now at the Division of Pure Physics, National Research Council, Ottawa, Canada.

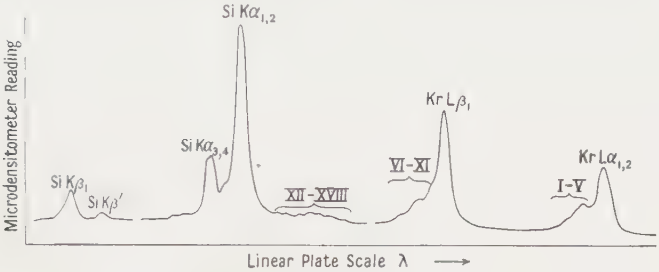

Figure 1. Composite tracing of an average microdensitometer record showing the krypton L-series lines together with silicon K-series lines emitted by the discharge tube.

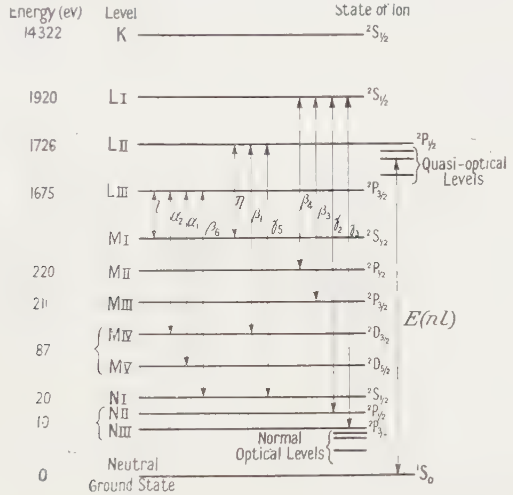

Figure 3. Diagram (not to scale) of the x-ray energy levels of krypton. Eleven dipole transitions are indicated together with a transition $E(nl)$ from a quasi-optical level to the ground state.

§ 2. WAVELENGTH MEASUREMENTS

The unavoidable silicon K-series lines $K\beta_1$ and $K\alpha_{1,2}$ (unresolved) emitted by the quartz discharge tube have been utilized as reference wavelengths, allowance being made for the wavelength shift due to chemical combination. Deodhar (1931) has determined the wavelength of $K\beta_1$ in the case of SiO_2 and his value of 6753 x.u. was accepted. Apparently there has been no low resolution measurement of $K\alpha_{1,2}$ in the case of SiO_2. Flemberg (1935) gives wavelength values for the resolved components of 7108·50 x.u. (α_1) and 7111·06 x.u. (α_2). It is reasonable therefore, in view of its known structure, to assign a wavelength of 7109 x.u. to the present unresolved $K\alpha_{1,2}$ doublet.†

Assuming a value of $d_1 = 9927{\cdot}58$ x.u. for the first-order lattice constant of the muscovite crystal (Siegbahn 1943) the wavelengths of the krypton L-series lines were calculated by methods similar to that described by Haglund (1942).

---

† This is consistent with the fact that, in the case of pure Si, the unresolved doublet wavelength of 7111·06 x.u. given by Larsson (1929) is slightly greater than the value 7110·92 x.u. for the α_1 component due to Flemberg (1935).

§ 3. THE SHAPE OF LINE Lβ_1 AND AN ANALYSIS OF ITS SATELLITE STRUCTURE

A plate was exposed with the β_1 line in exact focus. Four microdensitometer records were taken and their average converted to an intensity scale with the appropriate blackening curve. As shown in figure 4 there is partially resolved structure on the short wavelength side of the main peak. The intensity contour was analysed by assuming that each maximum corresponds to a component line having a natural shape of the type discussed by Weisskopf and Wigner (1930). In the present case the Weisskopf–Wigner line shape may be expressed in the symmetrical wavelength form

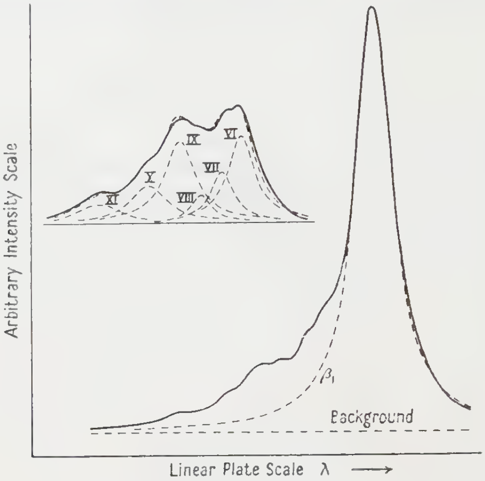

Figure 4. Analysis of the experimental contour in the region of the krypton line Lβ_1. After subtracting the contribution of line Lβ_1 and a linear background due to continuous radiation, the satellite complex is replotted on an expanded (×2) intensity scale. The full line is the experimental contour, the theoretical component lines and their envelope being drawn in broken line.

$$I(\lambda)=\frac{\gamma_\lambda}{2\pi}\frac{I_0}{(\lambda-\lambda_0)^2+\frac{1}{4}\gamma_\lambda{}^2}$$

where I_0 is the total line intensity, λ_0 is the position of the central maximum and γ_λ the full width of the line at half maximum intensity (half width). The various lines postulated on this basis are conveniently labelled VI–XI. Their half widths and relative peak intensities are collected in table 1 while their wavelengths are given in table 3. It is evident, from interpolation in a Moseley diagram, that line XI is the expected diagram line β_6.

Table 1. Analysis of Lβ_1 Satellite Structure

Line	Peak int. rel. to line Lβ_1	Half width x.u.	ev
β_1	100	15·3	3·3
VI	10·3	11·2	2·5
VII	6·1	9·7	2·1
VIII	3·3	8·1	1·8
IX	9·7	12·9	2·8
X	4·5	14·6	3·2
XI, β_6	2·2	16·2	3·6

Hirsh (1936) has studied the Lβ_1 satellite group over the atomic number range 30–48. His figure 4 shows a variation of the integrated relative energy of these satellites in accord with the Auger enhancement theory of Coster and Kronig (1935). The present analysis gives a value for the integrated relative energy of the krypton Lβ_1 satellites of about 0·23 which is somewhat greater than the value 0·15 found by interpolation in Hirsh's figure. The disagreement is possibly due to the photographic methods of intensity measurement involved rather than to an anomalous increase in Lβ_1 satellite energy for krypton.

Hirsh did not analyse the β_1 satellite structures he recorded photographically but referred to them as due to two components β_1' and β_1'' measured visually by Druyvesteyn (1928). Siegbahn (1931) lists wavelengths for β_1' and β_1'' over the atomic number range 33–46 while Richtmyer and Richtmyer (1929) measured a further two components β_1''' and β_1^{IV} in the range 38–46. Using these various values a semi-Moseley diagram (cf. Moore and Chalklin 1955) was constructed with Lβ_1 as parent line. By interpolation and extrapolation in this diagram the identities of the krypton satellites given in table 3 were established. It appears that this satellite group is more complicated than previous work would indicate.

§ 4. THE SHAPE OF LINE L$\alpha_{1,2}$ AND AN ANALYSIS OF ITS SATELLITE STRUCTURE

Figure 5 shows an analysis of the average record of a plate exposed with the $\alpha_{1,2}$ line in exact focus. The maxima in the short wavelength structure are not pronounced but do indicate a certain minimum number of components. In fitting the postulated lines I–V to the experimental contour a partial separation of the α_1 and α_2 components of the main peak must be allowed for. To do this the accepted intensity ratio of $\alpha_1 : \alpha_2 = 9 : 1$ was taken and a doublet separation of 6 X.U. used. The latter value is found by extrapolating the regular doublet law from the known separations at higher atomic numbers. The half widths and relative peak intensities of the various lines are given in table 2 and their wavelengths listed in table 3.

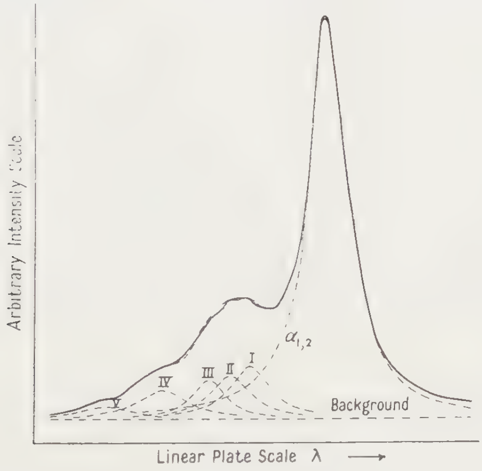

Figure 5. Analysis of the experimental contour in the region of the krypton line L$\alpha_{1,2}$. The full line is the experimental contour, a linear background due to continuous radiation and the theoretical component lines with their envelope are drawn in broken line.

The integrated relative energy of this satellite group (with respect to line α_1) is found to be 0·4. This is much greater than a value between 0·1 and 0·2 expected from extrapolation of the curve given by Hirsh (fig. 3, 1935) in his study of $L\alpha_1$ satellite intensity at higher atomic numbers. While errors in photographic intensity measurement cannot be dismissed, the magnitude of the discrepancy could mean that the values of integrated relative satellite energy given by Hirsh are too low. This would not alter his conclusion that the variation of the integrated relative satellite energy is in accord with the theory of Coster and Kronig (1935).

Table 2. Analysis of $L\alpha_{1,2}$ Satellite Structure

Line	Peak int. rel. to line $L\alpha_1$	Half width	
		X.U.	ev
α_1	100	14·7	3·0
α_2	11·1	15·4	3·2
I	15·5	15·5	3·2
II	12·7	15·5	3·2
III	11·3	12·4	2·6
IV	8·5	18·8	3·9
V	3·5	23·5	4·9

Richtmyer and Richtmyer (1929) have measured the wavelengths of five $L\alpha$ satellites α', α'', α''', α^{IV}, α^{V} in the atomic number range 37–46 and a sixth line α^{VI} for atomic numbers 41, 42, 44 and 46. These values were taken as the basis of a semi-Moseley diagram with α_1 as parent line. The identities of the krypton satellites given in table 3 were established by extrapolation in this diagram.

§ 5. THE DIAGRAM LINES $L\beta_4$, $L\gamma_5$ AND $L\beta_3$

On the long wavelength side of the silicon line $K\alpha_{1,2}$ and in the region where the krypton diagram lines β_4, γ_5 and β_3 are expected to be, there occurs a complex feature of low intensity (figure 1). It is assumed that the definite peaks in the density contour of this region correspond to a number of unresolved lines. They are labelled XII–XVIII and their wavelengths given in table 3. Lines XII, XIII and XIV were readily identified as the diagram lines β_4, γ_5 and β_3 respectively by interpolation in a Moseley diagram. The other lines in this region are discussed in § 7.

§ 6. THE LI, MIV,V AND NI ENERGY LEVELS

The quantum energies associated with the various krypton lines are given in the last column of table 3. They were calculated with the conversion factor 12 370 kilovolt X.U. given by Felt, Harris and Dumond (1953). The following relationships are of interest, energy values being rounded off in electron volts.

$$L\beta_4 \ : L_{I} - M_{II} = 1700 \quad (1)$$
$$L\beta_3 \ : L_{I} - M_{III} = 1710 \quad (2)$$
$$L\beta_1 \ : L_{II} - M_{IV} = 1639 \quad (3)$$
$$L\alpha_{1,2} \ : L_{III} - M_{IV,V} = 1588 \quad (4)$$
$$L\beta_6 \ : L_{III} - N_{I} = 1654 \quad (5)$$
$$L\gamma_5 \ : L_{II} - N_{I} = 1706 \quad (6)$$

Table 3. L-Series Lines of Krypton

Line	Identity	Wavelength (X.U.)	ν/R¶	Quantum energy (ev)
	$\alpha_{1,2}$	7788	117·00	1588·3
I	α'	7765	117·35	1593·0
II	α''	7758	117·46	1594·4
III	α'''	7751	117·56	1595·9
IV	α^{IV}	7737	117·78	1598·8
V	α^{V}, α^{VI}†	7718	118·07	1602·7
	β_1	7547	120·74	1639·0
VI	β_1'‡	7529	121·03	1642·9
VII		7523	121·13	1644·2
VIII	§	7516	121·24	1645·8
IX	β_1'', β_1'''	7508	121·37	1647·5
X	β_1^{IV}	7498	121·53	1649·7
XI	β_6	7481	121·81	1653·5
XII	β_4	7276	125·24	1700·1
XIII	γ_5	7251	125·67	1705·9
XIV	β_3	7236	125·93	1709·5
XV	LII–NIII	7222	126·17	1712·8
XVI		7205	126·47	1716·8
XVII	$^1S_0-(2p^55s, J=1)$	7181	126·89	1722·6
XVIII	$^1S_0-(2p^56d, J=1)$	7169	127·11	1725·4

†Either identity possibly correct, not resolved by analysis.
‡Probably components of β_1'.
§New β_1 satellite.
Either identity possibly correct, not resolved by analysis.
¶ν expressed in reciprocal X.U. $R=109\,737$ cm^{-1}.

Table 4. Energy Levels of Krypton in electron volts

Level	Fine and Hendee (1955)	Cauchois (1955)	Author
K	14323[a]	14322[a]	
LI	1931[b]	1904[c]	1920[j], 1921[k]
LII	1727[d]	1726[d]	
LIII	1675[e]	1675[e]	
MII		220[f]	
MIII		211[g]	
MIV			87[l]
MIV, V		87[h]	87[m]
NI			21[n], 20[o]
NII, III		10[i]	

a, From K-absorption transition; b, from least squares interpolation in Moseley diagram; c, from LI absorption transition; d–i, from K-absorption transition and $K\alpha_2$, $K\alpha_1$, $K\beta_3$, $K\beta_1$, $K\beta_5$ (quadrupole), $K\beta_2$ lines respectively, j, k, l, m, n, o, from relationships 1, 2, 3, 4, 5, 6 (in text) respectively.

In the second and third columns of table 4 are collected the known energy level values for krypton as determined by Fine and Hendee (1955) and Cauchois (1955). The methods for evaluating each level are also given. On substituting the MII, III and LII, III values given by Cauchois in the previous six relationships the level values listed in the fourth column of the table are found. It is seen that the present results allow each of the levels LI, MIV, V (unresolved) and NI to be evaluated from two independent transitions and that these pairs of values are mutually consistent. The present Lɪ value lies between the two values previously given for this level, neither of which is expected to be accurate. The present Mɪᴠ, ᴠ value confirms that deduced from a K-series quadrupole transition. The Nɪ level had not previously been determined.

§ 7. QUASI-OPTICAL X-RAY LINES

The observed lines XV–XVIII are not diagram lines and an explanation of their origins is required. If, instead of the x-ray value for the Nɪɪ, ɪɪɪ level 10 ev, a more accurate value of about 14 ev is taken (the first ionization potential of krypton) the quadrupole transition Lɪɪ–Nɪɪɪ (1712 ev) is a possible explanation of line XV. It is identified accordingly in table 3. The remaining three lines cannot be similarly explained. Their intensities relative to the adjacent diagram lines β_4, γ_5 and β_3 are probably too great for them to be satellites of the latter and, further, no such satellites have been observed in other elements.

Although the great majority of observed x-ray lines arise from transitions between ionic states due to inner ionization, there is no logical objection to the idea of a transition between an atomic state due to inner excitation and the ground state of the neutral atom. By inner excitation is meant the raising of an inner electron to an atomic level which is below the ionization limit. On the return of this electron to the inner vacancy the excited atom reverts to the ground state with the emission of a quantum of radiation. The upper states thus envisaged correspond to a series of quasi-optical levels which converge on the various inner ionization limits (x-ray absorption edges). Such a series of levels is drawn in figure 3 converging on the Lɪɪ ionization limit.

Since the quantum energies of lines XVI–XVIII come close to the value of the Lɪɪ level 1726 ev it is suggested that they might arise from inner excitation of a 2p electron. Complete removal of this electron would give rise to the $2p^5$ configuration, the atom being left in a ${}^2P_{1/2}{}^0$ state with an energy E (Lɪɪ) = 1726 ev above that of the ground state ${}^1S_0$. But if the excited electron resides in a quasi-optical level nl the resulting configurations $2p^5nl$ will give rise to various states $[{}^2P_{1/2}+nl]$ with energies $E(nl)$ which are less than E(Lɪɪ). Of these only odd states with $J=1$ arising from the configurations $2p^5ns$ $(n \geqslant 5)$ and $2p^5nd(n \geqslant 4)$ may combine with the ground state ${}^1S_0$ with the emission of radiation. Since the lower state of the transition is the ground state of the atom with zero energy, the emitted quanta must have the energy $E(nl)$. Evidently the difference $\Delta E = E(\text{L}_{\text{II}}) - E(nl)$ is the energy required to remove completely an nl electron from the krypton configuration $2p^5nl$. Assuming that the possible nl orbitals are sufficiently non-penetrating to be insensitive to the position of the hole in the atomic core, the energy ΔE may be compared with either the energy to remove completely an nl electron from the krypton configuration $4p^5nl$ or the energy to remove completely the valence electron from rubidium (atomic number 37) when in the ground or an excited state.

The values of ΔE corresponding to the allowed configurations $2p^5ns$ $(n \geqslant 5)$ and $2p^5nd$ $(n \geqslant 4)$ were calculated from both the Krɪ and Rbɪ term values given in *Atomic Energy Levels* (Moore 1952). Substitution in the expression $\Delta E = E(\text{L}_{\text{II}}) - E(nl)$ using the known value $E(\text{L}_{\text{II}}) = 1726$ ev then gave the various quantum energies $E(nl)$ to be associated with possible quasi-optical x-ray lines. Thus the krypton term values for the configurations $4p^55s$ and

$4p^5 6d$ lead to the quantum energies 1722·6 ev and 1725·3 ev respectively while the corresponding energies calculated from the rubidium term values for the configurations $4p^6 5s$ and $4p^6 6d$ are 1721·8 ev and 1725·4 ev. Either set of energies is in sufficient agreement with the measured values for lines XVII and XVIII to allow the identification given in table 3. It is recalled that lines XVII and XVIII were selected as among the most prominent in an unresolved complex. Other lines are probably present which fit in the same scheme of origin although line XVI does not do so.

§ 8. DISCUSSION OF RESULTS

The information obtained in this investigation shows that further study of the krypton L-spectrum with higher resolution would be fruitful. The diagram lines l, η, γ_2 and γ_3 have yet to be recorded. They would allow the MI level to be determined and possibly a better x-ray value for the NII, III level to be obtained. The suggestion that the $L\beta_1$ satellite group is unexpectedly complex needs confirmation, particularly in view of the present lack of an exact and generally applicable theory of satellite origins. The identification of lines XVII and XVIII with transitions between quasi-optical x-ray states and the neutral ground state is possibly of some interest. If correct it represents an emission phenomenon analogous to those established in ultra-violet absorption spectra by Beutler (cf. Herzberg 1944, p.167 *et seq.* for references and discussion) and in x-ray absorption spectra by Parratt (1939). The kind of transition proposed is essentially atomic in character and thus would be expected in the spectra of monatomic gases or vapours rather than in the spectra of solid emitters where the identities of the outer levels are lost by broadening in the crystal lattice.

ACKNOWLEDGMENTS

The author is indebted to Dr. G. Herzberg for the use of facilities at the National Research Council, Ottawa, Canada, during the preparation of this paper. Thanks are due also to Dr. R. Velasco who gave generously of his time in valuable discussions and to Dr. A. E. Douglas for his helpful criticism of the final manuscript.

REFERENCES

CAUCHOIS, Y., 1955, *J. Phys. Radium*, **16**, 253.
COSTER, D., and KRONIG, R. de L., 1935, *Physica*, **2**, 13.
DEODHAR, G. B., 1931, *Proc. Roy. Soc.* A, **131**, 633.
DRUYVESTEYN, M. J., 1928, *Dissertation*, Gröningen.
FELT, G. L., HARRIS, J. N., and DUMOND, J. W. M., 1953, *Phys. Rev.*, **92**, 1160.
FINE, S., and HENDEE, C. F., 1955, *Nucleonics*, **13**, 36.
FLEMBERG, H. K'SON, 1935, *Z. Phys.*, **96**, 167.
HAGLUND, P., 1942, *Ark. Mat. Astr. Fys.* A, **28**, No. 8.
HERZBERG, G., 1944, *Atomic Spectra and Atomic Structure* (New York : Dover).
HIRSH, F. R., 1935, *Phys. Rev.*, **48**, 722; 1936, *Ibid.*, **50**, 191.
LARSSON, A., 1929, *Uppsala Univ. Årsskr.*, **2**, 1.
MOORE, CH.E., 1952, *Atomic Energy Levels*, Vol. II (Washington : N.B.S. Circular 467).
MOORE, H. R., 1955, *J. Sci. Instrum.*, **32**, 324.
MOORE, H. R., and CHALKIN, F. C., 1955, *Proc. Phys. Soc.* A, **68**, 717.
PARRATT, L. G., 1939, *Phys. Rev.*, **56**, 295.
RICHTMYER, F. K., and RICHTMYER, R. D., 1929, *Phys. Rev.*, **34**, 574.
SIEGBAHN, M., 1931, *Spektroskopie der Röntgenstrahlen* (Berlin: Springer); 1943, *Nature, Lond.*, **151**, 502.
WEISSKOPF, V., and WIGNER, E., 1930, *Z. Phys.*, **63**, 54.

RESEARCH NOTES

The Mobility of He^+ Ions in Helium

By N. LYNN and B. L. MOISEIWITSCH
Department of Applied Mathematics, The Queen's University of Belfast

Communicated by D. R. Bates ; MS. received 8th February 1957

§ 1. Introduction

The laboratory investigation carried out by Tyndall and Powell (1931) resulted in a value of 20 $cm^2\ v^{-1}sec^{-1}$ for the mobility of helium ions in atomic helium at a temperature of 291°K and standard gas density ($2{\cdot}69 \times 10^{19}\ cm^{-3}$), while Massey and Mohr (1934) in a quantal study of the mobility of He^+ ions in He obtained a value of 11 $cm^2\ v^{-1}sec^{-1}$. In 1944 Meyerott (1944) suggested that Tyndall and Powell had measured the mobility of the molecular ion He_2^+ which is much larger than that of the atomic ion (Geltman 1953), and recent experiments (Biondi and Brown 1949) on the mobility of He^+ ions in their parent gas have given values in substantial agreement with the theoretical value of Massey and Mohr, whose calculations were, however, confined to one temperature. Chanin and Biondi (1955) have investigated experimentally the temperature dependence of the mobility of He^+ ions in He and it is consequently of interest to obtain theoretical values over a range of temperatures.

Recently, calculations have been carried out on the interaction energies between a He^+ ion and a He atom over a wide range of internuclear separations (Moiseiwitsch 1956, to be referred to as I). These energies have been used in the present paper to obtain the mobility of He^+ ions in atomic helium for the temperature range lying between 50°K and 1000°K. Very good agreement is found with the recent experimental work of Chanin and Biondi.

§ 2. Theory

The theory of slow inelastic collisions between heavy particles given by Bates, Massey and Stewart (1953) results in the equations

$$\frac{d^2g_l^{\pm}(R)}{dR^2}+\left\{k^2-\frac{2M}{\hbar^2}V^{\pm}(R)-\frac{l(l+1)}{R^2}\right\}g_l^{\pm}(R)=0 \qquad \ldots\ldots(1)$$

where $g_l^{\pm}$ is zero at the origin and for large R has the form

$$g_l^{\pm}\sim k^{-1}\sin(kR-\tfrac{1}{2}l\pi+\eta_l^{\pm}) \qquad \ldots\ldots(2)$$

and where V^+ and V^- are the interaction energies between a He^+ ion and a He atom corresponding to the states of g and u symmetry respectively, R is the internuclear distance, M is the reduced mass of the system, k is the wave number of the initial relative motion and $\eta_l^{\pm}$ are the phase shifts for the lth partial wave.

The charge transfer cross section is then given by

$$Q_{\mathrm{T}}=\frac{\pi}{k^2}\sum_{l=0}^{\infty}(2l+1)\sin^2(\eta_l^+-\eta_l^-) \qquad \ldots\ldots(3)$$

and the diffusion cross section by

$$Q_{\rm D}=\frac{4\pi}{k^2}\sum_{l=0}^{\infty}(l+1)\sin^2(\eta_l-\eta_{l+1}) \qquad \ldots\ldots(4)$$

where

$$\eta_{2r}=\eta_{2r}^{+}\text{ and }\eta_{2r+1}=\eta_{2r+1}^{-},$$

assuming that the nuclei obey Bose–Einstein statistics. The mobility can then be expressed in the form

$$\mu=eD/\boldsymbol{k}T \qquad \ldots\ldots(5)$$

where, according to the Chapman–Enskog theory (cf. Chapman and Cowling 1941), the coefficient of diffusion D is given by

$$D=\frac{3\sqrt{\pi}}{16n}\frac{1}{P_{12}}\left(\frac{2\boldsymbol{k}T}{M}\right)^{7/2}(1-\epsilon_0)^{-1} \qquad \ldots\ldots(6)$$

and

$$P_{12}=\int_0^{\infty}v^5Q_{\rm D}(v)\exp(-Mv^2/2\boldsymbol{k}T)dv, \qquad \ldots\ldots(7)$$

e being the ionic charge, $\boldsymbol{k}$ Boltzmann's constant, T the absolute temperature, n the number density of helium atoms, v the velocity of relative motion and ϵ_0 a small correction term which we shall ignore.

The scattering phase shifts for the collision process can be obtained by applying Langer's modification of Jeffreys' approximation (Langer 1937) to equation (1) and are given by

$$\eta_l^{\pm}=\tfrac{1}{2}\pi(l+\tfrac{1}{2})-kR_l^{\pm}+\int_{R_l^{\pm}}^{\infty}[F_l^{\pm 1/2}(R)-k]dR, \qquad \ldots\ldots(8)$$

where

$$F_l^{\pm}(R)=k^2-\frac{2M}{\hbar^2}V^{\pm}(R)-\frac{(l+\frac{1}{2})^2}{R^2} \qquad \ldots\ldots(9)$$

and $R_l^{\pm}$ is the largest positive zero of $F_l^{\pm}$.

Care has to be exercised in using this formula since for certain values of l it is found that F_l^{-} has three zeros. The necessary modification has been discussed by Buckingham and Dalgarno (1952).

Dalgarno and McDowell (1956) have suggested that, to a good approximation,

$$Q_{\rm D}=2(Q_{\rm T}+Q_{\rm P})\dagger \qquad \ldots\ldots(10)$$

where $Q_{\rm P}$ is a polarization correction given by

$$Q_{\rm P}\sim 2\pi\int_{\bar{P}}^{\infty}P\sin^2\left\{\frac{3C\pi}{8k^2P^4}\right\}dP \qquad \ldots\ldots(11)$$

in which $C\hbar^2/Me^2$ is the polarizability of a helium atom and $\bar{P}$ is the appropriate least value of the impact parameter P. An analytical formula for $Q_{\rm P}$ is given by Dalgarno, McDowell and Williams (to be published). It is of interest to investigate the accuracy of this approximation for the particular case with which we are concerned.

In I charge transfer cross sections were obtained by a method involving the application of the impact parameter method of Mott (1931) which should be

---

† Dr. Dalgarno informs us that he has investigated the accuracy of experimental charge transfer cross sections for positive ions in their parent gases by using formula (10) to calculate diffusion cross sections and hence mobilities.

accurate for energies of the incident He^+ ion greater than about 1 ev, but for lower energies it is necessary to calculate the charge transfer and diffusion cross sections from the exact expressions (3) and (4).

§ 3. DISCUSSION OF RESULTS

In I the electronic energies $E^+(R)$ and $E^-(R)$ for the $^2\Sigma_g$ and $^2\Sigma_u$ states of He_2^+ were calculated for a wide range of internuclear distances. Three trial wave functions, denoted in order of increasing complexity by (i), (ii) and (iii), were used. No account was taken of polarization in the evaluation of these energies. However, although polarization can be neglected with only slight error in the calculation of the charge transfer cross section, this is not the case for the diffusion cross section. Consequently, in this paper we have taken

$$V^{\pm}(R)=E^{\pm}(R)-\frac{\alpha}{(\sigma^2+R^2)^2}\text{ rydbergs} \qquad \ldots\ldots(12)$$

where $\alpha=1{\cdot}39$ is the value of the polarizability of the helium atom in units of a_0^3 ($a_0=5{\cdot}29\times10^{-9}$ cm) and σ is chosen to have the value 0·59.

It was suggested in I that function (iii) yielded the most satisfactory values of $E^{\pm}(R)$. These values were therefore used with Jeffreys' approximation to calculate the phase shifts $\eta_l^{\pm}$ for $k=2, 4$ (in units of a_0^{-1}), which were then substituted into expressions (3) and (4) to find the charge transfer and diffusion cross sections. The results are :

k	2	4
$\underset{\sim}{Q}_T$	44·5	39·4
$\underset{\sim}{Q}_D$	113·5	82·8

Cross sections are in units of πa_0^2.

For k values somewhat larger than 4, the values of $\underset{\sim}{Q}_T$ obtained in I for function (iii) should be sufficiently accurate, as should the values of $\underset{\sim}{Q}_D$ obtained from the approximate formula (10).

A close fit to the charge transfer cross section for an energy range corresponding to k between 2 and 1000 is found to be

$$\underset{\sim}{Q}_T=[49{\cdot}9-7{\cdot}87\ln k+0{\cdot}255(\ln k)^2]\pi a_0^2. \qquad \ldots\ldots(13)$$

This type of fit for the cross section is justifiable on theoretical grounds (cf. Demkov 1952, Dalgarno 1957). Similarly, a good fit to the diffusion cross section is

$$\underset{\sim}{Q}_D=[157{\cdot}3-72{\cdot}7\ln k+13{\cdot}68(\ln k)^2]\pi a_0^2. \qquad \ldots\ldots(14)$$

It should be noted, however, that this fit for $\underset{\sim}{Q}_D$ is satisfactory only for values of k between about 1·5 and 12 but this is more than adequate for the purposes of this paper.

For values of k rather less than 2 the cross sections begin to oscillate and it is no longer possible to obtain accurate values for them by Jeffreys' approximation. This makes it necessary to confine the calculations to temperatures greater than about 50°K.

Using expression (14) for the diffusion cross section in conjunction with (5), (6) and (7) an analytical expression for the mobility μ may be obtained without difficulty. Curve I of the figure shows how the mobility varies between 50° and 1000°K. The accuracy of this curve can be assessed by comparing with the experimental work of Biondi and Chanin (1954) and Chanin and Biondi (1955). In the earlier of these papers a value of 10·5 cm^2 v^{-1} sec^{-1} is given for the mobility of He$^+$ ions in He at a temperature of 300°K and standard gas density. In the second, which is in abstract form, the authors quote theoretical values of 17·5, 13·8 and 12·1 cm^2 v^{-1} sec^{-1} at 77°, 195° and 300°K, arrived at following a procedure due to Holstein (1952), and state that their experimental values are 15% lower than these calculated values. The values of μ obtained in this paper at standard gas density and corresponding temperatures are 14·9, 11·5 and 10·2 cm^2 v^{-1} sec^{-1} which are thus in very good agreement with the laboratory measurements of Biondi and Chanin. The values of $\underset{\sim}{Q}_{\mathrm{T}}$ corresponding to interaction (iii) in I should therefore be highly accurate.

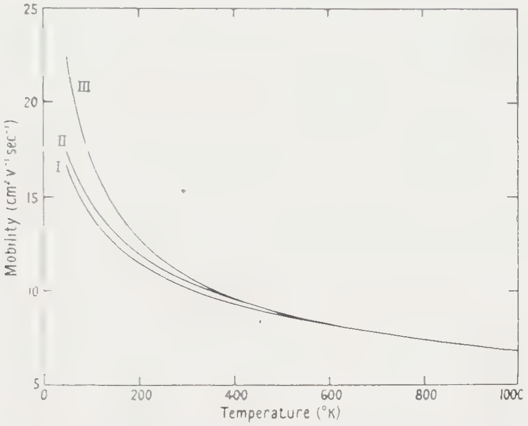

The mobility of He$^+$ ions in helium gas. Curve I obtained by using most accurate expression (14) for $\underset{\sim}{Q}_{\mathrm{D}}$, and curves II and III obtained by using $\underset{\sim}{Q}_{\mathrm{T}}$ given by (13) together with approximations (10) and (15) respectively.

Finally, it is of interest to investigate the accuracy of approximation (10) for $\underset{\sim}{Q}_{\mathrm{D}}$ and also the still more approximate expression for the diffusion cross section given by

$$\underset{\sim}{Q}_{\mathrm{D}} = 2\underset{\sim}{Q}_{\mathrm{T}} \qquad \ldots\ldots(15)$$

which arises from (10) when the effect of polarization is neglected. Using (13) for $\underset{\sim}{Q}_{\mathrm{T}}$, the resulting mobilities appear as curves II and III in the figure. It can be seen from curve II that (10) is very accurate over the whole range of temperatures considered in this paper, while from curve III it is evident that the polarization correction $\underset{\sim}{Q}_{\mathrm{P}}$ is not negligible for temperatures below 250°K.

ACKNOWLEDGMENT

It is a pleasure to thank Dr. A. Dalgarno for several useful discussions.

REFERENCES

BATES, D. R., MASSEY, H. S. W., and STEWART, A. L., 1953, *Proc. Roy. Soc.* A, **216**, 437.
BIONDI, M. A., and BROWN, S. C., 1949, *Phys. Rev.*, **75**, 1700.
BIONDI, M. A., and CHANIN, L. M., 1954, *Phys. Rev.*, **94**, 910.
BUCKINGHAM, R. A., and DALGARNO, A., 1952, *Proc. Roy. Soc.* A, **213**, 506.
CHANIN, L. M., and BIONDI, M. A., 1955, *Phys. Rev.*, **99**, 1658.

Chapman, S., and Cowling, T. G., 1941, *Mathematical Theory of Non-Uniform Gases* (Cambridge : University Press), 2nd Edn.
Dalgarno, A., 1957, *U.S.A.F. Cambridge Conference on Chemical Aeronomy* (New York : Pergamon Press) (in the press).
Dalgarno, A., and McDowell, M. R. C., 1956, *Proc. Phys. Soc.* A, **69**, 615.
Demkov, U. H., 1952, *Uchen. Zap. Leningr. Univ. Seria Phiz. Nauk*, **146,** 74.
Geltman, S., 1953, *Phys. Rev.*, **90,** 808.
Holstein, T., 1952, *J. Phys. Chem.*, **56,** 832.
Langer, R. E., 1937, *Phys. Rev.*, **51,** 669.
Massey, H. S. W., and Mohr, C. B. O., 1934, *Proc. Roy. Soc.* A, **144,** 188.
Meyerott, R. E., 1944, *Phys. Rev.*, **66,** 242.
Moiseiwitsch, B. L., 1956, *Proc. Phys. Soc.* A, **69,** 653.
Mott, N. F., 1931, *Proc. Camb. Phil. Soc.*, **27,** 553.
Tyndall, A. M., and Powell, C. F., 1931, *Proc. Roy. Soc.* A, **134,** 125.

Search for a Rare α-Emission in ^{228}Ra (MsTh 1)

By N. FEATHER, N. MILLER and S. W. PEAT
Natural Philosophy Department, Edinburgh University

The possibility of a branching in the thorium series at ^{228}Ra(MsTh 1) or ^{228}Ac(MsTh 2) was considered from time to time during the classical investigations into natural radioactivity. With ^{228}Ac, searches were made both for a rare α-emission and for the unknown isotope ^{224}Fr which would result from such a partial α-decay. The most careful of these (Hahn and Erbacher 1926) led to the conclusion that the α/β branching ratio of ^{228}Ac is less than $1{\cdot}5 \times 10^{-7}$, assuming that the half-value period of the ^{224}Fr is less than ten years. Studies of the systematics of α-decay in the heavy elements (Perlman, Ghiorso and Seaborg 1950, Glass, Thompson and Seaborg 1955) now permit well-founded conjectures to be made regarding the energies of α-disintegration to be anticipated in the decay of ^{228}Ra and ^{228}Ac, and the corresponding partial decay constants for α-emission. In this way the α/β branching ratio of ^{228}Ra may be estimated as 10^{-8}, within a factor of about 150 either way, reflecting an uncertainty of $\pm 0{\cdot}2$ Mev in the α-ray energy, and the α/β branching ratio of ^{228}Ac as 7×10^{-9} within a factor of 100 either way corresponding to a similar uncertainty, if the α-disintegration in this case is unhindered. If the α-disintegration is significantly hindered, as it probably is, the most probable α/β branching ratio of ^{228}Ac is more likely to be of the order of 10^{-10}. The search for the unknown products ^{224}Em and ^{224}Fr resulting from such branching thus presents a formidable problem. A method of great potential sensitivity suitable for tracing α-decay in ^{228}Ra is, however, available using nuclear emulsions, as follows.

The isotope ^{224}Em resulting from the α-decay of ^{228}Ra can safely be predicted to be β-unstable (by $0{\cdot}6 \pm 0{\cdot}3$ Mev), as also can the ^{224}Fr resulting from its β-decay (by $3{\cdot}0 \pm 0{\cdot}2$ Mev). Estimates of the half-value periods are less easy to make. In respect of ^{224}Em, which is the more important for our purposes, there is not much guidance to be obtained from a comparison with similar species. With its much smaller disintegration energy ($\sim 0{\cdot}05$ Mev), ^{228}Ra decays by an allowed transition, but the principal mode of disintegration of ^{234}Th (disintegration energy 0·20 Mev) is at least ten times slower than allowed. By contrast, the principal mode of ^{240}U (disintegration energy 0·36 Mev) is almost certainly allowed, but that of ^{246}Pu (disintegration energy 0·40 MeV) is again some three times slower. If the principal mode of disintegration of ^{224}Em were to the ground state of ^{224}Fr, the half-value period could be as short as one hour (within a factor of three either way due to uncertainty in the disintegration energy); on the other hand, if the principal disintegration mode had an energy of say 0·4 MeV, and were forbidden by a factor of 20, the half-value period might be as long as five days. In respect of ^{224}Fr a close estimate is not necessary for present purposes: the half-value period is probably a few minutes only, though it could be as long as a few hours. We may say, in conclusion, that whatever the half-value periods, within the above-stated limits, α-branching at ^{228}Ra will result in a fairly rapid return to the main chain at ^{224}Ra(ThX).

Let us suppose that all isotopes of Em which have grown within a solution of ^{228}Ra within a period of two weeks can be isolated by condensation in liquid air. On impregnating a nuclear emulsion with a solution of the residue, the presence of ^{224}Ra among the decay products of the emanation can be detected with certainty, against any likely background of active deposit, by virtue of the fact that the decay of ^{224}Ra gives rise to a 'star' of three or more α-tracks in the emulsion, as opposed to the single tracks characteristic of ^{212}Pb. Furthermore, simple chemical separations can eliminate the greater part of this active deposit before impregnation.

In our experiments, a solution containing 2 mC of ^{228}Ra in 5 ml. of 1 N hydrochloric acid was allowed to stand in a sealed system for at least two weeks, to allow any ^{224}Em present to approach secular equilibrium even on the longest estimates of its half-value period. Nitrogen was then bubbled through the solution for four hours. The emerging gas stream passed up a column 2 cm in diameter filled with glass beads and glass wool, and then through a trap surrounded with liquid oxygen, which contained 2 ml. of a frozen 1 N nitric acid solution. The efficiency of the column in trapping spray was checked by bubbling nitrogen through a solution containing 5 mC of ^{212}Pb(ThB) and examining the condensate for this activity with nuclear emulsions. None was found. In the experiments with ^{228}Ra, the trap was sealed after the bubbling terminated, and then allowed to warm up slowly and stand for 24 hours, whereupon the residue dissolved in the thawing nitric acid solution. An aliquot of this solution was removed and set aside for 14 days, to allow the ^{212}Pb to decay, and was then used to impregnate an emulsion directly, as an additional check on any carry-over of the parent activity, in spray or by volatilization, which proved to be negligible. The ^{222}Em (radon) derived from ^{226}Ra present in the ^{228}Ra was next removed by evaporating the main solution to dryness: its decay products could not in any case confuse the issue by giving rise to 'stars'. The residue was redissolved in nitric acid, carriers of Ba and Cs were added, and were separately freed from traces of Pb, Bi and Th isotopes, in the former case by eight successive precipitations of the barium as nitrate by fuming nitric acid in the presence of Pb and Bi carriers, in the latter by eight successive precipitations as carbonate of Ba, Pb and Bi carriers added to the solution, followed by precipitation of the Cs as perchlorate. Finally, the purified solutions of Ba and Cs were used to impregnate Ilford G5 emulsions, and these were left to stand for 14 days. The emulsion containing the Ba carrier would contain initially the bulk of the ^{224}Ra resulting from the hypothetical branching, if the half-value period of the intermediate ^{224}Fr were short: in that containing the Cs, ^{224}Ra would accumulate from the ^{224}Fr if the period of this body were, unexpectedly, greater than two days. Controls were made of emulsions impregnated with the distilled water used and with solutions of the Ba and Cs carriers.

In four successive runs of this type, a very weak ^{224}Ra activity appeared in the barium fraction, similar in intensity to the background contamination of the emulsion. It was identified by a significant increase in the number of four-track 'stars' in the emulsion, unaccompanied by any similar increase in five- or three-track 'stars'; furthermore, these 'stars' showed the correct proportion (about 66%) of long-track α-particles corresponding to the 8·78 MeV disintegration of ^{212}Po (ThC′). No activity significantly greater than background appeared in the caesium fractions.

Pending identification of the intermediate species ^{224}Em and ^{224}Fr this observation cannot be regarded as a confirmation that α/β branching takes place in ^{228}Ra, but it does permit of placing upper limits on the value of the branching ratio, which can be computed on various assumptions as to the half-value period of ^{224}Em. The figures in the table take account of the fact that there are two sources of ^{224}Em in the condensates: (i), that which accumulates in the 14-day period of standing prior to bubbling; (ii), that which accumulates in the four-hour bubbling period. They also include a factor of five to cover possible losses in the condensation and separation procedures.

Upper Limits of the α/β Branching Ratio of ^{228}Ra

Estimated half-value period of ^{224}Em	6 min	1 hr	10 hr	100 hr	200 hr
Upper limit	2×10^{-8}	$1{\cdot}5\times10^{-8}$	5×10^{-9}	3×10^{-9}	3×10^{-9}

When this investigation was started in 1953, Mrs. R. D. Kuppermann carried out the early observations. We wish to express our thanks to her for this collaboration.

References

Glass, R. A., Thompson, S. G., and Seaborg, G. T., 1955, *J. Inorg. Nucl. Chem.*, **1**, 3.
Hahn, O., and Erbacher, O., 1926, *Phys. Z.*, **16**, 531.
Perlman, I., Ghiorso, A., and Seaborg, G. T., 1950, *Phys. Rev.*, **77**, 26.

On a New Phenomenon in Activated Nitrogen

By J. BERKOWITZ
Department of Physics, University of Chicago

MS. received 3rd December 1956, *and in revised form 7th March* 1957

A new phenomenon associated with an a.c. arc discharge through nitrogen gas at several cm Hg pressure has recently been reported by Stanley (1955). He describes the phenomenon as follows:

"With nitrogen at a pressure of a few mm Hg and a current of about 10 mA an ordinary glow discharge was observed; a red positive column filled the capillary and the electrodes were immersed in the usual blue volume glow. At slightly higher pressure, a red core . . . appeared at the centre of the blue glow, and as the pressure was further increased the red core became larger, while the blue glow dwindled, until eventually the red core extended well beyond the boundary of the blue glow."

This 'red core' which is subsequently described as an orange beam, could be made at least 10 cm long, and exhibited the spectra of the First Negative and First and Second Positive bands of nitrogen. From the flow rate through his capillary, Stanley deduced that the lifetime of the beam was *c.* 5×10^{-4} sec, and hence concluded that the molecular states emitting this radiation were not flowing out of the arc, but had to be formed subsequently. By directing a second stream of nitrogen gas at the beam, he caused it to 'bend and waver', providing evidence that excitation was not being caused by low wavelength photons radiating from the discharge, but rather some material constituent of the gas stream.

Stanley suggested that this material constituent might be the metastable $A^3\Sigma_u^+$ state of N_2. This proposal was apparently motivated in large part by the experiments of Muschlitz and Goodman (1955) which yielded $2{\cdot}3 \times 10^{-4}$ second as the lifetime of this state.

It is difficult to reconcile the observed spectra with an energy carrier such as $A^3\Sigma_u^+$. The First Negative bands require 18·75 ev of excitation energy while the Second Positive bands must obtain 12 ev. Even the First Positive system is excited by *c.* 10 ev above the ground state, whereas the available electronic excitation energy of the $^3\Sigma$ is only *c.* 6 ev. If $^3\Sigma$ were the only species exciting the orange beam afterglow, a rather complicated accumulation of energy would need to be postulated to excite the First Negative bands.

Some recent electron impact work directed at determining the lifetime of the $^3\Sigma$ state (Lichten 1956) has produced evidence that the experiments of Muschlitz and Goodman may have been unintentionally producing the $a^1\Pi_g$ state. The electronic excitation energy of this state is slightly higher than that of $^3\Sigma$, but the energy deficits are substantially the same for the $a^1\Pi_g$. In addition, a multiplicity change would then be necessary to convert this to the radiating $^3\Pi_g$ state.

An alternative explanation for this phenomenon proposed herein considers the presence of molecular ions. Mass spectrometric study (Luhr 1933) has shown that ions corresponding to N_2^+, N_3^+ and N_4^+ can be expected under Stanley's experimental conditions. If ions of N_2^+ are present in sufficient concentration, they can give rise to the observed spectra by:

(1) Absorbing a relatively small amount of energy (3·17 ev), perhaps by electron interaction, to excite the First Negative bands. An alternative source of excitation of N_2^+ may involve collision with the $A^3\Sigma_u^+$ or $a^1\Pi_g$ metastable states.

(2) Supplying their energy of recombination with electrons (15·58 ev) to excite the Second and First Positive systems. This might occur by the sequence of reactions

(*a*) $N_2^+ + N_2 \longrightarrow N_4^+$,

(*b*) $N_4^+ + e^- \longrightarrow N_2^* + N_2$,

or by the one-step, three-body reaction

(*c*) $N_2^+ + e^- + N_2 \longrightarrow N_2^* + N_2$.

The asterisk refers to the upper state of the Second or First Positive band system.

If N_3^+ and N_4^+ emanate from the arc discharge in substantial concentration, reaction (*b*) might be expected to be most rapid. An alternative method of exciting the Second and First Positive band systems involves the dissociative recombination reaction

(*d*) $N_2^+ + e^- \longrightarrow N^* + N$,

where N^* refers to the ^2D or ^2P state of atomic nitrogen. The dissociative recombination process is purported to have a large cross section (Loeb 1955). Subsequent inverse predissociation of $N^* + N$ or $N + N$ can then give rise to the Second and First Positive systems.

The available experimental data (Loeb 1955) on electron–ion recombination are in approximate agreement with the lifetime of this glow reported by Stanley. For the case where recombination is the dominant process causing loss of electrons, we have

$$dn^+/dt = -\alpha n^+ n^-$$

where n^+, n^- are the concentrations of positive and negative charges (in this instance electrons) and α is the recombination coefficient. Assuming electrical neutrality in the beam, we have

$$-\frac{1}{n_2^+} + \frac{1}{n_1^+} = -\alpha t$$

where n_1^+, n_2^+ are the initial and final concentrations of positive charges. The important determinant in this calculation is the minimum detectable effect due to N_2^+, i.e. n_2^+. If we take this to be 10^9 ions cm^{-3}, and the initial concentration is at least one order of magnitude greater, we obtain $-10^{-9} = -\alpha t$.

The best value of α currently available (Loeb 1955) appears to be about 10^{-6}. This gives $t = 10^{-3}$ second, in rough agreement with Stanley's figure. The agreement is probably fortuitous, however. Reliable ion–electron recombination coefficients in very pure nitrogen gas are not available. If impurities having large electron affinities are present, most of the electrons will quickly be absorbed to form negative ions, and the positive ion decay will proceed via positive ion–negative ion recombination. In this regard, it is of interest to note that Stanley reports the spectra of NH, OH and NO impurities in his afterglow. Reaction 2(*d*) above is another mechanism which has the effect of removing N_2^+ from the reaction. The sparse experimental data available (Flügge 1956) indicate that either of the last named mechanisms may give rise to the observed afterglow lifetime. Hence, although no conclusion can be drawn regarding the mechanism of decay of N_2^+, current experimental results on nitrogen (under similar conditions of pressure, and probably purity, as those of Stanley's experiments) indicate a lifetime similar to that of Stanley's afterglow.

His observation that all three spectral bands appeared to have approximately the same decay time is further evidence for a single particle being responsible for all the excitations, as suggested above.

Herman, Salmona and Lucas (1956) have recently come to the conclusion that an afterglow of short duration in nitrogen may be ionically induced. No specific reference to any afterglow experiments is made by these authors other than to state that the lifetime they are considering is *c.* 10^{-4} second. Their analysis of the population of vibrational levels in the $C^3\Pi_u$ and $B^3\Pi_g$ electronic states suggests that the Second and First Positive band systems are emitted in a cascade process which may have been initiated by ion–electron recombination. They suspect the presence of other band systems in the infra-red and far ultraviolet regions, corresponding to energy levels above $C^3\Pi_u$. The distinction between direct and indirect recombination made by these authors is not altogether clear. In the case of direct recombination they assume the formation of the C or B states as direct products of the elementary ion–electron recombination process. The indirect recombination process appears to involve more highly excited electronic states than $C^3\Pi_u$, which they coalesce into a hypothetical state H. It is regrettable that Herman, Salmona and Lucas could not be more explicit in their discussion regarding the formation of the states equivalent to H. This recombination process would presumably either require a third body, as suggested above, or involve an inverse predissociation into a more stable molecular state.

Evidence for N_2^+ as the primary energy vehicle in this afterglow is thus threefold: (1) the excitation energy required, (2) the approximate lifetime, (3) the sequence of spectral bands observed.

If the radiation emanating from this orange beam is ionically induced, it provides a rather attractive system for the study of some recombination coefficient, depending upon which mechanism is dominant. The phenomenon described by Stanley appears to have the advantage of being free of wall effects. A mass spectrometric study similar to that performed on the Lewis–Rayleigh afterglow by Berkowitz, Chupka and Kistiakowsky (1956) would probably be of considerable help in shedding more light on the nature of the orange beam. A simpler and more direct experimental test would be an attempt to deflect the orange beam with electrostatic deflectors, if the discharge could be kept from striking the deflectors.

ACKNOWLEDGMENT

The author wishes to thank the Office of Ordnance Research, United States Army, for sponsoring this research.

REFERENCES

BERKOWITZ, J., CHUPKA, W. A., and KISTIAKOWSKY, G. B., 1956, *J. Chem. Phys.*, **25**, 457.

FLÜGGE, S., editor, 1956, *Handbuch der Physik*, Vol. 21, *Electron Emission. Gas Discharges I.* (Berlin : Springer), p. 483.

HERMAN, E., SALMONA, A., and LUCAS, S., 1956, *C. R. Acad. Sci., Paris*, **243**, 1029.

LICHTEN, W. H., 1956, *J. Chem. Phys.*, **26**, 306.

LOEB, L., 1955, *Basic Processes of Gaseous Electronics* (University of California Press), p. 562.

LUHR, O., 1933, *Phys. Rev.*, **44**, 459.

MUSCHLITZ, E. E., Jr., and GOODMAN, L., 1955, *J. Chem. Phys.*, **21**, 2213.

STANLEY, C. R., 1955, *Proc. Phys. Soc.* A, **68**, 709.

CONTENTS OF SECTION B

PAGE

Dr. S. M. MAKIN, Mr. A. H. ROWE and Mr. A. D. LECLAIRE. Self-Diffusion in Gold 545

Dr. C. HURST. Phase Changes of the Second Order 553

Dr. M. S. LONGUET-HIGGINS. A Statistical Distribution arising in the Study of the Ionosphere 559

Dr. J. M. LOCK. The Magnetic Susceptibilities of Lanthanum, Cerium, Praseodymium, Neodymium and Samarium, from 1·5°K to 300°K 566

Mr. H. N. V. TEMPERLEY. The Statistical Mechanics of the Steady State . . 577

Dr. J. E. PARROTT. Some Contributions to the Theory of Electrical Conductivity, Thermal Conductivity and Thermoelectric Power in Semiconductors . . 590

Dr. F. R. LIPSETT and Dr. R. KING. The Effect of Thin Films of Gold on the Mechanical Properties of Cadmium Single Crystals 608

Research Notes :

Mr. KRISHNAJI and Mr. G. P. SRIVASTAVA. Temperature Variation of Microwave Absorption Coefficient in Ethyl Chloride 621

Dr. D. A. CHRISTOFFEL. The Effect of Grain Size on the Magnetothermal Properties of Ferrites 623

Letters to the Editor :

Dr. B. BLEANEY and Dr. W. HAYES. Paramagnetic Resonance of Impurities in NaF 626

Mr. B. V. PARANJAPE. Field Dependence of Mobility in Semiconductors . 628

Reviews of Books 630

Contents of Section A 640

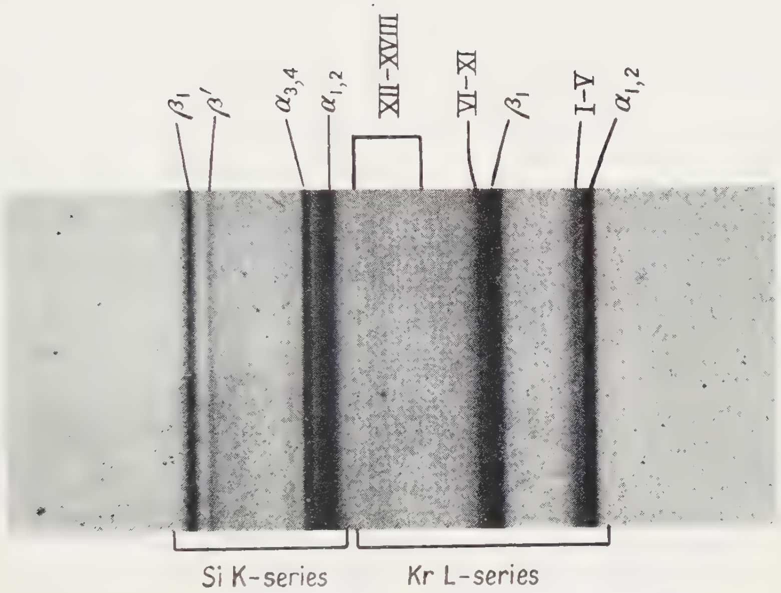

Figure 2. Spectrogram of the krypton L-series lines and some silicon K-series lines.

Hyperfine Structure in Manganese $^{55}_{25}$Mn

By G. K. WOODGATE and J. S. MARTIN
Clarendon Laboratory, Oxford

Communicated by H. G. Kuhn; MS. received 29th March 1957

Abstract. The hyperfine structure of the ground state $3d^54s^2\ ^6S_{5/2}$ of ^{55}Mn has been measured in a resonance experiment with an atomic beam. The value 5/2 for the nuclear spin has been confirmed by measurements in weak fields. The magnetic dipole interval factor is $A(^6S_{5/2}) = 72{\cdot}422 \pm 0{\cdot}002$ Mc/s. There is no departure from the interval rule outside experimental error.

---

§ 1. Introduction

The hyperfine structures of some of the lines in the spectrum of Mn I have been measured optically by a number of workers, for example, White and Ritschl (1930), Fisher and Peck (1939) and Murakawa (1955). Of these, only White and Ritschl assigned a non-zero splitting to the ground level, whose configuration is $3d^54s^2\ ^6S_{5/2}$. This ground level should have no hyperfine structure in the absence of perturbations, but according to White and Ritschl does have an interval factor $A(^6S_{5/2}) \simeq 60$ Mc/s.

We have determined this interval factor by a resonance experiment in an atomic beam for two reasons: first, a knowledge of this quantity together with the accurately known value of the nuclear magnetic moment of ^{55}Mn (Proctor and Yu 1951, Sheriff and Williams 1951) would lead to a value of the magnetic moment of the odd–odd isotope ^{56}Mn if the interval factor of the ground level of ^{56}Mn were to be measured in an experiment similar to ours; secondly, a better interpretation of the optical measurements of hyperfine structure in the excited states of ^{55}Mn can be made if the structure of the ground level (which is unresolved optically) is known.

§ 2. Apparatus

The apparatus was that used by Woodgate and Hellwarth (1956) with the following modifications : the target for radioactive detection was replaced by an electron-bombardment ionizing detector; a mass-spectrometer, electron-multiplier and synchronous detector were added, and a mechanical beam-chopper was fitted in the oven chamber.

The ionizer was a slight modification of the model first described by Wessel and Lew (1953). The ionized atoms were accelerated in the direction of the original beam into a mass spectrometer fitted on the end of the main vacuum chamber. The electron multiplier was of the Allen type with electrodes of beryllium–copper, and was obtained from the Atomic Energy Research Establishment, Harwell.

For the purpose of increasing the signal to noise ratio in this detection system, the beam was interrupted at a frequency of about 80 c/s as follows: a brass disc of three inches diameter with forty radial teeth and slots was mounted in front of the oven slit. This disc was fixed to a shaft which passed through the end wall of the oven chamber via a Wilson seal and was driven by a motor at about two revolutions per second. Fixed to the same shaft, but outside the vacuum chamber, was an iron disc similar to the brass beam chopper; its teeth passed between two small pole-pieces attached to an earphone magnet. The alternating voltage induced in the magnet coil was the reference signal for the synchronous detector. Phase adjustment consisted in changing the angular position of the pole-pieces with respect to the shaft axis.

Power oscillators made in the laboratory were used to excite the radio-frequency field. Frequencies between 200 Mc/s and 400 Mc/s were measured as follows: harmonics were generated from the 10 Mc/s signal of a G.E.C. standard frequency generator, and were mixed in a crystal diode with part of the signal from the power oscillator. The difference frequency was measured with a BC 221 frequency meter. The G.E.C. oscillator frequency never differed by more than 15 c/s from that of the laboratory frequency standard, and the BC 221 meter was checked against the G.E.C. oscillator. The accuracy of frequency measurement was better than 1 kc/s.

§ 3. THE SPECTRUM

The ground level of ^{55}Mn has the configuration $3d^54s^2\ {}^6S_{5/2}$ with a g_J of about 2. The nuclear spin is 5/2 (White and Ritschl 1930) and the nuclear magnetic moment is positive.

In zero field there are six hyperfine structure levels, labelled by $F=5$ to 0 of which the level $F=0$ is the lowest. These are split up by the application of an external magnetic field into thirty-six states which we label by F, m_F. Magnetic dipole transitions, denoted by the symbol $(F, m_F \longleftrightarrow F', m_F')$, in which $\Delta F=0, \pm 1$, $\Delta m_F = \pm 1$ (π transitions) or $\Delta F = \pm 1$, $\Delta m_F = 0$ (σ transitions), may be observed between the magnetic states, with the extra condition that m_J must change sign if the transition is to be observed in a straightforward 'flop-in' experiment such as ours. This condition simplifies the spectrum but does not reduce the amount of useful information obtainable.

§ 4. RESULTS

The π lines $(5, -2 \longleftrightarrow 5, -3)$, $(4, -1 \longleftrightarrow 4, -2)$ and $(3, 0 \longleftrightarrow 3, -1)$ which all have the same frequency at very weak fields were used to confirm that the nuclear spin of ^{55}Mn is 5/2. Their frequencies were measured at fields up to about 70 gauss, at which field the line $(5, -2 \longleftrightarrow 5, -3)$ was resolved from the lines $(4, -1 \longleftrightarrow 4, -2)$ and $(3, 0 \longleftrightarrow 3, -1)$. The results of a relatively imprecise measurement of these frequencies led to an estimated value for the magnetic interval factor $A(^6S_{5/2})$ of 70 to 75 Mc/s. No precise measurements were attempted at this or at a higher field because inhomogeneities in the C field (that in which transitions are induced) broadened the field-dependent lines. We are therefore unable to give an experimental value for g_J at present, but we hope to measure this quantity with an improved apparatus.

Of the five hyperfine structure separations in zero field, the upper three were calculated from measurements at very weak fields of the σ lines $(5, -2 \longleftrightarrow 4, -2)$, $(4, -1 \longleftrightarrow 3, -1)$ and $(3, 1 \longleftrightarrow 2, 1)$ which are independent of field to first order. The second order field dependence of the first two lines gave rise to very small corrections at the fields used (one to two gauss), and was calculated from perturbation theory. In order to measure the third line it was necessary to use a field large enough to resolve it from the two neighbouring lines (3, 2 ⟷ 2, 2) and (3, 0 ⟷ 2, 0). At this field (about 6·35 gauss) the above procedure was inadequate, and the secular equation had to be solved numerically. In this calculation of the corrections the effect of small terms involving g_I were neglected and g_J was assumed to have the value 2.

The three upper hyperfine structure separations in zero field for ^{55}Mn are shown in the following table, together with the number of measurements made on each of the lines from which the separations are derived.

Designation	$\Delta\nu_1(F=5 \longleftrightarrow F=4)$	$\Delta\nu_2(F=4 \longleftrightarrow F=3)$	$\Delta\nu_3(F=3 \longleftrightarrow F=2)$
Frequency (Mc/s)	$362{\cdot}123 \pm 0{\cdot}010$	$289{\cdot}676 \pm 0{\cdot}010$	$217{\cdot}260 \pm 0{\cdot}015$
Number of measurements	35	63	18

Each measurement was the mean of a pair of frequencies at equal intensity on either side of the peak of a resonance curve.

The field was measured by means of the field-dependent σ lines (2, 1 ⟷ 1, 1) and (2, −1 ⟷ 1, −1) of ^{41}K, and at the same time the field-independent line (2, 0 ⟷ 1, 0) of ^{41}K was measured. From this measurement the hyperfine structure separation for ^{41}K was calculated. The most reliable results for manganese were taken to be those for which the calculation of the hyperfine structure separation of ^{41}K gave an answer well within the limits of the published value 254·018 ± 0·006 Mc/s (Kusch and Taub 1949, Ochs, Logan and Kusch 1950). Thus, for manganese 10 of the 35 measurements of $\Delta\nu_1$ and 15 of those of $\Delta\nu_2$ were given greater weight than the others in taking averages. Three different radio-frequency loops were used, and the results for each line were consistent irrespective of the loop. The line width was about 170 kc/s. The limits of error of ± 10 kc/s are intended to be a reasonable fraction of the line width. These limits are in this sense arbitrarily chosen, but they are consistent with the day-to-day variations of the measurements. The larger limits, ± 15 kc/s, for $\Delta\nu_3$ include the errors introduced by the approximations made in calculating the larger field correction for this line.

Since the measurements lead to the determination of three hyperfine structure separations, these may be interpreted in terms of three constants: the magnetic dipole interval factor A, the electric quadrupole constant B, and the magnetic octupole constant C, where the notation is that of Jaccarino *et al.* (1954). These are

$$\begin{aligned} A &= 72{\cdot}422 \pm 0{\cdot}002 \text{ Mc/s},\\ B &= 0{\cdot}013 \pm 0{\cdot}028 \text{ Mc/s},\\ C &= 0{\cdot}0014 \pm 0{\cdot}0018 \text{ Mc/s}. \end{aligned}$$

B and C are therefore effectively zero within our limits of error, and there is no departure from the interval rule. C is likely to be much too small to be measured with the precision which we have reached. The vanishing of B is consistent with a perturbation of the ground state by another $^6S_{5/2}$ state for which there can be no quadrupole interaction.

In the light of our measurements, the values of A for the three terms quoted by Murakawa (1955) have to be modified by 10 to 15%, though his values of B remain unaffected (Brix 1952).†

We do not propose to measure the hyperfine structure of the odd odd isotope ^{56}Mn which emits β- and γ-rays with a half-life of 2·6 hours because we are not equipped to handle strongly radioactive material, but from other points of view this would be a feasible experiment. ^{56}Mn can be easily produced by neutron bombardment of ^{55}Mn. It is easy to evaporate, and would be detected by radioactive counting methods.

---

† We are grateful to Dr. G. Nöldeke for drawing our attention to the paper by P. Brix.

ACKNOWLEDGMENTS

One of the authors (G. K. W.) would like to thank Imperial Chemical Industries for a Research Fellowship; the other (J. S. M.) is indebted to the Rhodes Trust for the grant of a scholarship. We are also grateful to Dr. Lew for sending us the blueprints of his ionizer.

REFERENCES

BRIX, P., 1952, *Z. Phys.*, **132,** 579.

FISHER, R. A., and PECK, E. R., 1939, *Phys. Rev.*, **55,** 270.

JACCARINO, V., KING, J. G., SATTEN, R. A., and STROKE, H. H., 1954, *Phys. Rev.*, **94,** 1798.

KUSCH, P., and TAUB, H., 1949, *Phys. Rev.*, **75,** 1477.

MURAKAWA, K., 1955, *J. Phys. Soc. Japan*, **10,** 336.

OCHS, S. A., LOGAN, R. A., and KUSCH, P., 1950, *Phys. Rev.*, **78,** 184.

PROCTOR, W. G., and YU, F. C., 1951, *Phys. Rev.*, **81,** 20.

SHERIFF, R. E., and WILLIAMS, D., 1951, *Phys. Rev.*, **82,** 651.

WESSEL, G., and LEW, H., 1953, *Phys. Rev.*, **92,** 641.

WHITE, H. E., and RITSCHL, R., 1930, *Phys. Rev.*, **35,** 1146.

WOODGATE, G. K., and HELLWARTH, R. W., 1956, *Proc. Phys. Soc.* A, **69,** 581.

The Oscillator Strengths of the 1sσ–2pπ, 2pπ–2sσ and 2pπ–3dσ Transitions of HeH^{2+}

By A. M. ARTHURS and J. HYSLOP
Department of Applied Mathematics, The Queen's University of Belfast

Communicated by D. R. Bates ; MS. received 26th November 1956

Abstract. The oscillator strengths of the 1sσ–2pπ, 2pπ–2sσ and 2pπ–3dσ transitions of HeH^{2+} are calculated from the exact two-centre wave functions. A comparison is made with results obtained from the LCAO approximation with and without mixing, both the dipole length and dipole velocity formulae being used in each case.

§ 1. Introduction

Since the publication of the exact two-centre electronic wave functions for a number of states of HeH^{2+} (Bates and Carson 1956) various properties of the molecule have been investigated and comparison made with results obtained from approximate wave functions (Moiseiwitsch and Stewart 1956, McCarroll and Moiseiwitsch 1957, Dalgarno and Lynn 1957). In particular the oscillator strengths of the 1sσ–2sσ, 1sσ–3dσ and 2sσ–3dσ transitions have been evaluated (Dalgarno, Lynn and Williams 1956). These transitions are of the *parallel* type and it is desirable to extend the calculations to transitions of the *perpendicular* type.

§ 2. Calculations

2.1.

If the nuclei are regarded as held fixed at a distance R apart, the oscillator strength associated with the transition from a lower electronic state A to an upper electronic state B is

$$f(\mathrm{A{-}B}\,|\,R)=\tfrac{1}{3}E(\mathrm{A{-}B}\,|\,R)\;G(\mathrm{A{-}B})\,|\underset{\sim}{Q}(\mathrm{A}-\mathrm{B}\,|\,R)|^2, \qquad \ldots\ldots(1)$$

where $E(\mathrm{A}-\mathrm{B}\,|\,R)$ is the vertical energy difference, or photon energy, $E_{\mathrm{B}}-E_{\mathrm{A}}$, measured in rydbergs; $G(\mathrm{A}-\mathrm{B})$ is the orbital degeneracy factor† (Mulliken 1939); and $\underset{\sim}{Q}(\mathrm{A}-\mathrm{B}\,|\,R)$ is the transition integral given by

$$\underset{\sim}{Q}^{\mathrm{L}}(\mathrm{A}-\mathrm{B}\,|\,R)\,\mathbf{t}=\int \chi_{\mathrm{B}}{}^{*}(\mathbf{r}\,|\,R)\,\mathbf{r}\,\chi_{\mathrm{A}}(\mathbf{r}\,|\,R)\,d\mathbf{r} \qquad \ldots\ldots(2)$$

in the dipole length formulation, and by

$$\underset{\sim}{Q}^{\mathrm{V}}(\mathrm{A}-\mathrm{B}\,|\,R)\,\mathbf{t}=-\frac{2}{E(\mathrm{A}-\mathrm{B}\,|\,R)}\int \chi_{\mathrm{B}}{}^{*}(\mathbf{r}\,|\,R)\,\nabla\,\chi_{\mathrm{A}}(\mathbf{r}\,|\,R)\,d\mathbf{r} \qquad \ldots\ldots(3)$$

in the dipole velocity formulation (Chandrasekhar 1945), χ_{A} and χ_{B} being the electronic wave functions of the states indicated, $\mathbf{r}$ being the position vector of the electron relative to an arbitrary origin and $\mathbf{t}$ being some unit vector.

2.2.

The exact two-centre wave functions of HeH^{2+} can be written in the form

$$\chi(\mathbf{r}\,|\,R)=\Lambda(\lambda\,|\,R)\,M(\mu\,|\,R)\,\Phi(\phi), \qquad \ldots\ldots(4)$$

---

† G (A–B) is equal to 2 for $\sigma-\pi$ transitions, and 1 for $\pi-\sigma$ transitions.

in which λ and μ are confocal elliptic coordinates and ϕ is the azimuthal angle. Λ and M can be obtained from the tables of Bates and Carson (1956); and Φ is unity for σ-states and $\cos\phi$ or $\sin\phi$ for π-states.

With exact wave functions $\underset{\sim}{Q}^{\mathrm{L}}$ and $\underset{\sim}{Q}^{\mathrm{V}}$ are naturally identical and the superscripts may therefore be omitted. On substituting equation (4) into formula (2) (which is rather simpler than (3)), it is seen that for σ–π transitions

$$\underset{\sim}{Q}(\mathrm{A}-\mathrm{B}\,|\,R)=\pi(R/2)^4\left[\int_1^{\infty}\lambda^2(\lambda^2-1)^{1/2}\Lambda_{\mathrm{A}}\Lambda_{\mathrm{B}}\,d\lambda\int_{-1}^{+1}(1-\mu^2)^{1/2}M_{\mathrm{A}}M_{\mathrm{B}}\,d\mu\right.$$
$$\left.-\int_1^{\infty}(\lambda^2-1)^{1/2}\Lambda_{\mathrm{A}}\Lambda_{\mathrm{B}}\,d\lambda\int_{-1}^{+1}\mu^2(1-\mu^2)^{1/2}M_{\mathrm{A}}M_{\mathrm{B}}\,d\mu\right], \quad \ldots\ldots(5)$$

the wave functions being normalized according to

$$(R/2)^3\int_1^{\infty}\int_{-1}^{+1}\int_0^{2\pi}\Lambda^2M^2\Phi^2(\lambda^2-\mu^2)\,d\lambda\,d\mu\,d\phi=1. \quad \ldots\ldots(6)$$

While analytical evaluation of the integrations is possible, it is much less laborious to use numerical methods.

2.3.

The LCAO approximations to the wave functions of the $1s\sigma$, $2p\pi$, $2s\sigma$ and $3d\sigma$ states of HeH^{2+} have the form

$$\left.\begin{aligned}\chi(1s\sigma)&=\psi(1s_{\mathrm{a}})\\ \chi(2p\pi)&=\psi(2p_{x_{\mathrm{a}}})\\ \chi(2s\sigma)&=l(R)\,\psi(2s_{\mathrm{a}})+m(R)\,\psi(2p_{z_{\mathrm{a}}})\\ \chi(3d\sigma)&=m(R)\,\psi(2s_{\mathrm{a}})-l(R)\,\psi(2p_{z_{\mathrm{a}}})\end{aligned}\right\} \quad \ldots\ldots(7)$$

where

$$\left.\begin{aligned}\psi(1s_{\mathrm{a}})&=(8/\pi)^{1/2}\exp(-2r_{\mathrm{a}})\\ \psi(2p_{x_{\mathrm{a}}})&=(\pi)^{-1/2}r_{\mathrm{a}}\exp(-r_{\mathrm{a}})\sin\theta_{\mathrm{a}}\cos\phi_{\mathrm{a}}\\ \psi(2s_{\mathrm{a}})&=(\pi)^{-1/2}(1-r_{\mathrm{a}})\exp(-r_{\mathrm{a}})\\ \psi(2p_{z_{\mathrm{a}}})&=(\pi)^{-1/2}r_{\mathrm{a}}\exp(-r_{\mathrm{a}})\cos\theta_{\mathrm{a}}\end{aligned}\right\} \quad \ldots\ldots(8)$$

$\mathbf{r}_{\mathrm{a}}$ being the position vector of the electron referred to the helium nucleus A as origin, and l and m being parameters satisfying the normalization condition $l^2+m^2=1$ and determined by minimizing the electron energy given in rydbergs by

$$E=-\int\chi^*\left(\nabla^2+\frac{4}{r_{\mathrm{a}}}+\frac{2}{r_{\mathrm{b}}}\right)\chi\,d\mathbf{r}, \quad \ldots\ldots(9)$$

where $\mathbf{r}_{\mathrm{b}}$ is the position vector of the electron referred to the hydrogen nucleus B.

Substitution of equations (7) into formulae (2) and (3) gives

$$\left.\begin{aligned}\underset{\sim}{Q}^{\mathrm{L}}(1s\sigma\text{–}2p\pi\,|\,R)&=0{\cdot}372468\\ \underset{\sim}{Q}^{\mathrm{L}}(2p\pi\text{–}2s\sigma\,|\,R)&=-(1{\cdot}5)\,l(R)\\ \underset{\sim}{Q}^{\mathrm{L}}(2p\pi\text{–}3d\sigma\,|\,R)&=-(1{\cdot}5)\,m(R)\end{aligned}\right\} \quad \ldots\ldots(10)$$

$$\left.\begin{aligned}\underset{\sim}{Q}^{\mathrm{V}}(1s\sigma\text{–}2p\pi\,|\,R)&=\frac{1.11740}{E(1s\sigma-2p\pi|R)}\,,\\ \underset{\sim}{Q}^{\mathrm{V}}(2p\pi\text{–}2s\sigma\,|\,R)&=0\\ \underset{\sim}{Q}^{\mathrm{V}}(2p\pi\text{–}3d\sigma\,|\,R)&=0\end{aligned}\right\} \quad \ldots\ldots(11)$$

2.4.

At infinite nuclear separation the 2sσ, 3dσ and 2pσ states have the same energy, so that it is to be anticipated that considerable mixing of the LCAO representations of these states will occur at finite values of R. In addition then to the ordinary LCAO approximation of § 2.3, refinements of the LCAO wave functions, which take account of this mixing (Dalgarno and Lynn 1957), were used in the calculation of the 2pπ–2sσ and 2pπ–3dσ transition integrals. Apart from noting that no evidence was found in support of the expectation that interchange of the labelling of the 2sσ and 3dσ states would improve the agreement between the exact and approximate curves (cf. Dalgarno and Lynn 1957), it does not seem of value to present the results obtained for they are poorer than those derived from the ordinary LCAO approximation, being entirely of the wrong form.

§ 3. Results and Discussion

3.1.

Figures 1, 2 and 3 show the calculated values of the 1sσ–2pπ, 2pπ–2sσ and 2pπ–3dσ transition integrals, $\underset{\sim}{Q}$ being obtained from the exact wave functions and $\underset{\sim}{Q}^{L}$ and $\underset{\sim}{Q}^{V}$ from the LCAO approximation.†

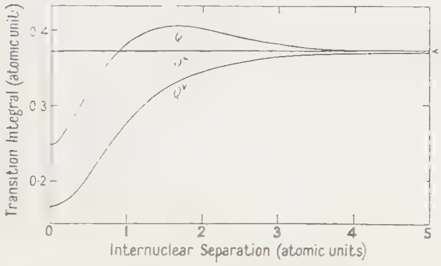

Figure 1. 1sσ–2pπ transition integral.

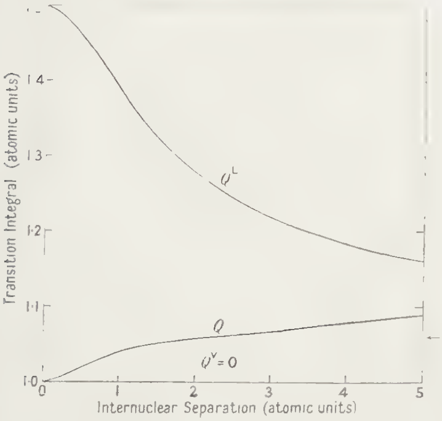

Figure 2. 2pπ–2sσ transition integral.

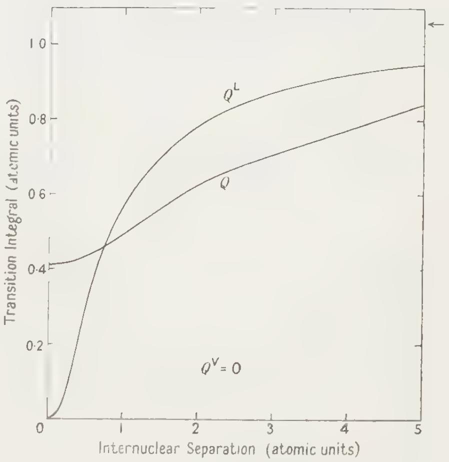

Figure 3. 2pπ–3dσ transition integral.

$\underset{\sim}{Q}$ refers to the exact values and $\underset{\sim}{Q}^{L}$ and $\underset{\sim}{Q}^{V}$ to the LCAO approximation. Arrows indicate the asymptotic values of the transition integrals.

---

† In computing $\underset{\sim}{Q}^{V}$ from formulae (3) the exact value of the photon energy was used rather than the approximate value.

The agreement between the exact and approximate values of the three transition integrals is unsatisfactory. For the 1sσ–2pπ transition the values of both $\underset{\sim}{Q}^{\mathrm{L}}$ and $\underset{\sim}{Q}^{\mathrm{V}}$ are reasonably accurate in the region $R > 2{\cdot}5$; but in the region $R < 2{\cdot}5$ $\underset{\sim}{Q}^{\mathrm{L}}$, which is constant, does not describe the essential features of the exact $\underset{\sim}{Q}$, which rises steeply from zero slope at $R=0$, while $\underset{\sim}{Q}^{\mathrm{V}}$ underestimates $\underset{\sim}{Q}$ considerably. In the case of the 2pπ–2sσ transition $\underset{\sim}{Q}^{\mathrm{L}}$ has entirely the wrong form, but is becoming more accurate with increase of R. The values of $\underset{\sim}{Q}^{\mathrm{V}}$ for the transitions 2pπ–2sσ and 2pπ–3dσ are both zero everywhere, except in the latter case where a point of indeterminancy occurs due to the crossing of the energy curves associated with the 2pπ and 3dσ states. For $R > 1{\cdot}5$, $\underset{\sim}{Q}^{\mathrm{L}}(2\mathrm{p}\pi\text{–}3\mathrm{d}\sigma \mid R)$ has roughly the same variation as $\underset{\sim}{Q}$, but for $R < 1{\cdot}5$, it falls off very rapidly to zero with decreasing R, crossing the exact curve in the region of $R = 0{\cdot}75$.

3.2.

The oscillator strengths obtained by substituting $\underset{\sim}{Q}$ into (1) are given in the table. $f(1\mathrm{s}\sigma\text{–}2\mathrm{p}\pi \mid R)$ is large as is to be expected since the transition is intense in both the united-atom and separated-atoms limits. Since the sum of the oscillator strengths of perpendicular transitions originating at the 1sσ level is 2/3, other transitions of the 1sσ–$nl\pi$ series must have considerable oscillator strengths. An analogous result holds in the case of the 1sσ_{g}–$nl\pi_{\mathrm{u}}$ series of $\mathrm{H}_2{}^+$ (Bates, Darling, Hawe and Stewart 1953). The 2pπ–2sσ and 2pπ–3dσ transitions are of the *sub-rydberg* type (Herzberg 1950) and the corresponding f values vary rapidly with nuclear separation. The change in sign of $f(2\mathrm{p}\pi\text{–}3d\sigma \mid R)$ occurs because of the crossing of the 2pπ and 3dσ energy curves.

Transitions involving the 2pσ state are of a type of special interest in astrophysical applications, and work on them and on other properties of HeH^{2+} is in progress.

Photon Energies ΔE and Oscillator Strengths f of some Transitions of HeH^{2+}

	1sσ–2pπ		2pπ–2sσ		2pπ–3dσ	
R (atomic units)	ΔE	f	ΔE	f	ΔE	f
0·00	6·75000	0·277	0·00000	0·0000	1·25000	0·0696
0·25	6·03512	0·310	0·07679	0·0260	1·23058	0·0708
0·50	5·14486	0·352	0·16233	0·0561	1·17969	0·0741
1·00	4·01008	0·392	0·24039	0·0868	1·02823	0·0831
1·5	3·46987	0·381	0·24661	0·0909	0·84910	0·0898
2·0	3·22510	0·346	0·22511	0·0840	0·65678	0·0864
2·5	3·11435	0·316	0·19526	0·0735	0·46391	0·0705
3·0	3·06230	0·296	0·16528	0·0628	0·29293	0·0491
3·5	3·03668	0·286	0·13844	0·0531	0·15928	0·0292
4·0	3·02346	0·280	0·11578	0·0449	0·06404	0·0128
4·5	3·01625	0·278	0·09723	0·0381	0·00076	0·0001
5·0	3·01203	0·277	0·08228	0·0326	−0·03842	−0·0091
∞	3·00000	0·277	0·00000	0·0000	0·00000	0·0000

ACKNOWLEDGMENTS

The writers are indebted to Professor D. R. Bates for suggesting this problem and for his continual interest and encouragement as the work progressed. They also wish to thank Dr. A. Dalgarno for helpful advice, particularly in connection with the approximate calculations.

Finally, they acknowledge the receipt of research grants from Antrim County Education Committee.

REFERENCES

BATES, D. R., and CARSON, T. R., 1956, *Proc. Roy. Soc.* A, **234,** 207.

BATES, D. R., DARLING, R. T. S., HAWE, S. C., and STEWART, A. L., 1953, *Proc. Phys. Soc.* A, **66,** 1124.

CHANDRASEKHAR, S., 1945, *Astrophys. J.*, **102,** 223.

COULSON, C. A., 1952, *Valence* (Oxford : Clarendon Press).

DALGARNO, A., and LYNN, N., 1957, *Proc. Phys. Soc.* A, **70,** 176.

DALGARNO, A., LYNN, N., and WILLIAMS, E. J. A., 1956, *Proc. Phys. Soc.* A, **69,** 610.

HERZBERG, G., 1950, *Spectra of Diatomic Molecules*, 2nd Edn. (London : Macmillan).

MCCARROLL, R. W., and MOISEIWITSCH, B. L., 1957, *Proc. Phys. Soc.* A, **70,** 507.

MOISEIWITSCH, B. L., and STEWART, A. L., 1956, *Proc. Phys. Soc.* A, **69,** 480.

MULLIKEN, R. S., 1939, *J. Chem. Phys.*, **7,** 14.

A Box Variational Method for Scattering Phases

By I. C. PERCIVAL
Department of Physics, University College London

Communicated by H. S. W. Massey; MS. received 4th March 1957

Abstract. The paper presents a variational method for calculating elastic s-wave scattering phases for short-range potentials, based on the Rayleigh–Ritz method for discrete energy levels, in which the approximate phase approaches the exact phase from below. The method is applied to scattering of electrons by the static field of the hydrogen atom.

§ 1. Introduction

Variational methods which have been used to determine elastic scattering phases (e.g. Hulthén 1944, Schwinger 1947, Kohn 1948) are based on variational principles for which the phase is stationary but not necessarily a maximum or a minimum. Kato (1951), Kohn (1954), Kikuta (1954) and others have shown how upper and lower bounds to the phase may be obtained, but the determination of these bounds usually requires additional labour.

The variational principle for the energy in a discrete spectrum is essentially a minimum principle. In the following sections this principle is applied to the system obtained by placing a scattered particle and a short-range spherical potential in a concentric spherical box. The result is a variational principle for s-waves, in which both phase and energy are allowed to vary, and the approximate phase approaches the exact phase from below.

§ 2. s-wave Scattering

The radial equation for s-wave scattering by a fixed spherically symmetric potential $V(r)$ is of the form

$$[H-E]F(k, r)=0, \qquad \text{......(1)}$$

where

$$H=-\frac{1}{2}\frac{d^2}{dr^2}+V(r), \qquad \text{......(2)}$$

k is the wave number, and $E=\frac{1}{2}k^2$ the energy of the scattered particle in appropriate units. The radial wave function $F(k, r)$ is zero at the origin and finite as $r \to \infty$. If for $\gamma < 2$

$$r^{\gamma}V(r) \to 0 \qquad (r \to \infty), \qquad \text{......(3)}$$

then $F(k, r)$ has the asymptotic form

$$F(k, r) \sim \sin(kr+\eta) \qquad \text{......(4)}$$

apart from an arbitrary constant multiplier. η is the zero-order scattering phase, and the s-wave contribution to the total cross section is $Q_S=(4\pi/k^2)\sin^2\eta$ in the same units as k^{-2}.

η is so far undefined to the extent that $\pm n\pi$ with n integral may be added to it without affecting any physical results. We shall define η uniquely as that solution of (4) which is a continuous function $\eta(k)$ of k such that $\eta \to 0$ as $k \to \infty$.

§ 3. Solutions within a Box

We initially make the additional assumption that for some R_0

$$V(r)=0 \qquad (r>R_0). \qquad \ldots\ldots(5)$$

This is probably never satisfied exactly for any physical system, but is a useful approximation for short-range potentials.

The energy spectrum for the system S_1 represented by equation (1) with the above boundary conditions will be similar to that of figure 1 (*a*). The number of discrete energy levels is dependent on V, and will be zero if V is repulsive. η and k are defined only for energies in the continuum.

Let S_1 be placed in a spherical box of radius R, centred at the origin, where

$$R>R_0 \qquad \ldots\ldots(6)$$

$$R>-\frac{\partial\eta}{\partial k}\cdot \qquad \text{(all } k\text{)}. \qquad \ldots\ldots(7)$$

It has been shown by Wigner (1955), (see also Corinaldesi and Zienau 1956) that (7) follows from (6) in the classical limit. Although the theory which follows requires the validity of (7), in practice a prior knowledge of $\partial\eta/\partial k$ is not generally necessary for the methods to be described, the inequality (6) being sufficient to enable a suitable choice of R to be made.

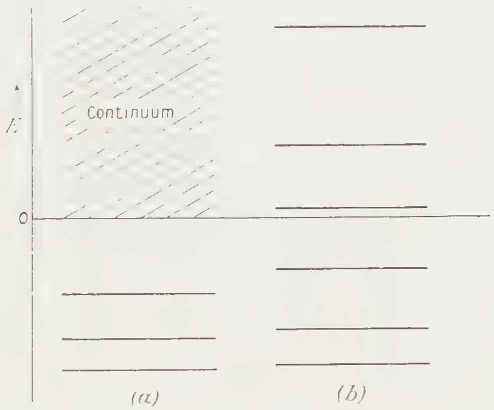

Figure 1. (*a*) Energy spectrum for typical system S_1 represented by the solutions of equation (1) with boundary conditions appropriate to the scattering problem. (*b*) Spectrum for system S_2 which consists of S_1 in a spherical box of radius R and is represented by solutions of equation (1) with fixed logarithmic derivative at the box.

The wave function F for the new system S_2 is defined only for $0\leqslant r\leqslant R$. Now let the logarithmic derivative at the box,

$$L=\frac{1}{F(k,r)}\frac{\partial F(k,r)}{\partial r}, \qquad (r=R) \qquad \ldots\ldots(8)$$

be fixed. The two cases which will be considered in detail are $L=0$, $L=\infty$. Then S_2 will have an energy spectrum such as that in figure 1 (*b*). Where the two systems S_1 and S_2 have the same energy E they will be represented inside the box by the same function $F(k, r)$, apart from a possible constant factor. Generally E will be in the continuous spectrum of S_1, and this is the only case that we shall consider.

§ 4. THE SPECTRUM AND THE PHASE

Let i be used to distinguish the states of S_2 for a given value of L, E_i being the ith energy level, and k_i the corresponding wave number of the system S_1 when $E_i \geqslant 0$. A set of wave functions $F(k_i, r)$ with $0 \leqslant r < \infty$ for the system S_1 may now be obtained by fitting the wave functions representing the states of S_2 on to the corresponding solutions of (1) for $r \geqslant R$ with boundary condition (8) at $r = R$. But these solutions are proportional to $\sin(k_i r + \eta_i)$, where $\eta_i = \eta(k_i)$, and the boundary condition furnishes the relation

$$\eta(k_i) = (I + n_i)\pi - k_i R, \qquad (n_i = 0, \pm 1, \pm 2, \ldots) \qquad \ldots\ldots(9)$$

where $I = i - \frac{1}{2}\delta_{L0}$ $(L = 0, \infty)$. It is proved in the Appendix that $n_i = 0$, so that

$$\eta(k_i) = I\pi - k_i R. \qquad \ldots\ldots(10)$$

Thus the phase $\eta(k_i)$ may be obtained from the boundary condition at the box, and the wave number k_i or the energy E_i, without any further knowledge of the function $F(k_i, r)$ within the box, and the spectrum of the system S_2 provides a set of scattering phases for S_1.

§ 5. THE RAYLEIGH–RITZ METHOD

The wave functions in a discrete spectrum, unlike those in a continuum, may be obtained by direct application of the variational principle for the energy. For the system S_2, $F(k_i, r)$ are those functions which are zero at the origin, satisfy the boundary condition (8), for which

$$\int_0^R F^*(k_i, r) F(k_i, r) dr = 1, \qquad \ldots\ldots(11)$$

and

$$E = \int_0^R F^*(k_i, r) H F(k_i, r) dr \qquad \ldots\ldots(12)$$

is stationary for variations in F consistent with the subsidiary conditions.

Approximate functions F may be obtained by restricting them to be of the form $\phi_i(a_{i1}, a_{i2}, \ldots, a_{iN}; r)$, where ϕ_i is a fixed function of the variables a_{ij} and r; a_{ij} are then determined from the variational principle.

When ϕ_i is of the form

$$\phi_i(a_{i1}, a_{i2}, \ldots, a_{iN}; r) = \sum_{j=1}^{N} a_{ij} u_j(r), \quad (i = 1, 2, \ldots, N) \qquad \ldots\ldots(13)$$

and $u_j(r)$ are an orthonormal set within the box obeying the required boundary conditions, the Rayleigh–Ritz method may be employed, whereby the approximate energy levels E_i' are obtained as the eigenvalues of the $N \times N$ matrix

$$H_{ij} = \int_0^R u_i^*(r) H u_j(r) dr. \qquad \ldots\ldots(14)$$

If $u_i(r)$ are finite for $R < r < \infty$ this may be put in the alternative form

$$H_{ij} = -\tfrac{1}{2}\int_0^R u_i^*(r) \frac{d^2}{dr^2} u_j(r) dr + \int_0^\infty u_i^*(r) V(r) u_j(r) dr. \qquad \ldots\ldots(15)$$

For positive E_i' an approximation $\eta'(k_i')$ for the scattering phase, where $k_i'^2 = 2E_i'$, is then obtainable from the equation

$$\eta'(k_i') = \pi I - k_i' R \qquad (L = 0, \infty). \qquad \ldots\ldots(16)$$

When $u_i(r)$, $(i = 1, 2, \ldots)$ form a *complete* orthonormal set, then $E_i' \to E_i$ as $N \to \infty$, $k_i' \to k_i$ and

$$\eta'(k_i') \to \eta(k_i), \qquad (N \to \infty). \qquad \ldots\ldots(17)$$

§ 6. The Phase Inequality

MacDonald (1933) has proved that if the successive energy levels of a discrete spectrum are

$$E_1 \leqslant E_2 \leqslant \ldots \leqslant E_N \leqslant E_{N+1} \leqslant \ldots, \qquad \ldots\ldots(18)$$

and a set of Rayleigh–Ritz approximate energy levels are

$$E_1' \leqslant E_2' \leqslant \ldots \leqslant E_N', \qquad \ldots\ldots(19)$$

then

$$E_i' \geqslant E_i \qquad (i=1, 2, \ldots, N). \qquad \ldots\ldots(20)$$

This is a generalization of the minimum property of the energy integral (11) when F is the ground state wave function.

Let the 'local phase' at R be

$$\zeta(k)=kR+\eta(k) \qquad \ldots\ldots(21)$$

and let

$$\zeta'(k_i')=k_i'R+\eta'(k_i'). \qquad \ldots\ldots(22)$$

Then ζ is a continuous function of k, so from (7) $\partial\zeta/\partial k>0$ and, using (20), $\zeta(k_i') \geqslant \zeta(k_i)$. But from equations (10) and (16)

$$\zeta'(k_i')=\zeta(k_i)=I\pi. \qquad \ldots\ldots(23)$$

Therefore

$$\zeta'(k_i') \leqslant \zeta(k_i') \text{ and } \eta'(k_i') \leqslant \eta(k_i').$$

In words, the approximate phase for the approximate energy obtained by the Rayleigh-Ritz method is never greater than the exact phase *for that energy*.

It also follows from (20), (21), (22) and (23) that

$$\eta'(k_i') \leqslant \eta(k_i), \qquad \ldots\ldots(24)$$

but this inequality is not of such practical value, since in using the method the exact k_i is not obtained. However, (17) and (24) show that the exact phase is stationary and a maximum.

§ 7. The Momentum Representation

Throughout this and subsequent sections it will be supposed that $L=0$ or $L=\infty$. In each case the most natural choice for $u_i(r)$ is the undistorted s-wave:

$$u_i(r)=\sqrt{\frac{2}{R}}\sin I\kappa r \qquad \ldots\ldots(25)$$

where $\kappa R=\pi$. ......(26)

The phases may conveniently be obtained from the eigenvalues $E_i^0=2\kappa^{-2}E_i'$ of the matrix with elements

$$H_{ij}^0=2\kappa^{-2}H_{ij}=I^2\delta_{ij}+2V_{ij} \qquad \ldots\ldots(27)$$

where

$$V_{ij}=U_{\frac{1}{2}(I+J)}-U_{\frac{1}{2}(I-J)} \qquad \ldots\ldots(28)$$

$$J=j-\tfrac{1}{2}\delta_{L0} \qquad \ldots\ldots(29)$$

$$U_q=\frac{2}{\kappa\pi}\int_0^R V(r)\sin^2 q\kappa r\,dr \qquad \ldots\ldots(30)$$

$$=\frac{2}{\kappa\pi}\int_0^\infty V(r)\sin^2 q\kappa r\,dr \qquad \ldots\ldots(31)$$

$$=-\frac{q}{\pi}\eta_{\text{Born}}(q\kappa). \qquad \ldots\ldots(32)$$

Thus the Born phases at intervals of $\frac{1}{2}\kappa$ may be used to obtain more exact phases for a set of slightly different energies using the matrix (27) with $L=0, \infty$.

This procedure is equivalent to the use of the *discrete* momentum representation *within the box*, and avoids the difficulties associated with the singularity in the integral equations of the continuous momentum representation obtained by letting $R \rightarrow \infty$. Calculation is reduced to a minimum if R is made as small as possible consistent with the inequalities (6) and (7) and the set of phases required.

§ 8. General Short-Range Potentials

In practice the condition (5) may be relaxed, and the box variational method applied to potentials which satisfy only (3). The box radius R should then be chosen so that $V(r)$ is 'small' for r greater than R, in the sense to be described.

The methods of § 5 and § 7 may then be carried out exactly as before. But (14) and (15) are not equivalent when (5) is not satisfied, and the question arises as to which gives the more accurate phase. We shall consider only the limit as $N \rightarrow \infty$. Then calculations based on equation (14) give the exact phase for the approximate potential

$$V'(r) \begin{cases} = V(r) & (r < R) \\ = 0 & (r > R). \end{cases}$$

If $V(r)$ for $r > R$ is sufficiently small to be considered as a perturbation on the Hamiltonian, the first-order error $\delta\eta(k_i)$ due to using $V'(r)$ in place of $V(r)$ is

$$\delta\eta(k_i) = \eta(V', k_i) - \eta(V, k_i) = \frac{2}{k_i}\int_0^\infty V(R+r)\sin^2(k_i r + I\pi)\,dr.$$

If $u_i^*(2nR \pm r)u_j(2nR \pm r)$ is independent of the integer n and the variable sign (e.g. $u_i = (2/R)^{1/2}\sin I\kappa r$), then calculations based on equation (15) give the exact phase for the potential

$$V''(r) \begin{cases} = V(r) + V(2R-r) + V(2R+r) + V(4R-r) + \dots & (r < R) \\ = 0 & (r > R). \end{cases}$$

Generally, the first-order error due to using $V''(r)$ in place of $V(r)$ will be small compared with $\delta\eta(k_i)$ above, although the actual error is not so simple to estimate. It may be concluded that for $u_i(r)$ of this type, if no correction is to be made to the phase, (15) is preferable to (14), and the corresponding equations (31) and (32) are preferable to (30).

§ 9. Application to Hydrogen

The box variational method was applied to the s-wave scattering of electrons by the static field

$$V(r) = -\left(1 + \frac{1}{r}\right)e^{-2r} \qquad \text{(atomic units)}$$

of the ground state of the neutral hydrogen atom, neglecting exchange. The momentum representation within a box of radius $R = \pi/2$ was used, with boundary conditions $L = 0, \infty$ at the box, and $N = 3$. The potential matrix was evaluated by equation (32), and no attempt was made to apply a correction to the phase. The only significant labour was the calculation of the Born phases for $k = 1, 2, \dots 6$ atomic units, and of the eigenvalues of two 3×3 matrices.

In figure 2 the results are compared with the Born and with the exact phases of McDougall (1932), which he obtained by numerical integration of the differential equation. For small k the agreement with the exact phases is good, in spite of the large 'tail' to the potential ($V(\pi/2)\simeq 0{\cdot}1$) and the small number of terms in the expansion (13). Poor values of the phase for large k, where i is near its maximum value N, are to be expected, since these are most affected by the truncation of the expansion at $i=N$. In this region the Born approximation is usually applicable.

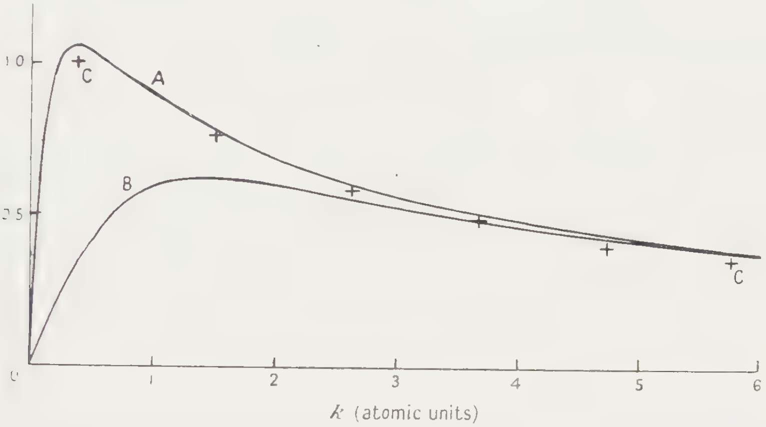

Figure 2. s-wave phases for scattering by the static field of the neutral hydrogen atom, neglecting exchange, plotted against wave number k, in atomic units. A, exact, from McDougall (1932). B, Born. C, box variation, using the momentum representation within the box: $R=\pi/2$ atomic units, $N=3$.

ACKNOWLEDGMENTS

I wish to thank Mr. L. Castillejo and Dr. M. J. Seaton for their helpful discussions and criticisms.

APPENDIX

To prove

$$\eta(k_i)=I\pi+k_iR, \qquad (\text{all } i). \qquad \ldots\ldots(\text{A1})$$

Let $\zeta=\zeta(k)$ be defined by equation (21). Then from (9)

$$\zeta(k_i)=(I+n_i)\pi \qquad (n_i=0,\ \pm 1,\ \pm 2,\ldots) \qquad \ldots\ldots(\text{A2})$$

and $\zeta(k)$ is a continuous function of k for which, by (7):

$$\frac{\partial\zeta}{\partial k}>0. \qquad \ldots\ldots(\text{A3})$$

The Rayleigh–Ritz method, with undistorted waves as basic functions (see § 7) may be applied to $F(k, r)$ within the box. If the rank N of the Hamiltonian matrix is sufficiently large and $0\ll i\ll N$, then

$$k_i'\simeq k_i \qquad \ldots\ldots(\text{A4})$$

$$\eta(k_i)\ll 1 \qquad \ldots\ldots(\text{A5})$$

$$I^2\kappa^2\gg U_q\kappa^2,\ U_I\kappa^2\ll 1 \qquad (\text{all } q) \qquad \ldots\ldots(\text{A6})$$

so that by applying perturbation theory to the Hamiltonian matrix it follows that

$$E_i' \simeq \tfrac{1}{2} I^2 \kappa^2 \qquad \ldots\ldots (A7)$$

$$k_i' \simeq I\kappa, \qquad \ldots\ldots (A8)$$

where the errors obtained by replacing the inequalities in (A4, A8) by equalities are small compared with unity. From (A4), (A5), (A8), (21) and (26), $\zeta(k_i) \simeq I\pi$. But n_i must be integral so by (A2), for sufficiently large i,

$$\zeta(k_i) = I\pi. \qquad \ldots\ldots (A9)$$

Now by using (A2) and (A3), the value of i may be reduced by unit steps, and the inequality $\zeta(k_i) \leqslant I\pi$ may be shown to hold for all i.

Suppose that

$$\zeta(k_i) < I\pi. \qquad \ldots\ldots (A10)$$

Then by (A9) there must be a highest i for which (A10) is valid. For this value of i, $\zeta(k_{i+1}) = (I+1)\pi$. But as ζ is a continuous function of k there will be some k'' between k_i and k_{i+1} such that $\zeta(k'') = I\pi$. This implies that the solution $F(k,'' r)$ of (1) has logarithmic derivative L at the box, which is impossible as E_{i+1} is the $(i+1)$th energy level of S_2.

Therefore

$$\zeta(k_i) = I\pi \qquad (\text{all } i)$$

$$n_i = 0 \qquad (\text{all } i)$$

and the result (A1) then follows from equation (9).

References

Corinaldesi, E., and Zienau, S., 1956, *Proc. Camb. Phil. Soc.*, **52,** 599.
Hulthén, L., 1944, *Kungl. Fysiog. Sällk. Lund Förh.*, **14,** 257.
Kato, T., 1951, *Progr. Theor. Phys.*, **6,** 394.
Kikuta, T., 1953, *Progr. Theor. Phys.*, **12,** 225.
Kohn, W., 1948, *Phys. Rev.*, **74,** 1763 ; 1954, *Rev. Mod. Phys.*, **26,** 292.
MacDonald, J. K. L., 1933, *Phys. Rev.*, **43,** 830.
McDougall, J., 1932, *Proc. Roy. Soc.* A, **136,** 549.
Schwinger, J., 1947, *Phys. Rev.*, **72,** 742.
Wigner, E. P., 1955, *Phys. Rev.*, **98,** 145.

Properties of the Hydrogen Molecular Ion VII : Magnetic Dipole Oscillator Strengths of the $1s\sigma_g$–$3d\pi_g$ Transition

By A. DALGARNO and R. McCARROLL
Department of Applied Mathematics, Queen's University of Belfast

Communicated by D. R. Bates ; MS. received 19th November 1956

Abstract. The magnetic dipole oscillator strengths of the $1s\sigma_g$–$3d\pi_g$ transition of H_2^+ are computed over a wide range of nuclear separations from the exact two-centre wave functions. A brief discussion is given of some related quantities and reasons are presented for supposing that the average values of the energy separations in second order expressions involving magnetic quantities are larger than for the analogous electric quantities.

---

§ 1. Introduction

A considerable collection of data on *electric* dipole transition probabilities of molecules has been provided in recent years by Bates and his collaborators (Bates 1951, Bates, Öpik and Poots 1953, Bates, Darling, Hawe and Stewart 1953, 1954, Lewis, McDowell and Moiseiwitsch 1955, Dalgarno, Lynn and Williams 1956) but no precise information is available on *magnetic* dipole transition probabilities.

Apart from their intrinsic interest, the matrix elements involved occur in theoretical expressions for the magnetic susceptibility (cf. Van Vleck 1932), for Λ- and ρ-type doubling (Van Vleck 1929) and for rotational magnetic moments (cf. Ramsey 1956).

§ 2. Theory

2.1.

The Einstein spontaneous emission coefficient $A(\mathrm{p}, \mathrm{q})$ for a magnetic dipole transition connecting an upper level p with a lower level q is given by the formula

$$A(\mathrm{p},\mathrm{q}) = \frac{32\pi^3\nu^3}{3c^3\hbar\,\omega_\mathrm{p}} S \qquad \ldots\ldots(1)$$

where c is the velocity of light, h is Planck's constant, ν is the frequency of the radiation emitted, ω_p is the statistical weight of the upper level, and S is the strength of the line, given by

$$S = \sum_{i,j} S(\mathrm{p}_i, \mathrm{q}_j) \qquad \ldots\ldots(2)$$

$S(\mathrm{p}_i, \mathrm{q}_j)$ being the strength of the component joining state p_i of one level to state q_j of the other and the summation being carried out over all components (cf. Condon and Shortley 1935). Condon (1934) has shown that

$$S(\mathrm{p}_i, \mathrm{q}_j) = \left| \int \Psi_{\mathrm{p}_i}^{\,*} \mathbf{M} \Psi_{\mathrm{q}_j}\, d\mathbf{r} \right|^2 \qquad \ldots\ldots(3)$$

with

$$\mathbf{M} = -\frac{e\hbar}{2mc}(\mathbf{L} + g\mathbf{S}) \qquad \ldots\ldots(4)$$

where **L** and **S** are the resultant orbital and resultant spin angular momenta, respectively, in units of $\hbar$, m and e are the electronic mass and charge, and the electronic g factor equals 2·00229 (Koenig, Prodell and Kusch 1952).

Neglecting spin–orbit interactions and rotational distortions, the selection rules for a diatomic molecule are

$$\Delta\Omega = \Delta(\Lambda+\Sigma) = \pm 1 \qquad \ldots\ldots(5)$$

Λ and Σ denoting the components of **L** and **S**, respectively, along the internuclear axis, and in addition for homonuclear molecules only g–g and u–u transitions are allowed (Van Vleck 1934).

In analogy with electric dipole radiation we introduce the dimensionless magnetic dipole oscillator strength

$$f_{\mathrm{m}}(\mathrm{p},\mathrm{q}) = \frac{4\pi m \Delta E}{3\hbar e^2 \omega_{\mathrm{q}}} S \qquad \ldots\ldots(6)$$

where ω_{q} is the statistical weight of the lower level. If energy is measured in rydbergs, (6) becomes

$$f_{\mathrm{m}}(\mathrm{p},\mathrm{q}) = \frac{\alpha^2 \Delta E}{12\omega_{\mathrm{q}} S} \qquad \ldots\ldots(7)$$

where α is the fine-structure constant and ΔE is the energy of the emitted radiation.

2.2.

The exact two-centre wave functions of the $1s\sigma_{\mathrm{g}}$ and $3d\pi_{\mathrm{g}}$ states of H_2^+ may be written

$$\Psi(1s\sigma_{\mathrm{g}}) = \Lambda_1(\lambda)\, M_1(\mu) \qquad \ldots\ldots(8)$$

$$\Psi(3d\pi_{\mathrm{g}}) = (\lambda^2-1)^{1/2}\Lambda_2(\lambda)\, M_2(\mu) \begin{Bmatrix} \sin\phi \\ \cos\phi \end{Bmatrix} \qquad \ldots\ldots(9)$$

where λ and μ are confocal elliptical coordinates, ϕ is the azimuthal angle and Λ_1 Λ_2, M_1, and M_2 can be obtained from the tables prepared by Bates, Ledsham and Stewart (1953), and if the z-axis is taken along the internuclear axis and the origin of coordinates is taken at the centre of mass of the nuclei, the components of orbital angular momentum may be written

$$L_x = i\sin\phi \frac{(\lambda^2-1)^{1/2}(1-\mu^2)^{1/2}}{(\lambda^2-\mu^2)} \left\{ \mu\frac{\partial}{\partial\lambda} - \lambda\frac{\partial}{\partial\mu} \right\} + i\cos\phi \frac{\lambda\mu}{(\lambda^2-1)^{1/2}(1-\mu^2)^{1/2}} \frac{\partial}{\partial\phi} \qquad \ldots\ldots(10)$$

$$L_y = -i\cos\phi \frac{(\lambda^2-1)^{1/2}(1-\mu^2)^{1/2}}{\lambda^2-\mu^2} \left\{ \mu\frac{\partial}{\partial\lambda} - \lambda\frac{\partial}{\partial\mu} \right\} + i\sin\phi \frac{\lambda\mu}{(\lambda^2-1)^{1/2}(1-\mu^2)^{1/2}} \frac{\partial}{\partial\phi} \qquad \ldots\ldots(11)$$

$$L_z = -i\frac{\partial}{\partial\phi}. \qquad \ldots\ldots(12)$$

The strength of the $1s\sigma_{\mathrm{g}}$–$3d\pi_{\mathrm{g}}$ electronic transition ($\Delta\Lambda = \pm 1$) is then given by twice the square of the matrix element

$$\frac{\pi R^3}{8} \left\{ \int_1^\infty (\lambda^2-1)\Lambda_2 \frac{\partial\Lambda_1}{\partial\lambda}\, d\lambda \int_{-1}^{+1} (1-\mu^2)^{1/2}\mu\, M_1 M_2\, d\mu - \int_1^\infty \lambda(\lambda^2-1)\Lambda_2\Lambda_1\, d\lambda \int_{-1}^{+1} (1-\mu^2)^{1/2} M_2 \frac{\partial M_1}{\partial\mu}\, d\mu \right\}. \qquad \ldots\ldots(13)$$

The evaluation of the integrations over λ in (13) is best done numerically. In practice the labour was not excessive since many of the derivatives had been computed previously for other purposes (McCarroll and McDowell 1955, Dalgarno and McCarroll 1956).

§ 3. Results and Discussion

3.1.

The magnetic dipole oscillator strengths obtained are shown in table 1 which includes for comparison purposes the electric dipole oscillator strengths f_e of the $1s\sigma_g$–$2p\pi_u$ transition (Bates, Darling, Hawe and Stewart 1953) and of the $1s\sigma_g$–$4f\sigma_u$ transition (Bates *et al.* 1954), the former of which is allowed in the united-atom limit ($R=0$) and the latter of which is forbidden. At the equilibrium separation of the $1s\sigma_g$ state, the order of magnitude of f_m is about 10^{-6} times that of the strong electric transition and about 10^{-2} times that of the weak electric transition. The variation with nuclear separation is in marked contrast to that of electric dipole oscillator strengths, for f_m increases without limit as R increases, the asymptotic form of (13) being $8\sqrt{2}R/81$ (see § 4). Radiation theory which leads to (1) is of course only applicable when the wavelength of the radiation is much greater than the linear dimensions of the molecule (cf. Condon and Shortley 1935).

Table 1. Oscillator Strengths of Some Transitions in $H_2{}^+$

R	0·0	0·4	0·8	1·2	1·6	2·0	3·0	4·0	5·0
f_m ($1s\sigma_g$–$3d\pi_g$)	0	$2·6\times10^{-10}$	$4·26\times10^{-9}$	$2·19\times10^{-8}$	$6·94\times10^{-8}$	$1·67\times10^{-7}$	$7·59\times10^{-7}$	$2·01\times10^{-6}$	$3·91\times10^{-6}$
f_e ($1s\sigma_g$–$2p\pi_u$)	0·28	0·32	0·37	0·41	0·44	0·46	0·48	0·465	0·43
f_e ($1s\sigma_g$–$4f\sigma_u$)	0	$1·3\times10^{-8}$	$3·2\times10^{-7}$	$2·5\times10^{-6}$	$1·2\times10^{-5}$	$4·1\times10^{-5}$	$4·4\times10^{-4}$	$2·7\times10^{-3}$	$1·1\times10^{-2}$

3.2.

The 'high frequency' term of the magnetic susceptibility of molecules is proportional to $\Sigma_i{}'|(i\,|\,\mathbf{L}\,|\,f)|^2\,(E_i-E_f)$ where f denotes the fth excited state with energy E_f and the prime indicates that the $f=i$ term is excluded from the summation (Van Vleck 1932). The summation is usually evaluated by supposing E_i-E_f may be replaced by a constant and applying the closure property. The choice of average value of E_i-E_f is largely arbitrary. Van Vleck and Frank (1929) choose it by analogy with the electric case whilst Hylleraas and Skavlem (1950) evaluate a rather similar summation by assuming E_i-E_f can be replaced by E_i; this latter procedure is equivalent to taking the first term of the Lennard-Jones expansion (1930).

For the $1s\sigma_g$ state of $H_2{}^+$, $\Sigma_f{}'\,|(i\,|\,\mathbf{L}\,|\,f)|^2=(i\,|\,L^2\,|\,i)$ has been computed by McCarroll and McDowell (1955) and the results are shown in table 2 together with $S=|(1s\sigma_g\,|\,\mathbf{L}\,|\,3d\pi_g)|^2$. It is clear that the $3d\pi_g$ state does not contribute greatly at $R=2$ to the summation so that the correct average for E_i-E_f must be very much larger than E_i, in contrast to the electric case for which most of the contribution usually arises from the lowest term. Generalization to other molecules is rather uncertain (see however § 4) since $H_2{}^+$ is hardly a representative system, but it is of interest to note that agreement between the theoretical evaluation of the magnetic shielding constant of H_2 by Hylleraas and Skavlem (1950) and the measurements of Ramsey (1950) can only be obtained by assuming the average value of $E_i - E_f$ to be about $5E_i$.

Table 2. Matrix Elements of the Orbital Angular Momentum

R	0·0	0·4	0·8	1·2	1·6	2·0	3·0	4·0	5·0
$(1s\sigma_g \mid L^2 \mid 1s\sigma_g)$	0·0	4×10^{-3}	$2·7 \times 10^{-2}$		$1·65 \times 10^{-1}$	$2·88 \times 10^{-1}$	$8·21 \times 10^{-1}$	1·78	
$\lvert(1s\sigma_g \mid \mathbf{L} \mid 3d\pi_g)\rvert^2$	0·0	$1·8 \times 10^{-5}$	$3·6 \times 10^{-4}$	$2·2 \times 10^{-3}$	$7·9 \times 10^{-3}$	$2·1 \times 10^{-2}$	$1·3 \times 10^{-1}$	$4·0 \times 10^{-1}$	$8·9 \times 10^{-1}$

§ 4. ASYMPTOTIC CONSIDERATIONS

4.1.

That a large value for the average of $E_i - E_f$ is to be anticipated follows from a consideration of the asymptotic form of the transition integrals. Suppose that the initial state of a homonuclear molecule consists at infinite separation of two atoms of nuclei A and B respectively described by normalized wave functions $\psi_a(\mathbf{r}_a)$ and $\phi_b(\mathbf{r}_b)$ where $\mathbf{r}_a$ represents the position vectors of all the electrons of atom A relative to A and $\mathbf{r}_b$ the position vectors of all the electrons of atom B relative to B. Suppose further that the final state consists of two atoms in states described by wave functions $\psi_a'(\mathbf{r}_a)$ and $\phi_b'(\mathbf{r}_b)$ respectively. Then the matrix element of L_y connecting the initial and final states is approximated by

$$(i \mid L_y \mid f) = \int X_i^* \, L_y X_f \, d\mathbf{r} \qquad \ldots\ldots(14)$$

where

$$\begin{aligned} X_i &= \frac{1}{\sqrt{2}} \{\psi_a \phi_b \pm \psi_b \phi_a\} \\ X_f &= \frac{1}{\sqrt{2}} \{\psi_a' \phi_b' \pm \psi_b' \phi_a'\} \end{aligned} \qquad \ldots\ldots(15)$$

depending upon the symmetry. The expression (14) simplifies to

$$\begin{aligned} (i \mid L_y \mid f) &= \int \psi_a^* \phi_b^* \, L_y \psi_a' \phi_b' \, d\mathbf{r} \\ &\pm \int \psi_a^* \phi_b^* \, L_y \psi_b' \phi_a' \, d\mathbf{r} \end{aligned} \qquad \ldots\ldots(16)$$

which reduces for g–g and u–u transitions to

$$(i \mid L_y \mid f) = \int \psi_a^* \phi_b^* \, L_y \psi_a' \phi_b' \, d\mathbf{r} \qquad \ldots\ldots(17)$$

when the exponentially decreasing terms arising from the identity of the nuclei are ignored. The operator L_{yj} corresponding to any electron j can be written either as

$$(L_{yj})_a + \tfrac{1}{2} i R \, \partial/\partial x_{ja} \quad \text{or as} \quad (L_{yj})_b + \tfrac{1}{2} i R \, \partial/\partial x_{jb}$$

where $(L_{yj})_a$ and $(L_{yj})_b$ are the y components of the orbital angular momentum of the jth electron about A and B, respectively, and x_{ja} and x_{jb} are the x-coordinates of the jth electron referred to A and B respectively. It follows that (17) can be written

$$(i \mid L_y \mid f) = i \frac{R}{2} \int \psi_a^* \phi_b^* \, \Sigma \frac{\partial}{\partial x_j} \psi_a' \phi_b' \, d\mathbf{r} \qquad \ldots\ldots(18)$$

where the origin of x need no longer be specified since (18) is independent of it.

The integral (18) is related directly to the *electric* dipole transition integral $Q(i-f)$ in the dipole velocity formulation (cf. Chandrasekhar 1945) according to

$$Q(i-f) = -\frac{2}{E_i - E_f}\int X_i^* \sum_j \frac{\partial}{\partial x_j} X_f \, d\mathbf{r} \qquad \ldots\ldots(19)$$

so that

$$(i\,|\,L_y\,|\,f) = i\frac{R}{4}(E_i - E_f)\,Q(i-f). \qquad \ldots\ldots(20)$$

It is immediately clear that the average value ϵ_{m} of $E_i - E_f$ in the formula

$$\sum_f{}' \; |(i\,|\,L_y\,|\,f)^2/(E_i - E_f) = \frac{|(i\,|\,L_y^2\,|\,i)|}{\epsilon_{\mathrm{m}}} \qquad \ldots\ldots(21)$$

will be much greater than that in the analogous electric expression

$$\sum_f{}' \; |(i\,|\,x\,|\,f)^2/(E_i - E_f) = \frac{|(i\,|\,x^2\,|\,i)|}{\epsilon_{\mathrm{e}}} \qquad \ldots\ldots(22)$$

for (21) can be written

$$\sum{}'(i\,|\,L_y\,|\,f)^2/(E_i - E_f) = \frac{R^2}{16}\sum(E_i - E_f)\,Q(i-f)^2 \qquad \ldots\ldots(23)$$

and (22) can be written

$$\sum_f{}' \; |(i\,|\,x\,|\,f)|^2/(E_i - E_f) = \sum\frac{Q(i-f)^2}{(E_i - E_f)}. \qquad \ldots\ldots(24)$$

The right-hand side of (23) can be summed using the Thomas–Kuhn electric dipole oscillator strength sum rule and gives

$$\sum{}' \, |(i\,|\,L_y\,|\,f)^2/(E_i - E_f) = \frac{R^2}{16}N \qquad \ldots\ldots(25)$$

where N is the total number of electrons in the molecule. Since for atoms in S states $|(i\,|\,L_y^2\,|\,i)|$ equals $(R^2/12)\,T_{\mathrm{e}}$ at infinite separation, T_{e} being the total electronic kinetic energy of the two atoms (Van Vleck 1936, Dalgarno and McCarroll 1956) it follows that for such cases

$$\lim_{R\to\infty} \epsilon_{\mathrm{m}} = \frac{4T_{\mathrm{e}}}{3N} = \frac{4}{3N}\,|E_i| \qquad \ldots\ldots(26)$$

by the quantal virial theorem. In the case of the ground state of H_2^+, $\epsilon_{\mathrm{m}}(\infty)$ is 4/3 whereas $\epsilon_{\mathrm{e}}(\infty)$ is easily shown to be 8/9 (cf. Dalgarno and Lewis 1956).

4.2.

The asymptotic form of the transition integral connecting the $1s\sigma_g$ and $3d\pi_g$ states of H_2^+ is readily obtained from (20) to be $i8\sqrt{2}R/81$. The contribution of this term to $(i\,|\,L^2\,|\,i)$ is therefore $0{\cdot}039R^2$ at infinity compared with the total of $0{\cdot}167R^2$, the limiting ratio being 0·43. However, at the equilibrium separation, the $1s\sigma_g$–$3d\pi_g$ transition contributes only 0·07 of the total, as table 2 demonstrates, so that, bearing in mind the weighting factor $(E_i - E_f)^{-1}$, it seems that the average value of ϵ_{m} at $R = 2$ may well be as large as three or four times its value at infinity.

ACKNOWLEDGMENT

The authors are grateful to Professor D. R. Bates for his stimulating interest in these calculations.

REFERENCES

BATES, D. R., 1951, *J. Chem. Phys.*, **19,** 1122.

BATES, D. R., DARLING, R. T. S., HAWE, S. C., and STEWART, A. L., 1953, *Proc. Phys. Soc.* A, **66,** 1124 ; 1954, *Ibid.*, **67,** 533.

BATES, D. R., LEDSHAM, K., and STEWART, A. L., 1953, *Phil. Trans. Roy. Soc.* A, **246,** 215.

BATES, D. R., ÖPIK, U., and POOTS, G., 1953, *Proc. Phys. Soc.* A, **66,** 1113.

CHANDRASEKHAR, S., 1945, *Astrophys. J.*, **102,** 223.

CONDON, E. U., 1934, *Astrophys. J.*, **79,** 217.

CONDON, E. U., and SHORTLEY, G. H., 1935, *The Theory of Atomic Spectra* (Cambridge : University Press).

DALGARNO, A., and LEWIS, J. T., 1956, *Proc. Phys. Soc.* A, **69,** 57.

DALGARNO, A., LYNN, N., and WILLIAMS, E. J. A., 1956, *Proc. Phys. Soc.* A, **69,** 610.

DALGARNO, A., and MCCARROLL, R., 1956, *Proc. Roy. Soc.* A, **237,** 383.

HYLLERAAS, E., and SKAVLEM, S., 1950, *Phys. Rev.*, **79,** 117.

KOENIG, S. H., PRODELL, A. G., and KUSCH, P., 1952, *Phys. Rev.*, **88,** 191.

LENNARD-JONES, J. E., 1930, *Proc. Roy. Soc.* A, **129,** 598.

LEWIS, J. T., MCDOWELL, M. R. C., and MOISEIWITSCH, B. L., 1955, *Proc. Phys. Soc.* A, **68,** 565.

MCCARROLL, R., and MCDOWELL, M. R. C., 1955, *Proc. Phys. Soc.* A, **68,** 810.

RAMSEY, N. F., 1950, *Phys. Rev.*, **78,** 699 ; 1956, *Molecular Beams* (Oxford : Clarendon Press).

VAN VLECK, J. H., 1929, *Phys. Rev.*, **33,** 467 ; 1932, *Electric and Magnetic Susceptibilities* (Oxford : Clarendon Press) ; 1934, *Astrophys. J.*, **80,** 161 ; 1936, *J. Chem. Phys.*, **4,** 327.

VAN VLECK, J. H., and FRANK, A., 1929, *Proc. Nat. Acad. Sci., Wash.*, **15,** 539.

Approximate Molecular Orbitals: VI—The 2pσ state of HeH^{2+}

By R. McCARROLL and B. L. MOISEIWITSCH
Department of Applied Mathematics, The Queen's University of Belfast

Communicated by D. R. Bates ; MS. received 9th August 1956

Abstract. Approximate wave functions for the 2pσ state of the HeH^{2+} molecular ion are obtained by the variational method. The values of the electronic total energies and potential energies computed using the approximate wave functions are compared with the exact values of these quantities.

Exact values of the dipole moment are also obtained.

---

§ 1. Introduction

In paper V of this series (Moiseiwitsch and Stewart 1956), approximate wave functions for the 1sσ and 2pπ states of the He H^{2+} molecular ion were obtained using the variational method. These two states are the lowest with zero and unit angular momentum respectively about the internuclear axis. The present paper is concerned with a similar investigation of the 2pσ state of HeH^{2+}. This presents greater difficulty than the two preceding cases as it is not the lowest state of its own particular symmetry. Thus, in applying the variational method, it is necessary to use approximate wave functions which are orthogonal to the ground 1sσ state.

An assessment of the accuracy of the approximate wave functions is made by comparing the values obtained for the electronic energies and potential energies with the corresponding values obtained by using the exact two-centre wave functions (Bates and Carson 1956).

§ 2. Choice of Wave Functions

Caution has to be exercised in the choice of approximate wave functions for the 2pσ state of HeH^{2-} as the dissociation products in this particular case are an H atom and an α particle, contrary to the 1sσ and 2pπ states treated in the previous paper which both give rise to a proton and an He^{+} ion. Because of this behaviour an obvious approximation is

$$\Psi(2\mathrm{p}\sigma)=\psi_0+C\psi_1+\lambda\psi_2+\mu\psi_3, \qquad \ldots\ldots(1)\dagger$$

where

$$\psi_0=\frac{1}{\sqrt{\pi}}\exp(-r_{\mathrm{b}}), \qquad \ldots\ldots(2)$$

$$\psi_1=\sqrt{\frac{8}{\pi}}\exp(-2r_{\mathrm{a}}), \qquad \ldots\ldots(3)$$

$$\psi_2=\frac{1}{\sqrt{\pi}}r_{\mathrm{a}}\cos\theta_{\mathrm{a}}\exp(-r_{\mathrm{a}}), \qquad \ldots\ldots(4)$$

$$\psi_3=\frac{1}{\sqrt{\pi}}(1-r_{\mathrm{a}})\exp(-r_{\mathrm{a}}), \qquad \ldots\ldots(5)$$

---

† Here and elsewhere normalization factors are omitted.

$\mathbf{r}_a$ and $\mathbf{r}_b$ being the position vectors of the electron relative to the helium nucleus A and the proton B. Here, ψ_0 is the wave function of the 1s state of a hydrogen atom and ψ_1, ψ_2 and ψ_3 are the 1s, 2s and $2p_z$ wave functions of He$^+$. The function (1) is then the usual LCAO approximation which takes account of degeneracy at infinite nuclear separation. The term involving ψ_1 has been introduced so as to make the function approximately orthogonal to the ground 1sσ state of HeH^{2+}. It follows immediately that

$$C = -\int \psi_0(r_b)\psi_1(r_a)d\mathbf{r}. \qquad \ldots\ldots(6)$$

In the limit of small internuclear separations the 2pσ state of the HeH^{2+} molecular ion tends to the $2p_z$ state of Li^{2+}. This suggests adopting as the united atom approximation

$$\Psi(2p\sigma) = \left(\frac{243\alpha^5}{32\pi}\right)^{1/2} r\cos\theta \exp\{-\alpha(2r_a + r_b)/2\} + A\Psi(1s\sigma) \qquad \ldots\ldots(7)$$

where $\mathbf{r}$ is the position vector of the electron relative to the centre of charge of the constituent nuclei and where the parameter A is chosen so as to make (7) orthogonal to the best wave function for the 1sσ state of HeH^{2+} obtained in paper V, which is of the form

$$\Psi(1s\sigma) = \exp\{-\alpha'(2r_a + r_b)\} + p'\exp(-2\beta' r_a). \qquad \ldots\ldots(8)$$

It is desirable to use a trial wave function which has the proper behaviour at both large and small internuclear distances. This may be achieved by using a combination of function (7) with the separated atoms function

$$\Psi(2p\sigma) = \left(\frac{\beta^3}{\pi}\right)^{1/2} \exp(-\beta r_b) + B\Psi(1s\sigma) \qquad \ldots\ldots(9)$$

where B is chosen so as to make (9) orthogonal to the ground 1sσ state function (8). Such a combined function may be written in the form

$$\Psi(2p\sigma) = \left(\frac{243\alpha^5}{32\pi}\right)^{1/2} r\cos\theta \exp\{-\alpha(2r_a + r_b)/2\} + p\left(\frac{\beta^3}{\pi}\right)^{1/2} \exp(-\beta r_b)$$
$$+ (A + pB)\Psi(1s\sigma). \qquad \ldots\ldots(10)$$

§ 3. Description of Calculations

The values of the parameters λ, μ in function (1), and the parameters α, β and p in functions (7), (9) and (10) have been determined for $0 \leqslant R \leqslant 5$ by minimization of the electronic energy of the system

$$E = -\int \Psi^*\left(\nabla^2 + \frac{4}{r_a} + \frac{2}{r_b}\right)\Psi d\mathbf{r} \bigg/ \int \Psi^*\Psi d\mathbf{r}. \qquad \ldots\ldots(11)$$

The functions considered were of type (1) and also of type (10) with

(i) $p = \infty$, $\beta = 1$;
(ii) $p = \infty$, β variable;
(iii) $p = 0$, $\alpha = 1$;
(iv) $p = 0$, α variable;
(v) $\alpha = 1$, $\beta = 1$, p variable;
(vi) α as determined by (iv) and β by (ii), p variable.

The values of the energy E obtained with these functions can be compared with the exact values of these quantities calculated by Bates and Carson (1956). A further comparison can also be made by using the exact and approximate wave functions to calculate the potential energy

$$V = -\int \Psi^*\left(\frac{4}{r_a}+\frac{2}{r_b}\right)\Psi\, d\mathbf{r} \Big/ \int \Psi^*\Psi\, d\mathbf{r}. \qquad \ldots\ldots(12)$$

Finally, the exact wave functions are also used to compute the dipole moment integral

$$Z = \int \Psi^* z_b \Psi\, d\mathbf{r} \Big/ \int \Psi^*\Psi\, d\mathbf{r} \qquad \ldots\ldots(13)$$

where z_b is the cartesian coordinate of the electron referred to an axis with origin at the proton and directed towards the α particle.

§ 4. RESULTS

The values of λ, μ obtained for function (1) and the values of α, β, A, B, p obtained for functions (i) to (vi) are given in table 1. Table 2 compares the approximate values of the electronic energy E given by function (1) and functions (i) to (vi) with the exact values of E, while in table 3 a similar comparison is made for the potential energy V. Finally, displayed in table 4, are the values of the dipole moment integral Z calculated with the exact wave functions. All quantities are given in Hartree units.

Table 3. Potential Energies, V

R Function	0·0	0·5	1·0	2·0	3·0	4·0	5·0
(1)		4·156	5·012	4·057	3·266	2·889	2·700
(1A)			7·256	4·787	3·282	2·864	2·752
(i)		5·266	5·071	4·141	3·388	3·012	2·802
(ii)		2·576	6·467	4·612	3·547	3·051	2·822
(iii)	4·500	4·574	4·566	3·997	3·502	3·329	3·451
(iv)	4·500	4·995	5·490	4·590	3·578	2·788	2·428
(v)	4·500	4·643	4·768	4·059	3·353	2·980	2·779
(vi)	4·500	4·965	5·787	4·600	3·497	3·003	2·793
Exact	4·500	5·063	5·794	4·834	3·716	3·105	2·780

Table 4. Exact Dipole Moments, Z

R	0·0	0·5	1·0	2·0	3·0	4·0	5·0
Z	0·000	0·092	0·191	0·325	0·509	0·657	0·670

§ 5. DISCUSSION

As was to be expected the accuracy achieved for the $2p\sigma$ state of HeH^{2+} is not so good as for the $1s\sigma$ and $2p\pi$ states treated in the previous paper.

At large R the contribution to the electronic energy from polarization is much greater for the $2p\sigma$ state than for the $1s\sigma$ or $2p\pi$ states. Functions (i) and (ii) make only a small allowance for it. Consequently the separated atoms approximation is not nearly so satisfactory for the $2p\sigma$ state as for the ground state or the $2p\pi$ state. Function (1), which includes contributions from the degenerate 2s and $2p_z$ states of He^+, makes fuller allowance for polarization and gives better results over the whole range of R than either function (i) or (ii).

Calculations using function (1) with the orthogonality parameter taken to be zero have been carried out by Dalgarno and Lynn (1957). The values of the electronic energy and potential energy obtained by them are given in rows (1A)

Table 1. Parameters

Function	*R*	0·00	0·25	0·50	0·75	1·0	1·5	2·0	2·5	3·0	3·5	4·0	4·5	5·0
(1)	λ			0·729		0·230		0·102		0·251		0·281		0·238
	μ			0·050		0·277		0·154		−0·075		−0·171		−0·174
(i)	B	−0·6495	−0·6643	−0·6564	−0·6003	−0·5048	−0·2941	−0·1580	−0·0918	−0·0602	0·0435	−0·0335	−0·0270	−0·0222
(ii)	β	0·80	0·79	0·81	1·02	1·27	1·27	1·20	1·13	1·08	1·05	1·02	1·01	1·01
	B	−0·5409	−0·5555	−0·5719	−0·6058	−0·5349	−0·2905	−0·1482	−0·0845	−0·0556	−0·0406	−0·0324	−0·0264	−0·0217
(iii)	A	0·0000	0·0049	0·0267	0·0613	0·1012	0·1442	0·1455	0·1400	0·1423	0·1534	0·1721	0·1978	0·2308
(iv)	α	1·00	1·03	1·09	1·16	1·21	1·25	1·24	1·20	1·06	0·83	0·70	0·63	0·58
	A	0·0000	0·0050	0·0292	0·0718	0·1166	0·1604	0·1532	0·1405	0·1414	0·1555	0·1784	0·2153	0·2688
(v)	p	0·0000	0·0759	0·2395	0·4314	0·6039	0·9584	1·2640	1·5138	1·7241	1·9191	2·1137	2·3095	2·5010
(vi)	p	0·0000	0·0639	0·1833	0·3795	0·6239	0·9106	1·0195	1·0998	1·5137	2·434	6·426	9·913	12·268

Table 2. Total Electronic Energies, $-E$

Function	*R* 0·00	0·25	0·50	0·75	1·00	1·5	2·0	2·5	3·0	3·5	4·0	4·5	5·0
(1)			2·181		2·513		2·577		2·282		2·022		1·823
(1A)					5·123		3·097		2·337		2·031		1·824
(i)	2·081	1·989	1·936	2·032	2·221	2·495	2·510	2·397	2·250	2·109	1·987	1·884	1·798
(ii)	2·146	2·064	1·987	2·033	2·302	2·602	2·566	2·420	2·258	2·105	1·987	1·884	1·798
(iii)	2·250	2·285	2·366	2·451	2·514	2·511	2·365	2·149	1·910	1·671	1·442	1·229	1·038
(iv)	2·250	2·286	2·381	2·497	2·589	2·604	2·435	2·183	1·913	1·694	1·545	1·439	1·359
(v)	2·250	2·286	2·378	2·497	2·600	2·681	2·603	2·449	2·282	2·130	2·000	1·892	1·803
(vi)	2·250	2·287	2·389	2·536	2·675	2·768	2·667	2·487	2·295	2·125	1·991	1·885	1·799
Exact	2·250	2·288	2·396	2·543	2·677	2·777	2·690	2·529	2·358	2·200	2·062	1·945	1·845

of table 2 and 3 respectively. For large R their results appear to be a slight improvement over those obtained with function (1) but for small R they are more in error.

Owing to degeneracy in the united atom limit, the $2p\sigma$ state is influenced to the first order in R by the 2s state of Li^{2+}. Though functions (iii) and (iv) take no account of this they give quite accurate values for the electronic energy at small R.

Both functions (v) and (vi) yield satisfactory results for all R, function (vi) giving electronic energies which are in error by less than 1% for $R \leqslant 2$ and by no more than $3\frac{1}{2}\%$ over the entire range of R investigated. The latter function also gives quite satisfactory values for the potential energy V.

Displayed in table 4 are values of the dipole moment integral calculated with the exact wave functions. It is unlikely that any of the approximate functions considered in this paper would give accurate values for Z and they have therefore not been used in the calculation.

The variation with R of the potential energy $V' = V + 4/R$, the kinetic energy T, and the total energy $E' = E + 4/R$ of the $2p\sigma$ state is illustrated in the figure.

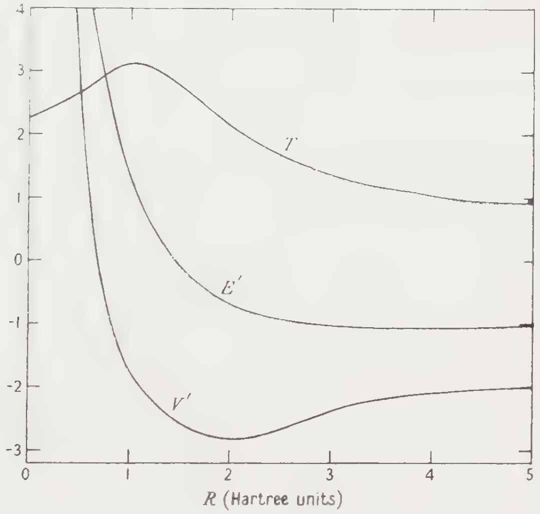

As the $2p\sigma$ state is attractive, T passes through a minimum in accordance with the theorem proved by Slater (1933).

ACKNOWLEDGMENT

We are indebted to Professor D. R. Bates for his continued interest and encouragement during this investigation.

REFERENCES

BATES, D. R., and CARSON, T. R., 1956, *Proc. Roy. Soc.* A, **234**, 207.
DALGARNO, A., and LYNN, N., 1957, *Proc. Phys. Soc.* A, **70**, 176.
MOISEIWITSCH, B. L., and STEWART, A. L., 1956, *Proc. Phys. Soc.* A, **69**, 480.
SLATER, J. C., 1933, *J. Chem. Phys.*, **1**, 687.

A Variation–Iteration Method for Short Range Potential Problems

By J. IRVING and F. B. BOUCHER
Mathematics Department, University of Southampton

MS. received 11*th April* 1957

Abstract. The device of cutting off the potential at a point where the asymptotic form of the wave function is valid permits the use of a simple trial wave function in the form of a polynomial in which some of the coefficients are variation parameters. The variation–iteration method is thereby simplified. As an illustration the bound-state deuteron problem is solved for a central Yukawa interaction and the results compared with those obtained by other authors.

§ 1. INTRODUCTION

THE integral equation formulation of the two-body problem and its solution by the variation–iteration method (Morse and Feshbach 1953) is well known. Svartholm (1945) for example has used the integral equation method in momentum space and determined the strength of the central interaction, with a given well-shape, to fit the deuteron ground state energy. On the other hand, Feshbach and Schwinger (1951) have formulated the deuteron problem, with a mixed central tensor interaction, as two coupled integral equations in configuration space and, with the aid of digital computation, solved these by the variation–iteration technique. In both formulations an initial trial function, satisfying appropriate boundary conditions, is chosen and then improved by iteration. In Svartholm's calculation a variation parameter is also introduced into the trial function. The method involves the evaluation of infinite range integrals which has usually to be carried out numerically and it is difficult to choose a trial wave function of a general form with the correct behaviour. Difficulties also arise in Feshbach and Schwinger's calculation due to the singularity of the integrands at the origin.

In the present paper the two-body problem is formulated as a finite range integral equation in configuration space by cutting off the potential at a point where the asymptotic form of the wave function is valid. This permits the use of an initial trial function in the form of a simple power series, whose coefficients are parameters. The series is chosen to have the correct behaviour at the origin and at the point where the potential is cut off. Any number of parameters can be introduced in a simple way. Accurate results can thus be obtained with only one iteration. The formulation may be advantageous for digital computation in the case of the coupled deuteron equations.

The method is illustrated in the case of the bound-state deuteron problem for a central Yukawa interaction. The technique can also be applied to the scattering problem and may be useful in the case of three- and four-body problems, though for the latter the integral equations are more complicated. It is also shown that the approximation in which the wave-function is assumed to be zero beyond the cut-off range gives results not significantly different from those obtained when the correct logarithmic derivative is used. This feature may be particularly advantageous in reducing the labour in the use of the three- and four-body problems.

§ 2. MATHEMATICAL FORMULATION

For a central interaction, the deuteron equation may be written in the form

$$\nabla^2\psi+(MV_0/\hbar^2)J\,(r/r_c)\,\psi-(M\,|\,E\,|\,/\hbar^2)\psi=0 \qquad \ldots\ldots(1)$$

where $|E|$ is the binding energy, M the nucleon mass, V_0 the well depth, $J\,(r/r_c)$ the well shape, r the interparticle distance and r_c the range of the forces.

Equation (1), with $x=r/r_c$, $\eta^2=Mr_c^2\,|\,E\,|/\hbar^2$ and $\lambda=MV_0r_c^2/\hbar^2$, reduces, in the case of the S-state, to

$$\frac{d^2\chi}{dx^2}+\lambda J\,(x)\chi-\eta^2\chi=0 \qquad \ldots\ldots(2)$$

where $\chi=r\psi$.

The asymptotic form of χ is thus $\exp\,(-\eta x)$, so that, if the potential is cut off at $x=x_0$, then $\chi'/\chi=-\eta$ at $x=x_0$. At the origin $x=0$, $\chi=0$. Constructing the Green's function in the usual way, equation (2) may then be written as the integral equation

$$\chi\,(x)=(\lambda/\eta)\left[\int_0^x e^{-\eta x}\sinh\eta\xi\,J\,(\xi)\,\chi\,(\xi)\,d\xi+\int_x^{x_0}\sinh\eta\,x\,e^{-\eta\xi}J\,(\xi)\,\chi\,(\xi)\,d\xi\right]. \qquad \ldots\ldots(3)$$

The simple trial function

$$\chi_0\,(x)=\alpha_1x+\alpha_2x^2+\alpha_3x^3+\,\ldots\ldots \qquad \ldots\ldots(4)$$

where α_1, α_2, ... are parameters, may then be used. This function satisfies the boundary condition at the origin, while the condition $\chi'/\chi=-\eta$ at $x=x_0$ gives a linear relation involving the parameters.

The first iterated wave function, $\chi_1\,(x)$ is obtained from

$$\chi_1\,(x)=e^{-\eta x}\int_0^x\sinh\eta\xi\,J\,(\xi)\,\chi_0\,(\xi)\,d\xi+\sinh\eta x\int_x^{x_0}e^{-\eta\xi}J\,(\xi)\,\chi_0\,(\xi)\,d\xi \qquad \ldots\ldots(5)$$

where $\chi_0\,(x)$ has the form of equation (4).

Two estimates, λ^0 and $\lambda^{1/2}$, of the eigenvalue are then obtained from the expressions

$$\lambda^0=\eta\int_0^{x_0}\{\chi_0\,(x)\}^2J\,(x)\,dx\Big/\int_0^{x_0}\chi_0\,(x)\,\chi_1\,(x)\,J\,(x)\,dx \qquad \ldots\ldots(6)$$

$$\lambda^{1/2}=\eta\int_0^{x_0}\chi_0\,(x)\,\chi_1\,(x)J\,(x)\,dx\Big/\int_0^{x_0}\{\chi_1\,(x)\}^2J\,(x)\,dx \qquad \ldots\ldots(7)$$

on minimization with respect to the variation parameters. From the theory of the variation–iteration method it is known that

$$\lambda^0\geqslant\lambda^{1/2}\geqslant\lambda_0.$$

where λ_0 is the true eigenvalue.

§ 3. NUMERICAL RESULTS FOR THE YUKAWA POTENTIAL J

To illustrate the method, approximations to the eigenvalue λ_0, which determines the well depth, are obtained for the Yukawa potential with $\eta=0{\cdot}25$. The simplest initial trial function is

$$\chi_0\,(x)=\alpha_1x+\alpha_2x^2$$

where α_2 is given in terms of α_1 by the boundary condition at $x=x_0$. Thus

$$\alpha_2 = -\{(1+\eta x_0)/(2x_0+\eta x_0^2)\}$$

α_1 being a normalization constant. It follows that in this particular case there are no variation parameters.

The formulae (6) and (7) yield, with $x_0=4$, the approximations $\lambda^0=2\cdot51$, $\lambda^{1/2}=2\cdot30$.

The trial function

$$\chi_0(x)=\alpha_1 x+\alpha_2 x^2+\alpha_3 x^3$$

on the other hand, has one variation parameter and gives the better values $\lambda^0=2\cdot266$, $\lambda^{1/2}=2\cdot239$. These results may be compared with the approximations $\lambda^0=2\cdot31$, $\lambda^{1/2}=2\cdot240$ obtained by Svartholm using the variation–iteration in momentum space. The true eigenvalue (Hulthén and Laurikainen 1951) is $\lambda_0=2\cdot2330$, so that the error in the best approximate value is $0\cdot3\%$. It is evident that the method described above can give the accuracy required in most deuteron calculations without excessive labour. The replacement of the true boundary condition at $x=x_0$ by the approximate condition $\chi(x_0)=0$ does not alter the results significantly. Comparable results are also obtained for $x_0=4$ and $x_0=5$, so that this provides another check on the calculation.

The method can also be applied to the coupled equations which arise when a mixed central-tensor interaction is used in the deuteron calculation, though it is, of necessity, more laborious. It does, however, remove the difficulties which occur in Feshbach and Schwinger's formulation due to the singular integrands. It is, also, more accurate than the variation–perturbation method of Cohen (1955) for the coupled and uncoupled equations.

If digital computation is used, it may be preferable to use the simplest trial function $\chi_0(x)=\alpha_1 x+\alpha_2 x^2$, which has no variation parameters, and iterate several times rather than use a function with several variation parameters and iterate once.

REFERENCES

COHEN, L., 1955, *Proc. Phys. Soc.* A, **68,** 419 and 425.
FESHBACH, H., and SCHWINGER, J., 1951, *Phys. Rev.*, **84,** 194.
HULTHÉN, L., and LAURIKAINEN, K. V., 1951, *Rev. Mod. Phys.*, **23,** 1.
MORSE, P. M., and FESHBACH, H., 1953, *Methods of Theoretical Physics*, Part I (New York : McGraw-Hill).
SVARTHOLM, N., 1945, *Thesis*, University of Lund.

Compound Nuclear Theory and the Optical Model

By J. BOWCOCK†
Department of Mathematical Physics, University of Birmingham

Communicated by R. E. Peierls; MS. received 5th March 1957

Abstract. A formalism is developed to relate the total cross section for low-energy nucleon–nucleus scattering to the cross section due to a potential well. By introducing the intermediate model of Lane, Thomas and Wigner for the compound nucleus states, a simple relation between these two cross sections is obtained. The method of extracting a potential well to replace the hard sphere scattering and the scattering from 'far distant' levels is given and then extended to find the well which describes the average total cross section.

§ 1. INTRODUCTION

THE idea that a particle upon entering a nucleus interacts strongly with the nuclear constituents and shares its energy rapidly among them enjoyed considerable support for some time after the discovery of the closely-spaced epithermal resonances (Moon and Tillman 1935). However, the striking successes of the shell model (Mayer 1949) and the experiments on average cross sections (Okazaki, Darden and Watton 1954, Walt and Barschall 1954) seem to indicate that the interaction with individual particles in the nucleus may not play as large a part as was believed previously. The more recent work of Brueckner (1955) on the nuclear many-body problem leads to the idea that it is the Pauli exclusion principle which effects this reduced interaction.

In an attempt to take into account a weaker interaction, Feshbach, Porter and Weisskopf (1954) introduced the optical model. The interaction is described by a complex potential $V(r) = -(42 + i2{\cdot}1)$ MeV of radius R, and this is successful in reproducing the average total neutron cross sections below several MeV and, less accurately, the neutron angular distributions at 1 MeV.

The present work originated in an attempt to give a theoretical basis to this semi-empirical complex potential. A general potential well is introduced and the cross sections derived from this are compared with the cross sections derived from the many-body problem. The intermediate model of Lane, Thomas and Wigner (1955) is then introduced by means of an eigenstate decomposition of the excited states of the compound nucleus. This enables us to choose the depth and imaginary part of a square well which will approximately reproduce the scattering and replace not only the hard sphere scattering but also scattering from the levels of the compound nucleus which lie far away from the actual energy. The method of solution is extended to find the well which would give the average total cross section. However, this solution requires a knowledge of a strength function $\overline{(\gamma_{0q}{}^{n})^2/D}$ which is not known from experiment. This information has therefore to be put in somewhat arbitrarily.

---

†Now at the Department of Physics, University of Wisconsin, Madison, Wis.

The extension of the theory to neutrons incident with an angular momentum other than $l=0$ is given and we find that the potential wells to describe the average total cross section from different l waves are solutions of different equations. The whole of the theory is carried out in the Kapur–Peierls formalism (1938) but since most work relating to this subject has been done in the Higner–Eisenbud formalism (1947) the transformation into this formalism is also given.

§ 2. Introduction of the Potential Well

2.1. *The Many-Body Problem*

Here we shall be concerned only with those cross sections which occur in the description of processes involved when a neutron of at most a few MeV energy is incident upon any nucleus. The neutron is taken to have zero angular momentum, the spins of all particles are neglected, and antisymmetrization between the incident particle and the other nucleons is not allowed for.

The Schrödinger equation for this process is

$$\mathscr{H}(\mathbf{r},\xi)\Psi(\mathbf{r},\xi)=E\Psi(\mathbf{r},\xi) \qquad \ldots\ldots(2.1)$$

where

$$\mathscr{H}(\mathbf{r},\xi)=H_0(\xi)-\frac{\hbar^2}{2m}\nabla_r{}^2+V(\mathbf{r},\xi) \qquad \ldots\ldots(2.2)$$

and

$$E=E_0+\frac{\hbar^2k^2}{2m}$$

where ξ represents the coordinates of all the nucleons of the target nucleus, E_0 is the energy of the ground state of the target nucleus, $\mathbf{r}$ represents the coordinates of the incident neutron with energy $\hbar^2k^2/2m$, $V(\mathbf{r},\xi)$ is the potential which the neutron meets and is zero beyond some radius R.

Writing $\Psi(\mathbf{r},\xi)=\Phi(\mathbf{r},\xi)/r$ our equation becomes

$$H'(\mathbf{r},\xi)\Phi(\mathbf{r},\xi)=E\Phi(\mathbf{r},\xi) \qquad \ldots\ldots(2.3)$$

where

$$H'(\mathbf{r},\xi)=-\frac{\hbar^2}{2m}\frac{d^2}{dr^2}+V(\mathbf{r},\xi)+H_0(\xi).$$

In the region $|\mathbf{r}|>r_0$, $\Phi(\mathbf{r},\xi)$ is of the form

$$\Phi(\mathbf{r},\xi)=\chi_0(\xi)\left\{\frac{\sin kr}{k}+S_0\exp(ikr)\right\}+\sum_c\chi_c(\xi)S_c\exp(ik_cr), \qquad \ldots\ldots(2.4)$$

if we assume that the energy of the system is such that the probability of more than one particle being found at a distance greater than r_0 from the centre of the nucleus is negligible. This is certainly true at the neutron energies we consider.

In (2.4), $\chi_c(\xi)$ are the states of the target nucleus, being solutions of

$$H_0(\xi)\chi_c(\xi)=E_c\chi_0(\xi), \qquad \ldots\ldots(2.5)$$

$\chi_0(\xi)$ is the wave function of the ground state and $\hbar^2k_c{}^2/2m$ is the energy of a neutron emitted when the target nucleus is left in the state $\chi_c(\xi)$.

In the internal region $|\mathbf{r}|<r_0$ we define a set of states $\phi_n(\mathbf{r},\xi)$ which satisfy

$$H'\phi_n(\mathbf{r},\xi)=W_n\phi_n(\mathbf{r},\xi) \qquad \ldots\ldots(2.6)$$

and have the boundary conditions that at $|\mathbf{r}|=0$, $\phi_n=0$ and at $|\mathbf{r}|=r_0>R$ they represent outgoing waves only. It can then be shown that

$$\int_{\text{int}}\phi_n(\mathbf{r},\xi)\phi_{n'}(\mathbf{r},\xi)\,d\mathbf{r}\,d\xi=\delta_{nn'} \qquad \ldots\ldots(2.7)$$

and that the eigenvalues W_n are complex, $E_n - i\gamma_n/2$, where γ_n is the total width of the level.

The continuity of the wave function across the boundary $|\mathbf{r}| = r_0$ gives

$$S_0 = \sum_n \frac{\hbar^2}{2m} \exp(-2ikr_0) \frac{\{\int \phi_n(r_0, \Omega, \xi) \chi_0(\xi)\, d\xi\, d\Omega\}^2}{W_n - E} - \exp(-ikr_0) \frac{\sin kr_0}{k} \qquad \ldots\ldots(2.8)$$

and the total cross section is then related to S_0 by

$$\sigma_{\mathrm{T}} = \frac{4\pi}{k} \mathscr{I} S_0. \qquad \ldots\ldots(2.9)$$

S_0 shows the well-known combination of resonance sum plus hard sphere scattering.

One point of interest is that the radius r_0 has been defined quite arbitrarily except for the condition $r_0 > R$. If this condition is satisfied for one particular value of r_0 it is also satisfied for any other r_0 greater than this. The contribution from the hard sphere scattering will change with r_0 but since σ_{T} is a physical quantity and must remain unaltered, this change is compensated by an equal variation in the sum over nuclear levels. Also as the resonance phenomena must be retained this variation occurs in the contribution from the levels of high excitation energy which is referred to as the contribution from the distant terms.

2.2. *Scattering by a Potential Well*

Since it is our intention in some way to relate the total cross section for the real scattering process to the total cross section due to a potential well we introduce at this stage the formula equivalent to (2.9) for the scattering due to an arbitrary potential well $U(r)$ of the same radius R as the nucleus.

This is

$$S_0{}^u = \sum_p \frac{\hbar^2}{2m} \exp(-2ikr_0) \frac{u_p{}^2(r_0)}{W_{0p} - E} - \exp(-ikr_0) \frac{\sin kr_0}{k}, \qquad \ldots\ldots(2.10)$$

where $u_p(r)$ is a solution of

$$\left(-\frac{\hbar^2}{2m} \frac{d^2}{dr^2} + U(r) \right) u_p(r) = \epsilon_p u_p(r) \qquad \ldots\ldots(2.11)$$

with boundary conditions that $u_p(r)$ is zero at $r = 0$ and that, at $|\mathbf{r}| = r_0$, $du_p(r)/dr = iku_p(r)$. W_{0p} is defined to be $\epsilon_p + E_0$. As before, $\sigma_{\mathrm{T}}{}^u = (4\pi/k) \mathscr{I} S_0{}^u$ and, comparing σ_{T} and $\sigma_{\mathrm{T}}{}^u$, we may write the identity

$$\sigma_{\mathrm{T}} = \sigma_{\mathrm{T}}{}^u + \frac{4\pi}{k} \mathscr{I} \left\{ \frac{\hbar^2}{2m} \exp(-2ikr_0) \left[\sum_n \frac{(\int \phi_n(r_0, \xi) \chi_0(\xi)\, d\xi\, d\Omega)^2}{W_n - E} - \sum_p \frac{u_p{}^2(r_0)}{W_{0p} - E} \right] \right\}. \qquad \ldots\ldots(2.12)$$

If we could find a particular $U(r)$ which makes the difference of the two sums in (2.12) zero over a certain energy range then this potential would reproduce exactly the real total cross section over this region. However, this is evidently impossible since the first sum contains the closely spaced resonances which are features of the many-body problem and cannot be given by a simple potential well. Instead we may require that $U(r)$ is chosen to reproduce the *average* total cross section, the average being taken over an energy region large compared with the distance between individual resonances but small compared with the width of a giant resonance.

An alternative is to consider the cross section in between individual resonances, to try to find a $U(r)$ to give this background.

§ 3. The Intermediate Model

In this section we attribute to the compound states $\phi_n(\mathbf{r}, \xi)$ properties which are similar to the assumptions of the intermediate model of Lane, Thomas and Wigner (1955). The model is constructed in terms of a decomposition of the eigenstates $\phi_n(\mathbf{r}, \xi)$,

$$\phi_n(\mathbf{r}, \xi) = \sum_{c,p} a_{cp}{}^n u_p(\mathbf{r}) \chi_c(\xi) \qquad \ldots\ldots(3.1)$$

where the $u_p(\mathbf{r})$ and the $\chi_c(\xi)$ are defined in the last section. There are then sum rules which apply to the $a_{cp}{}^n$ due to the completeness and orthonormality of the wave functions involved. In particular those we shall make use of are:

$$\begin{aligned}
&\sum_n a_{cp}{}^n a_{c'p'}{}^n = \delta_{cc'}\delta_{pp'} \\
&\sum_n a_{cp}{}^n a_{c'p'}{}^n (W_n - W_{cp}) = \langle cp|(V-U)|c'p'\rangle \\
&\sum_n a_{cp}{}^n a_{c'p'}{}^n (W_n - W_{cp})^2 = \langle cp|(V-U)^2|c'p'\rangle + (W_{c'p'} - W_{cp})\langle cp|(V-U)|c'p'\rangle.
\end{aligned} \qquad \ldots\ldots(3.2)$$

Here, $$W_{cp} = \epsilon_p + E_c.$$

The last equation (3.2) with $p = p'$ shows, in fact, that if we regard the quantity $(a_{0p}{}^n)^2$ as a function of n, hence of the energy W_n, its second moment about W_{cp} is finite, and equal to the right-hand side, which we shall later estimate to be of the order of W^2 where W is some quantity of the order of a few Mev. If the $a_{0p}{}^n$ were real, so that all terms in the sum would be positive, we could then conclude that $a_{0p}{}^n$ must be small unless $W_n - W_{0p}$ is at most of order W. With our definitions the coefficients are complex, but in general it is still true that the $a_{0p}{}^n$ are greatest where the real part of $W_n - W_{0p}$ is small and decrease when it exceeds W. This can, in detail, be verified only for each specific model and we shall assume, for what follows, that this is the case. W is, of course, large compared with the spacing D of compound levels, so that for given p, many of the $a_{0p}{}^n$ are appreciable. W may, however, be less than d, the spacing of single-particle levels, and in that case if $a_{0p}{}^n$ is appreciable all other $a_{0q}{}^n$ with $q \neq p$ must be small.

In the reduced neutron width

$$\gamma_0{}^n = \left(\frac{\hbar^2}{2m}\right)^{1/2} \int \phi_n(r_0, \xi)\chi_0(\xi)\, d\xi\, d\Omega, \qquad \ldots\ldots(3.3)$$

which gives $$(\gamma_0{}^n)^2 = \frac{\hbar^2}{2m}\left\{\sum_p a_{0p}{}^n u_p(r_0)\right\}^2;$$

we may then neglect cross terms and write

$$(\gamma_0{}^n)^2 = \frac{\hbar^2}{2m}\sum_p (a_{0p}{}^n)^2 u_p{}^2(r_0). \qquad \ldots\ldots(3.4)$$

These assumptions are identical with those of Lane, Thomas and Wigner (1955) except that our expansion (3.1) is made in terms of the eigenfunctions of a general potential $U(r)$ instead of the more specific potential

$$V = \int \chi_0(\xi) V(\mathbf{r}, \xi) \chi_0(\xi)\, d\xi$$

and that our one-particle states are defined with a complex boundary condition.

We introduce first the eigenstate decomposition (3.1) into (2.12) giving

$$\sigma_{\mathrm{T}} = \sigma_{\mathrm{T}}{}^{u} + \frac{4\pi}{k} \mathscr{I} \left\{ \frac{\hbar^2}{2m} \exp(-2ikr_0) \left[\sum_n \frac{(\sum_p a_{0p}{}^{n} u_p(r_0))^2}{W_n - E} - \sum_p \frac{u_p{}^2(r_0)}{W_{0p} - E} \right] \right\}$$

$$= \sigma_{\mathrm{T}}{}^{u} + \frac{4\pi}{k} \mathscr{I} \left\{ \frac{\hbar^2}{2m} \exp(-2ikr_0) T \right\}. \qquad \ldots\ldots(3.5)$$

Consider now the term

$$\sum_n = \frac{(\sum_p a_{0p}{}^{n} u_p(r_0))^2}{W_n - E} \sum_n \sum_p \frac{(a_{0p}{}^{n})^2 u_p{}^2(r_0)}{W_n - E} + \sum_n \sum_{p' \neq p} \sum_p \frac{a_{0p}{}^{n} a_{0p'}{}^{n} u_p(r_0) u_{p'}(r_0)}{W_n - E},$$

and for the moment neglect the cross terms. We write the following identity

$$\frac{1}{W_n - E} = \frac{1}{W_{0p} - E} + \frac{W_{0p} - W_n}{W_{0p} - E} + \frac{(W_{0p} - W_n)^2}{(W_{0p} - E)^3} + \frac{1}{W_n - E} \left(\frac{W_{0p} - W_n}{W_{0p} - E} \right)^3$$

$$\ldots\ldots(3.6)$$

and use the sum rules for the $a_{0p}{}^{n}$ to give

$$\sum_n \sum_p \frac{(a_{0p}{}^{n})^2 u_p{}^2(r_0)}{W_n - E} = \sum_p \frac{u_p{}^2(r_0)}{W_{0p} - E} \left\{ 1 + \frac{\langle 0p | V - U | 0p \rangle}{W_{0p} - E} + \frac{\langle 0p | (V - U)^2 | 0p \rangle}{(W_{0p} - E)^2} \right\}$$

$$+ \sum_p \sum_n \frac{(a_{0p}{}^{n})^2 u_p{}^2(r_0)}{W_n - E} \left\{ \frac{W_{0p} - W_n}{W_{0p} - E} \right\}^3. \qquad \ldots\ldots(3.7)$$

This equation reduces T to

$$T = \sum_p \frac{u_p{}^2(r_0)}{W_{0p} - E} \left(\frac{\langle 0p | V - U | 0p \rangle}{W_{0p} - E} + \frac{\langle 0p | (V - U)^2 | 0p \rangle}{(W_{0p} - E)^2} \right)$$

$$+ \sum_n \sum_p \frac{(a_{0p}{}^{n})^2 u_p{}^2(r_0)}{W_n - E} \left\{ \frac{W_{0p} - W_n}{W_{0p} - E} \right\}^3.$$

The factor $1/(W_n - E)$ which causes the many sharp resonances in the cross section at low energies is not contained in the first two terms of T which are therefore rather slowly varying functions of the energy E over an interval including many of the levels W_n. We consider in detail the third term to see from which W_n and from which p groups the major contributions come. Here for facility of argument all the factors involved are taken to be real but it may be shown, by separating the real and imaginary parts, that our conclusions are still valid even if the finiteness of the imaginary parts of the various quantities is allowed for. We suppose the energy of the incident neutron is such that E lies on a giant resonance centred on W_{0q} and we compare the contributions to the sum over p from q and $q+1$, i.e.

$$\sum_n \frac{(a_{0q}{}^{n})^2 u_q{}^2(r_0)}{W_n - E} \left\{ \frac{W_{0q} - W_n}{W_{0q} - E} \right\}^3 \quad \text{and} \quad \sum_n \frac{(a_{0,\,q+1}{}^{n})^2 u_{q+1}{}^2(r_0)}{W_n - E} \left\{ \frac{W_{0,\,q+1} - W_n}{W_{0,\,q+1} - E} \right\}^3.$$

For a simple potential well the factor $u_p(r_0)$ may be taken to be independent of p. Putting in the intermediate model of the nucleus, $(a_{0q}{}^{n})^2$ on the average, has as a function of W_n a peak at W_{0q} and falls to a comparatively small value over an energy interval less than $W_{0,q+1}-W_{0q}$. $(a_{0,q+1}{}^{n})^2$ has a similar form but centred on $W_{0,q+1}$. However in the q term the factors $1/(W_n-E)$ and $\{(W_{0q}-W_n)/(W_{0q}-E)\}^3$ attain large values over the region of W_n where $(a_{0q}{}^{n})^2$ is large, whereas in the $q+1$ term the equivalent factors $1/(W_n-E)$ and $\{(W_{0,q+1}-W_n)/(W_{0,q+1}-E)\}^3$ are small where $(a_{0,q+1}{}^{n})^2$ is sizeable.

Taking the single particle spacing to be of the order of 10 MeV and $|W_{0q}-E|\simeq 1$ MeV it is easy to see quantitatively that we may neglect the contributions from the $q+1$ term compared with that from the q term. The same argument applies to all values of p other than $p=q$. We are therefore justified in writing

$$\sum_p \sum_n \frac{(a_{0p}{}^{n})^2 u_p{}^2(r_0)}{W_n-E}\left\{\frac{W_{0p}-W_n}{W_{0p}-E}\right\}^3=\sum_n \frac{(a_{0q}{}^{n})^2 u_q{}^2(r_0)}{W_n-E}\left\{\frac{W_{0q}-W_n}{W_{0q}-E}\right\}^3. \qquad \ldots\ldots(3.8)$$

Our expression is now only a sum over n and has the property that the terms in n which give a non-negligible contribution to the sum extend only over a limited energy region. The reason for this is that $(a_{0q}{}^{n})^2$ becomes rapidly small when W_n differs from W_{0q} by an energy more than the half-width of the distribution of the average $(a_{0q}{}^{n})^2$. It is assumed for example that the average $(a_{0q}{}^{n})^2$ fall away exponentially. Some difficulties concerning the convergence of the sum $\sum_p \sum_n (a_{0p}{}^{n})^2 u_p{}^2(r_0)/(W_n-E)$ which appears in the original expression for the total cross section are thus removed.

Our cross section may now be written as

$$\sigma_{\mathrm{T}}=\sigma_{\mathrm{T}}{}^{u}+\frac{4\pi}{k}\mathscr{I}\left[\frac{\hbar^2}{2m}\exp(-2ikr_0)\left\{\sum_p \frac{u_p{}^2(r_0)}{W_{0p}-E}\left(\frac{\langle 0p|V-U|0p\rangle}{W_{0p}-E}\right.\right.\right.$$
$$\left.\left.\left.+\frac{\langle 0p|(V-U)^2|0p\rangle}{(W_{0p}-E)^2}\right)+\sum_n \frac{(a_{0q}{}^{n})^2 u_q{}^2(r_0)}{W_n-E}\left(\frac{W_{0q}-W_n}{W_{0q}-E}\right)^3\right\}\right] \qquad \ldots\ldots(3.9)$$

where we have again neglected the cross terms.

It was noted in § 2 that the radius r_0 is arbitrary so long as it is greater than a certain minimum value R. A change in r_0 produces a change in the hard sphere scattering which is compensated by an equal change in the contribution from the resonance sum. Suppose now we consider the scattering from the potential well $U(r)$. Then $\sigma_{\mathrm{T}}{}^{u}$ must remain unchanged with r_0 just as σ_{T}. The second expression on the right-hand side of (3.9) must also therefore remain unchanged as r_0 changes. If U can be chosen such that

$$\sum_p \frac{u_p{}^2(r_0)}{W_{0p}-E}\left[\frac{\langle 0p|V-U|0p\rangle}{W_{0p}-E}+\frac{\langle 0p|(V-U)^2|0p\rangle}{(W_{0p}-E)^2}\right]=0 \qquad \ldots\ldots(3.10)$$

whatever the value of r_0 then

$$\mathscr{I}\left[\exp(-2ikr_0)\sum_n \frac{(a_{0q}{}^{n})^3 u_q{}^2(r_0)}{W_n-E}\left\{\frac{W_{0q}-W_n}{W_{0q}-E}\right\}^3\right]$$

must also remain invariant under r_0. This is consistent with the fact that the compensation for change in hard sphere scattering comes from the far distant terms in the resonance sum which have been included in $\sigma_{\mathrm{T}}{}^{u}$ by the expansion (3.6). In the next section we shall discuss how equation (3.10) may be used.

The derivation of (3.9) included the neglect of the cross-terms in the double sum over p. We now discuss this approximation.

The neglected terms are

$$\sum_{n}\sum_{p'\neq p}\sum_{p}\frac{a_{0p}{}^{n}a_{0p'}{}^{n}u_{p}(r_0)u_{p'}(r_0)}{W_n-E}.$$

If we make the same expansion as used for the square terms we find that these terms reduce to

$$\sum_{p'\neq p}\sum_{p}\left\{\frac{\langle 0p|V-U|0p'\rangle}{(W_{0p}-E)^2}+\frac{\langle 0p|(V-U)^2|0p'\rangle}{(W_{0p}-E)^3}\right.$$
$$\left.+\sum_{p}\sum_{p'\neq p}\frac{a_{0p}{}^{n}a_{0p'}{}^{n}u_{p}(r_0)u_{p'}(r_0)}{W_n-E}\left\{\frac{W_{0p}-W_n}{W_{0p}-E}\right\}^3\right. \qquad \ldots\ldots(3.11)$$

Hence what we have neglected is

$$\sum_{p'\neq p}\langle 0p|V-U|0p'\rangle \text{ compared with } \langle 0p|V-U|0p\rangle, \qquad \ldots\ldots(3.11a)$$

$$\sum_{p'\neq p}\langle 0p|(V-U)^2|0p'\rangle \text{ compared with } \langle 0p|(V-U)^2|0p\rangle, \qquad \ldots\ldots(3.11b)$$

$$\sum_{n}\sum_{p'\neq p}\frac{a_{0p}{}^{n}a_{0p'}{}^{n}u_{p}(r_0)u_{p'}(r_0)}{W_n-E}\left\{\frac{W_{0p}-W_n}{W_{0p}-E}\right\}^3$$
$$\text{compared with } \sum_{n}\frac{(a_{0p}{}^{n})^2u_{p}{}^{2}(r_0)}{W_n-E}\left\{\frac{W_{0p}-W_n}{W_{0p}-E}\right\}^3. \qquad \ldots\ldots(3.11c)$$

If it is assumed that $\langle 0|V-U|0\rangle$ is a constant, independent of r then the neglected terms of (3.11*a*) are identically zero. The neglected terms of (3.11*b*) are also zero if we assume that $\langle 0|V^2|0\rangle-\langle 0|V|0\rangle^2$ also has no radial dependence. As a further test of the validity of the approximation $U(r)$ was chosen to be of the form $V_0\exp(-r/r_0)$ while $\langle 0|V|0\rangle$ was again taken to be constant. The neglected terms were found to amount to less than 5% of the included terms.

$$\sum_{n}\sum_{p'\neq p}\sum_{p}\frac{a_{0p}{}^{n}a_{0p'}{}^{n}u_{p'}(r_0)u_{p}(r_0)}{W_n-E}\left\{\frac{W_{0p}-W_n}{W_{0p}-E}\right\}^3$$

can be shown to give its major contribution from the term with $p=q$ by an argument identical with the one used above for the terms containing $(a_{0p}{}^{n})^2$. We may therefore write

$$\begin{aligned}\sum_{n}\sum_{p}\sum_{p'}\frac{a_{0p}{}^{n}a_{0p'}{}^{n}u_{p}(r_0)u_{p'}(r_0)}{W_n-E}\left\{\frac{W_{0p}-W_n}{W_{0p}-E}\right\}^3 &\simeq\sum_{n}\sum_{p'}\frac{a_{0q}{}^{n}a_{0p'}{}^{n}u_{q}(r_0)u_{p'}(r_0)}{W_n-E}\left\{\frac{W_{0q}-W_n}{W_{0q}-E}\right\}^3.\\ &\simeq\sum_{n}\frac{(a_{0q}{}^{n})^2u_{q}{}^{2}(r_0)}{W_n-E}\left\{\frac{W_{0q}-W_n}{W_{0q}-E}\right\}^3\\ &=\frac{2m}{\hbar^2}\sum_{n}\frac{(\gamma_{0q}{}^{n})^2}{W_n-E}\left\{\frac{W_{0q}-W_n}{W_{0q}-E}\right\}^3.\end{aligned}$$

§ 4. METHOD OF SOLUTION FOR POTENTIAL WELL

From (3.9) we see that if we can solve the equation

$$\sum_{p}\frac{u_{p}{}^{2}(r_0)}{W_{0p}-E}\left(\frac{\langle 0p|V-U|0p\rangle}{W_{0p}-E}+\frac{\langle 0p|(V-U)^2|0p\rangle}{(W_{0p}-E)^2}\right)=0 \text{ for } U(r) \qquad \ldots\ldots(4.1)$$

then this U will be a potential well which includes the scattering from the far distant terms as well as the hard sphere scattering. The method of solution is given and then extended to find a potential well which describes the total average cross section.

Solution of (4.1) is simplified by writing it as

$$\int \sum_p \frac{u_p(r)u_p(r_0)}{W_{0p}-E} \langle 0|V-U|0\rangle \sum_p \frac{u_{p'}(r)u_{p'}(r_0)}{W_{0p'}-E}\,dr$$
$$+\int \sum_p \frac{u_p(r)u_p(r_0)}{(W_{0p}-E)^2} \langle 0|(V-U)|^2)0\rangle \sum_{p'} \frac{u_{p'}(r)u_{p'}(r_0)}{(W_{0p'}-E)}\,dr=0. \qquad \ldots\ldots(4.2)$$

Here the additional terms with $p' \neq p$ have been included but these are taken to be negligible compared with the terms with $p'=p$. Indeed if V and U are square wells (as we shall use in the solution of our equation) then these extra terms vanish by the orthogonality of the u_p. The reason for writing our equation in this form is that the factor $\sum_p u_p(r)u_p(r_0)/(W_{0p}-E)$ has a simple interpretation which enables us to remove the sum over p. This is achieved by noting that the wave function describing the scattering due to the well $U(r)$ is a solution of

$$\left\{-\frac{\hbar^2}{2m}\frac{d^2}{dr^2}+(U-E)\right\}f(r)=0 \qquad \ldots\ldots(4.3)$$

throughout all r space. Also we have

$$\left\{-\frac{\hbar^2}{2m}\frac{d^2}{dr^2}+(U-E)\right\}\sum_p \frac{u_p(r)u_p(r_0)}{W_{0p}-E}=\delta(r-r_0) \qquad \ldots\ldots(4.4)$$

and hence

$$\sum_p \frac{u_p(r)u_p(r_0)}{W_{0p}-E}=\frac{2m}{\hbar^2}\exp(ikr_0)f(r) \qquad \ldots\ldots(4.5)$$

for $r<r_0$.

The sum

$$\sum_p \frac{u_p(r)u_p(r_0)}{(W_{0p}-E)^2}=Cg(r)$$

is also the solution of a simple equation

$$\left\{-\frac{\hbar^2}{2m}\frac{d^2}{dr^2}+(U-E)\right\}g(r)=\sum_p \frac{u_p(r)u_p(r_0)}{C(W_{0p}-E)}=f(r). \qquad \ldots\ldots(4.6)$$

With these substitutions equation (4.2) becomes

$$\langle 0f|V-U|0f\rangle+\langle 0g|(V-U)^2|0f\rangle=0. \qquad \ldots\ldots(4.7)$$

This may be rewritten as

$$\langle f|V_{00}-U|f\rangle+\langle g|(V_{00}-U)^2+\overline{\Delta V^2}|f\rangle=0. \qquad \ldots\ldots(4.8)$$

Here V_{00} signifies $\langle 0|V|0\rangle$ and $\overline{\Delta V^2}=\langle 0|V^2|0\rangle-\langle 0|V|0\rangle^2$.

V_{00} and $\overline{\Delta V^2}$ may be considered to be independent of the velocity of the incident neutron over the energy range we consider and by putting in shell model wave functions for $\chi_0(\xi)$ and assuming some two-body potential to describe the nucleon–nucleon forces both these quantities may be evaluated (Thomas 1955).

Equation (4.8) may be regarded as an equation for U if the quantities V_{00} and $\overline{\Delta V^2}$ are known. However, in this case the equation involves a complicated relation between the functions $f(r)$ and $g(r)$ and the potential $U(r)$. It was found simpler to solve the equation by assuming a value for $U(r)$, calculating the corresponding $f(r)$ and $g(r)$ and obtaining the values of V_{00} and $\overline{\Delta V^2}$ for given incident energies. A variation in the incident neutron energy will produce variations in V_{00} and $\overline{\Delta V^2}$ but since these are quantities which are taken to be constant it is the potential U which must vary with energy. It is relatively simple to vary U and the incident energy to obtain another sequence of values for V_{00} and $\overline{\Delta V^2}$ and hence for a given V_{00} and $\overline{\Delta V^2}$ we can ascertain how $U(r)$ varies with the energy of the incident neutron.

The form of $U(r)$ to be chosen is limited somewhat by the fact that we have used an intermediate model for the $a_{cp}{}^n$. However, the properties attributed to these coefficients are not likely to be valid if U is chosen to be a wildly varying function of r which has levels W_{0p}, $W_{0,p+1}$, lying closely together in some energy region. In this case if the energy E lay near W_{0p} both the coefficients $a_{0p}{}^n$ and $a_{0,p+1}{}^n$ would be large for the levels W_n near W_{0p}. To facilitate calculations $U(r)$ was chosen to be a square well, and V_{00}, $\overline{\Delta V^2}$ were also chosen of the same form. $\overline{\Delta V^2}$ is a quantity which is not likely to depend upon r, and V_{00} for heavy or intermediate nuclei should remain approximately constant over most of the nucleus.

Equation (4.8) then becomes

$$(V_{00}-U)^2+(V_{00}-U)\frac{\hbar^2K^2}{m}\times$$

$$\left[\frac{\left(\frac{r_0}{2}-\frac{\sin 2Kr_0}{4K}\right)\left(1-\frac{ik}{K}\tan Kr_0\right)}{(1-Kr_0\tan Kr_0-ikr_0)\left(\frac{r_0}{2}-\frac{\sin 2Kr_0}{4K}\right)+\left(\frac{r_0}{4}\cos 2Kr_0-\frac{\sin 2Kr_0}{8K}\right)\left(1-\frac{ik}{K}\tan Kr_0\right)}\right] \qquad \ldots\ldots(4.9)$$

where

$$\frac{\hbar^2K^2}{2m}=\frac{\hbar^2k^2}{2m}-U. \qquad \ldots\ldots(4.10)$$

This equation was solved numerically, taking U to be $-(42+iW)$ Mev and varying the incident neutron energy between 0 Mev and 30 Mev for several values of W. The results are shown in the figure. In the upper half of the graph where $\overline{\Delta V^2}$ is plotted against incident energy we see that for a given value of $\overline{\Delta V^2}$ the

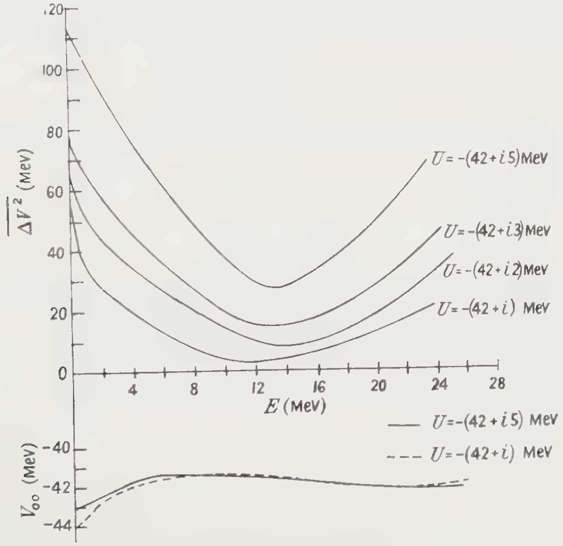

$\overline{\Delta V^2}$ is plotted against incident neutron energy for various complex wells. V_{00} is also plotted but in this case the curves lies so close that it is practicable to plot only two of them.

imaginary part of the complex well increases slowly to a maximum around 15 Mev after which it diminishes. On the other hand, for these particular values of U, V_{00} remains almost constant with varying incident energy differing from -42 Mev only by an amount of the order of 1 Mev over the whole range of variation. For a constant V_{00} of the order of -40 Mev the real part of U will remain approximately constant and close to this value. This behaviour is similar to that of the complex potential which describes the average total cross section (Peaslee 1955).

We have therefore succeeded in finding a potential which gives the contribution to the total cross section from far distant terms in the resonance sum and also includes the potential scattering. This leaves only those contributions from a finite number of levels around E to be evaluated. We may write these as

$$\frac{4\pi}{k}\mathscr{I}\left\{\exp(-2ikr_0)\sum_n \frac{(\gamma_{0q}{}^n)^2}{W_n-E}\left\{\frac{W_{0q}-W_n}{W_{0q}-E}\right\}^3\right\}.$$

Looking how to evaluate this sum we see that the unknowns are the widths $(\gamma_{0q}{}^n)^2$, the level positions E_n and the total level widths γ_n which occur in the imaginary part of W_n. The values of W_{0q} have been fixed by the potential $U(r)$. If we are in the continuum region we may assume an average behaviour of $(\gamma_{0q}{}^n)^2/D$, replace the sum by an integration and evaluate this term. In the case for which the calculation was done it happens that this term gives a contribution negligible compared to $\sigma_T{}^u$ and hence $\sigma_T{}^u$ gives the whole of the cross section. If we were in the resonance region we could substitute the experimental values for $(\gamma_{0q}{}^n)^2$, γ_n and E_n for the levels close to E and use some average behaviour to evaluate the other terms.

4.1. *Average Cross Sections*

The problem of finding a potential well to describe the average total cross section is more involved since our equation is now

$$\overline{C^2\langle f|V_{00}-U|f\rangle}+\overline{C^2\langle g|(V_{00}-U)^2+\overline{\Delta V^2}|f\rangle}+\overline{\sum_n \frac{(\gamma_{0q}{}^n)^2}{W_n-E}\left\{\frac{W_{0q}-W_n}{W_{0q}-E}\right\}^3}=0. \qquad \ldots\ldots(4.11)$$

We shall use the same definition of average cross sections as Feshbach, Porter and Weisskopf, i.e.

$$\overline{\sigma_T}=\frac{1}{I}\int_I \sigma_T(E)\,dE \qquad \ldots\ldots(4.12)$$

where I is an energy interval centred on E and large compared with the nuclear level spacing D, but small compared with the single particle spacing d. Since σ_T is related linearly to S_0 by (2.9) we write $\overline{\sigma_T}=(4\pi/k)S_0$. k is taken to be sufficiently far from zero so that it may be regarded as constant in the interval of averaging. Similarly, all those quantities which are slowly varying over this interval (f, g, $\exp(-2ikr_0)$) will also be taken as constant. Thus the expression we have to set equal to zero becomes

$$C^2\langle f|V_{00}-U|f\rangle+C^2\langle g|(V_{00}-U)^2+\overline{\Delta V^2}|f\rangle+\sum_p \frac{1}{I}\int_I \frac{(\gamma_{0q}{}^n)^2}{W_n-E}\left\{\frac{W_{0p}-W_n}{W_{0p}-E}\right\}^3 dE. \qquad \ldots\ldots(4.13)$$

In order to simplify the averaging process we consider that the averaging affects only those terms n for which W_n lies in the interval I and that in this interval the term $\{1/(W_{0p}-E)\}^3$ may be regarded as constant. The latter statement will be valid even if E lies near W_{0q} since in general W_{0q} has an imaginary part large compared to the interval I.

For these levels lying within I we have

$$\sum_{n>I} \int_{E_n-\Delta_1^n}^{E_n+\Delta_2^n} \frac{dE}{W_n-E}$$

where Δ_1^n, Δ_2^n are the energy lengths from E_n to each end of the interval I. After performing the integration we find

$$\left[\sum_{n>I} \frac{(\gamma_{0q}{}^n)^2}{I} \log\left\{\frac{(\Delta_2{}^n)^2+(\gamma_n)^2}{(\Delta_1{}^n)^2+(\gamma_n)^2}\right\} \right.$$
$$\left. +i \sum_{n>I} \frac{(\gamma_{0q}{}^n)^2}{I} \left\{\tan^{-1}\left(\frac{\Delta_2{}^n}{\gamma_n}\right) - \tan^{-1}\left(\frac{\Delta_1{}^n}{\gamma_n}\right)\right\} (\gamma_{0q}{}^n)^2 \right]. \qquad \ldots\ldots(4.14)$$

Assuming that $\gamma_n/\Delta_1{}^n$ and $\gamma_n/\Delta_2{}^n$ are both very small compared with unity this becomes

$$\log \prod_{n>I} \left(\frac{(\Delta_2{}^n)^2}{(\Delta_1{}^n)^2}\right)^{(\gamma_{0q}{}^n)^2/I} + i\pi\left(\overline{\frac{(\gamma_{0q}{}^n)^2}{D}}\right).$$

Since $(\gamma_{0q}{}^n)^2/I$ is a very small number

$$\prod_{n>I} \left(\frac{(\Delta_2{}^n)^2}{(\Delta_1{}^n)^2}\right)^{(\gamma_{0q}{}^n)^2/I} \simeq 1$$

and the first term vanishes. We are therefore left with the equation

$$C^2\langle f|V_{00}-U|f\rangle + C^2\langle g|(V_{00}-U)^2+\overline{\Delta V^2}|f\rangle + i\pi\overline{\frac{(\gamma_{0q}{}^n)^2}{D}}$$
$$+ \int_{n\phi I} \frac{(\gamma_{0q}{}^n)^2}{D} \left\{\frac{W_{0q}-W_n}{W_{0q}-E}\right\}^3 \frac{dE_n}{W_n-E}. \qquad \ldots\ldots(4.15)$$

Here the sum over n has been replaced by an integral extending over all values of n except those included in I. This, when solved, ought to lead to a complex potential. However, we have to put in additional information—the strength function $\overline{((\gamma_{0q}{}^n)^2/D)}$. If this were done the integral could be evaluated and then using the same technique as before we could find V_{00} and $\overline{\Delta V^2}$ as functions of the potential well and of the incident energy. This involves an extensive programme and has not been carried out. However, if it were carried out our empirical knowledge of the radius and magnitude of the complex well might be used to eliminate some suggested forms of the strength function.

One fact which emerges from (4.15) is that the shape and width of the strength function may be entirely different from those of the experimental giant resonances.

§ 5. EXTENSIONS OF THE THEORY

5.1. *Other l Waves*

The above approach may be easily extended to the case of neutrons incident with $l \neq 0$. Then the formula equivalent to (3.5) is

$$\sigma_{\mathrm{T}l}=\sigma_{\mathrm{T}l}{}^{u}+\frac{4\pi}{k}\mathscr{I}\left[-\frac{1}{2ik}\frac{\hbar^2}{2m}(f_l-f_l{}^*)\frac{A_l{}^*}{A_l}\left\{\sum_n\frac{(\sum_p a_{cpl}{}''u_{pl}(r_0))^2}{W_{nl}-E}-\sum_p\frac{u_{pl}{}^2(r_0)}{W_{0pl}-E}\right\}\right] \qquad \ldots\ldots(5.1)$$

where f_l and A_l are defined in Kapur and Peierls' paper.

Following the method of § 3 through for this expression and making the same assumptions for $(a_{0pl}{}'')^2$ as for $(a_{0p}{}'')^2$ we find

$$\sigma_{\mathrm{T}l}=\sigma_{\mathrm{T}l}{}^{u}+\frac{4\pi}{k}\mathscr{I}\left[-\frac{1}{2ik}\frac{\hbar^2}{2m}(f_l-f_l{}^*)\frac{A_l{}^*}{A_l}\left\{C_l{}^2\langle F_l|V_{00}-U|F_l\rangle\right.\right.$$
$$\left.\left.+C_l{}^2\langle G_l|(V_{00}-U)^2+\overline{\Delta V^2}|F_l\rangle+\sum_n\frac{(a_{0ql}{}'')^2u_{ql}{}^2(r_0)}{W_{nl}-E}\left\{\frac{W_{0ql}-W_{nl}}{W_{0ql}-E}\right\}^3\right]. \qquad \ldots\ldots(5.2)$$

q_l labels the giant resonance of the lth partial wave on which the energy E lies. The terms from values of p other than $p=q$ which occur in (5.1) have been included in the expression

$$C_l{}^2\{\langle F_l|V_{00}-U|F_l\rangle+\langle G_l|(V-U)_{00}{}^2|F_l\rangle\}$$

as before.

$F_l(r)$ and $G_l(r)$ are again simple functions being solutions of

$$\left\{-\frac{\hbar^2}{2m}\frac{d^2}{dr^2}+\frac{l(l+1)}{r^2}+U(r)-E\right\}F_l(r)=0,$$
$$\left\{-\frac{\hbar^2}{2m}\frac{d^2}{dr^2}+\frac{l(l+1)}{r^2}+U(r)-E\right\}G_l(r)=F_l(r).$$

If U is chosen to be a square well F_l is just a spherical Bessel function and G_l an expression involving such functions. It is interesting to note that if we wish to choose a $U(r)$ to satisfy the condition

$$\langle F_l|V_{00}-U|F_l\rangle+\langle G_l|(V-U)_{00}{}^2|F_l\rangle=0$$

then we have to solve a different equation for each l value. Therefore if we averaged (5.2) over the interval I in order to find a $U(r)$ to make $\sigma_{\mathrm{T}l}{}^{u}=\overline{\sigma_{\mathrm{T}l}}$ it appears that we would find a $U(r)$ which would depend upon the l value of the neutron. However, it may be that these various wells $U_l(r)$ are not very different from each other.

5.2. *Elastic Scattering*

We consider again for simplicity only the case of $l=0$ neutrons. The elastic cross section is then given by $\sigma_{\mathrm{el}}=4\pi|S_0|^2$ and by $\sigma_{\mathrm{el}}{}^{u}=4\pi|S_0{}^{u}|^2$ for the elastic scattering by a potential well. Previously we expanded S_{T} by $S_0=S_0{}^{u}+R$ where R is given in (3.9). We then found the $U(r)$ which reproduces the average total cross section by imposing the condition that $\overline{R}=0$. However, if we now consider the average elastic cross section we find

$$\overline{\sigma_{\mathrm{el}}}=\overline{4\pi|S_0|^2}=4\pi\overline{|S_0{}^{u}|^2}+4\pi\mathscr{R}(S_0{}^{u}\overline{R}{}^*)+\overline{|R|^2}$$
$$=4\pi|S_0{}^{u}|^2+\overline{|R|^2}$$

if $\overline{R}$ is chosen to be zero. Since there is no reason for $\overline{|R|^2}$ to be zero it seems that the $U(r)$ which gives the average total cross section will not also give the average elastic cross section. This may account for the less accurate agreement between the experimental average elastic cross sections and the elastic cross sections of the usual optical potential.

§ 6. R-MATRIX FORMALISM

The theory may be carried through quite easily in terms of the Wigner Eisenbud formalism. In this case the eigenvalues of the nuclear states are real. The eigenfunctions and eigenvalues of the compound nucleus are now denoted by $\phi_\lambda(\mathbf{r}, \xi)$, E_λ and the eigenfunctions and eigenvalues of the potential well by $v_p(\mathbf{r})$, W_{0p}.

The boundary conditions on the eigenfunctions are that the derivatives vanish at $r = r_0$. $v_p(\mathbf{r})$ and W_{0p} will still contain imaginary parts from the complex nature of $U(r)$.

Then
$$\sigma_{\mathrm{T}} = \frac{2\pi}{k^2} \mathscr{R}(1 - U_{\mathrm{T}})$$
where
$$U_{\mathrm{T}} = e^{-2ikr_0} \left\{ \frac{1 + ikR_{\mathrm{T}}}{1 - ikR_{\mathrm{T}}} \right\},$$
$$R_{\mathrm{T}} = \frac{\hbar^2}{2m} \sum_\lambda \frac{\{\phi\,(r_0, \xi)\chi_0(\xi)\,d\Omega\,d\xi\}^2}{E_\lambda - E}.$$

These expressions are strictly valid only in the case involving one channel. For scattering from $U(r)$, R_{T} is replaced by R_u where
$$R_u = \frac{\hbar^2}{2m} \sum_p \frac{v_p{}^2(r_0)}{W_{0p} - E}.$$

Just as before we write
$$\sigma_{\mathrm{T}} = \sigma_{\mathrm{T}}{}^u + \frac{4\pi}{k^2} \mathscr{R} \left\{ \frac{ik(R_u - R_{\mathrm{T}})}{(1 - ikR_u)(1 - ikR_{\mathrm{T}})} \right\}$$
and impose the condition that the average value of the second term is zero. By expanding the denominator of R_{T} we may write
$$\begin{aligned} R_{\mathrm{T}} = R_u - \sum_p \frac{v_p{}^2(r_0)}{(W_{0p} - E)^2} & \left\{ \langle 0p | V - U | 0p \rangle + \frac{\langle 0p | (V - U)^2 | 0p \rangle}{W_{0p} - E} \right\} \\ + \sum_n & \frac{(\alpha_{0q}{}^\lambda)^2 v_q{}^2(r_0)}{E_\lambda - E} \left\{ \frac{W_{0q} - E}{W_{0q} - E} \right\}^3 \\ = R_u & + R_1 + R_2 + R_3 \end{aligned}$$
where $\alpha_{0p}{}^\lambda$ are the expansion coefficients equivalent to $a_{0p}{}^n$. We have therefore
$$\sigma_{\mathrm{T}} = \sigma_{\mathrm{T}}{}^u + \frac{4\pi}{k^2} \mathscr{R} \left[\frac{ik(R_1 + R_2 + R_3)}{(1 - ikR_u)(1 - ik\{R_u + R_1 + R_2 + R_3\})} \right].$$

If we use the method of Thomas (1955) for averaging σ_{T} we find
$$\overline{\sigma_{\mathrm{T}}} = \sigma_{\mathrm{T}}{}^u + \frac{4\pi}{k^2} \mathscr{R} \left[\frac{ik(R_1 + R_2 + \overline{R_3})}{(1 - ikR_u)(1 - ik\{R_u + R_1 + R_2 + R_3\})} \right]$$
where
$$\overline{R_3} = i\pi \frac{\overline{(\gamma_{0q}{}^\lambda)^2}}{D} + \mathscr{P} \int \left(\frac{\overline{(\gamma_{0q}{}^\lambda)^2}}{D} \right) \left(\frac{W_{0p} - E_\lambda}{W_{0p} - E} \right)^3 \frac{dE_\lambda}{E_\lambda - E}.$$

Imposing the condition that $R_1 + R_2 + R_3 = 0$ gives an equation
$$\begin{aligned} C^2 \langle f | V_{00} - U | f \rangle + C^2 \langle g | (V_{00} - U)^2 + \overline{\Delta V^2} | f \rangle + i\pi \frac{(\gamma_{0q}{}^\lambda)^2}{D} & \\ + \mathscr{P} \int \left(\frac{(\gamma_{0q}{}^\lambda)^2}{D} \right) \left(\frac{W_{0p} - E_\lambda}{W_{0p} - E} \right) \frac{dE_\lambda}{E_\lambda - E} & = 0 \end{aligned}$$
which is very similar to (4.15).

The usual advantage of the Wigner–Eisenbud formalism is that most of the constants which appear are real and do not depend upon k through the boundary conditions. (If U is complex the W_{cp} and v_p will in general be complex although if U is a square well the v_p become real.) However, this reality does not appear to simplify the above theory at all, the complex relation introduced between the cross section and the R function being troublesome. This becomes even more complicated when more than one channel is open. The R function then becomes an R matrix and the cross sections are then given by expressions which become unmanageable. The Kapur–Peierls formalism, however, can be extended rather easily to the case with many open channels. In addition, the simple relations between the cross sections and the quantity S give a clearer picture of the relation between the real cross section and the cross section from a potential well.

Since the completion of this work, Dr. G. E. Brown has shown that the single particle levels are much more than 10 MEV apart in nuclei of intermediate A. Therefore, the intermediate model described in § 3 can be justified, and the region of validity of the development in § 4 is quite great. These points will be discussed in a forthcoming paper by Dr. Brown.

ACKNOWLEDGMENTS

The author wishes to thank Professor R. E. Peierls for suggesting the problem and for his encouragement and many helpful discussions during the course of the work. He also wishes to thank Dr. Erich Vogt for his interest and advice during the course of the work.

The award of a Maintenance Grant from the Department of Scientific and Industrial Research is gratefully acknowledged.

REFERENCES

BRUECKNER, K. A., 1955, *Phys. Rev.*, **97,** 153.
FESHBACH, H., PORTER, C. E., and WEISSKOPF, V. F., 1954, *Phys. Rev.*, **98,** 693.
KAPUR, L., and PEIERLS, R. E., 1938, *Proc. Roy. Soc.* A, **166,** 277.
LANE, A., THOMAS, R. G., and WIGNER, E. P., 1955, *Phys. Rev.*, **98,** 893.
MAYER, G. M., 1949, *Phys. Rev.*, **75,** 1949.
MOON, P. B., and TILLMAN, J. R., 1935, *Nature, Lond.*, **135,** 904.
OKAZAKI, A., DARDEN, S. E., and WATTON, R. B., 1954, *Phys. Rev.*, **93,** 462.
PEASLEE, 1955, *Ann. Rev. Nuclear Sci.* (Palo Atto: Annual Review Inc.)
THOMAS, R. G., 1955, *Phys. Rev.*, **97,** 224.
WALT, M., and BARSCHALL, H. H., 1954, *Phys. Rev.*, **93,** 1062.
WIGNER, E. P., and EISENBUD, L., 1947, *Phys. Rev.*, **72,** 29.

Addendum to the Paper "Calculation of the Interatomic Distance at which a Model of Compressed Solid Helium becomes a Metal"

By C. A. TEN SELDAM
Van der Waals Laboratorium, Gemeente Universiteit van Amsterdam, Netherlands

Communicated by N. F. Mott ; MS. received 22nd March 1957

In § 6 of the above mentioned paper (ten Seldam 1957) the exchange contribution to the energies of the top level of the first Brillouin zone, and of the lowest level of the second one, was calculated by formula (25), for the derivation of which the linear combinations $\phi_i(\mathbf{r})$, given by (22), were used.

In the text after (22) the remark was made, that the use of the four values of $\mathbf{K}_\alpha$ given (with $\mathbf{K}_\alpha a/\pi = 000$, 200, $\bar{1}11$ and $\bar{1}\bar{1}\bar{1}$) for *all* $\mathbf{k}_i$ would not result in the best possible four-plane-wave functions ϕ_i. In order to obtain better wave functions, one has to choose $\mathbf{K}_\alpha$'s which depend on the 48th part of the zone in which $\mathbf{k}_i$ lies. Thus in (22), (25) and in what follows after it, we must write $\mathbf{K}_{i\alpha}$, $\mathbf{K}_{j\beta}$, $\mathbf{K}_{i\gamma}$, $\mathbf{K}_{j\delta}$. The given values of $\mathbf{K}_{i\alpha} a/\pi$ hold for $\mathbf{k}_j$ in the top 48th part shown in the figure, i.e. for $\mathbf{k}_i a/\pi$ equal to any vector (ξ, η, ζ) for which $1 \geqslant \xi \geqslant \eta \geqslant \zeta \geqslant 0$, $\xi + \eta + \zeta \leqslant 3/2$. However, for $\mathbf{k}_i a/\pi = (-\xi, \eta, \zeta)$ the values of $\mathbf{K}_{i\alpha} a/\pi$ should be 000, 200, 111, 111; for $\mathbf{k}_i a/\pi = (\xi, \zeta, \eta)$ they are 000, $\bar{2}00$, $\bar{1}1\bar{1}$, $11\bar{1}$; etc. (the components of the $\mathbf{K}_{i\alpha}$ permuting and changing sign together with those of $\mathbf{k}_i$ through the 48 possibilities). The point $\mathrm{L}(\xi = \eta = \zeta = \frac{1}{2})$, which belongs to six 48th parts, has to be considered six times, with the $\mathbf{K}_{i\alpha}$'s pertaining to a different 48th part each time, and the sum of the results has to be divided by six. Similar considerations apply to the other points of high symmetry. (However, this 'hybridization' is necessary for the $\mathbf{k}_j$'s only: for the two values of $\mathbf{k}_i$ it follows from symmetry considerations that the same results will be obtained with either $\mathbf{k}_j$'s *and* $\mathbf{k}_i$'s hybridized or only the $\mathbf{k}_j$'s). The number of non-zero terms in (27) is sometimes 28, sometimes 26, the average value over 48 homologous points being $26\frac{2}{3}$.

Also, $(\pi/2a)^3 \Sigma_j g W_{ij}$ is calculated for $\mathbf{k}_j a/\pi = \frac{1}{2}(I, I', I'')$ (I, etc. arbitrary integers) and $\Sigma_j g = 32$. Again these results are corrected by the ratio of case V results for $\Sigma g = 256$ and 32 respectively. The results are given in the row marked VII of tables 1 and 2 (which correspond to tables 2 and 4 of the previous paper), together with case VI in which the same $\mathbf{K}_\alpha$'s were used throughout, case IV in which the integration region was the Fermi sphere and plane waves were used (cf. § 5 of previous paper), and case II, the 'ionic' calculation.

The pressures have been obtained as in § 8 of the previous paper.

The change in the results compared with those of case VI is largest for the point W (top level, first band). Analysis of the source of the difference indicates that the error in case VI, due to using constant $\mathbf{K}_\alpha$'s throughout, is greatest in the contribution of the 24 points $\mathbf{k}_j = \mathbf{k}_j(\mathrm{W})$ to $\Sigma_j g W_{ij}$. In the case of point L (lowest level, second band) the fact that the function ϕ_i is antisymmetric with respect to the points $\mathbf{k}_i a/\pi = \frac{1}{2}\frac{1}{2}\frac{1}{2}$ and $= -\frac{1}{2} -\frac{1}{2} -\frac{1}{2}$ tends to reduce the error.

Table 1. $V_x(\mathbf{k}_i) = W_i$ (contribution of exchange hole) $+ E_{em}$ (due to the difference in effective mass)

Energy (ryd)	Case	Integrated over	Functions used	κ_χ's used	Point L $a=2$	Point L $a=1{\cdot}5$	Point L $a=1{\cdot}25$	Point W $a=2$	Point W $a=1{\cdot}5$	Point W $a=1{\cdot}25$
$(V_x \mathbf{k}_i)$	IV	Fermi sphere	plane waves	—	−0·6428	−0·9017	−1·1204	−0·4985	−0·6895	−0·8460
$V_x(\mathbf{k}_i)$	VI	1st zone	lin. comb.	const. throughout	−0·4498	−0·6323	−0·7870	−0·5730	−0·7881	−0·9617
$V_x(\mathbf{k}_i)$	VII	1st zone	lin. comb.	dep. on $\mathbf{k}_i$	−0·4831	−0·6740	−0·8342	−0·7612	−1·0624	−1·3120
E^{e}_{m} ((19) of previous paper), included in all cases					−0·0292	−0·0403	−0·0479	−0·0487	−0·0672	−0·0798
ratio $W_i(\text{VI})/W_i(\text{IV})$					0·6998	0·7012	0·7027	1·1494	1·1430	1·1368
ratio $W_i(\text{VII})/W_i(\text{IV})$					0·7516	0·7475	0·7446	1·5270	1·5408	1·5508

Table 2. Results

Case	Remarks	$L(f_{1s})-W(f_1)$(ryd) $\equiv F$ $a=2$†	$a=1{\cdot}5$	$a=1{\cdot}25$	$a_{F=0}$ at	density (g cm^{-3})	pressure (megatm) p_0	p
II	‘ ionic ’ case	1·082	0·820	0·385	1·090‡	17·20	222	191
IV	(cf. table 1)	0·229	−0·027	−0·489	1·519	6·35	35·0	28·1
VI		0·496	0·341	−0·040	1·271	10·85	96·9	80·9
VII		0·651	0·573	0·263	1·105‡	16·51	207	177
Baltensperger's estimate of transition pressure								18

† a in atomic units ‡ extrapolation $a_{F=0} < 1{\cdot}25$

The resultant interatomic distance ($=2^{1/2}a$) at which overlap of the first two bands occurs, together with the corresponding density and pressure, are rather near to those for the Wigner–Seitz potential ('ionic' case). This suggests that the latter may be less unrealistic than previously thought.

Though done mainly in Amsterdam—within the framework of my work for the "Stichting voor Fundamenteel Onderzoek der Materie" (F. O. M.), which is made possible by financial support of the Nederlandse Organisatie voor Zuiver Wetenschappelijk Onderzoek (Z. W. O.)—this investigation is a continuation of work carried out during my stay in Cambridge, England (cf. acknowledgments of previous paper). Also for this paper I am indebted to Mr. V. Heine for helpful suggestions.

REFERENCES

TEN SELDAM, C. A., 1957, *Proc. Phys. Soc.* A, **70,** 97.

RESEARCH NOTES

Weak Collective Effects in the Nuclear Shell Model

By R. D. AMADO and R. J. BLIN-STOYLE
Clarendon Laboratory, Oxford

MS. received 28*th February* 1957

§ 1. Introduction

Eigenstates generated by considering particles moving independently in a spherically symmetric potential well are, according to the shell model of Mayer and Jensen (1955), good approximations for calculating the ground state and low energy properties of nuclei, particularly near closed shells. But even for nuclei differing by only one particle from a closed shell, weak collective effects have been found that can only be explained by calling into play most or all of the particles in the closed shell core. Hitherto, effects of this type have generally been interpreted in terms of weak collective coupling between the odd particle and the nuclear surface (Bohr and Mottelson 1953). An alternative approach, more nearly in the spirit of the shell model, is now proposed in which the residual two-body interaction between the odd particle and the core is used as a perturbation to mix in excited core configurations. The perturbed wave function can then be used to calculate the matrix element of some nuclear operator, and in this paper we are particularly interested in Q, the electric quadrupole operator, in which case the first order collective contribution is of the form

$$-\sum_i{}' \frac{\langle J|Q|i\rangle\langle i|(V-U)|J'\rangle}{E_i-E_{J'}} \qquad \ldots\ldots(1)$$

where the matrix element is taken between zero order shell model eigenstates $|J\rangle$ and $|J'\rangle$, and the $|i\rangle$ are the complete set of states of the zero order problem. If the odd particle is a neutron or neutron hole, there is no contribution from the average potential U, which generates the zero order states, and only the two-body interaction V need be retained. Furthermore, in this case, the sum in (1) can be taken over all states $|i\rangle$, including $|i\rangle=|J'\rangle$, since $\langle J|Q|J'\rangle=0$. We are thus interested in those states $|i\rangle$ which represent excitations of the core to 2^+ states differing from the ground state by only one particle. For an L–S closed shell these will result from excitations of a particle to a state two shells away in the oscillator sense and from higher excitations. For a j–j closed shell there may also be contributions from excitations to the other member of a spin–orbit doublet. If we assume that the combined effect of the large energy denominator, the selection of states by Q, and the potential coupling, all contribute to cutting off the sum quickly, then we can approximate it by closure, getting for (1)

$$-\frac{1}{\overline{E}}\langle J|QV|J'\rangle \qquad \ldots\ldots(2)$$

where $\overline{E}$ is a mean excitation energy. The closure approach has the great advantage of not requiring us to give in detail any but the ground state configuration.

It should be noted that (2) can also be arrived at from a closure wave function of the form

$$|\,\rangle = [1 - V/\bar{E}]|J\rangle.$$

This shows more clearly that the odd particle interacts with the core giving a sort of polarization of strength V and with 'stiffness' measured by $\bar{E}$. Wave functions of this general type have been used in variational calculations (Lennard-Jones 1930, Feingold 1956), but it is well to notice that $\bar{E}$ depends on the selection properties of the operator, in this case $\underset{\sim}{Q}$.

One expects to fit experiment with a mean excitation energy of the order of four times the separation between oscillator levels, the extra factor of two arising essentially from the velocity dependence of the potential well. That this factor should be there, thus improving the perturbation approximation, has been pointed out by Swiatecki (1956). A further point to be noticed is that, since the interaction V depends only on the relative coordinates, if $|J\rangle$ is an antisymmetric proper state of internal motion, then only antisymmetric excited states of internal motion will be coupled in, and no difficulties will arise with spurious states (Elliott and Skyrme 1955).

§ 2. APPLICATIONS NEAR THE LEAD CLOSED SHELL

This formulation has been applied to the weak collective effects near the lead doubly closed shell. To evaluate the matrix elements we use, instead of a sum over the core particles, a nuclear density distribution (Blin-Stoyle 1955) which reproduces the main features of the density distribution obtained from high energy electron scattering experiments (Hofstadter 1956). For the odd particle we use eigenstates in an infinite potential well. The interaction is treated in a range expansion going to one term beyond the delta function and its exchange dependence is taken as a Rosenfeld mixture (Rosenfeld 1948). The matrix elements are then evaluated in a straightforward manner, the radial integrals being done graphically. A fit can be made with experiment treating both $\bar{E}$ and the density edge thickness t as parameters.

In the one neutron hole nucleus ^{207}Pb, there is a 0·569 MEV E2 transition from the $f_{5/2}$ state to the $p_{1/2}$ ground state for which the lifetime is known. There is also a 1·72 MEV mixed M1–E2 transition from the $f_{7/2}$ to the $f_{5/2}$ state. One can assign an E2 lifetime to this transition from the mixing ratio by making the reasonable assumption that the M1 is of single particle strength. The details of the experimental data on ^{207}Pb are given by Alburger and Sunyar (1955). In ^{206}Pb the lifetime of the 2^+ to 0^+ E2 transition to the ground state has been measured by Stelson and McGowan (1955). For this case we have used a wave function for the 2^+ state calculated by Dr. Mary Kearsley (private communication 1956) that allows for configuration interaction between the two holes. In ^{209}Bi the quadrupole moment of the $h_{9/2}$ ground state is too big to be completely ascribed to the odd proton (Blin-Stoyle 1956). In calculating this case, however, the diagonal term must be subtracted from the closure sum since the odd particle is now a proton. Care must also be taken with antisymmetry. Thus for a delta function interaction the odd proton can only interact with the $Z/2$ protons in the core with spin opposite to it. Fitting the experimental results one finds that for an edge thickness $t = 0{\cdot}3$ (a value consistent with the electron scattering data), the mean excitation energies for the two transitions in ^{207}Pb and for the ground state moment of ^{209}Bi are all within 5% of 45 MeV, a value consistent with our expectations. Interestingly, for t very different from 0·3 there is no agreement. For ^{206}Pb, at $t = 0{\cdot}3$, the mean excitation energy is 35 MeV, but since ^{06}Pb differs by two particles from a closed shell, it might be expected to be a ittle 'softer' than ^{207}Pb or ^{209}Bi, and also the particle mixtures in the zero order wave functions may introduce some arbitrariness.

These results are more consistent with experiment than those obtained by True (1956) using the weak surface coupling approach of the collective or unified model of Bohr and Mottelson (1953). In the surface coupling approximation the core is treated as incompressible and thus all the effect of the odd particle is at the surface of the core. Further by quantizing the surface oscillations, the details of the effect of the odd particle are averaged out. In the configuration mixing approach with closure, on the other hand, the odd particle causes local fluctuations in the density throughout the core, and the formulation allows one to take into account the details of this effect. This seems to be a better approximation and, further, since details of the mechanism are more easily understood, one can come closer to understanding any failures of the formulation.

§ 3. APPLICATION TO ^{17}O

In ^{17}O the low-lying positive parity levels and the ground state magnetic moment are very well understood on a pure single particle shell model approximation. But the decay of the $2s_{1/2}$ first excited state to the ground state is E2 with a lifetime of the order of a single proton lifetime (Ajzenberg and Lauritsen 1955). Furthermore, the $d_{5/2}$ ground state has a very small negative quadrupole moment (Geschwind, Gunther-Mohr and Townes 1951). Recent work, however, indicates that a good deal of doubt still exists about the value of the moment (Stevenson 1957). Both of these electric effects are forbidden by a pure single particle model for an odd neutron. If one tries to explain these effects by giving the odd neutron an effective charge (this is the essential effect of a weak surface coupling calculation), one finds that ten times the effective charge is needed for the E2 transition over that for the ground state moment. Attempts have been made to reconcile the ground state moment as arising from centre of mass recoil, but as Elliott and Skyrme (1955, 1956) have shown, for proper internal states the recoil contribution vanishes identically, essentially because of antisymmetry. Furthermore, harmonic oscillator states are proper for one particle in the lowest shell outside completely filled shells. The effect of departure from harmonic oscillator has been investigated, and for the extreme case of an infinite square well, the recoil contribution can be as much as 10% of the classical recoil (Amado and Satchler, unpublished), but this is still too small to explain the ground state moment, and further the harmonic oscillator functions are considered to be a good approximation in the region of oxygen.

The configuration mixing approach with closure can be used to calculate these collective effects. A Gaussian radial dependence is taken for the force with a Rosenfeld exchange dependence. The wave functions are taken as determinants of harmonic oscillator single particle eigenfunctions. The matrix elements are then easily evaluated by expanding the interaction in spherical harmonics. We find that the mean excitation energy needed to fit the ground state moment is about seven times larger than the one needed to fit the E2. This result is independent of the exchange mixture and very insensitive to the range of the force. In fact since for oxygen the range of the force is of the order of the nuclear radius, reasonable variations in the form of the force or of the wave functions have almost no effect on the matrix elements.

If one neglects spin-orbit splittings, the closure approximation is exact in ^{17}O, since for harmonic oscillator functions the selection rules on matrix elements of $\underset{\sim}{Q}$ only allow excitations from the core of 1s to 1d, 1p to 2p, and 1p to 1f, all of which have an energy of twice the oscillator splitting. We have done a detailed calculation without closure of the separate contributions of each of the excitations in *j–j* coupling using the same interaction and wave functions as in the closure calculation. In all, of course, the result is the same as the closure, but it allows a more detailed view. We find that the 1p to 2p excitations contribute very little, and that the $1p_{3/2}$ to $1f_{7/2}$ gives the largest contribution, but in general the calculation yields no great surprises. One still finds that no reasonable values of the parameters will remove the factor of seven between the fitting of the E2 and of the ground state moment. Using semi-empirical values for the excitation energies, that is assuming that the energy of the negative parity states give an order of magnitude of the shell separation in oxygen, one finds that one can fit the transition probability quite well; but this of course still leaves a ground state quadrupole moment seven times larger than the one measured by Geschwind *et al.* A re-measurement of this moment is therefore of considerable interest.†

ACKNOWLEDGMENT

One of the authors (R. D. A.) is indebted to the Rhodes Trustees for the grant of a scholarship.

REFERENCES

AJZENBERG, F., and LAURITSEN, T., 1955, *Rev. Mod. Phys.*, **27,** 77.

ALBURGER, D. E., and SUNYAR, A. W., 1955, *Phys. Rev.*, **99,** 695.

BLIN-STOYLE, R. J., 1955, *Phil. Mag.*, **46,** 973 ; 1956, *Rev. Mod. Phys.*, **28,** 75.

BOHR, A., and MOTTELSON, B. R., 1953, *K. Danske. Vidensk. Selsk., Mat. Fys. Medd.*, **27,** no. 16.

ELLIOTT, J. P., and SKYRME, T. H. R., 1955, *Proc. Roy. Soc.* A, **232,** 561 ; 1956, *Nuovo Cim.*, **4,** 164.

FEINGOLD, A. M., 1956, *Phys. Rev.*, **101,** 258.

GESCHWIND, S., GUNTHER-MOHR, G. R., and TOWNES, C. H., 1951, *Phys. Rev.*, **83,** 209.

HOFSTADTER, R., 1956, *Rev. Mod. Phys.*, **28,** 214.

LENNARD-JONES, J. E., 1930, *Proc. Roy. Soc.* A, **129,** 598.

MAYER, M. G., and JENSEN, J. H. D., 1955, *Elementary Theory of Nuclear Shell Structure* (New York : Wiley).

ROSENFELD, L., 1948, *Nuclear Forces* (Amsterdam : North-Holland).

STELSON, P. H., and MCGOWAN, F. K., 1955, *Phys. Rev.*, **99,** 112.

STEVENSON, M. J., 1957, *Bull. Amer. Phys. Soc.*, Series II, **2,** 31.

SWIATECKI, W. J., 1956, *Phys. Rev.*, **101,** 1321.

TRUE, W. W., 1956, *Phys. Rev.*, **101,** 1342.

† *Note added in proof.* A new value has been obtained by R. A. Kamper, K. R. Lea and C. D. Lustig working under B. Bleaney (to be published) for the ground state quadrupole moment from the hyperfine structure of ^{17}O of $Q = -0{\cdot}027 \pm 0{\cdot}004$ barn. This is in agreement with our calculation and allows a consistent account of the ground state moment and the E2 transition.

The Scattering of Fast Charged Particles
III: On the Single Scattering of High Energy Positrons and Electrons at Small Angles

By K. R. ALLEN, K. PHILLIPS AND F. WHITTAKER
Research Department, Metropolitan-Vickers Electrical Co. Ltd., Manchester

MS. received 23rd January 1957, and in final form 13th March 1957

The Mott cross section for the Coulomb scattering of electrons of velocity β through an angle θ is expressed as:

$$\sigma=\frac{1}{K^2}\left[q^2(1-\beta^2)|F|^2\operatorname{cosec}^2\tfrac{1}{2}\theta+|G|^2\sec^2\tfrac{1}{2}\theta\right]$$

where $q=\alpha/\beta$, $K^2=m_0{}^2v^2/\hbar^2(1-\beta^2)$, $\alpha=Z\mathbf{e}^2/\hbar\mathbf{c}=Z/137$, $\beta=v/\mathbf{c}$.

Replacing Z by $-Z$ gives the cross section for positron scattering.

McKinley and Feshbach (1948) expanded F and G as a series in powers of α and α/β up to α^4. This was extended by Curr (1955) up to α^6.

These results were only calculated for scattering angles greater than 30°. More recently Doggett and Spencer (1956) have given tables of the scattering cross section for electrons and positrons for $Z=6$, 13, 29, 50, 82 and 92 at various energies. Accurate values of the scattering cross section at small angles are particularly useful in estimating the differences in the multiple scattering of electrons and positrons (Mohr 1954) and it is the purpose of this note to give the results of calculations for angles less than 30°.

We have for F and G, $F=F_0+F_1$ and $G=G_0+G_1$, where

$$F_0=\tfrac{1}{2}i\exp\left(iq\ln\sin^2\tfrac{1}{2}\theta\right)\frac{\Gamma(1-iq)}{\Gamma(1+iq)}$$

and

$$G_0=-iqF_0\cot^2\tfrac{1}{2}\theta$$

with

$$F_1=\tfrac{1}{2}i\sum_{k=0}^{\infty}\left[k^2D_k+(k+1)D_{k+1}\right](-)^kP_k(\cos\theta)$$

$$G_1=\tfrac{1}{2}i\sum_{k=0}^{\infty}\left[k^2D_k-(k+1)D_{k+1}\right](-)^kP_k(\cos\theta)$$

where $$D_k=\exp(-\pi ik)\frac{\Gamma(k-iq)}{\Gamma(k+1+iq)}-\exp(-\pi i\rho_k)\frac{\Gamma(\rho_k-iq)}{\Gamma(\rho_k+1+iq)}$$

and $\rho_k=(k^2-\alpha^2)^{1/2}$.

F and G can be expressed approximately as

$$F=F_0+A(\theta)\alpha^2+B(\theta)\alpha^3/\beta+C(\theta)\alpha^4/\beta^2+D(\theta)\alpha^4$$
$$G=G_0+E(\theta)\alpha^2+H(\theta)\alpha^3/\beta+I(\theta)\alpha^4/\beta^2+J(\theta)\alpha^4.$$

The values of the coefficients in these series have been summed numerically for values of θ from 5 to 30 degrees on the Manchester University Electronic Computer Mk.I. This machine has two types of storage; a quick access store (cathode-ray tubes) and a long term magnetic drum storage. For this problem the simplified system of coding (Autocode) described by Brooker (1955) was used. Even at the expense of longer machine time, it was well worth while to use Autocode, as this made the actual programming of the calculations so very much easier and speedier than would otherwise have been the case.

The coefficients in the F series converge as $1/k^2$ and can be readily evaluated; in the G series however, they are of the form

$$\sum_{k=1}^{\infty} \psi_n(k) P_k(\cos\theta)$$

where $\psi_n(k)$ are polygamma functions. If $\theta = \pi/m$, then for large values of k the Legendre polynomials $P_k(\cos\theta)$ change sign every m terms. Whenever $P_k(\cos\theta)$ changes sign the series $\Sigma_{k=1}^{\infty}\psi_n(k)P_k(\cos\theta)$ has an upper or a lower limit (according to whether $P_k(\cos\theta)$ has just been positive or negative). The programmes for each series were arranged to generate the Legendre polynomials and the polygamma functions as required during the calculation (by means of recurrence formulae) and to print out alternately at predetermined intervals an upper and a lower limit of the sum. The average of an upper and a lower limit gave a value S_{u} slightly greater than S_{∞}, and the average of a lower and an upper limit gave a value S_{l} slightly less than S_{∞}. The average, equal to $\frac{1}{2}(S_{\mathrm{u}} + S_{\mathrm{l}})$, gave an even better approximation to the value S_{∞}. When values of the successive averages $\frac{1}{2}(S_{\mathrm{u}} + S_{\mathrm{l}})$ and $\frac{1}{2}(S_{\mathrm{l}} + S_{\mathrm{u}})$ came equal (within the limits of accuracy required) then this value was taken as equal to S_{∞}. The speed of convergence varied considerably from one series to another. The series of some coefficients converged sufficiently after about 30 terms for $\theta = 30°$, whereas more than 1000 terms were needed for several series at $\theta = 5°$. The speed of calculation varied according to the complexity of the expression required for each series. For series H the calculation was at the rate of 500 terms per hour, the real and imaginary parts being summed simultaneously.

In an attempt to avoid the difficulties of the slow convergence of series G, Bartlett and Watson (1940) split the G_1 series into three parts. In the present calculation this was considered unnecessary as it would have only meant a more complicated programme for the computer. The coefficients have real and imaginary components and are tabulated in table 1 for angles 5, 10, 20 and 30

Table 1. Coefficients in the Series Expansion of F_1 and G_1

θ (deg)	5	10	20	30
A_{r}	−0·0671	−0·1312	−0·2515	−0·3616
A_{i}	0·0035	0·0112	0·0344	0·0639
B_{r}	0·0016	−0·0028	−0·0326	−0·0866
B_{i}	0·3021	0·4241	0·5086	0·4909
C_{r}	0·7716	0·8308	0·7233	0·5753
C_{i}	−0·0033	−0·0015	0·0011	−0·0110
D_{r}	−0·0036	−0·0137	−0·0512	−0·1073
D_{i}	−0·0077	−0·0242	−0·0716	−0·1287
E_{r}	17·220	8·2227	3·7401	2·247
E_{i}	−1·5661	−1·2200	−0·8754	−0·6758
H_{r}	0·2110	1·0449	1·3932	1·371
H_{i}	−44·60	−11·133	−0·6816	1·048
I_{r}	−43·863	1·1779	4·8230	2·979
I_{i}	−0·0110	−0·3606	0·1016	0·4695
J_{r}	1·8362	1·7368	1·5453	1·3635
J_{i}	3·4164	2·5693	1·7404	1·2765
K_{r}	−14·73	−7·012	−2·493	−1·6077
M_{r}	8·9755	5·1981	2·5844	1·5680

degrees, A_r and A_i are the real and imaginary part of A etc. The values of the coefficients at 30 degrees agree well with those given by Curr, but differ from McKinley and Feshbach in the cases of J_r and J_i, and H_r, I_r. H_i and I_r seem to diverge rapidly at 5 degrees and in order to check that this result was not spurious these coefficients were calculated at the intermediate angle of 7·5 degrees.

The ratio of the Mott (α^4 approximation) scattering to Rutherford can then be expressed as a series.

$$\begin{aligned} R = {} & 1 - \beta^2 \sin^2 \tfrac{1}{2}\theta + \alpha\beta R_1 + \alpha^2\beta^2 R_2' \\ & + (\alpha^3/\beta) R_3 + \alpha^3\beta R_3' + (\alpha^4/\beta^2) R_4 + \alpha^4 R_4' \\ & + \alpha^4\beta^2 R_4''. \end{aligned}$$

The values of the coefficients $R_{,,}$ are tabulated for angles 5, 10 and 20 degrees in table 2.

Table 2. Coefficients in the Series Expansion for R

θ (deg)	5	10	20
R_1	0·1311	0·2498	0·4511
R_2	0·0625	0·1702	0·4200
R_2'	0·0043	0·0157	0·0512
R_3	−0·3108	−0·4398	−0·4764
R_3'	0·0164	0·0651	0·2398
R_4	−0·3882	−0·6850	−0·9545
R_4'	−0·0577	−0·0970	−0·0177
R_4''	0·0008	0·0054	0·0328

For the purpose of comparison the ratio R to Rutherford scattering for positrons and electrons has been calculated for Z equal to 54 (xenon) based on the values of the coefficients $R_{,,}$ in table 2 and the variation with θ is shown in the figure. The values of R calculated from the results of McKinley and Feshbach are shown at 30 and 45 degrees and Curr's calculations (α^6 approximation) give values which differ from these by less than one per cent.

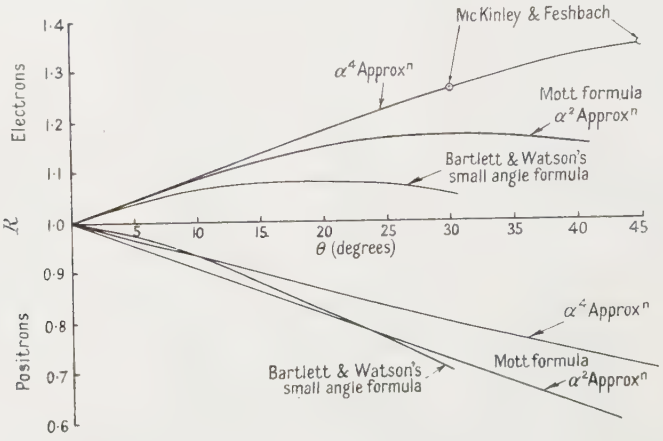

The ratio R of the theoretical values of the cross section to Rutherford scattering for electrons and positrons in xenon ($Z = 54$)

The ratio R has also been calculated from the Mott formula (α^2 approximation)

$$R = 1 - \beta^2 \sin^2 \tfrac{1}{2}\theta + \pi\alpha\beta \sin \tfrac{1}{2}\theta (1 - \sin \tfrac{1}{2}\theta).$$

These two results agree well up to about 10 degrees but for larger scattering angles the values of R diverge, the value given by the higher approximation being larger for both positrons and electrons.

Bartlett and Watson have given a small angle formula for high energies and have taken G_1 equal to G_1^{ϕ}, this being the part which has a singularity at $\theta = 0$.

The resulting expression for the scattering intensity is

$$|G|^2 = \frac{\cot^4 \frac{1}{2}\theta}{\cos^2 \frac{1}{2}\theta}\left[\frac{q^2}{4} + \frac{\pi\alpha^2 q}{4}\sin\tfrac{1}{2}\theta\cos\chi\right]$$

where χ is defined by

$$e^{i\chi} = \frac{\Gamma(\frac{1}{2} - iq)\Gamma(1 + iq)}{\Gamma(\frac{1}{2} + iq)\Gamma(1 - iq)}.$$

The value of R deduced from this formula gives a poor approximation to the other curves for angles greater than about 10°.

ACKNOWLEDGMENTS

The authors wish to thank Dr. Willis Jackson, Director of Research and Education, and Mr. B. G. Churcher, Manager of Research Department, Metropolitan-Vickers Electrical Co. Ltd., for permission to publish this paper.

REFERENCES

BARTLETT, J. H., and WATSON, R. E., 1940, *Proc. Amer. Acad. Arts Sci.*, **74**, 53.
BROOKER, R. A., 1955, *Brit. J. Appl. Phys.*, **6**, 307.
CURR, R. M., 1955, *Proc. Phys. Soc.* A, **68**, 156.
DOGGETT, J. A., and SPENCER, L. V., 1956, *Phys. Rev.*, **103**, 1597.
MCKINLEY, W. A., and FESHBACH, H., 1948, *Phys. Rev.*, **74**, 1759.
MOHR, C. B. O., 1954, *Proc. Phys. Soc.* A, **67**, 730.

Electron Collision Partial Cross Sections for the 1s–2s and 1s–3s Transitions of Atomic Hydrogen

BY D. R. BATES AND D. MISKELLY

Department of Applied Mathematics, Queen's University of Belfast

MS. received 28th December 1956

THE total cross section $\mathcal{Q}$ associated with the excitation of a particular state of an atom by electron impact may be written

$$\mathcal{Q} = \sum_{l=0}^{\infty} q_l \qquad \text{......(1)}$$

the partial cross section, q_l, being the contribution arising from the component of the incident wave which has the azimuthal quantum number indicated by the subscript (cf. Mott and Massey 1949). When applying Born's approximation the simplest procedure is of course to determine $\mathcal{Q}$ directly. However, it is also desirable to use the approximation to compute the larger q_l's separately. The information obtained is required in connection with some of the more refined theoretical treatments (cf. Massey 1956). Further, insight is gained by comparing the computed values with the limits set by the conservation theorem of Mott, Bohr, Peierls and Placzek (cf. Mott and Massey 1949) and by examining how rapidly the truncated series

$$\mathcal{Q}_N = \sum_{l=0}^{N} q_l \qquad \ldots\ldots(2)$$

converges to $\mathcal{Q}$ as N is increased. In this note we give general expressions for the partial cross sections for the 1s–2s and 1s–3s transitions of atomic hydrogen and present more extensive numerical results than hitherto available.

The mathematical analysis involved in deriving the partial cross sections from Born's approximation need not be described; but it may be mentioned that use is made of the formula

$$\int_0^\infty \mathrm{J}_{l+\frac{1}{2}}(ar)\mathrm{J}_{l+\frac{1}{2}}(br)\exp(-cr)dr = \frac{1}{\pi(ab)^{1/2}}\, Q_l\left(\frac{a^2+b^2+c^2}{2ab}\right) \qquad \ldots\ldots(3)$$

where $\mathrm{J}_{l+\frac{1}{2}}$ is the standard Bessel function and Q_l is the standard Legendre function of the second kind (Watson 1944).

Denoting the initial velocity of the free electron by v_i and the final velocity by v_f, putting

$$k_\mathrm{i} = 2\pi m v_\mathrm{i}/h, \qquad k_\mathrm{f} = 2\pi m v_\mathrm{f}/h \qquad \ldots\ldots(4)$$

and employing atomic units we find that

$$q_l(1\mathrm{s}\text{–}n\mathrm{s}) = p_l(1\mathrm{s}\text{–}n\mathrm{s})^2(\pi a_0^2) \qquad \ldots\ldots(5)$$

with

$$p_l(1\mathrm{s}\text{–}2\mathrm{s}) = \frac{2(l+1)}{k_\mathrm{i}(2k_\mathrm{i}k_\mathrm{f})^{5/2}(x^2-1)^2}[\{2x^2 - l(x^2-1)\}Q_l(x) - 2xQ_{l+1}(x)] \qquad \ldots\ldots(6)$$

in which

$$x = (4k_\mathrm{i}^2 + 4k_\mathrm{f}^2 + 9)/8k_\mathrm{i}k_\mathrm{f}; \qquad \ldots\ldots(7)$$

and with

$$\begin{aligned} p_l(1\mathrm{s}\text{–}3\mathrm{s}) = \frac{4(l+1)(2l+1)^{1/2}}{k_\mathrm{i}(3k_\mathrm{i}k_\mathrm{f})^{5/2}(y^2-1)^2}\Big[& 3(\{(l+2)y^2 - l\}Q_l(y) - 2yQ_{l+1}(y)) \\ & + \frac{16}{27k_\mathrm{i}k_\mathrm{f}(y^2-1)}(\{(l^2+5l-2)y - (l^2+5l+6)y^3\}Q_l(y) \\ & - \{(l^2+l-2) - (l^2+l+6)y^2\}Q_{l+1}(y))\Big] \end{aligned} \qquad \ldots\ldots(8)$$

in which

$$y = (9k_\mathrm{i}^2 + 9k_\mathrm{f}^2 + 16)/18k_\mathrm{i}k_\mathrm{f}. \qquad \ldots\ldots(9)$$

For a specific value of l considerable simplification may readily be effected: each $q_l(1\mathrm{s}\text{–}2\mathrm{s})$ may be expressed as an elementary function of x and $\log\{(x+1)/(x-1)\}$, and each $q_l(1\mathrm{s}\text{–}3\mathrm{s})$ as an elementary function of y and $\log\{(y+1)/(y-1)\}$.

In the computational work it is convenient to take the independent variable to be

$$\Delta k = k_\mathrm{i} - k_\mathrm{f}. \qquad \ldots\ldots(10)$$

Clearly the maximum permissible Δk is the square root of the excitation energy (in units of I_H) and occurs at the threshold of the process, while the minimum is zero and occurs at infinite energy. For the larger Δk extremely severe cancellation is encountered but the difficulties this causes may be avoided by expanding the logarithmic terms in power series.

The derived values of the first five partial cross sections and of the total cross sections are given in tables 1 and 2. It is apparent that the conservation theorem limits (cf. Mott and Massey 1949) are not approached closely: thus even q_0(1s–2s) and q_0(1s–3s) are never more than 0·22 and 0·04 times the appropriate limit.

Table 1. 1s–2s Transition. Cross sections in units of $10^{-1}\pi a_0^2$

Δk (atomic units)	k_i^2 (atomic units)	Partial cross sections					Total cross section
		q_0	q_1	q_2	q_3	q_4	$\mathcal{Q}$
0·80	0·755	0·549	$0{\cdot}002_6$	$0{\cdot}000_0$	$0{\cdot}000_0$	$0{\cdot}000_0$	0·551
0·75	0·766	0·963	0·015	$0{\cdot}000_1$	$0{\cdot}000_0$	$0{\cdot}000_0$	0·978
0·70	0·784	1·346	0·046	$0{\cdot}000_6$	$0{\cdot}000_0$	$0{\cdot}000_0$	1·393
0·65	0·813	1·666	0·106	$0{\cdot}002_4$	$0{\cdot}000_0$	$0{\cdot}000_0$	1·774
0·60	0·856	1·892	0·199	$0{\cdot}007_5$	$0{\cdot}000_2$	$0{\cdot}000_0$	2·099
0·55	0·916	1·995	0·327	0·019	$0{\cdot}000_8$	$0{\cdot}000_0$	2·342
0·50	1·000	1·958	0·479	0·043	$0{\cdot}002_6$	$0{\cdot}000_1$	2·483
0·45	1·120	1·781	0·633	0·083	$0{\cdot}007_4$	$0{\cdot}000_5$	2·505
0·40	1·294	1·488	0·752	0·142	0·018	$0{\cdot}001_9$	2·403
0·35	1·554	1·126	0·795	0·214	0·040	$0{\cdot}005_9$	2·181
0·30	1·960	0·755	0·732	0·279	0·074	0·016	1·859
0·25	2·641	0·435	0·567	0·302	0·114	0·035	1·465
0·20	3·901	0·204	0·348	0·257	0·136	0·060	1·042
0·15	6·631	0·071	0·153	0·152	0·113	0·070	0·637
0·10	14·440	0·015	0·039	0·050	0·050	0·043	0·301
0·05	56·626	0·001	0·003	0·004	0·006	0·006	0·078
0·00	∞	0·000	0·000	0·000	0·000	0·000	0·000

Table 2. 1s–3s Transition. Cross sections in units of $10^{-2}\pi a_0^2$

Δk (atomic units)	k_i^2 (atomic units)	Partial cross sections					Total cross section
		q_0	q_1	q_2	q_3	q_4	$\mathcal{Q}$
0·80	0·913	2·003	0·039	$0{\cdot}000_2$	$0{\cdot}000_0$	$0{\cdot}000_0$	2·043
0·75	0·936	2·625	0·101	$0{\cdot}001_1$	$0{\cdot}000_0$	$0{\cdot}000_0$	2·727
0·70	0·970	3·132	0·208	$0{\cdot}003_9$	$0{\cdot}000_0$	$0{\cdot}000_0$	3·344
0·65	1·018	3·478	0·368	0·011	$0{\cdot}000_1$	$0{\cdot}000_0$	3·857
0·60	1·083	3·626	0·581	0·027	$0{\cdot}000_6$	$0{\cdot}000_0$	4·235
0·55	1·173	3·553	0·832	0·059	$0{\cdot}002_0$	$0{\cdot}000_0$	4·447
0·50	1·297	3·263	1·091	0·115	$0{\cdot}006_2$	$0{\cdot}000_1$	4·476
0·45	1·471	2·792	1·306	0·201	0·017	$0{\cdot}000_7$	4·317
0·40	1·719	2·203	1·418	0·314	0·040	$0{\cdot}003_0$	3·979
0·35	2·088	1·581	1·377	0·434	0·084	0·011	3·488
0·30	2·662	1·012	1·169	0·517	0·148	0·031	2·882
0·25	3·621	0·560	0·839	0·512	0·212	0·068	2·212
0·20	5·393	0·255	0·481	0·396	0·232	0·109	1·538
0·15	9·229	0·087	0·199	0·215	0·172	0·116	0·923
0·10	20·200	0·018	0·048	0·064	0·068	0·062	0·430
0·05	79·457	0·001	0·003	0·005	0·007	0·008	0·111
0·00	∞	0·000	0·000	0·000	0·000	0·000	0·000

The ratios

$$R_N = \mathcal{Q}_N/\mathcal{Q} \qquad \ldots\ldots(11)$$

are plotted against Δk in figures 1 and 2. It is seen that corresponding curves for the 1s–2s and 1s–3s transitions are closely similar and that the truncated series converge rapidly.

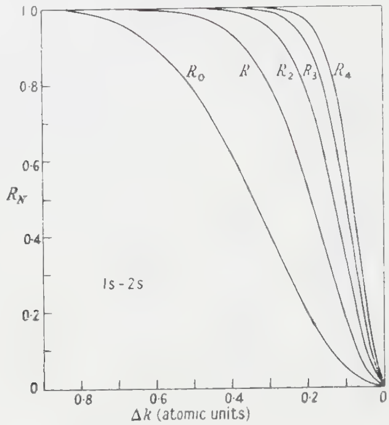

Figure 1. Ratio of truncated series of partial cross sections to total cross section for 1s–2s transition.

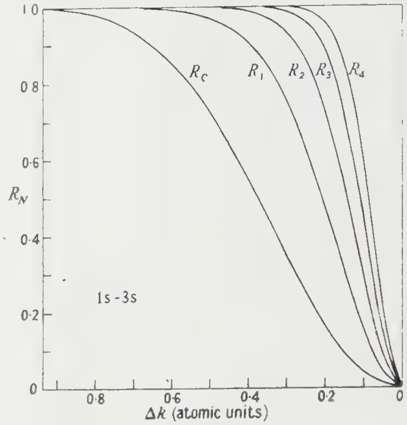

Figure 2. Ratio of truncated series of partial cross sections to total cross section for 1s–3s transition.

A different, and perhaps more useful, aspect of the results is viewed in table 3.

Table 3

	1s–2s transition		1s–3s transition	
N	$\mathcal{E}_N(5\%)$ (ev)	$\mathcal{E}_N(10\%)$ (ev)	$\mathcal{E}_N(5\%)$ (ev)	$\mathcal{E}_N(10\%)$ (ev)
0	11	12	13	14
1	16	20	20	24
2	26	34	33	43
3	41	55	53	70
4	62	80	78	102

This gives the incident energies, $\mathcal{E}_N(5\%)$ and $\mathcal{E}_N(10\%)$, below which the $\mathcal{Q}_N$'s differ from $\mathcal{Q}$ by less than the percentage indicated. These energies are smaller for the 1s–2s transition than they are for the 1s–3s transition, the ratios between corresponding pairs being approximately equal to the ratio of the excitation energies. It may be noted that the differences, $\mathcal{E}_{N+1} - \mathcal{E}_N$ are quite considerable.

ACKNOWLEDGMENT

This work was carried out under contract for the United Kingdom Atomic Energy Authority to whom thanks are due for permission to publish.

REFERENCES

MASSEY, H. S. W., 1956, *Rev. Mod. Phys.*, **28,** 199.

MOTT, N. F., and MASSEY, H. S. W., 1949, *Theory of Atomic Collisions* (Oxford : Clarendon Press).

WATSON, G. N., 1944, *Theory of Bessel Functions*, 2nd Edn. (Cambridge : University Press).

Experiments with a Polarized Muon Beam

By J. M. CASSELS, T. W. O'KEEFFE, M. RIGBY, A. M. WETHERELL
AND J. R. WORMALD
Nuclear Physics Research Laboratory, University of Liverpool

MS. received 2nd April 1957

LEE AND YANG (1956) recently drew attention to a lack of evidence for or against the natural idea that parity should be conserved in the weak fundamental particle interactions. In particular, parities might be mixed in the pion and muon decay processes. If so, the muons emitted from pions at rest should be longitudinally polarized, and this polarization could persist after the muons were brought to rest. In the subsequent muon decays, electrons would be emitted anisotropically. If the muon has spin $\frac{1}{2}$, for example, the electron angular distribution would be of the general form

$$I(\theta) = 1 + a \cos \theta \qquad \ldots\ldots(1)$$

where θ is the angle between the direction of emission of a muon and that of its decay electron.

Asymmetries of the type described by equation (1) were subsequently found by Garwin, Lederman and Weinrich (1957), so establishing the mixing of parities in both decay processes.† In their experiment the asymmetry was revealed by using a magnetic field, at right angles to the polarization axis, to precess the spins of the muons after they had come to rest in a carbon target. The precession frequency is $f = g\mathbf{e}H/4\pi m_\mu \mathbf{c}$, where m_μ is the mass of the muon and the other symbols, such as the g-factor, have their usual meanings. As a result of the spin precession, the electron intensity at a particular angle θ arising from muons which have spent a time t in the magnetic field becomes :

$$I(\theta,\ t) = \mathrm{e}^{-\lambda t}[1 + a \cos \{\theta + (g\mathbf{e}H/2m_\mu \mathbf{c})\, t\}]. \qquad \ldots\ldots.(2)$$

The convention here is that θ is measured clockwise by an observer looking along the magnetic field vector. The exponential factor takes account of the decay of the muons with the decay constant λ.

Garwin *et al.* found that g for the positive muon lay within 5% of the value of $2(1 + \alpha/2\pi + \ldots\ldots) \simeq 2{\cdot}002$ expected for a Dirac particle with spin $\frac{1}{2}$. An improved version of the experiment has now been set up at Liverpool, and a smaller limit has been set on any anomalous magnetic moment of the muon.

The apparatus shown in figure 1 was placed in a 110 MEV positive muon beam from the 156 in. cyclotron. The muons came from pions decaying near their point of production at a beryllium target inside the cyclotron. The arrangement strongly favoured forward decays along the line of the beam, so that the muons were expected to be polarized.

The muons were slowed down in paraffin wax absorbers and stopped in a copper or carbon target. The target lay in a magnetic field (perpendicular to the plane of the figure) produced by an H-type magnet with soft iron poles 6 in. in diameter. The field gap was 3 in. and a Rose shim ensured uniformity of the magnetic field over the target. The field was measured after the main cyclotron magnet and an auxiliary beam bending magnet had been switched on. The stopping of the muon in the target was signalled by a coincidence–anticoincidence pulse of the type 123 in the three scintillation counters. If the muon decayed by emission of the electron into counter 3, an anticoincidence pulse of the type 32 was produced. An electronic analyser then generated a pulse whose height was proportional to the time interval between these two signals and the output was sent to a 100 channel pulse analyser.

---

† The same conclusion has been reported from many other laboratories.

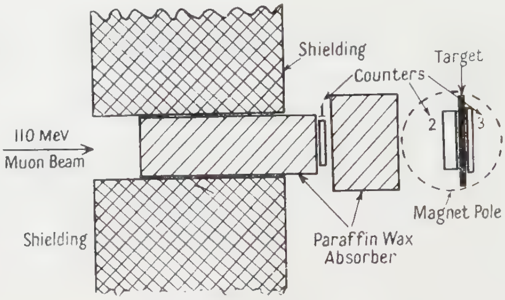

Figure 1. Layout of experimental apparatus.

The time distribution of the forward ($\theta = 0$) decay events in a field of $101{\cdot}9 \pm 0{\cdot}3$ gauss is shown in figure 2. In this plot the exponential decay factor has been removed, the muon lifetime being taken to be $2{\cdot}22\,\mu$sec (Bell and Hincks 1951). This value is incidentally verified to an accuracy to 1%. The modulation caused by the muon spin precession is very clearly evident. The fitted curve is of the type $A + B\cos(2\pi ft + \delta)$, with A, B, f and δ regarded as arbitrary parameters. A least squares fit gave $f = 1{\cdot}382 \pm 0{\cdot}006$ Mc/s and $\delta = 4{\cdot}9 \pm 4{\cdot}6°$. The beam is therefore longitudinally polarized, and the g-value is $2{\cdot}004 \pm 0{\cdot}014$. A subsidiary experiment at $\theta = -45°$ verified that g is positive and that the asymmetry pattern is not, for example, of the type $1 + a\cos 2\theta$ precessing at half the rate. The standard deviation in g ($0{\cdot}7$%) includes allowance for statistical fluctuations ($0{\cdot}4$%), errors in measuring the magnetic field ($0{\cdot}3$%), drifts in the time analyser electronics ($0{\cdot}5$%), and uncertainty in the value of m_μ ($0{\cdot}06$%; Cohen, Crowe and Du Mond 1956). It is clear that the present experimental result is entirely consistent with the theoretical value of the g-factor for a Dirac particle. Apart from radiative

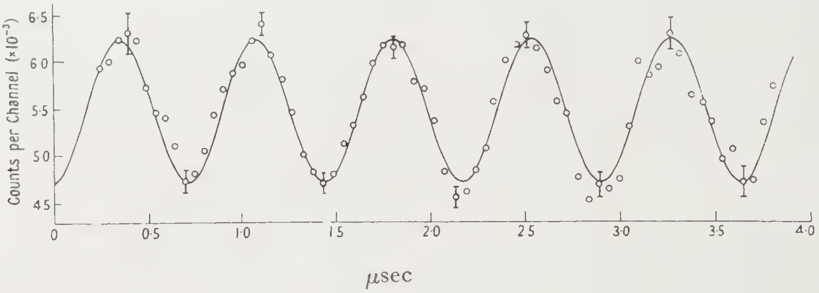

Figure 2. Time distribution of forward electrons from positive muons stopped in copper (87%) and carbon (13%). The magnetic field was 101·9 gauss. The exponential decay factor has been removed, and the first few points have been corrected for a slight non-linearity in the time analyser. Note the displaced zero.

corrections, a spin $\frac{3}{2}$ muon would theoretically have a g-factor of $\frac{2}{3}$ (Belinfante 1953).

It may be remarked that a much more accurate value of g/m_μ will surely be obtained by a resonance flip type of experiment, but the value of g itself should be sought in a comparison of the precession ($g\mathbf{e}H/2m_\mu\mathbf{c}$) and cyclotron ($\mathbf{e}H/m_\mu\mathbf{c}$) frequencies of muons in a magnetic field. The two frequencies are expected to differ only by the radiative correction.

The asymmetry coefficients *a* for copper and carbon are given in the table. Geometrical corrections have been applied for the solid angle subtended at the target by counter 3, which was large in order to establish the precessional modulation with the best possible statistical accuracy. The corrected value of *a* for muons stopped in the scintillator of counter 2 is also given in the table. This result was obtained by removing the ordinary target and requiring a coincidence event of the type 23 to signal the electrons:

Material	Asymmetry coefficient (*a*)
Copper	$-0{\cdot}24 \pm 0{\cdot}02$
Carbon (graphite)	$-0{\cdot}24 \pm 0{\cdot}04$
Polystyrene + 2% p-terphenyl	$-0{\cdot}06 \pm 0{\cdot}04$

The copper and carbon values are slightly lower than those reported by Garwin *et al.*, possibly because there was no absorber in front of the electron counter to bias it in favour of high energy electrons. The asymmetry coefficient in scintillator (polystyrene + 2% p-terphenyl) was much lower than in carbon or copper. The depolarization may be associated with the formation of muonium, a positive muon with an electron bound to it. The fine and hyperfine splitting in the muonium optical spectrum will certainly cause depolarization of large fractions of the total number of muons, in times of the order of 10^{-9} second. Fröhlich (private communication) has suggested that in conductors the electrons screen the Coulomb field of the muon so that no bound state is formed.

It is clear from figure 2 that negligible depolarization in copper or carbon occurs in the time interval from $\frac{1}{4}$ to 4 μsec. The same is probably true in scintillator, but this conclusion cannot be stated very strongly because of statistical limitations in the later precession cycles observed with this material.

A search was made for oriented triplet muonium formed in the scintillator, that is muonium with the electron and muon spins parallel. The system will have approximately the magnetic moment of the electron, with one unit of angular momentum, and it will therefore precess about a hundred times more rapidly in a magnetic field than a free muon. However, a run with the magnetic field reduced to 0·7 gauss showed no modulation greater than 2% at frequencies of the order of 1 Mc/s. Probably the triplet muonium was rapidly converted to the singlet ground state, as happens with triplet positronium in solids. Liquid or gas targets may be needed for this type of experiment.

We wish to record our thanks to many colleagues for helpful discussion and assistance in building the apparatus, and to the cyclotron crew for their willing co-operation. The numerical analysis of the data was greatly aided by Mr. Young, Miss Elmslie and Mr. Kirk of the Applied Mathematics Department. We are indebted to Dr. Mandl of the Atomic Energy Research Establishment for information about the radiative corrections to the muon magnetic moment, and to Dr. Lederman of Columbia University for sending us early details of his most

successful experiment. The search for triplet muonium was the direct result of stimulating discussions with Professor O. R. Frisch and Dr. K. F. Smith, of the Cavendish Laboratory, Cambridge.

References

Belinfante, F. J., 1953, *Phys. Rev.*, **92,** 997.
Bell, W. E., and Hincks, E. P., 1951, *Phys. Rev.*, **84,** 1243.
Cohen, E. R., Crowe, K. M., and Du Mond, J. W. M., 1956, *Phys. Rev.*, **104,** 266.
Garwin, R. L., Lederman, L. M., and Weinrich, M., 1957, *Phys. Rev.*, **105,** 1415.
Lee, T. D., and Yang, C. N., 1956, *Phys. Rev.*, **104,** 254.

Note added in Proof.—Further experiments with liquid carbon tetrachloride ($a = -0{\cdot}26 \pm 0{\cdot}05$), methyl alcohol ($a = 0{\cdot}16 \pm 0{\cdot}05$) and water ($a = -0{\cdot}15 \pm 0{\cdot}05$) have also failed to find a triplet muonium effect.

On the Interpretation of High Energy Fission

By L. MARQUEZ
Centro Brasileiro de Pesquisas Fisicas, Rio de Janeiro, Brazil

MS. received 5th *March* 1957

The process of high energy fission has been the subject of many research works. The process has usually been explained by a mechanism that assumes that the excitation energy is dissipated by evaporation of neutrons with fission then taking place (Goeckermann and Perlman 1949). It has been pointed out that there is an alternative mechanism in which the fission takes place as a consequence of the excitation energy left in the nucleus and that the neutrons are emitted from the excited fission fragments (Marquez 1954).

All the experiments on high energy fission carried out until recently were not directly sensitive to one or the other mechanism, but there has been done a very important experiment by Harding and Farley (1956) which goes directly into the mechanism of high energy fission. The experiment was to measure the ratio of the intensity N_0 of neutrons emitted parallel to the fission fragments to the intensity N_{90} of neutrons perpendicular to the fission fragments. They irradiated U with a beam of 147 MeV protons and found a ratio N_0/N_{90} of $1{\cdot}27 \pm 0{\cdot}11$.

In the interpretation of their result, they use a spectrum of neutrons emitted by the fission fragments calculated according to Le Couteur (1950). This spectrum has an average energy of 2·7 MeV and they conclude from this spectrum that the ratio N_0/N_{90} has to be 2·25 if the neutrons were emitted from the fission fragments. They go on to calculate what the ratio would be if some neutrons were emitted from the excited uranium nucleus and some from the fragments. For the latter they use the spectrum of neutrons from the fission of U with thermal neutrons and conclude that a ratio consistent with the experimental one would be obtained if, from the $13{\cdot}1 \pm 1{\cdot}6$ neutrons emitted in the fission of U with 147 MeV protons (Harding 1956), $2{\cdot}5 \pm 1$ are emitted from the fragments.

We would like to point out in this note that the average energy of the neutron emitted in the fission of U with 147 MeV protons is much greater than 2·7 MeV and that the ratio N_0/N_{90} of $1{\cdot}27 \pm 0{\cdot}11$ is compatible with the emission of all the neutrons from the fragments.

It has been shown by Belovitskii *et al.* (1955) that when U is irradiated with 150 MeV neutrons, only one from every 16 fissions shows a proton with an average energy of 18 MeV. They found a similar result when negative π-mesons produce fission when captured by U, and in this case the excitation energy is 140 MeV. If we assume that something similar happens when 147 MeV protons produce fission in U, we can estimate the average energy dissipated in protons as 1·5 MeV per fission.

In the thermal neutron fission of ^{235}U, about 5 MeV per fission are dissipated in the emission of gamma rays. Since it is expected that gamma-ray emission does not compete with neutron emission when this is energetically possible, we will take in our case 5 MeV for the energy of gamma rays.

If we assume that the kinetic energy of the fragments in the fission of U with 147 MeV protons is the same as in the fission with 90 MeV neutrons, we get from the data of Jungerman and Wright (1949), after applying the correction of Leachman (1952), the kinetic energy of 178 ± 6 MeV.

We can calculate now the average energy E of the emitted neutrons in the laboratory by conservation of energy:

$$147 + m(^{238}\mathrm{U}) + m(\mathrm{p}) = 178 + 6{\cdot}5 + m(^{112}\mathrm{Pd}) + m(^{114}\mathrm{Ag}) + 13m(\mathrm{n}) + 13E.$$

The masses in the equation are in MeV units. These masses are known fairly accurately from beta decay data and from masses of stable nuclides. This equation gives for the kinetic energy of the neutrons $6{\cdot}15 \pm 1{\cdot}5$ MeV in the laboratory and $5{\cdot}4 \pm 1{\cdot}5$ MeV in the system of the moving fragments.

If we calculate what should be the ratio N_0/N_{90} for neutrons of this energy if they are emitted from fragments with the average fragment energy, we get 1·23. The energy distribution of the neutrons emitted and the energy distribution of the fragments will change this ratio, probably making it greater, but it seems that the ratio $1{\cdot}27 \pm 0{\cdot}11$ is compatible with having all the neutrons emitted from the fragments. We have not tried to fit the data with a given spectrum because the ratio N_0/N_{90} depends critically on the low energy part of the spectrum. Any spectrum with an average energy of 5·4 MeV that does not have many neutrons on the low energy side will give the right ratio, and if it has many neutrons on the low energy side it will give a high ratio. This critical low energy region is the region from 0 to 1·5 or 2 MeV.

In conclusion, it seems that the experimental data are compatible with the emission of most of the neutrons from the fragments, and that it would be desirable to have a measurement of the energy distribution of the neutrons in the case discussed, and of the energy going in protons and gamma rays.

ACKNOWLEDGMENTS

We are indebted to the Conselho Nacional de Pesquisas of Brazil under whose auspices this work was done.

References

Belovitskii, G. E., Romanova, T. A., Soukhov, L. V., and Frank, I. M., 1955, *Zh. Exper. Teor. Fiz.*, **29,** 537.

Goeckermann, R. H., and Perlman, I., 1949, *Phys. Rev.*, **76,** 628.

Harding, G. N., 1956, *Proc. Phys. Soc.* A, **69,** 330.

Harding, G. N., and Farley, F. J. M., 1956, *Proc. Phys. Soc.* A, **69,** 853.

Jungerman, J., and Wright, S. C., 1949, *Phys. Rev.*, **76,** 1112.

Leachman, R. B., 1952, *Phys. Rev.*, **87,** 444.

Le Couteur, K. J., 1950, *Proc. Phys. Soc.* A, **63,** 259.

Marquez, L., 1954, *Nuovo Cim.*, **12,** 288.

LETTERS TO THE EDITOR

Bands Assigned to ZrF

While investigating the spectra of some zirconium compounds Afaf (1950) reported a group of bands in the blue which he assigned to the diatomic molecule ZrF. The bands were degraded to longer wavelengths and had, apparently, a complicated structure. The source employed by Afaf was a low voltage copper arc, the anode of which was hollowed out and charged with some ZrF_4.

In this laboratory we have made a search for these and other possible bands of ZrF. Several sources were employed including the hollow cathode discharge tube described by Hayes and Nevin (1955) which had proved very successful for producing the spectra of the manganese halides. But no trace of the spectrum assigned by Afaf to ZrF was obtained. Afaf's experiments with the copper arc were therefore repeated and the bands were readily excited. However, it was found that other fluorides such as MnF_2 brought up the spectrum with equal ease and intensity. Furthermore, when the copper electrodes were replaced by carbon pole pieces, the bands could not be excited, even when ZrF_4 was introduced into the arc. Hence on experimental evidence alone it appeared that the spectrum was not due to ZrF but probably some other molecule containing copper and fluorine.

A comparison of Afaf's wavelengths with those of the known systems of CuF was therefore made. This comparison is shown in the accompanying table in which the wavelengths of the CuF bands are taken from the absorption measurements of Ritschl (1927). The latter's classification of the bands and intensity estimates are also included.

ZrF(?) Bands		CuF Bands			
Int.	λ	Int.	λ	System	$v'-v''$
3	5061·18	4	5061·15	B	0–0
2	5052·27	3	5052·26	B	1–1
1	5044·08	2	5043·49	B	2–2
0	5034·16	1	5034·75	B	3–3
0	5026·15	1	5026·21	B	4–4
4	4933·95				
4	4933·38				
5	4932·11	5	4932·03	C	0–0
4	4926·88	3	4926·78	C	1–1
5	4921·58	3	4921·50	C	2–2
2	4920·22				
3	4916·33	2	4916·40	C	3–3
2	4914·76				
2	4911·37	2	4911·40	C	4–4
2	4906·18	1	4906·41	C	5–5
0	4899·24				
0	4897·88				
0	4897·25				

Some of Ritschl's bands of intensity comparable with those listed, such as system A and the 1–0 sequence of system B, are absent from the copper arc spectrum. But these are the very bands which were found to be absent or very weak in emission by Woods (1943).

It is seen that on the whole the correspondence between the two sets of wavelengths is very good and that there is little doubt that most of the strong features reported by Afaf are in fact heads of CuF bands. A few features cannot be assigned to CuF, but with the moderate dispersion used by Afaf and the present authors the arc spectrum looks somewhat confused and shows a considerable number of atomic lines. Under these circumstances it would not be difficult to pick out several spurious heads. In view of this and in the light of the experimental results described above, it would seem unlikely that a spectrum due to ZrF is in fact present.

In conclusion the authors would like to thank Professor Nevin for suggesting an investigation of the halides of zirconium and for his interest in the work.

Physics Department,
University College,
Dublin.
29th March 1957.

P. K. Carroll.
P. J. Daly.

Afaf, M., 1950, *Proc. Phys. Soc.* A, **63,** 544, 1156.
Hayes, W., and Nevin, T. E., 1955, *Proc. R. Irish Acad.*, **57,** 15.
Ritschl, R., 1927, *Z. Phys.*, **42,** 172.
Woods, L. H., 1943, *Phys. Rev.*, **64,** 259.

A Means of avoiding the 'Electron Rest Mass' Limitation in a Microtron

The maximum beam energy from any circular accelerator of given size depends upon the maximum value of the magnetic field. In a microtron (Veksler 1945, Redhead, LeCaine and Henderson 1950) this is subject to a limitation due to the rest energy of an electron, and the maximum field is that which makes the orbit revolution time increase by one cycle (of the accelerating electric field) when an energy increment of one rest mass is given once per revolution. It is possible to avoid this limitation if the total energy in the first orbit is made equal to the energy increment between successive orbits and this could be achieved by placing an emitter within the accelerating cavity such that an electron leaving this emitter will gain one rest mass less than an electron traversing the cavity.

The resonance conditions for a microtron are:

$$a = 2\pi W_i f / H\mathbf{e}c^2 \quad \text{and} \quad b = 2\pi \Delta W f / H\mathbf{e}c^2$$

where a, b are integers, f is the frequency of the accelerating field, H and $\mathbf{e}$ are in e.m.u., W_i is the total energy in the first orbit and ΔW the energy increment between successive orbits. If the injection voltage is small compared with the rest energy W_0 of an electron, then to sufficient approximation $W_i = W_0 + \Delta W$. The two conditions can now be combined to give

$$a - b = 2\pi W_0 f / H\mathbf{e}c^2$$

which takes the minimum value of unity determining the maximum usable magnetic field as $H = 2\pi W_0 f / \mathbf{e}c^2$ which is only of the order of 1000 gauss when $f = 3000$ Mc/s.

By employing a cavity in which field, or thermionic, electrons are provided from a plane within the cavity, the first resonance condition is altered, and if the source is positioned such that electrons in the first orbit have total energy ΔW (see diagram), $a = b = 2\pi \Delta W f / H\mathbf{e}c^2$ and there in no inherent field limitation, Further it is no longer necessary for ΔW to bear a simple relation to the rest energy.

The total energy gain ΔW across the cavity must now of course be greater than one rest mass, and to keep the first orbit as large as possible it is necessary for it to be relativistic, so that ΔW cannot be much less than two rest masses. The power requirement of such a resonator will be roughly double that usually required to make $\Delta W = W_0$, since it can be thought of loosely as two such resonators side by side. The resonator, then, could consist of a simple E_{010} cylindrical structure in which an emitting ring is supported by radial struts or a disc, and should have an appreciably higher shunt impedance than a cavity made re-entrant to provide field emission from the walls.

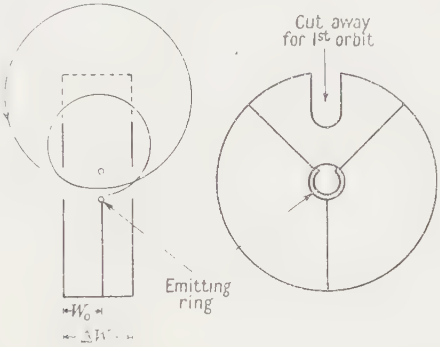

If operated in an $a = b = 1$ mode the problem of phase stability reduces to that for a microtron using a conventional resonator in the $a = 2$, $b = 1$ mode, which has been fully investigated (Henderson, Heymann and Jennings 1955). A comparable number of electrons from the first orbit should be accepted into stable higher orbits since the first transit conditions through the cavity can be made similar.

A serious difficulty is that the first orbit is now only one period in duration and correspondingly smaller, and it becomes difficult to allow it to clear the resonator. A tentative solution to this problem is to allow the first orbit to re-enter the cavity through a radial slot. This should not perturb the cavity performance appreciably and the beam will traverse it while the magnetic field is small and changing sign. Any electric field existing in this region will be in an accelerating sense, and small effects due to this could possibly be corrected by adjusting the voltage lag of the emitter.

A microtron which is at present under construction in this department is expected to provide a final beam of 28 MeV. It is hoped that the development of a resonator based on the principles outlined here will permit the magnetic field to be roughly doubled (at present ~1000 gauss) with corresponding increase to the final beam energy.

Department of Physics,
University College London.
25th April 1957.

D. K. Aitken.

Henderson, C., Heymann, F. F., and Jennings, R. E., 1953, *Proc. Phys. Soc.* B, **66,** 41.
Redhead, P. A., LeCaine, H., and Henderson, W. J., 1950, *Canad. J. Res.* A, **28,** 73.
Veksler, V., 1945, *J. Phys., Moscow*, **9,** 153.

Time Reversal in Beta-decay

Attention is drawn here to the fact that time reversibility, unlike spatial symmetry (Lee and Yang 1956), imposes useful restrictions on angular distributions in beta-decay only because of the adequacy of lowest order perturbation theory. We are concerned with ordinary or Wigner, rather than Schwinger, time reversal (Bell 1955 and references therein).

The time reverse of the decaying state is one of exponentially increasing amplitude in which there are incoming spherical waves of electrons and neutrinos and the initial nucleus is reassembled; we can hardly hope to observe this process. In scattering theory the corresponding difficulty is overcome by combining reversibility with unitarity to obtain reciprocity (e.g. Blatt and Weisskopf 1952), which relates direct and inverse transition probabilities. Such a relation would not be of much use here, for the inverse experiment would involve a three-body collision of electron, neutrino and nucleus.

To obtain useful results we appeal to explicit perturbation theory. Denoting by ψ the initial unperturbed state, and by V the interaction Hamiltonian, the real state is

$$\Psi=(1+GT)\psi \qquad \ldots\ldots(1)$$

with

$$T=V+VGV+VGVGV+\ldots\ldots\ldots \qquad \ldots\ldots(2)$$

$$\left.\begin{aligned} G&=\frac{Q}{e}\left(1+\left[\frac{-\Delta E}{e}\right]+\left[\frac{-\Delta E}{e}\right]^{2}+\ldots\ldots\ldots\right)\\ e&=i\epsilon+E_0-H_0\end{aligned}\right\} \qquad \ldots\ldots(3)$$

where Q is a projection operator excluding the initial state and $\Delta E=\langle\psi\,|\,T\,|\,\psi\rangle$ is the complex energy shift. If ΔE is ignored the interpretation of (1), as in scattering theory, is that the transition probability from ψ to a state ϕ is essentially $|\langle\phi\,|\,T\,|\,\psi\rangle|^2$. The neglect of ΔE is clearly unimportant for a given process in the lowest order in which it occurs. Time reversibility requires

$$\langle\phi\,|\,V\,|\,\psi\rangle=(\phi'\,|\,V\,|\,\psi')^{*} \qquad \ldots\ldots(4)$$

where ϕ' and ψ' are the time reverses of ϕ and ψ. In first order T and V are equal, so that

$$\langle\phi\,|\,T\,|\,\psi\rangle=(\phi'\,|\,T\,|\,\psi'\rangle^{*}. \qquad \ldots\ldots(5)$$

Correspondingly the transition probabilities satisfy

$$P(J,\,J_z,\,J',\,J_z{}',\,k_{\mathrm{e}},\,\sigma_{\mathrm{e}},\,k_\nu,\,\sigma_\nu)=P(J,\,-J_z,\,J',\,-J_z{}',\,-k_{\mathrm{e}},\,-\sigma_{\mathrm{e}},\,-k_\nu,\,-\sigma_\nu) \qquad \ldots\ldots(6)$$

where J and J' are the initial and final nuclear spins, and the k and σ are the momenta and spins of electron and neutrino. This is analogous to the relation (now known be to violated) which expresses spatial inversibility, only the k changing sign; the latter however depends on no approximation. In higher orders, because of the $i\epsilon$ in (3), (5) will not in general hold. If, however, we confine ourselves to the lowest order in which a given initial state can decay, intermediate states with $E_0=H_0$ do not occur; the infinitesimal $i\epsilon$ is then negligible, and (5) and (6) are again true. This is so for example in double beta-decay when single beta-decay is forbidden.

These results are unaltered if H_0 contains, for example, strong meson nucleon interactions which are themselves reversible; we then take ϕ and ψ to be the appropriate 'dressed' rather than 'bare' states. The results are, however, invalidated by the Coulomb interaction, which causes final state scattering and so brings into play the $i\epsilon$ in the Green's function.

With a beta-decay interaction of the usual type reversibility implies that the coupling constants can all be taken real (Pauli 1955, and references therein). That this leads to (6) in first order was verified in the recent explicit calculations of Jackson, Treiman and Wyld (to be published).

I am indebted to Dr. D. J. Candlin and Dr. T. H. R. Skyrme for remarks which stimulated these considerations.

Atomic Energy Research Establishment, J. S. BELL.
Harwell, Berks.
9th April 1957.

BELL, J. S., 1955, *Proc. Roy. Soc.* A, **231**, 479.
BLATT, J. M., and WEISSKOPF, V. F., 1952, *Theoretical Nuclear Physics* (New York: Wiley).
LEE, T. D., and YANG, C. N., 1956, *Phys. Rev.*, **104**, 254.
PAULI, W., 1955, *Niels Bohr and the Development of Physics* (London: Pergamon Press).

CORRIGENDUM

On the Moments of Inertia of Nuclei, by J. YOCCOZ (*Proc. Phys. Soc.* A, 1957, **70**, 388).

As the author of this paper is abroad, his proof corrections had not been received at the time of publication of the paper; the following corrections should therefore be made:

p. 389, l. 1 for Z read z.
p. 390, l. 11 for $1+\lambda P^{M}/(1+\lambda)$ read $(1+\lambda P^{M})/(1+\lambda)$.
l. 26 for $\chi(\theta^2+\pi)$ read $\chi(\theta+2\pi)$.
p. 391, l. 10 for " symmetric " read " asymmetric ".
p. 392, l. 21 this line should read: $S_1=\Sigma l+\frac{1}{2}$; $S_2=\Sigma m+\frac{1}{2}$.
l. 25 for $l^2/2\alpha^2$ read $e^2/2\alpha^2$.
p. 393, equation (11), for k in the denominator read K.
pp. 393–395 for I read $\mathscr{I}$ throughout.
p. 394, l. 5 omit " when ".
p. 397, the last reference should read:
WIGNER, E. P., 1931, *Gruppentheorie* (Braunschweig–Wien: Vieweg).

REVIEWS OF BOOKS

Changes of State, by H. N. V. Temperley. Pp. xi + 324. (London: Cleaver-Hume Press, 1956.) 50*s*.

The last twenty years have produced considerable research activity in the statistical mechanics of systems in which interactions play an essential part. The physical properties of such systems are of great interest, and they are usually associated with phase transitions of various kinds. Examples are the melting of solids, the condensation of liquids, the phenomena associated with the critical point of a liquid, the properties of solutions, and the various types of λ-point transition. Properties of this kind are often referred to as ' Co-operative Phenomena ', since the phase transitions arise from the co-operation of a large number of atomic systems.

Dr. Temperley's book is a review of attempts of various research workers at progress with problems in this field. The mathematical difficulties arising are considerable, and very few exact results are known. To a large extent, therefore, it is necessary to assess the usefulness of various approximations which have been devised. In addition to the topics mentioned previously there are chapters on order–disorder transitions, ferromagnetism and antiferromagnetism, ferroelectricity, superconductivity, and the transition of liquid helium.

The book will be of interest mainly to research workers in the field, and a basic knowledge of the methods of statistical mechanics is assumed. Although the author does not claim to provide an exhaustive review and some topics are omitted (e.g. the theory of conformal solutions), a large number of papers are discussed, and a useful summary is thus provided of the literature of the field. Such a review does not seem to be available elsewhere, and the author has definitely filled a gap which should act as a stimulus to further progress.

C. DOMB.

Handbuch der Physik, Vol. 1, *Mathematical Methods I*, edited by S. Flügge. Pp. vii + 364. (Berlin: Springer, 1956.) DM. 72.

The first two volumes of the new edition of the *Handbuch der Physik* are on Mathematical Methods. The first volume contains five articles, all in German. Three are by Lense on " Basic concepts of classical analysis, ordinary differential equations, theory of functions ", " Partial differential equations " and " Elliptic functions and integrals "; one is by Meixner on " Special functions of mathematical physics ", and one is by Schlögl on " Boundary value problems ".

The introductory article by Lense gives a clear and compact account of many of the basic concepts and facts of classical calculus. Definitions are given, theorems are stated in a logical order, and a vast amount of material is compressed into a relatively small space. Most of the text is easy to read and will be useful for reference to the physicist who wants only to refresh his memory or to inform himself mainly about facts. Real functions with one and several variables, differential and integral calculus, and infinite series are dealt with. One section reviews the theory of functions of a complex variable, and a very clear section gives an account of the basic facts of ordinary differential equations. An appendix deals with the Lebesgue integral.

Lense's article on partial differential equations (which is rather different from the same author's contribution in the 1928 edition) deals mainly with equations of the first order. Second order equations reappear in the other articles, but the subject is not adequately covered by the volume. The concepts related to the solutions of first order partial differential equations, their geometric interpretation and the theory of contact transformations are first explained for the more readily visualizable case of equations with two independent variables. The considerations are then extended to several variables and the connection with the Hamilton–Jacobi theory is established. The exposition is too concise to serve as a first introduction into the subject, but is suitable for reference.

Lense's third article gives a clear account of many of the features of elliptic functions and integrals. The exposition is descriptive, and in the nature of a summary, but this article can be read also as a first introduction. It presents in a nutshell the concepts and relationships of a special topic and gives useful orientation in a rather extended field.

Meixner reviews some of the properties of special functions, the hypergeometric function with its special and limiting cases (Bessel functions, spherical harmonics, Whittaker functions), the Matthieu functions and the spheroidal functions. The emphasis is on the general methods by which these functions can be handled. Information concerning a particular function therefore appears scattered throughout the paper. (When these special functions are actually to be used, one would rather consult the existing monographs). Definitions and properties, the related second-order linear differential equations and functional equations are treated; the account of the latter includes the factorization method and some of the main results of Truesdell's unified approach. Some references to recent contributions of physical interest are given. The separation of the three-dimensional wave equation in different curvilinear coordinates is presented in a systematic way, the differential equations of the special functions appearing through the separation.

Schlögl's article on boundary value problems deals with systems of orthogonal functions, integral equations, variational calculus and the boundary value problems of the differential equations of physics. A great many concepts are reviewed and there is more stress on the explanation of the concepts than on technical details. This would be an advantage, but for an introduction into the subject the article remains too summary. Concepts related to function spaces and expansions, Fourier series and integrals, and theorems and formal methods of solution for integral equations are reviewed. Boundary conditions for partial differential equations of the second order, characteristics, Green functions and eigenvalue problems are dealt with. Propagators of initial value problems are given for some simple cases.

The classical topics of mathematics which form the content of this volume are treated in many books, and the volume cannot be expected to compete in all its details with the existing expositions. It has its merits, however, and gives a handy collection of information which will be welcomed by the physicist.

J. G. VALATIN.

CONTENTS OF SECTION B

PAGE

Dr. J. G. Daunt. The Magnetic Refrigerator for Temperatures below 1°K . . 641

Mrs. J. Haselgrove. Oblique Ray Paths in the Ionosphere 653

Dr. T. H. Y. Yeung and Prof. J. Sayers. An R.F. Probe Technique for the Measurement of Plasma Electron Concentrations in the Presence of Negative Ions 663

Dr. W. E. Spear. Transit Time Measurements of Charge Carriers in Amorphous Selenium Films 669

Mr. J. C. Rivière. Contact Potential Difference Measurements by the Kelvin Method 676

Mr. M. Gardener, Mr. S. Kisdnasamy, Dr. E. Rössle and Dr. A. W. Wolfendale. The Neon Flash Tube as a Detector of Ionizing Particles . 687

Research Notes :

Dr. G. H. Cheesman and Mrs. C. M. Soane. The Lattice Constants of the Inert Elements 700

Mr. M. Prutton. Dielectric Constant and Conductivity of Guanidine Aluminium Sulphate during Switching 702

Dr. R. H. Jones. The Effect of Oxygen on an Evaporated PbSe Layer . . 704

Mr. P. S. Aggarwal and Mr. A. Goswami. A New Phase Structure of Molybdenum 708

Letters to the Editor :

Dr. R. R. Heikes and Dr. B. W. Roberts. Comments on the Manuel Model for MnBi 711

Reviews of Books 712

Contents of Section A 720

Fast Neutron Capture below 1 MeV: The Cross Sections for ^{238}U and ^{232}Th

By A. M. LANE and J. E. LYNN
Atomic Energy Research Establishment, Harwell, Berks.

Communicated by B. H. Flowers; MS. received 30th January 1957

Abstract. Recent measurements of neutron capture in ^{238}U and ^{232}Th with neutron energies up to 1 MeV reveal anomalies in the capture cross sections. We have attempted to fit these cross sections in terms of conventional compound nucleus theory, using the existing low energy resonance data to provide numerical values of the widths and other parameters. If one assumes some definite dependence of level density on energy, there are no free parameters left in the fitting. We have used the level density formula of Lang and Le Couteur, and find good absolute fits with the observed capture cross sections. It emerges in the fitting that the anomalies are a consequence of the small rate of increase of the number of inelastic scattering channels with energy. This small rate is a result of the rotational nature of the low-lying spectra of ^{238}U and ^{232}Th.

§ 1. Introduction

Only a small number of neutron capture cross sections have been measured for bombarding energies of more than 10 kev. Of these, two of the best studied cross sections are those of ^{238}U and ^{232}Th (see figures 1 and 2). Both of these sets of measurements show that the cross sections do not decrease steadily with increasing energy as might have been expected. In ^{232}Th there is an anomaly in the form of a plateau between about 200 kev and 700 kev. In ^{238}U the anomaly is more pronounced and there is actually a maximum or peak centred at 850 kev and with a 'width' of about 250 kev.

Remembering the existence of anomalies ('mountain resonances') in total neutron cross sections and their explanation in terms of long-range variations in neutron widths (Feshbach, Porter and Weisskopf 1954, Lane, Thomas and Wigner 1955) one might guess that the anomalies in the capture cross sections are to be explained in a similar way. However, it becomes clear when one considers the matter in detail that the capture cross sections are not sensitive to these variations. In any case the capture anomalies are much more narrow than the mountain resonances. The correct explanation for the anomalies seems to be more prosaic. As we shall see below, the form of the cross section is determined essentially by the ratio of the density of levels in the compound nucleus to the number of levels below the incident energy in the target nucleus. An increase in the former alone implies an increase in the cross section. An increase in the latter leads to a decrease in the cross section because of the extra competition in the decay of the compound states coming from the possibility of inelastic scattering. Normally the level densities in the target and compound nuclei increase at comparable rates, and this leads to a steady net decrease in the capture cross section. However, exceptional cases can occur. In particular, the nuclei ^{238}U and ^{232}Th are believed to have 'rotational' spectra. Thus, their level densities at low excitation energies actually *decrease* with increasing energy. It is this fact which enables the capture cross sections to remain constant or even increase up to an energy at which excited states of other than the simple rotational type begin to appear, i.e. where the level density becomes ' normal '.

In the following we first describe the theory of neutron capture cross sections, and then we present the relevant experimental material on capture in ^{238}U and ^{232}Th. Finally, we use the theory to fit the experimental data. In an appendix, we outline a corresponding theory for inelastic scattering cross sections and discuss its application to recent measurements on ^{238}U.

§ 2. THEORY OF NEUTRON CAPTURE CROSS SECTIONS

2.1. *Capture Cross Sections in the Isolated Level Approximation*

If resonance levels are well isolated, we can use the Breit–Wigner formula for the capture cross section near an isolated resonance λ of spin J. For the partial wave of angular momentum l this is

$$\sigma_{Jl} = \frac{(2J+1)}{2(2I+1)}\frac{\pi}{k^2}\frac{\sum_j \Gamma_{\lambda J(nlj)}\,\Gamma_{\lambda J(\gamma)}}{(E_\lambda - E)^2 + (\Gamma_{\lambda J}/2)^2} \qquad \ldots\ldots(1)$$

where k is the wave number of the incident neutron multiplied by 2π, E_λ is the resonance energy, I is the spin of the target nucleus (in its ground state), $\Gamma_{\lambda J(\gamma)}$ is the radiation width of the resonance, $\Gamma_{\lambda J(nlj)}$ is the entrance channel neutron width for channel spin j (which may take the values $j = I \pm \frac{1}{2}$ except in the case $I = 0$ when $j = \frac{1}{2}$), $\Gamma_{\lambda J}$ is the total width of the resonance and equals the sum of all the partial widths:

$$\Gamma_{\lambda J} = \sum_{l,j}\Gamma_{\gamma J(nlj)} + \sum_{n',l',j'}\Gamma_{\lambda I(n'l'j')} + \Gamma_{\lambda J(\gamma)} \qquad \ldots\ldots(2)$$

where $\Gamma_{\lambda J(n'l'j')}$ is the width for an inelastic scattering process which leaves the residual nucleus in a given excited state, the emitted neutron having orbital angular momentum l' consistent with parity conservation and the exit channel spin being j'.

Now the experimental data provide values of capture cross sections averaged over many resonances. Averaging equation (1) gives simply

$$\langle\sigma_{Jl}\rangle = \frac{(2J+1)}{(2I+1)}\frac{\pi^2}{k^2}\frac{1}{\langle D_{\lambda J}\rangle}\sum_j\left\langle\frac{\Gamma_{\lambda J(nlj)}\,\Gamma_{\lambda J(\gamma)}}{\Gamma_{\lambda J}}\right\rangle \qquad \ldots\ldots(3)$$

where $\langle D_{\lambda J}\rangle$ is the average spacing between resonances of given spin J and parity. The total capture cross section is obtained by summing $\langle\sigma_{Jl}\rangle$ over J and l.

2.2. *The Effects of Variation of Widths from Level to Level*

Since the average of a ratio is not in general equal to the ratio of the averages, it is not correct to replace $\langle\Gamma_{\lambda J(nlj)}\,\Gamma_{\lambda J(\gamma)}/\Gamma_{\lambda J}\rangle$ by $\langle\Gamma_{\lambda J(nlj)}\rangle\langle\Gamma_{\lambda J(\gamma)}\rangle/\langle\Gamma_{\lambda J}\rangle$ in (3). Rather one should proceed as follows. Suppose that there are altogether $\mu+1$ neutron channels (nlj) and $(n'l'j')$ for levels of given spin J and parity. Consider the contribution to (3) from the elastic channel (nlj) and define a quantity

$$\alpha_{lj} = \langle\Gamma_{\lambda J(\gamma)}\rangle/\langle\Gamma_{\lambda J(nlj)}\rangle$$

for this channel and similar quantities $\alpha_1, \ldots, \alpha_\mu$ for each of the other μ channels (elastic and inelastic). We may now define a quantity $S(\alpha_{lj};\ \alpha_1, \ldots, \alpha_\mu)$ as the dimensionless ratio

$$\left\langle\frac{\Gamma_{\lambda J(nlj)}\,\Gamma_{\lambda J(\gamma)}}{\Gamma_{\lambda J}}\right\rangle \Big/ \frac{\langle\Gamma_{\lambda J(nlj)}\rangle\langle\Gamma_{\lambda J(\gamma)}\rangle}{\langle\Gamma_{\lambda J}\rangle}$$

so that

$$\langle\sigma_{Jl}\rangle = \frac{\pi^2}{k^2}\frac{(2J+1)}{(2I+1)}\sum_j \frac{\langle\Gamma_{\lambda J(nlj)}\rangle\langle\Gamma_{\lambda J(\gamma)}\rangle}{\langle D_{\lambda J}\rangle\langle\Gamma_{\lambda J}\rangle} S(\alpha_{lj};\, \alpha_1, \ldots, \alpha_\mu). \qquad \ldots\ldots(4)$$

From the studies of low energy neutron resonances $\Gamma_{\lambda J(\gamma)}$ appears to be practically constant from level to level (Lynn and Pattenden 1955, Levin and Hughes 1956, Rae *et al.* to be published).

In this paper we shall assume $\Gamma_{\lambda J(\gamma)}$ to be constant, so that the value of S is determined by the distribution laws for the elastic and inelastic neutron widths and by the mean widths. The correct distribution law for neutron widths has been deduced from both theory and experiment to be (Porter and Thomas 1956) $p_1(x)dx = (2\pi x)^{-1/2}\,e^{-x/2}\,dx$. Another law which has sometimes been considered in this connection is $p_2(x)dx = e^{-x}\,dx$. Both of these laws are special cases ($\nu = 1$ and 2) of the so-called 'χ^2 family of distributions', each member of which † is characterized by a positive integral value of ν:

$$p_\nu(x)dx = (\nu/2)\Gamma(\nu/2)^{-1}\,(\nu x/2)^{(\nu-2)/2}e^{-\nu x/2}dx.$$

It is possible in principle to compute S for any given ν. In practice the computation becomes tedious for ν greater than 2 and μ greater than 1, but we are not interested in cases where $\nu \geqslant 2$. However, we are interested in cases where number of inelastic channels is quite large, say $\mu \geqslant 4$.

At energies below about 150 kev in ^{238}U and ^{232}Th μ is nearly always equal to 0 or 1 and in our calculations we have used values of S computed for the cases $\nu = 1$ and $\mu = 0, 1$ (see Appendix I). At higher energies μ becomes large enough for us to regard the total level width as being fairly constant. This is equivalent to S being of the order of unity, and that is what we have assumed in our calculations at the higher energies.

In order to check this assumption and obtain some qualitative idea of the effect of the distributions in neutron widths, we have computed the cross section under the extreme assumption that the μ inelastic widths at any given level λ are not independent but always have the same ratios. That is, we replace $S(\alpha;\, \alpha_1, \ldots, \alpha_\mu)$ by $S(\alpha;\, \beta)$ where $\beta = \sum \alpha_i$ for $i = 1$ to μ. The conclusion is that, although the value of the capture cross section for an individual pair of values of J and l may be changed by a factor greater than 2 by the presence of S, the total capture cross section is little changed, for individual terms in the sum are increased while others are decreased; for example, at 700 kev neutron energy, the total capture cross section is increased by about 30%. This correction in the actual case when the widths are independent ‡ can be expected to be very much less than 30%.

2.3. *Specification of Average Level Spacings and Widths*

We must now consider the specification of the various averages occurring in the formula for the capture cross section with special attention to the energy and spin dependences. We rewrite equation (4) summed over J and l in the form

---

† Members of this family can be defined as follows: given ν sets of samples $(y_1) \ldots (y_\nu)$, such that each set has a normal (Gaussian) distribution with mean value zero, then $p_\nu(x)dx$ is the probability of finding x in the interval $(x, x+dx)$ where x is defined as $x = y_1{}^2 + y_2{}^2 + \ldots + y_\nu{}^2$.

‡ We note here the possibility that the inelastic neutron widths considered in these calculations are in fact correlated as a result of the fact that the transitions they represent all lead to levels of a rotational band which have the same *intrinsic* wave function.

$$\sigma(E) = \frac{\pi^2}{k^2(2I+1)} \sum_{j=|I-\frac{1}{2}|}^{I+\frac{1}{2}} \sum_J (2J+1) \frac{\langle \Gamma_{\lambda J(\gamma)}(E) \rangle}{\langle D_{\lambda J}(E) \rangle}$$

$$\times \sum_{l=|J-j|}^{J+j} \frac{\langle \Gamma_{\lambda J(nlj)} \rangle / \langle D_{\lambda J} \rangle}{\langle \Gamma_{\lambda J} \rangle / \langle D_{\lambda J} \rangle} S(\alpha_{lj};\ \alpha_1, \ldots, \alpha_\mu) \qquad \ldots\ldots(5)$$

where J runs from zero through the positive integers if I is a half integer, and from $\frac{1}{2}$ through the odd half-integers if I is an integer or zero.

Average level spacing $\langle D_{\lambda J}(E) \rangle$.

Lang and Le Couteur (1954) have reviewed the available experimental data on level densities. They found that an adequate law of level density was given by the formula

$$\langle D_{\lambda J}(E) \rangle = C(2J+1)^{-1} \exp[(J+\tfrac{1}{2})^2/2ct](U+t)^2$$

$$\times \exp - \left\{ 2\left(\frac{AU}{11}\right)^{1/2} + \frac{3}{32}(11U)^{2/3} \right\}$$

where U is the excitation energy of the compound nucleus in MeV (and therefore equals $E + B_n$, where B_n is the binding energy of a neutron in the ground state of nucleus). A is the mass number of the compound nucleus, ch^2 is the moment of inertia of the assembly of particles carrying the angular momentum J and t is the nuclear temperature (in units of energy).

According to Lang and Le Couteur, for a nucleus of mass near $A \sim 239$, $t \sim 0{\cdot}5$ MeV and $2ct$ is about 35. The quantity C is a constant independent of energy and spin which is best determined empirically from the observed spacing of low energy neutron resonances.

Average radiation width $\langle \Gamma_{\lambda J(\gamma)}(E) \rangle$.

Usually the low energy neutron resonance data enable one to determine the mean radiation width at that energy. This value can be used to compute the mean capture cross sections at higher energies provided one specifies a dependence of the width on energy and spin.

Guided by the available evidence, we shall assume that there is no dependence on spin (Rae *et al.* to be published).

The evidence suggests a mild dependence on energy. In view of this we have estimated this energy dependence for the case of ^{239}U (see Appendix II) and have inserted this dependence into our predicted capture cross section. We estimate that the radiation width increases by about 16% on increasing the excitation energy U from 5 to 6 MeV.

Average neutron widths $\langle \Gamma_{\lambda J(nlj)} \rangle$.

The ratio $\langle \Gamma_{\lambda J(nlj)} \rangle / \langle D_{\lambda J} \rangle$ is related to the strength function $s_{J\,(lj)}$ (Thomas 1955) by

$$(\langle \Gamma_{\lambda J(nlj)} \rangle / \langle D_{\lambda J} \rangle) = 2P_l\, s_{J(lj)}$$

where P_l is the penetration factor for l-wave neutrons:

$$P_0 = \rho$$
$$P_1 = \rho^3/(1+\rho^2)$$
$$P_2 = \rho^5/(9+3\rho^2+\rho^4)$$
$$P_3 = \rho^7/(225+45\,\rho^2+6\rho^4+\rho^6)$$

Here $\rho = kR$, where R is the nuclear radius.

Although the strength function is energy dependent it is expected to change by at most a factor of two in an energy interval of 1 Mev (Feshbach, Porter and Weisskopf 1954). In addition it is not expected to depend strongly on j or J, although it may depend on l. The value of $s_{J(lj)}$ is best obtained empirically from the low energy neutron resonance data. In actual fact, the capture cross sections above 100 kev are not sensitive to this value because it occurs in both numerator and denominator and tends to cancel itself.

2.4. *The Effects of Interference between Resonances*

The assumption made in § 2.1 that the resonances are well isolated i.e. that $\langle \Gamma_{\lambda J} \rangle \ll \langle D_{\lambda J} \rangle$ is not exactly correct. In practice, there are always interference effects present. If these are not too severe we can use the prescription given by Thomas (1955) to take these effects into account. This prescription says simply that each mean width $\langle \Gamma_{\lambda J(nlj)} \rangle$ occurring in the cross section formula should be divided by a factor $|1 - R_{J(lj)} L_l|^2$ where $R_{J(lj)}$ is the so-called 'reduced R-function' for l-wave neutrons given by (Thomas 1955)

$$R_{J(lj)} = R^{\infty}_{J(lj)} + i\pi \, s_{J(lj)}$$

where $s_{J(lj)}$ is the strength function mentioned above and $R^{\infty}_{J(lj)}$ is such that $2 \tan^{-1} (P_l R^{\infty}_{J(lj)})$ is the deviation of the average scattering phase in the (lj) channel from that of hard-sphere scattering.

The factor L_l is defined in terms of the penetration factor P_l and the level-shift factor S_l for l-wave neutrons:

$$L_l = S_l + iP_l.$$

Although the factor $|1 - R_{J(lj)} L_l|^2$ is often appreciably different from unity its effect on capture cross sections is usually small because it must be inserted in both numerator and denominator, and therefore tends to cancel †.

§ 3. EXPERIMENTAL DATA ON THE NEUTRON BOMBARDMENT OF ^{238}U AND ^{232}Th

3.1. *Capture Cross Section Data*

The neutron capture cross section of ^{238}U is shown in figure 1. The experimental points are the results of Broda and Wilkinson (1945, unpublished), Rose (1955), workers at Los Alamos (published in the compilation of Hughes and Harvey 1955) and some relative values of Newson (private communication) normalized to the Los Alamos data.

The experimental data on ^{232}Th, shown in figure 2, are partly unpublished work reported by Hughes and Harvey (1955) but mainly the results of Hanna (to be published). Unfortunately, in both cases the unpublished work has been presented without any assignment of errors. It seems that all the data below 100 kev are less satisfactory than those at higher energies.

3.2. *Inelastic Scattering Data*

Batchelor (1956) has measured the inelastic scattering cross section of ^{238}U at various energies between 0·5 Mev and 1 Mev. He also investigated the spectra of the inelastically scattered neutrons. He found that the spectra of inelastically scattered neutrons at low incident neutron energies were consistent with a rotational level scheme of ^{238}U. He also found that, for higher energies, there is a level at about 700 kev above the ground state of ^{238}U to which strong inelastic scattering occurs.

---

† This is in contrast to the situation with inelastic neutron scattering cross sections where the factors occur twice in the numerator and only once in the denominator. Calculations for the reaction ^{238}U(nn′) at 500 kev show that the inclusion of the factor is important (see Appendix III).

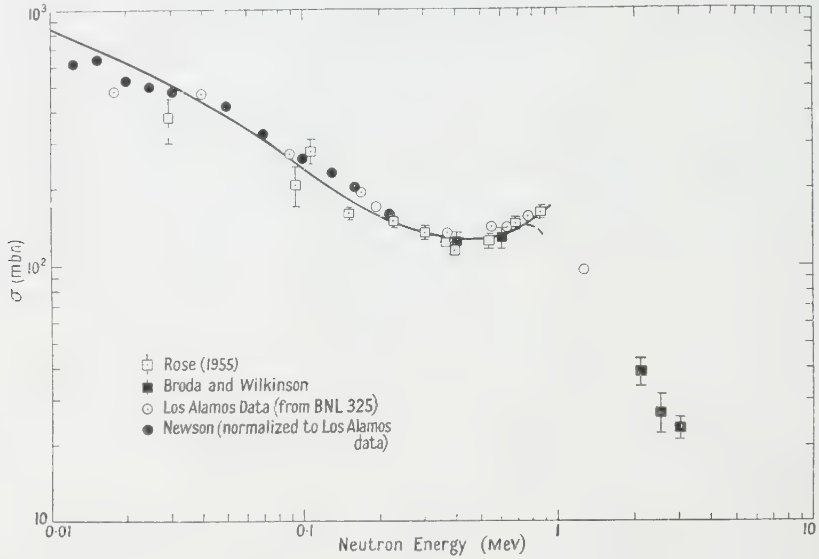

Figure 1. The neutron capture cross section of ^{238}U. The points are experimental. The curve is a theoretical one made with the numerical assumptions $R=9{\cdot}0\times10^{-13}$cm, Γ_γ/D at zero energy $=1{\cdot}35\times10^{-3}$, strength function $s_l=0{\cdot}036$ for all l values. The continuous curve is calculated allowing for inelastic scattering competition to the 0^+, 2^+, 4^+ states only (see figure 3). The broken curve shows the effect of allowing for additional inelastic scattering to the assumed 1^- and 3^- states at 700 kev and 775 kev.

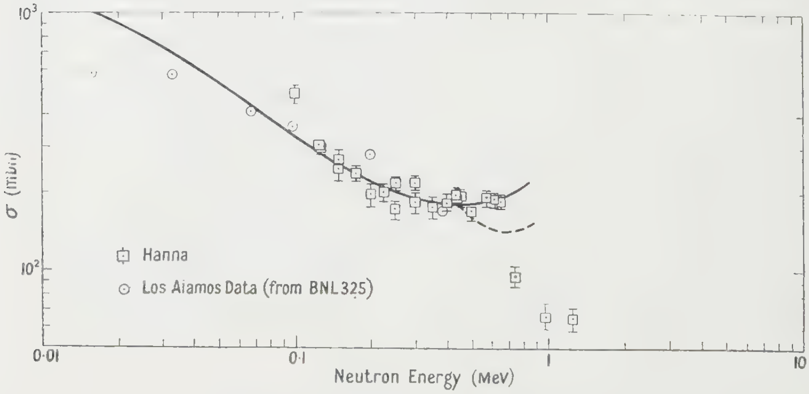

Figure 2. The neutron capture cross section of ^{232}Th. The points are experimental. The curve is a theoretical one made with the numerical assumptions $R=9{\cdot}0\times10^{-13}$ cm, Γ_γ/D at zero energy $=1{\cdot}88\times10^{-3}$, strength function $s_l=0{\cdot}036$ for all l values. The continuous curve is calculated allowing for inelastic scattering competition to the 0^+, 2^+, 4^+ states only (see figure 3). The broken curve shows the effect of allowing for additional inelastic scattering to the assumed 1^- and 3^- states at 425 kev and 500 kev.

A rotational spectrum in ^{238}U is to be expected from the observed rotational spectra of other even-even nuclei, in this mass region from about mass number 220 upwards (see, for example, Newton 1955 for a review of these properties). In the lowest rotational band of ^{238}U there is expected to be a 2^+ level at 45 kev and a 4^+ level at about 150 kev (see figure 3). A γ ray of 45 ± 3 kev has been observed in the Coulomb excitation of ^{238}U (Divatia *et al.* 1955) confirming the existence of the first level.

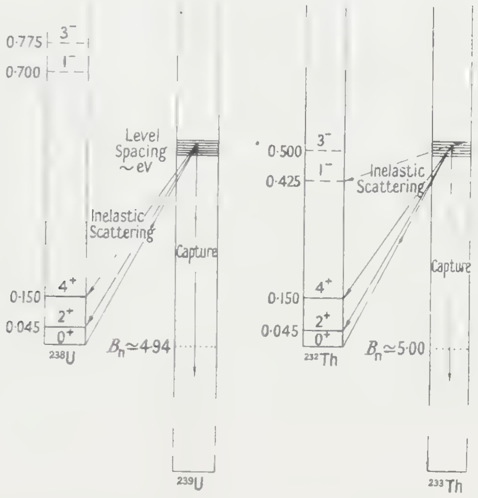

Figure 3. The level schemes of the target nuclei ^{238}U and ^{232}Th. As described in the text, these are partly experimental and partly inferred from systematics. Also indicated are the compound nuclei ^{239}U and ^{233}Th.

There is some evidence for the systematic occurrence of low lying 1^- states in the even–even nuclei in the region of mass number from $A = 222$ upwards. These states have been interpreted as being the lowest members of $K = 0^-$ rotational bands (1^-, 3^-, 5^-, ... states) corresponding to a pear-shaped deformation of the nucleus (Stephens, Asaro and Perlman 1955). Such a state has not been reported for ^{238}U, nor for ^{232}Th, but it may well be that the level Batchelor† observes in ^{238}U at about 700 kev is such a state. In this connection it is interesting to note that the presumed 1^- level in ^{238}Pu lies at 650 kev (Stephens, Asaro and Perlman 1955). The 1^- levels in the nuclei about $A = 226$ are at about 250 kev. As far as one can tell from the trend of the positions of the observed 1^- levels, we expect a 1^- level to lie at roughly 450 kev energy in ^{232}Th.

3.3 *Low Energy Resonance Data*

The low energy resonance data on ^{238}U and ^{232}Th have been compiled by Hughes and Harvey (1955). We have used these data to compute the various mean values that we need to know, and these values are listed in table 1.

---

† Batchelor reports a value of 0·8 barn for the inelastic scattering cross section of ^{238}U at 500 kev. We have attempted to reproduce this value by calculation in the course of this work. We shall report on this in Appendix III.

Table 1. Average values from the experimental data on the first eleven resonances found in the low energy bombardment of ^{232}Th and ^{238}U. $\Gamma_n{}^0$ signifies neutron width normalized to 1 ev. All quantities refer to states of spin $J=\frac{1}{2}^+$.

Nucleus	$\langle D\rangle$ (ev)	$\frac{\langle\Gamma_n^0\rangle}{\langle D\rangle}$	Strength function	Γ_γ (mv)	$\Gamma_\gamma/\langle D\rangle$ ($\times 10^3$)
^{232}Th	$18\ \pm 4$	$1{\cdot}0\ \pm 0{\cdot}5$	$0{\cdot}026 \pm 0{\cdot}012$	30 ± 10	$1{\cdot}65 \pm 0{\cdot}7$
^{238}U	$18{\cdot}5 \pm 4$	$1{\cdot}45 \pm 0{\cdot}7$	$0{\cdot}036 \pm 0{\cdot}017$	25 ± 5	$1{\cdot}35 \pm 0{\cdot}4$

§ 4. FITTING THE OBSERVED CAPTURE CROSS SECTIONS

We have computed theoretical capture cross sections in the spirit of the theory of § 2 in which one uses the low energy neutron resonance parameters (table 1). In addition to using these values, we have made the following numerical assumptions:

(i) The averaging factors S are replaced by unity above $E \sim 150$ kev. Below this energy they are computed assuming $\nu=1$ type distributions for neutron widths (Appendix I).

(ii) The low energy data give values for the strength function only for s-waves and so one must *assume* numerical values for higher partial waves. It is fortunate that, above 50 kev where the neutron width dominates the radiation width, only the *relative* values of the strength functions for the various l-values are important because the absolute value cancels in the numerator and denominator of the capture cross section. Furthermore, below 700 kev in ^{238}U, since all levels responsible for inelastic scattering have the same parity, one must specify only the relative strength functions for l-waves of the same parity. It is reasonable to assume that these are equal and this is what we have done. At the lowest energies, from 50 kev down to 10 kev, the cross section depends on the absolute values of the strength functions to some extent. Since the p-wave contribution is more sensitive to the value of the strength function than the s-wave one in this region, and since the p-wave contribution dominates in this region, one can use the observed cross section to determine the p-wave strength function. If this could be done accurately and if the s-wave strength function were much better known than is indicated by the errors in table 1, it would be very interesting to compare the two strength functions. According to theory (Feshbach, Porter and Weisskopf 1954) the p-wave value should be larger by a factor of 2 or so. Unfortunately the accuracy of the determinations does not enable us to do this at present. All we can say is that the p-wave strength function needed to fit the capture cross section up to 50 kev is of the same order as the poorly known s-wave value quoted in table 1. The actual values for the s and p wave strength functions that have been used in figures 1 and 2 are $s=0{\cdot}036$ for both†.

(iii) Inelastic scattering is assumed as follows. The level schemes of the target nuclei ^{238}U and ^{232}Th were discussed in § 3.2. In calculating the full curves of figures 1 and 2 we considered inelastic scattering to a 2^+ level at 45 kev and a 4^+ level at 150 kev‡. In the broken curve of figure 1 we have considered, in addition to these, inelastic scattering to a 1^- level at 700 kev and to a 3^- level at 775 kev in ^{238}U. The broken curve of figure 2 takes into account a 1^- level at 425 kev and a 3^- level at 500 kev in ^{232}Th.

---

† Reducing s to $0{\cdot}026$ for s and p waves reduces the 10 kev cross section by 12% and the 100 kev cross section by only 2%.

‡ One must be careful to take all contributing channel spins into account in assessing the total inelastic width.

§ 5. DISCUSSION

We emphasize that the theoretical fits shown in figures 1 and 2 are absolute fits and are not adjusted. In fact, one of the most interesting aspects of these fits is that there is very little freedom in making them, especially in the region above 50 kev and below the supposed 1^- levels. The most crucial single quantity is the level density, for which we have used the formulae and values of Lang and Le Couteur quoted in § 2. Both the energy and spin dependences that we have used are involved in an essential way in the fitting. For instance, altering the coefficient of $U^{1/2}$ in the exponential by a factor of $\sqrt{2}$ would lead to a discrepancy of a factor 2 at 850 kev. The spin dependence is essentially $2J+1$ for spins J not too large †. This factor combines with the $2J+1$ in the statistical g-factor giving $(2J+1)^2$. This can have appreciably large values for the higher J values and helps to compensate the smallness of the penetration factors for the higher partial waves, thereby leading to much higher contributions from these waves than one would normally expect. For example, f-waves contribute 16% of the cross section at 850 kev. If the $2J+1$ factor in the level density had been ignored, the cross section at 850 kev would have been smaller by about a factor of one half. *Therefore this factor plays an essential role in obtaining the fits and, to this extent, we can say that we have evidence for the presence of this factor.* Of course, the effect of ignoring the $2J+1$ factor could be compensated at any energy by increasing the coefficient of $U^{1/2}$ appropriately from its theoretical value. However, the overall shape of the predicted cross section curve is changed by doing this and the overall fit is not so good.

To summarize the fitting from 50 kev to 650 kev in ^{232}Th and to 850 kev in ^{238}U: the shape of the cross section curve is determined by a contest between increasing level density in the compound nucleus on the one hand and increasing inelastic scattering on the other. Because of the nature of the spectra of ^{232}Th and ^{238}U (both are rotational in character), the rate of increase of the latter quantity is smaller than usual, with the consequence that the usual fall-off in cross section with energy does not occur and, in the case of ^{238}U, the increasing level density of the compound nucleus actually causes a rise in the cross section.

Above 650 kev in ^{232}Th and 850 kev in ^{238}U, the new source of inelastic scattering to the presumed 1^- levels and their associated rotational bands (3^-, 5^-, ...) causes the cross sections to decrease. Without attempting detailed fits of the cross sections in these regions we have calculated the effects of the new inelastic scattering and found them to correspond qualitatively to the observed decreases in cross sections.

Finally, we remark that we have attempted to use the same type of theory to fit the observed inelastic neutron cross sections of ^{238}U. This work is described in Appendix III. The agreement between experiment and theory is not so definite. For instance, at 500 kev, taking account of interference between resonances reduces the predicted cross section by about 15%, but the values obtained are still rather higher than the observed value of 0·8 barn. The predicted cross section can be expected to be reduced even further by taking proper account of averaging over resonances (the F factors of Appendix III). However, it is not evident that the effect will be strong enough to bring about agreement. This is disturbing, especially because it is expected that a fair fraction of this observed value comes from direct excitation of the rotational states (Wandel, unpublished, Hayakawa and Yoshida 1955, Brink 1955).

---

† The cut-off factor $\exp[-(J+\frac{1}{2})^2/35]$ is not very significant. If we had ignored it, the theoretical cross section at 850 kev would be about 15% greater.

Note added in proof. The inelastic scattering cross section at 500 kev has recently been shown to be considerably larger than 0·8 barn. According to experimental results from Los Alamos, the correct value is about 1·7 barns (L. Cranberg, private communication). This number is in much better accord with our estimates. Furthermore, recent theoretical work at Los Alamos (L. Wilets, address at the Pittsburgh Conference on Nuclear Structure, June 1957) has found that the contribution to the cross section from direct rotational excitation is only a small fraction of the total.

ACKNOWLEDGMENTS

We are indebted to Dr. B. B. Kinsey for several helpful discussions and to B. Rose, Dr. R. Hanna and Professor H. Newson for results in advance of publication.

REFERENCES

BATCHELOR, R., 1956, *Proc. Phys. Soc.* A, **69,** 214.

BLATT, J. M., and WEISSKOPF, V. F., 1952, *Theoretical Nuclear Physics* (New York : Wiley).

BRINK, D. M., 1955, *Proc. Phys. Soc.* A, **68,** 994.

DIVATIA, R. H., DAVIS, A. S., MOFFAT, R. D., and LIND, D. A., 1955, *Phys. Rev.*, **100,** 1266 (A).

FESHBACH, H., PORTER, C. E., and WEISSKOPF, V. F., 1954, *Phys. Rev.*, **96,** 448.

HAYAKAWA, S., and YOSHIDA, S., 1955, *Proc. Phys. Soc.* A, **68,** 656.

HUGHES, D. J., and HARVEY, J. A., 1955, *Neutron Cross Sections*, Brookhaven Compilation, BNL 325.

LANE, A. M., LYNN, J. E., and STORY, J. S., 1956, *A.E.R.E Report T/M* 137.

LANE, A. M., THOMAS, R. G., and WIGNER, E. P., 1955, *Phys. Rev.*, **98,** 693.

LANG, J. M. B., and LE COUTEUR, K. J., 1954, *Proc. Phys. Soc.* A, **67,** 586.

LEVIN, J. S., and HUGHES, D. J., 1956, *Phys. Rev.*, **101,** 1328.

LYNN, J. E., and PATTENDEN, N. J., 1955, *Proceedings of the Geneva Conference on Peaceful Uses of Atomic Energy*, **4,** 210 (New York : United Nations)

NEWTON, J. O., 1955, *Progress in Nuclear Physics*, **4,** ed. O. R. Frisch (London : Pergamon Press), p. 234.

PEARSON, K., 1922, *Tables of the Incomplete* Γ*-Function* (London : Biometrika).

PORTER, C. E., and THOMAS, R. G., 1956, *Phys. Rev.*, **104,** 483.

ROSE, B., 1955, *A.E.R.E. Report*, NP/R 1743.

ROSE, M. E., MIRANKER, W., LEAK, P., and RABINOWITZ, G., 1953, *Brookhaven Report*, BNL 257.

STEPHENS, F. S., ASARO, F., and PERLMAN, I., 1955, *Phys. Rev.*, **100,** 1543.

THOMAS, R. G., 1955, *Phys. Rev.*, **97,** 224.

APPENDIX I

COMPUTATION OF THE FACTORS S_ν

S_ν is defined by

$$S_\nu(\alpha;\alpha_1,\ldots,\alpha_\mu)=\left\langle\frac{x}{x+x_1+\ldots+x_\mu+1}\right\rangle\Big/\frac{1}{1+\alpha/\alpha_1+\ldots+\alpha/\alpha_\mu+\alpha}$$

where $\alpha=\langle x\rangle^{-1},\ \alpha_i=\langle x_i\rangle^{-1}$

and where it is supposed that the x and x_i's have the χ^2 form of distribution with ν degrees of freedom (see § 2.2).

When $\nu=1$, $\mu=0$ we obtain from this definition

$$S_1(\alpha)=(1+\alpha)\frac{\alpha}{2\pi}\int_0^\infty\frac{x^{1/2}}{1+x}e^{-\alpha x/2}dx$$

$$=(1+\alpha)\frac{2\alpha}{\pi}\int_0^\infty\frac{v^2}{1+v^2}e^{-\alpha v^2/2}dv.$$

This may be expressed in terms of the integral

$$\Psi(u,t)=\frac{1}{2\sqrt{(\pi t)}}\int_{-\infty}^{\infty}\frac{\exp\{-(u-v)^2/4t\}}{1+v^2}\,dv$$

of which tables are available (Rose, Miranker, Leak and Rabinowitz 1953). We obtain

$$S_1(\alpha)=(1+\alpha)[1-\Psi(0,1/2\alpha)].$$

This function is shown in figure 4.

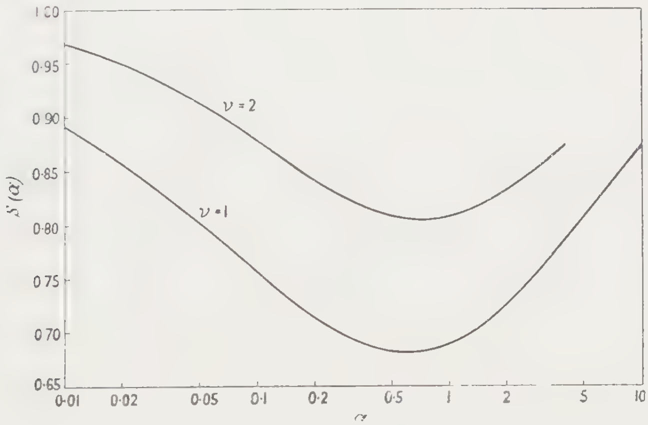

Figure 4. The averaging factor $S_\nu(\alpha)$ as a function of α for the case $\mu=0$ (no inelastic scattering channels) and $\nu=1$, 2.

The cases ($\nu=2$, $\mu=0$), ($\nu=2$, $\mu=1$) have been calculated elsewhere (Lane, Lynn and Story 1956). In the $\nu=2$, $\mu=0$ case

$$S_2(\alpha)=(1+\alpha)\{1-\alpha T_\alpha\}$$

where

$$T_\alpha=e^\alpha\int_\alpha^\infty\frac{e^{-t}}{t}\,dt.$$

Table 2. Values of $S_2(\alpha;\ \beta)$ for α in range 0 to 1·0 and β in range 0 to 1·0 assuming $\nu=2$

$\alpha \backslash \beta$	0	0·1	0·2	0·3	0·4	0·5	0·6	0·7	1·0
0	1·0	1·0	1·0	1·0	1·0	1·0	1·0	1·0	1·0
0·1	∞	0·966	0·887	0·865	0·857	0·854	0·853	0·853	0·855
0·2	∞	1·092	0·946	0·894	0·870	0·856	0·848	0·843	0·835
0·3	∞	1·193	1·004	0·932	0·895	0·873	0·859	0·850	0·834
0·4	∞	1·275	1·055	0·967	0·921	0·893	0·875	0·862	0·840
0·5	∞	1·342	1·099	1·000	0·947	0·913	0·891	0·875	0·848
0·6	∞	1·400	1·138	1·030	0·970	0·932	0·907	0·889	0·857
0·7	∞	1·449	1·173	1·056	0·991	0·951	0·923	0·902	0·867
0·8	∞	1·492	1·203	1·080	1·012	0·968	0·937	0·916	0·876
0·9	∞	1·529	1·231	1·102	1·030	0·983	0·951	0·928	0·886
1·0	∞	1·563	1·256	1·122	1·046	0·998	0·964	0·940	0·895

This is shown in figure 4. The $\nu=2$, $\mu=1$ case is given by

$$S_2(\alpha;\ \beta)=\left(1+\alpha+\frac{\alpha}{\beta}\right)\left\{\frac{\beta}{\beta-\alpha}-\frac{\alpha\beta}{(\beta-\alpha)^2}[(1+\beta-\alpha)T_\alpha-T_\beta]\right\}$$

where, for clarity, we have written β for α_1. Some values of this function are given in table 2.

We have had computed numerically a few values of $S_\nu\ (\alpha;\ \beta)$ when $\nu=1$, $\mu=1$. These are shown in table 3.

Table 3. Values of $S_1(\alpha;\ \beta)$ for α in range 0 to 1·0 and β in range 0 to 1·0 assuming $\nu=1$

$\alpha \backslash \beta$	0	0·2	0·4	0·6	0·8	1·0
0	∞	0	0	0	0	0
0·2	∞	0·8782	0·7725	0·7397	0·7262	0·7182
0·4	∞	1·0237	0·8395	0·7787	0·7483	0·7310
0·6	∞	1·1414	0·9066	0·8233	0·7811	0·7565
0·8	∞	1·2386	0·9637	0·8653	0·8148	0·7839
1·0	∞	1·3171	1·0125	0·9005	0·8428	0·8078

In Appendix III we introduce a quantity F which fulfils in the inelastic cross sections the same role as S in the capture cross sections. $F_\nu(\alpha;\beta)$ has been computed numerically for $\nu=1$, $\mu=1$ (table 4). Values of $F_\nu\ (\alpha;\ \beta)$ for $\nu=2$, $\mu=1$ have been tabulated elsewhere (Lane, Lynn and Story 1956) from the relation

$$F_2(\alpha;\beta)=\alpha\beta(\alpha+\beta+\alpha\beta)\left\{\frac{\beta+\alpha}{\alpha\beta(\beta-\alpha)^2}-\frac{1}{(\beta-\alpha)^3}[(2+\beta-\alpha)T_\alpha-(2-\beta+\alpha)T_\beta]\right\}.$$

Values are presented in table 5.

Table 4. Values of $F_1(\alpha;\ \beta)$ for α in range 0·04 to 0·8 and β in range 0·04 to 0·8 assuming $\nu=1$

$\alpha \backslash \beta$	0·04	0·08	0·40	0·80
0·04	0·5006	0·5149		
0·08	0·5149	0·5015	0·5676	0·6177
0·40		0·5676	0·5158	0·5339
0·80		0·6177	0·5339	0·5374

Table 5. Values of $F_2(\alpha;\ \beta)$ for α in range 0·4 to 0·9 and β in range 0·3 to 0·7 assuming $\nu=2$

$\alpha \backslash \beta$	0·3	0·4	0·5	0·6	0·7
0·4	0·6777	0·6772	0·6801	0·6842	0·6886
0·5	0·6827	0·6801	0·6811	0·6838	0·6870
0·6	0·6887	0·6842	0·6838	0·6852	0·6877
0·7	0·6947	0·6886	0·6870	0·6887	0·6893
0·8	0·7003	0·6931	0·6907	0·6905	0·6917
0·9	0·7056	0·6975	0·6943	0·6936	0·6942

APPENDIX II

ENERGY DEPENDENCE OF THE RADIATION WIDTH

According to Blatt and Weisskopf (1952, eqn (7.23), p. 649) the energy dependence of the radiation width for electric dipole radiation should be of the form

$$\Gamma_\gamma(E) \propto \rho(E+B_{\mathrm{n}})^{-1}\int_E^{E+B_{\mathrm{n}}} \epsilon^3\rho(E+B_{\mathrm{n}}-\epsilon)\,d\epsilon \qquad \ldots\ldots(6)$$

where $\rho(E+B_{\mathrm{n}})$ is the density of levels emitting dipole radiation to combine with a given lower state. The limits of the integral in (6) are fixed by the fact that ϵ represents the energy of the emitted radiation. Radiation which leaves the de-excited compound nucleus in a state above the neutron separation energy B_{n} will be followed predominantly by the emission of a neutron. Hence it will not be observed as part of the capture process which was measured, for ^{238}U and ^{232}Th, by activation techniques. The upper limit is the maximum energy of an emitted gamma ray.

The level density was approximated by $\rho(U) \propto \exp(aU)^{1/2}$ the value of a being adjusted to compensate for the neglect of the factor

$$(U+t)^{-2}\exp\left\{\frac{3}{32}(11U)^{2/3}\right\}.$$

The ratio

$$\frac{\Gamma_\gamma(E)}{\Gamma_\gamma(0)} = \frac{\exp\{(aB_{\mathrm{n}})^{1/2}\}\int_E^{E+B_{\mathrm{n}}} \epsilon^3 \exp\left[\{a(E+B_{\mathrm{n}}-\epsilon)\}^{1/2}\right] d\epsilon}{\exp\left[\{a(B_{\mathrm{n}}+E)\}^{1/2}\right]\int_0^{B_{\mathrm{n}}} \epsilon^3 \exp\left[\{a(B_{\mathrm{n}}-\epsilon)\}^{1/2}\right] d\epsilon}$$

was calculated by making the substitution $u=\{a(B_{\mathrm{n}}+E)\}^{1/2}-\{a(B_{\mathrm{n}}+E-\epsilon)\}^{1/2}$. The resulting integrals may now be broken down into incomplete gamma functions which are tabulated for example by Pearson (1922).

To give an idea of the variation in Γ_γ, we find that for $E=1$ MeV, $B_{\mathrm{n}}=5$ MeV and $a^{1/2}=9{\cdot}4$, $\Gamma_\gamma(E)/\Gamma_\gamma(0) \simeq 1{\cdot}16$, i.e. there is only a slight change in the radiation width over the energy range we are considering.

APPENDIX III

Calculation of Inelastic Scattering Cross Sections

The formula corresponding to (5) for inelastic scattering is

$$\sigma_{\mathrm{nn}'}(E) = \frac{\pi^2}{k^2(2I+1)} \sum_{j=|I-\frac{1}{2}|}^{I+\frac{1}{2}} \sum_J (2J+1) \sum_{l=|J-j|}^{J+j} \frac{(\langle\Gamma_{\lambda J(nlj)}\rangle/\langle D_{\lambda J}\rangle)}{(\langle\Gamma_{\lambda J}\rangle/\langle D_{\lambda}^{J}\rangle)}$$
$$\times \sum_{n',l',j'} (\langle\Gamma_{\lambda J(n'l'j')}\rangle/\langle D_{\lambda J}\rangle)\ F(\alpha_{lj};\ \alpha_1,\ldots,\alpha_\mu)$$

$F(\alpha_{lj};\ \alpha_1,\ldots,\alpha_\mu)$ is defined as the dimensionless ratio

$$\left\langle \frac{\Gamma_{\lambda J(nlj)} \sum_{n'l'j'} \Gamma_{\lambda J(n'l'j')}}{\Gamma_{\lambda J}} \right\rangle \Bigg/ \frac{\langle\Gamma_{\lambda J(nlj)}\rangle \sum_{n'l'j'} \langle\Gamma_{\lambda J(n'l'j')}\rangle}{\langle\Gamma_{\lambda J}\rangle}$$

α, $\alpha_1,\ldots,\alpha_\mu$ having the meanings assigned to them in § 2.2.

In a first estimate of the cross section ^{238}U(nn′) at 500 kev, we put the F factors equal to unity. In the same calculation we used the Thomas prescription for treating interference effects between resonances as described in § 2.4 and we tried the following numerical assumptions with the results quoted.

(i) $s_0 = s_2 = 0{\cdot}036$ and $s_1 = s_3 = 0{\cdot}072$; $R_\infty = 0$ for all l; $\sigma_{\mathrm{nn}'} = 2{\cdot}54$ barns.

(ii) $s_0 = s_1 = s_2 = s_3 = 0{\cdot}036$; $R_\infty = 0$ for all l; $\sigma_{\mathrm{nn}'} = 1{\cdot}83$ barns. (This calculation was repeated neglecting the interference effects, with the result $\sigma_{\mathrm{nn}'} = 2{\cdot}12$ barns).

(iii) $s_0 = s_2 = 0{\cdot}020$; $s_1 = s_3 = 0{\cdot}036$; $R_\infty = 0$ for all l; $\sigma_{\mathrm{nn}'} = 1{\cdot}39$ barns.

These values are appreciably greater than the experimentally observed value of 0·8 barn. The neglect of the F factors may be responsible for this. In table 4 we give values of the F factors, F for $\nu = 1$ and $\mu = 1$. These values lie between 0·5 and 0·6 for a large range of values of α and α_1. If $\nu = 2$ and $\mu = 1$ (table 5), F lies between 0·65 and 0·75 over a large range of values of α and α_1. It is laborious to compute F for values of μ greater than 1 and we have not done this. The values of F for μ equal to 1 suggest that one ought not to ignore the presence of these factors. It may be that taking account of the factors will reduce the predicted cross section to the observed value. However, even this may not be good enough, because one expects that a fair fraction of the observed value (0·8 barn) is due to a 'direct' process (Wandel, unpublished, Brink 1955, Hayakawa and Yoshida 1955) of which we have taken no account at all.

Tabulation of the Wigner 9*j* Coefficients

By J. W. STEPHENSON and K. SMITH

Department of Physics, North Carolina State College, Raleigh, N.C.

MS. received 1*st May* 1957, *and in final form* 3*rd June* 1957

Abstract. The tabulation of the Wigner 9*j* coefficient $\begin{pmatrix} a & b & e \\ c & d & f \\ g & h & k \end{pmatrix}$ is described. The calculation was performed on an electronic digital computing machine. The range of the parameters tabulated is $\frac{1}{2} \leqslant a, b, c, d \leqslant 7/2$; $0 \leqslant e, f, g, h, k \leqslant 7$.

---

§ 1. Introduction

The physical significance of the Wigner 9*j* coefficient (Wigner, unpublished, Jahn and Hope 1954), as the transformation function between two different coupling orders in pairs of any four-angular momenta, *a*, *b*, *c* and *d*, has been given by Arima, Horie and Tanabe (1954). These authors have also listed the properties of the coefficient.

Some tables of the coefficients have been prepared by other workers (Sharp 1953, Kennedy 1954, Matsunobu and Takebe 1955), but the ranges of the parameters were severely restricted. The latter's tables are confined to the ranges $a = b = \frac{1}{2}$, *f* and *k* between 0 and 4, and *c* and *d* between $\frac{1}{2}$ and 7/2. The Chalk River Reports give the coefficients for the following ranges of parameters: (Kennedy 1954): $b = d$, $e = f$, *b* and *e* take on integral and half-integral values from 1 to 5; $a, c = 1, 2$; *g*, *h*, *k* take on even values not exceeding 8. (Sharp 1953): $b = d = \frac{1}{2}$; *a* and *c* not exceeding 5, and for all values of the remaining parameters.

The present authors have tabulated the coefficient for *a*, *b*, *c* and *d* taking on the half-odd integral values from 1/2 to 7/2, and for integral values of *e*, *f*, *g*, *h* and *k* from 0 to 7. These tables can be obtained from the Secretary of the above department.

§ 2. Calculation of the Coefficients

All calculations were performed on an electronic digital computing machine (IBM-650) on the campus at N.C. State College.

The coefficient was computed using the identity:

$$\begin{pmatrix} a & b & e \\ c & d & f \\ g & h & k \end{pmatrix} = \sum_x (2x+1) W(gkbd; hx) W(ekcd; fx) W(gcbe; ax). \quad \ldots\ldots(1)$$

The explicit form of the *W* coefficient is given by Racah (1942).

From the triangular conditions imposed on the nine parameters it is possible to select a lower and an upper limit for *x* in the summation of equation (1), and to sum between these limits. The Racah coefficients were computed by a special sub-routine incorporated into the main programme. This sub-routine was specially constructed for this problem.

All of the computation, except the final summation, was performed in ten-digit floating decimal point form, while the speedometer arrangement and parameter selection section used fixed point arithmetic.

It is the present intention of the authors to compute those coefficients which have all their parameters integers.

REFERENCES

ARIMA, A., HORIE, H., and TANABE, Y., 1954, *Progr. Theor. Phys.*, **11,** 143.

JAHN, H. A., and HOPE, J., 1954, *Phys. Rev.*, **93,** 318.

KENNEDY, J.M., 1954, Atomic Energy of Canada, Ltd., CRT-569.

MATSUNOBU, H., and TAKEBE, H., 1955, *Progr. Theor. Phys.*, **14,** 589.

RACAH, G., 1942, *Phys. Rev.* **62,** 438.

SHARP, W. T., 1953, Atomic Energy of Canada, Ltd., CRT-556.

The Fission Cross Sections of ^{233}U, ^{235}U, ^{238}U and ^{239}Pu for Neutrons in the Energy Range 0·030 Mev to 3·0 Mev

By W. D. Allen and A. T. G. Ferguson

Atomic Energy Research Establishment, Harwell, Berks

MS. received 20th March 1957

Abstract. The fission cross sections of ^{233}U, ^{235}U, ^{238}U and ^{239}Pu have been measured as a function of neutron energy for neutrons in the energy range 0·030 Mev to 3·0 Mev. In addition, measurements of the ratios of the fission cross sections as a function of neutron energy have been made. The fission cross sections and the ratios have been shown to be consistent and a set of best values of the cross sections has been computed. The accuracy over most of the range is to about 3%, falling to 5% at the extremes.

§ 1. Introduction

We here report measurements of the fission cross sections of ^{233}U, ^{235}U and ^{239}Pu between neutron energies of 0·030 Mev and 3·0 Mev with an accuracy to about 3% in general. Somewhat larger errors are associated with the extremes of the energy range. The fission cross section of ^{238}U has been obtained from threshold up to 3·0 Mev.

Fission cross sections may be measured by placing a known amount of fissile material in a known neutron flux and counting the number of fissions. In the preceding paper (Allen and Ferguson, to be published) the development of techniques capable of measuring flux with an accuracy to 2–3% has been described. The source of neutrons was the bombardment of lithium or tritium with protons from the Harwell Van de Graaff machine. The quantity of fissile material suitable for absolute counting of fission fragments is about 1 mg. With this quantity of fissile material and under typical experimental conditions, the fission rate was too low to permit a series of measurements at a large number of neutron energies. In consequence absolute measurements were made at only two energies, viz. at 550 kev, where the yield of the Li(p, n) reaction had a maximum, and at 1500 kev, where the yield of the T(p, n) reaction became adequate. At other energies, only relative measurements, i.e. the variation with neutron energy of the fission cross section, have been made. For these, the accurate knowledge of the quantity of fissile material and the efficiency of counting fissions is not required. Therefore, the maximum possible amount of fissile material was used (e.g. 100 mg of ^{235}U) and high statistical accuracy obtained.

The erratic measurements encountered in some early experiments led us to adopt consistently a system of cross-checks. For ^{233}U, ^{235}U and ^{239}Pu, direct measurements of fission cross sections were made in different irradiation geometries and, using a back-to-back chamber, a cyclic set of three ratios of fission cross sections was measured. All these measurements were required to be self-consistent. This procedure was adopted for both relative and absolute measurements.

The fission cross section of ^{238}U and its variation with energy was found by comparison with ^{233}U.

In § 2 a description of the fission counters and their electronics and of the measurement of the epithermal background is given; this is followed in § 3 by a description of the absolute measurements. Section 4 gives an account of the measurements of the variation of the ratios of the cross section with energy and § 5 of the variation of the cross sections. Finally, there is a discussion of the results, their errors and significance.

§ 2. THE FISSION COUNTERS, ELECTRONICS AND BACKGROUND NEUTRONS

For the relative measurements one requires a counter which has a maximum quantity of fissile material in as small a space as possible. Such a counter (the 'multiplate counter'), incorporating 100 mg of ^{235}U in a volume of one cubic inch has already been described (Allen and Ferguson 1955). The quantity of ^{233}U and ^{239}Pu is limited by their α-activity to roughly 50 mg and 11 mg respectively. For neutrons in the energy range under investigation these counters had an average transmission of 93%. With a cadmium shield 0·015 in. thick in position the total attenuation of neutrons between source and fissile material was only $3\frac{1}{2}$% on the average. It was assumed that the neutrons scattered out of the direct beam were equal to those scattered in from the walls.

Measurements of the absolute values of the ratios of fission cross sections and their variation with energy are made in a counter (the 'back-to-back counter'), of which a radiograph is shown in figure 1. Like the multiplate counter above, it was made of 0·010 in. steel with insulators and base plate at a distance of about 6 in. from the fissile material. A removable Cd shield 0·015 in. thick excluded thermal neutrons. For the measurement of the variation of fission cross section ratios with energy, foils of 0·005 in. platinum were prepared with 4 mg of fissile material on each side. The material was on a 2 cm diameter circle. For absolute measurements of the ratios two 0·005 in. foils were mounted back to back. These were coated with a known quantity of about 1 mg or less of material. The counters were filled with 50 cm argon and 2·5 cm CO_2. With the absolute foils, the integral bias curves were very flat, the counting rate changing by 5% for a factor 2 change in bias. With the thicker foils the slope was steeper than this by a factor of 2 or 3, but still very satisfactory from the point of view of stable counting.

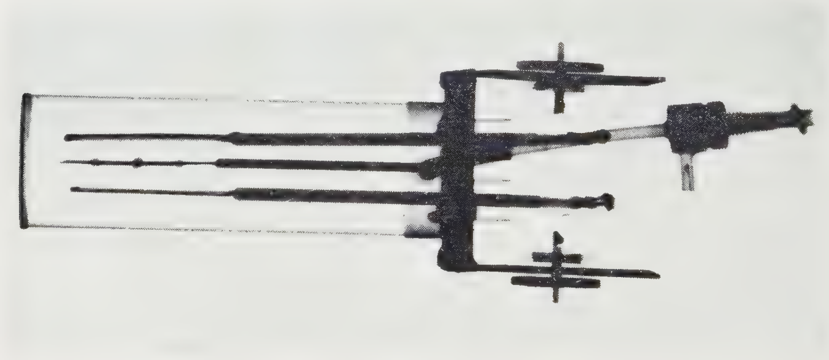

Figure 1. Radiograph of the back-to-back counter.

The change in ratio when the positions of the two foils relative to the target was interchanged by rotating the counter through 180° was about 2% for the two absolute foils. The mean value of the two measurements gave the ratio quoted. For the thick foils, deposited on either side of the same piece of platinum, the effect was about 1%.

A radiograph (figure 2) shows the counter design used for the absolute measurements of the fission cross sections. The negative high voltage electrode was spun from 0·005 in. brass and supported 8 in. from the base by a brass rod. The fission foil was mounted on this electrode, the large separation from the base plate ensuring that the number of neutrons back-scattered from the base was small compared with the direct beam. The walls of the counter were of 0·010 inch steel and the end dome of copper of similar thickness. The actual counting volume was thus hemispherical, giving optimum discrimination between fissions and α-particles. A 0·015 in. Cd sheath excluded thermal neutrons from the counters. The gas filling was 40 cm A + 2 cm CO_2. With the bias sufficiently high to exclude pulses due to α-particles, the ordinates of the integral bias curve for fission changed by about 2% for a factor of two increase in bias. To obtain the number of fissions above zero bias, the integral bias curve was assumed to be linear with bias and the observable portion was produced back to zero bias. This extrapolation gave a correction to the observed number of fissions. This correction had its maximum value (about 2%) for plutonium. The α-particles from plutonium were so numerous as to cause considerable 'pile-up' of pulses, necessitating a high bias for their exclusion. An additional correction had to be made for the fission fragments which do not escape from the material.

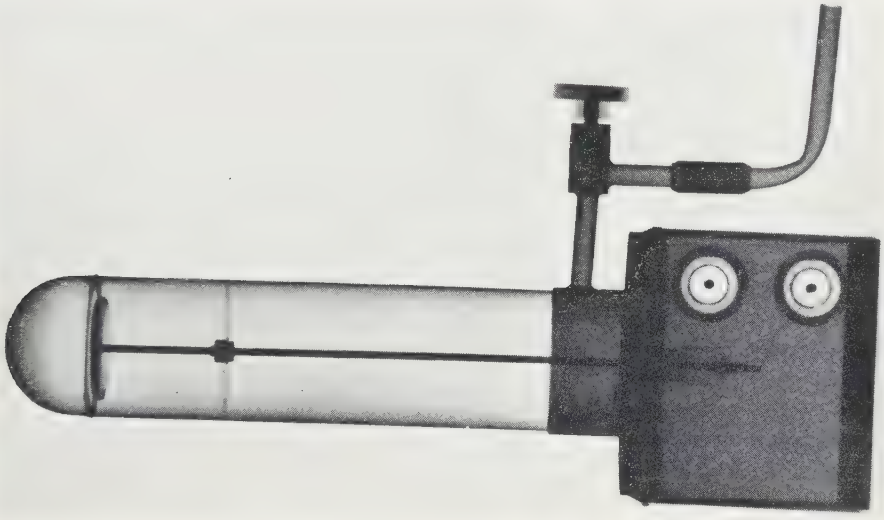

Figure 2. Radiograph of the counter used in measurement of absolute fission cross sections.

The main problems in electronics arise out of the high activity of α-particles and the low rate of fast neutron fission. Thus we require amplifiers with short time constants and a low rate of spurious pulses. Since we depend on counting above a bias, stability of gain and bias are important. The amplifier used (an A.E.R.E. type 1049B) had differentiating and integrating time constants of

0·08 μsec. To reduce spurious pulses head amplifier components, in particular the first valve, were specially selected, and ventilation of the components was improved. Many spurious counts seemed to come from the mains, so all the equipment was run from a stabilized generator. Because of the short pulses fast scalers had to be used. To avoid the loss of data accumulated during long runs in the event of scaler failure two scalers were used in parallel on the output of the amplifier.

Background neutrons may be divided into two main classes—those that result from a single scattering in or near the target and the very degraded neutrons scattered from the walls of the room (thermal or epithermal). By care in target design (see preceding paper) the former have been made negligible except for measurements at 120° to the proton beam. Even there, the number was less than 5% of the direct beam and the proportional counter allowed an accurate estimate of them. For a fission counter enveloped in 0·015 in. Cd sheet, the fission rate due to epithermals was from 1 to 2% of the direct rate at a distance of 4 in. from the target. It was measured by removing the counter to a distance of 40 in. where the direct flux was reduced by a factor of 100.

§ 3. THE ABSOLUTE CROSS SECTION MEASUREMENTS

For an absolute measurement one needs to choose a fission foil thickness in which the number of fissions can be accurately related to the quantity of material on the foil. For our experiments, one milligram was spread over an area 2 cm in diameter, the foil being placed 10 cm from the target. For this relatively small quantity a high neutron flux was required, therefore neutron energies of 550 kev, 1500 kev and 1800 kev were chosen. At 550 kev a lithium fluoride target 30 kev thick was used, at 1500 kev a tritium gas target 100 kev thick, and at 1800 kev a zirconium tritide target of thickness 50 kev. This choice of different neutron energies gave checks on the consistency of the measurements of the energy variation of the cross section. Further checks were provided by absolute measurements of the ratios of the fission cross section at 550 kev.

Two experimental arrangements were adopted.

In the first, called the direct method, the axes of the fission counter, long counter and recoil counter were generators of a 15° cone whose apex was at the target spot. This system has the advantage that only one run is necessary for flux and fission measurement. The chief objection is that with a rapidly varying

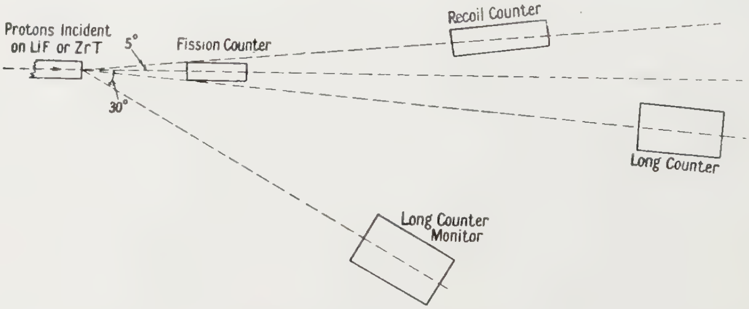

Figure 3. Geometrical arrangement for the study of the variation of the fission cross section with energy.

angular distribution of emergent neutrons, such as is obtained from Li, and with the fission counter close to the target, it is not easy to ensure that the respective angles of the fission and flux counter are identical.

In all the more recent experiments the 'substitution' method has been used instead. The geometry is shown in figure 3. The fission counter was mounted in such a way that it could readily be set at a distance of about 4 in. reproducible to 0·010 in. The flux counters were mounted in a vertical plane at angles of ± 5° to the proton beam. (The neutron energy and intensity at 5° differ very little from their values at 0°.) A second long counter acting as monitor was set up at an angle of 30° to the proton beam. In this method a run was taken with the fission counter in position, recording the number of fission counts and the number of monitor counts. Then the fission counter was removed and a further set of data taken recording the neutron flux in the long counter and recoil counter and again the number of monitor counts. It was established that the variation in monitor counts with and without a fission counter in place was negligible.

3.1. *Fission Foil Preparation*

All the foils were prepared on polished platinum blanks 1·25 in. diameter by the painting technique. In this method, the material is painted in many layers, being fired and rubbed with soft paper between each coat (Glover and Borrell 1954). The mass of fissile material was determined as follows.

^{233}U

The stock material was rather better than 99% pure chemically and isotopically. Four foils were prepared in which agreement between weight and mass by alpha assay in a low geometry counter was better than 1%. One of the four foils was then analysed by polarographic methods and the mass checked to better than 1%. With this material, the only possibility of error comes through foil irregularities affecting the 2π geometry fission counting. However, as the foils were flat and highly polished, this possibility was very remote.

^{235}U

The ^{235}U stock material contained about 80% ^{235}U, 1% ^{234}U and 19% ^{238}U. The isotopic constitution had therefore to be determined by a mass spectrometer, and the specific activity determined empirically. The accuracy was about ± 2% on the specific activity determination and rather better than 1% on the isotopic constitution. The activity was such that it enabled counting to be done both in the low geometry (solid angle 1/700) counter, and in the 2π geometry counter.

Three foils of ^{235}U were made, in all, of which the weight exceeded the mass determined from α-counting by 2–3%. Polarographic measurement of one foil, however, showed the presence of 2–3% by weight of impurity and gave an assay for the uranium in good agreement with the alpha counting. The latter was therefore accepted with a probable error of 1%.

^{238}U

For the relative measurements, ^{238}U whose ^{235}U content had been depleted by a factor of 40, was used. For absolute measurements, natural uranium was used because of the accurately known value of the specific activity (Kovarick and Adams 1955). Agreement in the three methods to 1% was again obtained.

^{239}Pu

The available plutonium contained some ^{238}Pu and ^{240}Pu. The ^{238}Pu activity was quite small and was distinguished by pulse analysis; the ^{240}Pu, however, which had a specific activity four times that of ^{239}Pu, was not so distinguished. Therefore the ^{240}Pu isotopic content—about $\frac{1}{2}$%—was determined mass-spectrometrically and allowed for. We used two foils, in which the mass of ^{239}Pu determined by α-counting and weighing agreed to within 1%. One Pu foil gave trouble later; it was deposited on 0·002 in. platinum. Weight and α-counting (low geometry) were consistent but the fission count was some 7–8% low. The foil, however, showed visible crinkles, and the discrepancy was attributed to the loss of fissions which, originating in a trough, buried themselves in the platinum backing.

3.2. *Results*

With the methods described above a series of measurements of the absolute cross sections was made of which an account is given below. Certain corrections which were common to all the foils used were made as follows:—

(i) A correction of $1\frac{1}{2}$% for fission fragments which do not escape from the uranium film.

(ii) Fissions induced by neutrons back-scattered from the foil support—calculated to be about $\frac{1}{2}$%.

(iii) The effect of scattering in the walls of the chamber and the Cd cover was thought to be negligible because, as the geometry approximated to a sphere, the numbers of neutrons lost or gained by scattering were equal.

(iv) The measured correction for fissions induced by epithermal neutrons was between $\frac{1}{2}$% and 1%.

(v) The ^{235}U and ^{238}U values were corrected for their respective contaminants of ^{238}U and ^{235}U.

With a tritium gas target as neutron source six values of the cross section of ^{239}Pu were obtained at a neutron energy of 1·5 Mev. These had an r.m.s. spread of under 2%. Similar measurements were made for ^{233}U and ^{235}U at a neutron energy of 1·8 Mev with neutrons from a ZrT target on a copper backing. By measuring the number of fissions produced by neutrons from a copper target these results were later corrected for the effect of neutrons from the ^{65}Cu(p, n) reaction in the target backing. This correction amounted to about 5% at the higher energy.

A set of measurements for all three isotopes was carried out at a neutron energy of 550 kev. In addition, at this energy absolute values of the ratios of cross section were determined, the method being described below (§ 5). In this case, foils of known mass were used, and the counting rate extrapolated to zero bias. By taking dimensions from the radiographs of the back to back counters absolute values of the cross sections were obtained, in addition to their ratios. The results taken together gave five independent estimates for each cross section. Certain inconsistencies appeared, which, after further ratio measurements in a thermal neutron flux were attributed to the thin ^{239}Pu foil described above. The results involving it were rejected. An analysis of the remaining results showed them to have a random error on each individual estimate of 3%. This quantity includes counting statistics, random errors in dimensions, random inconsistencies in the masses of the nine foils used, random errors in flux measurements, neutron energy, etc. all the random errors and inconsistencies. The corrections described above were applied to all the results. Combining the results at each energy, a final set of results was obtained which is set out in table 1.

Table 1. Fission Cross Sections (Barns)

Neutron Energy	^{233}U	^{235}U	^{238}U	^{239}Pu
550 kev	1·99 ± 0·04	1·22 ± 0·023	—	1·66 ± 0·01
1500 kev	—	—	—	1·93 ± 0·03
1800 kev	1·92 ± 0·03	1·38 ± 0·02	—	—
2000 kev			0·46 ± 0·01	

The errors quoted are only the statistical errors as described above. At an energy of 2·5 Mev an absolute measurement of the ratio of the fission cross section of ^{238}U to that of ^{233}U was obtained. From this and the ^{233}U cross section determined independently, the cross section of ^{238}U was deduced and is included in table 1.

Since the results at 550 kev had the greater statistical weight, and were free from the uncertainty of the correction for the effect of Cu(p, n) neutrons it was decided to normalize the measurements of the variation of cross sections to them. The resulting values of the cross section at 1500 and 1800 kev are in good agreement with the direct absolute measurements.

§ 4. THE ENERGY VARIATION OF THE RATIOS OF THE FISSION CROSS SECTIONS

Taken together with direct measurements of the cross section, measurement of ratios of the fission cross sections act as cross-checks and increase the statistical information. By measuring all three ratios, viz. the fission cross section of ^{239}Pu to the fission cross section of ^{235}U, the fission cross section of ^{233}U to that of ^{235}U and the fission cross section of ^{233}U to that of ^{239}Pu we have a set whose consistency we can readily check. These ratios are very sensitive to small changes in cross section with energy and reveal any fine structure present.

The counters were set up with the foils 2 in. from the target, the normal to the foil in a direction either at 0° or at 120° to the proton beam. At every energy two runs were taken in which about 10 000 fission counts were recorded in each foil though only about 5000 counts in regions where the neutron yield was low. Measurements of the variation of the ratio with energy were made from 30 kev to 3 Mev. An analysis at all energies where three or more sets of measurements were made indicated a standard deviation of $\pm 1{\cdot}5\%$ on each ratio measurement. This is very close to what we would expect from counting statistics alone. It indicates that errors arising from drifts of electronic discriminator levels and from random inaccuracies in the neutron energy must have been negligible. The consistency of the data has been estimated by comparing the product of two ratios with the third. The deviations from the mean of the two values at each energy was taken. The average value of the deviation was less than $\frac{1}{4}\%$. The root mean square of the deviation was $1{\cdot}5\%$ which is in accord with the errors of the measurements involved. Figure 4 shows the ratios obtained. At the higher energies a correction has been made for the contribution of the ^{238}U present in the ^{235}U foils.

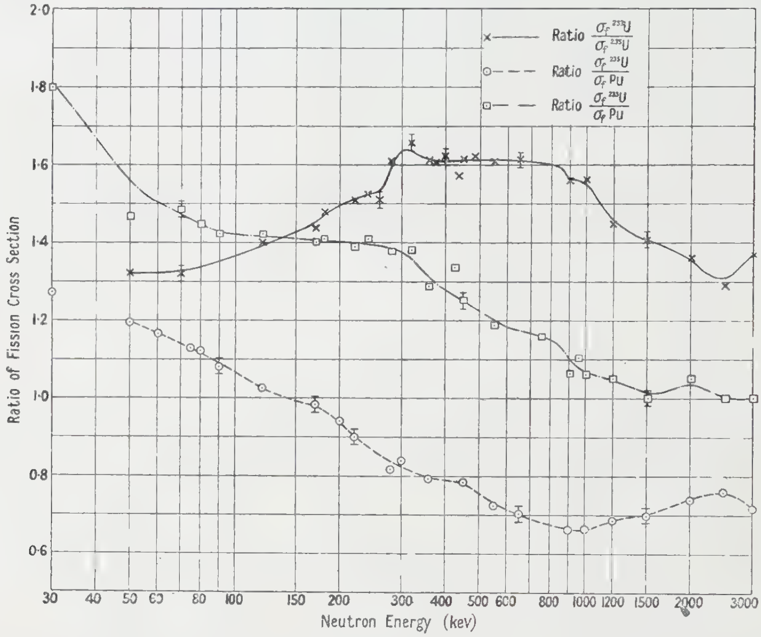

Figure 4. The ratios of the fission cross sections of ^{233}U, ^{235}U, ^{239}Pu.

The data have been normalized to the absolute value of the ratio of the cross sections, determined at 500 kev (§ 3).

By an identical method the ratio of the cross section of ^{238}U relative to ^{233}U was determined at a number of energies from threshold up to 3 Mev. These measurements were normalized to an absolute value obtained at 2·5 Mev, and, combining these results with the cross section of ^{233}U, the cross section of ^{238}U was found. The final results are shown in figure 5.

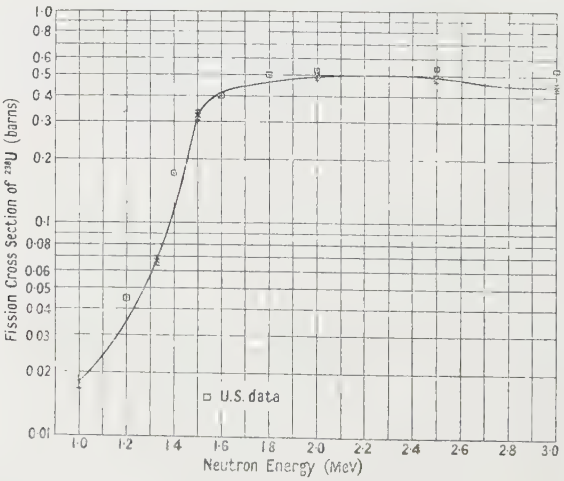

Figure 5. The fission cross section of ^{238}U.

§ 5. THE ENERGY VARIATION OF THE FISSION CROSS SECTIONS

The variation with neutron energy of the number of fissions in the multiplate chamber when it was placed in a known flux of monoenergetic neutrons was measured.

For neutron energies above 120 kev the substitution method was employed (see § 3), the fission counter being placed 4 in. from the target in a direction at 0° to the proton beam. In each measurement both the long counter and recoil counter were used to measure the neutron flux. The recoil counter enabled us to ensure the accuracy of the neutron energy and the purity of the neutron spectrum. (The presence of neutrons of higher or lower enegry gives rise to a distorted recoil spectrum.) While the recoil counter gave absolute flux measurements, the statistical accuracy of individual readings was only about $\pm 2\frac{1}{2}\%$. The stability and high efficiency of the long counter though not an absolute instrument allows relative flux measurements with small random errors. Combining all the recoil and long counter measurements at each energy gave a point by point calibration for the long counter with statistical errors of less than 1%. If the recoil spectrum was satisfactory the flux measured by the calibrated long counter was accepted. In this way, measurements were made between 120 kev and 625 kev with neutrons from a LiF target on a silver backing, and between 500 kev and 3·0 Mev with neutrons from a ZrT target. The backing of the latter was gold; it was mounted in a geometry identical to that of the LiF targets. In the region from 500 to 625 kev the measurements with the two targets agreed to within 1%. The neutron background was determined by bombarding a zirconium target on a gold backing. It was found by a long counter to be 2% of the yield of a similar target impregnated with tritium when the proton energy corresponded to 3 Mev neutrons from the latter.

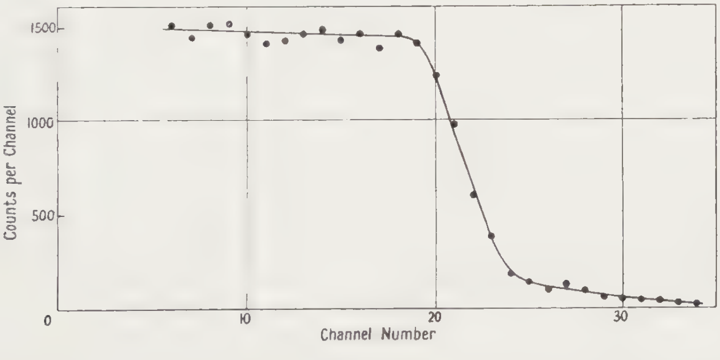

Figure 6. A typical recoil spectrum obtained with the counter in the 120° position. The tail at high energies is due to neutrons emitted at around 90° and scattered in the target. A correction is made for these neutrons.

For neutron energies below 120 kev it was necessary to carry out the measurements at 120° to the proton beam. Measurements were made down to an energy of 30 kev and carried on up to 300 kev in order to overlap the measurements at 0°. In this energy region we have used the recoil counter for flux measurements as it allows us to correct for the high energy neutrons scattered into this direction. Figure 6 shows a recoil spectrum taken at this angle, showing the high energy tail for which a correction is made. Simultaneous determinations of flux and numbers of fissions were made. In the region from 120 kev to 300 kev there was no systematic discrepancy in the variation with energy determined at 0° and 120°. The normalizing factor between the two sets of results had a random error of about 1%.

At each energy two counts of 5000–10 000 fissions were taken and so the statistical error in this quantity is small. In all measurements, both at 120° and 0°, the number of fissions due to epithermal neutrons was determined and a correction made. At some energies, e.g. 650 kev, 120 kev and several others, the measurements have been repeated many times, and from an analysis of these measurements an independent estimate of the total random error of the fission cross section measurement was obtained. These procedures gave the 'primary' set of measurements of the three fission cross sections, viz. those of ^{233}U, ^{235}U, ^{239}Pu, when normalized to the absolute best values at 550 kev; thus, at many energies we had three 'primary' cross sections and three ratios, each with an estimate of its random error. This set is over-determined; to obtain the best consistent set of results at each energy, the analytical procedure described by Morton *et al.* (1956) was applied. This gave a set of best values with their probable errors. The latter were in every individual case less than or equal to the errors quoted for the primary set showing the complete self-consistency of the data. The final cross sections are presented in figure 7. The errors shown are the resultant of all the random errors of the relative measurements, and are a measure of the self-consistency. In general, they are about $1\frac{1}{2}$% over the centre portion of the curve. The possible systematic errors will be discussed below.

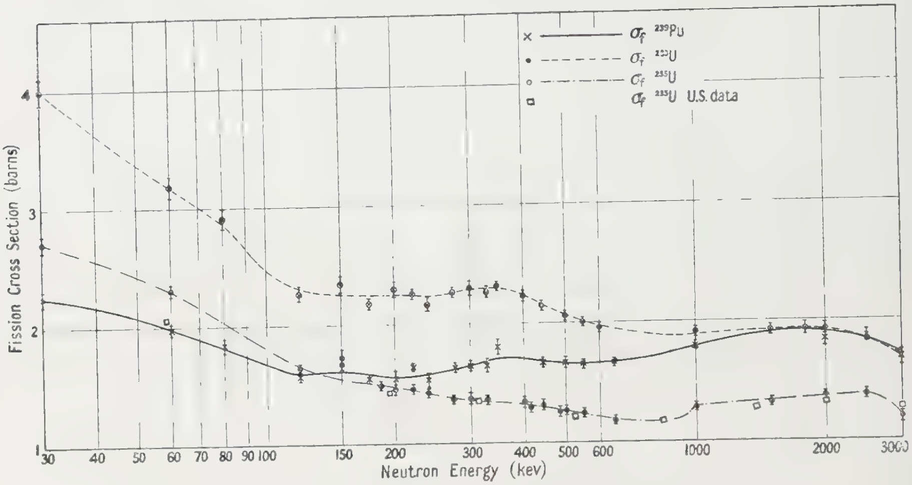

Figure 7. The fission cross sections of ^{233}U, ^{235}U, ^{239}Pu. The values taken from the curve in "Neutron Cross Sections" BNL. 325, are shown for comparison.

§ 6. DISCUSSION

6.1. *Errors*

In the sections on relative and absolute measurements an analysis of the results has been given taking account of all the random errors. On both the relative and absolute measurements these appear to be about 1½% over the major portion of the range giving a combined random r.m.s. error of about 2%. In our paper on the measurement of neutron flux we have felt that, in addition to the small random errors, there may be additional errors of 1·5 2%. The absolute masses of the fission foils, and uncertainties in the corrections may be of the same order. Even taking the larger values in all cases would give an error of about 3½% over the major part of the energy interval covered by our measurements. It is felt that an error of about 3% would not be unreasonable.

6.2. *Comparison with Other Work*

Until the Geneva Conference on the Peaceful Uses of Atomic Energy in July, 1955, no measurements had been published in this field. Data were presented there by workers in the U.S.A. and France, and briefly by the authors. In subsequent detailed comparison of U.S. data and ours, the agreement between 500 and 1500 kev was within 3–4%. Further revisions and checking have brought the results into even closer agreement. The technique adopted in the U.S.A. has been described by Diven (1953). Here a hydrogenous foil of glyceroltristearate and a film of ^{235}U are mounted back to back and the variation of the ratio of fissions to proton recoils observed between neutron energies of 500 kev and 1500 kev. An absolute measurement was made at 1250 kev. The most recent results from this source are given in the publication BNL 325 "Neutron Cross Sections" (1955) and by Henkel (private communication). A number of values for ^{235}U are plotted in figure 7. It may be seen that these agree with our measurements within 2%.

The American values for ^{239}Pu and ^{233}U are not shown in figure 6, but the agreement between 400 and 1200 kev is about the same as for ^{235}U. Below 400 kev, for ^{233}U, the Harwell figures are lower (by about 5%) than the American, while above 1200 kev the Pu figures are also lower by some 5–10%. A consequence of this latter feature in particular is that our ratios of ^{235}U : ^{239}Pu do not closely agree with those determined by Lamphere (1955, 1956) over the range 400–3000 kev. In view of the self-consistency checks in our work, both in sets of ratio determinations and by sets of absolute determinations at different energies, we find this a little surprising. The American work, which has been extended above 3 MeV, suggests that the falling off in cross section at that energy may not be as rapid as we observe. It is possible that at 3 MeV some systematic error in flux measurement has persisted. Our results on ^{238}U, which depend on a single comparison measurement, give a figure for the cross section appreciably below the American figure.

Fission cross section work has also been reported by groups of workers at Saclay (Szteinsznaider *et al.* 1955, Netter *et al.* 1956), but these do not include absolute measurements. Within the experimental inaccuracies, the agreement is fair.

Summing up the intercomparison of data, we can say that the agreement for all thermally fissile elements between 400 and 1200 kev is good. Below 400 kev, where our flux measurements depend on a recoil counter rather than a long counter, we consider our results are to be preferred. In the region 2000–3000 kev, our recoil counter is working in the limits of its range, and inaccuracies may be greater.

Table 2. The Consistent Set of values of Fission Cross Sections and Ratios

En	Pu	^{233}U	^{235}U	^{233}U/^{235}U	^{235}U/Pu	^{233}U/Pu
30	2·25 ± 0·06	4·0 ± 0·12	2·72 ± 0·08		1·27	1·80
50				1·32	1·195	1·47
60	1·98 ± 0·04	3·18 ± 0·10	2·32 ± 0·05		1·165	
70				1·32		1·49
75					1·13	
80	1·84 ± 0·06	2·91 ± 0·09			1·12	1·45
90					1·08	1·42
120	1·59 ± 0·03	2·28 ± 0·05	1·65 ± 0·03	1·40	1·05	1·42
150	1·73 ± 0·06	2·35 ± 0·07	1·68 ± 0·05			
175	1·55 ± 0·02	2·19 ± 0·02	1·51 ± 0·02	1·45	0·98	1·40
200	1·56	2·30 ± 0·07	1·47 ± 0·05		0·94	
220	1·64 ± 0·03	2·26 ± 0·03	1·48 ± 0·03	1·51	0·90	1·39
240	1·54	2·17	1·42 ± 0·03	1·53		1·41
275	1·65 ± 0·02	2·26 ± 0·02	1·38 ± 0·02	1·62	0·82	1·38
300	1·67 ± 0·03	2·30 ± 0·07	1·38 ± 0·04		0·84	
330	1·65	2·27	1·37 ± 0·03	1·66		1·38
350	1·80	2·32 ± 0·02	1·44	1·61		1·29
400		2·22 ± 0·04	1·34	1·65		
415			1·29 ± 0·02			1·34
445	1·68 ± 0·02	2·15 ± 0·02	1·32 ± 0·02	1·60	0·78	1·27
480		2·03	1·25 ± 0·02	1·625		1·25
500	1·68 ± 0·03	2·06 ± 0·03	1·26 ± 0·02	1·62		1·23
550	1·68 ± 0·02	2·00 ± 0·02	1·27 ± 0·02	1·61	0·723	1·19
650	1·68 ± 0·02	1·95 ± 0·02	1·19 ± 0·02	1·62	0·70	1·16
1000	1·80 ± 0·02	1·90 ± 0·02	1·22 ± 0·02	1·56	0·66	1·06
1500	1·93 ± 0·02	1·91 ± 0·02	1·33 ± 0·02	1·41	0·70	1·0
1800		1·91 ± 0·04				
2000	1·83 ± 0·04	1·90 ± 0·04	1·37 ± 0·03	1·365	0·74	1·05
2500	1·83 ± 0·05	1·82 ± 0·05	1·39 ± 0·03	1·29	0·76	1·0
3000	1·67 ± 0·06	1·65 ± 0·05	1·18 ± 0 04	1·37	0·70	1·0

6.3. *Comparison with Theory*

No quantitative theory of fission cross sections yet exists. However, the qualitative picture of A. Bohr (1955) and Hill and Wheeler (1953), has certain features which do not appear in our measurements. The theory predicts relatively rapid increases in the fission width whenever, with increasing energy, a new level in the saddle point system becomes available as a fission channel. In the same way there will be discrete changes in the neutron width as levels in the residual nucleus become available. Competition between the two processes gives rise to a series of relatively small upward or downward steps in the fission cross section. We find evidence for these, between 300 and 500 kev in ^{233}U and in ^{239}Pu between 600 kev and 1200 kev.

ACKNOWLEDGMENTS

The authors wish to thank Dr. D. J. Ferret, Mrs. K. M. Glover, Mr. G. R. Hall, Mr. F. Hudswell, and Dr. J. Milsted, of the Chemistry Division of A.E.R.E., for their cooperation in the preparation and assay of the foils of fissile material. They are indebted to Dr. D. A. Silverston who took part in many of the measurements, was responsible for the majority of the α-assay, and analysed the absolute results. The assistance of Dr. R. E. Meads is also acknowledged. They would like to thank Mr. K. W. Morton and members of the Computing Group for their work in computing best values. The development of head amplifiers free from spurious pulses was carried out by Mr. A. N. Thompson.

REFERENCES

ALLEN, W. D., and FERGUSON, A. T. G., 1955, *J. Nucl. Energ.*, **2,** 38.
BNL 325 (1955) *USAEC Compilation of Neutron Cross Sections.*
BOHR, A., 1955, *Geneva Conference on the Peaceful Uses of Atomic Energy*, Paper 8/P/911.
DIVEN, B. C., 1933, *U.S.A.E.C. Document LA-1336.*
GLOVER, K. M., and BORRELL, P., 1954, *A.E.R.E. Report C/R. 1359.*
HILL, D. L., and WHEELER, J. A., 1953, *Phys. Rev.*, **89,** 1102.
KOVARIK, A. F., and ADAMS, N. I., 1955, *Phys. Rev.*, **98,** 46.
LAMPHERE, R. W. 1956, *Phys. Rev.* **104,** 1654.
LAMPHERE, R. W., and GREENE, R. E., 1955, *Phys. Rev.*, **100,** 763.
MORTON, K. W., EGELSTAFF, P. A., and SANDERS, J. E., 1955, *A.E.R.E. Document N.R.D.C. 84.*
NETTER, F., JULIEN, J., CORGE, C., and BALLINI, R., 1956, *J. Phys. Radium*, **17,** 565.
SZTEINSZRAIDER, D., NAGGIAR, V., and NETTER, F., *Geneva Conference on the Peaceful Uses of Atomic Energy*, Paper P/355.

An Investigation of the Reaction $^{31}P(d, p)^{32}P$ by Magnetic Analysis

By A. W. DALTON, S. HINDS AND G. PARRY
Nuclear Physics Research Laboratory, University of Liverpool

Communicated by H. W. B. Skinner;
MS. received 25*th April* 1957, *and in final form* 14*th May* 1957

Abstract. The energy spectra of the protons emitted from a phosphorus target when bombarded by 8·9 MeV deuterons have been measured by magnetic analysis and a number of levels not previously reported have been observed. The angular distributions of 17 proton groups have been measured, and in most cases these have been fitted with theoretical stripping curves enabling parity and possible spin assignments to be made to some states of ^{32}P. Seven of these angular distributions show a dip below the Butler stripping curve at small angles, but otherwise correspond to $l=1$ transitions.

§ 1. INTRODUCTION

THE energy levels of ^{32}P have been accurately determined up to an excitation of 4·207 MeV by Van Patter, Endt, Sperduto and Buechner (1952) from an investigation of the proton energy spectrum from the $^{31}P(d, p)$ reaction. The angular distribution of the proton group leading to the ground state doublet of ^{32}P has been measured by Parkinson, Beach and King (1952), Black (1953) and also by Teplov (1956). Teplov also measured the angular distributions of the groups leading to the three lowest excited states of ^{32}P. The transition to the ground state doublet is of particular interest since it is a sensitive test for the shell model, as proposed by Bethe and Butler (1952).

Proton groups from the $^{31}P(d, p)$ reaction leading to several new excited states of ^{32}P have been observed. Angular distributions have been measured for many of the proton groups from this reaction, and attempts have been made to fit these with stripping curves, so enabling parities and possible spins to be assigned to many states of ^{32}P.

§ 2. EXPERIMENTAL TECHNIQUE

For these measurements the 9 MeV deuteron beam from the Liverpool 37 in. cyclotron was used to bombard a thin phosphorus target. This was prepared by evaporating red phosphorus, in vacuum, on to a 0·2 mg cm^{-2} gold backing held by the target frame. The reaction products emitted were analysed by the magnetic spectrograph described by Green and Middleton (1956 a), with a modified target chamber and improved monitoring of the exposures.

§ 3. TARGET CHAMBER

The target chamber was designed so that angles of observation between 5° and 135° could be obtained without any intermediate windows. Observations at large angles are important where the mechanism of the reaction process is uncertain, e.g. some (d, α) reactions.

The chamber, shown in figure 1, was of cylindrical shape, 6 in. in diameter and 4 in. deep, with a removable Perspex lid. The target frame was fixed to this lid so that the axis of the cylinder was in the plane of the target. The tube through which the reaction products reached the spectrograph magnet was fixed to a thin stainless steel strip, which could be moved over a slot cut out of the periphery of the cylinder while still maintaining a vacuum. This was effected by means of a rubber gasket between the steel strip and the cylinder. One end of a rigid arm supported the tube leading to the spectrograph, the other end being fixed to a large bearing which was coaxial with the chamber. This ensured that the spectrograph could see the target at all angles of observation.

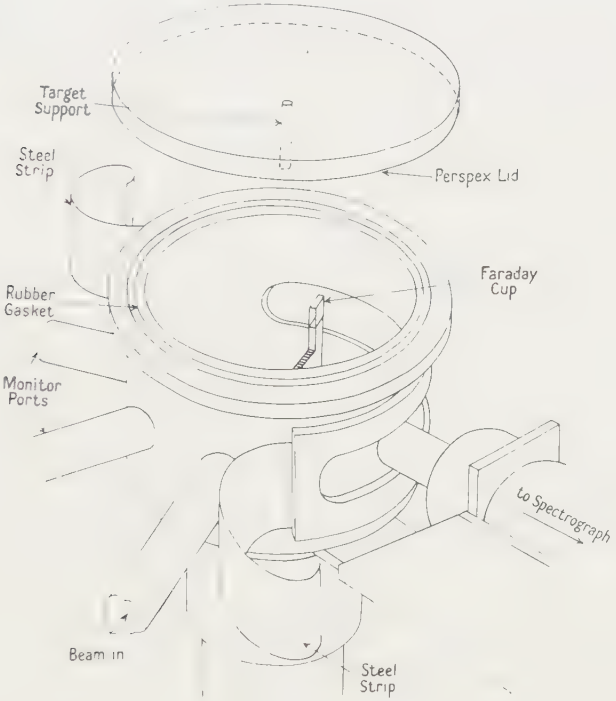

Figure 1. Diagram of the target chamber.

The exposures were monitored by catching the deuteron beam which had passed through the target in a Faraday cup, and integrating this current. The monitoring was checked by a photographic plate and scintillation counter which were fixed to look at the target through ports at angles of 135° and 90° respectively. The counter was useful in checking the stability of the target during the course of an exposure.

§ 4. Results

A typical proton energy spectrum obtained at an angle of observation of 15° is shown in figure 2. The groups labelled O_0 and O_1 are due to an oxygen impurity in the target, and correspond to transitions to the ground state and first excited state of ^{17}O. Similarly groups C_0, C_1 and C_2 arise from a carbon impurity. The strong group of protons, with an energy about 7·4 MeV, are the recoil protons from the elastic scattering of the incident deuterons by hydrogen in the target.

All these groups due to impurities were identified by their large energy shift with angle and also from their well-known angular distributions. The deuteron beam energy was calculated to be 8·9 Mev from the Q-value reported by Sperduto, Buechner, Bockelman and Browne (1954) for the group leading to the ground state of ^{17}O. This value gave excellent agreement between the measured and calculated energies for the proton groups leading to ^{32}P, from the Q-values reported by Van Patter *et al.* Good agreement was also obtained between the measured and calculated energies of the other groups due to target impurities. The proton groups from the reactions with phosphorus are indicated by the symbol ^{32}P of the final nucleus, and by the excitation energy in Mev of the final state. The yields of protons arising from states in ^{32}P reported by Van Patter *et al.*, at 1·316, 1·750, 2·650, 2·742, 2·999 and 3·141 Mev were found to be extremely weak. Angular distributions were measured for all the other proton groups previously reported and also for some groups leading to new states of ^{32}P which are listed in the table. The level at 3·45 Mev was not observed by Van Patter *et al.*, but they do not rule out the possibility of a level in this region. Also there is a γ-ray from the $^{31}P(n, \gamma)$ reaction reported by Kinsey, Bartholomew and Walker (1952) which cannot be fitted into the level scheme of Van Patter *et al.*, and which might indicate a level at 3·45 Mev. Levels were also observed at 4·66, 5·75, 6·20, 6·69 and 6·85 Mev (all $\pm 0{\cdot}1$ Mev), but the transitions to these were weak. The angular distributions are shown in figure 3, where the curves have been calculated from the deuteron stripping theory of Butler (1951). The radius of interaction chosen for all the curves was $(1{\cdot}7 + 1{\cdot}22A^{1/3})10^{-13}$ cm. Shown in the table are the most probable assignments for the number of units of angular momentum l taken into the nucleus by the absorbed neutron together with the parities and possible spins of the final states, J_f.

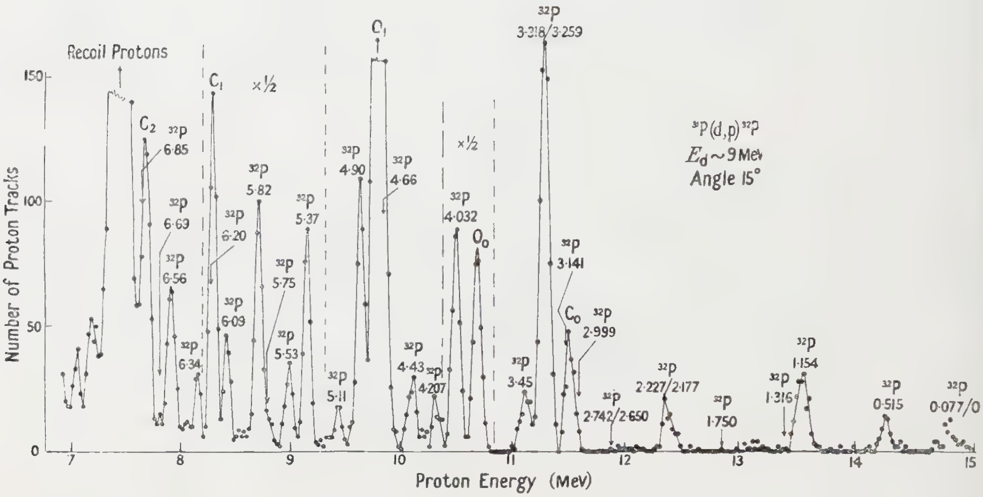

Figure 2. Proton energy spectrum at an angle of 15° resulting from the deuteron bombardment of a thin target of phosphorus.

A feature of the distributions is the number which have experimental points below the Butler curve at small angles, but otherwise agree with the curves for an $l=1$ transition. These distributions cannot be fitted with a mixture of l-values, and will be discussed later. The combined distribution of the groups leaving ^{32}P in excited states at 2·177 and 2·227 Mev shows a strong $l=0$ component, but there is probably some contribution from an $l=1$ transition. It is difficult to estimate the amount of the latter due to the uncertainty of the shape of these distributions at small angles as mentioned above. The distribution for the transition to the 5·11 Mev state is difficult to interpret, but at some angles there are indications from the spectra that the state is a doublet.

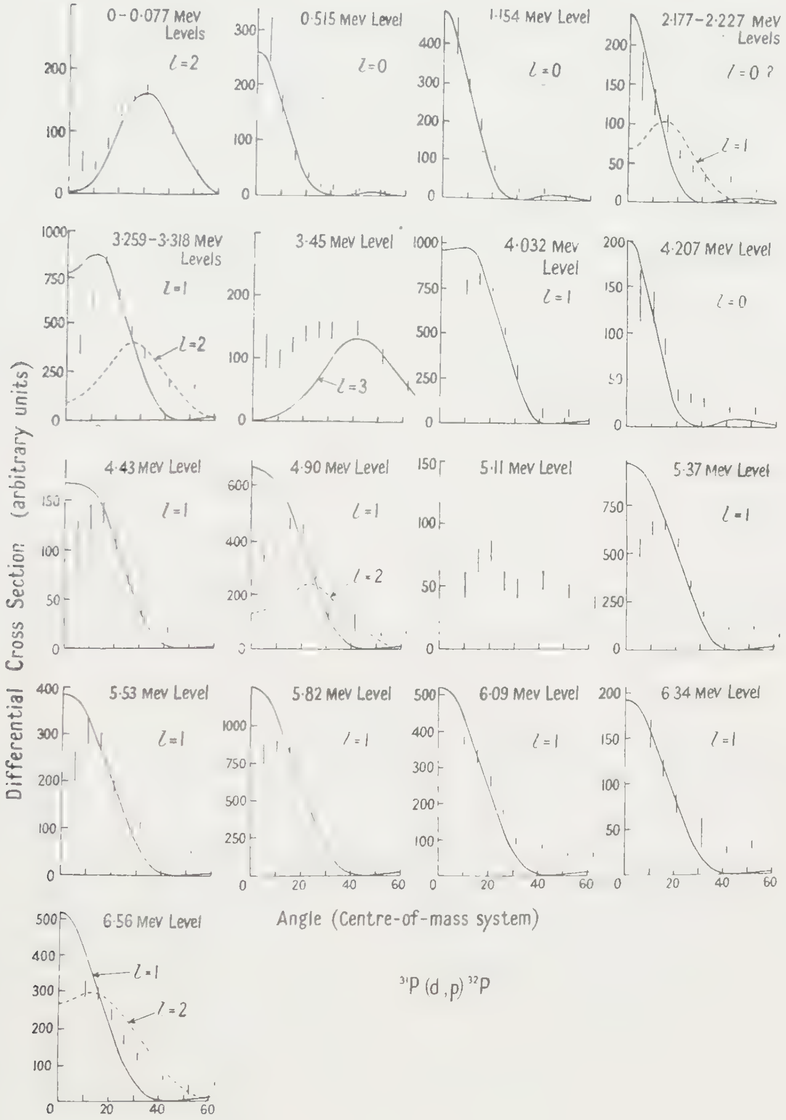

Figure 3. Angular distibutions of the proton groups. The cross sections for all distributions are in the same arbitrary units.

The values of the relative reduced widths, γ^2, for the transitions, combined with a factor $(2J_{\rm f}+1)$, are listed in the table. These ratios are only approximate since they have been obtained by directly fitting the stripping curve to the experimental points.

Energy levels		l		$\gamma^2(2J_{\rm f}+1)$
a	b		c	(relative units)
0		2	1^+ 2^+	7·2
0·077				
0·515		0	$0, 1^+$	0·7
1·154		0	$0, 1^+$	1·2
2·177		0 or 1	$0, 1^+$	0·6
2·227				
3·259		1†	$0, 1, 2^-$	8
3·318				
	3·45 ± 0·1	?		
4·032		1†	$0, 1, 2^-$	9
4·207		0	$0, 1^+$	0·8
	4·43 ± 0·1	1†	$0, 1, 2^-$	1
	4·90 ± 0·07	1†	$0, 1, 2^-$	5
	5·11 ± 0·1	?		
	5·37 ± 0·07	1†	$0, 1, 2^-$	7
	5·53 ± 0·07	1†	$0, 1, 2^-$	2
	5·82 ± 0·07	1†	$0, 1, 2^-$	8
	6·09 ± 0·07	1	$0, 1, 2^-$	3
	6·34 ± 0·1	1	$0, 1, 2^-$	1
	6·56 ± 0·07	1 or 2		

a, Van Patter, Endt, Sperduto and Buechner (1952). b, Present investigation. c, Parities and possible spins, $J_{\rm f}$, of the final states. † These distributions show a dip below the Butler stripping curve at small angles.

§ 5. Discussion

Angular distributions of products from stripping reactions which at small angles fall below the theoretical curve, but otherwise correspond to $l=1$ transitions, have been reported previously, e.g. Evans, Green and Middleton (1953), Holt and Marsham (1953) and Green and Middleton (1956 b). This effect is particularly noticeable for a bombarding energy of 8–9 Mev and Q-values between 0 and 2 Mev for (d, p) reactions and for negative Q-values for (d, n) reactions. In such cases the stripping contribution at small angles is relatively high and does not change much with angle over a small range in the forward direction, so that experimental deviations from the theoretical curve are easier to observe. In some cases a dip is not observed, though in the (d, p) work this could be due to experimental difficulties in obtaining good statistical accuracy on the observations at angles less than 15°. In particular for large negative Q-values the $l=1$ curve has a very sharp peak at 0°, so that even quite a large departure is difficult to observe since even though the experimental points may lie below the Butler curve, the deviation will not appear as a dip but only as a small change in slope.

Tobocman and Kalos (1955) have shown how allowance for Coulomb and nuclear effects can account for such deviations between Butler theory and experimental results. They also show that for large positive Q-values the experimental points may lie above the Butler curve at forward angles. This effect has been observed experimentally, but the contribution from a compound nucleus reaction could produce the same effect.

The angular distribution for the transition to the ground state doublet of ^{32}P is in agreement with the measurements of Parkinson *et al.* (1952), Black (1953) and Teplov (1956). Since the contribution of an $l=0$ transition is obviously very small, the departure from the shell model is small for this state.

In spite of this good agreement between the shell model and the configuration of the ground state, the low lying excited states do not appear to have simple shell model configurations. Huby and Newns (1955) have discussed the configuration of the ground state of ^{31}P and have shown that it cannot be pure $(s_{1/2})_0^2(s_{1/2})_{1/2}^1$ and must contain at least a component $(d_{3/2})_0^2(s_{1/2})_{1/2}^1$. The first bracket refers to the neutron shell and the second to the proton shell, and the suffixes give the resultant spin of the particles in each shell. Two $l=0$ transitions to ^{32}P are to be expected from the $(d_{3/2})_0^2(s_{1/2})_{1/2}^1$ component in ^{31}P and none from the other component. However, four $l=0$ transitions are observed leading to levels in ^{32}P below an excitation of 4·207 Mev. It is possible that the other two transitions may be explained by the ground state configuration of ^{31}P being so impure as to contain complex components such as $[(d_{3/2})^2(d_{3/2})^1]_{1/2}$ where the two neutrons and the proton are coupled together with a resultant spin of $\frac{1}{2}$. These may arise since ^{28}Si is not a good closed shell nucleus (Pryce 1954).

Regarding the $l=1$ transitions, one expects to find a state of ^{32}P with the configuration $(p_{3/2})^1(s_{1/2})^1$. Inglis (1953) has shown that this state is expected to be a doublet and so may possibly be identified with the levels at 3·259 and 3·318 Mev. However, there are a number of other $l=1$ transitions with comparable reduced widths and this again implies that the ground state configuration of ^{31}P must be very impure.

The position of the state in ^{32}P whose neutron configuration is predominantly $1f_{7/2}$ is most uncertain. Teplov (1956) has assigned this configuration to the 1·316 Mev state on the basis of the combined angular distribution of the protons from the ^{31}P(d, p) reaction leading to this state and to the 1·154 Mev state. We resolved the groups corresponding to these levels and found the intensity of the group leading to the 1·136 Mev level to be so weak that angular distribution measurements were not possible. It therefore seems unlikely that this transition proceeds by a stripping mechanism to a single-particle level. It is possible that the level at 3·45 Mev has the configuration $(f_{7/2})^1(s_{1/2})^1$ since the observed distribution could perhaps be due to an $l=3$ transition which has been badly distorted by Coulomb and nuclear effects. The observed yield of protons leading to the 3·45 Mev level is of the correct order of magnitude expected for a single-particle $l=3$ transition.

The reduced widths for most of the transitions are comparable and this prevents the usual procedure of assigning single-particle configurations to those transitions with large reduced widths. The lack of good single-particle levels may be explained by the configuration of the ground state of ^{31}P being extremely impure.

ACKNOWLEDGMENTS

The authors would like to express their gratitude to Professor H. W. B. Skinner for his encouragement and advice. We are grateful to Dr. H. C. Newns for helpful discussion on the interpretation of the results and to Dr. R. Middleton for his assistance in the design of the target chamber. We are also indebted to Miss H. B. Burrows, Miss P. M. P. Robinson and Mr. E. C. Hewitt for assistance in measuring the plates. Two of us (A. W. D. and S. H.) are grateful to the Department of Scientific and Industrial Research for maintenance grants.

REFERENCES

BETHE, H. A., and BUTLER, S. T., 1952, *Phys. Rev.*, **85,** 1045.
BLACK, C. F., 1953, *Phys. Rev.*, **90,** 381 (A).
BUTLER, S. T., 1951, *Proc. Roy. Soc.* A, **208,** 559.
EVANS, W. H., GREEN, T. S., and MIDDLETON, R., 1953, *Proc. Phys. Soc.* A, **66,** 108.
GREEN, T. S., and MIDDLETON, R., 1956 a, *Proc. Phys. Soc.* A, **69,** 16; 1956 b, *Ibid.*, **69,** 28.
HOLT, J. R., and MARSHAM, T. N., 1953, *Proc. Phys. Soc.* A, **66,** 565.
HUBY, R., and NEWNS, H. C., 1955, *Proc. Phys. Soc.* A, **68,** 758.
INGLIS, D. R., 1953, *Rev. Mod. Phys.*, **25,** 390.
KINSEY, B. B., BARTHOLOMEW, G. A., and WALKER, W. H., 1952, *Phys. Rev.*, **85,** 1012.
PARKINSON, W. C., BEACH, E. H., and KING, J. S., 1952, *Phys. Rev.*, **87,** 387 (L).
PRYCE, M. H. L., 1954, *Rep. Progr. Phys.*, **17,** 1. (London : Physical Society).
SPERDUTO, A., BUECHNER, W. W., BOCKELMAN, C. K., and BROWNE, C. P., 1954, *Phys. Rev.*, **96,** 1316.
TEPLOV, I. B., 1956, *Zh. eksper. teor. Fiz.*, **31,** No. 1(7), 25.
TOBOCMAN, W., and KALOS, M. H., 1955, *Phys. Rev.*, **97,** 132.
VAN PATTER, D. M., ENDT, P. M., SPERDUTO, A., and BUECHNER, W. W., 1952, *Phys. Rev.*, **86,** 502.

Electronic Absorption Spectra of Heterocyclic Systems I: A Comparison of Theoretical Methods: Pyridine and Pyrazine

By R. McWEENY†
Physical Chemistry Laboratory, King's College, Newcastle-upon-Tyne

MS. received 6th May 1957

Abstract. This work is concerned with the application of recent theoretical methods in elucidating the spectra of heterocyclic systems. It is now generally accepted that a satisfactory picture of the first few excited states can only be obtained by admitting limited configuration interaction. But this picture is also dependent upon the precise choice of *orbitals*—which, in a heterocyclic molecule, may range from Hückel molecular orbitals of the parent hydrocarbon to self-consistent orbitals of the substituted system and scarcely any information is available concerning the relative merits of different choices.

In the present paper (Part I) general methods are summarized, seven different choices of orbitals are suggested and discussed, and careful numerical comparisons are made in applications to pyridine and pyrazine. Useful conclusions emerge, in the light of which it is possible to consider more complicated systems. Such developments are taken up in a companion paper by Peacock (Part II).

§ 1. INTRODUCTION

In recent years the LCAO molecular orbital theory of the electronic structure and spectra of conjugated systems, more particularly of aromatic hydrocarbons, has made two major advances. The Hückel theory, in which the forms and energies of the molecular orbitals are calculated using a crude model of the π-electron system, and in which transition energies are equated to differences or orbital energies, has been replaced by a fairly complete self-consistent field theory, in which *best* orbitals (of LCAO form) are calculated and used in obtaining *total* energies of the various spectroscopic states. Secondly, the representation of these states by functions belonging to single electronic configurations has been abandoned, mixing of functions from different configurations now being admitted: this mixing is vital when the one-configuration approximations are degenerate (or near-degenerate) and gives the key to an understanding of the spectra of many hydrocarbons (Dewar and Longuet-Higgins 1954, Pople 1955) and their heteroderivatives (McWeeny and Peacock 1957). To summarize: these advances arise from the use of *best orbitals* (of LCAO self-consistent field form) and of limited *configuration interaction*, within a theoretical framework which is rather complete and contains relatively few empirical features.

It is of course true that configuration interaction provides an *alternative* to the use of best orbitals and that, if complete, configuration interaction were admitted the self-consistent field calculation would be quite superfluous. This is not necessarily the case when only a *selection* of configurations is employed: nevertheless, rather inferior molecular orbitals are often adopted on the grounds that even limited configuration interaction can compensate for their shortcomings. Careful comparisons of the accuracy of different approximations have been made in only one or two cases (e.g. Coulson, Craig and Jacobs 1951). In this paper such comparisons will be made in order to determine whether the self-consistent treatment can be dispensed with (at least in favourable cases) or whether it is essential, when configuration interaction is limited to the first few degenerate, or near degenerate, functions. This is a rather general question: it will be set in a specific and useful context by confining attention to the spectral shifts accompanying heterocyclic substitution in alternant hydrocarbons. Since very satisfactory results have already been obtained, using self-consistent field orbitals, for the nitrogen heterobenzenes (McWeeny and Peacock 1957), one important aim of the present work will be to reproduce such results as closely as possible, using a similar choice of configurations but orbitals which, at least for the ground state, are inferior to the self-consistent field molecular orbitals. The more general aim is to compare the merits of different methods of approximation with a view to selecting the simplest adequate theory of the spectra of heterocyclic molecules. In this paper attention will be confined to pyridine and pyrazine†: in a companion paper (Peacock 1957) the same methods will be applied in discussing the spectra of more elaborate systems.

---

† Now at the Departments of Mathematics, Physics and Chemistry, University College of North Staffordshire, Keele, Staffs.

§ 2. METHOD OF CALCULATION

We shall use A, B, C, . . . to denote, in descending energy order, the molecular orbitals which are doubly occupied in any particular one-configuration approximation to the ground state of the parent hydrocarbon. These will generally be determined as solutions of some eigenvalue problem (involving, for example, a self-consistent field or a Hückel one-electron Hamiltonian) and the remaining solutions, the 'virtual' orbitals, will be denoted by A′, B′, C′, ... in *ascending* energy order. This notation is particularly significant for alternant molecules where P and P′ are bonding and anti-bonding 'partners'; and it is generally convenient because, for instance, the transition A→B′ has exactly the same interpretation for all systems. Usually, the order of the levels will not change in heterocyclic substitution: but in any case it is most convenient for purposes of correlation to adopt a notation provided by the parent molecule (cf. McWeeny and Peacock 1957). The ground state function will be denoted by Φ_0 and the singlet and triplet functions of the configuration in which an electron has been taken from P and put into Q′ by $^1\Phi(P\to Q')$ and $^3\Phi(P\to Q')$, respectively. We shall admit only single excitations of this kind and, usually, only those involving the orbitals A, B, A′, B′: in this case it is convenient to use an abbreviated notation

$^{1,3}\Phi(A\to A')={}^{1,3}\Phi_1$, $^{1,3}\Phi(A\to B')={}^{1,3}\Phi_2$, $^{1,3}\Phi(B\to A')={}^{1,3}\Phi_3$, $^{1,3}\Phi(B\to B')={}^{1,3}\Phi_4$.

Matrix elements of the full Hamiltonian between such functions are easily obtained by standard methods and have been given by, for example, Pople (1955) and Pariser (1956). The formulae given by Pariser appear in completely reduced form, in terms of one- and two-electron integrals, and are consequently rather cumbersome. It seems preferable, particularly in a semi-empirical treatment, to preserve a close parallel with self-consistent field theory by writing these formulae in terms of an 'effective' Hamiltonian—even when this is *not* a strictly self-consistent quantity. The theory will then bear a close resemblance to that of Pople (1955), as extended to heterocyclic systems by McWeeny and Peacock (1957). This formulation is summarized in Appendix 1.

---

† Both molecules are substituted benzenes. Pyridine results when one carbon atom is replaced by nitrogen; pyrazine when two, diametrically opposite, carbons are replaced by nitrogens.

Using k_{rs} to denote the electron-interaction term in the matrix element H_{rs} between one-configuration functions Φ_r and Φ_s, and ϵ_{A}, ϵ_{AB}, for the diagonal and off-diagonal orbital-energy terms, the usual secular equation, which determines the configurational mixing is

$$\left.\begin{vmatrix} -E & \sqrt{2}\epsilon_{\mathrm{AA'}} & \sqrt{2}\epsilon_{\mathrm{AB'}} & \sqrt{2}\epsilon_{\mathrm{BA'}} & \sqrt{2}\epsilon_{\mathrm{BB'}} \\ & H_{11}-E & \epsilon_{\mathrm{A'B'}}+k_{12} & -\epsilon_{\mathrm{BA}}+k_{13} & k_{14} \\ & & H_{22}-E & k_{23} & -\epsilon_{\mathrm{BA}}+k_{24} \\ & \text{etc.} & & H_{33}-E & \epsilon_{\mathrm{A'B'}}+k_{34} \\ & & & & H_{44}-E \end{vmatrix} = 0 \right\} \qquad \ldots\ldots(1)$$

where $H_{11}=(\epsilon_{\mathrm{A'}}-\epsilon_{\mathrm{A}})+k_{11}$, $H_{22}=(\epsilon_{\mathrm{B'}}-\epsilon_{\mathrm{A}})+k_{22}$, $H_{33}=(\epsilon_{\mathrm{A'}}-\epsilon_{\mathrm{B}})+k_{33}$, $H_{44}=(\epsilon_{\mathrm{B'}}-\epsilon_{\mathrm{B}})+k_{44}$, are the one-configuration energies, relative to H_{00} as energy zero.

For an alternant hydrocarbon Φ_2 and Φ_3 are degenerate, and the combinations $\Phi_\alpha=2^{-1/2}(\Phi_2-\Phi_3)$ and $\Phi_\beta=2^{-1/2}(\Phi_2+\Phi_3)$ have been identified (Dewar and Longuet-Higgins 1954) as representing the states associated with the α and β absorption bands of Clar. It appears that, although this degeneracy is usually resolved when substituents are introduced, the same identification is substantially correct in the case of heteroderivatives (McWeeny and Peacock 1957). This means that (1) is reduced to *near*-diagonal form by making corresponding operations on rows and columns. Often, other near-degeneracies arise, either by accident or on account of symmetry (e.g. in benzene, anthracene, stilbene, etc.), and it is expedient to make a similar transformation of (1) for each degenerate pair. In other words, although (1) forms a suitable starting point, it is useful to take into account the main ('first-order') part of the configuration interaction by using correct zero-order combinations and an appropriately modified form of (1). The 'residual' configuration interaction then turns out to be so small that, as we shall see, it can be dealt with using perturbation theory.

§ 3. CHOICE OF ORBITALS

Since only limited configuration interaction is admitted, the orbitals employed in §2 should represent a good compromise between the best orbitals for the different states involved. The usual self-consistent field method determines only best orbitals for the approximate ground state, and although these may be satisfactory in describing the excited states it is possible that other choices may give a comparable (or even better) general picture.

The following possibilities suggest themselves:

(*a*) MO's for a Hückel model of the parent hydrocarbon;
(*b*) MO's for a Hückel model of the heterocyclic system;
(*c*) MO's for a 'standard excited state' (cf. Hall 1952) of the parent hydrocarbon;
(*d*) MO's of a standard excited state of the heterocyclic system;
(*e*) self-consistent field MO's for the parent hydrocarbon;
(*f*) self-consistent field MO's for the heterocyclic system;

(*g*) linear combinations of the MO's of (*f*), giving the same one-configuration ground state but different excited state approximations.

At first sight, it appears likely that (*f*) and (*a*) will yield, respectively, the best and the worst results, although it has been argued (Hall 1952), that a choice such as (*d*) (to which (*g*) may well be added) might give the best overall picture of the spectrum. But before passing to the calculations it is worth saying a few words about each approach.

Approximation (*a*).

This undoubtedly provides the simplest possible treatment: for the Hückel orbitals are already known for a large number of systems; *all* heteroderivatives can be discussed in terms of the one set of orbitals for the parent; and the special properties of alternant hydrocarbon systems can be fully exploited. The reductions due to alternant character are noted in Appendix 2, and apply also for approximations (*c*) and (*e*) which require no separate discussion.

Approximation (*b*).

It has been shown elsewhere that the self-consistent field solution for a heterocyclic system may most fruitfully be compared with a 'corresponding' Hückel approximation in which the Coulomb integral of a substituted atom *r* is changed by an amount (using the notation of Appendix 1)

$$\delta_r = \delta\omega_r + (R_{rr}\gamma_r - \tfrac{1}{2}\gamma_{\mathrm{C}}) \qquad \ldots\ldots(2)$$

($\mathbf{R} = \mathbf{T}\mathbf{T}^{\dagger}$ being the bonding matrix for singly occupied orbitals represented by the columns of $\mathbf{T}$). An improved approximation might therefore be achieved on replacing the hydrocarbon molecular orbitals by those of the corresponding Hückel model of the substituted system. These molecular orbitals are easily calculated but they no longer possess alternant properties and the reductions of Appendix 2 do not apply.

Approximation (*d*).

The standard excited state (Hall 1952) is that state in which the lower orbitals (bonding and anti-bonding) are each *singly* occupied by electrons with parallel spins. The LCAO self-consistent approximation to this state may then be obtained using an effective Hamiltonian (cf. McWeeny 1957)

$$\left.\begin{aligned} \mathbf{h}^{\mathrm{Ex}} &= \mathbf{f} + \mathbf{G}^{\mathrm{Ex}} \\ \text{where} \qquad G^{\mathrm{Ex}}{}_{ab} &= \sum_{r,s} R_{rs}[(as|g|br) - (as|g|rb)] \end{aligned}\right\} \cdot \qquad \ldots\ldots(3)$$

The exact standard excited state orbitals can be obtained by suitably extending the atomic orbital basis *a*, *b*, *c*, ... But at the present level of approximation, where the number of atomic orbitals is equal to the number of electrons, $\mathbf{T}$ is square and unitary and $\mathbf{R} = \mathbf{T}\mathbf{T}^{\dagger} = \mathbf{1}$. The Hamiltonian is then invariant against unitary mixing of the orbitals and either the atomic orbitals themselves or the full set of bonding and anti-bonding molecular orbitals may be used in the one-determinant wave function. With the approximations of the present work the standard excited state self-consistent field Hamiltonian is found to be (cf. (A1.4)).

$$h^{\mathrm{Ex}}{}_{aa} = \delta\omega_a + \sum_{r \neq a}(1 - Z_r)\gamma_{ar},\dagger \qquad h^{\mathrm{Ex}}{}_{ab} = \beta_{ab}. \qquad \ldots\ldots(4)$$

It is at once clear that the standard excited state orbitals are eigenvectors of a Hamiltonian whose character is very different from that of the ground state self-consistent field Hamiltonian. In this case the Hamiltonian involves only

---

† The orbital-energy zero is here simply ω_{C}.

framework quantities: near atom a an electron experiences simply the unscreened attraction represented by ω_a whereas in the ground state it experiences also repulsion from half the mobile charge upon the atom (namely the half associated with opposite spin); and this effect is exaggerated because the off-diagonals elements (which provide a natural energy unit—cf. Hückel theory) have values only about half as great as in the ground state—a fact obviously related to the absence of any net bond population in the excited state.

The standard-state orbitals are obtained by solution of $\mathbf{h}^{\mathrm{Ex}}\mathbf{T}^{\mathrm{Ex}}=\mathbf{T}^{\mathrm{Ex}}\boldsymbol{\epsilon}$, $\mathbf{T}^{\mathrm{Ex}}$ being an $m \times m$ unitary matrix and $\boldsymbol{\epsilon}$ an $m \times m$ diagonal matrix. The first $\frac{1}{2}m$ columns of $\mathbf{T}^{\mathrm{Ex}}$ are then taken over as a basis for the ground state calculation, in which each represents a *doubly* occupied orbital.

Approximations (f) *and* (g).

Calculations using self-consistent field molecular orbitals for the heterocyclic have been reported elsewhere (McWeeny and Peacock 1957) and require no further discussion.

The main objection to the use of self-consistent field molecular orbitals in predicting spectra might be that they over-emphasize the importance of the ground state: they are determined by the ground state charge distribution and the virtual orbitals, which are invoked in predicting excited states, occur merely as a by-product of the ground state calculation. The standard excited state method goes to the other extreme by utilizing the molecular orbitals of a highly excited state in which the charge distribution and effective Hamiltonian are completely unrepresentative of those in the ground and lower excited states. The best orbitals on the other hand, might resemble more closely the eigenvectors of a suitable 'compromise' Hamiltonian which does not over-emphasize the peculiarities of any particular state: and if these orbitals are constrained to be linear combinations of the occupied self-consistent field molecular orbitals of the ground state it will be possible in general to improve the excited states without sacrificing any accuracy in the ground state (which is invariant under such unitary mixing). Before attempting to develop any precise method of defining a 'best compromise' Hamiltonian, it seems worth examining whether the results are at all sensitive to limited mixing of the self-consistent field molecular orbitals. The mixtures which 'lie closest' to any given set of approximate orbitals may be obtained by a method developed elsewhere (McWeeny 1957). In the present investigation the self-consistent field mixtures which lie closest to the molecular orbitals of the Hückel model (b) have been constructed and utilized in the configuration interaction calculation.

§ 4. Examples: Pyridine and Pyrazine

In this section we shall apply the approximations introduced in § 3 to the molecules pyridine and pyrazine.

For the parent hydrocarbon we shall use the same choice of molecular orbitals and the same integral values as in previous work (McWeeny and Peacock 1957). Owing to the additional degeneracy we replace rows and columns 1 and 4 by p and β', where $\Phi_p=2^{-1/2}(\Phi_1+\Phi_4)$ and $\Phi_{\beta'}=2^{-1/2}(\Phi_1-\Phi_4)$, besides making the transformation 2, $3 \rightarrow \alpha$, β. $H_{pp}{}^0=\frac{1}{2}(H_{11}+H_{44}+2H_{14})$ etc. then give the energies of the p, α, β, β' states of the hydrocarbon, since the new determinant is exactly diagonal. These energies appear in table 1, and do not differ substantially from those obtained by Pople (1955) who used somewhat different integral values.

Table 1. Absolute Comparison of Energies (ev)

State	0	α	p	β	β'
Benzene	(0·0)	4·897	5·663	6·980	6·980
Pyridine (*a*)	−1·867	3·139	4·022	5·324	5·398
(*f*)	−1·883	3·127	3·945	5·273	5·274
Pyrazine (*a*)	−3·666	1·297	2·289	3·754	3·839
(*f*)	−3·748	1·151	2·182	3·311	3·613

In considering the substituted molecules we shall discuss in detail only the case of pyridine, using approximation (*a*), and again adopt the integral values given by McWeeny and Peacock (1957). All the other calculations follow the same pattern and require no further comment. The determinant (1) then factorizes, on account of symmetry, to give

$$\begin{vmatrix} -E & \sqrt{2}\,\epsilon_{\mathrm{AA'}} & 0 \\ \sqrt{2}\,\epsilon_{\mathrm{AA'}} & H_{11}-E & k_{14} \\ 0 & k_{14} & H_{44}-E \end{vmatrix}=0 \qquad \begin{vmatrix} H_{22}-E & k_{23} \\ k_{23} & H_{33}-E \end{vmatrix}=0. \quad \ldots\ldots(5)$$

Taking the same linear combinations of rows and columns as for the hydrocarbon, these determinants reduce to *near*-diagonal form:

$$\begin{vmatrix} -E & \delta\epsilon_{\mathrm{AA'}} & \delta\epsilon_{\mathrm{AA'}} \\ \delta\epsilon_{\mathrm{AA'}} & H_{pp}-E & H_{p\beta'} \\ \delta\epsilon_{\mathrm{AA'}} & H_{p\beta'} & H_{\beta'\beta'}-E \end{vmatrix}=0 \qquad \begin{vmatrix} H_{\alpha\alpha}-E & H_{\alpha\beta} \\ H_{\alpha\beta} & H_{\beta\beta}-E \end{vmatrix}=0. \quad \ldots\ldots(6)$$

where

$$\begin{aligned} H_{pp}&=H_{pp}{}^{0}-\delta\epsilon_{\mathrm{A}}{}^{(2)}+\tfrac{1}{2}\delta k_{11} & H_{\alpha\alpha}&=H_{\alpha\alpha}{}^{0}-\delta\epsilon_{\mathrm{A}}{}^{(2)} \\ H_{p\beta'}&=-\delta\epsilon_{\mathrm{A}}{}^{(2)}+\tfrac{1}{2}\delta k_{11} & H_{\alpha\beta}&=-\delta\epsilon_{\mathrm{A}}{}^{(1)} \\ H_{\beta'\beta'}&=H_{\beta'\beta'}{}^{0}-\delta\epsilon_{\mathrm{A}}{}^{(2)}+\tfrac{1}{2}\delta k_{11} & H_{\beta\beta}&=H_{\beta\beta}{}^{0}-\delta\epsilon_{\mathrm{A}}{}^{(2)} \end{aligned} \quad \ldots\ldots(7)$$

quantities with superscript 0 referring to the hydrocarbon and the small quantities $\delta\epsilon_{\mathrm{AA'}}$, $\delta\epsilon_{\mathrm{A}}{}^{(1)}$, $\delta\epsilon_{\mathrm{A}}{}^{(2)}$, δk_{11}, being defined in Appendix 2.

The advantage of introducing the α, β, p and β' combinations of the parent molecule—an advantage which persists in less trivial cases—is now evident. First order configuration interaction has in fact been admitted in going from (5) to (6) and off-diagonal elements have been so reduced in magnitude that their effects can adequately be described by perturbation theory. Writing down the energy expressions up to second order, the precise dependence of every energy level upon the various parameters (through $\delta\epsilon_{\mathrm{A}}{}^{(1)}$ etc.) becomes obvious. And in this way a qualitative discussion of the main effects of substitution in any alternant hydrocarbon becomes feasible.

From (A2.6) the one-configuration ground state is found to lie 1·833 ev below that of the hydrocarbon. The energy levels, referred to a common energy zero (the hydrocarbon ground state), follow immediately and appear in table 1.†

---

† The figures in the table were actually obtained by exact solution of (6): but the perturbation theory values differ by only one unit in the third decimal place. Actually, six figures were carried throughout the calculations in order that the *comparisons* should not be affected by spurious rounding-off errors. The *absolute* energy values are of course relatively inaccurate.

§ 5. RESULTS

Designating the ground state by 0 and the excited states by α, p, β and β' (i.e., by the names of the bands to which the related transitions correspond), the energies of the first few states of benzene, pyridine and pyrazine, predicted according to methods (*a*) and (*f*), are compared on the same absolute scale in table 1. The energy zero corresponds to the one-configuration energy of the parent hydrocarbon, benzene: and the two methods represent extremes of simplicity and elaboration.

Table 2. Comparison of Transition Energies (ev)

Band	α	p	β	β'
Benzene	4·897	5·663	6·980	6·980
Pyridine (*a*)	5·006(+0·109)	5·889(+0·226)	7·191(+0·211)	7·265(+0·285)
(*f*)	5·010(+0·113)	5·828(+0·165)	7·146(+0·166)	7·157(+0·177)
Pyrazine (*a*)	4·963(+0·066)	5·956(+0·293)	7·420(+0·440)	7·505(+0·525)
(*f*)†	4·898(+0·001)	5·929(+0·266)	7·059(+0·079)	7·361(+0·381)

The figures in brackets represent the actual shifts of the various bands relative to those of benzene.

† These results differ slightly from those reported by McWeeny and Peacock (1957), in which a small error, due to the use of an incorrect integral value, was subsequently detected : revision does not sensibly affect the conclusions of that paper.

The predicted transition energies for the three molecules are compared in table 2, along with the shifts (shown in brackets) resulting from the nitrogen substitution.

Finally, a detailed comparison of all approximation methods (*a*)-(*g*) has been made in the case of the one molecule, pyridine. The results, again on the same absolute scale, are given in table 3.

Table 3. Absolute Comparison of All Methods: Pyridine

State	Approximate Energies (ev)									
	(*a*)		(*b*)		(*d*)		(*f*)		(*g*)	
	(i)	(ii)	(i)	(ii)	(i)	(ii)	(i)	(ii)	(i)	(ii)
0	−1·833	−1·867	−1·879	−1·880	−1·762	−1·834	−1·883	−1·883	−1·993	−1·883
α	3·190	3·139	3·158	3·138	3·354	3·347	3·146	3·127	3·150	3·132
p	4·035	4·022	3·992	3·962	4·114	4·096	3·970	3·945	3·987	3·957
β	5·274	5·324	5·185	5·205	5·387	5·394	5·245	5·263	5·254	5·272
β'	5·351	5·398	5·305	5·337	5·354	5·444	5·250	5·274	5·268	5·297

(i) refers to ‘ diagonal ’ energies computed using the correct zero-order wave functions appropriate to the hydrocarbon (corresponding in this sense to first-order perturbation theory). (ii) includes the effect of off-diagonal elements (i.e., of the residual configuration interaction).

§ 6. CONCLUSION

From tables 1 and 2 it appears that the simplest possible treatment, based on the Hückel orbitals for the hydrocarbon, gives a surprisingly good approximation to the results obtained using the self-consistent field molecular orbitals of the nitrogen derivatives (and which we shall assume to be rather accurate). Even the spectral shifts are fairly well predicted by the simple method, except perhaps in the case of the pyrazine α band, and it might appear at first sight that the introduction of self-consistency is an unnecessary refinement.

On closer inspection, however, the accuracy of approximation (*a*) is seen to be of a different order in the two hetero-molecules. Thus, the energies of the ground and first four excited states of pyridine are inferior to those of self-consistent field theory by 0·016, 0·012, 0·077, 0·061 and 0·124 ev, respectively; but the corresponding figures for pyrazine are 0·082, 0·146, 0·107, 0·443 and 0·226 ev—which seems to imply that the fairly good agreement in table 2 is largely fortuitous in the case of this molecule.

This raises an important point concerning the selection of orbitals and configurations and indicates the dangers of a too hasty choice. The inadequacy of approximation (*a*) in the case of pyrazine is a direct consequence of the high symmetry of the molecule, for this excludes the possibility of improving the ground state by mixing with the chosen excited configurations. As a result, the pyrazine ground state energy is obtained essentially by first-order perturbation theory, using benzene orbitals, and the modification of the wave function associated with nitrogen substitution is completely ignored. In pyridine, on the other hand, configurational mixing *is* permitted and corrects the wave function so successfully that 70% of the ground state error is removed (as will be seen from table 3). Now in pyrazine the non-uniformities of charge are much larger than in pyridine and it is even more necessary to recognise them: since this cannot be done by configurational mixing it becomes necessary to admit orbitals which, in themselves, describe the charge shifts due to substitution (i.e. orbitals for the *hetero*-molecule). The only alternative would be to admit more highly excited configurations of benzene orbitals, which would destroy the simplicity of the approach.

Table 3 sheds further light on the relative merits of various approximations. The energy estimates in columns (i) are simply diagonal matrix elements of the Hamiltonian with respect to different basis functions and are not upper bounds to the true state energies: they are therefore of limited interest, beyond confirming that first-order configuration interaction, admitted at the outset by using (hydrocarbon) α, β, p, β' combinations, gives an adequate general picture of the spectrum. But the values listed in columns (ii) of table 3 (as indeed in table 1) represent upper bounds to the energies of all five states and therefore provide a direct and unequivocal test of the accuracy of different approximations.

It is clear that the usual self-consistent field molecular orbitals provide an exceedingly satisfactory account not only of the ground state but also of the first few excited states: for in only one instance (the β state) has a corresponding energy been surpassed in accuracy by using a different approximation. At the same time, approximations (*b*) and (*g*) are only slightly inferior, both being better than (*a*), in which the orbitals themselves take no account of charge non-uniformity. The only really poor result comes from the use of standard excited state orbitals which, as was pointed out in § 3, *over*-estimate the charge non-uniformity caused by the nitrogen. At the present level of approximation†, in terms of the finite set of (ortho-normalized) atomic orbitals a, b, c, ... all choices (*a*)–(*g*) would of course agree in their prediction of the standard excited state; but this state lies far above any of practical importance and its molecular orbitals evidently provide a relatively poor basis for precise calculations of the ground and first few excited states.

Our conclusions may now be drawn together and stated as follows:

---

† If it is assumed that the orthonormal set a, b, c, . . . *is* the set of localized transforms of the *exact* standard excited state molecular orbitals (a consistent and apparently legitimate choice), this qualification becomes unnecessary and the conclusion which follows appears to be inescapable.

(i) The orbitals of a parent hydrocarbon can, in suitable circumstances, provide a satisfactory basis for discussion of the derivatives. If the charge shifts due to substitution (or any other perturbation) can be described in terms of the selected set of configurations, the perturbation having matrix elements which will cause substantial mixing, then the limited configuration interaction calculation based upon the orbitals of the parent hydrocarbon (the unperturbed system) is likely to be adequate. If this is not the case, it is necessary to allow for the charge shifts, which on physical grounds must occur, by modification of the orbitals themselves (e.g. by introducing self-consistent field molecular orbitals for the perturbed system). This is a rather obvious criterion for assessing the validity of an approach based on hydrocarbon orbitals, and has related implications which are taken up in a companion paper (Part II).

(ii) The ground state self-consistent field molecular orbitals of the actual system give extremely satisfactory results for the first few excited states, configuration interaction being confined to degenerate or near-degenerate functions. None of the alternative calculations has given consistently better results.

(iii) The most accurate results are well reproduced using rather different linear combinations of the self-consistent field molecular orbitals (i.e. by relaxing the condition that the orbitals shall be *molecular* orbitals). This is useful when only the self-consistent field density matrix **R** is available (cf. McWeeny 1956 a, b); for linear combinations close to the molecular orbitals are extracted very easily (McWeeny 1957) while the exact molecular orbitals require solution of an eigenvalue problem. The use of molecular orbitals of a simple Hückel model of the substituted system is almost equally satisfactory, provided the electronegativity parameter is defined by equation (2).

(iv) The standard excited state molecular orbitals are rather unsatisfactory in calculations of the ground and first few excited states.

APPENDIX 1

Let **T** be the matrix whose columns represent the occupied orbitals A, B, C . . . and introduce $\mathbf{R}=\mathbf{T}\mathbf{T}^{\dagger}$ (so that $\mathbf{P}=2\mathbf{R}$ is the 'bonding matrix'). The 'effective' one-electron Hamiltonian is then defined in the atomic orbital basis *a*, *b*, *c*, . . . by the matrix

$$\mathbf{h}=\mathbf{f}+\mathbf{G} \qquad \ldots\ldots\text{(A1.1)}$$

where **f** is the 'bare framework' Hamiltonian (whose diagonal and off-diagonal elements are often denoted by α_a and β_{ab}) and **G** is an electron interaction matrix with elements

$$G_{ab}=\sum_{rs}R_{rs}[2(as|g|br)-(as|g|rb)]. \qquad \ldots\ldots\text{(A1.2)}$$

With currently accepted approximations (see, for instance, McWeeny 1956 b)

$$\left.\begin{aligned} f_{aa}&=\alpha_a=\omega_a-\sum_{b(\neq a)}Z_b\gamma_{ab} & \qquad G_{aa}&=R_{aa}\gamma_{aa}+\sum_{b(\neq a)}2R_{bb}\gamma_{ab} \\ f_{ab}&=\beta_{ab} & G_{ab}&=-R_{ab}\gamma_{ab} \end{aligned}\right\} \ldots\ldots\text{(A1.3)}$$

where ω_a measures the energy of an electron in orbital *a* on that part of the framework associated with ion *a* (and should be roughly constant from one molecule to another). γ_{ab} is the Coulomb integral $(ab|g|ab)$, and Z_b is the number of π electrons supplied by atom *b* ($=1$ for the carbon and nitrogen atoms of this paper). Using a subscript C to indicate a carbon value, it is convenient to introduce an orbital energy zero at $\omega_c + \frac{1}{2}\gamma_c$ by subtracting this quantity from the diagonal elements of f: we then have

$$\left.\begin{aligned} h_{aa} &= \delta\omega_a + (R_{aa}\gamma_{aa} - \tfrac{1}{2}\gamma_c) + \sum_{b(\neq a)} (2R_{bb} - Z_b)\gamma_{ab} \\ h_{ab} &= \beta_{ab} - R_{ab}\gamma_{ab} \end{aligned}\right\} \quad \ldots\ldots(\mathrm{A}1.4)$$

which means that $h_{aa}=0$ for a carbon atom in an alternant hydrocarbon. A suitable value of $\delta\omega$, for a nitrogen substituent, has been determined in previous work (McWeeny and Peacock 1957); in electron volts this becomes

$$\delta\omega = -1{\cdot}6765 \text{ ev.}$$

Denoting the columns of atomic orbital coefficients representing orbitals A, B, . . . by (A) (B) . . . the orbital energies are $\epsilon_P = \epsilon_{PP}$ where

$$\epsilon_{PQ} = (P)^\dagger \mathbf{h}(Q) \qquad \ldots\ldots(\mathrm{A}1.5)$$

and the off-diagonal elements $(P \neq Q)$ vanish only for strictly self-consistent molecular orbitals. Let us also denote the column whose r-element is the product $A_r{}^*B_r$ by (AB), and write $\boldsymbol{\gamma}$ for the square matrix of Coulomb integrals, so that $(PQ|g|RS) = (RP)^\dagger \boldsymbol{\gamma}\, (QS)$. Then the one-configuration energies of ground and excited states are

$$\left.\begin{aligned} H_{00} &= 2 \text{ tr } \mathbf{Rf} + \text{tr } \mathbf{RG} \\ {}^{1,3}(P \to Q'|H|P \to Q') &= H_{00} + (\epsilon_Q - \epsilon_P) \\ &\quad + [\left(\begin{smallmatrix}2\\0\end{smallmatrix}\right) (QP)^\dagger \boldsymbol{\gamma}(Q'P) - (PP)^\dagger \boldsymbol{\gamma}(Q'Q')] \end{aligned}\right\} \ldots\ldots(\mathrm{A}1.6)$$

and the off-diagonal matrix elements are

$$\left.\begin{aligned} {}^{1}(P \to Q'|H|0) &= \sqrt{2}\epsilon_{Q'P} \\ {}^{1,3}(P \to Q'|H|P \to S') &= \epsilon_{Q'S'} + [\left(\begin{smallmatrix}2\\0\end{smallmatrix}\right)(S'P)^\dagger \boldsymbol{\gamma}(Q'P) - (PP)^\dagger \boldsymbol{\gamma}(Q'S')] \\ {}^{1,3}(P \to Q'|H|R \to Q') &= -\epsilon_{RP} + [\left(\begin{smallmatrix}2\\0\end{smallmatrix}\right)(Q'R)^\dagger \boldsymbol{\gamma}(Q'P) - (PR)^\dagger \boldsymbol{\gamma}(Q'Q')] \\ {}^{1,3}(P \to Q'|H|R \to S') &= \qquad [\left(\begin{smallmatrix}2\\0\end{smallmatrix}\right)(S'R)^\dagger \boldsymbol{\gamma}(Q'P) - (PR)^\dagger \boldsymbol{\gamma}(Q'S')] \end{aligned}\right\} \ldots\ldots(\mathrm{A}1.7)$$

where the upper and lower figures in $\left(\begin{smallmatrix}2\\0\end{smallmatrix}\right)$ refer to singlet and triplet cases, respectively.

APPENDIX 2

When the parent molecule is an alternant, simplifications occur in using approximations (*a*), (*c*) and (*e*). Let $\mathbf{h}^0$ be the Hamiltonian, defined by (A1.4), of the parent hydrocarbon: then we can write for the hetero derivative

$$\mathbf{h} = \mathbf{h}^0 + \Delta, \qquad \epsilon_{PQ} = \epsilon^0{}_{PQ} + \delta\epsilon_{PQ}, \qquad k_{rs} = k^0{}_{rs} + \delta k_{rs} \qquad \ldots\ldots(\mathrm{A}2.1)$$

where Δ arises merely from a change of integral values and $\delta\epsilon_{PQ}$, δk_{rs} are computed using the orbitals of the hydrocarbon. Moreover, for an alternant, (P), (P'), $\mathbf{h}$ and Δ can be written

$$(P) = \begin{pmatrix} P_1 \\ P_2 \end{pmatrix} \quad (P') = \begin{pmatrix} P_1 \\ P_2 \end{pmatrix} \quad \mathbf{h} = \begin{pmatrix} \mathbf{h}_1 & 0 \\ 0 & \mathbf{h}_2 \end{pmatrix} \qquad \Delta = \begin{pmatrix} \Delta_1 & \Delta_{12} \\ \Delta_{21} & \Delta_2 \end{pmatrix} \; ..(\mathrm{A}2.2)$$

where the partitioning refers to 'starred' and 'unstarred' sets of atoms (sets 1 and 2, say). With the present approximation, $\beta_{rs}=0$ for r, s non-adjacent, Δ_1 and Δ_2 are diagonal; and it is then convenient to put $\delta\epsilon_{PQ} = \delta_{PQ}{}^{(1)} + \delta\epsilon_{PQ}{}^{(2)}$ where the two terms arise from the diagonal and off-diagonal parts of Δ ($\delta\epsilon_{PQ}$ being given as $(P)^\dagger \Delta(Q)$). Assuming also that the orbitals are real and that the only two-electron integral appreciably affected by substitution is the one-centre integral of the substituent itself, (γ_r say) we find

$$\epsilon_{\mathrm{AB}}{}^0 = -\epsilon_{\mathrm{A'B'}}{}^0, \qquad \epsilon_{\mathrm{A'B}}{}^0 = -\epsilon_{\mathrm{AB'}}{}^0,$$

$$\delta\epsilon_{\mathrm{AB}}{}^{(1)} = \delta\epsilon_{\mathrm{A'B'}}{}^{(1)} = \sum_r A_r B_r \delta_r,$$

$$\delta\epsilon_{\mathrm{AB}}{}^{(2)} = -\delta\epsilon_{\mathrm{A'B'}}{}^{(2)} = \sum_{r<s} (A_r B_s + A_s B_r)\delta\beta_{rs},$$

$$\delta\epsilon_{\mathrm{A'B}}{}^{(1)} = \delta\epsilon_{\mathrm{AB'}}{}^{(1)} = \sum_r (-1)^{\nu_r} A_r B_r \delta_r,$$

$$\delta\epsilon_{\mathrm{A'B}}{}^{(2)} = -\delta\epsilon_{\mathrm{AB'}}{}^{(2)} = \sum_{r<s} (-1)^{\nu_r} (A_r B_s + A_s B_r)\delta\beta_{rs},$$

$$k_{11}{}^0 = \binom{2}{0}(AA')^\dagger \gamma(AA') - (AA)^\dagger \gamma(AA) \qquad \delta k_{11} = \pm \sum_r A_r{}^4 \delta\gamma_r,$$

$$k_{12}{}^0 = k_{13}{}^0 = \binom{2}{0}(AA')^\dagger \gamma(AB') - (AA)^\dagger \gamma(AB) \qquad \delta k_{12} = \delta k_{13} = \pm \sum_r A_r{}^3 B_r \delta\gamma_r,$$

$$k_{14}{}^0 = \binom{2}{0}(AA')^\dagger \gamma(BB) - (AB)^\dagger \gamma(AB) \qquad \delta k_{14} = \pm \sum_r A_r{}^2 B_r{}^2 \delta\gamma_r,$$

$$k_{22}{}^0 = k_{33}{}^0 = \binom{2}{0}(AB')^\dagger \gamma(AB') - (AA)^\dagger \gamma(BB) \qquad \delta k_{22} = \delta k_{33} = \pm \sum_r A_r{}^2 B_r{}^2 \delta\gamma_r,$$

$$k_{23}{}^0 = \binom{2}{0}(AB')^\dagger \gamma(AB') - (AB)^\dagger \gamma(AB) \qquad \delta k_{23} = \pm \sum_r A_r{}^2 B_r{}^2 \delta\gamma_r,$$

$$k_{24}{}^0 = k_{34}{}^0 = \binom{2}{0}(AB')^\dagger \gamma(BB') - (AB)^\dagger \gamma(BB) \qquad \delta k_{24} = \delta k_{34} = \pm \sum_r A_r B_r{}^3 \delta\gamma_r,$$

$$k_{44}{}^0 = \binom{2}{0}(BB')^\dagger \gamma(BB') - (BB)^\dagger \gamma(BB) \qquad \delta k_{44} = \pm \sum_r B_r{}^4 \delta\gamma_r,$$

$$\ldots\ldots (\mathrm{A2.3})$$

where r is a substituted atom, and $\sum_r$ is a summation over all such atoms; $\delta\beta_{rs}$ is the change in (framework) resonance integral of bond r-s and $\sum_{r<s}$ is over all bonds affected by substitution; $\nu_r = 1$ or 2 according as r belongs to set 1 or set 2; and the $\binom{2}{0}$ and $\pm$ refer to the alternative singlet and triplet cases. Also

$$\delta_r = \delta\omega_r + \tfrac{1}{2}(\gamma_r - \gamma_{\mathrm{C}}), \quad \delta\gamma_r = (\gamma_r - \gamma_{\mathrm{C}}) \qquad \ldots\ldots (\mathrm{A2.4})$$

In the present work $\delta\gamma_r = 1{\cdot}4$ ev for a nitrogen atom and $\delta\beta_{rs} = -0{\cdot}19$ ev for a C–N bond. Using (A2.3), the secular problem with any number of substituents is directly related to that for the parent hydrocarbon. In comparing energies on the same absolute scale, it must be remembered that the one-configuration ground state energy, H_{00}, is affected by the changes in integral values due to substitution. Writing $H_{00} = H_{00}{}^0 + \delta H_{00}$, we find the general result

$$\delta H_{00} = \sum_r P_{rr}{}^0 \delta_r + 2\sum_{r<s} P_{rs}{}^0 \delta\beta_{rs} - \tfrac{1}{4}\sum_r (P_{rr}{}^0)^2 \delta\gamma_r \qquad \ldots\ldots (\mathrm{A2.5})$$

which becomes, for an alternant parent,

$$\delta H_{00} = \sum_r \delta_r + 2\sum_{r<s} P_{rs}{}^0 \delta\beta_{rs} - \tfrac{1}{4}\sum \delta\gamma_r \qquad \ldots\ldots (\mathrm{A2.6})$$

where, again, the summations are over all substituents and over all bonds affected by substitution.

References

Coulson, C. A., Craig, D. P., and Jacobs, J., 1951, *Proc. Roy. Soc.* A, **206,** 297.

Dewar, M. J. S., and Longuet-Higgins, H. C., 1954, *Proc. Phys. Soc.* A, **67,** 795.

Hall, G. G., 1952, *Proc. Roy. Soc.* A, **213,** 102.

McWeeny, R., 1956 a, *Proc. Roy. Soc.* A, **235,** 496; 1956 b, *Ibid*, **237,** 355; 1957, *Ibid.*, in the press.

McWeeny, R., and Peacock, T. E., 1957, *Proc. Phys. Soc.* A, **70,** 41.

Pariser, R., 1956, *J. Chem. Phys.*, **24,** 250.

Pople, J. A., 1955, *Proc. Phys. Soc.* A, **68,** 81.

An Analogue Method for Studying Multiple Scattering†

By J. C. BARTON‡, D. A. CAMPBELL§ and R. C. READ
University College of the West Indies

Communicated by R. Fürth; MS. received 8th March 1957

Abstract. A source of random motion was coupled to a mechanical differential analyser so that the output simulated the behaviour of a high energy charged particle undergoing multiple scattering. A large number of track analogues were drawn and their statistical behaviour studied. They provided an experimental test of the theory for the first passage problem of multiple scattering.

§ 1. Introduction

When a charged particle passes through matter it makes a large number of collisions with the atoms of the material. Even when the energy lost by the particle is small these collisions may still cause continual small changes in its direction. The path followed by any one particle is therefore uncertain and it is possible to study only the statistical distribution function which determines the probability of the particle reaching any particular point. The equation governing this distribution function was first derived by Fermi (see Rossi and Greisen 1941). In the two-dimensional case this equation is

$$\frac{\partial F}{\partial x}+\theta\frac{\partial F}{\partial y}=\mu\frac{\partial^2 F}{\partial\theta^2} \qquad \ldots\ldots(1.1)$$

where x and y are position coordinates, θ the angle, which is assumed to be small, between the track of the particle and the x-axis, $F=F(x, y, \theta)$ the distribution function, and μ half the mean square angle of scattering per unit length.

It is possible to find a solution to this equation only when the scattering material is of infinite extent. For particles starting from (0, 0, 0) the distribution function is:

$$F(x, y, \theta)=\frac{\sqrt{3}}{2\pi\mu x^2}\exp\left[-\frac{1}{\mu x^3}(3y^2-3xy\theta+x^2\theta^2)\right]. \qquad \ldots\ldots(1.2)$$

Unfortunately there are several problems of experimental importance in which it is the multiple scattering in a finite material that must be considered. Courant (1951) attempted to treat one such problem (the effective width of a collimating slit) theoretically, but his solution is clearly incorrect as the distribution function which he derives is not always positive. Since the work described in this paper was started two other theoretical papers, Chartres and Tidman (1955) and Barton (1957), have appeared and these treat certain aspects of the problem. Because of the difficulty of finding analytical solutions it seemed worth while to develop an analogue method. This paper describes the apparatus which has been built in order to simulate tracks and shows how, by studying a large number of tracks, their statistical behaviour can be deduced.

---

† An M.Sc. thesis by D.A.C., which was accepted by the University of London, included part of the material of this paper.

‡ Now at the Department of Physics, Birkbeck College, London.

§ Now at the Department of Physics, Royal Marsden Hospital, London.

§ 2. PRINCIPLE OF ANALOGUE METHOD

The Fermi equation for multiple scattering (1.1) and its solution (1.2) imply that the scattering angle is given by the Gaussian distribution law. The distribution law for the individual scattering processes is very different, being given by the Rutherford scattering law, but the Central Limit Theorem ensures that the angular distribution is Gaussian if the particles are scattered a sufficient number of times.

In order to produce an analogue of a scattered track it is therefore necessary to devise a mechanism which produces a Gaussian distribution of the variable which represents the scattering angle. There are undoubtedly many ways of realising a suitable mechanism; the one used was chosen chiefly on account of its relative simplicity. It consists of a device which generates a simple random walk in one dimension. The distribution function for the random walk problem is the binomial one and, provided that the number of steps is moderately large, this becomes very similar to the Gaussian one. It is not quite so obvious that the distribution in space will also be correct, but the following argument shows that it is approximately true.

We make the additional assumption that the steps of the random walk which cause variations in angle are made at equal intervals along the path of the track analogue (this assumption is not essential but corresponds to the most convenient experimental technique). Then the possible paths of particles for the first few steps are those shown in figure 1, where for clarity the angles have been greatly magnified.

Figure 1 is derived in the following way. In the first step the particle moves transversely one unit one way or the other. Thereafter it moves to a position at unit distance one side or other of the position which it would reach if it continued in the direction of its previous step. At each step there are two possibilities, so that after n steps there are 2^n possible positions (not necessarily distinct). If u_n units is the deviation after n steps, then

$$\begin{aligned} u_n &= u_{n-1} + (u_{n-1} - u_{n-2}) + x_n \\ &= 2u_{n-1} - u_{n-2} + x_n \end{aligned}$$

where $x_n = +1$ or -1, according to the two possibilities at the nth step.

Clearly

$$\begin{aligned} &u_1 = x_1 \\ &u_2 = 2u_1 + x_2 = 2x_1 + x_2 \\ &u_3 = 2u_2 - u_1 + x_3 = 3x_1 + 2x_2 + x_3 \\ &\cdot\ \cdot\ \cdot\ \cdot\ \cdot\ \cdot\ \cdot\ \cdot\ \cdot\ \cdot\ \cdot\ \cdot\ \cdot\ \cdot\ \cdot\ \cdot \\ &u_n = nx_1 + (n-1)x_2 + \ldots + x_n. \end{aligned}$$

Thus the possible deviations after n steps are given by numbers of the form:

$$\pm 1 \pm 2 \pm 3 \pm 4 \ldots \pm n, \qquad \ldots\ldots(2.1)$$

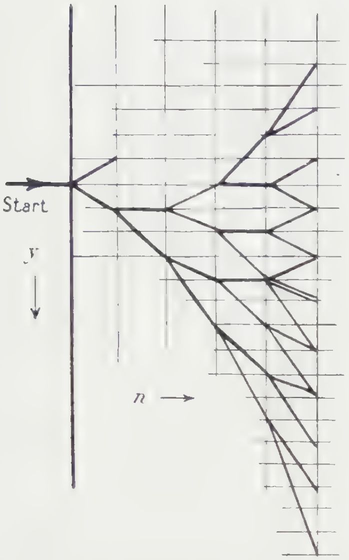

Figure 1. Possible paths of particles.

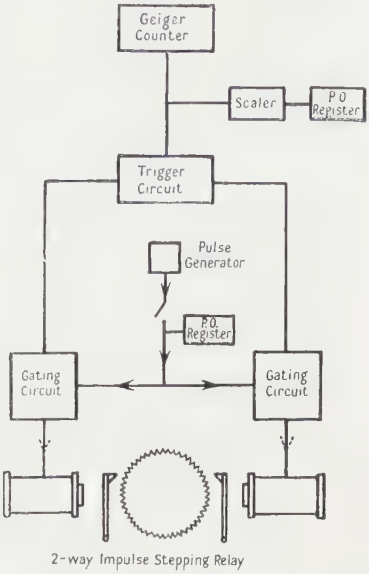

Figure 2. Random walk generator.

The moments of this distribution are calculated in the appendix (where it is also proved that the distribution approximates to the Gaussian distribution for large values of n.) The first few moments are

$$\begin{aligned} &\mu_1 = 0 \\ &\mu_2 = s_2 = \tfrac{1}{6}n(n+1)(2n+1) \\ &\mu_3 = 0 \\ &\mu_4 = 3s_2 - 2s_4 \end{aligned} \qquad \text{......(2.2)}$$

where $s_\nu = \sum_{r=1}^{n} r^\nu$. Accordingly, for large n,

$$\mu_2 \to \frac{n^3}{3} \quad \text{and} \quad \mu_4 \to \frac{n^6}{3}\text{ , etc.} \qquad \text{......(2.3)}$$

The solution of the Fermi equation for the distribution in y for any θ is

$$H(x, y) = \left(\frac{3}{4\pi\mu x^3}\right)^{1/2} \exp\left[-\frac{3y^2}{4\mu x^3}\right] \qquad \text{......(2.4)}$$

and the second and fourth moments are

$$\mu_2 = \tfrac{2}{3}\mu x^3 \quad , \quad \mu_4 = \tfrac{4}{3}\mu^2 x^6. \qquad \text{......(2.5)}$$

It is seen that these values agree with those of (2.3) if we set

$$n = (2\mu)^{1/3} x.$$

§ 3. Generation of Random Motion

Although several methods have been suggested for generating a random number electronically none of these schemes is very convenient for providing a mechanical motion. The method which was finally adopted is shown in figure 2. The mechanical motion is generated by a two-way impulse stepping relay; the output shaft of this device advances by a fixed amount in either direction according to which coil is energized. The randomness is derived from a Geiger–Müller counter. Its pulses provide the input for a bi-stable trigger circuit of the type which is commonly used in scalers and computers. The successive steps of the random walk are produced by a regularly recurring pulse which is routed to one or other coil of the stepping relay according to the state of the trigger circuit.

It is assumed that the time distribution of the arrival of cosmic ray and radioactive particles is truly random. Then if the average number of counts in a given time interval is r the probability $P(s)$ of observing s counts is given exactly by the Poisson distribution

$$P(s) = \frac{e^{-r} r^s}{s\,!}.$$

Consider two successive steps executed by the apparatus. If the trigger circuit has received an even number of pulses from the Geiger counter during the interval between the two steps then the two steps will be in the same direction. Alternatively, if there has been an odd number of counts the second step will be in the opposite direction.

Thus probability of two successive steps being in the same direction

$$\begin{aligned} &= \text{probability of an even number of counts} \\ &= P(0) + P(2) + P(4) + \dots \\ &= e^{-r}\left(1 + \frac{r^2}{2\,!} + \frac{r^4}{4\,!} + \dots\right) \\ &= \tfrac{1}{2}(1 + e^{-2r}). \end{aligned}$$

Similarly probability of two successive steps being in opposite directions

$$\begin{aligned} &= P(1) + P(3) + P(5) + \dots \\ &= \tfrac{1}{2}(1 - e^{-2r}). \end{aligned}$$

For a completely random motion these probabilities must each equal one half. We see that any value of r greater than 3 will satisfy this requirement to better than one part in a thousand. It is important to notice that the actual value of r is then immaterial.

This method of generating a random walk has been checked by comparing the distribution of the end-points of walks of a given number of steps with that expected theoretically. A detailed description of this test, and of other experiments on random walks, will be published later.

§ 4. Experimental Arrangement

The source of random motion is coupled to a model differential analyser, built in Meccano, which is similar to the one developed by Hartree and Porter

(1935). The connections which are necessary to simulate the tracks of scattered particles are shown, in the notation of Crank (1947), in figure 3. The output of the random walk device was used to displace the integrator carriage, the torque amplifier of another integrating unit being used to step up the power. If θ is the output of the random walk device, the output from the integrator is θx, so that the trace on the plotting table is a line with slope θ, i.e. a line making an angle with the x-axis of $\tan^{-1}\theta$. In order to reduce errors, the displacements of the carriage were made sufficiently large that the whole of the integrator disc was used. This entailed moving the carriage much more quickly than was possible with the normal lead screw method of displacement, so the lead screw was taken out, and the carriage was moved instead by means of a string passing over two drums. A pair of contacts were so arranged that they were closed twice for every revolution of a shaft which was coupled directly to the X traverse of the plotting table. The closure of these contacts was used to determine the time at which steps of the random walk were made. By this means the amount of scattering was determined only by the length of the track and was therefore independent of variations in the speed of the electric motor.

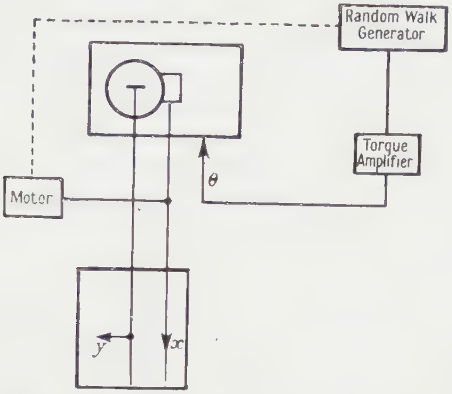

Figure 3. Connections of differential analyser.

The maximum length of tracks in the x-direction was 50 cm. The magnitude of the scattering depended on both the rate of occurrence of the random walk steps and the gearing used in the drive for the y coordinate. The theory of § 2 suggests that the number of steps should be large if even short lengths of the track are to be good representations of multiple scattering. In practice there were 5100 steps along the 50 cm of each track. For convenience of measurement the mean square values of θ and y were made as large as possible, but since the Fermi equation only applies for small angles of scattering the tracks obtained must be regarded as magnified in the y direction. Comparison between theory and experiment is still possible provided that $\tan\theta$ is used instead of θ. The actual value of μ was 0·00097 cm^{-1}.

§ 5. EXPERIMENTAL RESULTS

5.1. *Check of Fermi Distribution*

The apparatus was used to trace a total of 477 tracks starting with coordinates (0, 0, 0). y and $\tan\theta$ were measured for each track at its maximum length of

50 cm. If the apparatus was functioning correctly the distribution of these tracks should be given by equation (1.2) with the value of μ fixed by the instrumental constants.

The table shows the experimental and theoretical values for various quantities.

	Experiment	Theory
$\overline{y}$	$+0{\cdot}27 \pm 0{\cdot}41$ cm	0
$\overline{y^2}$	$9{\cdot}04 \pm 0{\cdot}29$ cm^2	$9{\cdot}00$ cm^2
$\overline{\tan\theta}$	$+0{\cdot}014 \pm 0{\cdot}014$	0
$\overline{\tan^2\theta}$	$0{\cdot}312 \pm 0{\cdot}009$	$0{\cdot}312$
$r=\dfrac{\overline{y\tan\theta}}{(\overline{y^2}\,\overline{\tan^2\theta})^{1/2}}$	$0{\cdot}851 \pm 0{\cdot}011$	$\dfrac{\sqrt{3}}{2}=0{\cdot}866$

In each case the error is the statistical one, as estimated by the theory. The agreement is remarkably good and shows that the apparatus imperfections are less important than statistical limitations. Of course this judgment might have to be reversed if a much larger number of tracks were studied.

5.2. *Symmetrical Double-sided First Passage Problem*

The problem considered here, which is important in the determination of absorption coefficients for high energy particles and in the use of nuclear plates for measuring a flux of particles, is illustrated in figure 4.

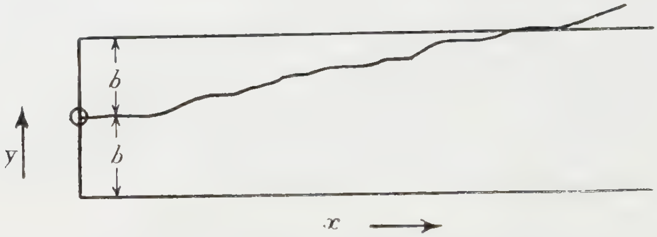

Figure 4. Double-sided first passage problem.

Particles all enter the piece of scattering material, which is assumed to be of width $2b$ in one direction and infinite in the other direction, at (0, 0, 0). It is required to find the proportion of particles which remain within the absorber at any distance x. The theoretical problem was first considered by Chartres and Tidman (1955) and a complete solution found by Barton (1957).

In principle the set of tracks obtained experimentally is sufficient to determine the first passage distribution for any value of b. However, if a large value of b is chosen a considerable proportion of the tracks have not crossed either boundary along their entire length of 50 cm. On the other hand a small value of b increases the uncertainty, due to the finite thickness of the pencil traces, of the position at which the track reaches either boundary. Balancing these two factors it seemed best to choose $b=1{\cdot}0$ cm.

The distribution of the lengths of the tracks up to their first passage across a boundary is shown in figure 5. The curve is obtained from the theory developed

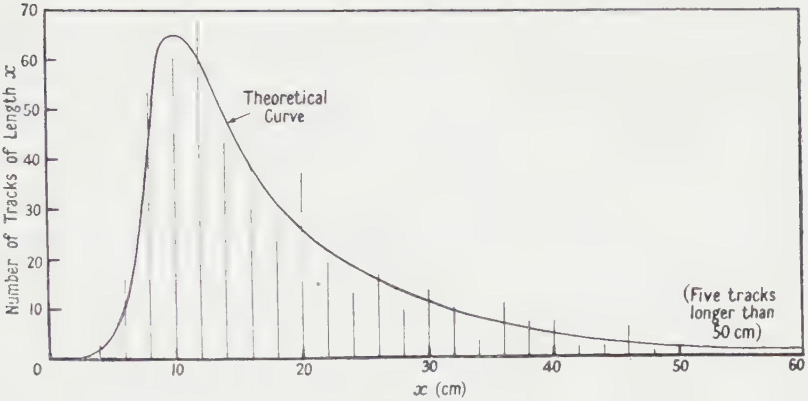

Figure 5. Distribution of the lengths of the tracks before crossing either boundary.

by Barton (1957). The mean length was found to be $17 \cdot 96 \pm 0 \cdot 51$ cm compared with the theoretical value of 18·0 cm. (The experimental figure has been adjusted by 1·2% to allow for the five tracks which remained inside the boundaries for their whole length.)

The behaviour of the tracks after they cross a boundary is also of interest. The tracks can be classified according to the number of boundary crossings which they make and this is shown schematically in figure 6. These results were helpful in the formulation of the theory referred to earlier. It is particularly interesting that behaviour of type (*e*) is commoner than type (*d*).

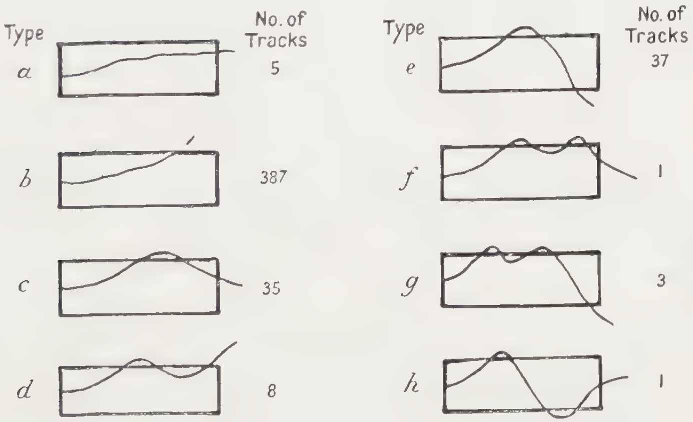

Figure 6. Classification of tracks according to their number of boundary crossings in a length of 50 cm.

§ 6. DISCUSSION

The results presented in the last section show that the imperfections of the apparatus, including back-lash in the Meccano gearing, were not serious enough to distort the tracks. The speed at which tracks could be drawn was limited by the rate at which the random walk generator operated reliably; seven steps per second was satisfactory and this enabled a 50 cm track to be drawn in about 12 minutes. A higher speed of operation would require improved mechanical design of the impulse stepping relay used in the random walk generator and of various parts of the differential analyser. It might then be better to use a combination of electronic and servo-mechanism techniques instead of a predominantly mechanical one.

The results can be applied to any value of the scattering constant by a suitable pair of scale transformations. Nor is it necessary to draw new tracks in order to study the first passage problem for different values of the initial coordinates, as it is sufficient to draw different boundaries for the same tracks. Thus the one set of tracks can be used to solve many problems.

As described the method only simulates the effect of true multiple scattering. It would not be difficult to include an occasional single scatter by using either another random motion device or, more simply, a variation of the 'Monte Carlo' method. In some problems the scattering increases along the length of the track as the particle loses energy. This could be simulated on the differential analyser by using two more integrating tables and appropriate inter-connections. It would also be possible to extend the method to deal with problems in which the restriction to small angles is no longer satisfied.

REFERENCES

BARTON, J. C., 1957, *Proc. Phys. Soc.* A, **70,** 253.

BROMWICH, T. J. I'A., 1926, *Theory of Infinite Series* (London : Macmillan), p. 299, ex. 2.

CHARTRES, B. A., and TIDMAN, D. A., 1955, *Proc. Phys. Soc.* A, **68,** 841.

COURANT, E. D., 1951, *Rev. Sci. Instrum.*, **22,** 1003.

CRAMER, 1946, *Mathematical Methods of Statistics* (Princeton : University Press), p. 176.

CRANK, J., 1947, *The Differential Analyser*, (London : Longmans Green).

HARTREE, D. R., and PORTER, A., 1935, *Mem. Manchr. Lit. Phil. Soc.*, **79,** 51.

ROSSI, B., and GREISEN, K., 1941, *Rev. Mod. Phys.*, **13,** 267.

APPENDIX

THE MOMENTS OF THE DISTRIBUTION

The probability of a deviation of u units after n steps is $1/2^n$ times the number of ways of choosing + and − signs in

$$\pm 1 \pm 2 \pm 3 \ldots \pm n$$

so as to get the number u. It is therefore the coefficient of t^u in the expansion of

$$G(t)=\frac{1}{2^n}\left(t+\frac{1}{t}\right)\left(t^2+\frac{1}{t^2}\right)\left(t^3+\frac{1}{t^3}\right)\ldots\left(t^n+\frac{1}{t^n}\right).$$

$G(t)$ is therefore the probability generating function of the distribution.

The moment generating function is obtained by putting $t=\mathrm{e}^{\alpha}$, and is therefore

$$M(\alpha)=\frac{1}{2^n}(\mathrm{e}^{\alpha}+\mathrm{e}^{-\alpha})(\mathrm{e}^{2\alpha}+\mathrm{e}^{-2\alpha})\ldots(\mathrm{e}^{n\alpha}+\mathrm{e}^{-n\alpha})$$

$$=\cosh\alpha\cosh 2\alpha\cosh 3\alpha\ldots\quad\cosh n\alpha.$$

Since

$$M(\alpha)=1+\mu_1\alpha+\frac{\mu_2}{2\,!}\alpha^2+\ldots,$$

the kth moment $\mu_k=M^{(k)}(0)$, by Maclaurin's theorem.

Now

$$\log M(\alpha) = \sum_{r=1}^{n} \log \cosh r\alpha.$$

Therefore

$$\frac{M'(\alpha)}{M(\alpha)} = \sum_{r=1}^{n} r \tanh r\alpha$$

whence $\mu_1 = M'(0) = 0$, as is otherwise obvious.

Differentiating k times, using Leibniz's theorem,

$$M^{(k+1)}(\alpha) = \sum_{p=0}^{k} \left[{}^kC_p M^{(k-p)}(\alpha) \frac{d^p}{d\alpha^p} \sum_{r=1}^{n} r \tanh r\alpha \right].$$

If t_p is the value of the pth derivative of $\tanh x$ when $x=0$, then

$$\frac{d^p}{d\alpha^p}(r \tanh r\alpha) = r^{p+1} t_p \qquad \text{when} \qquad \alpha = 0.$$

Therefore

$$M^{(k+1)}(0) = \sum_{p=0}^{k} \left[{}^kC_p M^{(k-p)}(0) t_p \sum_{r=1}^{n} r^{p+1} \right].$$

Writing s_ν for $\sum_{r=1}^{n} r^\nu$, we obtain the recurrence formula

$$\mu_{k+1} = \sum_{p=0}^{k} {}^kC_p \mu_{k-p} t_p s_{p+1}. \qquad \text{......(A)}$$

Now $t_p\, p\,!$ is the coefficient of x^p in the expansion of $\tanh x$, so t_p can be calculated (see e.g. Bromwich 1926). The first few values are $t_1 = 1$; $t_3 = -2$; $t_5 = 16$ etc., t_p being zero if p is even.

Therefore by equation (A)

$$\begin{aligned} \mu_2 &= \mu_0 t_1 s_2 + \mu_1 t_0 s_1 \\ &= s_2 && \text{(since } \mu_0 = 1) \\ \mu_3 &= 2\mu_1 t_1 s_2 && \text{(omitting terms for which } p \text{ is even)} \\ &= 0 && \text{(since } \mu_1 = 0). \end{aligned}$$

Clearly, all odd moments are zero anyway since the distribution is symmetrical.

$$\begin{aligned} \mu_4 &= \mu_0 t_3 s_4 + 3\mu_2 t_1 s_2 \\ &= 3s_2^2 - 2s_4 \\ \mu_6 &= \mu_0 t_5 s_6 + 10\mu_2 t_3 s_4 + 5\mu_4 t_1 s_2 \\ &= 16s_6 - 20 s_2 s_4 + 5(3s_2^2 - 2s_4)s_2 \\ &= 16s_6 - 30 s_2 s_4 + 15 s_2^3 \end{aligned}$$

and so on.

COMPARISON WITH THE GAUSSIAN DISTRIBUTION

The terms in the expression for μ_{2m} will be of the form

$$A s_2^a s_4^b \ldots s_{2m}^l$$

where A is a constant and $2a + 4b + \ldots + 2ml = 2m$.

Now s_ν is a polynomial in n of degree $\nu + 1$. Therefore, since the term of the form $A s_2^m$ is the only one with as many as m factors, it follows that this term is the only one whose degree is $3m$ (the others being of lesser degree).

To compare μ_{2m} with the $2m$th moment of the Gaussian distribution we must standardize by dividing by s_2^m which is a polynomial of degree $3m$ in n. If we now let n tend to infinity, all the terms in the expression for μ_{2m}/s_2^m will tend to zero except the one mentioned above. Denoting the limit by μ_{2m}^*, we have

$$\mu_{2m}^* = \lim_{n\to\infty} \frac{\mu_{2m}}{s_2^m} = \text{the coefficient of } s_2^m \text{ in expression for } \mu_{2m}.$$

If we regard the expression for μ_{2m} formally as a polynomial in variables $s_2, s_4, \ldots,$ we can obtain this coefficient by putting $s_2=1$, $s_4=0$, $s_6=0$, etc. Equation (A) gives

$$\mu_{2m} = \sum_{p=0}^{2m-1} {}^{2m-1}C_p t_p s_{p+1} \mu_{2m-p-1}.$$

With the given substitution, all terms but one of the right hand side vanish, and $s_2^m \mu_{2m}^* = {}^{2m-1}C_1 t_1 s_2 s_2^{m-1} \mu_{2m-2}^*$.

Thus $\mu_{2m}^* = (2m-1)\,\mu_{2m-2}^*$, so that $\mu_2^* = 1$, $\mu_4^* = 1 \cdot 3$, $\mu_6^* = 1\,.\,3\,.\,5$, and so on. These are the Gaussian moments.

But a distribution is uniquely determined by its moments if the series for the moment generating function is absolutely convergent for some positive value of the variable (Cramer 1900), and this is true in this case. Therefore the given distribution approximates to a Gaussian distribution as n tends to infinity.

RESEARCH NOTES

A Note on the Ising Model with Second Nearest Neighbour Interactions

By E. W. ELCOCK
Department of Natural Philosophy, University of Aberdeen

MS. received 17th April 1957

Although approximate series solutions are known (c.f. Domb and Potts 1951), as yet no closed expression has been found for the partition function of a two-dimensional Ising net with interactions between next nearest as well as nearest neighbours. The triangular net, with nearest neighbour interactions only, may be regarded as a deformed rectangular net with nearest neighbour interactions together with additional interactions along one of the diagonal directions (see figure 1 *a*). The known closed solution for the partition function of a triangular net with nearest neighbour interactions only may therefore be considered (see Newell and Montroll 1953, the notation of which will be used throughout) as a first step towards the solution of the nearest and next nearest neighbour rectangular net problem. However, the second nearest neighbour interactions in the rectangular net derived from the deformed triangular net have, considered alone, only one-dimensional character in that they form linear chains rather than a two-dimensional net. It is shown below that this limitation may be removed and that, by a generalization of the well-known star–triangle transformation, a problem may be solved in which the second nearest neighbour interactions themselves form a two-dimensional net.

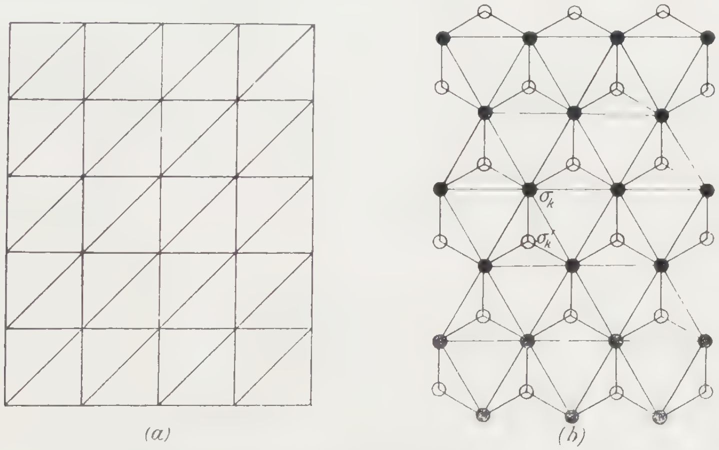

Figure 1. (*a*) The rectangular net formed by deformation of the triangular net, (*b*) the hexagonal net with nearest and those next nearest interactions considered in the text illustrated.

Consider the hexagonal net shown in figure 1 (*b*), and let it be regarded as composed of two interpenetrating triangular sub-nets, the nearest neighbours of a site on one sub-net all lying on the other sub-net. The coordinates of one sub-net will be represented by σ_k and the coordinates of the other by σ_k'. It is supposed that the interaction energy between (*a*), nearest neighbour particles

σ_j and σ_k' is $-J_1\sigma_j\sigma_k'$, (*b*), next nearest neighbour particles σ_j and σ_k comprising just one of the two sub-nets is $-J_2\sigma_j\sigma_k$, and (*c*) any other pair of particles is zero (see figure 1 (*b*)). The partition function for a net of N particles may be written in the form

$$Z = \sum_{\sigma_1=\pm1} \cdots \sum_{\sigma_{N/2}=\pm1} \left\{ \sum_{\sigma_1'=\pm1} \cdots \sum_{\sigma'_{N/2}=\pm1} \exp\left(\sum_{nn} K_1\sigma_i\sigma_j' + \sum_{nnn} K_2\sigma_k\sigma_l \right) \right\},$$

i.e.,

$$Z = \sum_{\sigma_1=\pm1} \cdots \sum_{\sigma_{N/2}=\pm1} \left[\exp\left(\sum_{nnn} K_2\sigma_k\sigma_l \right) \left\{ \sum_{\sigma_1'=\pm1} \cdots \sum_{\sigma'_{N/2}=\pm1} \exp\left(\sum_{nn} K_1\sigma_i\sigma_j' \right) \right\} \right], \qquad \ldots\ldots(1)$$

where $K_1 = J_1/\boldsymbol{k}T$ and $K_2 = J_2/\boldsymbol{k}T$. Considering now only the quantity in braces and applying the star–triangle transformation (Newell and Montroll 1953) we may write

$$\sum_{\sigma_1'=\pm1} \cdots \sum_{\sigma'_{N/2}=\pm1} \exp\left(\sum_{nn} K_1\sigma_i\sigma_j' \right) = 2^{N/2} \cosh^{3N/2} K_1 (\cosh^3 K_1^* + \sinh^3 K_1^*)^{-N/2}$$
$$\times \exp\left(\sum_{nnn} K_1^*\sigma_i\sigma_j \right), \qquad \ldots\ldots(2)$$

where K_1^* is given implicitly by the relation

$$\tanh^2 K_1 = \frac{\cosh K_1^* \sinh K_1^* (\cosh K_1^* + \sinh K_1^*)}{(\cosh^3 K_1^* + \sinh^3 K_1^*)}. \qquad \ldots\ldots(3)$$

Substituting from (2) in (1),

$$Z = 2^{N/2} \cosh^{3N/2} K_1 (\cosh^3 K_1^* + \sinh^3 K_1^*)^{-N/2} \sum_{\sigma_1=\pm1} \cdots \sum_{\sigma_{N/2}=\pm1} \exp\left(\sum_{nnn} (K_2 + K_1^*)\sigma_i\sigma_j \right),$$

i.e.,

$$Z = \frac{(2\sinh 2K_1)^{N/2}}{(2\sinh 2K_1^*)^{N/4}} Z_{\mathrm{T}}(K_{\mathrm{T}}), \qquad \ldots\ldots(4)$$

where $Z_{\mathrm{T}}(K_{\mathrm{T}})$ is the partition function of a triangular net with reduced nearest neighbour interaction $K_{\mathrm{T}} = K_2 + K_1^*$. The problem has thus been reduced to one for which the solution is known (Newell and Montroll 1953).

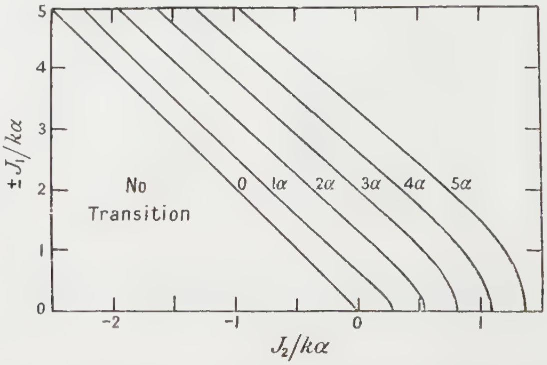

Figure 2. Iso-critical temperature lines for a hexagonal Ising net with nearest (J_1) and next nearest (J_2) interactions. The curves are labelled with values of the critical temperature T_c in arbitrary units.

It is perhaps of interest to exhibit the explicit dependence of the critical temperature on J_1 and J_2. From (3) it follows that $K_1^* \geqslant 0$. It follows from

(4) that the critical temperature is given by the solution of $4K_T = \log 3$, i.e. $4(K_2 + K_1^*) = \log 3$, or, from (3), by the solution of

$$4K_2 = \log [3/(2 \cosh 2K_1 - 1)]. \qquad \ldots\ldots(5)$$

Equation (5) has been solved numerically and the results are illustrated graphically in figure 2.

For $J_2 > 0$, J_2/J_1 such that J_2 is the dominant interaction, the method provides a rigorous closed solution of what must be regarded as a two-dimensional ferrimagnet.

REFERENCES

Domb, C., and Potts, R. B., 1951, *Proc. Roy. Soc.* A, **210,** 125.
Newell, G. F., and Montroll, E. W., 1953, *Rev. Mod. Phys.*, **25,** 353.

The Oscillator Strengths of the 1sσ–2pσ, 2pσ–2sσ, 2pσ–3dσ and 2pσ–2pπ Transitions of HeH^{2+}

By A. M. ARTHURS, R. A. B. BOND and J. HYSLOP
Department of Applied Mathematics, The Queen's University of Belfast

Communicated by D. R. Bates; MS. received 2nd *May* 1957

§ 1. Introduction

Calculations on the oscillator strengths of a number of transitions of HeH^{2+} have already been performed (Dalgarno, Lynn and Williams 1956, Arthurs and Hyslop 1957), using the exact two-centre electronic wave functions of Bates and Carson (1956). None of these transitions involves the *transfer* of the electron from one nucleus to the other and it is desirable to extend the calculations to transitions of the *charge-transfer* type (Mulliken 1939 a). Several charge-transfer transitions are of special interest in astrophysics, examples being the $\text{X}^2\Pi$–$\text{A}^2\Delta$ transition of CH and the $\text{X}^2\Pi$–$\text{A}^2\Sigma^+$ transition of OH. The associated transition integrals tend to be low at large internuclear distances because of the small overlap between the initial and final atomic orbitals; this is in marked contrast to the very intense transitions of the *charge-resonance* type† (Mulliken 1939 a, b).

§ 2. Calculations

If the nuclei are regarded as fixed at a distance R apart, the oscillator strength associated with the transition between two electronic states A and B may be written as

$$f(\mathrm{A}-\mathrm{B}|R) = \tfrac{1}{3}E(\mathrm{A}-\mathrm{B}|R)G(\mathrm{A}-\mathrm{B})|Q(\mathrm{A}-\mathrm{B}|R)|^2 \qquad \ldots\ldots(1)$$

the transition integral $Q(\mathrm{A}-\mathrm{B}|R)$ being given by

$$|Q| = |\textstyle\int \chi_\mathrm{B}^* \mathbf{r} \chi_\mathrm{A} \, d\mathbf{r}| \qquad \text{(dipole-length)} \qquad \ldots\ldots(2)$$

$$= 2|\textstyle\int \chi_\mathrm{B}^* \nabla \chi_\mathrm{A} \, d\mathbf{r} / E(\mathrm{A}-\mathrm{B}|R)| \qquad \text{(dipole-velocity)} \qquad \ldots\ldots(3)$$

(Chandrasekhar 1945), in the customary notation (cf. Arthurs and Hyslop 1957).

---

† The name 'charge-transfer spectra' has also been used to describe both charge-transfer and charge-resonance spectra. However, Mulliken (1939 a) originally defined charge-resonance spectra and charge-transfer spectra as related but distinct types of spectra, the prototypes of each being respectively H_2^+, ${}^2\Sigma_g^+$–${}^2\Sigma_u^+$ and H_2, ${}^1\Sigma_g^+$–${}^1\Sigma_u^+$.

With the exact wave functions in confocal elliptical coordinates, the analytical expressions for Q are identical to those presented in the earlier calculations of Dalgarno, Lynn and Williams (1956), for σ–σ transitions, and Arthurs and Hyslop (1957) for σ–π transitions. It is therefore not necessary to reproduce them here.

The simple LCAO approximations to the wave functions were also used. With these (2) and (3) reduce to combinations of the J-functions of Coulson (1942). In the case of the σ–σ transitions, only the dipole-velocity formula was applied since (because of the non-orthogonality of the approximate wave functions concerned) the dipole-length formula is dependent on the (arbitrary) origin of coordinates so that its computation is meaningless.

Photon Energies ΔE, Transition Integrals Q and Oscillator Strengths f of some transitions of HeH^{2+}

	1sσ–2pσ			2pσ–2sσ		
R	ΔE	Q	f	ΔE	Q	f
0·00	6·75000	0·248	0·139	0·00000	1·000	0·0000
0·25	5·97975	0·289	0·167	0·13216	0·977	0·0430
0·50	4·93558	0·360	0·213	0·37161	0·891	0·0984
1·00	3·39003	0·474	0·254	0·86044	0·641	0·1180
1·5	2·61404	0·482	0·203	1·10244	0·456	0·0765
2·0	2·33402	0·417	0·135	1·11619	0·341	0·0434
2·5	2·28069	0·333	0·0844	1·02892	0·264	0·0239
3·0	2·31333	0·263	0·0534	0·91425	0·209	0·0133
3·5	2·37369	0·207	0·0340	0·80143	0·166	0·0074
4·0	2·43905	0·168	0·0230	0·70019	0·135	0·0042
4·5	2·50068	0·136	0·0155	0·61280	0·107	0·0024
5·0	2·55538	0·111	0·0105	0·53893	0·0866	0·0013
∞	3·00000	0·000	0·0000	0·00000	0·0000	0·0000

	2pσ–3dσ			2pσ–2pπ		
R	ΔE	Q	f	ΔE	Q	f
0·00	1·25000	0·817	0·278	0·00000	0·000	0·0000
0·25	1·28595	0·794	0·270	0·05537	0·062	0·0001
0·50	1·38897	0·736	0·251	0·20928	0·122	0·0021
1·00	1·64828	0·630	0·218	0·62005	0·229	0·0217
1·5	1·70493	0·641	0·233	0·85583	0·329	0·0617
2·0	1·54786	0·731	0·276	0·89108	0·414	0·1019
2·5	1·29757	0·846	0·307	0·83366	0·472	0·1239
3·0	1·04190	0·948	0·312	0·74897	0·502	0·1261
3·5	0·82227	1·049	0·302	0·66299	0·509	0·1144
4·0	0·64845	1·141	0·282	0·58441	0·494	0·0949
4·5	0·51633	1·216	0·254	0·51557	0·462	0·0733
5·0	0·41823	1·259	0·221	0·45665	0·418	0·0532
∞	0·00000	0·000	0·000	0·00000	0·000	0·0000

The internuclear separation R is in units of a_0 ($0{\cdot}529 \times 10^{-8}$ cm) and the photon energy ΔE is in rydbergs.

§ 3. Results and Discussion

3.1.

The results obtained from the LCAO approximations will not be reproduced here for the derived oscillator strengths are consistently too small even at $R = 5a_0$

by a factor ranging from 4 for the 2pσ–2pπ transition to 25 for the 1sσ–2pσ transition, and for smaller R frequently are not even qualitatively correct.

The inaccuracy is due largely to the failure of the simple LCAO approximation for the 2pσ state to take account of the strong polarizing influence of the bare helium nucleus (cf. Dalgarno and Stewart 1956, McCarroll and Moiseiwitsch 1957). Since the energies of the 2pσ, 2sσ and 3dσ states are in exact resonance at infinite nuclear separation, it is to be anticipated that unusually severe mixing of the LCAO representations of these states will occur. This mixing is not allowed for by the simple LCAO wave functions adopted.

3.2.

The transition integrals and oscillator strengths derived from the exact two-centre wave functions are given in the table.

The value of f(1sσ–2pσ) is 0·254 when the internuclear separation is one atomic unit. In consequence, the remaining σ–σ transitions from the 1sσ level must be weak (the sum of the f's being only 0·079 by virtue of the Thomas–Kuhn sum rule). That this is so for the 1sσ–2sσ and 1sσ–3dσ transitions has been shown by Dalgarno, Lynn and Williams (1956). A similar conclusion was reached for the parallel transitions originating at the 1sσ_g level of H_2^+ (Bates, Darling, Hawe and Stewart 1954). However, for H_2^+ the required smallness of the oscillator strengths is achieved by the corresponding (Q, R) curves crossing the zero line, whereas this is not the case for HeH^{2+}.

Since the oscillator strength of the 2pσ-1sσ transition is negative, its large magnitude does not imply that the oscillator strengths of the upward transitions 2pσ–$nl\sigma$ are small. On the contrary, it necessitates that at least some of them be considerable since their sum must be almost $\frac{2}{3}$ for the Thomas–Kuhn sum rule to be satisfied. An analogous result holds in the case of the 2pσ_u–$nl\sigma_g$ series of H_2^+ (Bates, Darling, Hawe and Stewart 1954).

ACKNOWLEDGMENTS

The writers are greatly indebted to Professor D. R. Bates for suggesting this problem, and for his encouragement and interest throughout its progress. They are also grateful to Dr. A. Dalgarno for helpful discussions, particularly in connection with the approximate calculations.

Finally, two of them (J. H., A. M. A.) acknowledge research grants from Antrim County Education Committee.

REFERENCES

ARTHURS, A. M., and HYSLOP, J., 1957, *Proc. Phys. Soc.* A, **70,** 489.

BATES, D. R., and CARSON, T. R., 1956, *Proc. Roy. Soc.* A, **234,** 207.

BATES, D. R., DARLING, R. T. S., HAWE, S. C., and STEWART, A. L., 1954, *Proc. Phys. Soc.* A, **68,** 533.

CHANDRASEKHAR, S., 1945, *Astrophys. J.*, **102,** 223.

COULSON, C. A., 1942, *Proc. Camb. Phil. Soc.*, **38,** 210; 1952, *Valence* (Oxford : Clarendon Press).

DALGARNO, A., LYNN, N., and WILLIAMS, E. J. A., 1956, *Proc. Phys. Soc.* A, **69,** 610.

DALGARNO, A., and STEWART, A. L., 1956, *Proc. Roy. Soc.* A, **238,** 276.

HERZBERG, G., 1950, *Spectra of Diatomic Molecules*, 2nd Edn. (London : Macmillan).

MCCARROLL, R., and MOISEIWITSCH, B. L., 1957, *Proc. Phys. Soc.* A, **70,** 507.

MULLIKEN, R. S., 1939 a, *J. Chem. Phys.*, **7,** 20; 1939 b, *Astrophys. J.*, **89,** 283.

The Use of Extrapolated Quantum Defects as a Check on Calculated Phases for Scattering of Electrons by Positive Ions

By M. J. SEATON
Department of Physics, University College London

MS. received 24th April 1957

LET E_{nl} be the energy of a series electron and $-2Z/r$ be the asymptotic form of the potential $V(r)$ in which it moves, both measured in rydbergs (13·60 ev). Then $E_{nl}=-Z^2/\nu_{nl}^2$ defines the effective quantum number ν_{nl} and $\mu_{nl}=n-\nu_{nl}$ defines the quantum defect μ_{nl}. For the corresponding continuum (kinetic energy k^2 Rydbergs) the phase shift $\delta_l(k^2)$ is defined in terms of the asymptotic behaviour of the wave function:

$$F(k,l;r)\sim\sin\left\{kr-\tfrac{1}{2}l\pi+\frac{Z}{k}\ln(2kr)+\arg\Gamma\left(l+1-\frac{iZ}{k}\right)+\delta_l(k^2)\right\}.$$

Putting $V(r)=-u(r)-2Z/r$ where $r^2u(r)\to 0$ for $r\to\infty$, quantum defects and phases both provide measures of $-u(r)$, the non-Coulomb part of the potential. At the series limit

$$\delta_l(0)=\pi\mu_{\infty l} \qquad \ldots\ldots(1)$$

(Seaton 1955 a). A more general relation is contained in the theory of the quantum defect method (Ham 1955) developed for the study of solid state problems. If $u(r)=0$ for $r>r_1$ with r_1 finite and if all E_{nl} are known the phase can be deduced for all k^2. At low energies ($k^2\ll(2\pi Z)^2$) a more complicated expression reduces to

$$\delta_l(k^2)=\pi\mu_l(k^2) \qquad \ldots\ldots(2)$$

where $\mu_l(k^2)$ is the quantum defect extrapolated as a function of the energy. In practice the range of extrapolation is limited by incomplete knowledge of the E_{nl} and by the fact that a more complicated asymptotic form of the wave function should be considered at energies sufficiently large for inelastic collisions to occur.

Equation (1) has been used to check calculated zero-energy phases (Seaton 1955 a, b, Seaton and Osterbrock 1957). Using (2) similar checks may be made for k^2 non-zero. Table 1 shows that for Na $6p^6 k^2p$ the Hartree–Fock method (Seaton 1951) gives good results for the phase and the energy variation of the phase. The function $\pi\mu_1(k^2)$ is obtained from observed energy levels using formulae given by Ham.

Table 1. Na $6p^6 k^2p$

k^2	$\delta_1(k^2)$ Hartree–Fock		$\pi\mu_1(k^2)$ Empirical	
0·0	2·630		2·687	
		0·053		−0·055
0·2	2·577		2·632	

To within experimental accuracy the quantum defects for He 1sns ^{1}S and ^{3}S series may be represented as linear functions of energy, giving

Series	$\pi\mu_0(k^2)$	Lowest eigenvalue, E_{2s}
1sns ^{3}S	$0{\cdot}9319-0{\cdot}1263\,k^2$	$-0{\cdot}3505$
1sns ^{1}S	$0{\cdot}4372-0{\cdot}1089\,k^2$	$-0{\cdot}2919$

Although accurate at low energies these formulae cannot be correct at high energies since they give $\pi\mu_0(k^2)\rightarrow-\infty$ as $k^2\rightarrow\infty$ whereas it should go to zero. Tables 2 and 3 give comparisons with results of variational calculations (Bransden and Dalgarno 1953). In the exchange approximation anti-symmetrized product wave functions are used while in the exchange–polarization approximation (^{1}S only) an additional term is included depending on the inter-electronic distance r_{12}. As is usual, H and K refer to the methods of Hulthén (1944) and of Kohn (1948). It appears that the extrapolation formulae are unreliable for $k^2>1{\cdot}831$; compared with the energy of the lowest eigenvalue this represents a considerable range of extrapolation. For the ^{3}S case the agreement is satisfactory. The ^{1}S calculations are much more delicate. Poor agreement between the H and K methods is obtained in the exchange approximation (the K results being obviously incorrect) and the exchange–polarization approximation fails at low energies (the H method giving complex phases and the K method excessively large correction terms). Despite these difficulties it is seen that the H method in the exchange approximation continues to give reasonable results.

Table 2. He 1s k^2s, ^{3}S

k^2	$\delta_0(k^2)$ Exchange K and H	$\pi\mu_0(k^2)$ Empirical
0·241	0·959	0·902
0·607	0·824	0·855
1·157	0·807	0·786
1·831	0·762	0·701

Table 3. He 1s k^2s, ^{1}S

k^2	$\delta_0(k^2)$				$\pi\mu_0(k^2)$ Empirical
	Exchange		Exchange–polarization		
	H	K	H	K	
0·241	+0·419	−0·281	—	—	+0·411
0·607	0·404	+0·038	—	—	0·371
1·157	0·365	0·073	0·291	0·315	0·311
1·831	0·333	0·110	0·321	0·356	0·238

REFERENCES

BRANSDEN, B. H., and DALGARNO, A., 1953, *Proc. Phys. Soc.* A, **66**, 268.

HAM, F. S., 1955, *Solid State Physics*, Vol. 1. (ed. Seitz and Turnbull), (New York: Academic Press), p. 127.

HULTHÉN, L. H., 1944, *K. Fysiogr. Sällsk. Lund. Förh.*, **14**, No. 21.

KOHN, W., 1948, *Phys. Rev.*, **74**, 1763.

SEATON, M. J., 1951, *Proc. Roy. Soc.* A, **208**, 418; 1955 a, *C.R. Acad. Sci., Paris*, **240**, 1317; 1955 *b*, *The Airglow and the Aurorae* ed. Armstrong and Dalgarno, (London: Pergamon Press), p. 289.

SEATON, M. J., and OSTERBROCK, D. E., 1957, *Astrophys. J.*, **125**, 66.

LETTERS TO THE EDITOR

On the Rotational Analysis of Bands of the $A^3\Pi_{0^+} - X^1\Sigma^+$ System of TlCl

Within the last few years three different values for the internuclear distance in the ground state of the gaseous molecule TlCl have been published. Observations of the rotational spectrum in the microwave region (Mandel and Barrett 1955) lead to $r_e'' = 2{\cdot}4848 \pm 0{\cdot}0001$ Å, and Mandel and Barrett have pointed out that the results obtained by the molecular beam electric resonance method (Carlson, Lee and Fabricand 1952) are in excellent agreement if the observed line J $1 \leftarrow 0$ is attributed to $Tl^{37}Cl$ rather than to $Tl^{35}Cl$ as was done by Carlson, Lee and Fabricand.

A rotational analysis of bands of the $A^3\Pi_{0^+} - X^1\Sigma^+$ system (Kadesch, Moldenhauser and Winans 1956) gives $r_e'' = 2{\cdot}466$ Å, in poor agreement with the microwave value. However, the analysis (Kadesch 1956) is suspect from internal evidence, for plots of $\Delta_2 F(J)/(J+\frac{1}{2})$ are by no means linear. It is the purpose of this note to point out that good agreement with the microwave value can be obtained by simply altering the J-numbering of some of the observed branches.

R and P lines of the 0, 0 band, and P lines of the 1, 0 and 1, 1 bands of the species $^{205}Tl^{35}Cl$ were identified by Kadesch. If the values of J for the P branch of the 0, 0 band are increased by unity, there are obtained values of $\Delta_2 F''(J)$ in excellent agreement with those calculated from the microwave value of B_0'', with $D = 4B^3/\omega^2$: a selection of values is given in table 1.

Table 1. Values of $\Delta_2 F''(J)$ for $v'' = 0$: $^{205}Tl^{35}Cl$

	$\Delta_2 F''(J)$ (cm^{-1})			$\Delta_2 F''(J)$ (cm^{-1})	
J	obs.	calc.	J	obs.	calc.
5	1·98	2·01	35	12·94	12·94
10	3·83	3·83	40	14·80	14·75
15	5·60	5·65	45	16·58	16·57
20	7·47	7·48	50	18·37	18·38
25	9·30	9·30	55	20·22	20·19
30	11·13	11·12	60	22·02	22·00

Table 2. Constants for $^{205}Tl^{35}Cl$

State	$\Delta G_{\frac{1}{2}}$	B_e	α_e	D	r_e(Å)
$A^3\Pi_{0^+}$	201·60	$0{\cdot}09227_0$[a]	0·00131	$7{\cdot}_5 \times 10^{-8}$ [b]	$2{\cdot}472_9$
$X^1\Sigma^+$	281·88[c]	0·09147[c, d]	—	$4{\cdot}_4 \times 10^{-8}$ [d]	2·484[c, d]
		0·091396[e]	0·000397[e]	—	2·4848[e]

[a] with $B_0'' = 0{\cdot}091198$ cm^{-1}.
[b] with $D_0'' = 3{\cdot}76 \times 10^{-8}$ cm^{-1}.
[c] with $\alpha'' = 0{\cdot}000397$ cm^{-1}.
[d] from $\Delta_2 F''(J)/(J+\frac{1}{2})$: $D''_e = 4B_e^3/\omega_e^2 = 3{\cdot}7_6 \times 10^{-8}$ cm^{-1}.
[e] from the microwave spectrum, Mandel and Barrett 1955.

The constants for the upper state of the 0, 0 band may be obtained fro values of $R(J-1) + P(J)$ in the usual way. The J-numbering of the line in the P branch of the 1, 0 band may be determined by assuming that $P(J+1)_{1,0} - P(J+1)_{0,0}$ $(=\Delta G_{1/2} - \alpha' J(J+1))$ is linear in $J(J+1)$: the numbering in the 1, 1 band may be obtained similarly. The results are summarized in table 2.

Physical Chemistry Laboratory,
University of Oxford.
8th April 1957.

R. F. Barrow.

Carlson, R. O., Lee, C. A., and Fabricand, B. P., 1952, *Phys. Rev.*, **85**, 784.
Kadesch, R. R., 1956, *Dissertation*, University of Wisconsin.
Kadesch, R. R., Moldenhauser, J. C., and Winans, J. G., 1956, *Spectroscopia Molecular*, **5**, 18.
Mandel, M., and Barrett, A. H., 1955, *Phys. Rev.*, **98**, 1159.

REVIEWS OF BOOKS

Thermal Power from Nuclear Reactors, by A. S. THOMPSON and O. E. RODGERS. Pp. xiii + 229. (New York: John Wiley; London: Chapman and Hall, 1956.) 58*s*. (For a review see *Proc. Phys. Soc.* B., 1957, **70**, p. 713.)

Robert Hooke, by MARGERET 'ESPINASSE. Pp. vii + 192. (London: Heinemann, 1956). 21*s*.

All who have occasion to dip into the history of the formative century of modern science in almost any field—biology, physiology, chemistry, astronomy, physics—are bound to come across the work of Hooke which, as often as not, includes the decisive first step of systematic observation and experiment. In the history of scientific institutions he more than any other, as Curator of Experiments for the new Royal Society, provided the model for the scientific research of the future. Because he was so many sided it is difficult to see his life as a whole, though after the publication of his diaries we know more about his life than any other seventeenth century scientist. We are therefore particularly grateful to Mrs. 'Espinasse for her all-round study of Robert Hooke which presents him in the social environment of his time and helps to show the reasons both for his successes and his failures.

The failures were not in science, for he succeeded so well that in many fields his work was not bettered for a hundred years, but in getting due recognition for his work. The neglect of Hooke's achievements Mrs. 'Espinasse puts down mostly to the determined spite of Newton, under whose influence science in Britain took on for a century a highly mathematical, philosophical turn quite foreign to the lively practical interests of Hooke. But all through his life Hooke suffered, although for the most part he took it very well, from having to be second to other men, wealthier, more pushful and only scarcely more talented than himself. He started as an assistant to Boyle, and science owes the air pump and ' Boyle's law ' to him. In the Royal Society he suffered for years the animosity of the Secretary, Oldenburg. He saw his invention of the balance spring clock taken by Huyghens after some very dubious procedures on which Mrs. 'Espinasse throws much light. His greatest theoretical achievement, the enunciation of the inverse square law of gravitation, which he may well have done before Newton, only brought him trouble. Finally, in his architectural work he followed a most willingly acknowledged master, Wren. To be second to such giants is itself a title to greatness but Hooke certainly deserves more than that. The fame that is only now coming to him he missed in his time because he did not seek it; he was more interested in understanding and mastering nature and art than making a great name and place for himself. What he actually did for science is not to be found in any of his works taken separately, but rather in the general impulse he gave to experimental science, building up a tradition which, whether it acknowledged its debt to Hooke or not, has continued and flourished to this day. It still remains with its insistence on the primacy of experiment and its distrust of a prior theory specially characteristic of British science.

Mrs. 'Espinasse's book, admirably illustrated from the *Micrographia* and his other works, would furnish to those who know little of Hooke, except Hooke's law or Hooke's universal joint, an admirable picture of the man in the round; to those to whom he is already a favourite she presents a new aspect of his personality and has many penetrating things to say. Not everyone will agree with her judgment of Newton but we cannot doubt that he failed to give Hooke his due.

J. D. BERNAL.

Matrix Calculus, by E. BODEWIG. Pp. xii + 344. (Amsterdam : North Holland, 1956.) 53*s*.

The subject matter of this book is linear algebra—the solution of simultaneous linear equations, the inversion of matrices, and the determination of latent roots and vectors. It would be difficult to think of any branch of mathematics which has a wider range of application : all branches of engineering and applied physics and applied statistics depend heavily on it. It is a branch of mathematics which exists at several levels. At the foundation is the basic theory, as taught to, say, second year undergraduates, and on this are erected layers concerned with numerical problems arising from practical applications of the basic theory, in successively increasing degrees of sophistication. These are associated with ' failing cases '—the difficulties which arise in the attempted inversion of a nearly singular matrix, for example, or the evaluation of the vectors associated with nearly coincident latent roots.

It will be readily appreciated that this is a subject whose study has been greatly accelerated by the availability of electronic computers. Large stocks of results and methods are coming forward from all sides, and what one needs now is a critical comparative survey by an author whose all-seeing eye enables him to unify the mass of material available, without ever allowing his work to degenerate into a mere catalogue.

This is admittedly asking a lot. There are parts of Bodewig's book which are pure catalogue, but it must be admitted that there are also parts where he has succeeded in giving a critical unifying survey, notably in his discussion of the various iterative methods of solving linear equations. The quality of the writing fluctuates between these two levels throughout the book. Even the catalogue level, however, is of value in that the results listed are mainly recent and often difficult of access elsewhere, many having previously appeared only in the original papers. Of the 111 references cited in the bibliography, about two thirds are of post-war date. There is also a useful index.

The book is divided into four sections. Part I, Matrix Calculus, gives an account of basic matrix algebra; Part II deals with the solution of linear simultaneous algebraic equations, including a brief discussion of ill-conditioned systems, Part III with the inversion of matrices, and Part IV with eigenvalue problems, both direct and iterative methods being discussed throughout.

One slightly unexpected item is the detailed discussion of ' geodetic matrices ', that is to say, matrices of the type which arise in the normal equations of least squares obtained from the reduction of triangulated survey data.

An aspect of the book which invites comment is the Dutchness of the English in which it is written. It is probably fair to say that at no point is it impossible to penetrate to the author's meaning, but his usages are often confusing, being nearly enough right to have *a* meaning, but not quite the meaning intended. It has evidently been written direct in English by the author (a praiseworthy achievement) and never subsequently vetted.

One other idiosyncratic aspect of the book is the author's refreshing and unashamed enthusiasm for his notation. This depends on a consistent use of matrix concepts, with free use of partitioning, and with the basic building bricks of a matrix taken to be its vectors (rows or columns) and not its scalar elements. This is in the reviewer's opinion the correct way to teach and use matrices, though it is perhaps not as novel as the author claims.

To conclude, the book furnishes an adequate account of the basic theory and a reasonably complete summary of recent developments over the whole field of practical linear algebra. Workers having problems of numerical evaluation in this field will find it an extremely useful handbook. E. H. LLOYD.

Spheroidal Wave Functions (*including table of separation constants and coefficients*), by J. A. STRATTON, P. M. MORSE, L. J. CHU, J. D. C. LITTLE and F. J. CORBATÓ. Pp. xiii+613. (New York: John Wiley, and Technology Press of M.I.T., jointly; London: Chapman and Hall, 1956.) £5.

We are still far from having adequate tables of all special functions which arise when the scalar wave equation is separated in various three-dimensional coordinate systems. Wave functions associated with the rectangular box, the sphere and circular cylinder are fairly well tabulated; those for the elliptic and parabolic cylinders are either well advanced or being actively pursued, and the spheroids, prolate and oblate, are certainly comparable with these in importance.

This volume represents a stage—but only a stage—in the provision of spheroidal wave functions, and to those who have already benefited from the earlier tables of Stratton, Morse, Chu and Hutner, it is a welcome reminder that this effort, initiated some 25 years ago, is continuing. The task is a major one, because in addition to the continuous variables there are three parameters to consider, two integral parameters l and m (which in the language of quantum mechanics are the angular momentum and magnetic quantum numbers) and the continuous parameter h (or g) representing the number of wavelengths in the interfocal distance of the prolate spheroid, or in the focal diameter of the oblate spheroid.

The stage reached is that in which the regular radial wave function is expanded as a series in spherical Bessel functions, and the angular function in terms of Legendre functions. The coefficients in both series, and values of the mutual separation constant, are tabulated to 7 significant figures, for $l, m = 0(1)8$ ($l \geqslant m$) and h (or g) $= 0(0 \cdot 1)1(0 \cdot 2)8$. Thus these coefficients, combined with existing tables of spherical Bessel functions and Legendre polynomials, offer scope for numerous applications in physical problems. Nevertheless, it is expected (and to be hoped) that actual tables of spheroidal wave functions will become available in the future.

A feature of the present production is that both calculation and printing were carried out as a single process on the Whirlwind computer at the Massachusetts Institute of Technology. This gave rise to obvious technical problems in planning the printing layout of the tables, but the result is reasonably satisfactory. However, a more detailed index to the tables would have been useful

It is an interesting comment on modern developments that most of the programming was completed in six months, and the time of production on the machine was about ten hours. R. A. BUCKINGHAM.

Advanced Calculus, by R. C. Buck. Pp. viii + 423. (New York: McGraw-Hill, 1956.) (International Series in Pure and Applied Mathematics). 64*s*.

In this valuable book the author treats with care a number of subjects which are not easily accessible elsewhere, as well as a certain amount of more routine material. In the systematic account of Riemann integration, transformations of Euclidean space and their inverses and change of variable in integration and differentiation, the emphasis is always on several variables. Line and surface integrals are dealt with and there is an introduction to differential geometry, vector analysis and the theorems of Green, Gauss and Stokes, which are treated by means of the formalism of Cartan's exterior differential calculus. The book finishes with a short account of the calculus of variations and a 6-page appendix on the real number system.

Further topics treated include elements of limits, mean value theorems and l'Hôpital's rule, set theory and the study of continuous functions on compact and connected sets, and theory of series including power series and uniform convergence, but not Fourier series.

The treatment is rigorous and reasonably complete. In the more difficult cases the author refers to other monographs from time to time or gives the proof only in a simple special case. This technique is probably inevitable when dealing with, for instance, the complexities of Stokes' theorem. On the other hand it may be worth while in a future edition to include a proof that a linear transformation $T(x)$ in Euclidean space multiplies volumes by det T instead of referring the reader to an algebra textbook. For this result is used as a key theorem in all the subsequent work on transformations of multiple integrals in Chapter VI. Consequently, the reader is left in some doubt as to what has really been proved.

However, this is a minor criticism and is in any case a matter of taste. This book will be valuable for mathematicians and scientists who want the formulae and techniques of advanced calculus and are prepared to face some mathematical difficulties in order to see things done properly. There are many excellent examples to illustrate the text. These are starred in accordance with their difficulty. The ordinary one would be suitable for undergraduates in mathematics, and two star examples for exceptionally brilliant men. However, hints of solutions are given. There is an index and a list of suggested books for further reading at the back. The printing is excellent. W. K. HAYMAN.

BOOK NOTICES

Les fondements de la chimie théorique. Mecanique ondulatorie appliquée a l'étude des atomes et des molécules, by R. Daudel. Pp. x + 236. (Paris: Gauthier-Villars, 1956.) 3500 *fr*.

CONTENTS OF SECTION B

PAGE

Mr. M. Redwood. Dispersion Effects in Ultrasonic Waveguides and their Importance in the Measurement of Attenuation 721

Mrs. L. M. Roberts. The Atomic Heats of Calcium, Strontium and Barium between 1·5°K and 20°K 738

Mrs. L. M. Roberts. The Atomic Heats of Lithium, Sodium and Potassium between 1·5°K and 20°K 744

Dr. A. D. Buckingham. The Influence of a Strong Magnetic Field on the Dielectric Constant of a Diamagnetic Fluid 753

Mr. J. J. O'Dwyer. The High Temperature Dielectric Breakdown of Alkali Halides 761

Dr. J. A. Reynolds and Mr. J. M. Hough. Formulae for Dielectric Constant of Mixtures 769

Dr. T. S. Moss, Dr. S. D. Smith and Mr. T. D. F. Hawkins. Absorption and Dispersion of Indium Antimonide 776

Dr. W. A. Little. The Overhauser Effect in Solids 785

Dr. G. S. Bogle, Dr. J. N. Dodd and Mr. W. L. McLean. Hyperfine Structure Coupling Constant of the 6s6p $^3P_1$ Level of ^{199}Hg by Double Resonance . . 796

Research Notes :

Dr. F. W. G. Rose. The Mass Action Laws for the Reactions between Free Carriers and Impurities in Semiconductors considering the Electron Spin 801

Letters to the Editor :

Mr. P. D. Southgate. Internal Friction of Single Crystal Silicon from 25°C to 1100°C 804

Reviews of Books 807

Book Notices 814

Contents of Section A 816

Photoproduction of Pions at Complex Nuclei

By E. W. LAING and R. G. MOORHOUSE
Natural Philosophy Department, University of Glasgow

MS. received 14*th March* 1957, *and in revised form* 16*th May* 1957

Abstract. The production of charged pions at complex nuclei is calculated on the basis of a simple independent particle model for the nucleus. The primary photoproduction is assumed to be a single nucleon process in which the struck nucleon undergoes transitions into discrete or continuum states. Two points of view are adopted, (*a*) that production may take place inside the nucleus; (*b*) that only surface production is allowed, according to the model of Wilson and of Butler. Cross sections are obtained for two nuclei, ^{11}B and ^{40}Ca. Available experimental data are inconsistent with surface production.

§ 1. INTRODUCTION

In the photoproduction of pions from complex nuclei it is observed that the cross section is significently reduced from the cross section of the corresponding number of free nucleons. In an early calculation Lax and Feshbach (1951) take a Goldberger-Chew momentum distribution for the nucleons in the nucleus and insert, with some inevitable uncertaintv. the photoproduction cross section from free nucleons to find the cross section for photoproduction of pions from carbon. Agreement with experiment was obtained, the reduction from the corresponding free nucleon cross section being due to kinetic considerations of momentum distribution. Thirring (1953) in more extensive but rather similar work compared the photopion energy spectra and angular distributions from various nuclear momentum distributions, and concluded that an $\exp(-p^2)$ momentum distribution best fitted the existing experiments. However an anomalously large π^+/π^- ratio, which could not be simply explained, was observed (Littauer and Walker 1952). Butler (1952) assumed that pion production is suppressed in the nuclear core and gave arguments to show that agreement with the π^+/π^- ratio and the observed $A^{2/3}$ law for total photoproduction could thus be obtained. George (1956) finds evidence for this surface production model from his experiments on the photoproduction of stars and pions in nuclear emulsions. One aim of this present paper is to give more detailed calculations using the surface production model than have hitherto been presented. Our assumptions (1) (4) below are the same as those of Butler, except for (3); he uses plane waves for the struck nucleon.

Several assumptions will be made in calculating pion photoproduction at complex nuclei:

(1) That the primary photoproduction is essentially a single nucleon process.

(2) That the nucleons in the struck nucleus are taken to be bound in a potential well, which may be different for neutrons and protons. Interparticle forces and spin-orbit coupling are neglected. Thus we have a simple independent particle model for the nucleus.

(3) Consistent with assumptions (1) and (2), we assume that in the primary process the struck nucleon goes into a discrete or continuum state, and that the nuclear potential is unchanged during this transition.

(4) After production, the pion may be scattered or absorbed by other nucleons in the nucleus, and this effect may be taken into account by an optical model.

It is in assumption (1) that the major uncertainty lies. In the actual calculations the matrix element for production at a free nucleon is used; some points must, therefore, be noted: (i) Even if the other nucleons present do not affect the photoproduction, the process is off the energy shell for a free nucleon (the energy–momentum relations would be different from the free nucleon case, causing a change in the matrix element). This difficulty can be resolved only by a proper field theoretical treatment. (ii) The pion production in fact does not take place as if no other nucleons were present. Their presence is felt through operation of the Pauli principle and interparticle forces, which will be most important in the nuclear core and may lead to competing photodisintegration processes (Wilson 1952), which, combined with pion scattering and absorption inside the nucleus, will cause a suppression of pion production from the core. The extreme view that only nucleons at the nuclear surface contribute to pion production has been assumed by Butler (1952) who succeeds thereby in explaining qualitatively the $A^{2/3}$ law and the trend in the π^-/π^+ ratio found by Littauer and Walker (1952) for the range $7 \leqslant A \leqslant 209$.

In our calculation, we consider both surface and volume production, assuming that only the outer nucleon shells, on our model, contribute.

Concerning assumption (3) above, it is possible in a few cases to measure the cross section in which the struck nucleon is left in a discrete state. We take as an example for this the process (*a*) $^{11}\mathrm{B}(\gamma, \pi^-)^{11}\mathrm{C}$. Reactions of this bound state type have not hitherto been considered. Another type of reaction is that where continuum states must also be included. This occurs when we measure the pions only, and not the residual nucleus. For this case, we consider the processes (*b*) $^{40}\mathrm{Ca}(\gamma, \pi)^{40}\mathrm{X}$ and $^{40}\mathrm{Ca}(\gamma, \pi\mathrm{n})^{39}\mathrm{Y}$, where π is a charged pion, n the ejected nucleon, and X, Y are the appropriate residual nuclei. Some results for (*b*) have been reported by Hogg and Sinclair (1956). Preliminary results for (*a*) have also been obtained (Hughes and March 1957).

§ 2. GENERAL FORMALISM

The differential cross section for pion photoproduction at complex nuclei by a monochromatic photon beam is

$$\frac{d\sigma(\nu)}{d\mathbf{k}\,d\mathbf{q}} = \frac{1}{(2\pi)^2}\sum_f |\langle f|T|i\rangle|^2 \delta(E_f - E_i)\delta(\boldsymbol{\nu} - \mathbf{k} - \mathbf{q}) \qquad \ldots\ldots(1)$$

where $\boldsymbol{\nu}$ = photon momentum, $\mathbf{k}$ = pion momentum and $\mathbf{q}$ = momentum transferred to struck nucleon = $\mathbf{n}-\mathbf{p}$, where $\mathbf{p}$, $\mathbf{n}$ are initial and final nucleon momenta, E_i, E_f = total initial and final energies of system, $|i\rangle$, $|f\rangle$ = initial and final nuclear wave functions, T = general operator for photopion production at a system of nucleons.

The following approximations are made in T:

$$T = \sum_\lambda T_\lambda \qquad \ldots\ldots(2)$$

where T_λ = operator for pion production at the λth nucleon

$$=(\mathbf{K}\,.\,\boldsymbol{\sigma}^{(\lambda)}+L)\exp i(\boldsymbol{\nu}-\mathbf{k})\,.\,\mathbf{r}_\lambda \qquad \ldots\ldots(3)$$

(charge conservation is implied).

$\mathbf{K}$, L are functions $\mathbf{K}(\boldsymbol{\nu}, \mathbf{k}, \mathbf{p}, \mathbf{n})$ and $L(\boldsymbol{\nu}, \mathbf{k}, \mathbf{p}, \mathbf{n})$ which are approximated by $\mathbf{K}(\boldsymbol{\nu}, \mathbf{k}, 0, \boldsymbol{\nu}-\mathbf{k})$, $L(\boldsymbol{\nu}, \mathbf{k}, 0, \boldsymbol{\nu}-\mathbf{k})$. Investigation shows that this is a reasonable approximation when the uncertainty due to being off the energy shell for free nucleon production is remembered.

A consequence of equation (2) is that only single particle transitions are allowed between initial and final nuclear states. Use is made of this fact when $|i\rangle$ and $|f\rangle$ are expanded in terms of products of single particle wave functions. Thus, when we evaluate $\langle f|T_\lambda|i\rangle$ we expand the nuclear wave functions showing the explicit dependence on $\mathbf{r}_\lambda$ only. We then find that $\langle f|T_\lambda|i\rangle$ is independent of λ (provided of course that $|f\rangle$ and $|i\rangle$ are properly anti-symmetrized). Thus, we obtain

$$\langle f|T|i\rangle = N\langle f|T_\lambda|i\rangle \qquad \ldots\ldots(4)$$

where N is the number of nucleons (of appropriate charge) in the nucleus.

Finally, we have to perform the sum over final states, which in general include both bound states and continuum states of the struck nucleon. Further, if the struck nucleus has non-zero spin J, an average over the z-component J_z must also be performed.

§ 3. PION PHOTOPRODUCTION AT ^{11}B

In this case we consider only the reactions

$$(\alpha)\ {}^{11}\mathrm{B}(\gamma, \pi\ )^{11}\mathrm{C} \quad \text{and} \quad (\beta)\ {}^{11}\mathrm{B}(\gamma, \pi^-)^{11}\mathrm{C}^*.$$

Surface production of pions from the $1s_{1/2}$ shell will be negligible. Thus, only the outer $1p_{3/2}$ shell will be considered in the initial state. For comparison, volume production from the outer shell will also be evaluated. The final states of the struck nucleon are $1p_{3/2}$ for the reaction (α) and $1p_{1/2}$, $1d_{5/2}$, $2s_{1/2}$, $1d_{3/2}$, for the reaction (β). The nucleons are assumed to be bound in an oscillator central potential, and the difference in energy between the 1p and 1d shells is neglected, as also is the difference in neutron and proton binding energies, and the recoil energy of the struck nucleus.

Let

$$|M|^2 = \sum_f |\langle f|T|i\rangle|^2$$

(averaged over initial spin directions). Then

$$\frac{d\sigma(\nu)}{d\mathbf{k}\,d\mathbf{q}} = \frac{1}{(2\pi)^2}|M|^2\,\delta(\boldsymbol{\nu}-\mathbf{k}-\mathbf{q})\,\delta(\nu-\omega_k) \qquad \ldots\ldots(5)$$

where ν, ω_k = photon, pion energy and $\delta(\nu-\omega_k)$ is the result of the approximations above in E_i and E_f.

In this process, where only the ^{11}C is measured, we are interested finally in $\sigma(\nu)$. It is more convenient to eliminate $\mathbf{k}$ firstly, and obtain

$$\frac{d\sigma(\nu)}{d\mathbf{q}} = \frac{1}{(2\pi)^2}|M|^2\delta(\nu-\omega_k) \qquad \ldots\ldots(6)$$

where now, $\omega_k{}^2=(\boldsymbol{\nu}-\mathbf{q})^2+\mu^2=\nu^2+q^2-2\nu q\zeta+\mu^2$ and we have taken $\boldsymbol{\nu}=(\nu, 0, 0)$, $\mathbf{q}=(q, \Theta, \Phi)$ and $\zeta=\cos\Theta$.

We thus obtain for $\sigma(\nu)$

$$\sigma(\nu) = \frac{1}{2\pi}\int_{q_{\min}}^{q_{\max}} |M|^2 q\,dq \qquad \ldots\ldots(7)$$

where $q_{\min}, q_{\max} = \nu - (\nu^2 - \mu^2)^{1/2},\ \nu + (\nu^2 - \mu^2)^{1/2}$.

Using properly antisymmetrized wave functions $|i\rangle$ and $|f\rangle$ we obtain

$$(\alpha)\ |M|^2 = \tfrac{1}{4}\sum_{mm'} \left|\int d\mathbf{r}\, e^{i\mathbf{q}.\mathbf{r}}\, \mathcal{Y}^{m'\dagger}_{3/2,1,1/2}(\theta\phi)(\mathbf{K}\,.\,\boldsymbol{\sigma} + L)\mathcal{Y}^{m}_{3/2,1,1/2}(\theta\phi) f_1^{\,2}(r)\right|^2 \quad \ldots\ldots(8)$$

$$(\beta)\ |M|^2 = \sum_{mm'f} \left|\int d\mathbf{r}\, e^{i\mathbf{q}.\mathbf{r}}\, \mathcal{Y}^{m'\dagger}_{jl1/2}(\theta\phi)(\mathbf{K}\,.\,\boldsymbol{\sigma} + L)\mathcal{Y}^{m}_{3/2,1,1/2}(\theta\phi) f_l(\mathrm{r}) f_1(r)\right|^2 \quad \ldots\ldots(9)$$

where the f-summation is now over all possible j,l.

$\mathcal{Y}^{m}_{jl1/2}(\theta\phi)$ is a normalized angular momentum eigenfunction, $f_l(r)$ is the normalized radial function in an oscillator well corresponding to the 2s, 1p, 1d states for $l = 0$, 1, 2.

In both (8) and (9) there occurs a factor of the form

$$(\mathbf{K}\,.\,\boldsymbol{\sigma} + L)_{s's}(\mathbf{K}\,.\,\boldsymbol{\sigma} + L)_{tt'}$$

where $\mathbf{K} = (K_1, K_2, K_3)$, and s, s′, t, t′ are the spin variables. Conservation of the z-component of total angular momentum implies that $s - s' = t - t'$

$$\text{thus, either } s \neq s',\ \mathrm{s} = t,\ s' = t' \qquad \ldots\ldots(10)$$

$$\text{or } s = s',\ t = t'. \qquad \ldots\ldots(11)$$

Equation (10) implies that K_1, K_2 occur only in the combination $K_1{}^2 + K_2{}^2$; (11) implies that L, K_3 occur only in the combinations $(L + K_3)^2$, $(L - K_3)^2$, $L^2 - K_3{}^2$. However, by considering the terms in (m, m') and $(-m, -m')$ in $|M|^2$ we obtain the result that to every term in $|M|^2$ containing a factor $(L + K_3)^2$ there corresponds a term with $(L - K_3)^2$. Hence, (10) and (11) together show that L, K_i occur only in the combinations L^2, $K_3{}^2$, $K_1{}^2 + K_2{}^2$. We may express this in the relation

$$(\mathbf{K}\,.\,\boldsymbol{\sigma} + L)_{s's}(\mathbf{K}\,.\,\boldsymbol{\sigma} + L)_{tt'} \longrightarrow \qquad \ldots\ldots(12)$$
$$(L^2 - K_3{}^2)\delta_{ss'}\delta_{tt'} + (K_1{}^2 + K_2{}^2)\delta_{st}\delta_{s't'} + (2K_3{}^2 - K_1{}^2 - K_2{}^2)\delta_{st}\delta_{s't'}\delta_{ss'}.$$

We note also that

$$\sum_{s'} \delta_{s't'}(\mathbf{K}\,.\,\boldsymbol{\sigma} + L)_{s's}(\mathbf{K}\,.\,\boldsymbol{\sigma} + L)_{tt'} = (K^2 + L^2)\delta_{st}. \qquad \ldots\ldots(13)$$

It is found that the major contribution to $\sigma(\nu)$ is from the transitions $1\mathrm{p}_{3/2} \rightarrow 1\mathrm{d}_{3/2,\,5/2}$, calculation of which involves equation (13). For the other transitions, which involve equation (12), we can then approximate by assuming $K_3{}^2 = (K_1{}^2 + K_2{}^2)/2$. This makes a negligible difference to $\sigma(\nu)$. Equation (12) then becomes

$$(L^2 - \tfrac{1}{3}K^2)\delta_{ss'}\,\delta_{tt'} + \tfrac{2}{3}K^2\delta_{st}\,\delta_{s't'}. \qquad \ldots\ldots(14)$$

The effect of this approximation is to make $|M|^2$ independent of Θ, Φ. We may replace $\exp i\mathbf{q}\,.\,\mathbf{r}$ by $\exp iqr\cos\theta$ in equations (8) and (9). The evaluation of $|M|^2$ now proceeds according to standard methods. The sums over magnetic quantum numbers are effected by using properties of Clebsch–Gordan and Racah coefficients, yielding the general result

$$\sum_{mm'} \left|\int d\mathbf{r} \exp iqr\cos\theta\ \mathcal{Y}^{m'\dagger}_{jl1/2}(\theta\phi)(\mathbf{K}\,.\,\boldsymbol{\sigma} + L)\ \mathcal{Y}^{m}_{3/2111/2}(\theta\phi) f_l(r) f_1(r)\right|^2$$
$$= \sum_{\lambda} 4(2j+1)(l100|l1\lambda 0)^2[R^{\lambda}_{l1}(q)]^2$$
$$\times [3(2l+1)W^2(\tfrac{3}{2}1jl;\ \tfrac{1}{2}\lambda)(L^2 - \tfrac{1}{3}K^2) + \tfrac{2}{3}K^2] \quad \ldots\ldots(15)$$

where Clebsch–Gordan and Racah coefficients are in the usual notation.

$$R^{\lambda}{}_{l1}(q)=\int_{a}^{\infty} j_{\lambda}(qr)f_{l}(r)f_{1}(r)r^{2}dr \qquad \ldots\ldots(16)$$

where $a=0$ for volume production, $a=$ nuclear radius R for surface production.

For transitions to the d–shell, we obtain the simpler result

$$4(K^{2}+L^{2})\sum_{\lambda}(2l+1)(l100|l1\lambda0)^{2}[R^{\lambda}{}_{l1}(q)]^{2}. \qquad \ldots\ldots(17)$$

We note the radial functions used

$$\left.\begin{aligned} f_0&=N_0(2\beta r^2-3)\exp(-\tfrac{1}{2}\beta r^2)\\ f_1&=N_1 r\exp(-\tfrac{1}{2}\beta r^2)\\ f_2&=N_2 r^2\exp(-\tfrac{1}{2}\beta r^2)\end{aligned}\right\} \qquad \ldots\ldots(18)$$

where N_0, N_1, N_2 are normalization constants and β is fixed by imposing the condition

$$R^{2}=\langle r^{2}\rangle_{f_1}=5/2\beta. \qquad \ldots\ldots(19)$$

Taking $R=11^{1/3}$, in units $\hbar=c=\mu=1$ we obtain, from equation (19), $\beta=0{\cdot}5$. For volume production, $R^{\lambda}{}_{l1}(q)$ is an analytic function of q and $\sigma(\nu)$ can also be evaluated analytically. For surface production, $R^{\lambda}{}_{l1}(q)$ and $\sigma(\nu)$ are obtained by numerical methods.

To obtain numerical results we note that, with the photon energies available (variable $\nu_{\max}\leqslant 330$ MeV), together with the fact that a *total* cross section is required, it is reasonable to assume that the main contribution arises from S–wave mesons. Accordingly, we take

$$K^{2}+L^{2}=C/\nu\omega_{k}=C/\nu^{2} \qquad \ldots\ldots(20)$$

$C\ 2\pi$ is taken to be 10^{-28} cm^2 for agreement with the magnitude of photoproduction at free nucleons. In the cases where K^2, L^2 do not appear in the ‘free particle’ combination (20) we find that there is no appreciable difference in the cross section when we assume the two limiting cases $K^2\gg \mathrm{L}^2$ and $K^2\ll L^2$. Results of the calculation are given in table 1. ν is the photon energy in units of the pion mass. The suffices s, v denote surface and volume production respectively, and $\sigma(\nu)$ is given in units of 10^{-28} cm^2. Preliminary experimental results (Hughes and March 1957) indicate a lower limit to the cross section approximately 1×10^{-28} cm^2. This result cannot be explained by surface production alone.

Table 1. Total Cross Section $\sigma(\nu)$ for Photoproduction of Pions at ^{11}B

ν	1·2	1·4	1·6	1·8	2·0	2·2
$\sigma_s(\nu)$	0·39	0·37	0·29	0·24	0·21	0·18
$\sigma_v(\nu)$	2·20	2·10	1·79	1·44	1·16	0·96

§ 4. PION PHOTOPRODUCTION AT ^{40}CA

We consider in this section charged pion photoproduction at ^{40}Ca in which the final state of the struck nucleon can be either (i) bound or (ii) in the continuum. The initial nuclear state is now a closed shell, with zero angular momentum, and only complete shells are available for the final state of the struck nucleon.

In this part we are interested in the π^-/π^+ ratio and angular distribution of the emitted pions and because of the former, we must not neglect differences in the binding energies of protons and neutrons. However, the recoil energy of the residual nucleus is still negligible. In this calculation we evaluate the cross section $d\sigma(\nu)/d\mathbf{k}$ integrated over the bremsstrahlung spectrum $f(\nu)$,

$$\int_{\mu}^{\nu_{\max}} \frac{d\sigma(\nu)}{d\mathbf{k}} f(\nu)d\nu$$

where

$$\frac{d\sigma(\nu)}{d\mathbf{k}} = \sum_{f} \frac{1}{(2\pi)^2}|M|^2\delta(E_i-E_f) \qquad \ldots\ldots(21)$$

and

$$E_i-E_f=\nu-\omega_k+\Delta \qquad \ldots\ldots(22)$$

For case (i) (bound final nucleon), Δ is the difference in binding energies of the struck nucleon. For case (ii) (continuum state final nucleon), Δ = initial binding energy + final kinetic energy of the struck nucleon.

The wave functions are constructed in a similar manner to those of § 3, but instead of an oscillator potential we now use a square well, which is better suited to the treatment of the continuum. The radius of the well in ^{40}Ca is taken to be $4{\cdot}9\times10^{-13}$ cm and the depths (different for neutron and proton) are then fitted to give the correct binding energy of the last added neutron and proton (taken to be 15·9 and 8·4 MEV respectively). The result for $d\sigma(\nu)/d\mathbf{k}$ obtained by similar methods to those of § 3 is

$$d\sigma(\nu)/d\mathbf{k}=\frac{1}{(2\pi)^2}\sum_{nln'l'\lambda} 2(K^2+L^2)(2l+1)(2l'+1)(l'l00|l'l\lambda 0)^2[R^{\lambda}_{nl,n'l'}(q)]^2 \times\delta(E_i-E_f) \qquad \ldots\ldots(23)$$

with the same notation as before except that

$$R^{\lambda}_{nl,n'l'}(q)=\int_{a}^{\infty} j_{\lambda}(qr)f_{n'l'}(r)f_{nl}(r)r^2dr.$$

The summation over nl, $n'l'$ is over all initial and final orbital angular momentum states. In our case, nl = 1s, 1p, 2s, 1d (though for reasons given below the first two are omitted). When the struck nucleon goes into a bound state finally, $n'l'$ = 2p, 1f (π^+ production) and 1f(π^- production).

In the continuum case, $n'l'$ take any value, in principle. For the treatment of the nucleon continuum final states the method of partial waves should be used as in equation (23) to take into account the distortion by the potential wells. However, in our calculation, we have evaluated the differential cross section at meson angles $\Theta = 30°$, 90° 150° to the photon beam. We find that only at 30° is the number of partial waves necessary small enough to make the distorted wave treatment possible. It is at 30°, however, that the distortion is most important, since the momentum transfer $\mathbf{q}$ decreases with angle and so the effects of the potentials will be greatest.

Thus, at 90° and 150° a plane wave approximation is used for the continuum states.

We consider primarily production from the nuclear surface, that is, outside the nuclear radius R. For this, the 1s and 1p initial states make very little contribution as the number of nucleons in the surface in these states is small compared with the number of nucleons in the 2s and 1d states. Further, Δ (in equation (22)) is larger and the overlap integrals will, in general, be smaller. Consequently only contributions from initial 2s and 1d states are considered. At 30°, the method of partial waves is used.

At 90°, 150°, the final nucleon function is taken to be $(2\pi)^{-3/2} \exp i\mathbf{n}\,.\,\mathbf{r}$ and integration over all $\mathbf{n}$ gives from equations (21) and (23)

$$\frac{d\sigma(\nu)}{d\mathbf{k}} = \sum_{l=0,2} \int_0^{n_{\max}} \frac{2\pi n}{q}\, dn \int_{|q-n|}^{q+n} p\,dp\,|T_l(p)|^2 2(2l+1)(K^2+L^2) \qquad \ldots\ldots(24)$$

$n_{\max}$ is given by $\nu_{\max} = \omega_k + n_{\max}{}^2/2M + \mathrm{B.E.}$

$$T_l(p) = \frac{R^2}{p^2+\beta^2}[p j_{l-1}(pR) h_l^{(1)}(i\beta R) - i\beta j_l(pR) h^{(1)}{}_{l-1}(i\beta R)] \qquad \ldots\ldots(25)$$

where $\beta^2/2M$ is the binding energy of the lth state nucleon. $T_l(p)$ is essentially the Fourier transform of the part of the lth state wave function outside the nuclear radius R. K^2+L^2 in equation (24) is taken to be the matrix element for production of a meson at a free stationary nucleon by a photon of appropriate energy $\nu = \omega_k + n^2/2M + \mathrm{B.E.}$ We use the photoproduction data for positive pions given by Walker, Teasdale, Peterson and Vette (1955) and Tollestrup, Keck and Worlock (1955), and the π^-/π^+ ratio given by Watson, Keck, Tollestrup and Walker (1956).

For the sake of comparison, the photoproduction from the 1d and 2s shells is also evaluated, assuming production from the whole nucleus (volume production). In the continuum case at $\Theta = 30°$ the method of partial waves is again employed; at 90°, 150°, a plane wave approximation is used, with nucleon momentum n', n inside and outside the nucleus respectively, satisfying $n'^2 = n^2 + 2MV$, V being the appropriate well depth.

Results are given in tables 2 and 3 for a bremsstrahlung spectrum $f(\nu) = 330/\nu$ ($\nu_{\max} = 330$ MeV).

Table 2. Differential Cross Section, $d\sigma/d\Omega dE$, for Surface Production of Pions in ^{40}Ca

Pion angle (deg)	Pion energy (MeV)								
	π^+			π^-			π^-/π^+		
	60	100	120	60	100	120	60	100	120
30	—	16 + 2·1	—	—	7·6 + 0·8	—	—	0·47	—
90	28	12	5·3	19	7	2·8	0·70	0·59	0·54
150	—	1·3	—	—	1·2	—	—	0·92	—

Table 3. Differential Cross Section, $d\sigma/d\Omega dE$, for Volume Production of Pions in ^{40}Ca

Pion angle (deg)	Pion energy (MeV)								
	π^+			π^-			π^-/π^+		
	60	100	120	60	100	120	60	100	120
30	—	33 + 66	—	—	50 + 43	—	—	0·93	—
90	139	142	111	165	135	96	1·21	0·95	0·82
150	—	53	—	—	53	—	—	0·99	—

§ 5. PION SCATTERING AND ABSORPTION

Until now the pion has been treated as if it did not interact with the rest of the nucleus after having been photoproduced at one nucleon. In fact, both scattering and absorption take place, and this may be investigated using an optical model. We consider the effect of scattering and absorption on the surface production only, and to this end we consider the modification of $T_l(p)$ in equation (24). Thus we neglect here the distortion of the wave function of the ejected nucleon and bear in mind the fact that for surface production ejection of nucleons into discrete states is an unimportant process. We take as an example the modification of $T_0(p)$ which corresponds to production from the 2s shell. For no meson scattering or absorption

$$T_0(p)=\int_R^\infty dr\, r^2 h_0^{(1)}(i\beta r)(4\pi)^{1/2}[j_0(pr)] \qquad \ldots\ldots(26)$$

and this is equation (25) with $l=0$.

$$p=|\mathbf{p}| \text{ satisfies } \mathbf{p}=\mathbf{n}+\mathbf{k}-\boldsymbol{\nu}.$$

If λ_s is the mean-free-path for scattering, λ_a for absorption and we assume, as a good approximation in surface production, that for a meson produced at distance r from the centre the nucleus has radius r, then equation (26) is modified so that

$$\begin{aligned}[j_0(pr)]\rightarrow[j_0(pr)+\sum_{l=0}^{\infty} i^l Y_l^0(\Theta')j_l(p'r)\int_{\pi/2}^{\pi} 2\pi Y_l^0(\theta)\exp(2r\cos\theta/\lambda_a)\sin\theta d\theta \\ -\sum_{l=0}^{\infty} i^l Y_l^0(\Theta)j_l(pr)\int_{\pi/2}^{\pi} 2\pi Y_l^0(\theta)\sin\theta d\theta] \qquad \ldots\ldots(27)\end{aligned}$$

where $\mathbf{p}'=\mathbf{n}+\mathbf{k}(1+2/k\lambda_s)-\boldsymbol{\nu}$, $\Theta=$angle between $\mathbf{k}-\boldsymbol{\nu}$ and $\mathbf{p}$ and $\Theta'=$angle between $\mathbf{k}(1+2/k\lambda_s)-\boldsymbol{\nu}$ and $\mathbf{p}'$.

Equation (27) arises as follows: $j_0(pr)$ is the zeroth order partial wave from $\exp[i(\mathbf{n}-\boldsymbol{\nu}+\mathbf{k}).\mathbf{r}]$. When absorption and scattering inside the nucleus are included we take instead, the zeroth order partial wave of the function $\{\exp i(\mathbf{n}-\boldsymbol{\nu}+\mathbf{k}).\mathbf{r},\ \theta<\pi/2;\ \exp i\,[(\mathbf{n}-\boldsymbol{\nu}).\mathbf{r}+(1+2/k\lambda_s-2i/k\lambda_a)\,\mathbf{k}.\mathbf{r}],\ \theta>\pi/2\}$ where $\mathbf{r}=(r,\theta,\phi)$ and where $\theta=0$ is the direction of $\mathbf{k}$.)

Thus in the limit of small λ_a, corresponding to production from a hemispherical shell, equation (26) becomes

$$T_0(p)=(4\pi)^{1/2}\int_R^\infty dr\, r^2 h_0^{(1)}(i\beta r)[j_0(pr)-\sum_{l=0}^{\infty} i^l Y_l^0(\Theta)\int_{\pi/2}^{\pi} 2\pi Y_l^0(\theta)\sin\theta d\theta]. \qquad \ldots\ldots(28)$$

Now, as given in § 6, the characteristic angular distribution for surface production of pions is due to the fact that $T_l(p)$ has a sharp maximum for small p. This leads to a larger cross section for smaller q in equation (24), corresponding to smaller pion angles, than for larger q (larger pion angles).

The maximum in $T_0(p)$, for example, is due to the fact that $j_0(pr)$ in equation (26) has a maximum for small p. The correction (27) or (28) tends to smooth out that maximum, and hence the maximum in $T_0(p)$. Similar considerations apply to $T_2(p)$. Hence the effect of scattering and absorption on surface produced pions is to reduce the forward peaking.

§ 6. RESULTS AND DISCUSSIONS

It has been shown that pion production from a suitable complex nucleus, without nucleon emission, is large enough to be observed. The experiment depends on observing the final nucleus and consequently the suitability of a particular initial nucleus depends on the non-existence of other processes leading to the same final nucleus.

In § 3, results of our calculation on ^{11}B were given in table 1, and a comparison was made with preliminary experimental results. Although we have concluded that surface production alone is unable to account for the observed data, no definite assertion can be made at this stage. However, it is hoped that fuller experimental data will shortly be forthcoming to enable a more detailed comparison between theory and experiment. We note, however, that whereas, in the production at ^{40}Ca, the main contribution arises from the transitions to the continuum, here no such transitions are allowed. An immediate consequence of this is that here we are much farther off the energy shell for a free nucleon. It may not then be permissible to insert the free nucleon cross section, as was done in § 3.

In table 2 is given the differential cross section for surface photoproduction of pions from ^{40}Ca for various pion energies and angles. This includes only production from the 2s and 1d shells; as stated in § 4 the surface production from the 1s and 1p shells is less than 1/3 of that from the outer shells. The sum $a+b$ occurs in the 30° row; a and b are the cross sections for the struck nucleon making a transition into continuum and discrete states respectively. The calculations are with the outgoing nucleon wave undistorted at 90° and 150° but distorted at 30°, where the effect of distortion is most important due to the fact that few partial waves contribute. (If the undistorted results at 30° were substituted the cross sections would be increased by $\sim 40\%$). In table 3 are given the exactly corresponding quantities for production from the whole nucleus, including the surface; (volume production). Table 4 gives the available relevant experimental cross sections (Hogg and Sinclair 1956). As is well known volume production is unable to account for the π^-/π^+ ratio in symmetrical nuclei, and this is illustrated in table 3, while the relative success of surface production in this respect is shown in table 2. However, the magnitude of the experimental cross section is absolutely incompatible with our surface production model and is of the order of the volume production from the 2s and 1d shells. When the contribution from the 1s and 1p shells is taken into account the volume production will be about twice the experimental result.

Table 4. Experimental Differential Cross Section $d\sigma/d\Omega dE$ for Photoproduction of Pions in ^{40}Ca

Pion energy (MEV)

Pion angle (deg)	π^+		π^-		π^-/π^+	
	60	100	60	100	60	100
90	105	94	93	70	0·9	0·75

A surface production picture (Butler 1952) was hypothesized for the following reasons: (i) volume production gives too large a cross section which is difficult to explain away by absorption because of the long mean free path of pions in nuclear matter (Francis and Watson 1953); however, this has never been fully investigated; (ii) it explains the $A^{2/3}$ dependence of the cross section; (iii) it explains the π^-/π^+ ratio. Wilson (1952) put forward a possible explanation of surface production as a 'magic' two-nucleon absorptive effect in pion photoproduction in the region of high nucleon density. Our calculations indicate that most of the cross section is from the volume production; that is, it comes from the region of high nucleon density (note that the nucleon density, with the radius of the square well taken as the surface boundary, as in our calculations, rises rapidly to its maximum inside that boundary). However, no definite conclusion can be drawn because the result may be model-dependent. For example, with nucleon distributions as indicated by electron scattering experiments (Scott 1956) a much larger proportion of nucleons is in the region of low nucleon density or surface; here surface production may be able to account for a major part of the cross section. On the other hand, with a model of this type a rather extreme difference between the neutron and proton distributions would appear to be required to give the correct π^-/π^+ ratio. This merely illustrates the general difficulty of fitting both the magnitude of the cross section and the π^-/π^+ ratio.

Butler uses an independent particle model but with no particular type of potential well, and gives general arguments to obtain a surface production cross section. The calculations given here for calcium, with a square well potential, do not sustain these general arguments though for other types of potential, as noted above, agreement with Butler's results may be attained. Even the attainment of these results would still leave half the cross section as due to volume production, and thus the $A^{2/3}$ dependence and the π^-/π^+ ratio largely unexplained.

Tables 2 and 3 also indicate a characteristic and expected difference between surface and volume production. Surface production is peaked in the forward direction and very small at 150°, while volume production shows a maximum around 90°. This may afford a further means of distinguishing between surface and volume production, though we must bear in mind that the forward peaking is reduced by effects of pion absorption and scattering inside the nucleus.

ACKNOWLEDGMENTS

The authors would like to thank Dr. I. Hughes, Dr. P. V. March, Dr. H. Muirhead and Mr. D. Sinclair for valuable discussions on their experiments and Professor J. C. Gunn for his continued interest.

REFERENCES

BUTLER, S. T., 1952, *Phys. Rev.*, **87**, 1117.

FRANCIS, N. C., and WATSON, K. M., 1953, *Amer. J. Phys.*, **21**, 659.

GEORGE, E. P., 1956, *Proc. Phys. Soc.* A, **69**, 110.

HOGG, W. R., and SINCLAIR, D., 1956, *Phil. Mag.*, **1**, 466.

LAX, M., and FESHBACH, H., 1951, *Phys. Rev.*, **81**, 189.

LITTHAUER, R. M., and WALKER, D., 1952, *Phys. Rev.*, **86**, 838.

SCOTT, J. M. C., 1956, *Progr. Nucl. Phys.*, **5**, 157.

THIRRING, W., 1953, *Helv. Phys. Acta*, **26**, 465.

TOLLESTRUP, A. V., KECK, J. C., and WORLOCK, R. M., 1955, *Phys. Rev.*, **99**, 220.

WALKER, R. L., TEASDALE, J. G., PETERSON, V. Z., and VETTE, J. L., 1955, *Phys. Rev.*, **99**, 210.

WATSON, K. M., KECK, J C., TOLLESTRUP, A. V., and WALKER, R. L., 1956, *Phys. Rev.*, **101**, 1159.

WILSON, R. R., 1952, *Phys. Rev.*, **86**, 125.

The Measurement of Fast Neutron Flux over the Neutron Energy Range 0·03 Mev to 3·0 Mev†

By W. D. ALLEN and A. T. G. FERGUSON
Atomic Energy Research Establishment, Harwell, Berks.

MS. received 26*th March* 1957, *and in amended form* 4*th June* 1957

Abstract. Measurements of neutron flux in the neutron energy region 0·03 Mev to 3·0 Mev have been made using a proton recoil counter and a Hanson-McKibben type long counter. Several proton recoil counters filled with different gases at different pressures have given flux measurements self-consistent to 2%. The long counter has been calibrated against photo-neutron sources at a number of energies and also against the recoil counter. The variation of its efficiency as determined by the two methods is in satisfactory agreement. The absolute calibration of the long counter with respect to a RdTh–D_2O source whose strength was known to $\pm 2\frac{1}{2}\%$ agreed with the calibration with respect to the recoil counter to 1%. A similar cross check with an Ra–Be source gave an initial discrepancy of 15% but this was traced to an error in the source strength and variation with energy in the response of the long counter. These cross checks are satisfactory and over the major portion of the energy range the standard error is not more than ±3%.

§ 1. General Introduction

A knowledge of the neutron flux is essential in any measurement of a neutron reaction cross section. Frequently, as for example in the case of the fission cross section, uncertainties in the neutron flux are the principal source of error. The subject of fast neutron flux measurements has been reviewed by Barschall *et al.* (1952) whose general conclusion was that at that time no flux measurement had been made with an accuracy closer than ±5%. Our work is an attempt to make measurements of greater accuracy than this.

Two instruments have been used; the proton recoil proportional counter filled with a hydrogenous gas, and a 'long counter' after the design by Hanson and McKibben (1947). With the proportional counter, flux measurements using different gases at different pressures in different counters have been shown to be consistent within 2% except between 1·5 Mev and 3·5 Mev. Here the technique is approaching its limits, and in the absence of suitable cross checks, flux measurements are rather less certain. The relative efficiency of the 'long counter' has been measured at a number of neutron energies using photo-neutron sources intercompared in a $MnSO_4$ bath, and was also obtained by comparison with the recoil counter. The two methods were consistent within their errors. The absolute efficiency of the long counter was obtained (*a*) by comparison with the recoil counter, (*b*) by calibration with 200 kev neutrons from the Oxford RdTh–D_2O source whose strength was known to 2–3%. The two calibrations agree to within 1%. The consistency of the recoil counter measurements and cross checks between different instruments allow us to claim to be able to estimate neutron flux with an accuracy to 2–3%. We should not leave unmentioned the considerable discrepancy encountered in attempting to calibrate the long counter with an Ra -Be source, a practice widely adopted in fast neutron flux measurements. The error lay, admittedly, largely in the assumed strength of the source; but, even if this were accurately known, we would not be confident of an accuracy to better than ± 5%.

---

† This paper should have been published with the authors' paper in the August issue (*Proc. Phys. Soc.* A, 1957, **70**, 573) on fission measurement, which is the logical sequel to the present paper on flux measurement.

Our measurements have shown that the long counter is much less flat in response than has been assumed by other workers. We have found a slow increase of 13% in efficiency between 0·1 MeV and 1·0 MeV and a drop of approximately 10% between 2·5 MeV and 3 MeV.

The remainder of this paper is divided into three sections. Section 2 describes the principles of the proportional counter, the measurement of the energy expended per ion pair and the estimation of the total number of proton recoils from the observed pulse height spectra. In addition some notes on target techniques and neutron energy checks are presented. Section 3 gives an account of the work on the long counter. In the final section a discussion of the flux measurements and their analysis and errors is given.

This paper incorporates work described in rather greater detail in Harwell reports on the recoil counter (Allen and Ferguson 1955 a) and on the long counter (Allen 1955).

§ 2. PROPORTIONAL COUNTER MEASUREMENTS

2.1. *Principle of the Proportional Counter*

When a hydrogenous gas is bombarded with fast monoergic neutrons, recoil protons are produced in the gas. If the mass of gas, the n–p cross section and the number of recoils is known, the neutron flux can be calculated. Since the n-p scattering is isotropic in this neutron energy region, there is equal probability of recoils with energy between zero and the full neutron energy, i.e. the differential spectrum will be a rectangle. Because the neutrons are never accurately monoergic and the counter resolution is finite, the high energy limit is modified to the shape of a knee. Since the recoil protons have a finite range, many of them end in the walls or pass out of the sensitive region of the counter. These effects cause a rise in the differential spectrum at low energies referred to as 'end and wall effect'. The amount of the rise depends on the proton range and may be calculated.

The work described in this paper follows the pioneering work in this field of Skyrme, Tunnicliffe and Ward (1952, referred to hereafter as STW). For a description of the counters and the calculation of end and wall effect this paper should be consulted. These authors had shown that at a number of energies the observed spectrum of proton recoils agreed within the errors with that expected from calculation. However, when cross checks were applied by us, measuring the same flux with different counters, gases and gas pressures persistent discrepancies sometimes as large as 5% were encountered; we have tried to understand and eliminate these discrepancies.

2.2. *The Neutron Source and Target Techniques*

The neutrons of these experiments came from the bombardment of lithium and tritium with protons from the Harwell electrostatic generator. The performance of the latter, both in energy and current has improved greatly during the course of this work so that proton energies up to 4·5 MeV and currents of 25·0 μA have been obtained. Target techniques have also advanced so as to withstand such bombardment without deterioration. We should perhaps stress that we have established many points because the proportional counter is in fact a neutron spectrometer.

It was found that care was necessary in the design of target cans to avoid the scattering into the forward direction of neutrons given off from the target at around 90° to the proton beam. In the original arrangement, the target of LiF on 0·005 in. silver was mounted in an aluminium target can of thickness 0·03 in. A contamination of low energy neutrons was observed; at a neutron energy of 300 kev where the neutron angular distribution is isotropic this was a maximum, namely 6–8% of the direct yield. Our current practice, which has eliminated this effect, is to solder the 0·005 in. thick silver direct to brass target cans of 0·015 in. wall thickness: at the same neutron energy this gives a scattered neutron background of less than 1%.

For our experiments, lithium has been used in the form of LiF evaporated on 0·005 in. silver backings. It was found that these targets would sustain bombardment at the highest power (~100 watts) only if the silver was etched before evaporation and soldered directly to the target cans. The can was rotated and cooled by an air blast. It is, of course, well known that compared with LiF, Li metal has higher specific neutron yield and lower gamma ray yield. So far, however, we have rarely been satisfied with Li metal targets. Close to the neutron threshold, the proportional counter can detect flaws as small as 1% of the total bombarded area, when these differ by say 15 kev from the mean thickness. The non-uniformity of the metal targets has frequently been observed, and the targets have also appeared to deteriorate rapidly. The lithium was purified by distillation *in vacuo* before evaporation. Silver has been the main backing material used: with polished silver backings this sometimes gave initially satisfactory targets but deterioration was usually rapid. With etched silver the targets were durable but had the characteristics of a thick layer. Better results were obtained with thoroughly cleaned platinum, 0·010 in. thick, held by an O-ring at the end of the can.

We have used both tritium gas targets and zirconium tritide. The current which can be passed through the thin window of the gas cell has until very recently been limited to 2 μA, whereas, when rotated and cooled, ZrT targets can withstand bombardment by 25 μA without deterioration. Thus the neutron yield is about 20% of the gas target yield. The ZrT target has the advantage that it may be used in a geometry identical with that with lithium so that fission measurements could be made in the same experimental arrangement from 120 kev to 3·5 Mev. The absence of γ radiation and the large centre of mass effect make relatively thick ZrT targets attractive for measurements with neutrons in the energy range 30–500 kev produced at 120° to the proton beam. In their final form the ZrT targets were on gold backings 0·005 in. thick soldered with indium to the standard target cans.

A summary of our usual practice may be given as follows:

Neutron energy range (kev)	30–500	120–625	500–3500
Target	ZrT	LiF	ZrT
Angle of observation (deg)	120	0	0

2.3. *Neutron Energy Checks*

As the (n, p) cross section varies roughly as $E^{-1/2}$ in this energy range it is clearly essential to know the neutron energy accurately. In the early experiments it was found that the machine voltage as indicated by a generating voltmeter was nearly linear, e.g. the Li (p, n) threshold agreed with the T(p, n) threshold multiplied by 1·882/1·019 within 0·5%. Recent alterations to the Van de Graaff machine, including the installation of an electrode between outer tank and central electrode, has rendered the generating voltmeter inoperative. However, a vibrating coil magnetometer (Green, Hanna and Waring 1957) now measures the magnetic field and this has been calibrated with respect to known fluorine resonances. As a more direct check, well-known neutron resonances such as those of sulphur, oxygen and carbon have been observed, and these are consistent with the fluorine calibration.

Using neutrons from the proton bombardment of a ZrT target, the maximum pulse height in the counter as a function of neutron energy was measured over the range of neutron energies 250–1000 kev. The corresponding pulse height due to neutrons from a Na–Be (γ, n) source, was measured. The comparison of these data shows (figure 1) that the energy scale of the T(p, n) neutrons from the machine agrees with this spot check to within 1%. One should note that the energy of neutrons from a Ne–Be (γ, n) source widely quoted, viz. 0·83 Mev, is applicable only to the relatively thick sources used by Wattenberg (1947). This is a mean energy allowing for appreciable moderation of the neutrons. These checks all show that the neutron energy is close to that assumed. However, the accuracy required is high, and it is possible that neutron energy errors contribute 1% to the errors in the flux measurement.

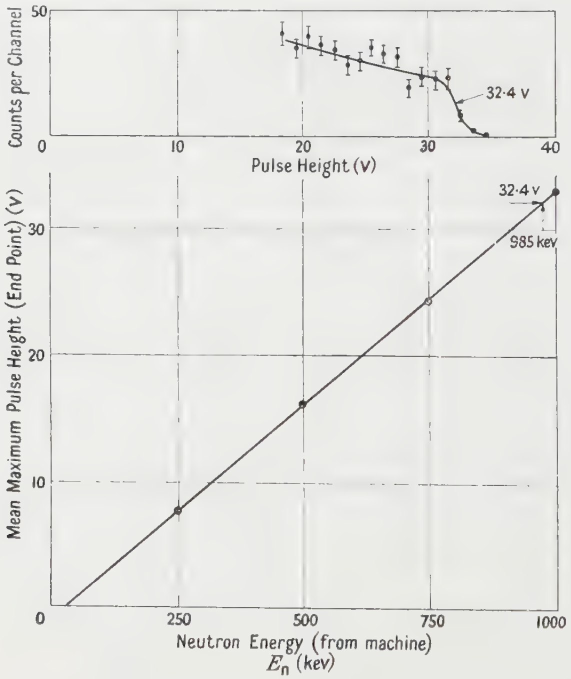

Figure 1. (*a*) Recoil spectrum of neutrons from Na–Be source. Counter filling 76 cm CH_4 at 0°c. (*b*) End points of recoil counter plotted against E_n as determined by machine potentiometer. Na–Be end point is 32·4 v corresponding to $E_n = 985$ kev. E_γ (^{24}Na)$=2·76$ Mev. Be (γ, n) threshold is 1·662 Mev; hence E_n (Na–Be source) from these figures is 8 (2·76−1·662)/9=0·975 Mev.

Because of the discrepancies between the curves of the n–p cross section quoted in the neutron cross section compilation, A.E.C.U. 2040 (1952) and its first supplement, it was decided to remeasure the n–p cross section in the energy range 80–550 kev. The measurements have been reported elsewhere (Allen and Ferguson 1955 b). The conclusion reached was that in this range, the theoretical cross section was accurate to 2%. The limit of experimental error was set by difficulties in chemical analysis.

2.4. *The Total Number of Proton Recoils*

It is not possible to estimate the number of proton recoils by integration as the lower part of the spectrum is obscured by pulses due to γ-rays and carbon recoils.

The technique of estimation described by STW was to find the total number of recoiling protons by integrating over the upper half of the recoil spectrum only. This, under certain assumptions, is a calculable fraction of the total number of proton recoils. The chief assumptions are (*a*) that the energy expended per ion pair is independent of energy, or its variation with energy is known, and (*b*) that one is using the correct range–energy relation.

If these conditions are satisfied the calculated and observed proton recoil spectra will be in good agreement and accurate estimation of the number of proton recoils can readily be made.

2.4.1. *The energy expended per ion pair.*

The energy expended per ion pair has been investigated by us for both hydrogen and methane over a wide range of energies. As this property is sensitive to the presence of electron capturing impurities in the counter considerable effort has been spent in eliminating them. The counters are entirely constructed of metal and glass. They are baked under vacuum for several days at a temperature of 100–150°c. The hydrogen is obtained from the hydrogen liquefier in the

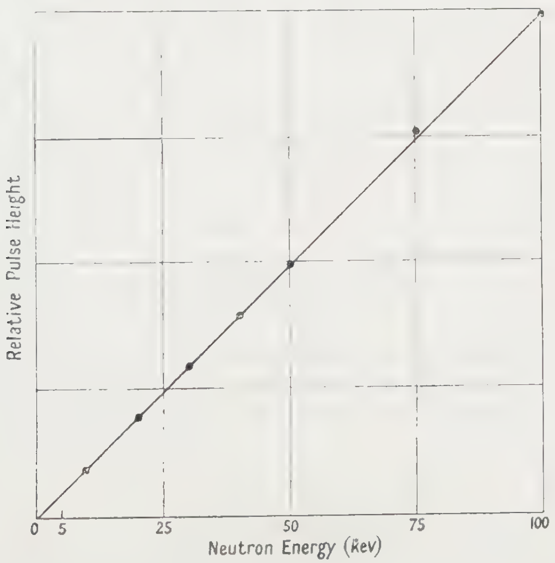

Figure 2. Counter filling 74 cm H_2 at 0°c. ZrT target at 135°.

Clarendon Laboratory, Oxford, and is finally purified by the formation and decomposition of uranium hydride. The methane is obtained from a fractional distillation column, and final removal of oxygen and water vapour is accomplished by storing the gas in 10 litre capacity glass flasks, on the walls of which a mirror of sodium has been evaporated: this technique is applied also to propane and xenon. We are indebted to Mr. D. West for suggesting this method.

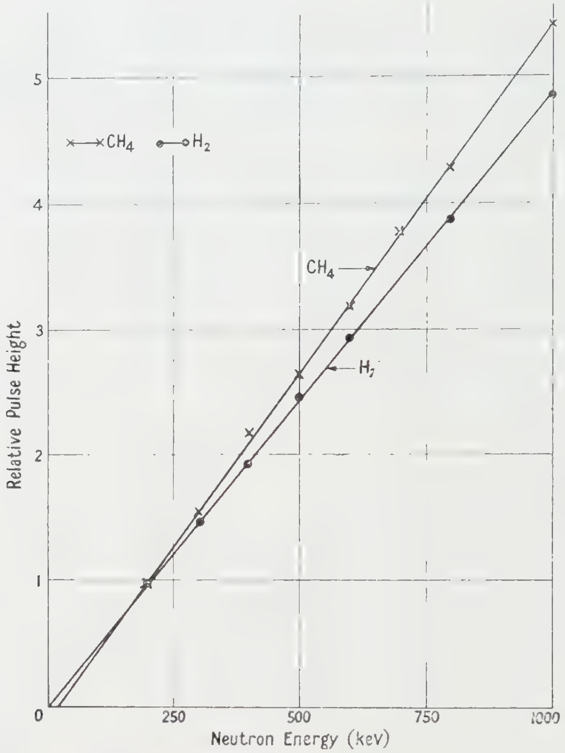

Figure 3. Range 0–1000 kev, target ZrT at 0°. Counter pressures 1 atmosphere. (Relative scales are not significant.)

The variation of ionizing power of recoil protons has been studied by varying the neutron energy and comparing it with the mean maximum pulse height of the recoils (point A, figure 5). The latter was taken to be the centre point of the knee of the differential spectrum. Errors in this measurement arise from errors in the machine voltage and in the electronics. We estimate the combined limits of errors to be about 1%. For purified hydrogen the graphs of figures 2 and 3 show that pulse height is a linear function of proton energy 1000 kev down to 10 kev, the intercept on the energy axis being certainly less than two kilovolts. Thus, at proton velocities equal to or less than those of the molecular electrons, i.e. proton energies about 20 kev, the percentage energy lost in ionization remains constant. This is remarkable in view of the work of Stier *et al.* (1954) who showed that at these energies a proton spends 80–90% of its path length in the neutral state.

In methane the results above 250 kev are consistent with a straight line having an intercept on the energy axis between 20–40 kev. At lower energies (see figure 4) the results, though within their errors they may be represented by a straight line, seem to converge towards the origin, having an intercept of 8 kev. The results as a whole would not be inconsistent with a parabola though their accuracy is inadequate to specify a unique curve. While every care has been taken to ensure gas purity, more evidence would be required to ascertain whether this was an intrinsic property of methane or was due to residual impurities.

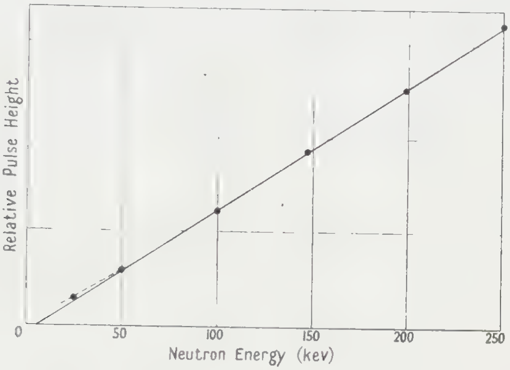

Figure 4. Counter filling 73 cm CH_4 at 0°c. ZrT target at 135°.

This result for methane implies that for low energies equal pulse height intervals correspond to increasing energy intervals as pulse height decreases. This gives a pulse height distribution similar to that which would be obtained if an increased range for the protons were assumed. The results show that, with the present techniques this effect should only be noticeable in CH_4 below about 400 kev and in hydrogen should be entirely negligible.

2.4.2. *Range–energy relation.*

In computing the expected shapes of the recoil spectra we have used the results of Weyl (1953) and Dunbar *et al.* (1953). Their measurements are in good agreement with the earlier work of Crenshaw (1942). STW used ranges extrapolated from the compilation of Bethe and Livingstone (1937). These are considerably greater at low energies than the more recent results, and the agreement that STW found between calculated and observed spectra in hydrogen at neutron energies below 200 kev can only be attributed to the fortuitous presence of impurities.

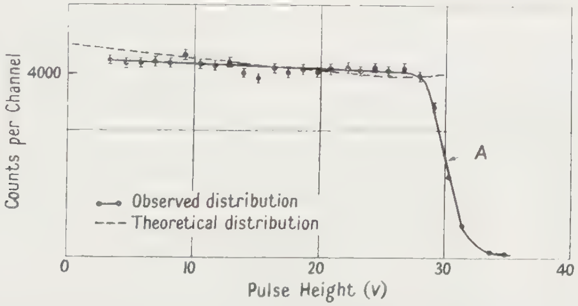

Figure 5. Comparison of theoretical and observed pulse heights. Counter pressure 134 cm H_2 at 0°c; maximum range of recoil protons (using Weyl's figures) is 0·45 cm.

2.4.3. *Comparison of theoretical and observed pulse height.*

For hydrogen, as might be expected from the results presented in the last section, extremely good fits of theoretical and observed spectra have been obtained. Figure 5 shows an example typical of many hundreds of such curves. Hydrogen is normally used at pressures of from 50 cm to 150 cm with neutrons from 550 kev downwards. With the combinations of neutron energies and pressures used in normal practice, the only discrepancies in the fit occur at low energies where the curves seem slightly flatter than predicted using the ranges of Weyl. That this effect is real was shown by reducing the gas pressure to 30 cm and the neutron energy to 100 kev. Here the range required to fit the data is only 0·75 of the ranges of Weyl. This effect may be tentatively explained in terms of nuclear collisions, although the effect is rather larger than that calculated by Dalgarno and Griffing (1955).

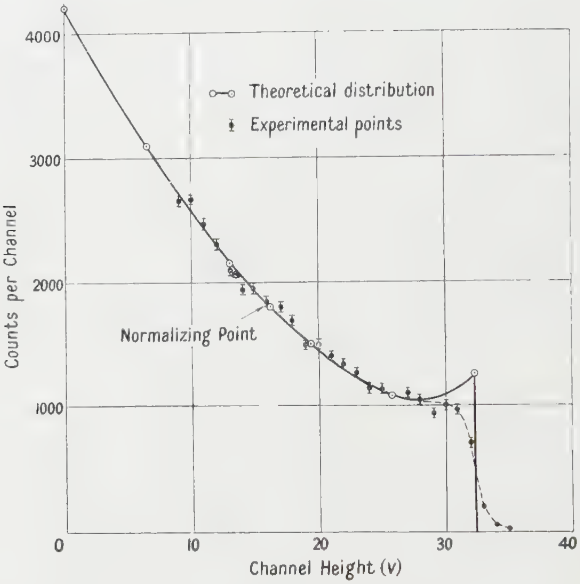

Figure 6. Counter pressure 139 cm CH_4 at 0°c. Maximum range of recoil protons 4·9 cm. Counter diameter 5 cm.

Methane has been used at pressures from 60 cm to 150 cm with neutrons of energy from 200 kev up to 2 Mev. The non-linearity in energy expended per ion pair has a negligible effect above 650 kev and very good fits to the theoretical curves are obtained (figure 6). Propane, though not studied so extensively as the other two gases has been used in the region above 1·5 Mev. Good fits have been obtained. Mixtures of hydrogen with argon and xenon have also proved satisfactory. Again our experience with these gas mixtures is limited, but this technique of obtaining higher stopping power shows more promise than the use of pure propane or methane at high pressures.

There is a broad region in which both the methane and hydrogen filled proportional counters may be used. Similarly, propane and methane counters have been intercompared between 1 Mev and 2·5 Mev.

2.4.4. *The consistent estimation of the total number of proton recoils.*

We have pointed out above that, given the range of protons in the counter gas, we can calculate the fraction of the total number of pulses due to proton recoils, which will have an amplitude in excess of half the maximum amplitude. This quantity is a very sensitive function of the range R.

We have seen, in 2.4.1 and 2.4.3, two phenomena which may in certain energy regions modify the spectrum in the same manner as a small change in range. These slight differences introduce errors in the estimate of the number of proton recoils. Thus, when we measure the same flux of neutrons by integrating all pulses above half the maximum height, at about 300 kev with a hydrogen filled and methane filled counter, we should expect a slight discrepancy. The departure from consistency of the energy per ion pair in methane leads to an underestimate of flux and the range effect in hydrogen leads to the reverse. Purification of the gases has reduced but not eliminated this effect.

If we consider the ordinate at half maximum pulse height for a unit spectrum (see STW) we find that it has the value 1 for $R=0$ and the value 0·97 for $R=2a$, the diameter of the sensitive volume of the counter. It is thus insensitive to small errors in the effective range. The product of this ordinate and the mean maximum pulse height gives a measure of the number of proton recoils. Our procedure is as follows. The experimental data are plotted and the agreement with the theoretical curve verified; if this is found satisfactory the number of proton recoils is determined. This method has given consistent results for all the gases we have tried over a wide variety of ranges, and has the additional merit of simplicity.

2.5. *Corrections to the Observed Flux*

2.5.1. *Background and scattering.*

The background of neutrons scattered in the room is determined by stopping the direct neutron beam with a paraffin cylinder 3 in. in diameter and up to 9 in. in length. The fraction of counts to be subtracted from a typical recoil spectrum is normally 1% or less at maximum pulse height, 6% at half height, rising to sometimes as much as 200% for the lowest pulses recorded.

The scattering in air which reduces the number of neutrons reaching the counter varies rapidly through the numerous resonances in oxygen and nitrogen. On the average it is about 2% for a source–counter distance of 40 in. The neutrons at other angles scattered into the counter will be allowed for as above, since they are indistinguishable from wall-scattered neutrons.

2.5.2. *Scattering in the counter.*

The end of the counter is calculated to scatter between $2\frac{1}{2}$ and 4% of incident neutrons; not all of these will miss the counting volume. On the other hand, there is in-scattering of neutrons from the walls and the base. These effects are difficult to estimate accurately and the overall correction was taken as zero.

2.5.3. $1/r^2$ *checks and the counter dimensions.*

The effective dimensions of each counter were determined from X-ray photographs. The agreement between different counters showed that there is no systematic error from this source; $1/r^2$ checks showed that the geometrical centre of the counter was the effective centre within 0·1 in. i.e. within 0·5% in flux. This entire method of flux determination has been criticized on the ground of the difficulty of locating the effective centre of the counter, but in our experience this is one of the least of the sources of error.

2.5.4. *Absorption of gas.*

Two possible corrections should be considered from the absorption of gas, especially hydrogen, in the walls of the counter. The first concerns the reduction of real pressure in the counter as a result of gas absorption, the second concerns the recoils from the absorbed layer into the sensitive volume of the counter. As regards the first possibility, manometer observation during filling showed no observable absorption in a period of the order of minutes, while extended observation of flux showed no systematic variation in a period of the order of weeks. Further, tests with counters filled with $\frac{1}{2}$, 1 and 2 atmospheres of hydrogen showed no variation of apparent flux with pressure consistent with wall absorption. We conclude therefore that the proportion of gas absorbed on the walls is not observable within the accuracy of observation. With this upper limit on the thickness of the absorbed layer, we can estimate the amount of the second correction. Since the layer on the walls is parallel to the neutron direction, we would expect to observe only those recoils which are ejected at an appreciable angle to the incident neutron beam. These recoils will have relatively low energy, i.e. they do not form part of the spectrum from which the flux is calculated. Even if they did, approximate estimates suggest that the correction required would be very small.

§ 3. THE BF_3 LONG COUNTER

The principles on which the 'long counter' of Hanson and McKibben (1947) is based are very different from those of the proton recoil counter. It has been shown to be insensitive to x-rays and hence well suited to calibration using photo-neutron sources. Thus its calibration might be related to international standards of neutron source strength. Further, many writers, e.g. Nobles *et al.* (1954) testify to its flatness of response over the whole energy region from 25 kev to the mean energy of the Ra–Be neutrons. The divergence from a truly flat response has been claimed to be as low as 1%. It therefore appeared to be an ideal instrument with which to check flux measurements with the proportional counter.

We have encountered many difficulties in the use of long counters for flux measurement which render them much less desirable than one might have expected from the information available when this work began. We have certainly not found them flat to the degree claimed and at high energies this view is now supported by recent work at Los Alamos (Henkel *et al.* 1956, private communication).

A survey of our conclusions about our present long counter has been given in the general introduction. The remainder of this section will be devoted to an account of the experiments necessary for the calibration of the long counter.

3.1. *Some Properties of the Long Counter*

If a counter is to be used in absolute flux determinations, it is essential to know the effective distance between source and counter. Measurements of the counting rate as a function of R, the distance from source to the front face of the counter, were made for a number of neutron energies. All the experiments on the long counter with neutron sources were carried out with the counter supported on a light frame, 8 feet above the concrete floor of a former aircraft hangar. The background due to neutrons scattered by the surroundings was measured by stopping out the direct neutrons with paraffin stoppers. Figure 7 shows the results of these measurements over the range of distances 20 in. to 110 in. The quantity $(I-I_0)^{-1/2}$ is plotted as a function of R where I and I_0 are the counting rates without and with the paraffin stopper respectively. Further investigations showed this relation to be linear down to a distance of 10 in. The value of R when $I-I_0$ is zero is R_0, which is the distance from the front face of the counter at which the counter is effectively centred. This distance is a function of neutron energy and its variation is shown in figure 8. It is interesting that a counter which depends on the slowing down of neutrons in paraffin can be represented so well over a wide range of energy by a point detector, although perhaps another way of making the same observation is that a $1/r^2$ check is quite insensitive.

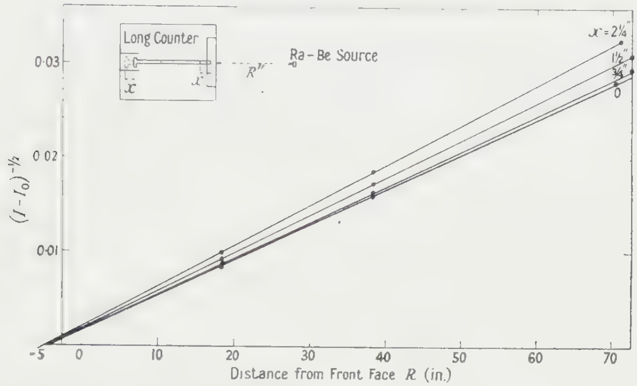

Figure 7. R is the distance of the source from the front face; x is the distance of withdrawal of the BF_3 counter from the fully forward position.

It was shown that the efficiency of the long counter is relatively insensitive to movements of the BF_3 counter of less than $\frac{1}{2}$ in. from its standard position, i.e. with the end of the counting volume in the plane of the surface of the paraffin

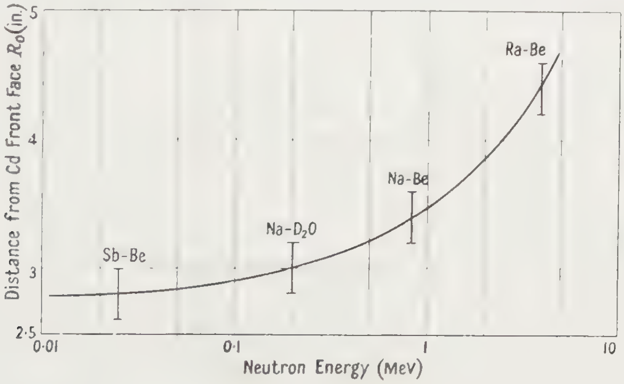

Figure 8. R_0, the distance from the front face of the counter at which the latter is effectively centred, as a function of neutron energy.

block. First, in the manner described above the effect on R_0 was determined, and it was found that even for a movement of several inches R_0 was unchanged. This might be expected since R_0 is close to the point at which the neutrons are effectively thermalized and from which the neutrons migrate to the BF_3 counter by thermal diffusion. Next, the variation in efficiency with counter movement was investigated over a distance of 3 in. for the neutrons from both the Sb–Be and the Na–Be source. The change for small movements ($\frac{1}{4}$ in.) was negligible in both cases, but for large displacements the efficiency fell off, the rate of fall being greater for neutrons of lower energy.

3.2. *The Calibration of the Long Counter*

The technique of intercomparing neutron sources in a bath of $MnSO_4$ solution (Fermi and Amaldi 1936) is now well known. In principle it depends on the thermalization of the neutrons and the subsequent capture of a constant fraction of them in the manganese. In these experiments the dimensions of the bath were $2\frac{1}{2}$ ft $\times$ $2\frac{1}{2}$ ft $\times$ 3 ft. The manganese activity was measured by inserting a set of seven Geiger counters in parallel. The efficiency of the latter was determined by daily comparison of response to a ^{60}Co source in a constant experimental arrangement.

Three photo-neutron sources were used in the final calibration viz. Na–Be, Sb–Be, Na–D_2O having neutron energies of 0·985, 0·025, and 0·2 MeV. Due to the size of these sources, moderation would be considerable especially in D_2O. The Be sphere was 4 in. diameter with six capsules of Na or Sb each $\frac{1}{4}$ in. diameter and $\frac{3}{4}$ in. long. The D_2O sphere was contained in a quartz sphere 4 in. in diameter with a $\frac{1}{2}$ in. diameter capsule of Na. The radioactive source strengths were about 1 curie giving $5\text{–}10 \times 10^6$ neutrons per second. Two Ra–Be (α, n) sources were available. The smaller gave about $2{\cdot}5 \times 10^6$ neutrons per second and was used in the $MnSO_4$ bath measurements on account of its small thermal absorption. The larger, the Harwell Standard Neutron source, gave approximately 10^7 neutrons per second but due to a reputed thermal absorption of 3% it was not used in the $MnSO_4$ bath, as the relative calibration required only the small source.

The source strength, measured by the manganese bath technique, is the integral over 4π of all the neutrons emitted. To compare this with the long counter it is necessary to measure the angular distribution of the neutrons emitted from the source. This was done for all the sources concerned. Certain corrections, however, must be applied to the bath measurements. (*a*) A correction for escape of neutrons from the bath is negligible for all sources except Ra–Be, for which it is estimated to be 2%. (*b*) The absorption of thermal neutrons by the source itself may require a correction. To estimate this for the beryllium sphere, its cross section was measured by the pile oscillator method; the absorption was found to be negligibly small. This was assumed for the quartz–D_2O sphere and the small Ra–Be source. (*c*) For the high energy neutrons from Ra–Be there are additional neutron losses due to (n, α) capture in oxygen and a correction for (n, α) and n, p) in sulphur. The larger of these, ^{16}O (n, α), is difficult to estimate: it is normally taken as 3% (Tavernier and Troyer 1954). Since the cross section is not known at all between 5 and 14 MeV, the uncertainty is large. We assume a correction of 6% + 3% due to capture in addition to 2% escape from the bath.

For the lower energy sources, the errors can be estimated from the consistency of sets of measurements in the $MnSO_4$ tank, errors in the long counter measurement etc. These give a standard deviation of $\pm 1\frac{1}{2}\%$ on an individual measurement and $\pm 3\%$ overall. There is a greater error in our knowledge of the relative efficiency with respect to Ra–Be neutrons, viz. $\pm 5\%$.

3.3. *The Calibration of the Long Counter with respect to the Proton Recoil Counter*

The intercomparison was carried out by mounting both counters at small angles ($\pm 5°$) with respect to the incident proton beam of the Van de Graaff generator. In a typical arrangement, the long counter would be at a distance of 80 in. and the recoil counter at 40 in. from the neutron producing target. The response of each to the same source was measured. Assuming that the true source strength was measured by the recoil counter, the efficiency of the long counter was obtained. In the neutron energy range 120 kev to 1500 kev, four separate measurements of the variation of the long counter efficiency have been made. The same smooth curve may be fitted to all of them. These four runs were taken at intervals over a period of nine months. During this time there was a slow drift in the absolute efficiency of the long counter of about 4%. Above 1500 kev, difficulties due to background were encountered and fewer reliable measurements were made. By relating each set of measurements to its mean the four sets of measurements were combined in a statistical analysis. From this analysis the best fitting polynomial curve was obtained with an estimate of the standard deviation of the curve at each point. These errors from the large numbers of observations are less than 0·5% in the region of 500 kev.

3.4. *The Relative and Absolute Efficiency of the Long Counter and the Accuracy of Flux Measurement*

Figure 9 shows the curve representing the relative efficiency of the long counter as a function of energy as determined by the recoil counter. The relative efficiency as determined by the photo-neutron sources is shown also, including the absolute calibration of 200 kev neutrons against the Oxford $RdTh-D_2O$ standard source. The relative calibration against the photo-neutron sources does not contribute to the accuracy of the measurement, but excludes the possibility of any gross systematic error. We should perhaps note in parenthesis

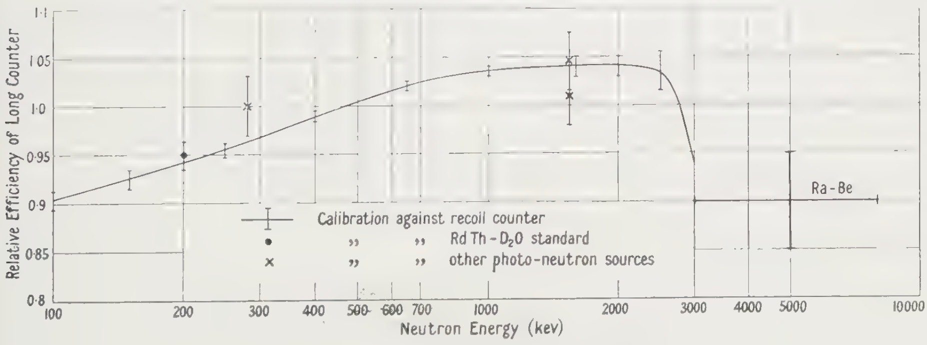

Figure 9. Relative efficiency of the long counter as a function of energy, as determined by the recoil counter.

that figure 9 differs from figure 3 of the earlier report on the long counter in that a 5% computational error was found in the Na–Be and Na–D_2O calibrations in the latter report.

The proton recoil counter provides an absolute calibration of the long counter over the whole energy range. A second calibration, against the Oxford RdTh–D_2O standard source, of 200 kev neutron energy, agreed with the proton recoil calibration within 1%. However, the latter was used only after considerable effort had been expended in accounting for a major discrepancy (about 14%) between the recoil counter calibration and the long counter as calibrated by the Harwell standard source Ra–Be (α, n). We have explained above that the nature of the corrections involved in the $MnSO_4$ bath makes such a calibration inevitably uncertain to within ±5%. None the less, the error was too large to be explained away in this manner. However, the discovery by Richmond and Gardner (1957) of an error of 7% in the value strength of the Harwell standard, and the computational error referred to above, fully account for the discrepancy. Flux measurements are commonly made by long counters calibrated against Ra–Be standard sources; our experience emphasizes that such measurements may be attended by considerable errors.

The two long counters have been compared over a large number of readings and the standard deviation of their ratio has been found to be 0·5%. Many measurements have been made of the long counter efficiency in terms of the recoil counter. An analysis of these shows a standard deviation on each measurement of ±2·5%. These fluctuations are therefore almost entirely in the recoil counter and include the effects due to different counters, gases and pressures, errors in pressure, temperature, neutron energy, distance etc. In the results used we have found no systematic variation between different counters and gases within the errors of the means. By taking a sufficient number of such observations and taking the mean, the random error in determining the efficiency of the long counter can be made very small. Since, as we have shown, the long counter is extremely stable, we can use it to make future determinations of flux with a probable random error of less than 1% and with the same absolute accuracy as the recoil counter. The absolute accuracy of the measurement depends ultimately on the knowledge of the hydrogen cross section. Over the energy range of these measurements a standard deviation of about 1% seems plausible for this quantity. The corrections to the estimated flux may be in error by a similar amount. The combined standard deviation of an absolute measurement by this method should not be greater than 2%. It is always difficult in an absolute measurement to estimate possible systematic errors and the validity of any such claims must depend on the accuracy of cross checks. Here we have a second line of evidence at one neutron energy, viz. the cross check with the Oxford standard neutron source. An accuracy to $\pm 2\frac{1}{2}\%$ is claimed for this source. Agreement between the two calibration is within 1%. The calibration against the Ra–Be source is also satisfactorily consistent. It is not possible in a rigorous way to combine these measurements; however, one would be justified in claiming that over the range from 100 kev to 1500 kev we can measure neutron flux with a standard deviation of not more than 3%. In the region from 30 kev to 100 kev this precision has not yet been attained due to lack of data. Here our present measurements have an accuracy estimated to be to within 5%. Above 1500 kev the technique in its present form is near its limits and accuracy is probably to within 5%.

ACKNOWLEDGMENTS

This work, having been spread over a long period, has had the contributions of many people. We have named some in the text, but also the help of J. Roberts in ensuring the self-consistency of the recoil counter, of D. Baker in the $MnSO_4$ bath tests and of D. A. Silverstone and R. E. Meads in recent measurements, are gratefully acknowledged.

REFERENCES

ALLEN, W. D., 1955, A.E.R.E. report, *NP/R* 1667.
ALLEN, W. D., and FERGUSON, A. T. G., 1955 a, A.E.R.E. report *NP/R* 1720; 1955 b, *Proc. Phys. Soc.* A, **68,** 1077.
A.E.C.U., 1952, 2040, *A Compilation of Neutron Cross Sections* (U.S. Dept. of Commerce).
BARSCHALL, H. H., ROSEN, L., TASCHEK, R. F., and WILLIAMS, J. H., 1952, *Rev. Mod. Phys.*, **24,** 1.
BETHE, H., and LIVINGSTONE, M. S., 1937, *Rev. Mod. Phys.*, **9,** 246.
CRENSHAW, C. M., 1942, *Phys. Rev.*, **62,** 54.
DALGARNO, A., and GRIFFING, G. W., 1955, *Proc. Roy. Soc.* A, **232,** 423.
DUNBAR, D. N. F., REYNOLDS, H. K., WENZEL, W. A., and WHALING, W., 1953, *Phys. Rev.*, **92,** 742.
FERMI, E., and AMALDI, E., 1936, *Phys. Rev.*, **50,** 899.
GREEN, G. W., HANNA, R. C., and WARING, S., 1957, *Rev. Sci. Instrum.*, **28,** 4.
HANSON, A. C., and MCKIBBEN, J. L., 1947, *Phys. Rev.*, **72,** 8.
NOBLES, R. A., DAY, R. B., HENKEL, R. L., JARVIS, G. A., KATURNIA, R. P., MCKIBBEN, J. Z., PERRY, J. R., Jr., and SMITH, R. K., 1954, *Rev. Sci. Instrum.*, **25,** 334.
RICHMOND, R., and GARDNER, B. J., 1957, A.E.R.E. report *R/R* 2097.
SKYRME, T. H. R., TUNNICLIFFE, P. R., and WARD, A. G., 1952, *Rev. Sci. Instrum.*, **23,** 204.
STIER, P. M., BARNET, C. F., and EVANS, G. E., 1954, *Phys. Rev.*, **96,** 973.
TAVERNIER, G. C., and DE TROYER, A. A., 1954, *Bull. Acad. Belg. Cl. Sci.*, **40,** 150.
WATTENBERG, A., 1947, *Phys. Rev.*, **71,** 497.
WEYL, P. K., 1953, *Phys. Rev.*, **91,** 289.

Electronic Absorption Spectra of Heterocyclic Systems II : Applications to some Two-ring Nitrogen Heterocyclics

By T. E. PEACOCK†

Department of Physical Chemistry, King's College, Newcastle upon Tyne, 1

Communicated by R. McWeeny; MS. received 6th May 1957

Abstract. The methods of a previous paper are applied in a theoretical analysis of the spectra of nitrogen derivatives of naphthalene and stilbene. The results provide, in every case, a satisfactory account of the main absorption bands and of the effects of nitrogen substitution. A simplified method, which permits very rapid estimates of shifts due to substitution in terms of data for the parent hydrocarbon, is found to be satisfactory and should be of general value.

§ 1. INTRODUCTION

In a preceding paper (McWeeny 1957, to be referred to as I) some recent approaches to the calculation of electronic energy levels in aromatic molecules have been examined and compared. These methods have in common a fairly complete theoretical framework (requiring the inclusion of all integrals and the admission of limited configuration interaction) but differ in their choice of one-electron orbitals. Preliminary applications were confined to the discussion of spectral shifts accompanying substitution in a benzene ring. In some cases the use of molecular orbitals of the parent hydrocarbon can give a satisfactory account of the shifts; but in others it is necessary to use orbitals appropriate to the substituted molecule itself, preferably in self-consistent field approximation, in order to recognize the charge non-uniformities caused by substitution. A simple criterion for determining whether a given orbital set is suitable as a basis for a perturbation calculation of this kind is as follows: If charge shifts resulting from the perturbation can be described in terms of the selected configurations (i.e. if the perturbation has substantial matrix elements between the ground state and some of the excited configurations admitted) then the limited configuration interaction calculation, based on the given orbital set, is likely to be adequate for predicting the effects of the perturbation. If this is not the case (e.g. if the matrix elements are small or vanish) it is necessary to allow for the charge shifts, which on physical grounds must occur, by modification of the orbitals themselves (e.g. by introducing self-consistent field orbitals).

In the present paper the methods of I will be extended to an interpretation of the spectral shifts accompanying nitrogen substitution in naphthalene (giving quinoline and isoquinoline) and *trans*-stilbene (giving *trans*-azobenzene). The methods of calculation are fully set out in I; the choice of orbitals will be made on the basis of the above criterion.

---

† Now at Department of Chemistry, University College of North Staffordshire, Keele, Staffs.

§ 2. SUBSTITUTION IN NAPHTHALENE AND STILBENE

2.1. *Naphthalene*

The molecule (figure 1) has symmetry D_{2h} and the energies and symmetries of the relevant molecular orbitals (A, B, A,′ B′) are as indicated in figure 2.

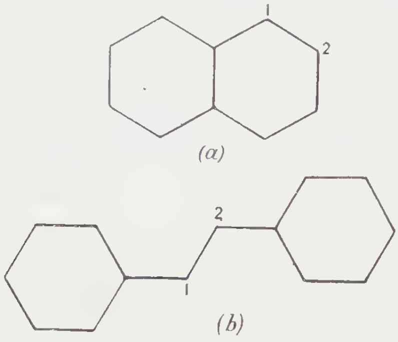

Figure 1. (*a*) Naphthalene. Substitution by nitrogen at 1 gives quinoline and at 2 gives isoquinoline ; (*b*) Stilbene. Substitution by nitrogen at 1 and 2 gives azobenzene.

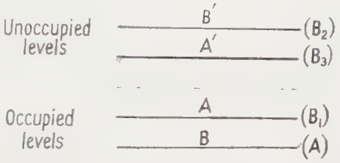

Figure 2. Naphthalene molecular orbitals.

The ground state function Φ_0 and the functions of the excited configurations, $\Phi(A \rightarrow A')$, $\Phi(A \rightarrow B')$, $\Phi(B \rightarrow A')$, and $\Phi(B \rightarrow B')$, are grouped according to symmetry species in table 1.

Table 1

Symmetry	A	B_2	B_3
Functions	Φ_0	$\Phi\,(A \rightarrow A')$	$\Phi\,(A \rightarrow B')$
		$\Phi\,(B \rightarrow B')$	$\Phi\,(B \rightarrow A')$

Since the excited functions considered differ in symmetry from that representing the ground state it would certainly not be satisfactory to base the calculation on Hückel orbitals, even in the case of the *hydrocarbon*; for electron interaction, regarded as a perturbation to the Hückel model (also with D_{2h} symmetry), would introduce charge shifts which could *not* be described in terms of the selected configurations, mixing still being ruled out by symmetry considerations. For this reason it is necessary to use self-consistent field orbitals in discussing even the parent hydrocarbon.

On the other hand, the nitrogen substitutions occurring in both quinoline and isoquinoline destroy the original symmetry and lead to heavy mixing, under the perturbation, of the functions listed in table 1. It therefore seems quite legitimate to discuss the *substitution* without further modification of the orbitals, i.e. in terms of the self-consistent orbitals of the parent hydrocarbon.

2.2. *Stilbene*

The molecule (figure 1) has the symmetry C_{2h}. In this case the four orbitals A, B, A′, B′, are inadequate for a description of the excited states, owing to the presence of accidental degeneracies or near-degeneracies. In the Hückel approximation it is immaterial whether the molecular model has the true symmetry (C_{2h}) or is distorted to a 'linear model' with symmetry D_{2h}, owing to the neglect of all but nearest neighbour interactions. And since distant-neighbour interactions are relatively unimportant it is useful to keep in mind a 'sub-classification' of orbital symmetries appropriate to the distorted molecule. The energies and symmetries of the Hückel molecular orbitals are indicated in figure 3 (symmetries on distortion appearing in brackets).

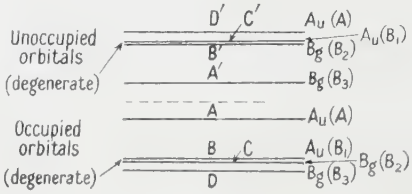

Figure 3. Stilbene molecular orbitals.

The functions of the excited configurations fall into the various symmetries species according to table 2.

Table 2

True symmetry	A_u		B_g	
Distorted symmetry	A	B_1	B_2	B_3
Functions	Φ (A → D′)	Φ (A → C′)	Φ (A → B′)	Φ (A → A′)
	Φ (B → C′)	Φ (B → D′)	Φ (B → A′)	Φ (B → B′)
	Φ (C → B′)	Φ (D → B′)	Φ (C → D′)	Φ (C → C′)
	Φ (D → A′)	Φ (C → A′)	Φ (D → C′)	Φ (D → D′)

Owing to the large number of configurations interacting with the A_u (A) ground state, mixing being allowed by symmetry even in the hydrocarbon, the introduction of stilbene self-consistent field molecular orbitals appears to be unnecessary: Hückel molecular orbitals should suffice in dealing with the parent molecule. At the same time it should be noted that this rather extensive interaction involves configurations which are 'normally' (e.g. in naphthalene) omitted and is therefore associated with the accidental degeneracy in stilbene. The point of introducing the symmetry sub-classification becomes apparent when matrix elements are calculated: those between functions whose symmetries differ in the distorted molecule turn out to be quite negligible and, in good approximation, the secular determinant factorizes accordingly.

The double substitution which yields azobenzene preserves the symmetry of the system and no new features arise in the calculation; there is still heavy mixing of ground and excited configurations, modified by the presence of the nitrogens, and there is every reason to expect that Hückel orbitals will be equally satisfactory in discussing both the parent molecule and its derivatives.

§ 3. RESULTS

The general interpretation of the so-called α, p, β and β′ bands of an alternant hydrocarbon has been discussed elsewhere (Dewar and Longuet-Higgins 1954, Pople 1955): and it has been pointed out that a similar interpretation appears to be satisfactory when nitrogen substituents are admitted (McWeeny and Peacock 1957, Peacock 1957)

The results for naphthalene and its hetero-derivatives are presented in table 3, where the symmetries and energies of the states associated with the α, p, β and β′ bands are listed. S and W indicates whether a band is strong or weak,† the observed transitions are given in the last column and the figures in brackets (in the case of naphthalene) show the complete failure of predictions based on Hückel orbitals.

Table 3

	State and Symmetry		Transition Energy (predicted) (in wave numbers $\bar{\nu}$)		Intensity	Observed Band ($\bar{\nu}$)
Naphthalene	α	(B_3)	35 900‡	(27 500)§	W	32 300
	p	(B_2)	36 600	(23 000)	S	36 500
	β	(B_3)	51 000	(43 500)	S	
	β′	(B_2)	53 700	(52 500)	S	
Quinoline	α		36 200		W	32 300
	p		37 500		S	37 000
	β		51 500		S	
	β′		54 000		S	
Isoquinoline	α		35 700		W	32 000
	p		37 900		S	38 000
	β		51 800		S	
	β′		55 000		S	

‡ The values reported here compare very well with those given by Pople (1955) and Pariser (1956) using slightly different parameters.

§ Similar calculation based on Hückel orbitals.

In the case of stilbene and its derivatives the designation is inadequate: the excited states may then be described by giving the functions of table 2 which predominate in their wave functions and indicating the signs with which they are combined. The state corresponding to a normal band would be described in this notation as $[\Phi(A \rightarrow B'), \Phi(B \rightarrow A'), (-)]$ or just $[(A \rightarrow B'), (B \rightarrow A'), (-)]$. The results for stilbene and azobenzene appear in table 4; only the states giving rise to transitions with non-zero oscillator strength are listed, and these are all of symmetry B_g.

§ 4. DISCUSSION

4.1. *Naphthalene and Quinolines*

α band. This occurs at $32\,300\bar{\nu}$ experimentally (Friedel and Orchin 1951) in all of the three molecules. It is also observed to be weak. Theory predicts the band to move only slightly under substitution, and for all three molecules it is at about 36 000 $\bar{\nu}$ and is also weak. Although the error between calculated and observed energies is considerable, the most significant fact is that the centre of the band does not move appreciably under nitrogen substitution.

---

† A qualitative assessment follows immediately from the considerations put forward by Dewar and Longuet-Higgins.

Table 4

State		Transition Energy ($\bar{\nu}$)	Intensity	Observed Transitions ($\bar{\nu}$)
Stilbene	[A → A′]	35 600	S	34 500 ~50 000
	[(B → B′) (C → C′) (−)]	51 400	W	
	[(B → B′) (C → C′) (+)]	66 900	S	
	[D → D′]	74 600	S	
	[(A → B′) (B → A′) (−)]	39 000	W	
	[(A → B′) (B → A′) (+)]	50 300	S	
	[(C → D′) (D → C′) (−)]	65 000	W	
	[(C → D′) (D → C′) (+)]	68 000	S	
Azobenzene	[A → A′]	34 000	S	22 000 32 000 ~50 000
	[(B → B′) (C → C′) (−)]	56 100	W	
	[(B → B′) (C → C′) (+)]	61 900	S	
	[D → D′]	76 900	S	
	[(A → B′) (B → A′) (−)]	38 600	W	
	[(A → B′) (B → A′) (+)]	50 700	S	
	[(C → D′) (B → C′) (−)]	66 900	W	
	[(C → D′) (D → C′) (+)]	66 900	S	

p *band.* Under substitution this band moves to higher energies for naphthalene 36 500 $\bar{\nu}$, for quinoline 37 000 $\bar{\nu}$, and for isoquinoline 38 000 $\bar{\nu}$. The predicted values are in agreement with these results.

β and β' bands. Very few experimental data exist for the β and β' bands although all three molecules absorb strongly as the vacuum ultra-violet is approached, in general agreement with the theoretical predictions.

It seems probable that the n→π transition, which will certainly occur, will be masked by the α band, and may well be a contributing factor in the large background absorption which occurs in this region.

4.2. *Stilbene and Azobenzene*

In these molecules the band system is more complicated, and we shall therefore discuss each *observed region* of absorption in turn.

The 35 000 $\bar{\nu}$ *band.* In stilbene this band is observed at 34 500 $\bar{\nu}$ (see Gillam and Stern 1954 for spectra of these two molecules) and can be associated with [A→A′](S) and [(A→B′), (B→A′) (−)](W) at 35 600 $\bar{\nu}$ and 39 000 $\bar{\nu}$, the former of which is intense. In azobenzene the peak occurs at 32 000 $\bar{\nu}$ and is much broader and less intense than in stilbene. The [A→A′](S) at 34 000 $\bar{\nu}$ and [(A→B′)(B→A′)(−)] (W) at 38 600 $\bar{\nu}$ will account for this band. The former will be unchanged in intensity and the latter increased in intensity at the expense of [(A→B′), (B→A′), (+)], as the coefficients of Φ(A→B′) and Φ(B→A′) will no longer be equal in magnitude, and the 'cancellation' pointed out by Dewar and Longuet-Higgins (1954) will be diminished. As these bands are close together they will be indistinguishable experimentally but the increased separation will mean a fall in the resultant peak height. The band will thus be shifted towards the visible and somewhat broadened by comparison with the band in the parent molecule. This is in complete accord with the experimental data in which the peak moves to 32 000 $\bar{\nu}$.

The 50 000 $\bar{\nu}$ *band*. In both molecules the peak appears at about 50 000 $\bar{\nu}$. In stilbene this can be associated with [(B→B′), (C→C′), (−)] (W) at 51 400 $\bar{\nu}$ and [(A→B′), (B→A′), (+)] (S) at 50 300 $\bar{\nu}$. This will give a strong band which is observed. In azobenzene the peak is broader and much less intense than in the parent. This can be accounted for by the shift of the [(B→B′), (C→C′)(−)] (W) to 56 100 $\bar{\nu}$. The peak will therefore derive its maximum intensity from [(A→B′), (B→A′), (+)] (S) at 50 700 $\bar{\nu}$ which has lost intensity to [(A→B′), (B→A′), (−)] in the manner already described. A broadening of the band and a diminished intensity is expected and in fact observed.

The 65 000 $\bar{\nu}$ *band*. In stilbene this is predicted at 67 000 $\bar{\nu}$ and in azobenzene also at about the same place. These bands are as yet unobserved.

The 22 000 $\bar{\nu}$ *band*. The absorption at 22 000 $\bar{\nu}$ is almost certainly due to an $n \rightarrow \pi$ transition. There is much experimental evidence in favour of this (see Mason 1955, Dewar 1956). According to the present calculation, there is no π electron level which could account for π absorption in this region of the spectrum.

§ 5. SEMI-EMPIRICAL METHODS

If the energies and assignments of the absorption bands of the parent are accepted from experiment it is clearly possible to use the methods of these papers for making rapid estimates of the shifts accompanying substitution. Taking the general case and assuming no degeneracies the Hamiltonian matrix for the parent, referred to α, p, β, β' functions, would be diagonal with empirically identified elements $H_{\alpha\alpha}{}^0$, $H_{pp}{}^0$, $H_{\beta\beta}{}^0$, $H_{\beta'\beta'}{}^0$. The *modification* arising from the introduction of hetero-atoms can then be estimated very simply, using Hückel orbitals and the formulae of I, Appendix 2, and the eigenvalue *shifts* can then be easily calculated by perturbation theory. Such a procedure has been tested for the quinolines and the results appear in table 5.

Table 5

Hydrocarbon expt.	Quinoline	Isoquinoline	Δ_{SE}†		Δ_P‡	
			$Q(\bar{\nu})$	$I(\bar{\nu})$	$Q(\bar{\nu})$	$I(\bar{\nu})$
36 500 $\bar{\nu}$	37 800 $\bar{\nu}$	37 600 $\bar{\nu}$	1300	900	900	1300
32 300	32 600	32 200	300	−100	300	−200
45 200	35 800	46 200	600	1000	500	800
59 700	59 900	61 200	200	1500	300	1300

†Δ_{SE} refers to shifts calculated using method of this section.
‡Δ_P refers to shifts calculated using method given in § 2.

The predicted shifts are in good agreement with those obtained using the self-consistent field orbitals of the hydrocarbon. It is possible that a perturbation treatment of this kind will prove a useful aid in the interpretation of absorption spectra of more complicated systems, for which self-consistent field solutions are not yet available.

ACKNOWLEDGMENTS

The author is indebted to Dr. R. McWeeny for many helpful suggestions, and the Academic Board of King's College for the award of a C. N. Levin postgraduate Studentship.

REFERENCES

DEWAR, M. J. S., 1956, *Special Publications of the Chemical Society*, No. 4, p. 64.

DEWAR, M. J. S., and LONGUET-HIGGINS, H. C., 1954, *Proc. Phys. Soc.*, A, **67,** 795.

FRIEDEL, R. A., and ORCHIN, M., 1951, *Ultraviolet Spectra of Aromatic Compounds* (London : Chapman and Hall).

GILLAM, A. E., and STERN, E. S., 1954, *Electronic Absorption Spectroscopy* (London : Arnold), (and references given therein).

McWEENY, R., 1957, *Proc. Phys. Soc.* A, **70,** 593.

McWEENY, R., and PEACOCK, T. E., 1957, *Proc. Phys. Soc.* A, **70,** 41.

MASON, S. F., 1955, Special Publications of the Chemical Society, No. 3, p. 139.

PARISER, R., 1956, *J. Chem. Phys.*, **24,** 250.

PEACOCK, T. E., 1957, *Nature, Lond.*, **179,** 684.

POPLE, J., 1955, *Proc. Phys. Soc.* A, **68,** 81.

The Radiative Capture of Alpha Particles in ^{15}N

By P. C. PRICE†
Cavendish Laboratory, Cambridge

Communicated by E. S. Shire; MS. received 11*th February* 1957, *and in final form* 6*th May* 1957

Abstract. The $^{15}N(\alpha, \gamma)^{19}F$ reaction has been examined with bombarding energy from 1·2 to 2·35 MeV. Three resonances have been found, two narrow and one of measurable width. The cascade schemes at each of the resonances have been partly elucidated, and the partial radiative widths of the resonances have been determined, except for a statistical factor. Some of the angular distributions have been measured, and conclusions have been drawn about the possible values of the spins and parities of the levels concerned. The relation of these results to the predictions of Elliott and Flowers is briefly discussed.

§ 1. INTRODUCTION

An account of the experimental work done on this nucleus before 1955 has been published in the review by Ajzenberg and Lauritsen (1955). Since the closing date of their survey two important papers have been published, which describe the results of inelastic scattering experiments with neutrons (Freeman 1956) and protons (Wilkinson, Toppel and Alburger 1956) respectively. These workers agree in adding another level to the scheme published by Ajzenberg and Lauritsen (1955). On the theoretical side, Elliott and Flowers (1955) have predicted the existence of several low-lying even parity states in ^{19}F, and have calculated the excitation energies of these levels as functions of a single parameter V_c. Figure 1 shows the experimental level scheme side by side with a graph of the energies of the levels predicted by Elliott and Flowers. The spins of the experimental levels are shown on the left, and the known radiative transitions are also shown : the principal transitions are drawn as continuous lines, and weaker transitions as interrupted lines.

One of the methods of investigating levels in ^{19}F which has not been undertaken before is the study of the $^{15}N(\alpha, \gamma)^{19}F$ reaction. § 2 contains a description of the apparatus and methods used in this study, and § 3 is an account of the experimental results. In § 4 their interpretation is discussed.

§ 2. EXPERIMENTAL METHODS

The experiments were all performed with the Cavendish electrostatic generator, which produces a beam of singly charged helium ions. The gamma rays were detected in NaI(Tl) crystals of two sizes (1·5 in. × 1·5 in. and 4 in. × 2 in. cylinders) mounted on good commercial photomultiplier tubes. The output of the photomultiplier was amplified in a commercial wide-band pulse amplifier, and fed into a Hutchinson–Scarrott pulse height analyser (Hutchinson and Scarrott 1951). The energy of the radiation was determined by comparison with six standard radioactive sources : ^{144}Ce (0·134 Mev), annihilation radiation (0·511 Mev), ^{137}Cs (0·662 Mev), ^{65}Zn (1·12 Mev), ThC″ (2·61 Mev), and the ^{15}N(p, α, γ)^{12}C reaction (4·43 Mev).

---

† Now at the Central Instrument Laboratory of Imperial Chemical Industries, Ltd.

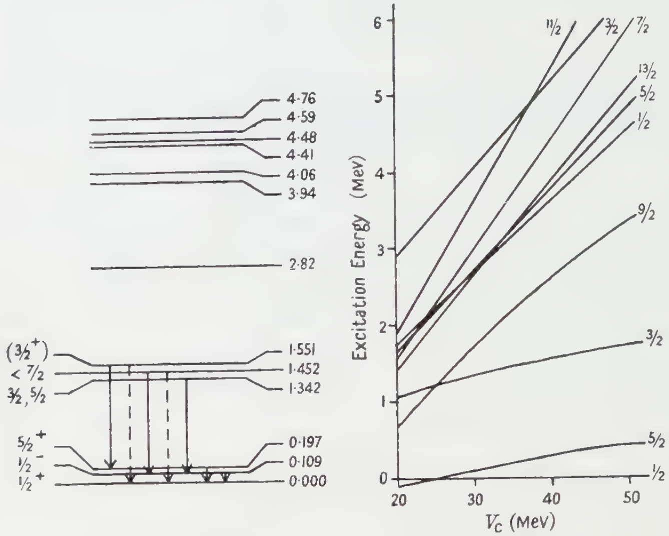

Figure 1. Levels in ^{19}F.

At the time of these experiments the Cavendish electrostatic generator was stabilized with an electron beam, which produced an intense x-ray background. In order to examine low energy gamma rays, it was necessary to shield the crystal ; this was done by placing the target chamber, crystal and photomultiplier tube in a large lead box. This box was 0·5 in. thick all round and additional lead was added on top. It was completely effective in excluding radiation less energetic than 0·5 Mev.

Two different kinds of nitrogen target were used. Thick tantalum nitride targets were made by heating tantalum foil to 1300°c in an atmosphere of dry ammonia, which was made from ^{15}N enriched ammonium nitrate by a method similar to that used by Malm and Beuchner (1950). Several types of thin target were tried, but the only useful ones were made by the Atomic Energy Research Establishment, Harwell, on their electromagnetic separator. They were about 20 kev thick (for alpha particles) on molybdenum backings.

§ 3. Results

A thick target yield curve was taken from 1·2 to 2·35 Mev. Two steps in this curve, at bombarding energies 1·53 and 1·62 Mev, were identified with the known resonances in ^{14}N(α, γ)^{18}F (Price 1955). Two new steps were observed at higher energies. More detailed yield curves were then taken between 1·6 and 2·0 Mev, and these showed that the upper step was double. Measurements were taken of the exact bombarding energies of the steps ; the energy scale was calibrated by examining the 0·669, 0·8735 and 0·9353 Mev resonances in ^{19}F(p, α, γ)^{16}O with the H_2^+ beam. The yield curve at each step was also examined to determine the width of the resonance.

Good reasons will be shown below for identifying these steps with resonances in ^{15}N(α, γ)^{19}F. Table 1 shows their energies and total widths ; the excitation energies have been calculated using the table of nuclear masses published by Li (1952).

Table 1

Bombarding energy (Mev)	1·681 ± 0·005	1·852 ± 0·003	1·883 ± 0·003
Excitation energy (Mev)	5·313 ± 0·020	5·447 ± 0·020	5·472 ± 0·020
Total width (kev)	<2	<1	4 ± 1

The spectrum of the radiation at each resonance was determined by examining the pulse height spectra in several ranges of quantum energy, covering altogether all quantum energies between 50 kev and 6 Mev. The intensity of the background radiation from the targets used was comparable with that of the significant radiation, and consequently it was necessary to observe the pulse height spectra at bombarding energies above and below that of the resonance in order to determine the spectrum of this background. Because of the proximity of the upper resonances, the experiments at these two resonances were combined.

The low intensity of the reaction did not permit the use of a crystal pair spectrometer, and the pulse height spectra were therefore interpreted by a detailed comparison with the pulse height spectra of the comparison sources, taken under identical conditions. The results of these experiments are summarized in table 2.

Table 2. Energies of Identified Spectral Lines (Mev)

1·68 Mev resonance	1·85 Mev resonance	1·88 Mev resonance
5·15 ± 0·04		5·18 ± 0·08
	4·0 ± 0·1	4·0 ± 0·1
	2·65 ± 0·02	
	1·27 ± 0·04	1·26 ± 0·04
	0·195 ± 0·008	0·187 ± 0·008
0·114 ± 0·005	0·110 ± 0·010	0·110 ± 0·006

It will be seen from that table that a line near 109 kev is found at each of the resonances, and a line near 197 kev at two of them. Low energy lines are not common in nuclear reactions, and the exact correspondence of energies suggests very strongly that each of the steps in the yield curve corresponds to a resonance in $^{15}N(\alpha, \gamma)^{19}F$. Furthermore, these steps were not observed in yield curves obtained with targets made by the same process with natural ammonium nitrate. The assignment of these resonances to this reaction can therefore be assumed.

The angular distributions and total yields of the more energetic lines were also measured. The total yields were obtained absolutely by comparison with the 90° yield of 4·43 Mev quanta from the $^{15}N(p, \alpha, \gamma)^{12}C$ reaction, which has been determined by Schardt *et al.* (1952). The determination of the angular distribution was straightforward at the 1·68 Mev resonance, but at the higher resonances it was necessary to determine the angular distribution and total yield of the events associated with each of the pulse height analyser channels, and to reduce these to the distributions and yields of the spectrum lines by the method of least squares. The calculation of the yields and angular distributions of the channels was facilitated by a special choice of the angles of observation (Price 1954), but the least squares calculation could not be similarly simplified. This part of the calculation was performed by Scientific Computing Services, Ltd.

The results are shown in table 3. The third column gives the yield as measured by $(2J+1)\Gamma_\gamma\Gamma_\alpha/\Gamma$, when J is the spin of the resonance, and Γ, Γ_α and Γ_γ are the total width, the alpha-particle emission width, and the partial width for emission of the appropriate gamma-ray respectively. The fourth column gives the coefficient A_2 in the angular distribution, normalized to the form $1+A_2P_2(\cos\theta)+A_4P_4(\cos\theta)+\ .\ .\ .$ None of the coefficients A_4 was found to be significantly different from zero.

Table 3

Resonance energy (MEV)	Transition energy (MEV)	Yield (ev)	A_2
1·68	5·2	6·6 ± 1·4	−0·08 ± 0·08
1·85	4·0	3·8 ± 0·8	−0·43 ± 0·06
	2·6	†7·0 ± 1·6	+0·28 ± 0·14
1·88	5·3	5·2 ± 1·4	+0·02 ± 0·06
	4·0	3·3 ± 0·7	0·00 ± 0·11

† This value is the yield for the transition, calculated on the assumption that this line is two transitions in cascade.

An attempt was made to obtain more information about the cascade scheme by coincidence experiments. These experiments all failed because of the high coincidence rate of the background radiation.

§ 4. INTERPRETATION

In assigning a cascade scheme and a set of possible values of spins and parities, it is possible to use not only the gamma-ray energies, but also the partial widths for gamma-ray and alpha-particle emission. This is because limits can be assigned for these widths which are functions of the spins and parities of the levels concerned.

Blatt and Weisskopf (1952), using the single-particle shell model, calculated formulae for the partial width of a radiative transition as a function of its energy and multipole order. Wilkinson (1956) has examined the observed radiative transitions in light nuclei with known multipole orders, and has found that the matrix elements (or ratios observed width/theoretical width) lie in certain ranges. If we assume that no dipole transition exists with a matrix element greater than double that of the largest yet discovered, and that no quadrupole transition exists with a matrix element greater than four times the present maximum (becaus the number of quadrupole transitions known is much smaller than the numbe of dipole transitions), we can then draw some probable conclusions on the spin and parities of the levels in ^{19}F.

Lane (1954) has published a similar survey of observed proton and alpha particle reduced widths. It seems reasonable to conclude from his results tha no alpha-particle emission width will be found greater than the ‘ Wigner limit ’ this assumption makes it possible to draw further conclusions on the spins an parities.

We shall now consider each of the resonances in turn. We shall first identif the cascade scheme, so far as the accuracy of the observations permits, and the consider what we can say about the spins and parities of the levels concerne

4.1. *The* 1·68 *MeV Resonance*

The width of the pulse height spectrum corresponding to the 5·15 MEV lir at this resonance is too narrow for the line to contain more than about 15% of

5·31 Mev component. The absence of a 197 kev line enables a similar limit to be put on the transition to the second excited state. We can therefore conclude that this resonance radiates predominantly to the 109 kev level. Less energetic transitions do not amount to more than 30% of the intensity of the principal line, and may not be present at all.

The intensity of the principal line is such that it must be a dipole or an E2 transition. The spin of this resonance must therefore be 1/2, 3/2, or $5/2^-$. The assignments $3/2^+$ and $5/2$ can be excluded because they do not fit the observed angular distribution, but none of the three remaining possibilities can be excluded. The value $3/2^-$ is less probable than the others, because a large amount of quadrupole mixing would be required in order to fit the observed angular distribution.

4.2. *The* 1·85 *MeV Resonance*

There is no trace of any line more energetic than 5 Mev at this resonance: the combined strength of all such lines does not exceed 10% of that of the line near 4 Mev.

This line cannot be definitely assigned to any one transition. The energy of the line with which it is probably in cascade (1·27 Mev) suggests that it is a transition to the 1·34 Mev level; but this does not seem to be consistent with the observed ratio of 109 kev to 197 kev radiation at this resonance, which is very low. It is possible that this is a single transition to the 1·55 Mev level; alternatively a state near 4 Mev may be involved.

The line at 2·65 Mev is not accompanied by any lines of comparable strength between 2·65 and 0·2 Mev, but it is of comparable strength with the 197 kev line. It seems, therefore, that the 2·65 Mev line must consist of two transitions cascading in series. Its energy and the fact that it is a narrow line indicates that the second of these two transitions goes predominantly to the 197 kev level. The energy of the state near 2·8 Mev cannot be deduced accurately, but it is consistent with the published value of 2·82 Mev (Ajzenberg and Lauritsen 1955).

It is not easy to assign spins and parities to the levels concerned with this resonance. We can conclude from the intensity of the 4 Mev line that it is unlikely (but not impossible) that it is the second transition of a cascade, and also that if it is a first transition, it must be a dipole or electric quadrupole transition. As we know that the highest spin that any of the levels near 1·5 Mev can possess is 5/2, we can conclude that the resonance is unlikely to have a spin greater than 9/2; furthermore, the transition 9/2 → 5/2 is inconsistent with the observed angular distribution, so it is unlikely to have a spin greater than 7/2.

The angular distributions are definitely anisotropic, which excludes the resonance spin of 1/2, but the possibilities are too numerous to enable any further conclusions to be drawn from the distributions.

The level at 2·82 Mev has a spin definitely greater than 1/2 and probably not greater than 9/2. This follows from the strength of the transition to this level, which indicates that it is a dipole transition, and from the fact that a 3/2 → 1/2 transition is excluded by the angular distribution.

4.3. *The* 1·88 *MeV Resonance*

The energy of the 5·3 Mev line is consistent with its identification with a transition to the 197 kev level, but not with either of the other transitions to the very low-lying states. The intensity of the transition to the 109 kev level cannot be more than 25% of the intensity of the principal line, and that of the ground state transition cannot be more than 10% of that intensity.

The energies of the lines at 4 Mev and 1·26 Mev are consistent with a cascade via the level at 1·34 Mev. The ratio of the intensities of the very low-lying lines is consistent with this interpretation.

In assigning spins and parities we have the advantage at this resonance of knowing the alpha-particle width. This is so great that the resonance cannot have a spin greater than $5/2^-$, $5/2^+$ or $7/2^+$. The last two values are improbable.

We also know that the 5·3 Mev line is so strong that it must be predominantly dipole radiation ; the resonance cannot, therefore, have a spin of 1/2. Moreover, the assignment of $5/2^-$ leads to an angular distribution for this line inconsistent with that observed.

We are left with the four possible assignments $3/2^+$, $3/2^-$, $5/2^+$ and $7/2^+$. The observed angular distributions are fitted better with the value of $3/2^+$ than with the other values, and also the large alpha-particle width is better reconciled with this spin than with the others. These constitute two good reasons for regarding this value as more probable than the others.

It should be mentioned that the angular distribution of the 4 Mev line is inconsistent with a $3/2 \rightarrow 3/2$ transition with change of parity. So if this resonance is $3/2^+$, the 1·34 Mev level cannot be $3/2^-$, and vice versa.

The conclusions given above are displayed in figure 2. The spins and parities given on the left of that figure are all the values consistent with the experimental results ; those in brackets are considered to be unlikely.

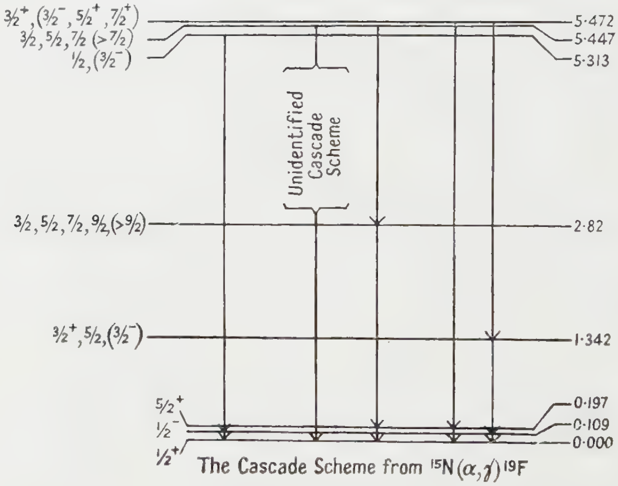

Figure 2. The cascade scheme from $^{15}N(\alpha, \gamma)^{19}F$.

Only one useful comparison can be made between this work and the predictions of Elliott and Flowers. This is on the spin of the 2·82 Mev level. This work excludes the possibility of a spin of 1/2, and provides two reasons for considering a high spin to be likely. Firstly, the level decays to the $5/2^+$ state rather than to either of the 1/2 states in the very low-lying group ; and secondly, the only one of the three resonances which decays to the 2·82 Mev level is also the only one which does not decay to any of the very low-lying states.

ACKNOWLEDGMENTS

The writer is obliged to Mr. E. S. Shire for suggesting the study of the radiative capture of alpha particles, and for his continued advice and encouragement. He also wishes to express his thanks to Trinity College, Cambridge, for a Research Scholarship and to the Department of Scientific and Industrial Research for a maintenance grant.

REFERENCES

AJZENBERG, F., and LAURITSEN, T., 1955, *Rev. Mod. Phys.*, **27,** 77.
BLATT, J. M., and WEISSKOPF, V. F., 1952, *Theoretical Nuclear Physics* (New York : Wiley).
ELLIOTT, J. P., and FLOWERS, B. H., 1955, *Proc. Roy. Soc.* A, **229,** 536.
FREEMAN, J., 1956, *Phil. Mag.*, **1,** 591.
HUTCHINSON, G. W., and SCARROTT, G. G., 1951, *Phil. Mag.*, **42,** 792.
LANE, A. M., 1954, *The Reduced Widths of Nuclear Energy Levels* (A.E.R.E., Harwell).
LI, C. W., 1952, *Phys. Rev.*, **88,** 1038.
MALM, R., and BUECHNER, W. W., 1950, *Phys. Rev.*, **80,** 771.
PRICE, P. C., 1954, *Phil. Mag.*, **45,** 237; 1955, *Proc. Phys. Soc.* A, **68,** 553.
SCHARDT, A., FOWLER, W. A., and LAURITSEN, C. C., 1952, *Phys. Rev.*, **86,** 527.
WILKINSON, D. H., 1956, *Phil. Mag.*, **1,** 127.
WILKINSON, D. H., TOPPEL, B. J., and ALBURGER, D. E., 1956, *Phys. Rev.*, **101,** 1485.

Elastic Scattering of Low Energy Nucleons by Complex Nuclei

By G. E. BROWN and C. T. DE DOMINICIS[†]
Department of Mathematical Physics, University of Birmingham

Communicated by R. E. Peierls; MS. received 9*th May* 1957, *and in final form* 6*th June* 1957

Abstract. The relation of the complex well which is used to describe average features of the scattering to dispersion theory is discussed. A model is employed in which the compound states have an underlying single-particle structure. It is shown that a complex well can be defined which reproduces the average scattering phase. The imaginary part of this well is simply related to the absorption.

§ 1. Introduction

Certain regularities are found in the scattering of low energy nucleons by complex nuclei. In particular, 'giant resonances' of width 1–4 mev are found in the average total cross section, the averaging being carried out over a band of energies of about 100 kev or so (this averaging is often carried out experimentally, since the incident beam usually contains an energy spread of this order). The positions and magnitudes of these giant resonances vary slowly and regularly with A, the atomic number. A summary of the experimental data is contained in the paper of Feshbach, Porter and Weisskopf (1954) who show that the average total cross section is reproduced by that calculated from a complex potential well of constant depth $(1+i\zeta)V_0$, where V_0 is -42 mev and ζ lies between 0·03 and 0·05, and of range $R=1{\cdot}45\times10^{-13}A^{1/3}$ cm.

In this paper, these regularities will be considered within the framework of nuclear dispersion theory. A picture proposed by Professor Peierls will be employed in which the compound nucleus levels, as a function of energy, have an underlying single particle structure. This picture has been used by Bowcock (1957) to provide a basis for the theory of Feshbach, Porter and Weisskopf. He shows, in particular, that between resonances in the complex well—the so-called single particle resonances—contributions to the scattering amplitude from the distant levels can be summed and that the amplitude from these is just that arising from a suitable complex well. Bowcock's work is reformulated here and it is shown that the complex well can reproduce the average phase even on the single particle resonances.

The object of this development is to provide a deeper understanding of the complex potential model of Feshbach, Porter and Weisskopf, and to show what can be learned by fitting the experimental data by results from a complex well.

[†] Now at Centre d'Études Nucléaires de Saclay.

§ 2. DESCRIPTION OF THE SCATTERING

The scattering will be described by a modified form of the Kapur–Peierls formalism†. For simplicity, scattering of a nucleon will be considered and it will be assumed that the same nucleon emerges with either the same energy (elastic scattering) or with a lower energy (inelastic scattering). The generalization to cases where more complex structures are in either the incident or scattered beam will be considered in a later paper. The treatment will be carried out in a somewhat symbolic fashion, with suppression of angular momentum and spin indices. Antisymmetrization between the initial nucleon and the nucleons in the nucleus is not carried out. This neglect does not seem to change the argument essentially.‡ The ground state of the initial nucleus will be represented by $\chi_0(\boldsymbol{\xi})$ where $\boldsymbol{\xi}$ stands for all nuclear coordinates, and the excited states by $\chi_j(\boldsymbol{\xi})$. For $r > R$ where R is some radius beyond which the potential $V(\mathbf{r}, \boldsymbol{\xi})$ vanishes, the wave function of the entire system is

$$\Psi = \chi_0(\boldsymbol{\xi})\psi_\alpha(\mathbf{r}) + S_\alpha{}^{ce}\chi_0(\boldsymbol{\xi})\psi_\alpha{}^{+}(\mathbf{r}) + \sum_{\alpha'} S_{\alpha\alpha',j}{}^{i}\chi_j(\boldsymbol{\xi})\psi_{\alpha'}{}^{+}(\mathbf{r}) \qquad \ldots\ldots(1)$$

where $\psi_\alpha(\mathbf{r})$ is the wave function which is regular at the origin defined in a complex potential $\hat{V}$ i.e.

$$\hat{H}\psi_\alpha(\mathbf{r}) = (T + \hat{V})\psi_\alpha(\mathbf{r}) = E\psi_\alpha(\mathbf{r}) \qquad \ldots\ldots(1.1)$$

and α is the 'channel label', denoting the totality of spin and angular momentum coordinates. Hence, $\psi_\alpha(\mathbf{r})$ is the product of an angular function and a radial function (see (3)). For s-waves, $r\psi_\alpha$ is just $e^{i\delta}\sin(kr+\delta)/2\sqrt{\pi}$ for $r > R$, where δ is the phase shift from the complex well. The functions $\psi_\alpha{}^{+}$ are solutions in the same potential, but chosen so that they represent outgoing waves; they become asymptotic to an angular function times $e^{i(kr+c)}/r$ as $r \to \infty$ where $k^2 = 2ME/\hbar^2$. The $\psi_{\alpha'}{}^{j}$ are defined by

$$(T + \hat{V})\psi_{\alpha'}{}^{j} = (E - E_j)\psi_{\alpha'}{}^{j} \qquad \ldots\ldots(1.2)$$

and an upper suffix + is sometimes used to indicate that the solution representing outgoing waves is chosen. It is seen from (1.2) that the $\psi_{\alpha'}{}^{j}$ also depend upon j through the energy. The $S_\alpha{}^{ce}$ is the coefficient of the elastically scattered wave not included in $\psi_\alpha(\mathbf{r})$ which determines what is usually called (Feshbach *et al.* 1954) the compound elastic scattering. The $S_{\alpha\alpha',j}{}^{i}$ is the coefficient of the wave scattered inelastically into the channel labelled by α' and j.

For $r < R$, Ψ can be represented by

$$\Psi = \chi_0(\boldsymbol{\xi})\psi_\alpha(\mathbf{r}) + \sum_{p} a_p \Phi^{(p)}(\boldsymbol{\xi}, \mathbf{r}) \qquad \ldots\ldots(2)$$

where $\Phi^{(p)}$ are a complete set of states which are defined to be eigenstates of the total Hamiltonian H, where

$$H = H_\xi + T + V(\mathbf{r}, \boldsymbol{\xi}) \qquad \ldots\ldots(2.1)$$

with H_ξ the Hamiltonian of the initial nucleus, T the kinetic energy of the incident nucleon and $V(\mathbf{r}, \boldsymbol{\xi})$ the potential between the incident nucleon and the nucleus (which is the sum of the nucleon–nucleon potentials between the incident particle and each particle in the nucleus in the realistic case). Thus we require as in Kapur and Peierls (1938)

---

† This modification was suggested by Professor Peierls.

‡ This point is discussed by Lane and Thomas (1957).

$$H\Phi^{(p)} = W_p \Phi^{(p)}. \qquad \ldots\ldots(2.2)$$

The $\Phi^{(p)}$ will be required to satisfy the boundary condition

$$\left[\int \chi_j(\xi) \frac{d}{dr} \Phi^{(p)}(\xi, \mathbf{r}) d\xi = f_{\alpha', j}{}^{+}(r, E-E_j) \int \chi_j(\xi) \Phi^{(p)}(\xi, \mathbf{r}) d\xi\right]_{r=R} \qquad \ldots\ldots(2.3)$$

with

$$f_{\alpha', j}{}^{+}(r, E-E_j) = \frac{d[r\psi_{\alpha', j}{}^{+}]/dr}{\psi_{\alpha', j}{}^{+} r}. \qquad \ldots\ldots(2.4)$$

The $f_{\alpha', j}{}^{+}$ is the logarithmic derivative for outgoing waves of energy $E-E_j$ at the edge of the nucleus; hence (2.3) and (2.4) express the requirement that the component of the scattered nucleon in $\Phi^{(p)}$ is an outgoing wave at the edge of the nucleus. The Φ's are chosen to obey the orthogonality and normalization conditions

$$\int_0^R \Phi^{(n)} \Phi^{(n')} d\tau = \delta_{nn'}. \qquad \ldots\ldots(2.5)$$

This normalization is different from that of Kapur and Peierls who use

$$\int_0^R |\Phi^{(n)}|^2 d\tau = 1, \qquad \ldots\ldots(2.6)$$

with the result that $\int_0^R \Phi^{(n)} \Phi^{(n)} d\tau = N_n$ where N_n is a complex constant. Since N_n vanishes only in exceptional cases (Peierls 1948), the $\Phi^{(n)}$ of Kapur and Peierls can be divided by $\sqrt{N_n}$ to give (2.5). This makes completeness relations (see (9.1)) simpler. The $\psi_\alpha(\mathbf{r})$ must be continuous at R. Equating the Ψ's from (1) and (2) at R determines the $S_\alpha{}^{ce}$ and $S_{\alpha\alpha', j}{}^{i}$. The ψ_α can be written as

$$\psi_\alpha(\mathbf{r}) = \Theta_\alpha(\theta) \phi_\alpha(r) \qquad \ldots\ldots(3)$$

where $\Theta(\theta)$ is a normalized function of all angle variables θ, and the ψ^{+}'s as

$$\psi_\alpha{}^{+}(\mathbf{r}) = \Theta_\alpha(\theta) \phi_\alpha{}^{+}(r)$$
$$\psi_{\alpha'}{}^{+}(\mathbf{r}) = \Theta_{\alpha'}(\theta) \phi_{\alpha'}{}^{+}(r). \qquad \ldots\ldots(3.1)$$

It is then found that

$$S_\alpha{}^{ce} = \frac{1}{\phi_\alpha{}^{+}(R)} \sum_p a_p \int_0^R d\xi \int d\theta \Phi^{(p)}(\xi, \mathbf{R}) \chi_0(\xi) \Theta_\alpha(\theta) \qquad \ldots\ldots(4)$$

where the integral is related to the square root of the reduced width. Also

$$S_{\alpha\alpha', j}{}^{i} = \frac{1}{\phi_{\alpha', j}{}^{+}(R)} \sum_p a_p \int_0^R d\xi \int d\theta \Phi^{(p)}(\xi, \mathbf{R}) \chi_j(\xi) \Theta_{\alpha'}(\theta). \qquad \ldots\ldots(4.1)$$

The a_p can now be determined by requiring the wave function to satisfy the Schrödinger equation inside the nucleus,

$$H\Psi = E\Psi \qquad \ldots\ldots(5)$$

which becomes, when Ψ is expressed as in (2),

$$(H-E)\chi_0(\xi)\psi_\alpha(\mathbf{r}) + \sum a_p (W_p - E) \Phi^{(p)}(\xi, \mathbf{r}) = 0. \qquad \ldots\ldots(5.1)$$

Multiplying by $\Phi^{(p)}$ on the left and integrating:

$$(W_p - E) a_p = -\int_0^R d\xi \int_0^R d\mathbf{r} \Phi^{(p)}(\xi, \mathbf{r}) (V - \hat{V}) \chi_0(\xi) \psi_\alpha(\mathbf{r}) \qquad \ldots\ldots(5.2)$$

where (1.1) and (2.5) have been employed. Consequently, S_α^{ce} and $S_{\alpha\alpha',j}^{i}$ are determined by (4), (4.1) and (5.2). Explicitly

$$S_\alpha^{\mathrm{ce}} = -\frac{1}{\phi_\alpha^{-}(R)} \sum_{\mathrm{p}} \int_0^R d\boldsymbol{\xi} \int_0^R d\mathbf{r}\, \frac{\Phi^{(\mathrm{p})}(\boldsymbol{\xi}, \mathbf{r})(V-\hat{V})\chi_0(\boldsymbol{\xi})\psi_\alpha(\mathbf{r})}{W_{\mathrm{p}}-E}$$

$$\times \int_0^R d\boldsymbol{\xi} \int d\theta \Phi^{(\mathrm{p})}(\boldsymbol{\xi}, \mathbf{R})\chi_0(\boldsymbol{\xi})\Theta_\alpha(\theta), \qquad \ldots\ldots(6)$$

$$S_{\alpha\alpha',j}^{i} = -\frac{1}{\phi_{\alpha',j}^{+}(R)} \sum_{\mathrm{p}} \int_0^R d\boldsymbol{\xi} \int_0^R d\mathbf{r}\, \frac{\Phi^{(\mathrm{p})}(\boldsymbol{\xi}, \mathbf{r})(V-\hat{V})\chi_0(\boldsymbol{\xi})\psi_\alpha(\mathbf{r})}{W_{\mathrm{p}}-E}$$

$$\times \int_0^R d\boldsymbol{\xi} \int d\theta \Phi^{(\mathrm{p})}(\boldsymbol{\xi}, \mathbf{R})\chi_j(\boldsymbol{\xi})\Theta_{\alpha'}(\theta). \qquad \ldots\ldots(7)$$

These formulae are exact. However, evaluation would require information about all of the compound states. We shall clearly have to make approximations. As noted earlier, a model will be employed here in which the compound states have an underlying single particle structure. In order to make these later approximations more transparent, we will now transform (6) and (7) to two different equivalent forms, each of which has some advantages for the later development.

The single particle aspects of the picture can be brought out by expanding the compound state functions in terms of single particle functions and residual nucleus functions χ_j in the way Bowcock (1957) has done. In the potential $\hat{V}(r)$ there will be a set of eigenfunctions $\hat{\psi}_m(\mathbf{r})$ defined by

$$\hat{H}\hat{\psi}_m = E_m\hat{\psi}_m \qquad \ldots\ldots(8)$$

$$\int_0^R \hat{\psi}_m^2(r)d\tau = 1,$$

and the boundary condition

$$\frac{d}{dr}[r\hat{\psi}_m(\mathbf{r})]|_R = f^{+}(R, E)\hat{\psi}_m(\mathbf{R})R \qquad \ldots\ldots(8.1)$$

with

$$f^{+}(r) = \frac{d[r\psi^{+}(\mathbf{r})]/dr}{\psi^{+}(\mathbf{r})r}$$

where the upper suffix + indicates that the outgoing wave boundary condition is chosen. The compound state wave functions can then be expressed as

$$\Phi^{(\mathrm{p})}(\boldsymbol{\xi}, \mathbf{r}) = \sum a_{jm}^{\mathrm{p}}\chi_j(\boldsymbol{\xi})\hat{\psi}_m^{j}(\mathbf{r}) \qquad \ldots\ldots(8.2)$$

where the upper suffix j indicates that in defining the boundary conditions on $\hat{\psi}$, E is to be replaced by $E-E_j$ in the f^{+} in (8.1). The eigenvalues of $\hat{\psi}_m^{j}$ will be labelled E_m^{j}. The particular choice of boundary conditions here is made so that resonances in the $\psi_\alpha(\mathbf{r})$ and $\psi_{\alpha'}^{j}(\mathbf{r})$ occur at energies equal to the real part of the energy eigenvalues of $\hat{\psi}_m$ and $\hat{\psi}_m^{j}$ respectively.

In order to understand later approximations, we shall be interested in the distribution of the a_{jm}^{p} with respect to energy. Lane, Thomas and Wigner (1955) discuss the distribution of quantities similar to the $|a_{jm}^{\mathrm{p}}|^2$†. In their model the quantities $|a_{jm}^{\mathrm{p}}|^2$ are large only if W_{p} is in the region of $E_m^{\ j}+E_j$. This simply expresses the fact that if the potential $V(\mathbf{r}, \boldsymbol{\xi})$ is not sufficiently strong or rapidly varying to break up the single particle structure of the levels, then the components $\chi_j(\boldsymbol{\xi})\psi_m^{\ j}(\mathbf{r})$ in $\Phi^{(\mathrm{p})}$ are large only in the neighbourhood of the resonance energy they would have if $V(\mathbf{r}, \boldsymbol{\xi})$ were equal to $\hat{V}$. More precisely, the criterion for the validity of this picture is that $\langle jm|(V-\hat{V})^2|jm\rangle$ where j and m indicate the core state and single particle function, respectively, is less than $(E_m^{\ j}-E_{m+1}^{\ \ j})^2$ where $E_{m+1}^{\ \ j}$ is the energy of the nearest single particle level with the same angular momentum. The distribution of the $(a_{jm}^{\mathrm{p}})^2$ employed here has been discussed by Bowcock (1957), who finds the same criterion for validity. This picture is illustrated in figure 1†. The second moment of this distribution is just $\langle jm|(V-\hat{V})^2|jm\rangle$.

---

† The picture employed here was, in fact, outlined by Professor Peierls to one of the authors (G.E.B.) in 1952 before the publication of the paper by Lane, Thomas and Wigner.

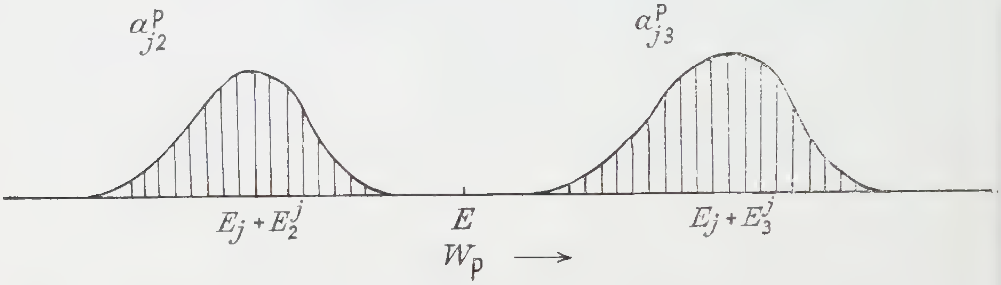

Figure 1. Each vertical line indicates the energy at which a_{j2}^{p} or a_{j3}^{p} are found in a compound state $\Phi^{(i)}$. The height of the vertical line is meant to indicate the magnitude of $|a_{j2}^{\mathrm{p}}|^2$ or $|a_{j3}^{\mathrm{p}}|^2$.

The picture shown in figure 1 would appear to be a good one. It will be shown in a following paper that the distance between levels of the same angular momentum is about 60 MeV in nuclei of intermediate A. Vogt and Lascoux (1957 to be published) have calculated the second moment for $A=100$ for various assumed nucleon–nucleon forces and find it to be about (8 MeV)^2. This is consistent with a reasonable concentration of the $(a_{jm}^{\mathrm{p}})^2$ about the single particle resonances.‡

Let us now consider elastic scattering, in which case we are interested in states $\Phi^{(i)}$ which have a large component of χ_0 and these will be in the neighbourhood of the E_m. Let us further assume, for the moment, that the energy E is

† It has been assumed here that the $|a_{jm}^{\mathrm{p}}|^2$ have approximately the same distribution as the $(a_{jm}^{\mathrm{p}})^2$. This is valid at low energies E, where the a_{jm}^{p} are almost real.

‡ To be precise, Vogt and Lascoux have used a representation in which the nuclear states are polarized by the scattered nucleon, and their states, therefore, contain r as a parameter; i.e., the nuclear state is $\chi(\boldsymbol{\xi}, \mathbf{r})$. The fact that their moment is much less than that originally obtained by Lane, Thomas and Wigner (1955) means that their representation is more nearly the correct one, i.e. that the a_{jm}^{p} are more concentrated about $E_j+E_m^{\ j}$ in their representation. Therefore, it should be used here. This can be done without altering the formal development, since the orthogonality and completeness relations are the same. Thus, Bowcock's picture is to be interpreted in the new sense and wave functions of the Vogt–Lascoux type are understood to be employed. This has the consequence that $\bar{V}=\int_0^\infty \chi^2(\boldsymbol{\xi}, \mathbf{r})V d\boldsymbol{\xi}$, a quantity to be employed later, is now velocity dependent, since it depends on the wave function of the scattered nucleon.

between the E_m as shown on figure 1. Substituting (8.2) in (6) gives

$$S_\alpha^{\mathrm{ce}} = -\frac{1}{\phi_\alpha^{+}(R)} \sum_{\mathrm{p}} \sum_{m} \sum_{j', m'} a_{0m}{}^{\mathrm{p}} a_{j'm'}{}^{\mathrm{p}} \int_0^R d\boldsymbol{\xi} \int_0^R d\mathbf{r}\, \chi_{j'}(\boldsymbol{\xi}) \hat{\psi}_{m'}{}^{j'}(\mathbf{r}) \\ \times \frac{(V-\hat{V})\chi_0(\boldsymbol{\xi})\psi_\alpha(\mathbf{r})}{W_{\mathrm{p}} - E} \int d\theta \hat{\psi}_m(\mathbf{R}) \Theta_{\alpha'}(\theta). \qquad \text{......(9)}$$

Since $a_{j'm'}{}^{\mathrm{p}}$ is large only if W_{p} is in the neighbourhood of $E_{j'} + E_{m'}{}^{j'}$, W_{p} in the denominator can be replaced, to a good approximation by $E_{j'} + E_{m'}{}^{j'}$. The sum over p can then be carried out with the use of

$$\sum_{\mathrm{p}} a_{jm}{}^{\mathrm{p}} a_{j'm'}{}^{\mathrm{p}} = \delta_{jj'} \delta_{mm'} \qquad \text{......(9.1)}$$

and the following expression is obtained

$$S_\alpha^{\mathrm{ce}} \simeq -\frac{1}{\phi_\alpha^{+}(R)} \sum_{m} \int_0^R d\boldsymbol{\xi} \int_0^R d\mathbf{r} \frac{\chi_0(\boldsymbol{\xi}) \hat{\psi}_m(\mathbf{r}) (V-\hat{V}) \chi_0(\boldsymbol{\xi}) \psi_\alpha(\mathbf{r})}{E_m - E} \\ \times \int d\theta \hat{\psi}_m(\mathbf{R}) \Theta_\alpha(\theta). \qquad \text{......(9.2)}$$

The function

$$g(\mathbf{r}, \mathbf{r}') \equiv \sum_m \frac{\hat{\psi}_m(\mathbf{r}) \hat{\psi}_m(\mathbf{r}')}{E_m - E} \qquad \text{......(10)}$$

which is a single particle Green's function will be considered now. This quantity satisfies the equations

$$\{\hat{H}(\mathbf{r}) - E\} g(\mathbf{r}, \mathbf{r}') = \delta(\mathbf{r} - \mathbf{r}') \qquad \text{......(10.1)}$$

and

$$\{\hat{H}(\mathbf{r}') - E\} g(\mathbf{r}, \mathbf{r}') = \delta(\mathbf{r} - \mathbf{r}').$$

Since g must be regular at the origin and at ∞ (outgoing waves), and continuous across $\mathbf{r} = \mathbf{r}'$, we must have

$$\begin{aligned} g(\mathbf{r}, \mathbf{r}') &= A \sum_\beta \psi_\beta(\mathbf{r}) \psi_\beta^{+}(\mathbf{r}') \qquad (r < r') \\ &= A \sum_\beta \psi_\beta^{+}(\mathbf{r}) \psi_\beta(\mathbf{r}') \qquad (r > r') \end{aligned} \qquad \text{......(10.2)}$$

where A is a constant which is determined by (10.1). Substituting for ψ and ψ^{+} from (3.1), and separating off the angle dependence it is found that (10.1) will be satisfied providing that

$$-\frac{A\hbar^2}{2Mrr'} \frac{d^2}{dr^2} \{r\phi_\beta^{+}(r) r'\phi_\beta(r') - r\phi_\beta(r) r'\phi_\beta^{+}(r')\} = \frac{1}{rr'} \delta(r - r') \qquad \text{......(10.3)}$$

implying that

$$-\frac{A\hbar^2}{2M} \{r'\phi_\beta(r') \frac{d}{dr} [r\phi_\beta^{+}(r)] - r'\phi_\beta^{+}(r') \frac{d}{dr} [r\phi_\beta(r)]\} = 1 \qquad \text{......(10.4)}$$

for $r = r'$. The normalization has not yet been specified. We choose it such that the Wronskian, which is the quantity in braces in (10.4) is equal to $-k$, where $(k)^2 = 2ME/\hbar^2$ and consequently

$$A\hbar^2 k/2M = 1 \quad \text{......(10.5)} \qquad \text{or} \qquad A = 2M/\hbar^2 k. \qquad \text{......(10.6)}$$

Hence

$$S_\alpha^{\mathrm{ce}} \simeq -\frac{2M}{\hbar^2 k} \int_0^R d\boldsymbol{\xi} \int_0^R d\mathbf{r}\, \chi_0(\boldsymbol{\xi}) \psi_\alpha(\mathbf{r}) (V - \hat{V}) \chi_0(\boldsymbol{\xi}) \psi_\alpha(\mathbf{r}). \qquad \text{......(11)}$$

The main error made in replacing W_{p} by E_m is in the neglect of contributions from the near levels. We shall see that this contribution determines the imaginary part of $\hat{V}$. This is small compared with the real part, which is determined by the contribution evaluated earlier, equation (11), but must be kept, and becomes of primary importance on the single particle resonances. However, rather than continue the expansion of which equation (11) gives the first term, we will obtain the exact remainder. We achieve this by using the identities

$$\frac{1}{W_{\mathrm{p}}-E}\Phi^{(\mathrm{p})}=\frac{1}{H-E}\Phi^{(\mathrm{p})}=\left\{\frac{1}{\hat{H}-E}-\frac{1}{H-E}(H-\hat{H})\frac{1}{\hat{H}-E}\right\}\Phi^{(\mathrm{p})}$$

$$=\sum_{j,m}\frac{a_{jm}{}^{\mathrm{p}}}{E_j+E_m-E}\left\{1-\frac{1}{H-E}(V-\hat{V})\right\}\chi_j(\boldsymbol{\xi})\hat{\psi}_m{}^j(\mathbf{r}) \qquad \ldots\ldots(12)$$

where $\hat{H}=T+\hat{V}$. Using (10.2) and (10.6) then gives

$$S_\alpha{}^{\mathrm{ce}}=-\frac{2M}{\hbar^2k}\int_0^R d\boldsymbol{\xi}\int_0^R d\mathbf{r}\,\chi_0(\boldsymbol{\xi})\psi_\alpha(\mathbf{r})(V-\hat{V})\left\{1-\frac{1}{H-E}(V-\hat{V})\right\}$$

$$\times\chi_0(\boldsymbol{\xi})\psi_\alpha(\mathbf{r}). \qquad \ldots\ldots(13)$$

Of course, (13) could have been obtained much more directly but the above development indicates that the second term in braces is small, and therefore we can treat it approximately.

§ 3. Average Scattering Amplitude

In order to facilitate the discussion, we now write equations like (13) in matrix form, with the following notation

$$\chi_j(\boldsymbol{\xi})=|j\rangle,\quad \chi_j(\boldsymbol{\xi})\psi_\alpha(\mathbf{r})=|j\alpha\rangle,$$

$$\Phi^{(\mathrm{p})}(\boldsymbol{\xi},\mathbf{r})=|\mathrm{p}\rangle,\quad \chi_j(\boldsymbol{\xi})\hat{\psi}_m(\mathbf{r})=|jm\rangle \qquad \ldots\ldots(14)$$

and $j=0$ will refer to the terms in which the residual nucleus is in the ground state. We will call an operator A diagonal if

$$\langle j|A|j'\rangle=A'\delta_{jj'} \qquad \ldots\ldots(14.1)$$

where A' is a number; hence it is diagonal in the states of the residual nucleus. Equation (13) can be rewritten

$$S_\alpha{}^{\mathrm{ce}}=-\frac{2M}{\hbar^2k}\left\{\langle 0\alpha|V-\hat{V}|0\alpha\rangle-\langle 0\alpha|(V-\hat{V})\frac{1}{H-E}(V-\hat{V})|0\alpha\rangle\right\}. \qquad \ldots\ldots(14.2)$$

It should be noted that $\langle 0\alpha|$ equals $|0\alpha\rangle$, and not $(|0\alpha\rangle)^*$ in this theory. In line with the discussion in § 1, we now average $S_\alpha{}^{\mathrm{ce}}$ over an energy interval I, such that

$$D\ll I \qquad \ldots\ldots(14.3)$$

where D is the order of the distance between compound nucleus levels. We shall choose $\hat{V}$ such that this average vanishes. Then,

$$\langle 0\alpha|V-\hat{V}|0\alpha\rangle=\left[\langle 0\alpha|(V-\hat{V})\frac{1}{H-E}(V-\hat{V})|0\alpha\rangle\right]_{\mathrm{Av}}. \qquad \ldots\ldots(15)$$

Using the unit operator $\mathrm{p}\rangle\langle\mathrm{p}$, (15) can be written

$$\langle 0\alpha|V-\hat{V}|0\alpha\rangle=\left[\sum_{\mathrm{p}}\langle 0\alpha|V-\hat{V}|\mathrm{p}\rangle\frac{1}{W_{\mathrm{p}}-E}\langle\mathrm{p}|V-\hat{V}|0\alpha\rangle\right]_{\mathrm{Av}}. \qquad \ldots\ldots(15.1)$$

Contributions to the right-hand side will come from states p whose energies are in the interval I and from states whose energies are outside. This latter contribution will be neglected for the moment. Then the average over I can be easily carried out, remembering that only the denominator is rapidly varying and that W_p has a small imaginary part. Then

$$\langle 0\alpha|V-\hat{V}|0\alpha\rangle = \sum_{p}{}^{I}\frac{i\pi}{I}\langle 0\alpha|V-\hat{V}|p\rangle^2 \qquad \ldots\ldots(16)$$

where the Σ^I is over all states p in the interval I.

In Feshbach *et al.* the averaging process is illustrated for the low energy region in which the levels are well separated. We consider first this case, and will establish a simple connection with their procedure.

The equations (15) and (15.1) are exact. We must, however, handle them approximately in order to evaluate $\hat{V}$. We specialize first to the region between single particle resonances, the advantage here being that the $\langle 0\alpha|p\rangle$ are small. We write

$$\hat{V} = \bar{V} - iW \qquad \ldots\ldots(17)$$

where

$$\bar{V} = \int_0^R \chi_0^2(\xi)V d\xi, \qquad \ldots\ldots(17.1)$$

then

$$\langle 0\alpha|0\alpha\rangle W = \sum_{p}{}^{I}\frac{\pi}{I}\langle 0\alpha|V-\hat{V}|p\rangle^2. \qquad \ldots\ldots(17.2)$$

In this low energy region $|p\rangle$ is mainly real. Further, $|0\alpha\rangle$ is real except for a complex factor; e.g., for s-waves and a square well potential of radius R

$$|\alpha\rangle = A\sin(K+i\kappa)r \qquad r<R \qquad \ldots\ldots(17.3)$$

where $K+i\kappa$ is the complex wave number inside the potential. The amplitude A, which is given by matching with the external wave function at the boundary, is given by

$$A = e^{i\delta}\frac{\sin(kR+\delta)}{\sin(K+i\kappa)R} \qquad \ldots\ldots(17.4)$$

where δ is the phase shift. Now κ is small in the low energy region ($\kappa \simeq (W/2\bar{V})K$) and can be neglected; since KR is nearly equal to $(n+\frac{1}{2})\pi$ at the centre of a giant resonance, the denominator in (17.4) is essentially unity here. In fact, for our present purpose a knowledge of the explicit form of A is not important because A^2 occurs on both sides of (17.2) and cancels out. In the region between resonances, we can set $\hat{V}$ equal to $\bar{V}$ on the right-hand side of (17.2) since the diagonal elements, $i\langle 0\alpha|W|p\rangle$ are certainly negligible here. Hence

$$W \simeq \sum_{p}{}^{I}\frac{\pi}{I}\frac{\langle 0\alpha|V-\bar{V}|p\rangle^2}{\langle 0\alpha|0\alpha\rangle}. \qquad \ldots\ldots(17.5)$$

and the right-hand side is real to a good approximation. In the appendix it is shown that the absorption σ_p into the compound state p is given by

$$\sigma_p = 2\pi C|\langle 0\alpha|V-\hat{V}|p\rangle|^2 \qquad \ldots\ldots(17.6)$$

where again we can replace $\hat{V}$ by $\bar{V}$. Therefore, W has a simple relation to the absorption, since we have established above that

$$\frac{\langle 0\alpha|V-\bar{V}|p\rangle^2}{\langle 0\alpha|0\alpha\rangle} \simeq \frac{|\langle 0\alpha|V-\hat{V}|p\rangle|^2}{|\langle 0\alpha|0\alpha\rangle|} \qquad \ldots\ldots(17.7)$$

in the region of separated resonances.

The contribution to the right-hand side of (15) from states p whose energies lie outside the interval I seems to be small, since the denominator is large in this case. Also, the largest terms have varying signs and tend to cancel.

It is not obvious that the matrix elements of W can be neglected on the right-hand side of (17.2) when the energy is on a single particle resonance, and we next establish that they can be. For convenience we write

$$\begin{aligned}\langle 0\alpha|V-\hat{V}|\mathrm{p}\rangle \frac{1}{W_{\mathrm{p}}-E}\langle \mathrm{p}|V-\hat{V}|0\alpha\rangle &= \langle 0\alpha|V-\bar{V}|\mathrm{p}\rangle \frac{1}{W_{\mathrm{p}}-E}\langle \mathrm{p}|V-\bar{V}|0\alpha\rangle \\ &+\frac{i}{W_{\mathrm{p}}-E}\{\langle 0\alpha|V-\bar{V}|\mathrm{p}\rangle\langle \mathrm{p}|W|0\alpha\rangle+\langle 0\alpha|W|\mathrm{p}\rangle\langle \mathrm{p}|V-\bar{V}|0\alpha\rangle\} \\ &-\langle 0\alpha|W|\mathrm{p}\rangle\frac{1}{W_{\mathrm{p}}-E}\langle \mathrm{p}|W|0\alpha\rangle. \qquad \ldots\ldots(18)\end{aligned}$$

Now $\langle 0|V-\bar{V}|0\rangle=0$, and hence the matrix element of $V-\bar{V}$ has only off-diagonal elements, whereas that of W has only diagonal elements. It seems reasonable to assume that the quantity in braces in (18) averages out to zero because of the varying signs of the matrix elements. The first term on the right-hand side of (18) is the same as we considered previously, but we neglected the last term in the region between resonances because there $|\mathrm{p}\rangle$ has a negligible component of $|0\mathrm{m}\rangle$, i.e. of states in the uncoupled representation with the nucleus in the ground state. We now evaluate the last term. We will write these matrix elements in terms of matrix elements between the single particle states m and separate off those referring to the resonance the energy is on.

Using (10.2) and considering s-waves by way of example,

$$\psi_\alpha(r)=\frac{\hbar^2 k}{2M}\mathrm{e}^{-ikR}R\sum_m\frac{\hat{\phi}_m(r)\hat{\phi}_m(R)}{E_m-E}. \qquad \ldots\ldots(19)$$

We are concerned only with the last term of (18), since the first term has only off-diagonal terms and not being directly affected by the increase in the components $|0m\rangle$ in $|\mathrm{p}\rangle$, it is still given by our previous expression. This last term is

$$\begin{aligned}\delta\langle 0\alpha|V-\hat{V}|0\alpha\rangle &\equiv \sum_{\mathrm{p}} -\left\{\langle 0\alpha|W|\mathrm{p}\rangle\frac{1}{W_{\mathrm{p}}-E}\langle \mathrm{p}|W|0\alpha\rangle\right\}_{\mathrm{Av}} \\ &= -W^2\left(\frac{\hbar^2 k}{2M}\right)^2 \mathrm{e}^{-2ikR}\frac{R^2(\hat{\phi}_m(R))^2}{(E_m-E)^2} \\ &\times\sum_{\mathrm{p}}\langle 0m|\mathrm{p}\rangle\frac{1}{W_{\mathrm{p}}-E}\langle \mathrm{p}|0m\rangle \qquad \ldots\ldots(20)\end{aligned}$$

where we have kept only the term in the sum (19) referring to the single particle resonance that the energy is on. Now,†

$$R^2\langle 0m|\mathrm{p}\rangle\langle \mathrm{p}|0m\rangle\frac{\hbar^2 k}{M}(\hat{\phi}_m(R))^2\simeq\gamma_{\mathrm{p}} \qquad \ldots\ldots(21)$$

---

† Strictly

$$\gamma_{\mathrm{p}}=R^2\frac{\hbar^2 k}{M}\sum_{m',m''}\langle 0m''|\mathrm{p}\rangle^*\langle \mathrm{p}|0m'\rangle\hat{\phi}_{m''}^*(R)\hat{\phi}_{m'}(R).$$

However, the energy is on the mth resonance, and the other giant resonances of the same angular momentum are very far away, so we can take $m''=m'=m$. Further, the matrix elements $\langle 0m|\mathrm{p}\rangle$ are essentially real in this low energy range. Therefore, equation (21) is true to a good approximation.

where γ_{p} is the partial width for elastic scattering. Then (20) becomes

$$\delta\langle 0\alpha|V-\hat{V}|0\alpha\rangle = -\left(\frac{W}{E_m-E}\right)^2\left(\frac{\hbar^2k}{2M}\right)\mathrm{e}^{-2ikR}\,\tfrac{1}{2}\sum\left\{\frac{\gamma_{\mathrm{p}}}{W_{\mathrm{p}}-E}\right\}_{\mathrm{Av}}$$

$$= -\frac{\hbar^2k}{2M}\left(\frac{W}{E_m-E}\right)^2\mathrm{e}^{-2ikR}\frac{i\pi}{2}\left(\frac{\gamma}{D}\right)_{\mathrm{Av}} \qquad \ldots\ldots(22)$$

where D is the distance between compound levels. The quantity $(\gamma/D)_{\mathrm{Av}}$ is usually called the strength function. On the resonance,

$$E_m - E = i\alpha_m = i(W + \beta_m/2),$$

where β_m is the natural single particle width (see (10.1) of the following paper; typical values of W and β_m are given in that paper). Since the right-hand side of (22) is imaginary, we can write

$$\delta\langle 0\alpha|V-\hat{V}|0\alpha\rangle = i\delta W\langle 0\alpha|0\alpha\rangle. \qquad \ldots\ldots(22.1)$$

We find

$$\delta W = -\frac{1}{\langle 0\alpha|0\alpha\rangle}\frac{\hbar^2k}{4M}\mathrm{e}^{-2ikR}\left(\frac{W}{E_m-E}\right)^2\pi\left(\frac{\gamma}{D}\right)_{\mathrm{Av}}. \qquad \ldots\ldots(22.2)$$

Now, from (17.3) and (17.4),

$$\langle 0\alpha|0\alpha\rangle \simeq \mathrm{e}^{2i\delta}(R/2)\sin^2(kR+\delta). \qquad \ldots\ldots(22.3)$$

Remembering that $2\hbar^2k/MR=\Gamma_m$ for an s-wave resonance, where Γ_m is the single particle width, we find that

$$\delta W = -\mathrm{e}^{-2i(\delta+kR)}\frac{\Gamma_m}{4\sin^2(kR+\delta)}\left(\frac{W}{E_m-E}\right)^2\pi\left(\frac{\gamma}{D}\right)_{\mathrm{Av}}. \qquad \ldots\ldots(23)$$

In the region of separated resonances, $\pi(\gamma/D)_{\mathrm{Av}}<1$, Γ_m is less than W and the factor $W/(E_m-E)^2$ is always smaller than unity, so that it would appear that $\delta W \ll W$, even on the single particle resonances and that we can neglect it. If this is so, (17.7) is valid even on the single particle resonance, and W is simply related to the absorption into compound states.

At higher energies the compound nucleus levels overlap and the imaginary parts of $|\mathrm{p}\rangle$ and $|\mathrm{m}\rangle$ become large, and the fact that all quantities are complex complicates this argument. It is, however, clear from equation (15.1) that a potential can be defined which reproduces the average phase, although it may no longer be true that the real part of $\hat{V}$ is $\bar{V}$. Now it is usually assumed that the average phase is the same as the phase in this region (Feshbach, Porter and Weisskopf 1954) since the widths of the compound levels are much greater than the spacings, and the phase is the sum of the phases from several levels. This argument is correct if fluctuations are neglected. If the average phase is the same as the actual phase, this latter is also reproduced by the complex well. But the total cross section is given by the imaginary part of the forward elastic amplitude. Hence, the complex well reproduces not only the elastic cross section, but also the total cross section. Therefore, the imaginary part of the potential reproduces the reaction cross section.

We will not discuss here the relation of the average phase to the average cross section, since this is done in detail in Feshbach, Porter and Weisskopf (1954).

§ 4. Discussion

We have shown in the preceding development that it is possible to obtain a complex potential which will reproduce the average scattering phase. The imaginary part can be simply interpreted as describing the disappearance of particles out of the incident beam into compound states.

It is interesting to see how the argument of § 3 depends on the validity of the intermediate model discussed by Lane, Thomas and Wigner (1955) and Bowcock (1957). This was used in showing that the part of $\bar{S}_\alpha$ which we could handle exactly (see equation (11)) was the main term, and that, therefore, we had to obtain the remainder to first order.

It should be noted, however, that equations (13) and (15) are exact, and that we could also carry through the development if the second term in braces in equation (13) were the main one. In this case, our potential would have a large imaginary part; this would tend towards the continuum model in which the particles are completely absorbed in the nucleus.

In a following paper, the scattering of a particle in a complex well will be described in order to derive several results used here, and in a further paper, a development similar to that used here will be applied to the inelastic scattering.

ACKNOWLEDGMENTS

The authors would like to thank Professor R. E. Peierls for many useful discussions about the model and formalism employed here. They are also grateful to Dr. A. M. Lane for several helpful suggestions.

APPENDIX

In this appendix we shall show how the right-hand side of equation (17.2) is related to compound state formation and decay in our modified version of the Kapur–Peierls dispersion theory.

We consider the inelastic scattering, which is given by

$$S_{\alpha\alpha',j}{}^{i} = -\frac{1}{\phi_{\alpha',j}{}^{+}(R)} \sum_{\mathrm{p}} \int_0^R d\boldsymbol{\xi} \int_0^R d\mathbf{r}\, \frac{\Phi^{(\mathrm{p})}(\boldsymbol{\xi},\mathbf{r})(V-\hat{V})\chi_0(\boldsymbol{\xi})\psi_\alpha(\mathbf{r})}{W_{\mathrm{p}}-E}$$

$$\times \int_0^R d\boldsymbol{\xi} \int d\theta\, \Phi^{(\mathrm{p})}(\boldsymbol{\xi},\mathbf{R})\chi_j(\boldsymbol{\xi})\Theta_{\alpha\alpha'}(\theta). \qquad \ldots\ldots \mathrm{A}(1)$$

Now $W_{\mathrm{p}} = \epsilon_{\mathrm{p}} - i\alpha_{\mathrm{p}}/2$, where ϵ_{p} and α_{p} are real, and we shall be interested in the width α_{p}. This can be obtained from the original equation

$$(H-W_{\mathrm{p}})\Phi^{(\mathrm{p})} = 0 \qquad \ldots\ldots \mathrm{A}(2)$$

and the conjugate equation

$$(H-W_{\mathrm{p}}{}^{*})\Phi^{(\mathrm{p})*} = 0. \qquad \ldots\ldots \mathrm{A}(2.1)$$

Changing these equations into equations on $r\Phi^{(\mathrm{p})}$ and $r\Phi^{(\mathrm{p})*}$, multiplying the first on the left by $r\Phi^{(\mathrm{p})*}$ and the second by $r\Phi^{(\mathrm{p})}$ and integrating, one obtains

$$i\alpha \int_0^R \Phi^{(\mathrm{p})*}\Phi^{(\mathrm{p})} d\tau = \frac{\hbar^2}{2M} \int_0^R d\boldsymbol{\xi} \int d\theta$$

$$\times \left\{ r\Phi^{(\mathrm{p})*} \frac{d}{dr}(r\Phi^{(\mathrm{p})}) - r\Phi^{(\mathrm{p})} \frac{d}{dr}(r\Phi^{(\mathrm{p})*}) \right\}\Bigg|_R . \qquad \ldots\ldots (\mathrm{A}2.2)$$

Using equation (2.3) and employing the expansion (8.2) this becomes

$$i\alpha = \frac{\hbar^2}{2M} \sum_{j,m,m'} a_{jm}{}^{\mathrm{p}*} a_{jm'}{}^{\mathrm{p}} R^2 \{\hat{\phi}_m{}^{j*}(R)\hat{\phi}_{m'}{}^{j}(R)[f^{+}(E-E_j,R) - f^{-}(E-E_j,R)]\}$$

$$\ldots\ldots \mathrm{A}(2.3)$$

where f^+ is the logarithmic derivative for outgoing waves and f^- the one for incoming waves. Using the Wronskian

$$(f^+-f^-)r^2\phi^+\phi^-=2ik_j \qquad \ldots\ldots \mathrm{A}(2.4)$$

where $(k_j)^2=2M(E-E_j)/\hbar^2$, we have

$$\alpha=\frac{\hbar^2}{M}\sum_{j,m,m'}k_j a_{jm}{}^{\mathrm{p}}a_{jm'}{}^{\mathrm{p}*}\frac{R^2\{\hat{\phi}_m{}^j(R)\hat{\phi}_{m'}{}^j(R)\}}{R^2\phi^+\phi^-(E-E_j,R)}. \qquad \ldots\ldots \mathrm{A}(2.5)$$

The $(R^2\phi^+\phi^-)^{-1}=(R|\phi^-|)^{-2}$ is just the penetration factor. Equation A(2.5) can be written $\alpha=\Sigma\alpha_j$ and α_j represents the width for leaving the residual nucleus in the jth excited state.

We calculate now the average cross section for inelastic scattering. In this we neglect cross terms, i.e. terms referring to different p, assuming that these cross terms will average to zero because of their varying phases. Then

$$\begin{aligned}\sigma=\sum_{\mathrm{p}}\sum_{j}\frac{1}{|\phi_{\alpha',j}{}^-(R)|^2}&\left|\int_0^R d\boldsymbol{\xi}\int_0^R d\mathbf{r}\Phi^{(\mathrm{p})}(\boldsymbol{\xi},\mathbf{r})(V-\hat{V}\chi_0)(\boldsymbol{\xi})\psi_\alpha(\mathbf{r})\right|\\ &\times\left|\int_0^R d\boldsymbol{\xi}\int d\theta\Phi^{(\mathrm{p})}(\boldsymbol{\xi},\mathbf{R})\chi_j(\boldsymbol{\xi})\Theta_{\alpha'}(\theta)\right|^2\\ &\times|1/(W_{\mathrm{p}}-E)|^2\frac{4\pi}{k^2}\frac{k_j}{k}(2l+1). \qquad \ldots\ldots \mathrm{A}(3)\end{aligned}$$

Using equation (8.2) and A(2.5) this can be written

$$\sigma=C\sum_{\mathrm{p}}\alpha_{\mathrm{p}}\frac{1}{|W_{\mathrm{p}}-E|^2}\left|\int_0^R d\boldsymbol{\xi}\int_0^R d\mathbf{r}\Phi^{(\mathrm{p})}(\boldsymbol{\xi},\mathbf{r})(V-\hat{V})\chi_0(\boldsymbol{\xi})\psi_\alpha(\mathbf{r})\right|^2, \qquad \ldots\ldots \mathrm{A}(4)$$

where

$$C=\frac{4\pi}{k^3}\frac{M}{\hbar^2}(2l+1).$$

Assuming that the incident beam is of width I

$$\bar{\sigma}=\frac{1}{I}\sum{}^I\sigma_{\mathrm{p}}$$

where

$$\begin{aligned}\sigma_{\mathrm{p}}&=C\int\left|\frac{1}{W_{\mathrm{p}}-E}\right|^2 dE\alpha_{\mathrm{p}}\left|\int_0^R d\boldsymbol{\xi}\int_0^R d\mathbf{r}\,\Phi^{(\mathrm{p})}(\boldsymbol{\xi},\mathbf{r})(V-\hat{V})\chi_0(\boldsymbol{\xi})\psi_\alpha(\mathbf{r})\right|^2\\ &=2\pi C\left|\int_0^R d\boldsymbol{\xi}\int_0^R d\mathbf{r}\Phi^{(\mathrm{p})}(\boldsymbol{\xi},\mathbf{r})(V-\hat{V})\chi_0(\boldsymbol{\xi})\psi_\alpha(\mathbf{r})\right|^2\\ &=2\pi C|\langle\mathrm{p}|V-\hat{V}|0\alpha\rangle|^2. \qquad \ldots\ldots \mathrm{A}(5.1)\end{aligned}$$

Since the sum in A(3) includes $j=0$, σ_{p} contains the compound elastic, as well as inelastic, scattering. Thus, the term occurring on the right-hand side of equation (17.2) is simply related to the inelastic plus compound elastic scattering.

REFERENCES

Bowcock, J., 1957, *Proc. Phys. Soc.* A, **70**, 515.
Brown, G. E., 1957, *Proc. Phys. Soc.* A, **70**, 681.
Feshbach, H., Porter, C. E., and Weisskopf, V. F. 1954, *Phys. Rev.*, **96**, 448.
Kapur, P. L., and Peierls, R. E., 1938, *Proc. Roy. Soc.* A, **166**, 277.
Lane, A., and Thomas, R. G., 1957, *Rev. Mod. Phys.*, **29**, in the press.
Lane, A., Thomas, R. G., and Wigner, E. P., 1955, *Phys. Rev.*, **98**, 693.
Peierls, R. E., 1948, *Proc. Camb. Phil. Soc.*, **44**, 242.

Note added in proof. The δW of equation (23) is, in fact, not negligible, because the $\sin(kR+\delta)$ occurring in the denominator is much less than unity, even on the resonance, for a well with an imaginary part. Further work has shown, however, that substitution of the right-hand side of equation (17.7) into equation (17.5) gives an equation relating W to σ_{p} which is valid even on the single particle resonance, although neither of these equations is valid separately, and, therefore, our conclusions are correct. This is because we have also neglected terms in the sum over p in equation (15.1) lying outside the interval I, and these are not negligible. We shall develop this point further later.

Resonances in a Complex Well

By G. E. BROWN
Department of Mathematical Physics, University of Birmingham

Communicated by R. E. Peierls; MS. received 9th May 1957, and in final form 23rd July 1957

Abstract. The scattering in a complex well of the type used in optical model calculations is described by dispersion theory. The positions and widths of the resonances are found.

§ 1. Introduction

A number of problems which arise in the scattering of low energy nucleons by complex nuclei involve replacing the nucleus by a complex potential, which is supposed to reproduce the average features of the scattering, and the solution then of the scattering in the complex potential (see Feshbach, Porter and Weisskopf, 1954). Whereas the solution of this latter problem is usually accomplished by solving the Schrödinger equation inside the potential and then matching the solution with the solution outside to determine the phase shifts, the scattering can also be described in the resonance formalism. This description is impractical for the numerical evaluation of the scattering, but is useful in making various arguments, some of which were necessary for the development in the preceding paper.

Firstly, the widths of the levels are of interest, because they govern the distance in which the scattering cross section can change appreciably. Secondly, the magnitude of the maximum contribution from any given partial wave—which comes from the peak of the relevant resonance—to the scattering cross section is of interest. Thirdly, the spacing of these resonances is crucial in determining the validity of the nuclear model proposed by Lane, Thomas and Wigner (1955) and Bowcock (1957). In this model, the giant resonances observed in the elastic scattering come from concentrations of compound states with certain characteristics just in the region of the resonances in the complex potential, as was discussed in the preceding paper. If the levels are far apart, the model is valid.

The dispersion formalism of Kapur and Peierls (1938) will be used ; in this formalism the resonance energy is complex. The maximum in the amplitude occurs when the incident energy is equal to the real part of the resonance energy, and the imaginary part of the resonance energy is just the half-width of the resonance.

§ 2. Development

In the Kapur–Peierls formalism, the single particle resonance states are defined by [†]

$$(T+\hat{V})\hat{\phi}_m(r)=E_m\hat{\phi}_m(r) \qquad \ldots\ldots(1)$$

$$\left.\frac{d}{dr}(r\hat{\phi}_m)\right|_R=ikR\hat{\phi}_m(R) \qquad \ldots\ldots(1.1)$$

[†] Here $\hat{V}$ is a complex potential, and $\psi_m(r)$ is an eigenfunction in this well. The notation is the same as in the preceding paper (Brown and De Dominicis 1957, to be referred to as I).

where only s-waves are considered from simplicity. Extension of the results to higher angular momentum will be indicated below. The solutions of (1) and (1.1) will be later compared with $\hat{\phi}_m^{(0)}$ defined by

$$(T+\hat{V})\hat{\phi}_m^{(0)}(r)=E_m^{(0)}\hat{\phi}_m^{(0)}(r) \qquad \ldots\ldots(2)$$

$$\frac{d}{dr}\left(r\hat{\phi}_m^{(0)}\right)\Big|_R=0. \qquad \ldots\ldots(2.1)$$

These $\hat{\phi}_m^{(0)}$ are similar to the eigenstates of the Wigner-Eisenbud formalism. Both the E_m and $E_m^{(0)}$, are complex ; although the boundary condition of $\hat{\phi}_m^{(0)}$ is real, $\hat{V}$ is complex. The functions $\hat{\phi}_m^{(0)}$ are considered because it is easier to handle them numerically, and it will be shown that it is easy to obtain some of the necessary results from them.

The E_m will now be found for the case where $\hat{V}$ is a square well

$$\begin{aligned}\hat{V}&=-U-iW \qquad && r<R_0\\ &=0. && r>R_0\end{aligned} \qquad \ldots\ldots(3)$$

Inside the well the complex wave number for the resonance state $K-i\kappa$ will be given by

$$(K-i\kappa)^2=\frac{2M}{\hbar^2}(E_m+U+iW). \qquad \ldots\ldots(3.1)$$

The boundary condition (1.1) can be written

$$(K-i\kappa)\cos(K-i\kappa)R=ik\sin(K-i\kappa)R. \qquad \ldots\ldots(4)$$

For simplicity the joining radius R in (1.1) has been chosen to be the edge of the well, R_0. It can be chosen differently, but this is immaterial for the qualitative features of the results derived here.

Now κR will be shown to be small for low energies ; equation (4) will be expanded to first order in this quantity. Then

$$(K-i\kappa)(\cos KR+i\kappa R\sin KR)=ik(\sin KR-i\kappa R\cos KR). \qquad \ldots\ldots(5)$$

This gives immediately

$$\kappa=\frac{k\sin KR}{KR\sin KR-\cos KR}. \qquad \ldots\ldots(5.1)$$

It will be shown that $\cos KR \ll KR\sin KR$ (see equation (5.3)) so that

$$\kappa\simeq k/KR. \qquad \ldots\ldots(5.2)$$

Using this value for κ, one obtains from (5)

$$\cos KR\simeq-\frac{k^2R\sin KR}{K(KR)^2} \qquad \ldots\ldots(5.3)$$

to lowest order in κR. Now KR is large, of the order of 10 even for medium A and zero incident energy, and so κ and $\cos KR$ are small. We now let $KR=K_0R+\delta KR$ where $r\hat{\phi}_m^{(0)}=\sin K_0R$, and $K_0R=(n+\frac{1}{2})\pi$ gives a solution to (2.1). To lowest order in κR it is found from (5.2) that

$$\delta K=k\frac{k}{K(KR)^2} \qquad \ldots\ldots(5.4)$$

and this δK is very small because of the large value of KR. Writing $E_m=\epsilon_m-\frac{1}{2}i\alpha_m$,

$$(\epsilon_m-\tfrac{1}{2}i\alpha_m+U+iW)=\frac{\hbar^2}{2M}(K-i\kappa)^2 \qquad \ldots\ldots(6)$$

giving with the use of (5.4)

$$\delta E \equiv \epsilon_m - \epsilon_m^{(0)} = \frac{\hbar^2}{2M}(2K\delta K - \kappa^2) = \frac{1}{(KR^2)}\,\epsilon_m \qquad \ldots\ldots(7)$$

to lowest order in $(KR)^{-1}$. Here δE is the difference in the real part of the resonance energy resulting from the different boundary conditions (1.1) and (2.1). It is usually small because of the $(KR)^2$ in the denominator. For $A=55$, $\epsilon_m = 10$ Mev, $U=42$ Mev and $R = 1{\cdot}45A^{1/3}\times 10^{-13}$ cm, δE is found to be of the order of 0·2 Mev.

Also, one has from (6) and (5.4)

$$\alpha_m = 2W + \frac{2\hbar^2 k}{MR}. \qquad \ldots\ldots(8)$$

The second term on the right-hand side is just $\Gamma_m = (\hat{\phi}_m(R))^2$ in the approximation of small κ.

Now, in going from (4) to (5) an expansion in κR was made and, although κ is always small, $\kappa R \to 1$ as $k \to K$. For large k, then, (7) and (8) are not accurate; however, (7) will give the correct order of magnitude for δE since κR is, at most, of the order of unity.

There is no need to rely on the approximate expression for α_m, because an exact one can be obtained in a way simpler than above, where the development was mainly to obtain δE. Taking (1) and the complex conjugate

$$(T+\hat{V}^*)\hat{\phi}_m^* = E_m^*\hat{\phi}_m^* \qquad \ldots\ldots(9)$$

one can easily change these into equations on $r\hat{\phi}_m$ and $r\hat{\phi}^*_m$. Then multiplying the first on the left by $r\hat{\phi}_m^*$ and the second on the left by $r\hat{\phi}_m$, integrating from 0 to R and subtracting, one obtains

$$\alpha_m = 2W + \beta_m \qquad \ldots\ldots(10)$$

where

$$\beta_m = \frac{k\hbar^2 R^2}{MN_m}\left|\hat{\phi}_m(R)\right|^2 \qquad \ldots\ldots(10.1)$$

and use has been made of (1.1).

Here

$$N_m = \int_0^R |\hat{\phi}_m(r)|^2 r^2\, dr. \qquad \ldots\ldots(10.2)$$

The N_m are not equal to unity because the normalization

$$\int_0^R \hat{\phi}_m{}^2 r^2\, dr = 1$$

is employed here as in I (see I (2.5)). For small κR which follows if $kR \ll KR$ from (5.2), the $\hat{\phi}_m$ are mainly real, N_m is nearly unity, and $\Gamma_m \simeq \beta_m$.

Using (10), the equation on the $\hat{\phi}_m$ is just

$$(T-U)\hat{\phi}_m(r) = \left\{\epsilon_m - \frac{i}{2}\beta_m\right\}\hat{\phi}_m(r). \qquad \ldots\ldots(10.3)$$

Now β_m is just the width which would result from eigenfunctions subject to (1.1) in a real potential U. Thus, for a square well, the eigenfunctions $\hat{\phi}_m$ are the same as those defined in a real well, equal to the real part of $\hat{V}$. Consequently, the demonstration of completeness (see Peierls 1947) for real potentials is equally valid for complex potentials, in the case of square wells.

Now $\hat{S}$ can be written

$$\hat{S}=\tfrac{1}{2}\exp(-2ikR)\sum_m \frac{\Gamma_m}{\epsilon_m-\tfrac{1}{2}i\alpha_m-E}-\exp(-ikR)\sin kR. \qquad \ldots\ldots(10.4)$$

The generalization to higher angular momentum can easily be made, by replacing ikR in (1.1) by the logarithmic derivative of the function which describes outgoing waves of the appropriate angular momentum. This results in Γ_m and β_m containing penetration factors which reduce both considerably if $l>kR$. Because of the large value of the α_m, the various terms in (10.4) do not give the pronounced resonances one usually finds in dispersion theory. At very low energies, W is approximately, 1·3 to 2 Mev and this governs the half-widths as long as β_m is reduced by the penetration factor. For a bombarding energy of about 10 Mev, the W needed to fit the experiments is of the order of 10 Mev. For $A=55$, $U=42$ Mev and $R=1{\cdot}45A^{1/3}\times10^{-13}$ cm, $\tfrac{1}{2}\beta_m$ and $\tfrac{1}{2}\Gamma_m$ are of the order of 5 Mev for s-waves, so that the half-width $\tfrac{1}{2}\alpha_m$ is about 15 Mev.

It is now easy to understand the behaviour of (10.4) as W becomes large. As soon as W is large enough so that the phase shift of the relevant partial wave has a large imaginary part, the contribution to $\hat{S}$ from this partial wave will remain essentially constant (almost complete absorption). Now if $E\simeq\epsilon_m$, i.e., the energy is on a resonance, the contribution to $\hat{S}$ from this particular resonance is equal to $i\Gamma_m/(W+\tfrac{1}{2}\beta_m)$ where $\beta_m\simeq\Gamma_m$ and this decreases as W becomes larger. Therefore, a large W has the effect of increasing the nett contribution from the distant resonances. This is especially true of the higher angular momenta, where Γ_m and β_m are small.

§ 3. POSITIONS OF THE LEVELS

It will be shown in this section that the single particle levels of the same total quantum number and parity, but different l, tend to group, so that in most of the energy region there are no single particle resonances. The positions of the energy levels will be determined by using the approximate boundary condition (2.1). It has been shown in § 1 that this gives the positions of the levels defined by (1.1) to within a fraction of one Mev, and this is adequate for our purposes.

The single-particle resonances in a square well will first be considered. Here s-resonances occur at $KR\simeq(n+\tfrac{1}{2})\pi$. We consider by way of example a nucleus of $A=55$ (Much of the 10–20 Mev proton scattering has been done on nuclei of $A\sim55$). Here an s-wave resonance occurs near zero energy for a well of depth 42 Mev and range $R=1{\cdot}45\ A^{1/3}\times10^{-13}$ cm (see Feshbach, Porter and Weisskopf 1954). Here $n=2$. If this formula is assumed to give an approximate idea of where the next s-resonance will be, choosing $n=3$ gives an energy of the order of 40 Mev. The actual energy of the resonance is at least about 20 Mev higher because of the decrease in depth of the potential with increasing bombarding energy (velocity dependence of the potential) which tends to increase the energies of the higher resonances. Also, the well chosen has, if anything, too large a radius. In a narrower and deeper well, the next resonance would be even higher. Hence, the next s-wave resonance will occur at 60–80 Mev.

The position of the lowest d-state resonance will now be considered. In a square well for $kr\ll2$, the d-state wave function will be given well by $\phi_{\mathrm{d}}\simeq A\sin(Kr-\pi)$, where A is a constant, the asymptotic form of the spherical Bessel function has been used here. But $\sin(Kr-\pi)=-\sin Kr$ and so the wave function is just a constant times the negative of the s-state wave function, and any boundary conditions on the logarithmic derivative of the s-state function will be equally well satisfied by the d-function. Since $Kr \sim 8$ at the edge of the well for our example of $A=55$ and zero energy, the approximation is quite good and will be even better for heavier nuclei. It is seen in Feshbach, Porter and Weisskopf (1954) that the s and d resonances do tend to occur near together in their calculations. In fact, direct calculation shows the low energy s and d resonances to be $4\frac{1}{2}$ MeV apart for $A=55$ and $2\frac{1}{2}$ MeV apart for $A=150$, where the s resonance again occurs at zero energy. The g resonance need not be considered, because its contribution is, in any case, very small at low energies as mentioned at the end of the last section.

The same argument also shows that the odd parity levels of low l fall together approximately half way between the even parity levels. Therefore, it is clear that in most of the energy region the energy is between single-particle levels.

At higher energies the single-particle levels become very broad and the cross section does not show maxima of the type associated with resonances at lower energies. However, the dispersion theory description would still seem to make sense, because the distance between levels increases at least as rapidly as the widths. Whereas the latter increase linearly with k, the distance between levels increases linearly with K. This is seen by noting that $\Delta KR=\pi$, where $\delta K$is the difference between wave numbers of two successive levels of the same angular momentum. But $\Delta E \simeq \hbar^2 K \Delta K/M = \hbar^2 K\pi/MR$, thus the levels remain well separated even at high energies.

§ 4. DISCUSSION

We have shown that the single-particle levels in a complex well are well separated for nuclei of intermediate A. This is very important for the success of the intermediate model proposed by Lane, Thomas and Wigner (1955) and Bowcock (1957) as was discussed in I.

It has also been shown that the widths of the single particle resonances are at least as large as $2W$, and since W is several MeV in the intermediate energy region, the complex potential (or optical model, as it is usually called) will give marked changes in cross sections, etc. only over a region of several MeV. (See, for example, the giant neutron resonance in Pb and the neighbouring elements). Further, large values of W tend to decrease the contributions to the scattering amplitude from resonances the energy is on, giving increased importance to contributions from distant levels.

ACKNOWLEDGMENTS

The author would like to thank Professor R. E. Peierls and Dr. A. M. Lane for useful discussions on this subject.

REFERENCES

BOWCOCK, J., 1957, *Proc. Phys. Soc.* A, **70,** 515.
BROWN, G. E., and DE DOMINICIS, C. T., 1957, *Proc. Phys. Soc.* A, **70,** 668.
FESHBACH, H., PORTER, C. E., and WEISSKOPF, V. F., 1954, *Phys. Rev.*, **96,** 448.
KAPUR, P. L., and PEIERLS, R. E., 1938, *Proc. Roy. Soc.* A, **166,** 277.
LANE, A., THOMAS, R. G., and WIGNER, E. P., 1955, *Phys. Rev.*, **98,** 693.
PEIERLS, R. E., 1947, *Proc. Camb. Phil. Soc.*, **44,** Pt. 2, 242.

Direct Interaction and Nuclear Dispersion Theory

By G. E. BROWN and C. T. DE DOMINICIS†
Department of Mathematical Physics, University of Birmingham

Communicated by R. E. Peierls; MS received 9th May 1957

Abstract. The problem of inelastic scattering of several MeV nucleons is formulated in nuclear dispersion theory. The case where the residual nucleus is left in a state of low excitation is considered in detail. Contributions from the distant compound-nucleus levels can be summed explicitly, and give an expression similar to that usually employed in the theory of direct interaction to calculate differential cross sections. Contributions from the near compound-nucleus levels contribute in a complex fashion, and cannot explicitly be summed. It is assumed that phase relations can usually be neglected for them, and they, then, are responsible for the compound-inelastic scattering.

§ 1. Introduction

The inelastic scattering of nucleons by complex nuclei in the energy range of several MeV exhibits certain regularities (see for example the report of the Brookhaven Conference 1955) over a wide range of elements. In particular, in cases in which the residual nucleus is left in a state of low excitation, the angular distributions of inelastically scattered particles are usually strongly peaked forward and the cross sections are much higher than would be predicted by the statistical theory of nuclear energy levels. These angular distributions vary slowly with energy, as would be predicted by parameters of single-particle levels, rather than by those of the compound nucleus levels. This scattering is often called scattering by 'direct interaction'. On the other hand, the major part of the scattering leaves the residual nucleus in a highly excited state and fits in well with the statistical theory.

The statistical theory of energy levels neglects phase relations between the different levels. It will be shown here that the phases from distant energy levels do not tend to cancel out, but add coherently to give effects which vary as the parameters of single particle levels. The contribution of these distant levels to the scattering will be summed explicitly, using dispersion theory. It is assumed that there is no coherence between the phases of the near compound-nucleus levels if a suitable average over energy is taken, and these then produce the scattering described by the statistical theory. Hence, both types of scattering follow, as they must, if they are not dropped along the way by bad approximations, since the initial dispersion theory contains a complete description of the nucleus.

A model in which the compound nucleus levels have an underlying single-particle structure (Lane, Thomas and Wigner 1955, Bowcock 1957) will be employed here, as in a preceding paper, which dealt with the elastic scattering (Brown and De Dominicis 1957, to be referred to as I). Most of the formal development necessary for the present treatment is given in I and in Brown 1957, (to be referred to as II).

---

† Now at Centre d'Études Nucléaires de Saclay.

This model of Lane *et al.* and Bowcock is valid as long as the potential is not strong enough to break up the underlying single-particle structure. This criterion is stated more precisely in the above papers as being that the root mean square moment of the perturbing potential is less than the distance between single-particle states. Although no detailed discussion of the validity of this model is attempted in these papers, the fact that the single-particle resonances are very far apart, as demonstrated in II, lends considerable support to it.

§ 2. DEVELOPMENT

For simplicity, scattering of a nucleon will be considered, and it will be assumed that the same nucleon emerges with the same energy (elastic scattering) or with a lower energy (inelastic scattering of a particle from channel α into channel α' leaving the residual nucleus in the excited state j as given by I(7). Using the expansion I(8.2) for the compound state $\Phi^{(p)}(\boldsymbol{\xi}, \mathbf{r})$ in terms of the eigenfunctions $\hat{\psi}_m(\mathbf{r})$ for the single nucleon in the complex well $\hat{V}(\mathbf{r})$ and $\chi_j(\boldsymbol{\xi})$ for the residual nucleus, one obtains

$$S^i_{\alpha\alpha',j} = -\frac{1}{\phi_{\alpha',j}(R)}\sum_{p}\sum_{m}\sum_{j',m'} a^p_{jm}\, a^p_{j'm'} \int_0^R d\boldsymbol{\xi} \int_0^R \frac{d\mathbf{r}\,\chi_{j'}(\boldsymbol{\xi})\hat{\psi}^{j'}_{m'}(\mathbf{r})(\hat{V}-V)\chi_0(\boldsymbol{\xi})\psi_\alpha(\mathbf{r})}{W_p - E}$$
$$\times \int d\theta\, \hat{\psi}^j_m(\mathbf{R})\Theta_{\alpha'}(\theta). \qquad \ldots\ldots(1)$$

An approximate expression for $S^i_{\alpha\alpha',j}$ can be obtained in the same way as I (9.2) for S^{ce}_α by remembering that a^p_{jm} is large only if W_p is in the neighbourhood of $E_j - E_m{}^j$ (see figure 1 of I). Then, by a treatment analogous to that described following equation (9.2) of I, one easily obtains

$$S^i_{\alpha\alpha',j} \simeq -\frac{2M}{\hbar^2 k_j}\int_0^R d\boldsymbol{\xi}\int_0^R d\mathbf{r}\,\chi_j(\boldsymbol{\xi})\psi_{\alpha'}(\mathbf{r})V\chi_0(\boldsymbol{\xi})\psi_\alpha(\mathbf{r})$$
$$\sigma_{\alpha\alpha',j} \simeq 4\pi\frac{2l+1}{k^2}\,|S^i_{\alpha\alpha',j}|^2\frac{k_j}{k} \qquad \ldots\ldots(2)$$

where $(k_j)^2 = 2M(E-E_j)/\hbar^2$.

This is just the result that would be obtained by using distorted waves for the nucleon and calculating the effect of V to first order; i.e. employing the Born approximation. We see now that this is reasonable in the model employed here, since the compound states $\Phi^{(p)}$ containing sizable components of the a^p_{jm} are spread about $E_j + E^j_m$ to an extent determined by the strength of V. We have used an approximation in which this spread is taken to be zero in calculating the denominator, and it turns out that this is equivalent to neglecting the distortion of the wave functions by $V - \hat{V}$ (first order Born approximation) as has been shown above.

The first thing to note in improving upon the above approximation is that the picture in figure 1 of I is highly idealized, and that —since there are 10^4–10^6 levels of the compound nucleus per MEV at several MEV excitation—a number of levels will occur in the region of E and will contribute strongly to the scattering, because the $E - W_p$ occurring in the denominator of (1) becomes very small. The contributions from these have been effectively neglected, since in setting W_p equal to the energy of the single particle resonance $E_j + E^j_m$ for the appropriate component in $\Phi^{(P)}$, the denominator has been made the same as that for the much larger number of resonances which occur near $E_m^j + E_j$.

The levels in the immediate vicinity of E have rapidly varying phases, and their contribution is of a very complex nature. It seems reasonable to assume that—if a suitable average over energy is taken in the experiment—phase relations from these near levels will tend to cancel out, except in exceptional circumstances, e.g. when one compound level gives a contribution which is a sizable proportion of the total scattering. Our assumption is weaker than that made usually in the statistical model, namely, that all phase relations can be neglected. We have seen above that this is incorrect for the distant levels. It seems reasonable for the near levels, however. With our assumption, the contribution from the near levels can be calculated immediately by the technique of Feshbach and Hauser (1952). The contribution from these will be called the compound-inelastic scattering. This scattering is symmetrical about 90°, if the phase relations can really be neglected. Here the residual nucleus will, in general, be left in a highly excited state, since the number of states available goes roughly as $\epsilon \exp(-\epsilon/T_{\mathrm{N}})$ where T_{N} is the nuclear temperature, of the order of 1–2 MeV, and ϵ is the excitation energy, which can usually be as large as five or ten times T_{N} or more. Hence, the direct interaction process will, in general, be the main one leaving the residual nucleus in states of low excitation, and the compound-inelastic scattering will leave the nucleus in highly excited states.

If E is on a single-particle resonance of angular momentum l, one would expect the coefficient of the corresponding spherical harmonic to be incorrectly given by (2) in the expression for the amplitude. Now l will be small compared with the total number L of angular momenta contributing to the direct interaction, and therefore, the change in the amplitude (2) will be slowly varying. This will not change the main pattern of the angular distribution but only the details, giving, for example, a slowly varying background of the type usually attributed in experiments to compound-inelastic scattering.

In fact, under the assumption employed here that there are no phase relations between the near levels, the giant resonance the particle is on contributes little to the scattering which leaves the nucleus in a low excited state, as in the case of the near levels discussed above. Therefore, if the energy is just on a giant resonance, one should substract off the contribution from that giant resonance from $S^i_{\alpha\alpha',j}$ given by equation (2).

In light nuclei the situation can become quite complex, because in addition to subtracting off the contribution from the resonance one is on, one may have to add on effects from the near levels which we have called compound-inelastic scattering. As indicated above, this can be neglected in heavy nuclei where the statistical considerations have some justification. For light nuclei and not too high energies, one cannot use the statistical theory and, indeed, there may be an appreciable chance of the nucleus being left in a low excited state as a result of compound-inelastic scattering.

In calculations of the direct interaction in the literature (see Austern, Butler and McManus 1953), the integration indicated in (2) is restricted to r greater than r_0, where r_0 is roughly the size of the usual nuclear radius, whereas we show it to go from 0 to ∞ (since V is zero beyond R, we could extend all of our upper limits of integration to ∞). These authors actually employ the impulse approximation, rather than the Born approximation, but their matrix element is not essentially different from that given here. These calculations are not, however, greatly different from what would be obtained by our prescription, since the ψ_α's are defined to be solutions in a complex potential, the imaginary part of which is quite large at the energies of interest. This has the effect of drastically reducing ψ_α inside the nucleus; in fact, the diameter of the nucleus of A of the order of 40 is several times the mean free path for protons at 10 MEV. Hence, results from employing (2) will not be radically different from previous calculations.† The absolute value of the cross section for direct interaction is, however, given unambiguously by (2), which is an advantage over most of the previous calculations which only gave angular distributions, except in the case of deuteron stripping where (2), with the integration cut off at r_0, was assumed to give the cross section.

The above development gives some insight into why the Born approximation works well for direct interaction processes. As seen from the above, it gives the correct results for the contributions from the distant compound nucleus levels, the total contribution of which, when summed, varies with the one-particle parameters. The criterion for the validity of the Born approximation in treating these contributions is roughly that the matrix elements of V are small compared with the distances between single-particle levels, and it is reasonable that this criterion is fulfilled. This has been gone into in detail in I. The Born approximation, however, drops the contribution from the near levels, which is responsible for the compound inelastic scattering, and in this sense is less complete than the present treatment.

ACKNOWLEDGMENTS

The authors would like to express their gratitude to Professor R. E. Peierls for many helpful discussions about the physical picture and the formalism used here. They also would like to thank Dr. S. T. Butler and Dr. W. Tobocman for many helpful comments, and Dr. R. Huby for clarifying the picture of deuteron stripping.

REFERENCES

AUSTERN, N., BUTLER, S. T., and MCMANUS, H., 1953, *Phys. Rev.*, **92,** 350.
BOWCOCK, J., 1957, *Proc. Phys. Soc.* A, **70,** 515, 708.
BROOKHAVEN CONFERENCE ON STATISTICAL ASPECTS OF THE NUCLEUS 1955, Report.
BROWN, G. E., 1957, *Proc. Phys. Soc.* A, **70,** 681.
BROWN, G. E., and DE DOMINICIS, C. T., 1957, *Proc. Phys. Soc.* A, **70,** 668.
FESHBACH, H., and HAUSER, W., 1952, *Phys. Rev.*, **87,** 366.
FESHBACH, H., PORTER, C. E., and WEISSKOPF, V. F., 1954, *Phys. Rev.*, **96,** 448.
KAPUR, P. L., and PEIERLS, R., 1938, *Proc. Roy. Soc.* A, **166,** 277.
LANE, A., THOMAS, R. G., and WIGNER, E. P., 1955, *Phys. Rev.*, **98,** 693.

---

† This point is discussed in detail by S. T. Butler (to be published), and was made clear through discussion with Dr. Butler.

Polarization Experiments in Proton–Proton Scattering

By T. V. KANELLOPOULOS† and G. E. BROWN
Department of Mathematical Physics, University of Birmingham

MS. received 23*rd May* 1957

Abstract. Possible proton–proton polarization experiments and the information that can be gained from them are reported here. In this paper we write down the formalism and list formulae from which a quantity which can be measured in such experiments can easily be obtained in terms of the theoretical quantities. We employ the formalism of the statistical matrix for spin $\frac{1}{2}$ particles and the representation of the scattering matrix in spin space. The chief aim of this paper is to present a complete set of formulae covering all experiments which appear to be possible in the near future. In a second paper we shall discuss in more detail a group of experiments which are now of great interest, namely, those involving analysis in coincidence.

In §1 we introduce the formalism to be employed and give an elementary discussion of polarization phenomena.

In §2 results of the algebra needed to carry out the analysis of experiments are given, and in §3, these are used to show what quantities the experiments determine.

§ 1. The Scattering Formalism

A complete description of the scattering of two spin $\frac{1}{2}$ particles is given by the scattering matrix M introduced by Wolfenstein and Ashkin (1952), and Dalitz (1952).

On the other hand the derivation of the formulae necessary for the analysis of polarization experiments is simpler with the help of the density matrix ρ for a mixture of states. The scattering matrix is given by Wolfenstein (1954) in the form

$$\begin{aligned} M = BS + C[(\boldsymbol{\sigma}_1\mathbf{n}) + (\boldsymbol{\sigma}_2\mathbf{n})] + N(\boldsymbol{\sigma}_1\mathbf{n})(\boldsymbol{\sigma}_2\mathbf{n})T \\ + \tfrac{1}{2}G[(\boldsymbol{\sigma}_1\mathbf{k})(\boldsymbol{\sigma}_2\mathbf{k}) + (\boldsymbol{\sigma}_1\mathbf{p})(\boldsymbol{\sigma}_2\mathbf{p})]T + \tfrac{1}{2}H[(\boldsymbol{\sigma}_1\mathbf{k})(\boldsymbol{\sigma}_2\mathbf{k}) - (\boldsymbol{\sigma}_1\mathbf{p})(\boldsymbol{\sigma}_2\mathbf{p})]T \end{aligned} \qquad \ldots\ldots(1)$$

where $\boldsymbol{\sigma}_1$ and $\boldsymbol{\sigma}_2$ are the spin matrices for the incident particle and target particle respectively; B, C, N, G and H are energy dependent functions of the scattering angle θ, in the centre-of-mass system; S and T, the singlet and triplet spin projection operators; and $\mathbf{n}$, $\mathbf{k}$, $\mathbf{p}$, unit vectors along the directions $\mathbf{k}_i \times \mathbf{k}_f$, $\mathbf{k}_f - \mathbf{k}_i$, and $\mathbf{k}_f + \mathbf{k}_i$, respectively. Here $\mathbf{k}_i$ and $\mathbf{k}_f$ are the propagation vectors for the incident and scattered particles. Wolfenstein's expression includes an additional term with coefficient D. This term causes a transition from singlet to triplet spin states and, therefore, in the case of proton–proton scattering, according to the Pauli exclusion principle, must be zero. The same is true for neutron–proton scattering if isotopic spin is to be conserved. We shall simply leave this term out.

---

† At present with CERN Theoretical Study Division, Copenhagen.

The coefficients B, C, N, H and G are functions of θ and are given in terms of phase shifts by Wright (1955).

The density matrix before scattering is

$$\rho_{\rm in} = \tfrac{1}{4}[1 + (\boldsymbol{\sigma}_1 \boldsymbol{\alpha})] \times [1 + (\boldsymbol{\sigma}_2 \boldsymbol{\beta})] \qquad \ldots\ldots(1.1)$$

where $\boldsymbol{\alpha}$ and $\boldsymbol{\beta}$ are the polarizations of the incident beam and target. After scattering

$$\rho_{\rm f} = M\rho_{\rm in}M^{\dagger}. \qquad \ldots\ldots(1.2)$$

The average value of any quantity related to any spin space operator Ω is given by:

$$\langle\Omega\rangle = \frac{\mathrm{Tr}\,(\rho\Omega)}{\mathrm{Tr}\,\rho} \qquad \ldots\ldots(1.3)$$

while $\mathrm{Tr}\rho_{\rm in} = 1$, the trace of $\rho_{\rm f}$ is not unity but equals the differential scattering cross section, i.e.

$$\mathrm{Tr}\rho_{\rm f} = \mathrm{Tr}(M\rho_{\rm in}M^{\dagger}) = I(\theta, \phi). \qquad \ldots\ldots(1.4)$$

The coefficients B, C, etc. of the scattering matrix are complex, and the relations which we obtain from (1.3) are quadratic forms of them. Therefore, at a given energy and scattering angle θ we need at least nine independent relations between the coefficients of the scattering matrix in order to determine the matrix, apart from a common phase factor.

In general, a given measurement, e.g. of the cross section, will give us a relation between the coefficients B, C, N, G, and H at the angle θ at which the measurement is carried out. We call this one 'piece of information'. Now, for the measurements of the cross section and ordinary polarization measurements, one obtains the same information by measurements at θ as at $180° - \theta$ because of symmetry of these quantities about 90° resulting from the fact that singlet and triplet states do not mix here. However, as we shall see, these states do mix in triple scattering, and here one obtains at $180° - \theta$ information different from that at θ. But this new information can be immediately related to give a new relation at θ because B and H are known to be even functions of $\cos\theta$, G and N to be odd functions and C to be an even function times $\sin\theta$ (Wolfenstein 1954). Hence, we can say that we obtain two pieces of information from each triple scattering experiment.

In the experiments to be described here, only one of the scatterings will be by hydrogen, the others by complex nuclei, such as carbon. These complex nuclei are efficient as polarizers, giving very nearly 100% polarization at a suitable angle and consequently are also efficient as analysers. It is well known that if a complex nucleus produces a polarization $\mathbf{P}'$ in scattering an unpolarized beam, then the asymmetry in scattering a polarized beam is just $\mathbf{P} \,.\, \mathbf{P}'$, where $\mathbf{P}$ is the polarization of the beam. The analyser can only determine the spin components perpendicular to the direction of motion of the particle incident on the analyser (Wolfenstein 1954), since scattering of an unpolarized beam by a complex nucleus can give only a polarization perpendicular to the scattering plane, and hence perpendicular to the direction of motion. These limitations can be overcome by using a magnetic field as will be described in §3.

We now give a brief summary of the amount of information that can be obtained in various cases.

(i) *Double scattering.*

In such experiments only measurements of the angular distribution are possible, and measurements of the asymmetry in scattering gives one piece of information in addition to the differential cross section, which can be obtained from single scattering. (Even if we had a polarized target, i.e. the most general case of double scattering, we could obtain only four pieces of information.)

(ii) *Triple scattering.*

In triple scattering the first scattering polarizes the beam; this usually occurs during extraction. The polarization of the beam is perpendicular to the direction of motion. The second scattering is the main one, and the third is the 'analysing' scattering by which we measure the components of the polarization of the 'outgoing' beam which are perpendicular to the direction of motion.

(*a*) With an unpolarized target and no magnetic fields, four pieces of information are obtainable in addition to those from (i) by measuring the components of polarization of the scattered and recoil beam. We shall not discuss the case of a polarized target below, but we mention that in this case twenty-three pieces of information could be obtained, if the orientation of its polarization could be changed arbitrarily †.

(*b*) The information that can be gained from triple scattering can be augmented by using magnetic fields which allow measurement of the longitudinal component of the outgoing scattered or recoil beam, or to obtain a longitudinal component of the incoming beam. It is then possible to obtain four pieces of information in addition to those from (*a*).

(iii) *Analysis in coincidence.*

In such experiments, both the spin of the scattered and recoil proton are measured after the main scattering. If the initial beam is unpolarized, one can obtain two pieces of information without a magnetic field, in addition to those listed above; with a magnetic field one can obtain yet another two.

With a polarized incident beam one can obtain three more pieces, without using a magnetic field, than with an unpolarized incident beam, i.e. five pieces in addition to those from (i) and (ii *a*). With a polarized incident beam and a magnetic field that can be placed either in the incident, recoil or scattered beam, one can obtain eight new pieces of information; i.e., eight in addition to those from all of the above experiments.

In all, then eleven pieces of information can be obtained without a magnetic field, and twenty-three with a magnetic field from the experiments listed in (i), (ii), and (iii).

Double scattering and some triple scattering experiments have been discussed in detail by Wolfenstein (1954) and others. The analysis in coincidence has been touched upon by various authors (Smorodinsky 1955, Oehme 1955, Stapp 1955), but the formalism in § 2 has not been written down in detail for this case. In analysis in coincidence, one measures the component of the polarization of the scattered beam in the direction $\mathbf{l}$ and that of the recoil beam in the direction $\mathbf{m}$ at the same time. This can be related to the quantity obtained, in terms of the scattering matrix, by calculating the average value of the operator $(\boldsymbol{\sigma}_1\mathbf{l})(\boldsymbol{\sigma}_2\mathbf{m})$. The average value of this operator is called the correlation 'function' and is denoted by $C(\mathbf{lm})$. Since experiments determining this quantity are now feasible and of great interest, we shall consider its characteristics in more detail in a following paper.

---

† Rose (1949) has suggested ways of polarizing the nuclei and arrived at the conclusion that a 20% to 40% polarization at the H nucleus is within the realm of practical possibility if suitable arrangements are made for cooling.

§ 2. GENERAL FORMULAE FOR NUCLEON–NUCLEON SCATTERING

We consider the scattering matrix M which is given by equation (1) and the density matrix ρ, by (1.1). Then the average value of any spin space operator Ω can be computed from the following terms:

$$\Lambda_1 = \mathrm{Tr}MM^{\dagger} = BB^* + 8CC^* + (G-N)(G^*-N^*) + 2NN^* + 2HH^* \quad \ldots\ldots(2.1)$$

$$\boldsymbol{\Lambda}_2 = \mathrm{Tr}\{MM^{\dagger}\boldsymbol{\sigma}_1\} = 4(CN^* + C^*N)\mathbf{n} \quad \ldots\ldots(2.2)$$

$$\boldsymbol{\Lambda}_3 = \mathrm{Tr}\{MM^{\dagger}\boldsymbol{\sigma}_2\} = 4(CN^* + C^*N)\mathbf{n} \quad \ldots\ldots(2.3)$$

$$\begin{aligned} \Lambda_4 &= \mathrm{Tr}\{MM^{\dagger}(\boldsymbol{\sigma}_1\mathbf{l})(\boldsymbol{\sigma}_2\mathbf{m})\} \\ &= (\mathbf{ln})(\mathbf{mn})[-BB^* + 8CC^* - (G-N)(G^*-N^*) + 2NN^* + 2HH^*] \\ &\quad + (\mathbf{lp})(\mathbf{mp})[-BB^* + (G-N)(G^*-N^*) - 2NH^* - 2N^*H] \\ &\quad + (\mathbf{lk})(\mathbf{mk})[-BB^* + (G-N)(G^*-N^*) + 2NH^* + 2N^*H] \\ &\quad + 4i[(\mathbf{lk})(\mathbf{mp}) + (\mathbf{lp})(\mathbf{mk})][C^*H - CH^*] \quad \ldots\ldots(2.4) \end{aligned}$$

$$\Lambda_5(\boldsymbol{\alpha}) = \mathrm{Tr}\{M(\boldsymbol{\sigma}_1\boldsymbol{\alpha})M^{\dagger}\} = 4[CN^* + C^*N](\boldsymbol{\alpha}\mathbf{n}) = (\boldsymbol{\Lambda}_2\boldsymbol{\alpha}) \quad \ldots\ldots(2.5)$$

$$\begin{aligned} \boldsymbol{\Lambda}_6(\boldsymbol{\alpha}) = \mathrm{Tr}\{M(\boldsymbol{\sigma}_1\boldsymbol{\alpha})M^{\dagger}\boldsymbol{\sigma}_1\} &= \mathbf{n}(\boldsymbol{\alpha}\mathbf{n})2\mathscr{R}[B(G^*-N^*) + 4CC^* + NN^* - HH^*] \\ &\quad + \mathbf{k}(\boldsymbol{\alpha}\mathbf{k})2\mathscr{R}[B(N^*-H^*) + (G-N)(N^*+H^*)] \\ &\quad + \mathbf{p}(\boldsymbol{\alpha}\mathbf{p})2\mathscr{R}[B(N^*+H^*) + (G-N)(N^*-H^*)] \\ &\quad + (\boldsymbol{\alpha}\times\mathbf{n})4\mathscr{I}\{C[B^* + (G^*-N^*)]\} \quad \ldots\ldots(2.6) \end{aligned}$$

$$\begin{aligned} \boldsymbol{\Lambda}_7(\boldsymbol{\alpha}) = \mathrm{Tr}\{M(\boldsymbol{\sigma}_1\boldsymbol{\alpha})M^{\dagger}\boldsymbol{\sigma}_2\} &= \mathbf{n}(\boldsymbol{\alpha}\mathbf{n})2\mathscr{R}[-B(G^*-N^*) + 4CC^* + NN^* - HH^*] \\ &\quad + \mathbf{k}(\boldsymbol{\alpha}\mathbf{k})2\mathscr{R}[-B(N^*-H^*) + (G-N)(N^*+H^*)] \\ &\quad + \mathbf{p}(\boldsymbol{\alpha}\mathbf{p})2\mathscr{R}[-B(N^*+H^*) + (G-N)(N^*-H^*)] \\ &\quad + (\mathbf{n}\times\boldsymbol{\alpha})4\mathscr{I}\{C[B^* - (G^*-N^*)]\} \quad \ldots\ldots(2.7) \end{aligned}$$

$$\begin{aligned} \Lambda_8(\boldsymbol{\alpha}, \mathbf{l}, \mathbf{m}) &= \mathrm{Tr}\{M(\boldsymbol{\sigma}_1\boldsymbol{\alpha})M^{\dagger}(\boldsymbol{\sigma}_1\mathbf{l})(\boldsymbol{\sigma}_2\mathbf{m})\} \\ &= (\boldsymbol{\alpha}\mathbf{n})\{(\mathbf{mk})(\mathbf{lp})2\mathscr{I}[B(G^*-N^*) + 2NH^*] \\ &\qquad - (\mathbf{mp})(\mathbf{lk})2\mathscr{I}[B(G^*-N^*) - 2NH^*] \\ &\qquad + 8[(\mathbf{mk})(\mathbf{lk}) - (\mathbf{mp})(\mathbf{lp})]\mathscr{R}CH^* \\ &\qquad + 8(\mathbf{mn})(\mathbf{ln})\mathscr{R}C^*N\} \\ &\quad + (\boldsymbol{\alpha}\mathbf{k})\{(\mathbf{mn})(\mathbf{lp})2\mathscr{I}[-B(N^*-H^*) + (N+H)(G^*-N^*)] \\ &\qquad + (\mathbf{mp})(\mathbf{ln})2\mathscr{I}[B(N^*-H^*) + (N+H)(G^*-N^*)] \\ &\qquad + (\mathbf{lk})(\mathbf{mn})4\mathscr{R}[B + (G-N)]C^* \\ &\qquad - (\mathbf{ln})(\mathbf{mk})4\mathscr{R}[B - (G-N)]C^*\} \\ &\quad + (\boldsymbol{\alpha}\mathbf{p})\{-(\mathbf{mk})(\mathbf{ln})2\mathscr{I}[B(N^*+H^*) + (N-H)(G^*-N^*)] \\ &\qquad + (\mathbf{mn})(\mathbf{lk})2\mathscr{I}[B(N^*+H^*) - (N-H)(G^*-N^*)] \\ &\qquad + (\mathbf{lp})(\mathbf{mn})4\mathscr{R}[B + (G-N)]C^* \\ &\qquad - (\mathbf{mp})(\mathbf{ln})4\mathscr{R}[B - (G-N)]C^*\}. \quad \ldots\ldots(2.8) \end{aligned}$$

Using equations (2.1)–(2.8) we find in the following particular cases:

(i) *Incident beam unpolarized—target unpolarized.*

$$\rho_{\mathrm{in}} = \tfrac{1}{4} \qquad \boldsymbol{\alpha} = \boldsymbol{\beta} = 0$$

$$\rho_{\mathrm{f}} = \tfrac{1}{4} M M^{\dagger}$$

Scattering cross section: $$I^{\mathrm{u}}(\theta) = \tfrac{1}{4}\Lambda_1 \qquad \ldots\ldots(2.9)$$

Polarization: $$I^{\mathrm{u}}(\theta)\langle \boldsymbol{\sigma}_1 \rangle_{\mathrm{f}}{}^{\mathrm{u}} = \tfrac{1}{4}\boldsymbol{\Lambda}_2 \qquad \ldots\ldots(2.10)$$

$$I^{\mathrm{u}}(\theta)\langle \boldsymbol{\sigma}_2 \rangle_{\mathrm{f}}{}^{\mathrm{u}} = \tfrac{1}{4}\boldsymbol{\Lambda}_3 = \tfrac{1}{4}\boldsymbol{\Lambda}_2 \qquad \ldots\ldots(2.11)$$

Correlation function: $$I^{\mathrm{u}} C^{\mathrm{u}}(\mathbf{l}, \mathbf{m}) = \tfrac{1}{4}\Lambda_4(\mathbf{l}, \mathbf{m}). \qquad \ldots\ldots(2.12)$$

Here the superfix u indicates that the initial beam is unpolarized; the suffix f indicates that the expectation value is taken with the final statistical matrix.

(ii) *Incident beam polarized—target unpolarized.*

$$\rho_{\mathrm{in}} = \tfrac{1}{4}[1 + (\boldsymbol{\sigma}_1 \boldsymbol{\alpha})]$$

$$\rho_{\mathrm{f}} = \tfrac{1}{4} M[1 + (\boldsymbol{\sigma}_1 \boldsymbol{\alpha})]M^{\dagger} = \tfrac{1}{4} M M^{\dagger} + \tfrac{1}{4} M(\boldsymbol{\sigma}_1 \boldsymbol{\alpha})M^{\dagger}$$

$$I^{\mathrm{p}}(\theta, \phi) = I^{\mathrm{u}}(\theta) + \tfrac{1}{4}(\boldsymbol{\Lambda}_2 \cdot \boldsymbol{\alpha}) = \tfrac{1}{4}[\Lambda_1 + (\boldsymbol{\Lambda}_2 \cdot \boldsymbol{\alpha})] \qquad \ldots\ldots(2.13)$$

$$4 I^{\mathrm{p}}(\theta, \phi) \, . \, \langle \boldsymbol{\sigma}_1 \rangle_{\mathrm{f}}{}^{\mathrm{p}} = \boldsymbol{\Lambda}_2 + \boldsymbol{\Lambda}_6(\boldsymbol{\alpha}) \qquad \ldots\ldots(2.14)$$

$$4 I^{\mathrm{p}}(\theta, \phi) \, . \, \langle \boldsymbol{\sigma}_2 \rangle_{\mathrm{f}}{}^{\mathrm{p}} = \boldsymbol{\Lambda}_2 + \boldsymbol{\Lambda}_7(\boldsymbol{\alpha}) \qquad \ldots\ldots(2.15)$$

$$4 I^{\mathrm{p}}(\theta, \phi) C^{\mathrm{p}}(\mathbf{l}\mathbf{m}) = \Lambda_4(\mathbf{l}, \mathbf{m}) + \Lambda_8(\boldsymbol{\alpha}, \mathbf{l}, \mathbf{m}). \qquad \ldots\ldots(2.16)$$

Here the superfix p indicates that the initial beam is polarized.

§ 3. DISCUSSION

We shall now discuss in detail the experiments listed under (i), (ii *a*), (ii *b*), and those in (iii) in §1 in which a magnetic field need be used only in the incident beam. We shall not discuss the analysis in coincidence experiments which require a magnetic field between scatterer and analyser, since this experiment would appear to be rather far in the future, but we have summarized in §2 the amount of information that can be obtained in this way, and the extension of the theory to this case is easy.

We assume in all that follows that the target is unpolarized and that the initial beam has polarization perpendicular to the direction of motion, although this can be bent by a magnet so that it has a component along the direction of motion. The system $OXYZ$ (see figure 1) is chosen to that OZ coincides with the direction of the incoming beam ($\mathbf{k}_{\mathrm{i}}$), and OY is parallel to the polarization of the beam, $\boldsymbol{\alpha}$. The scattering plane ($\mathbf{k}_{\mathrm{i}}$, $\mathbf{k}_{\mathrm{f}}$) = ($\mathbf{p}$, $\mathbf{k}$) = ($\mathbf{n}$) is fixed by the angle ϕ which the vector $\mathbf{n}$ forms with the positive direction of the axes OX. The scattering angle θ is kept constant throughout our consideration and therefore we know the energy of the emerging particles (scattered and recoil). We shall call s the analyser for the scattered beam and r the analyser for the recoil beam. Quantities referring to the scattered or recoil beam will be distinguished by the suffices s and r respectively.

For every position of the scattering plane the analysis can take place in only two planes for either the scattered or recoil beam, since the plane of analysis must be perpendicular to the direction of motion of the particle being analysed. For the s analyser the planes are (**n**) and (**k**) and for the r analyser they are (**n**) and (**p**), as shown in figures 1 and 2.

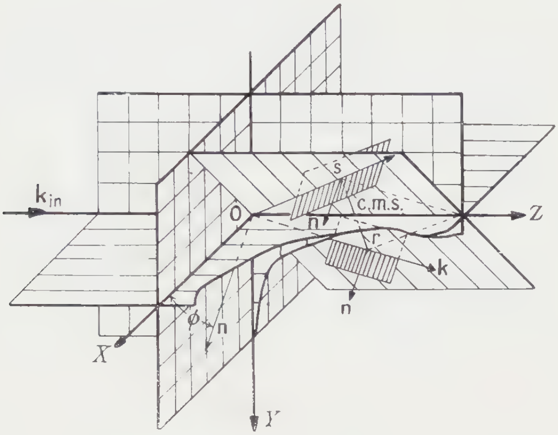

Figure 1.

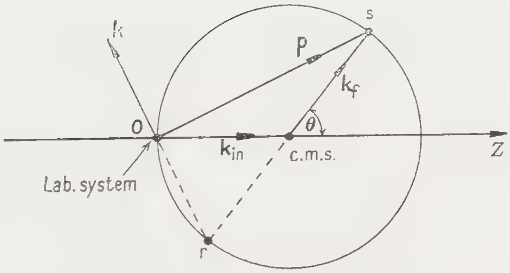

Figure 2.

Connection of the laboratory and centre of mass systems.

In a given analysing plane (**e**) we denote by I^+ and I^- the two differential cross sections, the I^+ always corresponding to the direction $\mathbf{k}^+$ such that (figure 3).

$$\mathbf{e} = \frac{\mathbf{k}_a{}^{\mathrm{in}} \times \mathbf{k}_a{}^+}{|\mathbf{k}_a{}^{\mathrm{in}} \times \mathbf{k}_a{}^+|}.$$

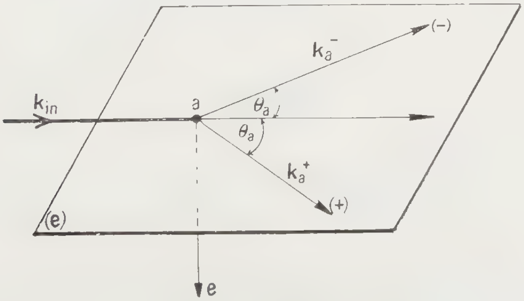

Figure 3.

With this assumption

$$\frac{I_a^+ - I_a^-}{I_a^+ + I_a^-} = C_a(\mathbf{P}\,.\,\mathbf{e}) \qquad \ldots\ldots(3.1)$$

where $\mathbf{P}$ is the polarization of the impinging beam, and C_a is the polarization produced by the scattering on the analyser 'a' if the impinging beam is unpolarized. The coefficients C_s and C_r for analysers are supposed to be known† and constant throughout our considerations, which are for a given set of angles θ, θ_s, and θ_r.

3.1. *Correlation Functions* $C(\mathbf{lm})$

We consider only‡ the case in which $\mathbf{l}$ and $\mathbf{m}$ are perpendicular to the scattered and recoil beam respectively.

We call M_s and M_r the scattering matrices for the two analysers. As they are targets of spin zero, we have

$$M_s = a_s + b_s(\boldsymbol{\sigma}_1\mathbf{l})$$

and

$$M_r = a_r + b_r(\boldsymbol{\sigma}_2\mathbf{m})$$

where a_s, b_s are functions of θ_s and a_r, b_r, functions of θ_r. The scattering matrix for the $(+\,+)$ measurement by coincidence is $M_rM_s = M_sM_r$. Therefore, if ρ_f is the density matrix after the main scattering, the number of events $N(+\,+)$ for $(+\,+)$ counting in coincidence will be

$$N(+\,+) = \frac{\mathrm{Tr}\,\{M_rM_s\rho_fM_s^\dagger M_r^\dagger\}}{\mathrm{Tr}\,\rho_f} = \frac{1}{\mathrm{Tr}\rho_f}\mathrm{Tr}\,\{\rho_f\,M_rM_r^\dagger M_sM_s^\dagger\}. \qquad \ldots\ldots(3.2)$$

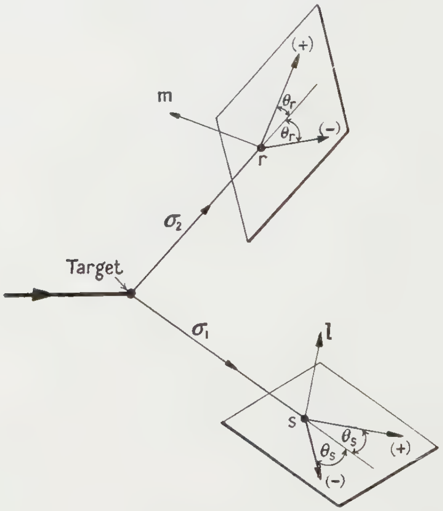

Figure 4.

Now

$$M_rM_r^\dagger = (a_ra_r^* + b_rb_r^*) + (a_rb_r^* + a_r^*b_r)(\boldsymbol{\sigma}_2\mathbf{m}) = A_r + B_r(\boldsymbol{\sigma}_2\mathbf{m})$$

$$M_sM_s^\dagger = (a_sa_s^* + b_sb_s^*) + (a_sb_s^* + a_s^*b_s)(\boldsymbol{\sigma}_1\mathbf{l}) = A_s + B_s(\boldsymbol{\sigma}_1\mathbf{l}). \qquad \ldots\ldots(3.3)$$

---

† For the sign of the polarization see Marshall and Marshall (1955).

‡ As we shall not consider here the case in which we use magnetic fields between targets and analysers, we do not need cases with $\mathbf{l}$ and $\mathbf{m}$ not perpendicular to the beams.

The A_r and B_r are related to the polarization, C_r that would be produced in scattering an unpolarized beam by the analyser, i.e. $B_r/A_r = C_r$, and similarly, $B_s/A_s = C_s$. One easily finds

$$C(\mathbf{l\,m}) = \langle(\boldsymbol{\sigma}_1\mathbf{l})(\sigma_2\mathbf{m})\rangle = \frac{1}{C_s C_r}\,\frac{N(++)+N(--)-N(+-)-N(-+)}{N(++)+N(--)+N(+-)+N(-+)} \qquad \ldots\ldots(3.4)$$

with C_s and C_r the polarization produced by scattering of unpolarized beam by the analysers under the same energetic and geometric conditions.

3.2. *The Effect of a Magnetic Field on the Polarization of a Beam*

In the non-relativistic treatment the Hamiltonian of the interaction of the magnetic field with the magnetic moment of the particles of a beam is of the form

$$\delta H = \lambda \boldsymbol{\sigma}\,.\,\boldsymbol{\mathfrak{H}} \qquad \ldots\ldots(3.5)$$

where $\lambda =$ constant. It can easily be shown that if the magnetic field $\boldsymbol{\mathfrak{H}}$ is perpendicular to the polarization $\mathbf{P}$, the rate of rotation of $\mathbf{P}$ relative to the direction of the (deflected) beam is given by

$$\frac{d\chi}{dt} = \frac{2\lambda'}{\hbar}\mathscr{H} \qquad \ldots\ldots(3.6)$$

where χ is the angle between $\mathbf{P}$ and the beam, and λ' is the anomalous moment of proton.

We consider now the measurements required for the cases (i), (ii*a*), (ii*b*), and (iii) mentioned in § 1 in the following order: double scattering, triple scattering, analysis in coincidence, giving in each case first the quantities which can be measured without a magnetic field, and then those for which magnetic fields are necessary.

As we shall not use magnetic fields between the target and analysers for the experiments of analysis in coincidence, we shall need only the following expressions which can be obtained easily from equations (2.1)–(2.8), i.e., we take only $C(\mathbf{n\,n})$, $C(\mathbf{n\,p})$, $C(\mathbf{k\,n})$, and $C(\mathbf{k\,p})$ from the correlation functions.

The following quantities will enter into the experiments we consider:

$$4\,I^p(\phi) = \Lambda_1 + \Lambda_5(\boldsymbol{\alpha}) \qquad \ldots\ldots(3.7)$$

$$4\,I^p(\phi)\,\langle\boldsymbol{\sigma}_1\rangle_f{}^p = \boldsymbol{\Lambda}_2 + \boldsymbol{\Lambda}_6 \qquad \ldots\ldots(3.8)$$

$$4\,I^p(\phi)\langle\boldsymbol{\sigma}_2\rangle_f{}^p = \boldsymbol{\Lambda}_3 + \boldsymbol{\Lambda}_7. \qquad \ldots\ldots(3.9)$$

We write the correlation coefficients explicitly:

$$\begin{aligned} 4I^p(\phi)\,C^p(\mathbf{n\,n}) &= -BB^* + 8CC^* - (G-N)(G^*-N^*) + 2NN^* + 2HH^* \\ &\quad + 8(\boldsymbol{\alpha}\,\mathbf{n})\,\mathscr{R}\,C^*N \qquad \ldots\ldots(3.10) \end{aligned}$$

$$\begin{aligned} 4I^p(\phi)\,C^p(\mathbf{n\,p}) &= (\boldsymbol{\alpha}\,\mathbf{k})\,2\mathscr{I}\,[B(N^*-H^*) + (N+H)(G^*-N^*)] \\ &\quad - (\boldsymbol{\alpha}\,\mathbf{p})\,4\mathscr{R}\,[B-(G-N)]\,C^* \qquad \ldots\ldots(3.11) \end{aligned}$$

$$\begin{aligned} 4I^p(\phi)\,C^p(\mathbf{k\,n}) &= (\boldsymbol{\alpha}\mathbf{k})\,4\mathscr{R}\,[B+(G-N)]\,C^* + (\boldsymbol{\alpha}\mathbf{p})\,2\mathscr{I}\,[B(N^*+H^*) \\ &\quad - (N-H)(G^*-N^*)] \qquad \ldots\ldots(3.12) \end{aligned}$$

$$4I^p(\phi)\,C^p(\mathbf{k\,p}) = 8\mathscr{I}\,CH^* - (\boldsymbol{\alpha}\mathbf{n})\,2\mathscr{I}\,[B(G^*-N^*) - 2NH^*]. \qquad \ldots\ldots(3.13)$$

All of the following measurements can be made at a given angle θ. Therefore, we indicate explicitly only the value of ϕ, which will be different for different experiments.

(i) *Double scattering.*

(*a*) We measure the differential cross sections $I(0^\circ)$, $I(90^\circ)$, $I(180^\circ)$ and $I(270^\circ)$ These values will be assumed to be known in the remaining measurements. From (2.13) we obtain

$$I^{\mathrm{p}}(0^\circ) = I^{\mathrm{p}}(180^\circ) = I_0. \quad (\boldsymbol{\alpha} \perp \mathbf{n})$$

Therefore we can put

$$\begin{aligned} BB^* + 8CC^* + (G-N)(G^*-N^*) + 2NN^* + 2HH^* &= \lambda_1 \\ \lambda_1 = 4I^{\mathrm{p}}(0^\circ) = 4I^{\mathrm{p}}(180^\circ). & \end{aligned} \qquad \ldots\ldots(4.0)$$

Again we have

$$\begin{aligned} I^{\mathrm{p}}(90^\circ) &= I^\circ + (CN^* + C^*N)\alpha \\ I^{\mathrm{p}}(270^\circ) &= I^\circ - (CN^* + C^*N)\alpha \end{aligned}$$

from which we obtain $CN^* + C^*N$. We put

$$\begin{aligned} CN^* + C^*N &= \lambda_2 \\ \lambda_2 &= \frac{I^{\mathrm{p}}(90^\circ) - I^{\mathrm{p}}(180^\circ)}{2\alpha}. \end{aligned} \qquad \ldots\ldots(4.1)$$

(*b*) Application of magnetic field does not yield anything new.

(ii) *Triple scattering.*

(*a*) *Without magnetic fields* $(\boldsymbol{\alpha} \perp \mathbf{k}_i)$.

1. $\phi = 90^\circ \quad \boldsymbol{\alpha} = \alpha\mathbf{n}$.

Measuring the $\mathbf{n}$ component of the polarization P_{s} of the scattered beam we find

$$(\mathbf{P}_{\mathrm{s}}\,\mathbf{n})_{90^\circ} = \langle \boldsymbol{\sigma}_1\,\mathbf{n} \rangle^{\mathrm{p}}_{90^\circ} = \frac{1}{C_{\mathrm{s}}} \frac{I_{\mathrm{s}}^{+}(90^\circ, \mathbf{n}) - I_{\mathrm{s}}^{-}(90^\circ, \mathbf{n})}{I_{\mathrm{s}}^{+}(90^\circ, \mathbf{n}) + I_{\mathrm{s}}^{-}(90^\circ, \mathbf{n})}.$$

From (3.8) we have

$$4I^{\mathrm{p}}(90^\circ)\langle \boldsymbol{\sigma}_1\,\mathbf{n} \rangle^{\mathrm{p}}_{90^\circ} = 4(CN^* + C^*N) + \alpha 2\mathscr{R}\,[B(G^* - N^*) + 4CC^* + NN^* - HH^*].$$

We can put

$$\begin{aligned} \mathscr{R}\,B(G^* - N^*) + 4CC^* + NN^* - HH^* &= \lambda_{3\mathrm{s}} \\ \lambda_{3\mathrm{s}} = \frac{2}{\alpha}\left[\frac{I^{\mathrm{p}}(90^\circ)}{C_{\mathrm{s}}} \times \frac{I_{\mathrm{s}}^{+}(90^\circ, \mathbf{n}) - I_{\mathrm{s}}^{-}(90^\circ, \mathbf{n})}{I_{\mathrm{s}}^{+}(90^\circ, \mathbf{n}) + I_{\mathrm{s}}^{-}(90^\circ, \mathbf{n})} - \lambda_2\right]&. \end{aligned} \qquad \ldots\ldots(4.2)$$

Working on the *recoil* beam in a similar way we obtain

$$\begin{aligned} -\mathscr{R}\,B(G^* - N^*) + 4CC^* + NN^* - HH^* &= \lambda_{3\mathrm{r}} \\ \lambda_{3\mathrm{r}} = \frac{2}{\alpha}\left[\frac{I^{\mathrm{p}}(90^\circ)}{C_{\mathrm{r}}} \times \frac{I_{\mathrm{r}}^{+}(90^\circ, \mathbf{n}) - I_{\mathrm{r}}^{-}(90^\circ, \mathbf{n})}{I_{\mathrm{r}}^{+}(90^\circ, \mathbf{n}) + I_{\mathrm{r}}^{-}(90^\circ, \mathbf{n})} - \lambda_2\right]&. \end{aligned} \qquad \ldots\ldots(4.3)$$

Measuring this quantity in the recoil beam for θ gives the same information as in the scattered beam at $180^\circ - \theta$.

For the same position of the scattering plane ($\phi = 90^\circ$) the other components of polarization for the scattered and for the recoil beam are zero, i.e. the polarization remains parallel to $\mathbf{n}$.

2. $\phi = 0, \quad \boldsymbol{\alpha} = -\alpha\,[\mathbf{k}\cos\tfrac{1}{2}\theta + \mathbf{p}\sin\tfrac{1}{2}\theta]$.

The $\mathbf{n}$ components of the polarization for the scattered and recoil beams give no new piece of information because $I^{\mathrm{p}}(0^\circ) = I_0$ and

$$4I^{\mathrm{p}}(0^\circ)\langle \boldsymbol{\sigma}_1 \rangle_{\mathrm{f}}^{\mathrm{p}} . \mathbf{n} = 4I^{\mathrm{p}}(0^\circ)\langle \boldsymbol{\sigma}_2 \rangle . \mathbf{n} = 4(CN^* + C^*N),$$

i.e. we get the polarization produced by scattering an unpolarized beam, which is already known from the double scattering.

For the **k** component of the polarization of the scattered beam we have

$$\langle \boldsymbol{\sigma}_1\, \mathbf{k} \rangle^{\mathrm{p}}_{0^\circ} = \frac{1}{C_{\mathrm{s}}} \times \frac{I_{\mathrm{s}}^{+}(0^\circ, \mathbf{k}) - I_{\mathrm{s}}^{-}(0^\circ, \mathbf{k})}{I_{\mathrm{s}}^{+}(0^\circ, \mathbf{k}) + I_{\mathrm{s}}^{-}(0^\circ, \mathbf{k})} = (\mathbf{P}_{\mathrm{s}} \,.\, \mathbf{k})_0.$$

From (3.8)

$$\begin{aligned} 4I^{\mathrm{p}}(0)\langle \boldsymbol{\sigma}_1\, \mathbf{k} \rangle^{\mathrm{p}}_{0^\circ} = {} & -\alpha \cos \tfrac{1}{2}\theta\, 2\mathscr{R}\,[B(N^* - H^*) + (G - N)(N^* + H^*)] \\ & - \alpha \sin \tfrac{1}{2}\theta\, 4\mathscr{I}\,[B^* + (G^* - N^*)]\, C \end{aligned}$$

we put

$$\begin{aligned} & -\mathscr{R}\,[B(N^* - H^*) + (G - N)(N^* + H^*)] \cos \tfrac{1}{2}\theta \\ & \qquad + 2\mathscr{I}\,\{C[B^* + (G^* - N^*)]\} \sin \tfrac{1}{2}\theta = \lambda_{4\mathrm{s}} \end{aligned}$$

$$\lambda_{4\mathrm{s}} = 2\frac{I^{\mathrm{p}}(0)}{\alpha C_{\mathrm{s}}} \times \frac{I_{\mathrm{s}}^{+}(0^\circ, \mathbf{k}) - I_{\mathrm{s}}^{-}(0^\circ, \mathbf{k})}{I_{\mathrm{s}}^{+}(0^\circ, \mathbf{k}) + I_{\mathrm{s}}^{-}(0^\circ, \mathbf{k})}. \qquad \ldots\ldots(4.4)$$

From the **p** component of the recoil beam we find

$$\begin{aligned} & -\mathscr{R}\,[-B(N^* + H^*) + (G - N)(N^* - H^*)] \sin \tfrac{1}{2}\theta \\ & \qquad + 2\mathscr{I}\,\{C[B^* - (G^* - N^*)]\} \cos \tfrac{1}{2}\theta = \lambda_{4\mathrm{r}} \end{aligned}$$

$$\lambda_{4\mathrm{r}} = 2\frac{I^{\mathrm{p}}(0^\circ)}{\alpha C_{\mathrm{r}}} \times \frac{I_{\mathrm{r}}^{+}(0^\circ, \mathbf{p}) - I_{\mathrm{r}}^{-}(0^\circ, \mathbf{p})}{I_{\mathrm{r}}^{+}(0^\circ, \mathbf{p}) + I_{\mathrm{r}}^{-}(0^\circ, \mathbf{p})}. \qquad \ldots\ldots(4.5)$$

This is the same quantity as would be obtained by measuring the **k** component of the scattered beam at $180^\circ - \theta$.

(*b*) *With a magnetic field on the incident beam.*

Now the polarization is $\boldsymbol{\alpha} = \boldsymbol{\alpha}_1 + \boldsymbol{\alpha}_2$ where $\boldsymbol{\alpha}_1$ is perpendicular to $\mathbf{k}_{\mathrm{in}}$ and $\boldsymbol{\alpha}_2$ is parallel to $\mathbf{k}_{\mathrm{in}}$. The two positions of the scattering plane ($\phi = 0^\circ$ and 90°) give the same relation. We choose as the simpler one the case $\phi = 90^\circ$. Now as

$$\boldsymbol{\alpha} = \alpha_1 \,.\, \mathbf{n} + \alpha_2 \{\mathbf{p} \cos \tfrac{1}{2}\theta - \mathbf{k} \sin \tfrac{1}{2}\theta\}$$

the components of polarization along **k** for the scattered beam and along **p** for the recoil beam are not zero.

We find from (3.8) that

$$\begin{aligned} 4I^{\mathrm{p}}(90^\circ)\langle \boldsymbol{\sigma}_1\, \mathbf{k} \rangle^{\mathrm{p}}_{90^\circ} = {} & -\alpha_2 \{2\mathscr{R}\,[B(N^* - H^*) + (G - N)(N^* + H^*)] \sin \tfrac{1}{2}\theta \\ & + 4\mathscr{I}\,\{C[B^* + (G^* - N^*)]\} \cos \tfrac{1}{2}\theta\} \end{aligned}$$

with†

$$\langle \boldsymbol{\sigma}_1\, \mathbf{k} \rangle^{\mathrm{p}}_{90^\circ} = \frac{1}{C_{\mathrm{s}}} \frac{I_{\mathrm{s}}'^{+}(90^\circ, \mathbf{k}) - I_{\mathrm{s}}'^{-}(90^\circ, \mathbf{k})}{I_{\mathrm{s}}'^{+}(90^\circ, \mathbf{k}) + I_{\mathrm{s}}'^{-}(90^\circ, \mathbf{k})}.$$

We put

$$\begin{aligned} & \mathscr{R}\,[B(N^* - H^*) + (G - N)(N^* + H^*)] \sin \tfrac{1}{2}\theta \\ & \qquad + 2\mathscr{I}\,\{C[B^* + (G^* - N^*)]\} \cos \tfrac{1}{2}\theta = \lambda_{5\mathrm{s}} \end{aligned}$$

$$\lambda_{5\mathrm{s}} = -2\frac{I^{\mathrm{p}}(90^\circ)}{\alpha_2 C_{\mathrm{s}}} \times \frac{I_{\mathrm{s}}'^{+}(90^\circ, \mathbf{k}) - I_{\mathrm{s}}'^{-}(90^\circ, \mathbf{k})}{I_{\mathrm{s}}'^{+}(90^\circ, \mathbf{k}) + I_{\mathrm{s}}'^{-}(90^\circ, \mathbf{k})}. \qquad \ldots\ldots(5.0)$$

† The prime (′) denotes that the measurements of $I^{\pm}$ are performed with a magnetic field on the incident beam. For the measurements with magnetic field between target and analysers we shall use double primed symbols.

As similarly for the recoil, ($\mathbf{p}$ component)

$$\mathscr{R}[-B(N^*+H^*)+(G-N)(N^*-H^*)]\cos\tfrac{1}{2}\theta$$
$$+2\mathscr{I}\{C[B^*-(G^*-N^*)]\}\sin\tfrac{1}{2}\theta=\lambda_{5\mathrm{r}}$$
$$\lambda_{5\mathrm{r}}=2\frac{I^{\mathrm{p}}(90^\circ)}{\alpha_2 C_{\mathrm{r}}}\times\frac{I_{\mathrm{r}}'^{+}(90^\circ,\mathbf{p})-I_{\mathrm{r}}'^{-}(90^\circ,\mathbf{p})}{I_{\mathrm{r}}'^{+}(90^\circ,\mathbf{p})+I_{\mathrm{r}}'^{-}(90^\circ,\mathbf{p})}. \qquad \ldots\ldots(5.1)$$

(*c*) *With a magnetic field between targets and analysers.*

For $\phi=90^\circ$ the polarization of the outgoing beams is in the $\mathbf{n}$ direction ($\equiv OY$). Therefore the magnetic field between target and analysers will be used only for $\phi=0$. It is understood that there is no magnetic field on the incident beam.

The direction of the magnetic field on the outgoing beams is along the X axis ($OX\equiv\mathbf{n}$). The $\mathbf{n}$ component of the polarization of the beams is unaltered while both the $\mathbf{k}$ and $\mathbf{p}$ components rotate by an angle χ_{s} for the scattered and χ_{r} for the recoil. These angles can be calculated from (3.6).

Measuring the $\mathbf{k}$ component of the beam after applying the magnetic field we find

$$(\mathbf{P}_{\mathrm{s}}''\,.\,\mathbf{k})_{0^\circ}=\frac{1}{C_{\mathrm{s}}}\times\frac{I_{\mathrm{s}}''^{+}(0^\circ,\mathbf{k})-I_{\mathrm{s}}''^{-}(0^\circ,\mathbf{k})}{I_{\mathrm{s}}''^{+}(0^\circ,\mathbf{k})+I_{\mathrm{s}}''^{-}(0^\circ,\mathbf{k})}=(\mathbf{P}_{\mathrm{s}}\,.\,\mathbf{k})\cos\chi_{\mathrm{s}}+(\mathbf{P}_{\mathrm{s}}\,.\,\mathbf{p})\sin\chi_{\mathrm{s}}$$

or

$$(\mathbf{P}_{\mathrm{s}}\,.\,\mathbf{p})_{0^\circ}=\langle\boldsymbol{\sigma}_1\,.\,\mathbf{p}\rangle^{\mathrm{p}}_{0^\circ}=\frac{1}{C_{\mathrm{s}}\sin\chi_{\mathrm{s}}}\left\{\frac{I_{\mathrm{s}}''^{+}(0^\circ,\mathbf{k})-I_{\mathrm{s}}''^{-}(0^\circ,\mathbf{k})}{I_{\mathrm{s}}''^{+}(0^\circ,\mathbf{k})+I_{\mathrm{s}}''^{-}(0^\circ,\mathbf{k})}\right.$$
$$\left.-\frac{I_{\mathrm{s}}^{+}(0^\circ,\mathbf{k})-I_{\mathrm{s}}^{-}(0^\circ,\mathbf{k})}{I_{\mathrm{s}}^{+}(0^\circ,\mathbf{k})+I_{\mathrm{s}}^{-}(0^\circ,\mathbf{k})}\cos\chi_{\mathrm{s}}\right\}. \qquad \ldots\ldots(6.0)$$

From (3.8) we can put

$$\mathscr{R}\{B(N^*+H^*)+(G-N)(N^*-H^*)\}\sin\tfrac{1}{2}\theta+2\mathscr{I}\{C[B^*+(G^*-N^*)]\}\cos\tfrac{1}{2}\theta=\lambda_{6\mathrm{s}}$$
$$\lambda_{6\mathrm{s}}=-\frac{2I^{\mathrm{p}}(0^\circ)}{\alpha C_{\mathrm{s}}\sin\chi_{\mathrm{s}}}\left\{\frac{I_{\mathrm{s}}''^{+}(0^\circ,\mathbf{k})-I_{\mathrm{s}}''^{-}(0^\circ,\mathbf{k})}{I_{\mathrm{s}}''^{+}(0^\circ,\mathbf{k})+I_{\mathrm{s}}''^{-}(0^\circ,\mathbf{k})}-\frac{I_{\mathrm{s}}^{+}(0^\circ,\mathbf{k})-I_{\mathrm{s}}^{-}(0^\circ,\mathbf{k})}{I_{\mathrm{s}}^{+}(0^\circ,\mathbf{k})+I_{\mathrm{s}}^{-}(0^\circ,\mathbf{k})}\cos\chi_{\mathrm{s}}\right\}. \qquad \ldots\ldots(6.1)$$

Similarly, for the recoil beam we have

$$\mathscr{R}\{-B(N^*-H^*)+(G-N)(N^*+H^*)]\cos\tfrac{1}{2}\theta$$
$$+2\mathscr{I}\{C[B^*-(G^*-N^*)]\}\sin\tfrac{1}{2}\theta=\lambda_{6\mathrm{r}}$$
$$\lambda_{6\mathrm{r}}=-\frac{2I^{\mathrm{p}}(0^\circ)}{\alpha C_{\mathrm{r}}\sin\chi_{\mathrm{r}}}\left\{\frac{I_{\mathrm{r}}''^{+}(0^\circ,\mathbf{p})-I_{\mathrm{r}}''^{-}(0^\circ,\mathbf{p})}{I_{\mathrm{r}}''^{+}(0^\circ,\mathbf{p})+I_{\mathrm{r}}''^{-}(0^\circ,\mathbf{p})}-\frac{I_{\mathrm{r}}^{+}(0^\circ,\mathbf{p})-I_{\mathrm{r}}^{-}(0^\circ,\mathbf{p})}{I_{\mathrm{r}}^{+}(0^\circ,\mathbf{p})+I_{\mathrm{r}}^{-}(0^\circ,\mathbf{p})}\cos\chi_{\mathrm{r}}\right\}. \qquad \ldots\ldots(6.2)$$

(iii) *Analysis in coincidence.*

In order to classify the experiments of analysis in coincidence we use three indices ϕ, $\mathbf{l}$, $\mathbf{m}$. The first fixes the position of the scattering plane, the second and the third are vectors perpendicular to the analysing planes for the scattered and recoil beam respectively.

(*a*) *Without a magnetic field.*

1. $\phi=0^\circ$, $\mathbf{l}=\mathbf{m}=\mathbf{n}$, $\boldsymbol{\alpha}=-\alpha\{\mathbf{k}\cos\tfrac{1}{2}\theta+\mathbf{p}\sin\tfrac{1}{2}\theta\}$.

We have from (3.10)

$$4I^{\mathrm{p}}(0^\circ)\,C_0^{\mathrm{p}}(\mathbf{n}\,\mathbf{n})=-BB^*+8CC^*-(G-N)(G^*-N^*)+2NN^*+2HH^*.$$

We put

$$-BB^*+8CC^*-(G-N)(G^*-N^*)+2NN^*+2HH^*=\lambda_7$$

$$\lambda_7=4I^{\mathrm{p}}(0^\circ)\,C_0^{\mathrm{p}}(\mathbf{n\,n}) \qquad \ldots\ldots(7.0)$$

2. $\phi=0^\circ, \mathbf{l}=\mathbf{n}, \mathbf{m}=\mathbf{p}$: From (3.11) we have

$$4I^{\mathrm{p}}(0^\circ)\,C_0^{\mathrm{p}}(\mathbf{n\,p})=-\alpha 2\mathscr{I}\,[B(N^*-H^*)+(N+H)(G^*-N^*)]\cos\tfrac{1}{2}\theta$$
$$+\alpha 4\mathscr{R}\,[B-(G-N)]\,C^*\sin\tfrac{1}{2}\theta.$$

We put

$$-\mathscr{I}[B(N^*-H^*)+(N+H)(G^*-N^*)]\cos\tfrac{1}{2}\theta+2\mathscr{R}\,[B-(G-N)]\,C^*\sin\tfrac{1}{2}\theta=\lambda_8$$

$$\lambda_8=\frac{2I_0^{\mathrm{p}}}{\alpha}\,C_0^{\mathrm{p}}(\mathbf{n\,p}). \qquad \ldots\ldots(7.1)$$

3. $\phi=0^\circ, \mathbf{l}=\mathbf{k}, \mathbf{m}=\mathbf{n}$: Equation (3.12) yields

$$4I^{\mathrm{p}}(0_0)\,C_0^{\mathrm{p}}(\mathbf{k\,n})=-\alpha 4\mathscr{R}\,[B+(G-N)]\,C^*\cos\tfrac{1}{2}\theta-\alpha 2\mathscr{I}\,[B(N^*+H^*)$$
$$-(N-H)(G^*-N^*)]\sin\tfrac{1}{2}\theta.$$

We put

$$2\mathscr{R}\,[B+(G-N)]\,C^*\cos\tfrac{1}{2}\theta+\mathscr{I}\,[B(N^*+H^*)-(N-H)(G^*-N^*)]\sin\tfrac{1}{2}\theta=\lambda_9$$

$$\lambda_9=-\frac{2I^{\mathrm{p}}(0^\circ)}{\alpha}\,C_0^{\mathrm{p}}(\mathbf{k\,n}). \qquad \ldots\ldots(7.2)$$

4. $\phi=0^\circ$, $\mathbf{l}=\mathbf{k}$, $\mathbf{m}=\mathbf{p}$: In this case we get

$$2\mathscr{I}\;CH^*=\lambda_{10}$$

$$\lambda_{10}=I^{\mathrm{p}}(0^\circ)\,C_0^{\mathrm{p}}(\mathbf{k p}). \qquad \ldots\ldots(7.3)$$

5. $\phi=90^\circ$, $\mathbf{l}=\mathbf{k}$, $\mathbf{m}=\mathbf{p}$, $\boldsymbol{\alpha}=\alpha\mathbf{n}$: From (3.13) we have

$$\mathscr{I}\,[B(G^*-N^*)-2NH^*]=\lambda_{11}$$

$$\lambda_{11}=\frac{2\lambda_{10}-2I^{\mathrm{p}}(90^\circ)\,C_{90}^{\mathrm{p}}(\mathbf{k\,p})}{\alpha} \qquad \ldots\ldots(7.4)$$

Measurement of the quantities $C_0^{\mathrm{p}}(\mathbf{n\,n})$ and $C_0^{\mathrm{p}}(\mathbf{k\,p})$ could equally well be carried out with an unpolarized incident beam; i.e. $C_0^{\mathrm{p}}(\mathbf{k\,p})=C^{\mathrm{u}}(\mathbf{k\,p})$, $C_0'^{\mathrm{p}}(\mathbf{n\,n})=C^{\mathrm{u}}(\mathbf{n\,n})$.

The case $\phi=90^\circ$, $\mathbf{l}=\mathbf{n}$, $\mathbf{m}=\mathbf{n}$ does not yield any new relation.

The case $\phi=90^\circ$, $\mathbf{l}=\mathbf{n}$, $\mathbf{m}=\mathbf{p}$ gives $C_{90}(\mathbf{n\,p})=0$.

The case $\phi=90^\circ$, $\mathbf{l}=\mathbf{k}$, $\mathbf{m}=\mathbf{n}$ gives $C_{90}(\mathbf{k\,n})=0$.

(*b*) *With a magnetic field on the incident beam.*

We expect to obtain new relations only from the cases $\phi=90^\circ$, $\mathbf{l}=\mathbf{n}$, $\mathbf{m}=\mathbf{p}$; and $\phi=90^\circ$, $\mathbf{l}=\mathbf{k}$, $\mathbf{m}=\mathbf{n}$.
Indeed for

1. $\phi=90^\circ$, $\mathbf{l}=\mathbf{n}$, $\mathbf{m}=\mathbf{p}$, $\boldsymbol{\alpha}=\boldsymbol{\alpha}_1+\boldsymbol{\alpha}_2=\alpha_1\mathbf{n}+\alpha_2\{\mathbf{p}\cos\tfrac{1}{2}\theta-\mathbf{k}\sin\tfrac{1}{2}\theta\}$.

From (3.11)

$$4I^{\mathrm{p}}(90^\circ)\,C_{90}'(\mathbf{n\,p})=-\alpha_2\sin\tfrac{1}{2}\theta\,2\mathscr{I}\,\{B(N^*-H^*)+(N+H)(G^*-N^*)\}$$
$$-\alpha_2\cos\tfrac{1}{2}\theta\,4\mathscr{R}\,[B-(G-N)]\,C^*.$$

We put

$$\mathscr{I}\,[B\,(N^*-H^*)+(N+H)(G^*-N^*)]\sin\tfrac{1}{2}\theta+2\mathscr{R}\,[B-(G-N)]\,C^*\cos\tfrac{1}{2}\theta=\lambda_{12}$$

$$\lambda_{12}=-\frac{2I^{\mathrm{p}}(90^\circ)\,C'_{90}\,(\mathbf{n}\,\mathbf{p})}{\alpha_2}. \qquad \ldots\ldots(8.0)$$

Finally,

2. $\phi=90^\circ, \mathbf{l}=\mathbf{k}, \mathbf{m}=\mathbf{n}$: From (3.12) we obtain

$$\mathscr{I}\,[B(N^*+H^*)-(N-H)(G^*-N^*)]\cos\tfrac{1}{2}\theta-2\mathscr{R}\,[B+(G-N)]\,C^*\sin\tfrac{1}{2}\theta=\lambda_{13}$$

$$\lambda_{13}=\frac{2I^{\mathrm{p}}(90^\circ)\,C'_{90}\,(\mathbf{k}\,\mathbf{n})}{\alpha_2}. \qquad \ldots\ldots(8.1)$$

The equations (4.0)–(6.2) give all the obtainable relations between the coefficients of the scattering matrix from experiments in which only one magnetic field has been used without analysis in coincidence.

The equations (4.0)–(4.5) and (7.0)–(7.4) give eleven relations and include all experiments without magnetic fields.

ACKNOWLEDGMENTS

We should like to thank Dr. R. H. Dalitz and Professor R. E. Peierls for many interesting discussions.

REFERENCES

DALITZ, R. H., 1952, *Proc. Phys. Soc.* A, **65,** 175.
OEHME, R., 1955, *Phys. Rev.*, **98,** 216.
MARSHALL, L., and MARSHALL, J., 1955, *Phys. Rev.*, **98,** 1398.
ROSE, M. E., 1949, *Phys. Rev.*, **75,** 213.
SMORODINSKII, Ya., 1955, *Dokl. Akad. Nauk., SSSR,* **104,** 713.
STAPP, H. P., 1955, *Thesis,* University of California, U.C.R.L. 3098.
WOLFENSTEIN, L., 1954, *Phys. Rev.*, **96,** 1654.
WOLFENSTEIN, L., and ASHKIN, J., 1952, *Phys. Rev.*, **85,** 947.
WRIGHT, S. C., 1955, *Phys. Rev.*, **99,** 996.

Analysis in Coincidence in Proton–Proton Scattering

By G. E. BROWN and T. V. KANELLOPOULOS†
Department of Mathematical Physics, University of Birmingham

Abstract. An elementary discussion of experiments involving analysis in coincidence is given. The case in which the incident beam is unpolarized is discussed in detail. Additional information that can be obtained if the incident beam is polarized is indicated, and the additional information which can be obtained with a magnetic field is briefly summarized.

§ 1. Introduction

In the preceding paper (Kanellopoulos and Brown 1957, to be referred to as I) we have given an account of possible polarization experiments in proton–proton scattering and have written down expressions which enable one to calculate easily any quantity that can be obtained from such experiments in terms of the coefficients of the scattering matrix. Detailed discussions of double scattering and triple scattering have been given previously (Wolfenstein 1954) but the experiments involving analysis in coincidence have just been briefly touched upon (Wolfenstein 1954, Oehme 1955, Smorodinsky 1955) and it is the purpose of this note to give an elementary discussion of what can be measured by experiments.

The experiments we have in mind here are those in which protons are scattered by hydrogen and both the scattered and recoil proton are again scattered by complex nuclei, which serve as analysers. These scatterings by complex nuclei tell us the spin directions of the protons scattered; the only restriction being that they can give information only about the spin components perpendicular to the direction of motion. A discussion of the scattering by complex nuclei has been given by Wolfenstein and Ashkin (1952) and by Dalitz (1952). We refer to the scattering by hydrogen as the main scattering and to those by the complex nuclei as the analysing scatterings. The beam incident on the hydrogen may be either unpolarized or polarized and we shall discuss both cases. In some cases, such as with the Birmingham proton synchrotron, the beam scattered out of the machine is polarized and, consequently, the experiments with incident polarized protons on the hydrogen involve no extra effort.

Such experiments as we describe have not yet been carried out, largely because they require a higher energy than double or triple scattering, in that both the scattered and recoil proton must be analysed, and efficient analysis requires the particle to have an energy of the order of 120 MeV or greater, since scattering of polarized protons by complex nuclei does not produce high asymmetries at energies lower than this. This means that even at energies of the order of 380 MeV, such as are available on the Liverpool cylotron, only main scatterings near 90° in the centre-of-mass system can be analysed, since otherwise one of the protons will have too small an energy.

† At present with C.E.R.N. Theoretical Study Division, Copenhagen.

§ 2. ANALYSIS IN COINCIDENCE WITH AN UNPOLARIZED INCIDENT BEAM

As we noted in § 3 of the preceding paper, the analysis in coincidence, with the analysers placed so as to measure spin components in the directions **l** and **m**, determine the quantity

$$C(\mathbf{l},\mathbf{m})=\langle \boldsymbol{\sigma}_1.\mathbf{l}\ \boldsymbol{\sigma}_2.\mathbf{m}\rangle \qquad \ldots\ldots(1)$$

where the ⟨ ⟩'s denote the expectation value of the enclosed quantity in the outgoing beam.

This quantity can be better understood by considering a simple example, the case in which the main scattering plane and both analysing planes are the same. This corresponds to a measurement of $C(\mathbf{nn})$ of I (3.13) with the polarization of the incident beam, $\boldsymbol{\alpha}$, zero.

We choose our axis of quantization perpendicular to the scattering plane, i.e. in the direction **n**. This is often the most convenient choice in discussing polarization experiments, rather than the incident direction of the particle, because dolarization produced in the scattering of unpolarized particles is always perpendicular to the scattering plane. The unpolarized incident beam can be represented by a mixture of equal amounts of the four states

$$\left.\begin{aligned}\chi_0&=(\alpha_1\beta_2-\beta_1\alpha_2)/\sqrt{2}\\ \chi_{11}&=\alpha_1\alpha_2\\ \chi_{10}&=(\alpha_1\beta_2+\beta_1\alpha_2)/\sqrt{2}\\ \chi_{1-1}&=\beta_1\beta_2\end{aligned}\right\} \qquad \ldots\ldots(2)$$

where α denotes a proton with spin up, β a proton with spin down, and the suffix 1 refers to the incident proton, 2 to the recoil proton.

Applying the scattering matrix M of I (1.1) to the χ's we find by an elementary calculation

$$\left.\begin{aligned}M\chi_0&=B\chi_0\\ M\chi_{11}&=(2C+N)\chi_{11}-H\chi_{1-1}\\ M\chi_{10}&=(G-N)\chi_{10}\\ M\chi_{1-1}&=-(2C-N)\chi_{1-1}-H\chi_{11}\end{aligned}\right\} \qquad \ldots\ldots(3)$$

where the direction of **p** has been taken as the x-axis, and that of **k** as the y-axis. (This is a different choice of axes than in I). The usual representation of the Pauli σ's has been employed in M.

Since the incident beam is an equal mixture of the four states (2), the average value of $\sigma_{1n}\,\sigma_{2n}$ in the outgoing beam is

$$C(\mathbf{nn})=\frac{\sum_j (M\chi_j)^{\dagger}\sigma_{1n}\sigma_{2n}M\chi_j}{\sum_j\ (M\chi_j)^{\dagger}M\chi_j} \qquad \ldots\ldots(3.1)$$

where the sum over j indicates a sum over the four states given in (2). This is just

$$C(\mathbf{nn})=\frac{\sigma_{11}+\sigma_{1-1}-\sigma_{10}-\sigma_0}{\sigma_{11}+\sigma_{1-1}+\sigma_{10}+\sigma_0} \qquad \ldots\ldots(3.2)$$

where σ_0 denotes the cross section for singlet scattering, and σ_{11} the cross section for scattering of the triplet state with projection 1 along the z-axis, etc. Equation (3.2) has a simple interpretation; in the states χ_{11} and χ_{1-1} the spins are parallel, and therefore the product $\sigma_{1n}\,\sigma_{2n}$ is positive, whereas in χ_{1-1} and χ_0 the spins are anti-parallel and $\sigma_{1n}\,\sigma_{2n}$ is negative.

Now, if the spin of the proton is up, it will be scattered to the right, let us say, by the analyser, and if it is down, to the left. It is then clear that the experimental quantity

$$\frac{RR+LL-LR-RL}{RR+LL+LR+RL}, \qquad \ldots\ldots(3.3)$$

where R indicates scattering to the right and L to the left, is equal to $C(\mathbf{nn})$. This assumes that the analysers are 100% efficient. Of course, in general, one will have to correct (3.3) for the lower efficiency of the analysers, so that if C_r and C_s are the polarizations that the analysers of the recoil and scattered beams would produce in unpolarized beams,

$$C(\mathbf{nn})=\frac{1}{C_rC_s}\,\frac{RR+LL-LR-RL}{RR+LL+LR+RL}. \qquad \ldots\ldots(3.4)$$

One very nice feature of $C(\mathbf{nn})$ occurs because σ_{10} is zero at 90°, since G and N are odd functions under the transformation $\theta \rightarrow 180^\circ-\theta$ (see Wolfenstein 1954). This means that at 90°,

$$C(\mathbf{nn})=\frac{\sigma_{11}+\sigma_{1-1}-\sigma_0}{\sigma_{11}+\sigma_{1-1}+\sigma_0} \qquad \ldots\ldots(4)$$

and therefore a measurement of this quantity at 90° in conjunction with total cross section measurements determines the triplet and singlet scattering cross sections at this angle. This gives important information about nuclear forces, for if there were only central forces between the two protons, there would be no triplet scattering at 90° and this quantity would be -1. The difference of this quantity from -1 gives some indication of the strength of spin-dependent forces, therefore. In the various sets of Berkeley phase shifts reported by Chamberlain *et al.* (1957) $C(\mathbf{nn})$ has the values 0·158, 0·711, 0·300, 0·490 and 0·425. It is seen, therefore, that spin-dependent forces are important here, and also that $C(\mathbf{nn})$ is quite different for most of the sets of phase shifts which fit all of the Berkeley experiments.

It is seen from equation (3.2) that $C(\mathbf{nn})$ depends on the squares of the absolute values of the amplitudes, not on cross products of various terms of the scattering matrix. Hence, it would not be expected to vary rapidly with energy. This is important if measurements at 380 MeV on the Liverpool cyclotron—where measurement of this quantity appears to be possible—are to relate to the Berkeley sets of phase shifts.

One can easily show that $C(\mathbf{lm})=C(\mathbf{ml})$ from the symmetry between the two protons, and consequently this limits the independent coefficients to $C(\mathbf{nn})$, $C(\mathbf{np})$, $C(\mathbf{nk})$, $C(\mathbf{pp})$, $C(\mathbf{pk})$ and $C(\mathbf{kk})$. Now $C(\mathbf{nk})$ can be obtained from equation (3.1) by replacing σ_{2n} by σ_{2k},

$$C(\mathbf{nk})=\frac{\sum\limits_j (M\chi_j)^\dagger\sigma_{1n}\sigma_{2k}M\chi_j}{\sum\limits_j (M\chi_j)^\dagger M\chi_j}. \qquad \ldots\ldots(5)$$

But this quantity is a pseudoscalar (it changes sign under spatial reflection), since $\boldsymbol{\sigma}$ and $\mathbf{n}$ are axial vectors, $\mathbf{k}$ is a vector and the other quantities are scalars. But it is not possible to construct a pseudoscalar from the three basic vectors $\mathbf{n}$, $\mathbf{k}$, $\mathbf{p}$, hence, $C(\mathbf{nk})$ must be zero. The same argument applies to $C(\mathbf{np})$.

The $C(\mathbf{pk})$ can be obtained in the same way as $C(\mathbf{nn})$. It is given by I (3.16). This quantity represents the correlation between the spin component of one particle in the x-direction and that of the other in the y-direction, and therefore it involves cross products of the coefficients of the scattering matrix, and is not given by such a simple picture as the $C(\mathbf{nn})$. Nevertheless, its measurement gives a new piece of information. For the Berkeley sets reported by Chamberlain *et al.* (1957), it has the values 0·363, 0·516, 0·251, 0·511 and −0·358.

The coefficients $C(\mathbf{pp})$ and $C(\mathbf{kk})$ are non-zero, but cannot be measured without a magnetic field because $\mathbf{p}$ is the direction of motion of the scattered particle in the laboratory system and $-\mathbf{k}$ is the direction of the recoil particle and the analysers cannot measure components of spin along the direction of motion. This can be remedied by employing a magnetic field to bend the component along the beam into the direction perpendicular to it. In general, magnets wil not bend the component along the direction of motion exactly perpendicular t it, but to some intermediate angle γ, with $\gamma < 90°$. Then it is more convenient to bend the longitudinal component into the $\mathbf{n}$ direction, in which case setting that analyser in the $\mathbf{n}$ plane gives just $\sin\gamma\, C(\mathbf{pp})$ or $\sin\gamma\, C(\mathbf{kk})$ depending on which coefficient is being measured; this is because $C(\mathbf{nk})$ and $C(\mathbf{np}$ are zero. If one bends the beam in the horizontal direction, one measures $\sin\gamma\, C(\mathbf{pp}) + \cos\gamma\, C(\mathbf{pk})$ or $\sin\gamma\, C(\mathbf{kk}) + \cos\gamma\, C(\mathbf{pk})$ and loses accuracy i elimination of $C(\mathbf{pk})$ if $\gamma \neq 90°$.

If the measurement of $C(\mathbf{pp})$ and $C(\mathbf{kk})$ must be carried out at $\theta = 90°$, as i the case in the 300 MeV region where only at this angle both particles have enoug energy to be analysed, no new information will be obtained. This is because th expectation value of $\sigma_{1k}\ \sigma_{2k}$ (or $\sigma_{1x}\ \sigma_{2x}$) is zero for the states χ_{11} and χ_{1-1}, an there is no scattering of the state χ_{10} at 90°. Also in the expression for $C(\mathbf{pp}$ and $C(\mathbf{kk})$ analogous to equation (3.1), cross products between χ_{11} and χ_{1-} vanish at 90°. Hence at this angle all of the contribution comes from the single state and $C(\mathbf{pp}) = C(\mathbf{kk}) = -\sigma_0/(\sigma_{11} + \sigma_{1-1} + \sigma_0)$ regardless of the nuclear forces, an hence the same information is obtained as in the measurement of $C(\mathbf{nn})$.

§ 3. EXTENSION TO OTHER CASES

We discuss now briefly the additional information that can be obtained if th initial beam is polarized. In this case, the polarization $\boldsymbol{\alpha}$, which is a pseud vector, enters into the problem, and with it and the unit vectors $\mathbf{p}$ and $\mathbf{k}$ it is eas to form pseudoscalars, so that $C(\mathbf{nk})$ and $C(\mathbf{pn})$ no longer need be zero. I fact, they are given in this case by I (3.14) and I (3.15) respectively. Further more, $C(\mathbf{kp})$ is different if the initial beam is polarized, and one obtains ne information by measuring it in this case. Although $C(\mathbf{nn})$ is also different for polarized beam, the difference is proportional to the polarization which measured in double scattering, and hence gives no new information. Thu three pieces of information can be obtained if the incident beam is polarized addition to the two that can be obtained from an unpolarized beam.

For completeness, we will mention the additional information that could obtained by using one magnetic field. If this is used on an incident polariz beam to produce a longitudinal component of polarization, two additional piec of information can be obtained. If it is employed between the main scatteri and an analysing scattering, to allow analysis of a longitudinal spin componen the $C(\mathbf{pp})$ and $C(\mathbf{kk})$ can be measured for an unpolarized incident beam, and addition, four additional new pieces of information can be obtained from polarized beam. Altogether then, thirteen pieces of information can be obtain from analysis in coincidence with a polarized incident beam and one magnetic field. Of course, many of these experiments are very difficult to carry out, and discussing them at the moment is somewhat academic.

ACKNOWLEDGMENTS

We would like to thank Dr. R. H. Dalitz and Professor R. E. Peierls for many interesting discussions.

REFERENCES

CHAMBERLAIN, O., SEGRÈ, E., TRIPP, R. D., WIEGAND, C., and YPSILANTIS, T., 1957, *Phys. Rev.*, **105**, 228.

DALITZ, R. H., 1952, *Proc. Phys. Soc.* A, **65**, 175.

KANELLOPOULOS, T. V., and BROWN, G. E., 1957, *Proc. Phys. Soc.* A, **70**, 690.

OEHME, R., 1955, *Phys. Rev.*, **98**, 216.

SMORODINSKII, Ya., 1955, *Doklady Akad. Nauk*, S.S.S.R., **104**, 713.

WOLFENSTEIN, L., 1954, *Phys. Rev.*, **96**, 1654.

WOLFENSTEIN, L., and ASHKIN, J., 1952, *Phys. Rev.*, **85**, 947.

CORRIGENDA

Compound Nuclear Theory and the Optical Model, by J. Bowcock (*Proc. Phys. Soc.* A, 1957, **70,** 515).

As the author of this paper is abroad, his proof corrections had not been received at the time of publication of the paper. The following corrections should therefore be made:

p. 515. Introduction, line 6, Watton should read Walton
p. 516, 1.5 Higner should read Wigner
eqn (2.5) the right-hand side should read $E_c\chi_c(\xi)$
p. 517, 1.13 σ_r should read σ_T
p. 519, first eqn, left-hand side should read $\bar{V}$
eqn between (3.5) and (3.6)

for $\sum_n = \frac{(\sum_p a_{0p}{}^n u_p(r_0))^2}{W_n - E} \sum$ read $\sum_n \frac{(\sum_p a_{0p}{}^n u_p(r_0))^2}{W_n - E} = \sum \ldots$

eqn (3.6), 2nd term on right-hand side should read

$$\frac{W_{0p} - W_n}{(W_{0p} - E)^2}$$

p. 519 to p. 527. For $(V-U)$ and $(V_{00}-U)$ read $(U-V)$ and $(U-V_{00})$
p. 520, last equation, for $(a_{0q}{}^n)^3$ read $(a_{0q}{}^n)^2$
p. 521, eqn (3.11), close brace at end of first line
p. 522, eqn (4.5), add at end of line $Cf(r)$
p. 523, eqn (4.9), add at beginning of line $0 = \Delta V^2 + \ldots .$
p. 524, 3 lines below (eqn 4.12), S_0 should read $\bar{S}_0$ in both cases where S_0 appears
2 lines before eqn (4.13), delete bracket after "interval"
eqn (4.13) last term should read

$$\ldots . \sum_n \frac{1}{I} \int_I \frac{(\gamma_{0q}{}^n)^2}{W_n - E} \left\{ \frac{W_{0q} - W_n}{W_{0q} - E} \right\}^3 dE$$

p. 526, eqn. (5.2), add closing brace before last square bracket
§5.2, 1.3, S_T should read S_0
p. 527, 5th line from bottom, replace W_{0p} by W_{0q}
4th line from bottom, replace R_3 by $\bar{R}_3$
2nd line from bottom, replace W_{0p} by W_{0q}
p. 528, 7th reference, for Watton read Walton.

REVIEWS OF BOOKS

Progress in Nuclear Energy—Series 2 : *Reactors*, Vol. 1, edited by R. A. CHARPIE, D. J. HUGHES, D. J. LITTLER and M. TROCHENS. Pp. x+492. (London : Pergamon Press, 1956.) £5 net.

This is the first volume in a series of annual reviews of progress in the field of nuclear reactors, and is devoted primarily to information published at the 1955 Geneva Conference. The first five chapters include Conference material on research reactors in the U.S.A. and the Soviet Union, and original reviews of research reactors in Canada and Europe. In the remaining six chapters, five of which are taken from the Conference proceedings, British and American authors discuss various existing, or suggested, types of power reactor. The book concludes with a list of the world's nuclear reactors.

Much of the treatment is descriptive and illustrated by some excellent diagrams and photographs. Nevertheless, a good deal of useful performance data and information about testing procedure is included, particularly in the sections on research reactors.

Chapters on aqueous homogeneous and sodium graphite reactors offer interesting summaries of feasibility study in this field. An excellent chapter is included on the pressurized water reactor at Shippingport, Pa, in which emphasis is laid on the complexity of the experimental development and design programme undertaken before the reactor was built, and which contains details about various test rigs and mock-ups. In contrast, a chapter on graphite-moderated gas-cooled reactors is far too brief to arouse the same degree of interest in the reader. In another chapter, operating experience of a boiling water reactor is summarized, and a final chapter contains a short review of some fast power reactors.

Despite its reliance on the previously published Geneva Conference papers, the book offers in convenient form an account of some representative existing and proposed types of reactor. As such, it is of use for reference rather than continuous reading.

J. F. PEARSON.

Rayonnements de particules atomiques, électrons et photons, by A. BERTHELOT. Pp. 192. (Paris : Masson, 1956.) 1800 *fr*.

This little monograph on the passage of high energy charged particles and quanta through matter contains much useful information. After some introductory chapters in which basic concepts are defined and expressions important in collision dynamics are set out an account is given of the passage of charged heavy particles through matter. The mean charge, stopping power, specific ionization, energy per ion pair, range, straggling and elastic scattering of such particles are discussed. A similar discussion of the passage of electrons through matter includes an account of the effect of electron-electron scattering, multiple electron scattering and the loss of energy due to bremsstrahlung production. The final chapters present expressions and figures for the absorption processes of gamma radiation. The numerous figures and tables enhance the value of the book for the experimental worker in nuclear and high energy physics although the lack of both author and subject indices is a serious inconvenience.

E. H. S. BURHOP.

Annual Review of Nuclear Science, Vol. 6, 1956, edited by J. G. BECKERLEY, M. D. KAMEN and L. I. SCHIFF. Pp. viii + 471. (Palo Alto, California: Annual Reviews Inc., 1956.) $7.50.

The latest addition to this well-known series is similar in layout, coverage and size to its predecessors. Most of the articles cover two or three years ending in April 1956, and including the period of the Geneva Conference on the Peaceful Uses of Atomic Energy. The papers of this conference have helped to make the present volume even more factual than usual.

The article by V. Sarabhai and N. W. Nerurkar on ' Time Variations of Primary Cosmic Rays ' is mainly descriptive, but attempts, not unsuccessfully, to introduce order into this wide and complex subject. It presents convincing evidence for the existence of large changes of the primary intensity. Two excellent articles (' Polarization of Fast Nucleons ' by L. Wolfenstein and ' Excitation of Nuclei by Charged Particles ' by N. P. Heydenburg and G. M. Temmer) deal with subjects of great interest to nuclear physicists, subjects which are certain to be treated in practically every review journal. The former is primarily theoretical and the latter experimental, but each gives a well-rounded and expert treatment of its topic. Nuclear data is now so extensive that considerable effort is required to reduce it to order. The complexity of the ordering process is illustrated in the account given by J. Mattauch, L. Waldmann, R. Bieri and F. Everling of the least-squares adjustment of the masses of light nuclides, and in the discussion by K. Way, D. N. Kundu, C. L. McGinnis and R. van Lieshout of general trends in the properties of medium weight nuclei ($A = 40$ to 140). A brief article by J. E. Mack and H. Arroe on ' Isotope Shift in Atomic Spectra ' distinguishes between effects due to nuclear mass and radius. Nuclear technique is represented by a readable account of low level counting (E. C. Anderson and F. N. Hayes), with applications to the study of double beta-decay and of the neutrino.

Two articles (' Generalized Acidity ' by R. A. Horne, C. D. Coryell and L. S. Goldring and 'Applications of Oxygen Isotopes inChemical Studies' by H.Taube) deal with chemical techniques; each is highly specialized. The chapter on ' Radiation Effects in Solids ' (H. Brooks) discusses with welcome candour the factors which make carbon and uranium difficult materials for the reactor engineer. The successful outcome of reactor engineering is dealt with in a comprehensive survey of ' Nuclear Reactors for Electric Power Generation ' by L. Davidson, W. A. Loeb and G. Young. The designs of reactors known to be under construction are tabulated and discussed one by one and the Russian work revealed at the Geneva Conference is introduced appropriately. The last two articles (' Cellular Radiobiology ' by L. H. Gray and ' Embryology ' by J. P. O'Brien) bring these subjects up to date; the two fields overlap to some extent. They give an interesting account of possible chemical means of protection against radiation damage, and of the known effects of radiation on the human embryo.

W. E. BURCHAM.

Digital Calculating Machines, by G. A. MONTGOMERIE. Pp. 262. (London and Glasgow: Blackie, 1956.) 30*s*.

This book is intended as an introduction to calculating machines of the digital type, which the author treats as follows: Chapter I (Introduction), Chapters 2–7 (Desk Calculating Machines), Chapter 8 (Punched Card Machines), and Chapters 10–12 (General Purpose Automatic Machines).

The first chapters give a very complete account of the principles of operation of all types of desk calculating machines including adding and listing machines, lever-set hand-operated machines such as the Brunsviga, key-set hand machines such as the Facit, and electrically operated machines such as the Marchant. The use of these machines for such operations as differencing, summation of products, synthetic division, and other calculations of a scientific and statistical nature are described. For this purpose a symbolic notation is employed to describe the operations of setting a number on a register, depression of the ' motor keys ', etc. This also forms a convenient introduction to the subject of ' programming ' for large-scale automatic machines, which is dealt with in the last chapter.

The chapter on punched card machines describes the principles of operation of both Powers–Samas and Hollerith equipment and the use of such equipment for solving linear simultaneous equations.

Chapter 9 describes how electromechanical relays and other items of telephone switchgear have been adapted to serve as computing elements in calculating machines, for example, the special purpose machine devised by MacEwan and Beevers (1942) for the summation of Fourier Series. Such machines are now, however, mainly of historical interest.

The chapters on large-scale machines deal mainly with the earlier machines such as the Harvard Mk. I and the ENIAC which serve to explain the principles of storage and number representation. In the last chapter the principles of ' programming ' (that is, the preparation of instruction schedules for machines) are explained with the help of an instruction table for a hypothetical machine. This serves to introduce the reader to such ideas as the counting of cycles of operation and the use of subroutines. R. A. BROOKER.

REFERENCE

MACEWEN, D., and BEEVERS, C. A., 1942, *J. Sci. Instrum.*, **19**, 150.

Table of the Fresnel Integral to Six Decimal Places, compiled by T. PEARCEY. Pp. 63. (Cambridge: University Press, 1956.) 12*s*. 6*d*.

In applications to theoretical physics and in particular the theory of diffraction, the Fresnel Integral is frequently needed to a precision greater than that of the four and five-figure tables which are readily available. The present tables are given to six-digit precision with seven places in the lower ranges. Tabulation is arranged so that elaborate interpolation is avoided.

The printing of the book is neat and the figures of comfortable size for easy reference.

CONTENTS OF SECTION B

PAGE

Mr. A. G. Clegg and Dr. M. McCaig. Processes occurring during the Heat Treatment of Alcomax 817

Dr. M. McCaig. The Unusual Magnetic Properties of Quenched Alcomax III . 823

Dr. M. Blackman. On the Thermal Expansion of Solids 827

Dr. N. J. Skinner and Dr. R. W. Wright. The Effect of the Equatorial Electrojet on the Ionospheric E_s and F2 Layers. 833

Dr. F. J. M. Farley and Mr. J. R. Storey. Time Variations of Extensive Air Showers 840

Dr. C. K. Coogan. The Measurement of the Optical Properties of Zinc Sulphide 845

Dr. L. Ward. The Temperature Coefficient of Reflectivity of Nickel . . 862

Dr. Sampooran Singh. Penetration by High Speed Metallic Jets . . . 867

Research Notes :

Dr. B. R. Judd. The Splittings induced in Levels by Crystal Fields of High Symmetry 880

Dr. B. Donovan and Dr. N. H. March. On the Absorption by Free Carriers in Semiconductors 883

Dr. L. W. Davies. Low–High Conductivity Junctions in Semiconductors . 885

Mr. D. E. Bradley, Dr. J. Franks and Miss P. E. Rush. Electron Microscopy of Tin Whiskers using Carbon Replicas 889

Dr. J. Franks. The Infra-Red Luminescence of Iodine 892

Letters to the Editor :

Prof. C. Domb and Dr. M. F. Sykes. High Temperature Susceptibility Expansions for the Close Packed Hexagonal Lattice 896

Mr. R. A. Kamper, Mr. K. R. Lea and Mr. C. D. Lustig. Hyperfine Structure and Nuclear Electric Quadrupole Moment of ^{17}O 897

Mr. K. S. Mendelson and Prof. R. Bray. Field Dependence of Mobility in p-Type Germanium 899

Reviews of Books 901

Contents of Section A 912

Electronic Levels of a Model of Liquid Potassium

By R. EISENSCHITZ and P. DEAN
Department of Physics, Queen Mary College, University of London

MS. received 20th May 1957

Abstract. As a one-dimensional model of a liquid a chain of atoms is considered in which the distances of nearest neighbours are independent random variables having a given probability distribution. · Electronic levels are derived using the tight binding approximation. The distribution of quantum states on the energy scale is obtained by applying known results from the mathematics of Jacobian matrices. Using atomic fields appropriate to the potassium atom it is shown that the conducting property of potassium and the insulating property of argon are preserved in the liquid state and that the band structure of the solid state is not essentially changed by the transition from the ordered to the disordered atomic structure.

§ 1. Introduction

The electron theory of crystals provides clear criteria for the conduction properties of solids in terms of the band structure of the energy spectrum. The existence of such bands is derived from the periodic nature of the lattices. It is a well known fact that insulators and good conductors preserve their properties in the liquid state. There is, as yet, no justification for the application of the band concept to liquids where the arrangement of the atoms is not periodic. Crystals with impurities in random positions are, with respect to their conducting properties, comparable to liquids.

A number of theoretical papers on this subject have been put forward. James (1949) and Gubanov (1954, 1955) applied perturbation theory to a perfectly periodic crystal in one and three dimensions and obtained a band structure, a result which is not conclusive as the band structure originates in the unperturbed system. James and Ginzbarg (1953) and Landauer and Helland (1954) considered one-dimensional chains by numerical methods. As a model of a disordered alloy two kinds of atom were assigned definite positions in chains of 40 or 150 atoms, their distribution being a representative sample of a random sequence. For a liquid model an array of atoms was considered in which the distances between neighbours were fixed, and again supposed to be a sample of a random sequence. The results, however, do not lend themselves to generalization.

In the present paper the energy spectrum of a one-dimensional chain of atoms is derived assuming that the interatomic distances are random variables for which a probability distribution is given. It should be added that a similar mathematical technique was applied in a recent paper by Schmidt (1957). Schmidt's method, however, applies only to special and not very realistic models and has, so far, not been fully evaluated.

§ 2. The Model

As a one-dimensional model of a liquid consider an array of N atoms of the same kind, the distances between nearest neighbours being random. We assume, as in the familiar theory of electrons in metals, that correlations between electrons are negligible, every electron moving independently of the others in the average field due to the array of ions and other electrons. This assumption has been made by virtually all previous workers.

Any given set of single-electron wave functions can be used for a basis as a representation of the energy matrix associated with the model. Identification of individual chain orbitals depends on diagonalization of the matrix. This problem, which has been solved for a strictly periodic lattice by various methods of approximation, seems to be intractable for a disordered chain.

It may, however, be sufficient to obtain a distribution function for the number of quantum states on the energy scale. This function can be found (cf. § 3), provided we have explicit knowledge of the position of every ion in the chain. If the positions of the ions are random any choice of values for interionic distances will be somewhat arbitrary. In the present paper this difficulty is overcome by specifying probabilities of interionic distances and finding the corresponding average energy spectrum.

In the theory presented below a definite assumption is made regarding the field due to a single ion, thus determining appropriate electronic orbitals. In addition, the distances between neighbouring ions are regarded as random variables, statistically independent, each having an identical probability distribution according to which the values of interatomic distance vary between approximately seven and eleven atomic units.

In mathematical terms the problem amounts to finding the distribution function of the eigenvalues of a matrix, the elements of which are not given explicitly but only in terms of a probability distribution.

§ 3. Mathematical Method

For matrices of a specially simple type the calculation of the distribution of eigenvalues has been solved in papers by Dyson (1953) and by Dean (1956). These matrices are of 'Jacobian' form, i.e. Hermitian matrices in which all the elements except those in the leading and two adjacent diagonals are zero.

Consider the matrix defined by

$$\left.\begin{array}{l} M_{ii}=a_i,\ M_{ii+1}=M^*{}_{i+1i}=b_i, \\ M_{ij}=0 \quad \text{for} \quad j\neq i,\ i\pm 1 \qquad (i,j=1,2,\ldots N). \end{array}\right\} \qquad \ldots\ldots(3.1)$$

Let $\mu_1, \mu_2, \ldots \mu_N$ be the N eigenvalues of this matrix. For large N the distribution of these eigenvalues can be represented by a continuous function $D(\mu)$.

Defining a generating function of an independent variable x by the relation

$$\Omega(x)=\int_0^\infty \ln(1+x\mu)D(\mu)\,d\mu \qquad \ldots\ldots(3.2)$$

this is expressed in terms of the matrix elements by

$$\Omega(x)=\lim_{N\to\infty}(1/N)\sum_{i=1}^{N}\ln[(1+a_i x)(1-g_i)] \qquad \ldots\ldots(3.3)$$

where g_i is a continued fraction of the form

$$g_i = \alpha_i[1-\alpha_{i+1}\{1-\alpha_{i+2}(\ldots-\alpha_{N-1})^{-1}\ldots\}^{-1}]^{-1} \qquad \ldots\ldots(3.4)$$

and

$$\alpha_i = |b_i|^2 x^2[(1+a_i x)(1+a_{i+1}x)]^{-1}. \qquad \ldots\ldots(3.5)$$

The generating function can then be inverted according to the relation

$$D(\mu) = (2\pi^2\mu)^{-1}\int_{-\infty}^{\infty}\cosh\pi\alpha\,d\alpha\int_0^{\infty}(x\mu)^{-1/2}\cos(\alpha\ln x\mu)\Omega'(x)\,dx \qquad \ldots\ldots(3.6)$$

where $\Omega'(x) = d\Omega(x)/dx$, thus yielding the required distribution function.

If the matrix elements are not given explicitly but only in terms of a probability distribution the procedure is modified as follows: let a_i, b_i $(i=1, 2, \ldots N)$ be governed by the probability function $P \equiv P(a_1a_2\ldots a_N;\ b_1b_2\ldots b_N)$ where $P\,da_1\,da_2\ldots da_N\,db_1\,db_2\ldots db_N$ is the simultaneous probability, for all i, of a_i lying in the range a_i to a_i+da_i and b_i lying in the range b_i to b_i+db_i. Our generating function is then given by a relation similar to (3.3) but in which the elements a_i and b_i are weighted according to their probabilities; thus

$$\Omega(x) = \int\ldots\int\ln[(1+a_1x)(1-g_1)]P\,da_1\,da_2\ldots da_N\,db_1\,db_2\ldots db_N. \qquad \ldots\ldots(3.7)$$

In the present paper P has the form $F(a_1)F(a_2)\ldots F(a_N)G(b_1)\ldots G(b_N)$ where $F(a_j)$ and $G(b_j)$ are probability distributions of a_j and b_j respectively.

We can find our new $D(\mu)$, which corresponds to an average over a statistical ensemble of chains, by inserting the $\Omega'(x)$ derived from (3.7) in (3.6).

§ 4. ENERGY MATRIX

In this paper the electronic levels of a liquid are derived using the tight binding approximation in which the distances between atoms are considered such that all overlap charges and energies between nearest neighbours are small quantities and are negligible for second nearest neighbours. This approximation, which is not too accurate in the solid state, can to some extent be justified for a liquid since the mean distance between neighbouring atoms is larger.

In the tight binding approximation the unperturbed states are specified by a chain orbital which is virtually identical with an atomic orbital specified by an energy parameter ϵ and a parameter κ. The set of states for which the value of ϵ is common can thus be represented by wave functions $\phi_{\epsilon\kappa}$ $(\kappa=1, 2, \ldots N)$, where ϕ is an atomic orbital. We use this set of wave functions, each member of which corresponds to an electron localized at one particular atom, as a basis for representation of the energy matrix.

The atomic orbitals ϕ were taken, for the ground state of potassium, from Hartree's tables of wave functions (Hartree 1934, 1938). These functions, however, are not orthogonal. A suitable basic set ψ, though, can be obtained from these functions ϕ by a well-known method of orthogonalization (cf. Courant and Hilbert 1953).

We write

$$\left.\begin{aligned} \psi_1 &= \phi_1 \\ \psi_2 &= \alpha_{21}\phi_1+\alpha_{22}\phi_2 \qquad . \\ &\cdot\quad\cdot\quad\cdot\quad\cdot\quad\cdot\quad\cdot\quad\cdot\quad\cdot\quad\cdot\quad\cdot \\ \psi_N &= \alpha_{N1}\phi_1+\alpha_{N2}\phi_2+\ldots+\alpha_{NN}\phi_N \end{aligned}\right\} \qquad \ldots\ldots(4.1)$$

where the constants α_{jk} are determined in terms of the overlap integrals $S_{ij}=\int\phi_i{}^*\phi_j\,d\mathbf{r}$ by standard methods. On account of the assumptions made in the tight binding approximation most of the constants α_{jk} vanish and (4.1) reduces to

$$\psi_j=\alpha_{jj-1}\phi_j+\alpha_{jj}\phi_j \quad (j=1,\,2,\,\ldots N) \qquad \ldots\ldots(4.2)$$

where

$$\left.\begin{aligned}\alpha_{jj-1}&=-S_{jj-1}(1-S^2_{jj-1})^{-1/2}\\ \alpha_{jj}&=(1-S^2_{jj-1})^{-1/2}\end{aligned}\right\}. \qquad \ldots\ldots(4.2)$$

and

We choose the zero of energy to be that of an electron at infinity so that the energy levels in the chain are negative.

Apart from integrals of the form S_{ij} we need, in calculation of the matrix elements, integrals

$$W_{ij}=\int\phi_i{}^*V_j{}'\phi_j\,d\mathbf{r} \qquad \ldots\ldots(4.4)$$

where

$$V_j{}'=\sum V(\mathbf{r}-\mathbf{r}_j)(1-\delta_{ij}) \qquad \ldots\ldots(4.5)$$

V being the potential of Hartree's self-consistent field. In accordance with our tight binding assumption we neglect all S_{ij} and W_{ij} integrals for which $j\neq i$ or $i\pm1$ and all squares and higher powers of the remaining integrals. Writing $H=-(h^2/2m)\nabla^2-\sum_j V(\mathbf{r}-\mathbf{r}_j)$ as the single electron Hamiltonian for the chain, the elements $H_{ij}=\int\psi_i{}^*H\psi_j\,d\mathbf{r}$ of the energy matrix reduce to

$$\eta_i=-H_{ii}=\epsilon_0+(1-S^2_{ii-1})^{-1}(W_{ii}-2S_{ii-1}W_{ii-1}) \qquad \ldots\ldots(4.6)$$

$$\lambda_i^{1/2}=-H_{ii+1}=[(1-S^2_{ii-1})(1-S^2_{i+1i})]^{-1/2}(W_{ii+1}-S_{ii+1}W_{ii}) \qquad \ldots\ldots(4.7)$$

$$H_{ij}=0 \quad \text{for} \quad j=i\pm2,\ i\pm3,\ \ldots$$

ϵ_0 being the ionization energy of a single atom.

The matrix $(-H_{ij})$ is thus of Jacobian form and the theory outlined in § 3 can be applied if we equate the quantities a_i with η_i and $|b_i|^2$ with λ_i. The distribution function obtained, corresponding to $D(\mu)$ in § 3, will be a distribution of energies which we write as $D(E)$. It is the object of this paper to find this energy distribution for two cases corresponding to different states of the potassium atom.

§ 5. THE ENERGY SPECTRUM

By means of equations (3.4), (3.5), (3.6) and (3.7) we can obtain, for the model which we consider, the distribution of the energy when interatomic distances are not fixed explicitly but are given in terms of a probability function. The evaluation of these equations is very much simplified by the fact that the squares λ_i of the non-diagonal elements of the energy matrix are very small, as is shown from figures below.

We can write (3.3), as applied to our model, in the form

$$\Omega(x)=\int\int\ldots\int\ln\,[(1+\eta_1x)(1-g_1)]F(\eta_1)F(\eta_2)\ldots G(\lambda_1)G(\lambda_2)\ldots d\eta_1\,d\eta_2\ldots d\lambda_1\,d\lambda_2\ldots$$

$$=\int\ln\,(1+\eta_1x)F(\eta_1)\,d\eta_1+\omega(x) \qquad \ldots\ldots(5.1)$$

where

$$\omega(x) = \iint \cdots \int \ln(1-g_1)F(\eta_1)F(\eta_2)\ldots G(\lambda_1)G(\lambda_2)\ldots d\eta_1\, d\eta_2 \ldots d\lambda_1\, d\lambda_2 \ldots \qquad \ldots\ldots(5.2)$$

On account of the smallness of the λ_i's the quantities α_i and hence g_i are very small and for all values of x and $\omega(x)$ may thus be regarded as a small correction. To a fair degree of accuracy, then, we may neglect $\omega(x)$ and write

$$\begin{aligned}\Omega(x) &\equiv \int \ln(1+xE)D(E)\,dE\\ &= \int \ln(1+x\eta)F(\eta)d\eta \qquad \ldots\ldots(5.3)\end{aligned}$$

and hence find that

$$D(E) = F(E) \qquad \ldots\ldots(5.4)$$

i.e. the distribution of the eigenvalues of the matrix is the same as the distribution of elements in the leading diagonal.

Since the λ's are small quantities compared to the η's it might appear that the problem is more amenable to treatment by standard perturbation theory. This, however, is not so, as the non-diagonal matrix elements

$$-H_{ii-1} = -H^*_{i+1i} = \lambda_i^{1/2},$$

are of the same order of magnitude as the differences of diagonal elements η_i.

As the result (5.4) might be considered almost too trivial, we make an estimate of the error due to neglecting the function $\omega(x)$; this can be done without much computing, use being made of the following numerical data (cf. next section). For the ground state (4s) of potassium ($\bar{\lambda}$ is the mean of λ)

$$\bar{\lambda} < 0{\cdot}002 \quad \text{and} \quad 0{\cdot}33 < \eta < 0{\cdot}5.$$

For the excited (5s) state

$$\bar{\lambda} < 0{\cdot}01 \quad \text{and} \quad 0{\cdot}25 < \eta < 0{\cdot}48$$

First we need a formula connecting the error $\omega(x)$ in the generating function with the error in the energy distribution. From (5.2) and (5.3) we get, quite generally,

$$\begin{aligned}\omega(x) &= \int_0^\infty D(E)\ln(1+Ex)\,dE - \int_0^\infty F(\eta)\ln(1+\eta x)\,d\eta\\ &= \int_0^\infty \Delta(E)\ln(1+Ex)\,dE \qquad \ldots\ldots(5.5)\end{aligned}$$

where $\Delta(E) = D(E) - F(E)$ is a correction distribution to be added to that found from (5.4) to give the true distribution. We notice that $\Delta(E)$ can have positive or negative values; however, for values of E at which $F(E)$ is zero it cannot be negative. It can be seen from (5.5) that $\Delta(E)$ may be found from $\omega(x)$ by a relation identical with (3.6).

By expanding the logarithm in (5.2) as a power series in α and replacing ratios of similar integrals as ratios of mean values of the integrands, it is easy to show that, if $R(x) = \omega(x)/\Omega(x)$ and $R_1(x) = \omega'(x)/\Omega'(x)$, then the maximum numerical values of $R(x)$ and $R_1(x)$ for all positive x are 0·006 and 0·007 respectively for the ground state, and 0·025 and 0·03 for the excited state. This, and further considerations which include knowledge that the zeroth and first moments of E with respect to $\Delta(E)$ are zero, lead to the conclusion that the effect of neglecting $\omega(x)$ is not serious; its inclusion would somewhat extend the limits of the spectrum as found from (5.4).

Having stated the mathematical technique used to determine the energy spectrum we now discuss its numerical evaluation.

§ 6. NUMERICAL COMPUTATION

The matrix elements η_i and $\lambda_i^{1/2}$ were calculated, as functions of interatomic distances, for the 4s and 5s states of the potassium atom. For the 4s state the potential and wave function according to Hartree's self-consistent field were used, as calculated by Hartree (1934, 1938). The same potential and a hydrogenic wave function were used for the 5s state, where the corresponding Hartree wave function is not yet known.

In evaluating the integrals W_{ii} and W_{ii+1} as defined in (4.4), a single term in the sum, due to the ion at $\mathbf{r}_i$, was taken into account, all other contributions being negligible. The integrals W_{ii}, W_{ii+1} and S_{ii+1} were calculated for four values of the interatomic distance, intermediate values being interpolated. The dependence of η_i and λ_i on interatomic distances was derived in accordance with (4.6) and (4.7). η_i is a function of two distances: $(r_{i+1}-r_i)$ and (r_i-r_{i-1}); it is plotted in figure 1, for the ground state, as a function of $(r_{i+1}-r_i)$, (r_i-r_{i-1}) being constant. Curves for the 5s state have a similar shape. The corresponding results for the λ_i are not shown as they are needed only for correction terms.

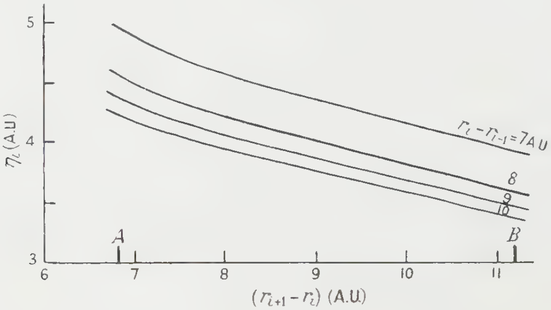

Figure 1. η_i as a function of $(r_{i+1}-r_i)$ for (*a*) $(r_i-r_{i-1})=7$ A.U.; (*b*) $(r_i-r_{i-1})=8$ A.U.; (*c*) $(r_i-r_{i-1})=9$ A.U.; (*d*) $(r_i-r_{i-1})=10$ A.U.
A and *B* denote extreme values of $(r_{i+1}-r_i)$ as given by equation (6.1).

The probability distribution function for the interatomic distances was chosen as

$$P(R_i)\,dR_i=(-0{\cdot}0731R_i^2+0{\cdot}3451)dR_i$$
$$-2{\cdot}173\leqslant R_i\leqslant+2{\cdot}173 \qquad (i=1,\,2,\,\ldots N) \qquad \ldots\ldots(6.1)$$

where $R_i=r_{i+1}-r_i-\bar{r}$, $\bar{r}$ being the mean interatomic distance which is equal to 9 atomic units. This function has a most probable value which corresponds to that for the nearest neighbours in the radial distribution function of liquid potassium (Gingrich 1943). The maximum cut-off value in (6.1) coincides with the first minimum in the radial distribution curve.

For the purpose of comparison, calculations of the energy spectrum were made for the strictly periodic chain of period $\bar{r}$. The formula for the distribution of energy in this case is

$$D(E)=(1/\pi)[4\bar{\lambda}-(E-\bar{\eta})^2]^{-1/2} \qquad \ldots\ldots(6.2)$$

which is in accordance with equation (57), p. 68, of Mott and Jones (1936).

§ 7. RESULTS

The energy spectra for two ‘bands’ of the liquid state are shown in figure 2; it can be seen that the 4s and 5s bands overlap considerably and hence overlap can be expected between the 4s and 4p bands. Comparable bands for the periodic chain also overlap (cf. figure 3). As the 4s state is only half filled in atomic potassium the conduction properties of the metal are independent of the separation of these bands.

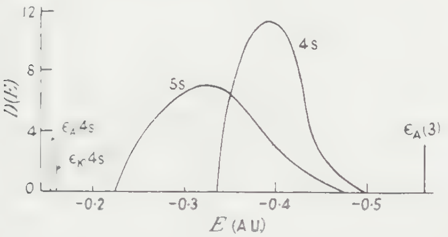

Figure 2. Energy bands for liquid potassium.

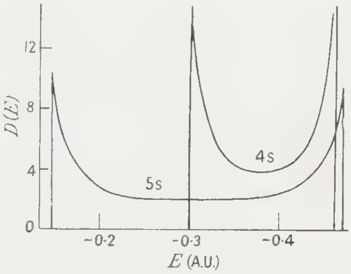

Figure 3. Energy bands for solid potassium.

The ground state of argon is a 3s–3p state and the lowest excited level is the 4s state. The energy of an electron in the ground state of the isolated atom is found to be $\epsilon_A(3)=-0{\cdot}564$ A.U.; for the excited state it is $\epsilon_A(4s)=-0{\cdot}154$ A.U. (Condon and Shortley 1953). This latter figure corresponds closely to the value for potassium ($\epsilon_K(4s)=-0{\cdot}159$ A.U.) showing that the 4s wave function for the two atoms do not differ very markedly, the increase in atomic radius for potassium being counteracted by the increase in nuclear charge. The results for the 4s band of the chain of potassium atoms are accordingly applicable to a chain of argon atoms.

The bracket $(W_{ii}-2S_{ii-1}W_{ii-1})$ in (4.6) must have the same sign as W_{ii}, the second term being of a smaller order of magnitude. Since W_{ii} and ϵ_0 are, in the usual convention, negative, it follows that the value of the energy ϵ_0 represents an upper limit to the corresponding band. In figure 2 the values of $\epsilon_A(3)$ and $\epsilon_A(4s)$ are shown. It is seen that there is a gap of approximately 0·1 A.U. between the lowest level of the 4s band and the energy $\epsilon_A(3)$ which is an upper limit of the lowest band of argon. It follows that there is an energy gap between the 3s–3p and the 4s bands of argon. This is an explanation of the fact that the insulating property of the argon crystal is preserved at melting.

The results of this paper cannot be checked against the work of previous authors, e.g. Landauer and Helland, who did not provide the spectrum of a chain of macroscopic length.

The present results give no indication of the formation of thinly spread states in the gaps between bands, known as impurity bands. In preliminary calculations we could, however, show that, if the tight binding approximation is applied, such impurity states exist for a crystal with a regularly spaced impurity. The theory outlined for the energy spectrum of a liquid is thus not in conflict with the well-known formation of impurity bands.

ACKNOWLEDGMENTS

One of us (P.D.) wishes to thank the Ministry of Education for the extension of a State Scholarship enabling him to carry out this research. We wish to thank the University of London Central Research Fund for the loan of a FACIT calculator.

REFERENCES

CONDON, G. U., and SHORTLEY, G. H., 1953, *The Theory of Atomic Spectra* (Cambridge : University Press), p. 328-9.

COURANT, R., and HILBERT, D., 1953, *Methods of Mathematical Physics* (New York : Interscience).

DEAN, P., *Proc. Camb. Phil. Soc.*, 1956, **52,** 752.

DYSON, F. J., 1953, *Phys. Rev.*, **92,** 1331.

GINGRICH, N. S., 1943, *Rev. Mod. Phys.*, **15,** 90.

GUBANOV, A. I., 1954, *Zh. Eksp. Teor. Fiz.*, **26,** 139, 1955 *Ibid.*, **28,** 401.

HARTREE, D. R., 1934, *Proc. Roy. Soc.* A, **143,** 506, 1938, *Proc. Camb. Phil. Soc.*, **34,** 550.

JAMES, H. M. 1949, *Phys. Rev.*, **76,** 1602; 1611.

JAMES, H. M., and GINZBARG, A. S., 1953, *J. Phys. Chem*,. **57,** 840.

LANDAUER, R., and HELLAND, J. C., 1954, *J. Chem. Phys.*, **22,** 1655.

MOTT, N. F., and JONES, H., 1936, *The Theory of the Properties of Metals and Alloys* (Oxford : Clarendon Press).

SCHMIDT, H., 1957, *Phys. Rev.*, **105,** 425.

A Phase-Shift Analysis of Nucleon Nucleon Scattering at 95 MeV

By R. J. N. PHILLIPS
Atomic Energy Research Establishment, Harwell, Didcot, Berks.

Communicated by B. H. Flowers; MS. received 25th June 1957

Abstract. A phase-shift analysis of n–p and p–p cross sections and polarizations at 95 MeV is made in terms of S, P and D partial waves. Three distinct small regions in the phase-shift space are found to be able to account for the data, at least approximately. Although the results indicate that F-wave effects are significant at this energy, test calculations suggest that they may be considered as a small perturbation.

---

§ 1. Introduction

In recent years there have been several attempts to analyse high-energy nucleon nucleon scattering in terms of phase shifts, as a first step toward elucidating this interaction (Garren 1953, 1954, 1955, Thaler and Bengston 1954, Klein 1955, Beretta *et al.* 1955, Stapp 1955, Feshbach and Lomon 1956, Ohnuma and Feldman 1956, Hull *et al.* 1956, Stapp *et al.* 1957, Clementel *et al.* 1957). At first it was hoped that S and P waves would be enough to describe the scattering up to 200 MeV, but later experiments have shown higher waves to be important even at 100 MeV. The most thorough analysis so far has been that of the 310 MeV p–p scattering experiments in terms of partial waves with $L \leqslant 5$, using high speed electronic computers (Stapp *et al.* 1957); however, this yields several distinct satisfactory solutions. When equally reliable analyses have been made at other energies, and further experimental data are included (in particular n–p scattering), it is hoped that there will emerge a unique set of phase shifts, varying continuously with energy.

This note describes a phase-shift analysis of n–p and p–p polarized and unpolarized cross sections at the nominal bombarding energy 95 MeV, carried out with the help of a desk computer. The data show a large polarization in the isotopic spin state $T=0$, which implies scattering in states with $L=2$ at least. On the other hand, F-waves should in general contribute a term in $\sin\theta\cos^3\theta$ to $[P(\theta)\sigma(\theta)]_{\mathrm{pp}}$, but a least-squares fit to the data gives a small value for this term, with an uncertainty nearly as large as the term itself. Since it was consistent with the data to ignore F-waves altogether, the analysis was carried out in terms of S, P and D waves alone. In principle, the problem was several times over-determined.

Because of experimental uncertainties one would not expect precise solutions, but rather small regions of fit to data in the space of phase shifts. Three such regions have been found.

The fits to data that have been secured are fair, but not wholly satisfactory, which suggests that F-wave effects may not be negligible. On the other hand, trial calculations suggest that such effects may be considered as a small perturbation, and that the present conclusions for S, P and D waves may be substantially correct.

§ 2. EXPERIMENTAL DATA, AND METHOD OF ANALYSIS

The unpolarized n–p cross section has been measured at 91 Mev by Stahl and Ramsey (1954); other work in this energy region is summarized in their paper. In figure 3 their results have been supplemented by those of Chih (1954) at 90 Mev and those of Thresher, Voss and Wilson (1955) at 105 Mev.

The n–p polarization at 95 Mev has been measured by Stafford, Whitehead and Hillman (1957).

The p–p polarization and unpolarized cross section have been measured at 98 Mev by Taylor and Wood (1957, to be published).† Their results are consistent with the earlier cross section measurements (at large angles only) of Kruse,

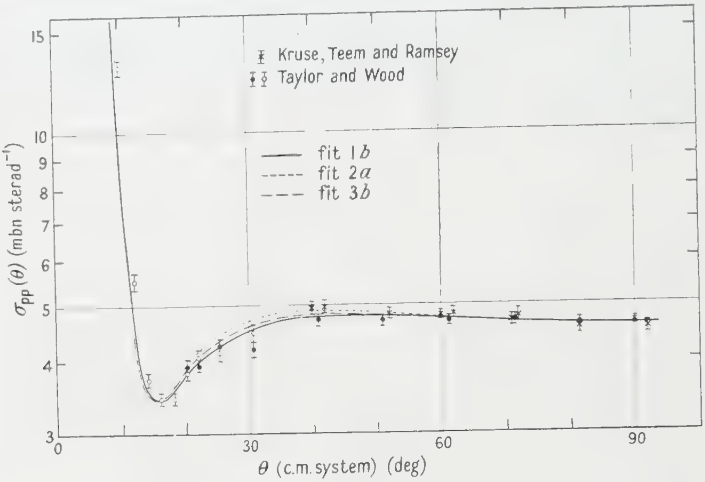

Figure 1. p–p unpolarized cross section.

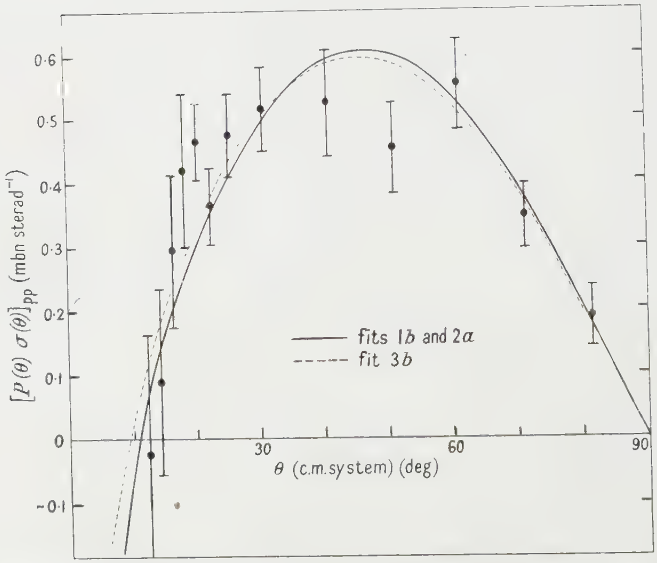

Figure 2. p–p polarized cross section. The experimental points are those of Taylor and Wood. Fits 1*b* and 2*a* nearly coincide, and are represented by a single curve.

---

† After this analysis was completed, further measurements were reported from Harvard (Wilson 1957), agreeing with those of Taylor and Wood.

Teem and Ramsey (1954, 1956) at 95 Mev. Taylor's cross section measurements have been taken normalized to 4·65 mbn sterad^{-1} at 90° in the centre-of-mass system; this differs from the normalization he gives by less than the standard error, when one has allowed for the small change in cross section with energy.

The experimental data are summarized in figures 1–4.

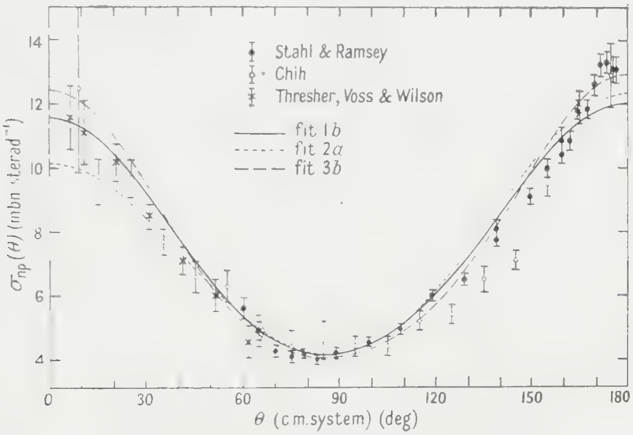

Figure 3. n–p unpolarized cross section.

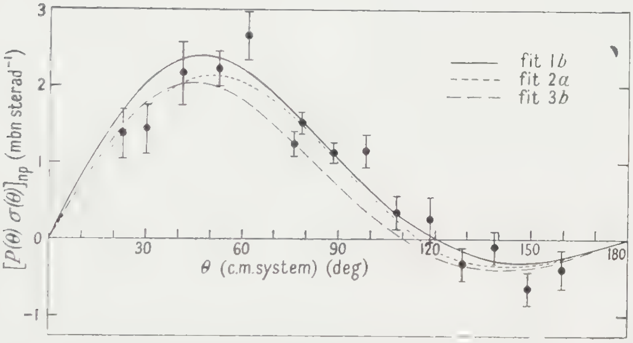

Figure 4. n–p polarized cross section. The experimental points are those of Stafford, Whitehead and Hillman (1957).

For S-, P- and D-wave scattering, the cross sections and polarizations have the general form

$$\sigma_{np}(\theta) = \sum_{n=0}^{4} a_n \cos^n\theta, \qquad \ldots\ldots(1)$$

$$[P(\theta)\sigma(\theta)]_{np} = \sin\theta \sum_{n=0}^{3} b_n \cos^n\theta, \qquad \ldots\ldots(2)$$

$$\sigma_{pp}(\theta) = \sum_{m=0}^{2} a_{2m}' \cos^{2m}\theta + \text{(electromagnetic terms)} \qquad \ldots\ldots(3)$$

$$[P(\theta)\sigma(\theta)]_{pp} = b_1' \sin\theta\cos\theta + \text{(electromagnetic terms).} \qquad \ldots\ldots(4)$$

The coefficients above can be written in terms of the ten relevant nuclear phase shifts (labelled δ_L for singlet, $\delta_L{}^J$ for triplet spin states†) and the ${}^3S_1$–${}^3D_1$

---

† The phase shifts for the $J=1$ triplet eigenstates are labelled by the L-values they take in the limit $\epsilon^1=0$.

mixture parameter ϵ^1 (in the convention of Blatt and Biedenharn (1952 a, b) with the sign as defined by Stapp (1955)). To write them out in full would take several pages, however, and the interested reader is referred to the literature where (3) and (4) have been given explicitly (e.g. Ohnuma and Feldman 1956), and where rules are given for deriving (1) and (2).†

The 'electromagnetic terms' above include the effects of interference with pure nuclear scattering. They may be neglected at angles greater than 30° (centre-of-mass) in p–p polarization, in view of the experimental errors. Such neglect is not justified in the unpolarized cross section, however; in typical examples from the present analysis, electromagnetic effects are 12% at 40°, 5% at 60° and 3% at 90° (centre-of-mass), and these figures could in principle be much larger. Experimental error, apart from the question of normalization, is only 2–3% at these angles.

p–p scattering is treated by simply adding the phase shifts for electromagnetic and pure nuclear scattering, and using charge independence to identify the pure nuclear phase shifts with those of n–p scattering. The usual relativistic coulomb and magnetic moment corrections are applied to the electromagnetic scattering (Garren 1955, 1956, Breit 1955, 1957, Ebel and Hull 1955). This is a perturbation treatment of electromagnetic effects, neglecting deformation of the wave function by nuclear forces. It is the only simple way of separating electromagnetic and pure nuclear effects; for a wholly correct treatment one would need to know the nuclear potential precisely.

The p–p data were first analysed in terms of the five ^{1}S, ^{3}P and ^{1}D waves. The polarization provides one piece of information, and the unpolarized cross section essentially four more (which may be taken as the values at 90°, 40°, 16° and 12° (centre-of-mass)). The ^{3}P phase shifts which satisfy the polarization data form a two-dimensional set; the corresponding ^{3}P contributions to σ (90°), σ (40°) and σ (16°), including electromagnetic effects, were recorded in a double-entry table. The corresponding contributions from general ^{1}S and ^{1}D phase shifts were recorded in another double-entry table. The tables were then compared systematically to find phase shifts that gave σ (90°), σ (40°) and σ (16°) in reasonable agreement with experiment. The phase shifts so defined formed continuous bands in the phase-shift space. Varying $P(\theta)\sigma(\theta)$ by as much as 20%, and the shape and normalization of $\sigma(\theta)$ by a few per cent, was found to make little difference to these bands.

The final criterion was to demand reasonable agreement with the observed cross section at 10° and 12°; because of the rapid change of the cross section with angle in this region, the angular resolution of the apparatus had to be folded into the theoretical curves. This should have selected small regions from the bands described above. However, for none of the bands was it possible to secure good agreement with the 10° and 12° measurements. It would have been unrealistic to use this criterion to select small regions of fit, and the final choice of $T=1$ phase shifts was therefore left to be decided by the n–p data.

It it not clear why there should be such poor agreement with the 10° and 12° observations: this question is discussed in an Appendix.

Scattering in the isotopic spin state $T=0$ is described by the six real parameters δ_1, $\delta_0{}^1$, $\delta_2{}^1$, $\delta_2{}^2$, $\delta_2{}^3$ and ϵ^1. The five coefficients a_0, a_2, a_4, b_1 and b_3, when compared with the corresponding p–p coefficients, gave five pieces of information about pure $T=0$ scattering. Hence the six parameters above were found to within a continuous degree of freedom (with several branches), together with considerable flexibility corresponding to the experimental uncertainties.

---

† See for example Stapp (1955). The formalism of § 1.1 is easily extended to the n–p system.

The four coefficients a_1, a_3, b_0 and b_2 are $(T=0,\ T=1)$ interference terms, and remain to be explained. The sets of $T=0$ and $T=1$ phase shifts described above were compared systematically, to find phase shifts that would explain these coefficients, at least approximately. The solutions were found to lie in three small regions in the phase-shift space. Examples are given in tables 1 and 2; they are to be understood as typical of these three small regions of fit to the data.

Table 1. $T=1$ phase shifts in degrees.

Fit No.	δ_0	δ_2	$\delta_1{}^0$	$\delta_1{}^1$	$\delta_1{}^2$
1*a*	35	1	−23·5	5	7
1*b*	32	0·5	−26	7·5	6
2*a*	26	−2	−22	15	6
2*b*	25	−4	−17	15	8
3*a*	30·5	−1	30	− 5	6
3*b*	31	−1	25	− 7	8
3*c*	31	0	16	−11	9
Marshak (100 MEV)	28·1	3·8	15·8	−14·0	9·8
Gammel (100 MEV)	21·7	5·5	10·5	−15·0	12·4
Feshbach	26	1	−28	2	5·5

Table 2. $T=0$ phase shifts in degrees.

Fit No.	δ_1	$\delta_0{}^1$	ϵ^1	$\delta_2{}^1$	$\delta_2{}^2$	$\delta_2{}^3$
1*a*	−37	33	20	−17	9	0
1*b*	−36	34	20	−16	11	1
2*a*	−35	39	20	−12	− 5	−1
2*b*	−24	49	25	− 5	−10	0
3*a*	−29	40	−5	−15	10	0
3*b*	−19	45	−5	−13	16	1
3*c*	−27	39	0	−13	16	1
Marshak (100 MEV)	−18·5	34·5	?	−16·8	19·3	6·1
Gammel (90 MEV)	−13·8	37·0	5·7	−13·2	18·7	3·8
Feshbach	−14	45	25	−10	—	—

The fits to data are illustrated in the figures 1–4.

§ 3. DISCUSSION

The fits to data given by the solutions above are fair, but not wholly satisfactory, which suggests that F-wave effects may be significant at this energy after all. If such effects behave like a small perturbation, however, the present results for S, P and D waves should be substantially correct. To test this possibility, some trial fits to the p–p data were made, including F waves. A least-squares fit to the data of Taylor and Wood gives

$$[P(\theta)\sigma(\theta)]_{\text{pp}} = \sin\theta\cos\theta[1{\cdot}00 \pm 0{\cdot}11 + (0{\cdot}16 \pm 0{\cdot}13)\cos^2\theta]\ \text{mbn sterad}^{-1}. \qquad \ldots\ldots(5)$$

Taking $b_1{}'=1{\cdot}0$ and $b_3{}'=0{\cdot}2$, and using either a $^3F_2$ or a $^3F_4$ wave (without

$^3P_2 - {}^3F_2$ mixing), solutions similar to fit 1 of table 1 were sought. Two examples are given in table 3, and it can be seen that introducing F waves has not greatly affected the lower partial waves. One is lead to conjecture that the F-wave scattering at 95 MeV may indeed be treated as a small perturbation. (This contrasts with the situation at 140 MeV, where F-wave effects cannot be treated in this way (Phillips 1957).)

Table 3. Examples using a single F-wave. $T=1$ phase shifts in degrees.

Fit No.	δ_0	δ_2	$\delta_1^{\,0}$	$\delta_1^{\,1}$	$\delta_1^{\,2}$	$\delta_3^{\,2}$	$\delta_3^{\,4}$
A	35	0·5	−24	6	6	—	0·2
B	37	0	−22	5	6	−1·2	—

It is interesting to note the similarities between the three regions of fit to the data; all agree qualitatively on δ_0, δ_1, $\delta_0^{\,1}$, $\delta_1^{\,2}$ and $\delta_2^{\,1}$. The values of δ_0 and $\delta_0^{\,1}$ are consistent with their well known behaviour at low energies. $\delta_2^{\,3}$ is small in all three regions, and has been put equal to zero in some examples. There is also agreement in making δ_2 small.

A static potential of simple shape, consistent with the low-energy data, must give δ_2 positive and of the order of 4° at least (Gammel and Thaler 1957a, unlike any of the fits above. However, δ_2 may well change by a few degrees when F waves and $^3P_2$–$^3F_2$ mixing are introduced.

There is little to choose between the three solutions on the basis of the present data. Fit 3 does not reproduce the n–p polarization as well as the others, but gives a somewhat better fit to the cross section; such differences may not be significant, since possible F-wave effects have been ignored. The results of Kruse, Teem and Ramsey (1954) for $\sigma_{\mathrm{pp}}(\theta)$ near 40° do not seem wholly compatible with those of Taylor and Wood; the examples given illustrate a variety of compromises (see figure 1), but the latter are in no way characteristic of the different regions of fit.

Fits 1 and 2 correspond roughly to the nuclear model of Feshbach and Lomon (1956), whereas fit 3 corresponds to Signell and Marshak's (1957) potential, and that of Gammel and Thaler (1957). The phase shifts given by these theories are included in tables 1 and 2 for comparison. It should be remembered that both the latter potentials lead to substantial F and G wave effects as well. At 310 MeV, the Gammel–Thaler potential agrees with solution 1 of Stapp *et al.* (1957).

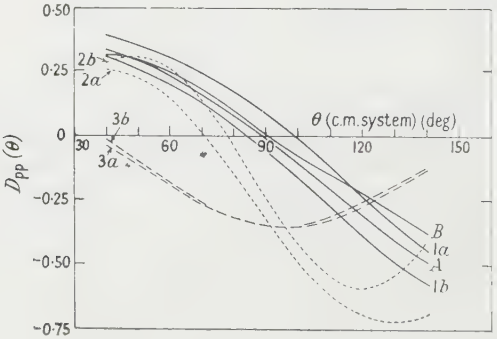

Figure 5. p–p depolarization. The predictions of the solutions in tables 1 and 3 are illustrated.

To discriminate between the present solutions, and to give more information about F-wave scattering, further experiments must be carried out. A measurement of p–p depolarization (Wolfenstein 1954) at 95 MeV is planned at Harwell. The predictions of the various solutions are shown in figure 5. It can be seen that the examples of table 3 differ little in this respect from the corresponding solutions without F waves†.

A rough preliminary analysis of the 95 MeV data has already been reported (Phillips 1956), in which a region of fit including the present fits 1 and 2 was found. However, it was necessary in this to make estimates of some quantities that had not then been measured, and the fairly close agreement with the present results is somewhat fortuitous.

The phase-shift analysis of this paper is in principle overdetermined. In practice, however, the experimental errors and the imperfections of the solutions prevent one from claiming that the basic hypotheses, including that of charge independence, have been verified. Nevertheless, it is reassuring that no large inconsistencies have appeared.

ACKNOWLEDGMENTS

The author would like to thank his colleagues at the Atomic Energy Research Establishment, in both theoretical and experimental branches, for many valuable discussions on this work. He is also greatly indebted to Dr. Hillman, Dr. Stafford, Mr. Taylor, Dr. Whitehead and Mr. Wood for early information about their experiments.

APPENDIX

σ_{pp} *at small angles*

When only S-, P- and D-wave scattering are important it can be shown that there is a maximum value for $\sigma(10^\circ)$ when $\sigma(\theta)$ is specified at three larger angles—say 16°, 40° and 90°. Furthermore, this maximum value is reached when $a_4' = 0$ (and hence $\delta_2 = 0$). For the 95 MeV data at 90°, 40° and 16°, the maximum value of $\sigma(10^\circ)$ is about 7 mbn sterad^{-1}, and the examples given above do not fall far short of this.

The angular resolution of the apparatus must now be included. In Taylor's experiment, a generous estimate of the beam divergence, with multiple scattering effects in target, windows, etc. is given by a Gaussian with $(\theta^2{}_{\mathrm{lab}})_{\mathrm{av}} = 1{\cdot}2$ degrees^2. The geometrical resolution of the telescope is given by a truncated triangle, full width 0·75° at the top and 1·75° at the base. The overall resolution is given roughly by folding the latter into the projected Gaussian distribution. In the examples given, the effect is to predict an 'observed' cross section at 10° (centre-of-mass) about 2 mbn sterad^{-1} higher than the true cross section.

The experimental result, however, is near 14 mbn sterad^{-1}, leaving a discrepancy of about 5 mbn sterad^{-1}.

When higher waves are included, the restriction on $\sigma(10^\circ)$ is lifted. However, of the examples of table 3, *A* gives very little improvement over the solutions without F-waves and *B* gives $\sigma(10^\circ)$ higher by 1 mbn sterad^{-1} only. It would appear that, if the discrepancy is to be explained by F-wave effects alone, these effects must be much larger than those suggested by the p–p polarization experiment.

---

† The predictions of the potentials of Marshak, Gammel and Thaler (not illustrated), which contain much larger higher-wave effects, still do not differ widely from those of fit 3 in the angular region shown.

It is possible that the experimental resolution may for some reason have been much worse than that estimated, but no firm conclusion can be reached at present.

REFERENCES

BERETTA, L., CLEMENTEL, E., and VILLI, C., 1955, *Phys. Rev.*, **98,** 1526.
BLATT, J. M., and BIEDENHARN, L. C., 1952 a, *Phys. Rev.*, **86,** 399; 1952 b, *Rev. Mod. Phys.*, **24,** 258.
BREIT, G., 1955, *Phys. Rev.*, **99,** 1581; 1957, *Ibid.*, **106,** 314.
CHIH, C. Y., 1954, *Thesis*, University of California, UCRL–2575.
CLEMENTEL, E., VILLI, C., and JESS, L., 1957, *Nuovo Cim.*, **5,** 907.
EBEL, M. E., and HULL, M. H., 1955, *Phys. Rev.*, **99,** 1596.
FESHBACH, H., and LOMON, E., 1956, *Phys. Rev.*, **102,** 891.
GAMMEL, J. M., and THALER R. M., 1957a, *Phys. Rev.*, **107**, 291; 1957b., *Phys. Rev.*, in the press.
GARREN, A., 1953, *Phys. Rev.*, **92,** 213, 1587; 1954, *Phys. Rev.*, **96**, 1709; 1955, USAEC *report NYU*–7102 *Thesis*, Carnegie Institute of Technology; 1956, *Phys. Rev.*, **101,** 419.
HULL, M. H., EHRMAN, J. B., HATCHER, R. D., and DURAND, L., 1956, *Phys. Rev.*, **103,** 1047.
KLEIN, C. A., 1955, *Nuovo Cim.*, **1,** 581; **2,** 38.
KRUSE, U. E., TEEM, J. M., and RAMSEY, N. F., 1954, *Phys. Rev.*, **94,** 1795; 1956, *Ibid.*, **101,** 1079.
OHNUMA, S., and FELDMAN, D., 1956, *Phys. Rev.*, **102,** 1641.
PHILLIPS, R. J. N., 1956, *Proceedings of the 6th Rochester Conference* (New York: Interscience); 1957, *Nuovo Cim.*, **5,** 1335.
SIGNELL, P. S., and MARSHAK, R. E., 1957, *Phys. Rev.*, **106,** 832.
STAFFORD, G. H., WHITEHEAD, C., and HILLMAN, P., 1957, *Nuovo Cim.*, **5,** 1589.
STAHL, R. H., and RAMSEY, N. F., 1954, *Phys. Rev.*, **96,** 1310.
STAPP, H. P., 1955, *Thesis,* University of California, UCRL–3098.
STAPP, H. P., YPSILANTIS, T. J., and METROPOLIS, N., 1957, *Phys. Rev.*, **105,** 302.
THALER, R. M., and BENGSTON, J., 1954, *Phys. Rev.*, **94,** 679.
THRESHER, J. J., VOSS, R. G. P., and WILSON, R., 1955, *Proc. Roy. Soc.* A, **229,** 492.
WILSON, R., 1957, *Proceedings of the 7th Rochester Conference* (New York: Interscience).
WOLFENSTEIN, L., 1954, *Phys. Rev.*, **96,** 1654.

Radiative Beta Decay of the Pion

By J. M. CASSELS, M. RIGBY, A. M. WETHERELL
AND J. R. WORMALD
Nuclear Physics Research Laboratory, University of Liverpool

MS. received 14th June 1957

Abstract. Theoretically about 1 pion in 10^3 is expected to decay by the process $\pi^+ \rightarrow P + \overline{N} \rightarrow e^+ + \nu + \gamma$, where the first stage is equivalent to a Yukawa reaction and the second to nuclear beta decay. A search for electron–photon coincidences from stopped positive pions has shown that in fact probably less than 1 pion in 10^5 decays in this way.

§ 1. INTRODUCTION

POSITIVE pions normally decay by the process $\pi^+ \rightarrow \mu^+ + \nu$ with a lifetime of $2{\cdot}5 \times 10^{-8}$ second, but it is reasonable to enquire whether beta decay in two stages also occurs,

$$\pi^+ \rightarrow P + \overline{N} \rightarrow e^+ + \nu \qquad \ldots\ldots(1)$$

where the bar indicates an anti-particle. Since the destruction of a particle is equivalent to the creation of an anti-particle, the existence of the first stage of reaction (1) is assured by the existence of the Yukawa reaction,

$$\pi^+ + N \rightarrow P. \qquad \ldots\ldots(2)$$

The second stage is similarly related to the beta decay of the neutron,

$$N \rightarrow P + e^- + \bar{\nu}. \qquad \ldots\ldots(3)$$

The effect of selection rules must of course be considered before the existence of the two stage process (1) can be predicted. The interaction responsible for the beta decay (3) certainly contains a tensor (T) term, and probably a scalar (S) one also. There is at present no clear evidence for vector (V), axial vector (**A**) or pseudoscalar (P) terms. Because the pion has zero spin and negative intrinsic parity it turns out that process (1) is forbidden except for the A and P interactions. There is therefore no compelling theoretical reason at present for believing in its existence, and in fact it has not been found experimentally (Friedman and Rainwater 1949, Lokanathan and Steinberger 1955).

The selection rules are altered for radiative beta decay, in which a photon is produced as well as the leptons,

$$\pi^+ \rightarrow e^+ + \nu + \gamma. \qquad \ldots\ldots(4)$$

This process is again forbidden for the S interaction, but it is allowed for the T interaction which certainly plays an important part in the beta decay (3) (Iwata, Ogawa, Okonogi, Sakita and Oneda 1955, Treiman and Wyld 1956).

The radiative beta decay rate, calculated to lowest order in pseudoscalar meson theory†, gives the logarithmically divergent result,

$$w(\pi^+ \rightarrow e^+ + \nu + \gamma) = (\mu/96\pi)\alpha(g_T\mu^2)^2G^2F^2$$
$$F = \pi^{-2}\ln(\Lambda/M) \qquad \ldots\ldots(5)$$

---

† We are very grateful to Drs. Dalitz, Gell-Mann, and Thirring for invaluable theoretical advice and, specifically, for the information set out in equations (5) to (10).

where $\hbar = c = 1$, μ is the pion mass, $\alpha = 1/137$ is the fine structure constant, $g_T\mu^2 = 2{\cdot}2 \times 10^{-7}$ is the tensor beta decay coupling constant, $G = \sqrt{15}$ is the pseudoscalar pion–nucleon coupling constant, M is the nucleon mass, and Λ the cut-off mass. If the cut-off is applied so that $\ln(\Lambda/M) \sim 1$, then $F^2 \sim \pi^{-4}$ (cf. Treiman and Wyld 1956), and

$$w(\pi^+ \to e^+ + \nu + \gamma) \sim 4 \times 10^4 \,\text{sec}^{-1}. \qquad \ldots\ldots(6)$$

This rate, when compared with the experimental value for the rate of decay into muons, gives a branching ratio,

$$\rho = \frac{w(\pi^+ \to e^+ + \nu + \gamma)}{w(\pi^+ \to \mu^+ + \nu)} \sim 10^{-3}. \qquad \ldots\ldots(7)$$

Some idea of the reliability of this calculation can be gained by enquiring into the decay rate of the π^0 by the process

$$\pi^0 \to P + \bar{P} \to 2\gamma. \qquad \ldots\ldots(8)$$

A similar calculation to lowest order yields the convergent result

$$w(\pi^0 \to 2\gamma) \doteq \left(\frac{\mu}{16\pi^2}\right) \alpha^2 G^2 \left(\frac{\mu}{M}\right)^2 = 2 \times 10^{16} \,\text{sec}^{-1}. \qquad \ldots\ldots(9)$$

The latest measurement of the Π^0 lifetime (Harris, Orear and Taylor 1957) shows that $w(\pi^0 \to 2\gamma)$ is probably greater than $2 \times 10^{15}\,\text{sec}^{-1}$. This does not contradict (9), and it is reasonable to expect the branching ratio ρ to be similarly within an order of magnitude of the value (7).

The matrix element for radiative beta decay through T interaction is

$$|\mathrm{M}|^2 \propto k(1 - \cos\theta)(1 - \cos\phi) \qquad \ldots\ldots(10)$$

where k is the photon energy divided by the pion rest energy, θ is the angle between the photon and electron momenta and ϕ is the angle between the photon and neutrino momenta. Various predictions of experimental interest have been obtained from (10) by putting in the appropriate phase space factors.

The overall energy spectrum of the electrons is given by

$$N_1(E) = 96E^2(1 - 2E), \quad \int_0^{1/2} N_1\,dE = 1 \qquad \ldots\ldots(11)$$

where E is the electron energy divided by the pion rest energy. The overal energy spectrum of the photons is

$$N_2(k) = 64k^3, \quad \int_0^{1/2} N_2\,dk = 1. \qquad \ldots\ldots(12)$$

The angular distribution of the photons relative to the electrons is, witl $u = \cos\theta$,

$$N_3(u) = 16(1-u)^{-5}\left\{2(1-u)(26 + 29u + 5u^2) + 3(1+u)(25 + 14u + u^2)\ln\left(\frac{1+u}{2}\right)\right\}$$

and

$$\int_{-1}^{1} N_3\,du = 1. \qquad \ldots\ldots(13)$$

The preference for emission of electron and photon in opposite directior (figure 1) is helpful for experiments which aim to detect them in coincidenc If events with $\theta = \pi$ are selected, the electron spectrum becomes

$$N_4(E, \theta = \pi) = 24E^2, \quad \int_0^{1/2} N_4\,dE = 1. \qquad \ldots\ldots(14)$$

All the corresponding photons have $k=\frac{1}{2}$. This would be an interesting point to check experimentally, since it is a direct consequence of the $(1-\cos\phi)$ factor in the T matrix element (10).

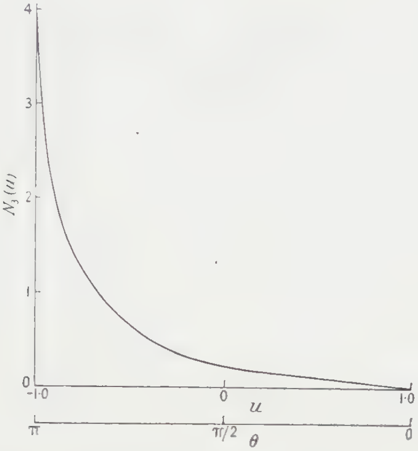

Figure 1. Angular correlation of the electron and photon emitted in pion radiative beta decay through tensor interaction.

§ 2. PREVIOUS EXPERIMENTS

Radiative beta decay might have been detected in either of the pion beta decay experiments already mentioned. Friedman and Rainwater (1949) examined the endings of 1419 meson tracks in nuclear emulsion, and found one event in which an electron might have been emitted from a pion. Their value for the branching ratio is therefore $\rho \lesssim 7\times10^{-4}$.

The experiment of Lokanathan and Steinberger (1955) was designed to detect the difference between the energy spectrum of the electrons emitted from pions and those emitted from muons. It happens that the difference is not very great for the continuous spectrum (11), and so the sensitivity of the experiment to radiative beta decay was probably reduced by a factor ten. Their result is then $\rho=(-3\pm9)\times10^{-4}$.

Both experiments, then, set upper limits to ρ which are about equal to the theoretical value (7).

§ 3. A COINCIDENCE EXPERIMENT

An attempt to detect the radiative beta decay by a coincidence method has been made with the apparatus shown in figure 2. A 96 MeV positive pion beam from the 156 in. Liverpool cyclotron was slowed down in the polyethylene absorber and stopped in the polyethylene target. The arrival of a pion was signalled by counter 1, and its subsequent radiative beta decay could have caused pulses in counter 2, detecting the electron, and counter 3, detecting electron pairs produced by the photon in the $\frac{1}{4}$ in. lead converter. The anti-coincidence counter 4 would not have been tripped by the photon. The whole event would therefore have given a coincidence–anticoincidence count of the type $1,23\bar{4}$, where the comma indicates that the pulse from counter 1 was delayed in order to bring it into coincidence with the pulses in counters 2 and 3.

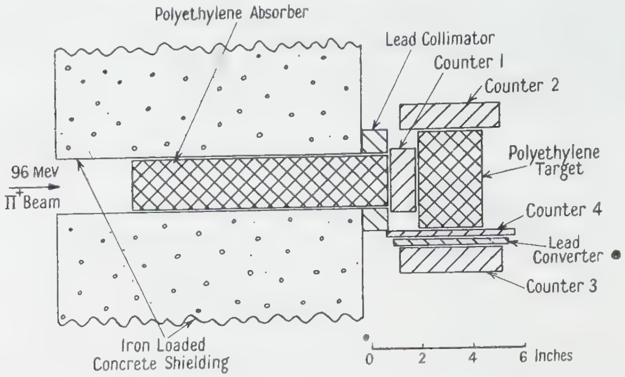

Figure 2. Apparatus for detecting pion radiative beta decay by electron–photon coincidences.

All four counters used E.M.I. 6260 photomultipliers and plastic scintillators (polystyrene + 2% p-terphenyl + 0·03% tetraphenyl butadiene). The 23 resolving time was 20 mμsec and the 4 resolving time 30 mμsec. The width and delay of the pulses from counter 1 were adjusted so that $1,23\bar{4}$ events were recorded when the $23\bar{4}$ count occurred between 11 and 62 mμsec after the 1 count. A monitor was provided by recording separately the pulses in counter 1.

The efficiency η for detecting radiative beta decay is the product of a number of the factors set out in table 1. According to the estimates there given

$$\eta = f_1 f_2 f_3 f_4 f_5 f_6 f_7 = 6 \times 10^{-3}. \qquad \ldots\ldots(15)$$

Table 1. Factors Used to Calculate Efficiency of the Experimental Arrangement

Factor	Definition	Estimated value
f_1	Fraction of monitor counts caused by pions stopping in target	0·65
f_2	Fraction of pions decaying between 11 and 62 mμsec after arrival in target	0·57
f_3	Chance of radiative beta decay electron leaving target	0·85
f_4	Solid angle subtended by counter 2, as fraction of 4π steradians	0·14
f_5	Solid angle subtended by counter 3, as fraction of 4π steradians	0·11
f_6	Efficiency of lead converter	0·40
f_7	Effect of opposite correlation of electron and photon emission directions (figure 1)	3·0
f_8	Fraction of pions which complete $\pi \to \mu \to e$ decay sequence between 11 and 62 mμsec after arrival in target	0·016
f_9	Fraction of muon decay electrons leaving target	0·80

A check on the estimates, and on the correct operation of the whole apparatus, was obtained by frequent counts of 1,2 events, 1,3 events and $1,3\bar{4}$ events (table 2).

Table 2. Tests of the Apparatus using Electrons from the $\pi \to \mu \to e$ Decay Sequence. Accidental coincidences have been eliminated by a linear extrapolation to zero counting rate.

	Counts per monitor count ($\times 10^4$)	
Type of count	Estimated	Observed
1, 2	12	10·1 ± 2·5
1, 3 (Pb out)	9	10·7 ± 2·5
$1, 3\bar{4}$ (Pb out)	0	0 ± 0·5

The first two types of event were caused by pions which completed the $\pi \to \mu \to e$ decay sequence between 11 and 62 mμsec after arrival, with the final electron leaving the target by way of counter 2 or 3. The chance ξ of a monitor count leading to a 1,2 event was, for example

$$\xi = f_1 f_4 f_8 f_9 = 1{\cdot}2 \times 10^{-3}. \qquad \ldots\ldots(16)$$

The 1,3 events were of course suppressed by bringing in the anti-coincidence $\bar{4}$.

The results of the search for $1,23\bar{4}$ events are summarized in table 3. Some counts were indeed observed, but most or all of them must be attributed to background effects. These were evaluated by running with the lead converter removed or with the counter 1 pulses delayed by an extra 52 mμsec (one r/f period of the cyclotron). The absence of the lead rendered counter 3 insensitive to photons, while the extra delay reduced f_2 in table 1 by a factor of 7·4.

Table 3. Summary of Experimental Records. The running conditions were: (A) lead converter in, normal delay between 1 and $23\bar{4}$; (B) lead out, normal delay; (C) lead in, 52 mμsec extra delay between 1 and $23\bar{4}$; (D) lead out, extra delay.

Monitor rate (sec^{-1})	Monitor counts ($\times 10^{-7}$)	Running condition	$1,23\bar{4}$ counts	Decay counts per monitor count ($\times 10^7$)	Background counts per monitor count ($\times 10^7$)
3800	11	A	38	$1{\cdot}13 \pm 0{\cdot}69$	$2{\cdot}30 \pm 0{\cdot}38$
	8	B	22		
	6	C	12		
	4	D	8		
1900	15	A	12	$-0{\cdot}04 \pm 0{\cdot}32$	$0{\cdot}84 \pm 0{\cdot}23$
	13	B	9		
	2	C	4		
	2	D	3		

The set of runs at a monitor rate of 3800 counts per second seemed to show a small genuine effect, which, however, was not confirmed by a more accurate set taken at 1900 counts per second. The background rate fell sharply, showing that it was principally caused by accidental coincidences.

The combined result of both sets is that the number of decay counts per monitor counts was

$$\eta\rho = (0{\cdot}16 \pm 0{\cdot}29) \times 10^{-7}. \qquad \ldots\ldots(17)$$

With the estimate of η given by (15), the branching ratio is found to be

$$\rho = (3 \pm 5) \times 10^{-6}. \qquad \ldots\ldots(18)$$

The experiment has obviously not established the existence of radiative beta decay, but it has considerably reduced the experimental upper limit on ρ. It can be said with 90% confidence that ρ is less than 10^{-5}, and with 99% confidence that it is less than $1{\cdot}5 \times 10^{-5}$.

§ 4. DISCUSSION

The experimental upper limit on ρ is thus about a factor of 100 below the theoretical estimate (7). A barely plausible explanation can be offered for this discrepancy.

First, it can be argued that the cut-off procedure used to evaluate (5) is arbitrary, and that a factor of ten error might have been made there. Secondly, the radiative beta decay should also occur through virtual states containing hyperons and anti-hyperons. Because of symmetries in the baryon–pion interaction, systematic cancellations of the several matrix elements might reduce the decay rate. The observed mass splittings of the baryons do not suggest a cancellation by more than a factor ten, and the example of the π^0 decay rate must be kept in mind.

An interesting third suggestion was made by Marshak (1957). The possibility of a V component in beta decay has recently been canvassed; since radiative beta decay is allowed for V interaction, the question of a cancellation in the second stage of the decay process has to be considered. Upon detailed investigation, however, the VT interference has turned out to be quite ineffective. (Sudarshan and Marshak, private communication).

If the experimental upper limit on ρ were to be lowered by another factor of ten, then the theoretical situation would begin to look somewhat desperate. Attempts to pursue the search down to this level are planned at Liverpool.

Finally, it may be remarked that the present limit has quite disastrous consequences for the simple universal Fermi interaction. This point has been thoroughly discussed by Treiman and Wyld (1956).

Acknowledgments

We wish to thank Mr. Halliday and the cyclotron crew for their willing co-operation throughout the experiment.

References

Friedman, H. L., and Rainwater, J., 1949, *Phys. Rev.*, **84**, 684.

Harris, G., Orear, J., and Taylor, S., 1957, *Phys. Rev.*, **106**, 327.

Iwata, K., Ogawa, S., Okonogi, H., Sakita, B., and Oneda, S., 1955, *Progr. Theor. Phys., Japan*, **13**, 19.

Lokanathan, S., and Steinberger, J., 1955, *Nuovo Cim.*, Suppl., **2**, 151.

Marshak, R. E., 1957, *Proceedings of the Seventh Annual Rochester Conference on High Energy Physics* (New York : Interscience Publishers).

Treiman, S. B., and Wyld, H. W., 1956, *Phys. Rev.*, **101**, 1552.

The Energy Spectrum of the 350 MeV Neutron Beam from the Liverpool Synchrocyclotron

By A. ASHMORE, R. G. JARVIS†, D. S. MATHER‡ and S. K. SEN §
Nuclear Physics Research Laboratory, University of Liverpool

Communicated by H. W. B. Skinner ; MS. received 22nd March 1957 *and in final form 8th August* 1957

Abstract. A knowledge of the energy spectrum of the neutron beam from the 156-inch cyclotron was required for cross section measurements. The spectrum of the recoil protons produced in n–p collisions was measured with a counter telescope containing a copper absorber of variable thickness. A calibration run was made in the external proton beam to measure the transmission of the absorber as a function of proton energy. It was found that the shape of the spectrum was consistent with the assumption that the neutrons are produced in 'elastic' proton–neutron collisions in the beryllium target. The shape is then determined by the amplitude of radial oscillations in the cyclotron and the energy lost by the protons in their multiple traversals of the target.

§ 1. Introduction

In a series of papers to be published, an account will be given of measurements that have been made of total cross sections, differential elastic cross sections, and absorption cross sections of nuclei for 350 MeV neutrons. The neutron beam was produced in the forward direction from the bombardment of a beryllium target in the cyclotron with protons of nominal energy 373 MeV. In the cross section measurements the neutron detector was a triple coincidence counter telescope which counted the recoil protons from a polythene scatterer. The energy threshold of the telescope was determined by the thickness of a copper absorber between the last two counters. In order to choose a suitable value for the thickness and to have a knowledge of the effective neutron energy spectrum used in the cross-section measurements, a measurement was required of the energy spectrum of the neutron beam.

Such measurements have been reported previously for various proton beam energies, by Kelly, Leith, Segrè, Wiegand (1950), Fox, Leith, Wouters and Mackenzie (1950), Bodansky and Ramsey (1951), Cladis, Hadley and Hess (1952); Nelson, Guernsey and Mott (1952), Goodell, Loar, Durbin and Havens (1953), Hoffmann and Strauch (1953), Randle, Cassels, Pickavance and Taylor (1953), Hartzler and Siegel (1954), Yodh (1955), Dzelepov, Karazinov, Golovin, Flyagin and Satarov (1955). The forms of the neutron spectra obtained have agreed in having a sharp rise from the highest energy to a peak followed by a long tail towards lower energies. The widths of the peaks have, however, differed considerably.

---

† Now with the General Electric Co. Ltd., London.

‡ Now at the Atomic Weapons Research Establishment, Aldermaston, Berks.

§ Now with Siemens-Schuckert Ltd., Erlangen, West Germany.

In our measurement the integral range distribution of the protons produced by the neutrons in n–p collisions was measured using a scintillation counter telescope containing a copper absorber variable in thickness. A polythene–carbon difference was used for the n–p scattering, and the mean scattering angle was 10 degrees. To correct for the loss of protons due to absorption and scattering in the copper absorber, a run was made with the counter telescope in the external proton beam, reduced to a suitably low level. The transmission of the absorber was measured as a function of the incident proton energy over the range of energies involved in the neutron spectrum measurement.

§ 2. Experimental Details and Procedure

2.1. *Geometry of the Neutron Beams*

The arrangement is shown in figure 1 (*a*). The beryllium target was $\frac{1}{4}$ in. thick in the direction of the proton beam and 1 in. high. It was situated at a radius of $69\frac{1}{4}$ in. where the nominal proton energy is 380 Mev. The neutrons emitted in the forward direction were collimated by 1 in. × 1 in. apertures in two steel plugs, 2 ft in length, placed one at each end of the 4 in. × 4 in. channel in the cyclotron shielding wall. In order to reduce the γ-ray contamination which was found to be present in the beam, a 4 in. thick lead filter was placed before the first collimator.

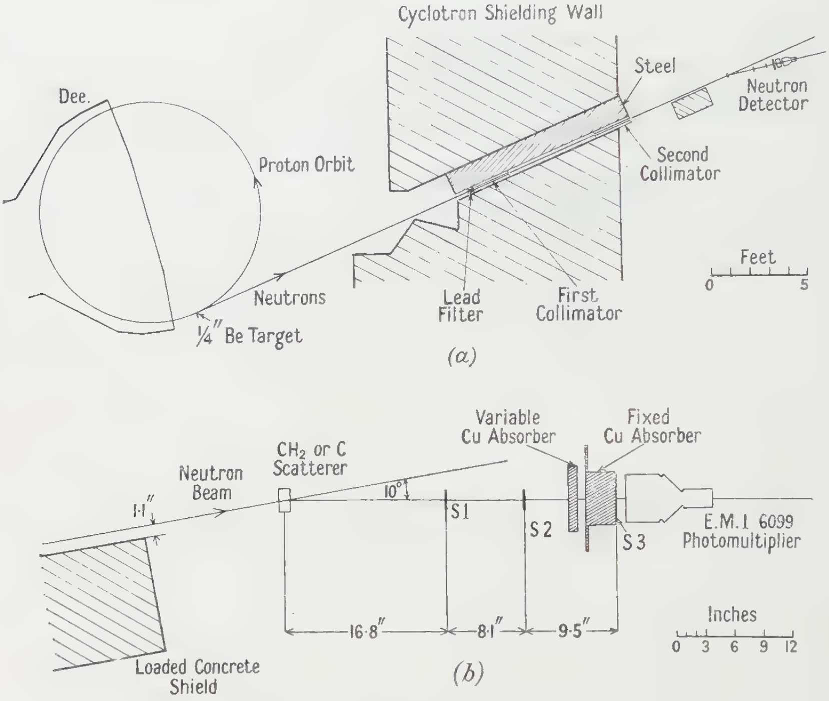

Figure 1. Experimental geometry.

2.2. *The Neutron Monitor*

The neutron monitor was a high pressure hydrogen filled ionization chamber located in the cyclotron room. This mainly detects recoil protons from low energy neutrons evaporated from the beryllium target. The current from the chamber was integrated using the circuit described by Lewis and Collinge (1953).

2.3. *The Neutron Detector*

Figure 1 (*b*) shows the arrangement of the neutron detector. A telescope of three scintillation counters was used to detect protons from a scatterer placed in the neutron beam, and the range spectrum of these protons could be obtained by varying the thickness of copper absorber between counters 2 and 3.

At the position of the scatterer the cross section of the collimated beam was 1·22 in. wide × 1·44 in. high. Scatterers 2·5 in. in diameter were used, of polythene (2·98 g cm^{-2}) and carbon (3·51 g cm^{-2}), having the same stopping power for protons. The axis of the counter telescope was set at an angle of 10 degrees to the direction of the neutron beam. The scintillation counters were then clear of the direct neutron beam. A 2 ft thick shield of iron loaded concrete blocks was used to reduce the background counts due to scattering from the mouth of the collimator.

All the scintillators were made from polystyrene containing tetraphenyl butadiene. In counters 1 and 2 the scintillators were $\frac{1}{4}$ in. thick and 2 in. in diameter, and were coupled by short Perspex light guides to E.M.I. 6260 photomultipliers placed below them. The scintillator in counter 3 was made larger (5 in. diameter) in order to keep down to negligible proportions the loss of protons due to scattering in the absorber. It was also made thinner ($\frac{1}{8}$ in.) so as to have as low an efficiency as possible for the detection of neutral secondaries from nuclear interactions of the protons in the absorber. The measurements in the proton beam (§ 2.6) showed that this effect was negligible. This scintillator was viewed with an E.M.I. 6099 photomultiplier placed so that its large ($4\frac{1}{2}$ in.) diameter photocathode was close to the back face of the crystal (figure 1 (*b*)).

The copper absorber consisted of a fixed section of thickness 67·9 g cm^{-2} which formed the front cover of the third counter, and a section variable in steps from 0·77 g cm^{-2} to 33·2 g cm^{-2}. This variable component was in the form of six plates 8 in. × $5\frac{3}{4}$ in. in cross section, which could be moved in and out of the telescope by means of cables actuated by pneumatic pistons, the latter being remotely controlled.

2.4. *Electronics*

The block diagram of the electronic equipment is shown in figure 2. The discriminators, trigger circuits and coincidence mixer were similar to those described by Collinge, Merrison and Eccleshall (1956).

An alternative form of head amplifier was used in which positive pulses from the last dynode of the photomultiplier were fed through a cathode follower into an EFP. 60 pulse-shaper. The pulses were clipped to a length of 2×10^{-8} sec by means of a 130 ohm open-circuited cable in the cathode as described by Chance (1949) and Wells (1952). Positive output pulses were taken from the EFP. 60 dynode and fed through a 130 ohm cable to the discriminator. The cathode follower was also used to reduce the effective capacity to earth at the output of the photomultiplier, and hence to enable larger voltage pulses to be obtained for the same degree of non-linearity of the photomultipler (Ashmore, Collinge and Sen 1957). Provision was made for counting the sum of the counts in the individual channels, thus enabling counting losses to be estimated.

When operating in the neutron beam the measured resolving time τ of the coincidence circuit was $2{\cdot}5 \times 10^{-8}$ sec. The dead time of the trigger circuit can be kept small if fired with pulses with heights considerably above the threshold value. For this reason the photomultipliers were operated at a voltage about 15% above the edge of their E.H.T. plateaux. Under these conditions the dead time in the individual channels was about 2×10^{-7} sec.

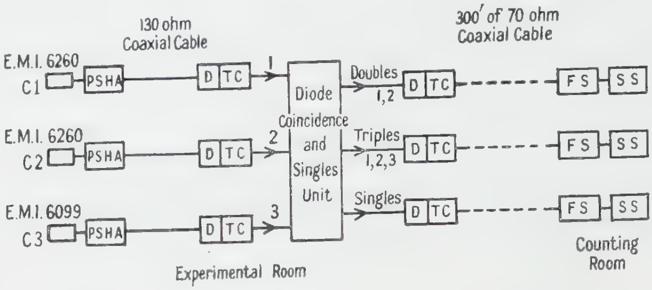

PSHA	Pulse shaping head amplifier	FS	Fast scale of 10
D	Discriminator	SS	Slow scaler
TC	Trigger circuit		

Figure 2. Electronics block diagram.

2.5. *Experimental Procedure*

The initial setting up and alignment of the target and detector system was carefully carried out using a theodolite and cross-wires in the collimators and on the counter supporting table. As a final check an X-ray film was exposed in the beam.

The electronic circuits were switched on several hours before each run to give steady conditions. The plateaux of the individual counters were then checked using triple coincidences and the photomultiplier EHT voltages suitably adjusted. Runs with different beam intensities showed that the efficiency of the neutron detector was independent of the beam intensity. In the spectrum measurement runs with the polythene, carbon and no scatterer were intermingled, each run covering the whole range of the variable absorber. The time was divided between the runs for approximately the best statistical accuracy.

The highest triple counting rates were 27, 12 and 0·3 per second with the polythene, carbon and no scatterer respectively. To obtain reasonable statistics for the neutron spectrum about 24 hours running time was required. Calculations showed that the loss of triples due to dead time effects was 0·85% in the worst case, while random coincidences were negligible.

2.6. *Measurements in the Proton Beam*

For these measurements the counter telescope, without the scatterer, was placed with its axis along the external proton beam. The beam was collimated to be about 1·5 in. in diameter and could be degraded in energy by means of carbon blocks placed just outside the proton exit on the cyclotron tank. Alignment of the counter telescope in the beam was done approximately by eye and the final adjustments made using X-ray films.

In the calibration runs a low proton beam intensity of about 500 per second was used so that the dead time losses in the counters were negligible. The ratio of triple coincidences to double coincidences in counters 1 and 2 gives a measure of the loss of protons in the absorber. This ratio, referred to hereafter as the absorber transmission factor, was measured as a function of the absorber thickness for several degraded proton energies. Runs were also made with an angle of 4 degrees between the axis of the telescope and the direction of the beam. This angle is about the maximum that a recoil proton from a scatterer can make with the telescope axis and still be detected.

§ 3. CALCULATION OF THE NEUTRON SPECTRUM FROM THE EXPERIMENTAL RESULTS

3.1. *Outline of Procedure*

The data obtained in the neutron beam measurement consist, for each absorber thickness, of the counting rates with the polythene scatterer (N_{CH}), the carbon scatterer (N_{C}) and no scatterer (N_{B}). Since the polythene and carbon scatterers were chosen to have the same stopping power for protons, the numbers of carbon atoms they contain are in the ratio 0·727 : 1. The counting rate N for protons from n–p collisions in the polythene scatterer is given by:

$$\begin{aligned} N &= (N_{\mathrm{CH}} - N_{\mathrm{B}}) - 0{\cdot}727\ (N_{\mathrm{C}} - N_{\mathrm{B}}) \\ &= N_{\mathrm{CH}} - 0{\cdot}727\ N_{\mathrm{C}} - 0{\cdot}273\ N_{\mathrm{B}}. \qquad \ldots\ldots(1) \end{aligned}$$

The values of N obtained with the different absorber thicknesses are shown in the table.

The following procedure was then adopted for the calculation of the neutron spectrum:

(1) The integral range distribution of protons given in the table was corrected for loss of protons in the absorber and converted to a differential energy distribution.

(2) The resolution curve of the neutron detector was calculated taking into account the thickness of the polythene scatterer and finite range of scattering angles over which protons were detected by the telescope.

(3) The energy distribution of the incident neutrons that would give the observed proton energy distribution was deduced using the calculated resolution curve of the detector.

Absorber thickness ($\mathrm{g\ cm^{-2}}$)		Number of protons per monitor count	
R_0	95·98	N_0	0
R_1	93·10	N_1	0·20 ± 0·04
R_2	90·22	N_2	1·54 ± 0·06
R_3	87·67	N_3	5·19 ± 0·07
R_4	84·79	N_4	10·97 ± 0·10
R_5	81·91	N_5	17·38 ± 0·14
R_6	79·03	N_6	22·24 ± 0·17
R_7	76·53	N_7	25·74 ± 0·19
R_8	73·65	N_8	29·62 ± 0·22
R_9	70·77	N_9	33·31 ± 0·24
R_{10}	67·89	N_{10}	36·45 ± 0·20

3.2. *Differential Energy Distribution of the Protons*

The integral range distribution of the protons was corrected for losses in the absorber and converted to a differential range distribution simultaneously. For this purpose the results of the measurements in the proton beam were used. A curve was plotted of the absorber transmission factor against absorber thickness for each incident proton energy. Now each curve is in effect an integral range curve and the mean range specifies the value of the degraded proton energy in terms of copper thickness. This is nore convenient, for the correction procedure adopted, than a value in Mev determined from the carbon degraded thickness and range–energy tables. Two sets of curves were obtained corresponding to angles between the telescope axis and the proton beam direction of 0° and 4°. The two curves obtained with the full proton beam energy are shown in figure 3. Since the curves for the two angles were similar, it was considered satisfactory to assume that the efficiency was independent of angle, and the 0° curves were used throughout the calculation. From these a further set of curves was constructed to give the absorber transmission factor T against the range in the copper absorber of the incident proton R, for each absorber thickness used in the neutron beam measurements.

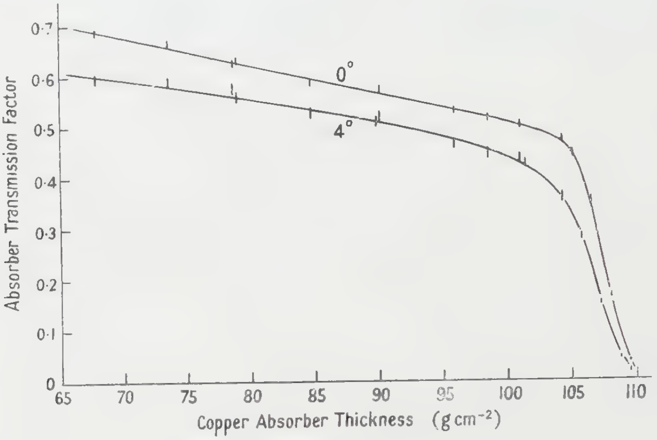

Figure 3. Absorber transmission curves.

Let ΔN_s be the number of protons entering the telescope with a range between R_s and R_{s-1}. For these protons and an absorber thickness R_r, a mean transmission factor T_{rs} can be obtained from the curves using the mean of the ranges R_s and R_{s-1}. Then

$$\begin{aligned} &N_0=0\\ &N_1=\Delta N_1 . T_{11}\\ &N_2=\Delta N_1 . T_{21}+\Delta N_2 . T_{22}\\ &N_3=\Delta N_1 . T_{31}+\Delta N_2 . T_{32}+\Delta N_3 . T_{33} \text{ etc.} \qquad \ldots\ldots(2) \end{aligned}$$

These equations were solved to give the quantities ΔN_1 etc. i.e. the differential range distribution of the protons corrected for losses in the absorber. The proton ranges were then converted to energy using the range–energy curves of Rich and Madey (1954) and the corrections of Mather and Segrè (1951). Allowance was made for energy loss in the scintillators and their aluminium caps. The resultant differential energy distribution of the protons, referred to hereafter as the recoil proton spectrum, is shown in figure 4.

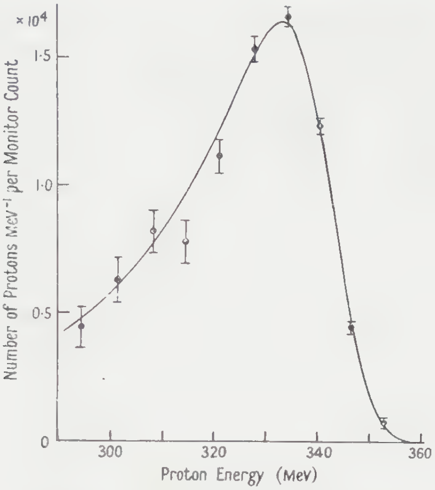

Figure 4. Recoil proton spectrum.

3.3. *The Resolution Curve of the Neutron Detector*

Referring to figure 5, the probability of a neutron producing, from an n–p collision in the element δm of the polythene scatterer, a proton at an angle between θ and $\theta+\delta\theta$ and which is detected by the telescope is given by

$$P(\theta)\delta\theta = 0{\cdot}086\delta m\left(\frac{d\sigma}{d\omega}\right)_\theta \delta\omega A_\theta \delta\theta \qquad \ldots\ldots(3)$$

where $(d\sigma/d\omega)_\theta$ is the n–p differential cross section in barns, in the laboratory system, for the proton at an angle θ, $\delta\omega$ is the solid angle subtended at the scatterer by the defining scintillator, $A_\theta\delta\theta$ is the proportion of the solid angle $\delta\omega$ between the angles θ and $\theta+\delta\theta$. The values of $d\sigma/d\omega_\theta$ were obtained by combining the results of Hartzler and Siegel (1954) at 400 Mev, and those of De Pangher (1954) at 300 Mev.

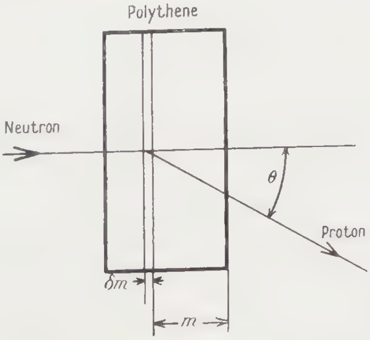

Figure 5. Neutron detection process.

The scattered proton has an energy less than that of the incident neutron due to the scattering through an angle θ and subsequent ionization loss in the polythene thickness m. For a constant difference in energy between the incident neutron and the emergent proton, the angles θ corresponding to different values of m were calculated and a graphical integration of the quantity $(d\sigma/d\omega)_\theta\, A_\theta$ was performed over the length of the polythene scatterer. This gives the relative probability $p(E_n - E_p)$ of a proton being detected with an energy E_p from a neutron of energy E_n and is the resolution curve shown in figure 6. For different incident neutron energies this curve will not be the same, but the variation is small enough to be neglected over the range of neutron energies involved. One calculation was therefore carried out for an incident neutron energy of 350 MeV.

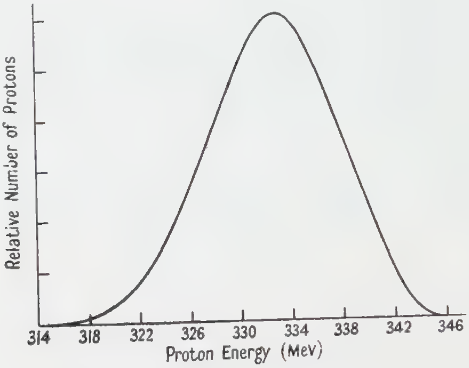

Figure 6. Detector resolution curve.

The area under the curve gives the total efficiency of the neutron detector as $3{\cdot}2 \times 10^{-5}$ exclusive of loss of protons in the copper absorber.

3.4. *The Neutron Spectrum*

The neutron spectrum $N(E_n)$ and the recoil proton spectrum $N(E_p)$ are related by the equation

$$N(E_p) = \int N(E_n)\, p(E_n - E_p)\, dE_n. \qquad \ldots\ldots(4)$$

It is thus a simple matter to calculate $N(E_p)$ from $N(E_n)$ by numerical integration, but considerably more difficult to solve for $N(E_n)$ when $N(E_p)$ is known as in the present case. A method of trial and error was adopted, having first made a reasonable estimate of the form of $N(E_n)$.

The difference between the proton beam energy (380 MeV) and the maximum energy of the recoil protons (356 MeV) is considerably greater than would be expected. It was suggested that the proton orbits might be displaced with respect to the centre of the magnet. To test this, a target almost diametrically opposite the neutron target was moved in until the neutron beam was cut off. This showed that the orbits were displaced from the magnet centre by $\frac{3}{4}$ inch towards the neutron target. The proton beam energy at the reduced radius is 373 MeV.

The recoil proton spectrum has an approximately exponential tail. It was assumed that this tail has the form:

$$N(E_p) \propto \exp[-(330 - E_p)/\epsilon] \text{ for } E_p < 330 \text{ MeV}.$$

A graph of log $N(E_p)$ against E_p gave the value of ϵ as 28 ± 2 MeV. The neutron spectrum must have a tail of the same form but starting from a higher energy of about 350 MeV. Due to multiple traversals of the beryllium target the protons traversing the target will also have an energy distribution of this form. ϵ in this case will be the energy lost by a proton making the mean number of traversals through the target. Using the theory of Cassels, Dickson and Howlett (1951) ϵ was found to be 30 Mev. This agrees with the value obtained from the recoil proton spectrum and suggests that the neutron spectrum is very similar to that of the protons traversing the target. Thus in the forward direction the neutrons are mainly produced in single 'elastic' proton–neutron collisions in the beryllium target. The neutron energies will be lower than the proton energies by 2 Mev owing to the Q-value of the process and the recoil energy of the nucleus.

There will be a further spread in energy of the protons traversing the target due to radial oscillations in the cyclotron orbits. This will mean that the protons incident on the target will be spread almost uniformly over a range of energies. It is convenient to take this range from E_0+2 Mev down to $E_{\mathrm{m}}+2$ Mev. The neutron spectrum then has the form

$$N(E_{\mathrm{n}})=C\{1-\exp[-(E_0-E_{\mathrm{n}})/\epsilon]\}/\{1-\exp[-(E_0-E_{\mathrm{m}})/\epsilon]\}$$
$$\text{for } E_0>E_{\mathrm{n}}>E_{\mathrm{m}}$$
$$N(E_{\mathrm{n}})=C\exp[-(E_{\mathrm{m}}-E_{\mathrm{n}})/\epsilon]$$
$$\text{for } E_{\mathrm{n}}<E_{\mathrm{m}}$$

where C is a numerical constant.

This form was assumed for the neutron spectrum, the values of E_0-E_{m} and ϵ were varied, and the resultant recoil proton spectrum calculated from equation (4). For each value of E_0-E_{m} the value of E_0 was adjusted to give the best fit. This analysis gave the values $\epsilon=28\pm 2$ Mev, $E_0-E_{\mathrm{m}}=10\pm 5$ Mev, $E_0=364\pm 2$ Mev, $E_{\mathrm{m}}=354\pm 3$ Mev. The value of E_0-E_{m} can be calculated independently from the length of the cyclotron beam pulse and the known variation of the radio frequency with time. From the random coincidence rate in the triple coincidence telescope the ratio of the period of the frequency modulation cycle to the length of the beam pulse was found to be $1/(50\pm 10)$. Making allowance for the uncertainty in E_0 and in the knowledge of the variation of radio frequency with time the value obtained for E_0-E_{m} was 14 ± 5 Mev. Combining this with the result of the numerical analysis, the neutron spectrum is defined by the values

$$\epsilon=28\pm 2\text{ Mev},\quad E_0-E_{\mathrm{m}}=12\pm 3\text{ Mev},\quad E_0=365\pm 1\text{ Mev},\quad E_{\mathrm{m}}=353\pm 2\text{ Mev}.$$

The neutron spectrum for the central values is shown in figure 7 and the curve in figure 3 is the recoil proton spectrum obtained with it. E_0 is 6 ± 1 Mev

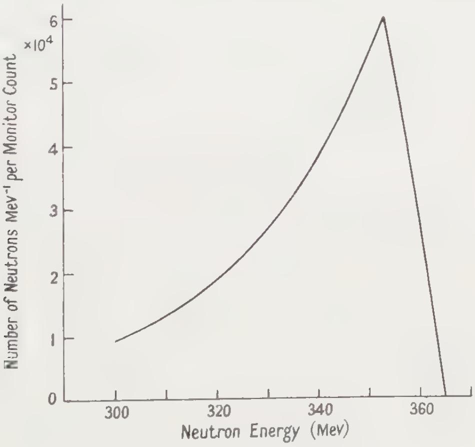

Figure 7. Neutron spectrum.

lower than the equilibrium orbit energy at the target radius. This would be explained if there were a minimum amplitude of radial oscillation corresponding to 6 MeV in energy.

The conclusion that the neutrons are produced in 'elastic' proton–neutron collisions was also reached by Hoffmann and Strauch (1953) in the interpretation of their results. They conclude that the neutrons are mainly produced in collisions between the incoming protons and the loosely bound neutron in the beryllium nucleus.

ACKNOWLEDGMENTS

The authors wish to thank Professor H. W. B. Skinner for his help and encouragement, Professor J. M. Cassels and Dr. J. P. Scanlon for valuable discussions, and the cyclotron crew for their willing co-operation. During the course of this work one of the authors (R. G. J.) was the holder of an I.C.I. Fellowship, one (D. S. M.) the holder of a University Fellowship, and one (S. K. S.) the holder of a West Bengal State Scholarship.

REFERENCES

ASHMORE, A., COLLINGE, B., and SEN, S. K., 1957, *Indian J. Phys.*, **31**, 261.
BODANSKY, D., and RAMSEY, N. F., 1951, *Phys. Rev.*, **82**, 831.
CASSELS, J. M., DICKSON, J. M., and HOWLETT, J., 1951, *Proc. Phys. Soc.* B, **64**, 590.
CHANCE, B., 1949, *Waveforms* (New York: McGraw-Hill), p. 244.
CLADIS, J. B., HADLEY, J., and HESS, W. N., 1952, *Phys. Rev.*, **86**, 110.
COLLINGE, B., MERRISON, A. W., and ECCLESHALL, D., 1956, *J. Sci. Instrum.*, **33**, 72.
DE PANGHER, J., 1954, *Phys. Rev.*, **95**, 578.
DZELEPOV, V. P., KAZARINOV, V. M., GALOVIN, B. M., FLYAGIN, V. B., and SATAROV, V. I., 1955, *Izvestia Akad. Nauk. S.S.S.R.*, **19**, 573.
FOX, R., LEITH, C., WOUTERS, L., and MACKENZIE, K. R., 1950, *Phys. Rev.*, **80**, 23.
GOODELL, W. F., LOAR, H. H., DURBIN, R. P., and HAVENS, W. W., 1953, *Phys. Rev.*, **89**, 724.
HARTZLER, A. J., and SIEGEL, R. T., 1954, *Phys. Rev.*, **95**, 185.
HOFFMANN, J. A., and STRAUCH, K., 1953, *Phys. Rev.*, **90**, 449.
KELLY, E., LEITH, C., SEGRÈ, E., and WIEGAND, C., 1950, *Phys. Rev.*, **79**, 96.
LEWIS, I. A. D., and COLLINGE, B., 1953, *Rev. Sci. Instrum.*, **24**, 1113.
MATHER, R., and SEGRÈ, E., 1951, *Phys. Rev.*, **84**, 191.
NELSON, B. K., GUERNSEY, G., and MOTT, G., 1952, *Phys. Rev.*, **88**, 1.
RANDLE, T. C., CASSELS, J. M., PICKAVANCE, T. G., and TAYLOR, A. E., 1953, *Phil. Mag.*, **44**, 425.
RICH, M., and MADEY, R., 1954, University of California UCRL-2301.
WELLS, F. H., 1952, *Nucleonics*, **10**, 28.
YODH, G. B., 1955, *Phys. Rev.*, **98**, 1331.

Nuclear Total Cross Sections for 350 MeV Neutrons

By A. ASHMORE, R. G. JARVIS†, D. S. MATHER‡ and S. K. SEN §
Nuclear Physics Research Laboratory, University of Liverpool

Communicated by H. W. B. Skinner; MS. received 5th July 1957, and in final form 8th August 1957

Abstract. Measurements have been made of the total cross sections of a number of elements for neutrons with a mean energy of $351 \cdot 5 \pm 2 \cdot 0$ MeV. The measured cross sections in millibarns were:

Carbon	$285 \cdot 3 \pm 1 \cdot 6$	Copper	1138 ± 9	Hydrogen	$35 \cdot 6 \pm 0 \cdot 7$
Oxygen	366 ± 3	Tin	1887 ± 15	Deuterium	$58 \cdot 9 \pm 1 \cdot 0$
Aluminium	$565 \pm 4 \cdot 5$	Lead	2828 ± 14	n–n	$23 \cdot 3 \pm 0 \cdot 7$

A comparison with previous measurements shows that the total cross sections of complex nuclei remain constant within the experimental error 1% between neutron energies of 270 MeV and 380 MeV. At 410 MeV they have risen significantly due to meson production.

§ 1. Introduction

The measurements that are described in this paper form part of a series that have been made of the cross sections of nuclei for 350 MeV neutrons. In a previous paper (Ashmore, Jarvis, Mather and Sen 1957), referred to hereafter as I, the measurement of the energy spectrum of the neutron beam was described. Papers to follow will deal with the differential elastic scattering cross sections and absorption cross sections, and the theoretical interpretation of the results of the series of experiments in terms of the Optical Model.

Measurements of the cross sections of nuclei for high energy neutrons have been mainly confined to the total cross sections. This is because of the simplicity and accuracy of the good geometry attenuation experiments in which they are measured. Total cross sections alone are an inadequate basis on which to make a theoretical analysis of the interaction of high energy neutrons with complex nuclei, although an attempt to do so has been made by Taylor (1953, 1954). The accuracy with which they can be measured, however, does mean that they are an important factor in any theoretical analysis. Also by the Optical Theorem (see Mapleton 1954) the imaginary part of the forward elastic scattering amplitude, $\mathscr{I}f(0)$, can be calculated from the total cross section σ_T using the equation

$$\mathscr{I}f(0) = k\sigma_T/4\pi \qquad \ldots\ldots(1)$$

where k is the wave number of the incident neutron. If the forward elastic scattering cross section is also measured an estimate is obtained of the relative magnitudes of the real and imaginary parts of the nuclear potential. This method was used by Wilson (1956) in his analysis of nuclear cross section measurements for neutrons with energies of 84, 135 and 290 Mev.

---

† Now with the General Electric Co. Ltd., London.

‡ Now at the Atomic Weapons Research Establishment, Aldermaston, Berks.

§ Now with Siemens Ltd., Schuckert Erlangen, West Germany.

The total cross sections of the elements remain almost constant from a neutron energy of 250 Mev until the effect of meson production becomes appreciable at about 400 Mev. Measurements in this energy region have been made by De Juren (1950) at 270 Mev, Fox, Leith and Wouters (1950) at 280 Mev and Nedzel (1954) at 410 Mev. Dzhelepov, Satarov and Galovin (1955) have measured total cross sections at several neutron energies between 380 Mev and 630 Mev, and Coor, Hill, Hornyak, Smith and Snow (1955) have measured them at an effective neutron energy of 1·4 Gev. References to measurements at neutron energies below 250 Mev are given by Nedzel (1954).

In the present measurements the total cross sections of hydrogen, deuterium, carbon, oxygen, aluminium, copper, tin and lead have been measured for neutrons with a mean energy of 351·5 ± 2 Mev. The method used was the usual attenuation experiment in good geometry. In the neutron detector recoil protons from a polythene scatterer in the neutron beam were detected in a triple coincidence scintillation counter telescope, set with its axis making an angle of 10 degrees with the neutron beam direction. A copper absorber between the last two counters of the telescope determined the threshold energy of the detector. The hydrogen cross section was obtained from the ratio of the neutron beam intensities after attenuation in polythene and carbon. Similarly, the deuterium cross section was obtained from measurements with heavy water and water. The oxygen cross section was obtained from the attenuation in water using the measured value of the hydrogen cross section.

§ 2. EXPERIMENTAL DETAILS AND PROCEDURE

2.1. *Experimental Arrangement*

The arrangements for producing, collimating, and monitoring the neutron beam and for detecting the neutrons were described in I. For the total cross section measurements only the polythene scatterer was used in the neutron detector, and the thickness of the copper absorber in the counter telescope was kept fixed at 78·73 g cm^{-2}. Figure 1 shows the plan of the experimental arrangement. The shielding wall of steel-loaded concrete blocks was used to reduce the background due to protons ejected from the attenuator into the counter telescope. This background would otherwise have been too high with the attenuators

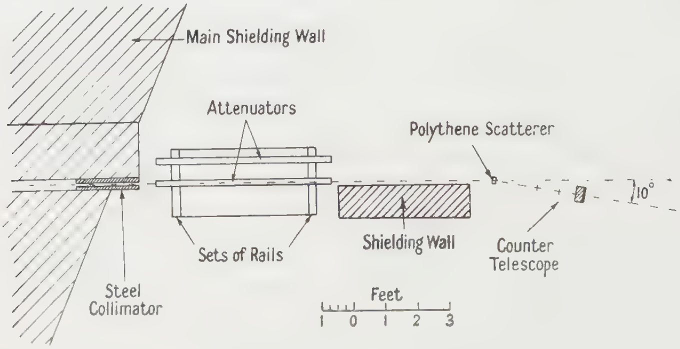

Figure 1. Experimental lay-out.

containing hydrogen or deuterium in the neutron beam. For the other attenuators the background was sufficiently low without the wall. Furthermore, for the heaviest elements it is necessary to make a correction for neutrons elastically scattered in the attenuator and by the wall into the detector. As this correction is difficult to estimate with sufficient accuracy the wall was only used for the measurements with the polythene, carbon, heavy water and water attenuators.

2.2. *The Attenuators*

The transmission T of the neutron beam through an attenuator of length m g cm^{-2} is related to the total cross section σ_{T} of the attenuator material by the equation

$$T = \exp(-\boldsymbol{N} m\sigma_{\mathrm{T}}/A) \qquad \ldots\ldots(2)$$

where $\boldsymbol{N}$ is Avogadro's Number and A is the atomic weight of the attenuator material. The thickness of the attenuators was usually chosen to give the best statistical accuracy. For the observed background of about 1% of the unattenuated beam the optimum value of T given by the curves of Rose and Shapiro (1948) is between 0·1 and 0·2. As can be seen from table 1 a value of $T \simeq 0{\cdot}2$ was the normal choice. Measurements were made with carbon and lead attenuators of several different lengths as a check that the attenuation was exponential. The transmission of the water attenuator (0·0855) from which the oxygen cross section was obtained was rather low because a reasonably high ratio was required between the transmissions through the heavy water and water attenuators for the deuterium cross section measurement.

Table 1. Total cross sections of the Elements for 350 MeV Neutrons

(1)	(2)	(3)	(4)
Hydrogen	11·99	0·771 ± 0·005	36·6 ± 0·90
	20·02	0·664 ± 0·010	34·2 ± 1·05
		Weighted Mean	35·6 ± 0·70
n–n	18·62	0·767 ± 0·006	23·3 ± 0·7
Deuterium			58·9 ± 1·0
Carbon	71·61	0·3645 ± 0·0033	282·0 ± 2·5
	119·34	0·1802 ± 0·0022	287·3 ± 2·0
		Weighted Mean	285·3 ± 1·6
Oxygen	166·3†	0·0854 ± 0·0013†	366 ± 3
Aluminium	123·10	0·2126 ± 0·0026	565 ± 4·5
Copper	142·7	0·2169 ± 0·0026	1138 ± 9
Tin	164·9	0·2092 ± 0·0025	1887 ± 15
Lead	95·8	0·4588 ± 0·0028	2826 ± 23
	192·1	0·2058 ± 0·0027	2873 ± 25
	238·0	0·1498 ± 0·0024	2787 ± 25
		Weighted Mean	2828 ± 14

† Values for the water attenuator.

(1) Element; (2) Attenuator length (g cm^{-2}); (3) transmission; (4) total cross section (mbn).

For the measurement of the hydrogen cross section, the lengths of the polythene and carbon attenuators were such that they contained almost exactly the same number of carbon atoms. Similarly, for the measurement of the deuterium cross section the lengths of the heavy water and water attenuators were such that they contained almost exactly the same number of oxygen atoms. The ratio of the transmissions in this measurement gives the difference between the deuterium and hydrogen cross sections. It is concluded from the discussion in §4 that at our neutron energy of 350 Mev this difference is close to the n–n cross section. It will therefore be referred to hereafter as the n–n cross section. The deuterium cross section was obtained from it by adding the measured hydrogen cross section. For the hydrogen and deuterium measurements the statistical error has a flat minimum for values of the transmission through the carbon or water between 0·07 and 0·35. As can be seen from table 1 values in this region were used. For the same running time the error in the hydrogen cross section is seven times greater and the error in the n–n cross section 16 times greater than the error in the cross section when the attenuator is a pure element. Although larger running times were used for the hydrogen and n–n measurements it was not possible to achieve the accuracy of the measurements in which the attenuators were pure elements.

All the attenuators had a diameter of approximately 2·5 inches, giving a good clearance round the neutron beam. Since the polythene and carbon attenuators were in several pieces they were placed in a thin-walled copper tube of internal diameter 2·5 inches. Similar tubes with copper windows in the ends were used as containers for the heavy water and water. A correction was made for the small effect of the copper windows on the transmission. The aluminium, copper, tin and lead attenuators were mounted on a V-block with a retaining strap over them.

The solid attenuators were carefully machined and their surface densities measured with an accuracy to 0·1% using vernier callipers and an accurate balance. As a check on their homogeneity the volume densities of the attenuators were measured. A significant variation in density was observed among the pieces making up the carbon attenuator. Measurements made by cutting up the pieces after the experiment was completed showed that the density was constant throughout each piece. Surface densities of the heavy water and water attenuators were obtained by measuring their lengths and using their known densities. The amount of impurity in the attenuators was in all cases less than 0·1%.

2.3. *The Attenuator Holder*

The attenuator holder was designed to allow either of two attenuators to be moved in and out of the neutron beam by remote control. Its arrangement can be seen in figure 1. Two sets of horizontal rails were mounted 4 feet apart on an angle iron framework at about 6 inches below the neutron beam level. These rails were arranged to run perpendicular to the neutron beam direction. Each set of rails carried two carriages with V-blocks, which could be withdrawn one to each end of the rails, or brought in one at a time to a fixed position determined by a stop between the rails. The driving force was supplied by Martonair compressed air pistons controlled by relays operated from the counting room.

The aluminium, copper, tin and lead attenuators were mounted, two at a time, on the carriages nearest the beam exit in the main shielding wall. For the copper tubes containing the longer attenuators a pair of carriages, one on each set of rails, was used. Horizontal and vertical screw movements of the V-block were provided to enable the attenuators to be aligned in the neutron beam.

§ 3. EXPERIMENTAL PROCEDURE

3.1. *Alignment*

Great care was taken with the initial alignment of the attenuator holder and the detector with the neutron beam direction. A theodolite situated about 10 ft beyond the detector position was used for this purpose. The neutron beam direction was defined by cross wires in the collimators at each end of the channel through the cyclotron shielding wall. The position and height of the theodolite were adjusted until the axis of its telescope was in the neutron beam direction. Adjustment of the attenuator carriages was done by using cross wires in a short length of $2\frac{1}{2}$ inch diameter tubing sitting in the V-block. The carriages were brought in turn into the fixed position against the stop and adjustments made with the horizontal and vertical screw movements on the V-block.

The counters had previously been arranged so that when they were mounted on the arm of the detector turntable their centres were in line. For alignment the counters were taken off the arm and cross wires were mounted on it so that they could be moved along the line defined by the centres of the counters. The height and position of the turntable were adjusted until these cross wires were aligned in the neutron beam at both ends of the arm. Alignment of the polythene scatterer was then done using the adjustments provided on its thin brass V-support. Finally, the beryllium target in the cyclotron was viewed through the theodolite and moved radially until its vertical edge intersected the line of the neutron beam. The counter arm was then fixed at an angle of 10 degrees to the neutron beam direction and the counters mounted on it.

As checks on the alignment an x-ray film was exposed in the neutron beam near the detector position, and the triple coincidence counting rate was measured as a function of the radial position of the target. These checks lead to a small adjustment being made in the radial setting of the target.

3.2. *Counting Sequence*

There is a small but appreciable variation in the relation between the counting rates in the monitor and the counter telescope. This is almost entirely due to changes in the form of the neutron spectrum as explained in §4. To reduce the effect of this variation the running time for a cross section measurement was divided into a series of measurements of the transmission T of short duration.

The running time was divided between unattenuated and attenuated beams approximately in the ratio $T^{1.2}:1$ required for best statistical accuracy. For the hydrogen and n -n measurements the same rule applies if T is taken to be the ratio of the neutron beam intensities transmitted through the two attenuators. Occasional runs were also done with the polythene scatterer of the detector removed to measure the small background and to check that it remained constant. These background runs were done with and without the attenuator in the neutron beam.

The beam intensity was made such that the counting losses did not exceed 1%. In the unattenuated beam the counting rate was about 7 sec^{-1}. For a transmission

$T=0{\cdot}2$, the cross section was measured with an accuracy to 0·8% in a running time of about $3\frac{1}{2}$ hours. This time will vary only slowly with T. For the hydrogen and n–n measurements the times required for 3% accuracy in the cross section were 12 hours and 36 hours respectively. The latter time is shorter than would be expected since, owing to there being similar counting losses with the water and heavy water in the beam, it was possible to run with increased neutron beam intensity. The short runs into which the running time was divided had a duration of between 15 and 20 minutes.

§ 4. EFFECTIVE NEUTRON SPECTRUM

It was shown in I that the energy spectrum of the neutron beam has the form

$$N(E_{\mathrm{n}})=\frac{C\{1-\exp[-(E_0-E_{\mathrm{n}}/\epsilon]\}}{\{1-\exp[-(E_0-E_{\mathrm{m}})/\epsilon]\}}\text{ for }E_0>E_{\mathrm{n}}>E_{\mathrm{m}}$$

$$N(E_{\mathrm{n}})=C\exp[-(E_{\mathrm{m}}-E_{\mathrm{n}})/\epsilon]\text{ for }E_{\mathrm{n}}<E_{\mathrm{m}}.$$

where C is a numerical constant. The experimentally determined values for the parameters were :

$$E_0-E_{\mathrm{m}}=12\pm3\,\text{Mev},\ \epsilon=28\pm2\,\text{Mev},\ E_0=365\pm1\,\text{Mev},\ E_{\mathrm{m}}=353\pm2\,\text{Mev}.$$

The effective neutron spectrum and mean neutron energy were calculated by numerical integration. For a neutron energy E_{n} the detector efficiency in the total cross section experiment is given by

$$F(E_{\mathrm{n}})=\int p_1(E_{\mathrm{n}}-E_{\mathrm{p}})T(E_{\mathrm{p}})dE_{\mathrm{p}}+\int p_2(E_{\mathrm{n}}-E_{\mathrm{p}})T(E_{\mathrm{p}})dE_{\mathrm{p}}\qquad\ldots\ldots(3)$$

where the suffix 1 refers to neutrons scattered from hydrogen and the suffix 2 to neutrons scattered from carbon in the polythene scatterer. $p_1(E_{\mathrm{n}}-E_{\mathrm{p}})$ is the resolution curve of the detector shown in figure 6 of I. $T(E_{\mathrm{p}})$ is the absorber transmission factor of the fixed copper absorber in the counter telescope for a proton of energy E_{p}. The variation of $T(E_{\mathrm{p}})$ with proton energy was measured by placing the counter telescope in the external proton beam in the arrangement described in § 2.6 of I.

It was found that the energy spectrum of protons from carbon observed in the neutron spectrum measurement could be reproduced within the statistical errors by assuming that

$$p_2(E_{\mathrm{n}}-E_{\mathrm{p}})=0\qquad\text{for }E_{\mathrm{n}}-E_{\mathrm{p}}<15\text{ Mev}$$

$$p_2(E_{\mathrm{n}}-E_{\mathrm{p}})=\text{constant}\qquad\text{for }E_{\mathrm{n}}-E_{\mathrm{p}}>15\text{ Mev}.$$

The value of the constant was obtained from the relative counting rates from the carbon and hydrogen in the polythene scatterer. From the neutron spectrum measurement these are in the ratio 0·243 : 1 for the thickness of copper absorber used in the total cross section measurements. Thus we require

$$\int N(E_{\mathrm{n}})p_2(E_{\mathrm{n}}-E_{\mathrm{p}})dE_{\mathrm{n}}=0{\cdot}243\int N(E_{\mathrm{n}})p_1(E_{\mathrm{n}}-E_{\mathrm{p}})dE_{\mathrm{n}}.$$

The detector efficiency $F(E_{\mathrm{n}})$ was then calculated as a function of neutron energy and the curve obtained is shown in figure 2. The mean neutron energy $\bar{E}_{\mathrm{n}}$ is given by

$$\bar{E}_{\mathrm{n}}=\int N(E_{\mathrm{n}})F(E_{\mathrm{n}})E_{\mathrm{n}}dE_{\mathrm{n}}\Big/\int N(E_{\mathrm{n}})F(E_{\mathrm{n}})dE_{\mathrm{n}}\qquad\ldots\ldots(4)$$

and the effective neutron spectrum $N_1(E_{\mathrm{n}})$ by

$$N_1(E_{\mathrm{n}})=N(E_{\mathrm{n}})F(E_{\mathrm{n}})/F(\bar{E}_{\mathrm{n}}).\qquad\ldots\ldots(5)$$

This spectrum is shown in figure 3 for the central values of $\epsilon = 28$ MeV, $E_0 = 365$ MeV and $E_m = 353$ MeV. The mean neutron energy for these values was found to be 351·5 MeV. Its standard deviation was estimated to be 0·5 MeV by calculating the effect of varying ϵ, E_0, E_m within the limits of their errors.

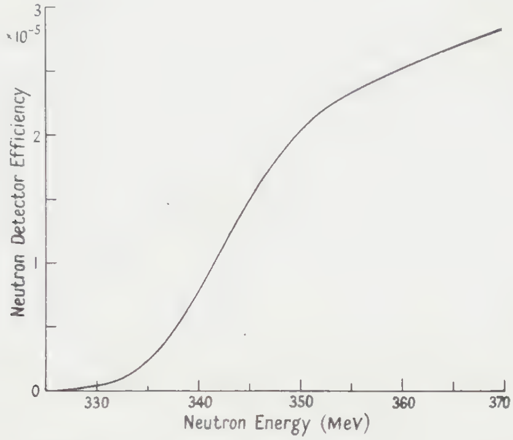

Figure 2. Neutron detector efficiency curve.

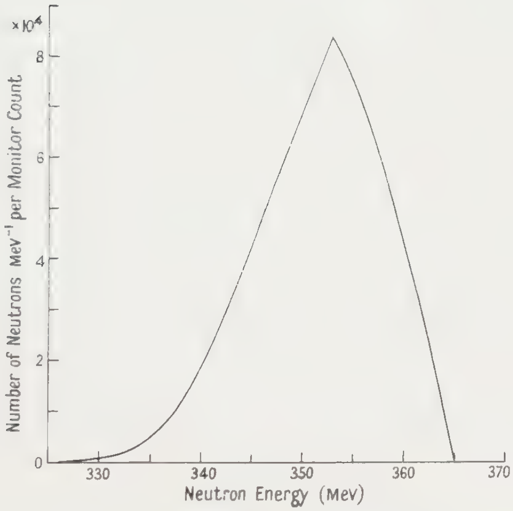

Figure 3. Effective neutron spectrum.

There is a further uncertainty in the mean neutron energy associated with changes in the relation between the counting rates in the monitor and the detector telescope. Such changes were infrequent and seemed to occur when the cyclotron was switched off. An analysis showed that the number of telescope counts per monitor count varied with a standard deviation of 5%. This effect is almost certainly due to a change in the radial oscillations of the cyclotron beam. This could change both E_0 and E_m. The change in the mean neutron energy corresponding to the change in counting rate is greatest for a general shift of the neutron spectrum towards lower or higher energies. This would involve a change in the minimum and maximum amplitudes of the radial oscillations. For this case a

5% change in the telescope counting rate corresponds to a change in the mean neutron energy of about 1 MeV. Finally, an allowance of at least 1 MeV must be made for the error in the range–energy relation for protons in copper. The final value of the mean neutron energy is then, $\bar{E}_n = 351{\cdot}5 \pm 2$ MeV.

§ 5. CORRECTIONS TO THE RESULTS

5.1. *Finite Size of the Detector*

The solid angle subtended by the detector at the attenuator position was $0{\cdot}32 \times 10^{-3}$ steradian for the metallic attenuators and $0{\cdot}50 \times 10^{-3}$ steradian for the longer attenuators in the copper tubes. A correction is required for neutrons that are elastically scattered within this solid angle. The method of Amaldi, Bocciarelli, Cacciapuati and Trabacchi (1946) was adapted to our experimental arrangement. The elastically scattered neutrons were assumed to have the angular distribution given by regarding the nucleus as a black sphere. This is in agreement with our measurements to be published. These measurements also showed that the forward scattering amplitude could be assumed to be wholly imaginary, so that the forward scattering cross section could be calculated from the total cross section by equation (1).

For the two longest lead attenuators the correction was about twice the statistical error. For the shortest lead attenuator and the tin and copper attenuators the correction was about equal to the statistical error. For the aluminium and carbon attenuators the correction was about one third of the statistical error. In estimating the errors in the cross sections an additional amount was included corresponding to a ±25% uncertainty in estimating this correction.

5.2. *Coulomb Scattering*

Coloumb scattering of the neutrons takes place because of the interaction of the Coulomb field of the nucleus with the magnetic moment of the neutron. The calculations of Schwinger (1948) show that this scattering is only appreciable for angles less than one degree. In the case of lead the contribution of Coulomb scattering to the measured cross section was found to be 4 mbn compared with the statistical error of 14 mbn. For lighter elements the Coulomb scattering was a decreasing proportion of the error. Coulomb scattering could therefore be neglected in calculating the results.

5.3. *Counting Losses*

As explained in I the sum of the singles rates in the three counters of the telescope was obtained simultaneously with the triple coincidence rate. This paper also gives the measured values of the dead time in each channel (2×10^{-7} sec) and the ratio of the period of the frequency modulation cycle to the length of the beam pulse (50 ± 10). Using these values the percentage loss of triples was estimated and a correction made to the measured transmission. This correction was largest for the lighter elements but never exceeded one third of the statistical error. The random coincidence rate was found to be negligible.

§ 6. RESULTS AND DISCUSSION

The results of our measurements are given in table 1. Quoted errors are the standard deviations deduced from the counting statistics with an additional allowance for the error in estimating the correction for the finite size of the detector.

If it can be assumed that the neutron and proton in the deuterium nucleus act as independent particles for high energy neutrons, then the n – n cross section is the true n–n cross section. The validity of this assumption has been discussed by Chew (1948, 1950) and by Gluckstern and Bethe (1951). These authors conclude that the interference term is not negligible. Brueckner (1953) has discussed the similar problem of the scattering of π-mesons in deuterium, and has shown that the effect of multiple scattering cannot be neglected. His results indicate, however, that for neutrons in the energy region under consideration the deuteron cross section should be equal to the sum of the neutron and proton cross sections within less than 10%. Glauber (1955) has shown that there is an additional effect due to the screening of one nucleon by the other when they are on the line of the incident particle. An analysis of this 'shadow effect' for the scattering of nucleons in the GeV energy region gives the deuterium cross section less than the sum of the neutron and proton cross sections by about 8%.

An analysis of the experimental results for the total cross sections of hydrogen and deuterium for high energy neutrons and protons has been made by Chen, Leavitt and Shapiro (1956). These authors conclude that for energies between 95 MeV and 410 MeV the difference between the deuteron cross section and the sum of the neutron and proton cross sections is very small. At 1·4 GeV the difference becomes appreciable and is of the sign and approximately of the magnitude calculated by Glauber (1955). The difference remains very small for energies up to 630 MeV as can be seen by comparing the experimental results of Dzhelopov, Satarov, and Galovin (1955) for neutrons, with those of Dzhelopov, Moskalev, and Medved (1955) for protons. Our value for the n–n cross section should thus be close to the true n–n cross section. It is in good agreement with the p–p cross section of 24·3 ± 1 mbn obtained by de Carvalho (1954) for 315 MeV protons.

The results are compared in table 2 with previous measurements, in the energy region over which the cross sections remain almost constant. There is no significant change in the total cross sections of complex nuclei as the neutron energy increases from 270 MeV to 380 MeV. There is possibly a small increase at

Table 2. Comparison of Measurements in the Neutron Energy Region over which Total Cross Section remains almost Constant

Element	Total cross section (mbn)				
	(1)	(2)	(3)	(4)	(5)
Neutron energy (MeV)	270	280	350	380	410
Carbon	288 ± 3	279 ± 4	285·3 ± 1·6	286 ± 2	297 ± 3
Oxygen	372 ± 7	380 ± 8	366 ± 3	376 ± 6	378 ± 5
Aluminium	555 ± 8	566 ± 18	565 ± 4·5	582 ± 8	587 ± 8
Copper	1145 ± 15	1190 ± 20	1138 ± 9	1170 ± 30	1187 ± 14
Tin	1870 ± 30	1830 ± 30	1887 ± 15	1880 ± 40	—
Lead	2840 ± 30	2890 ± 30	2828 ± 14	2810 ± 50	2890 ± 30
Hydrogen	38 ± 1·5	33 ± 3	35·6 ± 0·7	34 ± 2	33·7 ± 1·3
n–n	19 ± 2·6	16 ± 4	23·3 ± 0·7	23 ± 1·5	28 ± 4
Deuterium	57 ± 3	49 ± 5	58·9 ± 1·0	57 ± 2·5	62 ± 4

(1) De Juren (1950); (2) Fox *et al.* (1950); (3) present measurements; (4) Dzhelepov *et al.* (1955); (5) Nedzel (1954).

380 Mev although it is not large enough to be significant. At 410 Mev the total cross sections are significantly higher than at 350 Mev. The effect of meson production on the total cross sections thus first becomes apparent at 410 Mev. Owing to the greater errors in the hydrogen, n–n, and deuterium cross sections it is not possible to observe any significant difference between the values for different energies in table 2. Differences only become apparent at higher energies. In figure 4 the n–p, n–n, and carbon total cross sections from table 2 and from the measurements of Dzhelepov *et al.* (1955) are plotted against neutron energy. Carbon was chosen since the effect on the cross section of increased absorption in nuclear matter will be greater for a lighter nucleus. It will be seen from figure 4 that the n–p cross section remain constant within the errors from 170 Mev to 630 Mev, whereas the n–n and carbon total cross sections increase steadily above 380 Mev. The constancy of the n–p cross section is due to the increasing inelastic scattering associated with meson production being compensated by decreasing elastic scattering. The elastic part of the n–n cross section remains constant with increasing energy (Dzhelepov *et al.* 1955). It is clear that the rise in nuclear total cross sections for neutrons between 350 and 630 Mev is due to an increase in the absorption coefficient for neutrons in nuclear matter produced mainly by the increase in the n–n cross section.

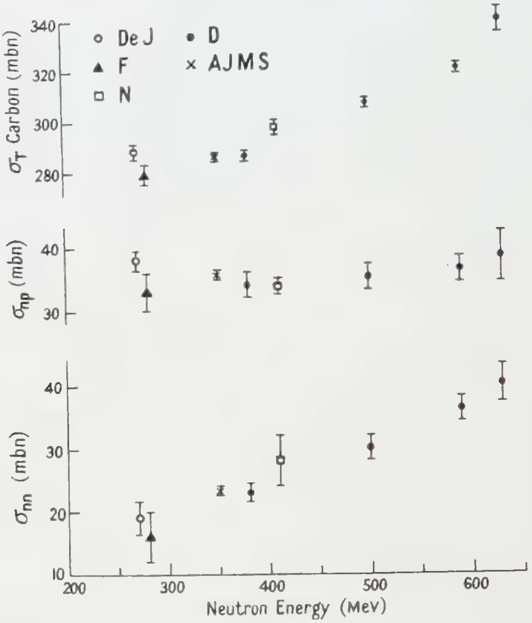

Figure 4. Variation with neutron energy of n–n, n–p and carbon total cross sections. De J, De Juren (1950); F, Fox *et al.* (1950); N, Nedzel (1954); D, Dzhelepov *et al.* (1955); AJMS, present measurements.

Acknowledgments

The authors wish to thank Professor H. W. B. Skinner for his help and encouragement, Professor J. M. Cassels and Mr. A. E. Taylor for valuable discussions, and the cyclotron crew for their willing co-operation. They are indebted to the Director of the Atomic Energy Research Establishment for the loan of the heavy water and of the containers used in the n–n cross section measurement. During the course of this work one of the authors (R.G.J.) was the holder of an I.C.I. Fellowship, one (D.S.M.) the holder of a University Fellowship, and one (S.K.S.) the holder of a West Bengal State Scholarship.

REFERENCES

AMALDI, E., BOCCIARELLI, D., CACCIAPUOTI, B. N., and TRABACCHI, G. C., 1946, *Nuovo Cim.*, **3**, 203.
ASHMORE, A., JARVIS, R. G., MATHER, D. S., and SEN, S. K., 1957, *Proc. Phys. Soc.* A, **70**, 735.
BRUECKNER, K. A., 1953, *Phys. Rev.*, **89**, 834.
DE CARVALHO, H. G., 1954, *Phys. Rev.*, **96**, 398.
CHEN, F. F., LEAVITT, C. P., and SHAPIRO, A., 1956, *Phys. Rev.*, **103**, 211.
CHEW, G. F., 1948, *Phys. Rev.*, **74**, 809; 1950, *Ibid.*, **80**, 196.
COOR, T., HILL, D. A., HORNYAK, W. F., SMITH, L. W., and SNOW, G., 1955, *Phys. Rev.*, **98**, 1369.
DE JUREN, J., 1950, *Phys. Rev.*, **80**, 27.
DZHELEPOV, V. P., MOSKALEV, V. I., and MEDVED, S. V., 1955, *Doklady Akad. Nauk, S.S.S.R.*, **104**, 380.
DZHELEPOV, V. P., SATAROV, V. I., and GALOVIN, B. M., 1955, *Doklady Akad. Nauk. S.S.S.R.*, **104**, 717.
FOX, R., LEITH, C., and WOUTERS, L., 1950, *Phys. Rev.*, **80**, 23.
GLAUBER, R. J., 1955, *Phys. Rev.*, **100**, 242.
GLUCKSTERN, R. L., and BETHE, H. A., 1951, *Phys. Rev.*, **81**, 761.
MAPLETON, R. A., 1954, *Phys. Rev.*, **96**, 415.
NEDZEL, V. A., 1954, *Phys. Rev.*, **94**, 174.
ROSE, M. E., and SHAPIRO, M. M., 1948, *Phys. Rev.*, **74**, 1853.
SCHWINGER, J., 1948, *Phys. Rev.*, **73**, 407.
TAYLOR, T. B., 1953, *Phys. Rev.*, **92**, 831; 1954, *Thesis*, Cornell University.
WILSON, R., 1956, *Phil. Mag.*, **1**, 1013.

RESEARCH NOTES

Wave Functions for Helium and Similar Atomic Systems

By A. L. STEWART
The Physics Department, The Queen's University of Belfast

Communicated by K. G. Emeléus; MS. received 4th June 1957

The problem of determining accurate wave functions of atomic systems is one of continuing interest (cf. Löwdin and Shull 1956, Holøien 1956). Of the several available methods, those based upon perturbation theory, which have the advantage that their accuracy can usually be assessed reliably from a comparison of the contributions from successive orders, have received little attention. Recent work on single electron atoms (Trees 1956, Dalgarno 1956) suggests that a perturbation treatment based upon zero order hydrogen-like wave functions may be quite accurate even if the perturbed wave function is calculated to only the first order. This note reports a perturbation treatment of the helium isoelectronic sequence.

The Schrödinger equation for the motion of two electrons in the field of a nucleus of charge ζ is

$$\left\{H+\frac{2}{r_{12}}+E\right\}\Psi=0 \tag{1}$$

with

$$H=-\nabla_1^2-\nabla_2^2-\frac{2}{r_1}-\frac{2}{r_2} \tag{2}$$

where $\mathbf{r}_1$, $\mathbf{r}_2$ and $\mathbf{r}_{12}$ are the electron–nucleus and electron–electron separations in units of the Bohr radius a_0 and E is the energy of the system in rydbergs. The interaction between the electrons, $2/r_{12}$, may be regarded as perturbing the system whose Hamiltonian is H in which case perturbation theory (cf. Dalgarno and Stewart 1957) gives the normalized wave function, correct to the first order, to be

$$\Psi_1=F_0+\{F_1-(F_0|F_1)F_0\} \tag{3}$$

where

$$(H-\mathscr{E}_0)F_0=0 \tag{4}$$

and

$$(H-\mathscr{E}_0)F_1+(2/r_{12}-\mathscr{E}_1)F_0=0. \tag{5}$$

Equations (4) and (5) yield immediately for the ground state of the system

$$F_0=\frac{\zeta^3}{\pi}\exp\{-\zeta(r_1+r_2)\},\ \ \mathscr{E}_0=-2\zeta^2 \tag{6}$$

and

$$\mathscr{E}_1=(F_0|2/r_{12}|F_0)=\frac{5}{4}\zeta \tag{7}$$

the energy being given, correct to the second order, by

$$E=\mathscr{E}_0+\mathscr{E}_1+\mathscr{E}_2, \tag{8}$$

where

$$\mathscr{E}_2=(F_0|2/r_{12}-\mathscr{E}_1|F_1). \tag{9}$$

Further, the value of any matrix element

$$\overline{M}=(\Psi|M|\Psi)$$

is obtainable to the first order as

$$\overline{M}=\overline{M}_0+\overline{M}_1 \tag{10}$$

where

$$\overline{M}_0=(F_0|M|F_0) \tag{11}$$

and

$$\overline{M}_1=2(F_0|M|F_1)-2(F_0|F_1)\overline{M}_0. \tag{12}$$

Equation (5) has been solved by Hylleraas and Midtdal (1956) by the Ritz variation method using a very complex trial wave function containing the inter-electron distance r_{12} explicitly. With this type of solution the labour of extending the procedure to many electron atoms is prohibitive and instead a linear combination of orbitals, constructed from a complete orthogonal set of Laguerre functions, is used here, the parameters being varied to minimize the functional

$$J_2=2(F_0|2/r_{12}-\mathscr{E}_1|F_1)+(F_1|H-\mathscr{E}_0|F_1). \tag{13}$$

Writing

$$F_1=\frac{2\sqrt{2}\zeta^3}{\pi}\sum_{n_1,n_2,l} a_{n_1n_2l}\psi_{n_1n_2l}$$

with

$$\psi_{n_1n_2l}=\mathrm{Z}_{n_1l}(2\zeta r_1)\mathrm{Z}_{n_2l}(2\zeta r_2)\mathrm{Y}_l(\theta),$$

$$\mathrm{Y}_l(\theta)=\left[\frac{2l+1}{2}\right]^{1/2}\mathrm{P}_l(\cos\theta)$$

and

$$\mathrm{Z}_{nl}(x)=\left[\frac{(n-l-1)!}{\{(n+l+1)!\}^3}\right]^{1/2}x^lL^{2l+2}_{n+l+1}(x)\exp(-x/2)$$

where θ is the angle between the vectors $\mathbf{r}_1$ and $\mathbf{r}_2$, P_l is the Legendre polynomial and L^{2l+2}_{n+l+1} is the associated Laguerre polynomial, the minimal procedure leads to a set of simultaneous equations for the coefficients $a_{n_1n_2l}$, which determine $\mathscr{E}_2$ through equation (9). The values of $\mathscr{E}_2$ achieved with a wave function which includes all possible orbitals such that $n_1+n_2<m$ is tabulated against m in table 1 and compared with the very accurate value obtained by Hylleraas and Midtdal.

Table 1. The Second Order Correction to the Energy using Wave Functions of Increasing Complexity

m	3	4	5	6	7	Hylleraas
$-\mathscr{E}_2$	0·195313	0·274089	0·288006	0·296344	0·301290	0·315311

The rate of convergence as the number of orbitals in the wave function is increased is initially rapid but becomes rather slow when $n_1+n_2=6$. In view of the simplicity of the calculation, however, the energy estimated using the wave function with $n_1+n_2<7$ is satisfactory, being closer to the minimum value than that obtained in any previous calculation using one electron orbitals. Thus an approximation due to Kessler (1955) yields the value $-0{\cdot}38$ rydberg for the second order energy correction whilst an expansion based on hydrogenic functions has been used by Gerhauser and Matsen (1955) to give $-0{\cdot}2514$ rydberg.

A severe test of the accuracy of approximate wave functions is provided by a comparison of the deduced value of the diamagnetic susceptibility χ with the observed value, since the relevant matrix element is weighted heavily in a region of space different from that which effectively determines the energy. With

$$M = -0{\cdot}793 \times 10^{-6}(r_1^{\,2}+r_2^{\,2}) \tag{14}$$

(10), (11) and (12) yield

$$\chi = -10^{-6}\left\{\frac{4{\cdot}76}{\zeta^2}+\frac{3{\cdot}79}{\zeta^3}\right\}\mathrm{cm}^3\,(\text{gramme ion})^{-1} \tag{15}$$

for the diamagnetic susceptibility of the helium sequence. The susceptibilities given by this formula are compared with the experimental data and with other approximate estimates in table 2. In the first and second columns are the susceptibilities calculated from (15) to zero and first order respectively, in the third those derived by Angus (1932) using semi-empirical Slater wave functions, in the fourth those derived by Stoner (1929) using self-consistent field wave functions, in the fifth column the estimates of Plato (1935), who used variationally determined wave functions of the form

$$\exp(-\alpha_1 r_1-\alpha_2 r_2)+\exp(-\alpha_1 r_2-\alpha_2 r_1)$$

and in the last column are the observed values.

Table 2. The Diamagnetic Susceptibility, $-\chi$ (10^{-6} cm^3 (gramme ion)$^{-1}$)

Ion	Stewart		Slater–Angus	Hartree–Stoner	Plato	Observed
	Zero Order	1st Order				
H^-	4·76	8·55	9·70	—	—	—
He	1·19	1·66	1·65	1·87	1·84	1·9†
Li^+	0·53	0·67	0·65	0·69	0·73	0·7‡
Be^{2+}	0·30	0·36	0·34	—	—	—

† Havens (1933). ‡ Brindley (1931), Klemm (1940).

The values given by first-order perturbation theory are seen to be satisfactory. They agree closely with those of Angus, both sets of results being slightly smaller than the estimates using Hartree wave functions which are in accord with Plato's work and with experiment. The accuracy achieved using Hartree wave functions may be fortuitous for there is evidence (Hoare and Brindley 1937, Hartree and Hartree 1938) that with the inclusion of exchange the derived values may be modified and the harmony with observation lost.

Calculations are in progress to improve the solution of equation (5) and to estimate the second-order correction to the diamagnetic susceptibility. These results and some applications to excited states will be reported in a subsequent communication.

ACKNOWLEDGMENTS

It is a pleasure to thank Dr. A. Dalgarno for his interest.

REFERENCES

ANGUS, W. R., 1932, *Proc. Roy. Soc.* A, **136,** 569.
BRINDLEY, G. W., 1931, *Phil. Mag.*, **11,** 787.
DALGARNO, A., 1956, *Proc. Phys. Soc.* A, **69,** 784.
DALGARNO, A., and STEWART, A. L., 1957, *Proc. Roy. Soc.* A, **240,** 274.
GERHAUSER, J. M., and MATSEN, F. A., 1955, *J. Chem. Phys.*, **23,** 1359.

Hartree, D. R., and Hartree, W., 1938, *Proc. Roy. Soc.* A, **166,** 450.
Havens, G. G., 1933, *Phys. Rev.*, **43,** 999.
Hoare, F. E., and Brindley, G. W., 1937, *Proc. Roy. Soc.* A, **159,** 395.
Holøien, E., 1956, *Phys. Rev.*, **104,** 1301.
Hylleraas, E., and Midtdal, J., 1956, *Phys. Rev.*, **103,** 829.
Kessler, P., 1955, *C. R. Acad. Sci., Paris*, **240,** 1314.
Klemm, W., 1940, *Z. Anorg. Chem.*, **244,** 377.
Löwdin, P. O., and Shull, H., 1956, *Phys. Rev.*, **101,** 1730.
Plato, G., 1935, *Ann. Phys., Lpz.*, **21,** 745.
Stoner, E. C., 1929, *Proc. Leeds Phil. Lit. Soc.*, **1,** 484.
Trees, R. E., 1956, *Phys. Rev.*, **102,** 1553.

Cyclotron Resonance over a wide Temperature Range

By D. M. S. BAGGULEY,† J. A. POWELL,‡
and D. J. TAYLOR†
† Clarendon Laboratory, Oxford
‡ Marconi Research Laboratory, Great Baddow, Chelmsford, Essex

MS. received 28*th June* 1957

Cyclotron resonance experiments with germanium and silicon at microwave frequencies have so far been confined to high purity samples at liquid helium temperatures (Dresselhaus, Kip and Kittel 1955, Dexter, Zeiger and Lax 1956). This is probably because the common impurities in these materials have excitation energies ΔE of the order 0·01 ev and carriers from these levels are so numerous as to give rise to plasma effects when the temperature is much above 4°K. The plasma effects obscure the cyclotron resonance. However, by doping the semiconductor with transition group metals, for example, iron, cobalt or gold, it is possible to introduce localized states well into the forbidden band ($\Delta E \sim 0{\cdot}15$ ev) and, if the carriers are derived from these levels, their number can be maintained reasonably small at temperatures as high as 90°K (Tyler *et al.* 1954, 1955, Dunlap 1955). By using this technique we have observed cyclotron resonance from hole carriers in germanium at temperatures above 90°K with microwave radiation of 8·8 mm wavelength. In this note we report some results obtained from germanium doped with gold over a temperature range from about 4°K to 90°K. These measurements are of particular interest since the cyclotron resonance experiments now extend into the temperature range where Hall coefficient and resistivity measurements may be available.

The samples were prepared by diffusing gold into single crystal sections of 60 ohm cm germanium (at 290°K) which was initially n-type. The gold doping converted the material to p-type and our method of excitation gave carriers of one sign only, namely holes. At 65°K and above, sufficient carriers were excited thermally, below 65°K the carriers were excited by applying a d.c. voltage across the sample. The microwave spectroscope employed a 50 c/s magnetic field modulation technique and the differential of the absorption line was traced out on a pen recorder. Typical records for a (111) direction in the crystal sample, which were obtained at 90°K and 65°K, are shown in figure 1.

At a temperature of 90°K and above, there was some plasma displacement of the cyclotron lines towards lower magnetic fields as the crystal orientation was changed and so it was not possible to investigate the angular dependence of the heavy mass carrier. At 90°K the resonance line from the light mass carrier was

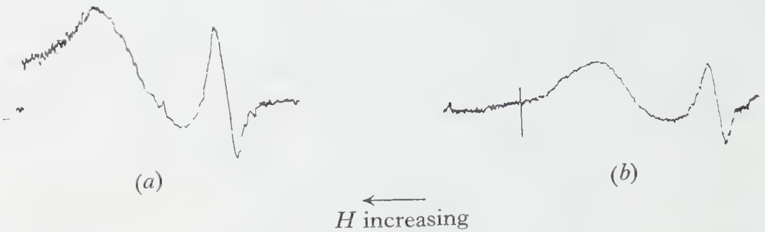

Figure 1. Cyclotron resonance absorption lines in gold-doped germanium (*a*) at 90°K, (*b*) at 65°K.

isotropic. At 65°K and below these plasma effects were not present and the observed angular dependence of the resonance lines for orientations in a (110) plane is shown in figure 2. In this diagram the values of m^* were obtained from the relation $m^* = \boldsymbol{e}H_r/\omega\boldsymbol{c}$ where H_r is the magnetic field where the pen recorder curve passes through zero, and $\omega/2\pi$ is the microwave frequency. No corrections were applied for any possible shifts in the resonant condition for these wide lines. The anisotropy which is observed with high purity p-type germanium at 4°K (Dresselhaus, Kip, and Kittel 1955) is also shown in figure 2. In contrast to

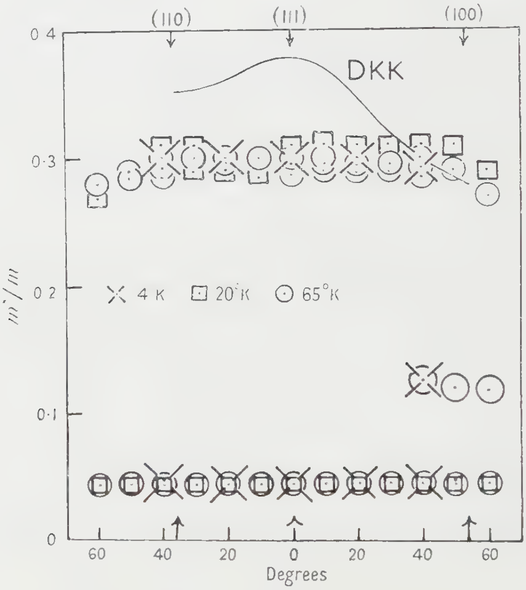

Figure 2. Effective masses from cyclotron resonance in gold-doped germanium. DKK, pure germanium at 4°K (Dresselhaus, Kip and Kittel 1955).

the high purity material, the gold doped sample shows an isotropic effective mass for the heavy holes ($m^*/m = 0{\cdot}30 \pm 0{\cdot}02$) as well as for the light holes ($m^*/m = 0{\cdot}045 \pm 0{\cdot}002$). Moreover, there is no change in effective mass with temperature and our values are in good agreement with those obtained from measurements on the high purity material. An additional weak line has been observed for crystal orientations near to a (100) direction. The line is not well resolved and the effective mass would be consistent with either a third harmonic of the heavy hole resonance or an electron resonance.

The collision time τ for the hole carriers can also be obtained from the width of the resonance lines by the relation $\Delta H/H_r \sim 0\cdot5/\omega\tau$ when $\omega\tau$ is of order unity. Here ΔH is half the separation in field between the maximum and minimum values of the differential absorption curve. Although there is considerable difference in the line widths when measured in terms of the magnetic field, the collision times are the same to the accuracy of these experiments for both the light and the heavy holes. The results are given in the table and it can be seen

Effective mass	Relaxation time $\tau(10^{-11}$ sec)			
m^*/m	90°K†	65°K	20°K	4°K‡
0·3	0·3	0·5	0·5	0·5
0·045	0·3	0·5	0·5	0·6

† Similar relaxation times have been obtained from preliminary measurements on iron-doped and cobalt-doped germanium at 90°K.

‡ The cavity was thermally connected to a liquid helium bath but the d.c. carrier excitation caused a small rise in temperature.

that τ is constant at temperatures below 65°K. It is also independent of crystal orientation. The lack of temperature dependence over so wide a range is surprising and suggests that the chief contribution to the collision time for the carriers in these samples arises from scattering by neutral impurities rather than from interaction with lattice waves or ionized centres which should give rise to a collision time having a 3/2 power law variation with the temperature. Taking the collision time $\tau = 0\cdot5 \times 10^{-11}$ sec, the number of neutral scattering sites may be estimated from our results to be 9×10^{15} per cm^3, if the effective mass is taken to be that corresponding to the heavy holes (Erginsoy 1950, Sclar 1956). This result is in good agreement with the measured solubility of gold in germanium namely, 3×10^{15} per cm^3 (Dunlap 1955). If the donor sites which were present initially in the sample (about 10^{13} per cm^3) are ionized by the gold impurities they should give rise to a relaxation time of order 10^{-10} sec at 20°K. This is too small a contribution to the line width to be detected in the present experiments.

The relative numbers of light and heavy holes (N_l, N_h) may be estimated from the extreme values for the differential absorption curve if an assumption is made about the line shape. This method enables the ratio N_l/N_h to be evaluated without performing a double integration of the pen recorder traces. We assume that the power absorption is given by

$$P \propto \frac{N\mathbf{e}^2\tau}{m^*}\left[\frac{1+\nu^2+\nu_c^2}{(1+\nu_c^2-\nu^2)^2+4\nu^2}\right] \equiv \frac{N\mathbf{e}^2\tau}{m^*} f(\nu,\nu_c)$$

where N is the number of carriers, $\nu = \omega\tau$, $\nu_c = \omega_c\tau = \dfrac{\mathbf{e}H}{m^*\mathbf{c}}\tau$ (Dresselhaus, Kip, and Kittel 1955). From this equation

$$\frac{\partial P}{\partial H} = \frac{\mathbf{e}\tau}{m^*\mathbf{c}} \times \frac{\partial P}{\partial \nu_c} = \left(\frac{\mathbf{e}^3\tau^2}{\mathbf{c}}\right)\frac{N}{(m^*)^2} \times \frac{\partial f}{\partial \nu_c}. \qquad \ldots\ldots(1)$$

At corresponding maxima or minima in the curve for $\partial P/\partial H$, the term $\partial f/\partial \nu_c$ has the same value for both the light and the heavy holes since in both of these cases, $\nu_c = \nu \pm 0\cdot5$ (τ is measured to be the same for each mass and we work at constant frequency so that $\nu = \text{constant}$). If S_l, S_h are two corresponding extreme values of $\partial P/\partial H$ for light and heavy holes respectively, we obtain from (1)

$$\frac{S_l}{S_h} = \left(\frac{m_h^*}{m_l^*}\right)^2 \frac{N_l}{N_h}. \qquad \ldots\ldots(2)$$

For our curves S_l/S_h is about unity at all temperatures so that $N_l \sim 0{\cdot}02 N_h$. On the other hand, if the population is determined by considerations of thermal equilibrium $N_l \sim 0{\cdot}06 N_h$. These values are probably in satisfactory agreement in view of the assumptions about the line shape involved in deriving equation (2).

The results obtained from these cyclotron resonance experiments at high temperatures may be compared with other estimates of the effective masses and with Hall mobility measurements. Benedict (1953) has estimated an average effective mass for holes of $(0{\cdot}3 \pm 0{\cdot}13)m$ from measurements of the high frequency conductivity and dielectric constant between 300°K and 160°K and a similar value was found in measurements extending down to 20°K (Fan 1955). Our cyclotron results, however, will give a rather lower value of about $0{\cdot}12m$ for the appropriate average effective mass for the conductivity experiments (Fan 1955). The Hall mobility μ can be obtained directly from the cyclotron results for the effective mass and the collision time. We obtain for the heavy holes $\mu_h = 29\,000 \text{ cm}^2 \text{ v}^{-1} \text{ sec}^{-1}$ at 65°K and $18\,000 \text{ cm}^2 \text{ v}^{-1} \text{ sec}^{-1}$ at 90°K whilst for the light holes $\mu_l = 190\,000 \text{ cm}^2 \text{ v}^{-1} \text{ sec}^{-1}$ and $120\,000 \text{ cm}^2 \text{ v}^{-1} \text{ sec}^{-1}$ at 65°K and 90°K respectively. The combined mobility appropriate to a Hall coefficient and resistivity experiment (Willardson, Harman and Beer 1954) is then $\mu = 42\,000 \text{ cm}^2 \text{ v}^{-1} \text{ sec}^{-1}$ at 90°K if $N_l = 0{\cdot}06 N_h$. This result does not compare very favourably with the value of about $6000 \text{ cm}^2 \text{ v}^{-1} \text{ sec}^{-1}$ measured by Dunlap (1955) with samples of high resistivity gold-doped germanium at 100°K. It is, however, comparable with measurements on relatively pure samples. Prince (1953), Morin and Maita (1954) obtain a hole mobility $\mu \sim 10^9 T^{-2{\cdot}3}$ over the temperature range 100°K to 300°K and if this relation is extrapolated to 90°K we obtain $\mu = 30\,000 \text{ cm}^2 \text{ v}^{-1} \text{ sec}^{-1}$.

The measurements that we have carried out so far have been confined to p-type germanium. By careful doping it is possible to obtain high resistivity n-type material (Dunlap 1955) and it should also be possible to extend the measurements to silicon where the common transition metals produce donor impurity sites. Such measurements on electron carriers are of considerable interest since the effective mass may be temperature dependent. It may also be possible to use analogous doping techniques in order to reduce the plasma effects which are so troublesome in intermetallic semiconductors.

References

Benedict, T. S., 1953, *Phys. Rev.*, **91,** 1565.
Dexter, R. N., Zeiger, H. J., and Lax, B., 1956, *Phys. Rev.*, **104,** 637.
Dresselhaus, G., Kip, A. F., and Kittel, C., 1955, *Phys. Rev.*, **98,** 368.
Dunlap, W. C., 1955, *Phys. Rev.*, **97,** 614.
Erginsoy, C., 1950, *Phys. Rev.*, **79,** 1013.
Fan, H. Y., 1955, *Solid State Physics*, Vol. I (New York : Academic Press).
Morin, F. J., and Maita, J. P., 1954, *Phys. Rev.*, **94,** 1525.
Prince, M. B., 1953, *Phys. Rev.*, **92,** 681.
Sclar, N., 1956, *Phys. Rev.*, **104,** 1559.
Tyler, W. W., Newman, R., and Woodbury, H. H., 1955, *Phys. Rev.*, **97,** 669.
Tyler, W. W., and Woodbury, H. H., 1954, *Phys. Rev.*, **96,** 874.
Willardson, R. W., Harman, T. C., and Beer, A. C., 1954, *Phys. Rev.*, **96,** 1512.

The Elastic Photoproduction of Neutral Pions from Helium

By E. H. BELLAMY, R. W. P. McWHIRTER† and P. PALIT
Department of Natural Philosophy, University of Glasgow

MS. received 10*th May* 1957, *and in final form* 6*th August* 1957

A study of the elastic photoproduction of π^0 mesons at H, D and ^{4}He is of particular interest, since a comparison of the production at these three nuclei should firstly provide information on the relative production at protons and neutrons, and secondly, might show modifications of the production at single nucleons due to the presence of other nucleons in the tightly bound helium nucleus.

The reaction

$$\gamma + {}^4\mathrm{He} \rightarrow \pi^0 + {}^4\mathrm{He} \qquad \ldots\ldots(1)$$

can be studied by detecting either the π^0 meson or the ^{4}He recoil particle. Except near threshold, the detection of the π^0 also involves the separation of π^0s produced in this reaction from those produced inelastically. Also since the π^0 is detected by measurements on one or both of the γ-rays resulting from its decay, it is extremely difficult to determine the angular and energy distributions of the initially produced π^0's. Goldwasser and Koester (1956) have made measurements on one of the γ-rays from the π^0 decay, the maximum beam energy of their machine being varied in steps of 10 Mev.

The alternative method, of measuring the ^{4}He particles, has been used by De Saussure and Osborne (1955). They detected the α-particles with photographic emulsions, where they are indistinguishable from ^{3}He particles. The latter may be produced by the reactions

$$\gamma + {}^4\mathrm{He} \rightarrow \mathrm{n} + {}^3\mathrm{He} \qquad \ldots\ldots(2)$$

or

$$\gamma + {}^4\mathrm{He} \rightarrow \begin{matrix} \pi^- + \mathrm{p} \\ \pi^0 + \mathrm{n} \end{matrix} + {}^3\mathrm{He}. \qquad \ldots\ldots(3)$$

The contribution of reaction (2) may be eliminated by a subtraction technique since all the ^{3}He particles of energy and angle of emission with respect to the bremsstrahlung beam which can be confused with the ^{4}He's from reaction (1) are produced by photons of energy less than 150 Mev.

It is not possible by such a technique to eliminate those ^{3}He's produced in the reactions (3). De Saussure and Osborne assumed that their contribution was negligible. Goldwasser and Koester state that their measurements give a cross section which appears to be 5 to 10 times smaller than that quoted by De Saussure and Osborne.

In order to improve the reliability of these measurements, it was decided to try and build a detector which would distinguish the ^{3}He from the ^{4}He particles. This was done by detecting them in two gridded ionization chambers which measured dE/dx and E. The α-particle energy at creation varied between 15 and 35 Mev. The resolution attained with this detector is shown in figure 1. At a laboratory angle of 90°, the kinematics of reaction (1) rule out the possibility of the emission of a ^{4}He particle. It is seen that the two types of particle are clearly separated. ^{3}He particles, being singly charged, are not recorded.

---

† Now at the Atomic Energy Research Establishment, Harwell, Berks.

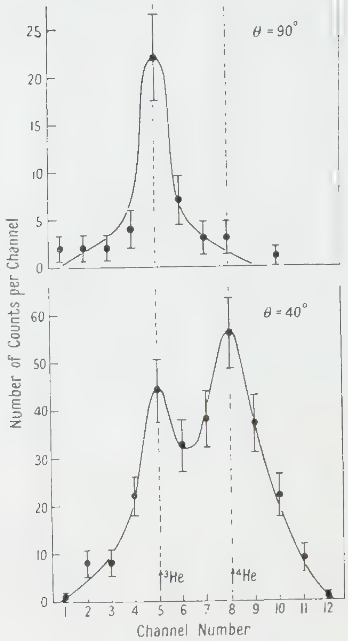

Figure 1. Resolution of the detector. θ is the laboratory angle of the recoiling particle with respect to the photon beam.

Our values of the cross section in centre-of-mass are found to be

$$\left(\frac{d\sigma}{d\Omega}\right)_{\phi=135^\circ} = 7{\cdot}5 \pm 0{\cdot}5\ \mu\text{bn sterad}^{-1}, \text{ averaged over a photon energy range } 257\text{–}310 \text{ MeV}$$

$$\left(\frac{d\sigma}{d\Omega}\right)_{\phi=90^\circ} = 12 \pm 1\ \mu\text{bn sterad}^{-1}, \text{ averaged over a photon energy range } 263\text{–}315 \text{ MeV}.$$

The excitation functions at these angles are shown in figures 2 and 3 and compared with calculations by Stoodley (1957, private communication) using an impulse

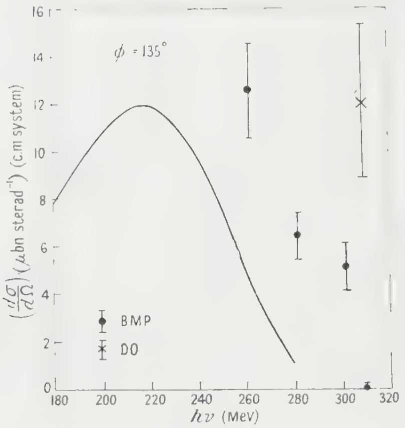

Figure 2.

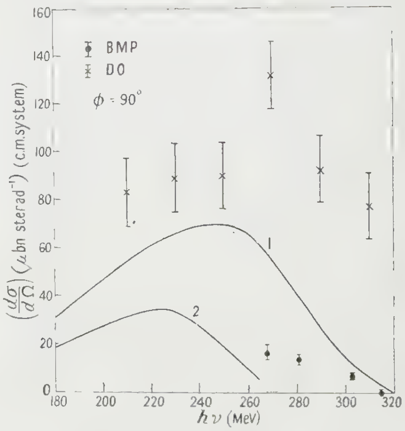

Figure 3.

Figure 2. The curve is based on impulse approximation calculation. ϕ is the centre-of-mass angle of the π^0. BMP, this experiment; DO, De Saussure and Osborne's result averaged over $280 < E_\gamma < 340$ MeV.

Figure 3. 1, impulse approximation; 2, impulse approximation with multiple scattering correction. ϕ is the centre-of-mass angle of the π^0. BMP, this experiment; DO, De Saussure and Osborne's results.

approximation. A multiple scattering correction has not been calculated at $\phi = 135°$, but is expected to be very small at this angle.

If all the ^{3}He particles detected in this experiment are attributed to reaction (2), the cross sections in the laboratory system are

$$90 < E_\gamma < 138 \text{ Mev} \quad \left(\frac{d\sigma}{d\Omega}\right)_{90°} = 9{\cdot}6 \pm 2\,\mu\text{bn sterad}^{-1}.$$

$$67 < E_\gamma < 96 \text{ Mev} \quad \left(\frac{d\sigma}{d\Omega}\right)_{40°} = 11{\cdot}8 \pm 1{\cdot}2\,\mu\text{bn sterad}^{-1}.$$

$$87 < E_\gamma < 117 \text{ Mev} \quad \left(\frac{d\sigma}{d\Omega}\right)_{20°} = 1{\cdot}4 \pm 1{\cdot}0\,\mu\text{bn sterad}^{-1}.$$

These values appear to be compatible with those found by De Saussure and Osborne, but there seems to be some inconsistency in the results quoted by these authors (figures 2, 3 and 4 of their paper).

The bremsstrahlung beam was measured with an ionization chamber identical with that used at Cornell (Corson *et al.* 1953), their calibration being used. An independent calibration against a pair spectrometer is planned.

Possible contributions to the ^{4}He particles detected from the scattering reactions

$$\gamma + {}^4\text{He} \rightarrow \gamma + {}^4\text{He}$$

$$\text{n} + {}^4\text{He} \rightarrow \text{n} + {}^4\text{He}$$

are both estimated to be negligible.

It is intended to extend these measurements to other angles.

We would like to thank the synchrotron crew under Dr. McFarlane for running the synchrotron for us and to Professor P. I. Dee for his encouragement throughout.

REFERENCES

CORSON, D. R., DE WIRE, J. W., McDANIEL, B. D., and WILSON, R. R., 1953, *The Cornell* 300 MEV *Synchrotron*, p. 62 (Ithaca: Cornell University).

DE SAUSSURE, G., and OSBORNE, L. S., 1955, *Phys. Rev.*, **99**, 843.

GOLDWASSER, E. L., and KOESTER, L. J., 1956, *Nuovo Cim.* Suppl., **4**, 950.

On the High Temperature Susceptibility for the Heisenberg Model of a Ferromagnetic

BY P. J. WOOD AND G. S. RUSHBROOKE

Physics Department, King's College, Newcastle-upon-Tyne, University of Durham

MS. received 10*th July* 1957

In a previous communication (Rushbrooke and Wood 1955, referred to subsequently as I) we discussed series expansions, in inverse powers of the temperature, of the susceptibility χ for the Heisenberg model of a ferromagnetic, for the special case in which the magnetic unit has spin $\frac{1}{2}$ in units of $\hbar$. In this present note we simply report the results of extending these calculations to the case of arbitrary spin S. Previous calculations for this more general model have been made by Brown and Luttinger (1955) and Brown (1956).

Thus, whereas in I we used the Hamiltonian

$$\mathscr{H} = -\tfrac{1}{2}J \sum_{\langle i,j \rangle} \boldsymbol{\sigma}^{(i)} . \boldsymbol{\sigma}^{(j)} - \beta \sum_{i} \boldsymbol{\sigma}^{(i)} . \mathbf{H}$$

we now use the more general Hamiltonian

$$\mathscr{H} = -2J \sum_{\langle i,j \rangle} \mathbf{S}^{(i)} . \mathbf{S}^{(j)} - g\beta H \sum_{i} S_3{}^{(i)}.$$

Introducing the reduced variables $\theta = kT/J$ and $\bar{\chi} = J\chi/Ng^2\beta^2$ we obtain expansions

$$\bar{\ }\theta = \tfrac{1}{3}S(S+1) \sum_{n=0}^{\infty} \frac{a_n}{\theta^n}$$

and

$$\frac{1}{\bar{\chi}\theta} = \frac{3}{S(S+1)} \sum_{n=0}^{\infty} \frac{b_n}{\theta^n}$$

where the coefficients, a_n and b_n, are the quantities requiring explicit calculation. In I we gave a_n and b_n for $n = 1, 2, .., 5$, for any lattice. Subsequently Domb and Sykes (1956) reported independent calculations of these values and gave also the results for $n = 6$.†

For the case of general spin Brown and Luttinger went as far as $n = 4$, and Brown extended the calculations to $n = 5$ for open lattices only. In this note we report the results of our calculations for any lattice (i.e. including close-packed lattices), also for $n = 1, 2, .., 5$. We confirm the results of Brown and Luttinger, but not those of Brown (1956). The discrepancy is very small. We believe that our results are in fact correct since they satisfy the checking procedure described below.

For brevity, we give the expressions for the b's in terms of the lattice parameters defined in I, denoting $S(S+1)$ by X. We also tabulate the a's for the special case $S = 1$, and for the lattices discussed in I. The results are

$$b_0 = 1 \qquad b_1 = -\tfrac{2}{3}zX \qquad b_2 = \tfrac{1}{9}zX(4X+3)$$

$$b_3 = \frac{4}{135}zX[(10p_1-4)X^2 + (5p_1-9)X - 6]$$

$$\begin{aligned} b_4 = \frac{4}{405}zX[&(80p_2 - 96p_1 - 16)X^3 + (40p_2 - 156p_1 + 64 - 40z)X^2 \\ &+ (-54p_1 + 96 - 45z)X + 45] \end{aligned}$$

$$\begin{aligned} b_5 = \frac{2}{42\,525}zX[&(2800p_3 - 3360p_2 - 3360p_1{}^2 - 1456p_1 + 800)X^4 \\ &+ (1400p_3 - 6160p_2 - 3360p_1{}^2 - 4200zp_1 + 12\,936p_1 + 1120z + 80)X^3 \\ &+ (-2940p_2 - 315p_1{}^2 - 3150zp_1 + 12\,978p_1 + 3570z - 3912)X^2 \\ &+ (2898p_1 + 3780z - 4752)X - 1728]. \end{aligned}$$

---

† We too have calculated a_6 and b_6 for $S = \frac{1}{2}$, and agree with the results of Domb and Sykes.

and

Lattice	a_1	a_2	a_3	a_4	a_5
Linear	$\frac{8}{3}$	$\frac{20}{9}$	$-\frac{64}{27}$	$-\frac{260}{81}$	$\frac{1088}{135}$
Honeycomb	4	$\frac{26}{3}$	$\frac{112}{9}$	$\frac{550}{27}$	$\frac{7072}{135}$
Plane square	$\frac{16}{3}$	$\frac{56}{3}$	$\frac{512}{9}$	$\frac{12\,344}{81}$	$\frac{457\,984}{1215}$
Plane triangular	8	$\frac{148}{3}$	256	$\frac{31\,900}{27}$	$\frac{2\,047\,232}{405}$
Diamond	$\frac{16}{3}$	$\frac{56}{3}$	$\frac{512}{9}$	184	$\frac{84\,736}{135}$
Simple cubic	8	$\frac{148}{3}$	$\frac{2624}{9}$	$\frac{44\,860}{27}$	$\frac{3\,803\,072}{405}$
Body-centred	$\frac{32}{3}$	$\frac{848}{9}$	$\frac{22\,016}{27}$	$\frac{546\,160}{81}$	$\frac{22\,383\,616}{405}$
Face-centred	16	$\frac{680}{3}$	$\frac{27\,392}{9}$	$\frac{1\,071\,800}{27}$	$\frac{205\,955\,584}{405}$

The disagreement with Brown's results amounts, in all cases, to a contribution $\frac{8}{1215}\,zp_2X^3(4X-3)$ in a_5; and this vanishes for $S=\frac{1}{2}$.

To check our results we have proceeded as follows. To determine the a's it is necessary to evaluate the traces of P^n and $P^{n-2}\underset{\sim}{Q}^2$ where

$$P=\sum_{\langle i,j\rangle}\mathbf{S}^{(i)}\,.\,\mathbf{S}^{(j)}\ \text{and}\ \underset{\sim}{Q}=\sum_{i}\mathbf{S}_3^{(i)}.$$

For the special case $S=1$, the eigenvalues of $P+\lambda\underset{\sim}{Q}$ were found directly for the following pseudo-lattices

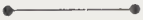

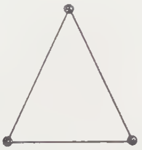

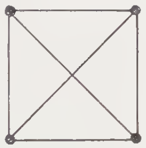

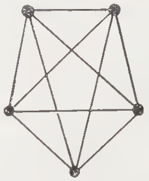

(cf. Rushbrooke and Scoins 1955). The required traces can then be computed, and on introducing the lattice parameters appropriate to these pseudo-lattices we can find expressions for a_1, a_2 . . , a_5 agreeing in each case with those previously calculated.

We end with a brief discussion of the Curie temperatures, θ_{C}, confining attention to the body-centred and face-centred cubic lattices and to the two cases $S=\frac{1}{2}$ and $S=1$. Basing the argument on the trend of $a_n^{1/n}$ we previously estimated, for $S=\frac{1}{2}$,

$$\text{face-centred}\ \theta_{\mathrm{C}}=4{\cdot}21$$
$$\text{body-centred}\ \theta_{\mathrm{C}}=2{\cdot}70.$$

We have re-examined these values, both in order to incorporate the values of a_6 and because we now believe that this method is liable to give rather too high an answer. We have, in fact, examined the behaviour of $a_n^{1/n}$, a_n/a_{n-1}, $(a_n/a_{n-2})^{1/2}$, and of the roots of the truncated expressions for χ^{-1}. We now incline to the results, for $S=\frac{1}{2}$,

$$\text{face-centred } \theta_C = 4{\cdot}15 \pm 0{\cdot}05$$
$$\text{body-centred } \theta_C = 2{\cdot}60 \pm 0{\cdot}05.$$

The values recently reported by Domb and Sykes (1957), 4·170 and 2·636, lie within our ranges: but we would hesitate ourselves to be more precise. For $S=1$ we similarly estimate

$$\text{face-centred } \theta_C = 11{\cdot}90 \pm 0{\cdot}05$$
$$\text{body-centred } \quad 7{\cdot}5 < \theta_C < 8{\cdot}0.$$

ACKNOWLEDGMENT

One of the authors (P. J. W.) would like to thank Messrs. George Angus and Co. Ltd. for the award of a Postgraduate Studentship.

REFERENCES

BROWN, H. A., 1956, *Phys. Rev.*, **104**, 624.
BROWN, H. A., and LUTTINGER, J. M., 1955, *Phys. Rev.*, **100**, 685.
DOMB, C., and SYKES, M. F., 1956, *Proc. Phys. Soc.* B, **69**, 486; 1957, *Proc. Roy. Soc.* A, **240**, 214.
RUSHBROOKE, G. S., and SCOINS, H. I., 1955, *Proc. Roy. Soc.* A, **230**, 74.
RUSHBROOKE, G. S., and WOOD, P. J., 1955, *Proc. Phys. Soc.* A, **68**, 1161.

LETTERS TO THE EDITOR

The β-Spectrum of Sulphur 35

While there have been suggestions to the contrary (Cook *et al.* 1948, Berggren and Osborne 1948, Cockcroft and Insch 1949), it now seems to be fairly well established (Albert and Wu 1948, Langer *et al.* 1950, Moljk and Curran 1954) that the β-disintegration of ^{35}S is allowed, corresponding to $\Delta I=0$ (no), the Fermi plot being linear from the end point down to at least 5 kev (Moljk and Curran 1954). The spectrum is known to be simple. It has been investigated, and the end-point energy determined, by the use of proportional counters and magnetic spectrometers using Geiger counters as detectors, as well as by a retarding potential method (Gross and Hamilton 1950). The precise value of the end-point energy is more in doubt than the linearity of the Fermi plot. Thus, end-point energies of $169{\cdot}1 \pm 0{\cdot}5$ kev (Cook *et al.* 1948) and $167{\cdot}0 \pm 0{\cdot}5$ kev (Langer *et al.* 1950) are to be found in the post-war literature.

In order to attempt to determine this energy more accurately, a supply of carrier-free ^{35}S was obtained from the Radiochemical Centre, Amersham, for examination by a magnetic spectrometer having a collecting power of 4% and a resolution of 2% (Richardson 1952). This spectrometer was calibrated against the internal conversion lines of Th (B + C), the F-line of which is particularly convenient having an energy of 148·08 kev. The calibration factor of the instrument was known to an accuracy of better than 1 part in 1000. The detector was an anthracene crystal and photomultiplier. A source of $5\,\mu\mathrm{g\,cm^{-2}}$ was prepared on a backing of V.Y.N.S. resin of thickness of the order of $5\,\mu\mathrm{g\,cm^{-2}}$ on to which a layer of gold of the order of $5\,\mu\mathrm{g\,cm^{-2}}$ had been evaporated so as to produce a conducting surface. We are indebted to Bakelite Ltd., Aycliffe Works, Co. Durham, for a supply of V.Y.N.S. resin (vinylite) which is a polyvinyl-chloride-acetate co-polymer soluble in cyclohexanone. From such a solution, very thin films of good tensile strength and chemical resistance can be produced (Pate and Yaffe 1955).

With the electronic settings employed it was already known that the counting efficiency of the detector fell below unity for electrons of energy less than 95 kev. For energies greater than 100 kev, however, the uncorrected Fermi plot for each of several runs on ^{35}S was linear within the limits of statistical accuracy, which was everywhere better than 1%. Taking the results as a whole, the end-point energy was determined to be $167{\cdot}4 \pm 0{\cdot}2$ kev. This end-point energy yields a $\log_1 ft$ value of 5·01 for 87·1 day ^{35}S and corresponds to a mean β-particle energy of $61{\cdot}0 \pm 0{\cdot}2$ kev.

Department of Natural Philosophy,
University of Edinburgh.

R. D. Connor.
I. L. Fairweather.

14th June 1957, and
in revised form 4th July 1957.

Albert, R. D., and Wu, C. S., 1948, *Phys. Rev.*, **74,** 847.
Berggren, J. L., and Osborne, R. K., 1948, *Phys. Rev.*, **74,** 1240.
Cockcroft, A. L., and Insch, G. M., 1949, *Phil. Mag.*, **40,** 1014.
Cook, C. S., Langer, L. M., and Price, H. C., Jr., 1948, *Phys. Rev.*, **73,** 1395.
Feuvrais, L., and Yuasa, T., 1954, *C.R. Acad. Sci., Paris*, **239,** 1627.
Gross, L., and Hamilton, D. R., 1950, *Phys. Rev.*, **80,** 484.
Langer, L. M., Motz, J. W., and Price, H. C., Jr., 1950, *Phys. Rev.*, **77,** 798.
Moljk, A., and Curran, S. C., 1954, *Phys. Rev.*, **96,** 395.
Pate, B. O., and Yaffe, L., 1955, *Canad. J. Chem.*, **33,** 15.
Richardson, H. O. W., 1952, *J. Sci. Instrum.*, **29,** 93.

CORRIGENDUM

The K Auger Yield for Tin, by J. A. V. Fairbrother, D. G. Parkyn and B. M. O'Connor. (*Proc. Phys. Soc.* A, 1957, **70,** 262.)

On page 264, immediately after equation (7), it is stated that a, b, c_{ij} and d are dependent on E_H and E_S. This is true only for a and b, and the method cannot be used, as suggested, for determining the P_{ij}'s. Since the paper is in no way dependent on this suggestion the determination of the Auger yield is not invalidated.

REVIEWS OF BOOKS

Physics, by J. S. Marshall and E. R. Pounder. Pp. viii + 905. (New York: Macmillan, 1957.) 59*s*. 6*d*.

The preface to this book may well induce a smug feeling of self-satisfaction in the British physicist when he reads the statement that the book is intended for first and second year University students and yet that ' calculus is not needed for an understanding of the text '. A brief glance at the contents would suggest that here it would be more suitable for school use.

In fact, however, these impressions would be quite wrong. Calculus is used extensively, and the reference in the preface merely means that mathematics is not used as a substitute for physics but as an ancillary to it. The treatment of thermodynamics is particularly good, and causes one rather to envy the opportunity that now exists in America for introducing physics as a new subject to more mature students than in this country. The book may well serve as a textbook for the courses introduced recently in several Universities for converting Arts students into scientists.

Use is made throughout of the metre, kilogramme and second as basic units, in preparation for their use in the rationalized m.k.s. system of units in electricity and magnetism. This system has practical advantages, but appears rather clumsy (see pp. 637 and 692) in basic definitions. Physicists here must soon make up their minds about its use, as the sheer weight of imported textbooks may soon force it upon them.

To summarize, the book can be strongly recommended to those who like to foster physical, as distinct from mathematical, insight into problems ; it may well brush the cobwebs from some dusty corners in many a physicist's mind.

H. LIPSON.

Science and the Nation, by Sir Edward Appleton. Pp. xi + 104. (Edinburgh: University Press, 1957.) 10*s*. 6*d*.

This slim little book represents the Reith Lectures for the B.B.C. almost in the form in which they were given in 1956. Sir Edward Appleton's concern is with the relations that exist between science and the nation as a whole. If, in his own words, " science is too serious a matter to be left entirely to the scientists ", then someone must tell ordinary people about the way that science works, and the conditions necessary for its proper functioning. This book is one lesson in this process of educating the public.

Sir Edward is well qualified for this kind of task, since he has had experience both as an academic scientist, and at the D.S.I.R., which may be said to be the mainspring of most governmental science. He describes the threefold field of science, in university, government and industry. There does not seem to be much wrong with university science except that, as compared with industry, each experimentalist has much too little technical help from skilled technicians. Thus in universities there is an average of one technician to two or three research workers; in industry there are three or four technicians to each research worker. Yet, wisely enough, Appleton does not want to change this ratio too drastically. For to work with your hands is to learn something of your subject that you would never learn otherwise; and in universities as distinct from industry, the number and speed of obtaining results are far less important than the training of people in the methods and understanding of research.

It is in the field of industry that most change is needed. Since 97% of firms in Britain employ less than 300 workers, it is almost impossible for them to carry out much research. Yet Appleton asserts that the few big companies which do research, do so not because they are big, but they are big because they did research, even when they were small. The future of the various Research Associations is here of the greatest moment, for they can help to bring the smaller firms up to scratch. It is a grave indictment of industry that only one in five of the directors on engineering boards in Britain has any genuine scientific or technical qualification. This is likely to be the biggest single factor operative to delay the proper technological development of the original ideas. We excel in the latter: we fail miserably in the former.

Appleton has much more to say along these lines. Most of it will be familiar to those of us who are ourselves scientists. But this sort of thing needs to be said repeatedly -and Sir Edward brings into his account a number of most interesting specific illustrations. This is a useful little book, even if—from the nature of things—it is not particularly profound in its analysis, and does not break much new ground in suggested remedies. C. A. COULSON.

Vorlesungen uber Atomphysik I, by J. PICHT. Pp. viii + 238. (Berlin: Deutscher Verlag der Wissenschaften, 1956.) DM. 18.60.

This first part of Professor Picht's lectures on atomic physics contains the main classical and quantal foundations. It covers such subjects as mechanics, the kinetic properties of gases, radiation theory and statistical mechanics. A large part of the book deals with the spectroscopy of atoms and molecules from the point of view of the Bohr theory and the correspondence principle. The treatment of these phenomena using the full apparatus of quantum mechanics is presumably reserved for the second volume.

The account of classical statistical mechanics is supplemented by a special chapter on Fermi and Bose–Einstein statistics. This is the traditional manner of handling the subject, though one does feel that this part of statistical mechanics (or for that matter the whole of it) might well be dealt with after a discussion of wave mechanics and of the symmetry properties of wave functions.

The book is written in a very concise manner, covering a wide field in the compass of a small volume. It would provide a very useful revision course for an advanced student of physics. M. BLACKMAN.

Temperature—Its Measurement and Control in Science and Industry. Vol. 2, edited by H. C. WOLFE. Pp. x + 467. (New York: Reinhold; London: Chapman and Hall, 1955). 96*s*.

The papers presented at the last Symposium on Temperature, which form the whole of this book, certainly illustrate both the rapidity with which science, particularly applied science or technology, can develop in a few years and also the interest which such development can hold for the non-specialist.

At the time of the previous Symposium (1939) experiments using liquid hydrogen and helium in any quantity were rare and adiabatic demagnetization was somewhat of a novelty. Eyebrows would certainly have risen at the idea of filling a liquid hydrogen bubble chamber with cubic metres of liquid. At the other end of the scale it was just being seriously realized that the working out of the details of stellar interiors depended on a knowledge of nuclear processes, and the advent of terrestrial nuclear explosions, with their extension of the upper limit of terrestrial temperatures by a large factor, was still in the future.

It will be best in discussing this volume to give a brief summary of its contents as, being similar to a journal, the title only offers very broad guidance to the subject matter. In fact, the attempt by the editors to give a partial division on logical grounds is inclined to separate as many common articles as it unites.

Section I covers general conceptual matters in temperature measurement from near the absolute zero (by the late F. E. Simon) up to astrophysical temperatures, with most emphasis on the newer extremes of temperature.

Section II gives the kind of practical details of precision thermometry in the ' middle ' range, which students and teachers in particular will find interesting to read. Much of the real meat of the Symposium is to be found in this section, quite well presented, and in sufficient detail to be easily followed.

Section III consists of two very topical papers on transient phenomena, one on the thermodynamics of irreversible processes and the other on the relaxation of partial temperatures, the latter being much to the fore in shock wave work.

Section IV is a rather diverse collection of subjects under the general heading of experimental measurements. We have a paper on susceptibility measurements below 1°K; one on flames and hot gases using radiation, and relevant to gas turbines, etc.; a large paper on temperature measurements in engineering processes, which will be useful to industrial concerns as a broad summary of well established methods; and three rather specialist papers on superconductivity, semiconductors and the velocity of sound, each used for temperature measurement.

Section V, the last section, is on miscellaneous topics and contains just three articles of exceptional interest. The first is on the temperatures produced in the explosion of an atom bomb, the second is on ionisation measurements at some of the highest steady temperatures ever reached (50 000–60 000°K), and the last on upper atmospheric temperatures as explored by rockets.

It will be seen that this book is by no means as dull as its title might lead one to expect, and it will be obvious that the emphasis is on ' science ' rather than ' industry '. It will be used none the less by industrial research departments, but as a source of up-to-date ideas rather than the practical details of temperature measurement or control in a particular application.

It will also be widely used as a good account of the current state of the subject, with the emphasis on modern developments, and will form a standard text for the next few years. R. LATHAM.

Cours de Mathématiques, by J. Bass. Pp. xii + 916. (Paris: Masson, 1956.) 8500 *fr*.

This is an encyclopaedic work of applicable mathematics, designed principally for physicists and engineers. It is, however, neither a mere reference book nor a dusty compilation of elementary mathematical methods. M. Bass has contrived to make his treatment sophisticated and reasonably rigorous without sacrificing simplicity, and has produced a self-contained course which is both useful and stimulating. It is, in fact, a pleasure to be able whole-heartedly to recommend a book of this kind—the only question being : to whom ? The book is apparently based upon courses given, in Paris and elsewhere, to intending students of physics and engineering, who have already done some mathematics but have not yet begun their scientific and technical studies. We know too little of the educational system in France to state precisely what this means : it must suffice to say that the initial standard of mathematics required is undoubtedly higher than that expected of entrants to British universities, and the book contains considerably more mathematics than our physics and engineering students generally acquire during their undergraduate years. We believe that a course of this kind should be a *sine qua non* for an honours degree in physics, at least, but as things stand at present we must reluctantly recommend the book only to *graduate* British students of physics and engineering. On the other hand the book would serve as a useful introductory course for students of mathematics.

The book is divided into eight sections, with two appendices. The first hundred pages are devoted to linear algebra, a topic which, in spite of its importance in physics, is often omitted from books of this nature. The section begins with the definitions and properties of rings, groups, and vector spaces, goes on to a detailed discussion of matrices, and ends with an account of the theory and some applications of cartesian tensors.

The integral calculus is developed with sufficient rigour in the following four sections, which also contain discussions of Fourier series, differential geometry, and the integral theorems of vector analysis, as well as a brief but valuable account of the operational calculus. Section six deals concisely with functions of a complex variable, and the remaining two sections give an enlightened treatment of ordinary and partial differential equations. A useful account of the calculus of variations is given as an appendix of some 20 pages, and also included as an appendix is a discussion of methods of constructing nomograms.

Even in a work of this length it is not possible to include everything which may be regarded as essential, and it is inevitable that the choice of the author will conflict with that of some of his readers. We feel, for instance, that the appendix on nomograms and a chapter describing various planimeters and mechanical integrators might well have been omitted, in favour perhaps of a discussion of Green's function, which is only accorded half a page. However, M. Bass justifies most of his sins of omission and commission in the Introduction.

An excellent feature of the book is the large number of examples, for which alone it should be invaluable to university teachers. These examples are, in fact, an important part of the course—the theory of integral equations, for instance, is hardly mentioned in the text but is developed to some extent in a number of examples. The solutions are not usually given, but hints are sometimes provided.

It must be confessed that the book has for the foreign reader a charm which may not be apparent to the native student. We find in figure 183, for example, a complicated arrangement of curves and lines, puzzling at first sight, but revealed by the text to be *un observateur couché sur Γ, dans le sens positif*—a human likeness which might well have graced the cave walls of Lascaux. It is also amusing, if a little unnerving, to find what we have long known as the ‘ divergence theorem of Gauss ’ in the guise of the ‘ formula of Ostrogradski ’. Similarly, the

Cauchy–Riemann conditions are credited to Cauchy only, but Riemann is compensated by the award of Stokes's theorem in two dimensions.

The price of the book, together with its linguistic disadvantage, make it unlikely that it will be a best-seller among English-speaking students, but it well deserves a place in all mathematical libraries. To those who can afford it—or, better, who can borrow it—we say, in the words of Professor G. Darmois, who has written the Preface : *Je pense que l'utilisateur de cet ouvrage éprouvera un sentiment de sécurité par l'ampleur des matières auxquelles il peut avoir accès, un sentiment de plaisir en résolvant les problèmes posés.* S. RAIMES.

Éléments de Mécanique Quantique, by Ph. PLUVINAGE. Pp. xii + 547. (Paris : Masson & Cie, 1955). 4000 *fr.*

Among all the varied studies which comprise quantum mechanics there is one, the quantum mechanics of electrons and nuclei, whose principles have hardly changed since they were first formulated about thirty years ago, and whose success in applications seems to establish it as a permanent part of physics. It applies directly only to atoms, molecules and solids and, even so, requires corrections when relativistic effects become important or the particles interact strongly with fields.

It is this important part of quantum mechanics which is the subject of this textbook. The first of its three parts gives a full account of the general principles of quantum mechanics and of their relation to classical mechanics. It uses the particle moving in one dimension as an illustration and treats the problems of a potential well, a simple oscillator, a free particle and a particle meeting a barrier. In the second part the extension to three dimensions is given and includes a discussion of curvilinear coordinates, separation of variables, spin and angular momentum, with applications to a rotating molecule, a hydrogen atom, and collisions with central fields. The final part is concerned with systems of particles and discusses the exclusion principle, the building up of atoms and the hydrogen molecule.

The book is addressed throughout to the experimental physicist and the mathematics required is explained carefully and simply. Orders of magnitude and the relation to experiment are illustrated by numerical examples in the text. Students will also appreciate the summaries at the heads of chapters and the exercises at the ends.

For a book of this size, however, there are some surprises in the selection of material. Thus, self-consistent field methods are dismissed in two pages and variational methods in little more and with applications only to He and H_2. Similarly, there is no mention of any modification or extension of perturbation theory and only a passing reference to the Dirac electron theory. Some acquaintance with these is essential for any further study of the subject and could have been included by abbreviating some of the sections entirely concerned with classical mechanics. These include a full chapter on probability in classical mechanics and numerous sections giving classical analogies to quantum mechanical results. These are interesting to read but scarcely necessary to a student.

This will be a useful addition to standard books on quantum mechanics. The presentation is so clear that it may be safely recommended as an introductory textbook for physicists or mathematicians. G. G. HALL.

CONTENTS OF SECTION B

PAGE

Dr. H. House. High Field Conduction Currents in Hexane 913

Dr. F. A. Lewis, Mr. J. Orr and Prof. A. R. Ubbelohde. Contact Effects resulting from Compression and Flash Sintering in Graphite Powders . 928

Dr. E. H. Grant. The Dielectric Properties of Methyl and Ethyl Alcohols in the Wavelength Range 3 cm–52 cm 937

Dr. A. K. Head. The Two-Mirror Aplanat 945

Dr. H. S. Story and Prof. R. W. Hoffman. Stress Annealing in Vacuum Deposited Copper Films 950

Dr. F. J. Hewitt. Radar Echoes from Inter-Stroke Processes in Lightning . 961

Prof. E. R. Andrew and Mr. N. D. Finch. Nuclear Magnetic Resonance Spectrum for Isosceles Triangular Configurations of Nuclei . . . 980

Mr. Y. Moriguchi and Prof. A. Okazaki. Current–Capacitance Characteristics of Metal Rectifiers 991

Research Notes :

Mr. D. J. Craik and Mr. P. M. Griffiths. A New Colloid for use with the Bitter Figure Technique 1000

Dr. H. H. Hopkins. The Numerical Evaluation of the Frequency Response of Optical Systems 1002

Dr. A. Goswami and Mr. Y. N. Trehan. The Thermal Decomposition of Cupric Oxide *in vacuo* 1005

Mr. R. Barrie. Magnetoresistance in Strong Magnetic Fields . . . 1008

Letters to the Editor :

Mr. C. Hilsum. Photoelectric Effects in InAs at Room Temperature . . 1011

Reviews of Books 1013

Contents of Section A 1024

The Low Energy Elastic Scattering of Neutrons by Deuterons

By P. G. BURKE† and H. H. ROBERTSON‡
† University College, London
‡ National Physical Laboratory, Teddington, Middx.

Communicated by H. S. W. Massey; MS. received 7th June 1957

Abstract. The elastic scattering of neutrons by deuterons at energies less than 16·6 MeV incident neutron energy has been calculated using a scattering equation similar to that of Buckingham and Massey and a central nuclear potential with Gaussian form. Five values of the effective range are considered, covering all values of physical significance. For analytical convenience, a deuteron wave function consisting of two Gaussians is used, the deuteron binding energy being minimized with respect to three parameters. S and P phases for several energies were evaluated with the aid of electronic computers (Pilot ACE and DEUCE) for Serber, ordinary and symmetrical exchange forces. From the total cross section below 2 MeV it appears that the potentials of larger effective range agree best with experiment, although the doublet scattering length considerably exceeds the experimentally estimated value for all these potentials, probably because of polarization effects at low energies. From the P phases, conclusions are drawn about the validity of the Born approximation used by Christian and Gammel. The problem is then resolved for the short range potential using an adaptation of the variational methods of Hulthén and Kohn. The results at low energies compare favourably with the exact solution obtained previously. It therefore seems that the variational method may be used successfully when polarization of the deuteron is explicitly allowed for, and further calculations including this effect and using the Kohn method are in progress.

§ 1. Introduction

It has long been recognized that the study of the low energy elastic scattering of neutrons by deuterons provides a powerful method for the investigation of nuclear forces and in this connection the theoretical aspect of the problem has received detailed treatment from amongst others, Buckingham and Massey (BM) (1941), Buckingham, Hubbard and Massey (BHM) (1952), Christian and Gammel (CG) (1953) and de Borde and Massey (de BM) (1955).

In any sophisticated phenomenological treatment of the problem it is now necessary to include a tensor force component in the interaction and, when this is done, the appropriate ranges and depths of the interaction are known within fairly close limits. However, owing to the extreme complexity involved in this inclusion, all previous work on the low energy n–d elastic scattering has been carried out with purely central forces. This procedure of representing the tensor force by an 'equivalent' central force has produced an ambiguity concerning the range to be taken for the interaction and there has consequently not been any generally adopted value. Thus, while CG used a short effective range consistent with all two-body data which do not depend essentially on the tensor force, BHM used a larger effective range potential found to give the best agreement with the observed properties of the light nuclei, e.g. binding energy of T^3. In order, therefore, to attempt to correlate the work of previous workers in the field and also to form some criterion concerning the best central force range to assume, it was decided to carry out calculations for five ranges extending over all physically feasible values.

S and P phases were evaluated and from the latter more accurate conclusions could be drawn than hitherto possible concerning the accuracy of the Born approximation used by CG. From Blatt–Jackson curves obtained using the quartet and doublet zero order phases for each of the potential ranges, it is found that the doublet scattering length is in disagreement with the experimentally determined value. Also it appears that this disagreement occurs for all the potential ranges considered and it is felt that the position will not be materially improved by using ranges outside the values assumed in this paper. It is probable, therefore, that the solution to this problem must be sought in the polarization of the deuteron by the neutron which, as pointed out by CG, is expected to be a predominantly doublet state effect.

On considering the work on atomic collisions, especially that of Massey and Moiseiwitsch (MM) (1951) concerning the scattering of electrons by hydrogen atoms, it seems likely that at least part of the polarization effect can be allowed for by a variational method where a term is inserted in the trial function dependent upon the relative orientation of the deuteron with respect to the incident neutron. This procedure requires a knowledge of the regions of applicability and failure of the variational method, and in order to achieve this, some of the phases found earlier by an exact method, are recalculated by a variational method and the appropriate conclusions drawn. It is hoped in a later paper to extend the calculations to allow explicitly for the polarization by a variational method.

§ 2. THEORY

The notation used in the paper BM is adopted here throughout. If the internucleonic interaction is assumed to be purely central and of the form

$$\mathscr{V}(r)=(mM+hH+bB+w)V(r) \qquad \ldots\ldots(1)$$

where M, H, and B are the usual Majorana, Heisenberg and Bartlett exchange operators and m, h, b and w are numerical constants which satisfy the relations $m+h+b+w=1$ and $m-h+w-b=x$ with $x=0{\cdot}6$, then the integro-differential equations which describe the scattering of neutrons by deuterons can be written in the form

$$(\nabla^2+k^2)F(\mathbf{r})=\alpha U(r)F(\mathbf{r}) + \int\left\{\beta Q(\mathbf{r},\mathbf{r}')+\gamma\left(P(\mathbf{r},\mathbf{r}')+\left(1+\frac{E_{\mathrm{n}}}{E_{\mathrm{d}}}\right)N(\mathbf{r},\mathbf{r}')\right)\right\}F(\mathbf{r}')\,d\mathbf{r}'. \qquad \ldots\ldots(2)$$

The values assumed by α, β and γ for scattering in the quartet and doublet state are given in table 1.

Table 1

	Quartet	Doublet
α	$2w+2b-m-h$	$2w-b+\frac{1}{2}m-h$
β	$2m+2h-w-b$	$2m-h+\frac{1}{2}w-b$
γ	1	$-\frac{1}{2}$

In terms of the normalized ground state wave functions of the deuteron the potential functions and kernels arising in (2) can be written

$$\left.\begin{aligned}
U(r) &= \frac{4M}{3\hbar^2}\int |\chi(R)|^2 V(|\mathbf{r}+\tfrac{1}{2}\mathbf{R}|)\,d\mathbf{R}\\
Q(\mathbf{r},\mathbf{r}') &= \frac{4M}{3\hbar^2}\left(\frac{4}{3}\right)^3 \chi(u)V(t)\chi(v)\\
P(\mathbf{r},\mathbf{r}') &= \frac{4M}{3\hbar^2}\left(\frac{4}{3}\right)^3 [-\chi(u)\{V(u)+V(v)\}\chi(v)]\\
&\quad+\left(\frac{4}{3}\right)^5\left[\chi(u)\nabla_v^2\chi(v)+\chi(v)\nabla_u^2\chi(u)+\chi'(u)\chi'(v)\frac{\mathbf{u}\,.\,\mathbf{v}}{uv}\right]\\
N(\mathbf{r},\mathbf{r}') &= \frac{4M}{3\hbar^2}\left(\frac{4}{3}\right)^3 E_{\mathrm{d}}\chi(u)\chi(v)\\
u=\tfrac{2}{3}|2\mathbf{r}'+\mathbf{r}|,&\quad v=\tfrac{2}{3}|\mathbf{r}'+2\mathbf{r}|,\quad t=\tfrac{2}{3}|\mathbf{r}-\mathbf{r}'|.
\end{aligned}\right\}\qquad\ldots\ldots(3)$$

In the derivation of equation (2) the function $\chi(R)$ is assumed to satisfy the equation

$$\int \chi(R)\left(-\frac{\hbar^2}{M}\nabla^2+V(R)-E_{\mathrm{d}}\right)\chi(R)\,d\mathbf{R}=0. \qquad\ldots\ldots(4)$$

This leads to a less reduced form for the kernels (3), than was obtained by BM, who used the exact solution of the deuteron wave equation for $\chi(R)$. The necessity for the use of equation (4) in preference to the more restrictive assumption concerning $\chi(R)$ follows from the fact that one of the variational forms derived in § 3 will be inserted for $\chi(R)$.

Finally making use of the following expansions for the kernels in (3)

$$\left.\begin{matrix} Q(\mathbf{r},\mathbf{r}')\\ P(\mathbf{r},\mathbf{r}')\\ N(\mathbf{r},\mathbf{r}')\end{matrix}\right\} = \sum_l \frac{2l+1}{4\pi rr'}P_l(\cos\theta)\left\{\begin{matrix} q_l(r,r')\\ p_l(r,r')\\ n_l(r,r')\end{matrix}\right. \qquad\ldots\ldots(5)$$

and

$$F(\mathbf{r})=\frac{1}{r}\sum_l f_l(r)P_l(\cos\Theta)$$

where Θ is the angle of scattering in the centre-of-mass frame, and θ is the angle between $\mathbf{r}$ and $\mathbf{r}'$. Then equation (2) becomes

$$\begin{aligned}
\frac{d^2f_l(r)}{dr^2}+\left(k^2-\frac{l(l+1)}{r^2}\right)f_l(r) &= \alpha U(r)f_l(r)\\
&\quad+\int_0^\infty\left[\beta q_l(r,r')+\gamma\left\{p_l(r,r')+\left(1+\frac{E_{\mathrm{n}}}{E_{\mathrm{d}}}\right)n_l(r,r')\right\}\right]f_l(r')\,dr'. \qquad\ldots\ldots(6)
\end{aligned}$$

It is necessary to find a solution of equation (6) satisfying the boundary conditions

$$f_l(0)=0,\qquad f_l(r)\sim\sin(kr-\tfrac{1}{2}l\pi+\delta_l). \qquad\ldots\ldots(7)$$

§ 3. FORMS ASSUMED FOR POTENTIAL INTERACTION AND DEUTERON WAVE FUNCTION

The potential interaction between the nucleons is assumed to have the form

$$V(r)=V_0\exp(-\mu r^2). \qquad \ldots\ldots(8)$$

Calculations are carried out for the five potential ranges corresponding to $\mu=0{\cdot}2(0{\cdot}1)0{\cdot}6\times10^{26}\,\text{cm}^{-2}$. The potential well depth V_0 is adjusted in each case to give the observed binding energy of the deuteron $E=-2{\cdot}226$ Mev, the results of this calculation being given in table 2.

In order that the kernels and potential function arising in equation (6) can be evaluated analytically, the ground state of the deuteron is represented by the sum of two Gauss terms:

$$\chi(R)=\frac{1}{n}(\exp(-\alpha R^2)+c\exp(-\beta R^2)) \qquad \ldots\ldots(9)$$

where n is the normalization factor, and α, β and c are parameters dependent on the range parameter μ.

The following inequality for the binding energy exists:

$$E\leqslant\int\chi(r)\left\{-\frac{\hbar^2}{M}\nabla^2+V(r)\right\}\chi(r)\,d\mathbf{r} \qquad \ldots\ldots(10)$$

where the form of $\chi(r)$ to be used in (10) is that given by (9). Written out explicitly in terms of α, β and c, (10) becomes

$$E\leqslant\frac{\dfrac{3\hbar^2}{2M}\left[\left(\dfrac{1}{2\alpha}\right)^{1/2}+8c\alpha\beta\left(\dfrac{1}{\alpha+\beta}\right)^{5/2}+c^2\left(\dfrac{1}{2\beta}\right)^{1/2}\right]+V_0\left[\left(\dfrac{1}{\mu+2\alpha}\right)^{3/2}+2c\left(\dfrac{1}{\mu+\alpha+\beta}\right)^{3/2}+c^2\left(\dfrac{1}{\mu+2\beta}\right)^{3/2}\right]}{\left(\dfrac{1}{2\alpha}\right)^{3/2}+2c\left(\dfrac{1}{\alpha+\beta}\right)^{3/2}+c^2\left(\dfrac{1}{2\beta}\right)^{3/2}}. \qquad \ldots\ldots(11)$$

For each value of the range μ, the values of α, β and c are determined to make the right-hand side of (11) a minimum. It was found that this minimum, E_{min}, was very insensitive to the value of the variable c and it was therefore not possible or indeed necessary to determine c to the same accuracy as the other variables. The values of α, β and c together with E_{min} for each range are given in table 2.

Table 2

$\mu(10^{26}\,\text{cm}^{-2})$	V_0(Mev)	$\alpha(10^{26}\,\text{cm}^{-2})$	$\beta(10^{26}\,\text{cm}^{-2})$	c	E_{min}(Mev)
0·2	−37·37	0·02618	0·1497	2·739	−2·167
0·3	−51·39	0·0318	0·204	2·73	−2·119
0·4	−64·98	0·0356	0·249	2·825	−2·073
0·5	−78·26	0·04067	0·3027	2·759	−2·0222
0·6	−91·33	0·04430	0·3484	2·779	−1·9695

Parameters associated with the deuteron wave function.

It can be seen from the fact that E_{min} approaches more closely the experimental value of the deuteron binding energy $E=-2{\cdot}226$ Mev as the range parameter μ decreases that (9) affords the best representation of the deuteron ground state for the long range potential. This may be due to the fact that the part of the wave function in the asymptotic region where the potential is negligible gives a smaller contribution to the expectation value of the Hamiltonian for the long range potentials and it is in this region that (9) is most obviously in error.

It should be noted that in order to make the formalism self-consistent, the value inserted for E_{d} in equations (3) and (6) is the appropriate $E_{\min}$ given in table 2.

§ 4. KERNELS AND POTENTIAL FUNCTIONS

Using the Gaussian forms (8) and (9) for the potential interaction and the ground state of the deuteron, then the potential function $U(r)$ and the kernels $q_l(r, r')$, $p_l(r, r')$ and $n_l(r, r')$ defined by equations (3) and (5) may all be evaluated analytically.

Defining the hyperbolic spherical Bessel function

$$\mathscr{I}_{l+1/2}(x) = (-1)^l \left(\frac{\pi x}{2}\right)^{1/2} \exp\left(-\frac{(l+\frac{1}{2})i\pi}{2}\right) J_{l+1/2}(ix)$$

the first two functions being

$$\mathscr{I}_{1/2}(x) = \sinh x, \qquad \mathscr{I}_{3/2}(x) = \frac{\sinh x}{x} - \cosh x$$

and writing $\mathscr{I}'_{l+1/2}(x)$ for $(d/dx)\mathscr{I}'_{l+1/2}(x)$, it can be shown that

$$\left.\begin{aligned}
U(r) = \frac{16\pi^2 M V_0}{3n^2h^2} &\left\{\left(\frac{\pi}{2\alpha+\mu/4}\right)^{3/2} \exp\left[-r^2 \frac{2\alpha\mu}{2\alpha+\mu/4}\right]\right. \\
&+ 2c\left(\frac{\pi}{\alpha+\beta+\mu/4}\right)^{3/2} \exp\left[-r^2 \frac{\mu(\alpha+\beta)}{\alpha+\beta+\mu/4}\right] \\
&\left.+ c^2\left(\frac{\pi}{2\beta+\mu/4}\right)^{3/2} \exp\left[-r^2 \frac{2\beta\mu}{2\beta+\mu/4}\right]\right\} \\
q_l(r, r') = A_1 \exp c_3 &\left\{\frac{1}{s_1} \exp(a_1+a_2)\mathscr{I}_{l+1/2}(2s_1)\right. \\
&+ \frac{2c}{s_1+t_1}(\exp(a_2+b_1)+\exp(a_1+b_2))\mathscr{I}_{l+1/2}(s_1+t_1) \\
&\left.+ \frac{c^2}{t_1}\exp(b_1+b_2)\mathscr{I}_{l+1/2}(2t_1)\right\} \\
n_l(r, r') = A_2 &\left\{\frac{1}{a_3} \exp(a_1+a_2)\mathscr{I}_{l+1/2}(2a_3)\right. \\
&+ \frac{2c}{a_3+b_3}(\exp(a_2+b_1)+\exp(a_1+b_2))\mathscr{I}_{l+1/2}(a_3+b_3) \\
&\left.+ \frac{c^2}{b_3}\exp(b_1+b_2)\mathscr{I}_{l+1/2}(2b_3)\right\} \\
p_l(\mathbf{r}, \mathbf{r}') = -A_1(\exp c_1 + \exp c_2) &\left\{\frac{1}{s_2} \exp(a_1+a_2)\mathscr{I}_{l+1/2}(2s_2)\right. \\
&+ \frac{2c}{s_2+t_2}(\exp(a_2+b_1)+\exp(a_1+b_2))\mathscr{I}_{l+1/2}(s_2+b_2) \\
&\left.+ \frac{c^2}{t_2}\exp(b_1+b_2)\mathscr{I}_{l+1/2}(2t_2)\right\} \\
&+ A_3\{\exp(a_1+a_2)(a_4\mathscr{I}_{l+1/2}(2a_3) - a_5\mathscr{I}'_{l+1/2}(2a_3)) \\
&+ c((d_1r^2 + d_2r'^2 + d_3)\exp(a_2+b_1) \\
&+ (d_2r^2 + d_1r'^2 + d_3)\exp(a_1+b_2))\mathscr{I}_{l+1/2}(a_3+b_3) \\
&- cd_4(\exp(a_2+b_1)+\exp(a_1+b_2))\mathscr{I}'_{l+1/2}(a_3+b_3) \\
&+ c^2\exp(b_1+b_2)(b_4\mathscr{I}_{i+1/2}(2b_3) - b_5\mathscr{I}'_{l+1/2}(2b_3))\}
\end{aligned}\right\} \quad \ldots\ldots(12)$$

where the following quantities have been defined

$$\left.\begin{array}{llll}
A_1=\dfrac{2048\pi^3MV_0rr'}{81n^2h^2} & A_2=A_1\dfrac{E_{\mathrm{d}}}{V_0} & A_3=\dfrac{4096\pi}{243n^2} & \\
a_1=-\dfrac{4}{9}\alpha(4r^2+r'^2), & b_1=-\dfrac{4}{9}\beta(4r^2+r'^2), & s_1=-\dfrac{4}{9}(\mu-4\alpha)rr', & \\
 & d_1=\dfrac{\alpha^2+4\beta^2+2\alpha\beta}{\alpha+\beta}, & & c_1=-\dfrac{4}{9}\mu(4r^2+r'^2), \\
a_2=-\dfrac{4}{9}\alpha(r^2+4r'^2), & b_2=-\dfrac{4}{9}\beta(r^2+4r'^2), & s_2=\dfrac{8}{9}(\mu+2\alpha)rr', & \\
 & d_2=\dfrac{4\alpha^2+\beta^2+2\alpha\beta}{\alpha+\beta}, & & c_2=-\dfrac{4}{9}\mu(r^2+4r'^2), \\
a_3=\dfrac{16}{9}\alpha rr', & b_3=\dfrac{16}{9}\beta rr', & t_1=-\dfrac{4}{9}(\mu-4\beta)rr', & \\
 & d_3=\dfrac{-\dfrac{9}{8}\left(\alpha^2+\beta^2+\dfrac{7}{2}\alpha\beta\right)}{(\alpha+\beta)^2}, & & c_3=-\dfrac{4}{9}\mu(r^2+r'^2), \\
a_4=\dfrac{7}{2}\alpha(r^2+r'^2)-\dfrac{99}{64}, & b_4=\dfrac{7}{2}\beta(r^2+r'^2)-\dfrac{99}{64}, & t_2=\dfrac{8}{9}(\mu+2\beta)rr', & \\
 & d_4=\dfrac{4\alpha^2+4\beta^2+5\alpha\beta}{\alpha+\beta}rr', & & \\
a_5=\dfrac{13}{2}\alpha rr', & b_5=\dfrac{13}{2}\beta rr', & n^2=\left(\dfrac{\pi}{2\alpha}\right)^{3/2}+2c\left(\dfrac{\pi}{\alpha+\beta}\right)^{3/2}+c^2\left(\dfrac{\pi}{2\beta}\right)^{3/2}. &
\end{array}\right\} \qquad \ldots\ldots(13)$$

§ 5. Method of Calculation

Programmes have been prepared (Robertson 1956) for the solution of equations of the form (6) and these were used to carry out the calculations on the Pilot ACE at the National Physical Laboratory. The programmes represent the integro-differential equation as a set of simultaneous equations with a maximum of thirty equally spaced points in the range of integration, and in the simplest mode of operation a truncation error exists in the finite difference representation.

The weak binding of the deuteron results in the deuteron 'size' exceeding quite appreciably the range of the potential. This effect is exemplified by the difference between μ and α in table 2. The p and n kernels which have parts depending only on the range of the deuteron, extend out much further than the q kernel. The rapidly varying nature of the q kernel near the origin requires a small interval of tabulation to enable the finite difference representation of the integro-differential equation to be convergent and, with the appropriate interval to accomplish this, there is still a contribution arising from the tail of the kernels which is not taken into account when the tabulation is limited to thirty points.

Ideally it would have been preferable either to divide the range into two parts and tabulate the kernel in the region near the origin at a small interval and in the asymptotic region at a large interval, or to include more than thirty equally spaced points in the range of integration. Both these methods would involve severe modifications of the available programme and it must also be remembered that if n is the number of points, the work of tabulating the kernels increases as n^2, and of solving the simultaneous equations as n^3. Approximate methods were thus used to avoid these modifications.

A preliminary investigation was carried out for the potential range corresponding to $\mu = 0{\cdot}6 \times 10^{26}\ \mathrm{cm}^{-2}$ for $l = 0$ and symmetric exchange forces. The kernels were tabulated and the equations solved for four intervals of integration $h = 0{\cdot}4, 0{\cdot}5, 0{\cdot}65, 0{\cdot}75 \times 10^{-13}$ cm, and for four energies corresponding to $k = 0{\cdot}075$, $0{\cdot}12$, $0{\cdot}2$ and $0{\cdot}4 \times 10^{13}\ \mathrm{cm}^{-1}$. In each case the phases were calculated using the values of the wave function at the last three pairs of points in the range, i.e. (f_{n-3}, f_{n-2}), (f_{n-2}, f_{n-1}) and (f_{n-1}, f_n). This gives three values of the phase η_{n-2}, η_{n-1}, and η_n which are identical if the kernels are sufficiently negligible at the end of the range of integration. If, however, the kernels have not completely died away an estimate of the asymptotic phase η_{lim} can be obtained by a formula due to Aitken (1937):

$$\eta_{\mathrm{lim}} = \frac{\eta_n \eta_{n-2} - \eta^2_{n-1}}{\eta_{n-2} - 2\eta_{n-1} + \eta_n}. \qquad \ldots\ldots(14)$$

This assumes that the approximate phases η_r are the successive partial sums of a geometric progression. Table 3 gives the results of this investigation, and figure 1 shows typical cases of the behaviour of the radial wave function.

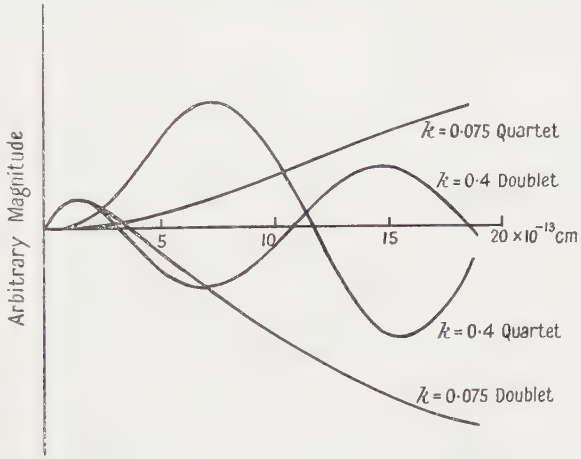

Figure 1. Radial wave functions corresponding to symmetrical exchange forces for $l = 0$ and the potential range $\mu = 0{\cdot}6 \times 10^{26}\ \mathrm{cm}^{-2}$.

From figure 1 the quartet wave functions are seen to be very small in the neighbourhood of the origin, that is in the region where the q kernel is most rapidly varying and thus the truncation error is small. The difficulty is therefore in this case removed by taking the interval appropriate to the p and n kernels. This view is borne out by a consideration of the phases η_{lim} corresponding to the intervals of integration $h = 0{\cdot}65$ and $0{\cdot}75$ (table 3). Thus it may be assumed that η_{lim} for $h = 0{\cdot}65$ quartet is given to about $\pm 0{\cdot}005^\circ$. From a consideration of η_{lim} for $h = 0{\cdot}4$ and $0{\cdot}5$ it appears that the Aitken limiting process gives reasonable results (within $0{\cdot}1^\circ$) for $h = 0{\cdot}5$ but not for $h = 0{\cdot}4$.

The doublet case is far more difficult since figure 1 shows that the wave function is large and rapidly varying in the neighbourhood of the origin, and thus the phases are strongly influenced by the truncation error in the q kernel integration, this effect increasing with increasing interval. From the point of view of this error alone, it is desirable to take as small an interval h as possible, but from the quartet phase case it was shown that the Aitken process was not

Table 3

Interval of Integration		Quartet 0·4	Quartet 0·5	Quartet 0·65	Quartet 0·75	Doublet 0·4	Doublet 0·5	Doublet 0·65	Doublet 0·75
$k=0{\cdot}075$	η_{n-2}	18·174	−21·100	−21·830	−21·854	−14·826	−13·039	−11·825	−10·547
	η_{n-1}	−18·580	−21·273	−21·841	−21·855	−14·591	−12·912	−11·819	−10·548
	η_n	−18·938	−21·411	−21·847	−21·856	−14·372	−12·811	−11·817	−10·549
	η_{lim}	−21·608	−21·955	−21·854	−21·856	−11·374	−12·419	−11·816	−10·549
$k=0{\cdot}12$	η_{n-2}	−29·014	−33·279	−34·238	−34·263	−23·299	−20·864	−19·258	−17·408
	η_{n-1}	−29·626	−33·521	−34·249	−34·263	22·950	−20·704	−19·252	17·409
	η_n	−30·161	−33·708	−34·255	−34·264	−22·631	20·583	−19·250	−17·409
	η_{lim}	33·878	−34·346	−34·262	−34·264	−19·239	−20·208	−19·249	−17·409
$k=0{\cdot}2$	η_{n-2}	−47·924	−53·147	−53·939	−53·949	−37·151	−34·809	−33·145	−30·702
	η_{n-1}	−48·766	−53·396	−53·943	−53·949	−36·712	−34·694	−33·145	−30·702
	η_n	−49·481	−53·571	−53·944	−53·949	−36·337	−34·618	−33·145	−30·702
	η_{lim}	−53·506	−53·985	−53·944	−53·949	−34·140	−34·470	−33·145	−30·702
$k=0{\cdot}4$	η_{n-2}	−88·459	−88·257	−87·916	−87·924	−67·079	−67·929	−66·362	−63·563
	η_{n-1}	−88·751	−88·187	−87·917	−87·924	−67·082	−67·953	−66·361	−63·563
	η_n	−88·886	−88·145	−87·918	−87·924	−67·121	−67·962	−66·361	−63·563
	η_{lim}	−89·002	−88·082	−87·918	−87·924	−67·079	−67·967	−66·361	−63·563

The phases η_{n-2}, η_{n-1}, η_n together with the Aitken asymptotic phase η_{lim} calculated for the four intervals of integration $h=(0{\cdot}4,\ 0{\cdot}5,\ 0{\cdot}65,\ 0{\cdot}75)\times 10^{-13}$ cm, for $l=0$ and a symmetrical exchange interaction for the potential range $\mu=0{\cdot}6\times 10^{26}\text{cm}^{-2}$.

reliable for $h<0{\cdot}5$. From the three reliable phases corresponding to $h=0{\cdot}5$, 0·65 and $0{\cdot}75\times10^{-13}$ cm it appears that the correct phase will not differ from that obtained for $h=0{\cdot}5$ by more than one degree.

An investigation was then carried out to determine equivalent intervals of integration for the other values of μ, the criterion used being that the kernels should have fallen off by about the same ratio as in the case considered above corresponding to $\mu=0{\cdot}6\times10^{26}\ \mathrm{cm}^{-2}$. The results are given in table 4. These intervals were used for all the partial waves considered.

Table 4

Interval of integration	0·65	0·65	0·6	0·5	0·5
$\mu(10^{26}\ \mathrm{cm}^{-2})$	0·2	0·3	0·4	0·5	0·6

§ 6. RESULTS

Phases were evaluated for three types of exchange force, symmetrical (MHWB), Serber and ordinary (WB). Two angular momenta corresponding to $l=0, 1$ were considered.

Table 5

		MHWB		Serber		WB	
	μ	Quartet	Doublet	Quartet	Doublet	Quartet	Doublet
$k=0{\cdot}075$	0·6	−21·955	−12·419	−21·944	−11·787	−21·806	−11·000
	0·5	−22·953	−12·264	−22·850	−11·456	−22·746	−10·738
	0·4	−23·940	−12·500	−23·780	−11·650	−23·639	−10·706
	0·3	−24·880	−13·008	−24·819	−11·906	−24·539	−10·864
	0·2	−26·783	−13·792	−26·670	−12·412	−26·126	−11·020
	BHM	−20	−17			−16	−14
$k=0{\cdot}12$	0·6	−34·346	−20·208	−34·313	−19·072	−34·066	−18·104
	0·5	−35·665	−20·207	−35·578	−18·981	−35·314	−17·956
	0·4	−37·115	−20·506	−36·938	−19·250	−36·614	−18·100
	0·3	−38·790	−21·491	−38·667	−19·868	−38·146	−18·337
	0·2	−41·636	−23·012	−41·426	−20·944	−41·443	−18·884
$k=0{\cdot}2$	0·6	−53·985	−34·470	−53·864	−32·838	−53·363	−31·419
	0·5	−55·600	−34·972	−55·445	−33·229	−54·795	−31·690
	0·4	−57·850	−35·824	−57·425	−33·941	−56·617	−32·240
	0·3	−60·274	−37·761	−59·999	−35·382	−58·817	−33·142
	0·2	−64·371	−40·736	−63·886	−37·696	−61·576	−34·649
	BHM	−53	−45			−43	−38
$k=0{\cdot}4$	0·6	−88·082	−67·967	−87·536	−65·308	−85·404	−62·955
	0·5	−90·896	−69·635	−89·104	−66·683	−86·761	−64·016
	0·4	−93·008	−72·013	−92·197	−68·673	−89·104	−65·595
	0·3	−96·871	−75·775	−95·729	−71·464	−90·896	−67·340
	0·2	−103·295	−81·692	−101·359	−75·839	−90·916	−69·935
	BHM	−94	−80			−84	−73

S phases in degrees. Results of BHM incorporated where available.

6.1. *S Phases*

Table 5 gives the results obtained for four energies varying up to 7 MEV incident neutron energy in the laboratory system. Where available the results of BHM using an exponential potential $V(r)=V_0\exp(-2r/a)$ are incorporated in the table. It is estimated that their range, $a=1{\cdot}73\times10^{-13}$ cm, corresponds to a value of μ in the neighbourhood of $\mu = 0{\cdot}3 \times 10^{26}$ cm^{-2}. It can be seen that there is very little dependence of the phases on the exchange nature of the forces, any difference there is tending to increase with increasing potential range, and increasing neutron energy.

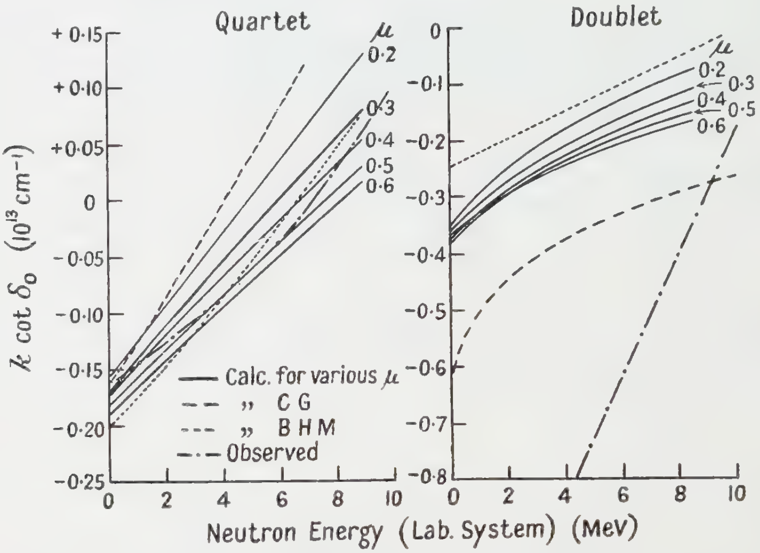

Figure 2. Comparison of the 'observed' and calculated zero-order phase shifts for n–d scattering. The full curves are for Serber forces for the five potential ranges $\mu = 0{\cdot}2,\ 0{\cdot}3,\ 0{\cdot}4,\ 0{\cdot}5,\ 0{\cdot}6 \times 10^{26}$ cm^{-2}.

In figure 2 values of $k \cot \delta_0$ for the Serber interaction are plotted against the incident neutron energy, for the quartet and doublet phases. For the low energy neutron–deuteron scattering a formula of the Blatt–Jackson type (1949) exists, i.e.

$$k \cot \delta_0 = -\frac{1}{a} + \frac{1}{2} r_0 k^2 + O(k^4). \qquad \ldots\ldots(15)$$

Also on the figure are plotted the curves calculated by BHM and by CG. The experimental values of $k \cot \delta$ have been derived by CG from an analysis of the observed differential cross sections and the zero energy scattering lengths. It is apparent from these curves that the dependence of the zero order phases on the potential range is small, although from a consideration of the quartet curves alone it would appear that over the energy range of approximately 2–8 Mev a potential corresponding to $\mu = (0{\cdot}4\text{–}0{\cdot}5) \times 10^{26}$ cm^{-2} is best. The slight deviation from linearity in the curves indicates a small contribution from the higher order terms $O(k^4)$ in (15).

The low energy scattering of neutrons by deuterons involves an important decision as to which of two allowed pairs of scattering lengths is correct. It was found by Wollan, Schull and Koehler (1951) that the lengths are either

$$a_{\mathrm{d}} = 8{\cdot}3 \times 10^{-12}\ \text{cm}, \qquad a_{\mathrm{q}} = 2{\cdot}4 \times 10^{-12}\ \text{cm} \qquad \ldots\ldots(16)$$

or

$$a_{\mathrm{d}} = 0{\cdot}8 \times 10^{-13}\ \text{cm}, \qquad a_{\mathrm{q}} = 6{\cdot}2 \times 10^{-13}\ \text{cm}. \qquad \ldots\ldots(17)$$

The scattering lengths obtained in this paper were read from the zero energy intercepts on the $k \cot \delta$ axis of figure 2, and are given for each range in table 6.

Table 6

$\mu(10^{26}\text{cm}^{-2})$	0·2	0·3	0·4	0·5	0·6
$a_q(10^{-13}\text{ cm})$	6·37	5·95	5·68	5·43	5·24
$a_d(10^{-13}\text{ cm})$	2·82	2·72	2·67	2·62	2·72

Scattering lengths a_q and a_d for Serber forces, obtained for each value of the potential range.

These seem to favour the second set of scattering lengths given by (17) and in this respect are in agreement with CG's results. The observed value of a_q given by (17) is very close to that obtained for the long range potential $\mu \sim (0{\cdot}2, 0{\cdot}3) \times 10^{26}\text{ cm}^{-2}$, however agreement is completely lacking for the doublet scattering length. Also, owing to the presence of a minimum in the variation of the doublet scattering length with the potential range occurring in the neighbourhood of $\mu = 0{\cdot}5 \times 10^{26}\text{ cm}^{-2}$, no better agreement can be expected outside the potential ranges considered. Only an explicit inclusion of polarization effects is therefore liable to improve this situation.

6.2. *P Phases*

Table 7 gives the P phases evaluated at three energies for three exchange forces. Also included in the table are the MHWB phases for $k = 0{\cdot}075 \times 10^{13}\text{ cm}^{-1}$

Table 7

		MHWB		Serber		WB	
	μ	Quartet	Doublet	Quartet	Doublet	Quartet	Doublet
$k=0{\cdot}2$	0·6	+16·925	−5·659	+17·726	−5·791	+21·944	−5·424
	0·5	+17·890	−6·590	+18·927	−6·153	+25·065	−5·881
	0·4	+19·252	−7·048	+20·640	−6·453	+30·071	−5·692
	0·3	+20·906	−7·767	+23·085	−6·837	+42·301	−5·492
	0·2	+23·499	−9·001	+27·594	−7·250	+83·306	−4·085
	CG	+13·5	−7·2	+14·0	−6·4	+15·5	−5·8
	BHM	+14·3	−4·58			+32·6	−0·57
$k=0{\cdot}4$	0·6	+22·461	−12·741	+25·995	−9·777	+39·875	−5·948
	0·5	+22·612	−13·189	+25·965	−9·280	+46·296	−3·822
	0·4	+23·286	−13·320	+27·554	−8·033	+56·115	+0·280
	0·3	+23·858	−14·493	+29·952	−6·463	+73·403	+8·576
	0·2	+24·497	−16·895	+34·047	−2·826	−83·215	+30·166
	CG	+23·8	−14·9	+27·0	− 9·7	+36·7	−5·8
	BHM	+31·5	−14·3			+77·3	−24·6
$k=0{\cdot}6$	0·6	+18·538	−11·418	+23·008	−1·710	+50·152	+11·7
	0·5	+18·513	−12·080	+24·563	+0·134	+57·686	+18·011
	0·4	+18·781	−11·881	+26·096	+3·722	+66·487	+27·277
	0·3	+18·451	−13·685	+27·974	+7·741	+77·350	+39·610
	0·2	+17·292	−17·463	+30·238	+13·608	+87·975	+53·560
	CG	+18·7	−14·55	+25·0	−4·5	+43·8	+2·9
	BHM	+17·2	−10·9				

MHWB

	$k=0{\cdot}075$		$k=0{\cdot}12$	
0·6	+ 1·609	− 0·635	+ 5·803	− 2·040
0·5	+ 1·920	− 0·682	+ 6·621	− 2·420
0·4	+ 1·989	− 0·727	+ 7·129	− 2·435
0·3	+ 2·315	− 0·838	+ 8·185	− 2·784
0·2	+ 2·910	− 1·040	+10·010	− 3·339

P phases in degrees. Results of BHM and CG incorporated where available.

and $k = 0{\cdot}12 \times 10^{13}$ cm^{-1}, evaluated in order to allow the total cross section curve to be plotted below 2 Mev. Where available the phases obtained by BHM and those of CG read from figure 1 of their paper are given. CG used a Gaussian interaction corresponding to $\mu = 0{\cdot}56 \times 10^{26}$ cm^{-2} and their results were obtained by use of the Born approximation.

It can be seen that the Born approximation gives results considerably better than previously suspected, but as pointed out by de BM it fails more noticeably for ordinary forces than for symmetrical exchange and Serber forces. Since α, the coefficient of the integral $J_1(\theta)$ arising in the Born approximation, CG equation (5), has its largest value for ordinary forces it is probable that the Born approximation representation of $U(r)$ as $J_1(\theta)$ contributes the largest proportion of this error. The dependence of the phase shift on the exchange nature of nuclear forces is very marked and increases with increasing potential range. Because the comparison of the S phases with the experimental results favours the long range potential, it should be easy to distinguish essentially exchange-type forces from ordinary forces, although it may be more difficult to decide whether Serber or symmetrical exchange forces represent actuality best.

6.3. *Total Cross Section*

The total cross section below 2 Mev is given in figure 3 for symmetrical exchange forces, phases for $l = 0$, 1 being included. Below 2 Mev the contribution to the total cross section from phases with $l \geqslant 2$ is negligible. It can be seen that the potential range corresponding to $\mu = 0{\cdot}3 \times 10^{26}$ cm^{-2} agrees very well over the whole energy range with the experimental results obtained by Nuckolls *et al.* (1946). BHM's curve evaluated for the long range potential gives too small a cross section. This is no doubt due to inaccuracies in their interpolation. The reason why an approximate total cross section which neglects polarization does not conflict with the experimental results at these low energies, is probably that the contribution from the polarization dependent doublet phases is so small.

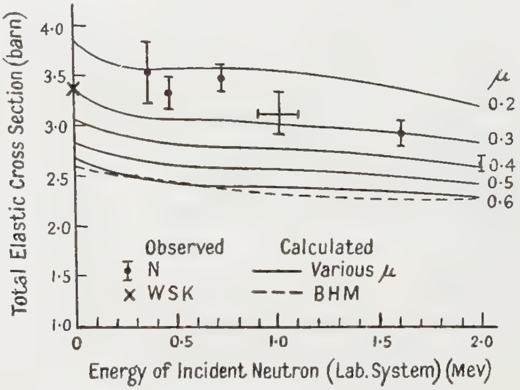

Figure 3. Comparison of the observed and calculated total elastic cross sections for neutron–deuteron scattering below 2 Mev in the laboratory system. The full curves are for symmetrical exchange forces for the five potential ranges $\mu = 0{\cdot}2$, $0{\cdot}3$, $0{\cdot}4$, $0{\cdot}5$, $0{\cdot}6 \times 10^{26}$ cm. N, Nuckolls *et al.*, WSK, Wollan, Shull and Koehler.

§ 7. VARIATIONAL METHOD

In the derivation of equation (2) all the continuous state terms in the expansion

$$\phi(\overline{12}, 3) = \chi(\mathbf{R})F(\mathbf{r}) + \int \chi_{\mathrm{K}}(\mathbf{R})F_{\mathrm{K}}(\mathbf{r})\,dK \qquad \ldots\ldots(18)$$

have been neglected. Here $\phi(\overline{12}, 3)$ is the space function, defined by BM representing the three nucleons, and $\chi(\mathbf{R})$ and $\chi_{\mathrm{K}}(\mathbf{R})$ are the ground state and continuous state wave functions of the deuteron respectively. This neglect is equivalent to assuming that the deuteron is unpolarized by the incident neutron. The use of the exact expansion (18) for $\phi(\overline{12}, 3)$ would result in an infinite set of coupled equations.

The variational method offers another method of allowing for the polarization of the deuteron. If a term is included in the trial function which would to some extent allow for the neglected continuous state terms of equation (18) then it can be expected that the resulting phases would give a better indication of this low energy scattering. This type of programme has been attempted with success in the domain of atomic collisions where in particular MM allowed for the polarization of hydrogen atoms by incident electrons. It was found there that the experimental results can be explained provided the variational method is used in a region of known applicability.

Thus, to provide a basis for an eventual extension of the work to allow for polarization, the approximate equation (6) without polarization has been solved using the variational methods of Hulthén and Kohn and the phases compared with those obtained by the exact solution in § 6.

The variational method starts from the integral

$$I_l = \int_0^\infty f_l^*(r) L f_l(r)\,dr \qquad \ldots\ldots(19)$$

where

$$Lf_l(r) = \left\{\frac{d^2}{dr^2} + k^2 - \frac{l(l+1)}{r^2} - \alpha U(r)\right\} f_l(r)$$
$$- \int_0^\infty \left\{\beta q_l(r, r') + \gamma\left(p_l(r, r') + \left(1 + \frac{E_{\mathrm{n}}}{E_{\mathrm{d}}}\right) n_l(r, r')\right)\right\} f_l(r')\,dr'. \qquad \ldots\ldots(20)$$

Since the polarization is essentially a low energy effect, this paper will only be concerned with S-wave scattering. The trial function is taken in this case to be

$$f_0(r) = (1 - b\exp(-\nu r^2))\sin kr + (a - c\exp(-\nu r^2))(1 - \exp(-\nu r^2))\cos kr \quad \ldots(21)$$

where ν is a range parameter, and a, b and c are the arbitrary variational parameters. It can be seen from equation (21) that $f_0(r)$ obeys the correct boundary conditions

$$f_0(0) = 0, \qquad f_0(r) \sim \sin kr + a\cos kr. \qquad \ldots\ldots(22)$$

Hulthén's method leads to the following equations

$$I_0(a, b, c) = 0, \qquad \partial I_0/\partial b = 0, \qquad \partial I_0/\partial c = 0 \qquad \ldots\ldots(23)$$

giving a quadratic equation for the phase $\delta = \tan^{-1} a$. Kohn's linear method uses the equations

$$\partial I_0/\partial a = -k, \quad \partial I_0/\partial b = 0, \quad \partial I_0/\partial c = 0, \quad \delta = \tan^{-1}(a + I_0/k). \quad \ldots\ldots(24)$$

In practice it is usually fairly easy to decide which of the two Hulthén phases is the correct one. This may be done for instance by a comparison with that obtained by Kohn's method.

In the above treatment the range parameter ν is regarded as a predetermined constant; however there is no indication so far concerning the numerical value to be assigned to it. Ideally it would be advantageous to be able to treat ν as a fourth variational parameter and so avoid the necessity of choosing a value for it. This method, however, would change the simultaneous equations given by (23) and (24) from their present linear and quadratic form into transcendental equations, the solution of which would be extremely difficult. It was therefore decided to solve the equations (23) and (24) for several fixed values of ν, these being chosen to include all physically significant ranges. The best value of the range parameter ν is then determined from a comparison of the variational phase with the phase obtained by the exact solution given in § 6.

The coefficients for the simultaneous equations (23) and (24) were obtained by representing the kernels $q_0(r, r')$, $p_0(r, r')$ and $n_0(r, r')$ as 30×30 matrices and $f_0{}^*(r)$ and $f_0(r)$ as row and column vectors respectively, the appropriate computation being done by means of standard matrix programmes on the DEUCE.

The variational calculation was carried out for one potential range corresponding to $\mu = 0{\cdot}6 \times 10^{26}\,\text{cm}^{-2}$ for the four energies corresponding to $k = 0{\cdot}075$, $0{\cdot}12$, $0{\cdot}2$ and $0{\cdot}4 \times 10^{13}\,\text{cm}^{-1}$. Only symmetrical exchange forces were considered since by reference to table 5 it can be seen that the S phases are largely independent of the exchange force used. The phase was evaluated for eleven values of ν in the range $(0{\cdot}02\text{–}0{\cdot}5) \times 10^{26}\,\text{cm}^{-2}$ for the quartet phases and for ten values in the range $(0{\cdot}03\text{–}0{\cdot}5) \times 10^{26}\,\text{cm}^{-2}$ for the doublet phases, these ranges including the parameters α and β arising in the deuteron ground state (table 2).

It has been shown in § 5 that at the interval of integration given in table 4 there is a contribution arising from the tail of the kernels which, in the case of the exact solution, is allowed for to some extent by Aitken's formula (14). Since in the variational calculation Aitken's method is no longer applicable then any phases obtained will possess a further uncertainty besides that inherent in the variational method. Reference to table 3 shows that this uncertainty is unlikely to exceed about $0{\cdot}5^\circ$.

In figure 4 are plotted the Kohn phase and the appropriate Hulthén phase as a function of $\log \nu$. The exact phase is given in each case. A significant feature of the results is that the Hulthén method gives imaginary phases for the shorter range trial functions. The reason for this lies in the inability of the trial function used to represent closely the radial wave function for these ν values, and its greater predominance in the quartet state is due to the nature of the quartet radial wave functions near the origin (figure 1). This particular feature of the quartet wave function is representable by the trial function (21) if ν is small and $b \simeq 1$.

The results in general show that the Kohn method is to be preferred to the Hulthén method in this particular problem. This statement is based on three features of the results, namely: (i) the Kohn method gives a phase for all ν values whereas the Hulthén method is limited to regions where it is real, (ii) the variation of the Kohn phase with ν is less rapid than the corresponding variation of the Hulthén phase and (iii) in general the Kohn phase lies nearer to the exact phase than the Hulthén phase.

Figure 4 shows that a minimum occurs in the doublet (Kohn phase, $\log \nu$) plots for $\nu = 0{\cdot}2 \times 10^{26}\,\text{cm}^{-2}$ and this minimum is stable with respect to variations in the energy. Since the quartet Kohn phase is also reasonable in this neighbourhood,

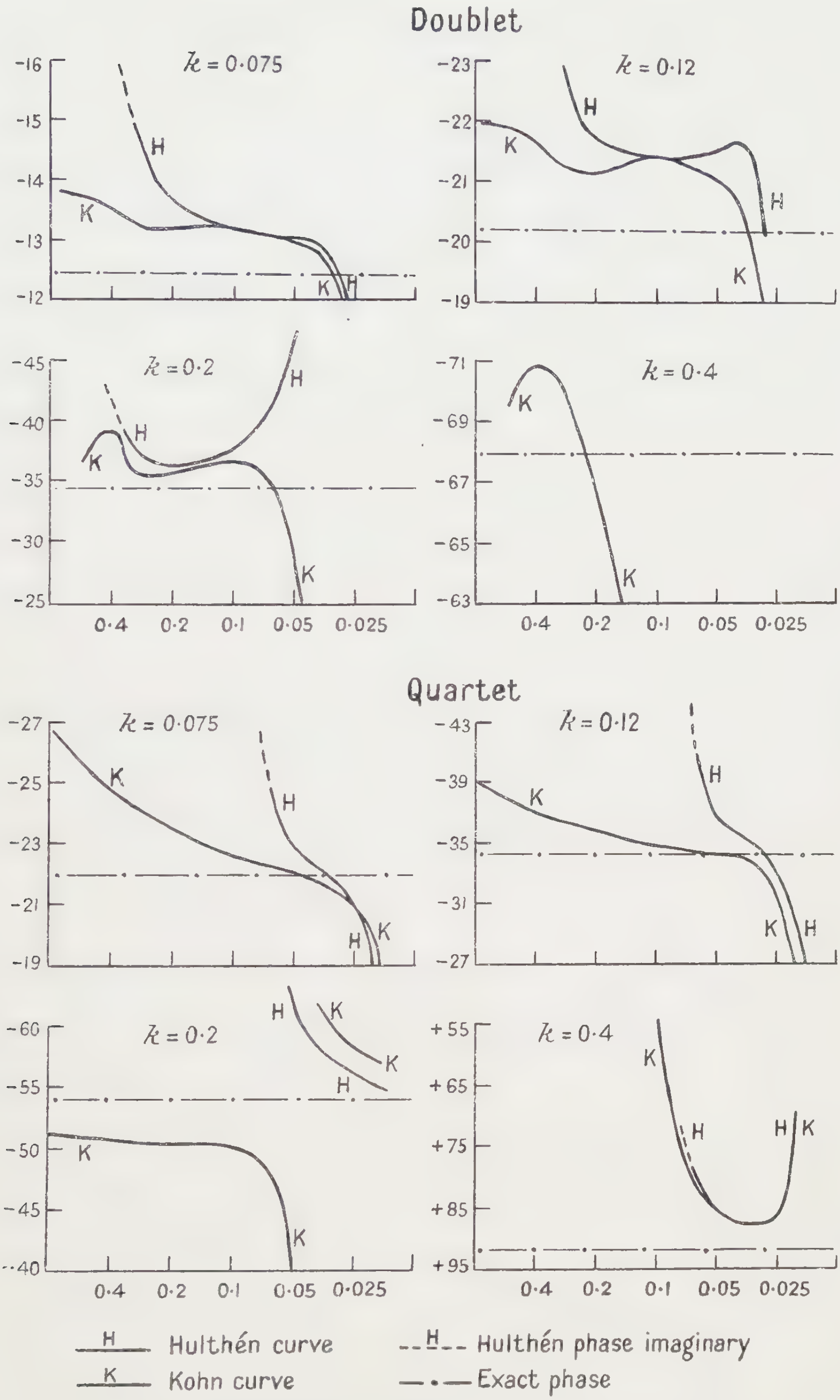

Figure 4. The variational phase in degrees plotted against the logarithm of the range parameter ν for the quartet and doublet states.

it is proposed to use this ν value for the polarization calculation. Phases for energies corresponding to $k \leqslant 0{\cdot}2 \times 10^{13}$ cm^{-1} will be obtained, this being the region where the polarization has most effect.

ACKNOWLEDGMENTS

We are greatly indebted to Professor H. S. W. Massey for suggesting the problem and for his continued interest shown throughout the course of the work, and to Dr. R. A. Buckingham for many helpful discussions and for checking parts of the formulation.

Some of the work described above has been carried out as part of the research programme of the National Physical Laboratory and our thanks are due to the Director for permission to publish.

Finally, one of us (P. G. B.) wishes to thank the University of London for a Granville Postgraduate Studentship.

REFERENCES

AITKEN, A. C., 1937, *Proc. Roy. Soc. Edinb.*, **57,** 269.
BLATT, J. M., and JACKSON, J. D., 1949, *Phys. Rev.*, **76,** 18.
DE BORDE, A. H., and MASSEY, H. S. W., 1955, *Proc. Phys. Soc.* A, **68,** 769.
BUCKINGHAM, R. A., HUBBARD, S. J., and MASSEY, H. S. W., 1952, *Proc. Roy. Soc.* A, **211,** 183.
BUCKINGHAM, R. A., and MASSEY, H. S. W., 1941, *Proc. Roy. Soc.* A, **179,** 123.
CHRISTIAN, R. S., and GAMMEL, J. L., 1953, *Phys. Rev.*, **91,** 100.
HULTHÉN, L., 1944, *K. Fysiogr. Sällsk. Lund Förh.*, **14,** 257.
KOHN, W., 1948, *Phys. Rev.*, **74,** 1763.
MASSEY, H. S. W., and MOISEIWITSCH, B. L., 1951, *Proc. Roy. Soc.* A, **205,** 483.
NUCKOLLS, R. G., BAILEY, C. L., BENNETT, W. E., BERGSTRALH, T., RICHARDS, H. T., and WILLIAMS, J. H., 1946, *Phys. Rev.*, **70,** 805.
ROBERTSON, H. H., 1956, *Proc. Camb. Phil. Soc.*, **52,** 538.
WOLLAN, E. O., SHULL, C. G., and KOEHLER, W. C., 1951, *Phys. Rev.*, **83,** 700.

Slowing Down of Neutrons in Infinite Homogeneous Media†

By N. CORNGOLD
Brookhaven National Laboratory, Upton, New York

MS. received 7th June 1957, *and in final form 30th July* 1957

Abstract. We have derived from the Boltzmann equation a new integral equation governing the slowing down of neutrons in a homogeneous mixture of atoms. The new equation reflects a view of the neutrons as propagating down the energy scale, whereas the Boltzmann equation expresses a collision balance. Unlike the Boltzmann equation the new equation lends itself to approximate solution by iteration and to the construction of an accurate variational principle for p, the resonance escape probability. Some numerical results are given.

---

§ 1. INTRODUCTION

THE nature of the slowing down of fast neutrons produced uniformly throughout homogeneous media composed of atoms of arbitrary mass was discussed ten years ago in a definitive paper by Placzek (1946). Placzek's paper was most successful in dealing with media which did not absorb neutrons. In a later review paper, Marshak (1947), using Laplace transform techniques, treated a large variety of slowing-down problems but in analysing absorbing media he dealt principally with absorption cross sections which varied slowly with energy. The very important case of absorption in resonances has not received adequate treatment in the literature.

In unpublished notes E. P. Wigner and A. M. Weinberg have recently shown that the Boltzmann equation for slowing down in an infinite media composed of one type of atom is equivalent to another, new, integral equation. The new equation is then used to obtain a correction to the usual expression for the capture probability in slowing down in such a media. The argument given by Wigner and Weinberg in deriving the new equation is essentially 'physical'. It is our purpose in this paper to show: (i) that the transformation to the new equation may be easily effected by the use of the Laplace transformation, (ii) that the Laplace transformation method enables one to construct the new equation for slowing down in arbitrary mixtures of atoms, a generalization that is not trivially obvious from the 'physical' argument, and (iii) that a variational principle, based on the equation, may be given for the capture probability. Examples that are given show that the variational method is accurate and may be of considerable practical importance.

We begin our development with rederivation of the Wigner–Weinberg equation. In fact, much of this work was completed before the author was aware of the unpublished work.

---

† Work performed under the auspices of the U.S. Atomic Energy Commission.

§ 2. MATHEMATICAL DEVELOPMENT

The traditional approach to the slowing-down problem in homogeneous media of infinite extent is based upon the Boltzmann equation for the collision density

$$\Phi(u) = \int_0^u du'\, K_m(u-u')\, h(u')\, \Phi(u') + S(u). \qquad \ldots\ldots(1)$$

Here u, the logarithmic energy, is related to neutron energy by $u = \ln(E_0/E)$, $\Phi(u)du$ is the number of collisions taking place per unit time in the interval between u and $u+du$ per unit volume of matter, and $S(u)du$ is the number of source neutrons introduced into unit volume in unit time with energies between u and $u+du$. The scattering medium is composed of atoms of mass m. The kernel $K_m(u-u')$ characterizes the scattering of neutrons by the atoms and is found to be

$$K_m(u-u') = \frac{\exp\{-(u-u')\}}{1-\alpha_m} \quad \text{when } q_m > u-u' > 0 \qquad \ldots\ldots(2)$$

$$= 0 \qquad \text{elsewhere} \qquad \ldots\ldots(3)$$

where $q_m = \ln[(m+1)/(m-1)]^2$ is the maximum logarithmic energy loss for a neutron upon collision and $1-\alpha_m = 4m/(1+m)^2$. Finally, $h(u)$ is the probability that a neutron-nucleus collision at energy u will be a scattering collision. In (1) $h(u)$ may be alternatively written as the ratio of scattering to total cross sections at energy u. For a detailed discussion of the derivation of (1) the reader may consult Marshak's review.

Equation (1) expresses a balance of collisions; the left-hand side represents collisions throwing the neutron out of energy u, the integral term in the right hand side represents collisions of faster neutrons, scattered into u. Except for the cases of very light scatterers (hydrogen, deuterium, ...) the integrand is zero except for energies quite close to u. That is, $q_m \ll 1$. In cases of practical interest, the source is at a fixed energy E_0, whence $S(u) = S\delta(u)$ and one is most concerned with neutrons that have made many collisions in the moderating material ($u \gg q_m$, $u > 1$). Equation (1) because of its 'local' character is poorly fitted to give information about $\Phi(u)$ in this energy region, when the source has been specified. Iteration upon the source function, or numerical integration requires that one follow the neutrons through their many collisions from source energy to u, a procedure that generally requires the assistance of a computing machine.

In the special case $h(u) = 1$, when there is no possibility for absorption, equation (1) may be solved. The solution, which we designate by $\psi_m(u)$ approaches, for large u, the constant value $1/\xi_m$. ξ_m is the average logarithmic energy loss per collision and is given by

$$\xi_m = 1 - \frac{q_m \exp(-q_m)}{1-\alpha_m} = 1 + \frac{(m-1)^2}{2m} \ln\left(\frac{m-1}{m+1}\right). \qquad \ldots\ldots(4)$$

For smaller $u(u \sim q_m)$ $\psi_m(u)$ varies rapidly and shows, in this domain, discontinuities in function and derivatives. We have assumed here, as we shall in what follows, that $S(u) = \delta(u)$.

We begin the derivation of the new equation by separating from $\Phi(u)$ a singular component composed of neutrons at source energy that have not yet made a first collision. We put $\Phi(u) = \phi(u) + \delta(u)$ and upon substitution of this expression into equation (1), obtain

$$\phi(u) = \int_0^u du'\, K_m(u-u') h(u') \phi(u') + h(0) K_m(u). \qquad \ldots\ldots(5)$$

Next, we apply a Laplace transformation to equation (5). If we denote the transformation

$$\int_0^\infty du\, e^{-\eta u} f(u) \text{ by } L\{f(u)\}=\tilde{f}(\eta) \qquad \ldots\ldots(6)$$

and remember the result of the convolution theorem

$$L\left\{\int_0^u du' f(u-u')\, g(u')\right\}=\tilde{f}(\eta)\,\tilde{g}(\eta), \qquad \ldots\ldots(7)$$

equation (5) becomes

$$\tilde{\phi}(\eta)=\tilde{K}_m(\eta)\, L\,\{h\phi\}+h(0)\,\tilde{K}_m(\eta). \qquad \ldots\ldots(8)$$

If we now write $h(u)=1-g(u)$, where $g(u)$ is the capture probability, equation (8) becomes

$$\tilde{\phi}(\eta)=\frac{h(0)\,\tilde{K}_m(\eta)}{1-K_m(\eta)}-\frac{\tilde{K}_m(\eta)}{1-\tilde{K}_m(\eta)}\, L(g\phi). \qquad \ldots\ldots(9)$$

Now we recognize that $\tilde{K}_m(\eta)/(1-\tilde{K}_m(\eta))$ is the transform of the solution ψ_m to the no-capture equation, whereupon inversion of (9) yields the new equation

$$\phi(u)=h(0)\,\psi_m(u)-\int_0^u du'\,\psi_m(u-u')\,g(u')\,\phi(u'). \qquad \ldots\ldots(10)$$

The physical content of the equation shows up if we transfer the integral term to the left-hand side. We then observe that $\phi(u)$, the solution in the case of capture is, when corrected by the integral term, equal to the solution of the no-capture case. The correction consists in adding neutrons to compensate for absorptions; e.g. the number of neutrons removed per unit time between u' and $u'+du'$ is $g(u')\,\phi(u')\,du'$. A source of the same strength will produce a 'disturbance' $g(u')\,\phi(u')\,du'\,\psi_m(u-u')$ at energy u. Thus, the picture is reminiscent of the multiple scattering of waves. Neutron density introduced at source energy 'propagates' according to $\psi_m(u)$. Variations in cross section disturb the propagation at u_1, u_2, ... producing secondary waves which propagate according to $\psi_m(u-u_1)$, $\psi_m(u-u_2)$, etc. The secondary waves interfere with the primary wave to produce the resultant, ϕ.

The mathematical operations leading from the Boltzmann equation (1) to the 'new' equation (10) may also be applied in the case of an N-component, homogeneous mixture of atoms. The Boltzmann equation is

$$\Phi(u)=\sum_{s=1}^{N}\int_0^u du'\, Km_s(u-u')\, h_s(u')\,\Phi(u')+\delta(u) \qquad \ldots\ldots(11)$$

where the Km_s are scattering kernels as described in equation (2). $h_s(u)$ has a somewhat different meaning. It is now the probability that a collision at energy u will be a scattering collision with an atom of type s. Thus

$$h_s(u)=n_s\,\sigma_{\text{scatt}}{}^{(s)}\Big/\sum_{r=1}^{N} n_r\,\sigma_{\text{tot}}{}^{(r)} \qquad \ldots\ldots(12)$$

and when absorption is absent, h_s is *not* equal to unity. In equation (12) n_r is the number of atoms of type r per unit volume.

Proceeding as in the previous case, we obtain for the transformed equation:

$$\tilde{\phi}(\eta)=\frac{\sum_s h_s(0)\,\tilde{K}_s(\eta)}{1-\sum_s h_s(0)\,\tilde{K}_s(\eta)}-\frac{\sum_s \tilde{K}_s(\eta)\, L\{g_s\phi\}}{1-\sum_s h_s(0)\,\tilde{K}_s(\eta)} \qquad \ldots\ldots(13)$$

with $g_s(u)$ defined by $h_s(0)-h_s(u)=g_s(u)$. In the case of a mixture, then, g_s is not proportional to the absorption by a type-*s* nucleus. g_s vanishes only if the absorption vanishes *and* the scattering is independent of energy.

If we define the function $\bar{\psi}_s$ by:

$$\mathrm{L}\{\bar{\psi}_s\}=\tilde{K}_s(\eta)/[1-\sum_r h_r(0)\,\tilde{K}_r(\eta)] \qquad \ldots\ldots(14)$$

or, equivalently

$$\bar{\psi}_s(u)=\sum_{r=1}^{N} h_r(0)\int_0^u du' K_r(u-u')\,\bar{\psi}_s+K_s(u) \qquad \ldots\ldots(15)$$

inversion of (13) yields:

$$\phi(u)=\psi(u)-\sum_s\int_0^u du'\,\bar{\psi}_s(u-u')\,g_s(u')\,\phi(u') \qquad \ldots\ldots(16)$$

with $\psi(u)=\Sigma_s h_s(0)\,\bar{\psi}_s(u)$.

In (16), $\psi(u)$ is the solution to the slowing-down problem in the mixture, provided that the cross sections are non-absorptive, and energy independent. $\bar{\psi}_s$ is another solution in the same non-absorptive mixture, but corresponds to a different initial condition. $\bar{\psi}_s$ describes the slowing down of neutrons whose first collision is with a nucleus of type *s*. Clearly, $\psi(u)=\Sigma_s h_s(0)\,\bar{\psi}_s(u)$. For sufficiently large u the $\bar{\psi}_s$ become identical with each other and with $\psi(u)$.

Equation (16) may be pictured in a manner similar to the discussion of equation (10). Neutrons propagate energy-wise from source energy according to the function $\psi(u)$. When absorption ($g_s>0$) or 'anomalous' scattering ($g_s<0$) occurs, the distribution is perturbed. A perturbation caused by collision with a type *s* nucleus may be compensated by the appropriate source $g_s(u')\,\phi(u')$. Neutrons propagating from this source do so according to $\bar{\psi}_s(u-u')$ since their first collision is with a type-*s* nucleus. The integral in (16) sums the effect of the compensating sources—the scattered waves.

§ 3. SOLVING THE NEW EQUATIONS

We are not able to give exact general solutions of (10) and (16), just as we are unable to solve equation (1) exactly. However, unlike equation (1), good approximate solutions to the new equations may be constructed by iteration. For equation (10) iteration yields a series solution: ($h(0)=1$)

$$\begin{aligned}\phi(u)=\psi_m(u)&-\int_0^u du'\,\psi_m(u-u')\,g(u')\,\psi_m(u')\\&+\int_0^u du'\,\psi_m(u-u')\,g(u')\int_0^{u'} du''\,\psi_m(u'-u'')\,g(u'')\,\psi_m(u'') \qquad \ldots\ldots(17)\\&-\ldots,\end{aligned}$$

which is composed of successively higher powers of absorption probability and will converge rapidly in all practical cases. The overall probability for capture of a neutron which is slowing down is seldom greater than 40%.

If, in equation (17) the functions ψ_m are replaced by their asymptotic values $\lim\limits_{u\to\infty}\psi_m(u)=1/\xi_m$, the series may be summed to give

$$\phi(u)=\frac{1}{\xi_m}\exp\left\{-\int_0^u g(u')\,du'\right\}. \qquad \ldots\ldots(18)$$

This expression is approximate, and well known. It is an exact solution of (17) only when the function $g(u)$ has resonances of vanishingly small width separated by $\Delta u \gg q_m$.

A quantity of considerable interest is the probability, p, that a neutron will escape capture during the slowing-down process. $g_s(u)$, which governs capture, differs from zero only in a small range of u (and energy), the 'resonance region'. A simple way to obtain p is to compare the asymptotic (large u) collision density obtained when capture is present with asymptotic density in the no-capture case. The ratio of densities is p. If we examine (16) in the limit $u\to\infty$, noting that $g(u)$ vanishes after we pass through the resonance region, we find the asymptotic values of ϕ and ψ related by

$$\phi_{\text{as}}=\psi_{\text{as}}-\lim_{u\to\infty}\sum_s\int_0^u du'\,\bar{\psi}_s(u-u')\,g_s(u')\,\phi(u'). \qquad \ldots\ldots(19)$$

$\bar{\psi}_s$, as we have noted, describes slowing-down in a mixture. Whether a neutron begins its life with a collision with a type s or a type r or $\cdot\cdot$ nucleus in the mixture its asymptotic behaviour will be the same. Thus $\lim\limits_{u\to\infty}\bar{\psi}_s(u)=\bar{\psi}_{\text{as}}$ independent of s. Since $\psi(u)=\sum\limits_s h_s(0)\,\bar{\psi}_s(u)$ and $\sum\limits_s h_s(0)=1$ in a medium characterized by non-absorptive, energy-independent cross sections,

$$\bar{\psi}_{\text{as}}=\lim_{u\to\infty}\bar{\psi}_s(u)=\psi_{\text{as}}=\lim_{u\to\infty}\sum_s h_s(0)\,\bar{\psi}_s(u).$$

The asymptotic value ψ_{as} is well known: it is $\psi_{\text{as}}=1/\xi_{\text{av}}$, $\xi_{\text{av}}=\Sigma_s h_s(0)\,\xi_s$. Hence

$$\phi_{\text{as}}=\frac{1}{\xi_{\text{av}}}\left[1-\int_0^\infty du'\sum_s g_s(u')\,\phi(u')\right]=\frac{1}{\xi_{\text{av}}}p. \qquad \ldots\ldots(20)$$

Using now (20) and (16) it is possible to construct the expression

$$J[\phi,\phi^+]=\frac{\displaystyle\int_0^\infty du\sum_s g_s(u)\phi^+(u)\phi(u)+\int_0^\infty du\sum_s g_s(u)\phi^+(u)\int_0^u du'\sum_l \bar{\psi}_l(u-u')g_l(u')\phi(u')}{\displaystyle\int_0^\infty du'\sum_s g_s(u')\phi(u')\int_0^\infty du'\sum_s g_s(u')\phi^+(u')} \qquad (21)$$

with the following properties: if $\phi(u)$ is a solution to (16), $J[\phi,\phi^+]=1/[\xi_{\text{av}}(1-p)]$. If $\phi(u)$ deviates by $\delta\phi(u)$ from the solution to (16) and $\phi^+(u)$ deviates by $\delta\phi^+(u)$ from the solution to an appropriate adjoint equation, the change in $J[\cdot\cdot]$, δJ, vanishes to second order in $\delta\phi$ and $\delta\phi^+$. Thus $J[\cdot\cdot]$ is stationary with regard to changes in ϕ and ϕ^+, and the right-hand side of (21) should give an accurate value for p when crude guesses for ϕ and ϕ^+ are substituted therein. We have constructed a variational principle for p.

While the proof of the stationary character of (21) will be relegated to the Appendix, we should mention here that the assumption has been made that for values of u in the resonance region, where $g_s(u)$ is non-zero, $\psi(u)$ has reached its asymptotic value, $1/[\xi_{\mathrm{av}}]$. If we do not wish to make this very plausible assumption, the correct $J[\phi, \phi^+]$ differs from (21) in that the factor

$$\int_0^\infty du' \sum_s g_s(u')\,\phi^+(u') \quad \text{is replaced by} \quad \int_0^\infty du' \sum_s g_s(u')\,\phi^+(u')\,\psi(u')$$

and for the correct ϕ, ϕ^+, $J[\phi, \phi^+]=1/(1-p)$. The stationary character is unaltered. With the assumption mentioned above, it is easy to show that

$$\phi(u)=\frac{1}{\xi_{\mathrm{av}}}\frac{1}{1-p}\int_0^\infty du' \sum_s g_s(u')\,\phi(u') - \int_0^u du' \sum_s \bar{\psi}_s(u-u')\,g_s(u')\,\phi(u') \quad \ldots\ldots(22)$$

while the discussion in the Appendix shows that $\phi^+(u)$ must satisfy

$$\phi^+(u)=\frac{1}{\xi_{\mathrm{av}}}\frac{1}{1-p}\int_0^\infty du' \sum_s g_s(u')\,\phi^+(u')$$
$$-\int_u^\infty du' \sum_s g_s(u)\,\bar{\psi}_s(u'-u)\,\frac{\sum\limits_l g_l(u')}{\sum\limits_l g_l(u)}\,\phi^+(u'). \quad \ldots\ldots(23)$$

If we specialize to a one-component mixture, (22) and (23) become

$$\phi(u)=\lambda\int_0^\infty du' g(u')\,\phi(u') - \int_0^u du'\,\psi_m(u-u')\,g(u')\,\phi(u')$$
$$\phi^+(u)=\lambda\int_0^\infty du'\,g(u')\,\phi^+(u') - \int_u^\infty du'\,\psi_m(u'-u)\,g(u')\,\phi^+(u') \quad \ldots\ldots(24)$$

with $\lambda=1/[\xi(1-p)]$.

§ 4. APPLICATIONS OF THE VARIATIONAL PRINCIPLE

A variation–iteration scheme, based on equations (21) and (22–23) or (24) will enable the investigator to obtain p to any desired degree of accuracy, in a systematic manner. In this scheme a zero-order set of trial functions is used to get $J[\phi_0,\phi_0{}^+]$ and p_0. Then ϕ_0, $\phi_0{}^+$ and p_0 are substituted into the right-hand sides of equations (22–23) or (24) in order to give ϕ_1, $\phi_1{}^+$. $J[\phi_1, \phi_1{}^+]$ then yields p_1 and the process continues. One might suppose the procedure to involve a large amount of computational effort. We shall show, however, that considerable accuracy is obtained—in some simple examples—with only the zero-order and first-order trial functions.

4.1. *A Mixture of Hydrogen and Infinitely Heavy Absorber*

The solution to this problem is well known. For hydrogen, $\psi_m=\psi_1\equiv 1$, and either iteration or differentiation of equation (16) leads to the solution

$$p=\exp\left\{-\int_0^\infty du\,g(u)\right\}=\mathrm{e}^{-A}. \quad \ldots\ldots(25)$$

Using $\phi_0=1$, $\phi_0{}^+=1$ in equation (21) we find

$$p_0=(1-\tfrac{1}{2}A)/(1+\tfrac{1}{2}A)=1-A+\tfrac{1}{2}A^2-\cdots \quad \ldots\ldots(26)$$

which agrees with the exact p up to terms in third order in the absorption. If we now iterate upon ϕ_0, $\phi_0{}^+$ and p_0, to get ϕ_1 and $\phi_1{}^+$, we find

$$p_1=(1-\tfrac{1}{2}A+\tfrac{1}{12}A^2)/(1+\tfrac{1}{2}A+\tfrac{1}{12}A^2), \quad \ldots\ldots(27)$$

which agrees with the exact p to terms in *fifth* order in the absorption. Indeed p_1 yields 5/6 of the fifth order term.

4.2. *A Mixture of Hydrogen and* ^{238}U

Here we shall compare the lowest order estimate of p, p_0, with exact numerical calculations for a mixture with 1 : 1 atom ratio of hydrogen to uranium, in which only a single absorption resonance of the uranium is considered. The numerical calculations, communicated to the author by Mr. K. T. Spinney, were based on a differential equation obtained from equation (11). We list also the results given by two other well-known approximations, the 'infinite absorber' (IA) in which the moderating effects of uranium are neglected and formula (25) is used, and the 'narrow resonance' (NR) in which the collision densities $\bar{\psi}_s$ are replaced by their asymptotic values $1/\xi_{\text{av}}$. The calculation of $J[\phi_0, \phi_0{}^+]$ which involves the construction of ψ_0 and ψ_1 (see Appendix) requires numerical integration, but much less labour is expended than in the 'exact' numerical calculation.

Resonance	$1-p$ (exact)	$1-p_0$ (variational)	$1-p$ (NR)	$1-p$ (IA)
36·9 ev	0·05820	0·05682	0·04739	0·06110
192 ev	0·007119	0·007630	0·005068	0·01228

§ 5. SUMMARY

We have derived from the Boltzmann equation a new integral equation governing the slowing down of neutrons in a homogeneous mixture of atoms. The new equation reflects a view of the neutrons as propagating down the energy scale, whereas the Boltzmann equation expresses a collision balance. The new equation lends itself to approximate solution by iteration and to the construction of an accurate variational principle for p, the resonance escape probability. Its greater tractability should help investigators in the study of slowing-down processes. In particular, interference effects in the capture by nearby levels will be elucidated.

REFERENCES

MARSHAK, R. E., 1947, *Rev. Mod. Phys.*, **19**, 185.
PLACZEK, G., 1946, *Phys. Rev.*, **69**, 423.

APPENDIX

1. THE VARIATIONAL PRINCIPLE

We wish to prove that $J[\phi, \phi^+]$ defined in equation (21) is stationary with respect to arbitrary, small variations of ϕ, ϕ^+ from the solutions to equations (22, 23).

$$J[\phi,\phi^+]\left\{\int_0^\infty du \sum_s g_s\phi\right\}\left\{\int_0^\infty du \sum_s g_s\phi^+\right\}$$

$$=\int_0^\infty du \sum_s g_s\phi\,\phi^+ + \int_0^\infty du \sum_s g_s\phi^+(u)\int_0^u du' \sum_l \bar{\psi}_l g_l \phi(u'). \qquad \ldots\ldots(28)$$

If we vary ϕ^+ by $\delta\phi^+$ from the solution to equation (23) and collect terms we find

$$\delta J\int_0^\infty du \sum_s g_s\phi^+ \int_0^\infty du \sum_s g_s\phi = \int_0^\infty du \sum_s g_s(u)\,\delta\phi^+(u)\,[F]$$

$$-F = J\int_0^\infty du \sum_s g_s\phi - \int_0^u du' \sum \bar{\psi}_l(u-u')\,g_l(u')\,\phi(u') - \phi(u). \qquad \ldots\ldots(29)$$

Since ϕ satisfies equation (22) and $J[\phi, \phi^+] = 1/[(1-p)\xi_{\mathrm{av}}]$ F must be zero. Since the coefficients of δJ do not in general vanish, $\delta J = 0$. If we instead vary ϕ by $\delta\phi$ from the solution to equation (22) we find

$$\delta J \int_0^\infty du \sum_s g_s \phi^+ \int_0^\infty du \sum_s g_s \phi = \int_0^\infty du \sum_s g_s(u)\, \delta\phi(u)\, [F]$$

$$F = \phi^+ - J \int_0^\infty du \sum_s g_s \phi^+ + \int_u^\infty du' \sum_s g_l(u)\, \psi_l(u'-u)\, \frac{\sum_s g_s(u')}{\sum_s g_s(u)}\ \phi^+(u'). \qquad \ldots\ldots(30)$$

Thus if ϕ satisfies equation (23) J will again be zero. We have shown, then, the stationary character of $J[\phi, \phi^+]$, when ϕ, ϕ^+ are the actual solutions to the integral equations.

2. CONSTRUCTION OF THE $\bar{\psi}_s$ FUNCTIONS

We shall indicate how one would construct the functions $\bar{\psi}_2$ and $\bar{\psi}_1$ relating to the slowing down of neutrons in a two-component mixture, here composed of uranium (subscript 2, and hydrogen (subscript 1).

By definition

$$\begin{aligned} \psi_s = {} & \frac{h_1(0)}{1-\alpha_1} \int_{\gamma_1(u-q_1)}^{u} du' \exp[-(u-u')]\ \psi_s(u') \\ & + \frac{h_2(0)}{1-\alpha_2} \int_{\gamma_2(u-q_2)}^{u} du' \exp[-(u-u')]\, \bar{\psi}_s(u') + \frac{1-\gamma_s}{1-\alpha_s} e^{-u}, \qquad \ldots\ldots(31) \end{aligned}$$

where $\gamma_s = \gamma_s(u) = 0$ for $u \leqslant q_s$

$= 1$ $u > q_s$.

If we write $h_s(0)/(1-\alpha_s) = c_s$, $e^u \bar{\psi}_s = y_s$ and then go to our example of hydrogen + uranium, (31) becomes

$$y_s = c_1 \int_0^u du'\, y_s(u') + c_2 \int_{\gamma_2(u-q_2)}^{u} du'\, y_s(u') + \frac{1-\gamma_s}{1-\alpha_s}. \qquad \ldots\ldots(32)$$

For $u \leqslant q_2$ $\quad y_s = (c_1+c_2) \int_0^u du'\, y_s(u') + \dfrac{1}{1-\alpha_s} \qquad \ldots\ldots(33)$

and $\quad y_s = \dfrac{\exp[(c_1+c_2)u]}{1-\alpha_s}.$

For $u > q_2$ $\quad y_s = (c_1+c_2) \int_0^u du'\, y_s(u') - c_2 \int_0^{u-q_2} du'\, y_s(u') + \dfrac{1-\gamma_s}{1-\alpha_s}. \qquad \ldots\ldots(34)$

Clearly, y_2 is discontinuous at $u = q_2$, while y_1 is continuous there. In addition, differentiation of (33) and (34) shows that the first derivative of y_2 is discontinuous at $u = q_2$, $2q_2$, the second derivative at $u = q_2$, $2q_2$, $3q_2$, etc. These results would be expected to follow at once from Placzek's discussion.

If we differentiate (34), re-arrange terms and, if $(n+1)q_2 \geqslant u \geqslant nq_2$, integrate between nq_2 and u, we find

$$x_s(u) = x_s(nq_2{}^+) - c_2 \exp\{-q_2(c_1+c_2)\} \int_{(n-1)q_2}^{u-q_2} x_s(u')\, du' \qquad \ldots\ldots(35)$$

where $\quad x_s(u) = (1-\alpha_s) \exp\{-(c_1+c_2)u\}\, y_s(u)$

and $\quad x_s(nq_2{}^+) = \lim\limits_{\epsilon \to 0} x_s(nq_2+\epsilon) \qquad \epsilon > 0.$

The 'limit from above' is introduced in order properly to take discontinuities into account. Equation (35) is the fundamental equation for the construction of

$\bar{\psi}_s$. Using the result $x_s=1$ for $u \leqslant q_2$ one can generate $x_s\ (u)$ for higher values of u through successive simple integrations in (35). The integrations may be done analytically or numerically.

Both $\bar{\psi}_1$ and $\bar{\psi}_2$ should approach the asymptotic value $1/\xi_{\mathrm{av}}$ for large u. While it is always difficult to extract the precise value of the constant from the Boltzmann equation, we can verify that (35) has a solution $x_s(u)=\exp \beta_s u$ where β_s is independent of s and has the value $\beta_s=1-(c_1+c_2)$, whence $\bar{\psi}_s(u)=\mathrm{const.}$

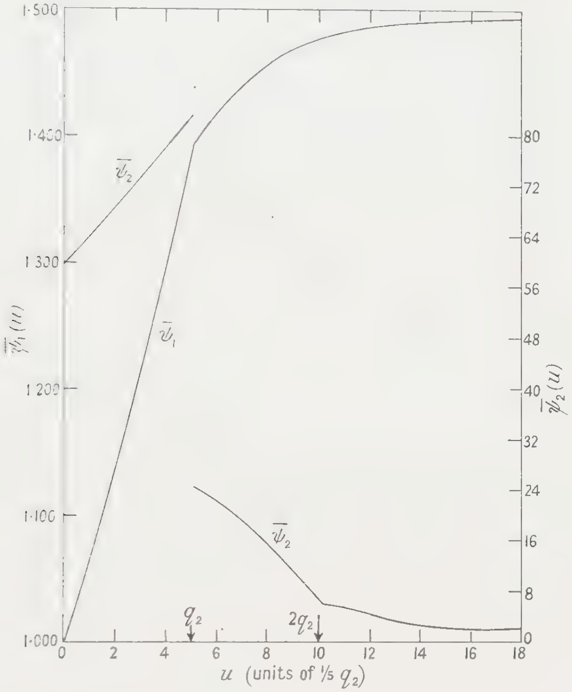

The functions $\bar{\psi}_1$ and $\bar{\psi}_2$ for 1 : 1 atom ratio of hydrogen to uranium.

The figure shows a graph of the functions $\bar{\psi}_1(u)$ and $\bar{\psi}_2(u)$ for the 1 : 1 atom ratio mentioned in the text. The functions $\bar{\psi}_1$ and $\bar{\psi}_2$ rapidly approach their asymptotic value.

Properties of the Helium Atom

By A. DALGARNO and N. LYNN
Department of Applied Mathematics, The Queen's University of Belfast

MS. received 24th June 1957

Abstract. The available theoretical values of the oscillator strengths of dipole transitions from the ground state of helium are modified so that they satisfy four different sum rules. They are then employed to evaluate the refractive index, the Verdet constant, the diamagnetic susceptibility, the Lamb shift, the average energy loss for fast particle impact and the van der Waals interaction between two helium atoms, good agreement being obtained with experimental data where comparison is possible.

§ 1. Introduction

In 1939, Margenau modified the theoretical values of the oscillator strengths of dipole transitions from the ground state of helium, so that they were in conformity with the Thomas–Kuhn oscillator strength sum rule and with the value of the polarizability deduced by Born and Heisenberg (1924) from the measurements by Cuthbertson and Cuthbertson (1911) of the refractive index. He then employed the modified oscillator strengths to calculate the van der Waals forces between two helium atoms. Recently, Kinoshita (1957) has accurately evaluated certain matrix elements which in conjunction with some sum rules suggested by Vinti (1932a) enable much of the uncertainty of Margenau's rather arbitrary procedure to be eliminated.

§ 2. Sum Rules

If $\mathbf{r}$ represents the coordinates of all the electrons of an atom, then the oscillator strength of a dipole transition from the ground state with wave function $\psi_0(\mathbf{r})$ to the nth excited state with wave function $\psi_n(\mathbf{r})$ is defined as

$$f_n = \frac{(E_0 - E_n)}{3} |(0|\sum_i \mathbf{r}_i|n)|^2 \qquad \ldots\ldots(1)$$

where E_0 and E_n are the binding energies of the ground and nth excited states respectively, measured in rydbergs, $\mathbf{r}_i$ is the position vector of the ith electron and

$$(0|\sum_i \mathbf{r}_i|n) = \int \psi_0{}^* \sum_i \mathbf{r}_i \psi_n \, d\mathbf{r}, \qquad \ldots\ldots(2)$$

length being measured in units of a_0 ($a_0 = 5{\cdot}292 \times 10^{9}$ cm).

The oscillator strengths satisfy the following sum rules:

(i) $\sum f_n/(E_0 - E_n)^2 = \alpha/4$

where α is the polarizability in units of $a_0{}^3$.

(ii) $\sum f_n/(E_0 - E_n) = (0|(\Sigma \mathbf{r}_i)^2|0)/3$.

(iii) $\sum f_n \qquad = N$

where N is the total number of electrons.

$$\text{(iv)}\qquad \sum f_n(E_0-E_n)=\tfrac{4}{3}\{E_0+\tfrac{1}{2}\sum_{i\neq j}(0\,|\,\mathbf{p}_i\cdot\mathbf{p}_j\,|\,0)\}$$

where $\mathbf{p}_i$ is the momentum of the ith electron.

$$\text{(v)}\qquad \sum f_n(E_0-E_n)^2=\frac{16\pi Z}{3}\sum_i(0\,|\,\delta^{(3)}(\mathbf{r}_i)\,|\,0).$$

where Z is the nuclear charge and $\delta^{(3)}(\mathbf{r})$ is the three-dimensional Dirac δ-function. In (i)–(v), the summation includes an integration over the continuum but excludes the $n=0$ term.

The first sum rule is the usual expression for the polarizability according to second-order perturbation theory (cf. Van Vleck 1932), the second is an immediate consequence of the matrix multiplication law and the third is the familiar Thomas–Kuhn oscillator strength sum rule. The last two are perhaps less well-known. They were introduced originally by Vinti (1932a) and may readily be established by the summation technique used recently by Dalgarno and Lewis (1955).

Values of α may be derived either from measurements of the refractive index or from measurements of the dielectric constant. The early refractive index measurements by Cuthbertson and Cuthbertson (1911, 1932) and by Koch (1913) yield a value of α equal to $2{\cdot}05\times10^{-25}\,\text{cm}^3$ (cf. Herzfeld and Wolf 1925), whereas the most recent measurement of the dielectric constant (Essen 1953, Hartshorn 1955) yields $\alpha=(2{\cdot}07\pm0{\cdot}01)\times10^{-25}\,\text{cm}^3$. We adopt the value $2{\cdot}06\times10^{-25}\,\text{cm}^3$.

No reliable values of $(0\,|\,(\sum\mathbf{r}_i)^2\,|\,0)$ appear to exist and we shall not make use of (ii) to derive f_n but shall instead evaluate (ii) from our values of f_n.

The third sum is simply 2 for helium, while the fourth and fifth may be obtained from the work of Kinoshita (1957) who computed

$$\sum_{i\neq j}(0\,|\,\mathbf{p}_i\cdot\mathbf{p}_j\,|\,0)\quad\text{and}\quad\sum_i(0\,|\,\delta^{(3)}(\mathbf{r}_i)\,|\,0)$$

using a 38-parameter trial wave function for the ground state of the helium atom, obtaining the values $-0{\cdot}6364$ and $3{\cdot}6212$ respectively in Hartree units for these terms.

§ 3. OSCILLATOR STRENGTHS

The earliest calculation of helium oscillator strengths was by Vinti (1932 b, 1933) who used the two-parameter Eckart (1930) wave function for the ground and first excited states and the modified hydrogenic approximation, in which the inner electron is regarded as moving in a field of charge two and the outer in a field of charge unity, for the higher discrete and continuum states. These calculations were later repeated by Körwien (1934) who obtained slightly different numerical results. In addition, Körwien used a hydrogenic approximation with a single screening parameter for ψ_0, ψ_n being as before, and also for transitions to 2^1P and 3^1P representations due to Hylleraas (1933) in terms of Laguerre polynomials. The work using Laguerre polynomials was repeated and extended by Hylleraas (1937), the numerical discrepancies being in this case more serious. Wheeler (1933) has calculated f-values using a six-parameter Hylleraas wave function (1929) involving the inter-electronic distance for ψ_0, the modified hydrogenic approximation for the continuum wave function and a three-parameter wave function for the 2^1P state. The continuum calculations were repeated by Huang (1948), again with slightly different numerical results. Huang also computed f-values using the dipole velocity and acceleration formulations (Chandrasekhar 1945), all earlier workers having used the dipole length formulation only.

The only calculations for transitions into doubly excited states are by Vinti (1932 b) who obtains a value 0·011 for the transition to $(2s\,2p)^1P$ and a value 0·0008 for the transition to $(3s\,3p)^1P$. By deliberately overestimating the contributions from more highly excited states Vinti shows that 0·043 constitutes an upper bound to the total f-value associated with doubly excited states. His analysis is not rigorous however and in particular does not take proper account of the continua associated with excited and ionized helium ions. A comparison of the electron impact calculations by Massey and Mohr (1935) on double excitation and by Dalgarno and McDowell (1956) on simultaneous excitation and ionization, suggests that the latter process may contribute an equal amount. Although it is not easy to find a flaw in Vinti's general arguments, it should perhaps be mentioned that an analysis of refractive index data for argon (Herzfeld and Wolf 1925) leads to the conclusion that f-values associated with doubly excited states may be large, whereas Vinti's analysis applied to argon leads to the opposite conclusion; argon is of course a much more complex system.

None of the sets of f-values, details of which are collected in tables 1, 2 and 3, satisfies all four sum rules (i), (iii), (iv) and (v), even if the contribution from doubly excited states is regarded as a disposable quantity. The rather unsystematic data suggest that the f-values are very sensitive to the choice of ψ_0 and that the f-values of transitions to the continuum are less sensitive than that of the resonance transition, the harmony of Huang's three sets of results for $\lambda > 150$ Å being satisfactory, though not entirely conclusive. We therefore adopt Huang's dipole velocity and acceleration value of 0·97 for $df/d\epsilon$ at the spectral head, ϵ being the energy of the ejected electron in rydbergs, and we further require that our derived continuum values do not differ from Huang's by more than 10 per cent for $\lambda > 150$ Å.

The functional form of $df/d\epsilon$ is severely limited by this requirement and by the finiteness of the summation (v) which requires that $df/d\epsilon$ falls off faster than λ^3. Several forms were investigated, the one finally adopted being

$$df/d\epsilon = A\lambda^4 \exp(-\beta\lambda) + B\lambda^{7/2} \exp(-\gamma\sqrt{\lambda}),$$

λ being measured in Å.

Hartree (1928) has shown that for highly excited states the f-values calculated on a central field approximation fall off as C/n'^3, where n' is the *effective* principal quantum number and Hargreaves (1929) has further shown that in consequence of continuity at the spectral head, the constant C is equal to twice the spectral head value of $df/d\epsilon$, a result which was confirmed explicitly for helium by Vinti (1932 b, 1933). We assume the formula to be valid for $n \geqslant 4$.

The locations of the doubly excited states are uncertain (cf. Bransden and Dalgarno 1953) and we suppose for simplicity that they are all located at 202·5 Å. The f-values for the transitions to the two lowest levels and to the totality of doubly excited levels and the constants appearing in the functional form adopted for $df/d\epsilon$ may then be determined by the requirement that, in addition to the conditions stated earlier, the four sum rules (i), (iii), (iv) and (v) be satisfied, the procedure being one of trial and error. Although the results, given in tables 1, 2 and 3, are less arbitrary than it may appear, it is difficult to estimate the possible error in any individual f-value. In particular, the derived total f-value of 0·143

Table 1.† Oscillator Strength of the Resonance Transition He(1^1S-2^1P)$-\lambda=584{\cdot}35$ Å.

1^1S wave function / 2^1P wave function	Hydrogenic	Eckart (1930)	Hylleraas (1929)	Hylleraas (1933)
Modified hydrogenic	0·189[1]	0·365[1]		
Eckart (1930)		0·349[2]		
Wheeler (1933)			0·266[3]	0·295[1] 0·356[4]
Hylleraas (1933)	0·169[1]	0·323[1]		

The value derived here is 0·239

1. Körwien (1934), 2. Vinti (1932 b), 3. Wheeler (1933), 4. Hylleraas (1937).

† For description of wave functions employed see text.

Table 2. *f*-Values obtained by Various Authors

Transition	Wavelength (Å)	Vinti (1932)	Körwien (1934)		Hylleraas (1937)	Present
1^1S-3^1P	537·05	0·093	0·055	0·089	0·072	0·081
1^1S-4^1P	522·2	0·0357	0·0230	0·0368	0·0282	0·0325
1^1S-5^1P	515·6	0·0177	0·0119	0·0173	0·0144	0·0162
1^1S-6^1P	512·1	0·0105	0·0068	0·0098	0·0082	0·0093
1^1S-7^1P	510·0	0·0063	0·0042	0·0061		0·0058
1^1S-8^1P	508·7		0·0028	0·0041		0·0039
1^1S-9^1P	507·7		0·0021	0·0028		0·0027
1^1S-10^1P	507·1		0·0015	0·0022		0·0020
$1^1S-\sum_{n=11} n^1P$						0·0088

Körwien (1934) has also computed $f(1^1S-3^1P)$ using the Hylleraas (1933) function for the excited state and the hydrogenic, the Eckart and the Hylleraas (1933) function for the ground state obtaining respectively 0·052, 0·086 and 0·079.

Table 3. $df/d\epsilon$-Values obtained by Various Authors

Wavelength (Å)	Wheeler (1933)	Vinti (1933)	Körwien (1934)		Huang (1948) (1)	(2)	(3)	Present
504·27	0·93	1·05	0·72	1·06	0·93	0·97	0·97	0·97
420	0·72	0·68	0·63	0·67	0·70	0·71	0·69	0·73
340	0·51	0·43	0·49	0·42	0·46	0·46	0·45	0·50
260	0·29	0·25	0·33	0·25	0·26	0·26	0·24	0·28
180	0·13	0·12	0·16	0·12	0·11	0·11	0·10	0·11
100	0·031	0·032	0·037	0·033	0·026	0·025	0·021	0·016
20	0·0010	0·00043	0·00032	0·00051	0·00037	0·00024	0·00019	0·00018

(1) Dipole length; (2) dipole velocity; (3) dipole acceleration. (Huang appears to have omitted a factor of 4 in his calculations using the dipole acceleration formulation. The corrected values are given in the table.)

for the doubly excited states may be made much smaller by modifying the continuum values appropriately. A more accurate treatment of the doubly excited levels does not seem warranted at this stage since the derived values are fairly sensitive to the value of $df/d\epsilon$ at the spectral head. A recalculation of this quantity using continuum wave functions more accurate than those of Huang (1948) is very desirable; our low value 0·239 for the resonance transition compared to Körwien's value 0·295 or Hylleraas' value 0·356 suggests that Huang's spectral head value is too large. However, these uncertainties have little effect on the values of the related quantities discussed in the following section.

The only direct measurements are by Dershem and Schein (1931) who give $df/d\epsilon$ at 44·6 Å as 0·0030 compared to our value of 0·0015 and by Lee and Weissler (1955) who give $df/d\epsilon$ between 496 and 240 Å, their $(df/d\epsilon, \lambda)$ curve agreeing within the limits of experimental error with all the calculated curves. Lee and Weissler also report a value 0·35 for the resonance transition but state that it is of doubtful accuracy.

§ 4. Related Properties

4.1. *The Index of Refraction*

The index of refraction n for radiation of energy E rydbergs is given at S.T.P. by

$$n^2-1=2{\cdot}002_4\times10^{-4}\sum f_n/\{(E_0-E_n)^2-E^2\}. \qquad \ldots\ldots(3)$$

For wavelengths λ long compared to that of the helium resonance line ($\lambda=584{\cdot}35$ Å) (3) may be expanded according to

$$n^2-1=2{\cdot}002_4\times10^{-4}\sum\frac{f_n}{(E_0-E_n)^2}\left[1+\frac{E^2}{(E_0-E_n)^2}+\frac{E^4}{(E_0-E_n)^4}+\ldots\right]. \qquad \ldots\ldots(4)$$

Substituting into (4) the derived f-values we obtain

$$n^2-1=6{\cdot}958\times10^{-5}\left(1+\frac{2{\cdot}32\times10^5}{\lambda^2}+\frac{6{\cdot}009\times10^{10}}{\lambda^4}+\ldots\right) \qquad \ldots\ldots(5)$$

λ being measured in Å. The measurements of Koch (1913) between 4109 Å and 2379 Å can be fitted by

$$n^2-1=6{\cdot}930\times10^{-5}\left(1+\frac{2{\cdot}35\times10^5}{\lambda^2}\right)$$

and those of Cuthbertson and Cuthbertson (1932) between 5462 Å and 2753 Å by

$$n^2-1=6{\cdot}932\times10^{-5}\left(1+\frac{2{\cdot}35\times10^5}{\lambda^2}\right).$$

The excellent agreement of these data with our formula is particularly gratifying since the second term depends strongly on the f-value of the important resonance transition.

4.2. *The Verdet Constant*

The Verdet constant V relates the rotation of the plane of polarization to the initiating magnetic field (cf. Van Vleck 1932) and is given for atoms in S states by the Becquerel formula

$$V=\frac{e^2}{2mc^2}E\frac{dn}{dE}, \qquad \ldots\ldots(6)$$

n being the refractive index. We find

$$V=\frac{4{\cdot}737\times10^{-3}}{\lambda^2}\left(1+\frac{5{\cdot}18\times10^5}{\lambda^2}+\ldots\right)\text{rad gauss}^{-1} \qquad \ldots\ldots(7)$$

whereas to within the limits of experimental accuracy the measurements of Ingersoll and James (1952) and of Ingersoll and Liebenberg (1954) can be fitted by

$$V=4{\cdot}7\times10^{-3}/\lambda^2\text{ rad gauss}^{-1}.$$

Okazaki (1942) has earlier checked the Verdet constant measurement of Bizette and Tsai (1937) by making use of the experimental refractive index data.

4.3 *The Diamagnetic Susceptibility*

The susceptibility per g mol is given by

$$\chi = -7{\cdot}92_6 \times 10^{-7}(0|\sum_i r_i^2|0) \qquad \ldots\ldots(8)$$

which for helium can be written

$$\chi = -7{\cdot}92_6 \times 10^{-7}\{3\sum f_n/(E_0 - E_n) - 2(0|\mathbf{r}_1 . \mathbf{r}_2|0)\}. \qquad \ldots\ldots(9)$$

Vinti (1932c) has calculated $(0|\mathbf{r}_1 . \mathbf{r}_2|0)$ to be approximately $-0{\cdot}073$ and the summation yields 2·297 so that we obtain $\chi = -1{\cdot}936 \times 10^{-6}$ in agreement with the most recently measured value (Havens 1933), which is $-(1{\cdot}933 \pm 0{\cdot}006) \times 10^{-6}$ when the change in the Curie constant for O_2 subsequent to Haven's work is taken into account.

4.4. *The Lamb Shift*

The Lamb shift is given in terms of an average excitation energy K_0 where

$$\log K_0 = \frac{\sum f_n(E_0 - E_n)^2 \log(E_0 - E_n)}{\sum f_n(E_0 - E_n)^2} \qquad \ldots\ldots(10)$$

(cf. Bethe and Salpeter 1957). With our f-values we obtain $K_0 = 146$ rydbergs in serious disagreement with the value $84{\cdot}3 \pm 5$ rydbergs computed by Kabir and Salpeter (cf. Bethe and Salpeter 1957). Although the disagreement at 44·6 Å between our f-value and the measured value casts doubt on the accuracy of the K_0 we obtain, which depends almost entirely on the f-values at very short wavelengths, the limits of error claimed by Kabir and Salpeter are surprisingly narrow, especially since K_0 depends exponentially upon the right-hand side of (10). Until details of their calculation become available, little further can be said about the discrepancy.

4.5 *The Average Energy Loss for Fast Impacts*

The average energy loss for fast impacts is given in terms of a mean excitation energy I (cf. Mott and Massey 1949), and by using the Born approximation with some additional assumptions valid at high velocities of impact Bethe (1930) has shown that

$$\log I = \frac{\sum f_n \log(E_0 - E_n)}{\sum f_n}. \qquad \ldots\ldots(11)$$

We obtain $I = 40{\cdot}2$ ev. The resulting energy loss for proton impacts is compared in table 4 with the experimental data of Reynolds, Dunbar, Wenzel and Whaling (1953). Agreement is satisfactory, most of the discrepancy at lower energies arising from the inadequacy of the Bethe formula which overestimates in this region (Dalgarno and Griffing 1955).

Table 4. Average Energy Loss for Proton Impacts in Helium (ev × 10^{-15} cm^2)

E(kev)	100	150	200	250	300	350	400	450	500	550	600
Theoretical	8·04	6·64	5·67	4·96	4·42	4·00	3·66	3·38	3·14	2·94	2·76
Experimental	7·30	6·37	5·55	4·91	4·41	4·01	3·69	3·42	3·18	2·99	2·81

4.6. *Van der Waals Force between two Helium Atoms*

The coefficient of the R^{-6} term in the series representation of the long range interaction between two similar neutral atoms is given by Margenau (1939) as

$$C = -24\sum_m\sum_n \frac{f_m f_n}{(E_0 - E_m)(E_0 - E_n)(2E_0 - E_m - E_n)} \qquad \ldots\ldots(12)$$

in Hartree units. The evaluation of (12) is elementary though tedious and we obtain $C=-3{\cdot}001$ which is to be compared with the previous most accurate calculation $C=-2{\cdot}90$ (Margenau 1939). The accuracy of C should be equal to that of the measured dielectric constant.

ACKNOWLEDGMENT

The authors are indebted to Professor D. R. Bates for his comments on an earlier draft of the manuscript.

REFERENCES

BETHE, H. A., 1930 *Ann. Phys., Lpz.*, **5**, 325.
BETHE, H. A., and SALPETER, E. E., 1957, *Handbuch der Physik*, **35** (Berlin : Springer).
BIZETTE, H., and TSAI, B., 1937, *C.R. Acad. Sci., Paris*, **204**, 1870.
BORN, M., and HEISENBERG, W., 1924, *Z. Phys.*, **23**, 388.
BRANSDEN, B. H., and DALGARNO, A., 1953, *Proc. Phys. Soc.* A, **66**, 911.
CHANDRASEKHAR, S., 1945, *Astrophys. J.*, **102**, 223.
CUTHBERTSON, C., and CUTHBERTSON, M., 1911, *Proc. Roy. Soc.* A, **84**, 13 ; 1932, *Ibid*, **135**, 40.
DALGARNO, A., and GRIFFING, G. W., 1955, *Proc. Roy. Soc.* A, **232**, 423.
DALGARNO, A., and LEWIS, J. T., 1955, *Proc. Roy. Soc.* A, **233**, 70.
DALGARNO, A., and McDOWELL, M. R. C., 1956, *Airglow and the Aurorae* (London and New York : Pergamon Press).
DERSHEM, E., and SCHEIN, M., 1931, *Phys. Rev.*, **37**, 1238.
ECKART, C., 1930, *Phys. Rev.*, **36**, 883.
ESSEN, L., 1953, *Proc. Phys. Soc.* B, **66**, 189.
HARGREAVES, J., 1929, *Proc. Camb. Phil. Soc.*, **25**, 75.
HARTREE, D. R., 1928, *Proc. Camb. Phil. Soc.*, **24**, 426.
HARTSHORN, L., 1955, *Precision Electrical Measurements* (London : H.M. Stationery Office).
HAVENS, G. G., 1933, *Phys. Rev.*, **43**, 992.
HERZFELD, K. F., and WOLF, K. L., 1925, *Ann. Phys., Lpz.*, **76**, 71, 567.
HUANG, S., 1948, *Astrophys. J.*, **108**, 354.
HYLLERAAS, E. A., 1929, *Z. Phys.*, **54**, 347 ; 1933, *Ibid.*, **83**, 739 ; 1937, *Ibid.*, **106**, 395.
INGERSOLL, L. R., and JAMES, W. L., 1952, *J. Opt. Soc. Amer.*, **42**, 985.
INGERSOLL, L. R., and LIEBENBERG, D. H., 1954, *J. Opt. Soc. Amer.*, **44**, 566.
KINOSHITA, T., 1957, *Phys. Rev.*, **105**, 1490.
KOCH, I., 1913, *Ark. Mat.*, **9**, 611.
KÖRWIEN, H., 1934, *Z. Phys.*, **91**, 1.
LEE, P., and WEISSLER, G. L., 1955, *Phys. Rev.*, **99**, 540.
MARGENAU, H., 1939, *Phys. Rev.*, **56**, 1000.
MASSEY, H. S. W., and MOHR, C. B. O., 1935, *Proc. Camb. Phil. Soc.*, **31**, 604.
MOTT, N. F., and MASSEY, H. S. W., 1949, *Theory of Atomic Collisions*, 2nd edn (Oxford : University Press).
OKAZAKI, A., 1942, *Proc. Phys.-Math. Soc. Japan*, **24**, 361.
REYNOLDS, H. K., DUNBAR, D. N. F., WENZEL, W. A., and WHALING, W., 1953, *Phys. Rev.*, **92**, 742.
VAN VLECK, J. H., 1932, *Theory of Electric and Magnetic Susceptibilities* (Oxford : University Press).
VINTI, J. P., 1932 a, *Phys. Rev.*, **41**, 432 ; 1932 b, *Ibid.*, **42**, 632 ; 1932 c. *Ibid.*, **41**, 813 ; 1933, *Ibid.*, **44**, 524.
WHEELER, J. A., 1933, *Phys. Rev.*, **43**, 258.

Inelastic Heavy Particle Collisions Involving the Crossing of Potential Energy Curves

V—Charge Transfer from Neutral Atoms to Doubly and Triply Charged Ions

By T. J. M. BOYD and B. L. MOISEIWITSCH

Department of Applied Mathematics, The Queen's University of Belfast

MS. received 15*th May* 1957, *and in amended form* 29*th July* 1957

Abstract. The Landau–Zener formula for the transition probability arising from the pseudo-crossing of potential energy curves is used to investigate charge transfer processes of the type $A+B^{3+}\rightarrow A^{+}+B^{2+}$ involving neutral helium atoms and triply charged ions of Be, Li, Al and Mg.

In addition, a method based on the Landau–Zener formula involving one experimentally determined parameter is used to calculate cross sections for processes of the type $A+B^{2+}\rightarrow A^{+}+B^{+}$. Good agreement is found with the cross sections obtained in the laboratory by Hasted and Smith for N^{2+} ions in He and Ne, and for A^{2+} ions in Ne.

§ 1. Introduction

In a recent series of papers (Bates and Moiseiwitsch 1954, Dalgarno 1954, Bates and Lewis 1955, Bates and Boyd 1956), the Landau–Zener formula (Landau 1932, Zener 1932), for the transition probability arising from the pseudo-crossing of potential energy curves, was employed to obtain cross sections and rate coefficients for a number of charge transfer processes. No comparison with experiment was possible in these papers. Recently, however, Hasted and Smith (1956) have made a laboratory investigation of charge transfer processes of the type

$$A+B^{2+}\rightarrow A^{+}+B^{+}(+\Delta E\,\mathrm{ev}) \qquad \ldots\ldots(1)$$

involving neutral atoms of helium, neon and argon. This work has made possible an assessment of the accuracy of the theory due to Landau and Zener, by using a method, based on their formula, involving one experimentally determined parameter.

An accurate ground state helium atom wave function has been published by Bartlett (1955) which has also enabled us to investigate charge transfer processes of the type

$$A+B^{3+}\rightarrow A^{+}+B^{2+} \qquad \ldots\ldots(2)$$

involving neutral helium atoms. Unfortunately collisions with doubly charged ions could not be treated due to the lack of sufficiently accurate wave functions for the ions of interest.

§ 2. THEORY

According to the Landau–Zener formula, if the potential energy curves corresponding to $A+B^{2+}$ and to $A^{+}+B^{+}$ cross at the internuclear separation R_x (in units of a_0) when the interaction between the initial and final states is neglected, the total cross section for process (1) is given by†

$$Q=4\pi R_x^{2}pI(\eta) \qquad \ldots\ldots(3)$$

in which

$$I(\eta)=\int_1^{\infty}\exp(-\eta x)\{1-\exp(-\eta x)\}x^{-3}\,dx \qquad \ldots\ldots(4)$$

and

$$\eta=247\sigma M^{1/2}\{\Delta U(R_x)\}^2/(\Delta E)^2E_{\mathrm{i}}^{1/2} \qquad \ldots\ldots(5)$$

where σ is 1 or 2 according as the process is of type (1) or (2) respectively, p is the probability that the particles approach along the specified potential energy curve, M is the reduced mass of the system on the ^{16}O-scale, $\Delta U(R_x)$ is the energy separation between the exact potential energy curves at R_x, E_{i} is the initial kinetic energy of relative motion, and ΔE is the energy difference, all energies being in ev. The above formulae are used in § 3 to obtain cross sections for charge transfer processes involving triply charged ions and helium atoms.

The maximum value 0·113 of the integral $I(\eta)$ occurs when $\eta=0{\cdot}424$ and to fair approximation

$$R_x=27{\cdot}2\sigma/\Delta E \qquad \ldots\ldots(6)$$

provided ΔE is not too large. Hence equation (3) enables us to calculate the maximum value of the cross section Q. Furthermore, if the value of E_{i} for which the cross section attains its maximum is known, η and hence Q can be obtained without difficulty as functions of E_{i} by using equations (5) and (3), since the required integral has been tabulated (cf. Plazcek 1946, Moiseiwitsch 1955). Values of the parameter η determined in this way are used to obtain charge transfer cross sections in § 4 where they are compared with the cross sections obtained in the laboratory by Hasted and Smith (1956).

§ 3. CHARGE TRANSFER TO TRIPLY CHARGED IONS

The following processes involving triply charged ions have been investigated in this paper

$$\mathrm{He}+\mathrm{Be}^{3+}\rightarrow\mathrm{He}^{+}+\mathrm{Be}^{2+}(2\,^3\mathrm{S}), \qquad \ldots\ldots(7)‡$$

$$\mathrm{He}+\mathrm{Be}^{3+}\rightarrow\mathrm{He}^{+}+\mathrm{Be}^{2+}(2\,^3\mathrm{P}), \qquad \ldots\ldots(8)$$

$$\mathrm{He}+\mathrm{Li}^{3+}\rightarrow\mathrm{He}^{+}+\mathrm{Li}^{2+}(2\mathrm{s}\text{ or }2\mathrm{p}), \qquad \ldots\ldots(9)$$

$$\mathrm{He}+\mathrm{Be}^{3+}\rightarrow\mathrm{He}^{+}+\mathrm{Be}^{2+}(2\,^1\mathrm{P}), \qquad \ldots\ldots(10)$$

$$\mathrm{He}+\mathrm{Al}^{3+}\rightarrow\mathrm{He}^{+}+\mathrm{Al}^{2+}(3\mathrm{s}\,^2\mathrm{S}), \qquad \ldots\ldots(11)$$

$$\mathrm{He}+\mathrm{Mg}^{3+}\rightarrow\mathrm{He}^{+}+\mathrm{Mg}^{2+}(3\mathrm{s}\,^3\mathrm{P}). \qquad \ldots\ldots(12)$$

---

† Small correction terms depending essentially on the polarizabilities of the particles concerned have been omitted from the formulae for the sake of brevity (cf. Bates and Moiseiwitsch 1954). However, these terms were taken into account in the calculations presented in this paper.

‡ If no spectroscopic designation is given, the particle is in its ground state.

The calculations closely resemble those described in previous papers of this series (cf. Bates and Moiseiwitsch 1954) and will not be described in detail in the present paper.

The ground state helium wave function was determined by fitting the function calculated by Bartlett (1955) at large distances, to a sum of exponentials, while the wave functions of the excited electron in the doubly charged product ions were obtained by using the Coulomb approximation (cf. Bates and Damgaard 1949). The values obtained for R_x, $\Delta U(R_x)$ and the overlap integral $S_{\rm if}$ between the initial and final wave functions are given in table 1. The variation of these quantities with R_x can be seen by referring to figures 1 and 2 where $\log \Delta U$ and $\Delta U/S_{\rm if}$ respectively are plotted against $1/R_x$. It is apparent from figure 1 that $\log \Delta U$ is a smooth function of $1/R_x$ in agreement with the investigation carried out by Bates and Boyd (1956), on processes involving the transfer of charge from an H$^-$-ion to various positive ions. Magee (1940) has suggested that $X = R_x \Delta U/S_{\rm if}$ is approximately constant except for large R_x. It can be seen from figure 2 that a better approximation is that X is a linear function of R_x provided R_x is not too large.

Table 1

Process	R_x (a_0)	ΔU $(e^2/2a_0)$	$S_{\rm if}$
(7)	5·05	$7{\cdot}1 \times 10^{-2}$	$4{\cdot}5 \times 10^{-2}$
(8)	7·34	$6{\cdot}6 \times 10^{-3}$	$5{\cdot}2 \times 10^{-3}$
(9)	8·49	$3{\cdot}2 \times 10^{-3}$	$2{\cdot}8 \times 10^{-3}$
(10)	9·61	$3{\cdot}2 \times 10^{-4}$	$3{\cdot}0 \times 10^{-4}$
(11)	14·08	$3{\cdot}2 \times 10^{-6}$	$4{\cdot}0 \times 10^{-6}$
(12)	20·17	$1{\cdot}7 \times 10^{-9}$	$2{\cdot}8 \times 10^{-9}$

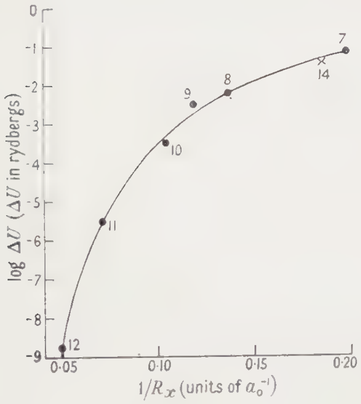

Figure 1.

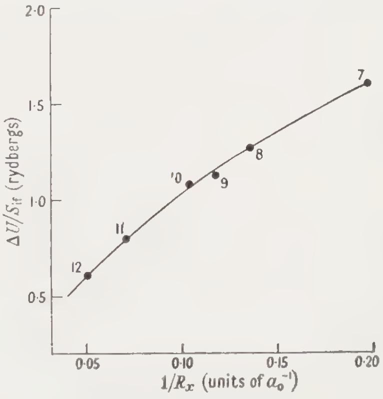

Figure 2.

Figure 1. Calculated values of ΔU (in rydbergs) for processes (7) (8), (9), (10), (11) and (12). The cross gives the value of ΔU for process (14) determined from the experimental data of Hasted and Smith (1956).

Figure 2. Calculated values of $\Delta U/S_{\rm if}$ (in rydbergs) for processes (7), (8), (9), (10), (11) and (12).

In figure 3 we give the cross sections calculated for processes (7), (8) and (9). The values of $\Delta U(R_x)$ are very small for the other three processes (10), (11) and (12) which have large values of R_x, and so the cross sections given by the

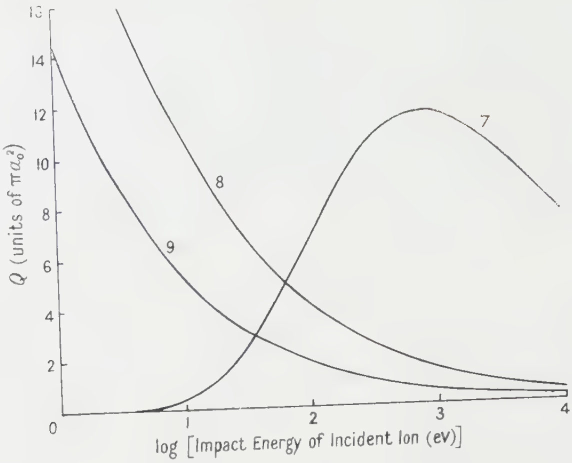

Figure 3. Cross sections Q (in πa_0^2) for the processes (7), (8) and (9).

Landau–Zener formula are minute except at very low energies. We therefore give only rate coefficients for them, obtained by averaging the product of the cross section and velocity of relative motion over a Maxwellian distribution. They are found to be constant down to very low temperatures and have the values

$$K_{10} = 1 \cdot 4 \times 10^{-11} \text{ cm}^2 \text{ sec}^{-1}, \; K_{11} = 6 \cdot 1 \times 10^{-15} \text{ cm}^2 \text{ sec}^{-1}$$

and

$$K_{12} = 7 \cdot 2 \times 10^{-21} \text{ cm}^2 \text{ sec}^{-1}$$

respectively.

§ 4. COMPARISON BETWEEN EXPERIMENT AND THEORY

Hasted and Smith (1956) have obtained cross sections for several charge transfer processes of type (1). For large R_x it can be seen from figure 1 that the value of $\Delta U(R_x)$ will be so small that the contribution to the cross section arising from curve crossing will be negligible compared with the contribution from other effects except for very low energies. This restricts comparison between the experimental cross sections of Hasted and Smith and the theoretical calculations based on the Landau–Zener method, to processes for which R_x is not too large. Consider the three processes

$$\text{Ne} + \text{A}^{2+} \rightarrow \text{Ne}^{+} + \text{A}^{+} \qquad \ldots\ldots(13)$$

$$\text{He} + \text{N}^{2+} \rightarrow \text{He}^{+} + \text{N}^{+} \qquad \ldots\ldots(14)$$

$$\text{Ne} + \text{N}^{2+} \rightarrow \text{Ne}^{+} + \text{N}^{+}. \qquad \ldots\ldots(15)$$

The values of R_x, corresponding to different states of the product ions for these processes, are given in table 2. Care has to be exercised in the interpretation of the experimental data due to the multiplicity of possible crossing points in processes (14) and (15). However, for process (14) the crossing points at $R_x = 8 \cdot 7$ and 28 are too large to give appreciable cross sections in the range of energies covered by Hasted and Smith. The crossing point at $R_x = 12 \cdot 4$ for process (15 can be dismissed for the same reason, and in addition for violation of Wigner's rule, while the contribution to the cross section arising from the crossing points at $R_x = 3{\cdot}4$ and $4{\cdot}4$ should be substantially smaller than that due to $R_x = 6{\cdot}8$.

Table 2

Process	State of Product Ion	R_x (a_0)
(13)	A^+ ^2P	4·5
(14)	N^+ ^3P	5·4
	^1D	8·7
	^1S	28
(15)	N^+ ^3P	3·4
	^1D	4·4
	^1S	6·8
	^5S	12·4

A comparison between theory and experiment is made in figure 4, the calculated cross sections being obtained on the basis of the Landau–Zener formula in the way described in § 2. The values of R_x were taken to be 4·5, 5·4 and 6·8 for processes (13), (14) and (15), and the maximum values of the cross sections were assumed to occur at the energies found experimentally by Hasted and Smith. It can be seen from figure 4 that the agreement between theory and experiment is good for these three cases, bearing in mind that the absolute accuracy claimed for the experiments was not closer than to ± 10%.

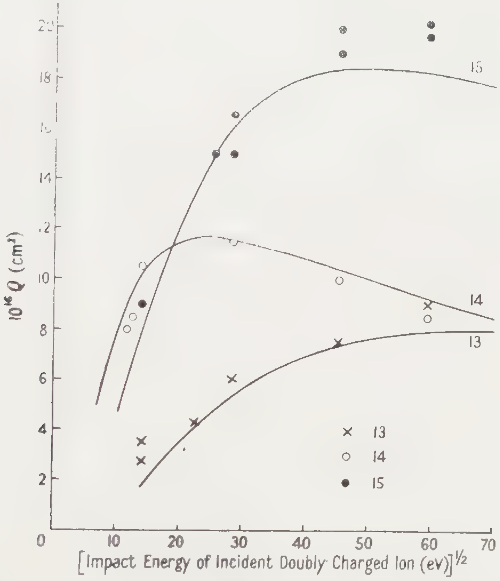

Figure 4. Comparison between the experimental cross sections of Hasted and Smith (1956) and the cross sections calculated by the Landau–Zener formula using one empirically determined parameter. The values of the experimental cross sections for processes (13), (14) and (15) are denoted by the points; the theoretical cross sections for the processes are given by the full lines.

The observed energy at which the maximum of a cross section occurs enables us to determine the value of $\Delta U(R_x)$. For process (14) the value of $\log \Delta U$

obtained in this way is given in figure 1 and it is in quite good agreement with that obtained from the investigation of triply charged ions in helium.

None of the other processes investigated by Hasted and Smith appear to have cross sections which can be explained on the basis of the Landau–Zener theory. It thus seems desirable that further experimental work should be carried out on processes involving the pseudo-crossing of potential energy curves in order to determine the range of validity of the theory more precisely.

ACKNOWLEDGMENT

It is a pleasure to thank Professor D. R. Bates for his interest in this investigation.

One of us (T. J. M. B.) wishes to thank the Ministry of Education for Northern Ireland for the award of a Scientific Research Grant.

REFERENCES

BARTLETT, J. H., 1955, *Phys. Rev.*, **98,** 1067.
BATES, D. R., and BOYD, J. M., 1956, *Proc. Phys. Soc.* A, **69,** 910.
BATES, D. R. and DAMGAARD, A., 1949, *Phil. Trans. Roy. Soc.* A, **242,** 101.
BATES, D. R., and LEWIS, J. T., 1955, *Proc. Phys. Soc.* A, **68,** 173.
BATES, D. R., and MOISEIWITSCH, B. L., 1954, *Proc. Phys. Soc.* A, **67,** 805.
DALGARNO, A., 1954, *Proc. Phys. Soc.* A, **67,** 1010.
HASTED, J. B., and SMITH, R. A., 1956, *Proc. Roy. Soc.* A, **235,** 354.
LANDAU, L., 1932, *Phys. Z. Sowjet.*, **2,** 46.
MAGEE, J. L., 1940, *J. Chem. Phys.*, **8,** 687.
MOISEIWITSCH, B. L., 1955, *J. Atmos. Terr. Phys.*, **23,** Special Supplement, Vol. 2, *Meteors*, ed. T. R. Kaiser.
PLAZCEK, G., 1946, *The Functions* $E_n(x)$ (National Research Council of Canada, Chalk River).
ZENER, C., 1932, *Proc. Roy. Soc.* A, **137,** 696.

Flash-Absorption Spectra of the Plasmas of Arcs and other Discharges

By W. R. S. GARTON and A. RAJARATNAM
Physics Department, Imperial College, London

MS. received 5th July 1957

Abstract. A technique is described in which a heavily loaded flash discharge is employed as a background source for observation of absorption spectra, when the absorbing gas column is strongly excited and, therefore, itself brightly luminous. Examples of the absorption spectra of the plasmas of several arc discharges, of both open and screw-stabilized type, are reproduced. Photometric determination of the total absorption under a number of lines, combined with relative emission intensities, yield values of line-reversal temperatures; some first results are reported for copper arcs.

§ 1. Introduction

Experiments on the optical absorption of a column of gas, excited electrically or otherwise, have produced many important results in several fields. The early work of Wood, Gaviola and others (Mitchell and Zemansky 1934), provided significant information on collision processes involving excited atoms. In a series of elaborate researches, Ladenburg (1933) examined, for example, the absorption spectrum of the positive column of a low pressure discharge interferometrically, using the results to derive excitation temperatures of the discharge and relative f-values of spectral transitions.

More recently, methods of flash-photolysis combined with flash-absorption spectroscopy have been successfully applied in studies of free radicals and reaction kinetics (Porter 1950, Norrish, Porter and Thrush 1953, Herzberg and Ramsay 1955, Nelson and Ramsay 1956). In such experiments, details of fast chemical processes—usually initiated by the photochemical action of a high intensity light flash of short duration—have been followed by means of the time variations in the absorption spectra of transient molecular species generated. In a few cases (White 1942, Nelson and Ramsay 1956) the primary excitation has been provided by a pulsed electrical discharge instead of by a light flash.

For investigations on the interactions of metastables in discharges and afterglows, elegant photoelectric techniques for the recording of absorption spectra, with high time resolution, have been recently developed at the Westinghouse Laboratories (Phelps and Pack 1955, Biondi 1955).

Work in progress in this laboratory shares some features with the researches cited, as regards objective, experimental method and applicability, but is aimed at observation of absorption spectra of strongly excited gases, with a view to determination of reversal temperatures of dense plasmas and measurement of relative oscillator strengths of transitions between energy levels of high excitation. Thus, while previous work has concerned absorption by a column of gas of modest brightness and population of higher excited states, our experiments relate to absorption spectra of sources which are themselves of high brightness and population temperatures. It is well known that a spectral line can be obtained reversed on a background continuum, only if the brightness temperature of the continuum exceeds the population temperature, in the absorbing gas, of that line. In arcs and other discharges, population temperatures in the range 5000° to 20 000°K are common, necessitating a very high brightness in any background source to be used. Since heavily loaded flash-discharge tubes can be built, which yield continua of brightness temperature in the range 30 000° to 50 000°K, according to current and wavelength, over the visible and near ultraviolet (Anderson 1932), it seemed likely that such a device could be used to register absorption spectra of the type sought. It is felt that sufficient success has been achieved to justify the following description of the experimental arrangement, and the first results.

§ 2. EXPERIMENTAL

The flash discharge is obtained by impulsive release of the energy on a condenser bank of several microfarads, charged to a high potential, through a constricted path in a gas at low pressure. The extremely bright 'Lyman continuum' emitted † was first investigated in detail by Anderson (1932). This continuum is fairly free of superposed emission and absorption lines over the visible and quartz ultraviolet, and extends, with diminishing intensity and increasing superposition of lines of Si, O etc., into the soft X-ray region. Convenient designs of flash tube for far ultraviolet absorption spectroscopy have been described by Worley (1942) and by Garton (1953); in the present experiments a tube of the latter pattern has been used. In brief, a condenser bank of 4 μF charged to 15 to 25 kV, is short-circuited once or twice per second through a low pressure gas in a 4–5·5 mm bore fused silica tube of 50 mm length, which is viewed end on. The nature of the filling gas is immaterial, so far as concerns intensity and its distribution; for far ultra-violet work, clean helium is used on account of its transparency, and though not essential, has some advantages when the tube is used at longer wavelengths.

The discharge repetition rate is limited by heating, and by the need to avoid excessively heavy charging gear, to no more than a few times per second. Rotating mirror photographs (Plate I, figure 1) and current oscillograms show the discharge to be oscillatory; only the first two half-cycles, each of about 5 μsec duration, are brightly luminous. To obtain the absorption spectrum of, for example, a continuously running arc, some means must therefore be used, to 'gate' the spectrograph slit to a period ranging, in practice, from a few μsec to several hundred μsec, according to the brightness of the absorbing source.

A block diagram of the experimental arrangement is shown in figure 2. The 'gating' of the spectrograph slit is performed by means of a pair of discs A, B, mounted on one axle and geared to rotate at one and at forty revolutions per second respectively. The discs carry radial slots which come into line with each other and with the slit S once per second, the slit thus remaining open for an adjustable period depending on the width of the slot in the fast disc. Diametrically opposite to the slot in each disc is a 10 μ slit; at the instant of exposure of the slit S, a pulse of light from a lamp L is passed to a photomultipler P, the signal from which passes, by way of a pulse amplifier G to the triggering electrode of the open 'trigatron' gap T, in series with the flash tube F. The photomultiplier pulse thus releases the charge on the main condenser bank C, through the flash tube, light from which passes to the slit S, via the absorbing light source D. An adjustable spark-gap T′ in parallel with the trigatron T, permits gentle starting. When care is taken in circuit layout, e.g., by reduction of stray inductance by the use of copper strip connections, the overall delay in the multiplier and trigger circuits amounts to only 1 μsec, and the shutter runs very reproducibly.

---

† The Lyman continuum is probably of different origin and more intense than that obtained with inert gas flash-tubes (Porter 1950)—which work at lower loadings cm^{-3}—ahd is freer of overlying emission lines above 2000 Å.

The absorption spectra of a number of arcs, of both free-burning and 'screw-stabilized' types, and of other discharge plasmas have been photographed, using Hilger medium-glass and-quartz prism instruments for exploratory work, and the third order of an Eagle mounted 3 metre grating for cases requiring high resolution, e.g., the measurement of line absorption coefficients. Intensity measurements and determination of absorption coefficients have been made by densitometry of a set of calibration exposures, registered on the same plate as the spectrum under study, and obtained by use of a stepped slit, with the grating spectrograph set at its secondary astigmatic focus. In this procedure it is, of course, essential that all exposures on a plate shall be made with the rotating shutter, as otherwise large errors would result from intermittency effects. Details of the various absorbing light sources are given individually under § 3.

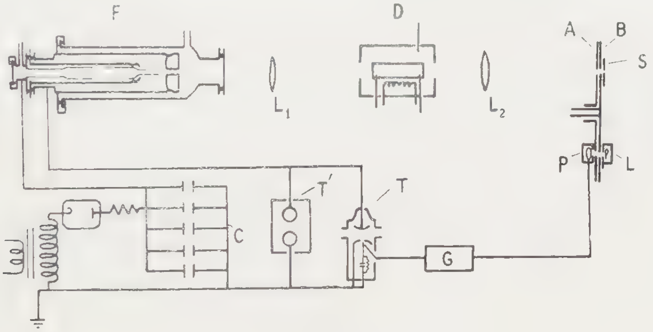

Figure 2.

§ 3. Results and Discussion

3.1. *Flash-Tube Brightness*

As stated in § 2, the flash-tube emission continuum is oscillatory in time, the first two half-cycles occupying a total of some 12 μsec and being responsible for most of the light. In the majority of the experiments described below the rotating shutter has embraced the first four half-cycles. It is of practical importance to know the order of magnitude of the effective brightness temperature of the flash source used under these conditions. Accordingly, determinations have been made, over the wavelength range 5100 to 3000 Å, of the flash continuum intensity, relative to that of the anode crater of a carbon arc run under standard conditions (Euler 1953). The results yield an effective brightness temperature for the first four half-cycles, ranging from 20 000°K at 5100 Å, to 30 000°K at 3000 Å; the peak and average brightness temperatures in the first half-cycle, though not yet measured by us, are obviously much higher (cf. Anderson 1932).

3.2. *Absorption Spectra of Free Burning Arcs*

Here the absorbing light source consisted of a simple vertical arc in air, between suitable solid electrodes (convection stabilized arc). A much reduced image of the flash discharge was formed by a concave aluminized mirror, instead of by the lens L_1 in figure 2, at the axis of the arc column, which in turn was imaged upon the spectrograph slit by L_2. The absorption spectra were thus obtained with 'side-on' illumination of the arc channel.

(*a*) *Carbon arc.* With arc currents between 6 and 12 A, strong absorption of the 0–0 sequence of the CN violet system was observed. The peak absorption in the 0–0 head, measured on grating spectra, amounted to 31% to 52% according to current.

(*b*) *The iron arc.* A 10 A arc between iron electrodes of $\frac{3}{8}$ in. diameter showed very heavy absorption of all strong and medium Fe I lines (figure 3, Plate 1). In the region of 2400 Å occurs a wide patch of apparently structureless absorption, of at present unknown origin, which certainly has no associated feature in the Fe emission spectrum. Some of the absorption lines present in the reproduction, start on energy states as high as 30 000 cm^{-1} (of the order of 3·8ev), above the Fe I ground level.

(*c*) *The copper globule arc.* This type of Cu arc (Milbourn 1934) has been recommended by Shenstone (1948) as the best source of development of the Cu arc spectrum. The arrangement consists of a pair of graphite poles, of which the lower is cathode, and carries a molten Cu–CuO bead; the arc runs stably and reproducibly.

At lower arc currents, of the order of 6 A, the flash-absorption spectrum contains all strong and many medium lines of Cu I, throughout the visible and quartz ultraviolet. The majority of these lines start on the metastable $d^9s^2\,{}^2D_{5/2,3/2}$ levels, which lie some 1·5 ev above the ground state; figure 4 (Plate II) shows the quartz ultra-violet absorption spectrum of the centre of the column of a 10 A globule arc. With an arc current of 12 A, and the flash imaged just above the cathode spot of the arc, the absorption is much more intense; under these conditions only the rather weak known emission lines of Cu I fail to appear in absorption. Some of the absorption lines here observed start on levels as high as 5 ev above the ground state, and terminate on doubly excited states lying above the Cu I ionization potential, which are known from the work of Shenstone (1948) and of Allen (1932), to auto-ionize readily. In this process, the atom raised to a doubly excited state makes a radiationless transition, leading to a positive ion and ejected electron. That interesting use may be made of absorption lines having auto-ionizing upper states will appear from the discussion in § 4. Some of these lines can be seen in figure 5 (Plate II) which shows absorption by the arc column just above the cathode spot, in the region of the Cu resonance lines, photographed in the third order of the grating spectrograph.

3.3. *Absorption Spectra of Screw-Stabilized Arcs*

It has long been known that an arc discharge undergoes interesting modifications when the convection currents, which largely control the behaviour of the free burning arc, are replaced by a current of air or other gas, forced into cylindrical or helical flow about the arc axis (Grotrian 1915, von Engel 1929). The most striking features of such an arc comprise a rise in plasma temperature, a high degree of axial stability and the facility with which the arc column can be drawn out to a much greater length than in the case of the free arc. The stabilized arc has special advantages for spectrocopic investigations, of which a number have been made (e.g. Huldt 1948). In the present absorption experiments, for instance, by using in 'end-on' fashion a horizontal arc between hollow electrodes, the absorption of a considerable length of steady plasma can be observed, and difficulties arising from the steep radial temperature gradient, which affect the 'side-on' aspect of an arc channel, can be avoided.

The form of arc used by us is a slightly modified version of a design due to Aarts (1952), the stabilizing action being produced by a screw shaped current of air or nitrogen. As the publication cited is not readily available in this country, a schematic diagram of our construction is shown in figure 6. The arc is drawn between two hollow cylindrical electrodes A, C, which slide in tapered graphite blocks G, G′, in turn supported by brass cylinders B, B′, which are double walled for water cooling. The cylindrical housing T contains a set of fixed vanes, by which gas injected excentrically is set into screw motion as indicated, and emerges through the chimney of the brass cylinder T′; T and T′ are separated by a length of Pyrex tubing P. To obtain the absorption spectra, the light from the flash capillary was focused along the axis of one of the hollow electrodes to form an image at the centre of the arc column; the light emerging through the other electrode was, in turn, imaged on the slit.

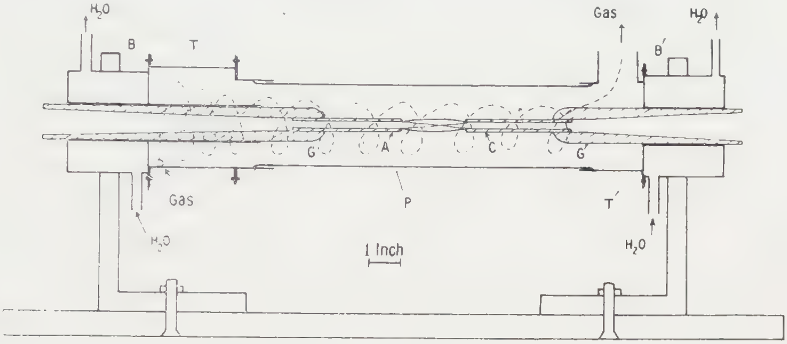

Figure 6.

(*a*) *Stabilized carbon arc.* The poles here consisted of tubes of graphite, of moderate purity. The absorption spectrum of figure 7 (Plate II), showing the CN 0–0 sequence in the grating third order, was obtained with an arc of 24 A, 32 mm long. The absorption is very intense, amounting to 98% in the 0–0 head; the rotational structure can be followed to about the R 100 line, and densitometry can be performed with reasonable accuracy as far as R70.

(*b*) *Stabilized copper arc.* The electrodes here consisted of a graphite cathode C, and an anode A of thick walled copper tubing. Currents up to 15 A were used, the limit being set by the need of avoiding too rapid melting of the copper electrode. Spectra of arcs of 5 cm length at 15 A were recorded, together with calibration exposures, to enable evaluation of absorption coefficients for the purposes of § 4. A disappointing observation has been that, in spite of the greatly increased path length, as compared with that at which the absorption spectrum of the open arc (figures 4 and 5) was obtained, the absorption is on the whole weaker. The reason is that, under the gas flow conditions used, the channel of the stabilized arc is much broader than that of the open arc, resulting in a lower concentration of copper vapour. A consequence has been that accurately measurable absorption of auto-ionization broadened lines has not been obtained to date with the stabilized arc. However, many of the normal lines are strongly absorbed, and these are used in § 4 to estimate reversal temperatures of this arc.

§ 4. DETERMINATION OF REVERSAL TEMPERATURES OF PLASMAS

It was stated in § 1 that a primary intention has been to employ flash-absorption spectra for the determination of reversal temperatures of discharge plasmas. Some preliminary results are here given of work which, though fairly advanced, requires some extension before being published in full.

The line-reversal method for determination of the temperature of a hot gas has been widely applied to flames, in which connection the literature has been summarized by Broida (1955) and by Gaydon and Wolfhard (1953). Briefly, if a column of hot gas, which is emitting a spectral line of an atomic species present, is backed by a light source giving a continuous spectrum, the spectrum of the transmitted radiation will show either a bright line on a weaker background or a dark line on a brighter background, according as the brightness temperature of the continuum is lower or higher than the 'excitation temperature' of the spectral line of the hot gas. If the two temperatures be equal, the discrete line vanishes into the continuum, and if the brightness temperature of the background source is known, the temperature of the hot gas is determined.

The reversal technique has been little used on discharge plasmas, and then only for those of feeble loading (Ladenburg 1933), presumably for lack of a background continuum of high enough brightness. While the flash tube is bright enough to overcome this difficulty, a somewhat modified procedure is necessitated by the fact that even the effective brightness temperature of the flash cannot be said to be known, since the progressive erosion of the silica capillary results in variation from one flash to the next.

The modified procedure is as follows. Let us consider a uniform column of hot gas at T°K, of length l in some particular direction, and containing atoms which emit a spectral line of central frequency ν_0. The measured total emission intensity of the line, in the preferred direction, will be

$$J = CB(\nu_0, T)\int_{\text{line}} (1 - e^{-k(\nu)l})d\nu \qquad \ldots\ldots(1)$$

where $B(\nu, T)$ is the Planck function of the mass of gas, $k(\nu)$ its absorption coefficient and C is a constant. The exponential term represents, of course, the presence of self-absorption. If we now suppose the gas to be backed by a light source of much higher brightness temperature, the total absorption (or equivalent breadth) of the absorption line is

$$W = \int \frac{I_0 - I}{I_0}\, d\nu = \int (1 - e^{-k(\nu)l})d\nu \qquad \ldots\ldots(2)$$

where I_0, I are the incident and emergent intensities.

If we work at a wavelength sufficiently short relative to the temperature T, then forced emission, represented by the term -1 in the Planck denominator, can be neglected, and from (1) and (2), $J/W = CB(\nu_0, T)$ reduces to

$$\log \frac{J}{W{\nu_0}^3} = \text{const} - \boldsymbol{h}\nu_0/\boldsymbol{k}T \qquad \ldots\ldots(3)$$

where the J's need be only relative emission intensities. Thus if we measure the latter by comparison with, for example, the standard carbon arc crater (Euler

1953), and also measure the total absorptions W for a number of spectral lines ν_0, the left-hand side of (3) can be plotted versus ν_0 ; the occurrence of a straight line plot will demonstrate that to speak of 'temperature', as regards the populations of the energy levels responsible for the spectral lines involved has meaning, and T can be derived from the slope. It will be seen that instead of establishing the precise reversal point, and using a known value of the brightness temperature of the background, we are here making an observation on each side of the reversal point, and averaging over a number of lines.

The method has been applied to the copper globule and screw-stabilized arcs, the more definite results relating to the latter form. An example, which represents the reduction of data from six plates, is given in figure 8. Each of the spectral lines used in this plot represents a transition between one of the $d^9s^2\ {}^2D$ metastable levels, and some higher level. It will be seen that two different straight lines can reasonably be drawn, respectively, through the sets of points which relate to ${}^2D_{5/2}$ and ${}^2D_{3/2}$ as lower level, save for the fact that one particular line of the group, $(d^94s^2\ {}^2D_{3/2}–d^94s4p\ {}^2F_{5/2})$, falls nowhere near either of the straight lines drawn. The fact that a single straight line plot is not obtained, within the limits of accuracy of the experiments, could be interpreted as indicating either serious departure from thermal equilibrium in the arc channel proper, or the presence of confusing effects due to cooler regions of copper vapour just within the ends of the hollow electrodes used. However, the latter possibility provides no obvious explanation of the large anomaly in the position of the experimental point for the line λ3279 ; there is some risk that this arises from a trace of Fe impurity in the carbon used for one electrode, since a strong Fe line lies nearby.

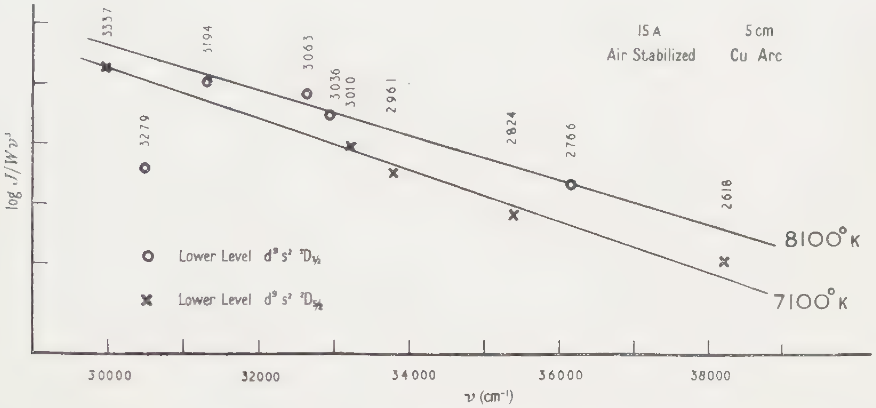

Figure 8. Air stabilized Cu arc ; 15A, 5 cm.

As mentioned under § 3.2 (*c*), particular interest attaches to application of the above reversal temperature method, to lines which show auto-ionization broadening. The reason for this interest is that the upper levels concerned in the emission of such lines are probably populated, in an arc, chiefly by radiationless capture—by the positive ions—of electrons from the adjacent series limit continua, rather than by direct excitation of neutral atoms from lower levels by atom–atom or electron–atom impacts. Consequently, reversal temperatures of spectral lines of this kind can be expected to reflect to some extent the electron temperature; if the latter differs substantially from the population temperatures of the normal levels of the atom, the fact should be evident on a log $J/W\nu^3$ plot, which embraces both lines which do and do not show auto-ionization. Though, as already mentioned, it has not yet been possible to investigate this point, using the screw-stabilized arc, because auto-ionization broadened lines have been obtained but weakly in absorption therein, some first results on the region immediately above the cathode spot of the globule arc are of interest. Data averaged from several plates are plotted in figure 9. The crosses here refer to lines not affected by auto-ionization, the circles to lines so affected ; the vertical stroke through each point denotes the spread of the results from the several plates. Though this spread is large for some lines, it is clear that a reasonable straight line plot can embrace, at most, only the shorter wavelength members of the group of lines not affected by auto-ionization. However, more striking than the fact that the longer wavelength lines of the same group fall away from the straight line drawn, is the occurrence of a very wide scatter of points relating to lines which are auto-ionization-broadened. This scatter is certainly not explicable by fluctuating arc conditions from one plate to the next. Qualitatively, these results merely point to a large departure from thermal equilibrium conditions in the cathode region of the globule arc, which is not surprising, since it is generally believed that the approximate thermal equilibrium, supposed to exist in the main body of an arc channel does not apply in the neighbourhood of the electrodes (cf. Edels 1950, Loeb 1939). However, there is evidently fair scope for a more detailed study of reversal temperatures of atmospheric pressure arcs and of other discharges, which may help to clarify quantitatively issues of this sort.

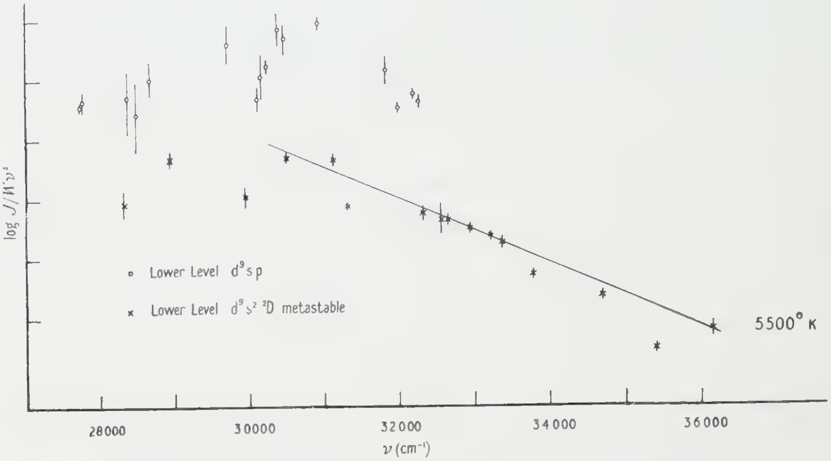

Figure 9. 11 A open copper globule arc, cathode region.

The technique described in this paper is expected to be useful also in determination of relative f-values of transitions between energy states, one or both of which may be highly excited, and in investigations of the time course of the concentrations of excited atoms in fairly heavy discharges, and in bright afterglows following discharge cut-off. It will be of particular interest to carry the work on the copper stabilized arc into the vacuum ultraviolet, since in this region strong absorption lines exist, which arise from transitions from the metastable $d^9s^2\ ^2D$ levels to higher auto-ionizing levels.

REFERENCES

AARTS, C. J. M., 1952, *Investigation of an Arc Discharge which is Stabilized with a Screw-shaped Stream of Air, Thesis,* Utrecht State University.

ALLEN, C. W., 1932, *Phys. Rev.*, **39,** 42, 55.

ANDERSON, J. A., 1932, *Astrophys. J.*, **75,** 394.

BIONDI, M., 1955, *Report of the International Symposium on Electrical Discharges in Gases, Delft* (The Hague: Nijhoff), p. 157.

BROIDA, H. P., 1955, *Temperature, its Measurement and Control in Science and Industry,* Vol. 2 (London: Chapman and Hall), p. 265.

EDELS, H., 1950, British Electrical and Allied Industries Research Association, *Technical Report* L/T230.

von ENGEL, A., 1929, *Z. tech. Phys.*, **11,** 505.

EULER, J., 1953, *Ann. Phys., Lpz.*, **11,** 203.

GARTON, W. R. S., 1953, *J. Sci. Instrum.*, **30,** 119.

GAYDON, A. G., and WOLFHARD, H. G., 1953, *Flames, their Structure, Radiation and Temperature* (London: Chapman and Hall), Chaps. 10–12.

GROTRIAN, W., 1915, *Ann. Phys., Lpz.*, **47,** 141.

HERZBERG, G., and RAMSAY, D. A., 1955, *Proc. Roy. Soc* A, **233,** 34.

HULDT, L., 1948, *Ark. Mat. Astr. Fys.*, **36,** No. 3.

LADENBURG, R., 1933, *Rev. Mod. Phys.*, **5,** 243.

LOEB, L. B., 1939, *Fundamental Processes of Electrical Discharges in Gases* (New York: Wiley), Chap. 11.

MILBOURN, M., 1934, *J. Inst. Metals*, **55,** 275.

MITCHELL, A. C. G., and ZEMANSKY, M. W., 1934, *Resonance Radiation and Excited Atoms,* (Cambridge: University Press), Chap. 2.

NELSON, L. S., and RAMSAY, D. A., 1956, *J. Chem. Phys.* **25,** 372.

NORRISH, R. G. W., PORTER, G., and THRUSH, B. A., 1953, *Proc. Roy. Soc.* A, **216,** 165.

PHELPS, A. V., and PACK, J. L., 1955, *Rev. Sci. Instrum.*, **26,** 45.

PORTER, G., 1950, *Proc. Roy. Soc.* A, **200,** 284.

SHENSTONE, A. G., 1948, *Phil. Trans. Roy. Soc.* A, **241,** 297.

WHITE, J. U., 1942, *J. Opt. Soc. Amer.*, **32,** 285.

WORLEY, R. E., 1942, *Rev. Sci. Instrum.*, **13,** 67.

Excitation Functions up to 980 MeV for Proton-Induced Reactions in some Light Elements

By J. L. SYMONDS†, J. WARREN‡ AND J. D. YOUNG§
Department of Physics, University of Birmingham

MS. received 20th June 1957

Abstract. A study has been made of some of the active products from the high energy bombardment of carbon, nitrogen, oxygen and fluorine. The ratios of cross sections to the $^{12}C(p, pn)^{11}C$ cross section were found and the excitation functions estimated. Deviations from a monotonic decrease of cross section with energy for some reactions have been found and are discussed. Evidence exists for a marked dependence of the (p, pn) cross section on the energy level structure of the residual nucleus.

---

§ 1. Introduction

The ^{11}C activity produced in carbon by high energy protons has been studied previously (Burcham, Symonds and Young 1955) and an excitation function presented for the cross section for energies up to 980 Mev. These results, together with those of other authors (Aamodt, Peterson and Phillips 1952, Crandall, Milburn, Pyle and Birnbaum 1956), have been summarized by Rosenfeld, Swanson and Warshaw (1956). The cross section for this reaction has been used as the basis for all the measurements presented and any absolute cross section quoted has been deduced from the ratio of its cross section to that for the production of ^{11}C from carbon. In all cases, the measured ratios are quoted as well as the deduced cross section.

Up to the present, the study of high energy proton-induced reactions in light nuclei has not covered a wide field. The main line of investigation generally has been through the use of cloud chambers and photographic plates. The present work was undertaken to investigate as many as possible of the light element reactions which result in β-active products. Proton energies from 420 to 980 Mev were used. By using bombardment times of different length, it was possible adequately to resolve activities whose half-lives were widely different. Most of the β-activities from carbon, oxygen, nitrogen and fluorine were resolved from the gross decay curves because of their widely differing half-lives.

In keeping with the notation of a previous paper (Chackett, Chackett, Reasbeck, Symonds and Warren 1956), we shall denote by subscript the chemical identity of the target while the residual nucleus investigated will be in brackets, e.g. $\sigma_N(^{11}C)$ would represent the cross section for the production of ^{11}C from nitrogen.

---

† Now with the Australian Atomic Energy Commission, Sutherland, New South Wales, Australia.

‡ Now at Enrico Fermi Institute, University of Chicago, Chicago, U.S.A.

§ Now at the Research Laboratory, Associated Electrical Industries Ltd., Aldermaston, Berkshire.

§ 2. Experimental Method

2.1. *General*

The main features of the proton synchrotron are described by Moon, Riddiford and Symonds (1955). The irradiations were all carried out in the re-entrant tube which was mounted in the vacuum box, as described by these authors in their figure 2, region E. Target holder arrangements were similar to those described by Burcham *et al.* (1955), the target foils being mounted vertically with the normal to their surface along the radius of the machine. Beam intensities of up to 10^9 protons cm^{-2} per pulse were obtained in the target region of the re-entrant tube, while the internal beam was about 10^{10} protons per pulse, with a pulse repetition rate of once in ten seconds. Proton energies from 420 to 980 MeV could be used in the re-entrant tube and the energies were known to about 1%. The beam was forced out onto the target as described by Moon *et al.* (1955).

2.2. *Target Preparation and Materials*

The beam intensities were monitored by polythene foils which were cut from sheet. These foils had an average thickness of 14 mg cm^{-2} and were 2 cm × 1 cm in size. Guard foils were also used to protect the monitor foils from nuclei knocked out from the material being studied and also to protect the stack of foils in the holder. The preparation of other sections of the target depended on the substance used.

Nitrogen.

Initially, the substance containing nitrogen which best suited all requirements was boron nitride (BN_3). This had the great advantage that boron produced no contaminating activities. Unfortunately, the only sample which could be obtained was found to contain a considerable proportion of oxygen, which eventually precluded the use of this material. Melamine (obtainable in Analar purity) was finally used. This was finely ground and compressed between polished faces in a hydraulic press to give a brittle sheet. The thickness varied from sample to sample but was approximately 60 mg cm^{-2} on average. The sheet was reduced to pieces 2 cm × 1 cm in size and, with care, these pieces could be mounted both in the holder and under the counter. The main disadvantage in the use of melamine was the correction which had to be made for the ^{11}C activity from the carbon in the melamine molecule. However, the allowance was easily made since the carbon was present in stoichiometric proportions.

Oxygen.

Finely divided boric acid (H_3BO_3) was available in Analar purity and this material could be compressed in the same way as the melamine samples. The sheet produced was generally a little thicker but not as brittle as the melamine and could be formed into a sheet of more consistent thickness.

Fluorine.

This was irradiated in the form of polytetrafluorethylene (CF_2) sheet which could be obtained in a thickness of 51·5 mg cm^{-2}. The sheet was easily handled and readily mounted with the polythene to form the stacks for irradiation.

Stack Preparation.

The foil to be counted was prepared in each case with a guard foil on either side. The three foils of the material under investigation had a group of three monitor foils of polythene on either side. The nine foils were then mounted in the holder as described. The polythene foils in front of and behind the sample foils provided a monitor of the beam intensity across the sample.

2.3. *Beta Counting*

While being counted, the active foils were supported by their corners only, to reduce the amount of back scattering to a minimum. The samples were counted with a screened GM4 end window (7 mg cm^{-2}) Geiger counter. Two carefully intercalibrated counting sets were used and care was taken to ensure that foils were always inserted in an identical position under the counter.

All measured activities, extrapolated to midtime of bombardment, were corrected for counter background and dead time losses. Self absorption in the sample was estimated by carrying out a series of measurements with foils of differing thickness. The correction to zero thickness was estimated from a curve fitted to the measured data and of the form $[1-\exp(-\mu t)]/\mu t$ where μ is the absorption coefficient for the particular beta particles in mg^{-1} cm^{2} and t is the sample thickness in mg cm^{-2}. The values of μ used were obtained from the work of Whitehouse and Putman (1953). It is possible that small systematic errors may result from this procedure but allowance is made for this in setting the total limit of error to the measurement. Corrections have also been made for absorption in the counter window and for the length of bombardment where necessary.

For some of the work, a 4π continuous flow methane proportional counter was developed. The investigation of the ratio $\sigma_C(^{10}C)/\sigma_C(^{11}C)$ using 5 mg cm^{-2} polythene foils was carried out with this equipment. All the work was to have been carried out with this type of counter but difficulty in producing very thin samples of substances other than polythene made the counting solid angle an unreliable 4π. Satisfactory corrections could not be made to give sensible results from the nitrogen and oxygen samples and this counter was abandoned in favour of the standard counting set.

2.4. *Resolution of the Gross Decay Curves*

From the gross decay curves for the light elements under discussion, the relative proportions of activity from the contributing isotopes may be readily extracted. Only in one instance was this impossible, viz. ^{14}O and ^{17}F. In the study of carbon, the ^{10}C activity was resolved from that of the ^{11}C by using one pulse for the former irradiation and twenty pulses for the latter. Nitrogen presented more of a problem since ^{13}N and ^{11}C have half-lives of 10·1 minutes and 20·5 minutes respectively. Analysis by three independent observers showed that it was possible to achieve good resolution accuracy. The same problem arose in the case of the oxygen but the analysis proved to be no more difficult. The ^{10}C and ^{15}O activities could be separated from ^{11}C and ^{13}N by using short and long bombardments. Fluorine was unusual in that no ^{13}N activity could be detected, and only an upper limit could be set to the cross section. The removal of this complication meant that all the other activities could be resolved except for ^{17}F and ^{14}O yields since these isotopes have identical half-lives.

§ 3. RESULTS

The results were obtained in several independent runs at each energy and each material. Tables 1, 2, 3, and 4 give the results expressed as the ratio of the particular cross section to that of $\sigma_C(^{11}C)$ at each energy. Relative errors are given with each table. These were estimated as the r.m.s. errors at any particular energy and isotope for those runs made. The total errors are an estimate of the overall errors for the measurements made with a given substance. These include both relative and possible systematic errors.

Table 1. Relative and Absolute Yields of ^{10}C from Carbon

(1)	(2)	(3)	(4)
980	0·114 ± 0·007	23·4	2·67
832	0·099 ± 0·007	25·8	2·55
648	0·108 ± 0·007	28·2	3·04
522	0·105 ± 0·007	30·8	3·23
420	0·102 ± 0·007	32·3	3·30
365	0·107 ± 0·013	33·2	3·55

(1) Proton energy (MEV), (2) $\sigma_C(^{10}C)/\sigma_C(^{11}C)$, (3) assumed $\sigma_C(^{11}C)$ (mbn), (4) estimated $\sigma_C(^{10}C)$ (mbn). Relative errors are quoted in column (2).

Table 2. Relative Yields of Various Isotopes from Nitrogen

(1)	(2)	(3)
980	0·46	0·88
835	0·47	0·98
772	0·41	0·74
710	0·41	0·63
648	0·35	0·66
522	0·33	0·71
420	0·34	0·70

(1) Proton energy (MEV), (2) $\sigma_N(^{13}N)/\sigma_C(^{11}C)$, (3) $\sigma_N(^{11}C)/\sigma_C(^{11}C)$. Relative errors : (2), ± 8%, (3), ± 10%; total errors : (2), ± 15%, (3), ± 15%.

Table 3. Relative Yields of Various Isotopes from Oxygen

(1)	(2)	(3)	(4)	(5)
980	1·60	0·32	0·44	0·14 ± 15%
835	1·50	0·24	0·41	—
648	1·08	0·22	0·28	—
522	1·30	0·22	0·34	—
420	0·95	0·20	0·26	0·19 ± 30%

(1) Proton energy (MEV), (2) $\sigma_O(^{15}O)/\sigma_C(^{11}C)$, (3) $\sigma_O(^{13}N)/\sigma_C(^{11}C)$, (4) $\sigma_O(^{11}C)/\sigma_C(^{11}C)$, (5) $\sigma_O(^{10}C)/\sigma_C(^{11}C)$. Relative errors : (2), 12%, (3), 10%, (4), 10%; total errors : (2), 20%, (3), 15%, (4) 15%.

Table 4. Relative Yields of Various Isotopes from Fluorine

(1)	(2)	(3)	(4)	(5)	(6)	(7)
980	0·85	0·55	0·35	0·17	0·05	<0·02
835	0·89	0·59	0·27	—	—	
726	1·25	0·47	0·35	—	—	
648	1·06	0·43	0·33	—	—	
522	0·85	0·53	0·31	—	—	
420	0·71	0·30	0·32	0·15	0·04	

(1) Proton energy (MEV), (2) $\sigma_F(^{18}F)/\sigma_C(^{11}C)$, (3) $\sigma_F(^{11}C)/\sigma_C(^{11}C)$, (4) $\sigma_F(^{15}O)/\sigma_C(^{11}C)$, (5) $\sigma_F(^{10}C)/\sigma_C(^{11}C)$, (6) $\sigma_F(^{14}O + ^{14}F)/\sigma_C(^{11}C)$, (7) $\sigma_F(^{13}N)/\sigma_C(^{11}C)$. Relative errors : (2), 8%, (3), 10%, (4) 15%, (5), 30%, (6), 30%; total errors : (2), 12%, (3) 15%, (4), 20%, (5), 30%, (6), 30%.

In all results relating to ^{18}F, a 3% correction has been added to correct for the ratio of K-capture to positron emission in that isotope (Drever, Moljk and Scrobie 1956).

Due to the method of irradiation in the re-entrant tube, it was felt that a check was necessary on the possible effects of secondary radiation background. To do this, fluon foils were irradiated inside the machine on a moving target. The target thickness was kept to an absolute minimum and the target was held in a clip holder (see similar comparison measurement in Chackett *et al.* 1955). The results of the comparison are given in table 5. There is no observable difference within experimental error.

Table 5. Background Check Runs on Fluorine

(1)	(2)	(3)
980	0·89	0·85
835	0·92	0·89
648	1·06	1·06

(1) Proton energy (MeV), (2) inside irradiation $\sigma_F(^{18}F)/\sigma_C(^{11}C)$, (3) re-entrant tube.
Estimated errors : (2), ±10%, (3), ±8%.

The results in all these measurements are all dependent on the cross section $\sigma_C(^{11}C)$ and we were faced with the problem of the choice of values at each energy. Due to a deviation from a monotonic decrease which we believe is present in the measurements of this cross section reported earlier (Burcham *et al.* 1955), two sets of data were taken for the basic cross section. The first estimation was based on the actual experimental values shown in column (2) of table 6 (*a*) with interpolated values for those energies where no experimental value existed. The second estimation was based on a straight line through the experimental values and these are given in table 6 (*b*), column (2). The relevant cross section data resulting from these figures and the cross section ratios of the previous tables are given in tables 6 (*a*) and 6 (*b*).

The experimental data in column (2) of table 6 (*a*) differs from the final results in the paper of Burcham *et al.* (1955). A more exacting check on the neutron contamination of the beam indicated that the correction made in that paper had been too large (Young 1956). It is believed that the figures quoted in the table are more nearly correct.

The data for the more complex reactions are given in Table 6 (*c*) using the cross section values of table 6 (*b*).

Table 6 (*a*). Estimated Cross Sections for (p, pn) Reactions
First Assumption (see text)

(1)	(2)	(3)	(4)	(5)
980	23·4	10·9	37	19·9
835	30·0	14·2	45	26·7
772	29·2†	11·9	—	—
726	28·0†	—	—	35·0
710	27·6†	11·5	—	—
648	25·5	8·9	28	27·0
522	33·2	10·8	43	28·2
420	32·3	10·9	31	22·9

(1) Proton energy (MeV), (2) $\sigma_C(^{11}C)$ (mbn), (3) $\sigma_N(^{13}N)$, (4) $\sigma_O(^{15}O)$, (5) $\sigma_F(^{18}F)$.
† indicates interpolated figures.

Table 6 (*b*). Estimated Cross Sections for (p, pn) Reactions
Second Assumption (see text)

(1)	(2)	(3)	(4)	(5)
980	23·4	10·9	37	19·9
835	25·8	12·2	39	23·0
772	26·8	10·9	—	—
726	27·5	—	—	34·4
710	27·7	11·3	—	—
648	28·2	9·9	30	29·9
522	30·8	10·0	40	26·2
420	32·3	10·9	31	22·9

(1) Proton energy (MeV), (2) $\sigma_C(^{11}C)$ (mbn), (3) $\sigma_N(^{13}N)$, (4) $\sigma_O(^{15}O)$, (5) $\sigma_F(^{18}F)$.

Table 6 (*c*). Cross Section Data for More Complex Reactions

(1)	(2)	(3)	(4)	(5)	(6)
980	7·5	10·3	20·6	12·9	8·2
835	6·2	10·6	25·2	15·2	7·0
772	—	—	19·8	—	—
726	—	—	—	13·2	9·6
710	—	—	17·4	—	—
648	6·2	7·9	18·6	12·1	9·3
522	6·8	10·5	21·9	16·3	9·6
420	6·5	8·4	22·6	9·7	—

(1) Proton energy (MeV), (2) $\sigma_O(^{13}N)$, (3) $\sigma_O(^{11}C)$, (4) $\sigma_N(^{11}C)$, (5) $\sigma_F(^{11}C)$, (6) $\sigma_F(^{15}O)$.
All cross sections quoted in mbn.

§ 4. DISCUSSION

4.1. *The* (p, pn) *Reactions*

Comparison of the results of table 6 for any particular energy shows that there is a remarkable difference in the magnitude of the cross section for the (p, pn) reaction in the four nuclei studied, varying from as low as 10 mbn for $\sigma_N(^{13}N)$ to 40 mbn for $\sigma_O(^{15}O)$. An explanation for this variation may be found in the energy level structure of the residual nuclei in each reaction.

We may consider any reaction at these high energies as the result of a two stage process. In the first stage, the incoming nucleon is considered as seeing only one nucleon in the target nucleus because of its high momentum and consequent small wavelength relative to the radius of the nucleus (Serber 1947). The two interacting nucleons may have further collisions in the nucleus before they finally leave and more nucleons may be knocked out. This process is followed by a second stage in which further nucleons may be evaporated to remove the excess energy deposited in the residual nucleus. Finally, the remaining nucleus reaches its ground state by gamma emission.

In light nuclei, due to their small nuclear radius, the first stage will not in general involve many nucleons. Moreover, if the deposited energy after stage one is in excess of about 25 MeV, these nuclei will generally break down into alpha particles, the requirement is that the initial collision should be with a neutron in the target nucleus and that only this neutron should be involved. Further, the interaction must result in a deposition of energy in the residual nucleus less than that required to excite the nucleus above its first particle emitting level. The excess energy will then be eliminated by gamma emission. The dependence of the magnitude of the cross section on the energy of the first particle emitting level above the ground state should therefore be very strong. In some cases, there are a few levels above these particle emitting states by which the excited nucleus may reach its ground state by gamma emission without involving the intermediate particle emitting state. These are important for example in the case of ^{13}N.

From the compilation of energy levels of light nuclei by Ajzenberg and Lauritsen (1955), we have drawn up table 7 which lists the energy level at which particle emission begins for the nuclei under consideration together with the type of particle emitted.

Table 7. Particle Emitting Levels in Light Nuclei

Residual nucleus	^{11}C	^{13}N	^{15}O	^{18}F
Energy level (MEV)	9·7	2·4	12·0	6·9
Particle emitted	α	p	α	p
(p, pn) cross section (mbn) at 980 MEV	23·4	10·9	37	19·3

Comparison of the figures of table 7 shows the qualitative agreement between the energy levels quoted and the magnitude of the particular (p, pn) cross section. It is interesting to note that if it were not for the presence of some gamma emitting levels above the 2·4 MEV level in ^{13}N, the cross section for its production could be much lower. A further point of interest is that most of the light nuclei preferentially emit alpha particles or protons from excited states rather than neutrons. This is important in the consideration of more complex reactions.

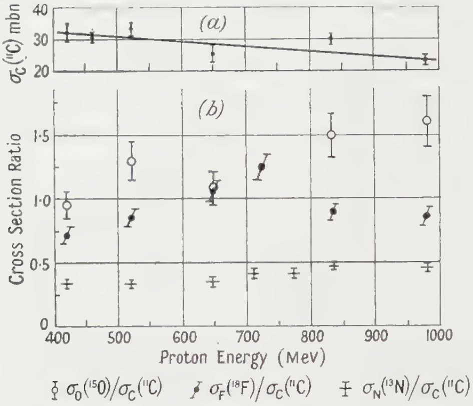

From table 6(*a*) and (*b*), it may be seen that there is a deviation from a monotonic decrease in the cross sections with increasing energy. This is particularly marked in the case of fluorine and the increase in the region of 750 MEV is well outside the limits of error. The possibility that the effect was instrumental was checked by the internal irradiation where we could expect with some confidence that the background was small. Consideration of the ratios in tables 2, 3 and 4 (and figure) shows that, in every case, the (p, pn) ratios depart from a slow change in this region of energy. Since the change is occurring at about 750 MEV, it might be supposed that it is associated in some way with meson production and the increase in the nucleon–nucleon total cross section (Chen, Leavitt and Shapiro 1956). The fact that the bump is more pronounced in the case of fluorine could be an effect caused by extra internal momentum of the nucleus, i.e. the bump would occur at a lower energy with fluorine than with the other nuclei. There is a trend in the measurements of Burcham *et al.* (1955) which indicates a bump in the region of 800 MeV in carbon. If the experimental figures are then accepted, the changes are more pronounced in the other cases (table 6(*a*)). Reference to the figures given for $\sigma_C(^{11}C)/\sigma_{Al}(^{24}Na)$, in Chackett *et al.* (1956), indicates that this rise may exist although the errors are somewhat too large on the 835 MeV point in that paper.

4.2. *More Complex Reactions*

The use of the energy level structure data may be carried further to give a qualitative explanation of the magnitude of some of the cross sections measured. We saw from table 7 that ^{13}N has a very low-lying level for particle emission, so that a very small amount of residual excitation will prevent the formation of ^{13}N. However, the yield of ^{13}N from oxygen is comparable with that from nitrogen. To reach ^{13}N from ^{16}O, one proton and two neutrons must be removed. If the initial process involved the target proton and incoming proton, the two extra neutrons may be removed by a form of pick-up process and two deuterons would appear. There is considerable likelihood that the residual ^{13}N nucleus would be left in its ground state (Selove 1956). A similar process may occur if the target nucleon is a neutron. There is evidence in other work (Fuller 1954) using cloud chambers that these high energy deuterons do emerge from light nuclei under bombardment with high energy particles.

The formation of ^{13}N from fluorine, on the other hand, requires the removal of two protons and four neutrons. The ejection of a neutron followed by alpha emission still leaves one neutron to be removed. Consideration of the ^{14}N energy levels indicates that this is quite probable but the nature of the process is such that the residual ^{13}N nucleus would not be left in the ground state in general. Investigation shows that other possible channels of formation are equally improbable in this instance. Even in the production of ^{13}N from aluminium, the cross section is only of the order of 1 mbn (Chackett *et al.* 1956).

Let us now consider reactions of the type (p, p2n). An example is the $\sigma_C(^{10}C)$ reaction whose small cross section is quoted in table 1. To form ^{10}C from carbon, the incoming proton must either directly knock out two neutrons, or knock out one neutron and allow the evaporation of the second after the first is removed. Like ^{13}N, ^{10}C has a low-lying particle emitting level and knock-out reactions are therefore likely to give low production cross sections for it. The evaporation of a neutron from ^{11}C is not very probable by comparison with alpha and proton emission, since the threshold is at about 20 MeV. All the more likely mechanisms thus result in low yields of ^{10}C in agreement with experiment. The same argument may be applied to ^{14}O and ^{17}F from oxygen and fluorine respectively.

The cross sections for these more complex reactions still show something of the rise at about 700–800 MeV but it is much less pronounced. This is especially so in those instances where a considerable number of particles are ejected and evaporated. The most pronounced effect is in the reaction producing ^{11}C from nitrogen. This is quite probably a combination of the fact that the ^{11}C is to a great extent produced by way of ^{13}N which is unstable to proton emission, and this proton could carry away a neutron to form a deuteron. The effects which appear in the (p, pn) reactions therefore appear in this case in the ^{11}C production.

ACKNOWLEDGMENTS

The authors wish to thank the proton synchrotron staff for help given in the preparation and irradiation of targets. They would also thank Professor W. E. Burcham for his assistance in the carbon studies and for the helpful discussions they have had with him. One of us (J. W.) wishes to thank the National Research Council of Canada and another (J. D. Y.) the Department of Scientific and Industrial Research for the award of grants.

REFERENCES

AAMODT, R., PETERSON, V., and PHILLIPS, R., 1952, *Phys. Rev*, **88,** 739.

AJZENBERG, F., and LAURITSEN, T., 1955, *Rev. Mod. Phys.*, **27,** 77.

BURCHAM, W. E., SYMONDS, J. L., and YOUNG, J. D., 1955, *Proc. Phys. Soc.* A, **68,** 1001.

CHACKETT, G. A., CHACKETT, K. F., REASBECK, P., SYMONDS, J. L., and WARREN, J., 1956, *Proc. Phys. Soc.* A, **69,** 43.

CHEN, F. F., LEAVITT, C. P., and SHAPIRO, A. M., 1956, *Phys. Rev.*, **103,** 211.

CRANDALL, W. E., MILBURN, G. P., PYLE, R. V., and BIRNBAUM, W., 1956, *Phys. Rev.*, **101,** 329.

DREVER, R. W. P., MOLJK, A., and SCROBIE, J., 1956, *Phil. Mag.*, **1,** 942.

FULLER, M. O., 1954, *University of California*, UCRL-2699.

MOON, P. B., RIDDIFORD, L., and SYMONDS, J. L., 1955, *Proc. Roy. Soc.* A, **230,** 204.

ROSENFELD, A. H., SWANSON, R. A., and WARSHAW, S. D., 1956, *Phys. Rev.*, **103,** 413.

SELOVE, W., 1956, *Phys. Rev.*, **101,** 231.

SERBER, R., 1947, *Phys. Rev.*, **72,** 1114.

WHITEHOUSE, W. J., and PUTMAN, J. L., 1953, *Radioactive Isotopes* (Oxford : University Press).

YOUNG, J. D., 1956, *Ph.D. Thesis*, University of Birmingham.

RESEARCH NOTES

Thermal Resistance due to Isotopic Mass Variation

By P. G. KLEMENS
Division of Physics, Commonwealth Scientific and Industrial Research Organization, Sydney

Communicated by G. H. Briggs; MS. received 16*th July* 1957 *and in final form* 28*th August* 1957

It has been pointed out by Slack (1957 a) and by Berman, Foster and Ziman (1957) that the mass variation due to the isotopic constitution of a solid can lead to a scattering of lattice waves which, in sufficiently pure dielectric solids, may in some cases contribute significantly to the thermal resistance at low temperatures.

At low temperatures the thermal resistivity is approximately additively composed of contributions due to the scattering of phonons (*a*) by the crystal boundaries, (*b*) by Umklapp processes arising from the lattice anharmonicities and (*c*) by lattice imperfections, which in many cases seem to be point imperfections. Thus the total thermal resistance is

$$W = AT^{-3} + BT^{-n}\exp(-\theta/\alpha T) + CT \qquad \ldots\ldots(1)$$

where T is the absolute temperature, θ the Debye temperature, B and α are intrinsic constants of the crystal, the power n is about 2 or 3, A depends upon the dimensions of the crystal and the surface conditions, and C depends upon the nature and concentration of the point imperfections (see, for example, Klemens 1956).

The parameter C has been calculated in terms of the phonon scattering cross sections (Klemens 1951). These cross sections in turn can be estimated in terms of the difference between the mass of an imperfection and that of a normal lattice point, in terms of a similar difference in the binding forces, and in terms of the distortion of the lattice about the imperfection (Klemens 1955). Thus

$$C = \frac{3(2\pi)^2}{0{\cdot}9}\frac{a^3}{\boldsymbol{h}v^2}\,nS^2 \qquad \ldots\ldots(2)$$

where a^3 is the volume of a unit cell, v is the velocity of the lattice waves, n is the relative concentration of imperfections and S^2 is a parameter proportional to the scattering cross section.

If an imperfection scatters only because of its mass difference

$$S^2 = \frac{1}{12}\left(\frac{\Delta M}{M}\right)^2 \qquad \ldots\ldots(3)$$

where M is the average mass of an atom (or unit cell) and $M+\Delta M$ the mass associated with an imperfection site (or cell). If there are a large number of imperfection sites, the quantity $n(\Delta M/M)^2$ in (2) and (3) must be replaced by

$$\left.\begin{aligned} \epsilon &= \sum_{\alpha} n_\alpha (M_\alpha - M)^2/M^2 \\ M &= \sum_{\alpha} n_\alpha M_\alpha \end{aligned}\right\} \qquad \ldots\ldots(4)$$

where the sum is over all types of atoms (or cells).

In crystals of great chemical and physical purity, the term CT in (1) can be neglected except in a narrow temperature region near the conductivity maximum, and the Umklapp resistance can be clearly observed because of the exponential temperature dependence of W. In many other crystals, some of them apparently pure, W varies approximately linearly with T, indicating the presence of point imperfections. Slack and Berman, Foster and Ziman have suggested that in such cases a major part of the point imperfection resistance is due to isotope scattering.

Slack (1957 a) has attempted to relate the observed point imperfection resistance of various crystals with theoretical values of C, calculated from (2), (3) and (4), using their known isotopic constitution. He found an order of magnitude agreement, but in general the observed values of C exceeded the theoretical values by a factor which varied from about 4 (germanium, potassium chloride) to more than 10 (quartz). Even allowing for some uncertainty in the separation of the Umklapp from the point imperfection resistance, this discrepancy is significant. Slack suggested that the calculation of the scattering cross section may be in error, because of approximations in the derivation of (3), and that S^2 ought to be increased by a factor of about 4 over the value given by (3). The remaining discrepancy is ascribed to other point imperfections.

Berman, Foster and Ziman accepted the values of the scattering cross sections calculated by Klemens (1955), but used a theory of Ziman (1956) to obtain an upper limit of the thermal resistance from those cross sections. This theory gives values of W about 50 times higher than given by Klemens (1951). The isotope resistances calculated by them exceed the observed resistances by large factors, ranging up to 20. Since the observed resistance cannot be smaller than the isotope resistance, Ziman's theoretical upper limit clearly overestimates the isotope resistance by a large factor.

Recent measurements of the lattice thermal conductivity of copper–gold alloys by Kemp, Klemens and Tainsh (to be published) allow a test of the theory. At temperatures above 40°K, the lattice thermal conductivity κ_g is of the form

$$1/\kappa_g = CT \qquad \ldots\ldots(5)$$

and it is seen by comparison with the semi-empirical theory of Liebfried and Schloemann (1954), which gives the magnitude of the Umklapp resistance, that the lattice thermal resistance is due to point imperfections. The most numerous point imperfections are the gold atoms, which scatter phonons mainly by virtue of their large mass. It can be shown that the difference in ionic radii between gold and copper is, in comparison with this mass difference, unimportant as a source of scattering, in contrast to copper–zinc alloys, where the mass difference is small, and the point imperfection resistance is due to the difference in ionic radii (Kemp, Klemens, Tainsh and White 1957). In the accompanying table the theoretical and experimental values of C are compared.

Table 1. Point Imperfection Resistance in Cu–Au Alloys

Alloy	ϵ	C_{theor}	C_{obs}
		(cm w^{-1})	
Cu– 7·5% Au	0·200	0·68	0·4
Cu–16·5% Au	0·331	1·12	0·5

The discrepancy is now smaller than that found by Slack, and in the opposite sense. It is interesting to note that the observed values of C are not proportional to ϵ but vary more slowly. This is to be expected if it is remembered that the perturbation treatment must fail when the perturbation becomes too strong. The quantity ϵ is a convenient parameter describing the strength of the perturbation. The scattering cross sections were derived on the assumption that $\epsilon \ll 1$ but now $\epsilon \sim 1$. If a perturbation treatment still converges, which it may, since $\epsilon < 1$, one would expect a further term in the thermal resistance proportional to ϵ^2. This suggests a relationship of the form

$$C = a\epsilon - b\epsilon^2. \qquad \ldots\ldots(6)$$

If a and b are determined from the observed values of C, then a should agree with the theoretical value of C/ϵ, obtained from (2), (3) and (4).

From the present data $a = 3$, $b = 5$, while the theory predicts $a = 3{\cdot}4$. Considering the inaccuracy in the determination of κ_g at liquid oxygen temperatures and the empirical nature of the extrapolation to small values of ϵ, the agreement with the theory must be regarded as satisfactory. In any case, one can now rule out the possibility that (3) would underestimate S^2 by a factor 4.

It is now necessary to explain the large values of C observed in crystals such as germanium and potassium chloride (Slack 1957 b). One may, of course, simply postulate that these materials contained unknown point imperfections in a concentration of between 10^{-5} to 10^{-4} per atom. In the case of potassium chloride this does not appear probable, but cannot be ruled out. In the case of germanium such an explanation appears difficult, as similar values of the thermal resistance were obtained by several authors (e.g. White and Woods 1955, Carruthers, Geballe, Rosenberg and Ziman 1957), and as any imperfections which may have been present were not detected electrically. Again, one cannot rule out the presence of an electrically neutral imperfection, present in all samples, such as perhaps substitutional carbon atoms.

It would be strange, however, if the apparent correlation between isotopic mass variation and thermal resistance should prove to be an accidental consequence of the presence of other point imperfections. It should be remembered that the theory of thermal resistance (Klemens 1951, 1956) in terms of scattering by static imperfections does not hold for all conditions. In this theory three-phonon interactions conserving quasi-momentum play an important role, and the present theory does not hold unless the strength of the three-phonon interactions relative to the scattering processes lies between an upper and a lower limit. These limits are at present not known, but in the limit of infinitely strong three-phonon interactions the resistance agrees with Ziman's (1956) theory, while in the absence of three-phonon interactions the conductivity becomes infinite. Most probably the present theory holds over a wide range of conditions, but it is possible that in cases where the scattering processes are relatively weak it underestimates the resistance. In the case of the copper–gold alloys the theory should give good results, but the discrepancies between the observed and calculated isotope resistances may be due to this cause, though perhaps only in part. Further experimental and theoretical work is needed to clarify this discrepancy.

REFERENCES

BERMAN, R., FOSTER, E. L., and ZIMAN, J. M., 1957, *Proc. Roy. Soc.* A, **237,** 344.

CARRUTHERS, J. A., GEBALLE, T. H., ROSENBERG, H. M., and ZIMAN, J. M., 1957, *Proc. Roy. Soc.* A, **238,** 502.

Kemp, W. R. G., Klemens, P. G., Tainsh, R. J., and White, G. K., 1957, *Acta Metallurg.*, **5**, 303.
Klemens, P. G., 1951, *Proc. Roy. Soc.* A, **208**, 108 ; 1955, *Proc. Phys. Soc.* A, **68**, 1113 ; 1956, *Handbuch der Physik,* **14,** No. 4. (Ed. by S. Flügge) (Berlin : Springer).
Leibfried, G., and Schloemann, E., 1954, *Nachr. Akad. Wiss. Göttingen,* **2a,** 71.
Slack, G. A., 1957 a, *Phys. Rev.*, **105,** 814; 1957 b, *Ibid.*, **105,** 832.
White, G. K., and Woods, S. B., 1955, *Canad. J. Phys.*, **33,** 58.
Ziman, J. M., 1956, *Canad. J. Phys.*, **34,** 1256.

The Integrated Cross Section from Threshold to 30 MeV for the Reaction ^{9}Be (γ, 2n) ^{7}Be

By K. H. LOKAN

Research School of Physical Sciences, Australian National University, Canberra

Communicated by E. W. Titterton, MS. received 29th *July* 1957, *and in final form* 23rd *August* 1957

The binding energy for the last neutron in ^{9}Be is known to be low (1·67 MeV) (Ajzenberg and Lauritsen 1955) and a good deal of evidence is available which suggests that an appropriate model for this nucleus might be that of a relatively loosely bound neutron moving in the field of two alpha particles. Such a model has been applied by several workers (Guth and Mullin 1949) and seems to have some general validity.

It is therefore interesting to look at the cross section for the (γ, 2n) process, for, while the low binding energy makes it relatively easy to remove the first neutron from the nucleus, the cross section for the removal of a second neutron might possibly be related to the cross section for the photo-disintegration of the alpha particle. From published mass values (Ajzenberg and Lauritsen 1955) the calculated threshold for the reaction is 20·56 MeV, and the residual nucleus is a conveniently long-lived isotope, so that the reaction should be amenable to a residual activation measurement.

In an attempt to estimate this cross section, a measurement was made in this laboratory with the 30 MeV Canberra Synchrotron. A block of beryllium, of dimensions 1 in. × 1 in. × 1 in. and weighing 29·57 grammes was irradiated for a total of sixteen hours in a bremsstrahlung beam with a maximum energy of 30 MeV. The beam was monitored using 1 in. × 1 in. tantalum foils, of thickness 0·005 in. irradiated simultaneously with the sample, tantalum being chosen for its convenient eight hour half-life. Gamma rays from the decay of ^{7}Be, produced in the reaction were detected with a NaI (Tl) scintillation counter. The irradiation was broken into three parts each of about five hours' duration, and for each, fresh monitor foils were taken.

The residual nucleus ^{7}Be has a 53·6 day half-life, decaying by K capture to ^{7}Li which, in 11% of cases, decays from an excited state by the emission of a 477 kev gamma ray (Ajzenberg and Lauritsen 1955). This gamma ray was readily detected, the measured energy being 475 ± 5 kev, and its half life, which was followed for some few weeks was confirmed to be 53 ± 3 days. The experimental data is shown in the figure.

The 8·15 hour beta activity from the tantalum monitor foils, arising from the reaction ^{181}Ta (γ, n) ^{180}Ta, was measured in a standard beta sensitive Geiger counter. Since the Stanford measurement of the reaction ^{63}Cu (γ, n) ^{62}Cu (Berman and Brown 1954) is taken as standard in this laboratory (Carver and Lokan 1957), a separate short irradiation of similar tantalum and copper foils was made at the same energy. The activities induced in these was measured with the same counter, to provide as a final monitor the activity which would have been induced in copper foils in the long irradiations. In each case the half-lives of the activities were checked and found to be as expected. The copper foils were counted also with the scintillation counter used to detect the ^{7}Be gamma ray, so that when corrections had been made for the different geometries of the block and foils, and for self-absorption in the beryllium, a figure for ‘ yield of ^{7}Be per copper disintegration ’ was obtained. Knowledge of the cross section for copper, and of the bremsstrahlung distribution for the machine, together with an assumption of a reasonable shape for the excitation function for the reaction, then leads directly to an estimate of the integrated cross section.

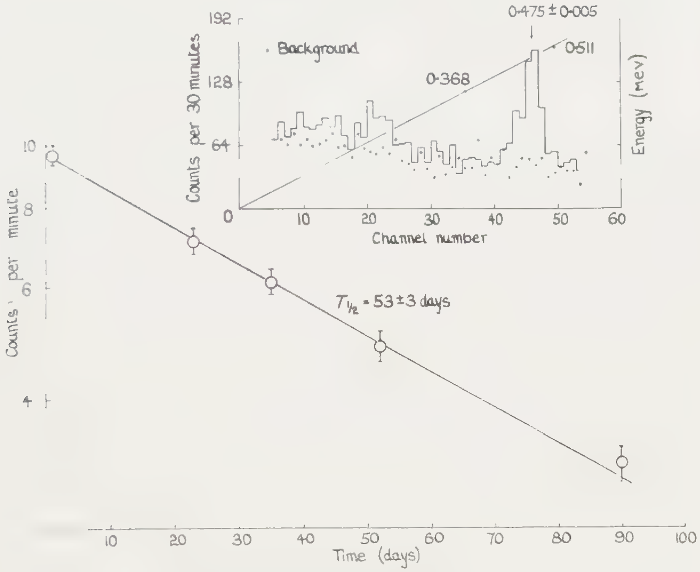

Energy and half-life of gamma ray from ^{7}Be.

The usual Schiff expression (Schiff 1951) for the intensity in the forward direction from a thin target was taken for the bremsstrahlung distribution, and an excitation function similar to that for the ^{4}He (γ, n) was assumed (Ferguson *et al.* 1954) peaking symmetrically about 24 Mev. It transpires that the estimate of the cross section is not sensitive to either of these assumptions, and the value obtained for the integrated ^{9}Be (γ, 2n) cross section from threshold to 30 Mev is

$$\int_{20 \cdot 56}^{30} \sigma(E)\, dE = (1 \cdot 2 \pm 0 \cdot 2) \text{ Mev mbn}$$

where the errors are those assigned to the measurements only.

Ferguson *et al.* (1954) have measured the ^{4}He (γ, n) excitation function, by detecting the neutrons and estimate the integrated cross section to 24 Mev to be 4 Mev mbn. The cross sections of the two reactions are therefore of the same order of magnitude.

REFERENCES

AJZENBERG, F., and LAURITSEN, T., 1954, *Rev. Mod. Phys.*, **27,** 77.
BERMAN, A. I., and BROWN, K. L., 1954, *Phys. Rev.*, **96,** 83.
CARVER, J. H., and LOKAN, K. H., 1957, *Aust. J. Phys.*, in the press.
FERGUSON, G. A., HALPERN, J., NATHANS, R., and YERGIN, P. F., 1954, *Phys. Rev.*, **95,** 776.
GUTH, E., and MULLIN, C. J., 1949, *Phys. Rev.*, **76,** 234.
SCHIFF, L. I., 1951, *Phys. Rev.*, **83,** 252.

LETTERS TO THE EDITOR

The Density Matrix and the Foundations of the Statistical Theory

In a recent paper (March 1957a), a variational method was developed for particles moving in a common one-dimensional potential. This approach necessitated constructing explicit variational wave functions and the aim was to approximate to the sum of the eigenvalues and the particle density. The resulting scheme was found to be closely related to von Weizsäcker's form of the statistical theory. However, it is known from previous work (see especially Berg and Wilets 1955) that the method of von Weizsäcker leads in some cases to energies which are much more in error than the results of the unmodified Thomas–Fermi theory. The present development arose from a search for a variational method more closely related to the original statistical theory and, we believe, represents the first completely quantum-mechanical discussion of the foundations of this theory (for a review of previous work on the fundamental basis of the statistical theory, see March 1957 b, § 9; see also Golden 1957).

The usual, somewhat loosely framed, statement that in the Thomas–Fermi approximation the wave functions are replaced locally by plane waves seems to find its most definite mathematical expression in the density matrix (cf. Fröman 1952). It seemed therefore natural to seek a variational scheme based on a density matrix obtained from such considerations; the need for introducing individual wave functions being thereby circumvented. Starting from the one-dimensional Schrödinger equation

$$-\frac{\hbar^2}{2m}\frac{d^2\psi}{dx^2}=[E-V(x)]\,\psi \qquad \ldots\ldots(1)$$

with wave functions ψ_n and corresponding eigenvalues E_n, and considering the case when the lowest N levels are singly occupied, we wish to approximate to the particle density $\sum_1^N \psi_n{}^*\psi_n$ and to the sum of the eigenvalues $\sum_1^N E_n$. To this end, we introduce the density matrix $\rho(x', x)$ which we define in the present case by

$$\rho(x', x)=\sum_1^N \psi_n{}^*(x')\,\psi_n(x). \qquad \ldots\ldots(2)$$

The sum of the eigenvalues may be expressed in the form

$$\mathscr{E}=-\frac{\hbar^2}{2m}\int\sum_1^N \psi_n{}^*\,\frac{d^2}{dx^2}\,\psi_n\,dx+\int\sum_1^N \psi_n{}^*\psi_n\,V dx, \qquad \ldots\ldots(3)$$

and we first of all rewrite this in terms of the density matrix. Obviously the potential energy may be written down directly in terms of the diagonal element (the particle density) but it is not possible to do this in the case of the kinetic energy. However, as may easily be verified, we have

$$\sum_1^N \psi_n{}^*\,\frac{d^2\psi_n}{dx^2}=\left[\frac{\partial^2\rho\,(x', x)}{\partial x^2}\right]_{x'=x} \qquad \ldots\ldots(4)$$

and thus we may write

$$\mathscr{E}=-\frac{\hbar^2}{2m}\int\left[\frac{\partial^2\rho\,(x', x)}{\partial x^2}\right]_{x'=x} dx+\int \quad x, x)\,V dx. \qquad \ldots\ldots(5)$$

We observe now that the exact density matrix would be expected to minimize (5) and that any physically allowable approximate density matrix, when inserted in (5), should lead to an upper bound for the sum of the eigenvalues.

We now proceed to construct a density matrix in keeping with the assumptions of the statistical theory, the following argument merely serving to suggest a variation function to insert in (5). The wave functions are approximated locally by plane waves and we therefore write

$$\rho(x',x)=\frac{1}{\boldsymbol{h}}\int \exp\left(-\frac{ipx'}{\hbar}\right)\exp\left(\frac{ipx}{\hbar}\right)dp \qquad \ldots\ldots(6)$$

where the allowed range of momenta is from $-p_0$ to p_0. Here p_0 depends on position and is related to the particle density, which we denote by $n(x)$ to simplify the notation, by

$$n(x)=2p_0(x)/\boldsymbol{h}. \qquad \ldots\ldots(7)$$

Evaluating the integral and taking the mean of x and x' as the appropriate point at which to evaluate the maximum momentum p_0 (or the density n), we have

$$\rho(x',x)=\frac{1}{\pi(x-x')}\sin\left[\pi(x-x')\,n\left(\frac{x+x'}{2}\right)\right] \qquad \ldots\ldots(8)$$

which, of course, is such that $\rho(x,x)=n(x)$. The expression (8) will now be made the basis for a variational evaluation of $\mathscr{E}$, the particle density $n(x)$ being the actual variational function.

It is a quite straightforward matter to calculate $[\partial^2\rho(x',x)/\partial x^2]_{x'=x}$ from (8) and the result may be written

$$\left[\frac{\partial^2}{\partial x^2}\rho(x',x)\right]_{x'=x}=-\frac{n^3\pi^2}{3}+\frac{1}{4}\frac{d^2n}{dx^2}. \qquad \ldots\ldots(9)$$

Thus we have, to this approximation,

$$\mathscr{E}=\frac{\hbar^2\pi^2}{6m}\int n^3\,dx-\frac{\hbar^2}{8m}\int\frac{d^2n}{dx^2}\,dx+\int nV\,dx \qquad \ldots\ldots(10)$$

and, as we have already remarked, this will be an upper bound to the correct sum provided n can be chosen such that (8) represents a physically acceptable approximation to the density matrix. It is clear that in the restricted variational scheme thus set up, we obtain the best possible approximation to the sum of the eigenvalues by choosing $n(x)$ to make (10) a minimum.

It will be observed that (10) is just the Thomas–Fermi expression for the sum of the eigenvalues in terms of the particle density, provided we can assume the term $-(\hbar^2/8m)\int(d^2n/dx^2)\,dx$ to be zero, which would be the case, for example, if dn/dx vanished at the end points of the range of integration. However, it may be remarked at this stage that the requirement that this integral shall be finite puts some restriction on the form of the variational function which can be taken for $n(x)$. This point seems of considerable importance, and will now be elucidated by considering a simple example—the linear harmonic oscillator. In this case the potential energy may be written

$$V=2\pi^2m\nu^2x^2 \qquad \ldots\ldots(11)$$

where ν is the classical frequency, and the density n which minimizes

$$\mathscr{E}_{\mathrm{TF}}=\frac{\hbar^2\pi^2}{6m}\int n^3\,dx+\int nV\,dx \qquad \ldots\ldots(12)$$

subject to normalization requirements may be expressed as

$$n_{\mathrm{TF}} = \frac{2}{\boldsymbol{h}}[2m(E_N - 2\pi^2 m\nu^2 x^2)]^{1/2} \qquad \ldots\ldots(13)$$

where

$$E_N = N\boldsymbol{h}\nu. \qquad \ldots\ldots(14)$$

Evaluating the energy (12) we then find

$$\mathscr{E}_{\mathrm{TF}} = (N^2\boldsymbol{h}\nu/2) \qquad \ldots\ldots(15)$$

which is the exact eigenvalue sum (cf. $\sum_0^{N-1}(n+\frac{1}{2})\,\boldsymbol{h}\nu$). This would appear to imply, at first sight, that by combining (13) and (8) we have the exact density matrix. This is demonstrably wrong, as the exact result is known in this case (Husimi 1940). The answer to this apparent contradiction lies in the term $-(h^2/8m)\int(d^2n/dx^2)\,dx$ of (10). It is easy to show that this does not remain finite with n given by (13) and thus the Thomas–Fermi density is not an allowable variation function, although it may be used, as is customary in the Thomas–Fermi theory, to obtain an approximation to $\mathscr{E}$ as given by (12). It therefore emerges from the theory presented here that a restrictive condition is ignored in using the Thomas–Fermi density in this case, and this is responsible for the fact that no upper bound property then holds.

Such a conclusion leads one to suppose that some of the well-known difficulties of the Thomas–Fermi theory, for example, the need for a 'boundary correction' in the Thomas-Fermi method for atoms (Scott 1952) and the fact that there is no satisfactory isolated atom in the Thomas–Fermi–Dirac theory, may be resolved along similar lines. Indeed, the writer has contended elsewhere that the variation principle of the Thomas–Fermi and Thomas–Fermi–Dirac theories is more general than the relations between density and potential (March 1957 b, § 4) and that by restricting the variational density employed to conform with general wave-mechanical requirements, the present difficulties can be avoided. The developments described here are in complete agreement with such a viewpoint and it is hoped to report the results of the further investigations, which are now proceeding, at a later date.

Note added in proof.—Further investigation now reveals that the requirement that the particle density shall be well behaved is not in general sufficient to ensure that use of equation (8) will yield an upper bound to the energy. The essential conclusion remains unchanged however; namely that the statistical method is based fundamentally on a variational density matrix in which the diagonal element is the actual variation function but that certain subsidiary conditions are neglected.

N. H. MARCH.

Department of Physics,
University of Sheffield.

15th July 1957.

BERG, R., and WILETS, L., 1955, *Proc. Phys. Soc.* A, **68,** 229.
FRÖMAN, P. O., 1952, *Ark. Fys.*, **5,** 135.
GOLDEN, S., 1957, *Phys. Rev.*, **105,** 604.
HUSIMI, K., 1940, *Proc. Phys.-Math. Soc. Japan*, **22,** 264.
MARCH, N. H., 1957 a, *Proc. Phys. Soc.* A, **70,** 169; 1957 b, *Advanc. Phys.*, (*Phil. Mag.* Suppl.), **6,** 1.
SCOTT, J. M. C., 1952, *Phil. Mag.*, **43,** 859.

REVIEWS OF BOOKS

Tables of Functions and of Zeros of Functions. U.S. Department of Commerce, N.B.S. Applied Mathematics Series 37. Pp xi+211. (Washington: U.S. Government Printing Office, 1954.) $2.25.

The volume contains a collection of eighteen short tables, which were published originally elsewhere. For this reason there is some diversity in the intervals of tabulation and also in the number of figures in the entries. More than half of the functions and zeros tabulated relate to Bessel functions and some of these are not easily accessible elsewhere. The functions tabulated include:

$$\int_0^x \mathrm{J}_0(t)dt\,; \quad \int_0^x \mathrm{Y}_0(t)dt\,; \quad \int_x^\infty \{\mathrm{J}_0(t)/t\}dt\,; \quad \tfrac{1}{2}(x)^{-n}!\,\mathrm{J}_n(x)\,;$$

the Struve functions $L_v(x),\ H_v(x)\,;\ x^n/n!\,;$

and $H(m, a, x) = \exp(-ix)F(m+l-ia,\ 2m+2;\ 2ix)$

where F is used to denote the confluent hypergeometric function ${}_1F_1$. Other tables give the first hundred Fourier coefficients of integral powers of x up to x^{10}, and sines and cosines for radian arguments between 100 and 1000. Since in this last the argument proceeds in steps of unity it is difficult to see any general use for this table.

The tables of zeros list zeros and weight factors of the first 16 Legendre polynomials and the first 15 Laguerre polynomials respectively. Apart from a table of the complex roots of $\sin z = z$, the rest of the zeros given are related to Bessel functions. These include the first five zeros of $\mathrm{J}_0(x)\mathrm{Y}_0(kx) = \mathrm{J}_0(kx)\mathrm{Y}_0(x)$, zeros of functions after fractional order and of their derivative, and the complex zeros of $\mathrm{Y}_0(z)$, $\mathrm{Y}_1(z)$ and $Y_1'(z)$.

Each table is proceeded by a concise account of the function and tabulation, which add considerable value to the tables themselves. Many of the tables included are frequently needed, and it is useful to have them published in good form in a standard series.

H. H. HOPKINS.

Tables of the Error Function and its Derivative. U.S. Department of Commerce, N.B.S. Applied Mathematics Series 41. Pp. xi+302. (Washington: U.S. Government Printing Office, 1954.) $3.25.

This volume is a re-issue, with a few corrections, of a table published in 1941. It represents a very comprehensive tabulation of the functions

$$H(x) = \frac{2}{\sqrt{\pi}} \int_0^x \exp(-\alpha^2)\, d\alpha \qquad H'(x) = \frac{2}{\sqrt{\pi}} \exp(-x^2)$$

to 15 places of decimals for the region $x = 0{\cdot}0$–56, and then to eight significant figures for $x = 4{\cdot}0$–$10{\cdot}0$. The intervals of tabulation in the different region are: 0·0000 (0·0001) 1·0000, then 1·000 (0·001) 5·600, and finally 4·00 (0·01) 10·0. Beyond $x = 5{\cdot}600$ in the 15-place part of the tables the additional entries necessary to reach $H(x) = 1$ and $H'(x) = 0$ to this accuracy are given. The layout, printing and binding are all of the high standard one now expects from the Bureau of Standards publications.

H H. HOPKINS.

Einführung in die Atomphysik, by W. FINKELNBURG. Pp. xi + 545. (Berlin : Springer, 1956.) DM 45.

Professor Finkelnburg's well-known text book on atomic physics was greatly expanded and largely rewritten for the third German edition, to which only small additions have been made in the fourth edition now before us. To write a book like that is a tremendous task, and it is a wonder that one person can do it. The volume includes not only atomic physics in its strictest sense, i.e. physics of free atoms, but also extensive chapters on the physics of nuclei, molecules and solids. Inspection shows that the author is a spectroscopist and an experimentalist; unavoidably subjects dear to his heart are treated with great care and contain more up-to-date material than others. For instance, Aston's mass spectrograph is described in some detail, including the focusing formula with its derivation. On the other hand in the brief section on β-spectra the difference in shape between allowed and forbidden spectra is barely hinted at; no formula is given and the spectrum shown as typical is actually a forbidden one.

But in an introduction to such a large subject one must not expect too much advanced material and it is always a debatable point where the line should be drawn. The volume before us certainly expounds all the important fundamental ideas with great care in typical German sentences expanding in stately convolutions. An excellent feature is the presence of nearly 300 figures, many of them good half-tone reproductions of spectra, track photographs and instruments. On the other hand there is no name index, and in my view such a book ought to contain references to important original papers, whose study is an indispensable part of the training of a scientist. O. R. FRISCH.

Elements of Partial Differential Equations, by I. N. SNEDDON. Pp. ix + 327. (New York : McGraw-Hill, 1957.) 52*s*. 6*d*.

This book is intended for applied mathematicians who are primarily concerned with obtaining actual solutions of partial differential equations, any existence theorems introduced being stated without proof.

The first part deals with first and second order equations and their solution by well established methods, e.g. those of Charpit, Jacobi, Monge and Cauchy, by separation of the variables and by integral transforms.

The second part goes on to treat systematically boundary value problems involving Laplace's equation, the wave equation and the diffusion equation, together with their appropriate Green's functions, examples being centred round specific problems in applied mathematics. The reader needs to be familiar with the elements of Legendre and Bessel functions, of which only the briefest of introductions are included.

The treatment throughout is very attractive and explanations are, for the most part, easy to follow. Each section includes an illustrative example worked out in full and there is a large collection of examples for solution. Although most of the subject matter is familiar there are a few topics not usually found in books at this level, e.g. Caratheodory's theorem and Reisz's solution of the wave equation.

A. N. GORDON.

English Translation of the Bulletin of the Academy of Sciences of the USSR. (New York: Columbia Technical Translations, No. 5, Vol. 19, 1955.) $20.

This volume gives an account of some of the proceedings of the Third All-Union Conference on the Physics of Cosmic Rays held during December, 1954, in Moscow. The theme of the Conference was the study of the physics of high-energy particles through the conjunction of investigations on cosmic rays and on artificial beams of particles. The topics discussed at the Conference were divided into the following categories :

(1) Interactions of cosmic ray particles having energies of the order of 10^{10}ev with atomic nuclei.

(2) Interactions of nucleons and photons of energies under 10^9ev with nucleons and atomic nuclei.

(3) Theory of high energy processes.

(4) Interaction of particles at ultra-high energies.

(5) New particles.

(6) Variations and origin of cosmic rays.

Of these, categories (1) and (2) have been published in *Izvestia* and translated by Columbia.

It is rather unfortunate that there has been such a long delay before the translation of the proceedings of this interesting Conference. Although the translation of JETP by the American Physical Society is particularly useful there is still a need for prompt translations of Conference reports. It is sad to relate that it is still difficult to get up to date information on work in the U.S.S.R; the difficulty in making personal contacts and the lack of a preprint scheme make adequate recognition of Russian contributions almost impossible.

Of the papers in this volume 12 refer to cosmic ray experiments and 3 to machine experiments with one theoretical paper and 4 short abstracts.

The first paper on cosmic rays is a review article by Vernov *et al.* on the interaction of nucleons with light nuclei at energies of 10^9–10^{12}ev. The production of the various components by primary protons is considered and an estimate made of the distribution of energy amongst these components. The idea of the ‘ kernel ’ charge of the nucleon—required to account for the comparatively low fraction of primary energy going into meson production—is well brought out. Most of the other papers on cosmic rays discuss the spectra of protons at various altitudes and their interactions with matter.

The machine experiments refer to the interactions of nucleons with energy below what was then the maximum energy attainable—660 MEV; similarly the four short abstracts describe photonuclear reactions produced by photons with energy below about 250 MEV.

The translations have been ably carried out and the diagrams are clear : the translations of the remaining categories are awaited with interest.

A. W. WOLFENDALE.

Spheroidal Wave Functions, By CARSON FLAMMER. Pp. ix + 220. (California : Stanford University; London : Oxford University Press, 1957.) 68*s*.

It has been known for a long time that the equation of wave motion and the Schrödinger wave equation are separable in spheroidal coordinates. But the spheroidal wave functions, as they are called, are clumsy complicated expressions, concerning which not many simple properties are known. The present book uses its first 85 pages in gathering together what is known, both for the scalar and vector functions. Asymptotic expansions, recurrence relations, power series expansions, integral relations, and continued fraction equations for the eigenvalues are all covered and their main properties set out in such a way that they really will be useful to the man who wants to use them. In passing, let it be said that this is not a book for the pure mathematician. The second half of the book, some 135 pages, is composed of no less than 166 tables of numerical values. As the author says " the tables are a hodgepodge of values for the spheroidal eigenvalues, expansion coefficients and the functions themselves ". Taken in conjunction with the 550 page tabulation of Stratton, Morse, Chu, Little and Corbato, there is about as much numerical material now available as one has any right to expect. The printing and type-setting of the present tables are excellent and very clear, though others beside this reviewer are likely to find the large scale absence of capital letters irritatingly modern.

C. A. COULSON.

Theories of Nuclear Moments, by R. J. BLIN-STOYLE. Pp. 88. (Oxford: University Press, 1957.) 8*s*. 6*d*.

This paper-backed monograph is the first of a series on research topics in physics to be published by the Oxford University Press under the title 'The Oxford Library of the Physical Sciences'. The series is intended for graduates and each volume is to be devoted to a survey of a single specialized topic. In the field of nuclear physics, this appears to be a new venture without immediate parallel in the existing literature, and it is therefore of considerable interest. There are, of course, several journals and annuals that regularly publish authoritative survey articles. For the discriminating reader, an important advantage of the monograph series over most existing publications is that they enable him to acquire individual articles.† Previously this has not been possible except when he has been able to persuade authors to part with copies of their limited supplies of reprints. In this connection, the price of the first book is astonishingly moderate and within reach of the average research student's pocket, unlike most contemporary books in advanced physics.

The monograph by Dr. Blin-Stoyle is a somewhat expanded version of an article by the same author in the Reviews of Modern Physics and augurs well for the series. It is a well-balanced survey of the whole subject of nuclear moments. After some preliminaries in which electromagnetic moments are defined, a chapter is devoted to experimental methods of measurement. This is followed by three chapters of theoretical discussion of those nuclear models that can make sensible predictions of moments, and the survey is concluded by five chapters of comparison of experimental values with theory. At the end of the book, there are two appendices on mathematical details and tables of moments, the latter being complete and up to date.

It would be incorrect to say that the monograph is 'exhaustive'; this would be a physical impossibility in a book of its size. Nevertheless, some description is given of all significant work done in the field. In particular, the outline of the theories of exchange moments is adequate enough for the general reader; the research specialist desiring more details is referred to the original papers. Much the same remarks apply to the discussion of nuclear models. One cannot expect to be able to use this book to learn about such models, but sufficient is said about them to provide understanding of their role in the prediction of nuclear moments. The comparison between experimental and theoretical moments in the concluding chapters is especially thorough and lucid, there being no necessity, in general, to consult any references for auxiliary information. A. M. LANE.

---

† In the case of *Reports on Progress in Physics* published by the Physical Society separate articles are available.

Scientific Uses of Earth Satellites, edited by JAMES A. VAN ALLEN. Pp. x+316. (University of Michigan Press; London: Chapman and Hall, 1956.) 63*s*.

In January 1956 the Upper Atmosphere Rocket Research Panel of the United States held a meeting to discuss the scientific uses of small artificial satellites of the earth. The volume under review is composed of the 33 papers which were read at this meeting. It is edited by the chairman of the Panel, J. A. van Allen. As he acknowledges in his preface, descriptions of proposed experiments are in general of an evanescent nature. Nevertheless, the decision to publish is to be commended. The difficulties arising in the exploitation of satellites are formidable; but the potential awards are great, and the remarkable achievements of the rocket scientists suggest that they will be reaped. Geophysicists and astrophysicists will warmly welcome these authoritative accounts of what might reasonably be attempted in the near future.

It is not feasible to report on each of the papers in the collection. All that can be done in the space available is to indicate the scope of a few representatives and to list the main topics covered by the remainder.

Several contributions are devoted to visual observations: light curves for diffusively reflecting and specularly reflecting spheres are compared (F. L. Whipple *et al.*), and consideration is given to the possibility of arranging for the emission of flashes which would enable optical tracking to be carried out at night (D. E. Hudson). Two others (F. L. Whipple *et al.*, J. L. Sedwick) are concerned with orbit theory: particular attention is paid to the effects of small deviations from the desired launching conditions and to the perturbations produced by the earth's oblateness and by atmospheric drag. It may be remarked incidentally that university mathematics lecturers can find in this field some stimulating problems suitable for undergraduates.

The following are also treated: instrumentation (H. J. Merrill, L. G. de Bey, H. K. Ziegler); terrestrial radiation and meteorology (P. R. Gast, V. J. Stakutis and J. X. Brennan, J. I. F. King, W. G. Stroud and W. Nordberg); air density determinations (L. M. Jones and F. L. Bartman, L. Spitzer, H. S. Sicinski *et al.*); ionospheric structure (W. W. Berning, G. Hok *et al.*, W. Pfister, F. B. Daniels, L. M. Hartman and R. P. Haviland); geomagnetism (E. H. Vestine, S. F. Singer, J. P. Heppner, L. Katz); auroral and cosmic radiations (W. H. Bennett, J. A. van Allen): meteors and interplanetary dust (H. E. la Gow, M. Dubin, S. F. Singer); Lyman alpha studies (T. A. Chubb *et al.*); measurement of solar emission in extreme ultraviolet (H. E. Hinteregger); ultraviolet stellar magnitudes (R. J. Davis).

A subject index is not supplied but otherwise the production is satisfactory.

D. R. BATES.

Handbuch der Physik, Vol. XXXII, *Structural Research*, edited by S. FLÜGGE. Pp. vii + 663. (Berlin: Springer.) £12 6*s*.

This is an attempt, which largely succeeds, at bringing into one volume the whole of the theory and practice of structure research which depends on the scattering of X-rays, electrons and neutrons by matter. Its great merit is its comprehensiveness, and although the thoroughness with which various topics are dealt varies considerably, the detailed references, given at the foot of each page, together with bibliographies at the end of each section, enable the reader to supplement the text without difficulty. The volume is divided into six parts, the first four being concerned with X-rays: 'Experimental Methods', by A. Guinier and G. von Eller (in French); 'Theoretical Principles' by J. Bouman (in English); 'Structure of Fluids and Amorphous Substances', by G. Fournet (in French); 'Size of Particles and Lattice Defects' by Beeman, Kaesberg, Anderegg and Webb (in English); 'Electron Diffraction' by H. Raether (in German); and 'Neutron Diffraction' by G. R. Ringo (in English). There is a detailed table of contents and a double index (German–English, English–German), as well as a separate index for the contributions in French. The system of cross references in the text is not explained, but it soon becomes obvious and is well designed for its purpose, at least within each section.

Doubtless every reader will find some aspects to criticize, while paying tribute to the overall accomplishment of the editor and contributors. In the section on experimental methods, retigraphs and powder photography are given excellent and full treatment, but the interpretation of oscillation photographs is quite inadequate (cylindrical coordinates and the Bernal chart are not even mentioned) and the paragraph on crystal setting by X-rays would no more to confuse than explain the process, especially as this is one of the few places where references are not given.

On absorption corrections it is said that prismatic crystals can be reduced approximately to the case of cylindrical ones. In fact this procedure, while having the support of tradition, can lead to considerable systematic errors.

In relation to a work of this size it would not be fair to list detailed omissions, which must be expected, but a rather more serious omission occurs in the section on low angle scattering of X-rays. The work of Ehrenberg and Franks on reflection from cylindrical mirrors is not mentioned, although their first results were published by 1952 and showed the achievement of three times the first order resolution and shorter exposure times than those quoted in this section, which purports to be complete up to 1955.

It is a pity that, although the 1952 International Tables are mentioned in the bibliography, the name 'Rhombohedric', which was there characterized as unsatisfactory, is given to the Trigonal system.

There are a number of minor misprints, the only ones of substance noticed being the substitution of y for x in the equation at the bottom of page 20 and the omission of a 2_1 axis in the figure on page 146.

The paper and printing, especially of the diagrams and photographs, leaves nothing to be desired and the reviewer has no hesitation in saying that every crystallographer should have access to this volume and use it as his first reference in any problem connected with structural research. J. W. JEFFERY.

CONTENTS OF SECTION B

PAGE

Dr. R. H. Jones. The Reaction of Oxygen with Lead Selenide . . . 1025

Mr. D. F. Marshall. The Dynamic Stress–Optic Coefficient of Perspex . 1033

Dr. A. Calverley. A Determination of the Surface Tension of Liquid Tungsten by the Drop–Weight Method 1040

Miss S. M. Crawford. The Variation with Temperature of the Dynamic Elastic Moduli of an Organic Glass at Two Frequencies 1045

Dr. R. J. Tayler. The Influence of an Axial Magnetic Field on the Stability of a Constricted Gas Discharge. 1049

Mr. M. Prutton. The Polarization Reversal Process in Guanidine Aluminium Sulphate Hexahydrate 1064

Dr. M. F. Culpin. The Viscosity of Liquid Indium and Liquid Tin . . 1069

Dr. M. F. Culpin. The Viscosity of Liquid Magnesium and Liquid Calcium . 1079

Research Notes :

Mr. J. R. A. Beale. Alloy-diffusion : A Process for making diffused-base Junction Transistors 1087

Mr. J. H. Smith and Dr. R. Street. Resistivity and Magnetoresistance of Au_2Mn 1089

Mr. R. R. Birss. The Saturation Magnetostriction of Nickel Single Crystals 1093

Dr. G. F. Alfrey and Mr. I. Cooke. Electric Contact to Zinc Sulphide Crystals 1096

Reviews of Books 1099

Contents of Section A 1104

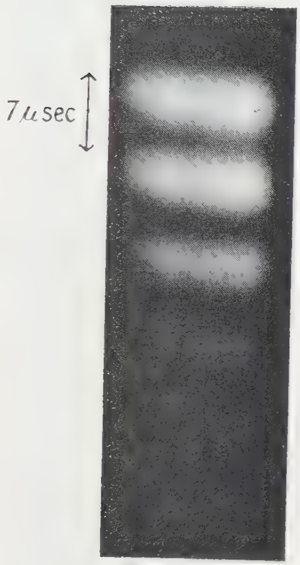

Figure 1.

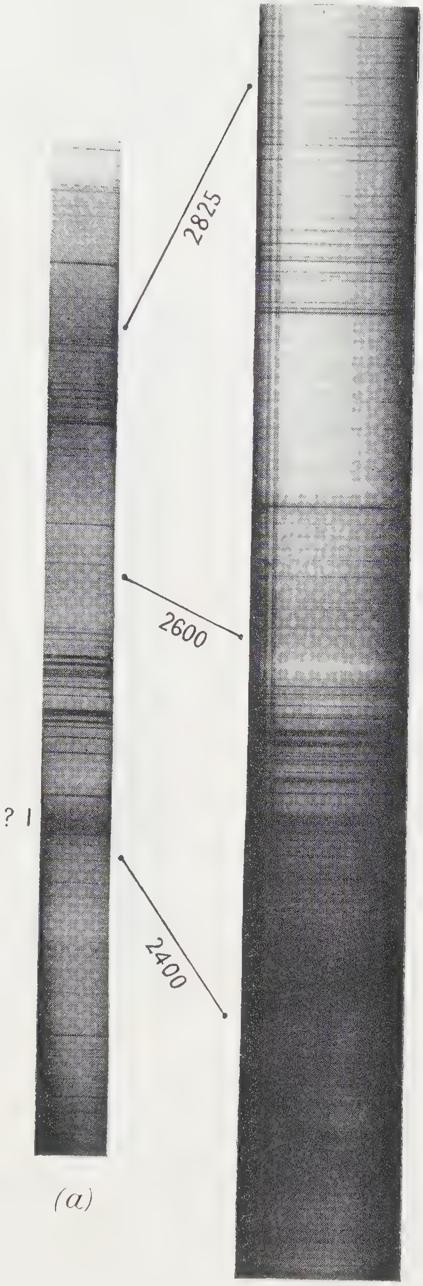

(a)

(b)

Figure 3.

Plate I.

Figure 1. Rotating mirror photograph of flash-discharge.
Figure 3. Absorption spectrum of free Fe arc ; (*a*) medium quartz, (*b*) 3 m grating.

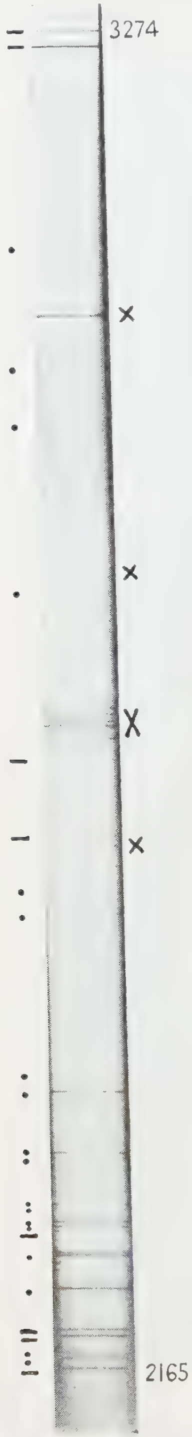

Figure 4.

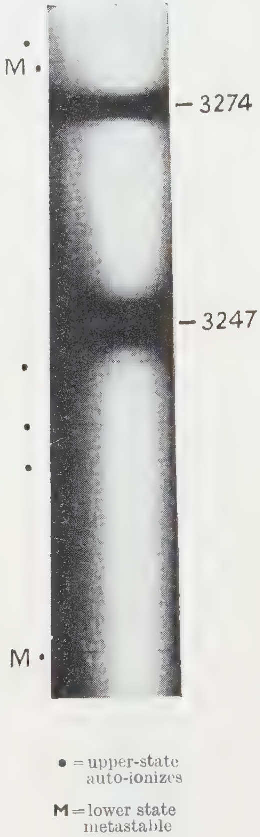

Figure 5.

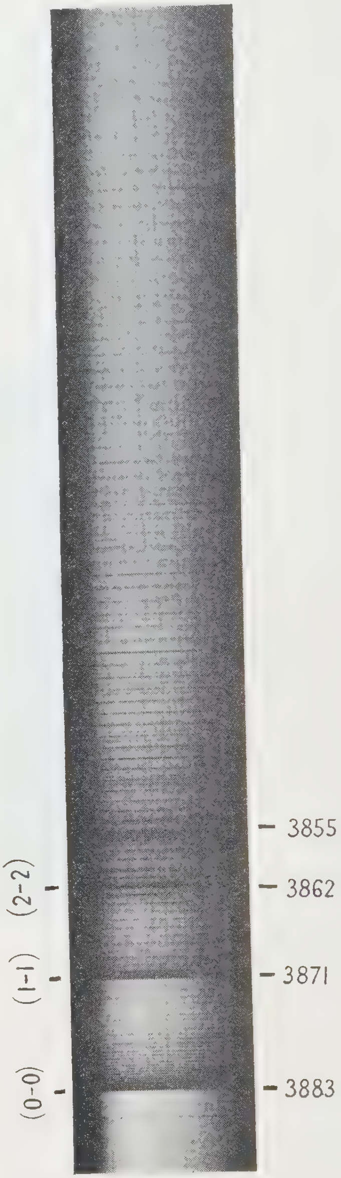

Figure 7.

PLATE II.

Figure 4. Absorption spectrum of 10 A Cu globule arc.

Figure 5. Absorption spectrum of cathode region of Cu globule arc; neighbourhood of resonance doublet.

Figure 7. Absorption spectrum of nitrogen screw-stabilized carbon arc showing CN violet 0–0 sequence.

Radiative Charge Transfer from H Atoms to He^{2+} Ions

By A. M. ARTHURS and J. HYSLOP
Department of Applied Mathematics, The Queen's University of Belfast

Communicated by D. R. Bates; MS. received 22*nd July* 1957 *and in final form* 26*th August* 1957

Abstract. The rate coefficient for radiative charge transfer from H atoms to He^{2+} ions is calculated at temperatures in the range 250°K to 64 000°K. It is found to be almost independent of temperature and to be very high (the mean value being about $1{\cdot}6\times10^{-13}\,cm^3\,sec^{-1}$). As a subsidiary part of the work, earlier computations on the exact two centre wave functions of the $1s\sigma$ and $2p\sigma$ states of HeH^{2+} and on the transition integral connecting these states are extended to internuclear separations up to 10 atomic units.

§ 1. Introduction

The semi-classical theory of radiative collisions between heavy particles developed by Kramers and ter Haar (1946) and Bates (1951) has been applied already to the study of the association processes

$$C+H\rightarrow CH+h\nu, \qquad \ldots\ldots(1)$$

$$C^-+H\rightarrow CH^-+h\nu, \qquad \ldots\ldots(2)$$

$$N^++N\rightarrow N_2^++h\nu, \qquad \ldots\ldots(3)$$

$$H^++H\rightarrow H_2^++h\nu, \qquad \ldots\ldots(4)$$

to the free–free process

$$H^++H\rightarrow H^++H+h\nu \qquad \ldots\ldots(5)$$

(Bates 1951), and to the deactivation process

$$He(2^1S)+He\rightarrow 2He+h\nu \qquad \ldots\ldots(6)$$

(Burhop and Marriott 1956). None of these involves a *transfer* of charge between the colliding systems as in

$$He^{2+}+H\rightarrow He^++H^++h\nu. \qquad \ldots\ldots(7)$$

In this paper we calculate the rate coefficient γ associated with (7), γ being defined according to

$$\frac{dn(He^+)}{dt}=\frac{dn(H^+)}{dt}=\gamma n(He^{2+})n(H), \qquad \ldots\ldots(8)$$

where the n's denote the concentrations of the species indicated. The only approximation made is to neglect the wave nature of the nuclei. It is to be anticipated that the results obtained from this calculation will be satisfactory in view of the substantial agreement between the semi-classical results of Bates (1952) for the inverse of processes (4) and (5) and the full quantal results of Buckingham, Reid and Spence (1952).

§ 2. Formula for the Rate Coefficient

Suppose a bare helium nucleus and a normal hydrogen atom approach each other. Let $A(r)$ be the Einstein transition probability from the potential energy curve $U_1(r)$ of the initial 2pσ state to the lower potential energy curve $U_2(r)$ of the final 1sσ state of the molecule HeH^{2+}, r being the internuclear separation. Averaging over a Maxwellian distribution at temperature T yields

$$\gamma = 8\pi^2\left(\frac{m}{2\pi \boldsymbol{k} T}\right)^{3/2}\iiint \exp\left(-\frac{mv^2}{2\boldsymbol{k}T}\right) v^3 A(r) p\left[v^2 - \frac{p^2v^2}{r^2} - \frac{2U_1(r)}{m}\right]^{-1/2} dv\,dp\,dr, \qquad \ldots\ldots(9)$$

where m is the reduced mass, v is the relative velocity of approach, p is the impact parameter and $\boldsymbol{k}$ is Boltzmann's constant. The integration over p is carried out first (Kramers and ter Haar 1946) between the limits 0 and p_M the greatest value of p consistent with the chosen v and r, and yields

$$\gamma = 8\pi^{1/2}\int_0^\infty I(r|T)A(r)r^2\,dr, \qquad \ldots\ldots(10)$$

where

$$I(r|T) = I_1(r|T) - I_2(r|T), \qquad \ldots\ldots(11)$$

$$I_1 = \int_{\epsilon_1}^{\epsilon_2} [\epsilon + H]^{1/2} \exp(-\epsilon)\,d\epsilon, \qquad \ldots\ldots(12)$$

$$I_2 = \int_{\epsilon_1}^{\epsilon_2} [\epsilon + H - \frac{\epsilon}{r^2} p_M^2 (\epsilon T)]^{1/2} \exp(-\epsilon)\,d\epsilon, \qquad \ldots\ldots(13)$$

$$\epsilon = mv^2/2\boldsymbol{k}T, \qquad H = -U_1(r)/\boldsymbol{k}T, \qquad \ldots\ldots(14)$$

the limits ϵ_1 and ϵ_2 corresponding to the minimum and maximum values of the velocity consistent with a specific internuclear separation.

Substituting the expression for the Einstein transition probability

$$A(r) = \frac{4G_2\boldsymbol{e}^2}{3\hbar^4\boldsymbol{c}^3}|Q(r)|^2[U_1(r) - U_2(r)]^3, \qquad \ldots\ldots(15)$$

in which G_2 is the orbital degeneracy factor of the lower state (Mulliken 1939)

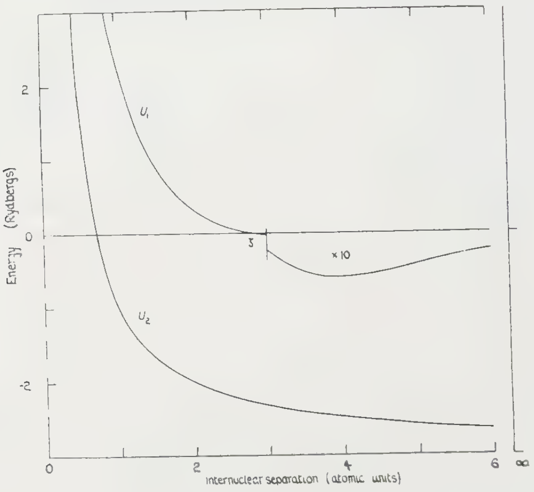

Figure 1. Potential energy curves U_1 and U_2.

and $Q(r)$ is the transition integral between the initial and final states, we have that

$$\gamma = 5{\cdot}64_5 \times 10^{-15} G_2 \int_0^\infty I(r|T)|Q(r)|^2[U_1(r) - U_2(r)]^3 r^2 \, dr \, \text{cm}^3 \, \text{sec}^{-1}, \qquad \ldots\ldots(16)$$

where r and $Q(r)$ are now in atomic units, $U_1(r)$ and $U_2(r)$ are in rydbergs and $I(r|T)$ is dimensionless.

To calculate γ we require the basic quantities U_1, U_2, I and Q.

The potential energies for r between zero and $5a_0$ are already known from the exact two centre calculations of Bates and Carson (1956); those for r between $5a_0$ and $10a_0$ were found by extending the exact calculations (see Appendix).

§ 3. Calculation of I

We consider the integral I in the two parts I_1 and I_2 as introduced in equations (11), (12) and (13). Consideration of the energy equation for the initial state of the system gives the lower limit ϵ_1 to be

$$\left.\begin{aligned} \epsilon_1 &= -H & \quad r &< \zeta \\ &= 0 & \quad r &> \zeta \end{aligned}\right\} \qquad \ldots\ldots(17)$$

where $U_1(\zeta) = 0$.

For the first part I_1, the upper limit ϵ_2 is infinite since all velocities of approach are possible. It follows that

$$\left.\begin{aligned} I_1 &= \frac{\sqrt{\pi}}{2} \exp(H) & \quad r &< \zeta \\ &= \frac{\sqrt{\pi}}{2} \exp(H)[1 - \operatorname{erf}\sqrt{H}] + \sqrt{H} & \quad r &> \zeta \end{aligned}\right\}. \qquad \ldots\ldots(18)$$

The second part I_2 may be written

$$I_2 = \int_{\epsilon_1}^{\epsilon_2} \mathscr{V}^{1/2}(r, \epsilon, T) \exp(-\epsilon) \, d\epsilon \qquad \ldots\ldots(19)$$

where

$$\mathscr{V} = \epsilon - \frac{U_1(r)}{kT} - \frac{\epsilon}{r^2} p_{\mathrm{M}}^2(\epsilon T) \qquad \ldots\ldots(20)$$

$$= \frac{\epsilon}{r^2}[L(r, \epsilon T) - p_{\mathrm{M}}^2(\epsilon T)] \qquad \ldots\ldots(21)$$

with

$$L = r^2\left[1 - \frac{U_1(r)}{k\epsilon T}\right]. \qquad \ldots\ldots(22)$$

In treatments previous to that of Bates (1951) it was supposed that

$$p_{\mathrm{M}}^2 = r^2\left[1 - \frac{U_1(r)}{k\epsilon T}\right] \qquad \ldots\ldots(23)$$

and hence concluded that I_2 vanishes. As pointed out by Bates this is not in general true. Consider the graph of L against r (figure 2). It is seen that L may pass through two minima and a maximum. For a fixed temperature the outer minimum C occurs for values of ϵ up to some ϵ_2; for $\epsilon > \epsilon_2$ the U_1 term in L becomes insignificant and the minimum C disappears. When this happens (23) is valid and so $\mathscr{V}$ is zero. If the region AB exists and r lies outside it $\mathscr{V}$ is also zero, but when r lies inside AB, p_{M}^2 is *not* given by (23). Instead, p_{M}^2 is equal to BC, since p_M is the greatest value of p for which the approach is possible. Here $L > p_M^2$, so that $\mathscr{V}$ is non-zero and positive for some range of ϵ corresponding to the r-region (δ, ρ). From the properties of L it may be shown that the region (δ, ρ) always lies beyond ζ. It follows then from equation (17) that ϵ_1 is zero.

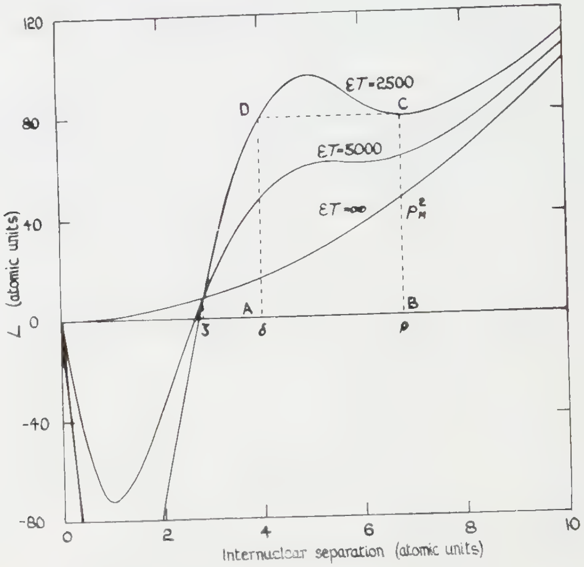

Figure 2. Plot of $L(r, \epsilon T)$ against r for $\epsilon T = 2500$, 5000, and ∞ (°K).

We next consider the determination of p_M^2. If a power law exists for U_1 then p_M^2 can be found analytically (cf. Bates 1951). In this problem U_1 can be fitted to a power law only for $r > 10a_0$ where it behaves like ar^{-4}. Thus for small values of ϵ (corresponding to large r) p_M^2 was found from the formula

$$p_M^2 = 2\left[-\frac{a}{k\epsilon T}\right]^{1/2}. \qquad \ldots\ldots(24)$$

For larger ϵ (i.e. $r < 10a_0$) U_1 does not obey a power law and p_M^2 was obtained by graphical methods from the (L, r) curves. Hence $\mathscr{V}$ was tabulated and I_2 evaluated by quadrature.

To repeat this procedure for every temperature would be a considerable task, but from (21) it can be seen that $\mathscr{V}$ satisfies the relation

$$\mathscr{V}\left(r, \frac{1}{n}\epsilon, nT\right) = \frac{1}{n}\mathscr{V}(r, \epsilon, T), \qquad \ldots\ldots(25)$$

so that it need only be tabulated for a single temperature.

§ 4. THE TRANSITION INTEGRAL

The values of the transition integral $\underset{\sim}{Q}(r)$ for $0 \leqslant r \leqslant 5a_0$ are known from the exact calculations of Arthurs, Bond and Hyslop (1957).

For r greater than $5a_0$, $\underset{\sim}{Q}(r)$ was first calculated from the dipole length, velocity and acceleration formulae (Chandrasekhar 1945), using the LCAO wave functions of McCarroll and Moiseiwitsch (1957) which take account of mixing and orthogonalization. The values of $\underset{\sim}{Q}^L$, $\underset{\sim}{Q}^V$ and $\underset{\sim}{Q}^A$ given by these formulae are presented in table 1 and can be seen to be converging very slowly. At large internuclear separations the dominant part of the transition integral is that which arises from the polarization term of the $2p\sigma$ wave function so that if the effect of polarization could be taken more completely into account Q^L, Q^V and Q^A might be in better agreement. Unfortunately, the accuracy of any one of Q^L, Q^V and Q^A could not be judged from these results. Hence it was decided to extend the exact calculations which are straightforward but laborious. Tables from which the exact wave functions can be obtained are given in the Appendix. The derived Q values are presented in table 1. It is seen that at $r=4a_0$ the approximate transition integrals all underestimate the true value of Q, while for r greater than $8a_0$ they overestimate (i.e. there is a complete cross-over), Q^L being more accurate than either Q^V or Q^A in the region beyond $6a_0$.

Table 1. Transition Integrals

r	Q^L	Q^V	Q^A	Q
4·0	0·1350	0·1465	0·1491	0·1681
5·0	0·1007	0·1085	0·1145	0·1108
6·0	0·0693	0·0741	0·0789	0·0711
7·0	0·0424	0·0451	0·0480	—
8·0	0·0235	0·0249	0·0264	0·0228
9·0	0·0122	0·0129	0·0136	—
10·0	0·0061	0·0064	0·0068	0·0058

Q refers to the exact values and Q^L, Q^V and Q^A to those based on the LCAO approximation. All quantities are in atomic units.

§ 5. RESULTS AND DISCUSSION

The rate coefficients γ given in table 2 were found from (16) by numerical integration. The computations should be accurate to within 1%. It is evident that γ is practically independent of the temperature in contrast with the rate coefficient for H_2^+ formation which is a rapidly increasing function of the temperature (Bates 1951). These different characteristics are due mainly to the form of the potential energy curves of the initial states; thus in the present problem the approach is along an attractive curve whereas in the case of H_2^+ formation the approach is along a repulsive curve.

Table 2. Rate Coefficients

T (°K)	250	500	1000	2000	4000	8000	16000	32000	64000
γ (10^{-13} cm^3 sec^{-1})	1·67	1·70	1·75	1·72	1·67	1·58	1·52	1·51	1·56

The magnitude of the rate coefficient describing process (7) is several orders of magnitude larger than those describing the other processes listed in (1) to (6). This arises from the fact that the Einstein A-coefficient is large and remains appreciable over a very wide r-range partly due to the unusually high photon energies for all internuclear distances (cf. figure 1).

Examination of the detailed variation of γ with temperature shows that there is an initial rise to a sharp maximum near 1000°K followed by a slow decrease to a minimum about 30 000°K. This behaviour at low temperatures emphasizes the part played by I_2 in the estimation of the interatomic field, for at these temperatures I_2 is almost as large as I_1 making $I=I_1-I_2$ very small. Neglect of I_2 would therefore result in a serious overestimate of γ at low values of T and further, because I_2 falls off rapidly as T increases, a *decrease* in γ would occur rather than the increase noted above. For moderate temperatures I_1 becomes dominant and γ then decreases. From the form of the potential energy curve it can be seen that a minimum in γ would be expected, followed by an increase at very high temperatures due mainly to the extension of the collision range to the repulsive part of the initial energy curve (cf. H_2^+).

At very low energies of approach charge transfer with emission of radiation would be expected to occur more readily than any other process. However, for velocities at which the perturbing influence of the relative motion on the system becomes appreciable, electron capture without emission of radiation will probably be dominant.

ACKNOWLEDGMENTS

Our thanks are due to Professor D. R. Bates for suggesting this problem and for his helpful advice throughout the course of the work. We also wish to thank the Antrim County Education Committee for research grants.

APPENDIX

EXACT WAVE FUNCTIONS OF HeH^{2+}

The electronic wave functions of HeH^{2+} may be written in the form

$$\Psi(\lambda,\mu,\phi)=\Lambda(\lambda)\,M(\mu)\,\Phi(\phi), \qquad \ldots\ldots(\mathrm{A1})$$

where ϕ is the azimuthal angle, λ and μ are the usual confocal elliptic coordinates, and

$$\Phi=\begin{matrix}\cos\\ \sin\end{matrix}(m\phi) \qquad (m=0,\,1,\,2\ldots), \qquad \ldots\ldots(\mathrm{A2})$$

$$\Lambda=(\lambda^2-1)^{m/2}\,(\lambda+1)^{\sigma}\,\exp(-p\lambda)\sum_{s=0}^{\infty} g_s\left(\frac{\lambda-1}{\lambda+1}\right)^{s}, \qquad \ldots\ldots(\mathrm{A3})$$

$$M=\exp(-p\mu)\sum_{t=m}^{\infty} f_t'\,P_t^m(\mu), \qquad \ldots\ldots(\mathrm{A4})$$

$$=\exp(+p\mu)\sum_{t=m}^{\infty} f_t''\,P_t^m(\mu). \qquad \ldots\ldots(\mathrm{A5})$$

The parameters p and σ and the coefficients g_s, f_t' and f_t'' of the $1s\sigma$ and $2p\sigma$ states have been computed at internuclear separations $R=6$, 8 and $10a_0$ (cf. Bates and Carson 1956). They are presented in the following tables. The electronic energies E (in rydbergs) and separation constants A' are also given.

For the $2p\sigma$ state the alternative expansion (A5) must be used when μ is close to -1. By combining (A4) and (A5) fitted at an arbitrary value of μ, M may be obtained accurately over the complete μ-range.

Table 1A. The Basic Parameters

	1sσ				2pσ			
R	p	σ	$-A'$	$-E$	p	σ	$-A'$	$-E$
6·0	6·24516	0·44112	5·95826	4·33356	3·90195	1·30654	11·61570	1·69169
8·0	8·24628	0·45520	7·96873	4·25007	4·90923	1·44438	15·73666	1·50628
10·0	10·24699	0·46385	9·97490	4·20003	5·92046	1·53359	19·79630	1·40207

Table 2A. The Coefficients of the λ Expansion (equation (A3) of text)

	1sσ			2pσ		
R	g_0	g_1	g_2	g_0	g_1	g_2
6·0	1	0·0075	0·0000	1	0·1131	0·0003
8·0	1	0·0061	0·0000	1	0·1107	0·0005
10·0	1	0·0051	0·0000	1	0·1036	0·0006

Table 3A. The Coefficients of the μ Expansion (equation (A4) of text)

1sσ

R	f_0'	f_1'	f_2'	f_3'	f_4'	f_5'	f_6'	f_7'	f_8'	f_9'	f_{10}'
6·0	1	0·96671	0·83252	0·65472	0·47301	0·31514	0·19428	0·11120	0·05927	0·02952	0·01377
8·0	1	0·97606	0·87339	0·72980	0·57166	0·42067	0·29132	0·19018	0·11723	0·06835	0·03776
10·0	1	0·98133	0·89825	0·77830	0·64020	0·50062	0·37256	0·26413	0·17856	0·11521	0·07103
R	f_{11}'	f_{12}'	f_{13}'	f_{14}'	f_{15}'	f_{16}'	f_{17}'				
6·0	0·00604	0·00250	0·00097	0·0004	0·0001	—	—				
8·0	0·01979	0·00986	0·00468	0·00212	0·00091	0·0004	0·0001				
10·0	0·04188	0·02365	0·01278	0·00666	0·00327	0·00166	0·0006				

2pσ

R	f_0'	f_1'	f_2'	f_3'	f_4'	f_5'	f_6'	f_7'	f_8'	f_9'	f_{10}'
6·0	0·39613	1	1·19520	1·04062	0·73073	0·43334	0·22305	0·10152	0·04143	0·01533	0·00519
8·0	0·37743	1	1·30469	1·27466	1·02608	0·70921	0·43096	0·23392	0·11476	0·05136	0·02113
10·0	0·36776	1	1·37116	1·43714	1·26307	0·96725	0·65919	0·40535	0·22717	0·11695	0·05566
R	f_{11}'	f_{12}'	f_{13}'	f_{14}'	f_{15}'	f_{16}'	f_{17}'	f_{18}'			
6·0	0·00162	0·00047	0·00013	0·00003	0·00001	—	—	—			
8·0	0·00804	0·00285	0·00094	0·00029	0·00009	0·00002	—	—			
10·0	0·02463	0·01018	0·00394	0·00144	0·00050	0·00016	0·00005	0·00002			

Table 4A. The Coefficients of the μ Expansion (equation (A5) of text)

2pσ

R	f_0''	f_1''	f_2''	f_3''	f_4''	f_5''	f_6''	f_7''	f_8''	f_9''	f_{10}''
6·0	−0·05177	1	−2·68799	3·95329	−4·09708	3·31270	−2·20628	1·25202	−0·61964	0·27206	−0·10737
8·0	−0·03852	1	−3·09855	5·28475	−6·43058	6·17532	−4·93181	3·38223	−2·03565	1·09244	−0·52916
10·0	−0·03100	1	−3·37552	6·31031	−8·51464	9·17085	−8·29767	6·50248	−4·50446	2·79922	−1·57809
R	f_{11}''	f_{12}''	f_{13}''	f_{14}''	f_{15}''	f_{16}''	f_{17}''	f_{18}''	f_{19}''	f_{20}''	
6·0	0·03849	−0·01264	0·00383	−0·00107	0·00029	−0·00003	—	—	—	—	
8·0	0·23360	−0·09474	0·03553	−0·01240	0·00404	−0·00125	0·00030	−0·00003	—	—	
10·0	0·81432	−0·38742	0·17098	−0·07037	0·02712	−0·00983	0·00337	−0·00108	0·00036	−0·00002	

REFERENCES

ARTHURS, A. M., BOND, R. A. B., and HYSLOP, J., 1957, *Proc. Phys. Soc.* A, **70,** 617.
BATES, D. R., 1951, *Mon. Not. R. Astr. Soc.*, **111,** 303; 1952, *Ibid.*, **112,** 40.
BATES, D. R., and CARSON, T. R., 1956, *Proc. Roy. Soc.* A, **234,** 207.
BUCKINGHAM, R. A., REID, S., and SPENCE, R., 1952, *Mon. Not. R. Astr. Soc.*, **112,** 382.
BURHOP, E. H. S., and MARRIOTT, R., 1956, *Proc. Phys. Soc.* A, **69,** 271.
CHANDRASEKHAR, S., 1945, *Astrophys. J.*, **102,** 223.
KRAMERS, H. A., and TER HAAR, D., 1946, *Bull. Astr. Insts Netherlands*, **10,** 137.
MCCARROLL, R., and MOISEIWITSCH, B. L., 1957, *Proc. Phys. Soc.* A, **70,** 507.
MULLIKEN, R. S., 1939, *J. Chem. Phys.*, **7,** 20.

Electron Scattering and Model Independence

By D. G. RAVENHALL and D. R. YENNIE
Department of Physics, Stanford University

MS. received 6th August 1957

Abstract. A critical examination is made of the hypothesis of model independence in high-energy electron scattering from nuclei. Results are presented which indicate that, contrary to this hypothesis, any differences in nuclear charge distributions result in differences in the electron angular distributions which become more and more pronounced as the energy is increased. The fallacies of the arguments leading to this hypothesis are noted, and comments are made on the scattering process.

Experiments on the elastic scattering of high-energy electrons by various nuclei, carried out at Stanford University in recent years, have on analysis yielded a considerable amount of information, some of it quite precise, about nuclear charge distributions (Hahn *et al.* 1956, Fregeau 1956; a complete bibliography of this subject is contained in the review article of Hofstadter (1956)). From the experiments on gold at 183 MeV, for instance, where charge distributions of the 'smoothed-uniform' type are assumed, the radius of this nucleus can be determined to within about 1%, and the surface thickness to within about 5%; the actual shape of the surface and the variation of the interior charge density cannot be fixed at all accurately, although some limits can be put on these properties, also. Similar results are obtained for light nuclei. In carrying out such an analysis it is clear that at any particular energy the limitations on the amount of information that can be obtained are imposed by the accuracy and angular extent of the experimental points, and that any improvement in the data will surely increase the precision of the final conclusions. It should be mentioned at this stage that the analysis used is a numerical partial-wave analysis of the Dirac equation containing the electrostatic potential of an assumed charge distribution (Yennie *et al.* 1954).

In disagreement with these results and conclusions, a series of papers have appeared which claim to show that there is an inherent physical limitation on the amount of detail of nuclear charge distributions that can show up in the calculated differential cross sections (Fowler 1955, Rosenfeld 1956-57 (and private communication), Regnier 1957). It is asserted that the optimum energy for revelation of the details of nuclear charge distributions is around 70 MeV, and it is implied that at energies much higher than this, all shapes will lead to the same cross section. This so-called 'model independence' is very reasonable when applied to energies so low that only one phase shift is appreciably modified by the finite nuclear size (Elton 1950, 1953, Acheson 1951, Feshbach 1951, Bitter and Feshbach 1953, Bodmer 1953, Glassgold 1955)† but that it should be true when very many phase shifts must be modified ($\simeq$10 to 12 for gold at 183 MeV) is at variance both with the results of our numerical work and with all of our physical ideas of the process involved. These tell us that angular distributions of the kind observed, consisting of regularly-spaced maxima and minima with a rapidly decreasing overall magnitude, can be thought of as the result of diffraction of a wave. It is typical of diffraction that the higher orders depend more and more on the fine details of the scattering potential. (In the first Born approximation they correspond to higher Fourier components.) Thus two different charge distributions must yield different cross sections if one looks at a high enough order of diffraction. The purpose of this note is to point out the fallacy in the arguments which have led to the idea of model independence and to make some comments on the scattering process in general.

---

† It should be noted that while some of these authors write with a view to upholding the model independence hypothesis at higher energies, the numerical cross sections presented usually seem to emphasize its limitation by exhibiting shape-dependence as soon as more than one phase shift is affected by the finite nuclear size.

It is necessary to calculate accurately a cross section which, over the angular range of interest for the experiments, varies in magnitude by a factor of 10^5 or more. Due to the smallness of the cross section at large angles, the sum of the Legendre series containing the scattering phase shifts involves some quite intricate cancellations of the contributions from the various partial waves. It is thus impossible to predict the cross section at large angles from only a rough knowledge of the phase shifts, and this is the defect of all of the model independence arguments. We shall demonstrate this by presenting examples of charge distributions whose phase shifts are very closely the same, and yet whose cross sections differ by large factors at some angles.

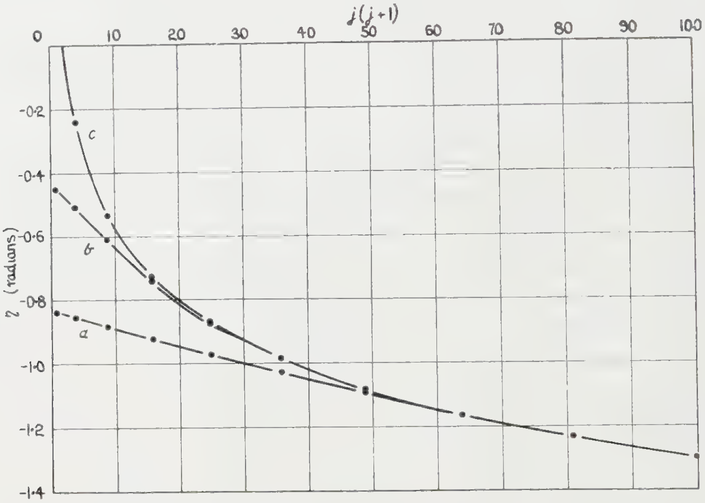

Figure 1. Phase shifts η versus $j(j+1)$, where j is the total angular momentum. The three cases illustrated are (a) the uniform distribution $kR=8$, (b) the uniform distribution $kR=4$, and (c) the point charge, all for gold. The phase shifts for the smoothed-uniform distribution (2), discussed in the text, are indistinguishable from curve (a) in this figure, and those for the three-parameter distribution (3) and the shell distribution (4) lie very close to (a).

From the results of numerical calculations with many charge distributions it is found that the phase shifts as functions of j, the total angular momentum, have the general character illustrated in figure 1. In this figure we have plotted against $j(j+1)$ the phase shifts for scattering from a point charge, and from uniform charge distributions with (a) $kR=4$ and (b) $kR=8$, all for gold ($Z=79$). It can be seen that as the energy increases the phase shifts do increase in magnitude, but the variation with j becomes smaller. This confirms Regnier's deduction (Regnier 1957) that in the limit of high energies the first few phase shifts tend to the same value. In fact any charge distribution at a particular energy has phase shifts which to a good approximation are characterized by just one parameter. This is the point made by the model-independence arguments. To examine the relationship between phase shifts and cross sections, we have considered four charge distributions, represented graphically in figure 2 : (1) the uniform distribution with

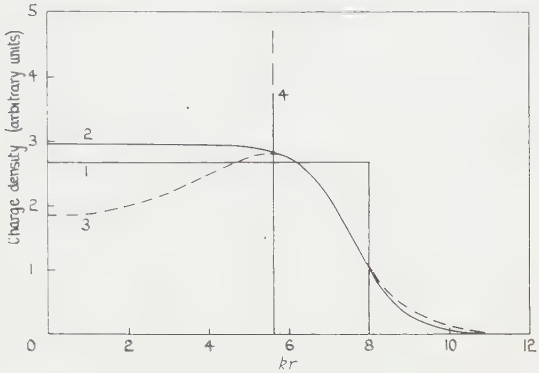

Figure 2. Charge densities for the four charge distributions discussed in the text : (1) the uniform shape $kR=8$; (2) the smoothed-uniform shape (Fermi shape) with $kc=7{\cdot}58$, $kt=2{\cdot}79$; (3) the three parameter shape with $kc=7{\cdot}07$, $kt=3{\cdot}30$, $w=1{\cdot}20$ (for notation, see Hahn *et al.* 1956); and (4) the shell distribution with $kR=5{\cdot}6$. They are all normalized so as to have the same volume integral.

$kR=8$, where k is the electron's wave number and R is the radius ; (2) the smoothed-uniform distribution with $kc=7{\cdot}58$, $kt=2{\cdot}79$, where c is the distance to the half-point, and t is the 90% to 10% distance ; (3) a distribution similar to (2), but with a depressed central density ; and (4) a shell of charge with $kR=5{\cdot}6$. All calculations are for gold ($Z=79$). The distributions (2) and (3) are of physcial interest since they correspond to shapes which fitted the experimental results at 183 Mev equally well (Hahn *et al.* 1955). With the parameters quoted above they correspond to scattering at 236 Mev. The phase shifts for the four shapes are given numerically in the table, and the cross sections are given in figure 3. A comparison of the table and figure 3 shows the following features : first, (1) and (2) have phase shifts which never differ by more than 0·006 radians, yet at large angles their cross sections can differ by a factor of 30 ; second, while the phase shifts of (2) and (3) differ by much larger amounts, their cross sections are much more similar ; third, the shell distribution (4) has phase shifts quite close to those of the other three shapes but its cross section in completely different. The second comparison illustrates a point mentioned earlier in this note, that any difference between charge distributions will become more pronounced in the higher orders of diffraction, and hence at higher energies.† It has significance also from the point of view of the future experiments at higher energies, of course. The general conclusion to be drawn is that the rough behaviour of the phase shifts is no guide whatsoever to the detailed cross sections at large angles. This clearly disposes of the hypothesis of model independence.

---

† Roughly speaking, the order of diffraction for the uniform distribution is the numerical value of $(1/\pi)\, 2kR \sin \frac{1}{2}\theta$. Thus increasing θ achieves the same result as increasing k.

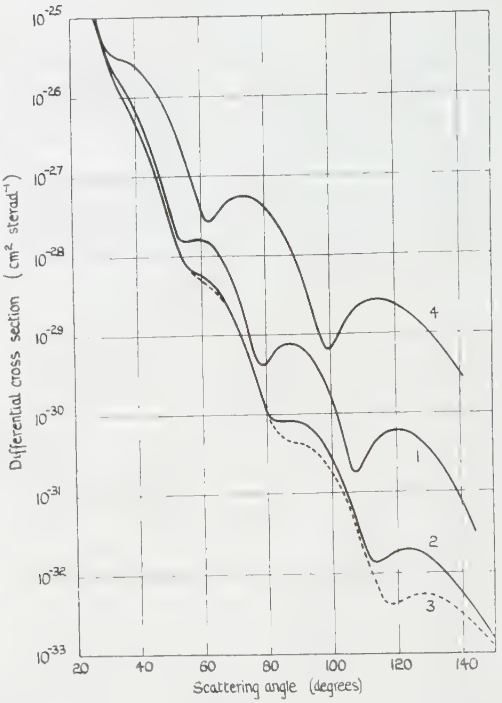

Figure 3. Differential cross sections for the four charge distributions discussed in the text and shown in figure 2.

In a problem in which many partial waves contribute to the scattering we feel that an approach which considers the three-dimensional properties of the wave functions is more promising. With this in mind we also have been interested in

Phase Shifts for Scattering from a point Charge and from the Four Charge Distributions Described in the Text. All are for Gold.

j	η_{point}	η_1	η_2	η_3	η_4
0·5	0·40736	−0·83553	−0·83580	−0·86671	−0·82006
1·5	−0·23797	−0·85289	−0·85481	−0·88201	−0·83253
2·5	−0·53303	−0·88136	−0·88352	−0·90764	−0·85521
3·5	−0·72659	−0·92116	−0·92438	−0·94356	−0·88041
4·5	−0·87098	−0·97034	−0·97541	−0·98968	−0·92664
5·5	−0·98623	−1·02902	−1·03568	−1·04562	−1·00054
6·5	−1·08218	−1·09683	−1·10266	−1·10900	−1·08480
7·5	−1·16438	−1·16829	−1·17179	−1·17536	−1·16473
8·5	−1·23628	−1·23710	−1·23866	−1·24044	−1·23632
9·5	−1·30020	−1·30033	−1·30089	−1·30167	−1·30020
10·5	−1·35772	−1·35773	−1·35790	−1·35822	−1·35772
11·5	−1·41001	−1·41001	−1·41005	−1·41017	−1·41001

the general features of phase shifts. Their behaviour for small j is closely connected with the gross properties of the electron wave function in the vicinity of the nucleus. For charge distributions close to uniform they are approximated quite closely by

$$\eta_j = a + bj(j+1) \qquad \ldots\ldots(1)$$

as can be seen from figure 1 and the table. By using a semi-classical analysis of the scattering the following approximate expressions can be obtained:

$$a = (Ze^2/\hbar c) - \langle \log 2kr \rangle, \qquad \ldots\ldots(2\,a)$$

$$b = (4k^2)^{-1}\,\langle r^{-2} \rangle, \qquad \ldots\ldots(2\,b)$$

where the expectation values are taken with respect to the charge density, normalized to $(Ze^2/\hbar c)$. The significance of these results is that the wave function near the nucleus can now be approximated by

$$\psi(\mathbf{r}) \simeq \left[1 - \frac{V(0)}{E}\right] \exp\left(ia + \frac{ib\mathbf{J}^2}{\hbar^2}\right) \psi_0(\mathbf{r}), \qquad \ldots\ldots(3)$$

where $\psi_0(\mathbf{r})$ represents a plane wave with direction of propagation parallel to the incident direction, but with its wave number altered due to the Coulomb potential by a factor $[1-(V(0)/E)]$. Hence a is the total phase of the wave function at the origin, and b represents a curvature of the incoming wave fronts. Relation (2*a*) has been noted previously by Regnier (1957)†. The usefulness of these observations lies in the fact that the approximation (3) forms a good zero-order wave function for the calculation by perturbation theory of various scattering processes, to which it restores to some extent the conceptual simplicity of the Born approximation (Yennie *et al.* 1957, see also Schiff 1956 a, 1956 b). This is the justification for some of our earlier remarks on the relation between scattering and diffraction. It should be noted that, while the approximation (3) describes the gross behaviour of the wave function near the nucleus, it does not contain in itself the scattering at large angles. Such scattering comprises only a minute part of the total cross section, and must be contained in the tiny departures of the actual phase shifts from approximation (1).

In conclusion, we should like to correct a misinterpretation of the electron-scattering results which apparently stimulated the investigation of model independence. This stated that the increase in the amount of information obtained as the energy is increased is much less than might be expected from classical impact-parameter considerations. We think it very difficult to state, as a number of parameters measured, just how much information has been obtained. It is true that with smoothed-uniform charge distributions, the type usually assumed, only two parameters—the radius and the surface thickness—can be determined accurately, while the shape of the surface is at present hardly measurable. This type of charge distribution was concentrated on because nuclei are commonly thought to look like that. Expressed in any other functional form a smoothed-uniform shape is quite complicated, and has the possibility of many parameters, yet in its natural form has only two. We have investigated a number of two-parameter distributions which certainly will not fit the 183 Mev experiments with any choice of parameters, and there must be many others. *The fact that the experiments at* 183 Mev *have narrowed down the range of possible shapes to distributions close to the smoothed-uniform type is then also information learned about the nucleus.* In this sense, the increased amount of information obtained by going to higher energies is all that one expects it to be, and we have every reason to believe that insofar as scattering from a static potential is all that is involved, this situation will persist as the energy is further increased.

† Regnier's criterion for the equivalence of charge distributions is effectively that the Born approximation expressions for their phase shifts be the same. In the high-energy limit the criterion becomes that of the equality of the values of a for the two distributions. As our results show, however, such equality is no guarantee of the equality of the cross sections at large angles. We might further remark that if Regnier's arguments are carried a stage further by summing the Legendre series containing the Born approximation phase shifts, the criterion becomes that of the equality of the three-dimensional Born approximation scattering amplitudes. In this form it is in fact much more reliable, but it need hardly be derived in this way.

ACKNOWLEDGMENTS

We wish to thank Professor Robert Hofstadter for calling our attention to this problem and for interesting discussions. The numerical computation of scattering cross sections was performed on the computer UNIVAC at the University of California Radiation Laboratory at Livermore. We thank the authorities of this laboratory, particularly Dr. Sidney Fernbach, for the use of this computer.

This research was supported in part by the U.S. Air Force through the Air Force Office of Scientific Research, Air Research and Development Command.

REFERENCES

ACHESON, L., 1951, *Phys. Rev.*, **82,** 488.
BITTER, F., and FESHBACH, H., 1953, *Phys. Rev.*, **92,** 837.
BODMER, A. R., 1953, *Proc.Phys.Soc.* A, **66,** 1041.
ELTON, L. R. B., 1950, *Proc. Phys. Soc.* A, **63,** 1115; 1953, *Ibid.*, **66,** 806.
FESHBACH, H., 1951, *Phys. Rev.*, **84,** 1206.
FOWLER, G. N., 1955, *Proc. Phys. Soc.* A, **68,** 559.
FREGEAU, J., 1956, *Phys. Rev.*, **104,** 225.
GLASSGOLD, A., 1955, *Phys. Rev.*, **98,** 1360.
HAHN, B., RAVENHALL, D. G., and HOFSTADTER, R., 1956, *Phys. Rev.*, **101,** 1131.
HOFSTADTER, R., 1956, *Rev. Mod. Phys.*, **28,** 214.
REGNIER, J., 1957, *Nuc. Phys.*, **3,** 340.
ROSENFELD, L., 1956-57, *Nuc. Phys.*, **2,** 450.
SCHIFF, L. I., 1956 a, *Phys. Rev.* **103,** 443; 1956b, *Ibid.*, **104,** 1481.
YENNIE, D. R., RAVENHALL, D. G., and TIEMANN, J. J., 1957, *Phys. Rev.*, in the press.
YENNIE, D. R., RAVENHALL, D. G., and WILSON, R. N., 1954, *Phys. Rev.*, **95,** 500.

The Reaction ^{3}He(d, p)^{4}He between 100 kev and 500 kev

By D. L. BOOTH†, R. S. HILL‡, F. V. PRICE and D. ROAF
Clarendon Laboratory, Oxford

MS. received 2nd August 1957, *and in revised form* 12*th September* 1957

Abstract. The cross section of the reaction ^{3}He(d, p)^{4}He has been investigated between 100 kev and 500 kev deuteron energy, using a thin gas target. No significant anisotropy was found up to 500 kev.

The total cross sections σ at deuteron energies E_d assuming isotropic angular distributions were

E_d	503·2	402·6	301·9	201·3	110·7
σ	0·476 ± 0·008	0·606 ± 0·050	0·482 ± 0·040	0·15 ± 0·01	0·023 ± 0·001

where E_d is in kev and σ in barns.

§ 1. Introduction

In previous investigations of the reaction $D + {}^3He = \alpha + p + 18{\cdot}4$ Mev uncertainties in the angular distribution and cross section have arisen from three principal causes: (i) Loss of energy by the bombarding ion in the windows used to isolate gas targets. (ii) Presence of neutral particles in the beam. (iii) Back scattering, energy loss and impurities in solid targets.

It is difficult to make reliable corrections for these effects. In the present work an attempt has been made to eliminate uncertainties on these three counts by using thin gas targets isolated from the main accelerator tube by narrow canals, and by measuring the deuteron beam current calorimetrically. Earlier measurements of this type on the ^{3}He(d, p)^{4}He reaction have been made in this laboratory at deuteron energies of less than 50 kev (Jarvis and Roaf 1953).

§ 2. Experimental

Singly charged deuterons from the Cockcroft–Walton accelerator were selected by a 10° magnetic analyser, using permanent magnets whose field was adjusted by a magnetic shunt. The target assembly was similar to that described by Booth, Hill, Price, Roaf and Salmon (1957), in which two accurately machined brass cones were used to define a cylindrical target volume 5 mm in diameter and 5 mm long. On opposite sides of this target volume two 4 in. by 2 in. Ilford E1 nuclear photographic plates were mounted symmetrically with respect to the beam axis; the plane of each plate was 2 cm from the axis of the beam. The energy losses of beam particles in crossing the target volume were of the order of 100 ev, and so quite negligible compared with the beam energy of 100 to 500 kev. The beam current was calculated from the value of the accelerating voltage and a measurement of the heat produced by the deuteron beam. To measure the accelerating voltage, a potentiometer was placed across the smaller of two resistances forming a potential divider whose ratio had been accurately calibrated at the ^{19}F(p, $\alpha\gamma$)^{16}O and ^{7}Li(p, γ)^{8}Be resonances (Preston, Shaw and

---

† Now at Atomic Power Department, English Electric Co. Ltd., Whetstone, Leicester.

‡ Now at Physics Division, Clarke Chapman Co. Ltd., Gateshead-on-Tyne.

Young 1954). During each experiment the pressure of the target gas was measured every 1·5 min. by a calibrated McLeod gauge. Samples of the target gas were analysed by Dr. K. I. Mayne in the laboratory's mass spectrometer. The ratio of the number of atoms of ^{3}He to the number of atoms of ^{4}He was $1{\cdot}78 \times 10^{-2}$.

The yield Y_ϕ of α-particles at an angle ϕ, measured with respect to the positive direction of the beam, into a solid angle ω (both ϕ and ω being measured in the laboratory system of coordinates) is given by

$$Y_\phi = 3{\cdot}618 \times 10^7 \frac{\epsilon}{V} \int_0^t \frac{pW}{T}\, dt\, G(\omega, \tau, \phi) \qquad \text{......(1)}$$

where W is the wattage produced by a deuteron beam of energy V kev passing through a target volume of τ cm^3 at a total gas pressure of $p\,\mu$ at T°K, and the atomic percentage of ^{3}He in the target gas is ϵ. The function $G(\omega, \tau, \phi)$ is determined solely by the target geometry and the angular distribution of the reaction.

At the energies covered by these experiments it is unlikely that higher powers than $\cos^2\theta$ appear in the angular distribution and the differential cross section was assumed to be of the form $J + K\cos\theta + L\cos^2\theta$, where θ is the angle in the centre-of-mass system corresponding to the laboratory angle ϕ, and J, K and L are energy-dependent parameters. From experimental values of Y_ϕ and computed values of $G(\omega, \tau, \phi)$, the values of J, K and L were determined.

The duration of each exposure was chosen to give a track density of not more than 10 particle tracks in each 0·01 mm^2. After processing the plates the numbers of α-particle tracks in certain selected small areas were counted using a Cooke, Troughton and Simms Type M4000 projection microscope which projected the image on to a screen at a distance of one metre giving an overall magnification of 700. In order to obtain satisfactory discrimination between the ^{3}He(d, p)^{4}He α-particles and the background of tritons from the D–D reaction, the range in the emulsion of each particle was calculated and the α-particles were identified by their range. Typical observed ranges of each particle were 10 to 12 microns for α-particles and 7 to 8 μ for tritons.

To select the area in which tracks were counted, reference lines were marked on each plate with a razor blade. Their precise positions in relation to the target volume defined by the cones were determined by replacing the marked plate in the camera and determining the coordinates of the points of intersection of these scribed reference lines by direct measurement with a travelling microscope. The error in determining the centre of each area counted was less than 0·1 mm.

Table 1. Differential Cross Section: $\partial\sigma/\partial\omega = J\left(1 + \frac{K}{J}\cos\theta + \frac{L}{J}\cos^2\theta\right)$

Deuteron Energy (kev)	J (bn sterad^{-1})	K/J	L/J
503·2	0·0353 ± 0·0012	0·046 ± 0·040	0·15 ± 0·08
402·6	0·0447 ± 0·0023	0·15 ± 0·05	0·18 ± 0·10
301·9	0·0357 ± 0·0019	0·07 ± 0·05	0·17 ± 0·10
201·3	0·01187 ± 0·00073	—	—
110·7	0·001824 ± 0·000057	—	—

The estimated errors are probable errors derived from the statistical spread of the measurements.

The value of the geometrical factor G was computed for each area in terms of J, K and L. By counting three areas subtending different angles, the values of J, K and L at each energy were derived (table 1). In the case of the two lowest energies, the values of K/J and L/J were less than the statistical error. To investigate more fully the possible anisotropy at 500 kev, seven areas were examined covering the range of angles from 34° to 147° (centre-of-mass); in no case were the values of these coefficients significantly greater than their probable errors.

The calculated values of the total cross section, assuming an isotropic distribution at all energies, is given in table 2. The values of these cross sections are slightly lower than those of Bonner, Conner and Lillie (1952) at energies greater than 300 kev, though the difference is not significantly greater than the errors in the measurements.

Table 2. Total Cross Section σ_{tot} when $K=L=0$

Deuteron Energy (kev)	σ_{tot} (bn)
503·2	$0{\cdot}476 \pm 0{\cdot}027$
402·6	$0{\cdot}606 \pm 0{\cdot}074$
301·9	$0{\cdot}482 \pm 0{\cdot}059$
201·3	$0{\cdot}15 \pm 0{\cdot}016$
110·7	$0{\cdot}023 \pm 0{\cdot}002$

The errors given include the estimated errors in the calibrations at different energies.

No attempt was made to modify a resonance formula to fit the observed excitation curve, as previous comparison of the experiment and theory (Yarnell, Louberg and Stratton 1953, Kunz 1955) for this reaction have yielded all the information likely to be useful until there is a theory of nuclear reactions which predicts formulae with fewer degrees of freedom in the choice of parameters.

REFERENCES

BONNER, T. W., CONNER, J. P., and LILLIE, A. B., 1952, *Phys. Rev.*, **88,** 473.

BOOTH, D. L., HILL, R. S., PRICE, F. V., ROAF, D., and SALMON, G. L., 1958, *J. Sci. Instrum.*, **35,** in the press.

JARVIS, R. G., and ROAF, D., 1953, *Proc. Roy. Soc.* A, **218,** 432.

KUNZ, W. E., 1955, *Phys. Rev.*, **97,** 456.

PRESTON, G., SHAW, P. F. D., and YOUNG, S. A., 1954, *Proc. Roy. Soc.* A, **226,** 206.

YARNELL, J. L., LOUBERG, R. H., and STRATTON, W. R., 1953, *Phys. Rev.*, **90,** 292.

The Binding Energy of ^{8}Be and ^{12}C

By S. J. Biel

Physics Department, University College London

Communicated by E. H. S. Burhop ; MS. received 30*th July* 1957, *and in revised form* 19*th September* 1957

Abstract. A general group-theoretic method is given for the enumeration of the integrals in the resonating group structure method of the alpha particle model of the alpha nuclei. The general methods are then applied to the calculation of the binding energies of ^{8}Be and ^{12}C. These calculations are carried out using Gaussian wave functions and a Gaussian central force potential, which is taken to be the mixture of the Wigner, Bartlett, Heisenberg and Majorana interactions. The variational method is used to fix the parameter determining the separation between the alpha particle clusters. Two types of exchange dependence of the potential are considered corresponding to symmetrical forces and to Serber forces respectively. The former gives no binding (both for ^{8}Be and ^{12}C) while the latter overestimates the binding energies. A mixture of about 30% of the symmetric force and 70% of the Serber force gives the correct values for the binding energies. A simple transformation is used to calculate the Coulomb energy from the previously evaluated integrals for the Gaussian potential.

§ 1. Introduction

The idea of an alpha particle model has arisen from the exceptional stability of the He-nucleus, which makes it a building brick of more complex nuclei. The original alpha particle model which considered a $4n$-nucleus as consisting of well-defined, fairly stable alpha clusters with attractive forces between them did not meet with much success (Rosenfeld 1948). These models assumed the additivity of the forces between the alpha clusters which were considered to be similar to the van der Waals attraction between the molecules of a liquid. Hafstad and Teller (1938) extended the alpha particle model to the $4n \pm 1$ nuclei.

However, it seems that in general, although low states of excitation of a nucleus can still be profitably treated by the more crude alpha particle model, one should treat the alpha clusters as transient structures and thus a proper allowance should be made for all possible groupings of nucleons into alpha clusters, leading to the idea of resonating group structure (Wheeler 1937). A simple calculation based on the method of resonating group structure of the interaction energy between two alpha particles was carried out by Margenau (1941) using Gaussian wave functions and potential. He obtained repulsion for all values of the alpha particle separation R. In the present paper the resonating group structure method is applied to the saturated alpha nuclei and on this basis the binding energies of ^{8}Be and ^{12}C are calculated. ^{8}Be is mainly treated for illustrative purposes as it has already been studied by Edwards (1952). One should also mention that recently a very interesting study of the alpha particle model of the $4n$-nuclei has been done by Herzenberg (1955, 1957) and Herzenberg and Roberts (1957). A particular feature of the studies is the quantitative treatment of polarization forces,

§ 2. GENERAL FORMULATION

The nucleus is divided into alpha particle groupings consisting of two protons and two neutrons. The distinction between the protons and neutrons is effected by means of the isotopic spin formalism. The state of any given nucleon is described by a vector $\mathbf{i}=(\mathbf{i}_1, \mathbf{i}_2, \mathbf{i}_3)$, where $\mathbf{i}_1$ refers to the ordinary spin and can have two values $\mathbf{i}_1=1$ or 2, $\mathbf{i}_2$ refers to the isotopic spin and again can have two values $\mathbf{i}_2=1$ or 2, $\mathbf{i}_3$ indicates the alpha cluster inside which the given nucleon is to be found. $\mathbf{i}_3$ can take as many values as there are alpha clusters inside the nucleus considered.

The wave function is totally antisymmetrized according to the Exclusion Principle, which involves summation over 8 ! permutations for ^{8}Be, 12 ! for ^{12}C etc. This follows from the fact that there are 8 and 12 different vectors of the type $\mathbf{i}$ in the cases of ^{8}Be and ^{12}C respectively.

The potential energy is obtained from the central two-body potential

$$\mathscr{F}(ij)=(\mathscr{W}+\mathscr{B}\,P_{ij}^{\sigma}-\mathscr{H}\,P_{ij}^{\tau}-\mathscr{M}\,P_{ij}^{\sigma}P_{ij}^{\tau})\,F(ij)+\frac{e^2}{r_{ij}}\epsilon_{ij}. \qquad \ldots\ldots(1)$$

$\epsilon_{ij}=1$ if i, j are protons, 0 otherwise. The explicit form of $F(ij)$ is immaterial for the general considerations which follow.

A certain fundamental order is now fixed for all the different vectors associated with the nucleons of a given nucleus. Thus for ^{8}Be one can take, for example,

$$(1,\,1,\,1)\,(1,\,2,\,1)\,(2,\,1,\,1)\,(2,\,2,\,1)\,(1,\,1,\,2)\,(1,\,2,\,2)\,(2,\,1,\,2)\,(2,\,2,\,2). \qquad \ldots\ldots(2)$$

Here (1, 1, 1) has the label 1, (1, 2, 1) has the label 2, (2, 1, 2) has the label 7, etc. With any permutation of these vectors is associated a certain wave function $\sigma_{i_1}^{(1)}\ldots\tau_{i_2}^{(1)}\ldots\psi(\ldots)$, where $\sigma^{(s)}$ are the ordinary spin functions, $\tau^{(s)}$ the isotopic spin functions and ψ is the space part of the wave function. By summing over all the permutations of the fundamental order with + or − sign according to the parity of a permutation a totally antisymmetrized wave function is obtained for the whole nucleus under consideration. Thus for ^{8}Be we have:

$$\Psi=\Sigma\,\epsilon_{ijklmnop}\,\sigma_{i_1}^{(1)}\ldots\sigma_{p_1}^{(8)}\,\tau_{i_2}^{(1)}\ldots\tau_{p_2}^{(8)}\,\psi\begin{pmatrix}1\,2\,3\,4\,5\,6\,7\,8\\ i_3\,\ldots\ldots\ldots\,p_3\end{pmatrix}. \qquad \ldots\ldots(3)$$

For the space part of the wave function a convention is adopted (following Edwards 1952) of writing together the coordinates of the nucleons inside the same alpha cluster. Thus (for ^{8}Be):

$$\psi\begin{pmatrix}1\,2\,3\,4\,5\,6\,7\,8\\ 2\,1\,2\,1\,1\,2\,1\,2\end{pmatrix}=\psi(2\,4\,5\,7;\ 1\,3\,6\,8). \qquad \ldots\ldots(4)$$

The space part of the wave function is assumed to be invariant for the interchanges of the particles inside the same alpha cluster and for the interchanges of the whole alpha clusters.

§ 3. ENUMERATION OF THE INTEGRALS

The binding energy is obtained from the equation

$$E=\frac{\int\Psi H\Psi}{\int\Psi\Psi} \qquad \ldots\ldots(5)$$

by minimizing E with respect to a parameter in Ψ. Here H is the Hamiltonian operator :

$$H=-\frac{\hbar^2}{4}\left(\frac{1}{M_n}+\frac{1}{M_p}\right)\sum_{\substack{\text{all}\\ \text{particles}}}\nabla_r^2+\sum_{\text{all pairs}}\mathscr{F}(ij). \qquad \ldots\ldots(6)$$

It is the purpose of the following sections to enumerate the normalization integrals occurring in $\int\Psi\Psi$, and the kinetic energy integrals occurring in

$$-\frac{h^2}{4}\left(\frac{1}{M_n}+\frac{1}{M_p}\right)\int\Psi\Sigma\nabla_r{}^2\Psi$$

and also to enumerate the potential integrals involved in evaluating

$$\int\Psi\sum_{\text{all pairs}}\mathscr{F}(ij)\Psi.$$

If P is a permutation of the vectors in the fundamental order, the corresponding permutation of the coordinates in ψ, the space part of the wave function, can be taken to be P^{-1}. The proof of this is trivial. For in the first alpha cluster those nucleons can be placed whose labels in the fundamental order are 1, 2, 3 and 4, in the second those whose labels are 5, 6, 7 and 8, and similarly with the other clusters. But this is just another way of saying that the corresponding permutation of coordinates in ψ is P^{-1}, if P is the permutation of the vectors in the fundamental order. It should be noted that it has been tacitly assumed that the fundamental order is fixed, quite naturally, in such a way that the first 4 vectors describe the particles inside the first alpha cluster, the next 4 inside the second alpha cluster and so on. The order given in equation (2) is of such a kind.

Grouping together all the terms in Ψ with the same ordinary and isotopic spin functions, sets are obtained containing $2\,!^4=16$ and $3\,!^4=1296$ terms in the cases of ^{8}Be and ^{12}C respectively. When the functions constituting the sets are expressed in terms of the corresponding vectors, associated with the nucleons of the nucleus under consideration, a set of permutations of the vectors of the fundamental order is obtained. All the permutations within such a set are said to belong to the same *pattern* (built on the same ordinary and isotopic spin functions). The pattern to which the identical permutation belongs will be called the *fundamental pattern*.

The permutations belonging to the fundamental pattern form a sub-group of the given symmetric groups of degrees 8 and 12 for ^{8}Be and ^{12}C respectively, for any permutation of the fundamental pattern only permutes certain letters among themselves, viz. the vectors with identical ordinary and isotopic spin components, and all the permutations of the type are included in the pattern. It follows that the product of any two permutations of the fundamental pattern is again a permutation of the fundamental pattern and since the symmetric groups are finite, this proves that the set considered is a sub-group.

It is important to notice that only the permutations belonging to the fundamental pattern form a sub-group. This follows from the fact that other patterns do not contain the identical permutation. The proof given above is not applicable in the case of a pattern other than the fundamental one, since although certain vectors are again permuted among themselves these permutations are not obtainable, within the pattern considered, from the identical permutation.

It will now be shown that the permutations constituting any given pattern are a left co-set of the sub-group consisting of the permutations belonging to the fundamental pattern. Since the totality of all the co-sets exhausts the whole symmetry group, it is sufficient to show that any co-set constitutes a pattern.

But, let

$$P=\begin{pmatrix}1 & 2 & 3 & \ldots\ldots & n\\ \dot{i}_1 & \dot{i}_2 & \dot{i}_3 & \ldots\ldots & \dot{i}_n\end{pmatrix};\quad Q=\begin{pmatrix}1 & 2 & 3 & \ldots\ldots & n\\ \dot{j}_1 & \dot{j}_2 & \dot{j}_3 & \ldots & \dot{j}_n\end{pmatrix}=\begin{pmatrix}i_1 & i_2 & i_3 & \ldots & i_n\\ \dot{j}_{i_1} & \dot{j}_{i_2} & \dot{j}_{i_3} & \ldots & \dot{j}_{i_n}\end{pmatrix}\qquad\ldots\ldots(7)$$

then

$$PQ=\begin{pmatrix}1 & 2 & 3 & \ldots\ldots & n\\ \dot{j}_{i_1} & \dot{j}_{i_2} & \dot{j}_{i_3} & \ldots & \dot{j}_{i_n}\end{pmatrix}.$$

This shows that j_k is replaced by j_{i_k}. But in the fundamental pattern all the vectors occupying the i_kth position have the same ordinary and isotopic spin components. Hence all the permutations obtained by multiplying the permutations of the fundamental pattern by a fixed permutation P have the same ordinary and isotopic spin components (the vectors corresponding to such permutations have these components) in the corresponding positions, i.e. the permutations constitute a pattern.

Finally it should be noted that the value of a multiple integral is invariant under any permutation of the variables in the integrand if these variables have the same ranges of variation.

§ 4. THE NORMALIZATION AND KINETIC ENERGY INTEGRALS

In the normalization integral $\int \Psi^* \Psi$ the only non-zero products come from the multiplication of similar patterns, i.e. no cross products of patterns occur. This follows from the properties of the ordinary and isotopic spin functions when we sum over the spins.

Consider a co-set of the fundamental pattern sub-group determined by a P. The space part of the functions of the corresponding pattern has the following form :

$$\epsilon_P \psi(P^{-1}) + \epsilon_{PP_1} \psi(P_1^{-1} P^{-1}) + \ldots\ldots + \epsilon_{PP_{n-1}} \psi(P_{n-1}^{-1} P^{-1}) \qquad \ldots\ldots(8)$$

(E, P_1, P_2, ..., P_{n-1} being the permutations belonging to the fundamental pattern; $n = 16$ and 1296 for ^{8}Be and ^{12}C respectively). Thus to obtain, from the space part of the functions of a pattern determined by P, the space part of the functions of the fundamental pattern, it is sufficient to multiply all the permutations of the coordinates by P on the right and to multiply the $\epsilon^{(s)}$ by ϵ_P ($\epsilon_{PP_k} = \epsilon_P \epsilon_{P_k}$ and ϵ_Q denotes the signature of the permutation Q). Since only the square of a pattern has to be considered the possible change of sign introduced when multiplying by P in case P is an odd permutation is immaterial. Hence using the invariance of the integrals under the permutations of coordinates, it follows that the contribution from the square of any pattern is equal to that of the fundamental pattern. Also

$$\int [\psi(E) + \epsilon_{P_1} \psi(P_1^{-1}) + \ldots + \epsilon_{P_{n-1}} \psi(P_{n-1}^{-1})] \epsilon_{P_k} \psi(P_k^{-1}) \quad (k = 0, 1, \ldots, n-1) \qquad \ldots\ldots(9)$$

($E = P_0$) are all equal to

$$\int \psi(E) [\psi(E) + \epsilon_{P_1} \psi(P_1^{-1}) + \ldots\ldots + \epsilon_{P_{n-1}} \psi(P_{n-1}^{-1})] \qquad \ldots\ldots(10)$$

$\psi(E) + \epsilon_{P_1} \psi(P_1^{-1}) + \ldots + \epsilon_{P_{n-1}} \psi(P_{n-1}^{-1})$ being the space part of the fundamental pattern. This follows from the fact that E, P_1, ..., P_{n-1} form a sub-group. Then

$$\int [\psi(E) + \epsilon_{P_1} \psi(P_1^{-1}) + \ldots\ldots + \epsilon_{P_{n-1}} \psi(P_{n-1}^{-1})]^2$$
$$= n \int \psi(E) [\psi(E) + \epsilon_{P_1} \psi(P_1^{-1}) + \ldots\ldots + \epsilon_{P_{n-1}} \psi(P_{n-1}^{-1})]. \qquad \ldots\ldots(11)$$

Since the interchanges of the whole alpha clusters leave the ψ-function invariant, the terms in $\psi(E) + \ldots\ldots + \epsilon_{P_{n-1}} \psi(P_{n-1}^{-1})$ can be collected into the sets of 2 and 6 equal functions in the cases of ^{8}Be and ^{12}C respectively. Thus for ^{8}Be we get:

$$\int [\psi(E) + \ldots + \epsilon_{P_{n-1}} \psi(P_{n-1}^{-1})]^2$$
$$= 2 \times 16 \int \psi(1234;\ 5678) [\psi(1234;\ 5678) - 4\psi(5234;\ 1678) + 3\psi(5634;\ 1278)]$$

after some further reductions using the invariance properties of ψ. Finally

$\int \Psi^*\Psi = 2\times 8\,!\int \psi_1[\psi_1 - 4\psi_2 + 3\psi_3]$ for ^{8}Be, with obvious notation. For ^{12}C we get:
$\int \Psi^*\Psi = 6\times 12\,!\int \psi_1[\psi_1 - 12\psi_2 + 9\psi_3 + 6\psi_4 + 8\psi_5 + 36\psi_6 + 36\psi_7 - 72\psi_8 - 12\psi_9]$

$\psi_1 = \psi(1\,2\,3\,4;\ 5\,6\,7\,8;\ 9\,10\,11\,12)$ $\qquad \psi_4 = \psi(5\,6\,3\,4;\ 9\,10\,7\,8;\ 1\ \ 2\,11\,12)$
$\psi_2 = \psi(5\,2\,3\,4;\ 1\,6\,7\,8;\ 9\,10\,11\,12)$ $\qquad \psi_5 = \psi(9\,2\,3\,4;\ 1\,6\,7\,8;\ \ 5\,10\,11\,12)$
$\psi_3 = \psi(5\,6\,3\,4;\ 1\,2\,7\,8;\ 9\,10\,11\,12)$ $\qquad \psi_6 = \psi(1\,6\,3\,4;\ 9\,2\,7\,8;\ \ 5\,10\,11\,12)$
$\psi_7 = \psi(5\,6\,3\,4;\ 9\,2\,11\,8;\ 1\,10\,7\,12)$
$\psi_8 = \psi(5\,2\,3\,4;\ 9\,10\,7\,8;\ 1\,6\,11\,12)$
$\psi_9 = \psi(9\,6\,7\,4;\ 1\,10\,3\,8;\ 5\,2\,11\,12)$

The kinetic energy integral is obtained simply by introducing the operator

$$-\frac{\hbar^2}{4}\left(\frac{1}{M_n} + \frac{1}{M_p}\right)\Sigma\,\nabla_r^{\,2}$$

in front of ψ_1, i.e. it operates on the first factor ψ_1 of the normalization integral.

§ 5. THE POTENTIAL ENERGY INTEGRALS

5.1. *Wigner Potential*

This does not involve exchanges of ordinary and isotopic spin coordinates. Hence the contribution from the Wigner potential is simply the sum of the squares of all the patterns multiplied by $S = \Sigma\, F(ij)$ (Σ taken over all combinations of ij, i.e. 28 for ^{8}Be and 66 for ^{12}C). Since S is clearly invariant under any permutation of a given symmetric group the problem is reduced to calculating the integral of the square of F_0, the space part of the fundamental pattern multiplied by S, i.e. $\int SF_0^{\,2}$ which is equal to $n\int\psi(E)\,SF_0$, using the group property of the fundamental pattern. Thus for the Wigner potential we get: $8\,!\int\psi(1\,2\,3\,4;\ 5\,6\,7\,8)\,SF_0$ as the total contribution for ^{8}Be. It should be noted that when a transposition (ij) is transformed by

$$P = \begin{pmatrix} 1 & 2 & \dots & i & \dots & j & \dots & n \\ k_1 & k_2 & \dots & k_i & \dots & k_j & \dots & k_n \end{pmatrix}$$

then another transposition is obtained which interchanges k_i and k_j, i.e.

$$P^{-1}(ij)\,P = (k_i k_j).$$

5.2. *Bartlett Potential*

Here ordinary spin coordinates are interchanged. Consider a pattern A. Three cases are to be considered.

(i) The square of the given pattern occurs multiplied by a $F(ij)$. (ii) The given pattern is multiplied by $F(ij)\times$ another pattern differing from it by the interchange of the ith and jth nucleons. (iii) The given pattern gives no contribution on account of the fact that after the interchange no pattern exists with the same ordinary and isotopic spin functions as the pattern considered.

Consider, for example, the pattern for ^{8}Be, which is the left co-set of the fundamental pattern determined by

$$P = \begin{pmatrix} 1\,2\,3\,4\,5\,6\,7\,8 \\ 1\,5\,2\,6\,3\,7\,4\,8 \end{pmatrix}.$$

In this case:

(i) The square of the pattern occurs for

$F(12)$, $F(13)$, $F(14)$, $F(23)$, $F(24)$, $F(34)$,
$F(56)$, $F(57)$, $F(58)$, $F(67)$, $F(68)$, $F(78)$.

(ii) The pattern is multiplied by a pattern with a single interchange for
$F(15)$, $F(16)$, $F(25)$, $F(26)$, $F(37)$, $F(38)$, $F(47)$, $F(48)$.

(iii) There is zero contribution for
$F(17)$, $F(18)$, $F(27)$, $F(28)$, $F(35)$, $F(36)$, $F(45)$, $F(46)$.

The corresponding results for the fundamental pattern are:

corresponding to (i)
$F(12)$, $F(15)$, $F(16)$, $F(25)$, $F(26)$, $F(56)$,
$F(34)$, $F(37)$, $F(38)$, $F(47)$, $F(48)$, $F(78)$,

corresponding to (ii)
$F(13)$, $F(17)$, $F(24)$, $F(28)$, $F(35)$, $F(46)$, $F(57)$, $F(68)$,

corresponding to (iii)
$F(34)$, $F(18)$, $F(23)$, $F(27)$, $F(36)$, $F(45)$, $F(58)$, $F(67)$.

The integral of the sum of the space parts of the expressions obtained in (i) is called the contribution from (i) to the pattern A. A similar definition is taken for the contribution from (ii) to the pattern A. By the total contribution of the pattern A is meant the sum of the contributions from (i) and (ii) as defined above. It will now be shown that the total contribution of any given pattern A is equal to the total contribution of the fundamental pattern. For let A be obtained from the fundamental pattern F by the application of a permutation P, and write this $\mathrm{A} = P\mathrm{F}$. Hence applying the permutation P to the space part of A, F_0 the space part of F is obtained (with a change of sign if P is odd, which is immaterial since there are always two factors in which such a change takes place). The operation $P = \binom{1\ \ 2 \ldots\ i \ldots\ j \ldots\ n}{k_1\ k_2 \ldots k_i \ldots k_j \ldots k_n}$ will change $F(ij)$ into $F(k_i, k_j)$ but the k_ith particle in the fundamental pattern has the same ordinary and isotopic spin functions as the ith particle of the pattern A. This shows that $F(k_i, k_j)$ is one of the $F(ij)^{(s)}$ when the computations of the corresponding type are carried out for the fundamental pattern. Since P will change two different $F(ij)^{(s)}$ into two different $F(ij)^{(s)}$ and since all the $F(ij)^{(s)}$ obtained in this way are obviously equal in number to all the $F(ij)^{(s)}$ obtained for the fundamental pattern the proposition has been proved for the computation of the contribution from (i). As regards the contribution from (ii) the fact that a transposition (ij) is transformed by $P = \binom{1 \ldots i \ldots j \ldots n}{k_1 \ldots k_i \ldots k_j \ldots k_n}$ into another transposition interchanging k_i and k_j, i.e. $P^{-1}(ij)P = (k_i k_j)$, together with the considerations given above show that the contribution from (ii) for A is the same as the corresponding contribution from the fundamental pattern. The required result has thus been completely established.

5.3. *Heisenberg Potential*

This case is completely analogous to that of the Bartlett potential.

5.4. *Majorana Potential*

Here there are two types of terms, one involving the multiplication of the square of a given pattern by $F(ij)$, the other type involving the multiplication of the given pattern by $F(ij) \times$ another pattern differing from it by the interchange of the ith and jth particles. The arguments given for the Bartlett potential apply here also and it is sufficient to consider the fundamental pattern only. For example, for the fundamental pattern of ^{8}Be one gets : (i) The square of the pattern occurs for $F(15)$, $F(26)$, $F(37)$, $F(48)$. (ii) The pattern is multiplied by a $F(ij) \times$ pattern, differing from the fundamental one by the interchange of the ith and jth particles, in all the remaining 24 cases.

5.5. *Coulomb Potential*

Using the methods given above, the enumeration of the Coulomb integrals is quite trivial. Again only the fundamental pattern need be considered, there are no exchanges of any coordinates, and it should only be remembered that the interactions occur only between protons.

It will now be shown that the sets of $F(ij)^{(s)}$ for the fundamental pattern in the cases (i) and (ii) of the B potential, H potential and M potential and also for the Coulomb interaction are all separately invariant under the permutations of the fundamental pattern. For whether a given $F(ij)$ belongs or not to one of the sets mentioned above, depends entirely on the ordinary and isotopic spin components of the ith and jth particles in the fundamental pattern and when a permutation P (belonging to the fundamental pattern) transforms i into k_i, the ith particle and the k_ith particle have the same ordinary and isotopic spin components. Thus when $F(ij)$ is transformed by P into $F(k_i k_j)$ this $F(k_i k_j)$ must necessarily be a member of the set to which $F(ij)$ belongs. Since two different $F(ij)^{(s)}$ will be transformed into two different $F(ij)^{(s)}$ this completes the proof of the proposition.

Using, for the case (ii) of the B, H and M potentials, the fact that a transposition (ij) is transformed by $P=\binom{1\dots i\dots j\dots n}{k_1\dots k_i\dots k_j\dots k_n}$ into another transposition interchanging k_i and k_j, i.e. $P^{-1}(ij)P=(k_i k_j)$, it is seen that the problem of calculating the contributions from the various potentials has been reduced to evaluating the sums of terms of the following forms :

$$\int\psi(E)\,F(ij)\,F_0 \qquad \text{and} \qquad \int\psi(E)\,F(ij)\,F_0^{ij};$$

where F_0^{ij} denotes the space part of the fundamental pattern F with the ith and jth coordinates interchanged.

Since the permutations interchanging the whole alpha groups (1 2 3 4), (5 6 7 8), ... belong to F it can be seen that, e.g., $\int\psi(E)\,F(12)\,F_0=\int\psi(E)\,F(56)\,F_0$.

Also a little consideration shows that if Q is of the form

$$Q=\begin{pmatrix}1\,2\,3\,4\,5\,6\,7\,8\,9\,10\,11\,12\\1\,4\,3\,2\,5\,8\,7\,6\,9\,12\,11\,10\end{pmatrix}$$

i.e. it interchanges two particles of the same order in each of the alpha groups and P is a permutation belonging to F, then $QPQ=R$ where R is another permutation belonging to F. Noting that for such a Q, $\psi(QT)=\psi(T)$ for every permutation T it is seen that, e.g., $\int\psi(E)\,F(17)\,F_0^{17}=\int\psi(E)\,F(16)\,F_0^{16}$. Thus all the contributions to the various potentials can be expressed in terms of the following four forms† :

$$\begin{array}{ll}\int\psi(E)\,F(12)\,F_0 & \int\psi(E)\,F(16)\,F_0\\ \int\psi(E)\,F(15)\,F_0 & \int\psi(E)\,F(16)\,F_0^{16}\end{array} \qquad \ldots\ldots(12)$$

which for ^{8}Be and ^{12}C are evaluated by direct enumeration. Some details of the results obtained, using ^{8}Be as an example, are given in the Appendix, including the discussion of the case when Ψ (i.e. its space part ψ) is taken to be complex instead of being real as has been tacitly assumed throughout the preceding discussion. It must be emphasized that all the general results obtained are

---

† The author has subsequently proved that for ^{8}Be, ^{12}C and ^{16}O

$$\int\psi(E)\,(F_0-F_0^{16})F(16)=\int\psi(E)\,F(15)F_0,$$

and this applies to the complex case treated in the Appendix. It appears that the proof can be generalized.

directly applicable to the complex case, the only difference occurring in the final evaluation of the four fundamental forms (12), there being some extra terms in the complex case.

§ 6. METHOD OF CALCULATION

The space part of the wave function has been taken as

$$\psi=\exp\left\{\left(-\frac{\lambda}{8}R_{12}^2\right)-\frac{\mu}{4}\left[\sum_{\substack{i=1\\ i<j}}^{4} r_{ij}^2+\sum_{\substack{i=5\\ i<j}}^{8} r_{ij}^2\right]\right\} \text{ for } {}^8\text{Be}$$

$$\psi=\exp\left\{-\frac{\lambda}{12}(R_{12}^2+R_{13}^2+R_{23}^2)-\frac{\mu}{4}\left[\sum_{\substack{i=1\\ i<j}}^{4} r_{ij}^2+\sum_{\substack{i=5\\ i<j}}^{8} r_{ij}^2+\sum_{\substack{i=9\\ i<j}}^{12} r_{ij}^2\right]\right\} \text{ for } {}^{12}\text{C}$$

where $R_{ij}^2=\sum_{x,y,z}(S_i-S_j)^2$ and $S_1=\sum_{i=1}^{4}x_i,\ S_2=\sum_{i=5}^{8}x_i,\ S_3=\sum_{i=9}^{12}x_i$

and $$r_{ij}^2=(x_i-x_j)^2+(y_i-y_j)^2+(z_i-z_j)^2.$$

The constant μ is fixed by the binding energy of an alpha particle and equals $4\alpha=0{\cdot}3156\times10^{26}\ \text{cm}^{-2}$. The value of α is taken from Hochberg, Massey and Underhill (1954). The internucleonic interaction is taken to be

$$F(ij)=a\exp(-\beta r_{ij}^2);\quad a=-45\ \text{MeV};\quad \beta=0{\cdot}2657\times10^{26}\ \text{cm}^{-2}.$$

The values of a and β are taken from the paper just quoted. The constants $\mathscr{W}$, $\mathscr{B}$, $\mathscr{H}$, $\mathscr{M}$ occur only in the following combinations

$$A=4\mathscr{W}+2\mathscr{B}-2\mathscr{H}-\mathscr{M}$$
$$B=-\mathscr{W}-2\mathscr{B}+2\mathscr{H}+4\mathscr{M}. \qquad \ldots\ldots(13)$$

Now

$$\mathscr{M}+\mathscr{H}+\mathscr{W}+\mathscr{B}=1$$
$$\mathscr{M}-\mathscr{H}+\mathscr{W}-\mathscr{B}=x \qquad \ldots\ldots(14)$$

where $x=0{\cdot}6$ is the ratio of the ^{1}S to the ^{3}S interactions in the deuteron. From (13) and (14)

$$A+B=\tfrac{3}{2}(1+x)=2{\cdot}4$$

and this is the value taken for $A+B$. If the exchange properties of the forces are similar to those of symmetric meson theory $\mathscr{M}=2\mathscr{B}$, $\mathscr{H}=2\mathscr{W}$ giving $A=0$; while if they correspond to the Serber interaction $\mathscr{M}=\mathscr{W}$, $\mathscr{H}=\mathscr{B}$ giving $A=B$.

To evaluate the various normalization, kinetic and potential integrals orthogonal transformations are applied which separate off the centre of mass and diagonalize the exponents of the normalization integrands. The Coulomb integrals can be obtained from the Gaussian potential integrals using the transformation

$$H_C=\int_0^\infty \frac{H(\beta)}{(\pi\beta)^{1/2}}\,d\beta \qquad \ldots\ldots(15)$$

where $H(\beta)$ is the Gaussian potential integral and H_C is the corresponding Coulomb integral (Edwards 1952). All the integrals encountered in the present work can be expressed in a closed form (Biel 1957, unpublished), where the tables of all the integrals both for ⁸B and ¹²C are given. When λ is put equal to zero in the expression (5) for E, the binding energies of two and three alpha particles are obtained in the cases of ⁸Be and ¹²C respectively. This follows from the fact that $\lambda=0$ corresponds to infinite separation between the constituent alpha particles of the nucleus considered. Thus when E has been minimized with respect to λ, the value of E corresponding to $\lambda=0$ is subtracted from that minimum value, giving the excess total energy over the number of the alpha particles inside the given nucleus. The graph in figure 1 gives the excess total energy over two alpha particles for ^{8}Be, while the graph in figure 2 gives the excess total energy over three alpha particles for ^{12}C.

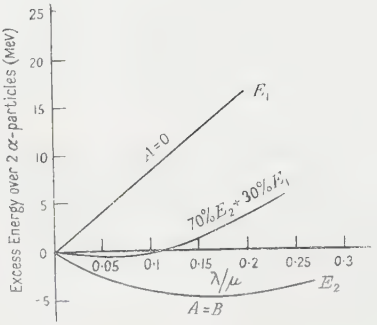

Figure 1.

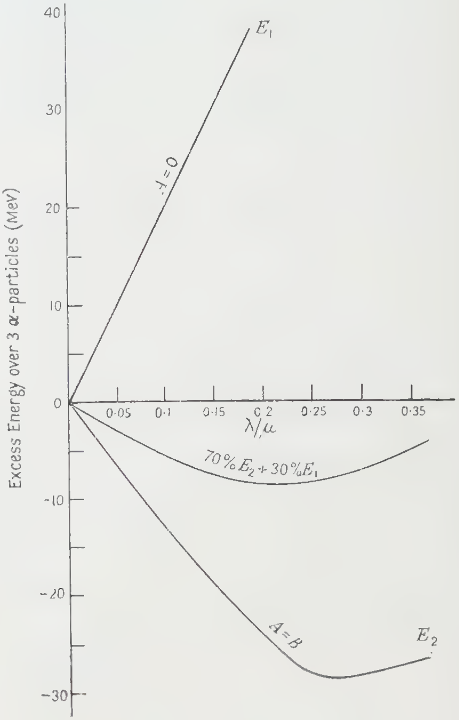

Figure 2.

§ 7. Discussion

The results obtained clearly indicate that neither the pure symmetric nor the pure Serber interaction can give agreement with the experimental binding energies for ^{8}Be or ^{12}C.

As regards the form of the potential function, comparison with the results of Edwards (1952) does not suggest any particular merit in taking the Yukawa type of interaction instead of the Gaussian form adopted in the present paper. Also the rather more involved wave function adopted by Edwards does not seem to have much justification as it rather refers to an excited state of ^{8}Be instead of the ground state. This might, however, explain the rather lower value he obtained for the binding energy.

The results of Edwards seem to indicate that the zero-exchange, single-exchange and double-exchange contributions to the kinetic and potential energies decrease rapidly in the order indicated. Our calculations do not confirm his result (see table). Similarly for ^{12}C no sharp differences can be observed in the order of magnitudes of the contributions from the various integrals (Biel 1957, unpublished).

It is seen from figure 1 and figure 2 that the Serber interaction gives too much binding, while the symmetrical type gives no binding at all. However, the same combination consisting of a 30% (slightly more than 30%) symmetrical force and a 70% (slightly less than 70%) Serber force mixture gives the correct binding energy for both ^{8}Be and ^{12}C.

Further investigations would be very instructive, particularly for the next $4n$-nucleus ^{16}O, to see whether the same proportion again gives the correct binding energy. The corresponding calculations would, however, be extremely involved though the exact extent of the complexity of the problem cannot be stated before a more detailed study of the problem, since there is a possibility that the fact that there is an even number of the alpha particles inside the nucleus may reduce the number of different integrals.

	λ/μ	0·0	0·05	0·1	0·15	0·2	0·25	0·3
$A=0$,	P.E. zero exchange	−172·5	−216·7	−302·9	−438·8	−649·0	−976·0	−1491·3
$A=0$,	P.E. single exchange	0·0	91·9	269·9	658·0	1267·1	2280·7	3966·1
$A=0$,	P.E. double exchange	0·0	−49·3	−169·9	−396·8	−797·1	−1485·0	−2656·3
$A=B$,	P.E. zero exchange	−172·5	−235·9	−355·3	−542·5	−833·5	−1289·6	−2014·4
$A=B$,	P.E. single exchange	0·0	123·5	403·6	903·8	1756·6	3188·5	5587·2
$A=B$,	P.E. double exchange	0·0	−68·2	−236·7	−556·0	−1123·0	−2103·2	−3780·8
	K.E. zero exchange	117·6	148·9	209·9	306·5	457·1	692·9	1067·3
	K.E. single exchange	0·0	−56·2	−187·2	−425·6	−837·8	−1537·7	−2721·2
	K.E. double exchange	0·0	29·6	105·2	252·3	519·0	987·7	1801·1
	Coulomb energy	1·8	3·1	3·4	3·7	3·8	4·1	4·4

All values are given in MeV. P.E. = potential energy, K.E. = kinetic energy.

The method of resonating group structure has been applied to the scattering of neutrons by deuterons by Buckingham and Massey (1941) and extended to include the scattering of protons by deuterons as well as to cover a wider range of energies in the following two papers (Buckingham, Hubbard and Massey 1952, de Borde and Massey 1955). The scattering of nucleons by alpha particles has been treated by Hochberg, Massey and Underhill (1954), using the method of resonating group structure. Swan (1953) applied the method to the scattering of neutrons by tritons and protons by ^{3}He. Work is in progress on the application of the method of resonating group structure to the alpha–alpha scattering following the general formulation of the present paper for ^{8}Be.

It is rather difficult to estimate, without detailed calculations, the effect the mixture of the present paper would have on the scattering phases, but since it can be expected that the results would be intermediate between those for the symmetric force and the Serber mixture, one would expect that in general this will improve the agreement with the experimental results.

In conclusion, it can be said that the method of resonating group structure seems to offer a very promising and fundamental approach to the problems of nuclear structure, being particularly well suited for the scattering problems.

ACKNOWLEDGMENTS

I would like to express my sincere thanks to Professor H. S. W. Massey and Dr. E. H. S. Burhop for suggesting the work and to thank them both for the interest they have shown during the progress of the work. I wish also to express my sincere gratitude to Mrs. J. Lawson for all the troubles she has taken in carrying out the rather involved numerical calculations for ^{12}C.

REFERENCES

DE BORDE, A. H., and MASSEY, H. S. W., 1955, *Proc. Phys Soc.* A, **68,** 769.

BUCKINGHAM, R. A., HUBBARD, S. J., and MASSEY, H. S. W., 1952, *Proc. Roy. Soc.* A, **211,** 183.

BUCKINGHAM, R. A., and MASSEY, H. S. W., 1941, *Proc. Roy. Soc.* A, **179,** 123.

EDWARDS, S. F., 1952, *Proc. Camb. Phil. Soc.*, **48,** 652.

HAFSTAD, L. R., and TELLER, E., 1938, *Phys. Rev.*, **54,** 681.

HERZENBERG, A., 1955, *Nuov. Cim.*, **1,** 986, 1008 ; 1957, *Nucl. Phys.*, **3,** 1.

HERZENBERG, A., and ROBERTS, A. S., 1957, *Nucl. Phys.*, **3,** 314.

HOCHBERG, S., MASSEY, H. S. W., and UNDERHILL, L. H., 1954, *Proc. Phys. Soc.* A, **67,** 957.

MARGENAU, H., 1941, *Phys. Rev.*, **59,** 37.

ROSENFELD, L., 1948, *Nuclear Forces* (Amsterdam : North-Holland), Chapter 13.

SWAN, P., 1953, *Proc. Phys. Soc.* A, **66,** 238, 740.

WHEELER, J. A., 1937, *Phys. Rev.*, **52,** 1083, 1107.

APPENDIX

The whole theory given in the present paper for the enumeration of the various integrals has been in terms of a real wave function Ψ. The theory is, however, obviously applicable to a wave function whose space part is complex. The problem is then reduced to evaluating the four fundamental forms:

$$\int\psi^*(E)F(12)F_0; \qquad \int\psi^*(E)F(16)F_0$$
$$\int\psi^*(E)F(15)F_0; \qquad \int\psi^*(E)F(16)F_0^{16} \qquad \text{(see eqn (12)).}$$

It is only in the reduction of these forms that certain differences may occur between the real and complex case.

This will be illustrated for ^{8}Be.

The total potential integral (without Coulomb interaction) is:

$$\left.\begin{aligned}8\times 8\,!\int\psi_1^*\{[F(12)(A+B)+F(15)A]\psi_1+\psi_2[(F(15)+F(26)-2F(23)-2F(12)\\ -2F(16))B-2(F(23)+F(26)\\ +F(12)+F(16))A]\\ +\psi_3[(F(12)+2F(13)+2F(17)-2F(15))B\\ +(F(12)+2F(13)\\ +2F(17)+F(15))A]\end{aligned}\right\}$$

for the complex case and

$$\left.\begin{aligned}8\times 8\,!\int\psi_1\{[F(12)(A+B)+F(15)A]\psi_1+\psi_2[(F(15)+F(26)-2F(23)-4F(12))B\\ -2(F(23)+F(26)+2F(12))A]\\ +\psi_3[(4F(13)+F(12)-2F(15))B\\ +(F(12)+F(15)+4F(13))A]\end{aligned}\right\}$$

for the real case. For in the real case:

$$\int\psi(1234;\ 5678)F(16)\psi(5234;\ 1678)=\int\psi(1234;\ 5678)F(12)\psi(5234;\ 1678)$$
$$\int\psi(1234;\ 5678)F(17)\psi(5634;\ 1278)=\int\psi(1234;\ 5678)F(13)\psi(5634;\ 1278).$$

For the Coulomb interaction we just give the final result for the real case:

$$\begin{aligned}e^2 4\times 8\,!\int\psi_1\{[F(12)+2F(15)]\psi_1-[4F(12)+2F(23)+F(15)+5F(26)]\psi_2\\ +[F(12)+4F(13)+4F(15)]\psi_3\}\end{aligned}$$

where $F(ij)=1/r_{ij}$.

The Decay of the Nitrogen Afterglow

By J. M. ANDERSON, A. D. KAVADAS† and R. W. McKAY
Department of Physics, University of Toronto, Canada

MS. received 28*th May* 1957, *and in revised form* 6*th August* 1957

Abstract. Accurate measurements of the decay of intensity of the nitrogen afterglow have been made over a range of intensity greater than 10^5 to one. Electronic methods of gating and control have permitted more accurate and reproducible measurements than any previously published. Series of observations are recorded for independent variation of temperature, pressure and oxygen impurity. All curves show three sections whose parameters vary independently of one another, an initial bimolecular decay, a second bimolecular decay and a final logarithmic decay when the glow is very faint. Constants of these processes are derived from graphs shown. Analysis of results is given by Anderson.

§ 1. Introduction

In spite of more than fifty years of publication concerning it, the nitrogen afterglow is not yet satisfactorily explained. Electronic methods of intensity measurement and of control and gating permit greatly increased accuracy and reproducibility in the study of such transient effects. The measurements below cover a range of intensity more than one hundred times greater than those reported by Rayleigh (1942) and have considerably greater accuracy.

§ 2. Method

A block diagram of the apparatus is shown in figure 1. The gas to be studied is placed in the discharge tube. This tube is inside the large copper tubing tank coil of a pulsed radio-frequency power amplifier. The amplifier is energized from a low power oscillator operating continuously. Gas pressure in the discharge

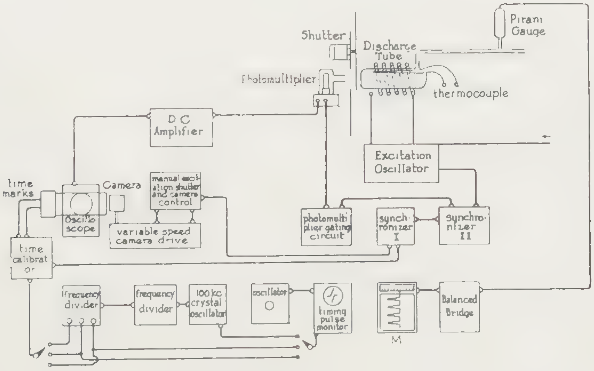

Figure 1. Block diagram of the equipment used.

---

† Now at University of Saskatchewan, Saskatoon, Saskatchewan, Canada.

tube is continually recorded using a specially developed fast response Pirani type gauge. Wall temperature is read from a meter attached to a thermocouple and isolated from the radio-frequency by suitable chokes. Light from the discharge tube is detected by the photomultiplier tube. To establish the zero light level regularly and check drifts, the light reaching the photomultiplier tube is interrupted periodically by a narrow vane on a shutter rotated by a small motor.

The output voltage of the photomultiplier is applied to the input of a d.c. amplifier with a stepped gain control. The output voltage of this amplifier is applied to the vertical plates of a cathode ray tube operated with no horizontal deflection. The image of the cathode ray tube spot is reflected from a half-aluminized mirror and focused on the steadily moving film of the camera. Light passing through this mirror allows the operator to watch the spot deflection and adjust manually the gain control on the amplifier to give a measurable deflection for as great a time as possible. Flashes of light passing from an illuminated slit through the half aluminized mirror in the other direction impress timing marks on the film at any desired interval. These timing flashes are produced by sub-multiple generator circuits controlled by a 100 kc/s crystal. These circuits end in an ordinary nuclear, scale of 1000, counter. The sub-multiple circuits feed regular pulses to this counter at the rate of 100 per second so that output pulses at intervals of 0·1, 1·0 and 10·0 seconds are avilable by simple switching of the counter scale. Other intervals are available by adjusting the sub-multiple circuits.

To avoid damaging the photocell and other components by the intense light of the exciting discharge, it was necessary to remove the applied voltage from the cell while the discharge was on and restore it immediately when the exciting power amplifier was pulsed off. This was accomplished by the photomultiplier gating circuit and synchronizing chassis II. To obtain completely repeatable results it was found necessary to operate the discharge tube cyclically for long periods to establish steady behaviour. The length of the on and off parts of the discharge cycle were controlled from the master pulsing unit in synchronizer II, or manually if desired. In the later stages of the work another synchronizing unit I was added to assure that the discharge always shut off and the photocell became active exactly at a timing mark. This added to the convenience of measurement of the recorded deflections.

The power supplies were all regulated, that for the power amplifier plate supply being a specially constructed supply with a two stage amplifier in the regulation system, capable of supplying 500 milliampères at any desired voltage from 700 to 1500. The regulation was necessary to ensure complete repeatability of excitation over long periods of time. The final system was very efficient and under optimum pressure conditions it is estimated that more than 500 watts were transferred to the discharge tube.

Because of the long times involved in the afterglow decay, d.c. coupling was necessary throughout. Constant current triodes were used to change the d.c. levels so that the photomultiplier supply (2500 volts negative) could be pulsed on and off by the same applied square wave which controlled the power amplifier screens (300 volts positive).

Gas temperatures were adjusted by varying the flow of cooling air fed into the light tight box enclosing the apparatus and also by varying the duration of the excitation part of the cycle. The extremes of temperature were attained only by precooling or heating the air. The upper limit of attainable temperature was set by the fire hazard. Wall temperatures varied by as much as ten degrees during an exposure but internal temperatures were probably much more constant close to the values stated.

The nitrogen used was produced by the bromine ammonia method. After being freed of water vapour and ammonia by passage over phosphorous pentoxide this gas produced strong afterglows without further purification. For further purification the nitrogen was passed over copper foil heated by an induction heater and passed into a bulb in which sodium vapour was produced by heating a pool of the metal. Large quantities of nitrogen were produced at one time and after purifying were stored in a one litre Pyrex reservoir whose walls were coated with metallic sodium from the purifying process. Commercial nitrogen was also tried and, after this purifying process, showed no difference in behaviour from that produced chemically.

§ 3. CALIBRATION

The sensitivity and linearity of the amplifying system were checked by applying d.c. voltages in known ratios to the amplifier input and photographing the cathode ray tube spot exactly as in an afterglow exposure. Deflections were measured on the developed film and plotted against the applied voltages. Constants were determined by least squares for the best straight line and best parabola fitting the results for each scale switch setting. The coefficient of the square term in the parabola was always negligibly small and the linear slope of the two curves agreed within the limits of error. The gain ratios were checked by independent measurement more than six months later and found to agree with the original values within one half of one per cent. Linearity of the light response of the photomultiplier and recording system was checked *in situ* for all but the two most sensitive ranges. In this calibration the photomultiplier was exposed to faint, diffusely reflected, light of approximately the correct colour. The intensity of the light falling on the diffusing surface was varied over about a factor of ten by rotating a Nicol prism relative to another left fixed. Factors greater than ten for one light value were considered insufficiently reliable due to rapid variation of the intensity at angles near 90°. The use of several intensities of light source gave overlapping values from several sets of readings and extended the calibration over several powers of ten. The process could not be extended to the most sensitive scales without removing the photomultiplier from its working position because stray light reaching the diffuser became comparable with the applied intensity. Since the plot of deflection against light intensity was straight at all intensities plotted and the amplifying and recording system had been shown linear on all scales, it was assumed that the response was proportional to intensity down to the lowest levels.

Using the sensitivity quoted in the manuals for type 931A photomultipliers, corrected to the wavelength for the afterglow, and the sensitivity of the recording system determined as above, the estimated overall sensitivity is $2{\cdot}44 \times 10^7$ quanta/sec striking the photomultiplier per millimetre deflection on the film. Using the fact that the cylindrical discharge tube was 35·5 cm long and 5 cm in internal diameter, and is placed with a flat window 2·5 cm in diameter, at a distance of 11 cm from the photosensitive surface, whose area is approximately 2 cm^2, it is possible to estimate the solid angle subtended by the photosensitive surface averaged over all points within the tube. Assuming that the glow is of equal intensity at all points in the tube, which is certainly very close to the truth from visual observation, and multiplying the average solid angle by the volume of the tube, it is found that the number of quanta per second striking the photosensitive surface is $5{\cdot}25 \times 10^{-2}$ times the number emitted per cm³. This quantity is subject to errors due to reflection at the walls of the tube and window. The outside walls of the tube were coated with chalk to give diffuse reflection and cut down loss of light but the efficiency of this device was probably not large. It seems likely that the figure quoted is fairly close to the true value. Combining these estimates, an instrumental constant G may be found. Its value is $2{\cdot}15 \times 10^{-9}$ mm quantum^{-1} cm^{-3} sec^{-1}.

The films were measured on a special comparator with motion in two directions at right angles. Tests showed that in a large number of settings on the same position the mean square deviation was 0·015 mm. Zero light positions on the film were taken from the points nearest to the time mark at which the intensity measurements were made. All light intensities of less than one millimetre are the average of five independent determinations.

§ 4. PROCEDURE

The success of this work was entirely due to the precautions taken to assure reproducibility. Stabilized power supplies and the automatic control assured reproducibility of electrical conditions to a very high degree. The nitrogen gas was prepared in large batches and stored under the conditions described above. Gas for each exposure was drawn from this supply. In the exposures for variation of pressure and temperature the following procedure was used. The discharge tube was pumped down to the order of 10^{-6} mm pressure as shown on a VG1A ionization gauge (not shown in figure 1). Nitrogen from the reservoir was admitted at a convenient pressure for starting the discharge. The discharge was operated on automatic control for a short time to stir the gas thoroughly. The tube was re-exhausted and nitrogen admitted to the pressure desired for experiment. The pressure was measured with the temperature adjusted to 40°c. The discharge was then put on automatic control and the on–off times and ventilating system adjusted to produce the temperature desired. Uninterrupted discharge could not be used as the temperature quickly rose beyond safe limits. On and off times were usually of the order of 10 to 60 seconds, the ratio being changed to aid in adjustment of the temperature.

It was found that the characteristics of the afterglow changed markedly during times up to two and one half hours after this process started but especially during the first thirty minutes or so. The gas when first admitted invariably showed little or no glow: no glow if especially rigorous outgassing and purifying had been carried out. Gradually, in the course of two hours, the glow increased in intensity and the form of the pressure variation, as shown on the Pirani gauge, reached a steady state. The condition reached after two hours and a half remained constant indefinitely. After three hours of such conditioning the film motion was started, and control was switched to manual. As the afterglow decayed, the spot deflection was monitored visually, and, starting with the lowest gain, the gain switch on the Tektronix 112 amplifier was changed to keep the deflection up to easily measurable values, until the most sensitive scale was reached, when the film was allowed to run and monitored until no deflection could be seen. The film was allowed to run considerably longer to allow the afterglow to die out completely. The apparatus was then put on automatic control once more while notes were made of the details of the exposure just finished. Frequently several exposures were made under identical conditions to check reproducibility but in the later stages this was so thoroughly established that the practice was discontinued. Because the intensity of the afterglow changed markedly with discharge conditions, it was thought that these might influence the other characteristics of the afterglow. For this reason several exposures were usually made under fixed conditions of pressure and temperature, but with different discharge frequencies. In each case electrical adjustments were made for the maximum power transfer to the gas. After final adjustments were made the automatic control was left on for some time until it was certain that steady state conditions had been reached before the film was exposed. This took much less time than the initial three hour conditioning. The same procedure was followed if temperature changes were to be studied at the same pressure. At the end of the series of exposures the discharge tube was pumped down and left in this condition until the next series.

The series of films on variation of oxygen impurity was preceded by a much more drastic outgassing of the discharge tube. The previous cleaning procedure was followed by thorough flaming of the tube under high vacuum. The gas in its reservoir was given a treatment of fresh sodium vapour and the copper foil reheated. This pure gas was then admitted to the tube and its pressure measured with the temperature at 40°c. As usual there was initially no visible glow. Even after the usual three hours conditioning the glow seemed very faint and of short duration. Unfortunately the film taken at this stage was destroyed before it could be measured.

Small percentages of electrolytic oxygen were then admitted from a short length of capillary tubing which could be refilled. The absolute percentages may well be quite considerably in error but the relative values should be quite accurate.

§ 5. RESULTS

The results are shown in figures 2 to 7 with numerical data in tables 1 to 3. With the above precautions reproducibility was excellent. Films taken under identical conditions yield graphs indistinguishable except as to position of points relative to the start of the exposure. Measurements of such curves agree at any one level to within an error of about 3% or 0·03 millimetres, whichever is larger. It is found that frequency and other discharge conditions have no effect on the slopes found for the curves. Films taken at different times and with different frequencies agree as to slopes of the curves within an error of the order of about 4 to 6%, the increase from the 3% above being probably due to not reproducing conditions accurately. Thus relations between the slopes of curves under different conditions might be expected to obey an interrelationship to this order of error. Error of any individual slope of course depends on the number and arrangement of the points used to determine it. Inspection of the curves will reveal some cases in which a larger error might be expected. The curves shown are taken with various frequencies from 6·6 to 9·5 Mc/s. The curves with the largest initial intensity were finally chosen in each case.

Figures 2, 4, 6 show plots of the natural logarithm of the intensity in millimetres against time for the whole curve. Figures 3, 5, 7 show the initial eighteen seconds of these same curves with $I^{-1/2}$ plotted against time. It is seen that all curves (except that for 0·4% oxygen, see below) show linear logarithmic plots at low intensities. All curves in which the points end short of the border of the graph have been carried down to an intensity of 0·2 mm on the film. In a few cases one point below this value has also been included. In the cases of 0·4% oxygen impurity the final point represents 0·16 mm (note scale factor of 10), the lowest value shown on any curve. Initial intensities rise to over 32 000 millimetres and, as above, intensity changes of 0·03 millimetres are significant so that the minimum significant intensity change is just short of one millionth of the maximum intensity used. In all the figures attention should be drawn to the fact that constants have been arbitrarily added to the ordinates of curves where necessary to keep the points separated.

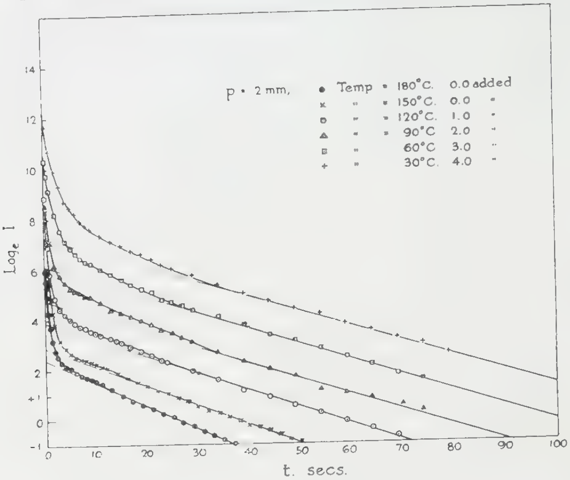

Figure 2. Graph of ln I against t, for varying temperature.

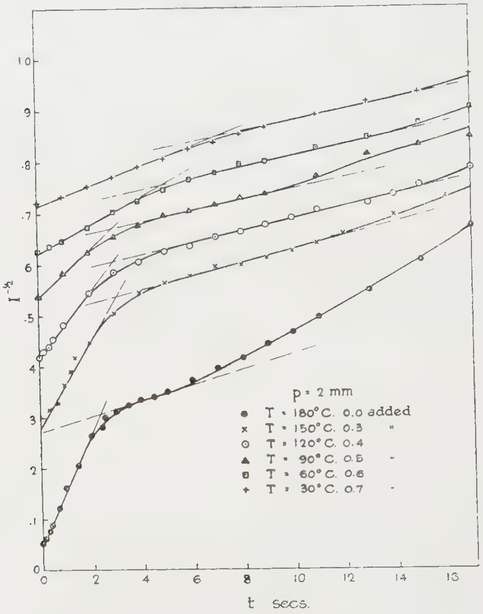

Figure 3. Graph of $I^{-1/2}$ against t, for varying temperature.

Figures 3, 5, 7 show that the initial decay gives two straight line relationships between $I^{-1/2}$ and t except in the case of the three lowest, and the highest, oxygen percentages. In the lower oxygen percentages, the first slope is missing or rudimentary, and in the highest case only the first slope exists, and this slope persists down to the lowest of all the intensities measured.

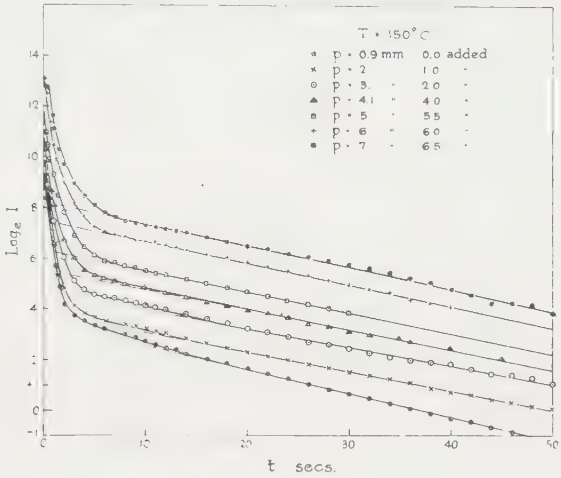

Figure 4. Graph of ln I against t, for varying pressure.

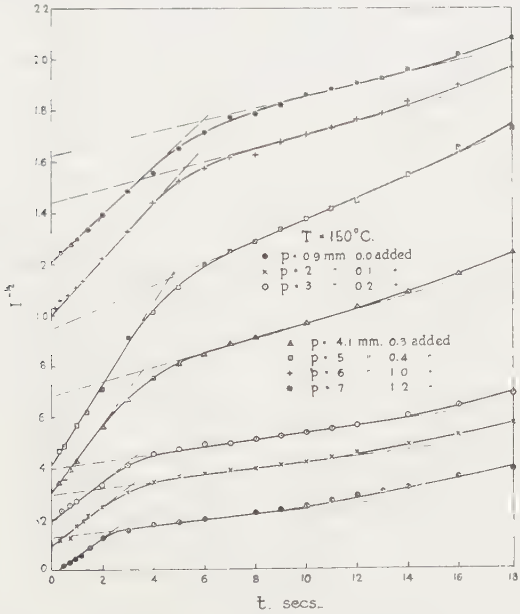

Figure 5. Graph of $I^{-1/2}$ against t, for varying pressure.

Slope determinations were made from large scale graphs 50 cm by about 70 cm in the x and y directions respectively. This scale is necessary to take full advantage of the accuracy of the experimental points. On this scale it was seldom possible to change the slope of the best straight line by as much as 3% without being quite evidently in error.

Even on the greatly reduced scale drawn for reproduction a peculiar feature is visible in figures 2, 4, 6. It is apparent in most of these curves that the curvature and in some cases the slope of these logarithmic curves is not a monotonically

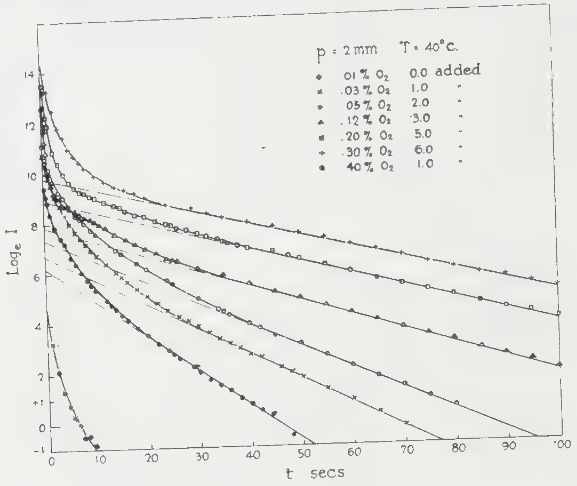

Figure 6. Graph of ln *I* against *t*, for varying oxygen added.

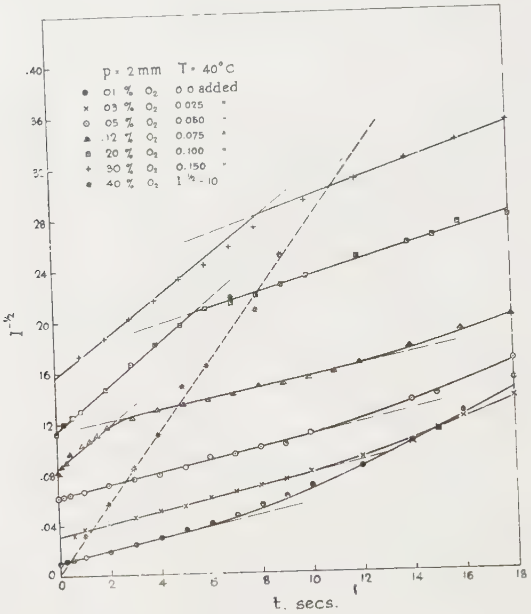

Figure 7. Graph of $I^{-1/2}$ against *t*, for varying oxygen added.

decreasing function of time. On any one curve this might be taken for random error but the repetition of the feature on all curves for the same gas condition, but widely different in initial intensity, and its appearance in altered size and form under different conditions makes it certain that the effect is real even though it is too small to be evaluated exactly in measurements of the present accuracy.

Numerical constants determined from large scale curves are presented in tables 1, 2, 3, in which variation of constants with variation of temperature, pressure and added oxygen are shown for the cases displayed in the graphs of figures 2 and 3, 4 and 5, and 6 and 7, respectively. R is the negative slope of the final logarithmic decay, S_1 is the slope of the initial straight line on the $I^{1/2}$ plots and S_2 is the second straight line slope on these same plots. I_{03} is the intensity obtained by extrapolating the logarithmic straight line back to zero time, I_{02} that obtained by extrapolating the second straight line on the $I^{1/2}$ curves (slope S_2) back to zero time and I_{01} is the estimated intensity of the component showing slope S_1 on the $I^{1/2}$ plots. The extrapolation of this straight line frequently showed an intercept of zero within the error of drawing, or even, in those films taken without synchronizer I, where the zero time is slightly uncertain, a small negative intercept. In these cases, the value of the initial intensity is simply listed as greater than the intensity of the first measured point. The value I_{01} is this initial intensity with I_{02} subtracted. These constants allow the experimental curves to be reproduced very closely. The exception to this reproduction is the behaviour mentioned above of the derivative and curvature of the logarithmic curves as the constant slope is approached. There is no indication, however, that the processes represented by S_1 and S_2 are anything other than additive.

Table 1. Variation of Constants with Change of Temperature, $p=2$ mm

Temp. (°c)	R ($\times 10^2$)	S_1 ($\times 10^2$)	S_2 ($\times 10^2$)	I_{01}	I_{02}	I_{03}
30	5·97	1·95	1·07	4900	210·0	26·3
60	6·22	2·79	1·08	3000	91·0	22·4
90	6·25	4·55	1·08	801	49·0	15·8
120	6·74	6·39	1·16	3880	33·9	17·4
150	7·64	7·71	1·32	>4200	23·8	17·8
180	9·21	10·8	1·50	500	15·2	11·2

Table 2. Variation of Constants with Pressure, $T=150$°c

p (mm)	R ($\times 10^2$)	S_1 ($\times 10^2$)	S_2 ($\times 10^2$)	I_{01}	I_{02}	I_{03}
0·9	9·60	7·21	1·11	>4300	59·0	34·6
2·0	7·64	7·71	1·32	>4200	23·8	17·8
3·0	7·44	7·80	1·45	> 950	25·5	16·2
4·1	7·60	13·7	2·85	> 520	6·9	4·5
5·0	8·08	16·2	4·36	> 240	3·4	2·3
6·0	8·44	11·0	2·61	>1150	5·1	4·6
7·0	8·80	9·50	2·29	> 480	7·3	6·0

Table 3. Variation of Constants with Oxygen Impurity, $p=2$ mm, $T=40$°c

% O_2	R ($\times 10^2$)	S_1 ($\times 10^2$)	S_2 ($\times 10^2$)	I_{01}	I_{02}	I_{03}
0·01	13·9	—	0·462	small	10000	525
0·03	9·89	—	0·478	7200	24500	248
0·05	8·52	—	0·466	3400	6920	190
0·12	6·04	1·62	0·428	15000	635	132
0·20	5·08	1·65	0·603	1400	186	50
0·30	4·94	1·55	0·703	25100	172	51
0·40	—	26·83	—	237	0	0

A study of the values listed in the tables indicates that the slopes of the various parts of the curves exhibit fairly smooth variation with each of the three variables in spite of wild fluctuations in the amplitudes, and in the ratios of the amplitudes to one another. It may be noted that I_{03} is always less than I_{02} as might be expected if they represented competing processes. I_{01} and I_{02} may have any ratio and seem to be quite independent of one another. I_{01} is almost certainly zero in absence of oxygen. I_{02} is also zero with the most highly purified gas until the discharge has been run for a conditioning period. The logarithmic component always appears when I_{02} exists but is absent when only I_{01} is present. The well known air after-glow due to chemical reaction of nitrogen and oxygen does not appear until about five times the maximum amount of oxygen used here is admitted. Further analysis of these curves is given by Anderson (1957).

ACKNOWLEDGMENTS

The authors are indebted to the Defence Research Board, Ottawa, Canada, for a grant of funds to one of us (J. M. A.) which permitted one of us to participate (A. D. K.) and permitted the purchase of some necessary apparatus.

REFERENCES

ANDERSON, J. M., 1957, *Proc. Phys. Soc.*, **70,** 887.
RAYLEIGH, LORD, 1942, *Proc. Roy. Soc.* A, **180,** 123.

The Nature of Active Nitrogen

By J. M. ANDERSON
Department of Physics, University of Toronto, Canada

MS. recieved 28*th May* 1957, *and in revised form* 8*th August* 1957

Abstract. It is shown that the first bimolecular process found experimentally in the decay of the nitrogen afterglow requires oxygen as a catalyst and draws both active bodies from a common population. An activation energy of 900 cm^{-1} is necessary for this afterglow process. The second bimolecular process involves two active bodies possessing monomolecular decays and drawn from different populations. Negligible activation energy is required for this afterglow process. This process is quenched by oxygen and requires a minute impurity believed to be hydrogen. The final monomolecular decay shows the usual diffusion–collision pressure dependence at higher temperatures and effectively diffusion dependence only at lower temperatures. The effects of diffusion are much reduced by a monomolecular layer of oxygen on the walls. An aggregate possessing a dissociation energy of 5600 cm^{-1} is involved in the final afterglow process. Reasons are given for believing that the first bimolecular process is recombination of nitrogen atoms in the presence of an oxygen molecular catalyst of the order of a few parts per million and that the second process is a collision of two different vibrationally excited ground states of the nitrogen molecule with a molecular hydrogen catalyst of the order of a few parts per million.

§ 1. INTRODUCTION

THE yellow glow persisting after an intense discharge in nitrogen has been the subject of publications for more than fifty years. Many theories have been proposed to account for the glow, among which are those of Sponer (1925), Cario and Kaplan (1929), Cario (1934), Mitra (1945) and Reinecke (1953). Since the yellow afterglow is such a prominent feature of active nitrogen any successful theory must account for its properties in detail, as well as for a number of other facts which seem well established.

The properties for which theory must account are as follows:

(*a*) A glow persists for a time up to the order of minutes after a high voltage discharge in 'pure nitrogen'. This glow consists principally but not exclusively of bands originating in the eleventh vibrational level above the $B^3\Pi$ state of the neutral nitrogen molecule. A small intensity in the afterglow exists coming from other vibrational levels of this state, chiefly the tenth, ninth, eighth and seventh.

The energy of the eleventh vibrational level is now accepted as being about 9·6 ev (Herzberg 1950). The intensity distribution of the afterglow bands follows the Franck–Condon principle as shown by McLennan, Ruedy and Anderson (1928) so that the final emitter of radiation is an unperturbed nitrogen molecule. In the same reference it is shown that the admixture of very large percentages of inert gas causes the maximum of emission of the afterglow to come from the tenth, ninth and eighth, etc., vibrational levels of this state successively as the percentage of nitrogen becomes smaller.

(*b*) When the glowing gas is pumped through a glass tube it was shown by Rayleigh (1911, 1940), that the glow disappears from a section heated by a bunsen burner but reappears in a cooler section beyond. The glow is enhanced if a section of the tube is cooled by liquid air.

(*c*) Abnormal chemical activity is associated with nitrogen emitting the afterglow as shown by Rayleigh (1911) and others. This chemical activity persists after the visible glow has ceased, and apparently involves a much larger percentage of the total number of gas molecules as shown by Willey and Rideal (1927).

(*d*) The decay curve of the afterglow intensity with time is not simple. Some investigators, e.g. Willey (1930), have found a bimolecular law, others such as Rayleigh (1935) have found the curve complex.

(*e*) Absolutely pure nitrogen fails to give an afterglow. This was first suggested by Comte (1913) partially verified by Rayleigh (1935), and has since been confirmed at Harvard (1955, verbal communication) and at Toronto as described by Anderson, Kavadas and McKay (1957, hereinafter AKM).

(*f*) No single particle has been suggested which could carry the full energy of the upper state of the afterglow. Therefore interaction of two energy carriers seems necessary.

§ 2. ANALYSIS

Instead of making a detailed theory of the mechanism of the afterglow it was decided to set up a quantitative description of the phenomenon leaving the details of the process unspecified. The simplest assumptions fulfilling the conditions above were adopted. These are: (1) Two energy carrying particles which may be the same or different from one another, interact together, possibly with third bodies. (2) This interaction results in the emission of one afterglow quantum. (3) Simultaneously with this process the energy carriers individually are giving up their energy without visible radiation. This process is assumed monomolecular.

Calling the population per unit volume of the two entities n_1 and n_2, these assumptions lead to the simultaneous differential equations

$$-\frac{dn_1}{dt}=kn_1n_2+k_1n_1, \quad -\frac{dn_2}{dt}=kn_1n_2+k_2n_2, \qquad \ldots\ldots(1)$$

kn_1n_2 is the number of afterglow quanta per cm^3 per second. The constants k_1 and k_2 represent the probability of each type of particle giving up its energy individually per unit time.

Dividing equations (1) by n_1 and n_2 respectively, integrating from zero to t with populations $n_1{}^0$ and $n_2{}^0$ at t equals zero, taking antilogarithms and multiplying the resultant equations we have

$$f=f(t)=kn_1n_2=kn_1{}^0n_2{}^0\exp\left[-(k_1+k_2)t-k\int_0^t(n_1+n_2)\,dt\right]. \qquad \ldots\ldots(2)$$

Defining the negative time derivative of the logarithm of f as a function $\phi(t)=\phi$ we have

$$\phi=\phi(t)=(k_1+k_2)+k(n_1+n_2). \qquad \ldots\ldots(3)$$

Because the energies involved in the process are so much greater than the temperature energy of the particles n_1 and n_2 must tend to zero as t increases.

Thus the limit of the function ϕ as t increases is a constant $R = k_1 + k_2$. Equation (3) may be written

$$k(n_1 + n_2) = \phi - R. \qquad \ldots\ldots(4)$$

Solving equations (2) and (4) as simultaneous equations in n_1 and n_2

$$n_1 \text{ and } n_2 = (1/2k)[(\phi - R) \pm \{(\phi - R)^2 - 4kf\}^{1/2}]. \qquad \ldots\ldots(5)$$

The intensity in quanta per second reaching the photomultiplier tube will be (AKM)

$$I = Gf(t) = Gkn_1n_2.$$

Here G is the apparatus constant determined in (AKM) equal to

$$2{\cdot}15 \times 10^{-9}\ \text{mm cm}^{-3}\ \text{sec}^{-1} \text{ per quantum}.$$

Since G is a multiplying constant it does not appear in equation (4). In equation (5) $f(t) = f$ must be replaced by I/G and if we put $k = s^2G$, the equation becomes

$$n_1 \text{ and } n_2 = (1/2s^2G)[(\phi - R) \pm \{(\phi - R)^2 - 4s^2I\}^{1/2}]. \qquad \ldots\ldots(6)$$

From equation (3) we see that one test of the correctness of the general mechanism assumed is that a plot of logarithm of intensity against time should tend to a straight line of constant slope.

To formulate a second test we must return to the original differential equations (1). Both n_1 and n_2 must decrease toward zero with time, the term kn_1n_2 decreasing more rapidly than the term k_1n_1 or k_2n_2. Thus if it is possible to produce sufficiently large initial populations the linear terms in equations (1) will be negligibly small compared to the term kn_1n_2 and the differential equations for short times after the creation of this large initial population will reduce to

$$dn_1/dt = -kn_1n_2 = dn_2/dt. \qquad \ldots\ldots(7)$$

Putting $n_1 = n_2 + C$, where C is a constant, integrating the two equations, forming the product $I = Gkn_1n_2$, and taking the reciprocal of the square root we have

$$\frac{1}{I^{1/2}} = \frac{1}{CI_0^{1/2}}\{n_1^0 \exp(\tfrac{1}{2}Ckt) - n_2^0 \exp(-\tfrac{1}{2}Ckt)\}. \qquad \ldots\ldots(8)$$

Expanding the exponentials, putting $(n_1^0 - n_2^0) = C$, using $I_0 = Gkn_1^0n_2^0$ where necessary and s as defined above

$$\frac{1}{I^{1/2}} = \frac{1}{I_0^{1/2}} + \frac{(n_1^0 + n_2^0)st}{2(n_1^0n_2^0)^{1/2}} + \frac{C^2k^2t^2}{8I_0^{1/2}} + \frac{n_1^0 + n_2^0}{2(n_1^0n_2^0)^{1/2}}\,\frac{C^2k^2s\,t^3}{24} + \ldots \qquad \ldots\ldots(9)$$

Equation (9) shows that for sufficiently great populations, a plot of $I^{-1/2}$ against t should show a straight line relationship, for times small enough that terms in squares and higher powers of t may be neglected. This constitutes the second test of the validity of the general form assumed since only a second order reaction will show this affect. The asymptotic slope depends not only on the bimolecular constant k but also on the initial population $r = (n_1^0/n_2^0)$. Any departure from the initial straight line must be towards higher values of $I^{-1/2}$.

Starting with equation (6) some progress in finding s is possible. Since the population numbers must be real the quantity under the root sign must be zero or positive

$$(\phi - R)^2 - 4s^2I \geqslant 0 \quad \text{or} \quad (\phi - R) \geqslant 2sI^{1/2}. \qquad \ldots\ldots(10)$$

If we use axes ϕ and $I^{1/2}$ as in figure 1 the straight line $(\phi - R) = 2sI^{1/2}$ divides the diagram into two parts, all points above the line corresponding to real values of n_1 and n_2, while all points below the line correspond to imaginary values of n and n_2 which cannot be experimentally attained. The equation $\phi - R = xsI^{1/2}$, where x is any constant, represents a straight line passing through the point $(0, R)$. Substituting in equation (6) shows that all points satisfying this relation correspond to a definite population ratio

$$r=\frac{n_1}{n_2}=\frac{x+(x^2-4)^{1/2}}{x-(x^2-4)^{1/2}} \quad \text{or} \quad x=\frac{(r+1)}{\sqrt{r}}. \qquad \ldots\ldots(11)$$

Lines of constant slope (xs) are loci of constant population ratio, $x=2$ corresponding to the case of equal populations. Substitution from (9) in (11) shows that this slope becomes $\frac{1}{2}xs$.

For any part of the intensity decay curve corresponding to the first two terms of equation (9), that is for $C=0$, the corresponding curve on the $(\phi, I^{1/2})$ diagram is a straight line. This curve is marked in figure 1. For two identical particles interacting, the slope of the straight line in figure 1 is $2s$ so that s becomes known. The appearance of this straight line is the criterion which must be satisfied for interaction of two identical energy carriers to produce the afterglow.

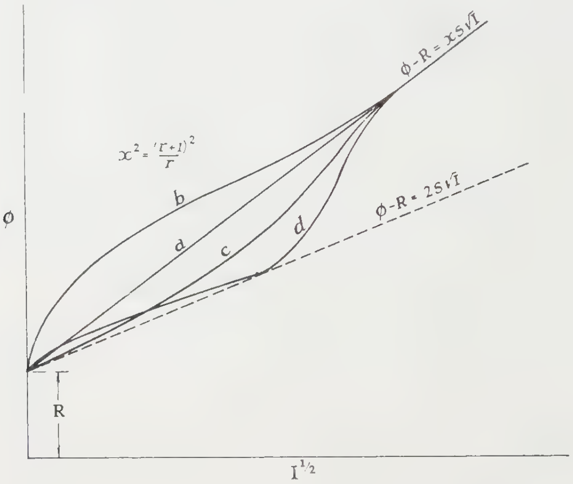

Figure 1. Possible forms for curves of ϕ against $I^{1/2}$.

If the two energy carrying entities are different it may be expected that the ratio of their populations will change with time. If the entity of greater initial population decays more slowly than that of initially smaller population the ratio r must increase with time, that is r must increase as I or $I^{1/2}$ decreases. For this case the locus of points on the experimental intensity decay curve must cut the loci of constant population ratio always from below as I decreases. This is shown in figure 1, curve *b*. Curvature indicates that the afterglow process involves the interaction of two particles of different properties.

If the entity of greater initial population decays more rapidly than the other, the ratio r and quantity x must decrease as the experimental intensity curve is traced from high to low intensity. Such a curve must cut the loci of constant ratio of population always from above. This could result in a curve such as figure 1 (curve *c*) which may meet the line of slope $2s$ at a finite or zero angle at the point $(0, R)$. These cases yield no information as to the values of x and s. The occurrence of curvature would indicate interaction of particles of different properties.

A fourth case exists in which the decay of the entity of greater initial population is so much more rapid than that of the other entity that equality of population is reached while the intensity of the glow is still appreciable. In such cases a curve such as figure 1 (*d*) results. Here the ratio is falling rapidly so that the experimental curve (*d*) approaches the locus of unit ratio with, say, n_1 greater than n_2 but the ratio decreasing toward unity. When n_1 equals n_2 a point on curve (*d*) must coincide with a point on the locus of unit ratio. As the ratio n_2/n_1 becomes greater than one the quantities in equation (6) interchange the signs before the square root. The curve from this point down to zero intensity will be of the same form as (*b*). In some cases ϕ may show a minimum value. In other cases ϕ may decrease monotonically but its rate of decrease may pass through a minimum. The case of curve (*d*) completely determines *s*.

§ 3. EXPERIMENTAL FACTS

In AKM it has been shown that the decay curve of the nitrogen afterglow divides into three parts: an initial bimolecular decay, linear in $I^{-1/2}$ against t having a slope S_1, a second bimolecular decay having an initial straight line portion on the $I^{-1/2}$ plots with a slope S_2 and a final part showing a straight line of slope R on a plot of natural logarithm of I against t. For brevity these will be referred to hereafter as the S_1, S_2 and R processes respectively. The numerical results of the experimental work (AKM) are shown in figures 2 and 3.

In addition to these results it was shown that extremely pure nitrogen gave no afterglow until it had been subjected to a very powerful intermittent discharge in a Pyrex vessel for about two hours. It was also pointed out that in most of the logarithmic decay curves plotted in the experimental paper the curvature did not approach zero monotonically and in several cases the first derivative of the curve passes through a local minimum before assuming its final value.

§ 4. DISCUSSION OF S_2 AND R PROCESSES

Processes S_2 and R fulfil all the required tests for the general form of mechanism discussed above. A straight line plot $I^{-1/2}$ against t exists in the early part of this section with the actual decay curve departing upward from this straight line as required and the final parts of all curves are accurately logarithmic over about two decades. From the curves of AKM it is evident that ϕ falls off less rapidly as I decreases and in some cases passes through a local minimum. This corresponds to curves *c* and *d* of figure 1 and indicates a bimolecular process involving two particles of different properties of which that which was originally the more abundant decays the more rapidly. One at least of these particles suffers monomolecular destruction.

In addition to this we know that some form of impurity must be involved since the most pure nitrogen shows no glow. It is readily shown using the formulae for the number of three-body collisions from Tolman (1927) and values of I_{02}, S_2, G (AKM) that such collisions by three independent particles are too rare to account for the glow by a factor of the order of 10^{15}–10^{17}. Some binding must exist between at least one of the energy carrying particles in the S_2 process and some impurity particle. The most probable substances for such an impurity are oxygen and hydrogen. As will be seen later oxygen, while necessary for the S_1 process, inhibits the S_2 process. Thus the impurity necessary for the S_2 process is *probably* hydrogen. This probability is increased by the fact that

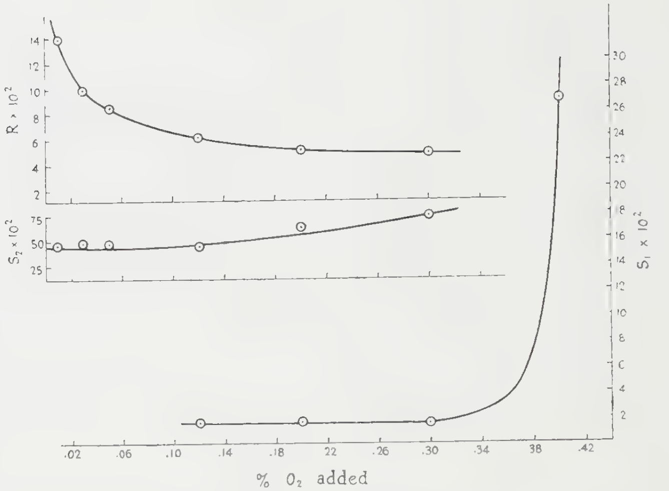

Figure 2. Variation of parameters with added oxygen, pressure 2 mm, temperature 40°C.

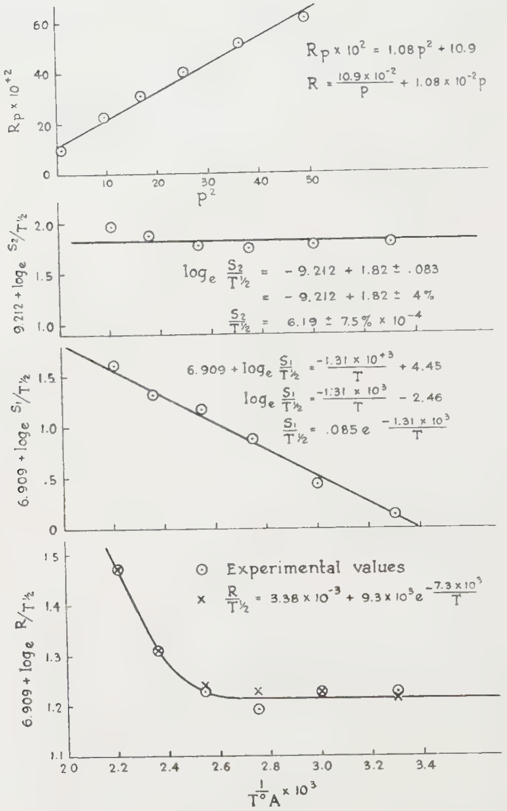

Figure 3. Deduction of equations for variation of parameters.

hydrogen is known to diffuse into and through Pyrex glass in appreciable quantities.

The bottom graph in figure 3 shows a plot of the natural logarithm of $R/T^{1/2}$ against $1/T$ where T is converted to absolute temperature. It is seen that the lower temperature values give a horizontal straight line while the higher temperature values rise steeply. The relation given

$$R/T^{1/2} = 3{\cdot}38 \times 10^{-3} + 9{\cdot}3 \times 10^{3} \exp(-7{\cdot}3 \times 10^{3}/T) \qquad \ldots\ldots(12)$$

fits the points within the accuracy of the experimental results.

In the top graph of figure 3, the product Rp is plotted against p^2 at a temperature of 150 C, that is, at the second highest temperature point in the lower graph of the same figure. Since the points fit a straight line within the expected limits of error we may represent the pressure variation of R at this temperature by the expression

$$R = \frac{10{\cdot}9 \times 10^{-2}}{p} + 1{\cdot}08 \times 10^{-2} p. \qquad \ldots\ldots(13)$$

This relation is of the well-known form found for destruction of metastable atoms by diffusion to the walls and destruction by collisions with unexcited particles. Since the theoretical form of the expression as given by Zemansky (1929) and many others is

$$R = \frac{D}{\lambda^2}\frac{1}{p} + Bp$$

where D is the diffusion coefficient at 1 mm pressure, B is the number of collisions made per second by a particle in gas at 1 mm pressure and λ is called the diffusion length of the discharge tube.

Substituting the dimensions for the discharge tube given in AKM, $1/\lambda^2$ is found to be 0·930, D for nitrogen in nitrogen is calculated using formulae in Tolman (1927) to be 320 c.g.s. units. The value of B again for nitrogen in nitrogen is similarly $5{\cdot}2 \times 10^6$. The unknown diameter of the complex particle involved will alter these constants somewhat but must leave the order of magnitude the same. Comparison of the constant $10{\cdot}9 \times 10^{-2}$ with the value of $D/\lambda^2 \simeq 300$ shows that the effective diffusion coefficient is lower by a factor of 3000 than the calculated value. The efficiency of collisions with unexcited nitrogen molecules is found to be one in 5×10^8 at this temperature. Reference to equation (12) shows that this extremely low collision efficiency is due to the fact that monomolecular destruction results only from collisions for which the available kinetic energy is greater than $7{\cdot}3 \times 10^3\boldsymbol{k}$ where $\boldsymbol{k}$ is Boltzmann's constant, that is, an energy of $10{\cdot}1 \times 10^{-13}$ erg or 5600 cm^{-1}. This energy may be taken as the dissociation energy of the complex particle involved. The values of R at lower temperatures show no requirement for excitation energy so that it may be presumed that the complex particle breaks up on diffusion to the walls without activation energy and with the release of the stored energy in the active particle.

Dissociation and recombination of the compound aggregates is necessary to account for Rayleigh's (1911, 1940) observation that the afterglow quenched by heating a portion of the tube again became visible in the cooler parts of the pumping line. Such a recombination indicates that the impurity particle is in a stable form in the tube, that is, it is molecular rather than atomic hydrogen. Straightforward arguments (unfortunately long) based on relative numbers of collisions available for the formation and destruction of aggregates show that the experimental results (AKM) for variation of pressure and of temperature can be explained by the action of a catalyst present to excess and that this excess requires in all cases a concentration of catalyst of less than 50 parts per million. The results for addition of impurity of oxygen, in which the cleaning and purification procedures were much more rigorous, are consistent with a reaction rate determined by a deficiency of catalyst which could then be present only to a few parts per million.

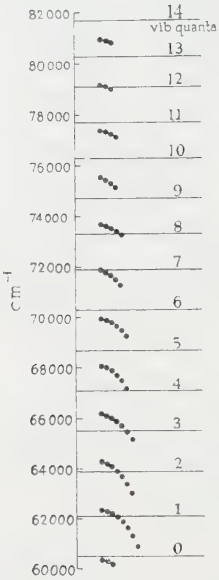

Figure 4. Vibrational energy levels of B$^3\Pi$ state of the nitrogen molecule with energies available from combined vibrational energies of the X$^1\Sigma$ state.

Support for this view of the reason for the exceptionally low values of S_2 in this impurity series may be found in the central graph of figure 3 in which S_2 is plotted against oxygen concentration. Because these impurity exposures were started with the highest possible purity and amounts of oxygen always added to the same gas, the graph against oxygen concentration is also a graph against time. The exposures were preceded by a three-hour conditioning period and separated by three-quarters of an hour of conditioning. Thus in the course of somewhat more than five and three-quarter hours during which these points were taken some increase in hydrogen might be expected even if none were admitted as a minute impurity with the oxygen impurity added. Thus S_2 might be expected to increase if its value were dependent on catalyst concentration. Exactly this form of increase is found. Some of the catalyst for the S_2 process may have entered with the added oxygen. Since the oxygen was electrolytic and no special purifying was done this seems possible.

The afterglow collision of the process S_2 requires no activation energy. The second graph of figure 3 shows that $S_2/T^{1/2}$ is a constant with a mean square deviation of 7·5%, which is only slightly above the value to be expected.

The effect of oxygen on the intensity and duration of the afterglow has been noted by many workers. This is shown, in figure 2, as successive percentages of oxygen are added to the highly purified and outgassed tube. In the top graph it is seen that the value of the logarithmic decay constant (at this temperature and pressure almost entirely due to diffusion) is very large for negligible quantities of oxygen, falls very rapidly and levels off at values between 0·2 and 0·3% oxygen added. When the oxygen is increased to 0·4% the glow almost disappears and its duration is very short. The decay is then completely bimolecular down to the lowest intensity level measured on any film, so that processes S_2 and R have disappeared.

Using the dimensions of the discharge tube and the diameter of the oxygen atom and dividing the area of the walls of the tube by the projected area of the oxygen atom it is found that $6{\cdot}9 \times 10^{17}$ oxygen molecules would be necessary to form a monomolecular layer on the walls. Using the value $6{\cdot}22 \times 10^{16}$ nitrogen atoms per cm^3 at 2 mm pressure and 40c and the volume of the vessel as 690 cm^3 it is found that the above number of atoms would amount to about 1·5% added oxygen. Since it is certainly impossible to pack oxygen atoms as closely as the calculation indicates and the absolute percentages of oxygen may be considerably in error, it seems certain that the added oxygen settled almost completely on the walls as a monomolecular layer inhibiting the destruction of the energy carrying particles of at least one kind and probably both kinds involved in the process S_2. Almost no oxygen appears in the body of the gas until the monolayer is completed between 0·3 and 0·4% added oxygen, as shown in figure 3.

§ 5. Mechanism of S_2 and R Processes

The form of the mechanism for processes S_2 and R is almost complete. One question remains. What is the nature of the energy-carrying particle? To settle this the possibilities must be eliminated. The particles cannot be nitrogen atoms recombining with or without catalysts. It has been shown that at least one of the particles involved in S_2 can be disposed of by a monomolecular process. Nitrogen atoms can only recombine in pairs, and no possibility of monomolecular decay exists. There is every indication, as will be shown below, that atomic recombination is responsible for process S_1.

Interactions involving metastable nitrogen atoms cannot account for afterglows of such long duration. All work on metastable atomic states such as that of Grant (1950), Eckl (1953) and Blevis (1957) at Toronto and Phelps and Molnar (1953) show that such states have lives of the order of milliseconds as compared to the required seconds or minutes. Heald and Beringer (1954) have shown, after careful search, that the populations of the ^{2}P and ^{2}D nitrogen atomic metastable states is unmeasurably small. Search for absorption from the $\text{A}^3\Sigma$ metastable state has been carried out without success by many workers, of whom one of the most recent is Worley (1948).

Molecular or atomic ions do not exist in the afterglow. Many observers have shown that the glowing gas contains no free charges if ionizable impurities are excluded. Benson (1952) has shown by modern methods that electron–ion recombination is not concerned in the afterglow.

These theories have also failed to take into account the observation by McLennan, Ruedy and Anderson (1928) that the maximum intensity of the afterglow moves toward the red as the nitrogen is diluted with increasingly great excess of inert gas. This indicates that, whatever the energy carrier involved, it must be able to give up its energy by collisions with inert gas molecules in such a way that depletion of energy carriers initially present leaves energy levels populated which are lower only by energies of the order of 2000 cm^{-1}. This requires that the carrier be molecular in character. The only energy-carrying particle fulfilling all the necessary conditions seems to be the nitrogen molecule in a high vibrational level of the $\mathrm{X}^1\Sigma$ ground electronic state.

Ample energy is available from this source, since Birge and Hopfield (1928) have traced these vibrational levels up to that with twenty-one quanta at 5·5 ev, while Herman (1945) has traced them still further to that with twenty-seven quanta at 6·6 ev. Since the eleventh vibrational level of the $\mathrm{B}^3\Pi$ state of the nitrogen molecule which gives maximum emission in the normal afterglow has an energy of only 9·6 ev a large number of possible combinations of pairs of such vibrationally excited molecules could provide the necessary energy. Figure 4 is a diagram of the vibrational energy levels of $\mathrm{B}^3\Pi$ state of the nitrogen molecule using data from Herzberg (1950). Black dots indicate energies available from addition of the energies of two vibrationally excited particles in the $\mathrm{X}^1\Sigma$ state. These fall in definite sequences which may be specified by the total number of vibrational quanta possessed by the two ground state molecules. Numbering from the bottom of figure 4, the sequences shown correspond to totals of twenty-seven quanta (below the zero level) up to thirty-nine quanta (above the fourteenth level). Energy within any one sequence is a maximum when the numbers of quanta contributed by each particle are most nearly the same. This energy is plotted at the left in each case. To the right are plotted the successive members of the sequence having the same total number of quanta but with the difference in contribution from the two molecules increasing. Since it seems unlikely that the very high levels found by Herman (1945) are heavily populated the sequences have been arbitrarily terminated at the twenty-first vibrational level.

The activation energy to be derived from kinetic energy is for the S_2 process either zero or smaller than $\boldsymbol{k}T$. Even small activation energies would suffice to give a large probability of transfer of the vibrational energy to the zero, sixth, seventh and eleventh vibrational levels which are among those involved in the afterglow emission. If collisions involving transfer of internal energy to kinetic energy also occur transitions to the first, second, third and eighth levels also become prominent. Thus a large part of the first positive band system in the visible region could well be emitted in the afterglow with local peaks depending on precisely which levels are involved. No other form of energy carrier seems to come close to satisfying all requirements.

Vibrational levels of the ground electronic state could display the monomolecular disappearance as required by the form of the light curves. In the majority of cases, if not in all, molecules in different vibrational levels would be involved and the active particles would be different as required. Little is known of the lifetime of such vibrational states although work is now under way in this laboratory.

Such an energy process might be expected to dissipate the energy of high vibrational states in such a way that the maximum of the afterglow emission would move to the red as observed (McLennan, Ruedy and Anderson 1928).

Even after the afterglow had disappeared, due to depletion of the higher states, large numbers of molecules might be expected to remain in the lower vibrational states but still with comparatively large amounts of stored energy. Such states might well account for the chemical activity associated with active nitrogen, persisting long after the glow has disappeared.

From the variation of S_2 and R with pressure (AKM) it is noted that the value of S_2 passes through a maximum near the point where R is a minimum. As shown in the early part of this paper S_2 is not a true bimolecular constant but is this constant multiplied by a factor increasing with the ratio of populations. At the pressures where the rate of destruction of those entities, of greatest initial population and most rapid decay, is least, it might be expected that the initial population ratio would increase and hence S_2 increase. That the maximum of S_2 does not coincide with the minimum of R may well be due to a similar but quantitatively different behaviour for the other and slower decaying active body.

§ 6. THE S_1 PROCESS

The S_1 process was shown in the experimental paper to vary with conditions quite independently of S_2. The results of the experiments for S_1 with variation of temperature and oxygen concentrations are shown in figures 2 and 3. The equation of figure 3 shows that the afterglow emission process S_1 involves an activation energy given by $1{\cdot}31 \times 10^3 = E/\boldsymbol{k}$ to be $1{\cdot}80 \times 10^{-13}$ erg per molecule or 900 cm^{-1}.

In figure 2, the bottom curve shows that the strength of emission due to the process S_1 is too small to allow of a slope being determined, if indeed it exists at all, at the lowest oxygen percentage. As discussed above in connection with the later processes S_2 and R, practically all the oxygen added goes to form a monomolecular layer on the walls, until the addition reaches between 0·3 and 0·4% when the layer is complete and oxygen appears in the body of the gas in appreciable concentration. The extremely small oxygen percentage present in the body of the gas below 0·3% added is still sufficient to affect the amplitude of S_1 very markedly, changing it from essentially zero at 0·01% added to 25 100 mm at 0·3% added (AKM). At 0·4% added the slope S_1 has risen to almost twenty times its value at 0·3% added and S_2 has disappeared completely. The initial amplitude at 0·4% oxygen added has fallen to 237 mm due probably to the very much smaller concentration of active bodies built up by the discharge.

No indication appears on any decay curve that the intensities of the processes S_1 and S_2 are other than completely independent. The curve at 0·4% shows the process down to the lowest measurable intensity and demonstrates the complete absence of curvature of the $(I^{-1/2}, t)$ curve, and of any trace of logarithmic decay at low intensities. Thus the S_1 process is a truly bimolecular process involving two particles of identical properties neither of which undergoes monomolecular decay. Thus the process is almost certainly due to recombinations of atoms. Oxygen appears to be necessary as a catalyst for the afterglow reaction.

As many observers have pointed out the present accepted value of the dissociation energy of nitrogen is just that necessary to excite the eleventh vibrational level of the $\mathrm{B}^3\Pi$ state of the molecule which emits a very large percentage of the light of the afterglow. Since independent three-body collisions are too rare by factors of the order of 10^{15} to account for the process, one of the atoms must make a preliminary binding with an oxygen particle. Since there is no evidence of upward curvature in the S_1 curves it seems likely that the oxygen particle must be a stable entity in the gas, that is, the particle involved must be the oxygen molecule and the initial entity must be of the form NO_2.

Since the oxygen available in the gas in the earlier stages of impurity addition is the extremely small percentage in equilibrium with the very stable adsorption sites on the walls, its value cannot be accurately estimated. Since it is certainly possible to pump such a discharge tube down to lower than 2×10^{-6} mm without appreciably depleting such a layer this may be taken as an upper limit of the partial pressure. Thus the actual percentage of oxygen present in the body of the nitrogen at 2 mm pressure must not be greater than one part per million. In the same way as the populations n_1 and n_2 were estimated in determining the catalyst concentrations for S_2 we may estimate that the population of atoms rises to the order of 10^{12} to 10^{13} cm^{-3} or of the order one in 10^3 to 10^4 of the nitrogen molecular population and for all points up to and including 0·3% oxygen added the reaction rate is certainly limited by the small concentration of the catalyst. Thus its tremendous rise between 0·3 and 0·4% is explained.

With the very great rise in concentration in the gas between 0·3% added and 0·4% added plenty of oxygen will be available to combine with and remove the catalyst hydrogen necessary for process S_2. Thus the active particles of process S_2 will still exist but will now give up their energy by processes other than emission of afterglow.

The meaning of the activation energy necessary in the final collision in process S_1, in which an NO_2 complex collides with a free nitrogen atom, is not clear. Whether this is to be treated as a dissociation energy of the complex or as an added energy necessary to produce the afterglow, or a combination of the two, cannot be decided with the present information.

The only relation which has not been discussed is that of S_1 against pressure (AKM). Here a maximum appears in S_1 not coinciding with either the minimum of the R curve or the maximum of the S_2 curve. Since S_1 is a truly bimolecular process no population ratio can vary to explain the change in slope. Precisely why the catalyst population should vary in this way is not evident. Chance occurrence does not seem possible since of the seven points all except that at 5 mm were checked by extra films which were of poorer quality but still quite useful. These extra films checked the ones published and definitely agreed as to the presence of a maximum. A possible action of the discharge in removing more oxygen from the wall films at intermediate pressures than at extreme pressures would seem a possible explanation.

Acknowledgments

Thanks are due to Dr. Richard Ruedy who first aroused the author's interest in active nitrogen many years ago. The author is indebted to the Defence Research Board, Ottawa, Canada, for a grant (DRB 9512-23) towards apparatus and salaries of assistants.

References

Anderson, J. M., Kavadas, A., and McKay, R. W., 1958, *Proc. Phys. Soc.* A, **71,** 877.
Benson, J. M., 1952, *J. Appl. Phys.*, **23,** 757.
Birge, R. T., and Hopfield, J. J., 1928, *Astrophys. J.*, **68,** 257.
Blevis, B. C., Anderson, J. M., and McKay, R. W., 1957, *Canad. J. Phys.*, **35,** 941.

Cario, G., 1934, *Z. Phys.*, **89**, 523.
Cario, G., and Kaplan, J., 1929, *Z. Phys.*, **58**, 769.
Comte, F., 1913, *Phys. Z.*, **14**, 74.
Eckl, D. J., 1953, *Canad. J. Phys.*, **31**, 804.
Grant, F. A., 1950, *Canad. J. Res.* A, **28**, 339.
Heald, M. A., and Beringer, R., 1954, *Phys. Rev.*, **96**, 645.
Herman, R., 1945, *Ann. Phys., Paris* (11), **20**, 241.
Herzberg, G., 1950, *Spectra of Diatomic Molecules* (Princeton : Van Nostrand).
McLennan, J. C., Ruedy, R., and Anderson, J. M., 1928, *Trans. Roy. Soc. Canad.*, **22**, 303.
Mitra, S. K., 1945, *Active Nitrogen—A New Theory* (Calcutta : India Press).
Phelps, A. V., and Molnar, J. P., 1953, *Phys. Rev.*, **89**, 1202.
Rayleigh, Lord (Strutt, J. W.), 1911, *Proc. Roy. Soc.* A, **85**, 219; 1912, *Ibid.*, **86**, 56; 1935, *Ibid.*, **151**, 567; 1940, *Ibid.*, **176**, 1; 1942, *Ibid.*, **180**, 123.
Reinecke, L. H., 1953, *Z. Phys.*, **135**, 361.
Sponer, H., 1925, *Z. Phys.*, **135**, 622.
Tolman, R. C., 1927, *Statistical Mechanics with Applications to Physics and Chemistry* (New York : Chemical Catalog Co. Inc.).
Willey, E. J. B., 1930, *J. Chem. Soc.*, 336; 1930, *Ibid.*, 1146.
Willey, E. J. B., and Rideal, E. K., 1927, *J. Chem. Soc.*, 669.
Worley, R. E., 1948, *J. Chem. Phys.*, **16**, 533.
Zemansky, M. W., 1929, *Phys. Rev.*, **34**, 213.

RESEARCH NOTES

Angular Distributions of Some Inelastically Scattered Deuteron Groups from ^{24}Mg and ^{28}Si

By S. HINDS†, R. MIDDLETON† and G. PARRY
Nuclear Physics Research Laboratory, University of Liverpool

Communicated by H. W. B. Skinner ; MS. received 31*st July* 1957

Angular distributions have been measured of some groups of deuterons inelastically scattered by ^{24}Mg. These distributions were obtained at a bombarding energy of 8·9 Mev, from the same exposures as were used for the investigation of the ^{24}Mg(d, p)^{25}Mg stripping reaction, reported by Hinds, Middleton and Parry (1958). In figure 1 is shown a deuteron spectrum measured at an angle of observation of 60° from the bombardment of a natural magnesium target. The various groups are labelled by the corresponding energy levels of the excited nuclei.

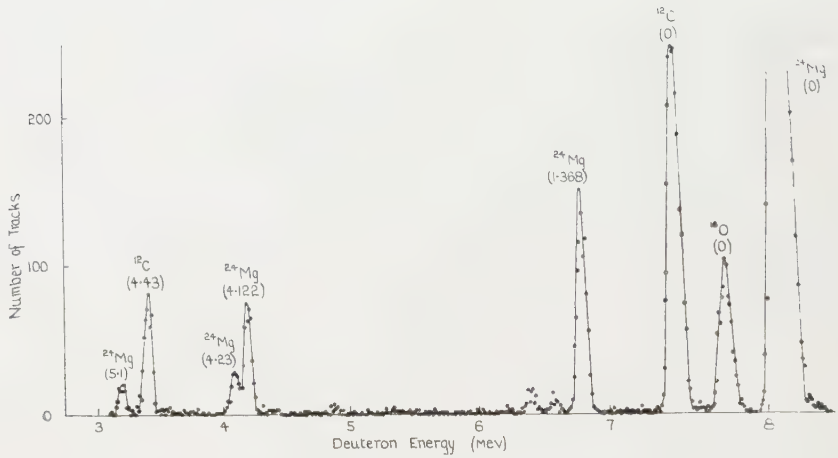

Figure 1. ^{24}Mg(d, d′)^{24}Mg*, angle 60°. $E_d = 8{\cdot}9$ Mev.

The angular distribution of the groups resulting from the excitation of the 1·368, 4·122 and 4·23 Mev levels of ^{24}Mg are shown in figure 2. The curves drawn have been calculated from the theory of inelastic deuteron scattering, developed by Huby and Newns (1951), using an effective radius of interaction a of $7{\cdot}0 \times 10^{-13}$cm. The distribution of the group corresponding to the excitation of the 1·368 Mev 2^+ level has previously been measured by Holt and Young (1949) at a bombarding energy of 7·5 Mev and there is good agreement between the two distributions, although the previous distribution was not measured in absolute units. There is reasonable agreement between the experimental and theoretical distributions for an $l = 2$ pattern only for the first maximum.

---

†Now at the Atomic Weapons Research Establishment, Aldermaston, Berks.

The 4·122 and 4·23 Mev levels are known to have even parity and spins of 4 and 2 respectively (Newton 1954) so that the selection rules for the above theory allow only $l=4$ and $l=2$, respectively, for the two transitions. The corresponding theoretical curves do not agree with the observed distributions.

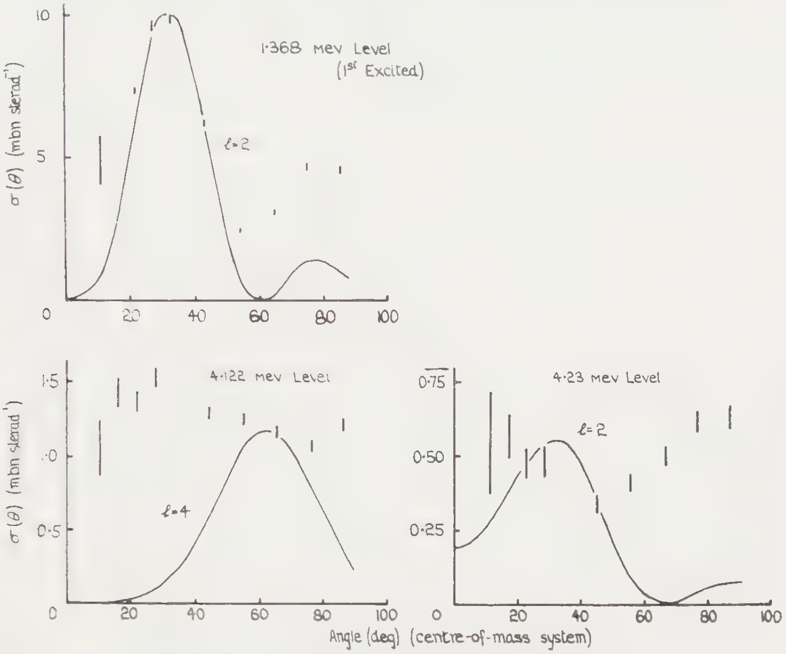

Figure 2. ^{24}Mg(d, d′)^{24}Mg*. $E_d=8{\cdot}9$ Mev.

The angular distribution of the inelastically scattered deuteron group exciting the 1·78 Mev 2^+ level of ^{28}Si, shown in figure 3, was obtained from an exposure using a quartz, SiO_2, target which was primarily used for an investigation of the ^{16}O(d, α)^{14}N reaction (Dalton, Hinds and Parry, to be published). The curve shown in the figure was calculated from the theory of Huby and Newns for $l=2$ using a value of a equal to $7{\cdot}0\times10^{-13}$ cm.

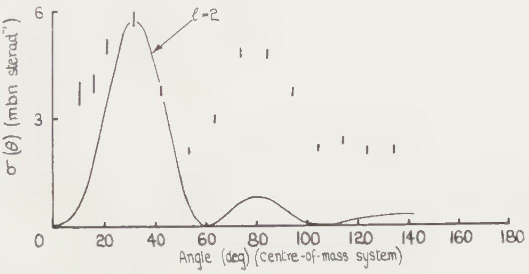

Figure 3. ^{28}Si(d, d′)^{28}Si*. $E_d=8{\cdot}9$ Mev. 1·78 Mev level (first excited).

The absolute cross sections for all the above distributions are considered to be accurate to ±25%.

There is a remarkable similarity between the distributions of the groups corresponding to the excitation of the first excited states of ^{24}Mg and ^{28}Si (at 1·368 and 1·78 Mev, respectively.) The only difference is that the ^{24}Mg group shows a higher intensity for the first maximum at about 30° than that for the ^{28}Si group.

REFERENCES

HINDS, S., MIDDLETON, R., and PARRY, G., 1958, *Proc. Phys. Soc.*, **71**, in the press.
HOLT, J. R., and YOUNG, C. T., 1949, *Nature, Lond.*, **164**, 1000.
HUBY, R., and NEWNS, H. C., 1951, *Phil. Mag.*, **42**, 1442.
NEWTON, J. O., 1954, *Phys. Rev.*, **96**, 241.

Absorption of Beta Particles in Liquids

By S. ABID HUSAIN†|| AND A. K. HILMI‡||

Communicated by J. L. Putman ; MS. received 8th July 1957

BETA particles passing through matter lose energy by ionizing and exciting the atomic electrons. This energy loss is a function of electron density. Husain and Putman (1957) have shown that the loss of energy of beta particles depends also on the atomic number because, due to nuclear collisions, the path length in the absorber is increased.

The absorption of beta particles in organic liquids was studied in order to see how far they show this effect.

For plotting the absorption curves for the liquids a liquid cell was made having a diameter of 2·46 cm. At the bottom of this cell an aluminium foil of thickness 2·35 mg cm^{-2} was fixed. An end-window Geiger counter (type EHM2) having a mica window of 2·3 mg cm^{-2} was placed in close contact with the bottom of the cell. The cross-sectional area of the liquid cell was the same as the area of the mica end-window. A ^{32}P beta source mounted on an aluminium tray was placed at a distance 6 cm from the window of the beta counter. The source tray was fixed in a polythene plug which forms the upper cover of the liquid cell in order to avoid the evaporation of the liquid.

Absorption of beta particles was noted by putting different thicknesses of the liquid in the cell which was carefully measured with a micropipette. This method is closely similar to the one used for solids where absorbers of different thicknesses are used.

The results, when plotted in terms of Z/A (mg cm^{-2}) (i.e. the electron density), did not give identical curves. But when they were plotted in terms of $Z^{4/3}/A$ (mg cm^{-2}) almost identical curves resulted.

In each case a liquid (say C_2H_5OH) was considered to consist of various components, in this case carbon, hydrogen and oxygen, and the factor $Z^{4/3}/A$ was applied to the respective weights of the three components in the compound.

The liquids used were methyl alcohol, ethyl alcohol, butyl alcohol, amyl alcohol, toluene, aniline, benzene, nitrobenzene, carbon tetrachloride and water.

Figures 1, 2 and 3 show a series of these curves. In each figure the curve for butyl alcohol is plotted as a full line to form a reference for comparison.

---

† Atomic Energy Commission, Karachi, Pakistan.
‡ Industrial Research Institute, Baghdad.
|| Now at Baghdad Pact Nuclear Centre, Salchiya, Baghdad.

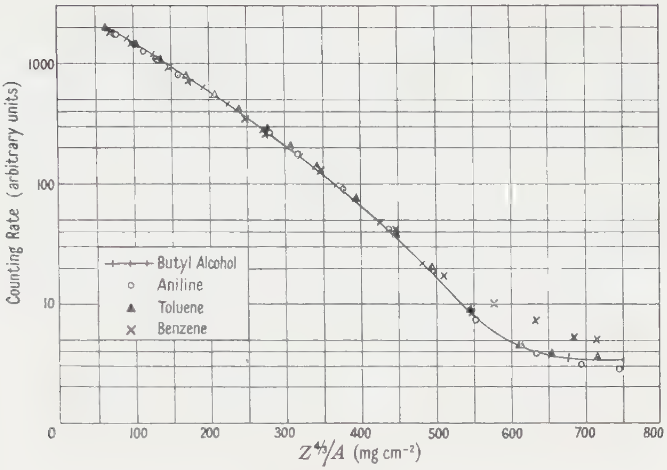

Figure 1.

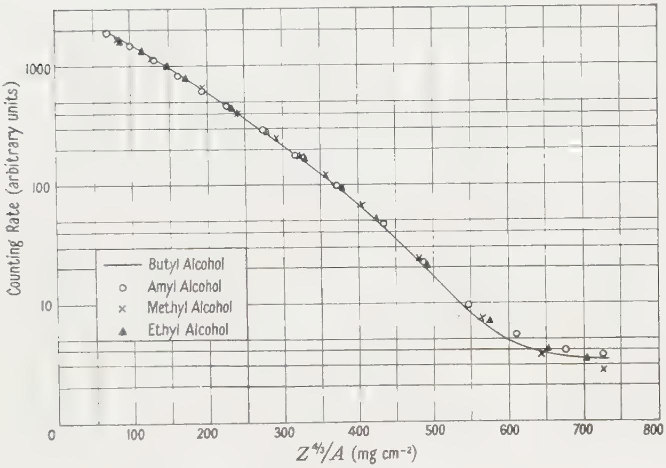

Figure 2.

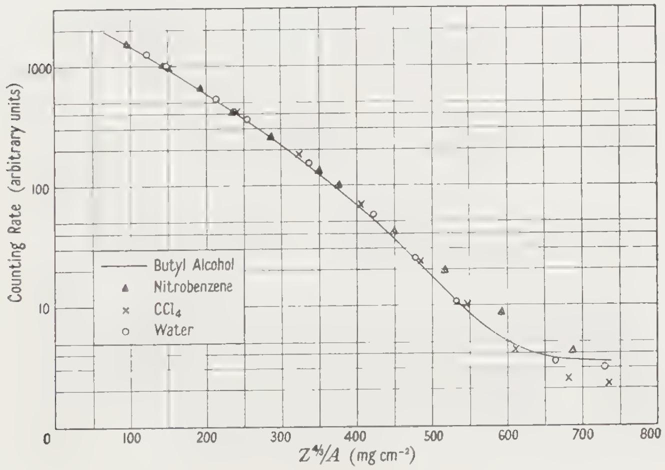

Figure 3.

It thus seems quite reasonable to believe that nearly identical absorption curves are obtained by plotting the absorption thickness in $Z^{4/3}/A$ (mg cm ^{2}) even when the absorber consists of more than one element, and that they also obey the empirical relationship $\log X = b - aZ^{4/3}$ as in the case of pure metals.

REFERENCES

HUSAIN, S. A., and PUTMAN, J. L., 1957, *Proc. Phys. Soc.* A, **70,** 304.

The Structure of the $X^7\Sigma$ State of MnH and MnD

BY W. HAYES†, P. D. MCCARVILL AND T. E. NEVIN
Physics Department, University College, Dublin

MS. received 6th August 1957

ROTATIONAL analyses of the (0, 0) and (0, 1) bands in the $A^7\Pi$–$X^7\Sigma$ system of MnH have been given by Nevin (1942, 1945) and of the (1, 0) band by Nevin and Doyle (1948). Nevin, Conway and Cranley (1952) have analysed the (0, 0) and (0, 1) bands in the corresponding MnD transition. A detailed comparison of the spectra of MnH and MnD has been given by Nevin and Stephens (1953). The purpose of this letter is to describe the results of the analysis of the (0, 2) bands of MnH and MnD. This work was undertaken in order to obtain improved values of the molecular constants of the $X^7\Sigma$ state.

The information available from the work on the (0, 0) and (0, 1) bands enabled the analyses to be carried out without much difficulty. The general experimental technique and method of analysis has already been described by Nevin (1942, 1945). P, Q and R branches were readily found in MnD but the MnH band was not as well developed and the P and R branches could not be located in the two high frequency components. In both cases, ^{S}R and ^{O}P branches were found in the five low frequency components but were not nearly as complete as in the (0, 0) and (0, 1) bands. In order to obtain precise information about the spin fine structure of the $X^7\Sigma$ state a search for ^{P}Q branches was undertaken. These were fragmentary and the $^PQ_{12}$ branch was the only one sufficiently developed to be of value. The MnD branch extended from $K=11$ to $K=26$ and the MnH branch from $K=4$ to $K=12$.

Table 1. Molecular Constants of the $X^7\Sigma$ State, $v''=2$

	MnH	MnD
B_v'' (cm^{-1})	5·2797	2·7550
D_v'' (cm^{-1})	$-3{\cdot}08\times10^{-4}$	$-8{\cdot}36\times10^{-5}$
H_v'' (cm^{-1})	$1{\cdot}02\times10^{-8}$	$2{\cdot}93\times10^{-9}$
γ (cm^{-1})	0·010	0·015

The rotational constants B_v'', D_v'' and H_v'' were calculated in the manner described by Nevin (1942, 1945) and are given in table 1. A comparison with the results obtained from the (0, 0) and (0, 1) bands indicates that the variation of B_v'' with v is non-linear. Using the relation:

$$B_v''=B_e''-\alpha_e''(v+\tfrac{1}{2})+\gamma_e''(v+\tfrac{1}{2})^2$$

---

† Now at the Clarendon Laboratory, Oxford.

one calculates improved values of B_e'', I_e'' and r_e'' in the case of MnD and of B_e'' in the case of MnH. The results are given below:

MnH $B_e''=5{\cdot}6841\ \text{cm}^{-1}$, $\alpha_e''=0{\cdot}1570\ \text{cm}^{-1}$, $\gamma_e''=-0{\cdot}00188\ \text{cm}^{-1}$.
MnD $B_e''=2{\cdot}8956\ \text{cm}^{-1}$, $\alpha_e''=0{\cdot}0514\ \text{cm}^{-1}$, $\gamma_e''=-0{\cdot}00196\ \text{cm}^{-1}$,
$I_e''=9{\cdot}663\times10^{-40}\ \text{g cm}^2$, $r_e''=1{\cdot}722\times10^{-8}\ \text{cm}$.

The term $f_i(K, J-K)$ which describes the spin fine structure of the $x^7\Sigma$ state is determined largely by the spin–rotation interaction. The spin–spin interaction gives a small contribution and when this is neglected the expression for the spin fine structure becomes

$$f_i(K, J-K)=\tfrac{1}{2}\gamma[2K(4-i)+(i-8)(i-1)]$$

and the separation of adjacent spin levels is

$$\Delta f''_{i,i+1}(K)=(4-i)\gamma+\gamma K.$$

In the present case the only reliable method of calculating γ was to apply the relationship

$$\Delta f''_{i,i+1}=f_i''(K)-f_{i+1}''(K)={}^{\mathrm{P}}\mathrm{Q}_{i,i+1}(K)-\mathrm{P}_i(K)$$

using the ${}^{\mathrm{P}}\mathrm{Q}_{12}$ and P_1 branches. The results appear in table 1.

The vibrational intervals $\nu_{0v''}$ of the ith component of the bands are obtained from the relationship:

$$\begin{aligned}\nu_{0v''}&=F_{ib}'(K)-\mathrm{R}_i(K-1)-F_i''(K-1)\\&=F_{ib}'(K)-\mathrm{P}_i(K+1)-F_i''(K+1)\\&=F_{ia}'(K)-\mathrm{Q}_i(K)-F_i''(K)\end{aligned}$$

where

$$F_v''(K)=B_v''K(K+1)+D_v''K^2(K+1)^2+H_v''K^3(K+1)^3.$$

Using these expressions, ν_{00}, ν_{01} and ν_{02} were calculated for different values of K and a mean taken. In this way, accurate values of the vibrational constants of the $x^7\Sigma$ state were obtained and are given below:

MnH $\omega_e''=1548{\cdot}0\ \text{cm}^{-1}$, $x_e''\omega_e''=28{\cdot}8\ \text{cm}^{-1}$.
MnD $\omega_e''=1102{\cdot}5\ \text{cm}^{-1}$, $x_e''\omega_e''=13{\cdot}9\ \text{cm}^{-1}$.

REFERENCES

Nevin, T. E., 1942, *Proc. R. Irish Acad.*, **48,** 1 ; 1945, *Ibid.*, **50,** 123.
Nevin, T. E., Conway, M., and Cranley, M., 1952, *Proc. Phys. Soc.* A, **65,** 115.
Nevin, T. E., and Doyle, P. G., 1948, *Proc. R. Irish Acad.*, **52,** 35.
Nevin, T. E., and Stephens, D. V., 1953, *Proc. R. Irish Acad.*, **55,** 109.

An Improved Born Approximation

By D. PARK
Department of Physics, Williams College, Williamstown, Massachusetts

MS. received 29th July 1957, *and in final form 27th September* 1957

It is well known that the first Born approximation to the solution of problems in scattering is not unitary, that is, it does not satisfy the requirement that the current be conserved. This fact typically shows itself in the failure of the cross section theorem, which relates the total cross section to the imaginary part of the forward scattering amplitude†. It is natural to ask whether by building into the approximation procedure the requirement that the solution be unitary, one could not at the same time improve the accuracy of the results. In this note we shall show a way in which the Born approximation can be modified so as to make it unitary, and illustrate by an example what appears to be a general property of the new formulae : that for values of the phase shift less than about 20°, they give a substantial improvement in accuracy.

It is easy to show that if one writes the total wave function as

$$\psi = \exp(i\mathbf{k} \,.\, \mathbf{r}) + \sum (2l+1) i^l g_l(r) P_l(\cos\theta)$$

then the scattering phase shifts δ_l are given for central forces by

$$\exp(2i\delta_l) - 1 = -2ik \int_0^\infty [f_l(r) + g_l'(r) + ig_l''(r)] U(r) f_l(r) r^2 \, dr \qquad \ldots\ldots(1)$$

where $U(r)$ is $2m/h^2$ times the scattering potential, $f_l(r)$ is $(\pi/2kr)^{1/2} J_{l+\frac{1}{2}}(kr)$, and g_l' and g_l'' are the real and imaginary parts of g_l. Let us denote by α_{l1}, α_{l2} and $i\beta_l$, with $\alpha_{l1} + \alpha_{l2} = \alpha_l$, the contributions to the integral in (1) arising from the parts f_l, g_l', and ig_l'' respectively. Then equating real and imaginary parts of (1) gives

$$\cos\delta_l \sin\delta_l = -k\alpha_l \qquad \ldots\ldots(2\,a)$$

$$\sin^2\delta_l = -k\beta_l \qquad \ldots\ldots(2\,b)$$

of which the second is essentially a statement of the cross section theorem. From these two relations we have

$$\tan\delta_l = -k(\alpha_l^2 + \beta_l^2)/\alpha_l \qquad \ldots\ldots(3\,a)$$

$$\alpha_l^2 + \beta_l^2 + \beta_l/k = 0. \qquad \ldots\ldots(3\,b)$$

The usual first Born approximation amounts to neglecting α_{l2} and β_l compared with α_{l1}, so that (3 *a*) gives

$$\delta_{l\mathrm{B}} = -\tan^{-1}(k\alpha_{l1}) \qquad \ldots\ldots(4\,a)$$

or

$$\delta_{l\mathrm{B}} \simeq -k\alpha_{l1} \qquad \ldots\ldots(4\,b)$$

while (3 *b*) is not satisfied. Empirically, (4 *b*) is found to be a little more accurate than (4 *a*), and since it is customary to regard this approximation as the first term of an expansion in powers of the coupling strength, the replacement is quite permissible.

But it is obvious that in dropping β_l, which violates (2 *b*) and (3 *b*), we are simplifying more than is necessary. In fact it is sufficient to neglect only α_{l2} and let β_l be determined by (2 *b*) and (3 *b*). Thus we take δ_l from (2 *a*), which is true regardless of β_l, and write in this new approximation

$$\delta_{l\mathrm{n}} = -\tfrac{1}{2}\sin^{-1}(2k\alpha_{l1}). \qquad \ldots\ldots(5)$$

In terms of the α_{l1} the scattered amplitude becomes

$$f_{\mathrm{n}}(\theta) = -k^{-1} \sum (2l+1) \{k\alpha_{l1} - \tfrac{1}{2}i[1 - (1 - 4k^2\alpha_{l1}^2)^{1/2}]\} P_l(\cos\theta). \qquad \ldots\ldots(6)$$

From this one obtains the total cross section by squaring and integrating it or by taking its imaginary part ; since no assumption violating (2 *b*) has been made, either procedure gives

$$\sigma_{\mathrm{n}} = (2\pi/k^2) \sum (2l+1)[1 - (1 - 4\,k^2\alpha_{l1}^2)^{1/2}]. \qquad \ldots\ldots(7)$$

---

† This theorem is readily established by comparison of the relevant phase-shift formulae when central forces are involved (Massey 1956); references and a more general discussion will be found in an earlier paper by the author (Park 1955).

To check the accuracy of (5), we have applied it to a number of scattering problems in which the exact value of the phase shift is known. We find it is considerably more accurate than (4 *b*) for phase shifts less than about 20°, but above this it is generally less accurate. As a typical example we give the S-wave scattering by a square-well potential $U(r)$ of depth λ and width r_0. Denoting kr_0 by x and $(\lambda+k^2)^{1/2}\, r_0$ by y, we find for the exact phase shift

$$\tan \delta_e = \frac{x \tan y - y \tan x}{y + x \tan x \tan y}$$

and for the first Born approximation, using (4 *b*),

$$\delta_B = \frac{y^2 - x^2}{2x}\left(1 - \frac{\sin 2x}{2x}\right).$$

The table shows the phase shifts at a given energy such that $x = \frac{1}{2}\pi$, as a function of the well depth measured by $y - x = \epsilon$. For phase shifts up to about 0·35 radian, or 20°, the new approximation has about one-fourth the error of the old. Beyond this range it deteriorates rapidly. In fact, it is clear from (5) that δ_{ln} cannot in any case exceed 45° and thus when δ_{lB} in (4 *b*) exceeds $\frac{1}{2}$ radian, or about 29°, the new approximation fails altogether.

Exact and Approximate Phase Shifts as a Function of Increasing Well Depth

ϵ	δ_e	δ_n	δ_B
0	0	0	0
0·1	0·105	1·104	0·103
0·2	0·222	0·220	0·213
0·3	0·353	0·359	0·329
0·35	0·420	0·446	0·389
0·4	0·488	0·562	0·451

REFERENCES

MASSEY, H. S. W., 1956, *Handbuch der Physik*, Vol. XXXVI, 238 (Berlin : Springer).
PARK, D., 1955, *Indian J. Theor. Phys.*, **3**, 83.

LETTERS TO THE EDITOR

Expressions for certain Wigner Coefficients

The existence of a closed formula for the Wigner coefficient $C^{j\;j\;j'}_{m\,m\,2m}$ (Stone 1956) makes it possible to derive a simplified summation for $C^{j+s\;j\;\;J}_{m+\mu\;m\;2m+\mu}$. Explicit expressions are given for $s=\frac{1}{2}$, 1.

Consider the following particular case of the relation between Wigner coefficients and Racah coefficients (Racah 1943):

$$C^{s\;j\;\;j+s}_{\mu\;m\;m+\mu}\,C^{j+s\;j\;\;J}_{m+\mu\;m\;2m+\mu} = \sum_{J'}\,[(2J'+1)(2j+2s+1)]^{1/2}\,W(sjJj\,;\,j+sJ')$$
$$\times\, C^{j\;j\;J'}_{m\,m\,2m}\,C^{s\;J'\;\;J}_{\mu\;2m\;2m+\mu}.$$

Both $C^{s\;j\;\;j+s}_{\mu\,m\;m+\mu}$ and $W(sjJj\,;\,j+sJ')$ can be written as one term (Racah 1942) and with the formula for $C^{j\;j\;J'}_{m\,m\,2m}$ (Stone 1956) one obtains

$$C^{j+s\;j\;\;J}_{m+\mu\;m\;2m+\mu}$$
$$= \sum_{\substack{J'+2j\\ \text{even}}} \frac{(-1)^{j-J'/2}(2J'+1)(j+\frac{1}{2}J')\,!}{(2j+J'+1)\,!\,(j-\frac{1}{2}J')\,!\,(\frac{1}{2}J'+m)\,!\,(\frac{1}{2}J'-m)\,!}\;C^{s\;J'\;\;J}_{\mu\;2m\;2m+\mu}$$
$$\times\left[\frac{\begin{array}{r}(2j+J+s+1)\,!\,(J+s)\,!\,(2j+s-J)\,!\,(J+J'-s)\,!\\ \times\,(j+m)\,!\,(j-m)\,!\,(s+\mu)\,!\,(s-\mu)\,!\,(J'+2m)\,!\,(J'-2m)\,!\end{array}}{\begin{array}{r}(J+J'+s+1)\,!\,(J-s)\,!\,(J+s-J')\,!\\ \times\,(J'+s-J)\,!\,(j+s+m+\mu)\,!\,(j+s-m-\mu)\,!\end{array}}\right]^{1/2}.$$

The summation is taken over $J'=J+s,\ J+s-1,\ \ldots,\ |J-s|$ and terms with $J'>2j$ vanish. $J'+2j$ must be even for a non-zero value of $C^{j\;j\;J'}_{m\,m\,2m}$.

Formulae for $C^{s\;J'\;\;J}_{\mu\;2m\;2m+\mu}$ are known for small values of s (Condon and Shortley 1935). When $s=\frac{1}{2}$ or $s=1$, $2j+J$ even, only one term in the summation survives. For $s=1$, $2j+J$ odd, there are two terms. The explicit forms for $s=\frac{1}{2}$, 1 are given below and have been verified in simple cases. Other coefficients can be found from the recurrence relations on m (Racah 1942).

$2j+l$ even:

$$C^{j+\frac{1}{2}\;j\;\;l+\frac{1}{2}}_{m+\frac{1}{2}\;m\;2m+\frac{1}{2}} = \left(\frac{l+2m+1}{j+m+1}\right)^{1/2} C,$$

$$C^{j+\frac{1}{2}\;j\;\;l+\frac{1}{2}}_{m-\frac{1}{2}\;m\;2m-\frac{1}{2}} = \left(\frac{l-2m+1}{j-m+1}\right)^{1/2} C,$$

where

$$C=\frac{(-1)^{j-\frac{1}{2}l}(j+\frac{1}{2}l)\,!}{(j-\frac{1}{2}l)\,!\,(\frac{1}{2}l+m)\,!\,(\frac{1}{2}l-m)\,!}\left(\frac{(2j+l+2)(2j-l)\,!\,(l+2m)\,!\,(l-2m)\,!}{2(2j+l+1)\,!}\right)^{1/2}$$

$2j+l$ odd:

$$C^{j+\frac{1}{2}\;j\;\;l+\frac{1}{2}}_{m+\frac{1}{2}\;m\;2m+\frac{1}{2}} = \left(\frac{l-2m+1}{j+m+1}\right)^{1/2} D,$$

$$C^{j+\frac{1}{2}\;j\;\;l+\frac{1}{2}}_{m-\frac{1}{2}\;m\;2m-\frac{1}{2}} = -\left(\frac{l+2m+1}{j-m+1}\right)^{1/2} D,$$

where

$$D=\frac{(-1)^{j-\frac{1}{2}l-\frac{1}{2}}(j+\frac{1}{2}l+\frac{1}{2})!}{(j-\frac{1}{2}l-\frac{1}{2})!\,(\frac{1}{2}l+m+\frac{1}{2})!\,(\frac{1}{2}l+m+\frac{1}{2})!}\times\left(\frac{(2j-l)!\,(l+2m+1)!\,(l-2m+1)!}{2(2j+l+2)!}\right)^{1/2}.$$

$2j+l$ even:

$$C^{j+1\ j\ \ l}_{m+1\ m\ 2m+1}=-\left(\frac{(l+2m+1)(l-2m)}{(j+m+2)(j+m+1)}\right)^{1/2}E,$$

$$C^{j+1\ j\ l}_{m\ \ m\ 2m}=\frac{2m}{[(j+m+1)(j-m+1)]^{1/2}}E,$$

$$C^{j+1\ j\ \ l}_{m-1\ m\ 2m-1}=\left(\frac{(l-2m+1)(l+2m)}{(j-m+2)(j-m+1)}\right)^{1/2}E,$$

where

$$E=\frac{(-1)^{j-\frac{1}{2}l-1}(j+\frac{1}{2}l)!}{2(j-\frac{1}{2}l)!\,(\frac{1}{2}l+m)!\,(\frac{1}{2}l-m)!}\times\left(\frac{(2l+1)(2j+l+2)(2j-l+1)!\,(l+2m)!\,(l-2m)!}{l(l+1)(2j+l+1)!}\right)^{1/2}.$$

$2j+l$ odd:

$$C^{j-1\ j\ \ l}_{m+1\ m\ 2m+1}=\frac{l(l+1)+(2m+1)(2j+2)}{2(\frac{1}{2}l+m+\frac{1}{2})!\,(\frac{1}{2}l-m-\frac{1}{2})!}\left(\frac{(l+2m+1)!\,(l-2m-1)!}{(j+m+2)(j+m+1)}\right)^{1/2}F,$$

$$C^{j-1\ j\ l}_{m\ \ m\ 2m}=\frac{2j+2}{(\frac{1}{2}l+m-\frac{1}{2})!\,(\frac{1}{2}l-m-\frac{1}{2})!}\left(\frac{(l+2m)!\,(l-2m!)}{(j+m+1)(j-m+1)}\right)^{1/2}F,$$

$$C^{j-1\ j\ \ l}_{m-1\ m\ 2m-1}=\frac{l(l+1)-(2m-1)(2j+2)}{2(\frac{1}{2}l-m+\frac{1}{2})!\,(\frac{1}{2}l+m-\frac{1}{2})!}\left(\frac{(l-2m+1)!\,(l+2m-1)!}{(j-m+2)(j-m+1)}\right)^{1/2}F,$$

where

$$F=\frac{(-1)^{j-\frac{1}{2}l+\frac{1}{2}}(j+\frac{1}{2}l+\frac{1}{2})!}{(j-\frac{1}{2}l+\frac{1}{2})!}\left(\frac{(2l+1)(2j-l+1)!}{l(l+1)(2j+l+2)!}\right)^{1/2}.$$

Union Christian College,
Alwaye,
S. India.

A. P. STONE.

14th August 1957.

CONDON, E. U., and SHORTLEY, G. H., 1935, *The Theory of Atomic Spectra* (Cambridge: University Press).
RACAH, G., 1942, *Phys. Rev.*, **62**, 438; 1943, *Ibid.*, **63**, 367.
STONE, A. P., 1956, *Proc. Camb. Phil. Soc.*, **52**, 424.

CORRIGENDUM

The β-spectrum of Sulphur 35, by R. D. CONNOR and I. L. FAIRWEATHER (*Proc. Phys. Soc.* A, 1957, **70**, 769).

Owing to an unfortunate error in normalization the value presented as the mean energy of β-particles of ^{35}S is incorrect. The re-calculated value is 48·8 ± 0·2 kev, and not 61·0 kev as previously given.

REVIEWS OF BOOKS

Neutron Transport Theory, by B. Davison (with the collaboration of J. B. Sykes). Pp. 450. (Oxford: University Press, 1957.) 75*s*.

This book gives a comprehensive account of the analytical methods of neutron transport theory. The reader is assumed to have a good background knowledge of mathematics, but although no previous knowledge of transport theory is necessary it is expected that most readers will have had some previous experience of elementary methods. The various methods are developed rigorously from the most general forms of the Boltzmann equation and the corresponding integral equation, and great attention is given to the underlying assumptions and approximations and thus to the conditions under which the different methods should be used. The style is uniformly good and clear and most chapters are fairly self-contained, with references only to a few general introductory chapters, so that the book is well designed for studying single chapters as well as for systematic reading.

The earlier parts of the book are a much expanded and more complete version of the author's well-known lecture series (*Transport Theory of Neutrons*, National Research Council of Canada, Atomic Energy Project, LT18, 1947). The methods studied include the diffusion approximation, the Serber–Wilson method, the spherical harmonics method, the method of discrete ordinates, perturbation theory, variational methods, Monte Carlo techniques, various multi-group theories, age theory and various methods for special types of problem, for example neutron fluxes at large distances from sources. The theories are usually given in their most complete form, suitable for the more complicated problems with several media, variable cross sections, anisotropic scattering, etc., as well as in the simpler forms more often needed. The chapters on the spherical harmonics method, which contain much original work, give a better account than is available elsewhere in the literature including instructions for forming the necessary auxiliary functions for the more complicated problems. The chief topics which have been omitted are the calculation of overall properties of inhomogeneous media, such as regular lattices, and time-dependent phenomena due to delayed neutrons. These are omitted as belonging more properly to reactor theory—a justifiable decision, particularly as no other applications are given in detail.

The discussion of various numerical approaches is not so complete as that of the analytical methods. This is partly because the numerical methods have been developed only very recently and, for example, the Carlson S_n method, which is proving to be very powerful, is only treated in a short appendix. For details of these methods the original papers will still be the best source, although very useful hints may be found in this book on the validity of the basic assumptions.

For the theoretician, this book will be an excellent basic textbook, both for reference and for study, for all the analytical methods required. It is also extremely well cross-referenced and indexed.

M. E. MANDL.

The Education of Physicists in Universities and Colleges of Technology. Being the proceedings of a Conference on " Degree and Diploma Courses in Applied Physics " organized jointly by The Institute of Physics and The London and Home Counties Regional Advisory Council for Higher Technological Education, and held on November 15–16, 1956, at The Institution of Electrical Engineers, Savoy Place, London, W.C.2. Pp. vi + 73. (London : The Institute of Physics, 1957.) 6*s*.

This booklet contains an account of what was said at a conference held in London in November of last year on " Degree and Diploma Courses in Applied Physics ". The speakers included Humphreys, Cockcroft, Blackett, Lipson and Topping to mention only a few, and the discussion ranged over a wider field than applied physics. A recurring theme of the meeting was the question whether the universities give to industry men trained in the way industry wants. And if not, is this the universities' fault, and should they change their method of teaching ? Or is it industry's fault and should they change the way they use their scientists ? Whatever the answer to this question, no one at the conference wanted degree courses in applied physics that were tied to any particular technology. Courses in applied physics were described which emphasized classical physics at the expense of nuclear and quantum science, but on the whole no one seemed to think that there was much wrong with the content of degree courses—not of the better ones, anyhow. The criticism that does seem to come from the industrial side is that the man from the university does not *want* a career in applied physics, and as for the man with a Ph.D., he won't look at it. From this attitude or this experience came the welcome expressed for diploma courses, courses taken after the first degree, lasting perhaps a year and which introduce students to a specialized technology or to engineering practice. It was hoped that such courses would develop a desire to become an applied scientist, and would produce men who would want to play a part in developing hardware that would sell. The discussion emphasized the need for the man who is, or who is willing to make himself, part physicist and part engineer and of whom there is said to be a particular shortage.

On the other hand, another point of view was expressed by some speakers. Blackett in particular stressed that what is important is to attract large numbers of talented young people into science, and it is more important to make an education in science something that they want to undertake than to vary the curriculum in the interests of particular users. The possibility of doing fundamental research and adding to knowledge is one of the things that has glamour for young men and attracts them to physics; every university teacher of the subject experiences this. Therefore it was argued that university courses must remain the avenue to fundamental research, and be seen to be just that. One needs—perhaps—a counter attraction, equally glamorous, in applied physics. Nuclear technology begins to provide it; why not other industries too ?

N. F. M.

CONTENTS OF SECTION B

PAGE

Mr. J. V. Evans. The Scattering of Radio Waves by the Moon 1105

Mr. J. P. Llewellyn and Dr. T. Smith. The Thermal Expansion of Iron Ditelluride 1113

Dr. R. W. Teale and Dr. G. Rowlands. Some Magnetothermal Relations for Ferromagnetics 1123

Dr. R. W. Smith and Prof. G. V. Raynor. The Effect of Liquid Media on the Grey Tin ⇌ White Tin Transformation in Commercially Pure Tin . . 1135

Dr. A. J. E. Foreman and Dr. W. M. Lomer. Lattice Vibrations and Harmonic Forces in Solids 1143

Dr. J. W. Christian and Mr. J. Spreadborough. Stacking Faults and Dislocations in Copper–Aluminium and Cobalt–Nickel Alloys 1151

Dr. H. H. Hopkins. Geometrical-optical Treatment of Frequency Response . 1162

Research Notes :

Mr. J. A. Lane. A Physical Interpretation of Impedance for Rectangular Waveguides 1173

Letters to the Editor :

Dr. P. T. Landsberg. Lifetimes of Excess Carriers in InSb 1175

Mr. K. D. Bowers, Mr. R. A. Kamper and Mr. C. D. Lustig. Paramagnetic Resonance Absorption in Iodine 1176

Reviews of Books 1178

Contents of Section A 1180

Subject Index, Section B, Vol. 70 1181

Index of Authors (with Titles), Section B, Vol. 70 1188

Index to Reviews of Books, Section B, Vol. 70 1196

PROCEEDINGS OF THE PHYSICAL SOCIETY
SECTION A, 1957—VOL. 70

SUBJECT INDEX

PAGE
Absorption bands, NO, in Schumann region, fine structure 219
Absorption of β-particles in liquids (R) 902
Absorption and dispersion of indium antimonide 776
Absorption spectra, electronic, of heterocyclic systems I: A comparison of theoretical methods: pyradine and pyrazine 593
Absorption spectra, electronic, of heterocyclic systems II: Applications to some two-ring nitrogen heterocyclics 654
Absorption spectra, *see also* Spectra
Alkali halides, dielectric breakdown of, at high temperatures 761
Alpha emission, rare, in ^{228}Ra (MsTh 1) (R) 478
Alpha particles, radiative capture of, in ^{15}N 661
Alpha particles and tritons emitted from deuteron bombardment of teflon, magnetic analysis 233
Angular distributions and correlations in γ-radiation following proton capture in ^{35}Cl, ^{37}Cl and ^{39}K 445
Angular distributions of inelastically scattered deuteron groups from ^{24}Mg and ^{28}Si (R) 900
Atomic heats of calcium, strontium and barium between 1·5 K and 20 K . . . 738
Atomic heats of lithium, sodium and potassium between 1·5°K and 20°K . . 744

Band spectra, bands assigned to ZrF (L) 549
Band spectra, structure of $X^7\Sigma$ state of MnH and MnD (R) 904
Band systems, $A^3\Pi_{0^+}$, $B^3\Pi_1-X^1\Sigma^+$ of gallium monofluoride, rotational analysis . . 34
Band systems, $A^3\Pi_{0^+}-X'\Sigma^+$ of TlCl, rotational analysis (L) 622
Beta decay, radiative, of pion 729
Beta decay, time reversal in (L) 552
Beta particles, absorption, as functions of atomic number (R) 304
Beta particles, absorption in liquids (R) 902
Beta spectrum of ^{35}S (L) . . . . 769 corr. 909
Binding energy of ^{8}Be and ^{12}C 866
Born approximation, improved (R) 905
Boundaries, first passage problems in theory of multiple scattering . . . 253

Carbon ions, bombardment of KI crystals, light output (R) 309
Charge transfer from neutral atoms to doubly and triply charged ions . . . 809
Charge transfer, radiative, from H atoms to He^{2+} ions 849
Collisions, atomic rearrangement, use of complete interaction Hamiltonian . . 26
Cloud chamber, high pressure, use of multiple scattering and effects of distortion in 17
Cloud chamber, high pressure, nuclear disintegrations produced by cosmic ray particles in 134
Collisions, inelastic, between heavy particles: V—Fast He ions 110
Collisions, inelastic, between heavy particles: VI—2s^{3}S–2p and 3p^{3}P excitations of fast He atoms 117
Collisions, inelastic, between heavy particles: VII—Electron loss from fast H atoms passing through He (R) 306
Collisions, inelastic, heavy particle, involving crossing of potential energy curves: V—charge transfer from neutral atoms to doubly and triply charged ions . . 809
Complex nuclei, elastic scattering of low energy nucleons by 668
Complex nuclei, photoproduction of pions at 629
Compound nuclear theory and optical model . . . . corr. 708
Cosmic ray air showers, extensive, structure; core detection and core structure 452

Cosmic ray particles and production of nuclear disintegrations in high pressure cloud chamber . . . 134
Coupling constant, hyperfine structure, of the $6s6p\,^3P_1$ level of ^{199}Hg by double resonance . . . 796
Cross section for 1s–2s excitation of hydrogen by electron impact, variational calculation (R) . . . 398
Cross section, integrated, from threshold to 30 Mev for reaction ^{9}Be (γ, 2n) ^{7}Be (R) . . . 836
Cross sections, nuclear, for 900 Mev protons . . . 209
Cross sections, nuclear total, for 350 Mev neutrons . . . 745
Cross sections, total, average neutron, of heavy elements at low energy . . . 51
Crystals, KI, under bombardment by C ions, light output (R) . . . 309
Crystals with NaCl type of lattice, homopolar effects . . . 123
Cyclotron resonance over wide temperature range (R) . . . 759

Density matrix, and foundations of statistical theory . . . 839
Deuteron bombardment of teflon, magnetic analysis of tritons and α-particles . . . 233
Deuterons from ^{24}Mg and ^{28}Si, inelastically scattered, angular distribution (R) . . . 900
Diamagnetic fluid, influence of strong magnetic field on dielectric constant of . . . 753
Dielectric breakdown of alkali halides at high temperatures . . . 761
Dielectric constant of a diamagnetic fluid; influence of strong magnetic field on . . . 753
Direct interaction and nuclear dispersion theory . . . 686
Discharges, flash-absorption spectra of plasmas of arcs and other discharges . . . 815
Dispersion and absorption of indium antimonide . . . 776
Dispersion theory, nuclear, and direct interaction . . . 686

Elastic scattering, *see* Scattering
Electron collisions, conversion of metastable He from singlet to triplet state . . . 288
Electron excitation of 3p levels of O I . . . 241
Electron rest mass, means of avoiding limitation in microtron (L) . . . 550
Electron scattering, *see* Scattering
Electron spin, consideration for mass action laws for reactions between free carriers and impurities in semiconductors (R) . . . 801
Electronic absorption spectra of heterocyclic systems I: A comparison of theoretical methods: pyradine and pyrizine . . . 593
Electronic absorption spectra of heterocyclic systems II: Applications to some two-ring nitrogen heterocyclics . . . 654
Electronic levels of model of liquid potassium . . . 713
Electronic structure and spectra of nitrogen heterobenzenes . . . 41
Electrons, and positrons, multiple scattering . . . 188
Electrons in metals, magnetic energy levels . . . 275
Electrons, scattering, *see under* Scattering
Elements, light, excitation functions up to 980 Mev for proton-induced reactions in . . . 824
Emulsion spectrograph: I—Design and theory . . . 146
Emulsion spectrograph: II—Construction and use for normal incidence . . . 154
Energy, binding, of ^{8}Be and ^{12}C . . . 866
Excitation functions up to 980 Mev for proton-induced reactions in some light elements 824
Excitation of discrete levels of atomic hydrogen by fast electrons . . . 460

Ferromagnetic, Heisenberg model, high temperature susceptibility (R) . . . 765
Fission, high energy, interpretation (R) . . . 546
Forces, second order long range, exact calculation (R) . . . 223

Gamma radiation following proton capture in ^{35}Cl, ^{37}Cl and ^{39}K . . . 84
Gamma radiation following proton capture in ^{35}Cl, ^{37}Cl and ^{39}K: II—Angular distributions and correlations . . . 445
Gamma rays, incoherent scattering from bound electrons of heavy elements . . . 337
Gamma rays, nuclear resonant scattering, in ^{199}Hg . . . 142
Graphite, polycrystalline, thermal inelastic scattering of cold neutrons in (L) . . . 314

PAGE
Hamiltonian, complete interaction, use in atomic rearrangement collisions . . . 26
Heisenberg model of ferromagnetic, high temperature susceptibility (R) . . . 765
Helium and similar atomic systems, wave functions (R) . . . 756
Helium atom, properties . . . 802
Helium atoms, inelastic scattering of electrons by . . . 299
Helium 1s2s^{1}S, simple analytic wave function . . . 296
HeH^{2+}, oscillator strengths of various transitions . . . 489, 617
HeH^{2+}, 2pσ state . . . 507
Helium, metastable, conversion from singlet to triplet state by electron collisions . . . 288
Helium, mobility of He$^+$ ions in He (R) . . . 474
Helium, solid, interatomic distance at which model of compressed solid He becomes metal . . . 97, 529
Heterocyclic systems, electronic absorption spectra of, I : A comparison of theoretical methods : pyridine and pyrazine . . . 593
Heterocyclic systems, electronic absorption spectra of, II : Applications to some two-ring nitrogen heterocyclics . . . 654
High energy fission, interpretation (R) . . . 546
High temperature dielectric breakdown of alkali halides . . . 761
Hydrogen, atomic, electron collision partial cross sections for 1s–2s and 1s–3s transitions (R) . . . 539
Hydrogen, atomic, excitation of discrete levels by fast electrons . . . 460
Hydrogen, capture of stopped negative pions by . . . 405
Hydrogen molecular ion, properties : VII—Magnetic dipole oscillator strengths of 1sσ_g–3dπ_g transition . . . 501
Hydrogen molecule, rotational transition by collision . . . 348
Hyperfine structure coupling constant of the 6s6p ^{3}P$_1$ level of ^{199}Hg by double resonance . . . 796
Hyperfine structure in $^{5}_{5}$Mn . . . 485

Indium antimonide, absorption and dispersion of . . . 776
Internal friction of single crystal silicon from 25°c to 1100°c (L) . . . 804
Ising model with second nearest neighbour interactions (R) . . . 615
Isotopic mass variation and thermal resistance (R) . . . 833

K Auger yield for tin . . . 262, corr. 770
Krypton, L-series emission spectrum . . . 466

Light output of KI crystals under bombardment by C ions (R) . . . 309
Liquids, absorption of beta-particles in (R) . . . 902
Long range forces, second order, exact calculation (R) . . . 223

Magnetic analysis, an investigation of the reaction ^{31}P(d, p)^{32}P . . . 586
Magnetic energy levels of electrons in metals . . . 275
Manganese, $^{55}_{25}$Mn, hyperfine structure . . . 485
Manganese, structure of x$^7\Sigma$ state of MnH and MnD (R) . . . 904
Mass action laws for reactions between free carriers and impurities in semiconductors considering electron spin (R) . . . 801
Meson, K-, decays through Fermi interaction . . . 321
Metal, interatomic distance at which solid He becomes metal . . . 97, 529
Metals, fluorescent yield, K Auger yield for tin . . . 262
Metals, magnetic energy levels of electrons in . . . 275
Microtron, means of avoiding ‘ electron rest mass ’ limitation (L) . . . 550
Mixtures, formulae for dielectric constant of . . . 769
Mobility of He$^+$ ions in He (R) . . . 474
Model independence, and electron scattering . . . 857
Molecular orbitals, approximate : VI—2pσ state of HeH^{2+} . . . 507
Molecular orbitals, curve crossing and orthogonality . . . 176
Moments of inertia, nuclear . . . 433
Moments of inertia of nuclei . . . 388, corr. 553

PAGE

Mu mesons, high energy, scattering in lead 421
Muon beam, polarized, experiments with (R) 543

Neutron beam, 350 Mev, from Liverpool synchrocyclotron, energy spectrum . . 735
Neutron cross sections, *see* Cross sections
Neutron flux, fast, measurement over neutron energy range 0·03 Mev to 3·0 Mev . 639
Neutrons, fast, capture below 1 Mev, cross sections for ^{238}U and ^{232}Th . . . 557
Neutrons, 14 Mev, interaction with medium weight nuclei 195
Neutrons in the energy range 0·03 Mev to 3·0 Mev; fission cross sections of ^{233}U, ^{235}U, ^{238}U and ^{239}Pu 573
Neutrons, low energy elastic scattering by deuterons 777
Neutrons, slowing down in infinite homogeneous media 793
Neutrons, *see also* Cross sections, Scattering
Nitrogen, activated, new phenomenon in (R) 480
Nitrogen, active, nature 887
Nitrogen afterglow, decay 877
Nitrogen heterobenzenes, electronic structure and spectra 41
Nuclear cross sections, *see* Cross sections
Nuclear disintegrations produced by cosmic ray particles in high pressure cloud chamber 134
Nuclear moments of inertia 433
Nuclear motion, collective model 381
Nuclear shell model, weak collective effects in (R) 532
Nuclear theory, compound, and optical model . . . . . 515, corr. 708
Nuclei, moments of inertia of . . . . 388, corr. 553
Nucleons, low energy, elastic scattering by complex nuclei 668

Particles, fast charged, emulsion spectrograph for determination of momenta: I—Design and theory 146
Particles, fast charged, emulsion spectrograph for determination of momenta: II—Construction and use for normal incidence 154
Particles, fast charged, scattering: II—Single scattering of 9·8 Mev positrons in xenon 355
Particles, fast charged, scattering: III—Single scattering of high energy positrons and electrons at small angles. 536
Particles, heavy, inelastic collisions between: V—Fast He ions 110
Particles, heavy, inelastic collisions between: VI—2s^{3}S–2p and 3p^{3}P excitations of fast He atoms 117
Particles, heavy, inelastic collisions between: VII—Electron loss from fast H atoms passing through He (R) 306
Particles, spin zero, dispersion relation for forward scattering by extended potential . 183
Photodisintegration of tantalum, direct excitation above giant resonance . . . 415
Photoproduction, elastic, of neutral pions from helium (R) 763
Photoproduction of pions at complex nuclei 629
Pion, radiative beta decay 729
Pions, neutral, elastic photoproduction from helium (R) 763
Pions, photoproduction of at complex nuclei 629
Pions, stopped negative, capture by hydrogen 405
Polarization of Gev protons scattered by complex nuclei 361
Polarization of protons scattered from carbon at 970 Mev (L) 165
Population of segments of random series including origin (L) 226
Potassium, liquid, model, electronic levels 713
Potential energy curve crossing, and inelastic heavy particle collisions: V—Charge transfer from neutral atoms to doubly and triply charged ions 809
Potential problems, short-range, variation–iteration method 512
Proton capture in ^{35}Cl, ^{37}Cl and ^{39}K, gamma radiation following 84
Proton capture in ^{35}Cl, ^{37}Cl and ^{39}K, γ-radiation following: II—Angular distributions and correlations 445

PAGE
Proton-proton scattering, analysis in coincidence in 703
Proton-proton scattering, polarization experiments in 690
Protons, elastic and inelastic, scattering by Mg 331
Protons from interaction of 14 MeV neutrons with medium weight nuclei 195
Protons, GeV, scattering by complex nuclei, polarization 361
Protons, 32 MeV, elastic scattering from gold 324
Protons, 900 MeV, nuclear cross sections for 209
Protons, scattered from carbon at 970 MeV, polarization (L) 165
Pyridine and pyrazine, *see* Heterocyclic systems.

Random series, including origin, population of segments (L) 226
Reaction, $^9Be(\gamma, 2n)^7Be$, integrated cross section from threshold to 30 MeV (R) 836
Reaction $^{12}C(d, p)^{13}C$ 68
Reaction $^3He(d, p)^4He$ between 100 and 500 keV 863
Reaction $^{31}P(d, p)^{32}P$, investigation by magnetic analysis 586
Reactions, proton-induced, in light elements, excitation functions for 824
Reactions, *see also* Stripping
Resonance, cyclotron, *see* Cyclotron
Resonances in a complex well 681
Rotational analysis of bands of the $A^3\Pi_{0+}$–$X^1\Sigma^+$ system of TlCl (L) 622

Scattering, elastic and inelastic, of protons by Mg 331
Scattering, elastic, of 32 MeV protons from gold 324
Scattering, elastic, low energy, of neutrons by deuterons 777
Scattering, elastic, of low energy nucleons by complex nuclei 668
Scattering, electron, and model independence 857
Scattering, forward, of spin zero particles by extended potential, dispersion relation for 183
Scattering, incoherent, of γ-rays from bound electrons of heavy elements 337
Scattering, inelastic, effectiveness of variational methods in problems 369
Scattering, multiple, in high pressure cloud chamber, and effects of distortion 17
Scattering, multiple, of positrons and electrons 188
Scattering, multiple, theory, first passage problem 253
Scattering, nuclear resonant, of gamma rays in ^{199}Hg 142
Scattering, nucleon–nucleon, at 95 MeV, phase-shift analysis 721
Scattering of electrons by positive ions, the use of extrapolated quantum defects as check on calculated phases 620
Scattering of fast charged particles: II—Single scattering of 9·8 MeV positrons in xenon 355
Scattering of fast charged particles: III—Single scattering of high energy positrons and electrons at small angles (R) 536
Scattering of high energy μ-mesons in lead 421
Scattering, n–α, contribution of tensor forces to 1
Scattering phases, s-wave, box variation method 494
Scattering, polarization of GeV protons scattered by complex nuclei 361
Scattering, proton–proton, analysis in coincidence in 703
Scattering, proton–proton, polerization experiments in 690
Scattering, thermal inelastic, of cold neutrons in polycrystalline graphite (L) 314
Scattering, *see also* Angular distribution, Protons
Semiconductors, mass action laws for reaction between free carriers and impurities considering electron spin. 801
Silicon, internal friction of single crystal from 25°C to 1100°C (L) 804
Spectra, and electronic structure, of nitrogen heterobenzenes 41
Spectra, flash-absorption, of plasmas of arcs and other discharges 815
Spectral lines, $L_{1,2}$, of lanthanum, remeasurement (L) 91
Spectrograph, emulsion: I—Design and theory 146
Spectrograph, emulsion: II—Construction and use for normal incidence 154
Spectrum, emission, L-series, of krypton 466
Statistical theory, foundations, and density matrix (L) 839
Stripping reactions, some aspects 62

PAGE

Sulphur, 35, β-spectrum of (L) . . . . 769, corr. 909
Susceptibility, high temperature, for Heisenberg model of ferromagnetic (R) . . 765
Synchrocyclotron, Liverpool, energy spectrum of 350 MeV neutron beam . . . 735
Tantalum, direct excitation above giant resonance in photodisintegration . . . 415
Tensor forces, contribution to n–α scattering 1
Thermal resistance due to isotopic mass variation (R) 833
Transition, rotational, of hydrogen molecule by collision 348

Variation–iteration method for short-range potentials 512
Variational calculation of cross section for 1s–2s excitation of hydrogen by electron impact (R) 398
Variational method, box, for calculating s-wave scattering phases 494
Variational methods, effectiveness for inelastic scattering problems 369

Wave functions for helium and similar atomic systems (R) 756
Wave mechanics, particle densities and sums of eigenvalues, variational method for calculation 169
Wigner coefficients, expressions for (L) 908
Wigner 9*j* coefficients, tabulation 571

Xenon, single scattering of 9·8 MeV positrons in 355

Zirconium fluoride, bands assigned to (L) 549

INDEX OF AUTHORS (WITH TITLES)

PAGE

Aitken, D. K. : A means of avoiding the ‘ electron rest mass ’ limitation in a microtron (L) . . . 550
Allen, H. R., with Sarma, N., and Govindjee, M. : A study of the reactions $^{12}C(d, p)^{13}C$ . . . 68
Allan, D. L. : Protons from the interaction of 14 MEV neutrons with medium weight nuclei . . . 195
Allen, K. R., Finlay, E. A., Lipsicas, M., Major, D., and Phillips, K. : The scattering of fast charged particles : II—On the single scattering of 9·8 MEV positrons in xenon . . . 355
Allen, K. R., Phillips, K., and Whittaker, F. : The scattering of fast charged particles : III—On the single scattering of high energy positrons and electrons at small angles (R) . . . 536
Allen, W. D., and Ferguson, A. T. G. : The fission cross sections of ^{233}U, ^{235}U, ^{238}U and ^{239}Pu for neutrons in the energy range 0·030 MEV to 3·0 MEV . . . 573
Allen, W. D. and Ferguson, A. T. G. : The measurement of fast neutron flux over the neutron energy range 0·03 MEV to 3·0 MEV . . . 639
Amado, R. D., and Blin-Stoyle, R. J. : Weak collective effects in the nuclear shell model (R) . . . 532
Anderson, J. M. : The nature of active nitrogen . . . 887
Anderson, J. M., Kavadas, A. D., and McKay, R. W. : The decay of the nitrogen afterglow . . . 877
Arthurs, A. M., Bond, R. A. B. and Hyslop, J. : The oscillator strengths of $1s\sigma$–$2p\sigma$, $2p\sigma$–$2s\sigma$, $2p\sigma$–$3d\sigma$ and $2p\sigma$–$2p\pi$ transitions of HeH^{2+} (R) . . . 617
Arthurs, A. M., and Hyslop, J. : The oscillator strengths of the $1s\sigma$–$2p\pi$, $2p\pi$–$2s\sigma$ and $2p\pi$–$3d\sigma$ transitions of HeH^{2+} . . . 489
Arthurs, A. M., and Hyslop, J. : Radiative charge transfer from H atoms to He^{2+} ions 849
Ashmore, A., Jarvis, R. G., Mather, D. S., and Sen, S. K. : The energy spectrum of the 350 MEV neutron beam from the Liverpool synchrocyclotron . . . 735
Ashmore, A., Jarvis, R. G., Mather, D. S., and Sen, S. K. : Nuclear total cross section for 350 MEV neutrons . . . 745

Bagguley, D. M. S., Powell, J. A., and Taylor, D. J. : Cyclotron resonance over a wide temperature range (R) . . . 759
Baliga, B. B., with Ghoshal, S. N. : Elastic scattering of 32 MEV protons from gold . 324
Barrow, R. F. : On the rotational analysis of bands of the $A^3\Pi_{0^+}$–$X^1\Sigma^+$ system of TlCl (L) . . . 622
Barrow, R. F., Dodsworth, P. G., and Zeeman, P. B. : Rotational analysis of bands of the $A^3\Pi_{0^+}$, $B^3\Pi_1$–$X^1\Sigma^+$ systems of gallium monofluoride . . . 34
Barrow, R. F., and Miescher, E. : Fine structure analysis of NO absorption bands in the Schumann region . . . 219
Barton, J. C. : The first passage problem in the theory of multiple scattering . . 253
Barton, J. C., Campbell, D. A., and Read, R. C. : An analogue method for studying multiple scattering . . . 605
Bates, D. R., and Miskelly, D. : Electron collision partial cross sections for the 1s–2s and 1s–3s transitions of atomic hydrogen (R) . . . 539
Bates, D. R., and Williams, A. : Inelastic collisions between heavy particles : VII—Electron loss from fast hydrogen atoms passing through helium (R) . . . 306
Baxter, P., and Stannard, F. R. : The use of multiple scattering and the effects of distortion in a high-pressure cloud chamber . . . 17
Bell, J. S. : Time reversal in beta-decay (L) . . . 552
Bellamy, E. H., McWhirter, R. W. P., Palit, P. : The elastic photoproduction of neutral pions from helium (R) . . . 763
Berenbaum, R., and Matthews, J. H. : Gamma radiation following proton capture in ^{35}Cl, ^{37}Cl, and ^{39}K : II—Angular distributions and correlations . . . 445

PAGE

Berenbaum, R., with Towle, J. H., and Matthews, J. H. : γ-radiation following proton capture in ^{35}Cl, ^{37}Cl and ^{39}K 84
Biel, S. J. : The binding energy of ^{8}Be and ^{12}C 866
Blin-Stoyle, R. J., with Amado, R. D. : Weak collective effects in the nuclear shell model (R) 532
Bond, R. A. B., with Arthurs, A. M., and Hyslop, J. : The oscillator strengths of $1s\sigma$–$2p\sigma$, $2p\sigma$–$2s\sigma$, $2p\sigma$–$3d\sigma$ and $2p\sigma$–$2p\pi$ transitions of HeH^{2+} (R) 617
Booth, D. L., Hill, R. S., Price, F. V., and Roaf, D. : The reaction ^{3}He(d, p)^{4}He between 100 kev and 500 kev 863
Booth, N. E., Ledley, B., Walker, D., and White, D. H. : Nuclear cross sections for 900 Mev protons 209
Boucher, F. B., with Irving, J. : A variation–iteration method for short range potential problems 512
Bowcock, J. : Compound nuclear theory and the optical model 515, corr. 708
Boyd, T. J. M., and Moiseiwitsch, B. L. : Inelastic heavy particle collisions involving the crossing of potential energy curves : V—Charge transfer from neutral atoms to doubly and triply charged ions 809
Boyd, T. J. M., Moiseiwitsch, B. L., and Stewart, A. L. : Inelastic collisions between heavy particles : V — Electron loss for fast He$^+$ ions passing through atomic hydrogen, and ionization of hydrogen atoms by fast He$^+$ ions 110
Brailsford, A. D. : The magnetic energy levels of electrons in metals 275
Bransden, B. H., and McKee, J. S. C. : A variation calculation of the cross section for the 1s–2s excitation of hydrogen by electron impact (R) 398
Brown, G. E. : Polarization of Gev protons scattered by complex nuclei 361
Brown, G. E. : Resonances in a complex well 818
Brown, G. E., and De Dominicis, C. T. : Elastic scattering of low energy nucleons by complex nuclei 668
Brown, G. E., and De Dominicis, C. T. : Direct interaction and under dispersion theory 686
Brown, G. E. and Kanellopoulos, T. V. : Analysis in coincidence in proton–proton scattering 703
Brown, G. E., with Kanellopoulos, T. V. : Polarization experiments in proton–proton scattering 690
Burcham, W. E. : Light output of potassium iodide crystals under bombardment by carbon ions 309
Burke, P. G., and Robertson, H. H. : The low energy scattering of neutrons by deuterons 777

Calvert, J. M., Jaffe, A. A., and Maslin, E. E. : An investigation of the reactions ^{12}C(d, n)^{13}N and ^{28}Si(d, n)^{29}P 78
Campbell, D. A., with Barton, J. C., and Read, R. C. : An analogue method for studying multiple scattering 605
Carroll, P. K., and Daly, P. J. : Bands assigned to ZrF (L) 549
Carver, J. H., Edge, R. S., and Lokan, K. H. : Direct excitation in the photodisintegration of tantalum above the giant resonance 415
Cassels, J. M., Fidecaro, G., Wetherell, A. M., and Wormald, J. R. : The capture of stopped negative pions by hydrogen 405
Cassels, J. M., O'Keefe, T. W., Rigby, M., Wetherell, A. M. and Wormald, J. R. : Experiments with a polarized muon beam (R) 543
Cassels, J. M., Rigby, M., Wetherell, A. M., and Wormald, J. R. : Radiative beta decay of the pion 729
Connor, R. D., and Fairweather, I. L. : The β-spectrum of sulphur 35 (L) 769, corr. 909
Corngold, N. : Slowing down of neuterons in infinite homogeneous media 793

Dalgarno, A., and Lynn, N. : Curve crossing and orthogonality of molecular orbitals 176
Dalgarno, A., and Lynn, N. : An exact calculation of second-order long range forces (R) 223
Dalgarno, A., and Lynn, N. : Properties of the helium atom 802

PAGE
Dalgarno, A., and McCarroll, R. : Properties of the hydrogen molecular ion : VII—Magnetic dipole oscillator strengths of the $1s\sigma_g$-$3d\pi_g$ transition 501
Dalton, A. W., Hinds, S. and Parry, G. : An investigation of the reaction $^{31}P(d, p)^{32}P$ by magnetic analysis 586
Daly, P. J., with Carroll, P. K. : Bands assigned to ZrF (L) 549
Dean, P., with Eisenschitz, R. : Electronic levels of a model of liquid potassium . 713
De Dominicis, C. T., with Brown, G. E. : Elastic scattering of low energy nucleons by complex nuclei 668
De Dominicis, C. T., with Brown, G. E. : Direct interaction and nuclear dispersion theory 686
Dickinson, N., with Kellermann, W. E., and Shaw, T. : On the structure of extensive cosmic ray air showers: core detection and core structure 452
Dodsworth, P. G., with Barrow, R. F., and Zeeman, P. B. : Rotational analysis of bands of the $A^3\Pi_{0^+}$, $B^3\Pi_1$–$X^1\Sigma^+$ systems of gallium monofluoride . . . 34

Edge, R. S., with Carver, J. H., and Lokan, K. H. : Direct excitation in the photo-disintegration of tantalum above the giant resonance 415
Eisenschitz, R., and Dean, P. : Electronic levels of a model of liquid potassium . . 713
El Bedewi, F. A., and Hussein, I. : Magnetic analysis of tritons and alpha particles emitted from the deuteron bombardment of teflon 233
Elcock, E. W. : A note on the Ising model with second nearest neighbour interactions (R) 615
El Nadi, Mohamed : Some aspects of the stripping reactions 62

Fairbrother, J. A. V., Parkyn, D. G., and O'Connor, B. M. : The K Auger yield for tin 262
Fairweather, I. L., with Connor, R. D. : The β-spectrum of sulphur 35 (L) 769, corr. 909
Feather, N. : Note on the population of segments of a random series which include the origin (L) 226
Feather, N., Miller, N., and Peat, S. W. : Search for a rare α-emission in ^{228}Ra(MsTh 1) (R) 478
Ferguson, A. T. G., with Allen, W. D. : The fission cross sections of ^{233}U, ^{235}U, ^{238}U and ^{239}Pu for neutrons in the energy range 0·030 Mev to 3·0 Mev 573
Ferguson, A. T. G., with Allen, W. D. : The measurement of fast neutron flux over the neutron energy range 0·03 Mev to 3·0 Mev 639
Fidecaro, G., with Cassels, J. M., Wetherell, A. M., and Wormald, J. R. : The capture of stopped negative pions by hydrogen 405
Finlay, E. A., with Allen, K. R., Lipsicas, M., Major, D., and Phillips, K. : The scattering of fast charged particles : II—On the single scattering of 9·8 Mev positrons in xenon 355

Garton, W. R. S., and Rajaratnam, A. : Flash-absorption spectra of the plasmas of arcs and other discharges 815
Ghoshal, S. N., and Baliga, B. B. : Elastic scattering of 32 Mev protons from gold 324
Govindjee, M., with Sarma, N., and Allan, H. R. : A study of the reactions $^{12}C(d, p)^{13}C$ 68
Greenlees, G. W., Haywood, B. C., Kuo, L. G., and Petravić, M. : The elastic and inelastic scattering of protons by Mg 331

Hayes, W., McCarvill, P. D., and Nevin, T. E. : The structure of the $X^7\Sigma$ state of MnH and MnD (R) 904
Haywood, B. C., with Greenlees , G. W., Kuo, L. G., and Petravić, M. : The elastic and inelastic scattering of protons by Mg 331
Henderson, C., and Scott, A. : The multiple scattering of positrons and electrons . 188
Hill, R. S., with Booth, D. L., Price, F. V., and Roaf, D. : The reaction $^3He(d, p)^4He$ between 100 kev and 500 kev 863
Hilmi, A., with Husain, S. A., : Absorption of beta particles in liquids (R) . . 902
Hinds, S., with Dalton, A. W., and Parry, G. : An investigation of the reaction $^{31}P(d, p)^{32}P$ by magnetic analysis 586

PAGE

Hinds, S., Middleton, R., and Parry, G. : Angular distributions of some inelastically scattered deuteron groups from ^{24}Mg and ^{28}Si (R) 900
Huck, R. J. : The effectiveness of variational methods for inelastic scattering problems 369
Husain, S. A., and Hilmi, A. K. : Absorption of beta particles in liquids (R) 902
Husain, S. A., and Putman, J. L. : The absorption of beta particles as a function of atomic number (R) 304
Hussein, I., with El Bedewi, F. A. : Magnetic analysis of tritons and alpha particles emitted from the deuteron bombardment of teflon 233
Hyslop, J., with Arthurs, A. M. : The oscillator strengths of the $1s\sigma$–$2p\pi$, $2p\pi$–$2s\sigma$ and $2p\pi$–$3d\sigma$ transitions of HeH^{2+} 489
Hyslop, J., with Arthurs, A. M.: Radiative charge transfer from H atoms to He^{2+} ions 849
Hyslop, J., with Arthurs, A. M., and Bond, R. A. B. : The oscillator strengths of 1s–2p, 2p–2s, 2p–3d and 2p–2p transitions of HeH^{2+} (R) 617
Hodgson, P. E., with Sugie, A., and Robertson, H. H. : The contribution of tensor forces to n–α scattering 1

Irving, J., and Boucher, F. B. : A variation–iteration method for short range potential problems 512

Jackson, J. D. : On the use of the complete interaction Hamiltonian in atomic rearrangement collisions 26
Jaffe, A. A., with Calvert, J. M., and Maslin, E. E. : An investigation of the reactions ^{12}C(d, n)^{13}N and ^{28}Si(d, n)^{29}P 78
Jarvis, R. G., with Ashmore, A., Mather, D. S., and Sen, S. K. : The energy spectrum of the 350 MeV neutron beam from the Liverpool synchrocyclotron 735
Jarvis, R. G., with Ashmore, A., Mather, D. S., and Sen, S. K. : Nuclear total cross sections for 350 MeV neutrons 745

Kanellopoulos, T. V., and Brown, G. E. : Polarization experiments in proton–proton scattering 690
Kanellopoulos, T. V., with Brown, G. E. : Analysis in coincidence in proton–proton scattering 703
Kavadas, A. D., with Anderson, J. M., and McKay, R. W. : The decay of the nitrogen afterglow 877
Kellermann, E. W., Shaw, T., and Dickinson, N.,: On the structure of extensive cosmic ray air showers : Core detection and core structure 452
Klemens, P. G. : Thermal resistance due to isotopic mass variation (R) 833
Knapp, V. : Nuclear resonant scattering of gamma rays in ^{199}Hg 142
Kothari, L. S., and Singwi, K. S. : Thermal inelastic scattering of cold neutrons in polycrystalline graphite (L) 314
Kuo, L. G., with, Greenlees, G. W., Haywood, B. C., and Petravić, M.,: The elastic and inelastic scattering of protons by Mg 331

Laing, E. W., and Moorhouse, R. G. : Photoproduction of pions at complex nuclei 629
Lane, A. M., and Lynn, J. E. : Fast neutron capture below 1 MeV : The cross sections for ^{238}U and ^{232}Th 557
Ledley, B., with Booth, N. E., Walker, D., and White, D. H. : Nuclear cross sections for 900 MeV protons 209
Lipsicas, M., with Allen, K. R., Finlay, E. A., Major, D., and Phillips, K. : The scattering of fast charged particles : II—On the single scattering of 9·8 MeV positrons in xenon 355
Lloyd, J. L., Rössle, E., and Wolfendale, A. W. : The scattering of high-energy μ-mesons in lead 421
Lokan, K. H. : The integrated cross section from threshold to 30 MeV for the reaction ^{9}Be(γ, 2n)^{7}Be 836
Lokan, K. H., with Carver, J. H., and Edge, R. S. : Direct excitation in the photodisintegration of tantalum above the giant resonance 415
Lynn, N., and Moiseiwitsch, B. L. : The mobility of He^{+} ions in helium (R) 474
Lynn, N., with Dalgarno, A. : Curve crossing and orthogonality of moleuclar orbitals 176

Lynn, N., with Dalgarno, A.,: An exact calculation of second order long range forces (R) 223
Lynn, N., with Dalgarno, A. : Properties of the helium atom 802
Lynn, J. E., with Lane, A. M. : Fast neutron capture below 1 Mev : The cross sections for ^{238}U and ^{232}Th 557

McCarroll, R. : The excitation of discrete levels of atomic hydrogen by fast electrons 460
McCarroll, R., and Moiseiwitsch, B. L. : Approximate molecular orbitals : VI—The $2p\sigma$ state of HeH^{2+} 507
McCarroll, R., with Dalgarno, A. : Properties of the hydrogen molecular ion : VII—Magnetic dipole oscillator strengths of the $1s\sigma_g$-$3d\pi_g$ transition 501
McCarvill, P. D., with Hayes, W., and Nevin, T. E. : The structure of the $x^7\Sigma$ state of MnH and MnD (R) 904
McKay, R. W., with Anderson, J. M., and Kavadas, A. D. : The decay of the nitrogen afterglow 877
McKee, J. S. C., with Bransden, B. H. : A variational calculation of the cross section for the 1s–2s excitation of hydrogen by electron impact (R) 398
McWeeny, R. : Electronic absorption spectra of heterocyclic systems : I—A comparison of theoretical methods : pyridine and pyrazine 593
McWeeny, R., and Peacock, T. E. : The electronic structure and spectra of some nitrogen heterobenzenes 41
McWhirter, R. W. P., Bellamy, E. H., and Palit, P. : The elastic photoproduction of neutral pions from helium (R) 763
Major, D., with Allen, K. R., Finlay, E. A., Lipsicas, M., and Phillips, K. : The scattering of fast charged particles : II—On the single scattering of 9·8 Mev positrons in xenon 355
Mandl, F.,: Dispersion relation for forward scattering of spin zero particles by an extended potential 183
March, N. H. : The density matrix and the foundations of the statistical theory (L) 839
March, N. H. : A variational method for the calculation of particle densities and sums of eigenvalues in wave mechanics 169
Marquez, L. : On the interpretation of high energy fission (R) 546
Marriott, R. : The conversion of metastable helium from the singlet to the triplet state by electron collisions 288
Marriott, R., and Seaton, M. J. : A simple analytic wave function for He $1s2s\,^1S$. 296
Martin, J. S., with Woodgate, G. K. : Hyperfine structure in manganese $^{55}_{25}$Mn . . 485
Maslin, E. E., with Calvert, J. M., and Jaffe, A. A. : An investigation of the reactions ^{12}C(d, n)^{13}N and ^{28}Si(d, n)^{29}P 78
Mather, D. S., with Ashmore, A., Jarvis, R. G., and Sen, S. K. : Nuclear total cross sections for 350 Mev neutrons 745
Mather, D. S., with Sen, S. K., Ashmore, A., and Jarvis, R. G. : The energy spectrum of the 350 Mev neutron beam from the Liverpool synchrocyclotron . 735
Matthews, J. H., with Berenbaum, R. : Gamma radiation following proton capture in ^{35}Cl, ^{37}Cl and ^{39}K : II—Angular distributions and correlations 445
Matthews, J. H., with Towle, J. H., and Berenbaum, R. : γ-radiation following proton capture in ^{35}Cl, ^{37}Cl and ^{39}K 84
Middleton, R., with Hinds, S., and Parry, G. : Angular distributions of some inelastically scattered deuteron groups from ^{24}Mg and ^{28}Si (R) 900
Miescher, E., with Barrow, R. F. : Fine structure analysis of NO absorption bands in the Schumann region 219
Miller, W. F., and Platzman, R. L. : On the theory of the inelastic sacttering of electrons by helium atoms 299
Miller, N., with Feather, N., and Peat, S. W. : Search for a rare α-emission in ^{228}Ra(MsTh 1) (R) 478
Miskelly, D., with Bates, D. R. : Electron collision partial cross sections for the 1s–2s and 1s–3s transitions of atomic hydrogen (R) 539
Moiseiwitsch, B. L., with Boyd, T. J. M. : Inelastic heavy particle collisions involving the crossing of potential energy curves : V—Charge transfer from neutral atoms to doubly and triply charged ions 809

PAGE
Moiseiwitsch, B. L., with Boyd, T. J. M., and Stewart, A. L. : Inelastic collisions between heavy particles : V— Electron loss for fast He$^+$ ions passing through atomic hydrogen, and ionization of hydrogen atoms by fast He$^+$ ions 110
Moiseiwitsch, B. L., with Lynn, N. : The mobility of He$^+$ ions in helium (R) 474
Moiseiwitsch, B. L., with McCarroll, R. : Approximate molecular orbitals : VI— The 2pσ state of HeH^{2+} 507
Moore, H. R. : The L-series emission spectrum of krypton 466
Moorhouse, R. G., with Laing, E. W. : Photoproduction of pions at complex nuclei 629

Nevin, T. E., with Hayes, W., and McCarvill, P. D. : The structure of the $X^7\Sigma$ state of MnH and MnD (R) 904
Nicholson, K. P., with Gayther, D. B. : The average neutron total cross sections of heavy elements at low energy 51

O'Connor, B. M., with Fairbrother, J. A. V., and Parkyn, D. G. : The K Auger yield for tin 262
O'Keefe, T. W., with Cassels, J. M., Rigby, M., Wetherell, A. M., and Wormald, J. R. : Experiments with a polarized muon beam (R) 543

Palit, P., Bellamy, E. H., and McWhirter, R. W. P. : The elastic photoproduction of neutral pions from helium (R) 763
Park, D. : An improved Born approximation (R) 905
Parkyn, D G., with Fairbrother, J. A. V., and O'Connor, B. M. : The K Auger yield for tin 262
Parry, G., with Hinds, S., and Middleton, R.: Angular distributions of some inelastically scattered deuteron groups from ^{24}Mg and ^{28}Si (R) 900
Peacock, T. E. : Electronic absorption spectra of heterocyclic systems : II— Applications to some two-ring nitrogen heterocyclics 654
Peacock, T. E., with McWeeny, R. : The electronic structure and spectra of some nitrogen heterobenzenes 41
Peat, S. W., with Feather, N., and Miller, N. : Search for a rare α-emission in ^{228}Ra(MsTh 1) (R) 478
Peierls, R. E., and Yoccoz, J. : The collective model of nuclear motion 381
Percival, I. C. : A box variational method for scattering phases 494
Percival, I. C. : Electron excitation of 3p levels of O I 241
Petravć, M., with Greenlees, G. W., Haywood, B. C., and Kuo, L. G. : The elastic and inelastic scattering of protons by Mg 331
Phillips, K. with Allen, K. R., Finlay, E. A., Lipsicas, M., and Major, D. : The scattering of fast charged particles : II—On the single scattering of 9·8 MEV positrons in xenon 355
Phillips, K., with Allen, K. R., and Whittaker, F. : The scattering of fast charged particles : III—On the single scattering of high energy positrons and electrons at small angles (R) 536
Phillips, R. J. N. : A phase-shift analysis of nucleon–nucleon scattering at 95 MEV 721
Platzman, R. L., with Miller, W. F. : On the theory of the inelastic scattering of electrons by helium atoms 299
Polkinghorne, J. C., Pursey, D. L., and Santa Maria, H. A. : K-meson decays through a Fermi interaction 321
Powell, J. A., with Bagguley, D. M. S., and Taylor, D. J. : Cyclotron resonance over a wide temperature range (R) 759
Price, F. V., with Booth, D. L., Hill, R. S., and Roaf, D. : The reaction ^{3}He(d, p)^{4}He between 100 kev and 500 kev 863
Price, P. C. : The radiative capture of alpha particles in ^{15}N 661
Pursey, D. L., with Polkinghorne, J. C., and Santa Maria, H. A. : K-meson decays through a Fermi interaction 321
Putman, J. L., with Husain, S. A. : The absorption of beta particles as a function of atomic number (R) 304

Rajaratnam, A., with Garton, W. R. S.: Flash-absorption spectra of the plasmas of arcs and other discharges 815

Randles, J. : Incoherent scattering of gamma rays from the bound electrons of heavy elements . . . 337
Ravenhall, D. G., and Yennie, D. R. : Electron scattering and model independence . 857
Read, R. C., with Barton, J. C., and Campbell, D. A. An analogue method for studying multiple scattering . . . 605
Rigby, M., with Cassels, J. M., Wetherell, A. M., and Wormald, J. R. : Radiative beta decay of the pion . . . 729
Rigby, M., with Cassels, J. M., O'Keefe, T. W., Wetherell, A. M., and Wormald, J. R. : Experiments with a polarized muon beam (R) . . . 543
Roaf, D., with Booth, D. L., Hill, R. S., and Price, F. V. : The reaction ^{3}He(d, p)^{4}He between 100 kev and 500 kev . . . 863
Robertson, H. H., with Burke, P. G. : The low energy scattering of neutrons by deuterons . . . 777
Robertson, H. H., with Sugie, A., and Hodgson, P. E. : The contribution of tensor forces to n–α scattering . . . 1
Rössle, E., with Lloyd, J. L., and Wolfendale, A. W. : The scattering of high-energy μ-mesons in lead . . . 421
Rushbrooke, G. S., with Wood, P. J. : On the high temperature susceptibility for the Heisenberg model of a ferromagnetic (R) . . . 765
Russell, P. C., and Stewardson, E. A. : A remeasurement of the L$\alpha_{1,2}$ lines of lanthanum (L) . . . 91

Santa Maria, H. A., with Polkinghorne, J. C., and Pursey, D. L. : K-meson decays through a Fermi interaction . . . 321
Sarma, N., Govindjee, M., and Allan, H. R. : A study of the reactions ^{12}C(d, p)^{13}C . 68
Scott, A., with Henderson, C. : The multiple scattering of positrons and electrons . 188
Seaton, M. J. : The use of extrapolated quantum defects as a check on calculated phases for scattering of electrons by positive ions (R) . . . 620
Seaton, M. J., with Marriott, R. : A simple analytic wave function for He 1s2s^{1}S . 296
ten Seldam, C. A. : Calculation of the interatomic distance at which a model of compressed solid helium becomes a metal . . . 97, 529
Sen, S. K., with Ashmore, A., Jarvis, R. G., and Mather, D. S. : The energy spectrum of the 350 Mev neutron beam from the Liverpool synchrocyclotron . . . 735
Sen, S. K., with Ashmore, A., Jarvis, R. G., and Mather, D. S. : Nuclear total cross sections for 350 Mev neutrons . . . 745
Shaw, T., with Kellermann, E. W., and Dickinson, N. : On the structure of extensive cosmic ray air showers : core detection and core structure . . . 452
Singwi, K. S., with Kothari, L. S. : Thermal inelastic scattering of cold neutrons in polycrystalline graphite (L) . . . 314
Skyrme, T. H. R. : Nuclear moments of inertia . . . 433
Smith, K., with Stephenson, J. W. : Tabulation of the Wigner 9*j* coefficients . . 571
Stannard, F. R., with Baxter, P. : The use of multiple scattering and the effects of distortion in a high-pressure cloud chamber . . . 17
Stephenson, J. W., and Smith, K. : Tabulation of the Wigner 9*j* coefficients . . 571
Stewardson, E. A., with Russell, P. C. : A remeasurement of the L$\alpha_{1,2}$ lines of lanthanum (L) . . . 91
Stewart, A. L. : Wave functions for helium and similar atomic systems (R) . . 756
Stewart, A. L., with Boyd, T. J. M., and Moiseiwitsch, B. L. : Inelastic collisions between heavy particles : V—Electron loss for fast He$^+$ ions passing through atomic hydrogens and ionization of hydrogen atoms by fast He$^+$ ions . . 110
Stone, A. P. : Expressions for certain Wigner coefficients (L) . . . 908
Sugie, A., Hodgson, P. E., and Robertson, H. H. : The contribution of tensor forces to n–α scattering . . . 1
Symonds, J. L., Warren, J., and Young, J. D. : Excitation functions up to 908 Mev for proton-induced reactions in some light elements . . . 824

Takayanagi, K. : Rotational transition of hydrogen molecule by collision . . 348
Taylor, D. J., with Bagguley D. M. S., and Powell, J. A. : Cyclotron resonance over a wide temperature range (R) . . . 759

PAGE

Towle, J. H., Berenbaum, R., and Matthews, J. H. : γ-radiation following proton capture in ^{35}Cl, ^{37}Cl and ^{39}K 84

Walker, D., with Booth, N. E., Ledley, B., and White, D. H. : Nuclear cross sections for 900 Mev protons 209
Warren, J., with Symonds, J. L., and Young, J. D. : Excitation functions up to 980 Mev for proton-induced reactions in some light elements 824
Wetherell, A. M., with Cassels, J. M., Fidecaro, G., and Wormald, J. R. : The capture of stopped negative pions by hydrogen 405
Wetherell, A. M., with Cassels, J. M., O'Keefe, T. W., Rigby, M., and Wormald, J. R. : Experiments with a polarized muon beam (R) 543
Wetherell, A. M., with Cassels, J. M., Rigby, M., and Wormald, J. R. : Radiative beta decay of the pion 729
White, D. H., with Booth, N. E., Ledley, B., and Walker, D. : Nuclear cross section for 900 Mev protons 209
Whittaker, F., with Allen, K. R., and Phillips, K. : The scattering of fast charged particles : III—On the single scattering of high energy positrons and electrons at small angles (R) 536
Williams, A., with Bates, D. R. : Inelastic collisions between heavy particles : VII—Electron loss from fast hydrogen atoms passing through helium (R) . 306
Wolfendale, A. W., with Lloyd, J. L., and Rössle, E. : The scattering of high-energy μ-mesons in lead 421
Wood, P. J., and Rushbrooke, G. S. : On the high temperature susceptibility for the Heisenberg model of a ferromagnetic (R) 765
Woodgate, G. K., and Martin, J. S. : Hyperfine structure in manganese ${}^{55}_{25}$Mn . . 485
Wormald, J. R., Cassels, J. M., Rigby, M., and Wetherell, A. M.,: Radiative beta decay of the pion 729
Wormald, J. R., with Cassels, J. M., Fidecaro, G., and Wetherell, A. M. : The capture of stopped negative pions by hydrogen 405
Wormald, J. R., with Cassels, J. M., O'Keefe, T. W., Rigby, M., and Wetherell, A. M.: Experiments with a polarized muon beam (R) 543

Yennie, D. R., with Ravenhall, D. G. : Electron scattering and model independence 857
Yoccoz, J. : On the moments of inertia of nuclei . . . . . . 388, corr. 553
Yoccoz, J., with Peierls, R. E. : The collective model of nuclear motion 381
Young, J. D., with Symonds, J. L., and Warren, J. : Excitation functions up to 980 Mev for proton-induced reactions in some light elements 824

Zeeman, P. B., with Barrow, R. F., and Dodsworth, P. G. : Rotational analysis of bands of the A$^3\Pi_{0^+}$, B$^3\Pi_1$–X$^1\Sigma_+$ systems of gallium monofluoride 34

INDEX TO REVIEWS OF BOOKS

PAGE

Academy of Sciences of the U.S.S.R. : *English translation of the Bulletin*, Vol. XIX, No. 5 844
Appleton, Sir Edward : *Science and the nation. The Reith lectures*, 1956 . . 771

Bass, J. : *Cours de mathématiques* 773
Beckerley, J. G., Kamen, M.D., and Schiff, L. I. : *Annual review of nuclear science* Vol. 6, 1956 710
Berthelot, A. : *Rayonnements de particules atomiques, électrons et photons* . . . 709
Bethe, H. A., and Morrison, P. : *Elementary nuclear theory* (2nd Edn) . . 401
Blin-Stoyle, R. J. : *Theories of nuclear moments* 845
Bodewig, E. : *Matrix calculus* 625
Booth, A. D., and Booth, K. H. V. : *Automatic digital calculators* (2nd Edn) . . 318
Born, Max : *Physics in my generation* 167
Buck, R. C. : *Advanced calculus* 627
Bugher, J. C., Coursaget, J., and Loutit, J. F. : *Progress in nuclear energy. Series VI. Biological sciences.* Vol. 1 401

Cartmell, E., and Fowles, G. W. A. : *Valency and molecular structure* 94
Charpie, R. A., Horowitz, J., Hughes, D. J., and Littler, D. J. : *Progress in nuclear energy. Series I. Physics and mathematics* 230
Charpie, R. A., Hughes, D. J., Littler, D. J., and Trocheris, N. : *Progress in nuclear energy. Series II. Reactors.* Vol. 1 709

Davison, B. : *Neutron transport theory* 910

'Espinasse, Margaret : *Robert Hooke* 624

Finkelnburg, W. : *Einführung in die Atomphysik* 843
Flammer, C. : *Spheroidal wave functions.* (Stanford Research Institute Monograph) 844
Flügge, S. (Ed.) : *Handbuch der Physik.* Band I. *Mathematical methods* 1 . . 554
Flügge, S. (Ed.) : *Handbuch der Physik.* Band XXXII. *Structural research* . 847

Giet, A. : *Abacs or nomograms* 317

Heitler, W. : *Elementary wave mechanics, with applications to quantum chemistry* (2nd Edn) 316
Hiscocks, E. S. : *Laboratory administration* 403

Institute of Physics : *The education of physicists in universities and colleges of technology* 911

Jauch, J. M., and Rohrlich, F. : *The theory of photons and electrons* 318

Marshall, J. S., and Pounder, E. R. : *Physics* 771
Marton, L., Marton, C., and Hall, W. G. : *Electron physics tables, N.B.S. circular* 571 (supersedes part II of *Mathematical table* 17) 95
McLachlan, N. W. : *Ordinary non-linear differential equations in engineering and physical sciences* 229
Montgomerie, G. A. : *Digital calculating machines* 711

Page, C. H. : *Physical mathematics* 402
Pearcey, T. : *Table of the Fresnel integral to six decimal places* 711
Picht, J. : *Vorlesungen über Atomphysik*, Band I 772
Pluvinage, P. H. : *Éléments de mécanique quantique* 775

PAGE

Schrödinger, E. : *Expanding universes* . . . 93
Schuler, M., and Gebelein, H. : *Five place tables of elliptic functions* . . . 316
Schuler, M., and Gebelein, H. : *Eight and nine place tables of elliptic functions* . 316
Sneddon, I. N. : *Elements of partial differential equations* . . . 843
Stratton, J. A., Morse, P. M., Chu, L. J., Little, J. D. C., and Corbató, F. J., *Spheroidal wave functions* . . . 626

Temperley, H. N. V. : *Changes of state* . . . 554

Umezawa, H. : *Quantum field theory* . . . 228
U.S. Department of Commerce, N.B.S. Applied Mathematics Series XXXVII : *Tables of functions and of zeros of functions.* . . . 842
U.S. Department of Commerce. N.B.S. Applied Mathematics Series XLI (Reissue of Mathematical Table 8) : *Tables of the error function and its derivative* 842

Van Allen : J. A. : *Scientific uses of earth satellites* . . . 846

Wheland, G. W. : *Resonance in organic chemistry* . . . 228
Wilson, A. J. C., Baenziger, N. C., Bijvoet, J. M., and Robertson, J. M. : *Structure reports for* 1942–1944 . . . 94
Wolfe, H. C. : *Temperature—its measurement and control in science and industry.* Vol. II . . . 772

(Zurich) : *Proceedings of the 2nd International Congress of the International Union for the Philosophy of Science.* Zurich, 1954. 5 vols. . . . 230

DATE DUE

OCT 21 '79 PER			

DEMCO 38-297